

# Atmospheric Exploration by Remote Probes

VOLUME 2

Proceedings of the Scientific Meetings of  
the Panel on Remote Atmospheric Probing

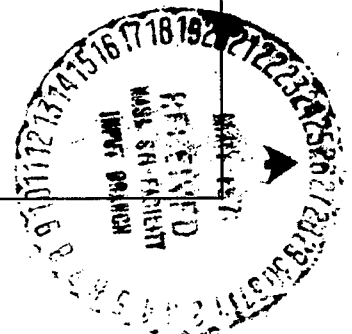
APRIL 18-20 and MAY 16-17, 1968

(NASA-CR-126787) ATMOSPHERIC EXPLORATION BY REMOTE PROBES. VOLUME 2: PROCEEDINGS OF SCIENTIFIC MEETINGS OF THE PANEL (National Academy of Sciences-National Research) Jan. 1969 710 p

N72-25347  
thru  
N72-25388  
Unclas  
30777

CSCL 04A G3/13

Reproduced by  
NATIONAL TECHNICAL  
INFORMATION SERVICE  
U S Department of Commerce  
Springfield VA 22151



# Atmospheric Exploration by Remote Probes

VOLUME 2

Proceedings of the Scientific Meetings of  
the Panel on Remote Atmospheric Probing

APRIL 18-20 and MAY 16-17, 1968

*Final Report of the*  
PANEL ON REMOTE ATMOSPHERIC PROBING  
to the  
COMMITTEE ON ATMOSPHERIC SCIENCES  
NATIONAL ACADEMY OF SCIENCES  
NATIONAL RESEARCH COUNCIL

January 1969

## COMMITTEE ON ATMOSPHERIC SCIENCES

Robert G. Fleagle, Chairman, University of Washington

Louis J. Battan, University of Arizona

Henry G. Booker, University of California-San Diego

George F. Carrier, Harvard University

Jule G. Charney, Massachusetts Institute of Technology

Michael Ference, Jr., Ford Motor Company

William W. Kellogg, National Center for Atmospheric Research

Paul E. Klopsteg (member emeritus), Glenview, Illinois

C. Gordon Little, Environmental Science Services Administration

Gordon J. F. MacDonald, University of California-Santa Barbara

Thomas F. Malone, Travelers Insurance Companies

William A. Nierenberg, Scripps Institution of Oceanography

Verner E. Suomi, University of Wisconsin

Edward Teller, University of California-Livermore

Philip D. Thompson, National Center for Atmospheric Research

John R. Sievers, Executive Secretary, National Research Council

PANEL ON REMOTE ATMOSPHERIC PROBING

David Atlas, Chairman, University of Chicago

Alan H. Barrett, Massachusetts Institute of Technology

Louis J. Battan, University of Arizona

Ralph Bolgiano, Jr., Cornell University

David C. Hogg, Bell Telephone Laboratories, Inc.

John N. Howard, Air Force Cambridge Research Laboratories

C. Gordon Little, Environmental Science Services Administration

Anthony J. Montgomery, Illinois Institute of Technology Research Institute

J. J. Stephens, Florida State University

Alan T. Waterman, Jr., Stanford University

Henry G. Booker, Special Consultant, University of California-San Diego

PRECEDING PAGE BLANK NOT FILMED

PREFACE

In December 1967, the Committee on Atmospheric Sciences of the National Academy of Sciences appointed a Panel on Remote Atmospheric Probing to undertake a review of all means capable of observing and measuring the physical composition and dynamical structure of the atmosphere from a distance, to assess the present and future potential of such methods, and to recommend steps leading toward the fullest realization of that potential.

The initiation of this study was stimulated by the recognition that further progress in the understanding and prediction of atmospheric phenomena on virtually all scales would be severely impeded by the inability of present-day direct measurement techniques to provide data in three-dimensions, in the required space and time density, and with the necessary coverage. It was also evident that activities in remote sensing had reached a level of development strongly suggesting that many of the observational requirements could be met in the not too distant future, if not now. It therefore seemed timely to conduct a broad evaluation of remote atmospheric probes.

The Panel conducted its studies in two phases. Phase 1 was comprised of two major scientific meetings, held during April 18-20 and May 16-17, 1968, during which members heard state-of-the-art reviews, critiques, and discussion by approximately 100 experts in various methods of indirect sensing and the relevant aspects of atmospheric effects on electromagnetic and acoustic propagation. These reviews and supplementary papers set forth important and imaginative approaches toward atmospheric probing which are of broad scientific interest. With the belief that they will be of value to atmospheric and propagation scientists generally, and to those interested in remote probing in particular, the Panel has assembled them in the form of technical proceedings in Volume 2 of the Panel's final report. These significant papers are reproduced in Volume 2 essentially as received from the authors, and do not necessarily represent the views of the Panel.

In Phase 2 of its study, the Panel met for a two week period at the National Center for Atmospheric Research to evaluate the various probing methods, to summarize their present and future potential, and to recommend

action that would provide for more effective development and application of techniques for atmospheric measurements. The Panel's evaluation and summary of the status of remote probing techniques for observing and measuring atmospheric characteristics, suggestions for essential research, and recommendations for ensuring progress in a field that offers both significant applications now, and exciting prospects for the near future in the atmospheric sciences, comprise Volume 1 of this report.

While the Panel certainly hopes that the steps recommended in Volume 1 of its final report will be implemented, it recognizes that competition for funding for scientific research is such that these steps may not be totally realized. Nevertheless, our efforts will have been abundantly rewarded if interested scientists are stimulated, as we have been, by the many exciting opportunities for advancing our knowledge of the atmosphere that are highlighted within these pages.

The Panel gratefully acknowledges the opportunity to undertake this study on behalf of the National Academy of Sciences-National Research Council, with interest of and support from the Atomic Energy Commission, the Environmental Science Services Administration, the Atmospheric Sciences Section of the National Science Foundation, and the Public Health Service under Task Order No. 9, NSF C-310, and from the National Aeronautics and Space Administration under W-12,596. The Panel also expresses its appreciation for the assistance and hospitality extended by the National Center for Atmospheric Research during its meetings there, and to Mr. W. B. Beckwith of United Air Lines for his assistance and cooperation in arranging for meeting space for the Panel at O'Hare International Airport.

David Atlas  
Chairman  
Panel on Remote Atmospheric Probing

January 1969

N72-25347  
88

Preface . . . . . v

SESSION 1: MICROWAVE LINE-OF-SIGHT PROPAGATION

Line-of-Sight Microwave Propagation  
 John W. Strohbehn . . . . . 48 1 ✓

Wave Propagation in a Random Medium  
 R. W. Lee and J. C. Harp . . . . . 49 21 ✓

Additional Line-of-Sight Methodology  
 C. I. Beard . . . . . 50 79 ✓

Comments on Papers by Drs. Strohbehn and Beard  
 Akira Ishimaru . . . . . 87 ✓

The Use of Satellite Beacons for Meteorological Research  
 Jules Aarons . . . . . 51 89 ✓

SESSION 2: OPTICAL LINE-OF-SIGHT PROPAGATION

Remote Atmospheric Probing by Ground-to-ground  
 Line-of-sight Optical Methods  
 Robert S. Lawrence . . . . . 52 91 ✓

Local Isotropy and Refractive Index Fluctuations  
 in the Surface Layer of the Atmosphere  
 Donald J. Portman . . . . . 53 111 ✓

Optical Propagation in a Near-Earth Environment  
 P. H. Deitz . . . . . 54 119 ✓

Incoherent and Coherent CW Laser Systems for  
 Remote Atmospheric Probing  
 R. F. Lucy . . . . . 55 125 ✓

Remote Probing of the Optical Strength of  
 Atmospheric Turbulence and Wind Velocity  
 D. L. Fried . . . . . 56 133 ✓

Critique of Paper by D. L. Fried  
 R. E. Huffnagel . . . . . 145 ✓

SESSION 3: LIDAR

Lidar			
R. T. H. Collis . . . . .	57	147	✓
Comments on "Lidar" by R. T. H. Collis			
Earl W. Barrett . . . . .		173	✓
Some Aspects of Remote Atmospheric Sensing by Laser Radar			
Richard M. Schotland . . . . .	58	179	✓
The Laser Radar Above 30 Kilometers			
B. R. Clemesha . . . . .	59	201	✓
Laser Radar Measurements of the Aerosol Content of the Atmosphere			
Gerald W. Grams . . . . .	60	207	NASA CR ✓
Comments on Bistatic Lidar			
John A. Reagan . . . . .	61	213	✓

SESSION 4: RADAR

Probing the Atmosphere with High Power, High Resolution Radars			
Kenneth R. Hardy and Isadore Katz . . . . .	62	217	NASA CR ✓
Further Remarks on Atmospheric Probing by Ultrasensitive Radar			
David Atlas . . . . .	63	245	✓
Atmospheric Probing by Doppler Radar			
Roger M. Lhermitte . . . . .	64	253	✓
Comments on Doppler Radar Applications			
Edwin Kessler . . . . .	65	287	✓
Comments on High-Power, High-Resolution Radars			
J. S. Marshall . . . . .	66	291	✓

SESSION 5: RADIO TROPOSPHERIC SCATTER

A Review of Transhorizon Propagation as a Possible Tool for Remote Probing of the Atmosphere Donald C. Cox . . . . .	.67	295	✓
Identification of Atmospheric Structure by Coherent Microwave Sounding William P. Birkemeier . . . . .	.68	337	✓
Theoretical Interpretations of Scatter Propagation Albert D. Wheelon . . . . .	.69	359	✓
Comments on the Possibility for Determining Detailed Atmospheric Structure from Trans-Horizon Radio Propagation Measurements Richard B. Kiebertz . . . . .	.70	367	✓

SESSION 6: MICROWAVE RADIOMETRY

A Selective Review of Ground Based Passive Microwave Probing of the Atmosphere William J. Welch . . . . .	.71	369	✓
Ground-Based Microwave Probing Ed R. Westwater and Martin T. Decker . . . . .	.72	397	✓
Passive Remote Sensing at Microwave Wavelength David H. Staelin . . . . .	.73	409	✓ NASA CR

SESSION 7: INFRARED RADIOMETRY

The Use of High-Frequency Infrared Radiometry for Remote Atmospheric Probing with High Vertical Resolution Lewis D. Kaplan . . . . .	24	435	✓
Determination of the Temperature Profile in an Atmosphere from its Outgoing Radiation Moustafa T. Chahine . . . . .	75	443	<del>WASA</del> CR
Towards an Optimal Inversion Method for Remote Atmospheric Sensing Jean I. F. King . . . . .	76	453	<del>WASA</del> CR
Experimental Approaches to Remote Atmospheric Probing in the Infrared from Satellites William R. Bandeen . . . . .	77	465	<del>WASA</del> JMX
Comments on the Paper by W. R. Bandeen S. Fritz . . . . .		507	<del>WASA</del> JMX
Some Comments on the Use of Infrared Radiometry for Remote Atmospheric Probing W. L. Godson . . . . .	78	511	✓
Remote Detection of CAT by Infrared Radiation Robert W. Astheimer . . . . .	79	517	✓

SESSION 8: CROSSED BEAM CORRELATION TECHNIQUES

Remote Sensing of Winds and Atmospheric Turbulence by Cross-Correlation of Passive Optical Signals A. J. Montgomery . . . . .	80	525	<del>WASA</del> CR
Noise Elimination by Piecewise Cross Correlation of Photometer Outputs Fritz R. Krause and Benjamin C. Hablutzel . . . . .	81	555	<del>WASA</del> JMX
Field Tests of the Optical Cross-Beam System V. A. Sandborn . . . . .	82	589	<del>WASA</del> CR

SESSION 9: SFERICS

Sferics  
E. T. Pierce . . . . . .83 595 ✓  
Comments on the Paper by E. T. Pierce  
Heinz W. Kasemir . . . . . .84 617

SESSION 10: ACOUSTICS

Acoustic Methods of Remote Probing of the Lower Atmosphere  
C. G. Little . . . . . .84 619 ✓  
Atmospheric Sound Propagation  
Richard K. Cook . . . . . .85 633 ✓  
Vertical Profiles of Wind and Temperature by  
Remote Acoustical Sounding  
Herbert L. Fox . . . . . .86 671 ✓  
Probing the Atmosphere with Infrasound  
Eric S. Posmentier and William L. Donn . . . . . .87 681 ✓  
The Hudson Laboratories Microbarograph System:  
Results and Future Trends  
I. Tolstoy and T. Herron . . . . . .88 691 ✓  
Author Index . . . . . . 697

SESSION **1**

Microwave  
Line-of-Sight  
Propagation

N72-25348

## LINE-OF-SIGHT MICROWAVE PROPAGATION

John W. Strohbehn

Radiophysics Laboratory  
Thayer School of Engineering  
Dartmouth College

### ABSTRACT

In the following paper a review of the uses of microwave line-of-sight propagation in remote atmospheric probing is given. The review concentrates on use of the following types of measurements: (1) the use of total electrical path length for measuring average density and water vapor content; (2) the use of amplitude and phase fluctuations over a single path for determining the form of the turbulence spectrum; (3) the use of angle-of-arrival data for measuring the decrease in refractivity; and (4) the use of multiple-element receiving antennas in determining wind speed, atmospheric parameters, and atmospheric models. The paper has not included a study of absorption effects, scattering by rain, fog, snow, or hail, or the effect of ducts.

A review is given of the connection between microwave measurements and meteorological parameters, and the basic electromagnetic theory on which the analyses are made. A few suggestions for future work in these areas is given.

### 1. INTRODUCTION

The major objective of the following paper is to assess the feasibility of microwave line-of-sight experiments in investigating significant meteorological problems. It is probable that such a paper will reveal more about the strengths, weaknesses, and prejudices of the author than about the feasibility of remote probing. A review of the literature reveals that the emphasis on the use of the radio experiments to study the atmosphere is somewhat unusual. The major effort in radio experiments has been

## Line-of-Sight Microwave Propagation

to predict the significant propagation characteristics affecting microwave systems with the smallest number and most easily obtainable meteorological parameters. In many situations the meteorological parameter studied has only an indirect relation to the meteorological parameter that directly influences the propagation of radio waves. Though this approach is of tremendous utility to the radio, communication, or systems engineer, it usually makes this type of data of relatively little significance when attempting to answer the reverse question about the feasibility of studying meteorological parameters with radio waves.

In selecting and discarding topics to include in this report some fairly arbitrary decisions had to be made. Furthermore, some topics were given a rather light treatment because of this reporter's lack of deep knowledge on the subject. The topic of atmospheric absorption and its use in studying the constituents of the atmosphere has been excluded on the grounds that it is an area that has been studied in some detail in the past, and can also be included under the heading of radiometry. The topics of scattering of microwaves by rain, snow, fog, or hail has been excluded for two reasons: First, it has been fairly extensively studied previously, and second, techniques such as high powered radars are much more useful in giving a detailed picture. The study of strong inversions or radio ducts has been excluded mainly because of a lack of knowledge, but could well be very relevant. This area also overlaps with beyond-the-horizon propagation, and possibly can be studied more effectively there.

The topics which have been included are: (1) studying the average total refractivity along a path by measuring absolute electrical path length; (2) studying the fluctuations in the atmosphere using phase fluctuations at one or two receiving sites; (3) studying the decrease of the refractive index with altitude by studying angle-of-arrival information; and (4) studying fluctuations in the atmosphere using a multiple-element array as a receiving antenna.

The paper has been divided into the following sections. In Part 2, the relation between meteorological parameters and microwave measurements, it is shown that radio measurements can only measure variations of the refractive index, and conclusions about meteorological parameters are inferences drawn from these measurements. In Part 3, theoretical background, it is shown that the formulas used in the microwave region are actually derived for the optical wavelength range and that further work is needed both in extending the results for longer wavelengths and in approximating actual experimental configurations. In Part 4, possible experiments, the experiments mentioned previously and their relation to meteorological quantities are discussed. In Part 5, related programs and future developments, a few suggestions for improving future work are given. In Appendix 1, the important formulas, pertinent equations and their limitations are reviewed.

## 2. THE RELATION BETWEEN METEOROLOGICAL PARAMETERS AND MICROWAVE MEASUREMENTS

From the point of view of the radiophysicist attempting to explain microwave measurements, the atmospheric quantity of direct interest is the dielectric constant,  $\epsilon$ , or equivalently the refractive index,  $n(\epsilon = n^2)$ . In this paper the term dielectric constant refers to the relative dielectric constant referred to the free space value,  $\epsilon_0$ . Since in the atmosphere  $n$  is very close to 1, it is common to define a more sensitive parameter, the refractivity  $N$ , as  $N = (n-1) \times 10^6$ .

The relationship between the refractive index and meteorological parameters is normally a function of the frequency of the electromagnetic wave and the constituents of the atmosphere, and may be expressed in the following form [Bean, 1966]

$$N = \frac{A'_{N1} P_{N1}}{T} + \frac{A'_{O} P_{O}}{T} + \frac{A'_{WV} P_{WV}}{T} + \frac{A''_{WV} P_{WV}}{T^2} \quad (2)$$

where  $P$  = pressure,  $T$  = absolute temperature,  $N1$  = nitrogen,  $O$  = oxygen, and  $WV$  = water vapor.

The constant  $A'$  gives the polarization effect due to distortion of charge distributions, and  $A''$  is the effect associated with the orientation of polar molecules. Neither nitrogen nor oxygen have permanent electric dipole moments, so that only water vapor contributes a significant  $A''$  term. Since the composition of dry air normally maintains a constant ratio of nitrogen to oxygen, eq.(2) may be written as

$$N = 77.6 \frac{P_{DA}}{T} + 72 \frac{P_{WV}}{T} + 3.75 \times 10^6 \frac{P_{WV}}{T^2} \quad (3)$$

where  $DA$  = dry air. The commonly accepted values for the constants have been inserted. It may be shown that the influence of other gases, mainly carbon dioxide, cause less than a 0.02 per cent error. Assuming normal atmospheric parameters, eq.(3) is considered valid for frequencies up to 30 GHz. The water vapor resonance at 22 GHz and the oxygen resonance at 60 GHz causing little effect below 30 GHz [Bean, 1966].

If rainfall and absorption effects are ignored, all information about meteorological or atmospheric parameters that can be learned from microwave measurements must be inferred from their influence on eq. (3). Microwave measurements can be used to measure average spatial and time values of  $N$  or spatial and time fluctuations about the average value. Inferences about the temperature, pressure, water vapor content, wind velocity,

## Line-of-Sight Microwave Propagation

turbulence or other atmospheric parameters must come from assumptions about the influence these parameters have on eq.(3). It is apparent that since  $N$  is a function of three parameters, PDA, PWV, and  $T$ , that it is impossible to unravel the influence of any one of these parameters without more measurements, or a priori knowledge about the influence of these parameters. Furthermore, since eq.(3) is reasonably independent of frequency in the microwave region below 30 GHz, multiple frequency experiments cannot easily overcome this limitation. It is worth noting that a combination of microwave and optical measurements can be very useful in separating water vapor and dry air effects.

Because of the fluctuations in temperature, pressure, and water vapor, the refractive index is a random function of both space and time:  $n(x,y,z,t)$ . If a time average is taken over some reasonable period (the amount of time will be dictated in practice by the phenomena that are being studied), then short term fluctuations are removed and gross average features become apparent. For example, it is often assumed that  $\langle n(x,y,z,t) \rangle$  is only a function of altitude,  $\langle n(x,y,z,t) \rangle = f(z)$ .

When studying average refraction effects, only the  $f(z)$  variation is taken into consideration. However, for some problems altitude effects may be negligible but local terrain effects lead to considering the differences in the average value of  $n$  at different locations,  $\langle n(x,y,z,t) \rangle = g(x,y)$ . For example, if a propagation path passes partly over land and partly over water it is reasonable to expect the average value of the refractive index to be different in the two locations.

In many applications the gross features are ignored and only the fluctuations are of interest. In these problems the expected value of  $n$  is often assumed to be constant,  $\langle n(x,y,z,t) \rangle = n_0$ , and the spatial or time fluctuations are studied. In most cases it is the spatial covariance function (or its associated Fourier transform) of  $n$  that is considered:

$$C_n(\underline{r}_1, \underline{r}_2) = \langle [n(\underline{r}_1) - n_0][n(\underline{r}_2) - n_0] \rangle$$
$$\Phi_n(\underline{k}) = \frac{1}{(2\pi)^3} \iiint_{-\infty}^{\infty} C_n(\underline{r}) e^{i\underline{k} \cdot \underline{r}} d\underline{r}$$
(4)

In general, of course, it is possible to combine the two effects and study them together. It does not appear that we have advanced far enough to take that step at this time. One comment should be made about the process of averaging. The amount of information to be gleaned from an experiment will be highly dependent on the investigator's skill at analyzing the data. It is customary to make many simplifying assumptions when proceeding with this analysis. Unfortunately it is not uncommon to make

an assumption that will hide a great deal, if not all, of the physical meaning of the data. For example, if data is averaged over widely varying meteorological conditions it is virtually impossible to relate the data to any meaningful atmospheric model. As another example, if there is a trend in the data over the sampling time, it can rarely be uncovered if the data analysis assumes a stationary process. Unfortunately there has been very little work concerned with the basic problems of geophysical data analysis. Data analysis, at the present time, relies mostly on the intuitive skill of the investigator.

If the atmosphere is pictured as a medium composed of eddies or blobs having different dielectric constants, and it is assumed that as the wind blows these eddies move with the air, but remain essentially unchanged ("frozen hypothesis"), then determination of the motion of the dielectric blobs corresponds to a measurement of the wind velocity. (This assumption appears to be more justified the smaller the size of an eddy.) On the other hand, it is conceivable that other changes could also give apparent velocity motions which are not related to the actual motion of the air. As an example, any type of wave motion, such as gravity waves, could produce this type of effect. Again, there is no method of separating these effects using radio measurements. Either meteorological measurements need to be made, or knowledge about the physical limitations of one source of apparent motion versus another source must be used.

The atmospheric physicist often encodes his knowledge of small scale atmospheric motions in terms of a velocity spectrum,  $\phi_v(\kappa)$ . In particular, it is often assumed that the conditions in the atmosphere can be described using a homogeneous and isotropic turbulence model. Under these conditions, it has been shown [Tatarskii, 1961], that the spectrum of a conservative passive additive will have the same form as the velocity spectrum. Using these results, it can be argued that the spectrum of the refractive index variations is identical in form to the spectrum of the velocity fluctuations. Therefore, measurements on the refractive index spectrum using microwave measurements can be directly related to the shape of the velocity spectrum.

### 3. THEORETICAL BACKGROUND

In assessing the theoretical formulations available to understand line-of-sight microwave propagation, it appears that there exists no careful formulations of the problem. Most workers have used either ray or geometrical optics or adapted diffraction theory results derived for optical wavelengths. Furthermore, the diffraction theory results have only been worked out in great detail for the plane wave case, and just recently expressions have appeared assuming a spherical wave and a finite antenna beam at the transmitter. Literature concerning the question "Given a particular set of experiments, what and how accurately can

## Line-of-Sight Microwave Propagation

various meteorological parameters be ascertained?" is virtually non-existent. (Even when radio experiments are used to infer meteorological parameters, it is unusual for the uncertainties or statistical significance of the results to be discussed).

The most complete treatment of the basic theoretical formulas is probably included in the monographs of Tatarski [1961, 1967]. In these works the different approaches to the electromagnetic problem are derived starting from Maxwell's equations, and it is possible to examine the approximations involved. Despite the orientation of these books towards optical propagation, it is explicitly stated where and why the derivations become invalid for longer wavelengths.

In the derivation of these equations, it is always assumed that only the scalar wave equation need be used. This assumption is equivalent to assuming that the scattered depolarized field is much smaller than the scattered field in the original direction of polarization. The condition under which this is assumed valid is for  $\lambda \ll \ell_0$ , where  $\ell_0$  is the inner scale of turbulence. For scale sizes smaller than  $\ell_0$ , it is assumed that there is no significant energy in the turbulence. In order for polarization effects to be important there must be a significant gradient in the refractive index, i.e., a significant change in the refractive index must occur in a distance of the order of a wavelength or less. In the atmosphere  $\ell_0 \approx 1$  to 10 millimeters, and at optical wavelengths the condition  $\lambda \ll \ell_0$  is easily satisfied. However in the microwave range the condition  $\lambda \ll \ell_0$  is no longer true, and it is necessary to make a much more careful analysis starting from the vector wave equation. To this person's knowledge such an analysis has not been done (a graduate student and the author are presently trying to solve this problem and have obtained some preliminary results.) It seems apparent that the restriction  $\lambda \ll \ell_0$  is much too strong when concerned with depolarization effects and it should be possible to relax it considerably. It therefore seems reasonable that the scalar wave equation should still be valid even over much of the microwave range. Unfortunately, this still does not immediately permit the use of the optical equations, since the condition  $\lambda \ll \ell_0$  is used in other places in the derivation. (See note at end of paper)

If a geometrical optics or ray tracing approach is used, the additional condition,  $L \ll \ell_0^2/\lambda$ , is required. This condition arises from analyzing the path lengths for which diffraction effects should become important when considering the scattered field. Even for  $\ell_0 = 10$  mm, this condition would appear to make geometrical optics of questionable validity for all microwave experiments. This statement, however, needs to be qualified. First of all, the restriction arises from considering when diffraction effects become important, but without carefully analyzing the importance of this effect on different quantities, e.g., amplitude or phase. By the very nature of diffraction it is

expected that it will affect the amplitude results much more strongly than the phase. Also it seems reasonable to expect that the diffraction effects are much more important when considering fluctuations about a mean value compared to considering the mean value itself. Secondly, the given conditions are sufficiency conditions. If the conditions are met the theoretician believes his results will agree with experimental observables. However, there is no way to guarantee that a much weaker set of conditions does not exist under which the derived results will still hold.

If a wave optics approach is used the present derivations relax the condition  $L \ll \ell_0^2/\lambda$ , but retain the condition  $\lambda \ll \ell_0$ . In the early optical work the Born approximation (single scatter theory) was used, but later workers have primarily concentrated on Rytov's method (multiple scatter theory). For microwave propagation there does not seem to be any inherent advantage of Rytov's method over the Born approximation, but the results from Rytov's method will be used as they are more carefully developed in the literature. Both approaches are essentially perturbation solutions of some form of the wave equation, and are only valid for fluctuations that are small compared to the mean value. This condition is well satisfied for almost all conceivable microwave paths in the earth's atmosphere. The importance of the assumption  $\lambda \ll \ell_0$  in these equations appears to need further work. This assumption is not only used in neglecting the depolarization term, but also to argue that the scattered radiation is confined to a small angle about the original direction of propagation. It is this further assertion that is difficult to justify. As the wavelength approaches the size of a turbulent "blob" or eddy, it is reasonable to expect wide-angle scattering. While this wide-angle scattering may not be important for phase effects, it may well be influential with respect to amplitude fluctuations. If wide-angle effects are important the influence of finite antenna beams must also be considered. In Appendix I a summary of the basic formulas and their restrictions are given.

Until recently all the theoretical developments were based either on ray tracing or plane waves. The more general problem of spherical waves and finite antenna beams has received very little attention. Recently there have been several papers [Schmeltzer, 1967; Carlson and Ishimaru, 1967], again concerned with optical propagation, that have studied this problem. As yet, the importance of these considerations in given experimental configurations is not well understood, and needs to be studied further. However, it is reasonable to expect that the restriction  $\lambda \ll \ell_0$  is much less important for spherical or beam waves than for plane waves.

The final type of study, which seems extremely scarce in the literature, is a theoretical analysis of the utility of microwave experiments in remote sensing. In other words, given some meteorological parameter that it is desired to investigate via microwave measurements, how accurately can the parameters be measured.

## Line-of-Sight Microwave Propagation

The following type of questions need to be answered: (1) Does the measurement determine a spatial average over the entire path or can localized properties be determined? If so, how localized? (2) How accurately may meteorological quantities, such as wind velocity, temperature, and humidity, be measured? (3) How sensitive is the measurement to different realistic models for the atmosphere? For example, can an experiment differentiate between a  $\kappa^{-11/3}$  turbulence spectrum versus a  $\kappa^{-4}$  or a  $\kappa^{-3}$  spectrum?

Unfortunately very little of this type of analysis appears in the literature, the most notable exceptions are papers by Muchmore and Wheelon [1955] and Strohbehm [1966], which are directly concerned with the sensitivity of line-of-sight experiments in determining the turbulence spectrum. Presently Robert Lee at Stanford is carrying out this type of analysis and some of his results are available elsewhere in this report.

It appears that there are two areas of theoretical work that need to be pursued before definitive statements about the possibilities and limitations of microwave line-of-sight propagation can be fully assessed with respect to remote probing of the atmosphere. First, there is the need for further basic theoretical work concerned with line-of-sight propagation in the microwave frequency range. This work will either verify the extension of geometrical optics or wave optics results into the microwave region, or will produce new expressions which should be used. This work will undoubtedly be done first assuming a plane wave source and must be extended to include the more practical case of spherical waves and finite antenna beams. Second, there is a need for careful theoretical analysis of what can and cannot be learned from specific experimental measurements. In other words, the type of analysis that will answer the kind of questions raised above.

### 4. POSSIBLE EXPERIMENTS

In analyzing the feasibility of using radio measurements as a tool for studying the atmosphere, a quick survey of the literature reveals that you are fighting the crowd. While there is a great deal of literature on different types of propagation experiments, the emphasis is on predicting the propagation effects with the simplest meteorological parameters possible. In a large number of papers there is no mention of meteorology at all; in others the objective is to predict the radio effects using the simplest meteorological measurement. While this objective is certainly entirely proper and desirable for communication and system studies, such as predicting range rate error or pointing error, it makes a great deal of the work of very minor importance for remote probing studies.

Therefore, in estimating the value of certain types of studies, it was necessary to make estimates based on very little direct

information and a large amount of guess work or intuition. As a result, the opinions given should be taken quite tentatively.

#### 4.1 Absolute Path Length Measurements

In geodesy it is necessary to determine the actual path length between two points as accurately as possible. When using radio means, the relation between the radio electrical length and the actual path length is given by

$$L_f = L(1 + \bar{N}_f \times 10^{-6}) \quad (5)$$

where  $L_f$  = radio electrical length measured at frequency  $f$ ,  $L$  = actual path length, and  $\bar{N}_f$  = the refractivity at frequency  $f$  averaged over the entire path. If  $L$  were known accurately enough then the above relation could be used to find the spatial average of  $\bar{N}_f$ , the quantity of interest in remote probing. However, the geodesist has found that it is easier and more accurate to find  $L$  by radio means, and one of his problems is to remove the error introduced by  $\bar{N}_f$ . Therefore it is unreasonable to expect that  $L$  will be known accurately, and that  $\bar{N}_f$  can be determined directly from eq.(5). Part of the problem must be to include a method of determining  $L$  as part of the radio measurement. One method is to use the dispersive characteristics of  $\bar{N}_f$ , i.e., the variation of  $\bar{N}$  with frequency is known and may be used to determine  $L$ . This approach has been attempted using centimeter and millimeter wavelengths but has been discontinued [Sullivan, 1965]. However, dispersive effects are much stronger for optical frequencies and hence this experiment can be performed more accurately there. Thompson [1968] has shown that a three-wavelength experiment, two in the optical and one in the microwave, can be used to determine total density and water vapor density to about 0.5 per cent, or better than 1N unit for  $\bar{N}$ . He projects that these accuracies could be improved by one or two orders of magnitude for the total density. It is possible that the same technique could be performed in the millimeter and submillimeter band using the dispersion effects that occur because of the water vapor and oxygen lines. However, with the present state of technology, the dual optical-microwave system seems more suitable. This technique will not be discussed in more detail here as it appears that it will be more thoroughly covered in another paper.

#### 4.2 Relative phase measurements, using one or two receivers

There has been a large amount of work on this problem from the point-of-view of determining phase variations and resulting errors in angle-of-arrival. Unfortunately, from the point of view of remote probing, very little of this data has been analyzed with the objective of critically studying the atmosphere. The major use of such data would be in the determination of the

## Line-of-Sight Microwave Propagation

form of the spectrum of the refractive index fluctuations. When employing one receiver almost nothing can be inferred without an independent measurement of the wind velocity. Given the wind velocity and assuming the "frozen hypothesis" is valid, it is

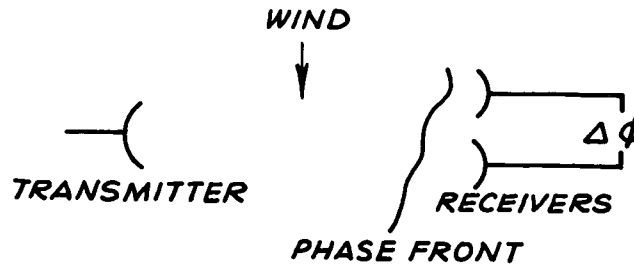


Fig. 1 Phase Measurements

possible to interpret the phase fluctuations in terms of refractive index variations. However, in this interpretation it is necessary to take into account the effect of the antenna aperture in averaging the phase fluctuations [Norton, 1965]. The major problems in interpreting this type of experiment are the following: (1) It is impossible to test the validity of the frozen hypothesis; (2) The interpretation assumes the atmospheric conditions are homogeneous over the entire path. For almost any reasonable microwave propagation path this assumption will be highly suspect, and there is no way to isolate non-homogeneous conditions from other effects using radio results. (3) There is some evidence that phase measurements are the least sensitive in discriminating between different atmospheric models [Muchmore and Wheelon, 1955; Strohhahn, 1966]. However, the covariance function measured in this way is a measure, in some sense, of the outer scale of turbulence. The interpretation of such data must be done carefully since for these scale sizes the turbulence is rarely isotropic.

When using two receiving systems, the phase differences at the two receiving sites may be used to estimate the average wind velocity over the path or may be combined to give angle-of-arrival information. This combination has essentially the same drawbacks as the phase measurements, except there is evidence that angle-of-arrival measurements are more sensitive than phase in discriminating between atmospheric models.

Even though these types of measurements are extremely valuable in interpreting the effect of the atmosphere on different proposed radio systems, it seems that they are much less valuable in the

area of remote probing. For remote probing many of the ambiguities of the single or double path measurement can be resolved by a multiple-element array, as will be discussed in another section

#### 4.3 Refraction Measurements

In estimating the angle-of-arrival errors introduced by the atmosphere when tracking airplanes or space vehicles it is important to take into account the amount of bending of the rays because of the decrease in the average refractive index as a function of altitude above the earth's surface. Again the objective of most of the work has been to estimate the propagation

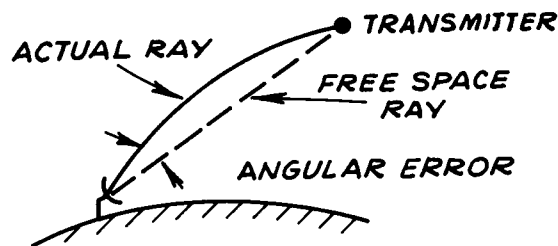


Fig. 2. Refraction Measurements

effect using as simple an atmospheric parameter as possible. In this problem it has been found that a reasonable prediction can be made by using a linear equation to relate  $\tau$ , the amount of bending of the ray, and  $N_s$ , the refractivity at the surface [Bean, 1966]. There also have been efforts at using more complicated models and radiosonde data in making predictions.

It is an intriguing possibility to turn the problem around and to investigate the possibility of tracking an object whose exact position is known and use the results to predict the decrease of the average refractive index with altitude. Whether such measurements would be sensitive enough to distinguish between a linear or exponential decrease of refractivity is not clear. However, it seems somewhat doubtful because of the ability to predict the bending from as simple a measurement as the surface refractivity. Furthermore, the major contribution to the bending is near the earth's surface, where a linear approximation can be made to the exponential decrease. There is also a noise problem in the sense that small scale inhomogeneities will cause fluctuations in the angle-of-arrival. The method should also be

## Line-of-Sight-Microwave Propagation

applicable to studying elevated ducts. In the above discussion it has been assumed that the measurements are made from a vehicle that is transmitting. It is obvious that the same type of measurements can be made using a radar. It should also be noted that in the millimeter region atmospheric absorption prohibits transmission at low angles of elevation (high refraction effects) [Straiton, 1965].

### 4.4 Array Measurements

The use of microwave arrays in measuring atmospheric parameters is just beginning to be fully realized. With present equipment it is now feasible to measure and record amplitude and phase information at eight or ten different receiving antennas.

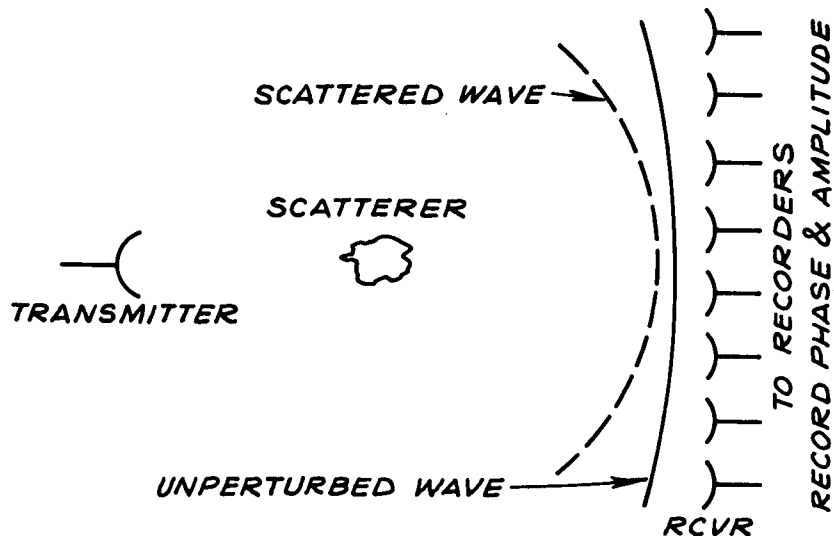


Fig. 3. Multiple Element Array

Because of the multiplicity of measurements made there is the possibility of resolving the ambiguities present in a single antenna measurement and the possibility of investigating properties which must be assumed as true under simpler measurement configurations. These advantages are obtained at the expense of more complicated and expensive equipment and the necessity for highly sophisticated data reduction techniques. However, for investigating processes as complex as those in the atmosphere, these complications seem extremely worthwhile. In analyzing the possibilities of array measurements in determining meteorological parameters it seems worthwhile to divide the discussion into three categories: (1) the measurement of apparent wind speed; (2) the determination of meteorological parameters at different points along the path, given that some atmospheric model is assumed, and (3) the determination of an atmospheric model.

When considering the measurement of apparent wind speed, the remarks made in Section 2 should be repeated. A radio measurement can only determine the apparent motion of the refractive index fluctuations in space. The interpretation of these motions as a blob of air moving with the average wind or as a wave motion in the refractive index caused by another type of mechanism cannot be distinguished by radio measurements alone. Therefore, when discussing the measurement of wind speed below, the more general interpretation given above is implied. It appears to this author that the influence of wave motions in causing apparent wind speed changes is not well understood and could bear further investigation.

According to some as yet unpublished work by Robert Lee of Stanford, it is believed possible to obtain the projected component of the windspeed across the path at 10 different positions along the propagation path with an accuracy on the order of 10 per cent (As yet this technique has not been proven.) This wind speed is more or less instantaneous in time but spatially averaged over some segment of the propagation path. The multiple element array is ideally suited to this type of measurement.

The second approach is to assume some form of an atmospheric model, for example, assume  $\Phi_n(\kappa)$  is of the form [Tatarskii, 1967]

$$\Phi_n(\kappa) = 0.033 C_n^2 \kappa^{-11/3} e^{-\kappa^2/\kappa_m^2}$$

$$\kappa_m = 5.92/\ell_0$$

where  $C_n^2$  is a measure of the intensity of the turbulence. Note that making such an assumption implicitly rules out a number of mechanisms as contributing to the propagation problem. The form assumed implies that the atmosphere can be described by locally homogeneous isotropic turbulence. This assumption rules out stratification effects and anisotropy as playing a major role. Given that the assumption is made, however, it is possible to determine a parameter, such as  $C_n^2$  at different points along the path. The above approach, which is extremely useful when the form of the atmospheric model is reasonably universal, must be used with some caution in the real world. While the form of the spectrum given above is probably the best model available, it is in no sense universal and is only expected to exist under certain reasonably restrictive conditions. Therefore this type of approach should only be used when other considerations make the model reasonable.

The third approach is to attempt to use the measurements to actually determine the form of  $\Phi_n(\kappa)$  under different meteorological conditions. This is a much more difficult problem than the preceding, since there are a number of parameters to be determined.

## Line-of-Sight Microwave Propagation

Furthermore,  $\Phi_n(\kappa)$  is defined for all wavenumbers from 0 to  $\infty$ , but the best a given experiment can accomplish is to measure  $\Phi_n(\kappa)$  over some range of  $\kappa$ .

The following comments are taken from a private communication from Robert Lee at Stanford. From amplitude covariances the microwave array type of experiment is sensitive to blob sizes about one-half the Fresnel zone radius (on the order of 6 meters for an 8 mm wavelength and 25 kilometer path). The range of wavenumbers is typically one octave. Phase covariances are mainly controlled by the largest scale sizes and information can be learned about the region around  $L_0$ , the outer scale of turbulence, again approximately one octave, is important. It is expected that the effects of anisotropy can be determined and also the decay time of eddies.

From the above remarks it is apparent that measurements using multiple-element arrays should be extremely useful in measuring atmospheric parameters. It should be noted that the above analysis was based on the assumption that wave optics formulas of the type given in the Appendix are valid in the microwave region. There must be some reservations about this formulation until a more careful analysis of the problem for microwaves has been completed. Furthermore, the conclusions given still must be regarded as tentative in nature, as there is a need for much more work in this area of analysis and interpretation of experimental results.

It should be remarked that similar measurements at optical wavelengths will make available much the same information as for the millimeter. Phase measurements should reveal substantially the same information and for the same scale sizes. Amplitude measurements, however, will emphasize much higher wavenumbers, close to the  $l_0$  range of the spectrum. In this sense optical and millimeter measurements should be complementary.

### 5. RELATED PROGRAMS AND FUTURE DEVELOPMENTS

The major work in the area of microwave line-of-sight research is being performed at the Institute for Telecommunications Sciences and Aeronomy, the University of Texas, and Stanford University (see Bibliography). The work at ITSA seems to be primarily mission oriented in the sense that the work is more oriented towards predicting the effect of propagation on systems and less oriented toward remote probing. The work at the two universities is more oriented towards the remote probing aspects. It should be noted that at times it is difficult to separate the two orientations. There are of course numerous single-path experimental facilities. The most sophisticated multiple-element array is that of Lee and Waterman at Stanford [1966].

I envision the experimental progress in this area in the next decade or so to be very similar to the progress of the last ten years--slow. At present there are only a few facilities capable of performing sophisticated experiments and analyzing the data. Even during times of relative scientific wealth it was difficult to secure money for experiments that were oriented towards fundamental research in atmospheric physics. The support, even for many of the best programs, has been justified on the basis of applications. It appears that in the immediate future this situation will get worse, perhaps relaxing toward the end of the next five years. For example, to my knowledge, there are no plans for more multiple-element arrays. Furthermore, there is no indication that the rather unfortunate situation of the past where few good radio experiments were combined with good meteorological experiments will drastically change in the future.

There are a few general recommendations that I would like to make. First, that efforts be made to see that radio measurements of a given type are made in a number of different meteorological situations. For example, when designing a radio experiment serious consideration should be given to making such experiments semi-portable when possible. In particular, it would be desirable to have several multiple-element arrays in reasonably different climates and different terrains. Secondly, there is a tremendous need for better meteorological measurements in conjunction with radio measurements. As a particular suggestion, an agency through which one could secure either funds for or temporary loans of meteorological equipment would be extremely valuable. It is not uncommon for certain agencies to fund radio experiments for systems studies, but not allow funding for meteorological equipment. If a scientist had a readily available and sympathetic second source for this type of equipment, it is quite possible better measurements would be made.

With regard to theoretical investigations there are several interesting problems that require further development. First, there is a need for a closer look at the basic theoretical expressions for amplitude and phase fluctuations and their validity in the microwave range. Second, there has been very little work in the area of the effect of finite antenna beamwidths, etc., on the basic expressions. Third, there is a great need for careful analysis of exactly what can be learned about the atmosphere from microwave experiments. In general, it would be surprising if there were suddenly any great interest in attacking these problems. However, there is an indication that there are at present a few workers who are investigating some of these problems, and it is reasonable to expect that some progress will be made in the next few years.

## 6. APPENDIX: THE IMPORTANT FORMULAS

## A. Geometrical Optics

Restrictions:  $\lambda \ll \ell_0$ ,  $\sqrt{\lambda L} \ll \ell_0$ , where  $\lambda$  = wavelength,  $L$  = path length and  $\ell_0$  = inner scale of turbulence.

Phase formulas:

$$S(\underline{r}) = k \int_0^r ds n(\underline{s}) \quad (A1)$$

$$S_1(\underline{r}) = k \int_0^r ds \delta n(\underline{s}) \quad (A2)$$

$$C_S(\rho) = \langle S_1(L,0)S_1(L,\rho) \rangle \quad (A3)$$

$$C_S(\rho) = 2k^2 L \int_0^\infty C_n[(x^2 + \rho^2)^{1/2}] dx = 2\pi \int_0^\infty F_S(\kappa) J_0(\kappa\rho) \kappa d\kappa \quad (A3)$$

$$F_S(\kappa) = 2\pi k^2 L \Phi_n(\kappa) \quad (A4)$$

where

- $S$  = total phase change
- $S_1$  = fluctuation of phase about its mean value
- $k = 2\pi/\lambda$ ,  $\lambda$  = wavelength
- $L$  = path length
- $C_S(\rho)$  = covariance function of the phase fluctuations
- $\rho = [y^2 + z^2]^{1/2}$  = distance between two receivers
- $C_n(r)$  = covariance function of the refractive index
- $F_S^n(\kappa)$  = two-dimensional spectrum of the phase fluctuations (two-dimensional Fourier transform of  $C_S(r)$ )
- $\Phi_n(\kappa)$  = Three-dimensional spectrum of the refractive index fluctuations (three-dimensional Fourier transform of  $C_n(r)$ )
- $\kappa$  = spatial wavenumber

The first equation (A1) may be used to calculate the average phase change  $\langle S(\underline{r}) \rangle = k \int ds \langle n(\underline{s}) \rangle$  and is particularly useful in studying the beam bending due to refraction. In this case it is usually assumed that  $n(\underline{s})$  is only a function of height above the earth's surface. Eq. (A2) gives the phase fluctuation about its mean value. Eqs. (A3) are derived from (A2) and give the covariance of the phase fluctuations at two receivers, both a distance  $L$  away from the transmitter, and separated by a distance  $\rho$ . If the covariance function,  $C_S(\rho)$ , is known for all values of  $\rho$ , a two-dimensional Fourier transform leads to the two-dimensional spectrum of the phase fluctuations,  $F_S(\kappa)$ . It is obvious that complete knowledge of  $F_S(\kappa)$  would lead to complete knowledge of  $\Phi_n(\kappa)$ . However, experimentally it is only possible to measure  $F_S^n(\kappa)$  over some range of wavenumbers.

Amplitude formulas:

$$\chi(\underline{r}) = \ln[A(\underline{r})/A_0(\underline{r})] = \frac{1}{2k} \int_0^x dx' \nabla_T^2 S_1(x', y, z) \quad (A5)$$

$$C_{\chi}(\rho) = \langle \chi(L,0)\chi(L,\rho) \rangle$$

$$C_{\chi}(\rho) = \frac{L^3}{6} \int_0^{\infty} \nabla_{T_1}^2 \nabla_{T_2}^2 C_n [(x^2 + \rho^2)^{1/2}] dx \quad (A6)$$

$$F_{\chi}(\kappa) = \frac{\pi L^3}{6} \kappa^4 \Phi_n(\kappa) \quad (A7)$$

where  $A(\underline{r})$  = amplitude at point  $\underline{r}$ ;  $\nabla_T^2$  = transverse Laplacian.

In eq.(A5),  $A(\underline{r})$  is the total amplitude. If it is assumed that  $A(\underline{r}) = A_0(\underline{r}) + A_1(\underline{r})$ , and  $A_1(\underline{r}) \ll A_0(\underline{r})$ , then  $\ln[A(\underline{r})/A_0(\underline{r})] \approx [A_1(\underline{r})/A_0(\underline{r})]$ . However, it is also very common to define  $\chi(\underline{r}) = \ln[A(\underline{r})/A_0(\underline{r})]$ , where  $\chi(\underline{r})$  will be called the log-amplitude. It should again be noted that perfect knowledge of  $C$  or  $F$  would lead to exact knowledge of the form of  $\Phi_n(\kappa)$ , but again experimentally this is not possible. It is worth noting that the amplitude spectrum emphasizes a different range of wavenumbers than the phase spectrum.

### B. Rytov's Method (Wave Optics)

$$\text{Restrictions: } \lambda \ll \ell_0, L \ll \ell_0^4/\lambda^3$$

Phase formulas:

$$F_S(\kappa) = \pi k^2 L \left(1 + \frac{k}{\kappa^2 L} \sin \frac{\kappa^2 L}{k}\right) \Phi_n(\kappa) \quad (A8)$$

$$C_S(\rho) = 2\pi \int_0^{\infty} F_S(\kappa) J_0(\kappa\rho) \kappa d\kappa \quad (A9)$$

Amplitude formulas:

$$F_{\chi}(\kappa) = \pi k^2 L \left(1 - \frac{k}{\kappa^2 L} \sin \frac{\kappa^2 L}{k}\right) \Phi_n(\kappa) \quad (A10)$$

$$C_{\chi}(\rho) = 2\pi \int_0^{\infty} F_{\chi}(\kappa) J_0(\kappa\rho) \kappa d\kappa \quad (A11)$$

The above formulas, which may be found in Tatarski [1961], are derived using Rytov's method of smooth perturbations. It is noted that both of the restrictions given above would limit the validity to wavelengths in the millimeter range or shorter, and to very short path lengths. However, the above restrictions are, in a sense, sufficiency conditions, and it is possible that they may be relaxed considerably. However, at present there is no theoretical basis for relaxing these restrictions. It is possible to make intuitive or physical arguments that the phase fluctuations should follow equations (A8) and (A9) reasonably well. For amplitude fluctuations it seems reasonable to expect more significant changes in the forms of the equations for longer wavelengths. The use of the above formulas in this paper is mainly based on the fact that they are the only ones available.

## Line-of-sight Microwave Propagation

N O T E: Recent unpublished results by Clifford and Strohbehm have shown that the restriction  $\lambda \ll \ell_0$  may be relaxed with no significant change in the appropriate formulas for microwaves, i.e. equations derived for the optical case (when  $\lambda \ll \ell_0$ ) are still valid in the microwave case (when  $\lambda \gg \ell_0$ ).

### REFERENCES

- Bean, B.R. and E.J. Dutton (1966), Radio Meteorology, NBS Monograph 92, Supt. of Documents, Washington, D.C., pp. 435.
- Carlson, F.P. and A. Ishimaru (1967), "Beam wave propagation in a random medium," and "Spherical wave propagation in non-stationary media," presented at 1967 Fall URSI Meeting, Ann Arbor, Michigan.
- Deam, A.P. and B.M. Fannin (1955), "Phase-difference variations in 9350-megacycle radio signals arriving at spaced antennas," Proc. IRE, 43, 1402-1404.
- Du Castel, F. (ed.) (1965), Progress in Radio Science, 1960-1963, II, Elsevier Publishing Co., New York, pp. 291.
- Flock, W.L., R.C. Mackey, and W.D. Hershberger (1960), "Propagation at 36,000 Mc in the Los Angeles basin," IRE Trans. on Antennas and Propagation, AP-8, 235-241.
- Herbstreit, H.W. and M.C. Thompson (1955), "Measurements of the phase of radio waves received over transmission paths with electrical lengths varying as a result of atmospheric turbulence," Proc. IRE 43, 1391-1401.
- \_\_\_\_ (1956), "Measurements of phase of signals received over transmission paths with electrical lengths varying as a result of atmospheric turbulence." IRE Trans. on Antennas and Propagation AP-4, 352-358.
- Janes, H.B. and M.C. Thompson, Jr. (1964), "Errors introduced by the atmosphere in microwave range measurements." Radio Science J. of Res. NBS/USNC-URSI 68, 1229-1235.
- Lee, R.W. and A.T. Waterman, Jr. (1966), "A large antenna array for millimeter wave propagation studies," Proc. IEEE 54, 454-58.
- Muchmore, R.B. and A.D. Wheelon (1955), "Line-of-sight propagation phenomena, I," Proc. IRE 43, 1437-1449.
- Norton, K.A. (1965), "Effects of tropospheric refraction in earth-space links" Progress in Radio Science, 1960-63, Du Castel (ed.).
- Saxton, J.A. (Ed.) (1962), Radio-Wave Propagation in the Troposphere, Elsevier Publishing Co., New York, pp. 199.
- Saxton, J.A. (Ed.) (1964), Advances in Radio Research, I, Academic Press, New York, pp. 226.
- Schmeltzer, R.A. (1967), "Means, variances, and covariances for laser beam propagation through a random medium," Qrtly of Applied Math, XXIV, 339-354.

- Straiton, A.W. and H.W. Smith (1950), "Progression of micro-wave radio scintillations at wind speed on an overwater path," Proc. IRE (Correspondence) 28, 825-826.
- \_\_\_\_ (1965), "Propagation characteristics of millimeter radio waves", Progress in Radio Science, 1960-1963, Du Castel (Editor).
- Strohbehm, J.W. (1966), "The feasibility of laser experiments for measuring atmospheric turbulence parameters," J. Geophys. Res. 71, 5793-5808.
- Sullivan, J.F. and H. Richardson, Final Report on line integral refractometer, Mitre Corp. Rept. MTP-19, 1965.
- Tatarski, V.I. (1961), Wave Propagation in a Turbulent Medium, McGraw-Hill, New York, pp. 285.
- \_\_\_\_ (1967), Propagation of waves in a turbulent atmosphere, Nauka, Moscow, pp. 548 (In Russian).
- Thompson, M.C., Jr.; H.B. Janes and A.W. Kirkpatrick (1960), "An analysis of time variations in tropospheric refractive index and apparent radio path length," J. Geophys. Res. 65, 193-201.
- Thompson, M.C., Jr. and L.E. Wood (1965), "The use of atmospheric dispersion for the refractive index correction of optical distance measurements." Oxford Symposium on Electromagnetic Distance Measurement, 165-172.
- Thompson, M.C., Jr. (1968), "Space averages of air and water vapor densities by dispersion for refractive correction of electromagnetic range measurements," J. Geophys. Res. 73, 3097-3102.
- Tolbert, C.W. and A.W. Straiton (1953), "Propagation characteristics of 0.86 cm radio waves," 1953 Proc. Conf. on Radio Meteorology, Austin, Texas.
- \_\_\_\_, A.W. Straiton, and C.D. Tipton (1953), "Propagation studies at 8.6-millimeter wavelength on 3.5- 7- and 12-mile paths," University of Texas, Austin, EERL Rept. 69.
- \_\_\_\_, A.W. Straiton, and C.D. Tipton (1953), "Propagation of 8.6-millimeter radio waves over a 50-mile path," University of Texas, Austin, EERL Rept. 70.
- \_\_\_\_, C.O. Britt, C.D. Tipton, and A.W. Straiton (1954), "Propagation of 4.3-millimeter radio waves on 3.5- and 7.0-mile paths," University of Texas, Austin, EERL Rept. 75.
- \_\_\_\_, B.M. Fannin, and A.W. Straiton (1956), "Amplitude and phase difference fluctuations of 8.6-millimeter and 3.2-centimeter radio waves on line-of-sight paths," University of Texas, Austin, EERL Rept. 78.
- \_\_\_\_, C.O. Britt, and A.W. Straiton (1957), "Antenna pattern fluctuations at 4.3-millimeter wavelengths due to atmospheric inhomogeneities," University of Texas, Austin, EERL Rept. 96.
- Wheelon, A.D. (1955), "Near field corrections to line-of-sight propagation," Proc. IRE 43, 1459-1466.

## Line-of-Sight Microwave Propagation

- (1957), "Relation of radio-measurements to the spectrum of tropospheric dielectric fluctuations," J. Applied Physics 28, 684-693.
- (1959), "Radio wave scattering by tropospheric irregularities," J. Res. NBS-D Radio Propagation 63D, 205-233.
- (1959), "Radio scattering by tropospheric irregularities," J. Atmos. Terres. Physics 15, 185-205.

N72-25349

## WAVE PROPAGATION IN A RANDOM MEDIUM

R. W. Lee and J. C. Harp

Stanford Electronics Laboratories  
Stanford University

### ABSTRACT

A simple technique has been used to derive statistical characterizations of the perturbations imposed upon a wave (plane, spherical or beamed) propagating through a random medium. The method is essentially physical rather than mathematical, and is probably equivalent to the Rytov method. The limitations of the method are discussed in some detail; in general they are restrictive only for optical paths longer than a few hundred meters, and for paths at the lower microwave frequencies. Situations treated include arbitrary path geometries, finite transmitting and receiving apertures, and anisotropic media. Results include, in addition to the usual statistical quantities, time-lagged functions, mixed functions involving amplitude and phase fluctuations, angle-of-arrival covariances, frequency covariances, and other higher-order quantities.

### 1. INTRODUCTION

An increasing amount of interest has been focused in recent years upon the problem of electromagnetic wave propagation in media whose properties are random functions of space and time. The atmosphere of the earth is such a medium, and this interest has been aroused both by technological pressure for more efficient utilization of the radio-through-optical spectrum, and by the recognition that the effects produced by the atmosphere upon waves propagating through it are useful measures of the nature of the atmosphere. In order that perturbations observed on propagated waves may be interpreted in terms of atmospheric parameters, it is necessary to evolve a sound theoretical framework, based upon a realistic model of the atmosphere. The atmospheric model used must be amenable to the necessary mathematical operations of the theoretical analysis, but must at the same time possess sufficient degrees of freedom to represent adequately the actual random medium.

## WAVE PROPAGATION IN A RANDOM MEDIUM

While this last requirement has not always been met in attempts to develop the theory of propagation through random media, notable progress has been made. The work of Tatarski (1961) is a satisfactory basis for plane-wave situations, and that of Schmelzter (1967) extends the work to spherical-wave, finite-aperture situations. Both authors use the Rytov method, developed 30 years ago in connection with work on the diffraction of light by ultrasonic beams. Considerable discussion has attended the use of this method, primarily concerning the range of validity of the approximation. In particular, the sufficiency conditions obtained in the mathematical approach (that the aggregate of the perturbations on the wave be much less than the magnitude of the wave, and that all refractive perturbations be large compared to a wavelength) have been considered by some to be unnecessarily severe. If the requirement that all refractive perturbations be much larger than a wavelength is taken at face value, application of these theories is restricted to wavelengths of less than about 1 mm, since it is known that inhomogeneities at least as small as a few mm are present in the atmosphere.

In the development that follows a very simple technique will be used to obtain a wide variety of statistical characterizations of the perturbations produced by a random medium upon a wave propagating through it. The method is basically physical and geometrical, rather than mathematical; as a result, when approximations are made, they arise in a physical context, making it possible to assess more easily the implications of the approximations.

Briefly, the technique consists of resolving the 3-dimensional refractivity field of the medium into thin slabs perpendicular to the propagation path, and further resolving the 2-dimensional refractivity field within a slab into Fourier components of varying wavenumber and angle in polar coordinates. The effect produced upon the wave by one of these Fourier components is then determined, a simple matter because the component acts exactly like a phase diffraction-grating. The resolution is then retraced, and perturbations produced by Fourier components of differing wavenumber, angle and position along the path are summed statistically.

The resulting solution is composed of three multiplicative terms: the power spectrum of the refractive irregularities, a term relating the fluctuations at one point in the receiving plane to those at another point, and a term which is a measure of the relative efficiency of an irregularity of a given size, located at a given position along the transmission path, in producing perturbations at the receiver. This latter term is generally referred to as a "filter function," serving as it does to weight selectively the spectrum of refractive irregularities.

This method is used in Sections 2 and 3 to obtain spatial covariance- and structure-functions for the plane- and spherical-wave situations; a discussion of the region of validity of this development is given in Section 4. The theory is extended in succeeding sections to include anisotropic media (Section 5), temporal quantities (Section 6), additional higher statistical functions (Section 7), finite transmitting and receiving apertures (Section 8), and non-transparent media (Section 9). Section 10 is devoted to examples of "filter functions," just described. These functions depend upon the path geometry and the measurement being made, and are quite important factors in the interpretation of measurements in terms of atmospheric parameters. Finally, Section 11 consists of a discus-

sion of the techniques available for extracting from experimental measurements information about the medium—information concerning not only quantities averaged over the transmission path, but concerning the spatial distribution of such quantities as well.

## 2. PROPAGATION OF AN INFINITE PLANE-WAVE

A plane-wave propagating in the  $z$ -direction with wavenumber  $k \exp(-ikz)$  is incident upon an infinite slab bounded by the planes  $z = r$  and  $z = r + dz$ . The slab imposes upon the wave a phase perturbation which is sinusoidal in  $x$ , and of peak magnitude  $kadz$ :

$$\Delta \phi = kadz \cos (u(x+b)) \quad (2.1)$$

where  $u$  is the wavenumber of the perturbation, and  $ub$  is the phase of the perturbation at the  $z$ -axis. At this point we shall make the assumption that  $k \gg |\bar{u}|$  for all wavenumbers in the refractivity spectrum (see Figure 2.1).

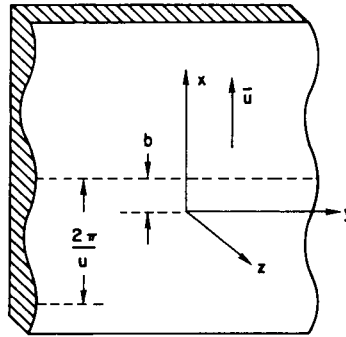


Figure 2.1

Upon exiting from the slab the incident wave is then

$$\exp(-ikr) \cdot \exp \{ -ika dz \cos (u(x+b)) \}. \quad (2.2)$$

Assuming that the perturbation is small ( $ka dz \ll 1$ ), (1.2) may be written

$$\begin{aligned} & \exp(-ikr) \{ 1 - ika dz \cos (u(x+b)) \} \\ &= \exp(-ikr) - \frac{ika dz}{2} \exp(-ikr) \exp(iu(x+b)) \\ & \quad - \frac{ika dz}{2} \exp(-ikr) \exp(-iu(x+b)). \end{aligned} \quad (2.3)$$

The first term of (2.3) represents the original wave, undiminished in the weak-scattering approximation. The second term represents another plane-wave, propagating at an angle  $\theta$  with respect to the  $z$ -axis and an angle  $\gamma$  with respect to the  $x$ -axis, where

$$\begin{aligned} \gamma &= \arccos (u/k) \\ \theta &= \arccos (\sqrt{1 - u^2/k^2}) \end{aligned}$$

## WAVE PROPAGATION IN A RANDOM MEDIUM

The projection of  $\bar{k}$  on the z-axis is  $k \cos \theta = \sqrt{k^2 - u^2}$ , the effective wavenumber  $k'$  of the scattered wave. The wave is, of course, invariant in y. The third term of (2.3) represents another plane-wave, the mirror image of the second wave as reflected in the plane  $x=b$  (see Figure 2.2). At the plane  $z=L$ , these three become:

$$\begin{aligned} & \exp(-ikr) \exp(ik(L-r)) \\ & \exp(-ikr)(-ikadz/2) \exp\{-ik'(L-r)-iu(x+b)\} \\ & \exp(-ikr)(-ikadz/2) \exp\{-ik'(L-r)+iu(x+b)\} \end{aligned} \quad (2.4)$$

The resulting field  $dE_t$  at the plane  $z=L$  is the sum of these three waves.

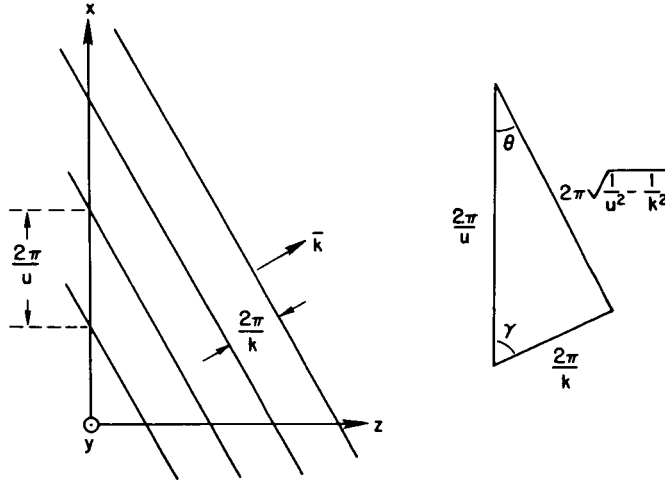


Figure 2.2

Dropping the common phase term  $\exp(-ikr)$  and setting  $L-r=s$ , the sum becomes

$$\begin{aligned} dE_t &= \exp(-iks) - (ikads/2) \exp\{-ik's-iu(x+b)\} \\ & \quad - (ikads/2) \exp\{-ik's+iu(x+b)\} \\ &= \exp(-iks) - ikads \cdot \exp(-ik's) \cos(u(x+b)) \end{aligned} \quad (2.5)$$

Factoring and dropping the phase term  $\exp(-iks)$ ,

$$dE_t = 1 - ika \cdot ds \cdot \exp\{-is(k'-k)\} \cos(u(x+b)). \quad (2.6)$$

The observed perturbation of the field in the plane  $z=L$  is the difference of the magnitudes of the perturbed and unperturbed fields.

$$\begin{aligned} dP_a &= |dE_t| - 1 = [\mathcal{R}^2(dE_t) + \mathcal{I}^2(dE_t)]^{1/2} - 1 \\ &= ka \cdot ds \cdot \cos[u(x+b)] \cdot \sin[s(k'-k)]. \end{aligned} \quad (2.7)$$

Terms in  $a^2$  are neglected. Note that the perturbation of the field is sinusoidal in  $x$ , displaced in phase by  $ub$ , with period  $2\pi/u$ ; that is, the field perturbation is a projection on the plane  $z=L$  of the perturbing sinusoidal lens.

The perturbation of the phase front in the plane  $z=L$  is

$$\begin{aligned} dP_p &= \tan^{-1} [\mathcal{I}(dE_t)/\mathcal{R}(dE_t)] \\ &= ka \cdot ds \cdot \cos[u(x+b)] \cos[s(k'-k)]. \end{aligned} \quad (2.8)$$

The spatial-covariance function  $C(d)$  of the field perturbations is the ensemble average of the products of all perturbations observed at a point  $x_1$  with all perturbations at another point  $x_2$ . Assuming that the average product of perturbations of differing wavenumber  $\bar{u}$  is zero (since if the refractivity field is random, the Fourier components of that field are uncorrelated) there remain the cross-products resulting from a given wavenumber  $\bar{u}$  at two points  $s_1$  and  $s_2$  on the path. The sum of such cross-products for all  $s_1$  and  $s_2$  is

$$dC_a(d) = k^2 \int_0^L \sin(s_1(k'-k)) \int_0^L \sin(s_2(k'-k)). \quad (2.9)$$

$$\langle a(u, s_1) \cos(u(x_1 + b_1)) \cdot a(u, s_2) \cos(u(x_2 + b_2)) \rangle ds_1 ds_2.$$

We see that the quantity within the  $\langle \rangle$  brackets is simply the correlation between parallel slabs containing the same  $u$  and separated by  $s_1 - x_1$ . This is just the average product of two expressions

$$\begin{aligned} & \langle [d\Psi_r(u, s_1) \exp(iux_1) + d\Psi_r(-u, s_1) \exp(-iux_1)]. \\ & [d\Psi_r(u, s_2) \exp(iux_2) + d\Psi_r(-u, s_2) \exp(-iux_2)] \rangle. \end{aligned} \quad (2.10)$$

The integral (2.9) may be simplified to:

$$\begin{aligned} dC_a(d) &= 2k^2 \int_0^L \sin(s_1(k' - k)) \int_0^L \sin(s_2(k' - k)). \\ & \cos(u(x_1 - x_2)) F_r(u, s_1 - s_2) ds_1 ds_2. \end{aligned} \quad (2.11)$$

This integral has been handled by Tatarski (1961, Chapter 8) for the case  $k \gg u$ , with the result:

$$dCa(d) = 4\pi k^2 \int_0^L \Phi(u) \sin^2 \frac{u^2 s}{2k} ds \cos(u(x_1 - x_2)), \quad (2.12)$$

where  $s = (s_1 + s_2/2)$  and  $\Phi(u)$  is the three-dimensional power spectrum of the turbulence,  $\Phi(u_x, u_y, u_z)$ , evaluated at  $u_z = 0$ .

The total covariance  $C_a(d)$  is the integral of  $dC_a(d)$  over all wavenumbers  $\bar{u}$ .

$$C_a(d) = 4\pi k^2 \int_0^\infty \int_0^L \Phi(u) \cdot \sin^2 \left( \frac{u^2 s}{2k} \right) \cos(u(x_1 - x_2)) ds d\bar{u}. \quad (2.13)$$

Taking  $d\bar{u} = u \cdot du \cdot d\phi$ , noting that the projection of the receiver separation  $d$  upon  $\bar{u}$ ,  $d \cdot \cos \phi$ , is the difference  $(x_1 - x_2)$  of the  $x$ -coordinates of the two receivers, and limiting the integration in  $\bar{u}$  such that  $|\bar{u}| \leq k$ ,

$$C_a(d) = 4\pi k^2 \int_0^k du \int_0^L ds \int_0^\pi d\phi u \Phi(u) \cos(du \cdot \cos\phi) \sin^2[u^2 s/2k] \quad (2.14)$$

Performing the integration in  $\phi$ , assuming  $\Phi(u)$  to be independent of  $\phi$ :

$$C_a(d) = 4\pi^2 k^2 \int_0^k du \int_0^L ds u \Phi(u) J_0(du) \sin^2(u^2 s/2k). \quad (2.15)$$

This is the form given by Tatarski (1961, p. 168). If  $\Phi(u)$  is independent of  $s$ , (2.13) reduces to

$$C_a(d) = 2\pi^2 k^2 L \int_0^L du u \Phi(u) J_0(du) \left[ 1 - \frac{k}{u} \sin \frac{u^2 L}{k} \right]. \quad (2.16)$$

Amplitude variance is obtained by setting  $d = 0$ .

$$C_a(0) = 4\pi^2 k^2 L \int_0^k du \int_0^L ds u \Phi(u) \sin^2(u^2 s/2k). \quad (2.17)$$

Phase covariance follows from (2.8) by simply replacing the  $\sin [s(k' - k)]$  term by  $\cos [s(k' - k)]$  in the foregoing development. For example,

$$C_p(d) = 4\pi^2 k^2 \int_0^k du \int_0^L ds u \Phi(u) J_0(du) \cos^2[u^2 s/2k]. \quad (2.18)$$

Again, if  $\Phi(u)$  is independent of  $s$ , this reduces to

$$C_p(d) = 2\pi^2 k^2 L \int_0^k du u \Phi(u) J_0(du) \left( 1 + \frac{k}{u} \sin \frac{u^2 L}{k} \right). \quad (2.19)$$

The latter is the form given by Tatarski (1961, p. 143). Structure-functions follow from the definition

$$D_i(d) = 2(C_i(0) - C_i(d)).$$

Thus,

$$D_a(d) = 8\pi^2 k^2 \int_0^k du \int_0^L ds u \Phi(u) [1 - J_0(du)] \sin^2(u^2 s/2k). \quad (2.20)$$

$$D_p(d) = 8\pi^2 k^2 \int_0^k du \int_0^L ds u \Phi(u) [1 - J_0(du)] \cos^2(u^2 s/2k). \quad (2.21)$$

and the wave structure-function,

$$\begin{aligned}
 D(d) &= D_a(d) + D_p(d) = 8\pi^2 k^2 \int_0^k du \int_0^L ds u \Phi(u) [1 - J_0(du)] \quad (2.22) \\
 &= 8\pi^2 k^2 L \int_0^k du u \Phi(u) [1 - J_0(du)], \Phi(u) \neq f(s).
 \end{aligned}$$

### 3. PROPAGATION OF A SPHERICAL-WAVE

The development of the spherical-wave case closely follows that of the preceding section. A spherical-wave expanding from the origin at (O,O,O), with wavenumber  $k$ , has near the  $z$ -axis at  $z = s$  the magnitude

$$\frac{L}{s} \exp(-ik \sqrt{s^2 + x^2 + y^2}).$$

The magnitude is normalized to unity at  $z = L$ , the plane of the receiving points. This wave is incident upon an infinite slab in the plane  $z = s$ , of thickness  $dz$ . As in the plane wave case, the slab imposes upon the wave a perturbation in phase, sinusoidal in  $x$  (cf. (2.1) and Figure 2.1), of peak magnitude  $k a dz$ :

$$d_{\text{phase}} = k a dz \cos(u(x + b)) \quad (3.1)$$

where  $u$  is the wavenumber of the perturbation, and  $b$  is the phase of the perturbation at the  $z$ -axis. Upon exiting from the slab the incident wave becomes

$$\frac{L}{s} \exp(-ik \sqrt{s^2 + x^2 + y^2}) \exp(-ik a dz \cos(u(x + b))). \quad (3.2)$$

Since the perturbation is assumed to be small ( $k a dz \ll 1$ ), (3.2) may be written

$$\begin{aligned}
 &\frac{L}{s} \exp(-ik \sqrt{s^2 + x^2 + y^2}) (1 - ik a dz \cos(u(x + b))) \quad (3.3) \\
 &= \frac{L}{s} \exp(-ik \sqrt{s^2 + x^2 + y^2}) - \frac{ikaLdz}{2s} \exp(-ik \sqrt{s^2 + x^2 + y^2}) \exp \\
 &\quad - \frac{ikaLdz}{2s} \exp(-ik \sqrt{s^2 + x^2 + y^2}) \exp(-iu(x + b))
 \end{aligned}$$

Near the  $z$ -axis ( $x, y \ll s$ ), (3.3) may be written

$$\begin{aligned}
 &\frac{L}{s} \exp(-ik \sqrt{s^2 + x^2 + y^2}) - \frac{idaLdz}{2s} \exp\left[-ik \left(s + \frac{x^2}{2s} + \frac{y^2}{2s}\right)\right] \exp[-iu(x + b)] \quad (3.4) \\
 &\quad - \frac{ikaLdz}{2s} \exp\left[-ik \left(s + \frac{x^2}{2s} + \frac{y^2}{2s}\right)\right] \exp[-iu(x + b)] \\
 &= \frac{L}{s} \exp\left[-ik \sqrt{s^2 + x^2 + y^2}\right] - \frac{ikaLdz}{2s} \exp(iub) \exp\left[-ik \left(s + \frac{y^2}{2s} + \frac{x^2}{2s} - \frac{ux}{k}\right)\right] \\
 &\quad - \frac{ikaLdz}{2s} \exp(iub) \exp\left[-ik \left(s + \frac{y^2}{2s} + \frac{x^2}{2s} + \frac{ux}{k}\right)\right]
 \end{aligned}$$

## WAVE PROPAGATION IN A RANDOM MEDIUM

Completing the square of the x-terms, and factoring the remainder:

$$\begin{aligned} \frac{L}{s} \exp \left[ -ik \sqrt{s^2 + x^2 + y^2} \right] & \quad (3.5) \\ - \frac{ikaLdz}{2s} \exp(iub) \exp \left[ \frac{iu^2 s}{2k} \right] \exp \left( -ik \left[ s + \frac{y^2}{2s} + \frac{[x-us/k]^2}{2s} \right] \right) \\ - \frac{ikaLdz}{2s} \exp(-iub) \exp \left[ \frac{iu^2 s}{2k} \right] \exp \left( -ik \left[ s + \frac{y^2}{2s} + \frac{[x+us/k]^2}{2s} \right] \right) \end{aligned}$$

The first term of (3.5) is the original spherical-wave, undiminished in the weak-scattering approximation. The next two terms represent two additional spherical waves, originating from the points  $[us/k, 0, 0]$  and  $[-us/k, 0, 0]$ , differing in amplitude from the original wave by the factor

$$ka \frac{dz}{2},$$

and in phase by the factor  $\exp \pm (iub) \exp [iu^2 s/2k]$ . Note that it is required that

$$2s^2 \gg \left( x + \frac{us}{k} \right)^2.$$

This is satisfied if  $x$  is small and  $k \gg u$ . In the plane  $z = L$  the sum of these three spherical-waves is

$$\begin{aligned} dE_t = \exp \left( -ik \left( L + \frac{x^2}{2L} + \frac{y^2}{2L} \right) \right) & \quad (3.6) \\ - \frac{ikadz}{2} \exp(iub) \exp \left( \frac{iu^2 s}{2k} \right) \exp \left[ -ik \left( L + \frac{y^2}{2L} + \frac{(x-us/k)^2}{2L} \right) \right] \\ - \frac{idadz}{2} \exp(-iub) \exp \left( \frac{iu^2 s}{2k} \right) \exp \left[ -ik \left( L + \frac{y^2}{2L} + \frac{(x+us/k)^2}{2L} \right) \right] \end{aligned}$$

Factoring and dropping the common phase term  $\exp [ -ik (L + y^2/2L) ]$ ,

$$\begin{aligned} dE_t = \exp \left[ \frac{-ikx^2}{2L} \right] - \frac{ikadz}{2} \exp \left[ \frac{iu^2 s}{2k} \right] & \left( \exp(iub) \exp \left( \frac{-ik}{2L} \left[ x - \frac{us}{k} \right]^2 \right) \right) \\ + \exp(-iub) \exp \left( \frac{-ik}{2L} \left[ x + \frac{us}{k} \right]^2 \right) & \quad (3.7) \end{aligned}$$

Dropping another common phase factor  $\exp [-ikx^2/2L]$  and combining terms,

$$\begin{aligned} dE_t = 1 - \frac{ikadz}{2} \exp \left[ \frac{iu^2 s}{2k} \right] \exp \left[ \frac{-iu^2 s^2}{2kL} \right] & \left( \exp(iub) \exp \left[ \frac{iuxs}{L} \right] + \right. \\ \exp(-iub) \exp \left[ \frac{-iuxs}{L} \right] & \left. \right) \\ = 1 - ikadz \exp \left[ \frac{iu^2 s(L-s)}{2kL} \right] \cos \left[ u \left( \frac{xs}{L} + b \right) \right]. & \quad (3.8) \end{aligned}$$

The observed field perturbation at  $(x,y,L)$  is the difference of the magnitudes of the perturbed and unperturbed fields

$$\begin{aligned} dPa &= |dE_t| - 1 = \left[ \mathcal{R}^2 (dE_t) + \mathcal{I}^2 (dE_t) \right]^{1/2} - 1 \\ &= kadz \sin \left[ \frac{u^2 s(L-s)}{2kL} \right] \cos \left[ u \left( \frac{xs}{L} + b \right) \right]. \end{aligned} \quad (3.9)$$

Terms in  $a^2$  are neglected. As in the plane-wave case, the perturbation of the field is sinusoidal in  $x$  (and independent of the  $y$ -coordinate of the receiver), but the period is  $2\pi L/su$  (rather than  $2\pi/u$ ). That is, the period of the perturbation of the field in the plane  $z = L$  is the projection of the period of the perturber in the plane  $z = s$ .

The perturbation of the phasefront in the plane  $z = L$  is

$$\begin{aligned} dP_p &= \tan^{-1} \left[ \frac{\mathcal{I} dE_t}{\mathcal{R} dE_t} \right] \\ &= kadz \cos \left[ \frac{u^2 s(L-s)}{2kL} \right] \cos \left[ u \left( \frac{xs}{L} + b \right) \right]. \end{aligned} \quad (3.10)$$

The spatial-covariance function of amplitude  $dC_a(d)$  becomes (cf. (2.9)):

$$\begin{aligned} dC_a(d) &= k^2 \int_0^L \sin \left[ \frac{u^2 s_1(L-s_1)}{2kL} \right] \int_0^L \sin \left[ \frac{u^2 s_2(L-s_2)}{2kL} \right] \\ &\cdot \left\langle \left\{ a(u,s_1) \cos \left[ u \left( \frac{x_1 s_1}{L} + b_1 \right) \right] \right\} \cdot \left\{ a(u,s_2) \cos \left[ u \left( \frac{x_2 s_2}{L} + b_2 \right) \right] \right\} \right\rangle. \end{aligned} \quad (3.11)$$

Once again, as in Section 2, the  $\langle \rangle$  term is identifiable with equation (I.6) of Appendix I. Following the development in Section 2, with the one additional assumption that  $L \gg \lambda$ , we obtain an expression for (3.11):

$$dC_a(d) = 4\pi k^2 \int_0^L \Phi(u) \sin^2 \left[ \frac{u^2 s(L-s)}{2kL} \right] \cos \left[ u \frac{(x_1 x_2)}{L} s \right] ds. \quad (3.12)$$

Integrating this expression over all  $\bar{u}$  as was done in Section 2, we obtain:

$$C_a(d) = 4\pi^2 k^2 \int_0^\infty \int_0^L u \Phi(u) J_0 \left( \frac{dus}{L} \right) \sin^2 \left[ \frac{u^2 s(L-s)}{2kL} \right] ds du. \quad (3.13)$$

This is the form given by Schmeltzer (1967, p. 354) as used by Fried (1966, p. 1381). In the case of  $d = 0$  (variance), (3.13) was first derived by Tatarski (1961, p. 183).

If the refractive fluctuations are finite only over the range  $L - H < s < L$ , the covariance becomes

$$C_a(d) = 4\pi^2 k^2 \int_0^k du \int_{L-H}^L ds u \Phi(u) \text{Jo} \left[ \frac{dsu}{L} \right] \sin^2 \left[ \frac{u^2 s(L-s)}{2kL} \right] \quad (3.14)$$

Making  $L$  arbitrarily large (removing the transmitter to infinity),  $\frac{s}{L} \rightarrow 1$  over the range of integration, and

$$C_a(d) = 4\pi^2 k^2 \int_0^k du \int_{L-H}^L ds u \Phi(u) \text{Jo}(du) \sin^2 \left[ \frac{u^2 (L-s)}{2k} \right] \quad (3.15)$$

Making the substitution  $h = L - s$ ,  $dh = -ds$ ,

$$C_a(d) = 4\pi^2 k^2 \int_0^k du \int_0^H dh u \Phi(u) \text{Jo}(du) \sin^2 \left[ \frac{u^2 h}{2k} \right] \quad (3.16)$$

which is the plane-wave result (2.13).

Phase-covariance follows from (3.10), simply by replacing the  $\sin^2(\cdot)$  term in (3.13) by  $\cos^2(\cdot)$ :

$$C_p(d) = 4\pi^2 k^2 \int_0^k du \int_0^L ds u \Phi(u) \text{Jo} \left[ \frac{dsu}{L} \right] \cos^2 \left[ \frac{u^2 s(L-s)}{2kL} \right] \quad (3.17)$$

Structure functions (cf. (2.18), (2.19), and (2.20)) are:

$$D_a(d) = 8\pi^2 k^2 \int_0^k du \int_0^L ds u \Phi(u) \left( 1 - \text{Jo} \left[ \frac{dsu}{L} \right] \right) \sin^2 \left[ \frac{u^2 s(L-s)}{2kL} \right] \quad (3.18)$$

$$D_p(d) = 8\pi^2 k^2 \int_0^k du \int_0^L ds u \Phi(u) \left( 1 - \text{Jo} \left[ \frac{dsu}{L} \right] \right) \cos^2 \left[ \frac{u^2 s(L-s)}{2kL} \right] \quad (3.19)$$

$$D(d) = 8\pi^2 k^2 \int_0^k du \int_0^L ds u \Phi(u) \left( 1 - \text{Jo} \left[ \frac{dsu}{L} \right] \right) \quad (3.20)$$

The amplitude covariance function (3.13), evaluated for several cases, is shown in Figure 3.1. The refractivity spectrum  $\Phi(u)$  assumed in the evaluations was a simple power-law spectrum, with an exponent of  $-11/3$  (Kolmogorov) or  $-4$ . Other parameters used were  $L = 28$  km,  $k = 716$  (35 GHz). The covariance functions are normalized by dividing by  $C_a(0)$ . The central pair of curves in Figure 3.1 is for the normal spherical-wave situation, a single transmitter and two spaced receivers separated by  $d$  (0 to 20 m). A similar curve for the Kolmogorov spectrum has been published by Fried (1967, p. 178).

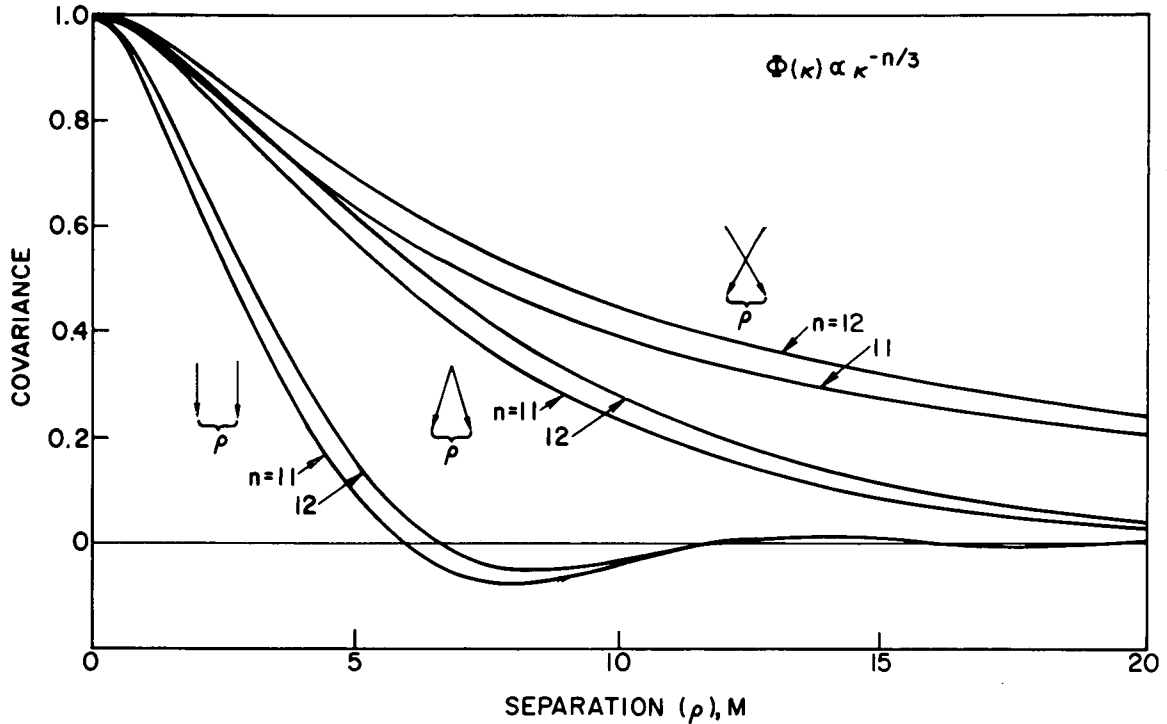


Figure 3.1. Amplitude covariance as a function of path separation  $\rho$ , for three path geometries.

The other two pairs of curves in Figure 3.1 are for crossed- and parallel-path geometries; that is, the two receivers are coupled to two separated transmitters, each transmitter-receiver system being independent of the other. To treat such geometries theoretically, it is only necessary to recognize that the quantity  $ds/L$  in (3.13) represents the separation between the two paths connecting the transmitter to the receivers. In the parallel-path situation (viz. the plane-wave case) this separation is constant along  $s$ , and the Bessel function in (3.13) becomes  $J_0(du)$ . In the crossed-path case, it becomes

$$J_0 \left[ \frac{du(L-2s)}{L} \right] .$$

Another family of theoretical evaluations of (3.13) is shown in Figure 3.2. The same path parameters are used, with additional curves for other refractivity spectra plotted. Also shown in the figure are experimental results obtained over a path described by Lee and Waterman (1966, pp. 454-458). The data represent 32-hour means, with 10th and 90th percentiles of 100-sec measurements. The mean values follow the theoretical curves well as to form, although the Kolmogorov spectrum does not give the best fit.

Evaluation of the phase structure function (3.19) has been performed by Fried (1967, p. 179). For a Kolmogorov refractivity spectrum, over the region in separation  $d$  of interest here the structure function follows a power-law with a slope of  $5/3$ . Experimental measurements of the phase structure function, over the path just mentioned, are plotted in Figure 3.3. The data represent 100-sec samples, taken at random over a two day period. Differences in magnitude among the curves reflect variations in the magnitude of the refractivity spectrum (that is, changes in  $C_n^2$ ). The curves shown in Figure 3.3 approximate a  $5/3$  slope.

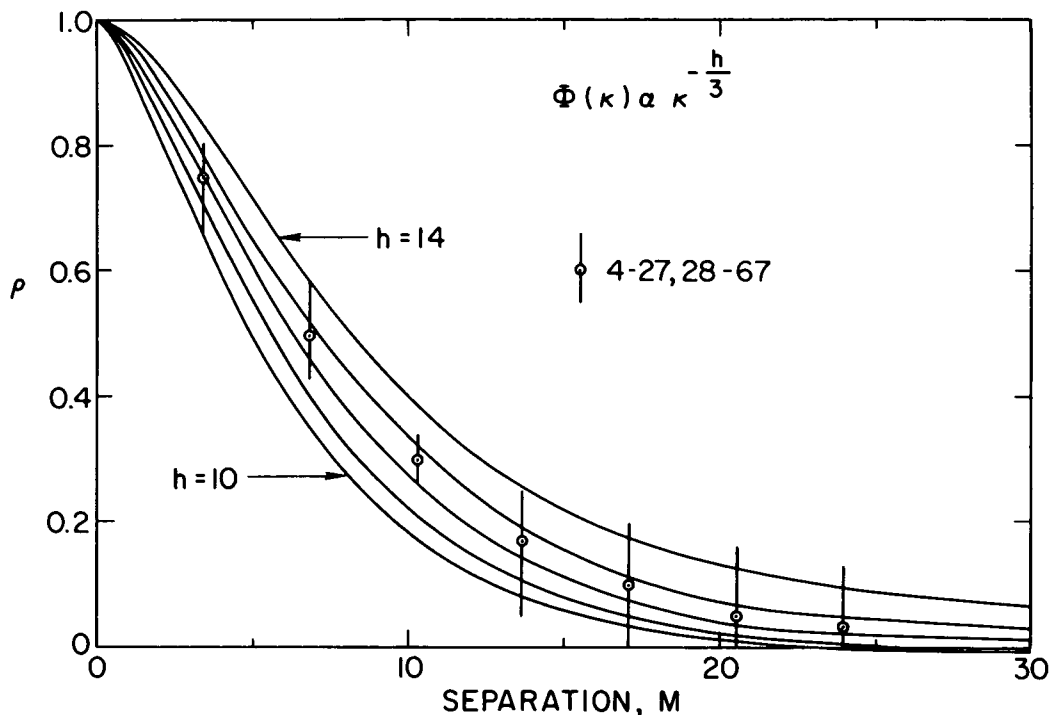


Figure 3.2. Amplitude covariance functions for different spectra  $\Phi(u)$ , with experimental data.

#### 4. ON THE LIMITATIONS OF THE THEORY

Whether or not this theoretical framework (or any theory, for that matter) is suitable for application to a given experimental situation depends upon the validity of two classes of assumptions. The first class involves the accuracy of the assumptions made concerning the parameters of the physical world as introduced into the theory—in this case, the nature of the refractivity field as approximated by a three-dimensional spectrum and associated statistical characterizations. The second class consists of those assumptions (usually called approximations) which arise out of the mathematical necessity, in the process of obtaining mathematically simple (if physically unrealistic) solutions. The preceding theoretical development possesses considerable advantage over more abstract mathematical approaches in this respect, in that approximations of the sort just mentioned arise in a clear physical context, making evaluation of the implications of the approximations relatively simple. An analysis of both classes of assumptions follows, for the development of Sections 2 and 3, with the intent being to obtain not only sufficiency conditions, but necessary conditions for the application of the results.

Without doubt the most important assumption made in the development of the theory is that the scattered energy is small compared with the incident wave. The necessity for this assumption arises for two reasons. Taking the plane-wave development of Section 2 (the same argument holds equally well for the spherical- or beamed-wave cases), this assumption allows the exponential of (2.2) to be expanded into (2.3); this not only makes possible the rest of the development, but carries an important implication as well. That

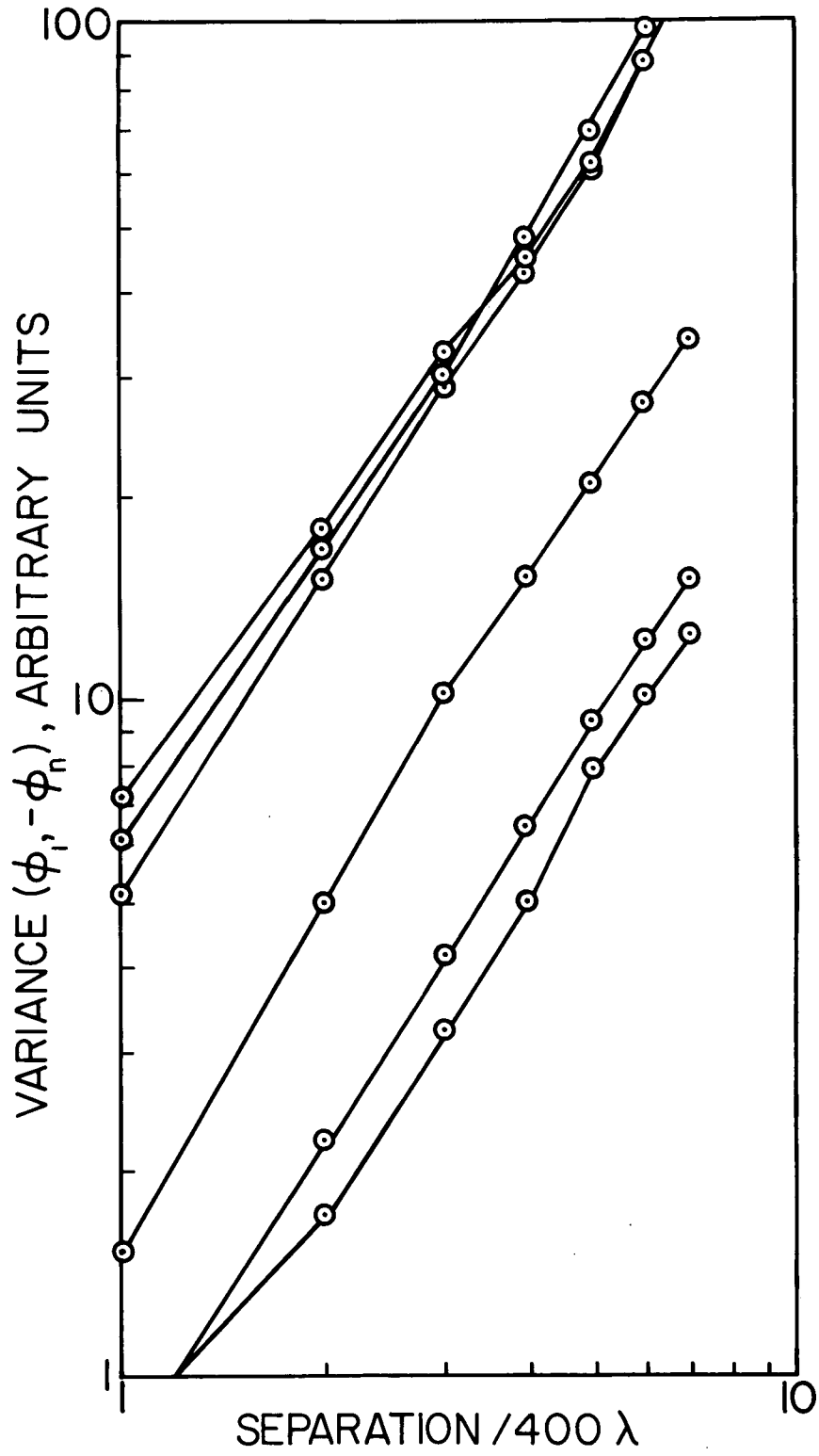


Figure 3.3. Phase structure-functions measured.

is, the expansion used results in the original wave propagating without the loss of energy, while finite energy appears as a scattered component. Clearly energy is not conserved; in actual practice the incident unperturbed wave will decay with distance. The assumption of weak scattering allows two other phenomena to be ignored: multiple scattering (wherein a scattered wave of the type noted in (2.4) can itself be scattered from another slab), and higher order scattering (corresponding to the higher grating orders). The second occasion wherein weak scattering is invoked occurs at the end of the development, when variance is obtained. It is implicit in (2.7) that since the unperturbed field is normalized to unity, the perturbations calculated are ratios of perturbed to unperturbed fields. When the sum of many such perturbations is identified with the covariance, as in (2.15), this identification rests upon the assumption that the sum of the perturbations is less than the unperturbed field. That is, not only must the individual perturbations be small, but their sum must be small. There can be no doubt that the theory breaks down when the variance of the received field approaches unity in terms of the mean field.

It is appropriate to note here that the theory as developed here treats the received field (as normalized by the mean field) rather than the logarithm of the field, as used by Tatarski (1961) and others using the approach of Rytov. Nonetheless, the results obtained here agree in general with the results of log-amplitude treatments. This agreement can be attributed to the weak-scattering assumption for as long as the variance of the received field is appreciably less than unity, there is no significant difference between the logarithm of the field and the departure of the field from unity.

The nature of the limitation imposed by this basic assumption upon application of the theory depends upon the intensity of the refractivity spectrum, as well as upon wavelength and path length. For the lower atmosphere, pathlengths are limited to (typically) hundreds of meters at optical wavelengths, and to hundreds of km at centimeter wavelengths.

It is generally assumed during use of the Rytov method that the wavelength  $2\pi/k$  is much smaller than the smallest dielectric irregularity; that is,  $k \gg u_{\max}$ . (4.1)

It is generally agreed that a lower limit on irregularity size exists in the atmosphere ( $l_0$ , the "inner scale" of turbulence), and is of the order of millimeters. Taken at face value this assumption limits the use of the theory to wavelengths shorter than a millimeter or so. In order to extend the validity of the theory to longer wavelengths, it is necessary to consider the effect of wavenumbers  $u$  ranging from about  $k/10$  (where  $k$  can be considered much greater than  $u$ ) to infinity. First consider the region  $u$  greater than  $k$ .

It can be seen from (2.3) that the sinusoidal phase-perturber of Figure 2.1 is equivalent to a sinusoidal amplitude-perturber lagging  $90^\circ$  in phase. The perturbation emerges from the equivalent of a transmission grating, with adjacent "slits" differing in phase by  $180^\circ$  due to the cosine term. The angles defined in Figure 2.2 are simply the grating-lobe angles. With this background, the effect of reducing the grating spacing is evident. As the spacing decreases (corresponding to higher wavenumber  $u$ ) the grating angles become larger (corresponding to the perturbing wave arriving from farther off path) until, for  $k = u$ , they are  $\pm 180^\circ$ . When  $u$  exceeds  $k$  there are no longer solutions which result in constructive interference for any angle, and, in fact, the effective wavenumber of the emerging perturbation  $k'$  becomes imaginary, as can be seen from the definition.

$$k' = \sqrt{k^2 - u^2} . \quad (4.2)$$

In this situation the additional waves caused by the perturbation (the so-called evanescent waves) do not propagate more than a few wavelengths. Hence the integration in  $u$  (cf. (2.15)) may be safely terminated at  $k$ , rather than infinity, and no limitation need be imposed upon  $k$ . We are left with the region  $k = u$  to  $k \gg u$ . This is the region of wide-angle scattering, scattering which is usually ignored, being removed from mathematical developments by the use of a "cone of integration." There are at least three reasons for concluding that this region of the refractivity spectrum can be safely ignored. In the first place, in practical experiments, finite antenna aperture provides a physical "cone of integration." Narrow beamwidths are not required; tens of degrees suffice (equivalent to an aperture of a few wavelengths). Secondly, in the case of a spherical wave the divergence of the wavefront reduces the effect of wide-angle scattering both through an effective increase in the scatter angle, and through increased attenuation of waves scattered at large angles (since the scattered waves are themselves spherical waves, and hence undergo  $1/r$  decay, unlike infinite plane waves). Finally, in the case of the plane wave, solutions can be obtained for the scattering in the region of the spectrum, including the effects of depolarization (Lee and Harp, 1969, and Strohbehn and Clifford). These solutions show that, provided the propagation path is reasonably lossy (this condition is met at all wavelengths from the microwave to the optical regions), contributions from this portion of the refractivity spectrum will be negligible.

A final point concerns an assumption implicit in Sections 2 and 3—that Fourier components along the axis of the path (as opposed to transverse components making up the slab) have no effect upon the wave. This is clearly the case as far as the amplitude of the wave is concerned; a wave propagating through a uniform slab emerges with its wavefront unperturbed. However, the wavefront will suffer delay (or advancement) in phase. If the period of the Fourier component (or series of slabs, alternately retarding and advancing the wave) is small compared with the path length, the net phase perturbation will be near zero (it is at most that caused by a half-cycle of the Fourier component). If on the other hand the period is comparable to or greater than the path length, and the amplitude of the Fourier component is large enough, significant phase changes can occur. Such phase changes will affect all points in the plane of the receiver, and can be thought of as changes in the average refractive index of the atmosphere in the vicinity of the path. As such, they can be excluded from analysis concerned with scattering, and included simply as a slowly changing correction to phase-path, resulting from air-mass changes, etc.

## 5. PROPAGATION IN ANISOTROPIC MEDIA

In the preceding sections it has been assumed that the refractivity spectrum  $\Phi(u)$  was independent of  $\phi$ , the angle between  $\bar{u}$  (the Fourier component of the refractivity field in a slab perpendicular to the path) and the plane containing the transmitter and the two receiving points. This assumption—that  $\Phi(u)$  is isotropic—is not strictly valid in the atmosphere, particularly for small values of  $u$ . In this section we will consider two approaches to the treatment of anisotropic refractivity spectra  $\Phi(u, \phi)$ .

In the simplest case,  $\Phi(u, \phi)$  is a separable function of the two variables  $u$  and  $\phi$ :

$$\Phi(u, \phi) = f(\phi) \Phi'(u) \quad (5.1)$$

In this case the spectral shape of  $\Phi(u, \phi)$  is constant for all values of  $\phi$ , and only the overall magnitude changes with angle. The function  $f(\phi)$  may be resolved into its Fourier components in harmonics of  $2\phi$  over the range  $0 < \phi < \pi$ , giving the general form for the spectrum

$$\Phi(u, \phi) = \Phi(u) \{1 + a_1 \cos(2\phi + 2b_1) + a_2 \cos(4\phi + 4b_2) \dots + a_n \cos(2n\phi + 2nb_n)\} \quad (5.2)$$

where  $a_n$  are the Fourier coefficients of  $f(\phi)$  and  $b_n$  are the phases of the components (the angles between the axes of the components and the plane containing the transmitter and the receiving points). The Fourier coefficient  $a_0$  is absorbed into the spectrum  $\Phi(u)$ .

Taking the case of elliptical anisotropy ( $a_n, b_n = 0$  for  $n > 1$ ) and performing the integration of (2.14)

$$\begin{aligned} & \int_0^\pi \Phi(u, \phi) \cos(du \cos \phi) d\phi \\ &= \Phi(u) \int_0^\pi \{1 + a_1 \cos(2\phi + 2b_1)\} \cos(du \cos \phi) d\phi \\ &= \Phi(u) \int_0^\pi \cos(du \cos \phi) d\phi + a_1 \Phi(u) \int_0^\pi (\cos 2\phi \cos 2b_1 - \sin 2\phi \sin 2b_1) \cos(du \cos \phi) d\phi \end{aligned} \quad (5.3)$$

The integral of the term involving  $\sin 2\phi$  being zero, we are left with

$$\pi \Phi(u) \{J_0(du) + a_1 \cos(2b_1) J_2(du)\} \quad (5.4)$$

The  $n^{\text{th}}$  term in the case of general anisotropy gives rise to a similar term, of the form

$$\pi \Phi(u) a_n \cos(2nb_n) J_{2n}(du) \quad (5.5)$$

and the general result for amplitude covariance is:

$$\begin{aligned} C_a(d) &= 4\pi^2 k^2 \int_0^k du \int_0^L ds u \Phi(u) \{J_0(du) + a_1 \cos(2b_1) J_2(du) + \dots \\ &+ a_n \cos(2nb_n) J_{2n}(du)\} \sin^2 [u^2 s / 2k] \end{aligned} \quad (5.6)$$

The form of this result is applicable to phase covariance, the spherical-wave case, and higher-order functions. (5.6) has been evaluated for elliptical anisotropy in the spherical-wave geometry, and the results are shown in Figure 5.1. The parameters used were: path length  $L = 28$  km, wavenumber  $k = 716$  (35 GHz). The spatial covariance function is plotted for  $a_1 = 0$  (central curve; isotropic case),  $a_1 = 1$  with  $b_1 = 0$  (upper curve), and

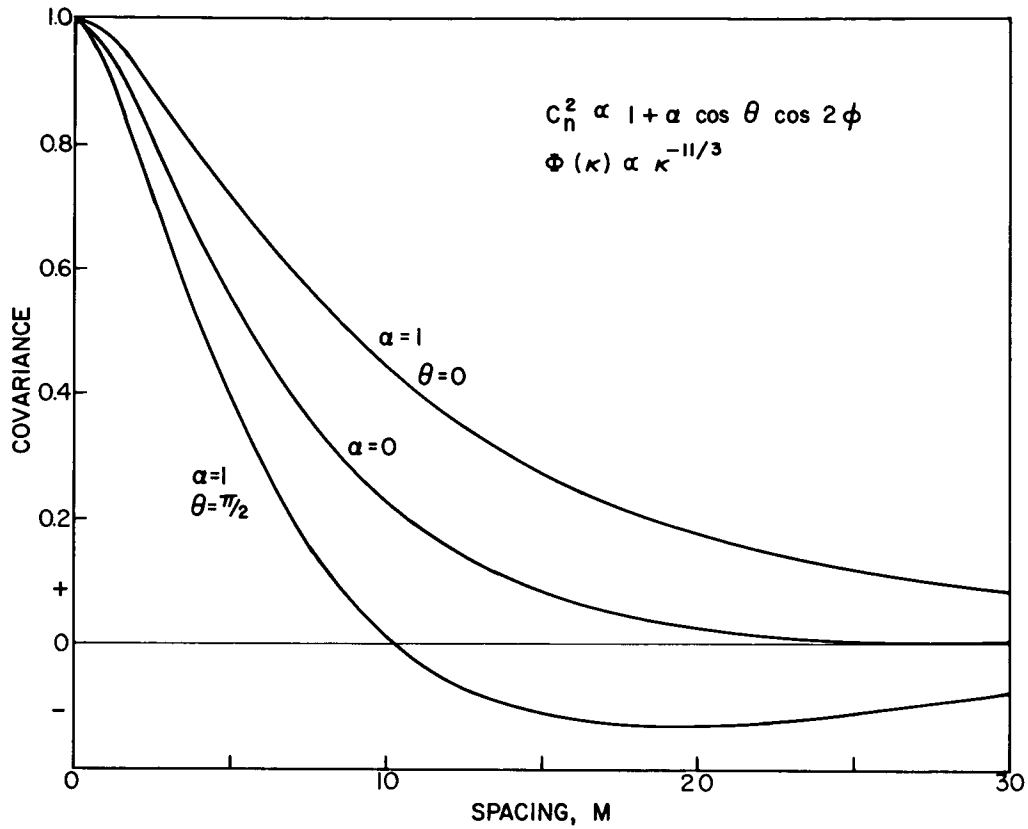


Figure 5.1. Amplitude covariance functions for three anisotropic spectra.

and  $a_1 = 1$ ,  $b_1 = \pi/2$ . In an experimental situation the two curves for  $a_1 = 1$  correspond to aligning the separation between the receivers parallel to and perpendicular to the major axis of the anisotropy. The resulting changes in covariance are quite marked, and affect the basic shape of the function as well as the magnitude. Note that the two curves for the anisotropic case are symmetrically displaced from the isotropic curve.

A second approach to anisotropy is to consider  $\Phi(u, \phi)$  to be composed of two orthogonal components, each of which is separable in  $u$  and  $\phi$ :

$$\Phi(u, \phi) = \Phi_h(u) \sin^2(\phi + b) + \Phi_v(u) \cos^2(\phi + b) \tag{5.7}$$

$\Phi_h(u)$  and  $\Phi_v(u)$  might be the spectrum as measured in the atmosphere in the horizontal and vertical planes, and  $b$  the angle between  $\bar{u}$  and the plane containing the transmitter and receiving points. This relationship is quite appropriate to the situation in the free atmosphere, where in general there are only three unique axes, defined by the vertical, the horizontal and the direction of the wind. Note that only two degrees of freedom are necessary for the calculations here, since longitudinal components of the refractivity field are assumed to have negligible effect. Expanding (5.7):

$$\begin{aligned} \Phi(u, \phi) = & \Phi_h(u) (\sin^2 \phi \cos^2 b + \cos^2 \phi \sin^2 b + \frac{1}{2} \sin 2\phi \sin 2b) \\ & + \Phi_v(u) (\cos^2 \phi \cos^2 b + \sin^2 \phi \sin^2 b - \frac{1}{2} \sin 2\phi \sin 2b) \end{aligned} \tag{5.8}$$

Performing the integrations as in (5.3):

$$\int_0^{\pi} \sin^2 \phi \cos (d u \cos \phi) d\phi = \frac{\pi}{2} [J_0(du) + J_2(du)] \quad (5.9)$$

$$\int_0^{\pi} \cos^2 \phi \cos (d u \cos \phi) d\phi = \frac{\pi}{2} [J_0(du) - J_2(du)] \quad (5.10)$$

As before, the terms involving  $\sin 2\phi$  do not contribute to the integral. Using (5.9) and (5.10) in conjunction with (5.8):

$$\begin{aligned} & \int_0^{\pi} \Phi(u, \phi) \cos (du \cos \phi) d\phi = \\ & \frac{\pi}{2} [J_0(du) + J_2(du)] [\cos^2 b \Phi_h(u) + \sin^2 b \Phi_v(u)] \\ & + \frac{\pi}{2} [J_0(du) - J_2(du)] [\sin^2 b \Phi_h(u) + \cos^2 b \Phi_v(u)] \\ & = \frac{\pi}{2} J_0(du) [\Phi_h(u) + \Phi_v(u)] + \frac{\pi}{2} J_2(du) \cos(2b) [\Phi_h(u) - \Phi_v(u)] \end{aligned} \quad (5.11)$$

The amplitude covariance (plane-wave) becomes:

$$C_a(d) = 2\pi^2 k^2 \int_0^k du \int_0^L ds u \{ J_0(du)(\Phi_h + \Phi_v) + J_2(du) \cos(2b) (\Phi_h - \Phi_v) \sin^2 [u^2 s / 2k] \} \quad (5.12)$$

The same remarks as to generality apply here as to (5.6). If the spectra  $\Phi_h$  and  $\Phi_v$  differ only by a multiplicative constant, (5.12) reduces to (5.6), with  $\Phi(u) = \Phi_h + \Phi_v$  and  $a_1 = \Phi_h - \Phi_v / \Phi_h + \Phi_v$ . Both  $\Phi_h$  and  $\Phi_v$  of (5.7) can be anisotropic spectra in the sense of (5.2). Integration over  $\phi$  is still straightforward, the result being quite general. The spectrum can then be elliptically anisotropic as far as changes in the behavior of  $\Phi(u, \phi)$  in  $u$  with  $\phi$  are concerned, and arbitrarily anisotropic in  $\phi$  for each of the components. Completely general anisotropy can be treated by allowing the coefficients  $a_n$  and  $b_n$  in (5.6) to functions of  $u$ .

## 6. TIME-LAGGED FUNCTIONS

Temporal variation of the field at a point in the receiving plane is the result of two distinct processes. The dielectric field over the region between the transmitter(s) and receivers is changing with time through various mechanisms—advection, convection, turbulent motions, and so on—resulting in corresponding changes in the field. Such changes take place on the time scale of the meteorological processes involved, typically from seconds (turbulent motions) to very large time scales (air mass changes). It is reasonable to expect that the fine scale structure of the dielectric field is more susceptible to rapid variation than large-scale structure. Such changes in the dielectric

field (and the resulting changes in received field) are in general anisotropic, inhomogeneous and non-stationary, and are therefore very difficult to treat both experimentally and theoretically.

The second process resulting in temporal variations of the dielectric field is simply motion of the atmosphere itself, either real (wind) or apparent (as due to the motion of a source). If, to take an example, the atmosphere between a transmitter and a receiver was unchanging except for a simple translation in a direction perpendicular to the transmission path, then the field at the receiver would change in exactly the same manner as if the receiver and transmitter had themselves translated, the atmosphere remaining stationary. This transformation of spatial functions to temporal functions, or Taylor's hypothesis (Taylor, (1938)), is quite convenient from both a theoretical and experimental point of view. It allows (approximately) the equivalent of measurements at many points in space to be made (expensive to do directly), simply by observing the time behavior of a quantity, providing that the velocity of the atmosphere is known.

In general, however, wind velocity in the atmosphere is not sufficiently uniform over the experimental path for a simple "frozen atmosphere" approach to yield accurate results. The next higher approximation is to consider the velocity to be a known function over the path, if this is possible in the appropriate theory.

Approaches based upon Taylor's hypothesis are approximations in two senses. First, wind velocity is assumed to be uniform at all points in a plane transverse to the path—a relatively safe assumption, since only a limited region surrounding the axis of the path itself is important. In addition, temporal variations arising from causes other than wind are neglected. The validity of this assumption depends upon the particular measurement being made. In general, measurements are sensitive only to a limited region of the spectrum of refractivity fluctuations (see Section 10), and as a result temporal variations caused by a given windspeed will lie in a given frequency range. Whether Taylor's hypothesis is appropriate will then depend upon whether significant changes occur in the appropriate region of the spectrum of refractivity fluctuations, in a time scale similar to that expected for changes due to wind. It is sufficient to note there that this condition is often satisfied to the extent that useful measurements can be made.

The extension of the theoretical development of Sections 2 through 5 to include temporal functions involving windspeed is quite straightforward. In (2.14) the quantity  $d$  represents the spatial separation of the paths to the two receivers (in this case the source is at infinity, and  $d$  is independent of path position). Since time-lagged covariance is by definition the covariance of the fluctuations at one point with the fluctuations at another point at a different time, the quantity  $d$  can be identified as the apparent spatial separation between the two paths, including both the physical separation and the apparent separation caused by drift with the wind of one of the points. That is,  $d = d_0 + V(s)t$ , where  $V(s)$  is the velocity at position  $s$  in the path, and  $t$  is the time-lag for which covariance is to be obtained. This substitution is quite general, and may be applied wherever  $d$  appears (usually in the argument of a Bessel function). For instance, in the spherical-wave case, a typical argument is (cf. (3.13)):

$$J_0 \left[ u \left( \frac{ds}{L} + V(s)t \right) \right] \quad (6.1)$$

Note that  $V(s)$  is the component of the wind velocity transverse to the transmission path, the effects of longitudinal winds being quite small. In the case where  $\bar{d}$  and  $\bar{V}(s)$  are not parallel, the appropriate vector addition is necessary.

As an example, a family of theoretical time-lagged amplitude covariance functions is shown in Figure 6.1. The curves were calculated from the results of Section 3 (cf. (3.13)), using for  $\Phi(u)$  the Kolmogorov spectrum  $\Phi(u) \propto u^{-11/3}$ . Path length is 28 km,  $k = 716$ , and  $V(s) = 5$  m/s. Covariance functions are shown for 8 values of  $d$  from 0 (highest curve) to 24 m. The variation of covariance with separation  $d$  at  $t = 0$  follows the curve in Figure 3.1 for the diverging-path geometry (with  $n = 11$ ). In addition, the peaks of the covariance functions in Figure 6.1 follow the curve in Figure 3.1 for the crossed-path geometry, for separations half as great. That is, maximum time-lagged covariance is obtained when the uniform drift due to the wind has effectively moved one of the transmission paths across the other, such that they cross in the center. In this situation, the separation at the ends of the path is half the separation at  $t = 0$ . Figure 6.2 shows a typical family of curves identical in formal and path geometry to that of 6.1, but experimentally obtained rather than theoretical.

The peak-covariances of many families of the type shown in Figure 6.2 were measured over a two day period, on the path already described. The results are shown in Figure 6.3, plotted together with three theoretical curves of the type shown in Figure 3.1 (crossed-path geometry). The figures on the three curves represent the exponent of the refractivity spectrum assumed. The mean data points agree well with the theoretical curves, but individual data points differ greatly, as can be seen from the 10th and 90th percentiles. This is perhaps reasonable, for while the average wind velocity may be uniform along the path, the wind at any time may be highly non-uniform. As will be seen from the theoretical examples to follow, the first effect of a linear variation of

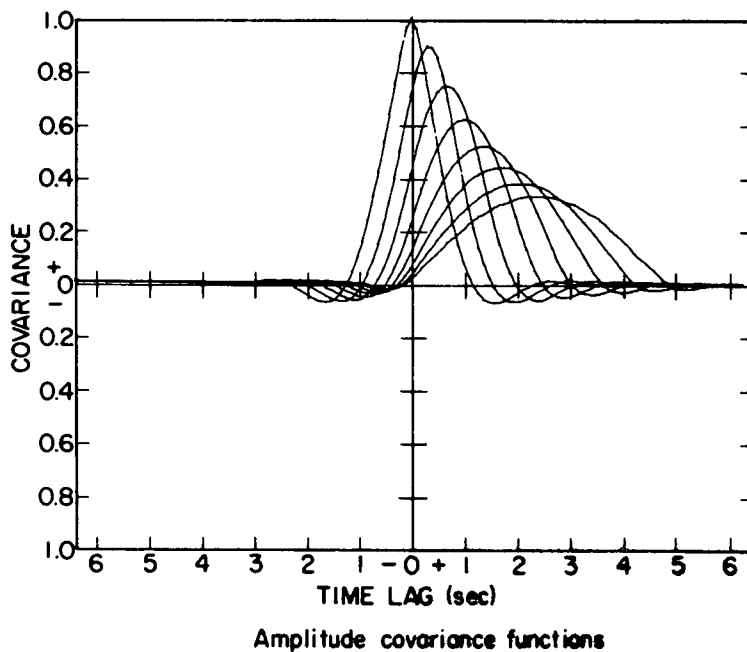


Figure 6.1. Covariance vs. time lag for uniform wind field.

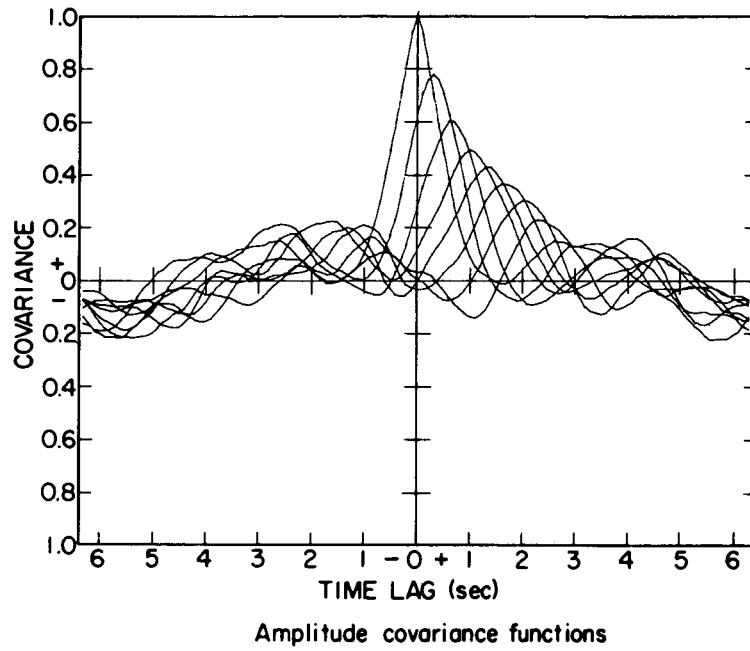


Figure 6.2. Measured covariance functions.

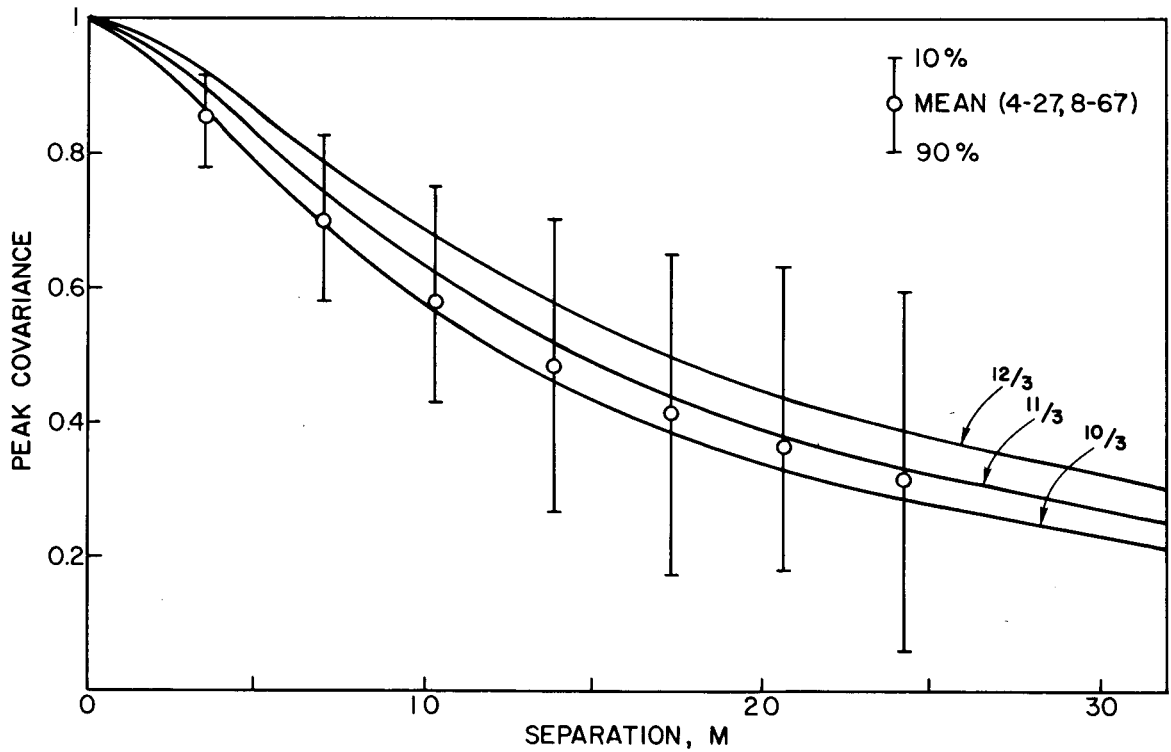


Figure 6.3. Peak time-lagged covariance vs. receiver separation, theoretical and experimental.

wind velocity along the path is to increase or decrease the peak covariances, depending upon whether the variation tends to rotate the air mass about the transmitter, or receiver, respectively.

In general the wind velocity is not uniform along the path, and in addition the refractivity spectrum may also vary along the path. As an example, Figure 6.4 shows another family of experimentally-obtained covariance functions, taken when the path was far from uniform. The curves are much more complex than those of Figure 6.2, and in fact exhibit double-peaks.

To give an indication of the effect of non-uniform wind velocity upon amplitude covariance functions, a few specific cases for which the covariance functions have been evaluated are included here. They differ from Figure 6.1 only in that different assumptions have been made concerning the wind field.

As an example of a double-peaked family of functions, Figure 6.5 was obtained for a wind field uniform at 5 m/s over the path from the transmitter to mid-path, and 7/8 of this value for the remainder of the path. Figure 6.6 was obtained for a wind field uniform at 5 m/s over the first half of the path, as is Figure 6.5, but in this case the velocity was -5 m/s over the last half of the path; that is, the windspeed was uniform, but the direction reversed at mid-path. Contributions from the two regions of the path are clearly evident in the figure. A more subtle change in the windfield was used to obtain Figure 6.7—the windspeed increased linearly from 4 m/s at the transmitter to 6 m/s at the receiver. As a result, the covariance peak value is increased, since the wind field tended to rotate the air mass about the transmitter. If the wind field were zero at the transmitter and increased linearly with distance from it, then (in the "frozen medium" approximation) the peaks of the covariance functions would all be unity, since rotation would bring a given

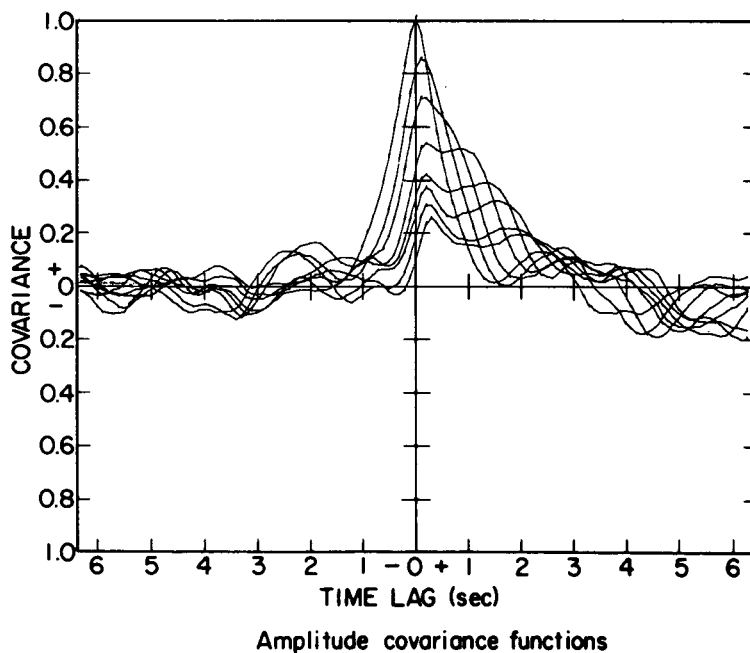


Figure 6.4. Measured covariance functions for non-uniform wind field.

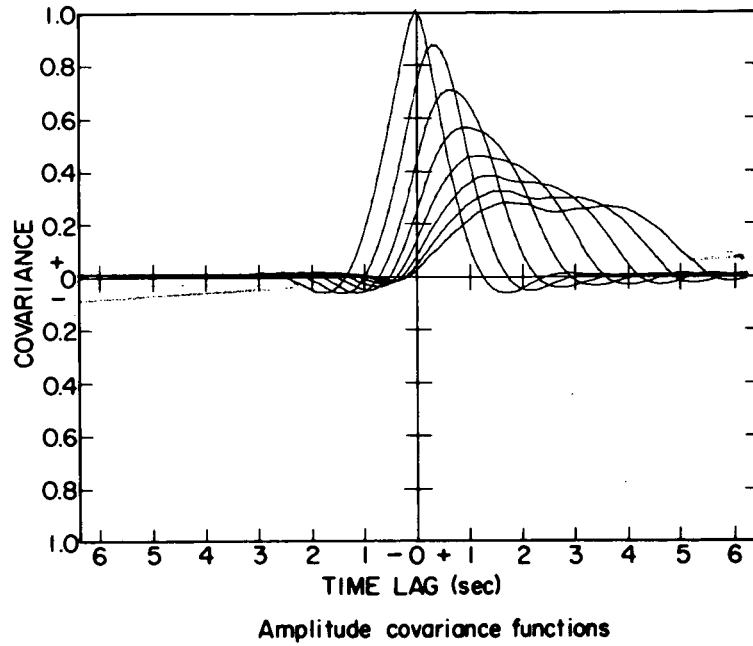


Figure 6.5. Theoretical covariance functions for bimodal wind field.

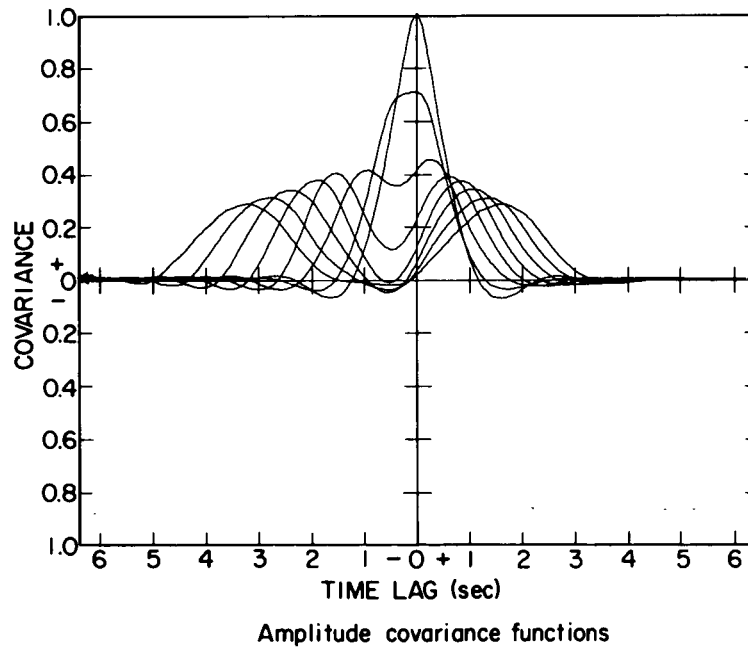


Figure 6.6. Theoretical covariance functions for wind field with direction reversal at mid-path.

# WAVE PROPAGATION IN A RANDOM MEDIUM

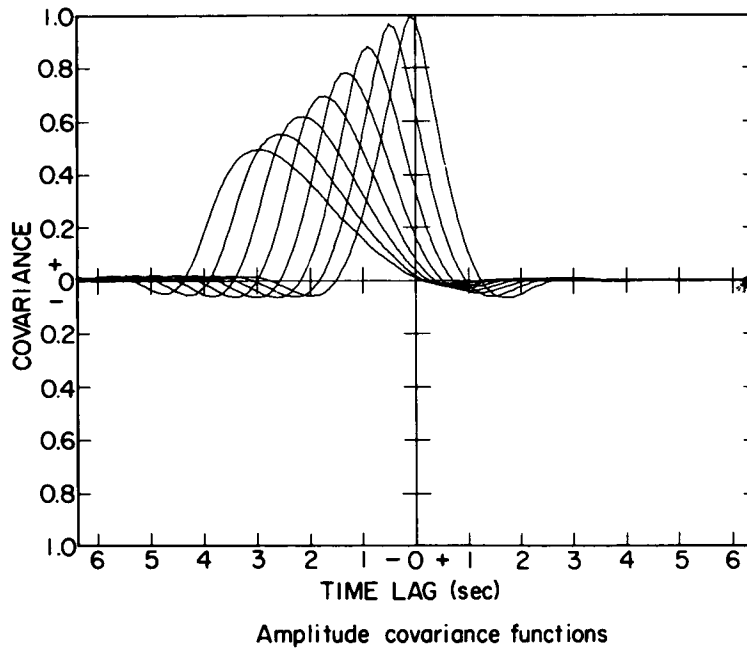


Figure 6.7. Theoretical covariance functions for wind field with uniform shear.

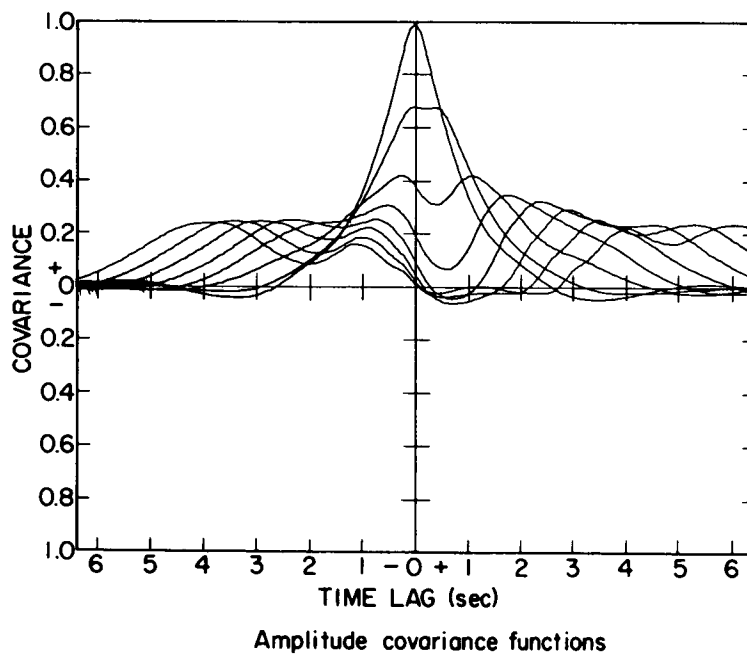


Figure 6.8. Theoretical covariance functions for wind field rotating about mid-path.

region of the atmosphere successively between the transmitter and the several receiving points. Finally, Figure 6.8 was obtained for a wind field effectively rotated around mid-path—the velocity at the transmitter was 8 m/s, decreasing linearly to zero at mid-path, and further decreasing to -8 m/s at the receiver. As can be seen from the figure, the result is quite complex.

## 7. HIGHER STATISTICAL FUNCTIONS

Simple covariances and structure-functions are by no means the only quantities characterizing the wave perturbations which are of interest. The number of possibilities is limitless, and this section is devoted to some important examples, which may serve as guides for generalization.

Hitherto the quantities calculated have involved the relationship between perturbations of the wave at two points in the receiving plane. A natural extension is to consider more than two points, an extension which will be seen to have considerable experimental application. Consider the covariance of difference-pairs—that is, the covariance of the difference of amplitude at two points with the difference between two other points. If the four points are co-linear, the pairs are separated by  $d$ , and members of a pair separated by  $e$ , it is easily shown that

$$C(d,e) = 2C(d) - C(d+e) - C(d-e) . \quad (7.1)$$

When applied to amplitude or phase covariance, the Bessel term of (3.18) and (3.22) becomes

$$J_0 \left( \frac{dsu}{L} \right) \rightarrow 2J_0 \left( \frac{dsu}{L} \right) - J_0 \left( \frac{(d+e)su}{L} \right) - J_0 \left( \frac{(d-e)su}{L} \right) . \quad (7.2)$$

The same result may of course be obtained directly by starting with the magnitude of the perturbation, taking differences, and proceeding as before. As an example of the utility of (7.2), combined with (3.17), several computed phase-covariance functions are shown in Figure 7.1. The upper four curves show the normal (2 point) covariance function; for all cases a Kolmogorov spectrum was assumed—the cases differ only in the value of  $u$  at which the power-law spectrum was terminated at the lower end (the "outer-scale"  $L_0$ ). Such termination is of course required in order that the phase-covariance be finite. Path parameters were  $L = 2.8 \times 10^4$ ,  $k = 716$ . The values chosen correspond to values of  $L_0$  from 50 to 100 m. The lower four curves represent 4-point covariance functions of the type just described. The same values of  $L_0$  were used, the relative narrowness of the function reflecting the emphasis that the differential-process places upon small-scale perturbations. The value of  $e$  used was 3.5 m. The two points on the plot represent averages of experimental data obtained on the path already described. The particular utility of such difference-pair covariances in this case is evident, since phase-difference between two points on the wavefront is much easier to measure experimentally than absolute phase.

In the event that the four points in such a measurement are not co-linear, or equally-spaced, the results may be expressed as four terms involving the four separations; an important situation involves the four points in a rectangular situation:

# WAVE PROPAGATION IN A RANDOM MEDIUM

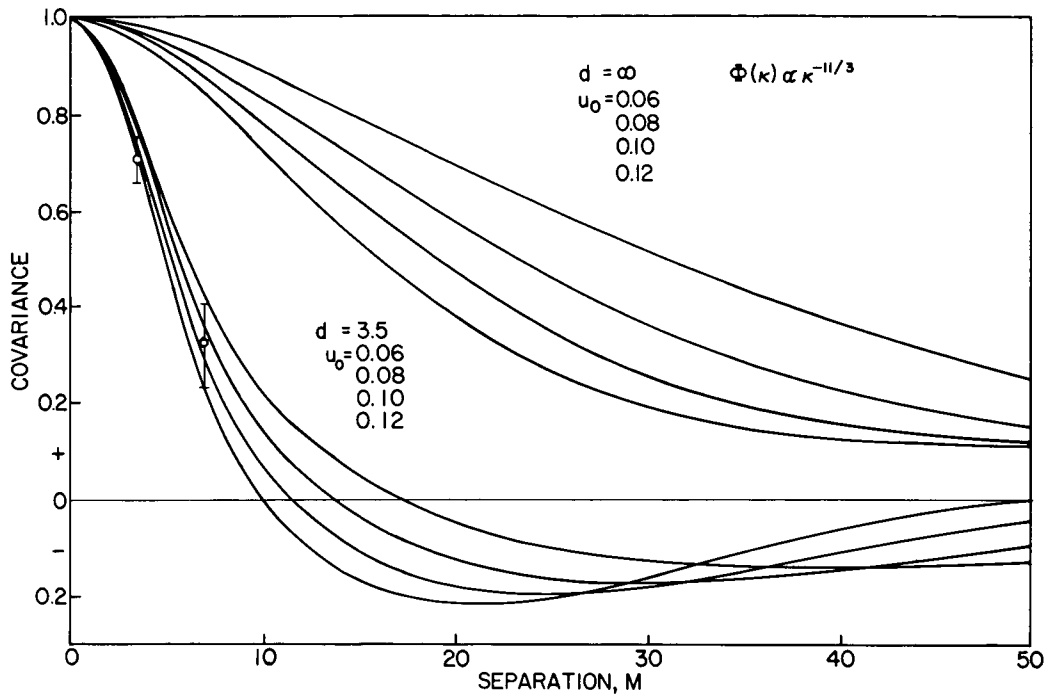


Figure 7.1. Phase and phase-difference covariance functions, for different values of the "outer scale."

$$J_0 \left( \frac{dsu}{L} \right) \rightarrow 2J_0 \left( \frac{dsu}{L} \right) - 2J_0 \left( \sqrt{d^2 + e^2} \frac{su}{L} \right) \quad (7.3)$$

If the separation  $e$  in (7.2) and (7.3) is made arbitrarily small, and the resulting covariance is normalized by  $1/e$ , the result is the covariance of the slope of the quantity. Performing this operation on (7.2), the result is

$$\frac{2}{2L} \frac{su}{2} \left( J_0 \left( \frac{dsu}{L} \right) - J_2 \left( \frac{dsu}{L} \right) \right). \quad (7.4)$$

Using (7.4) with (3.17), covariance of the slope of the phasefront is obtained; that is, covariance of that component of angle-of-arrival parallel to the separation  $d$ . When the operation is performed on (7.3), the result differs only in that the minus sign of (7.4) becomes a plus sign, and covariance of the perpendicular component of the slope is obtained.

With the exception of the wave structure-function, all quantities calculated thus far have involved either the amplitude or phase perturbations on the wavefront, but not both. This separation is somewhat artificial; mixed quantities are easily obtained. As an example, the covariance of the amplitude fluctuations at one point in the receiving plane with the phase fluctuations at another point is

$$C_{ap}(d) = 2\pi^2 k^2 \int_0^k du \int_0^L ds u \Phi(u) J_0 \left( \frac{dsu}{L} \right) \sin \left( \frac{u^2 s(L-s)}{kL} \right) \quad (7.5)$$

Similarly, the covariance between the amplitude at one point and the difference between the phases at two other points differs from (7.5) in that

$$J_0\left(\frac{dsu}{L}\right) \rightarrow J_0\left(\frac{d + \frac{e}{2}su}{L}\right) - J_0\left(\frac{\left(d - \frac{e}{2}\right)su}{L}\right) \quad (7.6)$$

Where the amplitude is measured at (0), and the phase at  $d + e/2$  and  $d - e/2$ . A plot of this function, calculated for a Kolmogorov spectrum (with  $e = 3.5$  m, other parameters as before), is shown in Figure 7.2. An experimentally obtained function of a similar nature is shown in Figure 7.3. It shows the covariance between the amplitude and the phase difference at two points separated by 3.5 m, as a function of time-lag.

The covariance between the amplitude and angle-of-arrival may be similarly obtained. It differs from (7.5) in that

$$J_0\left(\frac{dsu}{L}\right) \rightarrow \frac{us}{2L} J_1\left(\frac{dsu}{L}\right) \quad (7.7)$$

As might be expected, this is also an odd-function.

As a final example, the amplitude covariance between waves with different wave-numbers  $k_1$  and  $k_2$  is

$$C_f(d) = 4\pi^2 k_1 k_2 \int_0^L ds \int_0^{\sqrt{k_1 k_2}} du u \Phi(u) J_0\left(\frac{dsu}{L}\right) \sin\left(\frac{u^2 s(L-s)}{2k_1 L}\right) \cdot \sin\left(\frac{u^2 s(L-s)}{2k_2 L}\right) \quad (7.8)$$

An evaluation of this integral for a Kolmogorov spectrum is shown in Figure 7.4. Note that the covariance (for  $d = 0$ ) is quite high over several octaves.

WAVE PROPAGATION IN A RANDOM MEDIUM

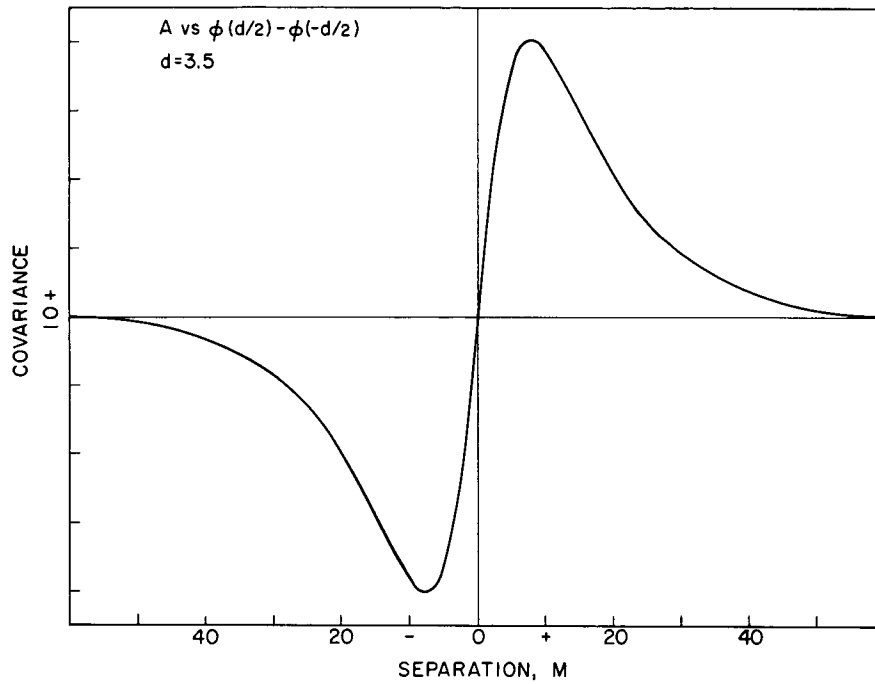
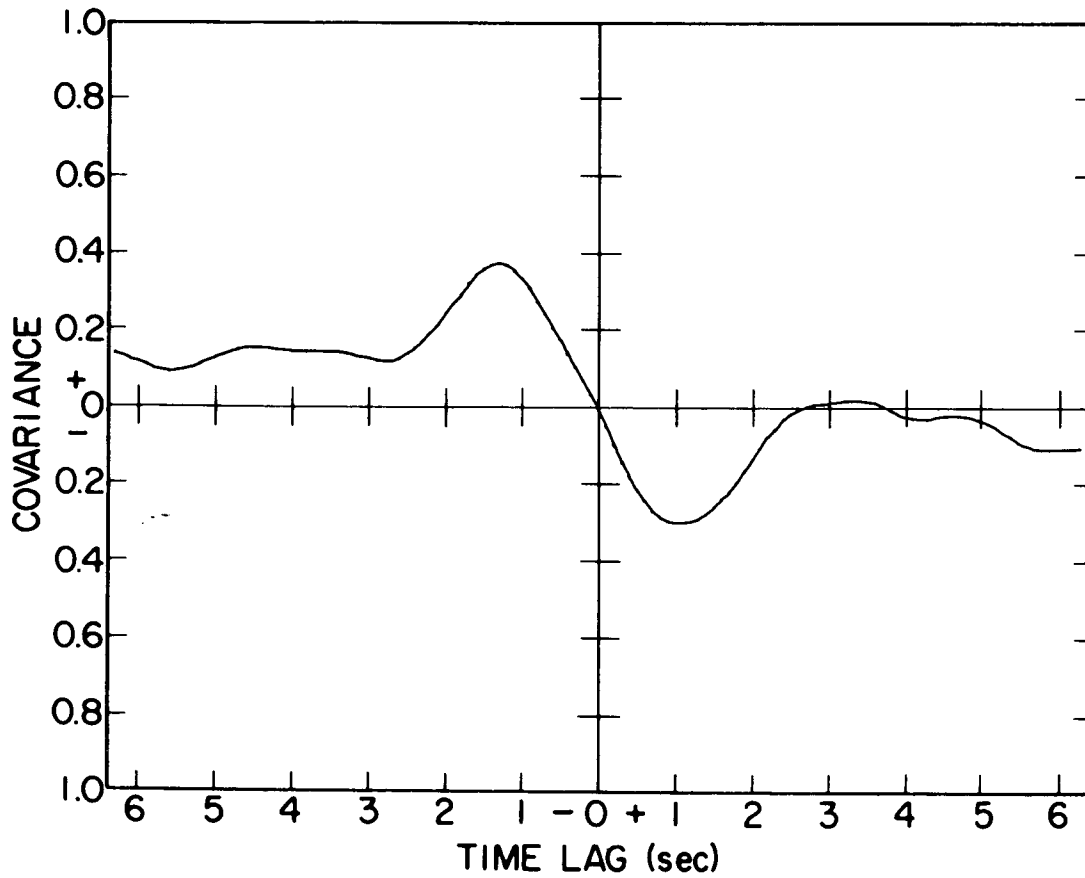


Figure 7.2. Amplitude vs. phase-difference covariance function.



A vs  $\Delta\phi$  covariance functions

Figure 7.3. Experimental amplitude vs. phase-difference covariance function.

C.2

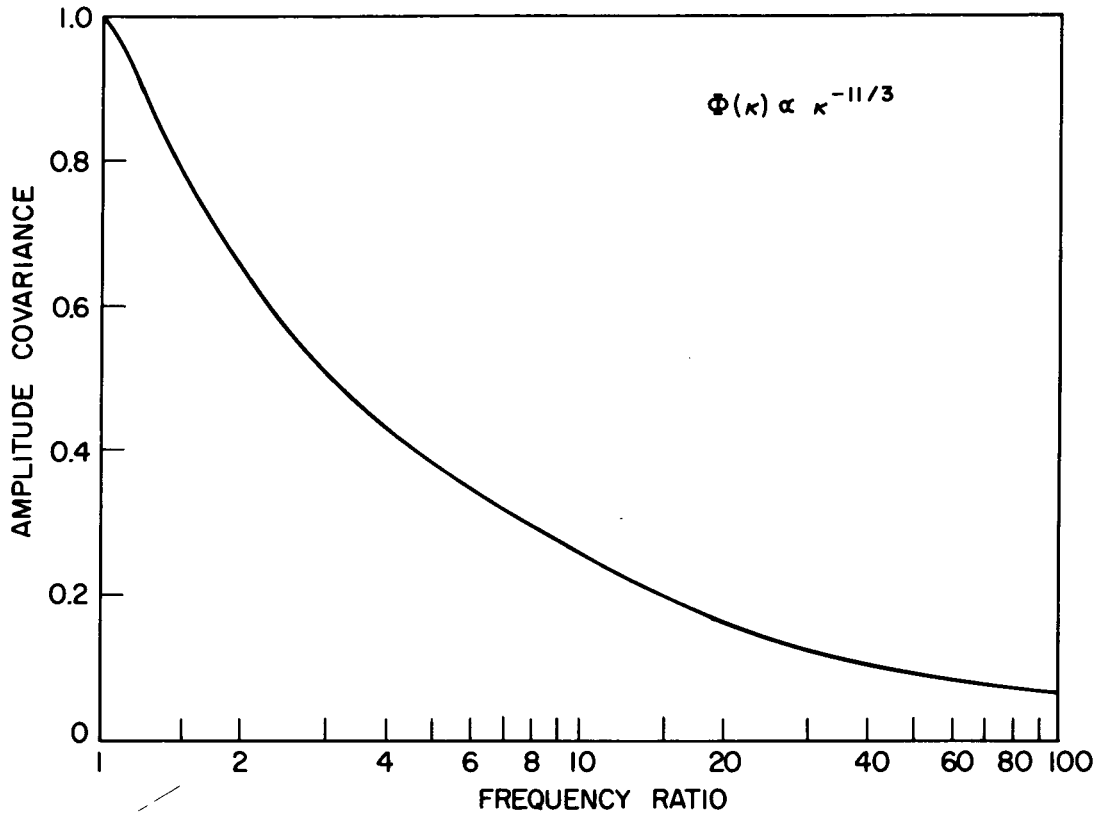


Figure 7.4. Amplitude covariance vs. frequency separation.

## 8. FINITE TRANSMITTING AND RECEIVING APERTURES

In the previous sections receiving apertures have been considered to be points; in the development which follows finite apertures are equated with assemblages of such points, with some weighting factor. In the geometry of the figure power is radiated from an aperture in the plane  $z = 0$ , through a perturbing slab of the kind already discussed (located at  $z = s$ ), to a point receiver located at  $(x_o, y_o, L)$ . The weighting factor at the aperture will be taken to be Gaussian.

$$W = \frac{1}{2\pi\sigma_t^2} \exp \left[ -\frac{x^2 + y^2}{2\sigma_t^2} \right], \quad (8.1)$$

where  $\frac{1}{2\sigma_t^2} = \frac{1}{2} - \frac{ik}{F}$

The physical size of the aperture is  $\sigma_t$  (the standard deviation of the Gaussian), and the focal length is  $F$  (i.e., if  $F = \infty$ , the phase illumination across the aperture is uniform). The differential field  $dE_t$  at  $P$  from a point at  $(x_t, y_t, 0)$  on the aperture is (cf. (3.8)):

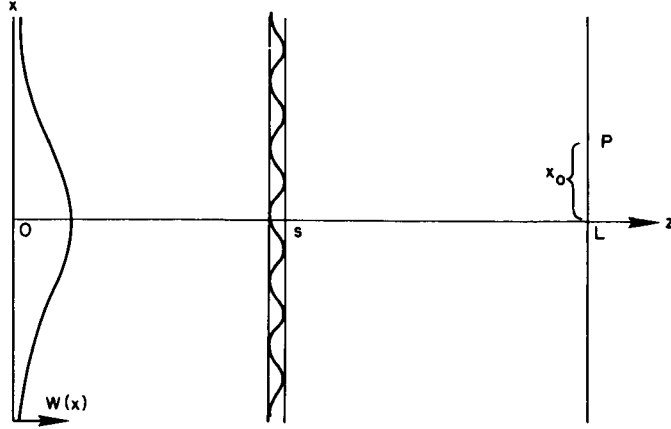


Figure 8.1.

$$dE = \frac{\exp(-ikL)}{L} \exp \left[ \frac{-ik}{2L} (x_o - x_t)^2 + (y_o - y_t)^2 \right] \cdot W dx_t dy_t \cdot \left[ 1 + ika \cdot dz \cdot \exp \left( \frac{iu^2 s(L-s)}{2kL} \right) \cos \left( \frac{x_o us}{L} + \frac{x_t(L-s)}{L} + bu \right) \right]. \quad (8.2)$$

As in the spherical-wave case, the perturbation at  $s$  lies along the  $x$ -axis. The total differential field  $dE_t$  at  $p$  is simply the integral of (8.2) over all points  $x_t$  and  $y_t$  on the transmitting aperture

$$dE_t = \frac{\sigma^2 \exp(-ikL)}{\sigma_t^2 (L+ik\sigma^2)} \exp \left[ \frac{-ik(x_o^2 + y_o^2)}{2(L+ik\sigma^2)} \right] \cdot \left[ 1 + ikadz \exp \left( \frac{iu^2 s(L-s)}{2kL} \right) \exp \left( \frac{-u^2 (L-s)^2 \sigma^2}{2L(L+ik\sigma^2)} \right) \cos \left( x_o u \frac{s+ik\sigma^2}{L+ik\sigma^2} + bu \right) \right]. \quad (8.3)$$

Since  $a$  is a small quantity, terms in  $a^2$  can be neglected, and the field perturbation at  $P$  is (cf. (2.7)),

$$dP_a = \mathcal{R} \left[ ikadz \exp \left( \frac{iu^2 s(L-s)}{2kL} \right) \exp \left( \frac{-u^2 (L-s)^2 \sigma^2}{2L(L+ik\sigma^2)} \right) \cos \left( ux_o \frac{s+ik\sigma^2}{L+ik\sigma^2} + bu \right) \right]. \quad (8.4)$$

The phase perturbation is of course the imaginary part of the quantity in (8.4). The amplitude covariance is obtained by summing the products of the perturbations at two points. Choosing one point at  $(x_o, y_o, L)$  and the other at  $(O, O, L)$ , and proceeding as in (3.11),

$$\begin{aligned}
 dC_a(x_o) &= \frac{1}{2} \mathcal{R} \left\{ k^2 \int_0^L i \cdot \exp \frac{(iu^2 s_1 (L-s_1))}{2kL} \exp \frac{(-u^2 (L-s_1)^2 \sigma^2)}{2L(L+ik\sigma^2)} \right. \\
 &\quad \left. \int_0^L i \cdot \exp \frac{(iu^2 s_2 (L-s_2))}{2kL} \exp \frac{-u^2 (L-s_2)^2 \sigma^2}{2L(L+ik\sigma^2)} \right. \\
 &\quad \left. \langle a(u, s_1) \cos \left( ux_1 \frac{s_1 + ik\sigma^2}{L+ik\sigma^2} + b_1 u \right) \cdot a(u, s_2) \cos \left( ux_2 \frac{s_2 + ik\sigma^2}{L+ik\sigma^2} + b_2 u \right) \right\rangle ds_1 ds_2 \\
 &\quad + k^2 \int_0^L (s_1 \text{ terms}) \int_0^L (s_2 \text{ terms})^* \\
 &\quad \left. \langle a(u, s_1) \cos (\dots + b_1 u) \quad a^*(u, s_2) \cos (b_2 u) \rangle ds_1 ds_2 \right\}, \tag{8.5}
 \end{aligned}$$

where \* denotes the complex conjugate. In expression (8.5) we have used the relation:

$$\mathcal{R}(A) \cdot \mathcal{R}(B) = \frac{1}{2} \mathcal{R}[A(B + B^*)], \tag{8.6}$$

where A and B are complex quantities.

As in the spherical-wave case, we may perform the cross product integration in (8.5) under the conditions,  $k \gg u$  and  $L \gg \lambda$ , with the result:

$$\begin{aligned}
 dC_a(x_o) &= 2\pi^2 \mathcal{R} \left\{ \int_0^L u \Phi(u) \left[ \exp \left( \frac{iu^2 s(L-s)}{2kL} \right) \exp \left( \frac{-u^2 (L-s)^2 \sigma^2}{2L(L+ik\sigma^2)} \right) \right] \right. \\
 &\quad \left. ([\dots] - [*]) \cos \left( ux_o \frac{s + ik\sigma^2}{L+ik\sigma^2} \right) ds \right\}, \tag{8.7}
 \end{aligned}$$

where [\*] denotes the complex conjugate of the previous quantity in similar brackets.

The total covariance is the integral of (8.7) over all wavenumbers  $\bar{u}$ . Proceeding as in the spherical-wave case (cf. (3.13)), where  $d\bar{u} = udu d\phi$ , and recognizing the x-coordinate separation of the receiving points  $(x_o)$ , as  $d\cos(\phi)$ ,

$$C_a(d) = 2\pi^2 k^2 \mathcal{R} \int_0^k du \int_0^L ds u \Phi(u) \text{Jo} \left( \frac{du(s+ik\sigma^2)}{L+ik\sigma^2} \right) \exp(Q) (\exp(Q^*) - \exp(Q)) \tag{8.8}$$

$$\text{where } Q = \left( \frac{-u^2 (L-s)(s+ik\sigma^2)}{2ik(L+ik\sigma^2)} \right).$$

Phase-covariance is obtained similarly.

$$C_p(d) = 2\pi^2 k^2 \mathcal{R} \int_0^k du \int_0^L ds u \Phi(u) \text{Jo} \left( \frac{du(s+ik\sigma^2)}{L+ik\sigma^2} \right) \exp(Q) (\exp(Q^*) + \exp(Q)) \quad (8.9)$$

These results are essentially identical to those of Schmeltzer (1967). They differ only in the assumption of  $\exp(-ikr)$  for the form of a propagating wave, rather than  $\exp(+ikr)$ , with the result that the solutions are conjugate to those of Schmeltzer.

If  $\sigma^2$  is real—that is, if the transmitting aperture is focused at infinity—(8.8) and (8.9) may be written

$$c_p^a(d) = 2\pi^2 k^2 \mathcal{R} \int_0^k du \int_0^L ds u \Phi(u) \text{Jo} \left( \frac{du(s+ik\sigma^2)}{L+ik\sigma^2} \right) \exp \left( \frac{-u^2(L-s)\sigma^2}{L^2+k^2\sigma^4} \right) \cdot \left[ 1 \mp \exp \left( \frac{iu^2(L-s)(sL+k^2\sigma^4)}{k(L^2+k^2\sigma^4)} \right) \right] \quad (8.10)$$

A logical extension of these results is to consider the receiving as well as the transmitting apertures to be finite. The result of similar development for Gaussian receiving and transmitting apertures is

$$C_p^a(d) = 2\pi^2 k^2 \mathcal{R} \int_0^L du \int_0^k ds u \Phi(u) \text{Jo} \left( \frac{du(s+ik\sigma_t^2)}{L+ik(\sigma_t^2+\sigma_r^2)} \right) (RR^* \mp RR) ,$$

$$R = \exp \left( \frac{iu^2 s(L-s)}{2kL} \right) \exp \left[ \frac{iu^2}{2L} \left( \frac{(L-s)^2 \sigma_t^2}{L+ik\sigma_t^2} + \frac{L\sigma_r^2 (s+ik\sigma_t^2)^2}{(L+ik\sigma_t^2)(L+ik(\sigma_t^2+\sigma_r^2))} \right) \right] \quad (8.11)$$

where  $\sigma_t$  and  $\sigma_r$  refer to the transmitting and receiving apertures.

The plane-wave situation can be obtained from (8.11) by allowing  $\sigma_t$  to approach infinity,  $\sigma_t$  being real:

$$C_p^a(d) = 2\pi^2 k^2 \int_0^k du \int_0^L ds u \Phi(u) \text{Jo}(du) \exp(-u^2 \sigma_r^2) \left[ 1 \mp \cos \left( \frac{u^2(L-s)}{k} \right) \right] \quad (8.12)$$

This expression differs from the plane-wave, point-receiving-aperture result by the term  $\exp(-u^2 \sigma_r^2)$ , which has the effect of reducing contributions from high wavenumbers  $u$ .

If the transmitting aperture is not infinite, but the receiver is nevertheless well within the near-field of the transmitter aperture (a common situation in optical experiments), then  $k\sigma_t^2 \gg L$ , and (8.11) may be approximated ( $\sigma_t^2$  real).

$$C_{\frac{a}{p}}(d) = 2\pi^2 k^2 \int_0^k du \int_0^L ds u \Phi(u) J_0 \left[ \frac{du\sigma_t^2}{\sigma_t^2 + \sigma_r^2} \right] \exp \left[ \frac{-u^2 \sigma_t^2 \sigma_r^2}{\sigma_t^2 + \sigma_r^2} \right] \cdot \left[ 1 \mp \cos \left( \frac{u^2(L-s)}{k} \right) \right]. \quad (8.13)$$

In obtaining (8.5) it was assumed that one of the receiving points lay on the z-axis; if this is not the case, (8.5) may be rewritten

$$\begin{aligned} dC_{\frac{a}{p}}(x_1 - x_2) &= \frac{1}{2} \mathcal{R} \left\{ k^2 \int_0^L i \cdot \exp \left( \frac{i u^2 s_1 (L-s_1)}{2kL} \right) \exp \left( \frac{-u^2 (L-s_1)^2 \sigma^2}{2L(L+ik\sigma^2)} \right) \cdot \right. \\ &\quad \int_0^L (s_2 \text{ terms}) \cdot \langle a(u, s_1) \cos \left( u x_1 \frac{s_1 + ik\sigma^2}{L+ik\sigma^2} + b_1 u \right) \cdot \\ &\quad a(u, s_2) \cos \left( (x_2, s_2 \text{ terms}) + b_2 u \right) \rangle ds_1 ds_2 \\ &\quad + k^2 \int_0^L (s_1 \text{ terms}) \cdot \int_0^L (s_2 \text{ terms}) \cdot \\ &\quad \left. \langle a(u, s_1) \cos(\dots) \cdot a^*(u, s_2) \cos(\dots) \rangle ds_1 ds_2 \right\}. \quad (8.14) \end{aligned}$$

As before, we may reduce this integral under the one additional assumption  $x_1, x_2 \ll L$  (cf. (8.7)).

If  $\bar{d}_1$  and  $\bar{d}_2$  are the vectors from (O,O,L) to the two receiving points, and  $\phi$  and  $(\phi + \theta)$  are the angles between these vectors and the axis of the perturbation, then,

$$x_1 = |\bar{d}_1| \cos(\phi), \quad (8.15)$$

$$x_2 = |\bar{d}_2| \cos(\phi + \theta).$$

Expressing the total covariance  $C(d)$  as the integral of (8.14) over all  $\bar{u}$ , and performing the  $\phi$  integration (cf. (8.8)):

$$C_{\frac{a}{p}}(d) = 2\pi^2 k^2 \mathcal{R} \int_0^k du \int_0^L ds u \Phi(u) \left( |\exp Q|^2 J_0 \left[ u |\bar{d}_1 R - \bar{d}_2 R^*| \right] \mp (\exp Q)^2 J_0 \left[ u R |\bar{d}_1 - \bar{d}_2| \right] \right), \quad (8.16)$$

$$\text{where } R = \frac{s+ik\sigma^2}{L+ik\sigma^2} \text{ and } Q = \frac{-u^2(L-s)}{2ik} R$$

This result is essentially that of Ishimaru (1968). It may be extended to include finite receiving as well as transmitting apertures:

$$C_{\frac{a}{p}}(d) = 2\pi^2 k^2 \mathcal{R} \int_0^k du \int_0^L ds u \Phi(u) \left( |P|^2 J_0 \left[ u |\bar{d}_1 S - \bar{d}_2 S^*| \right] \mp P^2 J_0 \left[ u S |\bar{d}_1 - \bar{d}_2| \right] \right) \quad (8.17)$$

where

$$P = \exp \left( \frac{i u^2 s (L-s)}{2kL} \right) \exp \left[ \frac{u^2}{2L} \left( \frac{(L-s)^2 \sigma_t^2}{L + i k \sigma_t^2} + \frac{L \sigma_r^2 (s + i k \sigma_t^2)^2}{(L + i k \sigma_t^2)(L + i k (\sigma_t^2 + \sigma_r^2))} \right) \right]$$

$$S = \frac{s + i k \sigma_t^2}{L + i k (\sigma_t^2 + \sigma_r^2)}$$

The development of expressions for anisotropic spectra  $\Phi(u)$  of Section 5 may be applied readily to the finite aperture treatment of this section. The anisotropic spectrum (5.7) can be included in the  $\phi$ -integration preceding (8.5) or (8.16), with results of the form of (5.12) obtaining.

## 9. PROPAGATION IN A RANDOM LOSSY MEDIUM

Thus far the propagation medium has been considered to be transparent—that is, the refractive index has been assumed to be real. Strictly speaking this is not the case in the atmosphere, although it is a good approximation in the microwave and optical portions of the spectrum. For other regions of the spectrum, particularly the millimeter-wave and infrared regions, moderate to very severe attenuation occurs, primarily resulting from molecular absorption lines (especially those of the water molecule).

Extension of the techniques used in Sections 2 and 3 to a medium with a complex refractive index is straightforward, and indeed the results may be simply guessed at the start. Considering a single Fourier component of the refractivity field as acting as a diffraction grating, we have noted that an additional pair of waves is generated by the grating, and that these waves lag the original wave by  $90^\circ$  at the grating. The sum of the three waves varies in amplitude as the sine of a function depending upon the distance from the grating (2.7). If the refractive perturbation  $a$  (cf. (2.3)) is now made complex, an additional pair of waves is created, propagating at the same angles as those caused by the real portion of the refractive index, but in phase with the original wave at the grating. Since these waves lack the  $90^\circ$  phase shift at the grating, their sum with the original wave is a cosine function of the distance from the grating. Note that this cosine relationship is that appropriate for the phase fluctuations due to the real part of the refractive index. In the final result, the relationships between amplitude and phase perturbations resulting from the imaginary portion of the refractive index, are identical to those for the phase and amplitude, respectively, resulting from the real part; that is, the role of a given scatterer is reversed in the two cases.

Derivation of results for the spherical-wave geometry follows. Naturally the same approach is valid for the plane-wave situation. From (3.8),

$$dE_t = 1 - ika dz \exp\left(\frac{iu^2 s(L-s)}{2kL}\right) \cos\left[u\left(\frac{xs}{L} + b\right)\right] \quad (9.1)$$

If  $a$  (the magnitude of the phase perturbation) is complex,

$$a = \sqrt{\Phi_r(u)} + \sqrt{\Phi_i(u)} = R + iI \quad (9.2)$$

and  $c$  is the correlation coefficient between the real and imaginary parts of  $a$ , then the perturbation of amplitude in the plane  $z = L$  is

$$dP_a = ka dz \cos\left(u\left(\frac{xs}{L} + b\right)\right) \left[ R \sin \frac{u^2 s(L-s)}{2kL} + I \cos \frac{u^2 s(L-s)}{2kL} \right] \quad (9.3)$$

Performing the cross-product integration of (3.11),

$$\begin{aligned} dC_a(x_1-x_2) = 4\pi k^2 \int_0^L ds \cos\left(\frac{su}{L}(s_1-x_2)\right) \cdot \left[ R^2 \sin^2 \frac{u^2 s(L-s)}{2kL} \right. \\ \left. + I^2 \cos^2 \frac{u^2 s(L-s)}{2kL} + cRI \sin \frac{u^2 s(L-s)}{2kL} \right] \quad (9.4) \end{aligned}$$

and the total covariance is:

$$\begin{aligned} C_a(d) = 4\pi^2 k^2 \int_0^k du \int_0^L ds J_0 \frac{dsu}{L} \cdot u \cdot \left[ \Phi_r(u) \sin^2 \left( \frac{u^2 s(L-s)}{2kL} \right) \right. \\ \left. + \Phi_i(u) \cos^2 \left( \frac{u^2 s(L-s)}{2kL} \right) + c\sqrt{\Phi_r(u)\Phi_i(u)} \cdot \sin \left( \frac{u^2 s(L-s)}{kL} \right) \right] \quad (9.5) \end{aligned}$$

If the real and imaginary spectra are related by a multiplicative constant such that  $\Phi_i(u) = m^2 \Phi_r(u)$ , then

$$\begin{aligned} C_a(d) = 4\pi^2 k^2 \int_0^k du \int_0^L ds u \Phi_r(u) J_0 \left( \frac{dsu}{L} \right) \cdot \left[ \sin^2 \left( \frac{u^2 s(L-s)}{2kL} \right) \right. \\ \left. + m^2 \cos^2 \left( \frac{u^2 s(L-s)}{2kL} \right) + cm \sin \left( \frac{u^2 s(L-s)}{kL} \right) \right]. \quad (9.6) \end{aligned}$$

Phase covariance is obtained by simply interchanging  $\sin^2(\cdot)$  and  $\cos^2(\cdot)$  terms:

$$\begin{aligned} C_p(d) = 4\pi^2 k^2 \int_0^k du \int_0^L ds u \Phi_r(u) J_0 \left( \frac{dsu}{L} \right) \cdot \left[ \cos^2 \left( \frac{u^2 s(L-s)}{2kL} \right) \right. \\ \left. + m^2 \sin^2 \left( \frac{u^2 s(L-s)}{2kL} \right) + cm \sin \left( \frac{u^2 s(L-s)}{kL} \right) \right] \quad (9.7) \end{aligned}$$

Other quantities are similarly obtained. For example, the wave structure function:

$$D(d) = 8\pi^2 k^2 \int_0^k du \int_0^L ds u \Phi_r(u) \left[ 1 - J_0\left(\frac{dsu}{L}\right) \right] \left[ 1 + m^2 + 2cm \sin\left(\frac{u^2 s(L-s)}{kL}\right) \right] \quad (9.8)$$

In the likely case where either  $\Phi_r(u)$  or  $\Phi_i(u)$  dominates, the cross-term  $2cm \cdot \sin(\ )$  will not be important (as it is oscillatory about zero in both  $u$  and  $s$ ).

In order to estimate the value of  $m$ , the ratio of the magnitudes of the real and imaginary fluctuating components of the refractive index, consider the following argument:

A plane-wave propagating along the  $z$ -axis in a medium of refractive index  $n$ ,  $\exp(-iknz)$ , where  $n = A + iB$ , experiences an excess phase-path over free-space of  $z(A-1)$ , and a transmittance of  $\exp(-kzB)$ . If the predominant mechanism for refractivity variations is local density change (as by temperature fluctuations), then changes in excess phase path will occur in proportion to the logarithm of changes in transmittance. That is, the fluctuating component of  $(A-1)$  will be of approximately the same ratio to the average excess phase path  $(A_0-1)$ , as the fluctuating component of  $\exp(-kzB)$  is to the average transmittance  $\exp(-kzB_0)$ . Thus

$$m = \frac{B_0}{(A_0 - 1)} = - \frac{\log_e(\text{Transmittance})}{kL(A_0 - 1)} \quad (9.9)$$

At the surface of the earth  $A_0 - 1 = .0003$ ; thus

$$m = - \frac{\log_e(\text{Transmittance})}{.0003kL} = .06 \lambda \text{ (attenuation)} \quad (9.10)$$

where  $\lambda$  is the wavelength in meters, and the attenuation is measured in db/km.

It appears unlikely that  $m$  can approach unity in practical situations, for (9.10) implies that losses of 16 db/1000 wavelengths would be required. To give some more realistic examples, for  $\lambda = 10^{-2}$ m and a loss of 0.3 db/km,  $m$  would be about  $2 \times 10^{-4}$ ; for  $\lambda = 10^{-6}$  and a loss of 30 db/km,  $m$  would be about  $2 \times 10^{-6}$ . Thus, in these cases, the lossy portion of the refractive index could be safely ignored as far as the wave structure function or phase covariances are concerned.

This is not necessarily the case, however, for amplitude covariances, even with such low values of  $m$ , due to the nature of the "filter functions" present in the integral (9.6). While the contribution of the real part of the refractive index to amplitude covariance is zero at  $u = 0$  and rises to a peak at blob sizes of about a Fresnel zone (because of the  $\sin^2$  term in (9.6)), the filter function for the imaginary part is quite different. In the latter case the weighting is maximum at  $u = 0$ , and is minimum at the peak of the contribution from the real part. As a result, amplitude fluctuations originating from variations of the imaginary part of the refractive index, at low values of  $u$ , are emphasized by the spectrum  $\Phi(u)$ , which rises steeply for low  $u$ . Thus, while  $m^2$  may be only  $10^{-6}$ , the spectrum may be stronger by a factor of  $10^4$  or more at the lower  $u$ . When such contributions to amplitude covariance are appreciable, they will tend to broaden the covariance function, as well as increase the variance. The data points in Figure 3.2, for example, may be slightly affected.

## 10. "FILTER FUNCTIONS" FOR VARIOUS QUANTITIES

It is instructive to consider the integrands of the expressions derived in the preceding sections as composed of three types of multiplicative terms. The first term is simply the power spectrum of the refractive irregularities, the energy input to the scattering process. This term is the only connection between the integrand and the medium—the other portions of the integrand are dependent only upon the geometry of the situation (with some exceptions to be noted presently). In this section,  $\Phi(u)$  is taken to be  $u$  times the spectrum appearing in previous sections. Hence, for a Kolmogorov turbulence, this section takes  $\Phi(u) = u^{-8/3}$  rather than  $u^{-11/3}$ .

The second term is unique in being a function of the path-separation in (for example) covariance functions. It serves to relate the perturbations present at one point in the receiving plane to those at another point, and in general goes to unity as the two points become coincident (as in the case of variance). In the expressions derived in this paper this term is always a Bessel function of the first kind. In two cases not considered in this section (time-lagged functions and anisotropic media), atmospheric parameters also enter into this term.

The third term, the subject of this section, is generally referred to as a "filter function," since it weights selectively the first term. It is a measure of the effect produced by an irregularity of a given wavenumber  $u$ , at a given position  $s$  along the path; that is, it measures the scattering efficiency of the perturber. The "filter function" is a function of the geometrical factors  $s, u, L$  (path length),  $k$  (wavenumber of the electromagnetic wave), and  $\sigma$  (the size of the transmitting aperture). In many of the examples to follow, the second term mentioned above will be included in the "filter function," adding the receiver separation  $d$  to the variables.

The importance of "filter functions" becomes clear when attempts are made to interpret experimental measurements in terms of atmospheric parameters. A single measurement obviously cannot uniquely determine a number of parameters, and it is necessary to determine those parameters to which the measurement is most sensitive. If the more sensitive parameters are well known, attention can be directed to less sensitive parameters; if not, unique determination of the less sensitive parameters is not possible. As an example, measured spatial amplitude-covariance functions readily yield values for a very general parameter, the slope of the refractivity spectrum. However, the appropriate "filter function" (Figure 10.17) shows that such a measurement is sensitive to only a narrow range of wavenumber  $u$ . Thus the measured spectral slope is probably only representative of that portion of the spectrum in the vicinity of the peak of the "filter function."

The remainder of this section is devoted to examples of "filter functions" of four distinct types. The first type is the simple "filter function" as defined above. It is the evaluation of the integral in question (less the refractivity spectrum  $\Phi(u)$ ) over all variables with the exception of  $u$ , and is plotted as a function of  $u$ , for several values of the path separation  $d$ . The second type is similar to the first, but is plotted for several values of the receiving or transmitting aperture  $\sigma$ . The third type consists of either of the first two types, multiplied by a Kolmogorov spectrum  $\Phi(u) = u^{-8/3}$ . While the first

two types of "filter functions" serve to demonstrate the sensitivity of a given measurement to perturbations of various sizes, the third type gives a more realistic idea of the relative importance of various wavenumbers in a practical situation, where the refractivity spectrum is strongly biased toward large irregularities. The fourth type of "filter function" consists of the evaluation of the integral in question over all variables (including  $u$ ) except  $s$ , position along the path. The result, plotted as a function of  $s$ , expresses the relative importance of different portions of the transmission path in the production of a given perturbation, assuming a uniformly random medium. A Kolmogorov spectrum is assumed.

The simplest and most well known "filter function" is that for the plane-wave, amplitude-covariance case, first given by Tatarski (1961, p. 149) for the case  $d = 0$ . It is shown in Figure 10.1 for three values of  $d$ . The quantity plotted is the evaluation of (2.15) over the variable  $s$ . The amplitude covariance is insensitive to small wavenumbers  $u$ , and the effect of high wavenumbers is reduced by increasing receiver separation  $d$ . The corresponding evaluation for phase-covariance is shown in Figure 10.2. It differs from the preceding case in that small wavenumbers are important; in fact, it is easily shown that those irregularities which are most effective in the production of amplitude fluctuations are least effective in the production of phase perturbations.

Another pair of amplitude- and phase-covariance "filter functions" is shown in Figures 10.3 and 10.4. In this case, the parameter is receiver aperture, and the relevant integral is (8.12), evaluated over  $s$ . Increased aperture has an effect similar to that of increased path separation, but is even more effective in reducing the importance of high wavenumbers, due to the rapid falloff of the Gaussian. Figures 10.5 and 10.6 differ from the preceding two only in that the results have been multiplied by  $u^{-8/3}$ , to simulate a typical spectrum  $\Phi(u)$ . The curve in Figure 10.5 for amplitude variance peaks at about  $u\sqrt{L/k} = 1.6$ , or for a period of the perturbation of  $1.6\sqrt{\lambda L}$ , in terms of the Fresnel zone radius. Contributions from higher wavenumbers decrease rapidly.

The effect upon the variance of amplitude can be easily seen, since variance is simply the area under the curves. Finite receiver aperture has less effect in the case of phase covariance, since large perturbations are most important. The area under the curves of Figure 10.6 is not finite for a  $u^{-8/3}$  spectrum; in the atmosphere the spectrum ceases to increase with decreasing wavenumber at what is called the "outer scale," resulting in finite phase variance.

Spatial "filter functions" for amplitude and phase covariance are shown in Figures 10.7 and 10.8, a Kolmogorov spectrum being assumed (with an "outer scale" assumed in the case of phase covariance). Note that regions near the receiver ( $R$  in the figures) contribute little to amplitude fluctuations, and a maximum amount to phase fluctuations.

The "filter-functions" of other quantities are of interest, since they are potentially sensitive to different regions of the refractivity spectrum or different portions of the transmission path. That for amplitude-phase covariance (cf. (7.5)) is shown in Figure 10.9, and in Figure 10.10 is shown multiplied by a  $u^{-8/3}$  spectrum. The "spatial filter function" for this quantity is shown in Figure 10.11. The "filter function" for angle-of-arrival covariance (cf. (7.4)) is shown alone in Figure 10.12, and with an assumed

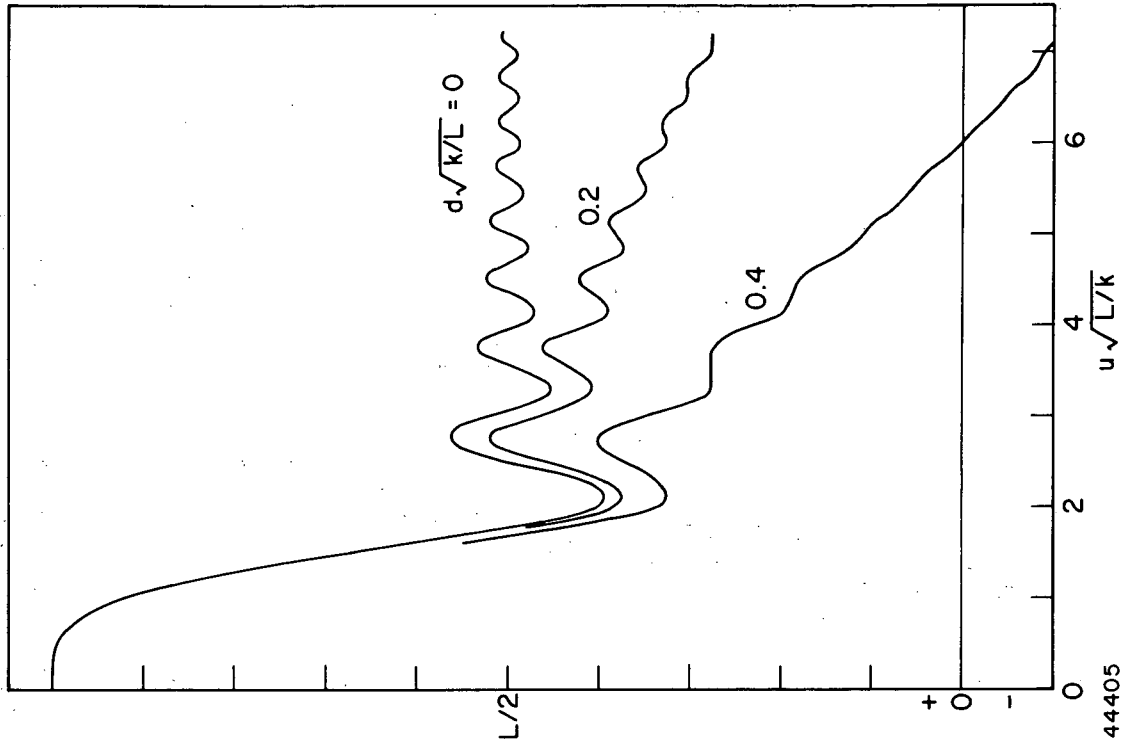


Figure 10.1. Plane-wave amplitude covariance "filter function" for three values of receiver separation.

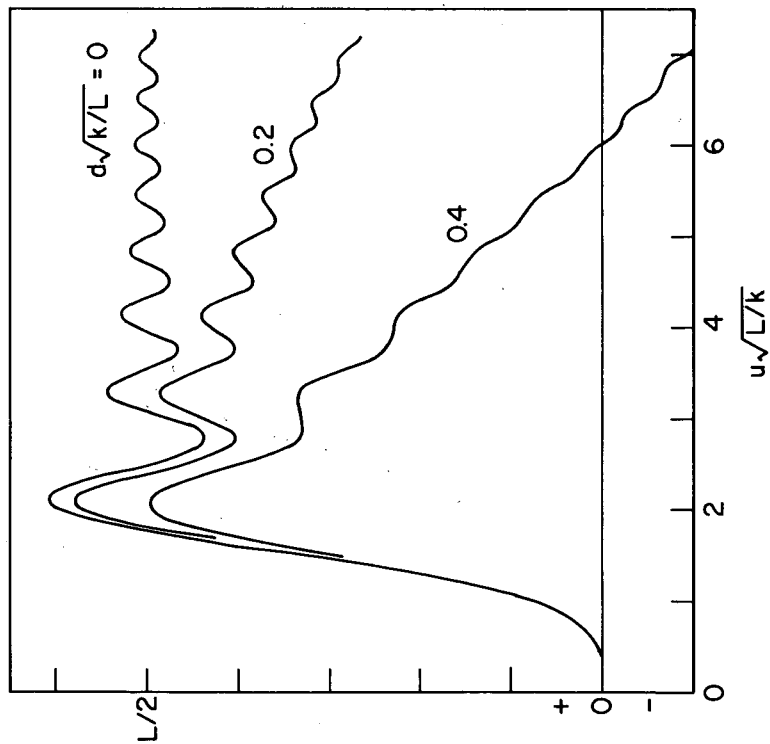


Figure 10.2. Plane-wave phase covariance "filter function" for three values of receiver separation.

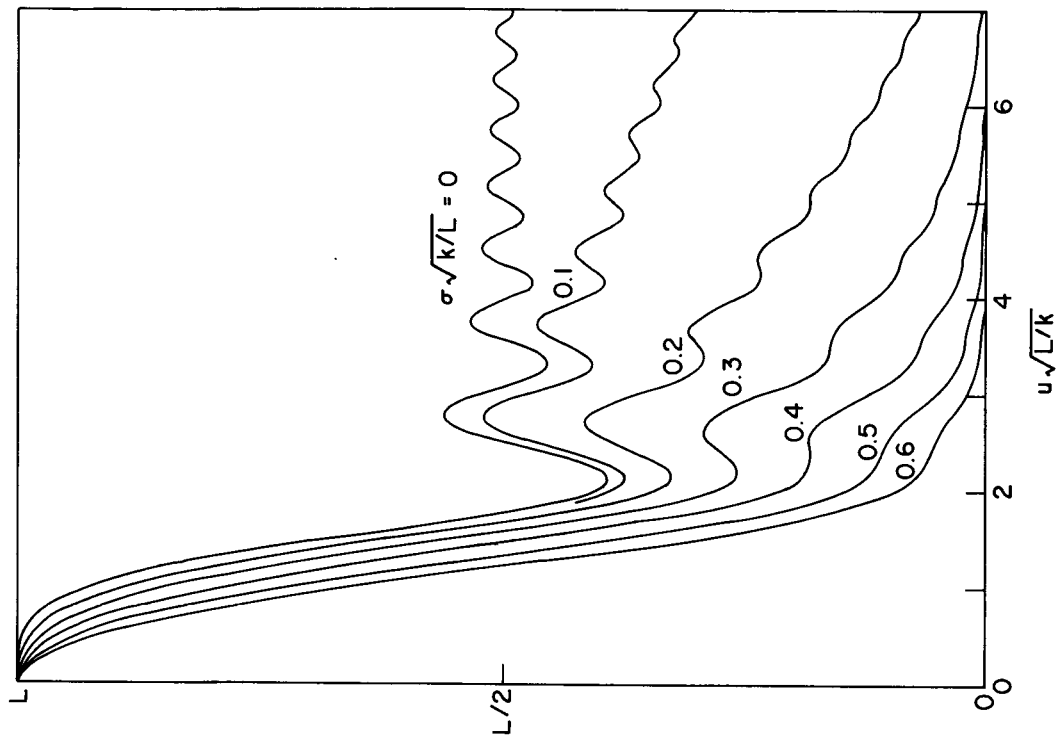


Figure 10.3. Plane-wave amplitude covariance "filter function" for several values of receiving aperture  $\sigma$ .

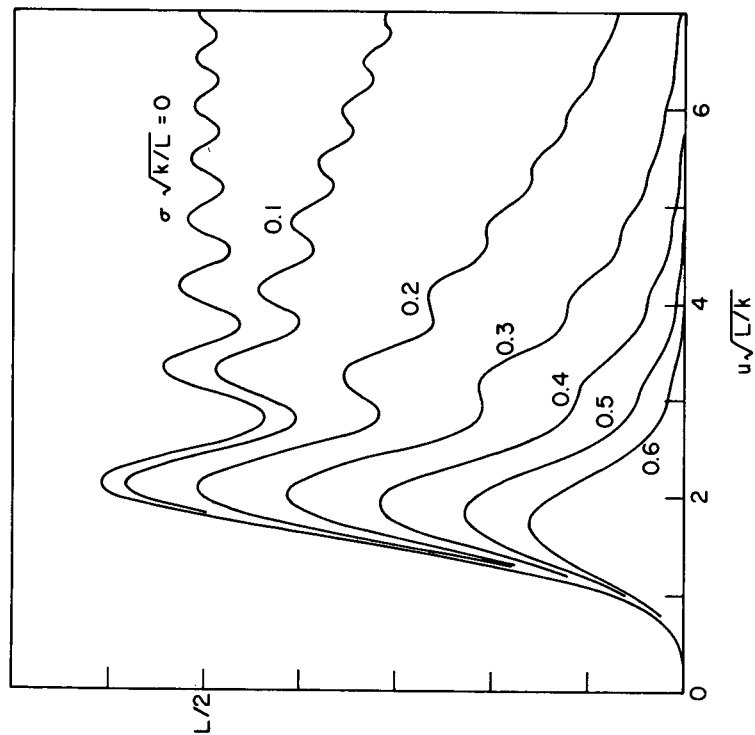


Figure 10.4. Plane-wave phase covariance "filter function" for several values of receiving aperture  $\sigma$ .

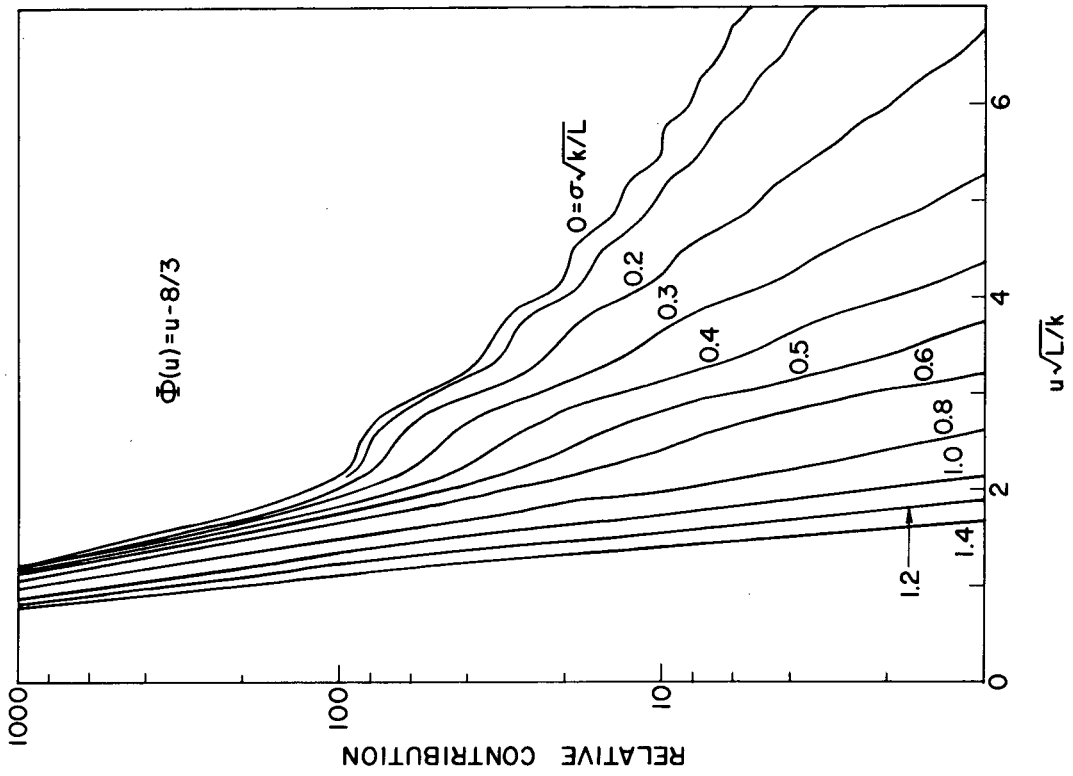


Figure 10.6. Plane-wave phase covariance "filter function" multiplied by  $\Phi(u)$ , for several values of receiving aperture  $\sigma$ .

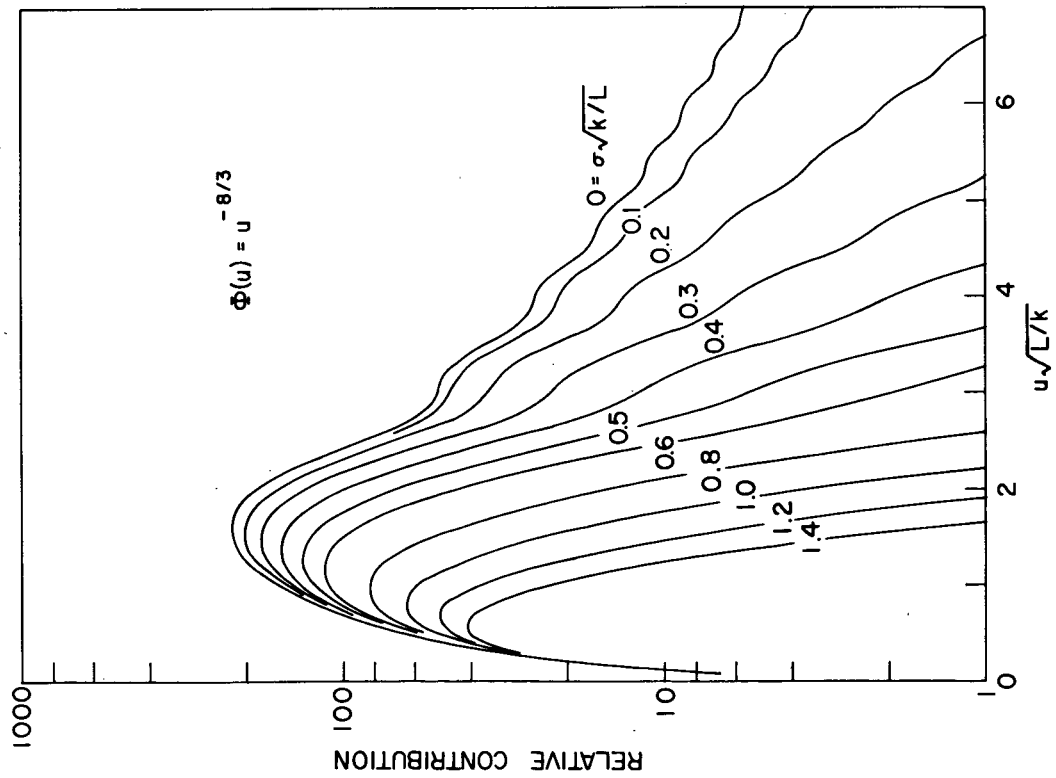


Figure 10.5. Plane-wave amplitude covariance "filter function" multiplied by  $\Phi(u)$ , for several values of receiving aperture  $\sigma$ .

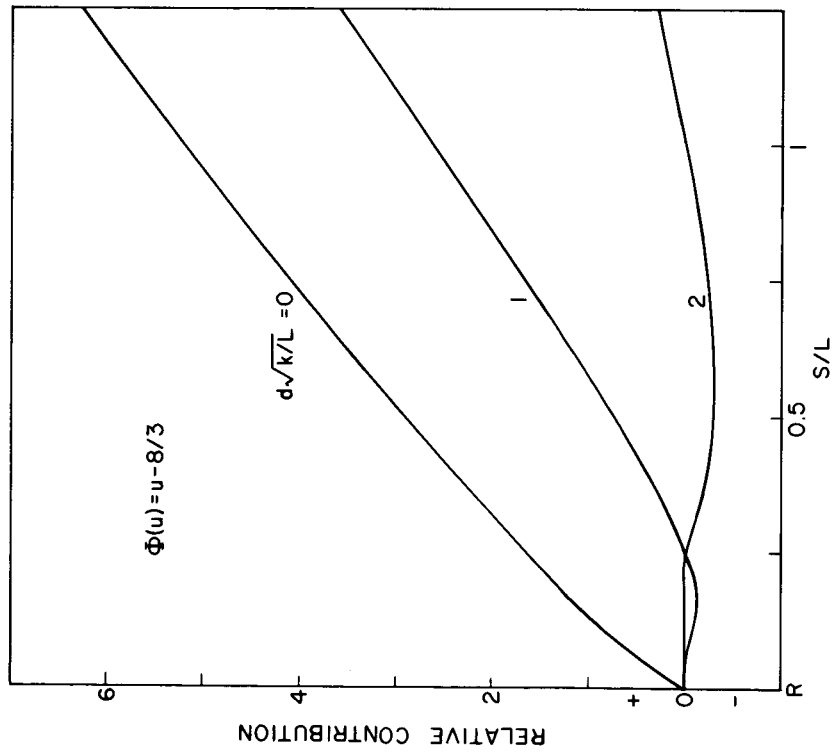


Figure 10.7. Plane-wave amplitude covariance "spatial filter function."

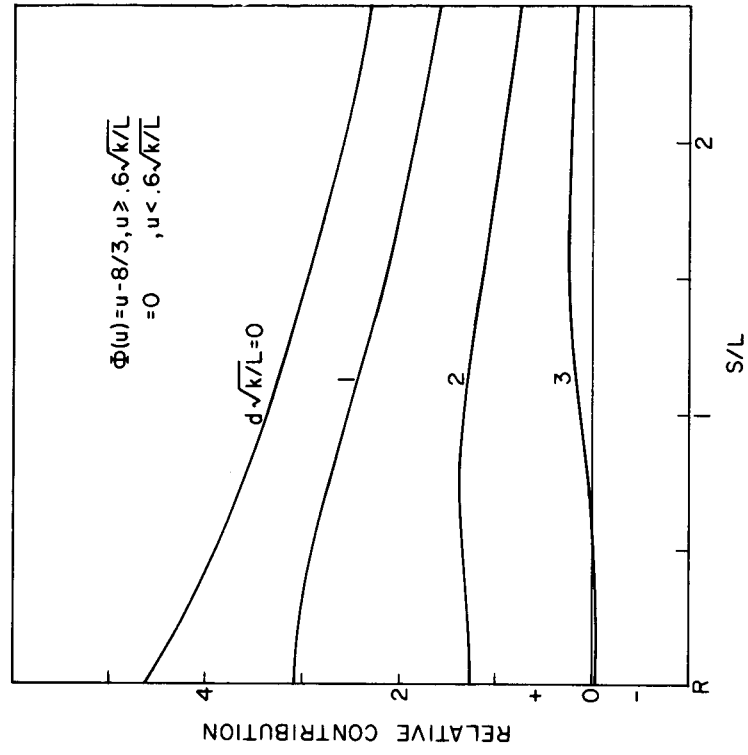


Figure 10.8. Plane-wave phase covariance "spatial filter function."

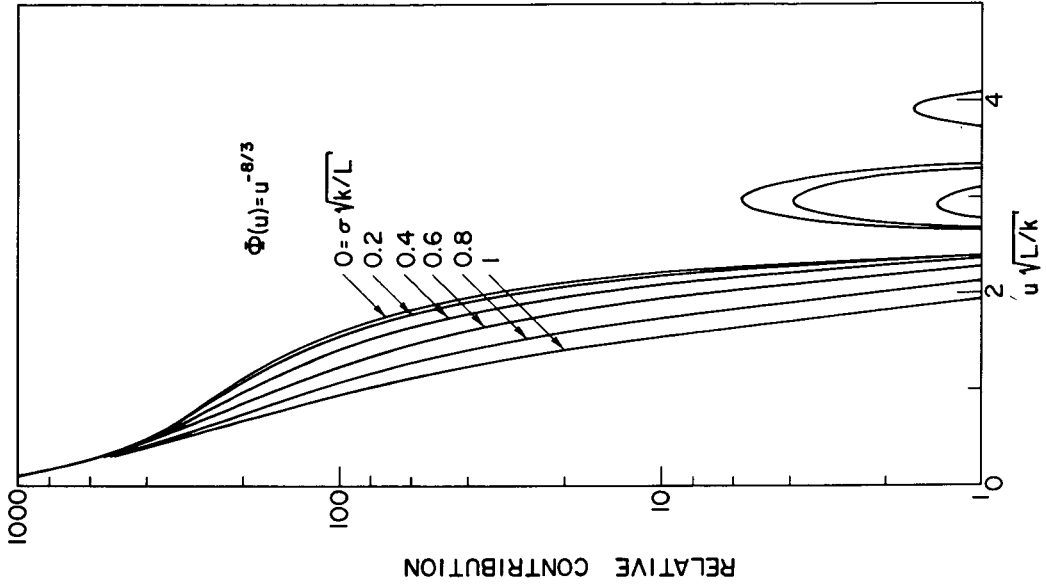


Figure 10.10. Plane-wave amplitude vs. phase covariance "filter function" multiplied by  $\Phi(u)$ , for several values of receiving aperture  $\sigma$ .

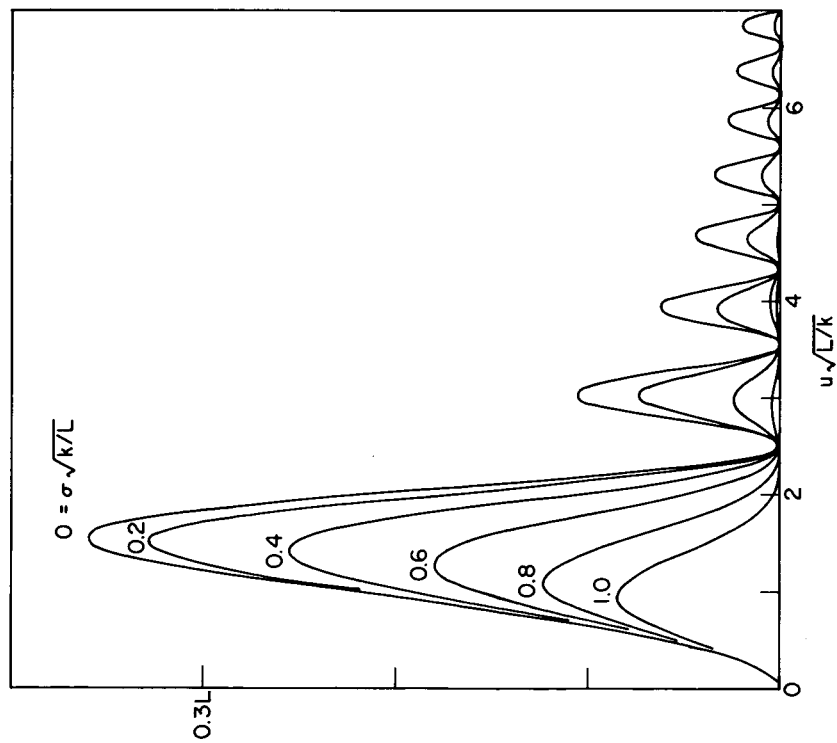


Figure 10.9. Plane-wave amplitude vs. phase covariance "filter function" for several values of receiving aperture  $\sigma$ .

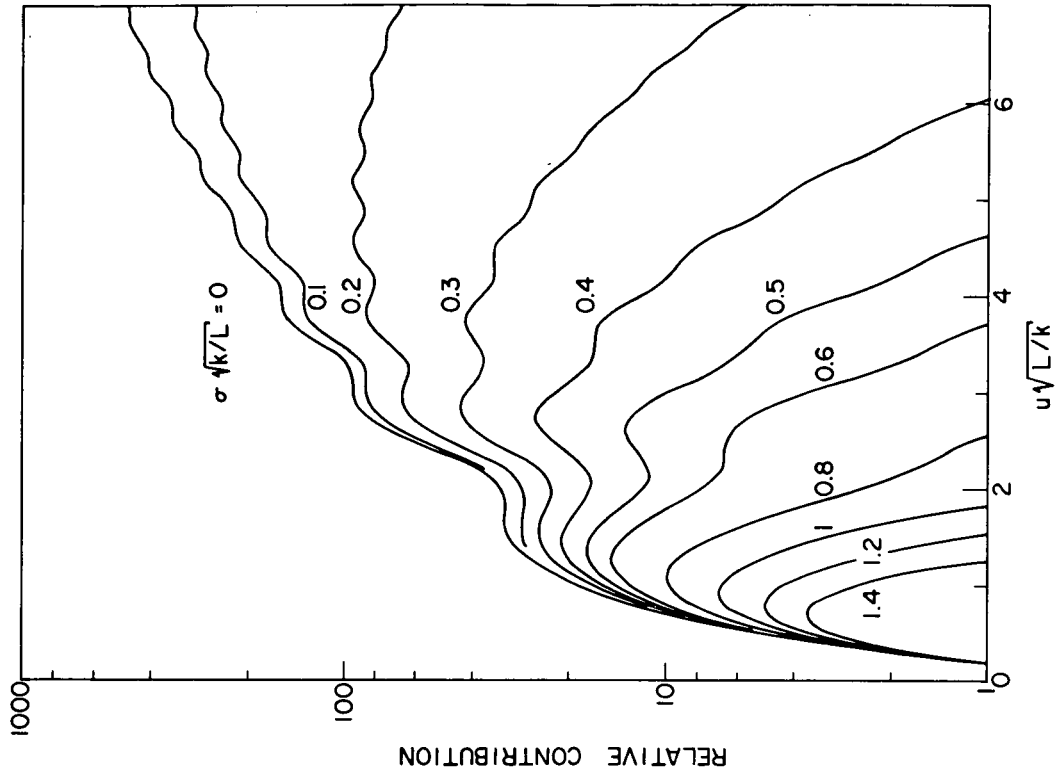


Figure 10.12. Plane-wave angle-of-arrival covariance "filter function" for several values of receiving aperture  $\sigma$ .

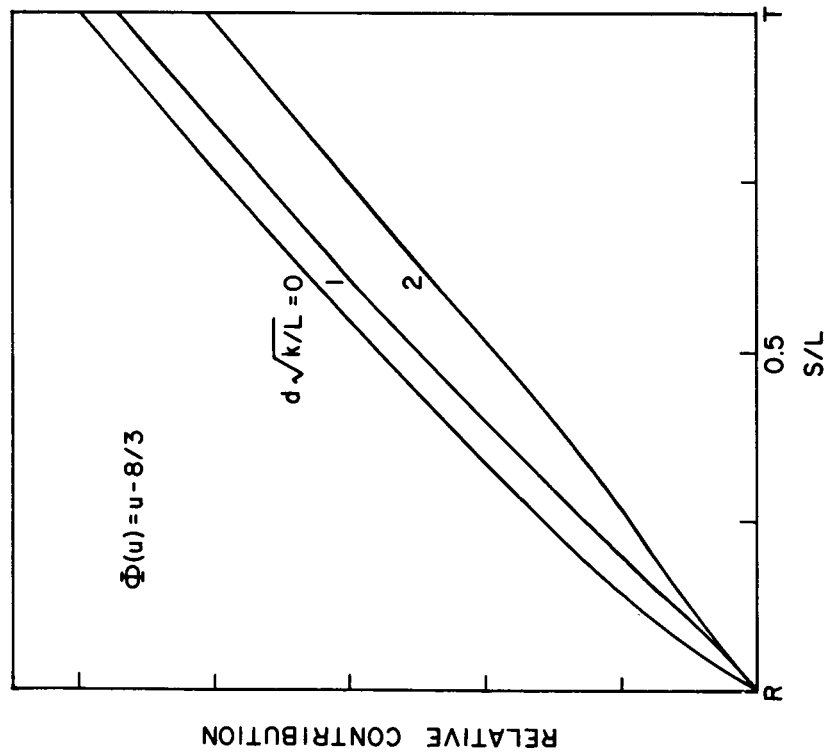


Figure 10.11. Plane-wave amplitude vs. phase covariance "spatial filter function."

spectrum in Figure 10.13. The "spatial filter function" is shown in Figure 10.14, where the case  $d = 0$  is not shown. The variance is not finite for a  $u^{-8/3}$  spectrum, unless the aperture or path separation is finite, or the spectrum terminates at some maximum wavenumber. There is no convergence problem at the low end of the spectrum in this case.

Thus far, plane wave situations have been considered. As an introduction to the spherical-wave geometry, attention is drawn to the basic amplitude-covariance integral (3.13). The "filter function" portion of this integral is the  $\sin^2$  term, the zeroes of which are plotted as solid lines in Figure 10.15. Zeroes of the Bessel function in (3.13) are plotted as dashed lines. When a  $u^{-8/3}$  spectrum is mentally superimposed upon Figure 10.15, the relative contributions can be imagined in two dimensions—in  $s$  and in  $u$ . It can be seen, for example, that the Bessel function serves to reduce the contribution of high wavenumber perturbations near the receiver ( $s/z = 1$ ), while having little effect near the transmitter. Similarly, the  $\sin^2$  term serves to emphasize large perturbations near mid-path, and smaller-scale perturbations towards the ends of the path. In quantitative terms, the  $\sin^2$  term places major emphasis upon those perturbations which are equal in size to the Fresnel ellipsoid, which of course is small near the ends of the path and largest in the center. At high-wavenumbers the situation is very complex, some wavenumbers contributing negatively to the covariance, others positively and some not at all, since they are very poor scatterers.

Amplitude and phase-covariance "filter functions," as obtained from (3.13) by integration over  $s$ , are shown in Figure 10.16 for two values of  $d$ ; they are rather similar to those in the plane wave case (Figures 10.1 and 10.2); finite receiver separation is quite effective in reducing the contribution of high-wavenumber perturbations. The same quantities, multiplied by an assumed spectrum, are shown in Figure 10.17, and the "spatial filter functions," obtained by integrating (3.13) in  $u$  (with an assumed spectrum), are shown in Figures 10.18 and 10.19. The peak of the amplitude-variance curve in Figure 10.17 occurs at  $u\sqrt{L/k} = 3$ , or for a period of the perturbation of about  $0.8\sqrt{\lambda L}$ , in terms of the Fresnel-zone radius (vis.  $1.6\sqrt{\lambda L}$  in the plane-wave case), and of course contribution from high wavenumbers is greatly reduced due to the steep slope of the spectrum. Note in Figure 10.18 that increasing receiver separation tends to emphasize that portion of the path near the transmitter, and in any case the very ends of the path are unimportant. In the case of phase variance (Figure 10.19,  $d = 0$ ), the whole path is almost equally important (for the outer-scale chosen; a smaller outer-scale would reduce the importance of mid-path).

As an example of another function, the "filter function" for amplitude-phase covariance is shown alone in Figure 10.20, and multiplied by an assumed spectrum in Figure 10.21. The "spatial filter function" is shown in Figure 10.22; it is similar to the amplitude-covariance case, but is less sensitive to increased receiver separation. The "filter function" for spherical-wave angle-of-arrival variance is shown alone in Figure 10.23, and multiplied by an assumed spectrum in Figure 10.24. As in the plane-wave case, this integral is not convergent for a  $u^{-8/3}$  spectrum unless the aperture or separation is finite. Thus, in the "spatial filter function" shown in Figure 10.25, the case  $d = 0$  is not given. Figure 10.25 is unique among the spherical-wave, "spatial filter functions" given here, in its emphasis upon the region near the receiver, and lack of emphasis near the transmitter.

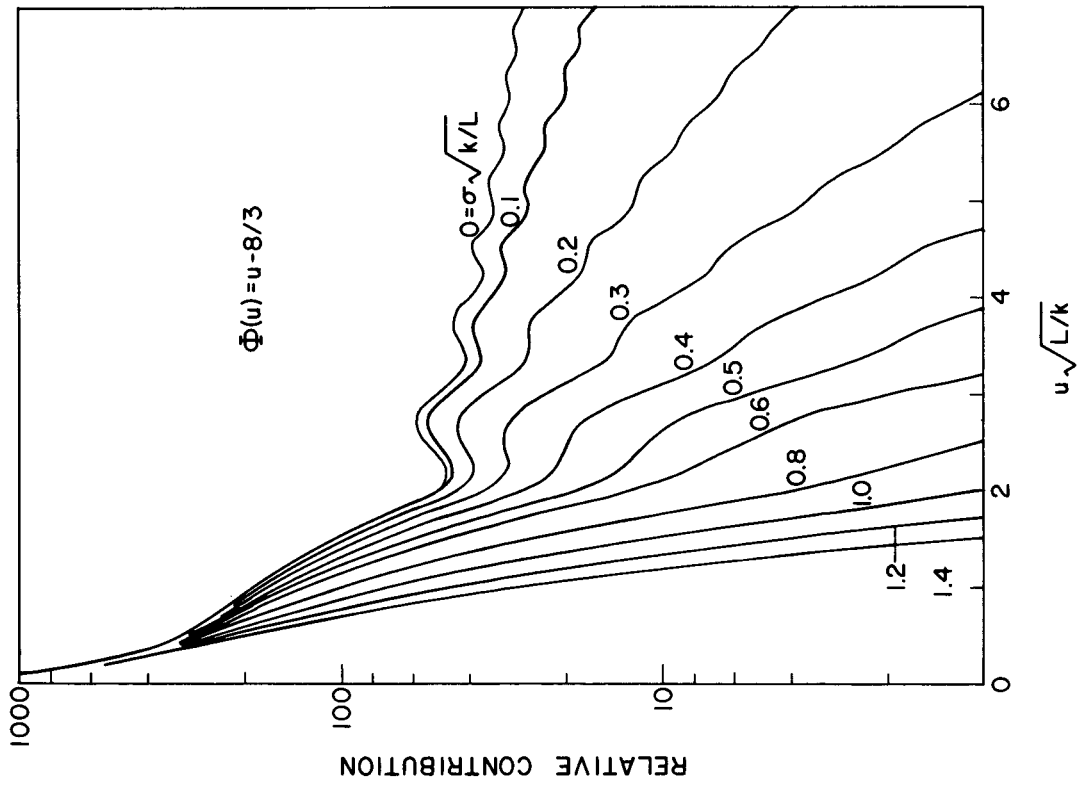


Figure 10.13. Plane-wave angle-of-arrival covariance "filter function" multiplied by  $\Phi(u)$ , for several values of receiving aperture  $\sigma$ .

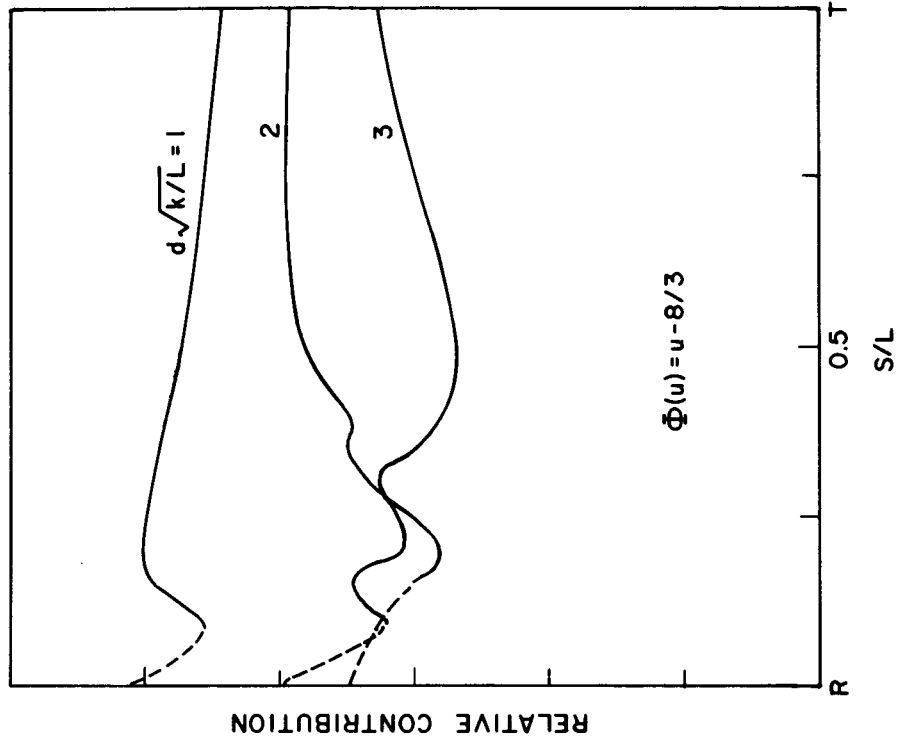


Figure 10.14. Plane-wave angle-of-arrival "spatial filter function."

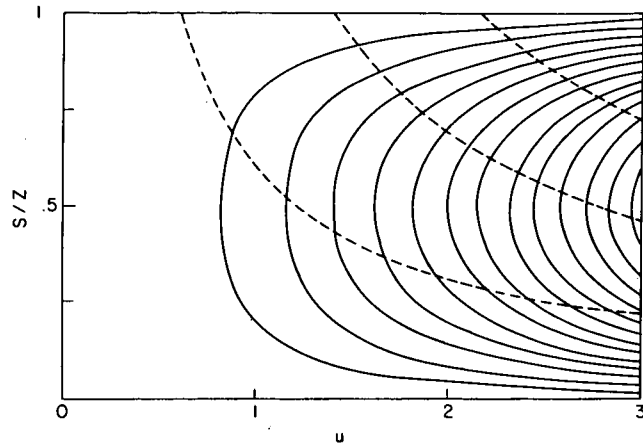


Figure 10.15. Zeroes of the function  $J_0(dsu/L) \sin^2(u^2s(L-s)/2kL)$ , with  $L = 28000$ ,  $k = 716$ ,  $d = 4$ .

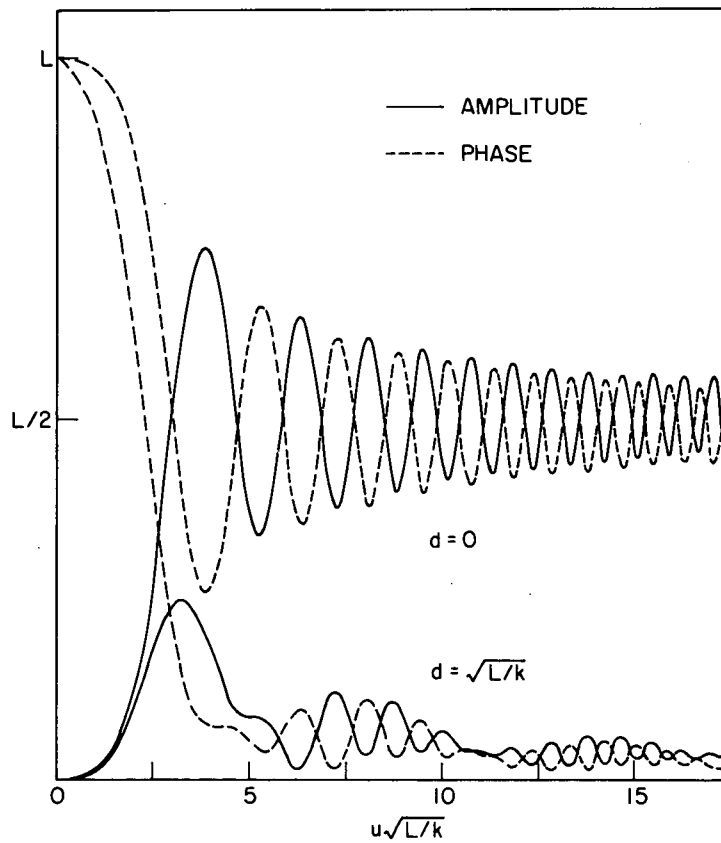


Figure 10.16. Spherical-wave amplitude and phase covariance "filter functions" for two values of receiver separation  $d$ .

# WAVE PROPAGATION IN A RANDOM MEDIUM

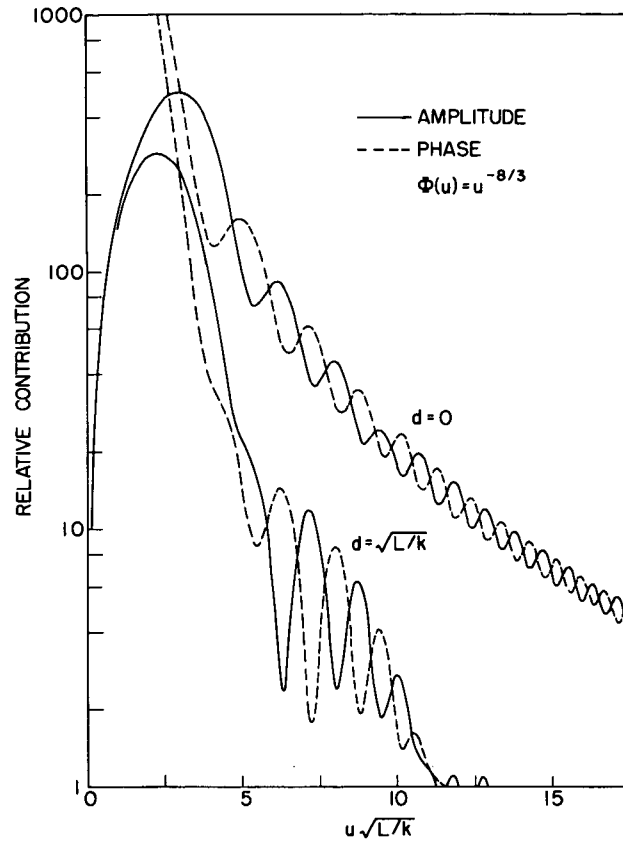


Figure 10.17. Spherical-wave amplitude and phase covariance "filter functions" for two values of receiver separation  $d$ .

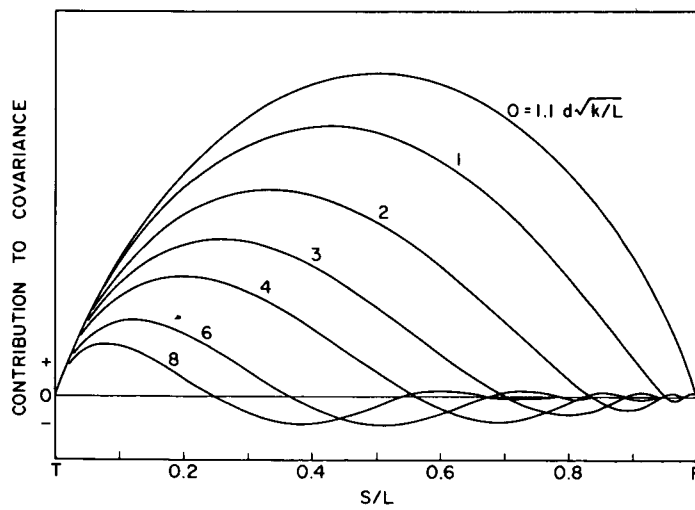


Figure 10.18. Spherical-wave amplitude covariance "spatial filter function."

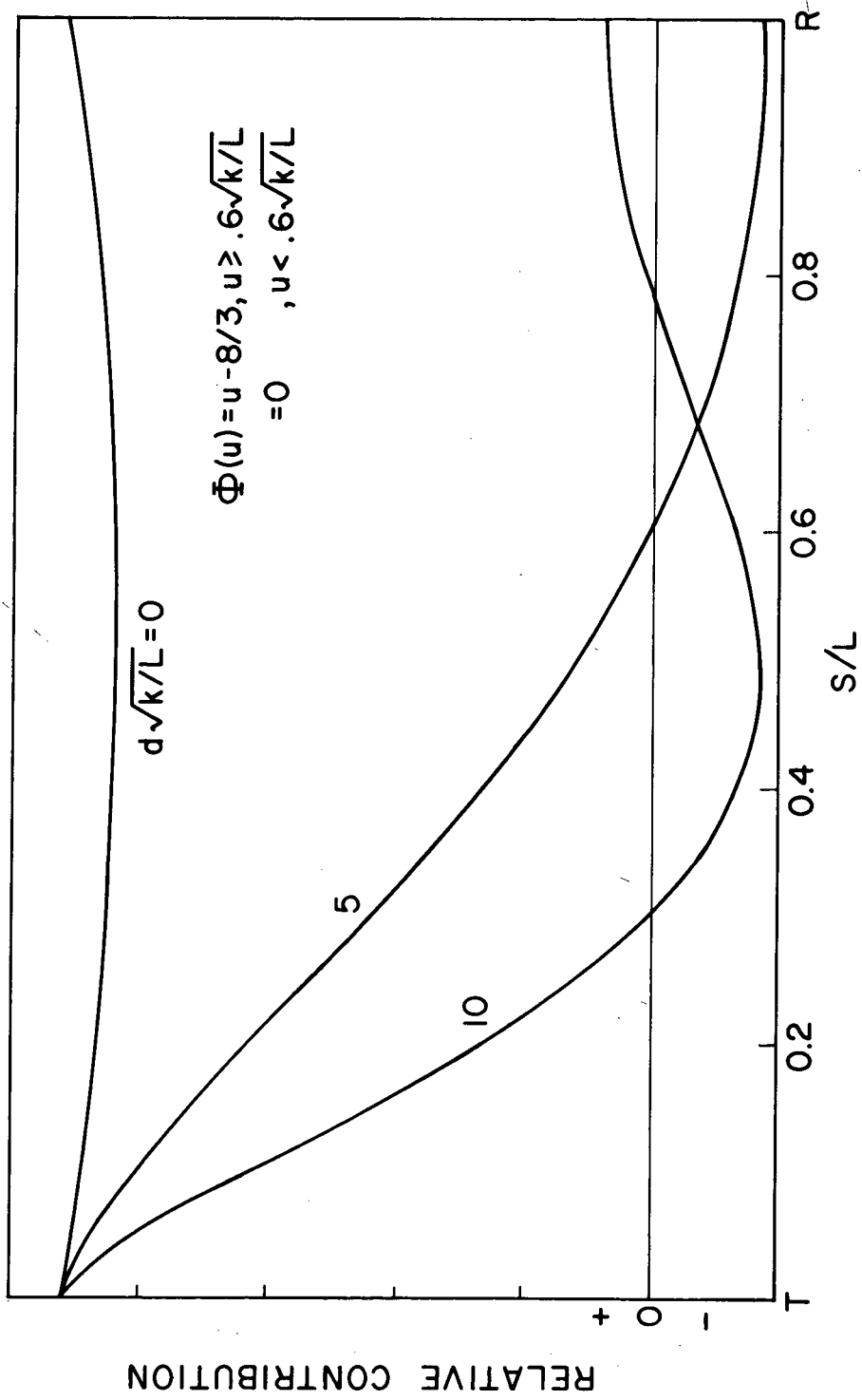


Figure 10.19. Spherical-wave phase covariance "spatial filter function."

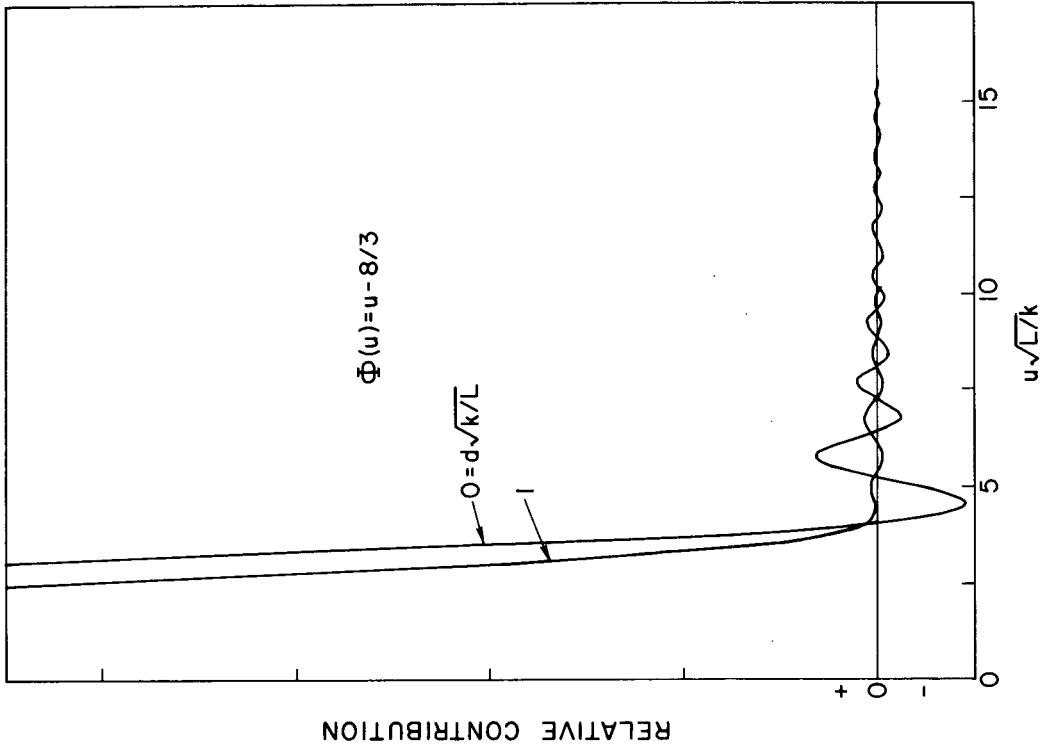


Figure 10.21. Spherical-wave amplitude vs. phase covariance "filter function" multiplied by  $\Phi(u)$ , for two values of receiver separation  $d$ .

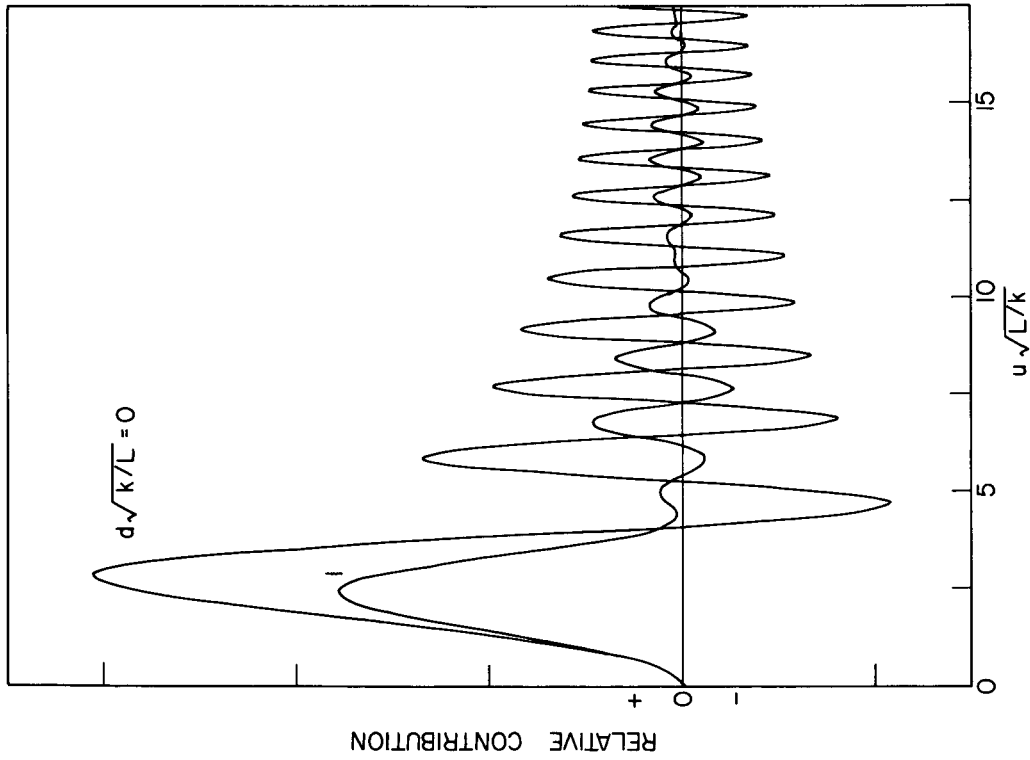


Figure 10.20. Spherical-wave amplitude vs. phase covariance "filter function" for two values of receiver separation  $d$ .

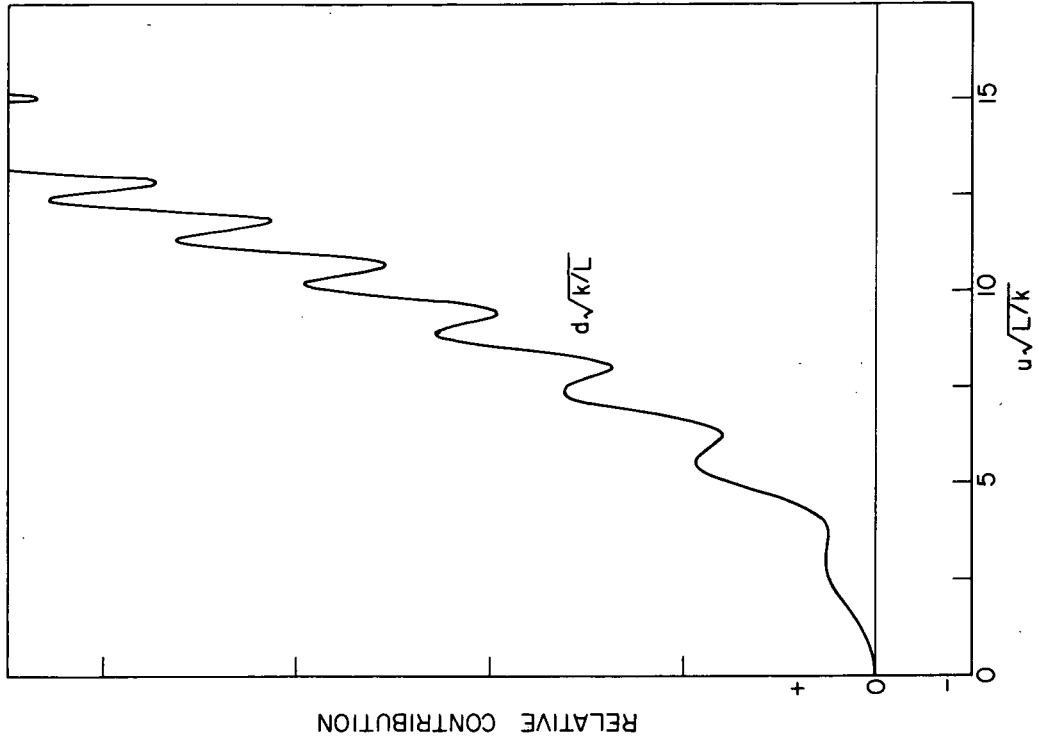


Figure 10.23. Spherical-wave angle-of-arrival covariance "filter function" for receiver separation  $d = 0$ .

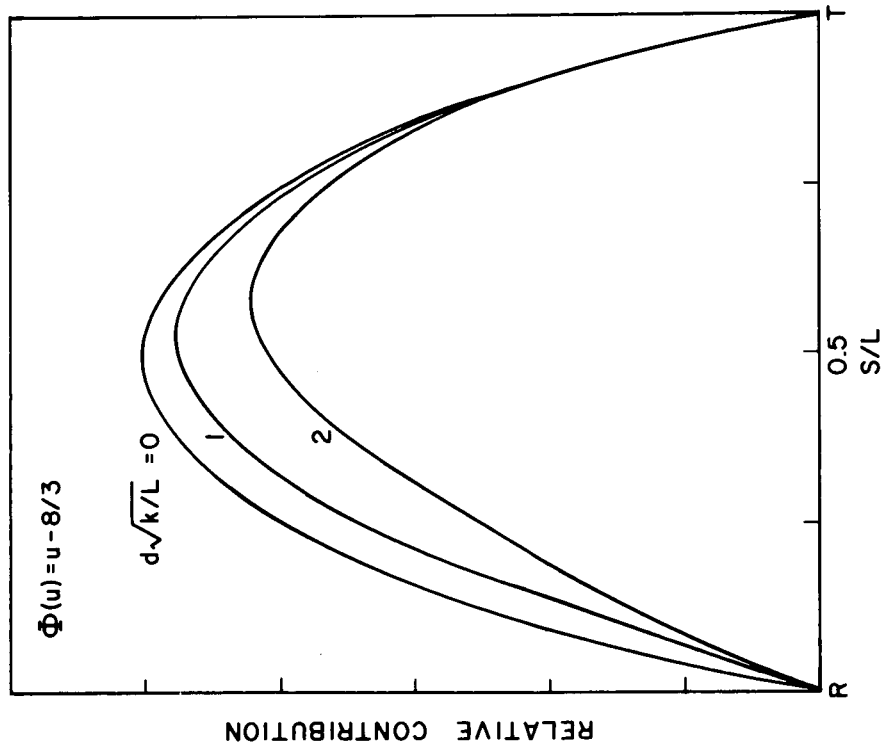


Figure 10.22. Spherical-wave amplitude vs. phase covariance "spatial filter function."

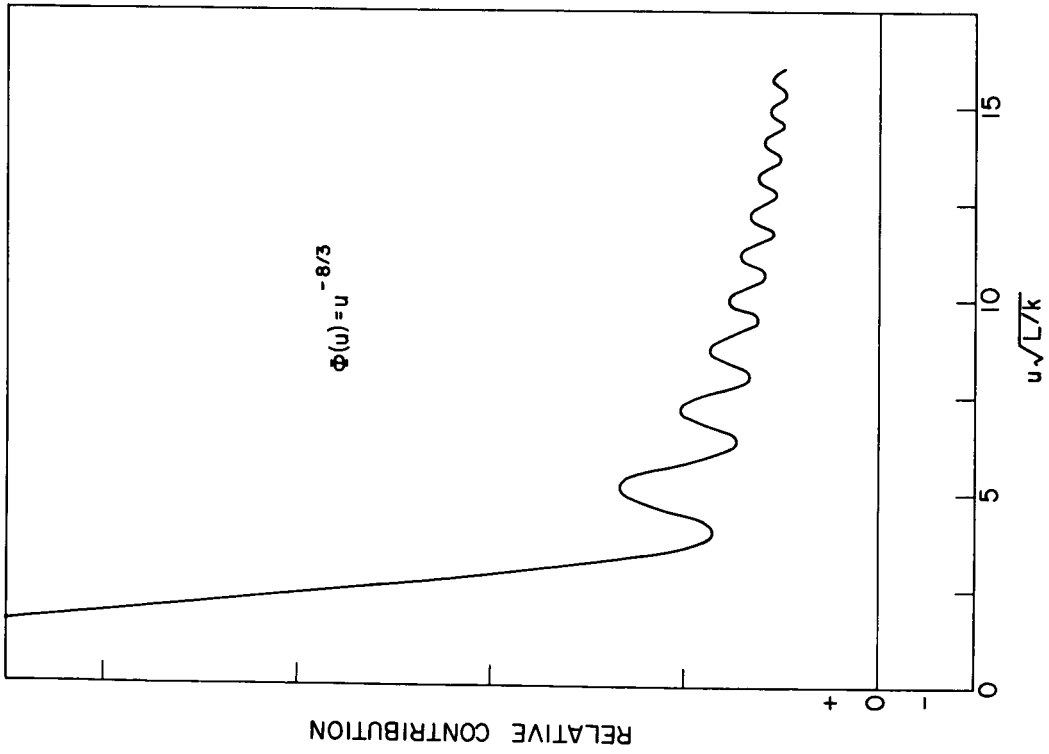


Figure 10.24. Spherical-wave angle-of-arrival covariance "filter function" multiplied by  $\Phi(u)$ , for receiver separation  $d = 0$ .

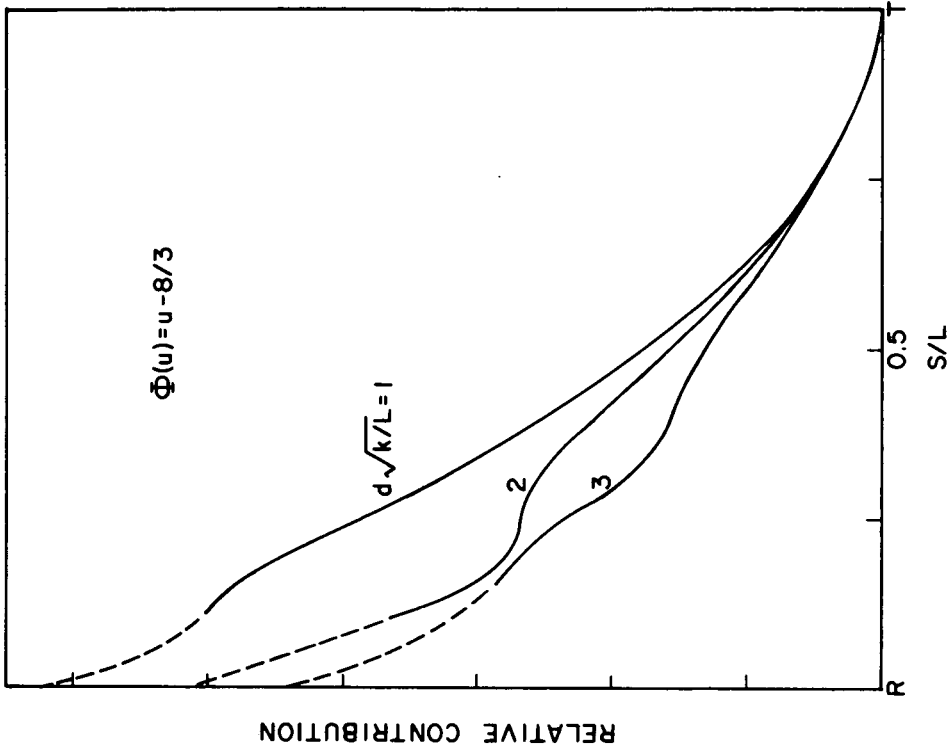


Figure 10.25. Spherical-wave angle-of-arrival covariance "spatial filter function."

These examples of "filter functions" demonstrate that, to some extent, the region of the medium or the range of wavenumber of interest can be emphasized by proper choice of the quantity measured. Perhaps more importantly, they also demonstrate that conclusions based upon measurements are valid only over a certain range of wavenumbers, or perhaps over a certain portion of the transmission path.

## 11. THE USE OF PROPAGATION MEASUREMENTS IN ATMOSPHERIC PROBING

Considerable interest exists in the application of microwave and optical propagation measurements to the determination of various atmospheric parameters, both because such measurements can be made without actually placing an instrument at the point of measurement, and because the potential exists for measuring quantities otherwise very difficult to measure at all. The basic problems involved in relating propagation measurements to atmospheric parameters are three. First, a suitable analytical framework must be developed, expressing the relationship between the parameter of interest and the measurements; this has been the subject of the preceding sections of this report. Secondly, measurements of sufficient quality must be obtained. Finally, suitable mathematical techniques must be used to obtain from the measurement the desired information about the atmosphere. This latter problem is not trivial; the expressions derived in the preceding sections equate the measured quantity with an integral over atmospheric parameters, and thus the problem is to solve an integral equation (and generally a family of such equations). In only a few of the cases of interest is it possible to invert the integral analytically and we shall generally be forced to use iterative, numerical techniques.

Atmospheric parameters of interest may be conveniently divided into two categories—quantities averaged over the transmission path, and quantities about which spatial information is desired. The simplest quantity of the first type is the magnitude of the refractivity spectrum,  $C_n^2$ . This quantity may be obtained simply by measuring the variance of the amplitude of the received signal. It must be borne in mind, however, that this quantity as measured is a weighted average—weighted along the path and weighted in wavenumber  $u$ , as described by the "filter functions" plotted in Section 10. Thus, if the refractivity spectrum is not uniform along the path, or is not of the form assumed (Kolmogorov, for instance), the results will be difficult to interpret. A more sophisticated approach to measuring the magnitude of the refractivity spectrum is to consider the form of the spectrum to be unknown, and solve for the form as well as the magnitude (assuming spatial uniformity of the spectrum). To take a simple case, consider plane-wave amplitude covariance, as governed by (2.13). Rewriting that expression,

$$C_a(d) = \int_0^k du u \Phi(u) J_0(du) \int_0^L F(u,s) ds \quad (11.1)$$

where  $\Phi(u)$  is the unknown quantity, and  $C_a(d)$  the measured quantity. This expression can be inverted explicitly as a Hankel transform.

$$u \Phi(u) = \int_0^\infty d' J_0(d'u) C_a(d') dd' / \int_0^L F(u,s) ds \quad (11.2)$$

Similar analytical inversions are possible in the spherical-wave case, but only for parallel-path situations (where the variable  $s$  does not appear in the argument of the Bessel function). Such a situation occurs in the case of time-covariances, when the windfield is uniform. Covariance is then measured as a function of  $Vt$ , rather than  $d$ , and the inversion proceeds in the same fashion as above. In the general spherical-wave situation, analytic transformation is not possible, but simple numerical techniques are available. For instance, the spectrum,  $\Phi(u)$ , can be assumed to have some form—as a series of step functions in  $s$  with unknown amplitudes at each step. The covariance at each separation  $d$  can then be written as a summation of integrals over the various steps in  $s$ , the whole set then forming a family of linear simultaneous equations. This is easily solved, and  $n$  measurements of covariance provide  $n$  degrees of freedom in the result.

Such measurements and subsequent transformations have proved to be of great value at the upper limit of the refractivity spectrum where, with very short optical paths, it is possible to measure the rather sharp cutoff of the spectrum. It should be equally valuable to examine the lower end of the spectrum where the suitable technique would be (as can be seen from the filter functions in Section 10) measurements of phase covariance over parallel paths. It would also be of interest to investigate the "inertial subrange" for departures from the expected Kolmogorov spectrum. Here the appropriate tool would be millimeter-wave amplitude covariance measurements.

As an example of another more-or-less spatially averaged quantity, wind velocity can be measured to a degree by correlation techniques. It can be seen from (6.2) that the time-lag for which the time-autocorrelation function ( $d = 0$ ) falls to a given value is inversely proportional to the velocity  $V$ . In Figure 11.1 is plotted the reciprocal half-width of the amplitude time-correlation function, vs. time, as observed on the array described previously (Lee and Waterman, 1966). This quantity should thus be proportional to the velocity, and that it is to a degree can be seen by comparison with Figure 11.2, taken from measurements made 250 m under the propagation path.

We now consider the second category mentioned above, quantities whose spatial distribution is to be studied. The simplest such quantity is the magnitude of the refractivity spectrum,  $C_n^2$ . In either the plane- or spherical-wave case we are faced with a linear integral equation of the first kind. We proceed as before, and assume that  $C_n^2$  is a series of step functions in  $s$ , and the amplitude of the several steps is unknown. A family of linear, simultaneous equations results, the solution of which furnishes the desired dependence of  $C_n^2$ , with the resolution dependent upon the number of measurements available.

The above examples are relatively simple, and present no mathematical problems, but are nevertheless quite useful. As a final example, we will consider a much more difficult problem, that of determining windspeed as a function of position  $s$ .

As can be seen from (6.2), velocity appears in the argument of the Bessel function which is always present in the covariance integrals. Thus the problem is that of inverting a family of non-linear integral equations, rather than linear integral equations. The general techniques for solution remain the same—assuming a form for the solution, with unknown parameters, and then solving a set of simultaneous equations for those parameters.



In the general case of non-linear integral equations, however, these simultaneous equations are themselves non-linear, and therefore must be solved by iterative numerical techniques. While such solutions are not difficult in principle, they are mathematically messy, and certain techniques can be used to simplify the process, at the expense of some detail in the results. One such technique is to linearize the integral involved by differentiation. The time-derivative of the time-lagged amplitude covariance function (plane-wave) is of the form

$$C'(d,0) = \int_0^k u^2 \Phi(u) J_1(du) du \int_0^L V(s) F(u,s) ds \quad (11.3)$$

as evaluated at  $t = 0$ . Note that this is a linear equation of exactly the type considered earlier, and the solution follows the same lines.  $V(s)$  may, for instance, be obtained as a stepwise-linear function of  $s$ , with as many steps as measurements. Information is lost in the process of differentiation—that information obtained at larger time-lags—and thus resolution is reduced. This information may be utilized by considering higher derivatives of the correlation function, still evaluated at  $t = 0$ . The set of simultaneous equations resulting from measurements of the second derivative are equations in  $V(s)^2$ , for example; that is, they are linear equations in  $V(s)^2$ . This process may be carried to still higher derivatives, until the derivatives are no longer meaningful. In practice, the measured time-lagged correlation functions would be fit to high-order polynomials, and the derivatives of these polynomials taken, thus making use of large time-lag covariances. Other techniques for solution exist, and may be exploited, but in general, simultaneous equations of even higher complexity (including cross-terms between the unknowns) result.

There are other problems involved in the interpretation of measurements along the lines suggested above, which deserve mention here. In the first place, such transformations are by nature sampled-data processes. Measurements are made at a finite number of points, separated in time and distance by finite increments. Hence the results obtainable from such transformations are subject to inherent limitations of resolution and region of validity. For example, in the determination of the spectrum  $\Phi(u)$  by measurement of the spatial-covariance function and subsequent transformation, a lower-limit upon the separation in  $u$  of the resulting independent estimates of the spectral density is imposed by the maximum separation  $d$  available. This limit is easily derived, and is of the order  $2\pi/d_{\max}$ . Similarly, an upper limit is set upon  $u$  by the smallest separation, of order  $2\pi/d_{\min}$ . Energy from higher wavenumbers will "fold over" and contaminate estimates for lower wavenumbers. This process is exactly analogous to spectral analysis of time-sampled data. The accuracy of the resulting spectral-density estimates is also limited by the width of  $u$  included in the estimate ("bandwidth")—the narrower the bandwidth, the greater the statistical fluctuation of the spectral density estimates.

The second problem concerns the sensitivity of the measurement to the atmospheric parameter being estimated. Taking as an example the transformation (11.2), the quantity in the denominator can be recognized as the "filter function" appropriate to the measurement. If the measurement is relatively insensitive to the desired parameter (as very large or very small  $u$  in the case of amplitude covariances), the filter function is quite small, and its inverse quite large. Uncertainties in the measured quantity then become

very important, and the process is quite "noisy." Thus care must be exercised in choosing the range over which the unknown quantity is to be estimated.

A final problem concerns noise present in the measurements or generated in subsequent analysis. This noise can arise from several sources—finite signal-to-noise ratio, lack of stationarity in the atmosphere, and round-off errors in the mathematical transformation, to name a few. The effect of such noise sources can be estimated by propagating artificial errors through the transformation process.

Optimum solution of these problems is a difficult task, but general principles can be stated. Clearly, as many spacings and time-lags as possible should be used. It is highly desirable to over-constrain the unknowns, and obtain a least-squares solution, to reduce the effects of noise. By the same token, it is desirable to allow as few unknowns as possible, to enhance their statistical significance. To achieve this to the highest degree possible, full use should be made of all a priori knowledge concerning the medium, so that the assumed form of the solution may be tailored so as to require a minimum number of degrees of freedom. For example, if it is known that a certain quantity varies more rapidly near the termini of the path, the assumed step-function-series solution for this quantity should have broader steps near mid-path than at the ends. Such tailoring should not be carried too far, however, as there is danger of forcing a solution of the desired type.

## 12. CONCLUSION

The theory of line-of-sight propagation in random media, to which much of this report has been devoted, appears to be reasonably adequate for application to the determination of atmospheric parameters. It should be noted, however, that the theory cannot handle such non-random atmospheric phenomena as sharp layers or refractivity gradients, nor can it handle other than weak-scattering situations (such as long optical paths).

Experimental techniques are advancing rapidly, and have reached the point where the transformation techniques described above can be attempted. By far the most promising systems—and the only systems which provide the requisite number of separations required in the transformations—are arrays of receivers, sampling the received wave at several points in space simultaneously. Such arrays in the centimeter and millimeter region exist at Stanford, measuring both the phase and amplitude of the wavefront, and are contemplated or under construction elsewhere in both the microwave and optical regions.

Mathematical techniques exist for the transformation of the measurements in terms of atmospheric parameters. The quantities measured must be selected carefully, bearing in mind their sensitivity to variations of the parameters of interest, as evidenced by "filter functions." The statistical and other limitations inherent in the process must be considered, and maximum use should be made of available information about the medium, to reduce the number of unknowns in the problem. Finally, all assumptions regarding the refractivity spectrum, stationarity, isotropy, etc., must be regarded as suspect until and unless they can be justified by actual measurement.

## WAVE PROPAGATION IN A RANDOM MEDIUM

This work is supported by AFCRL contract F04701-68-C-0110.

### BIBLIOGRAPHY

- Fried, D. L., 1966: J. Opt. Soc. Am., 56, 1380.
- Fried, D. L., 1967: J. Opt. Soc. Am., 57, 175.
- Hodara, H., 1966: Proc. IEEE, 54, 368.
- Ishimaru, A., 1968: Amplitude fluctuations of a beam wave in a locally homogeneous medium, presented at 1968 Spring URSI, Washington, D.C., April 11, 1968.
- Lee, R. W. and Waterman, A. T., 1966: Proc. IEEE, 54, 454.
- Lee, R. W. and Harp, J. C., To be published in 1969.
- Schmeltzer, R. A., 1967: Quart. Appl. Math., 24, 454.
- Strohbehn, J. W. and Clifford, S. F., Private communication.
- Tatarski, V. I., 1961: Wave propagation in a turbulent medium, McGraw-Hill Book Company, New York.
- Taylor, G. I., 1938: Proc. Roy. Soc. London, Ser. A, 164, 476.

U72-25350

ADDITIONAL LINE-OF-SIGHT METHODOLOGY TO THAT PRESENTED  
BY JOHN W. STROHBEHN IN "THE USE OF LINE-OF-SIGHT  
MICROWAVE PROPAGATION IN REMOTE ATMOSPHERIC PROBING"

C. I. Beard

Boeing Scientific Research Laboratories  
Seattle, Washington 98124

ABSTRACT

These remarks present some promising microwave and infrared techniques, not covered in Strohbehn's preceding paper, which are now being tested in line-of-sight tropospheric scattering. Newly measured parameters of the incoherent scattered microwave field are sensitive to wavefront sphericity, to wind speed, and to the eddy wavenumber spectrum. A recommendation for advancing the state of the art is given by a proposed experimental program.

1. INTRODUCTION

These remarks were made following the paper by Strohbehn (1968). Since the writer is in general agreement with Strohbehn's points, except for the topic in Section 6 below, the following remarks present information on some promising line-of-sight measurement procedures additional to those given by Strohbehn. These techniques have only relatively recently been applied to line-of-sight tropospheric paths; the information on them is mainly in Company reports and thus not widely distributed. Therefore, the intent of these comments is primarily to supplement and complement the presentation of Strohbehn by bringing this material to the attention of the Panel. The topics are listed in the following Sections; references given by Strohbehn are not repeated to save space.

2. MEASUREMENT OF INTEGRATED MICROWAVE INDEX OF REFRACTION

Since microwave methods respond only to the microwave index of refraction of the atmosphere, Professor Strohbehn touched on some measurement methods. In addition to the approaches at ITSA/ESSA and MITRE, however, the writer wants to acquaint this Panel with a different type of method, an infrared

transmissometer, developed by Tank (1967) at Boeing Scientific Research Laboratories (BSRL). Briefly, an infrared line-of-sight beam is split into three parts, each filtered by a bandpass filter; one is in a window at 2.12 microns ( $\mu$ ), one is in an oxygen absorption band at 1.27  $\mu$ , and the third is in a water vapor band at 1.86  $\mu$ . Ratios of the  $O_2$  and  $H_2O$  intensities to the window intensity are taken to cancel scintillation; these ratio signals then provide the instantaneous values of the line-integrated values of the dry and wet terms of the index of refraction equation, and they can be combined to give  $n$ . In connection with Strohbahn's comment that M. C. Thompson has suggested a method of measuring the integrated index of refraction using two optical wavelengths and one at microwaves, it should be added that the three wavelength IR system results are to be combined with K-band (20-26 GHz) results of Kreiss (1967) to improve the overall accuracy of the determination of  $n$ .

In future line-of-sight experiments some one of these methods for measuring integrated index of refraction along the path should be included. This is especially true for the longer paths, say 10 to 50 miles, on which microwave measurements have actually been made in the past as a function of meteorological data taken at each end of the path but without really knowing the intervening medium. In those days the methods mentioned above were not available, but now there is no excuse except the deepening money crisis. (See Section 4 for related remarks.)

### 3. SPHERICAL WAVES

In different places of Strohbahn's report (Parts II and V), he has mentioned the little attention given to spherical wavefronts and the need for more work. The writer wants to support this view and add an additional voice to the need for more work in this direction. This opinion is based on experimental results showing the importance of sphericity (Beard, 1962). Since the subject is important to the interpretation of experimental results, the following references to theoretical work by deWolf (1967), Twersky (1963), and Ishimaru (1968) are being added to those given by Strohbahn. Further remarks on sphericity will be made in Section 6.

### 4. AGENCY FOR METEOROLOGICAL EQUIPMENT

Strohbahn's suggestion for "an agency through which one could secure either funds for or temporary loans of meteorological equipment" is a suggestion which should be given the full backing of this Panel. The need for such equipment and thus for such an agency becomes obvious upon reading the published literature describing microwave propagation experiments, line-of-sight or otherwise. Equipment such as the path-integrated index of refraction methods mentioned in Section 2, microwave cavity refractometers, etc., whose primary functions are to obtain meteorological parameters, are too costly for the budgets of many experimenters. One of the Panel participants mentioned that NCAR has a program of this type; this is commendable. The writer strongly recommends that this Panel make, or recommend the making of, a study of the type and level of overall program desirable. An effective lending program could significantly raise the national level of the quality and

meaning of propagation research.

## 5. ARRAY MEASUREMENTS

An antenna array with which the field is sampled at several points in space simultaneously (essentially) is obviously a desirable, worthwhile device as shown by the results of Lee and Waterman (1966). The mathematical extensions developed by Lee, as reported on quite favorably by Strohbehn, offer new possibilities, especially that of measuring the transverse wind at ten positions along the path.

Consideration should also be given to the "depth of focus" and the "diameter" of the focused volume in comparison to the eddy scale sizes, to the number of such eddies within the contributing focused volume, and to the amplitude and phase structure of the focused field over the eddies included in this volume. Such information, along with the type of statistical treatment to be used with this information, are also needed to estimate the resolution and accuracy of the method. It is to be hoped that resolution tests will be performed against measured wind velocities at the path altitude at various locations along the path length. The system capabilities obviously warrant tests of this type.

The second use of the array given by Strohbehn is to determine  $C_n^2$  at different points along the path. The only comment here is to point out that this approach involves an even more restrictive assumption (that of a wavenumber spectrum for locally-homogeneous, isotropic turbulence) than those assumptions for the single receiver (Taylor's hypothesis and homogeneity). The third array approach, of trying to determine the wavenumber spectrum, is a task the "phase quadrature" experiment (described in Section 6 below) is also set up to investigate.

## 6. PHASE QUADRATURE MEASUREMENT, USING ONLY ONE RECEIVER

The author wants to acquaint the Panel with a new way of extracting useful information from the single path, only one receiver configuration. Professor Strohbehn has essentially "written off" this type of experiment for three reasons. His first, that Taylor's hypothesis must be assumed, does not seem too critical in view of some confirming tests reported in the literature. The second, the assumption of homogeneity over the path length, is a severer requirement to satisfy. The third reason results from his considering only relative phase variations of the total received field (and/or angle of arrival variations with two receivers); he rightly states that these are insensitive to atmospheric models. The writer wants to point out that by considering the full amount of information available in the system, one can obtain the statistics of the phase quadrature components of the incoherent scattered field itself, which is the entity produced by the fluctuating medium and thus most sensitive to it.

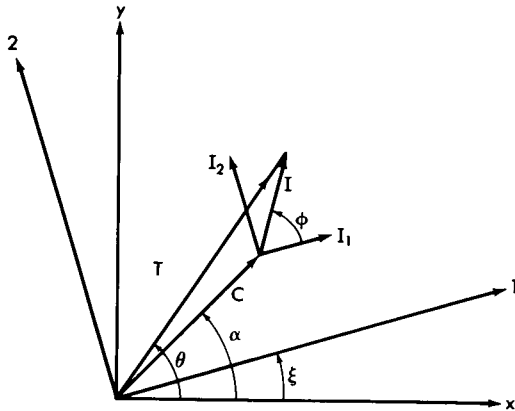


Figure 1. Phasor Diagram of the Received Field and its Components.

Figure 1 showing the phasor diagram is included merely for clarity. T is the instantaneous magnitude of the total received field at an instantaneous phase  $\theta$ , I is the instantaneous magnitude of the random incoherent field with phase quadrature components  $I_1$  and  $I_2$ , and C is the magnitude of the time-average coherent field at a fixed phase  $\alpha$ , with all phases referred to, say, the transmitted field along the x-axis. The fields are resolved along two phase quadrature axes, 1 and 2, which can be rotated to any desired angle  $\xi$ . Because of the coherent field on a line-of-sight path, it is qualitatively clear from Figure 1 that the phase ( $\theta$ ) of the total field is not sensitive to the statistics of the incoherent field; Beard (1962) has shown this insensitivity quantitatively in a laboratory type of "line-of-sight" path at the same time that the phase quadrature components were measured to show the actual incoherent field statistics.

The phase quadrature method determines several parameters which may be useful in characterizing the medium:

1) The statistics of the phase quadrature components of the incoherent scattered field (such as probability distributions, variances, spectra, correlations, etc.).

2) The incoherent power  $\overline{I^2} = \sigma_1^2 + \sigma_2^2$ .

3)  $K^2 \equiv (\sigma_2^2 / \sigma_1^2)_{\max} =$  the maximum ratio of the variances of the phase quadrature components ( $K^2 \equiv \geq 1$ ).

4) The phase rotation angle ( $\xi$  in Figure 1) of the axes to obtain the maximum value of  $K^2$ ; this is the rotation angle of the equiprobability ellipse.

Examples of a few of these parameters are becoming available from a tropospheric experiment (Beard, 1968) which was set up just for the purpose of investigating the relationship of these parameters to the scattering medium. On a 3.57 km path the phase quadrature components show that the incoherent field lies almost entirely at a phase angle of  $\pm 90^\circ$  with respect to the coherent field,  $K^2 \gg 1$ , and this component is closely normally distributed. This result agrees with the near field model of Wheelon and Muchmore (1955) and is consistent with the scale sizes encountered. In Figure 2 is shown a calculated power spectrum for this larger quadrature component (at  $\pm 90^\circ$  to C); the interesting feature is that it drops four orders of magnitude with a  $-8/3$

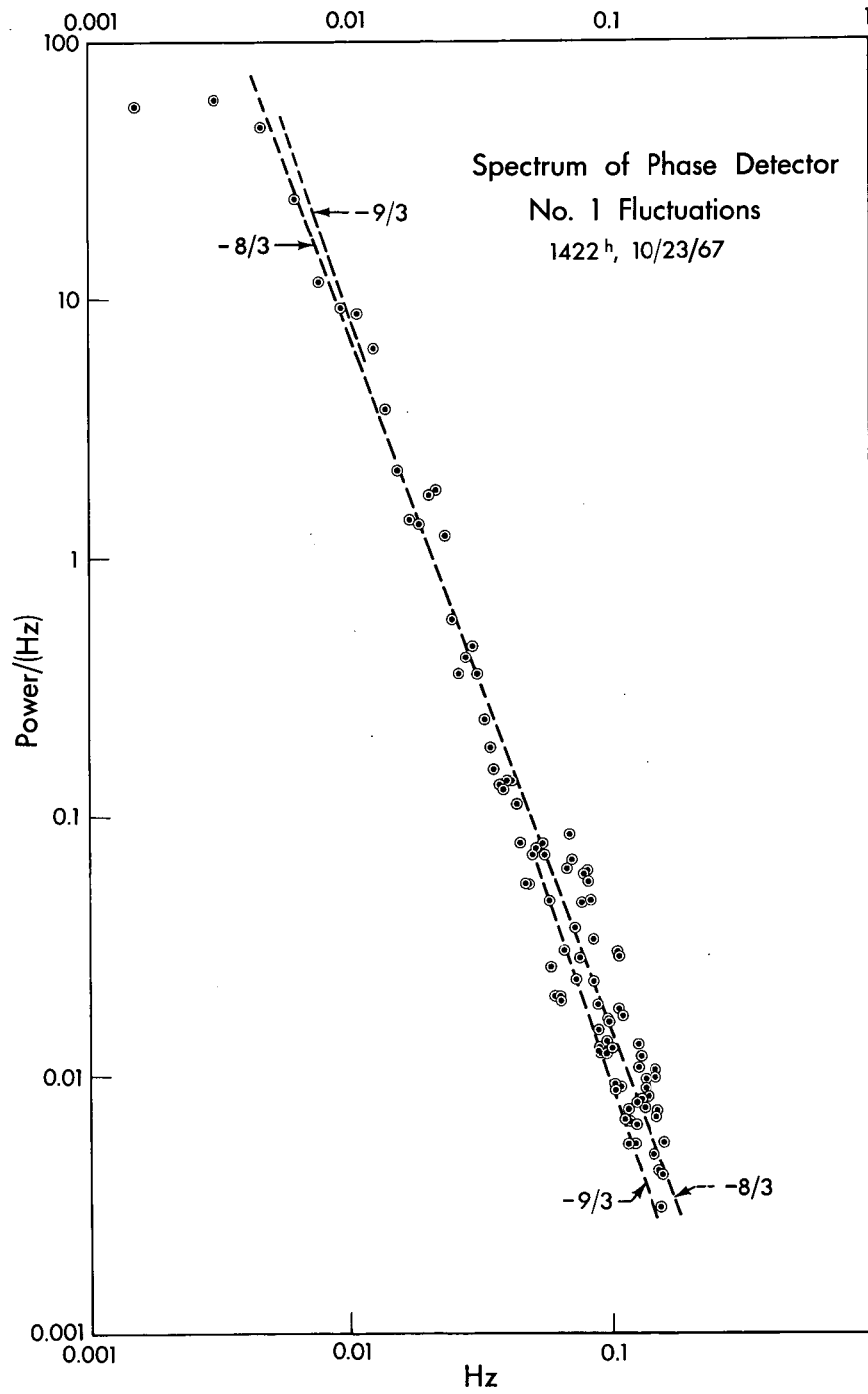


Figure 2. Power spectrum of the incoherent field component in phase quadrature to the coherent field.

(or possibly  $-9/3$ ) slope, but definitely not a  $-7/3$  or  $-10/3$  slope. (A one-dimensional  $\kappa^{-5/3}$  spectrum integrated along the path becomes a  $\kappa^{-8/3}$  spectrum.) This result relates to the question of Strohbehn (page 14 of his paper), "Can an experiment differentiate between a  $\kappa^{-11/3}$  turbulence spectrum versus a  $\kappa^{-4}$  or a  $\kappa^{-3}$  spectrum?" It might also be mentioned that even in this first spectrum, the scale size information extends over a range of approximately 1.5 decades. Whether information content down to scale sizes limited by aperture smoothing can be obtained depends on signal-to-noise ratios obtainable from magnetic tape reduction in the future.

There is an indication that there may be a relationship of the incoherent power to the wind speed, but with the few data available one should say only that the point looks worth pursuing.

One of the promising exploratory features of this method is the use of the ratio  $K^2 = (\sigma_2^2 / \sigma_1^2)_{\max}$ . This ratio is sensitive to the sphericity of the illuminating and receiving wavefronts (Beard, 1962), and it is most sensitive in the "mid-field" region. Since  $K^2$  is sensitive to the eddy scales, this writer advances the hypothesis that  $K^2$  can be used to explore the eddy wavenumber spectrum by examining  $K^2$  for various frequency "slices" of the power frequency spectra of the two phase quadrature components of the incoherent field. The low fluctuation frequencies should be associated with the larger scale sizes, and the high fluctuation frequencies with the small scales.  $K^2$  should thus be large at the low frequency end of the spectrum since near-field conditions are approached, and  $K^2$  should decrease toward the high-spectral frequencies as far-zone conditions are approached for smaller scale sizes. The one test that has been made with the spectra of the two components is encouraging and warrants a full test of the hypothesis.

The fourth parameter  $\xi$ , the phase rotation of the equiprobability ellipse, may be rotated with respect to the coherent field (Beard, 1962), and the writer has also found that the rotation angle may change with sphericity in rough surface scattering. Whether such behavior occurs in this particular tropospheric experiment is not known yet and awaits digital reduction of the magnetic tape data.

Since the "mid-field" region is related to a phase delay  $k\ell^2/8L$ , where  $k = 2\pi/\lambda$ ,  $\ell$  is the eddy scale size, and  $L$  is the path length, there are clearly three variations on the line-of-sight theme to change the sphericity:

- a) A multi-wavelength experiment (with the same antenna beamwidths) seems best since the meteorology remains constant.
- b) Two paths of different length  $L$ ; the obvious difficulty is to traverse nearly the same atmospheric conditions.
- c) The third method is to make measurements in various weather conditions, letting the weather change the scale sizes.

In summary, in this method of measuring the phase quadrature components of the received field at one receiver, four parameters of the incoherent scattered field are determined. Various of these parameters are sensitive to the eddy wavenumber spectrum, the wind speed, and to the sphericity of the transmitting

and receiving wavefronts. A hypothesis is advanced to use one of these parameters,  $K^2$ , as a means of exploring the eddy size wavenumber spectrum.

## 7. A PROPOSED EXPERIMENT

Out of this comparison emerges the outline of a line-of-sight experiment *supreme*. It incorporates the most encouraging features of the newer programs and must be performed over a fully meteorologically instrumented path. It should include the following:

- a) A phase and amplitude array experiment (Section 5 above) in both the horizontal and vertical planes, operating simultaneously.
- b) A "phase quadrature" experiment (Section 6 above) on the field received by the center antenna of the array and operated simultaneously with the array. (A phase reference link from the transmitter to the receiver is required.)
- c) A path-integrated microwave index of refraction measurement (Section 2 above) made simultaneously with (a) and (b) above, possibly by the infrared-K-band system now in operation.
- d) Comprehensive meteorological measurement of the path, for example, wind velocity at the path altitude at various points along the path, wide spectral response recordings of many parameters such as temperature and humidity, microwave refractometer index of refraction, wind shear, shadowgraph photographs for transverse scale sizes, etc.

The very magnitude of this program in terms of complexity and variety of equipment, expense, manpower, data processing, etc., indicates that a cooperative program and/or facility of some kind might not be inappropriate.

## REFERENCES

- Beard, C. I., 1962: Statistics of phase quadrature components of microwave fields transmitted through a random medium. *IRE Trans. Ant. & Prop.*, AP-10, 721-731.
- Beard, C. I., 1968: Phase quadrature components of the 10.4 GHz scattered field on a short tropospheric path. Presented at the April 1968 URSI Meeting, Washington, D. C.; see also Beard, C. I., 1967: Microwave scattering from atmospheric inhomogeneities, *Boeing Scientific Research Laboratories Review*, p. 50-52.
- deWolf, D. A., 1967: Spherical wave propagation through a random continuum. *Radio Science*, 2, 1513-1515.
- Ishimaru, A., 1968: Amplitude fluctuations of a beam wave in a locally homogeneous medium. Presented at the April 1968 URSI Meeting, Washington, D. C.
- Kreiss, W. T., 1967: Radio meteorology. *BSRL Review*, p. 53.
- Strohbehn, J. W., 1968: The use of line-of-sight microwave propagation in remote atmospheric probing. Presented at the Remote Atmospheric Probing Panel of CAS-NAS, April 18, 1968.

ADDITIONAL LINE-OF-SIGHT METHODOLOGY

- Tank, W. G., 1967: The measurement of integrated refractivity for evaluating atmosphere-induced radar ranging errors. *BSRL Report*, D1-82-0639.
- Twersky, V., 1963: Signals, scatterers, and statistics. *IEEE Trans. Ant. & Prop.*, AP-11, 668-680.
- Wheelon, A. D., and R. B. Muchmore, 1955: Line-of-sight propagation phenomena--II. scattered components. *Proc. IRE*, 43, 1450-1458.

## COMMENTS ON PAPERS BY DRs. STROHBEHN AND BEARD

by  
Akira Ishimaru

Department of Electrical Engineering  
University of Washington  
Seattle, Washington

I have a number of points to make concerning the presentations of both Drs. Strohbehn and Beard. They are as follows:

1. On the assumption  $\lambda \ll l_0$ .

There are two possible ways to relax this assumption.

- (a) The assumption is basically equivalent to taking the saddle point approximation of the integral; therefore the assumption may be relaxed (Bremmer, 1964).
- (b) Tatarski's argument of using  $\lambda \ll l_0$  is based on the plane wave case. Other waves, such as spherical and beam waves may not require this condition. In particular, the beam wave theory does not seem to require such an assumption.

2. Importance of the filter function for beam waves.

The spectrum of the field at an observation point is a product of a filter function and a power spectrum of the index of refraction. The filter function for the plane wave is well known (Tatarski). But the filter function for the beam wave has an additional factor involving the size of the beam. Thus, depending on whether the beam size is large or small compared with the inner and outer scale of turbulence and the Fresnel radius for the distance, we would expect different spectral behaviors; this may be useful in probing atmospheric characteristics.

It may also be noted that the beam spreading and the fluctuation characteristics of the focused beam, which is now under study, may yield additional information.

3. Measurement of the structure function.

Since atmospheric turbulence is basically nonhomogeneous, and is better approximated by Kolmogorov local homogeneity, its characteristics may be better measured by structure functions rather than by covariance functions. The amplitude fluctuations are basically homogeneous due to the effect of the filter function, but the phase fluctuation is affected much more by the outer scale of turbulence. Thus, the measurement of the phase structure function may be more useful.

4. Difference between the average and effective refractive indices.

Recently, Tatarski and Keller made an extensive study on the propagation of the average field and corresponding effective refractive index,  $n_{\text{eff}}$ . For example, for scalar waves

$$(\nabla^2 + k^2 n^2) = 0, \text{ and}$$

$n = \bar{n} + n_1$ , where  $\bar{n}$  = average index of refraction and  $n_1$  is the fluctuation. Then

$$(\nabla^2 + k^2 n_{\text{eff}}^2) \bar{u} = 0$$

where  $\bar{u}$  is the average field, and  $n_{\text{eff}}$  does not equal  $\bar{n}$  but depends on the correlation function of  $n_1$ . This difference may have to be taken into account when considering the absolute path, especially when the fluctuation is significant.

5. Regarding Dr. Beard's experiment.

Dr. Beard's phase quadrature experiments seem to be quite consistent with the theoretical results outlined by Dr. Strohbehn. As is well known, at short distance, the mean square fluctuation increases as  $L$  (distance) while the mean square amplitude fluctuation increases much more slowly as  $L^3$ . On the other hand, at large distances, the mean square phase and amplitude fluctuations are about the same. Beard's results appear to correspond with these predictions. On the other hand, the Russian workers observed that the log-amplitude seems to obey Gaussian statistics in their optical experiments. This should be compared with the statistics which Dr. Beard is investigating.

REFERENCE

Bremmer, H., 1964: Random volume scattering. *Radio Science*, 68D, 967-981.

N72-25 351

THE USE OF SATELLITE BEACONS FOR METEOROLOGICAL RESEARCH

Jules Aarons

Air Force Cambridge Research Laboratories

Bedford, Massachusetts

Atmospheric absorption measurements have been made in the past using microwave radiation from the sun, the moon, and discrete radio sources for the measurements. Oxygen and water vapor are the principal constituents absorbing the energy. Absorption is readily observed at 3 GHz and higher frequencies.

Another tool which might be used to measure absorption is microwave beacon transmissions from synchronous and near synchronous satellites. With a fixed angle of elevation of a synchronous satellite complete diurnal coverage of the integrated absorption is available. With refined interferometric equipment, angle of arrival studies can also be made and phase deviations measured.

The transmissions now available are of limited utility for consistent observations because of their low power. Large antennas and phase lock ground equipment are needed for an adequate signal to noise ratio.

Among the beacons now transmitting in the microwave region are the following:

(1) Intelsat 2 F-3 Object 1967 26A - Beacon #1 at 4058.15 MHz, Beacon #2 at 4182.00 MHz. It is now positioned at 5° West Longitude. COMSAT Corporation, Washington, D.C., is responsible for this satellite and several others which are also transmitting on the same frequencies and located in either the Atlantic or Pacific areas.

(2) IDCS Beacons - a series of twenty satellites which are in a near synchronous orbit and transmit on 7299.5 MHz. The Defense Communications Agency (DCA), Mr. William de Hart, Code 480, Washington, D.C., is responsible for this series.

The technical output of a study of this type is the integrated absorption over the whole path length. This has limited utility for meteorological research but may have utility for cataloging long term changes of oxygen and water vapor at a particular area. The measurements, of course, need calibration by other techniques in order to determine the various height contributions to the absorption.

A more subtle measurement may be made of atmospheric irregularities by means of the interferometric technique. The beacon signal has phase information and the interferometric measurements of phase differences can yield new irregularity data at high angles of elevation through the total atmosphere; present ground based transmitter and angle of arrival measurements have only horizontal paths or relatively limited geometry (mountain-valley).

SESSION **2**

Optical  
Line-of-Sight  
Propagation

N 72-25352

# REMOTE ATMOSPHERIC PROBING BY GROUND-TO-GROUND LINE-OF-SIGHT OPTICAL METHODS

Robert S. Lawrence  
ESSA Research Laboratories, Boulder, Colorado

## ABSTRACT

We describe qualitatively the optical effects arising from refractive-index variations in the clear air and discuss the possibilities of using those effects for remotely sensing the physical properties of the atmosphere. The effects include scintillations, path-length fluctuations, spreading of a laser beam, deflection of the beam, and depolarization. The physical properties that may be measured include the average temperature along the path, the vertical temperature gradient, and the distribution along the path of the strength of turbulence and the transverse wind velocity.

Line-of-sight laser-beam methods are clearly effective in measuring the average properties, but less effective in measuring distributions along the path. Fundamental limitations to the resolution are pointed out and experiments are recommended to investigate the practicality of the methods.

## 1. INTRODUCTION

This paper deals with the optical effects arising from variations of the refractive index of the clear atmosphere. It does not consider the effects of absorption or scattering by either aerosols or molecules. Thus, there will be no discussion of radiometry, spectroscopy, or spectrophotometry.

The atmospheric effects that remain include the modification of the optical path by the mean refractive index along the line of sight and the distortion of an optical wave by the temporal and spatial variations in the refractive index. Sections 2 through 4 summarize those atmospheric effects that may

## PROBING BY OPTICAL METHODS

be relevant to the problem of remote probing. The remaining sections describe briefly some methods for using the effects.

### 2. EFFECTS OF TURBULENCE

#### 2.1 The Refractive-Index Variations

The twinkling of stars and the variable blurring of their images in a telescope are caused by the small-scale and rapidly varying density fluctuations associated with atmospheric turbulence. Density is the pertinent physical property because the optical refractivity,  $n-1$ , is proportional to density. In the open atmosphere the variation in density of a small parcel of air depends only on variation of its temperature because pressure differences are smoothed out with the velocity of sound. Thus, in what follows, we shall be safe in making no distinction between the refractive-index fluctuations and the temperature fluctuations. Notice, however, that these fluctuations are not necessarily identical to the velocity fluctuations measured by the hot-wire probes so commonly used in studies of turbulence. If the atmosphere is in neutral thermal stability, i.e. if the temperature lapse rate is adiabatic, strong mechanical turbulence may exist with little or no optical effect.

The direct relationship between temperature fluctuations and optical effects suggests the use of small, high-speed thermometers to measure directly the strength and the structure of turbulence as it affects light waves. Resistance thermometers having dimensions less than a millimeter and response times less than a millisecond are regularly used by ERL in Boulder to "calibrate" the atmosphere whenever optical measurements are in progress (see Ochs, 1967).

As we shall see later, the thermal irregularities that are most effective in producing optical effects range in size from a few millimeters to about ten centimeters. Over this range of sizes, and indeed to much larger scales, the turbulence follows closely the Kolmogorov-Obukov model which predicts that the power spectrum of temperature fluctuations will vary as the  $-5/3$  power of the wave number. Measurements made at Boulder have shown the "inertial sub-range," in which the  $-5/3$  spectrum holds, to extend to irregularities as small as 2 or 3 mm. At smaller sizes, the spectrum steepens as viscous damping destroys the turbulence.

#### 2.2 Intensity Effects on a Light Wave

Let us consider the behavior of a light wave as it travels outward from a point source through the turbulent atmosphere (Figure 1). The wave front is initially spherical, as at A. Upon passing through irregularities to reach position B it becomes distorted. Since absorption and wide-angle scattering are negligible, the energy density of the wavefront B is still uniform and equal to its free-space value. Thus an ordinary square-law detector located at B would be unaffected by the irregularities and incapable of measuring

them. The irregularities in the wave front can, of course, be measured by a phase-sensitive detector such as an interferometer.

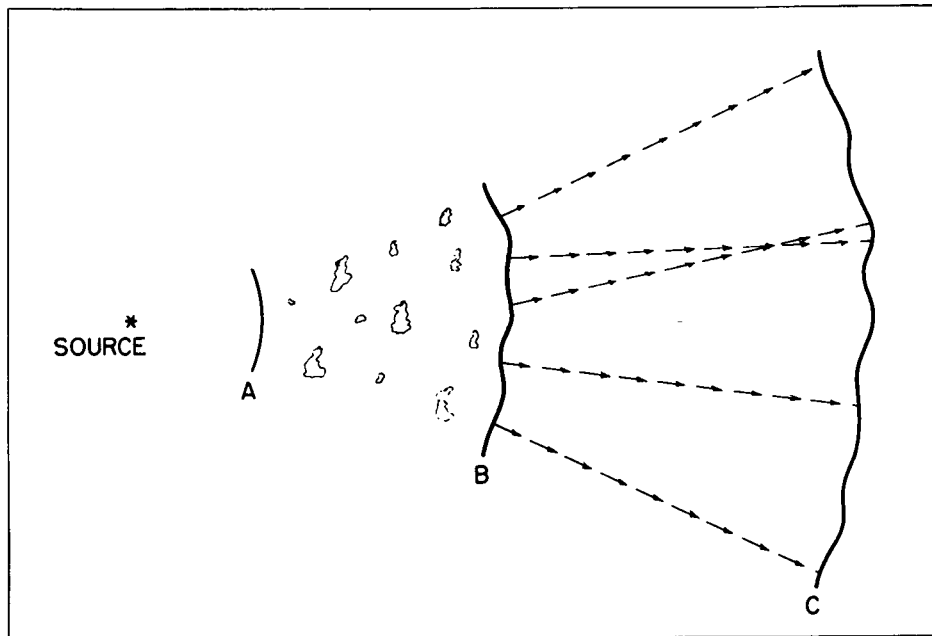


Figure 1. Schematic diagram of the propagation of a spherical light wave through a turbulent atmosphere. Phase fluctuations at B develop into phase and intensity fluctuations at C.

As the wave progresses from B toward C, the various portions of the distorted wave front travel in slightly different directions and eventually begin to interfere. The interference is equivalent to a redistribution of energy in the wave and causes intensity fluctuations (scintillations) which can be detected by a square-law detector. On the way from B to C the wave front passes through additional refractive-index irregularities and so suffers additional phase perturbations. These new irregularities are, however, relatively ineffective in producing intensity fluctuations.

Let us examine the criteria that determine which of the turbulent irregularities along a line of sight are most effective in producing intensity fluctuations. In Figure 2, consider an irregularity of radius  $r$  at an arbitrary point A on the line of sight between the source S and the receiver R. That irregularity can be fully effective in producing intensity variations only if the extreme ray paths, SAR and SBR, involving it differ in length by at least half a wavelength, i. e. the irregularity must be at least equal in size to the first zone of a Fresnel zone plate situated at A. This minimum effective size is, in fact, the optimum size for the irregularity. Larger irregularities at the same point are rendered ineffective by the smaller ones just as a lens is rendered ineffective by a ground-glass surface.

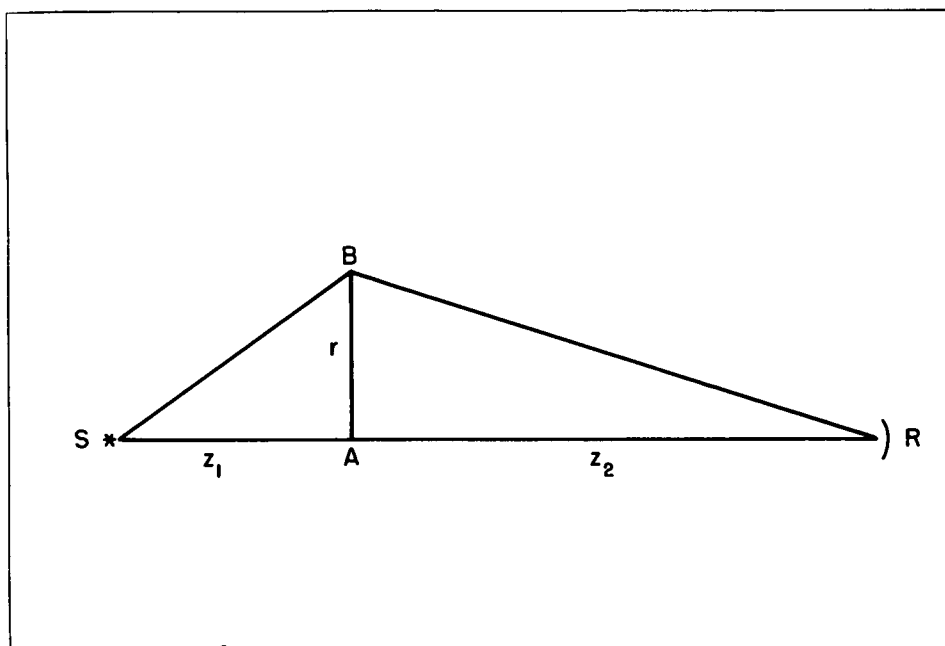


Figure 2. The geometry involved in determining the irregularity size most effective in producing scintillations.

Working out the geometry of Figure 2, we find that the radius of the most effective irregularity is  $r \approx \sqrt{q\lambda}$ , where  $\lambda$  is the wavelength and  $q = \frac{z_1 z_2}{z_1 + z_2}$  depends upon the position of A. This radius is plotted in Figure 3 for a wavelength of 6328 Å and a path length of 10 km.

If we assume, for the moment, that the turbulence is uniformly distributed along the path and has a Komogorov spectrum, it is clear that the mean-square fluctuation of refractive index attributable to irregularities of optimum size varies systematically along the path. There is, therefore, a weighting function that expresses the relative effectiveness of turbulence in producing intensity fluctuations as a function of position along the path. From Figure 3 it is clear that this weighting function must reach a maximum at the midpoint of the path and must drop symmetrically to zero at the ends. An expression for this function has been derived (Fried, 1967a). It is

$$E = \int_0^{-\infty} x^{-11/6} \sin^2 \left( \frac{q\lambda}{4\pi} x \right) dx .$$

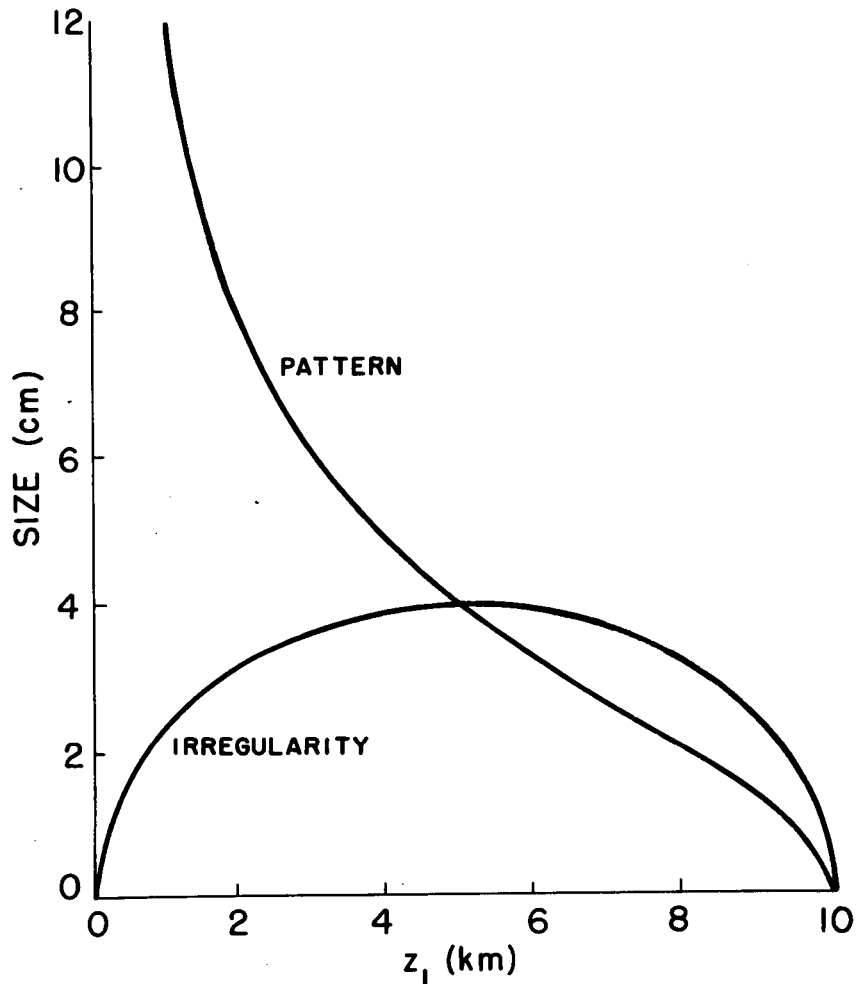


Figure 3. The radius of the most effective irregularity at various points along a 10 km path, and the resulting pattern size.

Figure 4 compares this integral, evaluated numerically as a function of position along the path, with the best-fitting parabola. In summary, the relative effectiveness of a uniformly turbulent atmosphere in producing intensity scintillations is approximately a parabolic function of position along the path, being a maximum at the midpoint and zero at the ends.

Next, let us examine the scale sizes of the intensity patterns at the receiver due to the optimum-sized refractive-index irregularities located at various points along the path. Referring to Figure 5 and recalling that the

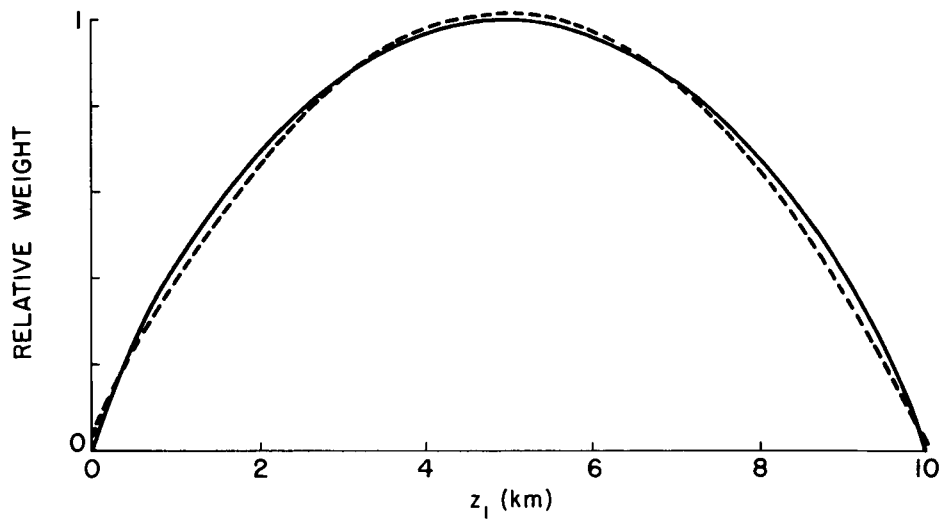


Figure 4. The relative effectiveness of Kolmogorov turbulence at various points along a 10 km path in producing intensity fluctuations. The dashed curve is the best-fit parabolic approximation.

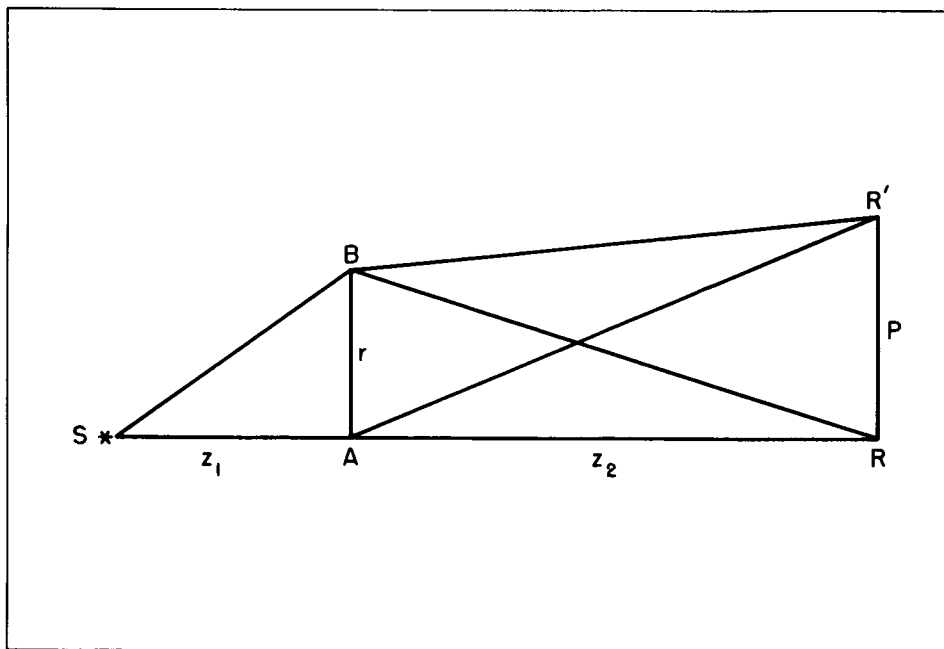


Figure 5. The geometry involved in determining the pattern size produced by the most effective irregularities.

radius  $r$  of the optimum-sized irregularity of  $A$  was such that  $SBR$  exceeded  $SAR$  by a half wavelength, we can see that the size  $p$  of the pattern at the receiver is determined by the requirement that  $SBR'$  must equal  $SAR'$ . Then, when destructive interference is present at  $R$ , constructive interference will occur at  $R'$ . Working out the geometry, we find that the pattern is larger than the turbulent irregularity by the factor  $p/r = \frac{1}{2} (1 + z_2/z_1)$ . The pattern size  $p$  is shown in Figure 3 for a 10 km path.

We have seen that the diffraction process that produces intensity fluctuations in the light wave selects only certain optimum sizes from the broad spectrum of irregularities available in Kolmogorov turbulence. The optimum size selected depends on the position along the path, and each position produces a predominant, and unique, pattern size at the receiver. When the weighting function shown in Figure 4 is combined with the pattern-size function of Figure 3, there results the composite spectrum of sizes observable in the intensity pattern. Notice that, for turbulence distributed uniformly along the path, this composite spectrum of sizes depends only on the wavelength and the path length; it is not indicative of any preferred size of turbulent eddies in the atmosphere. An expression for this spectrum, or rather, its Fourier transform, the covariance function, has been derived by Fried (1967b), and is compared with observational data in Figure 6. In the figure,

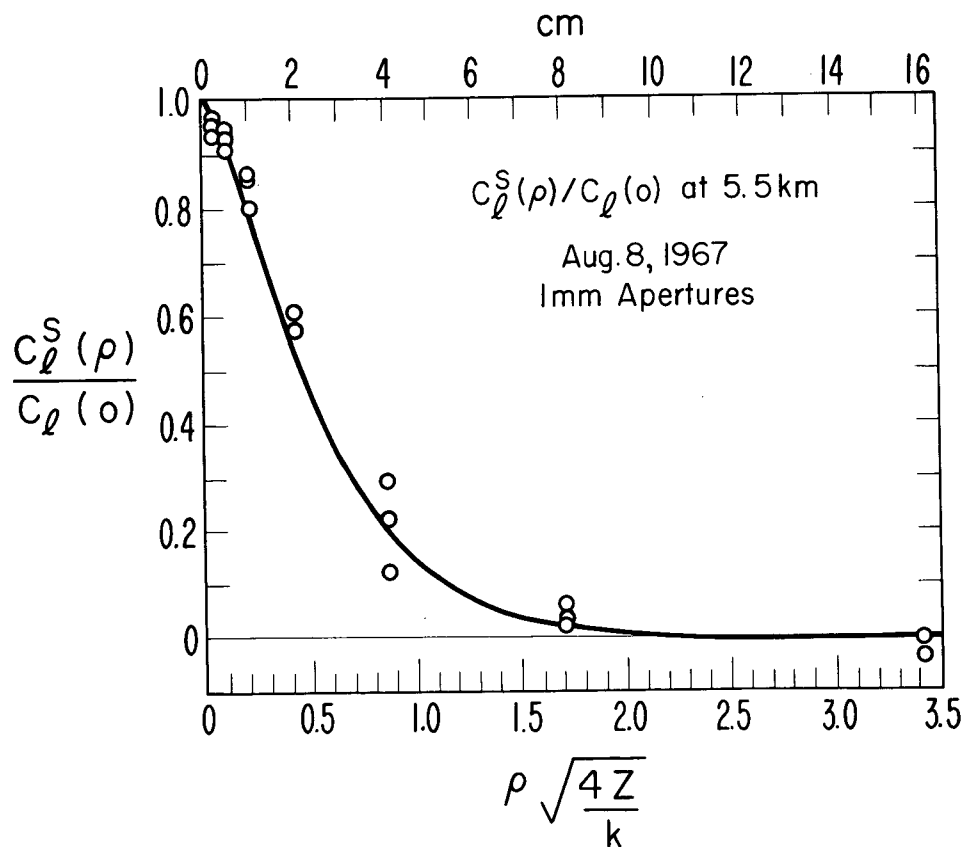


Figure 6. The covariance function of intensity fluctuations calculated (from Fried) and observed over a 5.5 km path.

the normalized covariance of log-amplitude measurements made on spaced detectors is plotted as a function of detector spacing  $p$ .

The temporal fluctuations of intensity observed at a point arise from two causes. First, the intensity pattern at the receiver plane is continuously changing in detail because of the random velocities of the various turbulent eddies in the atmosphere. Second, the entire pattern drifts past the detector as the result of the transverse component of the mean wind. The power spectrum of intensity fluctuations is closely related to the spatial spectrum of the intensity pattern, and derived from it by including the effect of the mean transverse wind. As in the case of the spatial spectrum, the power spectrum resulting from uniformly distributed turbulence depends only on the wavelength of the light and the path length, shifted in frequency in proportion to the transverse wind velocity.

Incidentally, though the topic is outside the scope of this paper, the power spectrum changes radically if raindrops enter the beam. This effect has not been investigated but might prove useful in remotely measuring the presence of rain, or maybe even the drop size distribution.

As we have seen, the spectrum of pattern sizes and the power spectrum of temporal fluctuations depend on the wavelength of the light, but they are not ordinarily indicative of any preferred size of turbulent eddies in the atmosphere. Thus, when dealing with a Kolmogorov spectrum of turbulence, we should not expect to obtain independent information by observing on two or more wavelengths simultaneously. However, such multiple-wavelength observations might prove useful in investigating departures from the Kolmogorov spectrum. A possible application is the use of short paths and multiple frequencies to observe the steepening of the turbulent spectrum for small eddies where viscous damping becomes effective.

### 2.3 Optical Path Length Fluctuations

The cumulative effect of the phase distortions of the wavefront combines with the random velocities of the turbulent eddies to produce temporal fluctuations in the phase of the received light wave or, what is equivalent, changes in the optical length of the path. Over short paths where the intensity effects are not fully developed, the path-length changes can be measured by interferometry. A typical 4-second sample of such measurements over a 25-meter path is shown in Figure 7. The second-to-second fluctuation of such a path is of the order of a few parts in  $10^8$  after long-term (10-second) trends have been removed.

As the path length is increased so that the intensity effects become well developed, interferometer measurements begin to suffer from ambiguities during the intensity minima. Then it is more convenient to measure path length by modulating the light beam, much as Fizeau did with his toothed wheel when measuring the velocity of light. With a modulated beam, the group path length rather than the phase path length is measured because of

the optical dispersion of air. A 110-second sample of such a measurement, using 10 cm modulation wavelength over a 5 km path, is shown in Figure 8. Here the second-to-second fluctuation is a few parts in  $10^9$  after the slow drift is removed.

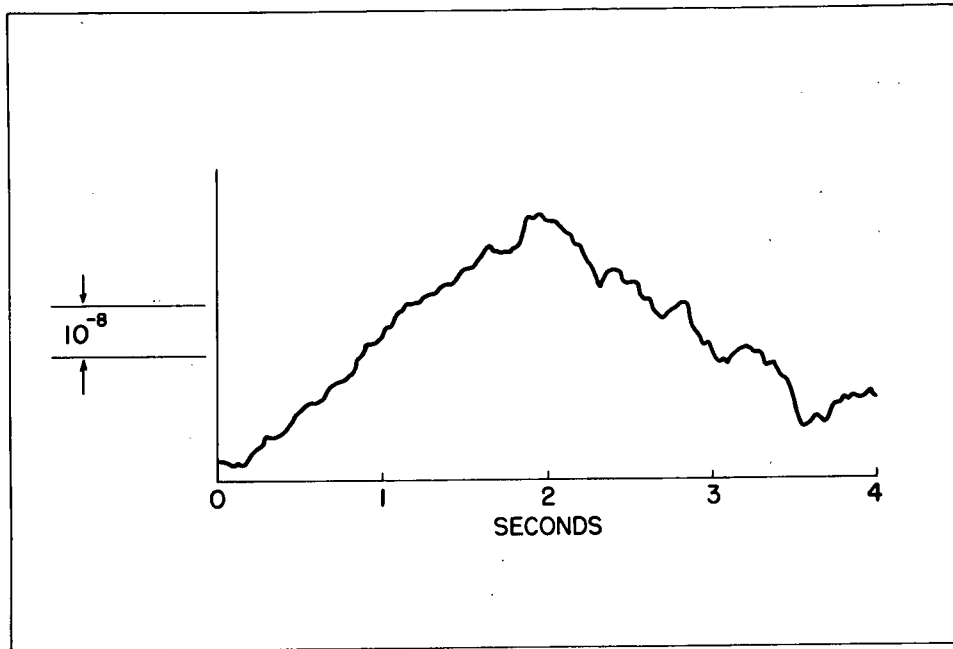


Figure 7. A typical four-second measurement of optical path-length changes over a 25 m path.

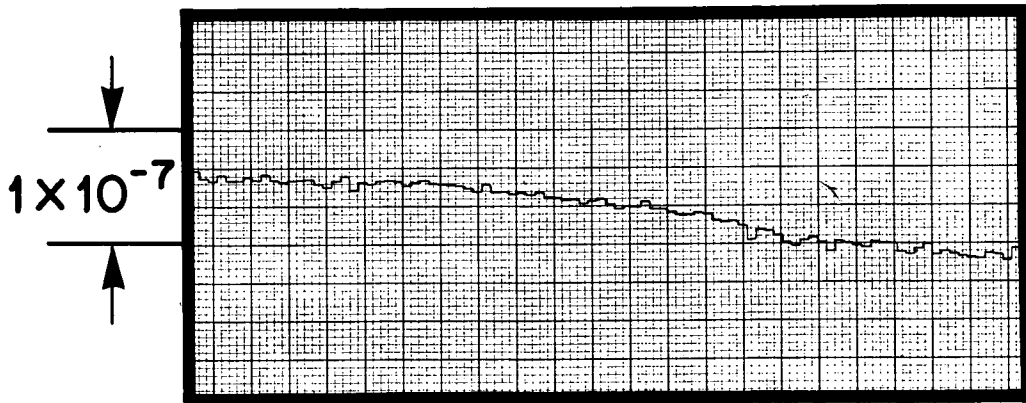


Figure 8. A typical 110-second recording of optical path-length changes over a 5 km path. The individual measurements are one-second averages.

## PROBING BY OPTICAL METHODS

### 2.4 Spreading of a Laser Beam

If the light is restricted to a narrow beam from a well collimated laser, the phase fluctuations in the wavefront which, at position B of Figure 1, cause portions of the wave to propagate in slightly different directions will produce a measurable spreading of the beam. Rigorous analysis of this effect is surprisingly difficult, though an approximate geometrical solution has been presented by Beckmann (1965).

The weighting function for beam spreading is very different from that for intensity fluctuations. We can see its approximate nature from the following simple argument. Referring to Figure 9, consider a laser source L which,

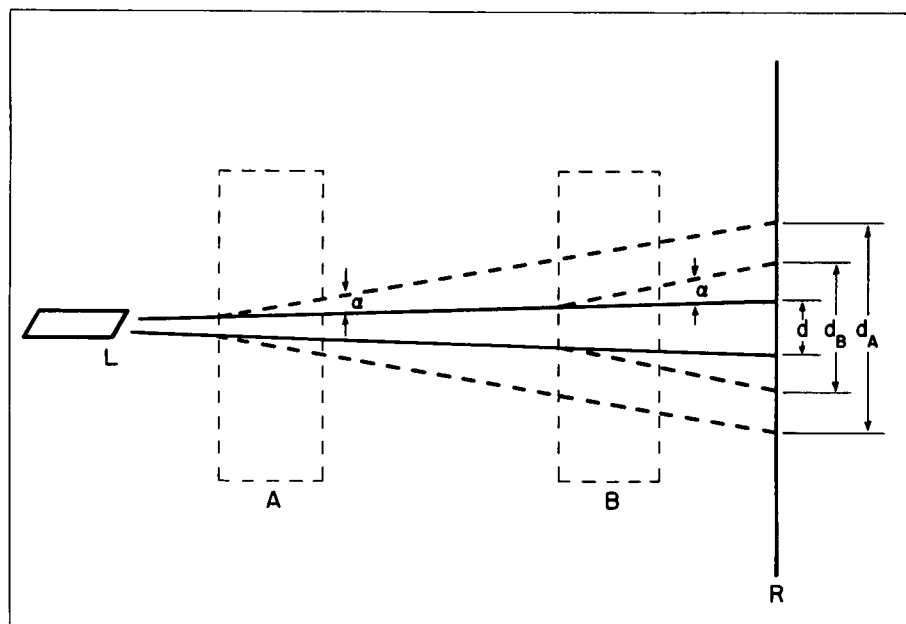


Figure 9. The geometry involved in determining the relative effectiveness of turbulence at various points along the path in producing beam spread.

in the absence of an atmosphere, would produce a spot of diameter  $d$  on the receiving screen R. If a parcel of turbulent atmosphere (not a single refractive-index irregularity but a complete, bounded region containing a Kolmogorov spectrum of irregularities) were inserted in the beam at point A, it would cause some additional beam spreading of angle  $\alpha$  and would result in a spot at R of diameter  $d_A$ . If, instead, the same parcel of turbulent atmosphere is located at point B, the beam spreading caused by it will still have the same angle  $\alpha$ , but now the spot on the receiving screen will be only  $d_B$  in diameter. Thus, if the inherent angular divergence of the laser beam is much smaller than the atmospheric effect  $\alpha$ , the weighting function that describes the effectiveness for beam spreading of turbulence at various positions along the path is linear. It is a maximum at the laser and drops to zero at the receiver.

Figure 10 shows the typical diurnal variation of beamwidth as measured over 5.5 and 15 km paths near Boulder, Colorado. The laser beam was expanded and collimated so that its intrinsic divergence was only  $5 \mu\text{rad}$ . The average height above ground of the paths is 50 and 80 m respectively.

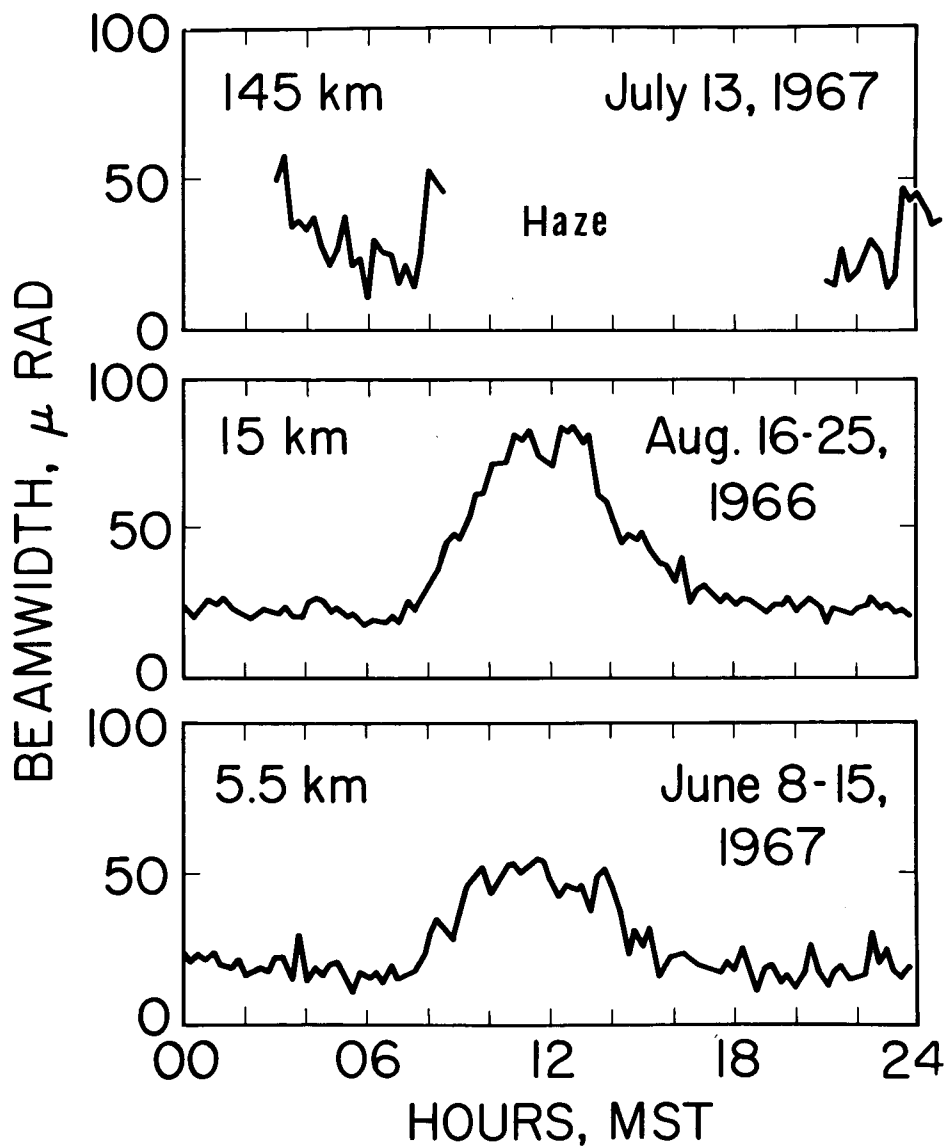


Figure 10. Typical diurnal variation of beam width observed over three paths near Boulder, Colorado.

## PROBING BY OPTICAL METHODS

Figure 11 presents some slight evidence in support of a linear weighting function for beamwidth. The line and the solid dots show the close relationship between beamwidth observed over an irregular 5 km path on a sunny summer afternoon and the mean square temperature fluctuation measured along the beam with a high-speed thermometer mounted on an airplane. Here,

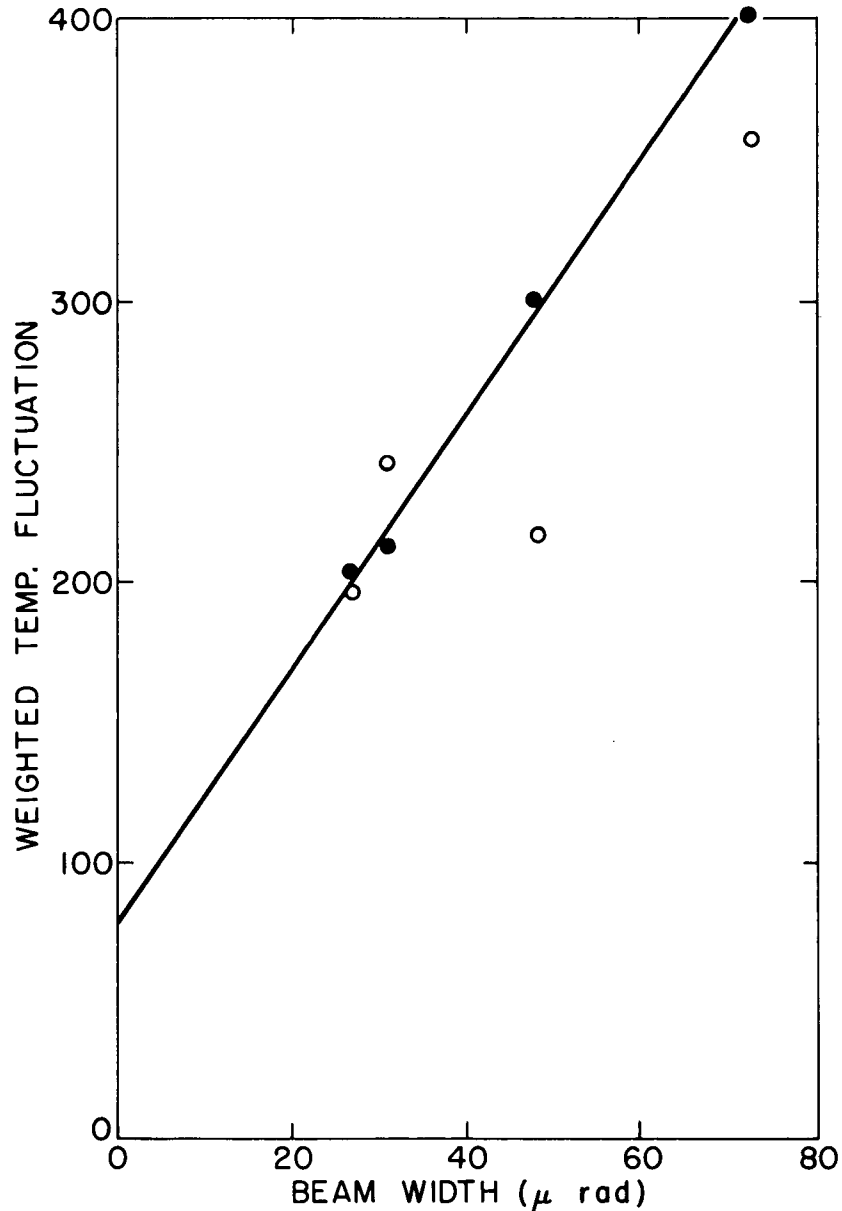


Figure 11. The dark circles show the close relationship between observed beamwidth and properly weighted airborne measurements of turbulence along a 5 km path. The open circles show how the relationship deteriorates when an improper weighting function is used.

linear weighting of the temperature measurements has been used, counting the fluctuations near the laser most heavily and those near the receiver not at all. The open circles show how this close relationship is lost if reverse linear weighting is used, as would be appropriate were the laser and receiver interchanged. Although the experiment is still to be done, we may infer that the beamwidth would be very different on this path if measured in the opposite direction.

### 3. EFFECTS OF LARGE-SCALE REFRACTIVE-INDEX VARIATIONS

Large-scale variations in the refractive index of the atmosphere are primarily controlled by temperature and barometric pressure. The large-scale phenomena that are most important to ground-to-ground optical propagation are changes in the average temperature along the path, changes in the barometric pressure, and changes in the vertical gradient of temperature. Minor effects result from changes in the water-vapor content of the atmosphere and from horizontal temperature gradients.

A laser beam sufficiently narrow to be dominated by turbulent spreading typically wanders from its mean position by several times its own diameter. This wandering is primarily in the vertical direction because of the predominance of vertical temperature gradients. Figure 12 illustrates this effect with

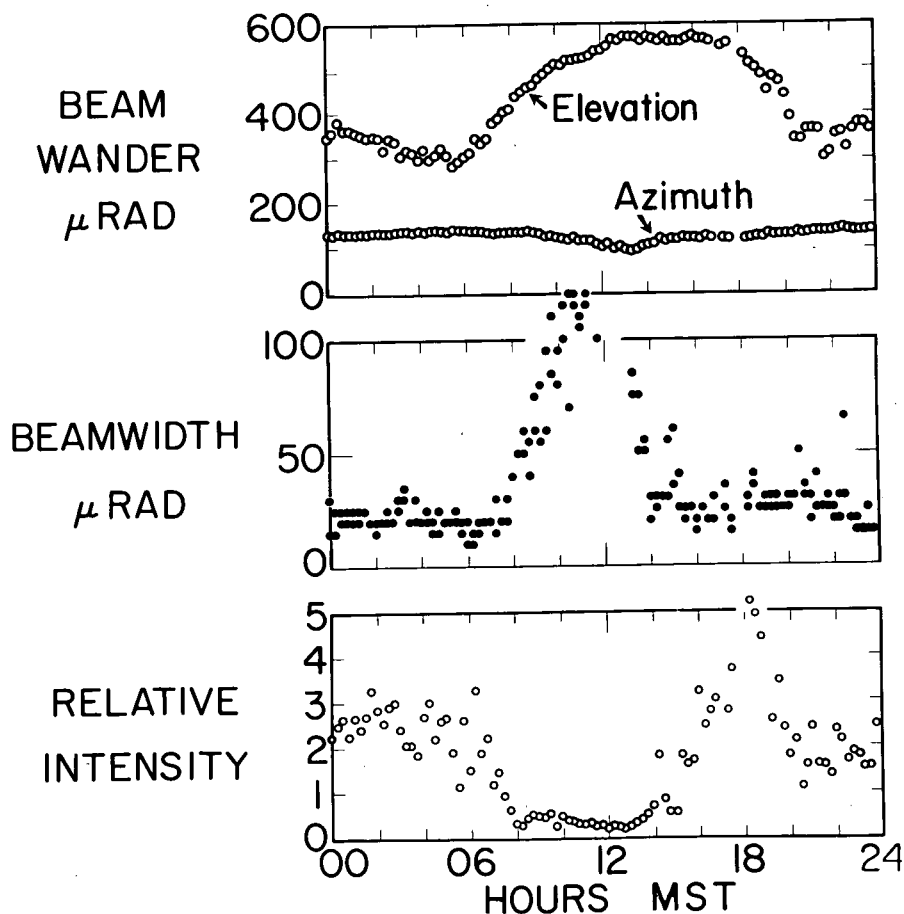


Figure 12. A typical day's measurements, made every 15 minutes, of beam width and beam wander over a 15 km path.

## PROBING BY OPTICAL METHODS

a series of beam positions measured every 15 minutes during a typical day. When, upon occasion, the beam passes through a temperature inversion, the vertical deflections are greatly enhanced as in the case of a mirage. In addition, it is common in these cases to observe nearly periodic vertical oscillations, presumably caused by gravity waves.

The average density of the air along the path determines the optical path length. A change of 1 K in temperature or of 3 mb in pressure is sufficient to affect the optical path length  $nL$  by one part in  $10^6$ . Notice that this is several hundred times greater than the second-to-second fluctuation typically caused by turbulence. Figure 13 shows an example of this effect measured over a 3 km round-trip path. The reference temperature was measured with a thermometer at the center of the path.  $\Delta(nL)$  is the difference in optical path length between red light and blue light.

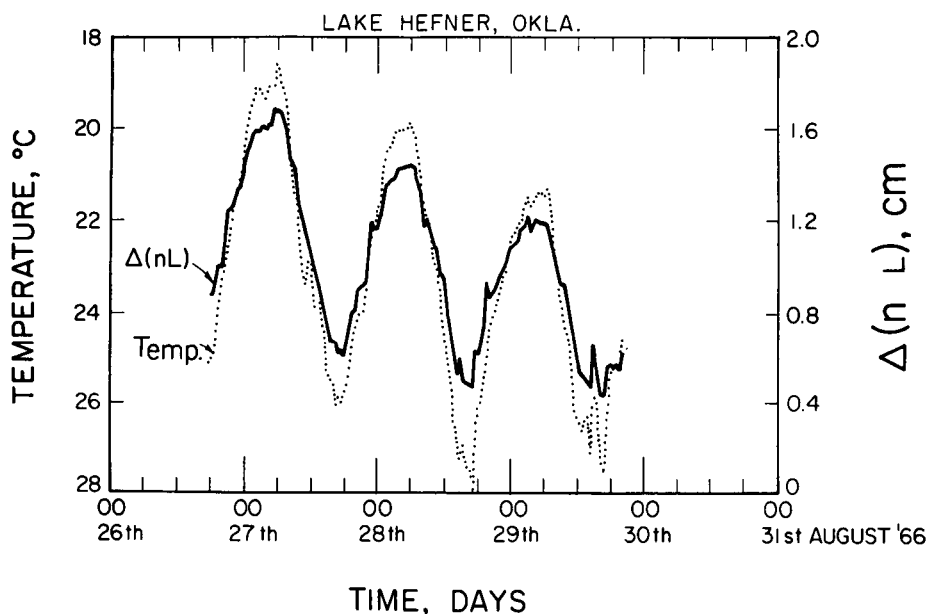


Figure 13. The relationship between optical path length over a 1.5 km path and the temperature measured at the midpoint. In this plot the relative scales have not been properly adjusted, so the variation of path length appears too small.

### 4. POLARIZATION EFFECTS

In theory, the turbulent irregularities in the atmosphere should depolarize a linearly polarized light wave. The effect has been calculated by Saleh (1967) and estimated to be about  $10^{-9}$  per km. He was unable to observe the depolarizing effect of the atmosphere on a 2.6 km path, even with an equipment sensitivity of -42 db. We conclude that at the present time polarization effects are of no practical interest for optical remote sensing of the clear atmosphere using line-of-sight paths.

## 5. THE DETERMINATION OF AVERAGE TEMPERATURE

If we assume that the barometric pressure is known, the average temperature along a fixed open-air path can be determined by comparing the optical path length with the known true geometrical length. The apparatus for doing this could, in principle, be as simple as that shown in Figure 14. This is a

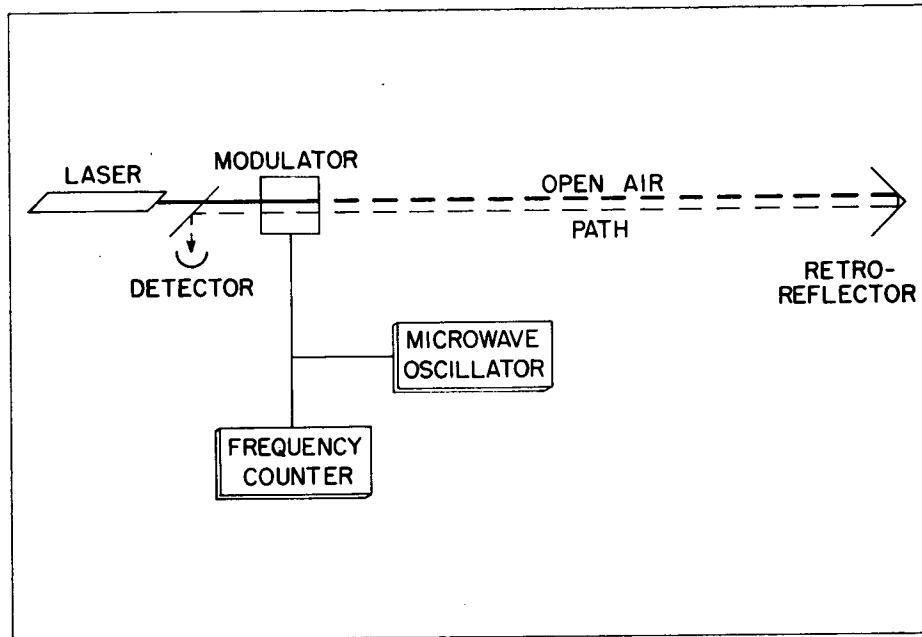


Figure 14. A block diagram of a simple device for measuring average temperature over a fixed path.

modern version of Fizeau's classical experiment. A laser beam is passed through an amplitude modulator and traverses the open-air path to a retro-reflector. It returns through the modulator and is deflected by a beam splitter to a detector. A small adjustment of the modulation frequency is made to minimize the detector output, and the modulation frequency is then measured by the counter. In practice, it would be desirable to provide a means for servo-controlling the oscillator to maintain a null output. The frequency read from the counter provides the optical path length. This can be converted to temperature given only the barometric pressure.

We have already noted that the second-to-second fluctuation in path length caused by turbulence corresponds to a temperature change of less than 0.01 K along the whole path. Thus, turbulence will not be a limitation to measurements of average temperature unless the required accuracy is better than about 0.1 K. For 0.1 K temperature accuracy, the barometric pressure must be measured to 0.3 mb. and both the modulation frequency and the fixed geometrical length of the path to 1 part in  $10^7$ . The effect of varying composition of the air, particularly the effect of water vapor, has been discussed in detail by Owens (1967a). For temperatures near 20° C., a relative humidity error of 15 percent results in a temperature error of 0.1 K.

## PROBING BY OPTICAL METHODS

Determination of the geometrical length to one part in  $10^7$  is at, or perhaps just beyond, the limit of the state of the art, and requires the averaging of a large number of optical measurements taken under various carefully measured weather conditions. In summary, absolute temperature measurements with an accuracy of 1 K or, perhaps, 0.1 K are feasible, and temperature-difference measurements to 0.01 K are possible if the humidity along the path can be measured sufficiently well.

If the path is not fixed, or if the path length is unknown, a more complicated variant of the optical path-length method can be used, utilizing the dispersion of the atmosphere. In round numbers, the atmosphere reduces the velocity of blue light by 330 parts per million while it reduces the velocity of red light by only 300 ppm. Both these numbers are proportional to atmospheric density and therefore, for a given barometric pressure, inversely proportional to temperature. Simultaneous measurement of optical path length with both red and blue light provides the two equations needed to solve for the path length and the temperature. A discussion of this method and its accuracy has been given by Owens (1967b). Briefly, temperature measurements to 1 K are feasible and, with a little elaboration to remove ambiguities, would produce as a byproduct distance measurements accurate to one part in  $10^6$ .

A quite different application of the two-frequency principle suggests itself and is now being investigated in Boulder. Simultaneous measurement of apparent path length with optical and microwave frequencies over a fixed path yields the average temperature and the average water-vapor content. The method has been described by Bean and McGavin.

### 6. THE DETERMINATION OF VERTICAL TEMPERATURE GRADIENT

The beam wandering discussed in section 3 and illustrated in Figure 12 provides a direct indication of temperature gradients along the path. The predominant temperature gradients are in the vertical direction so it is these that are most readily measurable. The sensitivity of the method increases in proportion to path length and, for a 10 km path, a temperature gradient of 1 k/100 m. results in a beam deflection of about  $75 \mu\text{rad}$ . This angle is comparable to moderately strong turbulent broadening of the beam and is easily measurable.

### 7. THE DETERMINATION OF TURBULENCE ALONG THE PATH

We have seen in section 2 that the turbulence along the path must be weighted linearly to account for its effect upon beamwidth, while it has a symmetrical, nearly parabolic weight in its effect upon intensity fluctuations. If the turbulence is uniformly distributed along the path there will be a fixed relationship between beamwidth and log-amplitude variance, at least until the turbulence becomes sufficiently strong to saturate the scintillations. If the turbulence is not uniformly distributed, this relationship will not hold in general. Thus, the simultaneous observation of beam spread and log-amplitude variance

can be used to check the uniformity of the turbulence along a path. There is not, however, enough information in such a pair of measurements to invert the integral and learn any appreciable details of how the turbulence is distributed along the path.

The covariance function of intensity scintillations was shown in Figure 6. The discussion in section 2 showed how this function (or its Fourier transform, the spatial spectrum of the fluctuations) results from the combined effects of the turbulence along the path. The turbulence at each point contributes to the spectrum a limited range of pattern sizes distributed closely around the sizes shown, for example, in Figure 3. Accordingly, if turbulence were absent over a portion of the path, the spectrum of the intensity fluctuations would be distorted in a characteristic way. Figure 15 illustrates this

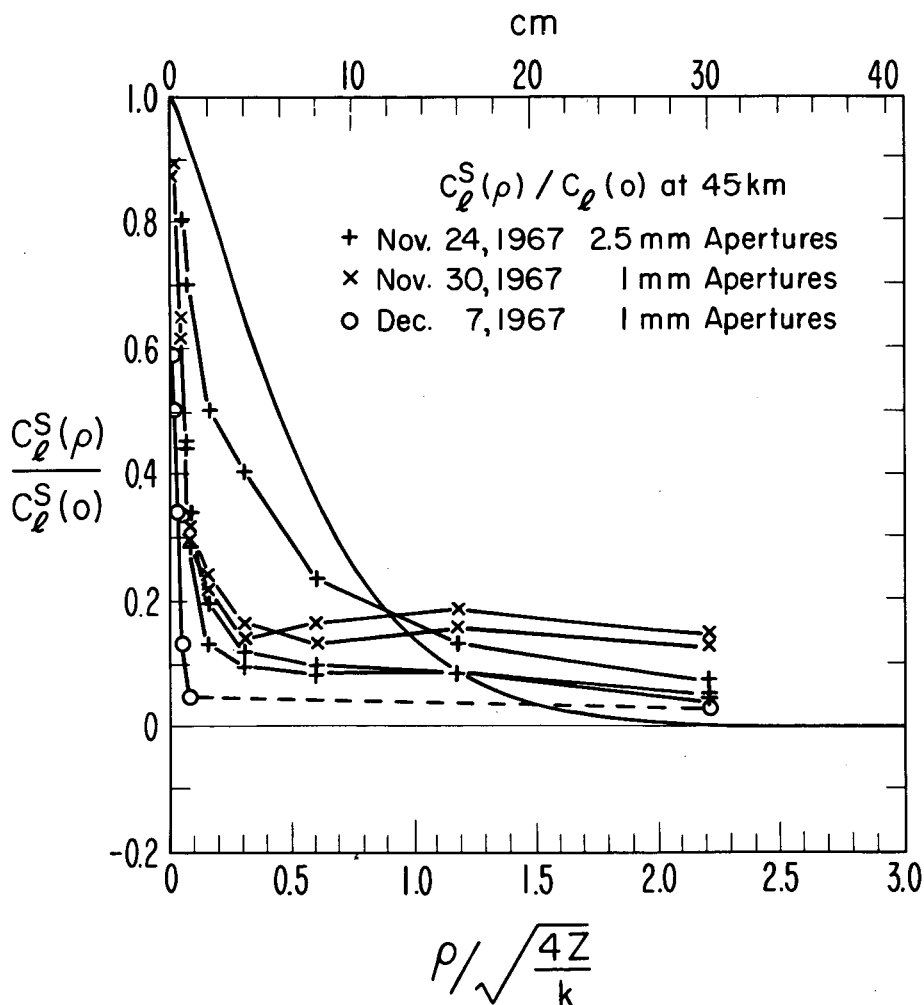


Figure 15. Measurements of the covariance function of scintillations over a 45 km path demonstrate poor agreement with the theoretical curve. This is explained by the concentration of turbulence near the end-points of the path.

## PROBING BY OPTICAL METHODS

effect with measurements taken over a 45 km path near Boulder, Colorado. The smooth, unmarked curve is the theoretical covariance function for uniformly distributed turbulence, taken from Fried (1967b) and plotted for the particular path length and wavelength. The six broken curves, connecting observations made on three different nights, differ systematically from the theoretical curve. The sharp spike with a width of less than 1 cm represents small-scale structure caused by turbulence near the receiver. The long tail, sometimes even peaking in the vicinity of 18 cm, represents large-scale structure caused by turbulence near the transmitter. The absence of scale sizes between these two extremes indicates an absence of turbulence at the middle of the path. This is exactly what might be expected because the path lies between two mountain tops and, except near the end points, is never less than 150 meters above the ground. It is well known that turbulence generally decreases rapidly with height above the ground; Hufnagel (1966) indicates that the turbulence may be expected to have 1600 times less optical effect per unit path length at 150 meters height than at ground level.

Thus, we have a possible method for determining the distribution of turbulence along the path. Like so many remote-sensing techniques, it involves the inversion of an integral to obtain the desired answer. The measurements, themselves, are statistical in nature and so contain a random element, i. e. they are inherently noisy. The noise cannot be reduced indefinitely by extending the observation period because the open atmosphere is notorious for yielding non-stationary time series. Although guesses can be made at the present time, it remains for experiment to disclose how accurate the method can be. Such experiments are in progress at Boulder. Our expectation is that the turbulence distribution can be represented in terms of a third or fourth order polynomial, but probably not in much more detail. Inclusion of beam-spread measurements might yield a slight improvement.

### 8. THE DETERMINATION OF TRANSVERSE WINDS

As a uniform wind blows across the path, it is obvious that the pattern drift velocity will be greater for a pattern caused by irregularities near the laser than for a pattern arising near the receiver. Also, as shown in Figure 3, the former pattern will have a larger scale. Thus, for a uniform wind, the large-scale intensity fluctuations will drift past the receiver more rapidly than will the fine-scale structure.

Now consider the correlation between the intensity fluctuations observed by two point detectors separated by a variable horizontal distance transverse to the optical path. For any given time lag there is a spacing of the detectors that will maximize the correlation. The ratio of this spacing to the time lag determines the drift velocity of those components of the intensity pattern having a size comparable to or larger than the detector spacing. (Notice that the drift velocity is not the same as the apparent velocity that would result from holding the spacing fixed and varying the time lag to maximize the correlation. The difference between these two velocities has been discussed

at length by Briggs, Phillips and Shinn (1950)). It has proved possible to check these ideas with a laboratory setup where two hair driers were arranged to blow hot, turbulent air across a 10-meter laser beam. It was quite easy to observe a bi-modal time-lagged correlogram, the two humps corresponding to the air streams from the two fans. Outdoor experiments, calibrated by a large number of anemometers, are in preparation.

The correlation between the two detectors is a surface parametric in time lag and detector spacing. From the theory of wave propagation through turbulent media it must be possible to express this correlation as an integral of the transverse wind velocity and the strength of turbulence along the path. The determination of wind velocity from scintillation observations then becomes the familiar remote-sensing problem of inverting the integral. Notice that the wind determination is intimately tied to the determination of the distribution of turbulence. As in the previous problem, we can only guess what will be the practical accuracy achievable by this method. Once again, we must deal with observations that are, by their very nature, severely contaminated by noise. Again I suspect that the best we can do may be to determine the coefficients of a third or fourth order polynomial describing the distribution of transverse wind velocities along the path.

## 9. SUMMARY

We have presented, in a mostly qualitative manner and with heuristic arguments, a description of the principal effects of the clear atmosphere upon optical propagation. Several of these phenomena offer possibilities for the remote sensing of atmospheric properties, and we have mentioned in particular the measurement of average temperature, average vertical temperature gradient, and the distribution of turbulence and transverse wind velocity along the path. The first of these has been tested in the field. The second and third have been demonstrated qualitatively with outdoor data, and the fourth has been demonstrated only in the laboratory.

Observation of integrated effects over a line-of-sight path is naturally more practical for the determination of average values over the path than it is for the determination of distributions along the path. While the former may confidently be pursued, the latter should be approached with cautious optimism. We have seen that the appropriate weighting functions and the spectrum of turbulence are smoothly varying. This means that the contribution to the integral from a parcel of atmosphere located at a particular point on the path is irrevocably mixed with the contribution from nearby parcels. Thus it is, in principle, impossible to determine distributions in great detail. We have guessed that four or five independent parameters will be the limiting resolution, but actual tests must be made in the open atmosphere.

## PROBING BY OPTICAL METHODS

### ACKNOWLEDGEMENTS

We thank G. R. Ochs and Dr. J. C. Owens for helpful discussions and permission to use unpublished samples of their data. We also thank Dr. C. G. Little who has helped us to recognize the importance and possibilities of remote sensing and has worked to provide the facilities required to undertake their investigation.

### REFERENCES

- Bean, B. R. and McGavin, R. E., 1967: Electromagnetic phase variability as a measure of water vapor and temperature variations over extended paths, Proceedings of the AGARD-EPC Symposium of Phase and Frequency Instability in Electromagnetic Wave Propagation, Ankara, Turkey, 1967, to be published.
- Beckmann, P., 1965: Signal degeneration in laser beams propagated through a turbulent atmosphere, Radio Science 69D, 4, 629-640.
- Briggs, B. H., Phillips, G. J., and Shinn, D.H., 1950: The analysis of observations on spaced receivers of the fading of radio signals, Proc. Phys. Soc. B63, 106-121.
- Fried, D. L., 1967a: private communication
- Fried, D. L., 1967b: Propagation of a spherical wave in a turbulent medium, J. Opt. Soc. Am. 57, 2, 175-180.
- Hufnagel, R. E., 1966: An improved model turbulent atmosphere, Appendix 3 of: Restoration of Atmospherically Degraded Images, Woods Hole Summer Study, July 1966, National Academy of Sciences, National Research Council.
- Ochs, G. R., 1967: A resistance thermometer for measurement of rapid air temperature fluctuations, ESSA Tech. Rep't. IER 47-ITSA 46.
- Owens, J. C., 1967a: Optical refractive index of air: dependence on pressure, temperature, and composition, Applied Optics 6, 51-59.
- Owens, J. C., 1967b: Recent progress in optical distance measurement: lasers and atmospheric dispersion, Proc. International Symposium Figure of the Earth and Refraction, Osterreichischen Zeitschrift fur Vermessungswesen 25, 153-161.
- Saleh, A. A. M., 1967: An investigation of laser wave depolarization due to atmospheric transmission, IEEE J. Quantum Electronics QE-3, 11, 540-543.

M2-25353

LOCAL ISOTROPY AND REFRACTIVE INDEX FLUCTUATIONS  
IN THE SURFACE LAYER OF THE ATMOSPHERE

Donald J. Portman  
The University of Michigan

ABSTRACT

In the air layer near the ground, atmospheric probing by optical means is influenced by turbulent fluctuations of refractive index. Spectral characteristics of the fluctuations may be significant, for example, in determining mean vertical temperature variations by measuring mean refraction of a horizontal beam. Theoretical and experimental evidence for the existence of local isotropy is briefly examined and conflicting results are found. Recent measurements of temperature spectra support earlier hot wire anemometer and optical scintillation measurements that show little evidence of local isotropy at 1 to 1.5 meters over an extensive uniform and level grass covered field.

1. INTRODUCTION

Characteristics of turbulent fluctuations of refractive index in an optical path usually cannot be ignored to understand or to predict atmospheric effects on optical propagation. Neither can they be ignored if one wishes to deduce atmospheric information from the effects. In the preceding paper, Lawrence gives examples to illustrate the latter point. This note is intended to raise a question about our knowledge of the spectral characteristics of refractive index fluctuations in the layer of air near the ground, a part of the atmosphere often used to study how turbulence influences optical propagation. The specific point to be examined is whether or not there exists a significant size range of turbulent motions that are isotropic at heights of 1 to 2 meters over an extended horizontal plane of uniform roughness. For isotropic turbulence, refractive index spectra may be expected to be proportional to the frequency, or wave number, raised to the  $-5/3$  power in accordance with the theories of Kolmogorov (1941) and Obukhov (1949). For horizontally homogeneous turbulence with thermal stratification it is reasonable to expect wind and temperature spectra to depend on buoyancy forces. This is the case of interest here because only when there is a mean vertical temperature

## ISOTROPY AND REFRACTIVE INDEX FLUCTUATIONS

gradient will there be significant index of refraction fluctuations. Monin (1962) considered this influence and concluded that temperature spectra, for both lapse and inversion conditions, decrease with frequency at a rate less than that for isotropic turbulence.

### 2. TURBULENT REFRACTIVE INDEX FLUCTUATIONS AND MEAN REFRACTION MEASUREMENTS

The significance of isotropy for remote probing of the atmosphere may be illustrated with the example given by Lawrence (loc. cit.) of determining the space average temperature variation with height by measuring the mean refraction of an optical beam. Fleagle (1950) derived a relationship to show that the apparent difference in height between a distant object and its image is proportional to the square of the viewing distance for a given average temperature difference. Practical use of the relationship is hindered, however, by the fact that turbulent index of refraction fluctuations cause the image to fluctuate in size, brightness and position making it difficult, if not impossible, to measure accurately the image position. Tatarski (1961) shows that the variance of the logarithmic intensity fluctuations is proportional to the  $11/6$  power of the path length if the small scale turbulence is isotropic and the spectrum of index of refraction fluctuations follows the  $-5/3$  law in accordance with Kolmogorov's inertial subrange. The result is that the turbulence imposed intensity fluctuations increase with path length nearly as fast as the apparent height difference itself so that an increase in path length may not in fact produce a measurement advantage indicated by Fleagle's equation.

If, on the other hand, the turbulence is not isotropic fluctuation effects may vary with the path length raised to a power different from  $11/6$  and advantages or disadvantages will be experienced accordingly. Portman et al., (1962) reported experimental results for path lengths between 122 and 610 meters (1.5 meters high) in which the power of the path length was found to correspond to 1.56, 1.76 and 1.80 for Richardson numbers of +0.03, +0.011 and -0.065, respectively. The findings indicate a small advantage to be gained by increasing path length to increase precision in measuring optical beam refraction.

For longer paths and stronger turbulence these effects may not be significant since experimental results given by Siedentopf and Wisshak (1948), Gracheva and Gurvich (1965) and Gracheva (1967) show that the path length influence is absent for paths greater than about 1 km. Thus, increasing the optical path beyond 1 km should give advantage in measuring thermal stratification optically. The theories of Tatarski (1967) and of deWolf (1968) show that the critical length depends on the power of the path length. Both authors assume it to be  $11/6$  (again, from the  $-5/3$  law) but if the actual power is less than  $11/6$ , the critical length is less and vice versa. In all cases the critical length depends on the strength of turbulent fluctuations as well as the wave length of light.

### 3. THEORETICAL BASIS FOR ISOTROPY

The question of the existence of the Kolmogorov inertial subrange within a few meters of the ground has been examined both theoretically and experimentally. Most results seem to establish its reality at heights of a meter and above in spite of the fact that Kolmogorov's basic conditions for its existence apparently are absent. This is to say, neither wind shear in the mean motion

nor buoyant energy, the two sources of turbulent energy, satisfy the Kolmogorov requirement that turbulent energy feeding be characterized by scales much larger than those characterizing the smallest motions. It is difficult not to agree with Corrsin (1958) and Monin (1965) in their suggestions that both shear and buoyancy must work at all scales of motion in the layer of air near the ground.

Corrsin's analysis is for shear flow in the absence of buoyancy forces. By considering the characteristic times required for turbulent energy to cascade to smaller scales and to transfer to other components of motion, he concludes that the low wave number limit,  $\kappa_l$ , and upper wave number limit,  $\kappa_u$ , of the inertial subrange are given by the inequalities

$$\kappa_l \gg \varepsilon^{-1/2} \left( \frac{1}{2} \frac{d\bar{u}}{dz} \right)^{3/2}, \quad \kappa_u \ll \left( \frac{\varepsilon}{\nu^3} \right)^{1/4}$$

These reduce to

$$\kappa_l \gg (kz)^{-1} \left( \frac{1}{2} \right)^{3/2}, \quad \kappa_u \ll \left( \frac{u_*^3}{\nu^3 kz} \right)^{1/4}$$

for the usual relationships

$$\varepsilon = \frac{u_*^3}{kz} \quad \text{and} \quad \frac{d\bar{u}}{dz} = \frac{u_*}{kz}$$

for the constant flux layer next to the ground. If the height  $z = 100$  cm, von Karman number  $k = 0.4$ , and kinematic viscosity  $\nu = 0.15 \text{ cm}^2 \text{ sec}^{-1}$ , and for a friction velocity  $u_* = 45 \text{ cm sec}^{-1}$ , corresponding to a two meter wind speed  $u = 500 \text{ cm sec}^{-1}$ , the conditions are, approximately,

$$\kappa_l \gg 0.009 \quad \text{and} \quad \kappa_u \ll 28$$

It appears, therefore, that an inertial subrange of limited extent, say  $0.1 < \kappa < 2.8$ , is to be expected in neutral conditions at 1 meter above ground if the double inequality signs can be interpreted as representing an order of magnitude.

Lumley and Panofsky (1964) extend the analysis to include buoyancy effects. With some assumptions (generally valid only in near neutral conditions) they conclude that in stable stratification the existence of the inertial subrange can, on the average, be assumed for heights above 1 meter. For unstable stratification their estimate is that

$$\text{or} \quad z \geq 100 \nu / u_*$$

$$z \geq 1/3 \text{ cm for } u_* = 45 \text{ cm sec}^{-1} \text{ and } \nu = 0.15 \text{ cm}^2 \text{ sec}^{-1}$$

if the inertial subrange is to exist.

## 4. EXPERIMENTAL FINDINGS

Experimental information on the existence of the inertial subrange may be found in several forms. The most commonly cited are spectral relationships for wind component and temperature fluctuations. In general one dimensional spectral densities are found to be proportional to the  $-5/3$  power of frequency or wave number. (See, for example, Gurvich, 1962; and Tsvang, 1960.) Other conditions used to test the hypothesis are the absence of Reynolds fluxes of heat and momentum for the subrange and the fact that the spectral densities of the cross wind (transverse) components are  $4/3$  times that of the along wind (longitudinal) component in accordance with the analysis of von Karman and Howarth (1938) for isotropic turbulence.

MacCreedy (1962) examined data from a number of sources to describe the inertial subrange within 200 meters of the ground. His summary indicates that the inertial subrange at one meter extends between eddies on the order of 0.1 and 150 cm. He found, also, that one-dimensional velocity spectra characteristically are proportional to  $-5/3$  power of wave number at wave numbers lower than those at which isotropy can be said to exist, a fact that is significant if one attempts to identify the inertial subrange from one-dimensional velocity spectra alone.

In a recent study of turbulence spectra, Busch and Panofsky (1968) examined Round Hill data (heights of 15, 16, 40, 46 and 91 meters) in regard to the Karman-Howarth  $4/3$  relationship. They concluded that: "in regions over which the spectra obey  $-5/3$  power laws, the ratio of the lateral to the longitudinal spectra shows fair agreement with the  $4/3$  ratio predicted by the Kolmogorov hypothesis for the inertial subrange. The vertical-longitudinal ratio has a similar tendency." Examination of their diagrams, however, shows that almost all data for the lower values of  $z/\lambda_N$ , in which  $\lambda_N$  is the Nyquist spatial frequency, *i.e.*, the highest frequency possible to measure for each level, all fall well below the  $4/3$  value. In fact, for the vertical-to-longitudinal spectral density ratios, 50 percent of the data have values equal to or less than unity. For the transverse-to-longitudinal spectral density ratios, more than 50 percent of the data have values less than  $4/3$ . It is difficult to see how the authors arrived at their conclusion on this criterion for the inertial subrange.

Hot wire anemometer measurements were made by Biggs (1966) at a meter above a horizontal and uniformly cut grass surface at Willow Run airfield. (See Portman, Ryznar and Waqif, 1968.) Spectra for  $u$ ,  $v$ , and  $w$  were obtained for five 12-minute periods. Richardson numbers for four of the periods were all about  $-0.01$  and for the fifth about  $+0.07$ . All spectra showed an approximate  $-5/3$  power wave number dependency between wave numbers of 0.01 and 1.0 rad/cm but in all five cases the longitudinal ( $u$ ) spectral densities were greater than comparable spectral densities for the transverse components.

Temperature spectra were not measured, unfortunately, for the above periods of hot wire measurements. More recent measurements, however, have been made at the same location and are soon to be reported. Preliminary analysis for averaged six minute temperature spectra yield the following results:

<u>No. of spectra averaged</u>	<u>Richardson No.</u>	<u>Slope on a ln power-ln wave no. plot</u>
6	-0.025	-1.25
5	+0.015	-1.33
7	-0.027	-1.11, -1.50*
5	-0.062	-1.13, -1.50*

\* The first number applies for wave numbers less than  $2.5 \times 10^{-2}$  rad/cm and the second for wave numbers greater than  $2.5 \times 10^{-2}$  rad/cm.

Hot wire anemometer measurements to accompany these data have not yet been processed. These results deviate significantly from the  $-5/3$  power law and support the earlier hot wire anemometer measurements, made at the same location under similar conditions, in showing no evidence of isotropy.

Brightness fluctuations within a laser beam (scintillation) were measured along with temperature and wind component spectra at the Willow Run field station. (The optical path was 500 meters long and about 1.5 meters above ground.) Scintillation spectra are related to refractive index spectra (Tatarski, 1961) and it might be expected that deviations from isotropy would appear in the measured scintillation spectra. For one set of measurements (Portman, Ryznar and Waqif, 1968) it was found that spectra for inversion conditions showed a marked suppression of low frequency scintillation and those for lapse conditions showed a weak low frequency enhancement, both in comparison to Tatarski's isotropic model. Subsequent measurements, however, have been partially inconsistent with this finding. It appears that representation of the refractive index spectra by a simple power law may be inadequate to relate temperature spectra, such as those given above, to scintillation spectra. If such is the case, it is evident that the spectral regions significant for optical diffractive effects are not isotropic for these conditions.

## 5. CONCLUSIONS

Spectral characteristics of index of refraction fluctuations in the layer of air near the ground are significant for understanding atmospheric influences on optical propagation, and therefore, for probing the atmosphere with optical techniques. Both theoretical and experimental findings are inconclusive in regard to whether or not an inertial subrange of significant wave number interval actually exists at heights of 1 to 2 meters above ground. Most experimental evidence is based on the observation of a  $-5/3$  power dependency on wave number, a relationship that is known to exist in anisotropic regions of the spectrum. Relationships between wind component spectral densities, careful examination of temperature spectra, and certain optical scintillation measurements, however, do not support the existence of the inertial subrange at this height. Since wave number limits of the inertial subrange are expected to increase in separation with increasing height, optical experiments that are strongly dependent on the existence of isotropy and a  $-5/3$  power law should be conducted at heights well above the ground. There is an important need for more information on the structure of turbulence near the ground and how the spectral characteristics of refractive index fluctuations depend on both the structure and the height above ground.

## ISOTROPY AND REFRACTIVE INDEX FLUCTUATIONS

### ACKNOWLEDGEMENTS:

Measurement and analysis of recent Willow Run observations of wind, temperature and scintillation were the work of Messrs. Edward Ryznar, Kenneth Davidson and Allen Davis. Their contributions are gratefully acknowledged.

### REFERENCES

- Biggs, W. G., 1966: Measurement and Analysis of the Structure of Turbulence near the Ground with a Hot Wire Anemometer System. Ph.D. thesis. Dept. of Meteor. and Ocean., The University of Michigan., 128 pp.
- Busch, N. E. and H. A. Panofsky, 1968: Recent spectra of atmospheric turbulence. Quart. J. Roy. Meteor. Soc., 94, 132-148.
- Corrsin, S., 1958: Local isotropy in turbulent shear flow. NACA RM 58B11, 15 pp.
- de Wolf, D. A., 1968: Saturation of irradiance fluctuations due to turbulent atmosphere. J. Opt. Soc. Amer., 58, 461-466.
- Fleagle, R. G., 1950: The optical measurement of lapse rate. Bull. Amer. Meteor. Soc., 31, 51-55.
- Gracheva, M. E., 1967: Investigation of statistical properties of strong fluctuations of light intensity in the atmospheric layer near the earth. (English Transl.) Izv. V.U.Z. Radiofizika, 10, 775-788.
- and A. S. Gurvich, 1965: Strong fluctuations in the intensity of light propagated through the atmosphere close to the earth. (English Transl.) Izv. V.U.Z. Radiofizika, 8, 511-515.
- Gurvich, A. S., 1962: The pulsation spectra of the vertical component of wind velocity and their relations to the micrometeorological conditions. (English Transl.) Akad. Nauk SSSR, Trudy, No. 4, 101-136.
- Kolmogorov, A. N., 1941: The local structure of turbulence in an incompressible viscous fluid for very large Reynolds numbers. C.R. (Doke.) Akad. Sci. USSR, 30, 301-305.
- Lumley, J. L., and H. A. Panofsky, 1964: The Structure of Atmospheric Turbulence. New York, Interscience, 239 pp.
- MacCready, P. B., Jr., 1962: The inertial subrange of atmospheric turbulence. J. Geophys. Res., 67, 1051-1059.
- Monin, A. S., 1962: On the turbulence spectrum in a thermally stratified atmosphere. (English Transl.) Izv. Akad. Nauk SSSR, Geophys. Ser. 1962, 397-407.
- , 1965: On the influence of temperature stratification upon turbulence. Proc. Intern. Colloq. Atmos. Turb. and Radio Wave Prop. Moscow, Nauka, 375 pp.

- Obukhov, A. M., Structure of the temperature field in a turbulent flow. Izv. Akad. Nauk SSSR, Geogr. and Geophys. Ser. 1949, 58-70.
- Portman, D. J., F. C. Elder, E. Ryznar and V. E. Noble, 1962: Some optical properties of turbulence in stratified flow near the ground. J. Geophys. Res. 67, 3223-3235.
- , E. Ryznar and A. Waqif, 1968: Laser scintillation caused by turbulence near the ground. U. S. Army Cold Regions Res. and Eng. Lab. Res. Report 225, 77 pp.
- Siedentopf, H. and Wisshak, 1948: Die Scintillation on der Strahlung terrestrischer Lichtquellen and ihr Gang mit der Tageszeit. Optik, 3, 430-443.
- Tatarski, V. I., 1961: Wave Propagation in a Turbulent Medium. New York, McGraw-Hill. (Trans. by R. A. Silverman), 285 pp.
- Tatarski, V. I., 1967: Propagation of Waves in a Turbulent Atmosphere. Moscow, Nauka, 548 pp. (In Russian).
- Tsvang, L. R., 1960: Measurements of temperature pulse frequency spectra in the surface layer of the atmosphere. Izv. Akad. Nauk SSSR, Geophys. Ser. 1960, 1252-1262.
- von Karman, T. and L. Howarth, 1938: On the statistical theory of isotropic turbulence, Proc. Roy. Soc., A164, 192-215.

## OPTICAL PROPAGATION IN A NEAR-EARTH ENVIRONMENT

Paul H. Deitz

U. S. Army Ballistic Research Laboratories

## ABSTRACT

This paper describes optical measurements of the magnitude of scintillation as a function of the range and refractive index structure coefficient,  $C_n$ . The results are compared with the Tatarski and deWolf geometrical optics saturation equations. In addition, a variation in the Kolmogorov turbulence model is suggested to account for certain observed optical and meteorological parameters.

## 1. INTRODUCTION

During the past year, experiments were initiated to test the well-known log-amplitude variance equation of Tatarski, describing the effect of scintillation. Tests made first with a pulsed ruby laser as a source were later extended to include measurements with a helium-neon laser. During a majority of the tests, the refractive index structure coefficient,  $C_n$ , was measured by means of a high-speed, temperature-differential system. These experiments clearly show a saturation of scintillation magnitude with increasing range and  $C_n$ . In addition, some of the characteristics of propagation under temperature inversion conditions were investigated. A change in the Kolmogorov turbulence model is suggested to account for certain observed optical and meteorological parameters.

## 2. THEORY AND BACKGROUND

Central to the development of the log-amplitude variance equation is the employment by Tatarski of the Rytov approximation. Higher order terms in the Born series formulation of the wave equation are dropped. Thus Tatarski (1960) obtains in this approximation an expression giving the log-intensity variance of a plane wave as

$$\sigma^2 = 1.23 C_n^2 k^{7/6} L^{11/6} \quad (1)$$

where  $C_n$  is the index structure coefficient,  $k$  is the wave number of the light, and  $L$  is the path length. The solution of the wave equation for spherical wave propagation using the same approximations, given by Fried (1967), is identical to Eq. (1) except for the constant which is evaluated as 0.496.

This formulation went essentially untested until experiments were performed by Gracheva and Gurvich (1965) in which temporal fluctuations of intensity were monitored over ranges from 125 to 1750 meters using a mercury arc source. Simultaneous with the optical data, Richardson's number was measured. Through this parameter,  $C_n$  was inferred by a method reported by Tsvang (1962). These experiments showed that the variance did not increase indefinitely with  $L$  and  $C_n$ , but reached a maximum. Tatarski (1967) developed formulation to show that saturation could be achieved theoretically. One such evaluation gives the log-intensity variance as

$$\sigma^2 = 4\{1 - (1 + 6\sigma_1^2)^{-1/6}\} \quad (2)$$

where

$$\sigma_1^2 = \frac{\pi^2 \cdot 0.033 \Gamma(7/6)}{24} C_n^2 L^3 k_m^{7/3} \quad (3)$$

Here  $\Gamma$  indicates a gamma function,  $C_n$  is the index structure coefficient,  $L$  is the path length, and  $k_m$  is the Obukov scale. Tatarski finds the product of  $k_m$  and the inner scale,  $l_0$ , equal to 5.48.

More recently, deWolf (1968) has predicted a saturation of scintillation magnitude by evaluating higher order terms in the Born series formulation of the scalar integral wave equation. He gives the variance as

$$\sigma^2 = \ln\{2 - \exp(-\sigma_1^2)\} \quad (4)$$

where  $\sigma_1^2$  is the variance for the plane wave solution given earlier in Eq. (1).

### 3. EXPERIMENTAL METHOD

The optical measurement method employed here utilizes a photo-optical technique to record directly a 61-cm cross section of a received optical beam. The receiving system used is essentially a telescope with the image plane located at a position conjugate to the entrance aperture of the system rather than to the far field. Thus, a photograph is made of the distribution of energy across a 61-cm aperture. After appropriate calibration, the film is scanned with a densitometer and computer-corrected to give unidirectional scans of intensity versus distance (in object space). The scanning aperture of the densitometer corresponds to an aperture a few millimeters in object space so that the highest spatial frequencies can be resolved.

In order to measure  $C_n$ , instrumentation was utilized which incorporates two high-speed thermometers. These are arranged in a Wheatstone bridge circuit to give a difference signal proportional to the temperature gradient between the two probes. The RMS value of this signal can be used to compute a mean value of  $C_T$ , the thermal structure coefficient, and hence  $C_n$ .

4. MEASUREMENT RESULTS

A pulsed ruby laser was used to make measurements over ranges of 200 to 1500 meters at a beam height of 2 meters above ground. Figure 1 shows a typical cross-section photograph taken at a range of 1000 meters. The magnification of the image can be judged from the diameter of the observable field (61 cm). One-dimensional scans from such photographs, converted to energy as a function of distance, were used to compute a variance using the formulation

$$\sigma^2 = \ln\left\{1 + \frac{\sigma_1^2}{(\bar{I})^2}\right\} \quad (5)$$

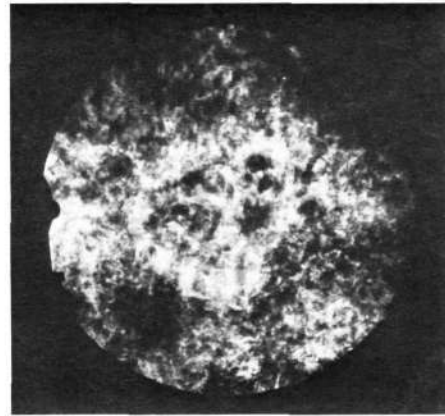


Figure 1. Cross Section of Pulsed Ruby Laser at 1000 Meters

where  $\sigma_1$  is the normal variance and  $\bar{I}$  is the mean intensity.

Tests were made in which the log-intensity variance was measured for various path length and  $C_n$  values. The results of these tests are shown in Figure 2. Here the measured standard deviations, derived using Eq. (5), are plotted against the square root of Eq. (1), corrected to the Fried coefficient. The Tatarski and deWolf formulations (Eqs. (2) and (4)) are also shown. One of the indications

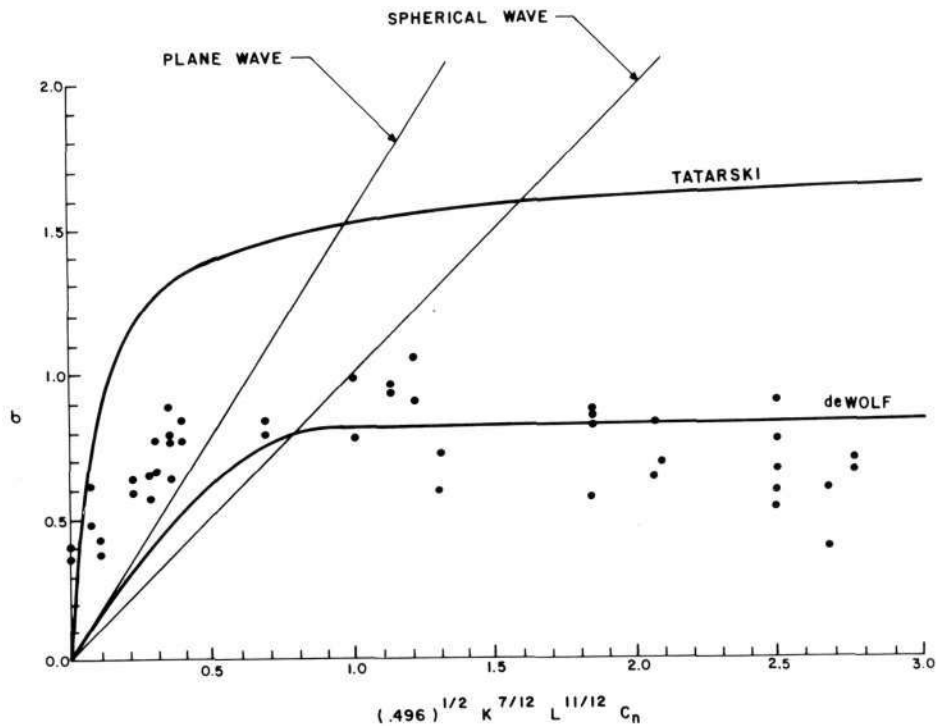


Figure 2. Measured Standard Deviations as a Function of Range, L, and Refractive Index Structure Coefficient,  $C_n$

of these data is that beyond a range of about 500 meters (depending on the magnitude of  $C_n$ ) the strength of the optical turbulence ( $C_n$ ) cannot be quantified by an optical measurement using, for instance, Eq. (1).

##### 5. METEOROLOGICAL MODEL

The cross sectional energy distribution in an optical beam (such as indicated in Figure 1) may be thought of as the realization of the spectral interaction of an optical filter function and a three-dimensional spectrum of turbulence. Tatarski (1960: see Fig. 11, p. 140) has formulated an optical filter function for an infinite plane wave which acts as a high bandpass filter on the turbulence spectrum (which is a low bandpass filter) given by Kolmogorov (1941). Carlson and Ishimaru (1968) have indicated that the optical filter function for beam-wave propagation is different than for infinite wave propagation; i.e., for high wave numbers the optical filter function does not damp to unity, but rather peaks at some wave number and then diminishes to zero. The peak of the filter function is set by the beam diameter of the diffraction-limited transmitter and moves to lower wave numbers for larger diameters. Thus, depending on the beam width, various turbulence domains are sharply weighted as to their contribution to the beam modulation. These results suggest a method of probing the index medium to ascertain the strength of fluctuations in various turbulence domains (integrated over the optical path within the range of saturation).

The importance of these spectral interactions is indicated by the character of data gathered using a helium-neon laser. Figure 3 shows a beam cross-section photograph made of a CW laser (2-millisecond exposure) at a range of 650 meters. This picture was taken during a summer afternoon under high temperature lapse conditions. The image is composed of small intensity cells with sharp edges.

Figure 4 shows a photograph made with the identical optical configuration after nightfall during a temperature inversion. There are pronounced variations in the intensity regions, but the scale for the variations is larger and the edges of the intensity cells are not as sharp. In addition, a low-contrast fringe pattern can be observed in the image. This effect is caused by an interference filter element in the optical receiver which is acting as a Fabry-Perot

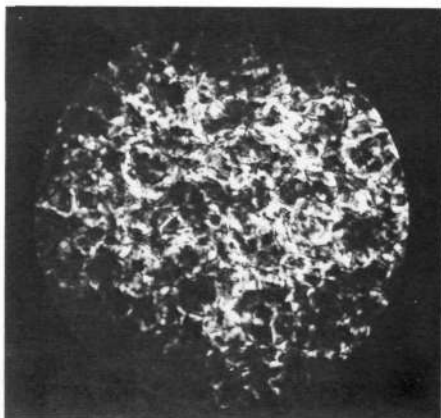


Figure 3. Cross Section of Helium-Neon Laser at 650 Meters, Lapse Conditions

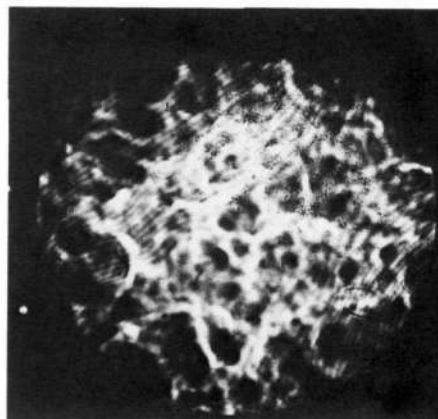


Figure 4. Cross Section of Helium-Neon Laser at 650 Meters, Inversion Conditions

etalon. The fringes indicate a large transverse coherence width made observable by a large temporal coherence length. Secondly, there are diffraction patterns of high spatial frequency in the upper right-hand corner of the image due apparently to dust particles or a smudge on one of the lenses of the receiving system.

It may be conjectured that a change in the statistics of the turbulence is responsible for the variation in the optical parameters. Measurements taken with the  $C_n$  apparatus under inversion conditions indicate an outer scale of turbulence (here meant to be the largest scale size for which the "two-thirds law" applies) on the order of or less than 30 cm. It can be expected that as the outer scale of turbulence decreases less energy is injected into the medium, and viscous forces tend to dissipate the energy at a larger inner scale. Measurements of temperature spectra by Tsvang (1960) lend support to this view. During inversion conditions, both a decrease in the outer scale and an enlargement of the inner scale are indicated.

Such a change in the Kolmogorov model may explain the observed optical characteristics. The amplitude and phase filter functions of Tatarski (1960: Eqs. (7.87) and (7.88), p. 151) indicate that the high wave number turbulence contributes most to amplitude fluctuations and that the low wave number turbulence contributes most to phase fluctuations. An expansion of the inner scale will tend to increase the intensity correlation interval. Spatial correlations of beam photographs have shown this shift. A reduction in size of the outer scale will tend to increase the dimension over which the phase front is unperturbed. As this dimension approaches the size of the diffracting object (dust particle or lens anomaly referenced to object space), diffraction images will begin to appear.

## 6. SUMMARY

Log-intensity variances have been measured for optical paths from 200 to 1500 meters over a range of  $C_n$  values. For high  $C_n$  conditions, the variance is seen to saturate at about 500 meters. Beyond this range, the optical variance cannot be used to compute a strength parameter for the turbulence.

In addition, the significance of the optical filter function and the Kolmogorov turbulence model is discussed. A modification of the Kolmogorov spectrum is suggested to account for the character of optical data gathered during temperature inversion conditions. Because of the close relationship between the optical propagation effects and the underlying meteorology, the importance is stressed of performing careful experiments in which both meteorological and optical parameters are examined.

## 7. ACKNOWLEDGMENT

The author gratefully acknowledges the assistance of Mr. N. J. Wright in the gathering and reduction of the data.

## REFERENCES

- Carlson, F. P., and A. Ishimaru, 1968: To be published.  
 deWolf, D. A., 1968: Saturation of irradiance fluctuations due to turbulent atmosphere. *J. Opt. Soc. Am.* 58, 461.

OPTICAL PROPAGATION IN A NEAR-EARTH ENVIRONMENT

- Fried, D. L., 1967: Propagation of a spherical wave in a turbulent medium (see Eq. (1.13)). *J. Opt. Soc. Am.* 57, 175.
- Gracheva, M. E., and A. S. Gurvich, 1965: Strong fluctuations in the intensity of light propagated through the atmosphere close to the earth. *Izv. Vuzov, Radiofizika* 8, 717.
- Kolmogorov, A. N., 1941: The local structure of turbulence for very large Reynold's numbers. *Proc. Acad. Sci. USSR*, Vol. 30, No. 4.
- Tatarski, V. I., 1960: *Wave Propagation in a Turbulent Medium*. New York, McGraw-Hill Book Company, Chapters 9 and 12.
- Tatarski, V. I., 1967: On strong fluctuations of the amplitude of a wave propagating in a medium with weak random inhomogeneities. *Radiofizika* 10, 48.
- Tsvang, L. R., 1960: Measurements of temperature pulse frequency spectra in the surface layer of the atmosphere. *Izvestia, ANSSSR, Geophys. Ser.*, No. 8, 1252.
- Tsvang, L. R., 1962: *Tr. IFA, Atmospheric Turbulence* 4, 137.

N72-25235

INCOHERENT AND COHERENT CW LASER SYSTEMS FOR  
REMOTE ATMOSPHERIC PROBING

R. F. Lucy

Sylvania Electronic Systems  
Applied Research Laboratory  
Waltham, Massachusetts 02154

ABSTRACT

This report summarizes typical laser systems now available for atmospheric probing. Experiments comparing coherent and incoherent receiving techniques are described and typical performance data presented.

1. INTRODUCTION

A narrow CW laser beam could be used to remotely probe the refractive effects in the atmosphere. These refractive effects at optical wavelengths are produced by temperature differences and motion of the air over the transmission path between the laser beam source and the optical receiver. With an optical probe only average effects produced by the path may be discernible. Single and multiple probes can be employed. A description of theory, experiments, and references have been presented to the panel by other contributors.

Experimenters will have not only a choice of wavelength but a choice of receiver and transmitter configurations. Beamwidths, background noise radiation, transmitter apertures, and receiving apertures and pointing requirements are important considerations, as well as transmitter power and receiver sensitivity. In addition, the environment near the receiver and transmitter may require special design in order to minimize strong effects at the interface between the experiment and the atmosphere to be probed.

## 2. TRANSMITTERS

The transmitter would probably generate a simple spherical or plane wave over a predetermined aperture, and diffraction, as well as geometrical, optics effects must be considered. The transmitter beam may be either convergent, divergent or diffraction-limited plane parallel. Conical or cylindrical beam geometries are also an option to the experimenter. Wavelengths, such as 4880 Å, 5145 Å, 6328 Å, 3.39 $\mu$  and 10.6 $\mu$ , are now available in single mode, CW lasers. Optical modulators<sup>1</sup> are available and a variety of optical modulation techniques, including amplitude, phase, frequency, and polarization modulation, can be implemented. The modulation can be applied from dc up to several gigahertz.<sup>2</sup>

## 3. INCOHERENT RECEIVERS

At the receiver the experimenter can use either or both incoherent and coherent detection methods.<sup>3,4</sup> The incoherent detector, will measure the incident instantaneous optical power and produce current or voltage proportional to the optical power. If the aperture optics focuses the power received onto a simple detector, then the integral of the power over the aperture is measured. In addition, angle-of-arrival data may also be obtained by measuring focused signal motion in the optics focal plane. Narrow-band optical filters tuned to laser frequencies and field stops to minimize the receiver field of view will be required to keep scattered sunlight and other unwanted radiation from interfering with the measurements. Unwanted radiation can produce noise that will limit receiver sensitivity. The need for a restricted field of view introduces a pointing requirement in an incoherent receiver.

The minimum aperture size or system resolution realizable will be strongly influenced by the available power density, receiver sensitivity needed, experiment accuracy, and required receiver bandwidth. Thus, resolution of signal structure over the aperture may be limited. Both imaging and point detectors can be used. A scanning point detector, such as an image dissector in the visible, or mechanical scan device in the infrared, can be employed to dissect a large optical receiver aperture, reduced in size by the optics, into smaller elements. Television image tubes are also applicable in the visible. In any event, the detector integration time and scan period must be faster than expected time variations due to the transmission path.

#### 4. COHERENT RECEIVERS

A coherent receiver may offer additional advantages not realized by incoherent receivers.<sup>3,4</sup> A coherent receiver uses a local phase reference that allows phase difference measurements to be made over the aperture. (This capability at an optical wavelength scale may allow a microprobe technique to be developed.) The received wave is added to the locally generated wave and then squared by the optical square law detector. The photocurrent or voltage represented by the cross product term is proportional to the scalar product of the local electromagnetic field and the received electromagnetic field. If the two fields are oscillating at different frequencies, then the resultant photocurrent or voltage beat is at the difference frequency. The coherent receiver is both amplitude and phase sensitive. Point-to-point phase differences across the incoming optical wave can be observed by simultaneously detecting the beat frequency relative to the local reference and comparing the phase of the two beat frequency signals. Alignment between the local and received signals is extremely critical.<sup>5</sup>

The wavefront over the receiver aperture is nonuniform as a result of propagating through the atmosphere. In communications receivers this represents noise;<sup>6</sup> in a remote probe this represents the measured quantity. When the signals of many phases and amplitudes are collected and heterodyned with the local reference, currents of many phases and amplitudes determined by the received optical wave are generated. If many portions of an aperture containing different phases and amplitudes are simultaneously imposed on a single detector, then the resultant beat frequency will be the vector sum of all the currents. Since there will probably be numerous phases, the resultant beat signal can be averaged out. The sensitivity of this receiver could thus be much less than a corresponding incoherent receiver. Angle-of-arrival fluctuations produced by the atmosphere near the receiver aperture will severely degrade the receiver performance. The commonly used antenna theorem<sup>5</sup> for a coherent aperture requires that the product of receiver field of view and aperture area should be equal to or less than the square of the wavelength if the receiver coherent efficiency is to be large. Consequently, at longer wavelengths receiver pointing accuracy and aperture atmosphere interfaces are less demanding and apertures can be larger than at shorter wavelengths.

## INCOHERENT AND COHERENT CW LASER SYSTEMS

When using large collecting apertures, the coherent receiver may demonstrate poor performance. However, when using apertures that are less than the coherence size of the received wave, a coherent system can be used to measure small angle fluctuations produced by the atmosphere with great sensitivity.

A major advantage of a coherent system over an incoherent system is that in the coherent system random noise from the detector and radiation background can be discriminated against.<sup>3,4</sup> When operating at the shorter wavelengths where the sun is a prime noise source, this approach may be invaluable. In addition, when operating at longer infrared wavelengths where detectors may be noisy, the coherent technique is necessary if a sensitive system is to be implemented.<sup>3</sup>

### 5. COMPARISON OF COHERENT AND INCOHERENT TECHNIQUES AT 6328 Å

Several experiments were performed at 6328 Å to obtain quantitative data due to atmospheric-induced scintillation on a coherent optical receiver system.<sup>7</sup> Parameters that were varied included transmitter aperture, receiver aperture, and transmitter beam divergence. The signal intensity variations, as well as the envelope of the heterodyne signal, were simultaneously recorded on magnetic tape for further computer processing. Of particular interest was the comparison of incoherent and coherent modes of detection. A comparison was also made for different weather conditions.

Three configurations demonstrating transmitter options were employed and are shown in Figure 1. In Experiment A all the energy was focused into the receiver aperture and the transmitter aperture was varied. In Experiment B a nearly plane wave was formed at the transmitter aperture and the receiver aperture was varied. In Experiment C a small transmitter aperture and a diverging beam were used and the receiver aperture was varied. Transmitter and receiver were separated by 1 kilometer. The beam traversed over a path consisting of buildings, parking lots, and trees. In all cases the beam was at least 5 meters above the underlying terrain and objects. In every case it was found that the coherent system signal fluctuations, due to atmospheric turbulence, was considerably greater than in the incoherent system. This result shows the greater sensitivity of the coherent system to the time-varying wavefront breakup produced by atmospheric turbulence.

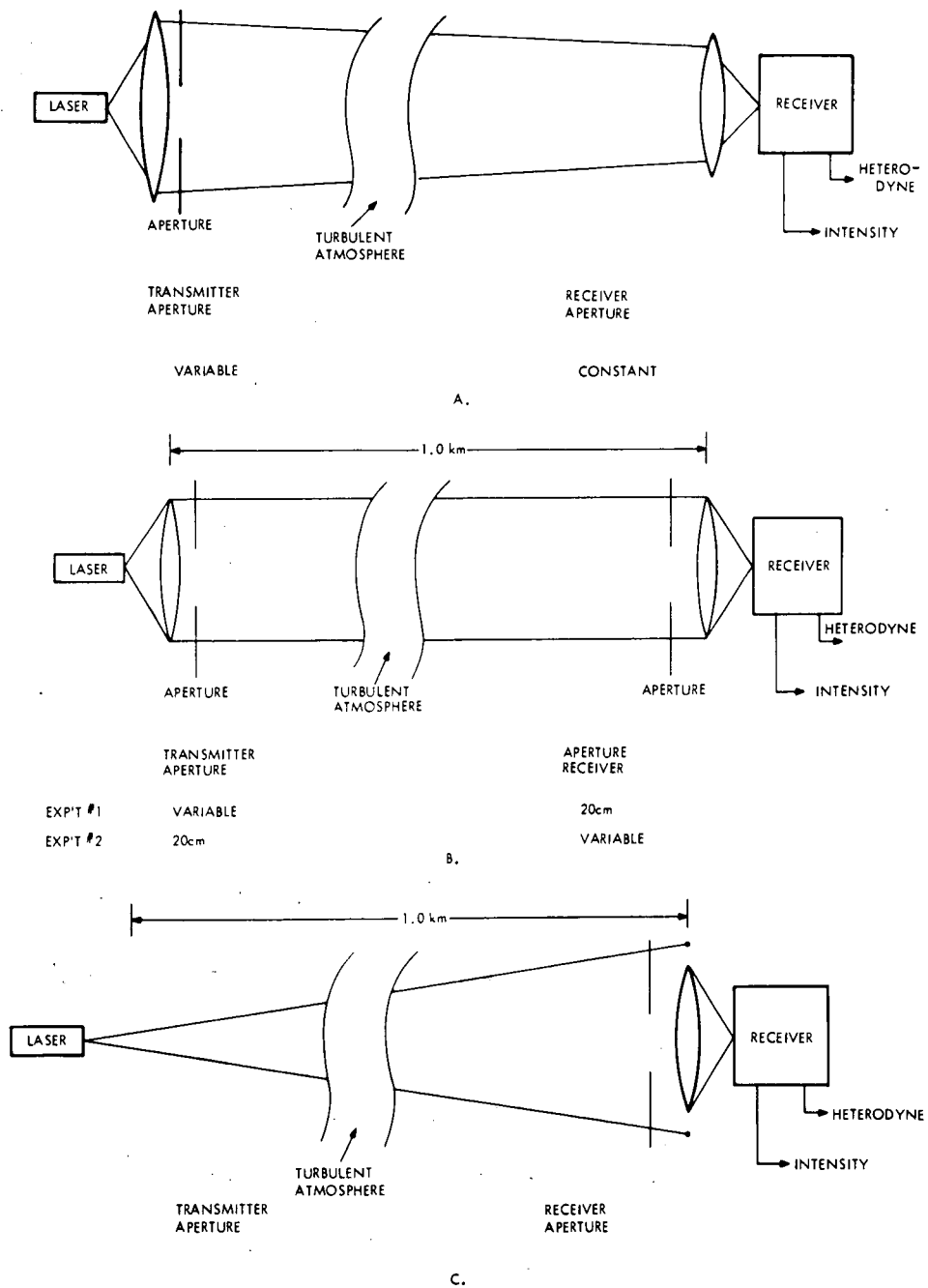


Figure 1. Signal fading experiment to compare coherent and noncoherent detection.

## INCOHERENT AND COHERENT CW LASER SYSTEMS

Figure 2 shows comparative cumulative probability data for the parallel beam case when the receiver was apertured. The data corresponds to a 1-minute sample taken near noontime on a sunny day. The rapid decrease in signal probability from unity toward zero is indicative of the larger effects in the coherent output as compared to the incoherent output. This is due to the additional phase sensitivity of the coherent system. Figure 3 compares performance on a clear sunny day to a light rainy day. The signal fluctuation spectra for the data of Figure 3 is shown in Figure 4. Note that the coherent system appears to have a greater number of higher frequency components. This may be due to the effect of the wind.

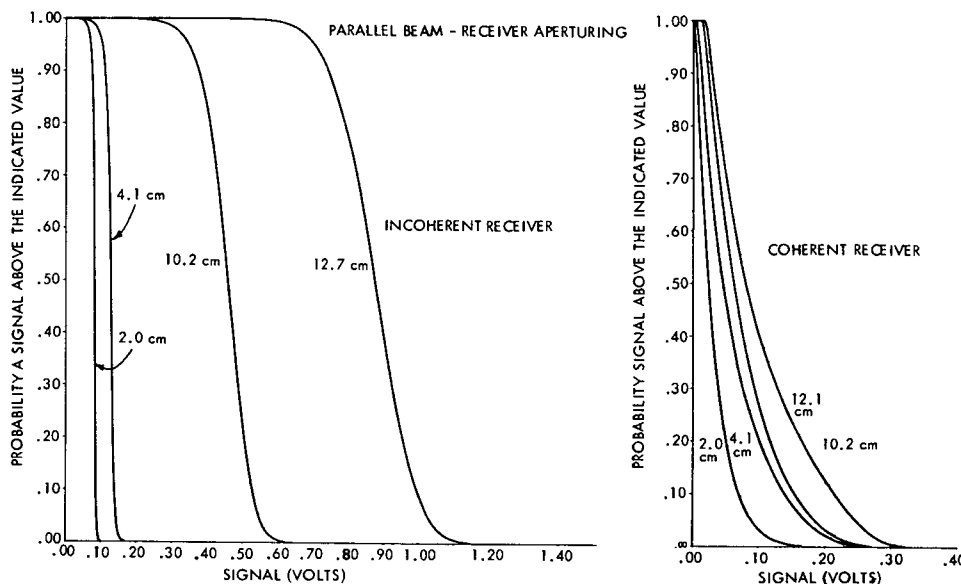


Figure 2. Comparison of incoherent and coherent signal probabilities.

### 6. COHERENT EXPERIMENT AT 10.6 MICROMETERS

An experiment to provide initial evaluation of atmospheric turbulence effects on coherent propagation at 10.6 micrometers was performed. The experiment utilized homodyne detection and was set up utilizing the 6328 Å optical superheterodyne receiver optics. A moving corner reflector, 1 kilometer from the equipment, was used to reflect the transmitted signal back to the receiver.

Signal fluctuations produced by the atmosphere were easily observed in the return signal. From visual estimates the approximate depth of many of these fluctuations was about 6 dB below the peak and occurred at rates from about 1 Hz to 20 Hz. It was significant to note that the measured peak mixing efficiency was as high as 38 percent. Typical mixing efficiencies measured at 6328 Å on a similar day have been found previously to be only

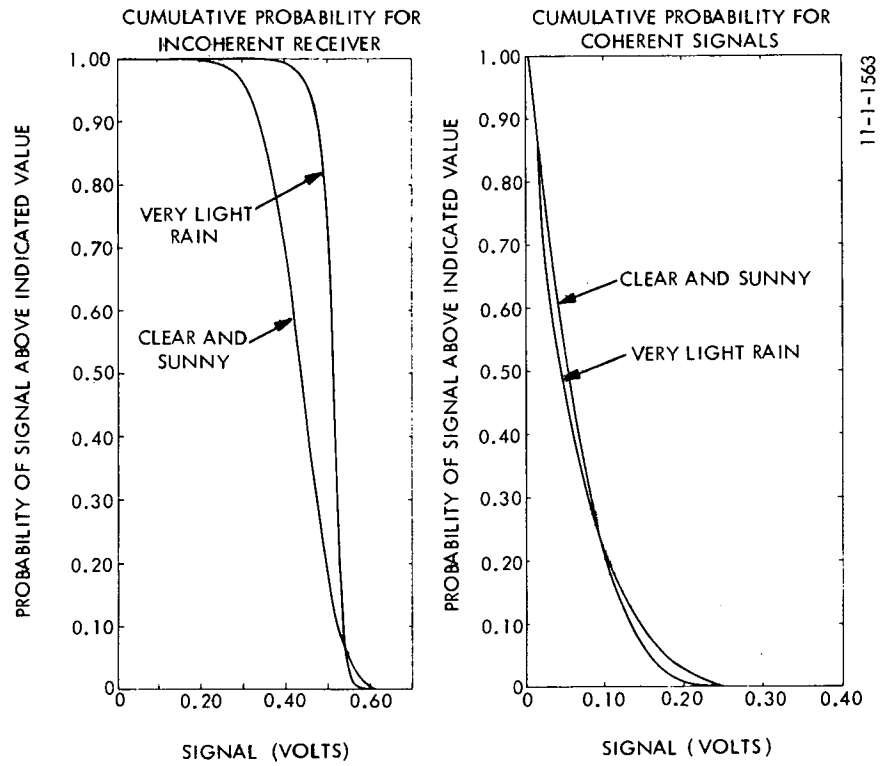


Figure 3. Effects of weather on signal probabilities.

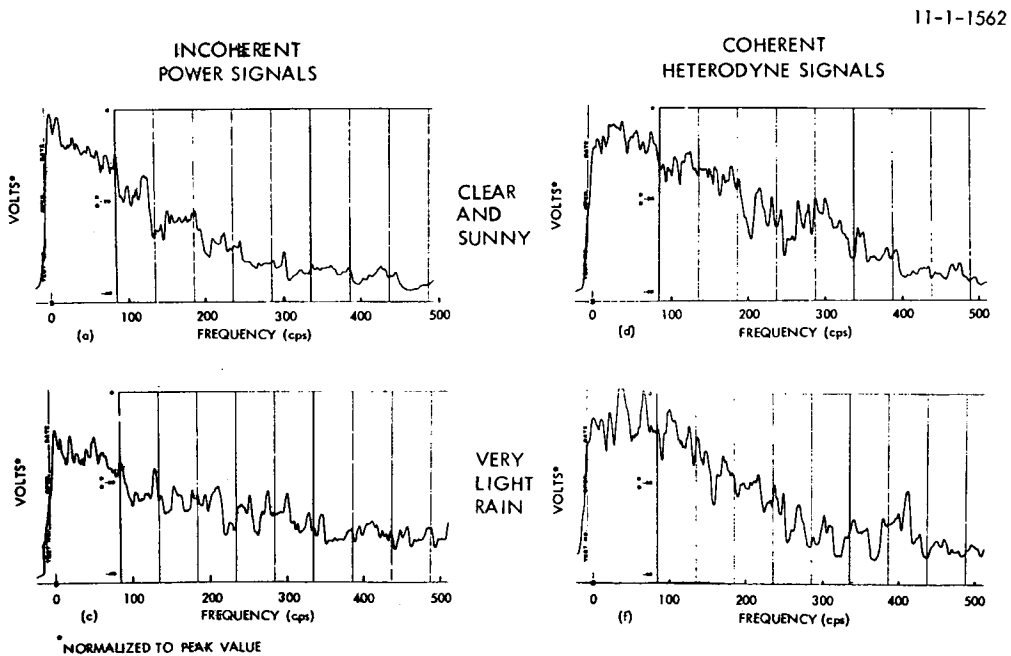


Figure 4. Comparison of signal fluctuation spectra.

## INCOHERENT AND COHERENT CW LASER SYSTEMS

a few percent.<sup>7</sup> This data, when compared with the performance of similar experiments at 6328 Å, shows the anticipated reduced angular sensitivity at the longer wavelength.

### 7. CONCLUSIONS

The technology to implement remote probing experiments using narrow laser beams as a tool is available. Plane or spherical, narrow frequency, optical beams can be formed to propagate through a turbulent atmosphere to a receiver. Detection techniques are available to measure the spatial and temporal amplitude, phase, direction, and polarization characteristics of the beam at the receiver. Use of a coherent system, that is extremely sensitive to phase and angle fluctuations, may offer atmospheric probing technique for microscale measurements.

### 8. RECOMMENDATIONS

A closely unified theoretical and experimental effort should be initiated to develop the techniques of atmospheric probing using narrow laser beams.

### REFERENCES

1. Rattman, W. J., Bicknell, W. E., Yap, B. K., Peters, C. J., Nov. 1967: Broadband, low power electrooptic modulator. IEEE J. Quantum Elec., QE-3, 550-554.
2. Bicknell, W. E., Yap, B. K., Peters, C. J., Feb. 1967: 0-3 GHz Traveling wave electrooptic modulator. Proc. IEEE, 55, 2, 225-226.
3. Fried, D. L., Seidman, J. B., Feb. 1967: Heterodyne and photon counting receivers for optical communications, Appl. Optics, 6, 245-250.
4. Biernson, G., Lucy, R. F., Jan. 1963: Requirements of a coherent laser pulse doppler radar. Proc. IEEE, 51, 202-213.
5. Siegman, A. E., Oct. 1966: The antenna properties of optical heterodyne receivers. Appl. Optics, 5, 1588-1594.
6. Fried, D. L., June 1967: Atmospheric modulation noise in an optical heterodyne receiver. IEEE J. Quantum Elec., QE-3, 213-221.
7. Lucy, R. F., Lang, K., Peters, C. J., Duval, K., Aug. 1967: Optical superheterodyne receiver. Appl. Optics, 6, 8, 1333-1342.

A72-25 356

REMOTE PROBING OF THE OPTICAL STRENGTH  
OF ATMOSPHERIC TURBULENCE AND OF WIND VELOCITY

by

D. L. Fried  
Electro Optical Laboratory  
Electro Sensor Systems Division  
Autonetics, A Division of  
North American Rockwell Corporation  
Anaheim, California

ABSTRACT

A procedure for determining the optical strength of turbulence of the atmosphere and the wind velocity at various altitudes by measuring the spatial and temporal covariance of scintillation is developed. Emphasis is placed on the development of the formal relationships that have to be inverted to obtain the desired results. For determination of optical strength of turbulence, it is a linear integral equation that is developed. However, for determination of remote wind velocity, a nonlinear integral equation is obtained. A computer approach for solving each of the equations is suggested. The configuration and performance requirements of the measurement apparatus are discussed.

1. INTRODUCTION

It is the objective of this paper to explore analytic techniques for utilizing measurements of turbulence-induced effects on optical propagation as a basis for remote probing of the atmosphere. Our attention is centered on the problem of vertical rather than horizontal probing, although the analytic techniques are sufficiently general that they might be applied with certain changes to either case.

In the interest of establishing the basis for an economical and a truly remote probing technique, we have eschewed the possible use of a balloon terminal either as an optical target or as one end of an optical propagation link. We have restricted our attention to the use of a stellar source, and have placed heavy reliance on the potential of a sophisticated computer-signal-processing oriented ground station. With this approach, we have not only been able to establish the basis for remote measurement of the optical strength of atmospheric turbulence-- a quantity of great interest to those of us concerned with optical propagation in the atmosphere, but have also been able to lay the conceptual and analytic groundwork for remote measurement of wind velocities aloft -- a matter of very real interest in a variety of fields of endeavor. Our work on the remote measurement

## PROBING OPTICAL TURBULENCE AND WIND VELOCITY

of wind velocity is, in a sense, an attempt to formalize and extend the earlier work of Barnhart, Keller, and Mitchell (1959), and to lift the requirement for their assumption that all stellar scintillation is generated by turbulence in a fairly narrow altitude range with a single characteristic wind velocity.

We have approached our problem in two steps: first, by studying the relationship between the spatial covariance of scintillation, as measured by the conventional log-amplitude covariance, and the distribution along the propagation path of the optical strength of turbulence, as measured by the refractive-index structure constant. From this examination, we have found that we can obtain a linear integral equation relating the two functions. This considers the log-amplitude covariance as the known function -- it is a quantity we plan to measure -- and treats the refractive-index structure constant as an unknown function of position along the path of propagation. By inverting this integral equation, we are able to solve directly for the optical strength of turbulence along the propagation path. When the propagation path is that for star light, we have, in effect, a vertical probe of the atmosphere.

In the second part of our approach to the remote probing problem, to obtain information on the wind velocities in the atmosphere, we have generalized our interest in the log-amplitude covariance function to include its temporal as well as spatial dependence. The temporal dependence provides us with a "handle" on the wind velocities. (It is an interesting feature of a computer-oriented signal processing set-up that obtaining the temporal as well as the spatial dependence of the log-amplitude covariance, as compared with obtaining only the spatial dependence, requires only a change in the computer program and no additional hardware or data-taking time.) In this case again, an integral equation is obtained relating the spatial and temporal dependence of the log-amplitude covariance function to the wind velocity function. In this treatment, the wind velocity function is a vector function with functional dependence on position along the propagation path. (The vector function is the two-dimensional vector projection of the actual wind velocity vector on a plane perpendicular to the propagation direction. A correction for the projection of the actual wind feature can be introduced after the vector function has been obtained, by assuming that the true winds are horizontal, or nearly so.) It is an awkward aspect of this part of the work that the integral equation from which we expect to obtain the wind velocity function is very nonlinear. As a consequence, the task of inverting the equation, even approximately, on a computer is expected to be formidable. However, we see no reason in principle that the integral equation can not be adequately approximated by a set of nonlinear simultaneous equations and these solved by the use of relaxation techniques. With a modern, high speed computer, this should be quite economical.

In the next section, we shall define the quantities of interest with sufficient detail to provide a basis for planning their measurements. We will follow this with a pair of sections that develop the formal relationships of interest. Finally, we shall devote several sections to problems related to consideration of the actual implementation of the necessary measurement processes.

## 2. DEFINITIONS

Basically, the measurements we intend to make are of the irradiance produced by star light from some star at a variety of points with various separations. The measurements are to be continuous in time so that we have data on the temporal as

well as the spatial aspects of the star light irradiance. Although we will get into more detail on the measurement equipment configuration in a subsequent section, for the present it is sufficient to consider that we are dealing with a pair of photoelectric detection telescopes, each of whose signals is recorded on magnetic tape for subsequent computer data processing. Each telescope has a very restricted field-of-view, which is guided by the telescope mount to keep the star of interest in the field-of-view. The two telescopes are placed on the same mount in such a manner that the separation of their collection apertures can be adjusted. The collection apertures are intended to be of zero dimension, although for practical reasons a one-millimeter aperture is contemplated. The optical train in each telescope contains an interference filter which permits only radiation in a narrow spectral band to be observed. Ideally, the band should be of zero width, but for practical reasons we plan to use a 10% bandwidth. It can be shown (Fried (1967)) that the effect of using a non-zero spectral bandwidth is virtually negligible as far as scintillation effects are concerned, although it may be desirable at some later date to incorporate any slight changes in theory that go with the non-monochromatic signal. For this paper we shall use a monochromatic theory without reservation. We denote the center of the wavelength band by  $\lambda$ , with an associated wavenumber,  $k = 2\pi/\lambda$ .

We shall use the notation  $\vec{\rho}$  to denote the vector separation between the pair of miniature telescope collection apertures. We will let  $z$  denote a distance from the telescope along the path of propagation. Working with a stellar source at a zenith angle  $\theta$ , the height of a point at  $z$  is approximately  $h = z \cos \theta$ .

We denote the photocurrent out of each of the telescopes by  $i_1(t)$  and  $i_2(t)$ ,  $t$  being the time at which the photocurrent is observed. The logarithmic quantities  $\ell_1(t)$  and  $\ell_2(t)$ , called the log-amplitudes, are computed from the relationships

$$\ell_1(t) = 1/2 \ln [ i_1(t) / \langle i_1 \rangle ] , \quad (1a)$$

$$\ell_2(t) = 1/2 \ln [ i_2(t) / \langle i_2 \rangle ] , \quad (1b)$$

where  $\langle i_1 \rangle$  and  $\langle i_2 \rangle$  are the average values of  $i_1(t)$  and  $i_2(t)$ , respectively. (The angle brackets  $\langle \rangle$  are used here and hereafter to denote an ensemble average, although in practice we shall feel free to invoke the ergodic hypothesis and consider the brackets to denote a time average.) From  $\ell_1(t)$  and  $\ell_2(t)$  we calculate the spatial-temporal log-amplitude covariance,  $C_\ell(\vec{\rho}, \tau)$ , according to the equation

$$C_\ell(\vec{\rho}, \tau) = \langle [ \ell_1(t) - \langle \ell_1 \rangle ] [ \ell_2(t + \tau) - \langle \ell_2 \rangle ] \rangle . \quad (2)$$

For convenience in dealing with the spatial dependence of log-amplitude covariance for zero time delay, we shall use the notation  $C_\ell(\rho)$  rather than  $C_\ell(\vec{\rho}, 0)$ . Because of the isotropy of the statistics of turbulence, we are able to suppress the dependence on the vector aspect of  $\vec{\rho}$  and merely show a dependence on the scalar value  $\rho$ . (For a non-zero value of  $\tau$  the vector wind velocity becomes significant and it is the interaction of this vector with  $\vec{\rho}$  that required the dependence on the vector nature of  $\vec{\rho}$ .)

The optical strength of turbulence is measured by the refractive-index structure constant. The refractive-index structure constant is defined in relation to the

Kolmogorov theory of turbulence in the inertial subrange. According to this theory, the difference of two turbulently varying quantities has a mean square value which varies in proportion to the two-thirds power of their separation. The refractive-index structure constant is the constant of proportionality when the turbulently varying quantity is the refractive index. We denote the refractive-index structure constant at the position  $z$  along the propagation path by  $C_N^2(z)$ . At present there is very little data on the value of  $C_N^2$  as a function of altitude and effectively no data on how it varies with time of day and year, and with geographic location, or even how and if it varies statistically under apparently similar conditions. It is the first objective of the suggested measurements to permit compilation of data on  $C_N^2$  at various altitudes.

We shall use the notation  $\vec{V}(z)$  to denote the projection of the actual wind velocity vector at a distance  $z$  along the propagation path upon a plane perpendicular to the propagation direction. We shall speak of this as the wind velocity, although in all cases we shall eventually want to know what the vector in a horizontal plane is whose projection is  $\vec{V}(z)$ , for that vector is the true wind velocity. It is the second objective of the stellar scintillation measurements that we recommend, to provide data from which  $\vec{V}(z)$ , and ultimately the true wind velocity, can be determined.

### 3. DETERMINATION OF THE REFRACTIVE-INDEX STRUCTURE CONSTANT

In this section, we will establish the basic mathematical relationship between the refractive-index structure constant and the log-amplitude covariance for zero time delay, i.e., for  $\tau = 0$ . This will eventually permit determination of  $C_N^2$  from stellar scintillation data. We start with the basic relationship obtainable from Tatarski (1961), that

$$C_\ell(\rho) = 0.652 k^2 \int_0^L dz C_N^2(z) \int_0^\infty d\sigma \sigma^{-8/3} J_0(\sigma\rho) \left(1 - \cos \frac{\sigma^2 z}{k}\right) \quad (3)$$

which applies for propagation of an infinite plane wave\* of wavenumber  $k = 2\pi/\lambda$  traveling a distance  $L$ . (The  $z$ -integration is from collector to source.) For a stellar source we replace  $L$  by infinity, but keep carefully in mind the fact that  $C_N^2$  falls to zero about as rapidly as the square of the atmospheric density, so there is no problem of convergence of the integral.

It is a surprising fact that the double integral in Eq. (3) has never been evaluated by doing the  $\sigma$ -integration first. (For some reason an assumption about the  $z$ -dependence of  $C_N^2$  has always been made and the  $z$ -integration performed first.) This time we wish to perform the  $\sigma$ -integration first. This will yield some function of  $k$ ,  $z$ , and  $\rho$ , which will appear as the kernel in the  $z$ -integration side of an integral equation connecting  $C_\ell(\rho)$  and  $C_N^2(z)$ .

---

\* It should be carefully noted that most ground-to-ground propagation paths involve a source quite different from an infinite plane wave source and that the results developed here from Eq. (3) will be grossly inadequate for interpretation of such measurements. Often the theory for a spherical wave source will be applicable.

To perform the  $\sigma$ -integration, we use the two integral formulas that

$$\int_0^{\infty} u^{\alpha} J_0(\beta u^{1/2}) du = \left(\frac{4}{\beta^2}\right)^{\alpha+1} \frac{\Gamma(\alpha+1)}{\Gamma(-\alpha)}, \quad (4a)$$

and that

$$\int_0^{\infty} u^{\alpha-1} \cos u J_0(\beta u^{1/2}) du = \Gamma(\alpha) \operatorname{Re} \left[ \exp\left(-i\frac{\pi\alpha}{2}\right) {}_1F_1\left(\alpha; 1; i\frac{\beta^2}{4}\right) \right]. \quad (4b)$$

Eq. (4b), which apparently does not exist in any of the tables of definite integrals, can be obtained by a slight modification of the application of Ramanujan's formula presented in Appendix A of the paper by Fried and Cloud (1966). In fact, it can be recognized as the conjugate result to that developed in the reference. Eq. (4a) comes directly from that reference.

By making the transformation of  $u = \sigma^2 z/k$  in Eq. (3), and replacing  $L$  by  $\infty$  to restrict our attention to propagation of star light, we get

$$C_{\mathcal{L}}(\rho) = 0.326 k^{7/6} \int_0^{\infty} dz z^{5/6} C_N^2(z) \int_0^{\infty} du u^{-11/6} J_0\left(\sqrt{\frac{k\rho^2}{z}} u\right) \times (1 - \cos u). \quad (5)$$

With the aid of Eq.'s (4a) and (4b), we perform the  $u$ -integration, thus obtaining

$$C_{\mathcal{L}}(\rho) = 0.326 k^{7/6} \int_0^{\infty} dz z^{5/6} C_N^2(z) \left\{ \left(\frac{k\rho^2}{4z}\right) \frac{\Gamma(-5/6)}{\Gamma(11/6)} - \Gamma(-5/6) \operatorname{Re} \left[ \exp\left(i\frac{5\pi}{12}\right) {}_1F_1\left(-5/6; 1; i\frac{k\rho^2}{4z}\right) \right] \right\}. \quad (6)$$

We recognize that everything in the curly brackets in Eq. (6) may simply be considered as some function of  $k\rho^2/4z$ . Thus we can rewrite Eq. (6) in the desired integral equation form, namely

$$C_{\mathcal{L}}(\rho) = k^{7/6} \int_0^{\infty} dz z^{5/6} C_N^2(z) \mathfrak{F}\left(\frac{k\rho^2}{4z}\right), \quad (7)$$

PROBING OPTICAL TURBULENCE AND WIND VELOCITY

where the function  $\mathfrak{F}(x)$  is defined in terms of the power series

$$\mathfrak{F}(x) = \frac{-x^{5/6}}{\Gamma(11/6)} + \sum_{n=0}^{\infty} (a_n + b_n x) x^{2n}/(2n)! \quad (8)$$

The power series coefficients are defined by the recurrence relationships

$$a_n = -a_{n-1} \left[ \frac{(2n - 17/6)(2n - 11/6)}{(2n - 1)(2n)} \right], \quad (9a)$$

$$b_n = -b_{n-1} \left[ \frac{(2n - 11/6)(2n - 5/6)(2n - 1)}{(2n)(2n + 1)^2} \right], \quad (9b)$$

and the initial values

$$a_0 = (-0.326) \cos(5\pi/12) \Gamma(-5/6) \quad (10a)$$

$$b_0 = (11/6) (-0.326) \sin(5\pi/12) \Gamma(-5/6). \quad (10b)$$

The first few values of  $a_n$  and  $b_n$  are listed in Table I.

TABLE I  
Coefficients for the Power Series Determination of  
 $\mathfrak{F}(x)$  According to Eq. (8)

The notation a(b) denotes  $a \times 10^b$

n	$a_n$	$b_n$
0	5.403 (-1)	3.696 (0)
1	3.752 (-2)	-3.993 (-2)
2	-7.903 (-3)	8.219 (-3)
3	3.476 (-3)	-3.009 (-3)
4	-1.978 (-3)	1.437 (-4)
5	1.286 (-3)	-7.999 (-4)
6	-9.080 (-4)	4.926 (-4)
7	6.778 (-4)	-3.257 (-4)
8	-5.268 (-4)	2.270 (-4)
9	4.221 (-4)	-1.648 (-4)
10	-3.464 (-4)	1.236 (-4)

From this point on, we may consider  $\mathfrak{F}(x)$  to be a known and tabulated function, which makes Eq. (7) a very straightforward linear integral equation connecting the measured function,  $C_\ell(\rho)$  to the function  $C_N^2(z)$ , which is to be determined. As an integral equation, we have somewhat of a problem in obtaining  $C_N^2(z)$ . However, by replacing the integration in Eq. (7) with a summation over a set of finite ranges of  $z$ , and by replacing the functions  $C_\ell(\rho)$  and  $C_N^2(z)$  with a finite set of values, known or to be determined, we convert Eq. (7) to a set of linear simultaneous equations. This is an easy matter for a computer to handle and we can expect data on  $C_N^2(z)$  whose quality is limited only by how well we have chosen the set of  $\rho$ 's for measurement of  $C_\ell(\rho)$ , by how high our signal-to-noise ratio is for determination of  $C_\ell(\rho)$ , and by how effectively we designate the ranges of  $z$  in replacing the integration by a summation. The choice of ranges will depend on our a priori estimate of how  $C_N^2(z)$  varies with altitude. This should be nearly proportional to the variation of the square of the density of the atmosphere -- with allowance for a possible anomaly in the vicinity of the tropopause, as has recently been suggested by Hufnagel (1966). It will also depend on how  $\mathfrak{F}(x)$  varies and on our choice of values of  $\rho$ . Optimally, the choice of the set of  $\rho$ 's will be governed by the values of  $z$  for which  $C_N^2(z)$  is desired. For initial work, however, we expect that almost any choice of values for  $\rho$  for the measurement of  $C_\ell(\rho)$  and any reasonable separation of the range of  $z$  to replace the integral with a sum will yield a reasonably representative set of results. The really important matter will be the signal-to-noise ratio achieved in measuring  $C_\ell(\rho)$ . Of all of the adjustable features of the data-taking and data reduction procedure, this will have the most pronounced effect on the quality of the set of  $C_N^2$  that we obtain. The signal-to-noise ratio can be changed by varying the length of the data-taking. We shall have to be careful in the design of the actual experiment that we have enough equipment to take all the data we need in a short enough total period, and yet allow enough time for each measurement.

#### 4. DETERMINATION OF WIND VELOCITY

For this section, let us assume that the procedure suggested in the previous section has been successfully implemented -- that measurements of the log-amplitude covariance,  $C_\ell(\rho)$  have been obtained and that the appropriate linear simultaneous equations have been solved so that we now have accurate results for the refractive-index structure constant,  $C_N^2(z)$ . We now wish to consider what we could do with measurements of the temporal dependence of the refractive-index structure constant, i.e., with  $C_\ell(\rho, \tau)$  to compute the projected wind velocity,  $\vec{V}(z)$ . The key equation to carry this out is the time-dependent version of Eq. (3), which has the form

$$C_\ell(\vec{\rho}, \tau) = 0.652 k^2 \int_0^\infty dz C_N^2(z) \int_0^\infty d\sigma \sigma^{-8/3} J_0(\sigma |\vec{\rho} - \vec{V}(z)\tau|) \times (1 - \cos \frac{\sigma^2 z}{k}). \quad (11)$$

This equation does not appear in any of the published literature. Although the most straightforward way to obtain it is to derive it in detail from the stochastic propagation equations for log-amplitude at points 1 and 2 and times  $t$  and  $t + \tau$ ,

utilizing the hypothesis of frozen turbulence (i.e., that the wind transports the turbulent structure across the propagation path more rapidly than the structure breaks up and reforms), for the purpose of this presentation we shall argue that Eq. (11) follows as an obvious extension of Eq. (3) when we consider the contribution to the log-amplitude of the turbulence at any particular value of  $z$ . With the hypothesis of frozen turbulence, we note the equivalence of the contribution to the scintillation pattern at time  $(t)$  and position  $(\vec{R})$ , to the contribution at time  $(t + \tau)$  and position  $(\vec{R} + \vec{V}\tau)$ . With this in mind, the Eq. (11) follows directly from Eq. (3).

We can now use the same mathematical manipulations as in Section 3. This time they yield the result, in analogy to Eq. (7), that

$$C_{\ell}(\vec{\rho}, \tau) = k^{7/6} \int_0^{\infty} dz z^{5/6} C_N^2(z) \mathfrak{F}\left(\frac{k|\vec{\rho} - \vec{V}(z)\tau|}{4z}\right) . \quad (12)$$

Recognizing that now our problem is, given  $C_{\ell}(\vec{\rho}, \tau)$  and  $C_N^2(z)$  -- solve for  $\vec{V}(z)$ , we see that we are dealing with a rather formidable nonlinear integral equation. If we had to solve this equation, in the formal sense, it is doubtful that any further progress could be made on the problem. However, the use of numerical techniques reduces the problem to one of approximation, and that we may expect to be able to accomplish. By replacing the integration with a summation over a set of ranges of  $z$ , we obtain a set of nonlinear simultaneous equations to solve. Although there is no closed form solution possible for the set of general nonlinear simultaneous equations, as there is for the linear simultaneous equations, (for which matrix inversion produces a solution-generating operator), by the use of a relaxation procedure or some other iterative method, it should be possible to solve for  $|\vec{\rho} - \vec{V}(z)\tau|$  as a function of  $z$ . How quickly the solution procedure will converge will depend on the quality of the starting estimate for  $\vec{V}(z)$ .

The calculations would start with data on  $C_N^2(z)$  obtained from measurements of  $C_{\ell}(\vec{\rho})$  and would probably use the data for  $C_{\ell}(\vec{\rho}, \tau)$  and  $C_{\ell}(\vec{\rho}', \tau)$  where  $\vec{\rho}$  and  $\vec{\rho}'$  have the same magnitude but are perpendicular. Values of  $\tau$  would range from  $\tau = 0$  to a value of  $\tau$  sufficiently large as to make  $C_{\ell}(\vec{\rho}, \tau)$  vanish. This will be sufficient to permit calculation of  $\vec{V}(z)$ . Since data for other values of  $\vec{\rho}$  and  $\vec{\rho}'$  will be available, these measurements will also be processed to provide a consistency check and to improve the accuracy of the solutions for  $\vec{V}(z)$ .

## 5. MEASUREMENT OF SIGNAL-TO-NOISE RATIO

At this point, it is appropriate to examine the actual measurement and determine what kind of signal-to-noise ratio we can expect. Stellar scintillation measurements have previously been done with optics of one or more inches diameter. For order of magnitude evaluation of the intensity covariance, such a large aperture might have been acceptable, and it certainly helped the signal-to-noise ratio; but for the precision application which we have in mind for the data, we must plan to use much smaller apertures. Our apertures must be small enough that they do not average over the irradiance pattern. Examining the data in reference 1, it appears that a one-millimeter diameter would be suitable. As we have indicated

earlier, to avoid the complication in the theory of spectral spread, we plan to use a fairly narrow spectral bandwidth. Based on the results in reference 2, we have elected a 10% bandwidth at  $5250 \text{ \AA} \pm 250 \text{ \AA}$ . To be certain that we do not miss any of the rapid scintillation fluctuations, we plan to use a 1 kHz electronic bandwidth. These three quantities, the aperture diameter, the spectral bandwidth, and the electronic bandwidth, virtually determine the signal-to-noise ratio we will have on the photocurrent.

We plan to use an S-20 photocathode image dissector type photomultiplier, with a quantum efficiency in this spectral range of  $\eta = 4 \times 10^{-2}$  amps/watt. The use of the image dissector is simply to provide a very small photocathode area and in that way reduce the dark current to a negligible amount. By working with a very limited field-of-view, we can keep the background photocurrent down to a negligible amount even for daytime operation.

Since we are using a photomultiplier, there will be no significant amount of noise generated after the photocathode, so we can identify the shot noise in the average stellar current as the only noise. If the average stellar signal photocurrent is  $I$ , then the signal-to-noise ratio in dB will be

$$S/N = 10 \log_{10} (I/2 e \Delta f) \quad (13)$$

where  $e = 1.6 \times 10^{-19}$  coulombs is the electron charge and  $\Delta f = 10^3$  Hz is the electronics bandwidth. We consider as typical stellar sources the stars Vega or Arcturus, both of nearly zero-magnitude. A zero-magnitude star produces an irradiance of about

$$W = 10^{-11} \text{ watts/m}^2 - \text{\AA}$$

in the spectral range of interest. With combined atmospheric and optics transmission of  $T = .5$ , a collector diameter  $D = 10^{-3}$  m, and a spectral bandwidth  $\Delta\lambda = 500 \text{ \AA}$ , we see that the stellar signal average photocurrent will be

$$I = \eta \left( \frac{\pi}{4} D^2 \right) \Delta\lambda T W, \quad (14)$$

from which it follows that the photocurrent is  $I \approx 7.9 \times 10^{-17}$  amps. This yields a signal-to-noise ratio of -6.1 dB.

At first one is inclined to say that this proves that the measurement can't be made -- there isn't enough signal-to-noise ratio. However, we must remember that we are trying to make an accurate determination of the log-amplitude covariance, not of the instantaneously fluctuating signal! To see the difference, consider the fact that every one of the two thousand samples per second that goes with  $\Delta f = 10^3$  Hz contributed coherently to the final value of the log-amplitude covariance itself, but the noise in each sample, being independent of the noise in each other sample, contribute in quadrature to the error in the measured covariance.

After 300 seconds of operation, we may expect that the noise voltage will be up above the instantaneous voltage by  $\sqrt{300 \times 2000} \approx 800$ , while the covariance voltage will accumulate about  $(800)^2$  for a net improvement in signal-to-noise ratio of about 58.1 dB. Thus, after five minutes of operation we should have a value of the log-amplitude covariance which has a signal-to-noise ratio of about 52 dB. This should be entirely adequate.

## 6. MEASUREMENT PROCEDURE

In the preceding sections, we have spoken of the measurement of the log-amplitude covariance,  $C_L(\vec{\rho}, \tau)$  in terms of the use of a pair of one-millimeter aperture photoelectric telescopes on a tracking mount and pointed at a star. The implication was that the signals from the two telescopes were directly correlated by some suitable electronic device. In practice, this would be much too slow and inefficient a procedure. By the time a complete set of data was obtained, so much time would have elapsed that it is doubtful that conditions would be the same for the first and last part of the set. It is questionable whether or not there would be any self-consistency within the data set. Instead of such a one-at-a-time type of measurement, we visualize the entire set of data being obtained simultaneously in about five minutes of running time.

There would be no real-time conversion of the scintillation signals to log-amplitude covariances. Instead, all of the raw data would be stored on magnetic tape and later entered into and reduced in a digital computer. This would, amongst other things, permit a limited number of telescopes to provide data for calculation of log-amplitude covariance for a much larger number of combinations of values of  $\vec{\rho}$  and  $\tau$ . The output from any one telescope can be paired in the computer with several other telescopes to provide data for several values of  $\vec{\rho}$ . For example, a string of thirteen telescopes spaced 1, 1, 1, 1, 1, 1, 7, 7, 7, 7, 7, 7 units between each would permit the computer to select pairs covering any separation from one-unit to 48-units apart -- 48 values of  $\vec{\rho}$  covered with thirteen telescopes. Another string of thirteen crosswise to the first string (using a common element so there is a total of only 25-telescopes) would provide all possible data of interest. The computer, by shifting the data from any telescope, can simulate a time delay  $\tau$  and in that way calculate all the time dependent features of the log-amplitude covariance without increasing the equipment or measurement time requirements above the requirements for determination of just  $C_L(\rho)$ .

The tape recorder capacity to accommodate all of this data is not very extensive. By using three twenty-channel multiplexers, we can record all of the data on three 20 kHz FM tape recorder channels, with a blank space recorded between each signal sample, just to insure the impossibility of data crosstalk between telescopes.

Although we have spoken of the equipment as a collection of 25 one-millimeter diameter telescopes on a common mount, with the implication that each unit involved separate optics and separate boresighting, in practice it will probably prove to be much more economical to use a single large telescope, perhaps twelve inches in diameter, with a single narrow band filter and focal plane stop to define the limited field-of-view. The light passing through the focal plane stop would be allowed to diverge and when it had reached some suitably large diameter, would be sampled by positioning the 25 photomultipliers (or by positioning 25 one-millimeter diameter diagonal mirrors or fiber optics tubes to "tap-off" the light for the photodetectors.) The balance of the light could be used to provide a signal for tracking the star. The total configuration would be relatively simple and trouble-free. There would be, for instance, no significant pointing problems for any of the individual sensors.

## 7. COMMENTS

All of this analysis is based on two assumptions which, while we believe they are satisfied, should be pointed out here. First, all of our analysis assumes that the Kolmogorov spectrum for turbulence in the inertial subrange is the appropriate spectrum. There is quite reliable evidence to support this for the high spatial frequencies of interest in optical propagation, for regions near the ground. For much lower spatial frequencies, this has also been demonstrated for higher altitudes. While it seems quite plausible to extend this information to higher altitudes with the higher spatial frequencies associated with optical propagation, it must be recognized that the applicability of the Kolmogorov spectrum is not demonstrated by any measurements.

The second assumption is that the theory for optical propagation in a randomly inhomogeneous medium, as we have used it, is valid. Recently there has been considerable controversy about this. However, it is almost universally agreed that for small enough scintillation effects, the results of theory should be valid. As Hulett (1967) has pointed out, measured values of scintillation for stars near the zenith are quite small. For this reason, we believe there is no reason to question the accuracy of propagation theory as we have applied it in this paper.

We believe that a firm foundation exists for exploiting our understanding of optical propagation and the flexibility of modern data handling electronics to develop an economical method of remote probing of the atmosphere. The expense of development of this method will be fully justified by the cost reduction in obtaining winds aloft data. We further believe that the reduced cost and the ease with which this data is obtained will result in expanded coverage of winds aloft measurements and will thereby promote a better understanding of meteorological interactions.

## REFERENCES

- P. E. Barnhart, G. Keller, and W. E. Mitchell, Jr., "Investigation of Upper Air Turbulence by the Method of Analyzing Stellar Scintillation Shadow Patterns," Final Technical Report on Air Force Contract AF 19(604)-1954 with AFCRL, July 1959. (Available as ASTIA Document AD 231378.)
- D. L. Fried, "Spectral and Angular Covariance of Scintillation for Propagation in a Randomly Inhomogeneous Medium," pp. 33-76 in "Final Report - Theoretical Analysis of Atmospheric Effects on Optical Propagation," Contract NAS 8-18035 (1967) performed for NASA, George C. Marshall Space Flight Center, Huntsville, Alabama.
- D. L. Fried and J. D. Cloud, "Propagation of an Infinite Plane Wave in a Randomly Inhomogeneous Medium," *J. Opt. Soc. Am.* 56, 1667 (1966)
- R. E. Hufnagel, Appendix III, Vol. 2 of "Restoration of Atmospherically Degraded Images," Woods Hole Summer Study, July 1966, published by the National Research Council of the National Academy of Sciences.

## PROBING OPTICAL TURBULENCE AND WIND VELOCITY

H. R. Hulett, "Turbulence Limitations in Photographic Resolution of Planet Surfaces," J. Opt. Soc. Am. 57, 1335 (1967).

V. I. Tatarski, "Wave Propagation in a Turbulent Medium," McGraw-Hill Book Co., Inc., New York (1961).

CRITIQUE OF PAPER BY D. L. FRIED

R. E. Hufnagel

The Perkin-Elmer Corporation

Dr. Fried is to be congratulated for his skill and perseverance in solving this difficult inversion problem. A few months before this meeting, I learned of a similar work by Arthur Peskoff (1968) who has independently solved the same problem. It will be interesting to compare these two methods. My comments below apply to both methods.

I believe that it will be very difficult in practice to get accurate and detailed inversions from real-life experimental data. To explain why this might be so, we note, first, that all scintillation experimental data tend to look somewhat alike (thus implying that it can't contain much information of interest). To illustrate this, we need only note that the autocorrelation function for scintillation as computed by Chernov (1960) using a Gaussian shaped turbulence spectrum is very similar to the scintillation autocorrelation function obtained by Tatarsky (1961) who used a Kolmogoroff description of turbulence. A second difficulty arises from the often observed nonstationarity of turbulence statistics.\* This means that one cannot reliably average observations over long time periods to gain effective signal to noise enhancement. On the other hand, since the theory in its proposed form requires the use of small diameter telescopes, and a narrow spectral filter, the noise problem will be severe, and accurate inversion will be difficult. Still another difficulty is that present inversion theories assume isotropic Kolmogoroff turbulence statistics. It is very likely that above the atmospheric boundary layer that these statistics are often not valid -- especially in thin turbulent strata, which do appear to exist (Hufnagel, 1966).

On a constructive note, however, there are some ways in which we can make this remote sensing method more accurate and reliable. The first and foremost principle to employ is to make use of all available *a priori* information. For example, it is relatively easy to learn the wind velocity profile through standard radiosonde techniques. Rather than ask this proposed remote inversion method to determine the wind velocity profile in addition to the turbulence (as has been proposed), one should instead use an independently measured wind profile as *a priori* information to

---

\* If the turbulence is indeed nonstationary, it would be well to inquire again about just what descriptors you are trying to measure anyway.

## CRITIQUE OF PAPER BY D. L. FRIED

aid the inversion method. Secondly, we know something already of the general distribution of turbulence with altitude and should use this information. Also, since the ground layer turbulence can be easily measured *in situ*, one could use this information to subtract its known contribution from the total observed scintillation statistics.

It is certainly apparent that an error analysis for this inversion method is required. Also, I would strongly recommend that a limited program of *in situ* measurements be made to learn more about the true nature of the turbulence before we attempt to rely on indirect remote sensing methods, such as proposed here.

On a different subject, we should note that in the discussions today we have talked only about using intensity scintillation measurements as an indicator of remote effects. Similar methods have been developed for other types of optical disturbances, such as, image blurring (Hufnagel, 1967). These alternate methods can well complement the scintillation methods described here.

## REFERENCES

- Chernov, L.A., 1960: Wave propagation in a random medium, McGraw-Hill Book Co., New York.
- Hufnagel, R.E., 1966: An improved model atmosphere, appendix III of: Restoration of atmospherically degraded images, Woods Hole Summer Study, July 1966, National Academy of Science, National Research Council (available from D.D.C.).
- Hufnagel, R.E., 1967: Measurement of atmospheric turbulence via observation of instantaneous optical blur functions, presented at AGARD/EPC (NATO) conference in Ankara, Turkey, October 9-12, 1967. To be published in Proceedings.
- Peskoff, A., 1968: Theory of remote sensing of clear air turbulence profiles, to be published in J. Opt. Soc. Am. (summer 1968).
- Tatarsky, V.I., 1961: Wave propagation in a turbulent medium, McGraw-Hill Book Co., New York.

SESSION 3

Lidar

N72-25357

## LIDAR

R. T. H. Collis

Stanford Research Institute

### ABSTRACT

Lidar is an optical 'radar' technique employing laser energy. Variations in signal intensity as a function of range provide information on atmospheric constituents, even when these are too tenuous to be normally visible. The theoretical and technical basis of the technique is described and typical values of the atmospheric optical parameters given. The significance of these parameters to atmospheric and meteorological problems is discussed. While the basic technique can provide valuable information about clouds and other material in the atmosphere, it is not possible to determine particle size and number concentrations precisely. There are also inherent difficulties in evaluating lidar observations. Nevertheless, lidar can provide much useful information as is shown by illustrations. These include lidar observations of: cirrus cloud, showing mountain wave motions; stratification in 'clear' air due to the thermal profile near the ground; determinations of low cloud and 'visibility' along an air-field approach path; and finally the motion and internal structure of clouds of tracer materials (insecticide spray and explosion-caused dust) which demonstrate the use of lidar for studying transport and diffusion processes.

Lidar is a generic, rather than a specific, technique and thus can be applied in a variety of forms to a wide range of research and operational problems. Research applications include: the investigation of dust in the high atmosphere; studies of air motion and turbulence revealed by cirrus and other clouds; boundary layer phenomena, as shown by variations in turbidity in the mixing layer; turbulence and diffusion processes using suitable indicators; and investigations of the effects of cirrus and other particulate

layers on measurement of radiation in and through the earth's atmosphere. Operational applications include: ceilometry, transmissometry, and the monitoring and tracking of atmospheric pollutants. Much progress is readily possible within the state-of-the-art, although higher pulse-rate lasers of higher average power are needed, together with the application of modern data-handling techniques and the development of quantitative methods of interpreting lidar data.

## 1. INTRODUCTION

The advent, in 1960, of the laser as a source of energy, opened up many possibilities for new techniques of probing the atmosphere or for improving and extending established techniques. The properties of this new form of energy were remarkable even at an early stage of technology. The energy, at optical or near optical frequencies was monochromatic, coherent, and, with the development of Q-switching techniques, could be generated in very short pulses of very high power. A number of scientists soon recognized the applicability of this device to atmospheric studies and described a variety of ways in which the special characteristics of laser energy could be exploited. These ranged from straightforward radar-type applications to more sophisticated concepts in which the wave nature and coherence of the laser energy were utilized. (See Schotland et al., 1962, Goyer and Watson, 1963, for example.)

The first actual use of lasers in atmospheric studies appears to be Fiocco and Smullin's use of a ruby laser "radar" to detect echoes from the atmosphere at heights up to 140 kms in June and July 1963. (Fiocco and Smullin, 1963.) At about the same time however, the late Dr. M. G. H. Ligda had initiated a program at Stanford Research Institute in which a similar pulsed ruby laser "radar" system, or lidar\*, as Ligda called it, was used to probe the lower atmosphere and study meteorological phenomena. (Ligda, 1963)

Since that time, such simple 'radar' techniques have been applied by a number of workers to map and track concentrations of particulate matter and to study the density profile of the atmosphere by reference to gaseous backscattering. Meanwhile, others have been implementing some of the concepts involving the wave nature and coherence of laser energy. These include the use of multiple wavelength lidars to determine by reference to differential absorption the atmosphere's gaseous composition and also the use of Doppler techniques to determine motion in the atmosphere or, from molecular velocities, its temperature.

This paper will consider only the simple 'radar' approach and be concerned with the application of determinations of the intensity of backscattering of lidar energy to atmospheric studies and the solution of meteorological problems.

---

\*The word lidar, an acronym analogous to radar, from Light Detection And Ranging, was earlier used by Middleton and Spilhaus (1953) in connection with pulsed-light ceilometers.

ILLUSTRATIONS SIGNIFICANT TO TEXT MATERIAL  
HAVE BEEN REPRODUCED USING A DIFFERENT  
PRINTING TECHNIQUE AND MAY APPEAR AGAIN IN  
THE BACK OF THIS PUBLICATION

## 2. THE BASIC LIDAR TECHNIQUE

Energy generated by giant-pulse (Q-switched) lasers is highly monochromatic, essentially coherent, and is concentrated in very short, high-power pulses. This energy is directed by refracting or reflecting lens systems in a beam. Energy backscattered by the atmosphere within the beam is detected by an energy sensitive transducer (normally a photomultiplier tube) after being collected by suitable receiver lens systems. The monochromaticity of the energy makes it possible, by the use of narrow-band filters, to limit 'noise' in the form of energy of solar origin, to a minimum. The coherence of the energy makes it possible to achieve very narrow transmitter beams. A typical lidar system is shown in Figure 1; its characteristics are given in Appendix. (Northend *et al.*, 1966)



Figure 1. MARK V 1967 Neodymium LIDAR

The essential features of lidar detection of atmospheric targets are described in the following equation:

$$P_r = \frac{P_t c \tau \beta'_{180} A}{8\pi r^2} \exp -2 \int_0^r \sigma(r) dr, \quad (1)$$

where

$P_r$  is received power

$P_t$  is transmitted power

## LIDAR

- c is the velocity of light
- $\tau$  is pulse duration
- r is range
- $\beta'_{180}$  is the volume backscattering coefficient of the atmosphere at range r (having dimensions of area/unit volume). (Following radar practice,  $\beta'_{180}$  is defined as an area that would intercept the same amount of energy as would yield the same return at the lidar if radiated isotropically at range r, as is, in fact, received from unit volume of the atmosphere at that range).
- A is the effective receiver aperture
- $\sigma$  is the extinction coefficient

The basic lidar observation consists of an evaluation of received signal power  $P_r$  in terms of range and direction. The minimum detectable signal level is determined by either the system noise and that due to solar energy entering the receiver, or the sensitivity of the detector system. At laser wavelengths, even with systems of modest performance, the smallest hydrometeors may be readily detected, as well as the microscopic particles of the 'clear' aerosol.

It will be immediately apparent that unless the volume backscattering coefficient,  $\beta'_{180}$ , and the extinction coefficient,  $\sigma$ , are uniquely related, it is not possible to evaluate the intensity information in absolute terms. However, within certain limits the relationship between these parameters is sufficiently consistent to enable the significance of the variation of received signal with range to be unequivocal and of direct value. This is particularly the case where the lidar beam encounters strongly scattering targets after passing through relatively clear air, as occurs in observing clouds of particulates. Again, minor variations of signal intensity with range are immediately obvious and reveal layers and inhomogeneities in a continuously scattering atmosphere.

In practice, the signal from the photomultiplier is normally displayed on an oscilloscope as a function of range—the familiar A-scope presentation of radar practice. The single transient signal from a single shot may be photographed or magnetically recorded. Polaroid photography allows early inspection of the data in the former case, but the use of magnetic video disc memory makes a continuously viewable oscilloscope display available immediately as well as providing an input for more sophisticated analysis procedures and displays.

Although up to the present, data has largely been converted manually to punched cards or tape for subsequent computer processing and presentation, automatic data input techniques can readily be implemented. In the case of the very weak signals from high altitudes, where the signal is a function of the rate of generation of single photoelectrons, more sophisticated, automatic data processing techniques have already been employed (for example, McCormick et al., 1966, describe the on-line input of lidar data to a digital computer).

The limited data rate of the early lidar systems (with intervals between pulses measured in seconds if not in minutes) has restricted the resolution of observations in time,

and has precluded the development of scanning systems capable of developing two-dimensional sections of the type familiar in radar practice. (The lower data rate has perhaps been responsible for an earlier application of quantitative analyses than was the case with weather radar.) Both quantitatively and qualitatively however, lidar has made it possible to study remotely in three dimensions many atmospheric phenomena that hitherto could only be observed grossly or examined piecemeal.

### 3. ATMOSPHERIC OPTICAL PARAMETERS

Electromagnetic energy incident upon a volume of atmospheric gases and the liquid and solid particles suspended therein is scattered and absorbed. The magnitude of these effects is dependent upon the size and number of the particles present and their refractive index (and in this context gaseous molecules may be considered as particles) and also upon the wavelength of the incident energy. (In the case of laser energy, its highly monochromatic nature is an important consideration, for as shown by Twomey and Howell, (1965) the effects of critical wavelength/particle-size ratios are not averaged out so readily as is the case with broadband light sources.)

Of the energy scattered, that which is returned in the direction of the lidar, is evaluated in terms of the volume backscattering coefficient,  $\beta'_{180}$  ( $\ell^{-1}$ ). Energy removed from the direction of propagation, either by scattering or by absorption, can be evaluated most conveniently in terms of the extinction coefficient  $\sigma$  ( $\ell^{-1}$ ). This in turn can be considered in terms of the extinction due to scattering,  $\sigma_s$ , and the extinction due to absorption,  $\sigma_a$ . The important scattering and absorption mechanisms are now discussed.

#### 3.1 Rayleigh Scattering

Rayleigh scattering from the molecular atmosphere is important for it provides a method by which atmospheric densities may be derived from lidar measurements. In addition, it also provides a convenient datum, to which other scattering and absorption effects may be related, in the upper atmosphere, particularly where layers of purely gaseous composition can be identified.

For wavelengths well separated from the absorption lines of the atmospheric constituents, the Rayleigh scattering cross section  $C_{\text{RAY}}$  of an individual scattering center is given (Van de Hulst, 1957) by:

$$C_{\text{RAY}} = \frac{8\pi}{3} \left(\frac{2\pi}{\lambda}\right)^4 \alpha^2 \frac{6 + 3\delta}{6 - 7\delta}, \quad (2)$$

where

$\lambda$  = wavelength of incident radiation

$\delta$  = depolarization factor due to the anisotropy of the atmosphere

$\alpha$  = molecular polarizability of scatterer

# LIDAR

For the atmospheric gases, the factor  $\delta$  has a value near 0.035; therefore the fraction  $(6 + 3\delta)/(6 - 7\delta)$  is about 1.061. The polarizability  $\alpha$  is approximately  $2 \times 10^{-30} \text{ (m}^3\text{)}$ , and thus:

$$C_{\text{RAY}} = 3.96 \times 10^{-56} \lambda^{-4} \text{ (m}^2\text{)} \quad (3)$$

and at the ruby wavelength  $\lambda = 0.694\mu$ , for example,

$$C_{\text{RAY}} (\lambda = 0.694\mu) = 1.71 \times 10^{-31} \text{ (m}^2\text{)}. \quad (4)$$

The total scattering cross section per unit volume of a purely gaseous atmosphere is this elementary cross section multiplied by the number density  $N$  of molecular scatterers per unit volume.

$$\sigma_{\text{RAY}} + N C_{\text{RAY}} \quad (5)$$

This quantity  $\sigma_{\text{RAY}}$  is also called the Rayleigh attenuation coefficient. It is that quantity which, when multiplied by the incident power density and the effective illuminated volume, gives the total power scattered in all directions from the incident radiation beam.

For pure Rayleigh scattering it can be shown that  $3/8\pi$  per steradian of this total will be scattered back toward the source. As a result of the convention used in defining radar cross sections (see Sec. 2 above) it follows that for Rayleigh scattering the volume backscattering cross section  $\beta'_{180}$ , can be obtained from:

$$\beta'_{180 \text{ RAY}} = 4\pi \frac{3}{8\pi} N C_{\text{RAY}} = 1.5 \sigma_{\text{RAY}} \quad (6)$$

Thus the factor  $k$ , which is the ratio of backscattering,  $\beta'_{180}$ , the extinction coefficient,  $\sigma$ , is for Rayleigh scattering a trusted constant (3/2) and not subject to the fluctuations encountered when the scattering particles become large compared to the wavelength. The significance of the value,  $\beta'_{180 \text{ RAY}}$  in determining the density of the upper atmosphere is indicated in Table I.

Table I lists values for  $N$  from the U.S. Standard Atmosphere, 1962 (U.S. Government Printing Office, 1962) and for  $\beta'_{180 \text{ RAY}}$  for sea level to 20 km elevation in 5 km increments.

Table I. Volume scattering coefficients for Rayleigh component of atmospheric scattering for ruby LIDAR ( $\lambda = 0.6943\mu$ )\*

Height (km)	$N$ ( $\text{m}^{-3}$ )	$\beta'_{180}$ ( $\text{m}^{-1}$ )	$\sigma_{\text{RAY}}$ ( $\text{m}^{-1}$ )
0	$2.55 \times 10^{25}$	$6.55 \times 10^{-6}$	$4.37 \times 10^{-6}$
5	$1.52 \times 10^{25}$	$3.93 \times 10^{-6}$	$2.62 \times 10^{-6}$
10	$8.60 \times 10^{24}$	$2.21 \times 10^{-6}$	$1.47 \times 10^{-6}$
15	$4.06 \times 10^{24}$	$1.04 \times 10^{-6}$	$.69 \times 10^{-6}$
20	$1.85 \times 10^{24}$	$4.75 \times 10^{-7}$	$3.2 \times 10^{-7}$

\*Rayleigh scattering is proportional to  $\lambda^{-4}$

### 3.2 Mie Scattering

Mie scattering is of far greater significance than Rayleigh scattering in the lower atmosphere. It applies to particulate matter having dimensions of magnitude similar to the wavelength of the incident radiation. For large particles the elementary scattering cross section  $C_{\text{MIE}}$  is of the order of twice the geometrical cross section. The scattering pattern in the Mie case does not resemble the symmetrical-dipole pattern of Rayleigh scattering, but can be quite irregular and complicated (Middleton, 1953; Van de Hulst, 1957; Deirmendjian, 1964). The ratio of the backscattered to the total scattered energy is thus highly variable as a function of the particle-size to wavelength ratio and the dielectric characteristics of the particle. This is illustrated in Figure 2 which shows the relationship between backscattering and total scattering and the size parameter,  $\alpha$ , for single spherical particles having a real refractive index of 1.33 (i.e., that of water). (The size parameter  $\alpha = 2\pi a/\lambda$  where  $a$  is the radius.)

It will be seen that neither backscattering nor total scattering show significant general dependence on wavelength or particle size. Usually Mie scattering is predominantly forward so that in an assemblage of particles of different sizes,  $k$ , in the relation  $\beta'_{180} = k\alpha$ , is often less than unity. Because the effects of particle size differences tend to average out in such assemblages, useful approximate values can be determined for  $k$  and used in evaluating the lidar signal. Stanford Research Institute calculations for water sphere distributions typical of natural water clouds give an average value of  $k = 0.625$ . This value, together with the Attenuation Coefficients given in Elterman's Clear Standard Atmosphere (Elterman, 1964), have been used to compute values for the aerosol contribution to total backscattering for various altitudes as plotted in Figure 3. (The value  $k = 0.625$  is most accurate for water spheres, but is a reasonable approximation for other aerosol components.)

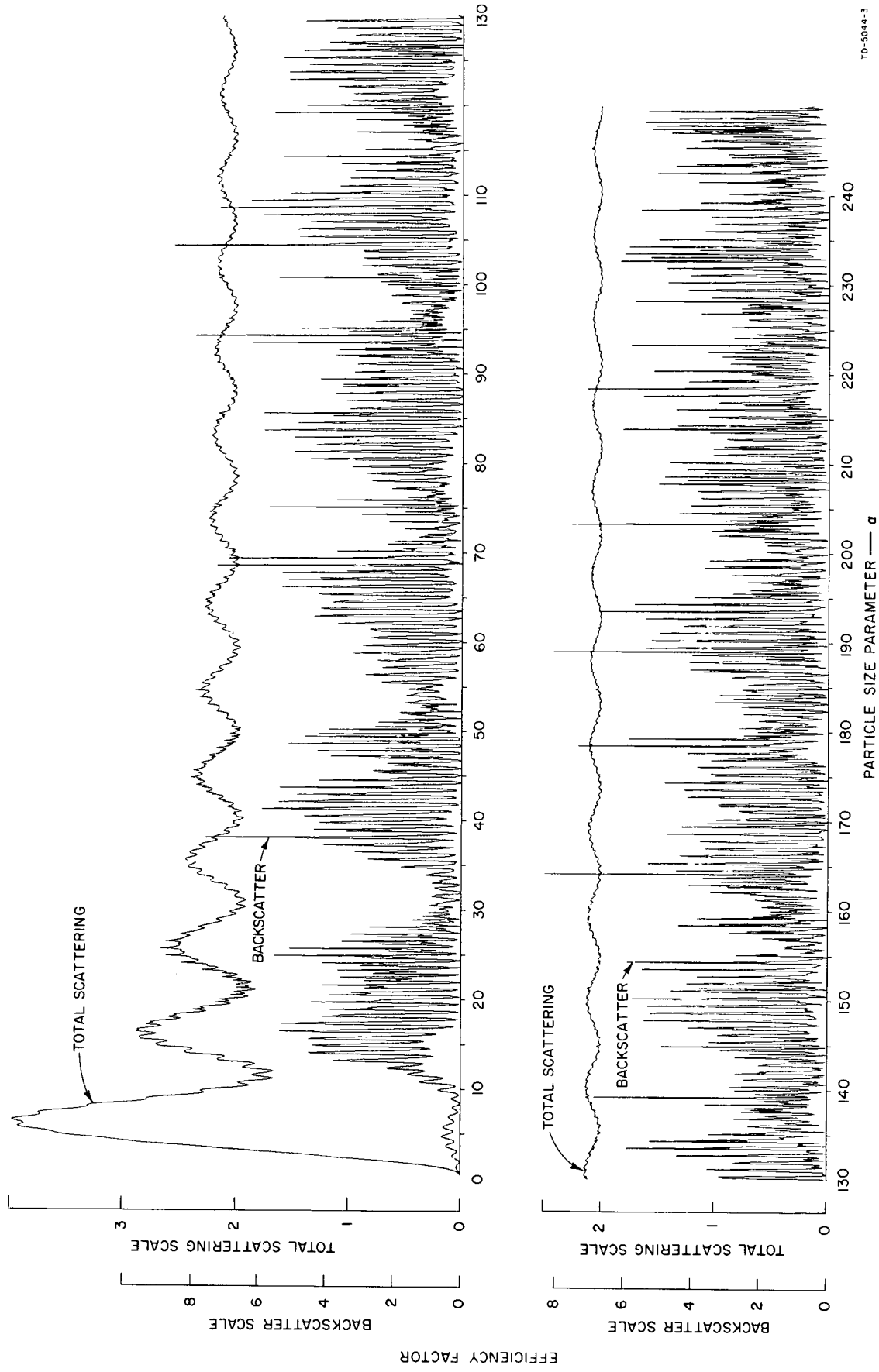
From this figure it is apparent that even on "clear" days (i.e., those with a horizontal visibility of about 25 km at sea level for the Elterman model) the aerosol backscattering predominates over the molecular backscattering for all elevations below 4 km.

Table II lists a range of typical water-cloud and haze conditions, together with the associated computed aerosol extinction coefficients, and anticipated volume backscatter coefficients,  $\beta'_{180}$ , under the assumption that  $k = 0.625$ .

Note however the generalizations involved in these examples (see Sec. 4 below).

### 3.3 Backscattering by Atmospheric Turbulence

The possibility of directly detecting atmospheric turbulence by lidar as a function of backscattering by dielectric inhomogeneities has attracted some attention. Among others, Munick (1965) has shown however, that this mechanism is far too feeble to encourage any hopes in this direction. For temperature and molecular number density values typical of altitudes of 10 km and a large temperature structure coefficient (representative of turbulent conditions near the ground), he shows that the backscattering due to turbulence at ruby wavelengths would be some 7 orders of magnitude less than that due to molecular backscattering!



TD-5044-3

Figure 2. Scattering efficiency factor as function of particle size parameter (refractive index: 1.33). Efficiency factor is ratio of respective scattering cross section to geometric cross section.

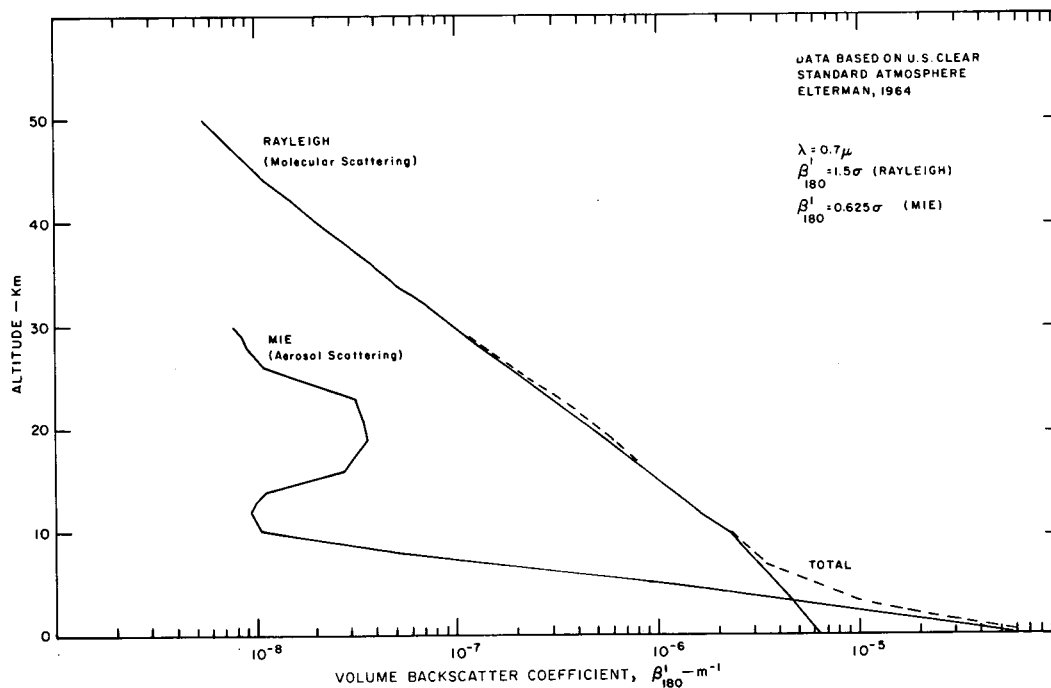


Figure 3. Volume backscatter coefficients for a clear standard atmosphere (for Ruby Lidar  $\lambda = 0.6943 \mu$ ) Based on U.S. Clear Standard Atmosphere (Elterman, 1964). Note that a recent revision (Elterman, 1968) indicates a substantially larger aerosol content above approximately 4 km. The total backscattering profile based on these data would have the same general characteristics but would have values larger by a factor of approximately two above about 4 km up to the 30 km level.

Table II. Predicted volume backscatter and extinction coefficients for water clouds and hazes. For Ruby Lidars ( $\lambda = 0.6943 \mu$ ) ( $k = 0.625$ )

	$\sigma_{\text{MIE}}$ ( $\text{m}^{-1}$ )	$\beta'_{180 \text{ MIE}}$ ( $\text{m}^{-1}$ )
Dense Water Cloud	$3.2 \times 10^{-1}$ to $1.6 \times 10^{-2}$	$2 \times 10^{-1}$ to $1 \times 10^{-2}$
Light Water Cloud	$1.6 \times 10^{-2}$ to $4.0 \times 10^{-3}$	$1 \times 10^{-2}$ to $2.5 \times 10^{-3}$
Thick Haze	$4.0 \times 10^{-3}$ to $1.1 \times 10^{-3}$	$2.5 \times 10^{-3}$ to $7 \times 10^{-4}$
Moderate Haze	$1.1 \times 10^{-3}$ to $4.8 \times 10^{-3}$	$7 \times 10^{-4}$ to $3 \times 10^{-4}$
Light Haze	$4.8 \times 10^{-3}$ to $1.6 \times 10^{-4}$	$3 \times 10^{-4}$ to $1 \times 10^{-4}$

### 3.4 Absorption

In addition to scattering, the gaseous atmosphere, and to a certain extent the industrially polluted aerosol absorbs energy. The attenuation due to this is generally insignificant in comparison to scattering losses, and  $\sigma_{\text{total}} \approx \sigma_{\text{S}}$ . Absorption is, of course, highly wavelength-dependent (especially at absorption line centers as exploited in spectroscopic lidar techniques), but may be neglected for many purposes in the basic

lidar application. Since in the operation of ruby lasers, heating can result in emission at the water vapor line centered on  $.69438 \mu$  where the attenuation rate is some five times greater, some workers have found it desirable to control the laser operating temperature to avoid this (Kent et al., 1967).

#### 4. THE SIGNIFICANCE OF LIDAR MEASURED OPTICAL PARAMETERS

##### 4.1 Meteorological Significance

It is important to recognize that the magnitudes of the coefficients discussed above, and the relationships between the volume backscattering coefficients and attenuation coefficients are by no means absolute. They are given merely to provide general orders of magnitude and illustrate the relationships between the parameters in question.

For many meteorological and atmospheric applications, number and size spectrum of the aerosol particles is all-important. Although in certain cases, e.g., the measurement of visibility, the evaluation of the optical parameter as such, in this case the extinction coefficient,  $\sigma$ , will have direct significance. The quantitative contribution that lidar observations can make to meteorological studies is limited by the degree to which the optical parameters can be interpreted in terms of atmospheric characteristics.

Thus, in the case of the higher atmosphere, i.e., above 30-40 km, if the absence of particulate material can reasonably be inferred from the data, an evaluation of the volume backscattering coefficient is essentially a direct method of measuring atmospheric density. (Kent et al., 1967, Sandford, 1967). In 'clear' air in which particulate matter is present, the volume backscatter coefficient and the extinction coefficient can only be related to the particulate loading of the atmosphere within certain limits. Barrett and Ben-Dov (1967) discuss these in connection with lidar applications in air pollution measurements. They show that variations in assumed aerosol distribution parameters will produce relatively small errors (less than a factor of 2) in evaluation of particle concentrations from volume backscatter coefficient determinations.

While this degree of accuracy may be acceptable in air pollution studies, for other purposes it is obviously too uncertain. Fenn (1967) for example shows the limitations inherent in the relationship between atmospheric backscattering and the extinction coefficient in connection with the measurement of visual range. Twomey and Howell (1965 and 1967) also discuss the difficulties of deriving information on particle size distribution from optical measurements with special reference in their earlier paper to the monochromatic aspects of laser energy.

##### 4.2 The Evaluation of Lidar Measured Optical Parameters

The discussion of the meteorological significance of optical parameters in 4.1 above has been carried on with the tacit assumption that the volume backscattering coefficients and the extinction coefficient can be evaluated. As noted in Section 2, the separation and evaluation of these terms cannot readily be accomplished from lidar observations, for unless a unique relationship exists between the volume backscattering coefficient and the extinction coefficient the lidar equation is unsolvable. The difficulties discussed above

(4.1) in connection with the interpretation of the significance of optical parameters apply in an especially critical way to attempts to interpret the lidar equation. Particularly because of the monochromatic nature of the energy, (Twomey and Howell, 1965) the relationship between backscattering and total scattering in the Mie region - i.e., for the particle sizes commonly involved in atmospheric aerosols and such features as cloud and fog, is highly variable. For a single scatterer, a diameter variation of, say, 1/100 can change the backscattering coefficient by a factor of 20. Although the averaging that occurs in the case of a volume of multi-size particles tends to stabilize the relationship ( $k$ ) between the volume backscattering coefficient and extinction coefficient (see Sec. 3) at single wavelength, uncertainties in the relationship remain. Analysis techniques that rely on assumptions of any specific value of  $k$  are consequently apt to be in error. The difficulty lies in the fact that, unlike weather radars, (particularly those of wavelength of 10 cm or longer) any significant backscattering of lidar energy by atmospheric targets involves considerable attenuation.

Various analytical techniques have been proposed. For example, where the atmosphere is homogeneous, the derivative of the logarithm of the range-corrected received signal with respect to range, yields the attenuation coefficient in absolute terms.

$$\frac{d \log_e P_r r^2}{dr} \equiv -2\sigma \quad (7)$$

Barrett and Ben-Dov (1967) in the appendix to their paper describe the derivation and solution of an integral equation based on the initial assumption of a specific value of  $k$ .

The authors point out the instability inherent in approaches of this type, but show how errors can usually be confined to reasonable limits. At Stanford Research Institute (SRI) a similar approach has been taken but has been developed in the following form.

The data from the lidar signature is reduced in terms of the atmospheric optical parameters in a form which is called the lidar S-function\* defined as:

$$S(r) \equiv 10 \log \frac{P_r(r) r^2}{P_r(r_o) r_o^2} \equiv 10 \log \frac{\beta'_{180}(r) T_a^2(r)}{\beta'_{180}(r_o) T_a^2(r_o)} \quad (8)$$

---

\*The concept of the S-function was developed from the Spatial Backscatter Function (SBF) previously used at SRI (See Sec. 5). The SBF was defined as:

$$SBF(r) = 10 \log \beta'_{180}(r) T_a^2(r) \quad (9)$$

where  $\beta'_{180}$  has dimensions of  $\text{km}^{-1}$ . The S-function has the advantage of being dimensionless.

## LIDAR

where  $T_a(r)$  = one-way atmospheric transmission

$$= \exp \left( - \int_0^r \sigma(r') dr' \right) \quad (10)$$

and  $r_0$  is a reference range.

When the backscatter is related to the extinction by

$$\beta'_{180}(r) = k_1 \sigma(r)^{k_2} \quad (11)$$

the derivative of the expression for  $S(r)$  yields a first-order, non-linear differential equation

$$\frac{d\sigma}{dr} - c_1 \frac{dS}{dr} \sigma - c_2 \sigma^2 = 0 \quad (12)$$

where  $c_1 = 1/4.34 k_2$  and  $c_2 = 2/k_2$ . The transform  $\eta \equiv 1/\sigma$  reduces the equation to linear form for which the solution may be written as:

$$\sigma(r) = \sigma(r_0) e^{c_1 S(r)} \left[ 1 - c_2 \sigma(r_0) \int_{r_0}^r e^{c_1 S(r')} dr' \right]^{-1} \quad (13)$$

where knowledge of  $\sigma(r_0)$  is required for solution.

Even in the absence of complete solutions, it is noteworthy that, unlike much of the work on weather radar, quantitative approaches are being developed and utilized in handling and displaying lidar data. This is encouraging for it appears that this will lead to progress both in the analytical technique and in the exploitation of modern data processing and presentation resources.

## 5. APPLICATION OF LIDAR OBSERVATIONS TO METEOROLOGICAL PROBLEMS AND ATMOSPHERIC STUDIES

### 5.1 General

Techniques for remotely probing the atmosphere can be directed towards measuring the temperature, density or composition (in terms of water vapor, ozone or carbon dioxide) of its gases, or to delineating and identifying the nature of its particulate content. In addition, the motions of the atmosphere are also of concern - both in terms of wind motion and turbulence.

What can lidar observations accomplish in these areas?

Direct evaluations of the backscattering profile in the upper atmosphere are believed to be capable of providing information on density profiles with sufficient accuracy to show seasonal variations in molecular density, at least in the layer from 50 to 80 kms, (Kent et al., 1967 and Sandford, 1967). However the possibility of unexpected particulate intrusions and the difficulty of making accurate measurements of returns from the tenuous upper atmosphere, make this approach rather uncertain, and in any case, it cannot be used when there are low clouds.

Other direct applications include the detection of the presence, height, shape, and in certain cases, thickness of clouds or haze layers. The evaluation of the atmospheric optical parameters ( $\beta'_{180}$  and  $\sigma$ ) can also be considered direct observations which provide descriptive information on the atmosphere and its structure.

Finally from the nature of atmospheric structure, observed in this way, it may be possible to infer the motion of the atmosphere which has given rise to such a structure. Motion, however, is most readily inferred by observing the displacement of recognizable natural features or specifically introduced indicator materials (e.g., smoke).

## 5.2 Illustrative Examples

The uses of lidar for these purposes can best be appreciated from the following illustrative examples. These are selected from a wide range of applications to demonstrate the salient features of lidar application to this context and show the current state-of-the-art.

### 5.2.1 Cloud and Cloud Structure

A good example of the use of lidar in a qualitative role is provided by observations made of cirrus cloud in the Owens Valley, California, early in 1966. (Collis et al., 1968). The SRI Mk. V Ruby Lidar (see Appendix for details) was located near Independence and used to make a series of observations in a vertical plane parallel to the direction of air flow. The objective was to observe the features and dimensions of waves caused by the Sierra range. Figure 4 shows an example of the cloud structure observed in this way. The readiness with which the length and amplitude of the waves can be evaluated is obvious. Note that lidar echoes were obtained at slant ranges over 20 km for cirrus cloud, in daylight with the relatively modest system. The limited data rate (1 pulse per minute) however, restricts the resolution of the cross section both in space and time. Atmospheric structure revealed in this and similar cross sections (even of sub-visible inhomogeneities) offer a new capability for studying atmospheric motion with possible implications in the study of turbulent motion. (See Lawrence et al., 1968 for a report of lidar observations associated with turbulence experienced by an aircraft.)

Of course, denser lower clouds can readily be mapped by lidar (Collis, 1965). More quantitative studies of cirrus clouds are also being carried out at SRI in connection with radiometric measurements such as those made by satellite. An example of quantitative data reduced from lidar observations is shown in Figure 5. (Manually extracted data is processed and presented by computer and automatic plotter. Quantitative data are available on punched tape for further manipulation). Data such as these are compared with satellite cloud photographs and upper air soundings. As a subsequent experiment, it is hoped to compare them with radiometric data acquired by the Nimbus satellite.

### 5.2.2 Inhomogeneity in the 'Clear' Air

Variations in the turbidity of what appears to the eye to be clear air may readily be determined by lidar. Figure 6 shows a time/height cross section made at Menlo Park, California in 1967 by making a series of vertical lidar observations over an extended period. The data in the form SBF values (see 4.2 above) show the stratification clearly.

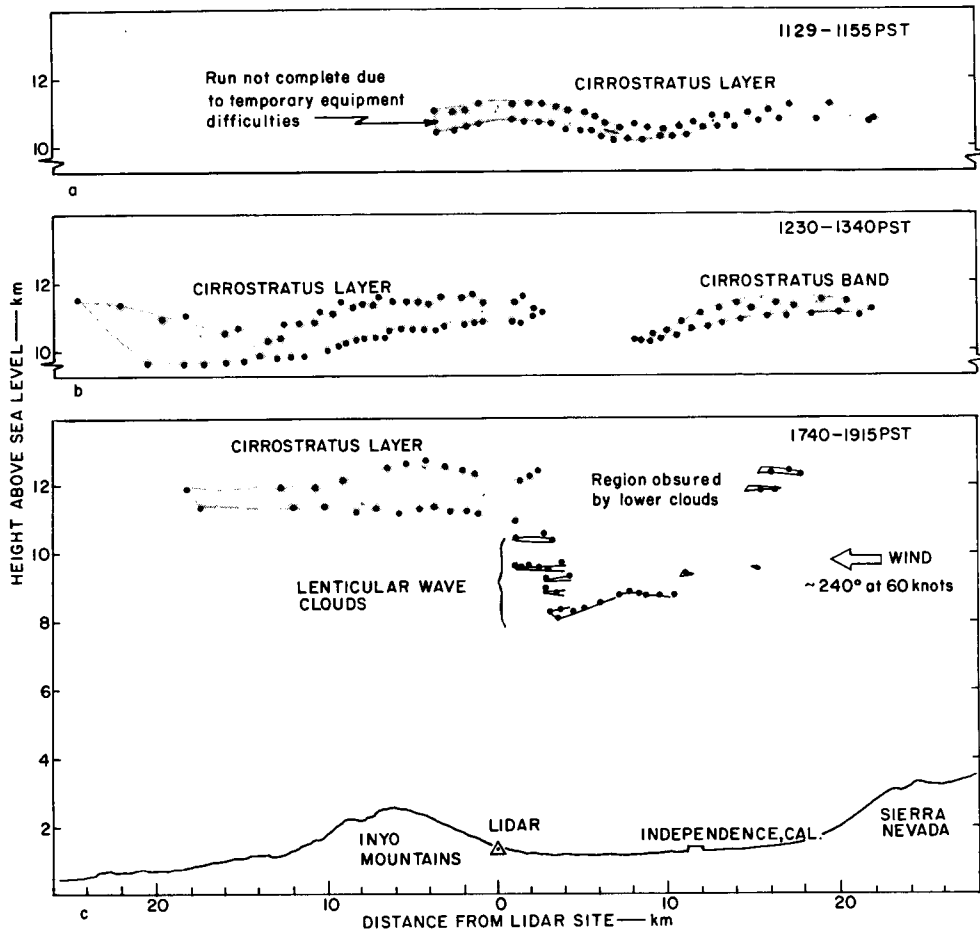


Figure 4. LIDAR observation of wave clouds in the lee of the Sierra Nevada, 1 March 1967. Data were obtained by scanning ruby lidar in the vertical and noting echoes at successive angles of elevation (indicated by data points).

The turbid air in the lower layer is separated from the overlying clean air at the level of the temperature inversion base (approx. 300 m). The transition layer between the turbid and clean air is marked in the illustration by the pair of lines roughly parallel to the time axis. This layer was particularly well defined during the period where the lines are heavy. The diurnal effects are apparent as relative humidity increased before sunrise, at which time vestiges of visible stratus cloud were observed to form.

Such lidar observations clearly offer contributions in observing and monitoring the effects of thermal stratification in the atmosphere and possible changes in its relative humidity. In addition, of course, remote quantitative observation may be made of the density of the particulate pollution loading and its changes with time (Barrett and Ben-Dov, 1967).

At higher levels, i.e., in the stratosphere and mesosphere, a number of workers have reported the detection of particulate layers, some of which are claimed to be associated with noctilucent clouds. (See Fiocco and Smullin, 1966; Fiocco and Grams, 1966; McCormick, P. D. et al., 1966; Collis and Lidga, 1966; Kent et al., 1967; and Sandford, 1967.)

5.2.3 Air Motion

If a suitable indicator or tracer material is injected into the atmosphere, lidar makes it possible to monitor its dispersal quantitatively and conveniently. For example, Figure 7 shows how a cloud of insecticide released by a low-flying aircraft moved down a wooded hillside, under the influence of air drainage. This example from observations made in Idaho in 1966 in connection with U.S. Forest Service studies of insecticide application shows the position of the cloud (which was quite invisible to the eye) along a fixed line of sight just above the tree tops at successive intervals of time. The velocity of the flow can readily be evaluated. In this case, the cloud remained fairly compact, but in other drops made under different meteorological conditions, the cloud dispersed rapidly. In such cases, especially as studied in a subsequent program conducted in 1967 (Figure 8) it was possible also to monitor the dispersal in the vertical, and by measuring changes in volume backscattering coefficient, to assess fall-out and diffusion (Collis and Oblanas, 1967).

Another example of transport studies is illustrated in Figure 9 which shows successive horizontal cross sections through a cloud of dust caused by an explosion in Montana in 1966 (Oblanas and Collis, 1967). These sections were made initially by allowing the cloud to drift through the lidar beam at successive fixed headings and thereafter by scanning in the horizontal plane. Even at the time of the dense first section, the dust suspension was too tenuous to be visible to the eye.

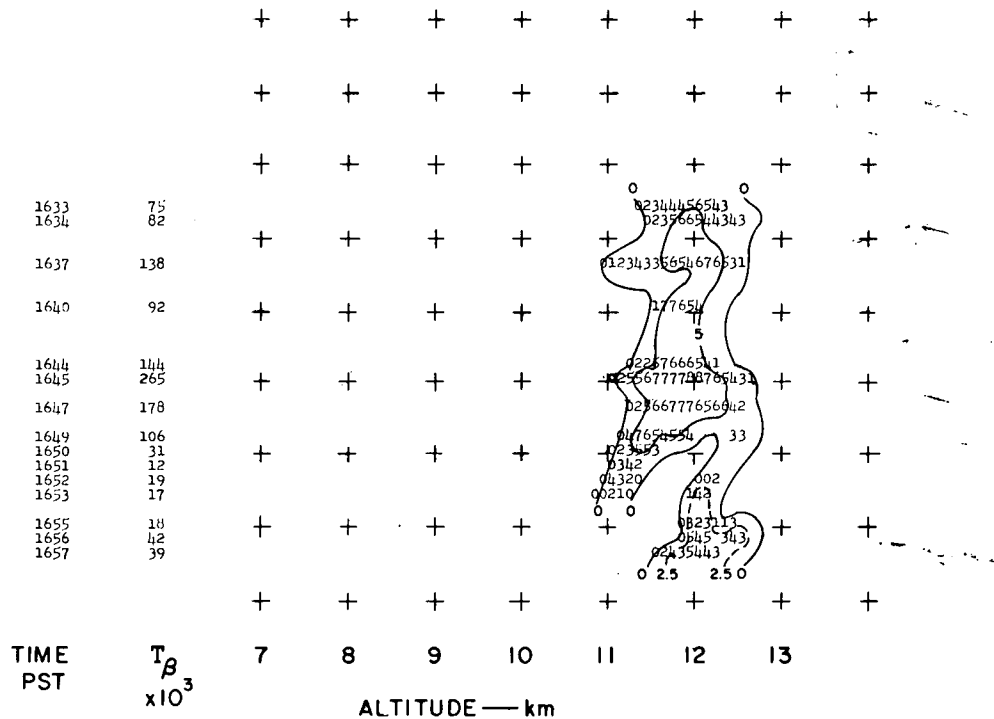


Figure 5. Graphical-quantitative representation of LIDAR cloud observations, Menlo Park, 8 December 1967. The automatically plotted data show volume backscattering coefficient values (for altitude increments of 100 m) expressed in a logarithmic code. The parameter shown as a number against each time indication similarly describes the transmission measured through the cirrus layer. Input data were manually reduced from Polaroid photographs.



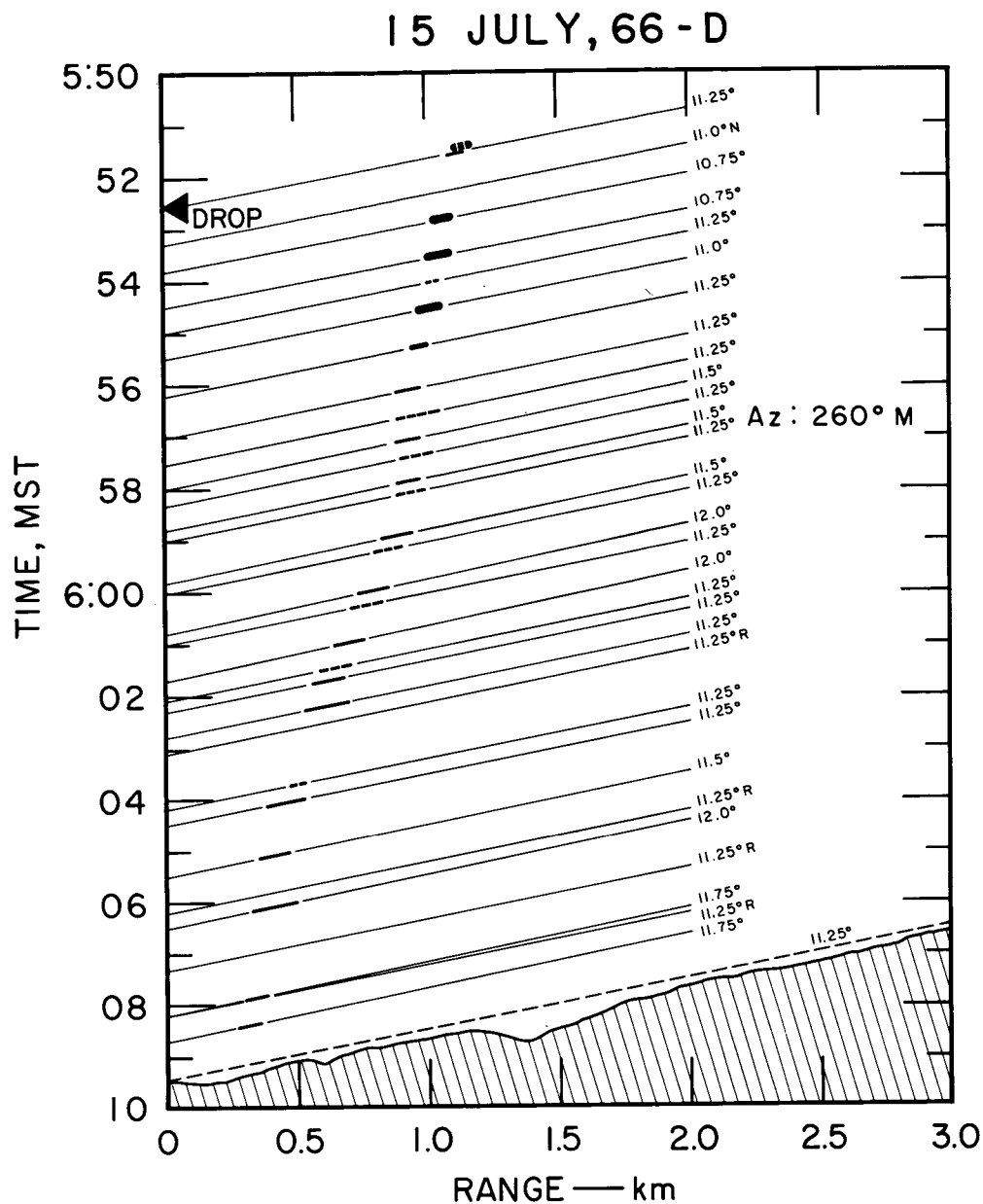


Figure 7. LIDAR observations of insecticide sprayed, by aircraft, Idaho, June 1966. Two lidars were used, ruby and neodymium. The echoes (continuous and dashed marks respectively) were detected in the positions shown at about the level of the tree tops (indicated by a dashed line). The insecticide was dropped at approximately 0552 MST (in concentration of 1qt/acre, droplet size of order 100 microns) from an aircraft flying about 60 m above the surface in a direction normal to the section represented. Note that the ordinate shows time and the diagram thus shows the results of lidar observations made at successive intervals as indicated. The insecticide was quite invisible to the eye.

LIDAR

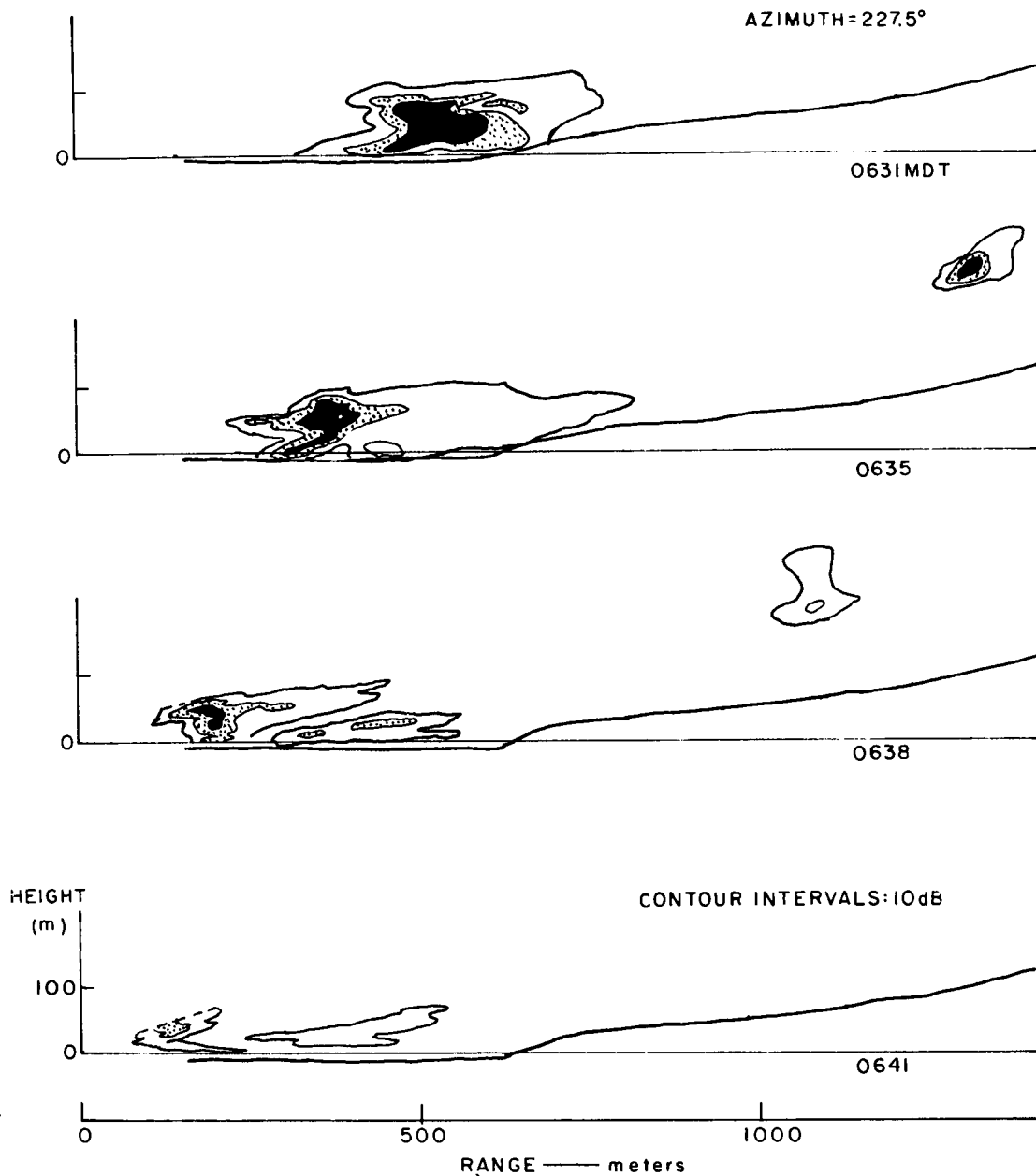


Figure 8. LIDAR observations of insecticide clouds, Idaho, June 1967. In this case a neodymium lidar was scanned in the vertical and observations were made at  $1^\circ$  intervals of elevation every 5 seconds. (The insecticide was sprayed in a similar manner to that described in Figure 7, but in this case the concentration was of the order of 0.5 pt/acre, with droplet sizes around 50 microns.) (The small cloud on the right of the illustration was smoke, also trailed by an aircraft.) The successive cross-sections (in which the internal structure is shown by relative backscattering coefficient isolines at 10 db intervals) show the motion and rate of dispersal of the insecticide (which was quite invisible to the eye).

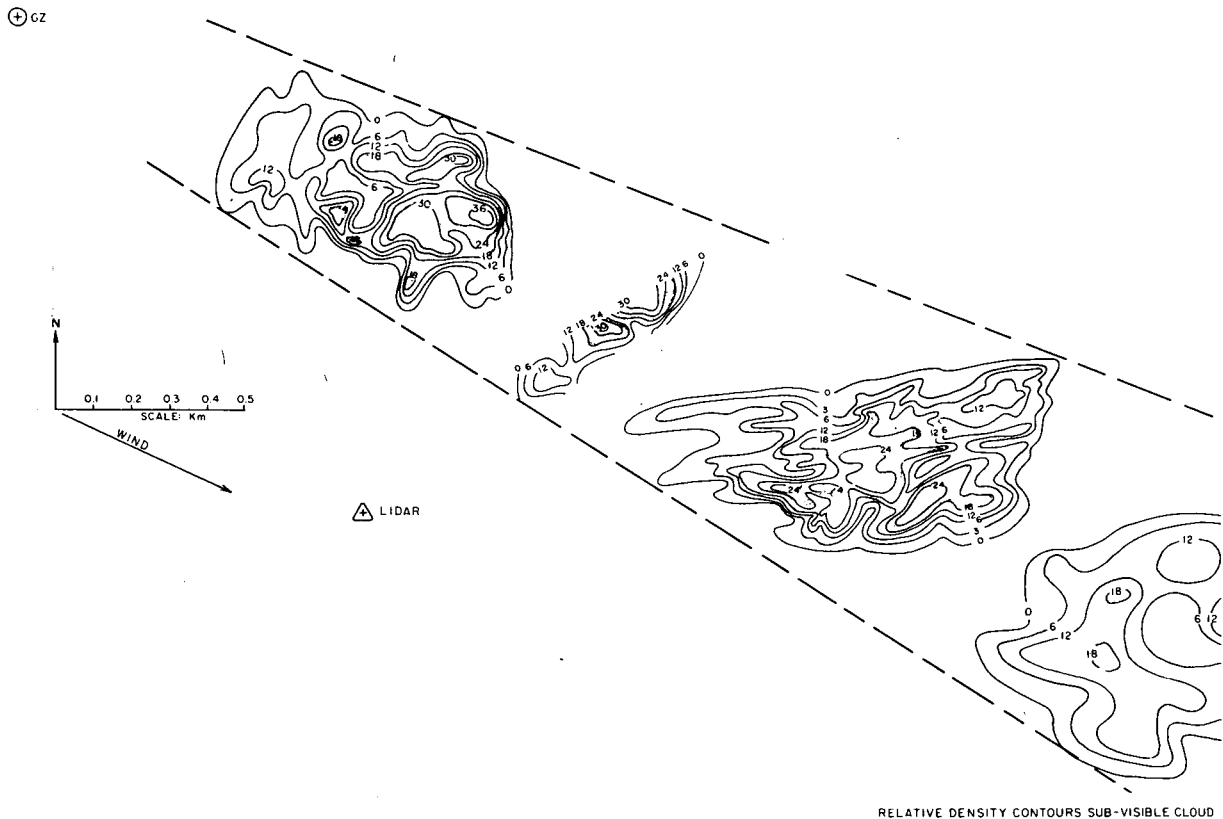


Figure 9. Series of four horizontal cross sections showing approximate relative density distributions of subvisible dust cloud. Cross sections were made with a neodymium lidar. (Observations time are centered at 3.0, 4.0, 6.0, and 8.3 minutes after the explosion which took place at Ground Zero (GZ) as indicated.) Dust was caused by the explosion of 20 tons of nitromethane at Fort Peck, Montana, November 1966. Even at the time of the first cross-section, however, no dust could be seen by the eye.

Similar sections have been made of explosion clouds using an airborne lidar (Collis and Oblanas, 1968) and work is continuing at SRI on applications of this type. Hamilton (1965) has also described lidar tracking observations of effluent from power station smoke stacks.

#### 5.2.4 Fog and Low Cloud

A recent example of lidar observations of fog and low cloud is illustrated in Figure 10. It is of particular significance because it demonstrates the important contribution lidar can make in an operational role. At Hamilton AFB, California, the landing approach path on a well used runway lies over the waters of San Francisco Bay and adjoining marshes. The conventional rotating beam ceilometer located near the touch down point is only capable of monitoring cloud base immediately overhead. Conditions at this point are frequently not representative of conditions along the approach path. In experimental observations made with an SRI ruby lidar, the nature of the cloud base was monitored out along the approach to distances of up to 2 km in conditions of fog and low ceiling (visibilities of the order of 1000 m). The illustration shows a typical cross section

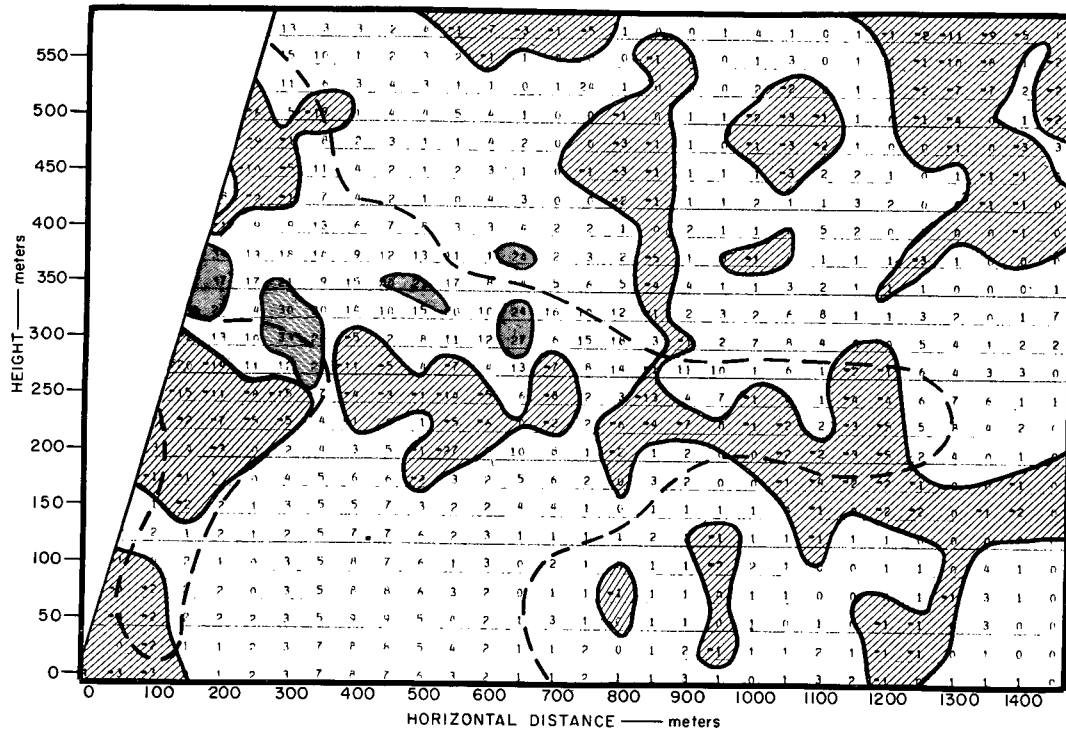


Figure 10. LIDAR observations of low cloud and reduced visibility conditions, Hamilton AFB, January 8, 1968. This is an analysis based on interim evaluations of extinction coefficient made by computer from manually entered data from a series of lidar observations. The parameter shown is  $\sigma$  ( $\text{km}^{-1}$ ). Negative values show areas of rapidly increasing volume backscattering coefficient (i.e., dense cloud). Dotted line shows limit of area (i.e., within 700 m at the surface) of higher confidence in the data.

derived from a series of lidar observations scanning in the vertical. In addition to the delineation of the level of the diffuse cloud base, (c, 200 m) computations of quantitative parameters related to 'visibility' are shown over the section in question. Apart from the ability of lidar to observe cloud bases considerably displaced from its vicinity, this example illustrates the further potential of lidar for evaluating the important, but hitherto inaccessible operational parameter "slant visibility."

## 6. LIDAR CONTRIBUTIONS TO ATMOSPHERIC STUDIES AND METEOROLOGICAL PROBLEMS

It is important to recognize that the lidar technique applies broadly to a wide range of atmospheric and meteorological studies. We are dealing here with a generic rather than a specific technique.

The technique may be adapted and applied to a very diverse range of problems and it is hoped that these will be broadly evident from the above discussion and illustrations. The following seem particularly appropriate areas for lidar contributions:

General Research

1. Structure of dust layers in upper atmosphere, noctilucent clouds, etc. (20 to 150 km), atmospheric density (50-80 km).
2. Wave motion and turbulent air flow over orographic features and generally, as revealed by clouds and particulate inhomogeneities (at all levels up to say 15 kms).
3. Boundary layer structure (variations in low-level inversion levels, etc.) especially in relation to factors significant to air pollution in urban areas.
4. Turbulent mixing and diffusion processes, using indicator materials.
5. The effect of visible and sub-visible cirrus clouds and other aerosol layers on radiative transfer of energy within and through the atmosphere.

Operational

1. Ceilometry
2. 'Visibility' measurement, particularly over elevated slant paths for aircraft operations.
3. Wind profile measurement (using rocket disseminated trails of tracer material).
4. Tracking atmospheric pollutants from specific sources, e.g., insecticide spraying, nuclear tests, and smoke stacks.

## 7. FUTURE DEVELOPMENTS

Progress in the atmospheric and meteorological studies noted above (Sec. 6) could undoubtedly be made with little or no further technological development. There is much room for progress in the technological basis of the lidar technique, however. In certain fundamental aspects, advances in laser energy generation for example, progress will emerge as a result of new discoveries which can confidently be expected in this burgeoning field. In other aspects, many possibilities for progress are already readily apparent and achievable within the current state-of-the-art. The restrictive factors here are largely economic.

In the area of new developments, there is a need for higher repetition rate lasers providing higher average powers and higher data rates than are currently available. In this context, particularly for operational applications, eye safety considerations are important. Fortunately all requirements would be well met by a relatively low peak power with a high pulse repetition frequency, but it would be desirable in addition for such lasers to operate at wavelengths which are outside the visual range.

## LIDAR

The development of high pulse rate lasers would lead to the development of systems capable of scanning in two dimensions to obtain nearly instantaneous atmospheric cross-section from stationary viewpoints, or more complete data from moving platforms such as aircraft or satellites. While such high-PRF systems would facilitate the development of graphical displays comparable to those used in weather radars, a more desirable development would be the input of such data to a computer for automatic quantitative processing and display. Techniques for handling data in this way are readily adaptable from currently available technology—but further progress must be made in developing techniques for recovering significant data from lidar operations.

Apart from the more obvious advantages of such data handling and presentation techniques, they open up the way to the powerful resources of modern information analysis procedures and the better coordination of lidar observations with other types of observations.

### ACKNOWLEDGMENTS:

In preparing this review, I have drawn heavily upon the contributions of my colleagues at Stanford Research Institute and I am especially indebted to Dr. Warren Johnson, Dr. E. Uthe, and Mr. W. E. Evans for their assistance.

I am very conscious of having dealt only cursorily with the work of others elsewhere. Having relied mainly upon published descriptions of their work, my account is necessarily out of date in this respect.

## Appendix

STANFORD RESEARCH INSTITUTE  
TYPICAL LIDAR CHARACTERISTICS

	<u>Mark V</u>	<u>Mark I</u>
	<u>Transmitter</u>	
Laser Material	Neodymium-Glass	Ruby
Wavelength ( $\mu$ )	1.06	.6943
Beamwidth (mrad)	0.2	0.5
Optics	6-inch Newtonian Reflector	4-inch Refractor
Peak Power Output (MW)	50	10
Pulse Length (ns)	12	24
Q Switch	Rotating Prism	Saturable dye
Max. PRR (pulses/min)	12 (1967) 1-2 (1966)	1-2
	<u>Receiver</u>	
Optics	6-inch Newtonian Reflector	4-inch Refractor
Field of View (mrad)(maximum)	3.0	2.0
Pre-Detection Filter		
Wavelength Interval ( $\mu$ )	.01	.0017
Detector	RCA 7102 (S-1 Cathode)	RCA 7265 (S-20 Cathode)
Post-Detection		
Filter Bandwidth (MHz)	30	30

## REFERENCES

- Barrett, E. W. and O. Ben-Dov, 1967: Application of LIDAR to air pollution measurements, J. Appl. Meteorology, 6, p. 500.
- Collis, R. T. H., 1965: LIDAR observations of clouds, Science, 144, p. 978.
- Collis, R. T. H. and M. G. H. Ligda, 1966: Note on LIDAR observations of particulate matter in the stratosphere, J. Atmos. Sc., 23, p. 255.
- Collis, R. T. H. and J. W. Oblanas, 1967: LIDAR observations of forest spraying operations, SRI Final Report, Contract 26-120, Forest Service, U.S. Dept. of Agric.
- Collis, R. T. H. and J. W. Oblanas, 1968: Airborne LIDAR observations-Pre Gondola II, U.S. Army Engineer Nuclear Cratering Group Report PNE-1119.
- Collis, R. T. H., F. G. Fernald and J. Alder, 1968: LIDAR observations of Sierra wave conditions, J. Appl. Met., 7, p. 227.
- Deirmendjian, D., 1964: Scattering and polarization properties of water clouds and hazes in the visible and infrared, Appl. Optics, 3, p. 187.
- Elterman, L., 1964: Atmospheric attenuation model, 1964, in the ultraviolet, visible and infrared regions for altitudes of 50 km, #46 Environmental Res. Papers, Air Force Cambridge Research Laboratories, AFCRL-64-740.
- Elterman, L., 1968: UV, visible, and IR attenuation for altitudes to 50 km, 1968, Environmental Res. Papers, No. 285, Air Force Cambridge Research Laboratories, AFCRL-68-0153.
- Fenn, R. W., 1966: Correlation between atmospheric backscattering and meteorological visual range, Appl. Optics, 5, p. 293.
- Fiocco, G. and L. D. Smullin, 1963: Detection of scattering layers in the upper atmosphere, Nature, 199, p. 1275.
- Fiocco, G. and Grams, 1966: Observations of the upper atmosphere by optical radar in Alaska and Sweden during the summer 1964, Tellus, 18, p. 34.
- Goyer, G. G. and R. Watson, 1963: The laser and its application to meteorology, Bull. A. Met. S., 44, p. 564.
- Hamilton, P. M., 1966: The use of LIDAR in air pollution studies, Air and Wat. Pollut. J., Pergamon Press, Oxford, Eng., 10, p. 427.
- Kent, G. S., B. R. Clemesha and R. W. Wright, 1967: High altitude atmospheric scattering of light from laser beam, J. Atmos. and Terr. Phys., 29, p. 169.

- Lawrence, J. D., M. P. McCormick, S. H. Melfi and D. P. Woodman, 1968: Laser backscatter correlation with turbulent regions of the atmosphere, App. Phys. Letters, 12, p. 72.
- Ligda, M. G. H., 1963: Meteorological observations with pulsed laser radar, Proc. 1st Conf. on Laser Technology, U.S. Navy, San Diego, Sept. 1963, p. 63.
- Long, R. K., 1963: Atmospheric attenuation of ruby lasers, Proc. IEEE, 51, p. 859.
- McCormick, P. D., S. K. Poultney, V. Van Wijk, C. O. Allen, R. T. Beltinger and J. A. Perschy, 1966: Backscattering from the upper atmosphere 75-160 km detected by optical radar, Nature, 209, p. 798.
- Middleton, W. E. K., 1958: Vision Through the Atmosphere, Univ. of Toronto Press.
- Middleton, W. E. K. and A. F. Spilhaus, 1953: Meteorological Instruments, Univ. of Toronto Press, p. 208.
- Munick, R. J., 1965: Turbulent backscatter of light, J. Opt. Soc. Amer., 55, p. 893.
- Northend, C. A., R. C. Honey and W. E. Evans, 1966: Laser radar (LIDAR) for meteorological observations, Rev. Sci. Instruments, 37, p. 393.
- Oblanas, J. W. and R. T. H. Collis, 1967: LIDAR observations of the Pre Gondola I Cloud, U.S. Army Engineer Nuclear Cratering Group, Report PNE-1100.
- Sandford, M. C. W., 1967: Laser scatter measurements in the mesosphere and above, J. Atmos. and Terr. Phys., 29, p. 1657.
- Schotland, R. M., A. M. Nathan, E. A. Chermack and E. E. Uthe, 1962: Optical sounding, Technical Report #2, New York University Report, Contract DA-36-039-SC87299, U.S. Army, E.R.D.L.
- Twomey, S. and H. B. Howell, 1965: The relative merit of white and monochromatic light for determination of visibility by backscattering measurements, Appl. Optics, 4, p. 501.
- Twomey, S. and H. B. Howell, 1967: Some aspects of the optical estimation of microstructure in fog and cloud, Appl. Optics, 6, p. 2125.
- U.S. Government Printing Office, 1962: U.S. Standard Atmosphere.
- Van de Hulst, H. C., 1957: Light Scattering by Small Particles, J. Wiley and Sons, New York, New York, p. 82.

PRECEDING PAGE BLANK NOT FILMED

COMMENTS ON "LIDAR" BY R. T. H. COLLIS

Earl W. Barrett  
Atmospheric Physics and Chemistry Laboratories  
ESSA Research Laboratories  
Boulder, Colorado 80302

Dr. Collis has given an excellently clear and concise summary of the basic theory of lidar backscatter measurements, and of the various ways in which lidar data can be used in support of atmospheric research and meteorological observations. I cannot find any major points of disagreement with his presentation. My remarks are, therefore mainly concerned with emphasizing various points in his discussion which call most strongly for additional research and development. In the course of my remarks I will, however, occasionally give opinions which are sometimes more optimistic and sometimes more pessimistic than those which he has expressed.

My comments will fall into two general categories; those dealing with hardware problems and those dealing with evaluation, interpretation, and utilization of data.

I concur with Dr. Collis's statement that one of the most urgent needs is for lasers with high repetition rates, in order to avoid the necessity for photographic recording and subsequent tedious manual reduction of data. I believe, however, that unless the average output power can be increased by orders of magnitude, raising only the pulse rate will not allow the acquisition of any more information per unit time than is presently possible. For example, consider two lidars, one with a PRF (pulse repetition frequency) of 1 per second and a peak pulse power of 1 MW, and the other with a PRF of 1000 per second and peak power of 1 KW. I do not wish to pose as an expert on information theory, but it seems to me that the following argument holds: The signal-to-noise ratio, on a single shot, will be 30 db. poorer for the second lidar than for the first. It will therefore be necessary to average electronically 1000 pulses from the second lidar to establish the same S/N ratio. But this will require precisely one second, so that no time whatever will be saved.

What is really needed is a more efficient method of exciting the useful energy levels in solid-state laser materials. The present method of optical excitation with flashtubes is really a brute-force conversion of noise into information. As such, it is a statistically improbable phenomenon and therefore hopelessly inefficient. The average power of a solid-state laser is ultimately limited by two factors: The thermal conductivity of the rod material, and the surface-to-volume ratio of the rod. The first is beyond our

power to influence, so that only the latter is adjustable. The limit of improvement in this area has probably been reached already by use of fiber-optic bundles of doped glass, with interstices for coolant flow, in neodymium lasers. Hence the only hope for the future lies in finding better means of pumping. We thus have identified a prime research target.

With regard to choice of wavelength, it is evident that a compromise must be made with respect to various practical factors. A long wavelength reduces the Rayleigh and sky-light background, and is therefore desirable when aerosol or cloud measurements are the objective, but is contra-indicated for upper-atmosphere density measurements. Also, the efficiency of photodetectors falls off deplorably at wavelengths exceeding 1 micron, as do the transmittances and reflectances of lenses and mirrors. The multiplicity of absorption lines for water and CO<sub>2</sub> also introduce complications in data interpretation. At short wavelengths, sky-noise and Rayleigh background increase, and absorption by most atmospheric constituents sets in as the ultraviolet is approached. I therefore feel that the ruby wavelength represents the best possible compromise at present, with the neodymium running a close second (because of its higher possible PRF), if one is limited to a single general-purpose instrument.

The need for automation in the handling of lidar data is very apparent to anyone who has strained his eyes reading ranges and intensities to tenths of millimeters from Polaroid photographs of A-scopes. This is the rate-determining step in the entire process. In my own work on aerosols, the raw data are impressed on the film in one or two microseconds; the print is ready for inspection in 15 seconds, and is dry enough for handling in 15 minutes. Reading-off and tabulating some 30 significant levels from a print takes about an hour; punching these on cards consumes another half hour. The computer then finishes the job in about 1 1/2 seconds. Direct analog-to-digital conversion would save nearly two hours per sounding.

Dr. Collis's suggestion that a video magnetic recorder be used for storage and repetitive playback to a sampling-type digitizer is an excellent one in principle, but does have certain limitations, in my opinion. Video signals have a nominal bandwidth of 4 MHz, which implies a time resolution of the order of 250 nanoseconds or a range resolution of 125 feet. This may be adequate for some purposes, but certainly not for all. The matter of waveform distortion is also serious; what is adequate for playback of an entertainment video signal is, in most cases not sufficiently "high fidelity" for lidar work. Two sources of waveform distortion are easily identified. Although the DC component of a signal can be recorded on tape or disc, the playback is essentially a mathematical differentiation so that some low-frequency information is inevitably lost. Since any single-shot phenomenon, however short, has a spectral peak at zero frequency, it follows that some distortion will be introduced, in the form of a "sag" in the reproduced signal. Even though this may only amount to a few parts per million of the

peak amplitude, it may be unacceptably large in view of the 60-db dynamic range involved in a single lidar sounding. The other source of distortion is the variation in magnetic properties from point to point on the recording medium. I have not experimented with video recorders; I have, however, recorded a steady tone from a signal generator on a professional-quality audio tape recorder and observed 1-db fluctuations in level on playback. This would, in my opinion, be unacceptably large for quantitative lidar work. There is also ample chance for distortions of one or more per cent in the needed amplifications and signal mixings involved in magnetic recorders and playbacks. My philosophy is that, the less circuit elements between the photodetector and the Polaroid camera, the more reliable the information obtained.

Probably the most satisfactory arrangement would be real-time analog-to-digital conversion of the voltage appearing across the photodetector load resistance, followed by transfer of the digitized data to an on-line computer. The feasibility of this again depends on the range resolution desired. If one takes 25 feet as a target figure, the A-D conversion must be done every 50 nanoseconds; the 60-db dynamic range calls for 5-significant-figure digitization. I have not yet found any off-the-shelf system which will meet these requirements; my friends in the electronics profession are, in general, rather pessimistic about the possibility of meeting them in the near future. This is another research problem of pressing importance.

Turning now to the evaluation problems, I note that Dr. Collis's main point here is that the lidar equation is unsolvable unless the relationship between  $\beta'_{180}$  and  $\sigma$ , i. e., the backscatter and the total scatter, can be specified. I am in complete agreement with this statement. I believe, however, that he may be slightly too pessimistic when he states, on p. 157 of his paper that "----any significant scattering of lidar energy by atmospheric targets involves considerable attenuation." I have evaluated a number of soundings taken in rather dirty air, with and without the extinction term, and have found that in most cases the results differed by only a few per cent at the longer ranges. There are notable exceptions, particularly in stagnant maritime-tropical air under a subsidence inversion, when the error becomes as great as 50 per cent.

To illustrate this point, I have augmented Dr. Collis's Table II by computing some values of  $\beta'_{180}$  and  $\sigma$  (for the aerosol contribution alone) for my "standard aerosol", which has a radius range of 0.04 to 10.0 microns, a mass-median radius of 0.63 micron, is distributed in accordance with the Junge " $r^{-3}$  law", and has an index of refraction of 1.5. Rather than categorizing the haze as light, moderate, or heavy, or by number density, I have used visibility (in the sense of Koschmieder) as the parameter. The basis for the calculation is the scattering table of De Bary et al (1965). The results are tabulated below.

TABLE I

Haze Scattering (Aerosol Component)

<u>V (mi)</u>	<u><math>\beta'_{180}</math> (<math>m^{-1}</math>)</u>	<u><math>\sigma</math> (<math>m^{-1}</math>)</u>
20	$4.36 \times 10^{-5}$	$9.00 \times 10^{-5}$
15	$5.89 \times 10^{-5}$	$1.21 \times 10^{-4}$
10	$9.03 \times 10^{-5}$	$1.86 \times 10^{-4}$
5	$1.22 \times 10^{-4}$	$2.51 \times 10^{-4}$
2	$4.68 \times 10^{-4}$	$9.64 \times 10^{-4}$
1	$9.39 \times 10^{-4}$	$1.93 \times 10^{-3}$
1/2	$1.88 \times 10^{-3}$	$3.88 \times 10^{-3}$

$$(\beta'_{180} = (943V^{-1} - 4) \times 10^{-6}, V \text{ in miles; } \sigma = 2.06\beta'_{180}, k = 0.486)$$

It is clear that, if the visual range is greater than 20 miles, the error made by dropping the extinction term in the lidar equation will be less than 18 per cent at a distance of 1 km. It has been my experience that, once one ascends above the polluted boundary layer, the subjective visibility is much greater than 20 miles in most meteorological situations (excluding clouds); it is usually 100 miles or more. This is confirmed by the lidar data at Chicago. For most vertical soundings, therefore, even a rough estimate of Dr. Collis's  $k$  will yield sufficiently accurate calculations of  $\beta'_{180}$  even at long ranges. For slant observations at low elevation angles in the boundary layer, or when one is stretching the capability of the technique by trying to measure quantitatively the aerosol concentration in the stratosphere, I agree that greater precision is required.

Dr. Collis's frequent reference to the work of Twomey and Howell, in pointing out the uncertainties in the proper value of  $k$ , brings me to my last main point. When I first saw their plot of  $\zeta$  (Dr. Collis's  $k$ ) as a function of particle radius for a wavelength of 0.7 micron, I was quite shocked. It struck me that the plot looked much more like noisy experimental data than like the solution of a neat mathematical model. I have not singled out these authors for special criticism; I have simply developed considerable skepticism about all computations based on the Mie theory. I do not mean to imply that the theory, as such, is unsound; I refer, rather, to the appallingly numerous opportunities for the entrance of computational noise when the usual algorithms (as I have seen them) are used. The scattered intensity (for each polarization) consists of the square of an infinite series of amplitudes, each multiplied by a function of the scattering angle. The convergence rate of this series is known to be very slow; the possibility of significant truncation error is therefore great. Furthermore, the individual amplitudes are each a ratio of differences of two numbers. These numbers, in turn, are products of Bessel functions, which are (I suspect) calculated in practice by means of recursion equations; this invites

cumulative error. I suspect that the major source of computational noise lies in those ratios of (possibly small) differences of (possibly large) numbers which occur in the amplitudes. In addition, when the scattering by polydisperse aerosols is to be computed, a numerical integration over the size distribution must be carried out. This smooths out irregularities, to be sure, but offers additional opportunity for quantitative error.

I feel, therefore, that further work must be done to recast the Mie algorithms into forms less sensitive to computational noise; probably by transformation to new variables. I have been spending considerable time recently on just this problem, with, however, a notable lack of success so far. I would like very much to enlist the aid of applied mathematicians in this, which I identify as the third major obstacle standing in the way of more effective utilization of the lidar.

With reference to the observation of Dr. Collis that the quantitative approach has entered rather earlier in the history of lidar than in that of radar, I agree that the low PRF of the lidar, which precludes the eye-catching but qualitative intensity-modulated areal displays, has been an important factor. I should like to suggest some possible other contributors. One of these is the considerable body of experience already acquired with radar. Another is the fact that meteorological uses of radar were first discovered during wartime, by military users, and were promptly slapped under tight security classification. Still another is the fact that, since lidar operates in or near the visible spectrum, the qualitative phenomena involved are already familiar to the eye and hence are less interesting and novel. Furthermore, the quantitative application of radar which was most obvious, and hence most studied, is the measurement of precipitation; the radar has had a much cheaper competitor in the rain gauge. As a converse proposition, many of the qualitative functions the lidar can perform can be done more cheaply by other means (such as ceilometers).

To Dr. Collis's list of present and prospective uses for the lidar, I would like to add one or two more. The water-vapor line at 0.69438 micron, which is a nuisance in most other applications of the ruby lidar, offers the possibility of remote humidity soundings by comparison of the returns from two lidars, one tuned inside the line and the other outside. I believe that Dr. Schotland will discuss this particular application in detail in his paper, so I will not say more. I will mention another effect of humidity which is also a bother in aerosol work, but which is helpful when the lidar is used to monitor the height of subsidence inversions. The sorption of water by hygroscopic and hydrophilic aerosol particles increases their sizes and hence their scattering cross-sections, as the humidity increases. The effect is to produce the analog of the "bright band" of radar meteorology, because the humidity normally reaches a maximum at the inversion base, while both the humidity and aerosol count decrease rapidly through the inversion.

## COMMENTS ON "LIDAR" BY R. T. H. COLLIS

If any agreement can be reached on a mean drop-size distribution function for young, non-precipitating clouds, the lidar could be used for mapping the liquid-water content of the clouds from the ground. The figures would be rough, to be sure, but who would claim any remarkable accuracy for the present aircraft-mounted probes used for this purpose?

The lidar can also be used to study meso- and micro-scale atmospheric circulations when these affect the spatial distribution of aerosols. If time permits, I would like to show a few slides which show how the diurnal lake-breeze cycle at Chicago affects the distribution of pollutants, after the following concluding remark.

Dr. Collis and I are in agreement that there are state-of-the-art limitations, both physical and mathematical, to the quantitative application of lidar in remote atmospheric measurement, and that some of these are not likely to be removed in the immediate future. I have emphasized three such major blocks in my comments. I believe that, since we must live with these limitations, it behooves us to seek out and stress those applications where the lidar has no true economic competitor, such as the mapping of aerosols and the others we have mentioned, because, certainly, rough data are preferable to no data at all. I close, then, by proposing that the motto of the lidar guild in meteorology should be "Help stamp out research aircraft and meteorological towers".

N72-25358

## SOME ASPECTS OF REMOTE ATMOSPHERIC SENSING BY LASER RADAR

Richard M. Schotland

New York University\*

### ABSTRACT

An analysis has been made of some aspects of atmospheric sensing by laser radar spectroscopy. A discussion of the laser radar equation is presented which leads to methods for obtaining atmospheric information by spectroscopic means. Calculations are presented which investigate the potential of Doppler, Raman and differential absorption techniques. It is concluded that atmospheric measurements based upon Doppler and Raman approaches are restricted to qualitative studies at the present time primarily because of the limitations imposed by existing laser sources and detectors. It is probable that these limitations will be removed in the near future and it is recommended that exploratory experiments be continued. The differential absorption method for obtaining the spatial distribution of atmospheric gases is well developed for such gases as water vapor and oxygen where the basic laser frequency lies close to the center of the particular absorption line. Further investigation is recommended in the field of laser frequency shifting. Additional information is also required on the shape of the absorption line, particularly in the region where the line reflects both pressure and Doppler broadening.

### 1. INTRODUCTION

The purpose of this paper is to consider the potential of the laser radar as a ground based remote sensor of the earth's atmosphere. Perhaps the simplest approach to this subject may be had by a consideration of the transfer equation which relates the power transmitted by the laser to that which is captured by coaxial receiving optics.

---

\*Contribution No. 62 of the Geophysical Sciences Laboratory, Department of Meteorology and Oceanography, New York University, New York, 10468.

$$P_r = \left( \frac{P_T}{\pi Z^2 \theta^2} \right) \cdot \left( \sigma_\pi \cdot n(Z) \right) \cdot \left( \frac{\Delta Z}{2} \cdot \pi Z^2 \theta^2 \right) \cdot \tau \cdot \frac{A_r}{Z^2} \quad (1)$$

Radiance at Z	Scatter cross section per unit length	Scattering volume	Transmis- sion of at- mosphere	Capture solid angle
------------------	---	----------------------	--------------------------------------	---------------------------

where

- $P_r$  = received power
- $P_T$  = transmitted power
- $A_r$  = receiver aperture
- $Z$  = slant range
- $\sigma_\pi$  = molecular backscatter cross section
- $n(Z)$  = molecular number density
- $\Delta Z$  = pulse length
- $\tau$  = two way atmospheric transmission
- $\theta$  = receiver beam width

When this equation is applied to the atmosphere it takes the normalized form:

$$Z^2 \frac{\bar{H}_{r\lambda}}{P_{T\lambda}} = \Delta Z \left[ \frac{2\pi^2 \gamma^2}{\lambda^4} n(Z) + \frac{\lambda^2}{8\pi^2} \int_0^\infty i(r, \lambda) N(r) dr \right] \tau \quad (2)$$

$$\tau = \exp -2 \left[ \int_0^Z \beta_G dz + \int_0^Z \beta_A dz + \int_0^Z \rho(Z) K_\lambda dz \right] \quad (3)$$

In this equation the following definitions hold:

- $\bar{H}_{r\lambda}$  = average irradiance at the receiver at wavelength  $\lambda$
- $P_{T\lambda}$  = pulse power of the transmitter at wavelength  $\lambda$
- $Z$  = slant range to the pulse volume
- $\lambda$  = laser wavelength
- $i(r, \lambda)$  = Mie scattering function
- $n(Z)$  = molecular number density at range  $Z$

$N(r, Z)$  = spectral distribution of aerosol particles at range  $Z$

$\beta_G$  = molecular scatter cross section/unit volume

$\beta_A$  = aerosol scatter cross section/unit volume

$K_\lambda$  = molecular absorption cross section (area/unit mass)

$\gamma$  =  $2\pi$  molecular polarizability

$\rho(Z)$  = atmospheric density

### 1a. Atmospheric Constituents

The atmosphere is composed primarily of nitrogen (78.5%) and oxygen (20.95%). These gases are well mixed and maintain the same percentages on a volume basis throughout the troposphere and stratosphere. The major variable gases of meteorological interest are water vapor, ozone, and carbon dioxide. These gases can vary rapidly both in time and in space.

The surface air contains large numbers of small particles whose sizes range from  $10^{-2}$  microns to 2 microns. Total number densities may be as large as  $10^5$  per cubic centimeter. The bulk of these particles have radii less than 0.1 micron and a typical count for particles greater than 0.5 micron would be 1 per cubic centimeter. The particle density normally decreases with height in an exponential manner as shown in Figure 1. The refractive index of these particles is complex with a real part in the range 1.5 to 1.7. Little is known of the spectral variability of either the real or imaginary portions of this quantity.

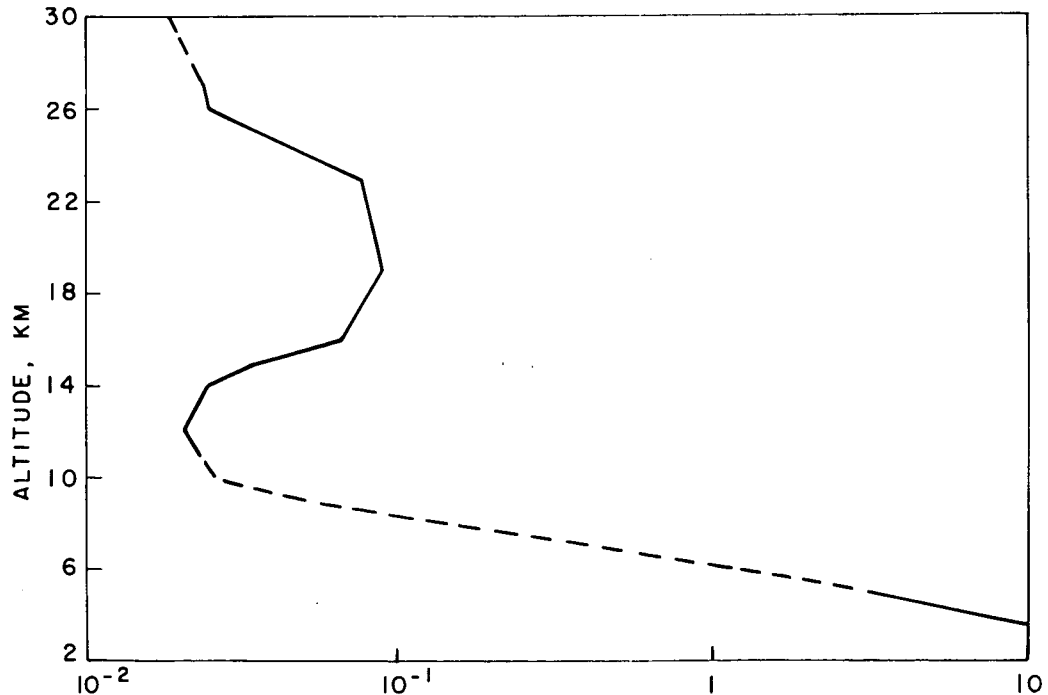


Figure 1. Variation of particle concentration with height.

## 1b. Atmospheric Spectral Properties

Elterman has computed the sea level particle scattering coefficient as a function of wavelength. These values have been plotted by Breece, *et al.* (1966) and are presented here as Figure 2. It should be noted that the scattering coefficient changes very slowly in the region below 1 micron. At wavelengths near 10 microns the aerosol particles will be in the Rayleigh range and the wavelength dependence will be  $\lambda^{-4}$ .

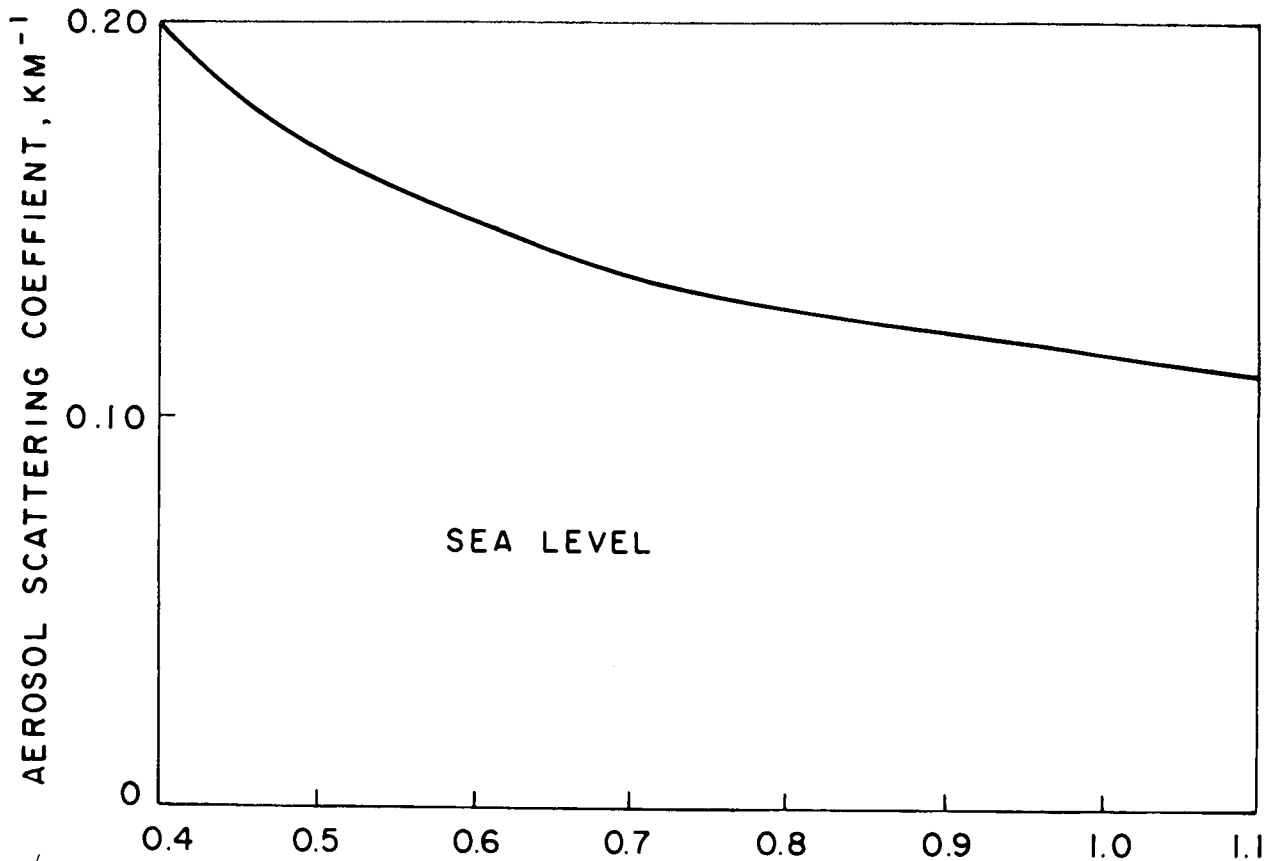


Figure 2. Variation of aerosol particles scattering coefficient with wavelength.

The magnitude of the particle backscatter at  $\lambda = .7\mu$  is an order of magnitude greater than that due to molecular scatter at ground level. However, due to the rapid decrease of particle density with height the two terms become essentially equal at 3 kilometers and remain so throughout the troposphere as shown in Figure 3 (Breece, *et al.* 1966).

The strong absorption bands of water vapor, carbon dioxide and ozone in the infrared and of ozone in the ultraviolet regions of the spectrum are well known to the meteorologist as they play important roles in the thermodynamics of the atmosphere. It is normally assumed that the atmosphere is essentially transparent from 0.3 to 0.9 microns. However, reference to high resolution telluric spectra shows that narrow, intense absorption lines due to water vapor, oxygen, ozone are dispersed throughout this region of the spectrum. A sample of such a spectrum taken at N. Y. U. by Bradley is shown in Figure 4. It should be noted that the atmospheric absorption for water vapor (one way) at  $6943.80\text{\AA}$  is nearly 60% and the line width is essentially  $0.05\text{\AA}$  at half width. Reference will be made to this isolated line in a latter portion of this paper.

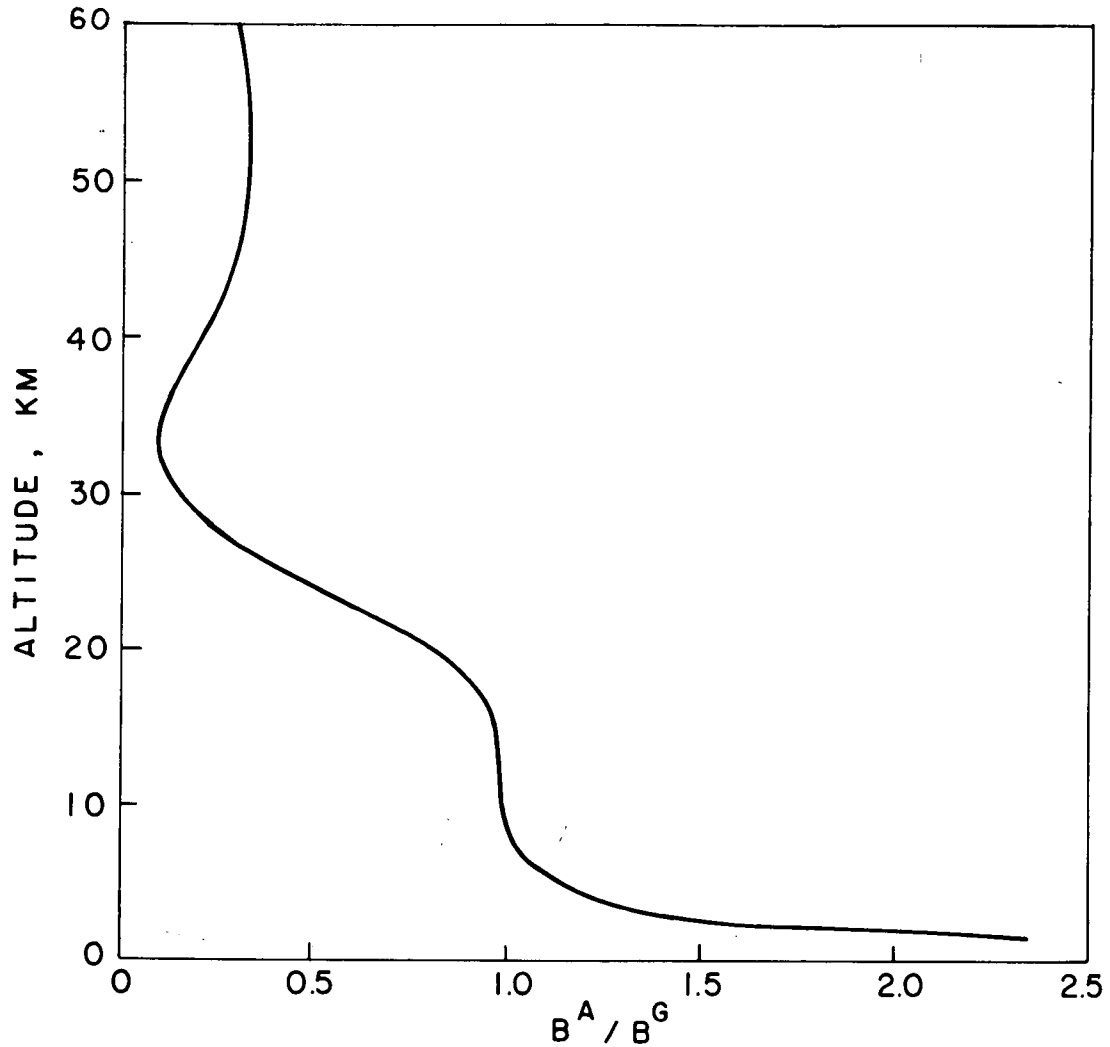


Figure 3. Ratio of particle to Rayleigh scattering coefficients as a function of height.

#### 1c. Energy Background Level

In the discussion which follows it will be necessary to compute signal to noise ratios of various proposed systems in order to establish their feasibility. Generally, these systems, if they are to be considered useful from a meteorological standpoint, must be operable during day as well as night hours. Consequently, the noise contribution due to the presence of background radiation must be known. The background radiation may be computed from the relationship

$$P_B(\lambda) = A_R J(\lambda) \Delta \omega$$

where

- $P_B(\lambda)$  = background radiation (watts)
- $A_R$  = receiving aperture ( $\text{cm}^2$ )
- $J(\lambda)$  = radiance ( $\text{watts}/\text{cm}^2/\text{sr}/\text{micron}$ )
- $\Delta \omega$  = solid viewing angle

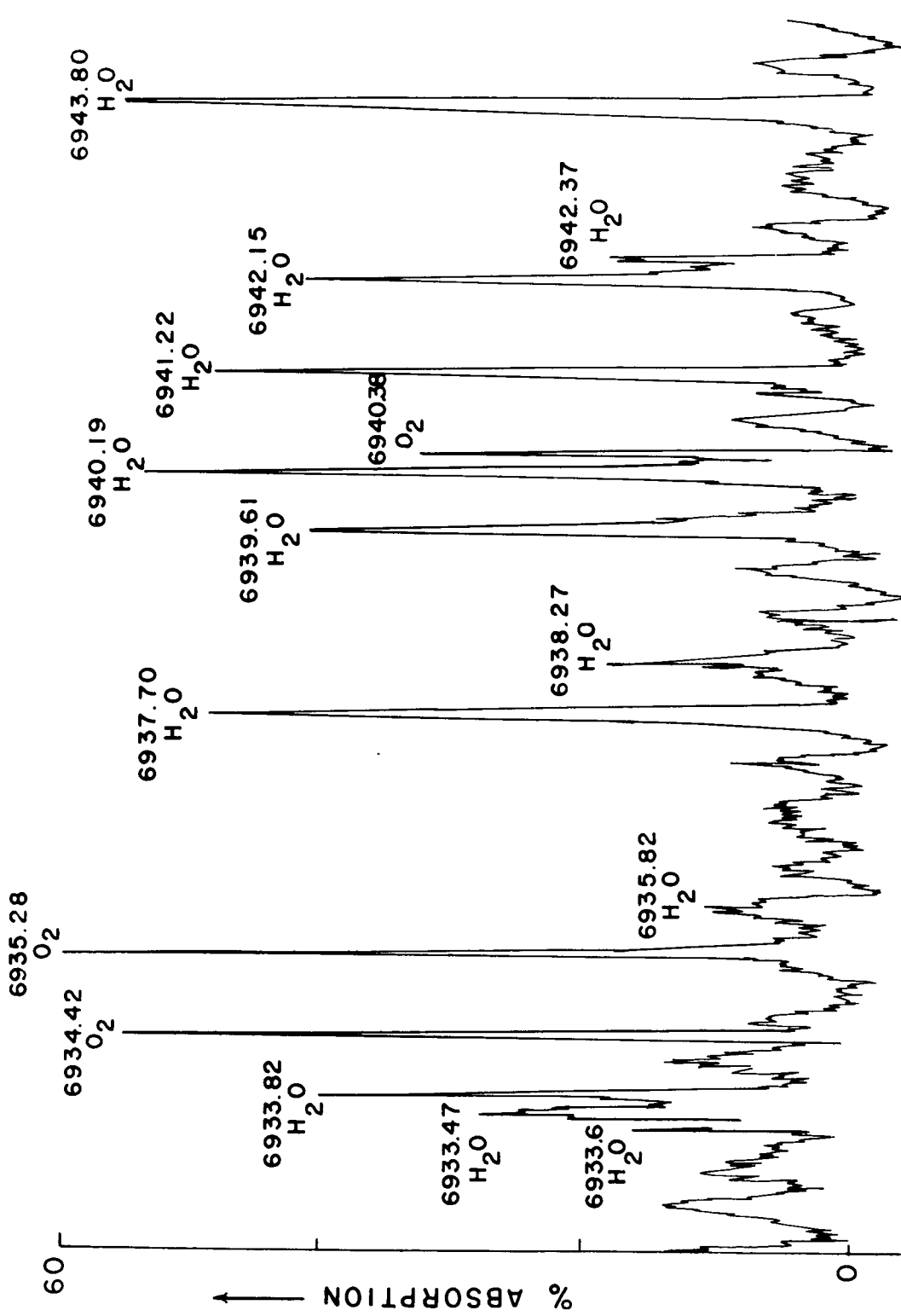


Figure 4. Telluric absorption spectrum (6933-6945Å) April 10, 1967.

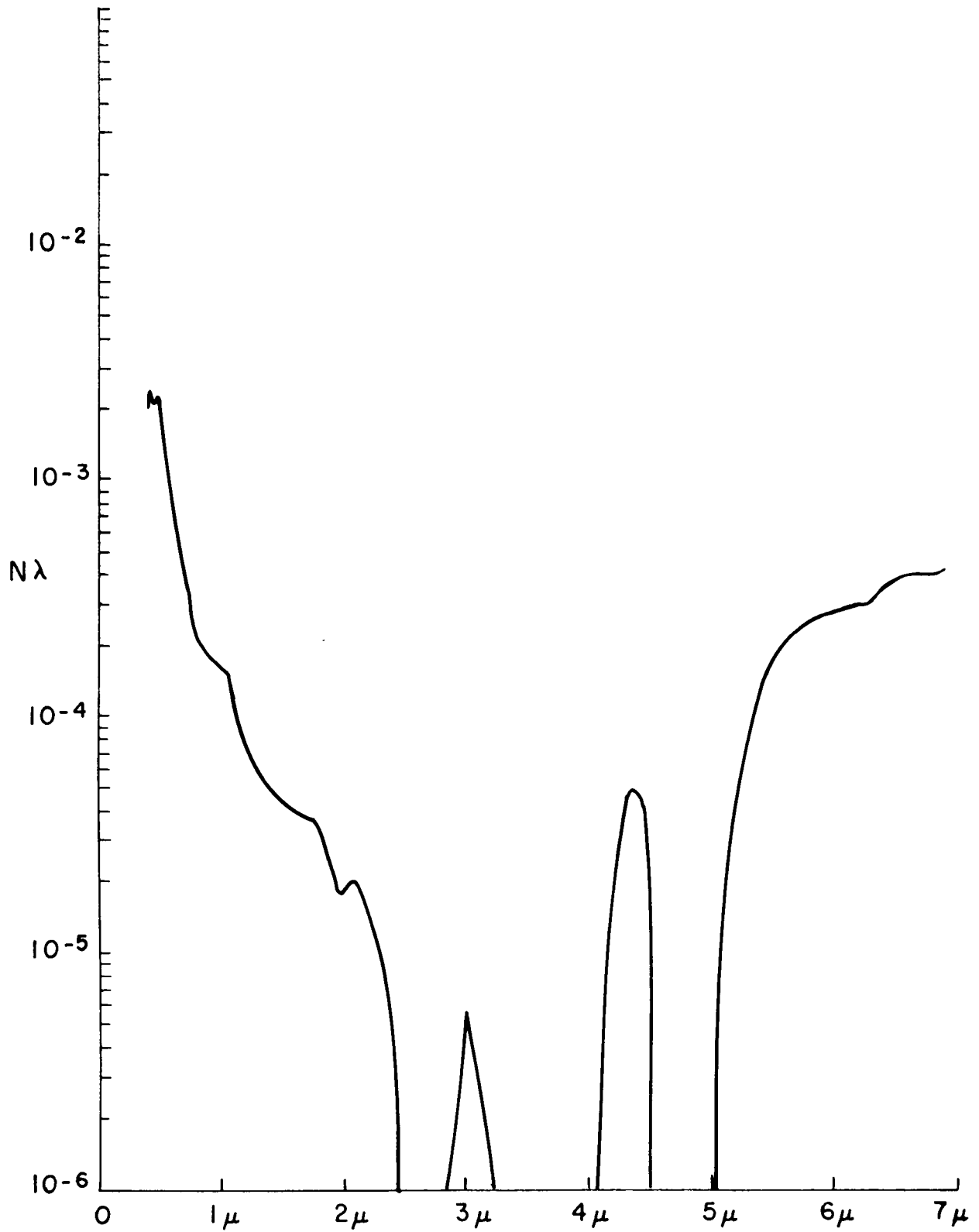


Figure 5. Spectral radiance of background radiation for a blue sky as a function of wavelength.

A graph of  $J(\lambda)$  versus  $\lambda$  of blue sky observed by Vanderhei and Taylor (1960) is given in Figure 5. A value of  $10^{-3} \text{w/cm}^2/\text{sr}/\text{micron}$  is characteristic of the ruby laser region.

## 2. CAPABILITIES OF LASER SYSTEMS

One of the goals of a remote sensing device would be to provide information equivalent to that obtained by the standard radiosonde under all weather conditions. It is clear that the laser radar will not penetrate thick cloud decks. This limitation is imposed by the available energy in laser pulses. For example, assume a cloud deck of 300 meters thickness and of  $3 \text{ gram/meter}^3$  liquid water content. In order to penetrate this cloud and provide a path for the return scattered energy it would be necessary to evaporate the water in the path of the beam. If the beam were 0.1 meter x 0.1 meter in cross section this would require a pulse containing approximately 21,000 joules of energy. Present day systems provide energy levels (Q switch) of a maximum of 10 joules. It does not seem possible in the foreseeable future to provide energy of the requisite amount through combinations of increased pulse energy and repetition rates.

What can the laser radar do aside from deriving qualitative indications of  $n(Z)$  and  $N(Z)$ ? We would like to operate the laser radar in a manner which would permit the separation of the quantities  $n(Z)$ ,  $\rho(Z)$  and  $T(Z)$ . The following approaches to such measurements will be considered in the remainder of the paper

$n(Z)$  and  $N(Z)$  via Raman scattering

$\rho(Z)$  via differential absorption of scattered energy

$T(Z)$  via Doppler power spectrum of the scattered energy.

$v(Z)$  via Doppler power spectrum of the scattered energy.

### 2a. Doppler Power Spectrum

The transfer equation stated in the introduction of this paper relates the energy returned to the laser radar to that which is transmitted. The scattering process is an interaction mechanism between the traveling laser energy and the molecules and particles which comprise the atmosphere. These constituents are in random motion and their velocities are governed by the Maxwell-Boltzmann relationship

$$dN(v) = \frac{1}{N} \frac{dv}{\sqrt{2\pi}} \sigma_v \exp \left[ - \frac{(v - \bar{v})^2}{2\sigma_v^2} \right] \quad (4)$$

where

$\bar{v}$  = mean wind

$v$  = random particle velocity

$\sigma_v$  = standard deviation of the thermal wind due to Brownian motion

$N$  = number of particles/unit volume

$dN(v)$  = number of particles in the range  $dv$  at the velocity  $v$

The scattered radiation although initially nearly monochromatic will be Doppler broadened by virtue of the velocities of the scattering components. The Doppler shift may be expressed for these particles as

$$f_d = \frac{\vec{v}_i}{\lambda} \cdot (\hat{r} + \hat{t})$$

where

$\vec{v}_i$  = particle velocity

$\hat{r}$  = unit vector to the receiver

$\hat{t}$  = unit vector to the transmitter

for a coaxial system

$$f_d = \frac{2v_i}{\lambda}$$

This relationship may be used with the Maxwell-Boltzmann expression to transform the normalized transfer equation into a power spectrum for the backscattered radiation. Use is made at this point of the relationship

$$\sigma_v^2 = \frac{kT}{m} \quad (5)$$

where

$k$  = Boltzmann's constant

$T$  = temperature

$m$  = scattering mass

$$I = \frac{R^2}{P_T} \frac{\partial H_R}{\partial f_d} = \frac{\gamma^3 \pi^2}{\lambda^2} \frac{\Delta Z_n(Z)}{[2\pi R^* T]^{1/2}} \exp \left[ -\frac{\lambda_o^2 f_d^2}{8R^* T} \right] \quad (6)$$

This relationship (Schotland, et al. 1962) is plotted in Figures 6 and 7. It is assumed that the plot has been centered about  $\bar{f}_d = \frac{\bar{v}}{\lambda}$ .

It should be said at this point that the spectrum may not transform simply as shown. Dicke (1953) has suggested a collision narrowed Lorentz form. This expression does not deviate appreciably at halfwidth from the Boltzmann form for molecular scatter, but does so markedly for particles larger than  $0.1\mu$  (Schotland, et al. 1967). The Boltzmann form also has been used by Zirkel (1966) and Breece, et al. (1966). It is important that this point be clarified.

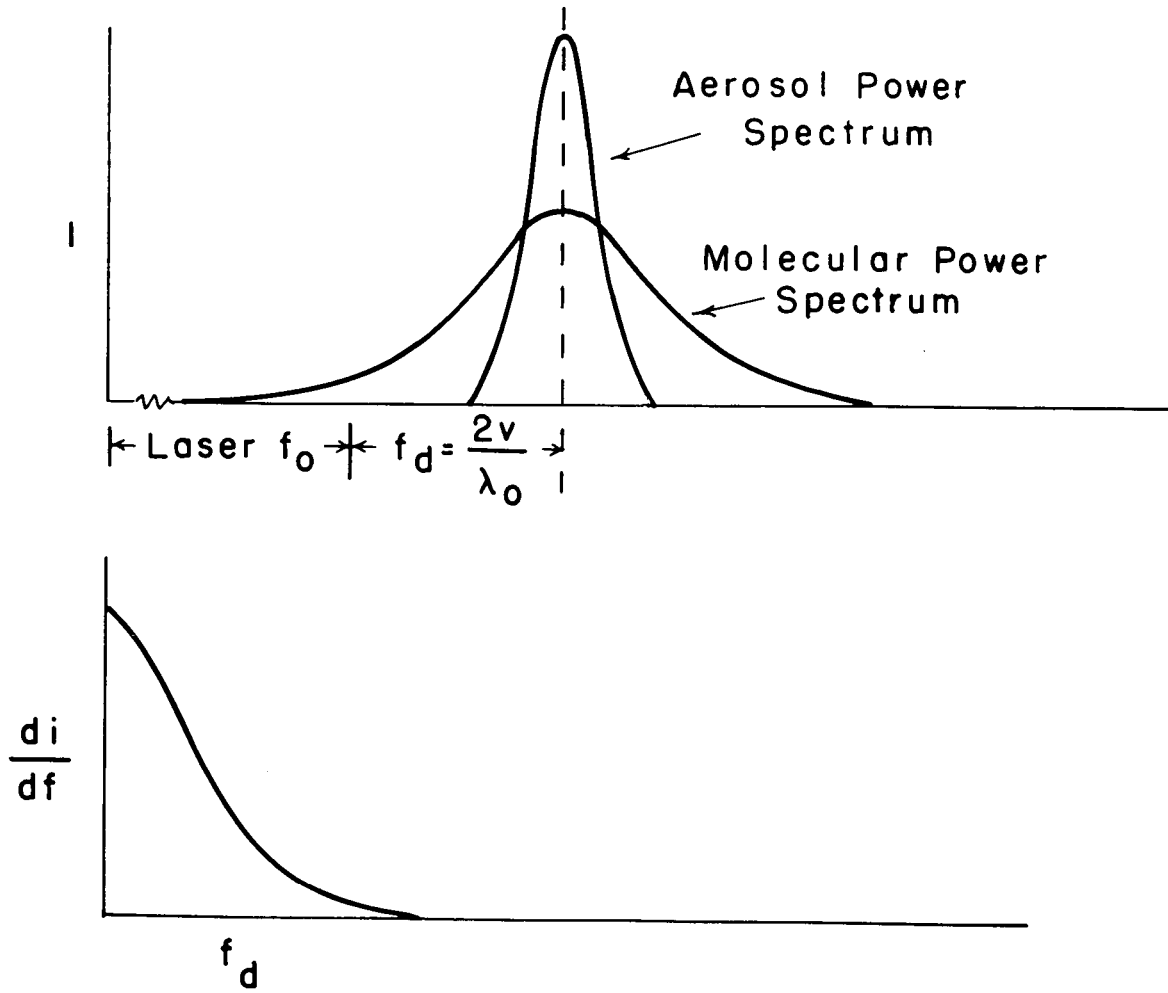


Figure 6. Representation of molecular and aerosol power spectra.

The normalized power spectrum for particles in the Rayleigh range is

$$R^2 \frac{\partial H_R}{\partial f_d} = \frac{9\pi^2 K^2}{\lambda^3} \Delta Z V^2 N(Z) \frac{1}{\sqrt{2\pi}\sigma_v} \exp\left[-\frac{\lambda^2 f_d^2}{8\sigma_v^2}\right] \quad (7)$$

where  $V$  = volume of scattering particle.

$$K = \frac{m - 1}{m + 2}, \quad m = \text{refractive index.}$$

This form of the equation is useful at the  $\text{CO}_2$  laser wavelength ( $10.6\mu$ ).

In order to observe the power spectrum it is necessary to limit the receiving aperture to the coherence area of the sources. This area,  $A_c$  is of the order of  $\lambda^2/\Omega$  where  $\Omega$  is the solid angle of the scattering volume viewed from the receiver. This restriction implies that the beamwidths of the transmitted signal must be extremely narrow if practical values of  $A_c$  are to be obtained. Fried (see Breece, et al. 1966)

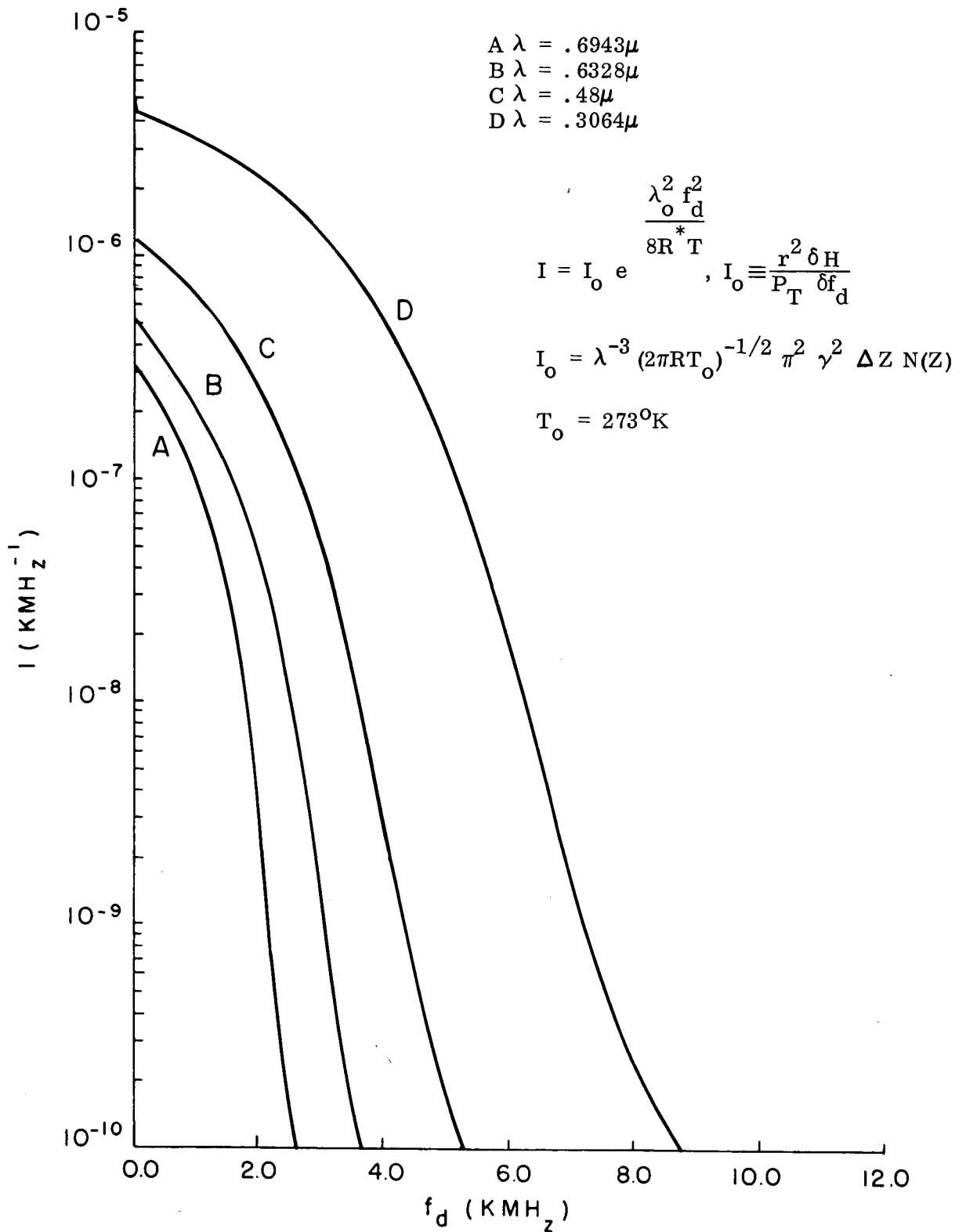


Figure 7. Normalized molecular Doppler spectrum.

has demonstrated that the transmitting optics should be diffraction limited and equal in area to that of the receiver for optimum results.

Another problem area in the application of Doppler techniques to the atmosphere results from the perturbation of the wavefront of the radiation by the atmosphere. The diameter of the receiving telescope should not exceed a value  $r_o$  given by Fried (1965) as

$$r_o = 1.2 \times 10^{-8} \lambda^{6/5} R^{-3/5} C_N^{-6/5} \quad (8)$$

where

$\lambda$  = wavelength

$R$  = range (two way)

$C_N^2$  = Tatarski's structure constant

The strong dependency on  $\lambda$  should be noted. As an example  $r_o$  for day operation is of the order of 7 cm for  $\lambda = .7\mu$  while it may be as large as  $10^2$  cm at  $10\mu$ .

In order to discuss the potential of the laser radar for Doppler application, the line purity of typical lasers must be considered. At the present time two classes of lasers can be considered useful. They are the pulsed crystal and the  $CO_2$  gas laser.

According to Hercher (private communication) the line width of pulsed crystal lasers can be of the order of  $30 \times 10^6$  Hz, when operated in the Q-switch mode. This line width is of the order of the pulse spectrum so that no improvement appears possible except through the use of longer pulses. The energy available is approximately 0.1 joule in projected laser systems.

From a discussion with equipment manufacturers it appears that the line width of a  $CO_2$  gas laser is of the order of  $0.008\text{\AA}$  ( $2.4 \times 10^6$  Hz) at a power level of 100 watts.

Modulation schemes have been proposed whereby the Doppler shift occurs at the modulation frequency. This technique has the twin advantages of strong spectral purity and a coherence area dictated by the modulation frequency. However, present modulation schemes are limited to  $10^9$  Hz ( $\lambda = 30$  cm). Therefore the Doppler shifts are generally small:  $f_d/v = 6$  Hz/m/sec.

### 3. APPLICATIONS OF THE DOPPLER SYSTEM

It has been suggested that the Doppler technique be used to measure the following parameters.

1. Temperature from the width of the molecular spectrum
2. Wind velocity via the mean Doppler shift using heterodyne techniques
3. Velocity gradient using square-law detection of the backscattered radiation from two laser pulses separated in range

Problems 1 and 2 were analyzed by Schotland, *et al.* (1962) and although times have improved and a better understanding of the problem is available, the conclusion is still pessimistic.

Consider the temperature problem. If

$$I = \frac{Z^2}{P_T} \frac{\partial H}{\partial f_d}$$

$$I(f_0) = 3.4 \times 10^{-16} \text{ for } \lambda = 0.7\mu$$

Then at the half power point which is sufficiently removed from the aerosol contribution,

$$I\left(\frac{1}{2}\right) \sim 1.7 \times 10^{-16}$$

$$\Delta P_R = 1.7 \times 10^{-16} \times \frac{P_T}{Z^2} A_c \times \Delta f$$

Phase limitations limit  $A_c$  to approximately  $50 \text{ cm}^2$ . Assume  $\Delta f = 10^7 \text{ Hz}$  and a range of  $1 \text{ km}$ .

$$\Delta P_R = 1.7 \times 10^{-16} \times 10^7 \times 10^{-10} \times 50 \times 10^7$$

(I<sub>0</sub>)                      (Δf)              (Z<sup>2</sup>)              (A)              (P)

$$\Delta P_R = 8.5 \times 10^{-11} \text{ watts}$$

Substitution of this power into the S/N relation assuming  $P_B = 0$  yields  $S/N = 3$  which is not very satisfactory. It should be noted that with coherent detection the S/N ratio is basically equivalent to that obtained with  $P_B = 0$ .

An estimate of the desired signal/noise value for thermal measurement can be obtained by logarithmically differentiating the expression for I.

$$\frac{dI}{I} = \frac{dT}{T} \left[ \frac{\lambda_o^2 f_d^2}{8R^* T} - \frac{1}{2} \right]$$

Thus for  $\frac{\lambda_o^2 f_d^2}{8R^* T} = 1$ , a  $2^0$  temperature precision at the level of  $300^0\text{K}$  requires a precision in the measurement of I of  $1/300$ . This level of accuracy could be obtained at a maximum range of only  $10 \text{ m}$ .

Bistatic systems using c. w. lasers such as the Argon or the  $\text{CO}_2$  units can be used with synchronous detection techniques for the temperature measurements. The difficulty with this approach is that with present capabilities the integration times necessary to yield reasonable S/N ratio are of the order of minutes. Another method which can be used to obtain the change in Doppler width involves the direct use of an interferometer. The advantage of this approach is that the conditions on phase coherence

are relaxed - permitting much larger receiving apertures. The interferometer provides information only on the spectral width and therefore this method cannot be used for velocity studies.

Doppler techniques to measure the mean wind and the radial wind gradient are basically dependent upon the ability of the system to "see" these shifts in the presence of the spectrum variability of the laser source. The Doppler shift sensitivity may be expressed as  $f_d/v = 2/\lambda$ .

$\lambda$	.7 $\mu$	10.6 $\mu$
$f_d/v$	$3 \times 10^6 \text{ m}^{-1}$	$2 \times 10^5 \text{ m}^{-1}$

If a velocity measurement accurate to 1 m/sec is desired, the expected shift will be of the order of 0.1 of the spectral noise of state of the art laser systems. This uncertainty does not lead to a useful measurement. At the present time a laser is not available which will deliver 0.1 joule with a bandwidth of  $30 \times 10^6$  Hz. It appears that such a system could be developed with existing technology.

Recently Fiocco and DeWold (private communication) performed an experiment in which they used a pressure scanned Fabry-Perot interferometer to observe the Doppler spectrum of an aerosol. Although this system cannot be used as it stands for atmospheric probing, the work does demonstrate the reality of the Doppler spectra.

Similar conclusions were also reached by Cummins, et al. (1964) who used optical mixing techniques to study the Doppler power spectrum in liquids.

It is recommended that an experimental program be initiated to study the thermal Doppler spectrum. In particular the shape of the spectrum should be considered in relationship to the Lorentz versus Gaussian forms.

### 3b. Raman Scattering Technique

In general, the radiation which is backscattered is returned at a wavelength similar, except for Doppler shift, to the existing wavelength. At times the scattering molecule will undergo a change of state during the scattering process and the scattered energy will be returned at a different wavelength. This process is known as Raman scattering. The average Raman cross section is of the order of  $4 \times 10^{-3}$  that of the Rayleigh cross section for atmospheric gases. The changes of molecular state are related to the vibration and rotation spectra of the molecules and the magnitude and wavelength shift will be specific for a given molecule. Since the Raman cross section (non-stimulated) is small, the technique will probably be useful only for the major atmospheric components such as  $N_2$  and  $O_2$ .

An example of the signal to noise ratio in the measurement of the vertical distribution of  $O_2$  is calculated below. It is assumed that a ruby laser operating at 6943 $\text{\AA}$  has been frequency doubled with an efficiency of 25 percent. The  $\nu = 0$  to  $\nu = 1$  vibration state corresponding to a line shift of  $1550 \text{ cm}^{-1}$  will be used in the computation.

System parameters

$$A_R = 4 \times 10^3 \text{ cm}^2$$

$$\Delta\Omega = 10^{-5} \text{ sr}$$

$$\Delta\lambda = 4 \times 10^{-4} \mu$$

$$J_\lambda = 2 \times 10^{-3} \text{ watts/sr/}\mu\text{/cm}^2$$

$$P_T = 0.5 \times 10^8 \text{ watts}$$

$$\Delta f = 10^6 \text{ hz}$$

$$C = \text{photomultiplier responsivity} = .15 \text{ amp/w.}$$

The signal to noise ratio for shot noise limited system such as a photomultiplier is given by the following expression:

$$\frac{S}{N} = \frac{P_R C \tau}{[2e \Delta f C \tau (P_R + P_B)]^{1/2}} \quad (9)$$

where  $e$  = electronic charge

Substitution of the above parameters into the S/N relationship results in the following values: for ranges  $Z = 3$  and  $6 \text{ Km.}$ ,  $S/N \approx 80$  and  $18$ , respectively.

It appears that the measurement is feasible. Some work has been done by Cooney at R.C.A. (private communication) using a straight ruby laser system and filter suitable for the  $N_2$  molecule. His results have not been published but it appears that he has observed the Raman profile.

There is a difficulty with this model. While Raman scattering is specific for a particular molecule, the attenuation function is not. Thus the returned signal will be modulated by the total atmospheric cross section. A possible solution to this problem would be to monitor the unshifted backscatter (or an additional line) and use this quantity as a correction to the Raman measurement.

Consider the relationship

$$I_1 = \frac{R^2_{H_R}}{P_T} = \frac{L}{2} [\sigma_{RAY} + \sigma_P] \tau^2 \quad \text{for the unshifted line} \quad (10)$$

$$I_2 = \frac{R^2_{H_{RAM}}}{P_T} = \frac{L}{2} [\sigma_{RAM}] \bar{\tau}^2 \quad \bar{\tau}^2 = \tau \text{ for the Raman line} \quad (11)$$

$$\frac{I_1}{I_2} = k_1 + k_2 \frac{\sigma_P}{\sigma_{RAY}} \quad \text{i. e. the ratio of particle to Rayleigh cross section is available} \quad (12)$$

Cooney (private communication) points out that temperature information is incorporated in the ratio of the intensities of the Stokes and anti-Stokes lines. It is not clear at the present time if the intensity of the anti-Stokes line is of sufficient magnitude to insure a useful measurement.

### 3c. Differential Absorption of Scattered Energy

The expression for atmospheric transmission which appears in the radar transfer equation includes a term  $\exp -2 \int_0^Z \rho K_\lambda dz$ . This function represents the molecular absorption due to atmospheric gases. The atmospheric spectrum presents an abundance of narrow lines ( $0.1\text{\AA}$ ) of moderate strength due to  $\text{H}_2\text{O}$ ,  $\text{O}_2$ ,  $\text{O}_3$ , and  $\text{CO}_2$ . Figure 4 represents a portion of the telluric spectrum from 6934 to 6944 $\text{\AA}$  obtained by Bradley. The predominant lines in this region are due to  $\text{H}_2\text{O}$  and  $\text{O}_2$ . A technique has been developed at N. Y. U. over the past 10 years to measure the vertical distribution of absorbing gases by measuring the differential absorption of the backscattered radiation from a pulse emitted by an optical radar. The technique was initially applied to  $\text{O}_3$  in 1958 using a pulsed Xenon source. However, the results were marginal due to the poor spectral brightness of the source. The development of the laser has provided an energy source which is ideal for this type of measurement. Basically the laser is tuned to an absorption line center and then to an adjacent window region.

An example of simulated radar data is presented in Figure 8 which represents the transfer equation evaluated for 6943.80 $\text{\AA}$  water vapor line. Line parameters are due to Benedict.

The inversion of the optical return to obtain the vertical profile of water vapor proceeds as follows:

$$R(Z) = \frac{P_R(\lambda_L)}{P_R(\lambda_W)} = \frac{F_T(\lambda_L)}{F_T(\lambda_W)} \exp \left[ -2 \int_0^Z \rho_v(Z) K_\lambda(\lambda_i) dz \right] \quad (13)$$

$$\frac{\partial}{\partial Z} \ln R(Z) = -2 \rho_v(Z) K_w(\lambda_i) dz \quad (14)$$

$$\therefore \rho_v(Z) = \frac{1}{2K_w(\lambda_i)} \frac{\partial}{\partial Z} \ln R(Z) \quad (15)$$

The accuracy of the determination of the water vapor profile by the differential absorption technique is limited primarily to the uncertainties in the measurement of the gradient of the power return and by the incomplete knowledge of the water vapor absorption coefficient. The power measurement, at least from the first four kilometers of the atmosphere, does not represent a problem area.

The variance of the deduced water vapor density may be expressed in terms of the variances of the absorption coefficient and returned power gradients as follows:

$$\sigma_w^2 = \frac{\rho^2(Z)}{K^2} \sigma_K^2 \left[ \frac{1}{P_L^2} \sigma^2 (\partial P_L / \partial Z) + \frac{1}{P_W^2} \sigma^2 (\partial P_W / \partial Z) \right] \quad (16)$$

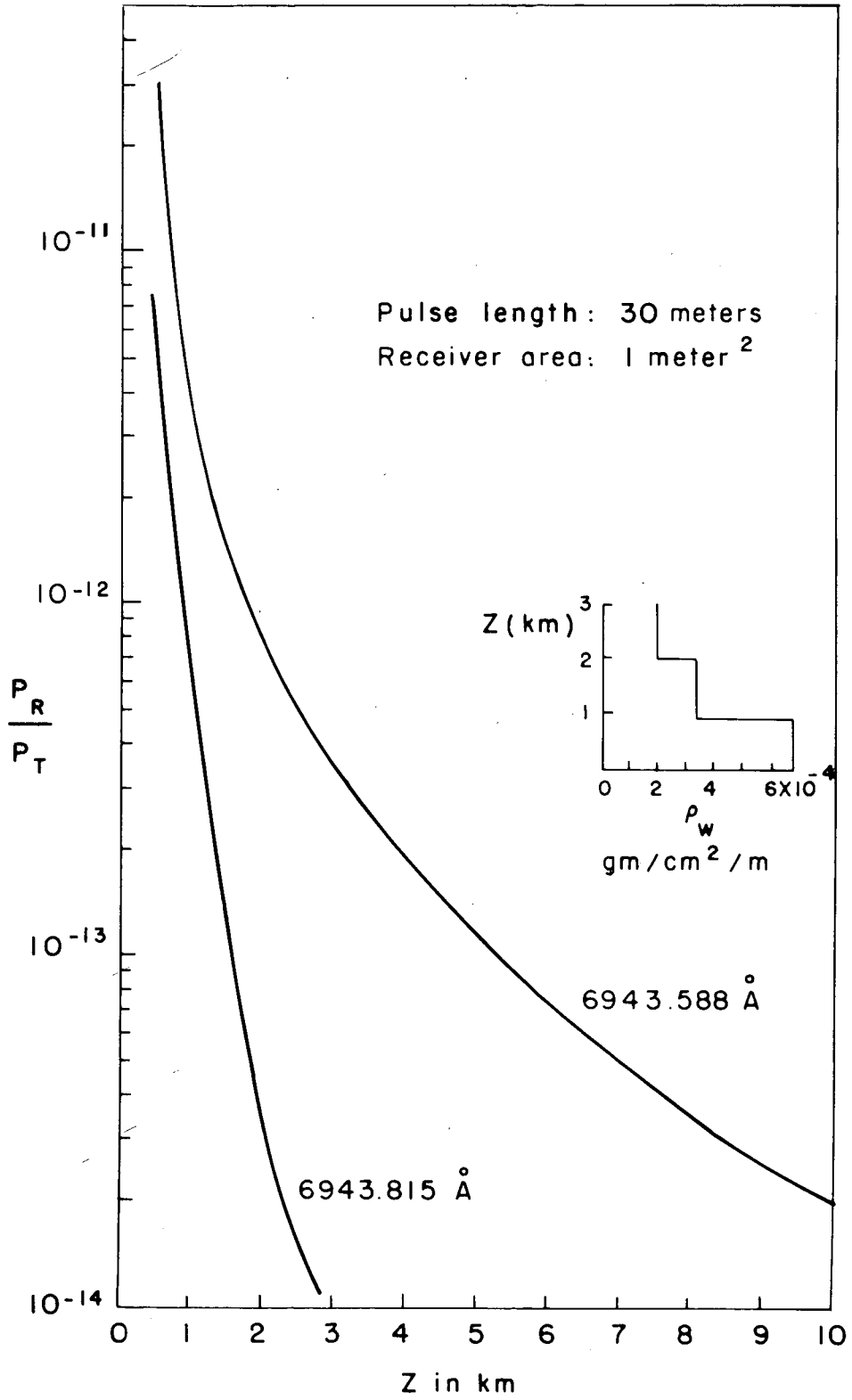


Figure 8. Transfer function for .7μ

where

- $\sigma_w^2$  = water vapor variance
- $\sigma_K^2$  = the absorption coefficient variance
- $\sigma^2(\partial P/\partial Z)$  = the power gradient variance

The variance of the absorption coefficient is due to two factors. The first factor is that an uncertainty exists in the measurements of the line parameters and in the effects of pressure and temperature broadening upon line shape. The values for the line width and strength according to Benedict are thought to be correct to  $\pm 33\%$  while the line strength has an uncertainty of  $\pm 25\%$ . The second factor that contributes to the variance in the absorption coefficient is the uncertainty in the frequency of the laser. From the work that has been done at N. Y. U., it appears that a laser frequency setting uncertainty of  $\pm 0.01\text{\AA}$  is possible. If the laser is tuned to line center and the half width of the water vapor is taken to be  $0.04\text{\AA}$ , then the fractional uncertainty in  $K\lambda$  is of the order of 5 percent. However, if the laser should be tuned to the inflection point of the curve, the fractional uncertainty can be as large as 29%.

The variance of the water vapor density due to the power gradient term arises primarily from the shot noise produced by the photomultiplier-detecting system. The variance of radiant noise power may be written

$$\sigma_N^2 = \frac{2e}{R} (P_r + P_B) \Delta f \tag{17}$$

where

- e = electron charge
- C = photomultiplier responsivity
- $\Delta f$  = measurement system bandwidth
- $P_B$  = background power

The variance of  $\frac{\partial P}{\partial Z}$  can be expressed as

$$\sigma^2(\partial \rho / \partial P) \cong \frac{2\sigma_N^2}{\Delta Z^2} \tag{18}$$

Substitution of the expression for variance of  $(\partial P/\partial Z)$  into the equation for the variance of  $\rho_w$  yields

$$\sigma_w^2 = \frac{\rho^2(Z)}{\Delta K^2} \sigma_K^2 + \frac{e \Delta f}{R \Delta K^2 \Delta Z^2} \left[ \frac{P_L + P_B}{P_L^2} + \frac{P_w + P_B}{P_w^2} \right] \tag{19}$$

The value of  $\sigma_w$  has been computed using the model atmosphere of Figure 8 and the following constants:

$$P_B = 5 \times 10^{-8} \text{ watts}$$

$$P_t = 2 \times 10^7 \text{ watts (over } 25 \times 10^{-9} \text{ sec)}$$

$$A = 10^3 \text{ cm}^2$$

$$\Delta f = 2\Delta Z/c = 4$$

$$\Delta Z = 120 \text{ meters}$$

The results are plotted in Figure 9 separately for the contributions due to  $\sigma_{\partial P/\partial Z}$  and to  $\sigma_K$ . The uncertainty in  $\sigma_K$  was assumed to arise solely from the frequency stability of the laser. It is apparent that in the first two kilometers the uncertainty in  $\sigma_w$  arises from  $\sigma_K$ . However, the contribution from  $\sigma_{\partial P/\partial Z}$  increases rapidly above two kilometers and is the dominating factor at three kilometers. The uncertainty in  $\rho_w$  due to  $\sigma_{\partial P/\partial Z}$  can be reduced by increasing both the output energy of the laser and the aperture of the receiver.

The major problem area in developing a field laser radar system of this type centers about the frequency stability of the laser. It is necessary to center the laser on line center with an accuracy of  $\pm .01\text{\AA}$ . Initial experiments were undertaken using the thermal tuning characteristic of the ruby laser to locate the line center. The thermal sensitivity of a ruby laser is  $0.065\text{\AA}/^\circ\text{C}$  which implies a rod thermal stability of  $0.1^\circ\text{C}$  if the wavelength tolerance of  $.01\text{\AA}$  is to be maintained. This proved difficult to achieve at high laser repetition rates and consequently resonant cavity frequency stabilizers are now used. These devices also permit rapid frequency shifting of the laser. A sample of  $R(Z)$  data for water vapor obtained using a thermally tuned laser is given in Figure 10.

It is possible in principle to generate both the window and line center wavelength by using an appropriate Raman shifter as suggested by Dobbins and La Grone, (1967). However, no calculations are available in which the power output and line width of the appropriate Raman shifted energy are available. This work should be continued since Raman shifting will provide access to a variety of atmospheric lines.

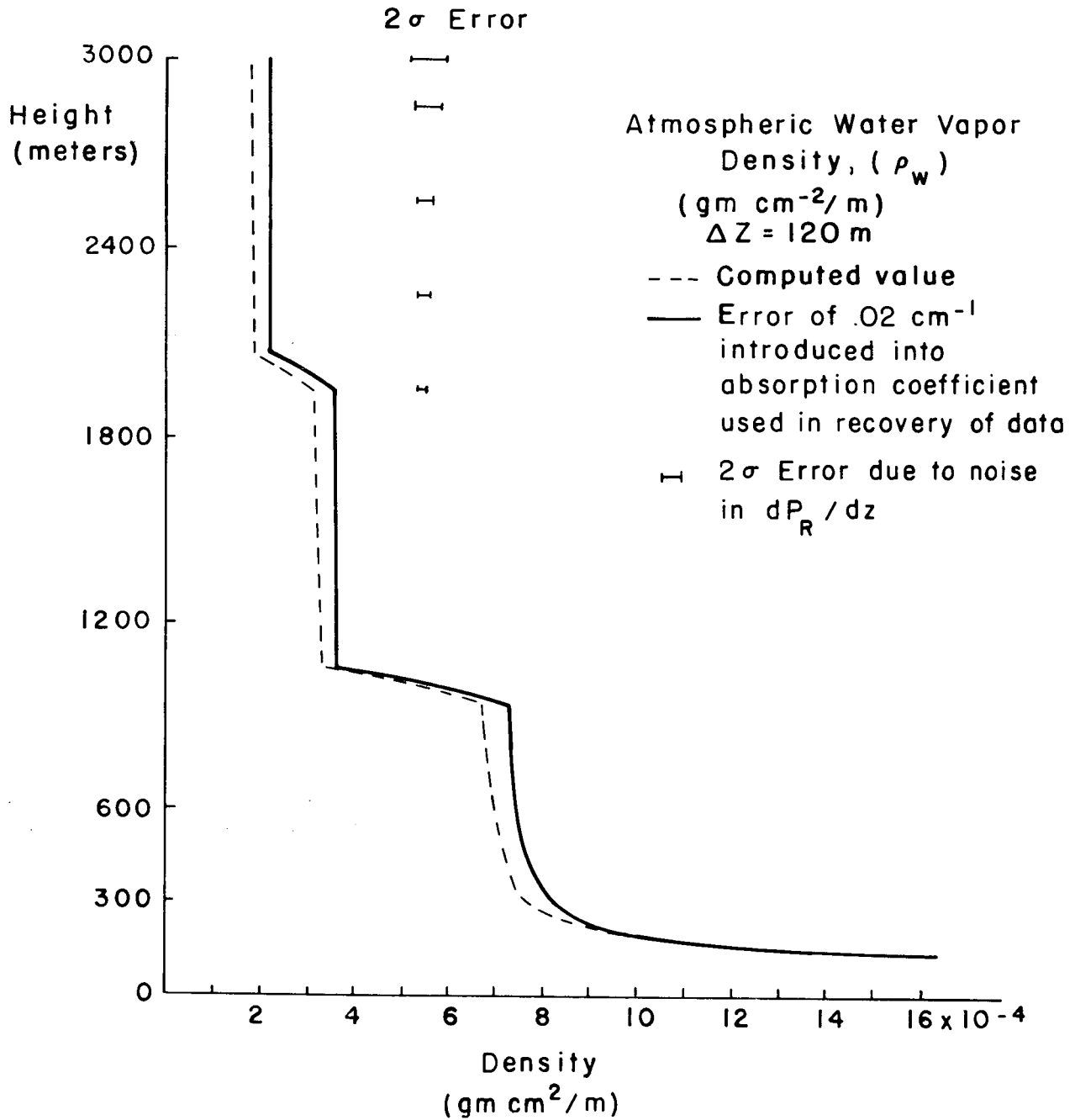


Figure 9. Uncertainty in atmospheric water vapor density measurement.

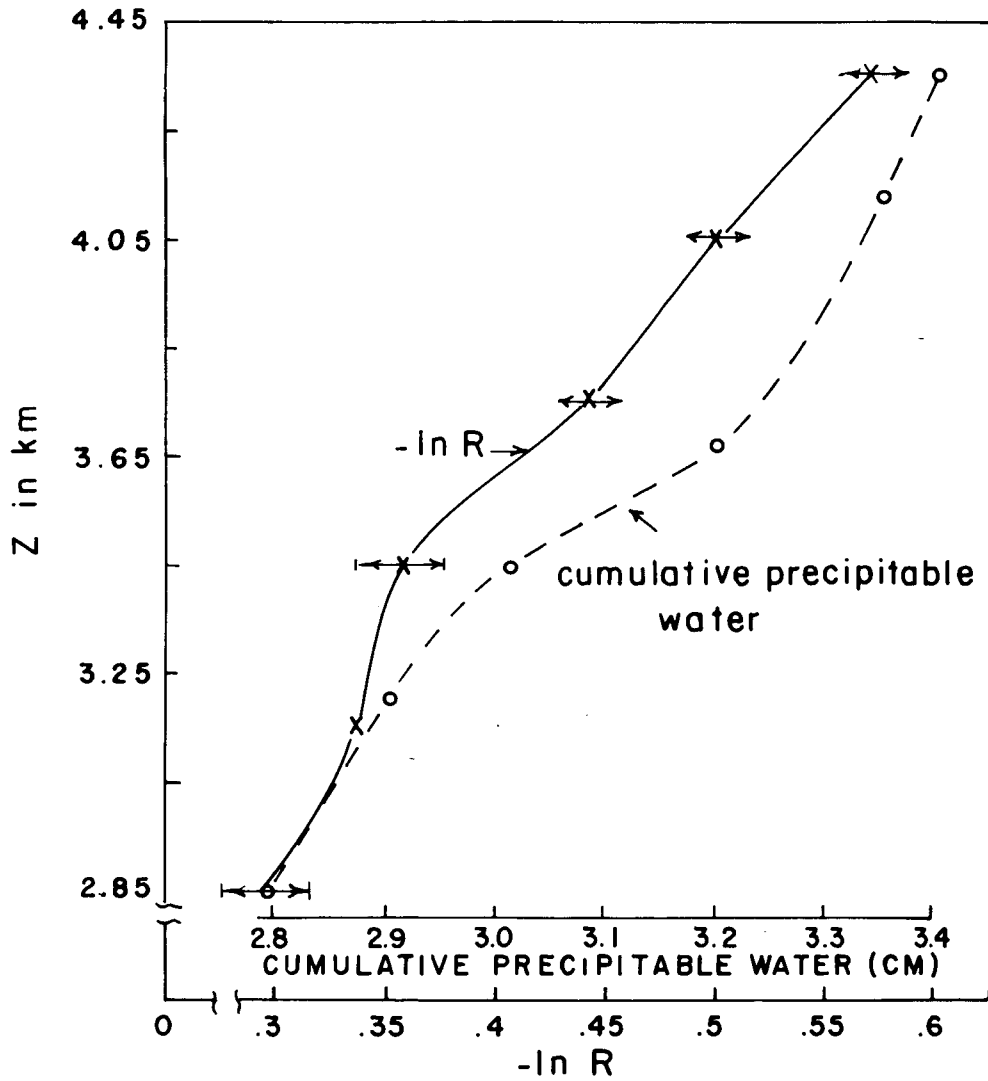


Figure 10. Comparison of observed cumulative precipitable water as a function of height with laser return.

REFERENCES

- Breece, R. C., D. L. Fried, J. B. Seidman, 1966: Remote measurement of differential atmosphere. Institute of Navigations Proc. Conf. Clear Air Turbulence, Society of Automotive Engineers, Inc., Washington, D. C., 135-162.
- Cummins, H. Z., N. Knabe, Y. Yeh, 1964: Observation of diffusion broadening of Rayleigh scattered light. Columbia University, Physics Review Letters, 12, 150-153.
- Dicke, R. H., 1953: Physical Review, 89, 472.
- Dobbins, D. L., A. H. LaGrone, 1967: Number density determination of O<sub>2</sub>, H<sub>2</sub>O and CO<sub>2</sub> by high intensity laser beam. Conference Record, South Western Institute of Electrical and Electronics Engineers, Institute of Electrical and Electronics Engineers, Inc., New York, 5·3·1-5·3·10.
- Fried, D. L., 1965: Conference on atmospheric limitations to optical propagation. Central Radio Propagation Laboratory and National Center for Atmospheric Research, Boulder, Colorado, 192-264.
- Schotland, R. M., J. Bradley, A. M. Nathan, 1967: Optical sounding III. Technical Report 67-2, ECOM-02207-F, Fort Monmouth, New Jersey.
- Schotland, R. M., A. M. Nathan, E. A. Chermack, E. E. Uthe, D. Chang, 1962: Optical sounding. Technical Report No. 3, U.S. Army Electronic Research Development Laboratory, Fort Monmouth, New Jersey, 58 pp.
- Vandehai, P. T., B. J. Taylor, 1960: Spectral ground and sky backgrounds. Background Measurements IRMP-56, Geophysical Research Directorate Research Notes, No. 46, Geophysical Research Directorate, Bedford, Massachusetts.
- Zirkel, R. E., 1966: The feasibility of optical radar to detect clear air turbulence. Institute of Navigation, Proc. Conf. Clear Air Turbulence, Society of Automotive Engineers, Inc., Washington, D. C., pp. 55-68.

# THE LASER RADAR ABOVE 30 KILOMETRES

B.R. Clemesha

Department of Physics

University of the West Indies

Kingston 7, Jamaica

## ABSTRACT

This is a short 'state of the art' report on laser radar observations of the atmosphere at heights greater than 30 km.

## 1. INTRODUCTION

Much of the work so far reported on applications of the laser radar technique has been concerned with the troposphere and lower stratosphere. This is due in part to the general interest in this region and in part to the fact that comparatively modest equipment can be used. A number of groups have, however, been applying the technique to the region between 30 km and 140 km. This work is being done with two principal aims: (i) the measurement of atmospheric density and scale height, (ii) the observation of dust between the heights of 60 km and 140 km.

The first work of this nature was reported from M.I.T. by Fiocco and Smullin (1963) who claimed to have observed dust layers at various levels between 70 and 140 km. Subsequently McCormick *et al.*, (1966) working at Maryland reported similar results. These early measurements are now generally considered unreliable as they are based on radar returns containing spurious signals, which have been largely eliminated in later work. These spurious signals were due to fluorescence from the laser and enhanced noise from the photomultiplier detector (Sandford, 1967; Clemesha, Kent and Wright, 1967). Later results from a number of workers are reviewed below.

## 2. MEASUREMENTS BELOW 70 KILOMETRES

Some recent results for the region between 30 km and 70 km are shown in figure 1. Here results from Kingston, Jamaica (Kent, Clemesha and Wright, 1967), Maryland, U.S.A. (McCormick *et al.*, 1967, Silverberg and Poultney,

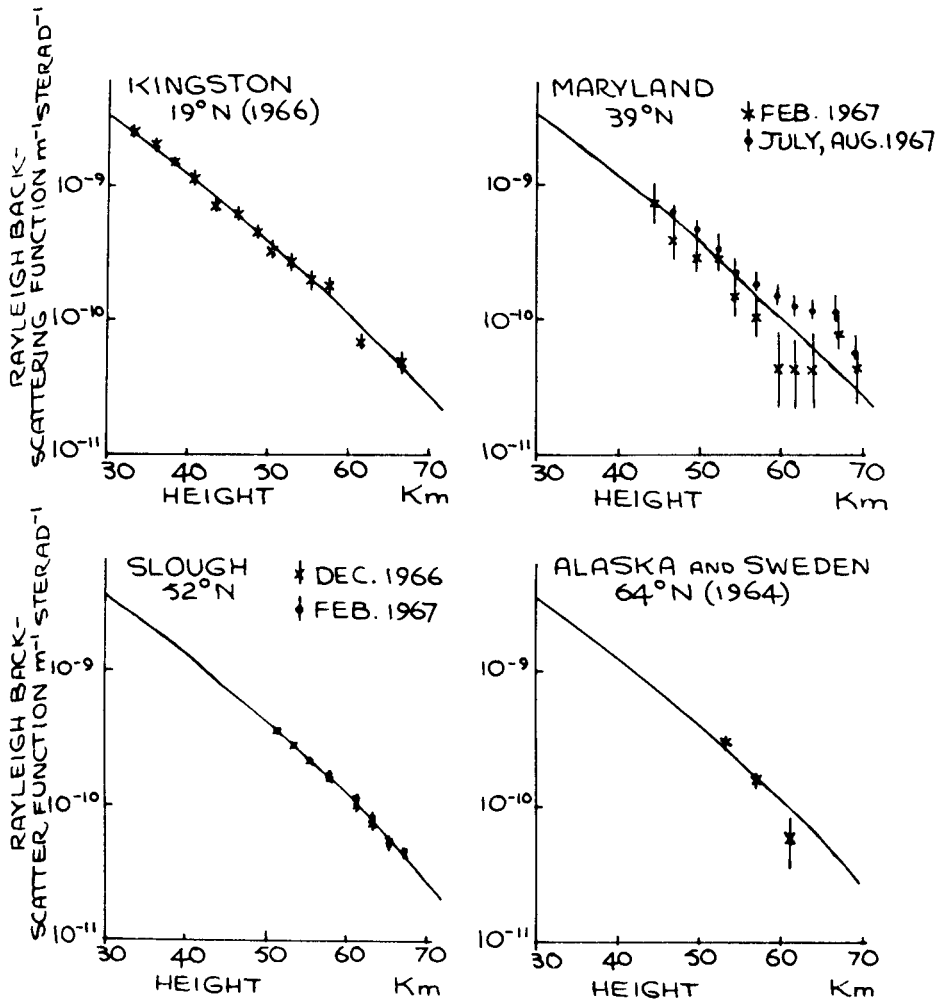


FIG.1. RECENT MEASUREMENTS OF THE RAYLEIGH BACK-SCATTER FUNCTION BETWEEN 30 AND 70 KILOMETRES.

$\ast \updownarrow$  EXPERIMENTAL RESULTS.  
 ——— FITTED STANDARD ATMOSPHERES.

1967), Alaska and Sweden (Fiocco and Grams, 1966) are presented in the same diagram for the purpose of comparison. Note that in each case these results have been fitted to a calculated curve for a standard atmosphere. Absolute measurements are not available because of the difficulty involved in an absolute calibration of the laser radar. It may be seen that the height variation of the experimentally observed scattering function matches the predicted variation in all cases with the exception of the summer results from Maryland, which possibly indicate the presence of particulate material above 60 km. In the absence of particulate material the scattering function is directly proportional to atmospheric density.

The accuracy of the measurements is limited by the very weak signals received from great heights. These signals are measured by photon counting techniques and contain a statistical uncertainty when the number of photons counted is small. The most accurate results have been published by Sandford, 1967 and Kent, Clemesha and Wright, 1968. The latter workers state (Kent, Clemesha and Wright, 1968) that they can measure the scale height precisely enough to obtain temperatures with an error of  $\pm 5^{\circ}\text{C}$  at 30 km increasing to  $\pm 25^{\circ}\text{C}$  at 50 km. Our present knowledge of the behaviour of the atmosphere between 30 km and 90 km is very poor and hence data of this sort of accuracy are just good enough for the technique to provide new information on seasonal, and perhaps diurnal variations in density and temperature. With regard to diurnal variations it must be remembered that day time sky brightness limits the maximum height to which measurements can be made to about 30 to 40 km, high altitude measurements can only be made at night.

So far no routine measurements of this nature appear to have been made over a sufficient period of time to provide new information. This is partly due to equipment difficulties at this early stage in the development of the technique.

The measurements which we in Kingston have made have in fact been part of a feasibility study for a much more powerful radar which is presently (May 1968) about to go into operation. This system should give  $\pm 10\%$  accuracy for density measurements at 100 km, improving to  $\pm 2\%$  at heights of 70 km and below. We hope that these measurements will fill a considerable gap in our present knowledge of the 30 km to 100 km region.

There does exist one problem in respect of the atmospheric density measurements. The determination of density from the laser radar return assumes that the scattering is entirely due to atmospheric molecules. There is some evidence (see for example Volz and Goody, 1962) for the existence of dust particles at all heights up to 70 km. If the scattering from dust is more than a small fraction of the molecular scattering there will result errors in the computed densities. So far the laser radar measurements do not indicate the presence of dust between 30 and 60 km, although the stratospheric aerosol layer is observed (Fiocco and Grams, 1964). One way to resolve this problem would be to make near simultaneous observations on different frequencies (to date all published results have been based on work using the 0.6943 micron ruby laser wavelength).

### 3. MEASUREMENTS ABOVE 70 KILOMETRES

Some results of laser radar returns from above 70 km are shown in figure 2. These results are from the same workers as those shown in figure 1. By far the most accurate data are from Slough, showing meaningful measurements

LASER RADAR ABOVE 30 KILOMETRES

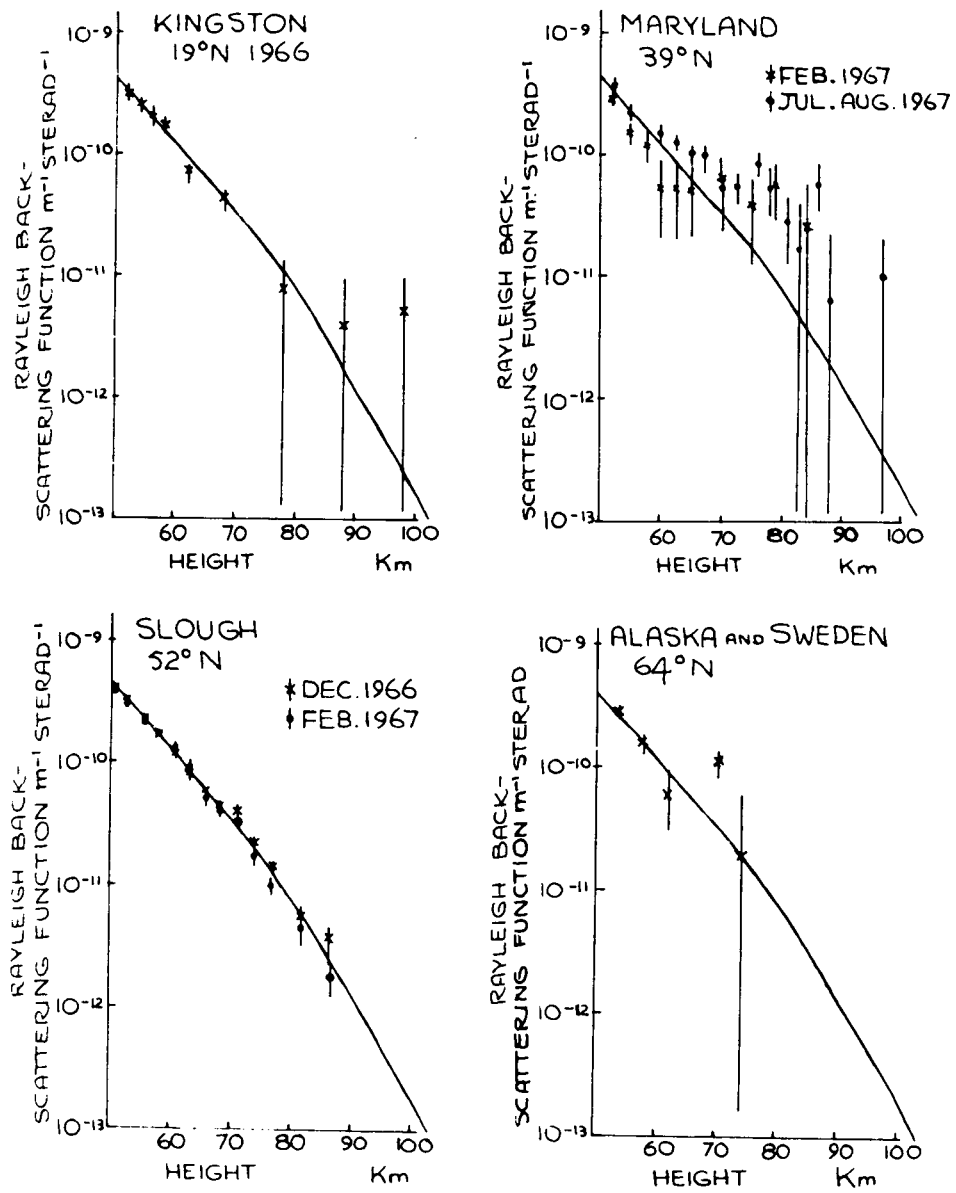


FIG. 2. RECENT MEASUREMENTS OF SCATTERING ABOVE 50 KILOMETRES.

\* ♦ EXPERIMENTAL RESULTS.  
 — STANDARD ATMOSPHERES.

up to 85 km. Both Maryland and the M.I.T. group (Alaska and Sweden) claim that their results show scattering which is significantly in excess of the expected molecular scatter at certain heights. This enhancement is interpreted as being the result of dust particles in the atmosphere at these heights. Slough sees a slight enhancement near to 70 km on some occasions. At Kingston we observe no echoes significantly in excess of the predicted molecular return.

At the present time there is some controversy as to whether or not the excessive scattering from this region is genuine. The importance of the problem lies not only in the intrinsic significance of dust particles at this height, but also in the effect of dust on attempts to derive atmospheric densities from the observed scattering cross-sections. It has been pointed out (see for example Fiocco and Grams, 1964) that the entry of meteoric particles into the atmosphere could explain the existence of the dust, and that the height of observation is close to the mesopause, where noctilucent clouds are observed. On the other hand it is rather disturbing that the most accurate measurements (Sandford, 1967) show the least enhancement. The basic problem is simply that the dust is observed at heights where the laser return is very weak, and hence most likely to be contaminated by an undetected noise source, as was certainly the case with early measurements. The final solution to this problem must await the advent of more powerful radars.

#### 4. CONCLUSIONS

1. Present high sensitivity laser radars are capable, if used on a routine basis, of providing new information on molecular density and temperature in the height range 30 km to 60 km. The presence of the stratospheric aerosol precludes the possibility of measuring molecular density below this height in a simple experiment.

2. An increase in sensitivity by 2 to 3 orders of magnitude over radars currently in use would enable density measurements to be made rapidly and conveniently at heights from 30 km to 100 km, provided the atmosphere is not contaminated by dust. At least one group is currently building a radar with this sensitivity.

3. There is controversial evidence for the existence of aerosols in the 60 km to 90 km height range.

ACKNOWLEDGEMENTS: The laser radar work being carried out at Kingston is supported by the United States Air Force, Office of Aerospace Research, under AFOSR Grant No. AF-AFORR-616-67.

#### REFERENCES

Clemesha, B.R., Kent, G.S. and Wright, R.W.H. 1967(b): Nature 214, 261-262.

Fiocco, G. and Grams, G. 1964: J. Atmos. Sci. 21, 323.

Fiocco, G. and Grams, G. 1966: Tellus XVIII 34.

Fiocco, G. and Smullin, L.D. 1963: Nature, 199, 1275.

Kent, G.S., Clemesha, B.R. and Wright, R.W.H. 1967: J. Atmos. Terr. Phys. 29,  
169-181.

LASER RADAR ABOVE 30 KILOMETRES

Kent,G.S., Clemesha, B.R. and Wright, R.W.H. 1968: Scientific Report No.19  
Physics Department, University of the West Indies.

McCormick,P.D., Poultney, S.K., Von Wijk, U., Alley,C.O.,Bettinger, R.T. and  
Perschy, J.A. 1966: Nature 209 798-799

McCormick,P.D., Silverberg,E.C., Poultney, S.K., Von Wijk, U., Alley, C.O. and  
Bettinger, R.T. 1967: Nature 215 1262-1263.

Sandford, M.C.W. 1967(b): J.Atmos.Terr.Phys. 29 1657-1662.

Silverberg,E.C. and Poultney,S.K. 1967: University of Maryland Tech.Rep. 765.

Volz,F.E. and Goody,R.M. 1962: J.Atmos.Sci. 19 385-406.

N7A-25360

LASER RADAR MEASUREMENTS OF THE AEROSOL CONTENT  
OF THE ATMOSPHERE\*

Gerald W. Grams

National Aeronautics and Space Administration  
Electronics Research Center  
Cambridge, Massachusetts

ABSTRACT

This report reviews the experimental program conducted by Professor Giorgio Fiocco and his group at the Research Laboratory of Electronics of the Massachusetts Institute of Technology. A summary of the results of laser radar observations of atmospheric aerosols is presented along with a description of the laser radar system devised during the study and of the data handling techniques utilized for the analysis of the data of the temporal and spatial distribution of atmospheric aerosols. Current research conducted by the group is directed toward the analysis of the frequency spectrum of laser radar echoes to obtain absolute measurements of the dust content of the atmosphere by resolving the molecular and aerosol contributions to the laser radar echoes.

---

\*This research was conducted at the Massachusetts Institute of Technology and was supported in part by the National Aeronautics and Space Administration under grants NGR-22-009-114 and NGR-22-009-131.

## 1. INTRODUCTION

One of the simplest techniques for probing the atmosphere with lasers uses the backscattered radiation from a pulsed laser to detect layers of dust particles in the atmosphere. In the experiments that have been performed, the optical backscattering cross-section of the atmosphere is measured as a function of range, and the presence of aerosol layers is established by locating significant deviations from the laser radar return expected for dry, clean air.

The first experiments to use lasers for ground-based remote measurements of atmospheric parameters were conducted by Fiocco and Smullin (1963). In their preliminary studies, echoes from scattering layers from heights of 60 to 140 km were detected during the summer of 1963. These echoes were tentatively attributed to dust particles of extraterrestrial origin (Fiocco and Colombo, 1964); this interpretation is corroborated by the observed correlation between the laser radar echoes from 110 to 140 km and ionospheric sporadic-E (Fiocco, 1965). Numerical calculations of the ionization resulting from neutral-neutral collisions of the ambient gas induced by incoming extraterrestrial particles (Fiocco, 1967) have verified that the influx of cosmic dust can produce ionization in amounts comparable to that required in the E-region at night and in some types of sporadic-E irregularities. Since subsequent laser radar measurements have not always detected the presence of scattering layers at high altitudes, considerable variability of the influx of extraterrestrial particles is indicated. There is further evidence of increased meteoric activity during the summer of 1963 obtained by techniques other than laser radar observations (see, for example, McIntosh and Millman, 1964; Ellyett and Keay, 1964).

A two-year study to evaluate the average and time-variant characteristics of stratospheric aerosols has been conducted with a laser radar (Fiocco and Grams, 1964; Grams and Fiocco, 1967). Most of the observations were conducted at Lexington, Massachusetts during 1964 and 1965; some data were also obtained during the summer of 1964 at College, Alaska. The vertical distribution of the aerosol particles was obtained by comparing the laser radar return with the return expected from a molecular atmosphere, using the observed echoes from 25 to 30 km altitude to calibrate the instrument. The data consistently showed a maximum in the relative concentration of aerosols between 15 and 20 km altitude. The observations showed that the stratospheric aerosol layer exhibited little temporal variability, with a generally decreasing trend during the two-year observation interval. At the observation site in Lexington, Massachusetts, the observed return from the layer was approximately 1.9 times the expected return from clear, dry air. The daily rms fluctuation of this scattering ratio was approximately 0.3 and hourly fluctuations were smaller. For the observations at College, Alaska, the maximum scattering ratio was ~1.7 with daily fluctuations of about 0.15. The study was conducted during a period following the eruption of the Mount Agung volcano in early 1963; thus, the results may represent anomalous conditions in the lower stratosphere and are likely to be associated with the temporal and spatial distribution of volcanic debris.

The observed scattering ratios have been related to the number of particles per unit volume illuminated by the laser beam by evaluating Mie-scattering functions for backscattered radiation. The calculated concentration of  $\sim 1 \text{ cm}^{-3}$  for particles larger than about  $0.3\mu$  radius is in agreement with independent studies by other investigators, especially with the particle counts of Rosen (1964). Comparisons with earlier measurements obtained by other investigators using a variety of different techniques indicated that the concentration of stratospheric aerosols was about one order of magnitude higher than before the eruption of Mount Agung; this has also been confirmed by the results of other investigators (see, for example, Volz, 1965).

The observations have been compared with other meteorological parameters in the lower stratosphere. The center of mass of the layer was usually very close to 16 km; day-to-day changes in the tropopause height were accompanied by a tendency for small vertical displacements of the layer. The laser radar observations performed in Alaska agree with the concept that the height of the layer approximately follows latitudinal changes in the tropopause height. A significant negative correlation was found between dust concentrations derived from the results of the laser radar study and ozone concentrations obtained by the Air Force Cambridge Research Laboratories (Hering, 1964; Hering and Borden, 1964, 1965). The anticorrelation was also obtained between the measurements of the dust concentration and measurements of total atmospheric ozone obtained at Bedford, Massachusetts; this result provided additional statistical evidence of a relation between the aerosol layer and stratospheric ozone.

During summer 1964 laser radar experiments were performed in Alaska and Sweden for the purpose of observing the aerosol content of the mesosphere during noctilucent cloud displays (Fiocco and Grams, 1966). In these experiments strong echoes were observed near 70 km and were taken as an indication that measurable processes involving a wide range of mesospheric heights were involved. New experiments to obtain measurements of the aerosol content of the mesosphere at times when noctilucent clouds might be present were conducted in the summer of 1966 near Oslo, Norway (Fiocco and Grams, 1968). The measurements indicate that the altitude region 60-70 km contains an appreciable amount of particulate material in the summertime at high latitudes during periods of noctilucent cloud activity, as suggested by the earlier laser radar results. Observations of the transient features of a noctilucent cloud were also obtained with the apparatus: the height of the cloud varied from 75 to 73 km during the observation interval; the geometric thickness of the cloud was appreciably less than 1 km, and the optical thickness was about  $10^{-4}$ . An estimate of the meridional flux of particulate material at high latitudes was obtained from the measurements by relating the average vertical distribution of aerosols observed by the laser radar during the summer to the general circulation of the upper atmosphere; estimates of the mass flux of extraterrestrial dust based on this data are in agreement with results obtained by other techniques.

## LASER RADAR MEASUREMENTS

A large number of laser radar measurements related to the aerosol content of the mesosphere were obtained in Lexington, Massachusetts, in 1964 and 1965. The data are being analyzed and the results will soon be available.

### 2. INSTRUMENTATION AND DATA ANALYSIS

The measurements were made with a Q-switched ruby laser used as the transmitter and a 40-cm diameter telescope of the Dahl-Kirkham type as the receiver for a monostatic laser radar system. In the system used for the most recent experiments, the laser emits pulses of approximately 2 joules of less than 100 nsec duration at a maximum pulse repetition frequency of  $0.5 \text{ sec}^{-1}$ . The radiation is collimated by a transmitting telescope, 10 cm in diameter with 1-meter focal length. The laser is Q-switched through the use of a rotating prism. The instrument includes two synchronized rotating shutters: one is mounted on the transmitter to prevent any fluorescence from the laser after the pulse is radiated; the other synchronized shutter is incorporated into the detector to prevent exposing the photomultiplier to the intense return obtained from scattering at short distances. A temperature-controlled water-cooling system is used to maintain the laser unit and the narrow-band interference filters in the detection system at constant temperature through closed-loop circulation of distilled water. A polarizing filter is included in the receiver to reduce twilight-sky background: the filter is adjusted to match the polarization of the laser radiation; the observations are carried out at the zenith and the apparatus can be rotated around the vertical axis to minimize the polarized sky-background. The EMI 9558A photomultiplier used in the photodetector is refrigerated by circulation of methanol cooled by mixing with dry ice.

To record the data the apparatus utilizes a 35 mm automatic radarscope camera, modified for use with a dual-beam oscilloscope. Two traces, displaying the amplified photomultiplier current, are recorded simultaneously with different sweep rates: one trace displays the signal from 0 to 200 km altitude; the other displays records of either the signal from 0 to 40 km, to provide data on stratospheric aerosols, or the 60 to 90 km signal, to observe detailed features of mesospheric scattering layers. For altitudes above ~30 km, the backscattered signal is so small that a continuous photomultiplier current is no longer recorded. Thus, the high-altitude traces are analyzed by counting the number of individual photoelectrons recorded in specified range intervals, with the range determined by measuring the time difference between the instant the laser was pulsed and the instant the photoelectron was emitted. The data are reduced with the aid of a semi-automatic film reader incorporating an analog-to-digital converter. Coordinates related to the signal intensity for the 0-40 km traces and to the instant of emission of each photoelectron displayed on the high-altitude traces are digitized and punched on data processing cards for subsequent computer analyses.

A considerable reduction in the effort required to digitize the photographic records of the laser radar data is now possible. A computer has been incorporated into a photointerpretive system

for analyzing information recorded on 35-mm film. This system has been used extensively to analyze spark chamber data (Rudloe, Deutsch, and Marill, 1963); it has now been programmed to digitize the coordinates of the photographed oscilloscope traces. Some of the laser radar data have already been digitized with the programmable film reader, and the time and effort required to analyze the measurements have been substantially decreased.

### 3. CURRENT RESEARCH

Although the studies of the aerosol content of the atmosphere would benefit from the use of lasers of higher average power, the use of more sensitive photodetection systems, or, perhaps, the judicious use of on-line computer systems, it is apparent that the technique used to study atmospheric aerosols suffers from certain limitations in the interpretation of the laser radar returns. In particular, observations of the optical backscattering cross-section of the atmosphere do not provide absolute measurements of the atmospheric aerosol content or of the density of the molecular atmosphere unless the effects of scattering by aerosols and atmospheric molecules can be separated. For this reason, spectral analyses of the light scattered by atmospheric constituents are being conducted.

The main effect on the scattered light is the frequency shift due to the Doppler effect resulting from the motion of the scatterers. As a result of the random thermal motions of atmospheric molecules, the scattered spectrum will be broadened with respect to the radiated spectrum. Measurements of the width of the spectral line are related to the temperature of the gas and could therefore be used as the basis of a system for remote measurements of atmospheric temperature (DeWolf, 1967), while bulk shifts of the scattered spectrum could provide information on wind motion.

Aerosols also contribute to the scattered spectrum. However, the velocities associated with the random Brownian motions of aerosols are much smaller than the thermal velocities of the molecular component of the atmosphere, and the scattered energy from the aerosols is contained in a narrower band of the spectrum than the scattered energy from the atmospheric molecules. Thus, analyses of the frequency spectrum of laser echoes from atmospheric constituents would make it possible to distinguish between the contribution from the aerosols and from atmospheric molecules, if the spectral analysis can be performed with sufficient resolution.

Some preliminary laboratory experiments in which the spectrum of the radiation scattered from a laser beam has been analyzed to provide a measurement of the aerosol component have been reported (Fiocco and DeWolf, 1968). In these experiments the light from a continuous-wave He-Ne laser was scattered from air containing naturally-occurring aerosol particles and from air containing artificially-produced dense fogs. The spectral distribution of the light was measured with a pressure-scanned Fabry-Perot interferometer. Although the apparatus used for these studies requires considerable improvement, a direct measurement of the ratio of aerosol-to-molecular scattering was obtained. This technique provides an

## LASER RADAR MEASUREMENTS

absolute measurement of the aerosol-to-molecular scattering and therefore provides the information required for the definite interpretation of laser radar echoes.

### REFERENCES

- DeWolf, J. B., 1967: On the measurement of atmospheric temperature by optical radar. M.S. thesis, M.I.T., Cambridge, Mass.
- Ellyett, C. D., and C.S.L. Keay, 1964: Meteors: an unexpected increase in 1963. Science, 146, 1458.
- Fiocco, G., 1965: Optical radar results and ionospheric sporadic E, J. Geophys. Res., 70. 2213-2215.
- Fiocco, G., 1967: On the production of ionization by micro-meteorites. J. Geophys. Res., 72, 3497-3501.
- Fiocco, G., and G. Colombo, 1964: Optical radar results and meteoric fragmentation, J. Geophys. Res., 69, 1795-1803.
- Fiocco, G. and J.B. DeWolf, 1968: Frequency spectrum of laser echoes from atmospheric constituents and determination of the aerosol content of air. J. Atmos. Sci., 25, 488-496.
- Fiocco, G. and G. Grams, 1964: Observations of the aerosol layer at 20 km by optical radar. J. Atmos. Sci., 21, 323-324.
- Fiocco, G. and G. Grams, 1966: Observations of the upper atmosphere by optical radar in Alaska and Sweden during the summer 1964. Tellus, 18, 34-38.
- Fiocco, G. and G. Grams, 1968: Optical radar observations of mesospheric aerosols in Norway during the summer 1966. J. Geophys. Res. (submitted for publication).
- Fiocco, G., and L.D. Smullin, 1963: Detection of scattering layers in the upper atmosphere (60-140 km) by optical radar. Nature, 199, 1275-1276.
- Grams, G. and G. Fiocco, 1967: Stratospheric aerosol layer during 1964 and 1965. J. Geophys. Res., 72, 3523-3542.
- Hering, W.S., 1964: Ozonesonde observations over North America. Rept. AFCRL-64-30(I), Air Force Cambridge Research Laboratories.
- Hering, W.S., and T.R. Borden, Jr., 1964: Ozonesonde observations over North America. Rept. AFCRL-64-30(II), Air Force Cambridge Research Laboratories.
- Hering, W.S., and T.R. Borden, Jr., 1965: Ozonesonde observations over North America. Report. AFCRL-64-30(III), Air Force Cambridge Research Laboratories.
- McIntosh, B.A., and P.M. Millman, 1964: Radar meteor counts: anomalous increase during 1963. Science, 146, 1457.
- Rosen, J.M., 1964: The vertical distribution of dust to 30 kilometers. J. Geophys. Res., 69, 4673-4676.
- Rudloe, H., M. Deutsch, T. Marill, 1963: PIP: a photo-interpretive program for the analysis of spark-chamber data. Commun. Assoc. Computing Machinery, 6, 332-335.
- Volz, F.E., 1965: Note on the global variation of stratospheric turbidity since the eruption of Agung Volcano, Tellus, 17, 513-515.

N72-25-361

## COMMENTS ON BISTATIC LIDAR

John A. Reagan

Department of Electrical Engineering  
The University of Arizona  
Tucson, Arizona 85721

In our discussions thus far, we have ignored, for the most part, the question of how effectively lidar can be employed to determine information about the sizes and concentrations of atmospheric aerosols. This is admittedly a difficult question to answer due to the complicated scattering problem which is encountered. But the question is quite relevant in view of the fact that lidar offers one of the most apparent remote probing techniques for studying the properties of aerosols. Some preliminary work on lidar measurements of aerosol distributions has already been attempted by Barrett and Ben-Dov (1967) by making use of backscattered lidar measurements. However, since light scattered by particulates depends on a number of scatterer properties, the amount of information which can be derived about the nature of the particles by measuring only the backscattered intensity of the scattered light is quite limited. It is therefore worthwhile to consider other experimental techniques which take greater advantage of the information available in the scattered signal. In this regard, I would like to comment on the possibility of using bistatic lidar systems.

Monostatic lidar is limited to measurements in only the backscattered direction. In contrast, bistatic lidar provides a means for measuring not only the intensity but also the polarization of light scattered at various angles other than  $180^\circ$  (backscattering). Bistatic lidar, therefore, presents a method for obtaining additional pieces of experimental information which can, in principle, be used to infer more about the size distribution and number density of aerosols than can be inferred from monostatic measurements. In particular, it appears that elliptical polarization measurements can be quite useful in this respect. For example, recent theoretical and experimental work presented by Eiden (1966) indicates that the ellipticity of angularly scattered light which is initially linearly polarized is quite sensitive to the size distribution and index of refraction of aerosol particles for wavelengths close to the typical lidar wavelength, 0.6943 microns (ruby). Moreover, measurements of the

## COMMENTS ON BISTATIC LIDAR

ellipticity of scattered light can unambiguously be attributed to aerosols alone, since molecular scattering does not give rise to elliptical polarization of the scattered signal as long as we are dealing with single scattering. Polarization measurements are also advantageous in that the ellipticity of the received scattered signal can be obtained from the ratios of relative intensity components. This eliminates the difficult problem of having to make absolute intensity measurements. Also, lasers provide excellent linearly polarized sources.

I want to stress, however, that I am not suggesting that bistatic lidar can be used to uniquely determine the size distribution and number density of an arbitrary distribution of particulates. First of all, while bistatic lidar provides a means for obtaining several more measurements than can be made with a monostatic system, an unfeasibly large number of measurements would be required to completely determine the scatterer distribution. Secondly, as recently pointed out by Twomey and Howell (1967), the measurements must be made quite accurately, typically with an error of 1 percent or less, to obtain a few pieces of independent information about the scatterers. It appears, however, that bistatic measurements made at several scattering angles coupled with logical a priori assumptions about the general mathematical form of the particle size distribution can provide useful estimates about the distribution of particulates in the atmosphere. Moreover, through polarization measurements, it may be possible to distinguish certain meteorological phenomena which influence the vertical distribution of particulates; namely, variations in the temperature distribution which bring about a collection of particulates in the vicinity of stable layers and regions of high humidity which give rise to swelling in size of hygroscopic particles.

With regard to existing or planned bistatic lidar installations, I understand that Dr. Paul Palmer at Brigham Young University has assembled a system which became operational about a month before this meeting. Also, I am attempting to set up a bistatic system at the University of Arizona. At present, I am working with Dr. Benjamin Herman, University of Arizona, on a theoretical study to investigate the ambiguity involved in attempting to invert bistatic lidar measurements to infer information about the sizes and concentrations of particulates as a function of height. We hope to have an operational bistatic system for probing to heights of about 10 kilometers by the end of this year.

References

1. Barrett, E. W. and P. Ben-Dov (1967), Applications of the Lidar to air pollution measurements, J. Appl. Met., 6, 500-515.
2. Eiden, R. (1966), The elliptical polarization of light scattered by a volume of atmospheric air, App. Optics, 5, 569-575.
3. Twomey, W. and H. B. Howell (1967), Some aspects of the optical estimation of microstructure in fog and cloud, App. Optics, 6, 2125-2131.

SESSION **4**

Radar

N72-25-362

PROBING THE ATMOSPHERE WITH HIGH POWER, HIGH RESOLUTION RADARS

Kenneth R. Hardy  
Air Force Cambridge Research Laboratories

and

Isadore Katz  
Applied Physics Laboratory  
The Johns Hopkins University

ABSTRACT

Observations of radar echoes from the clear atmosphere are presented and the scattering mechanisms responsible for the two basic types of clear-air echoes are discussed. The commonly observed dot echo originates from a point in space and usually shows little variation in echo intensity over periods of about 0.1 second. The results of the most recent investigations of these clear-air dot targets are consistent with the conclusion that most, if not all, of the dot echoes are caused by insects or birds.

The second type of clear-air radar echo appears diffuse in space, and signal intensities vary considerably over periods of less than 0.1 second. The echoes often occur in thin horizontal layers or as boundaries of convective activity; these are characterized by sharp gradients of refractive index. The reflectivity-wavelength dependence of these echoes is consistent with the theory of scattering by fluctuations in refractive index, and the signal intensities can be accounted for by the spectral characteristics of refractive-index variations observed directly.

Some features of clear-air atmospheric structures as observed with radar are presented. These structures include thin stable inversions, convective thermals, Bénard convection cells, breaking gravity waves, and high tropospheric layers which are sufficiently turbulent to affect aircraft.

1. INTRODUCTION

Radar echoes from a clear atmosphere, usually called "angels," have existed almost from the time that radar was first used. Many and varied are the reports in the literature of angel phenomena, and there have been numerous attempts to arrive at a plausible and satisfactory explanation of their origin. A fairly complete background of the entire angel problem is presented in the reviews by Plank (1956), Atlas (1959), Atlas (1964), and Atlas and Hardy (1966). If the vast amount of work reported in these papers were to be summarized as briefly as possible, that summary would indicate that there are just two types of radar echoes from the clear atmosphere (excluding the effects of anomalous propagation). One type appears to originate from a dot or point target whereas the other type extends over a region of considerable horizontal extent. The objective of this paper is to summarize some of the key properties of the two types of clear-air echoes and to present the results of several recent radar investigations of the clear-air echo patterns as observed with three ultra-sensitive radars at Wallops Island, Virginia. Although these radars may be fruitfully used to investigate clouds and precipitation (especially during the early stages of their development), their primary utility is for the observation of the clear-air. Thus, we will restrict the present discussion to clear-air structures.

2. THEORY

The scattering of electromagnetic waves by a turbulent medium has been studied extensively by various investigators (e.g., Booker and Gordon, 1950; Villars and Weisskopf, 1954; Tatarski, 1961). Since clear-air echoes have been observed from regions of the atmosphere where the variations in refractive-index are large, it is useful to state briefly some of the theoretical results which have been obtained. Thus, Tatarski (1961) has derived the expression:

$$\eta = 0.39 C_n^2 \lambda^{-1/3} \tag{1}$$

where  $\eta$  is the radar reflectivity,  $C_n^2$  is a measure of the intensity of the refractivity fluctuations, and  $\lambda$  is the radar wavelength. Tatarski also derives the expression

$$C_n^2 = a^2 L_o^{4/3} (\overline{dn/dz})^2 \tag{2}$$

where  $a^2$  is a nondimensional proportionality parameter,  $L_o$  the outer scale or eddy size which defines the outer limit of the inertial subrange of turbulence, and  $(\overline{dn/dz})$  the mean vertical gradient of potential refractive index.

Saxton, et al., (1964) used the same theory as described by Tatarski to derive an expression for the radar reflectivity in terms of  $F_n(k)$ , the one dimensional normalized spectral density of the mean-square fluctuations of refractivity,  $\langle (\Delta n)^2 \rangle$ . Their equation is

$$\eta = \frac{\pi}{8} \langle (\Delta n)^2 \rangle k^2 F_n(k) \tag{3}$$

where  $k$  is wavenumber and is related to the radar wavelength ( $\lambda$ ) by  $k = 4 \pi/\lambda$ . Lane (1967) has pointed out that Eq. 3 is a particularly useful form because

the reflectivity can be evaluated from direct estimates of  $\langle (\Delta n)^2 \rangle > F_n(k)$  which are derived from spectral analysis of the field of refractive index. This direct estimate of reflectivity can then be compared to the reflectivity measured with a radar as we will do in Section 5.

Atlas, et al., (1966) give an equation

$$L_0 = (\epsilon/\beta^3)^{1/2} \quad (4)$$

where  $\beta$  is the vertical gradient of the mean horizontal wind and  $\epsilon$  the rate of energy dissipation. The quantity  $\epsilon$  is an indicator of turbulence because energy dissipation at high rates is accomplished by increased turbulence.

Combining Eqs. (2) and (4) and substituting into Eq. (1), we find that

$$\eta = 0.39 a^2 \epsilon^{2/3} \beta^{-2} (\overline{dn/dz})^2 \lambda^{-1/3} \quad (5)$$

Equation (5) shows that, if the mean gradients of horizontal wind and potential refractivity are known, an estimate of the turbulence intensity can be obtained by evaluating  $\epsilon$  from measurements of the reflectivity,  $\eta$ .

Finally, if there are particles in the atmosphere which are small relative to the radar wavelength, then the reflectivity is given by

$$\eta = \pi^5 |K|^2 \lambda^{-4} \sum D^6 \quad (6)$$

where  $K$  is related to the complex index of refraction of the particle,  $D$  is the particle diameter, and the sum is taken over a unit volume. Equation (6) is the Rayleigh approximation; it can be applied with very small errors for clouds and raindrops when radar wavelengths greater than 3 cm are used. Comparing Eqs. (1) and (6), one sees that particle scatter can be distinguished from scatter due to variations in refractive index by measuring the reflectivity at more than one radar wavelength.

### 3. TYPES OF CLEAR-AIR RADAR ECHOES

A multiwavelength radar facility at Wallops Island has been used since 1965 to investigate the nature of clear-air radar echoes. Characteristics of the radars have been tabulated by Hardy, et al., (1966). Briefly, the wavelengths of the radars are 3.2, 10.7, and 71.5 cm, and the minimum detectable cross-section at a range of 10 km is approximately  $6.0 \times 10^{-4}$ ,  $2.5 \times 10^{-5}$ , and  $3.4 \times 10^{-5} \text{ cm}^2$ , respectively.

TABLE 1 illustrates how the Wallops Island radars can readily identify scatterers which are small relative to the wavelength (Rayleigh scatterers) or the scattering expected from refractive index variations. If the pulse volumes are filled with Rayleigh scatterers, then the signal at 3.2-cm wavelength will be about 5 db greater than at 10.7 cm and 30 db greater than at 71.5 cm. On the other hand, if the reflectivity of the scattering medium has a wavelength dependence of approximately  $\lambda^{-1/3}$ , as appears likely from observations of the clear atmosphere reported by Hardy, et al., (1966) and Atlas, et al., (1966a), then the 3.2-cm signal will be about 15 db lower than

TABLE 1

Ratios of Signal Strengths Expected from Two Types of Scatterers  
Applicable Only for the Wallops Island Radars

Wavelength (cm)	Ratio of 3.2-cm received power above minimum detectable to that at 10.7 and 71.5 cm (db)	
	Rayleigh scatterers ( $\lambda^{-4}$ dependence)	Scattering from refractive index fluctuations ( $\lambda^{-1/3}$ dependence)
3.2	0	0
10.7	5	-15
71.5	30	-20

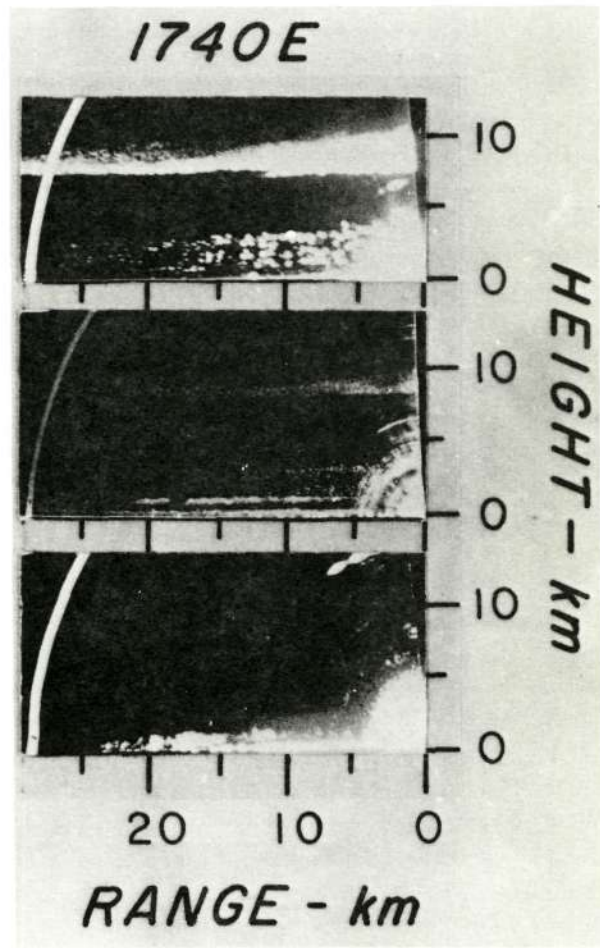
at 10.7 cm and 20 db lower than at 71.5 cm. Thus, if the signal is stronger at the longer wavelength, it is certain that the mechanism giving rise to the radar echoes is not scattering by Rayleigh particles. The data which follow are interpreted qualitatively with the aid of TABLE 1.

Figure 1 shows simultaneous photographs of the range height indicators (RHI) of the three Wallops Island radars, taken while the beams were scanning synchronously in elevation angle. Except for an overcast cirrus layer, the sky was clear at the time of this observation. The cirrus cloud appears between a height of 7 and 10 km; it is easily identified as it is strongest at 3.2-cm wavelength (top photo), weaker at 10.7-cm wavelength (middle photo), and not visible at 71.5-cm wavelength (bottom photo). Such a drop-off in signal strength with wavelength is expected for Rayleigh scatterers as indicated in TABLE 1. The fact that the numerous dot echoes, appearing between 1 and 3 km in height, are seen most prominently with the 3.2-cm radar and not at all with the 71.5-cm radar indicates that the targets are small relative to the radar wavelength. This observation on the dot echoes, as well as many other types of measurement (for example, the tracking by radar of single known insect species), has led to the conclusion that most of the dot targets are insects (Glover and Hardy, 1966; Glover, *et al.*, 1966).

In Figure 1, the thin layers seen near the surface and at 1 km with the two longer wavelength radars are not attributed to particle scatter. If this were so, the layers would appear much stronger at the shorter wavelength (TABLE 1). Instead, the layers are caused by backscatter from variations in refractive index (Hardy, *et al.*, 1966). These authors show that the wavelength dependence of the echo layers is consistent with the theory of scatter by refractive-index variations [Eq. (1)]. In addition, it has been confirmed that these clear-air radar layers are associated with increased refractivity fluctuations as measured directly with refractometers mounted on aircraft or suspended below a helicopter (Konrad and Randall, 1966).

Another pattern of echo formation is generally found under conditions of

Fig. 1 Photographs of range-height indicators (RHI). The photographs were taken at 3.2-, 10.7-, and 71.5-cm wavelengths (top to bottom) along an azimuth of 260 deg. for 1740 E.S.T. 3 Sept 1966 at Wallops Island, Virginia. The cirrus cloud appears at the shorter wavelengths, whereas the longer wavelength detects only the clear-air variations in refractive index. The numerous dot echoes which appear uniformly distributed between 1 and 3 km at the two shorter wavelengths are due to single insects.



surface heating, both over land and over water. This pattern along with other clear-air structures will be discussed in the following sections.

#### 4. DOT ANGELS

Dot or point angels, as their name implies, appear as point targets on a PPI or RHI scope photograph (Fig. 1). They are also very commonly observed with a fixed vertically-pointing radar beam. An example of dot angels as observed with a 0.86 cm TPQ-11 vertically-pointing radar is shown in Fig. 2. This time-height record was obtained by intensity modulating a scope which was photographed while the film moved continuously at a slow rate. Because of the way the TPQ-11 signal is recorded (Petrocchi and Paulsen, 1966), each dot target appears as a short vertical line. The full vertical lines are at 5-minute intervals and the horizontal dashes correspond to 5000-foot height markers. The lower 3000 to 4000 feet appears filled with dot angels, particularly in the lower half of the figure. In addition, however, there is a distinct tendency for the dot angels to concentrate near heights of 6500 and 8000 feet. The tendency for preferred heights has also been noted by Plank (1956) and Hardy, *et al.*, (1966).

Prior to 1962, there was little known about the wavelength dependence of the

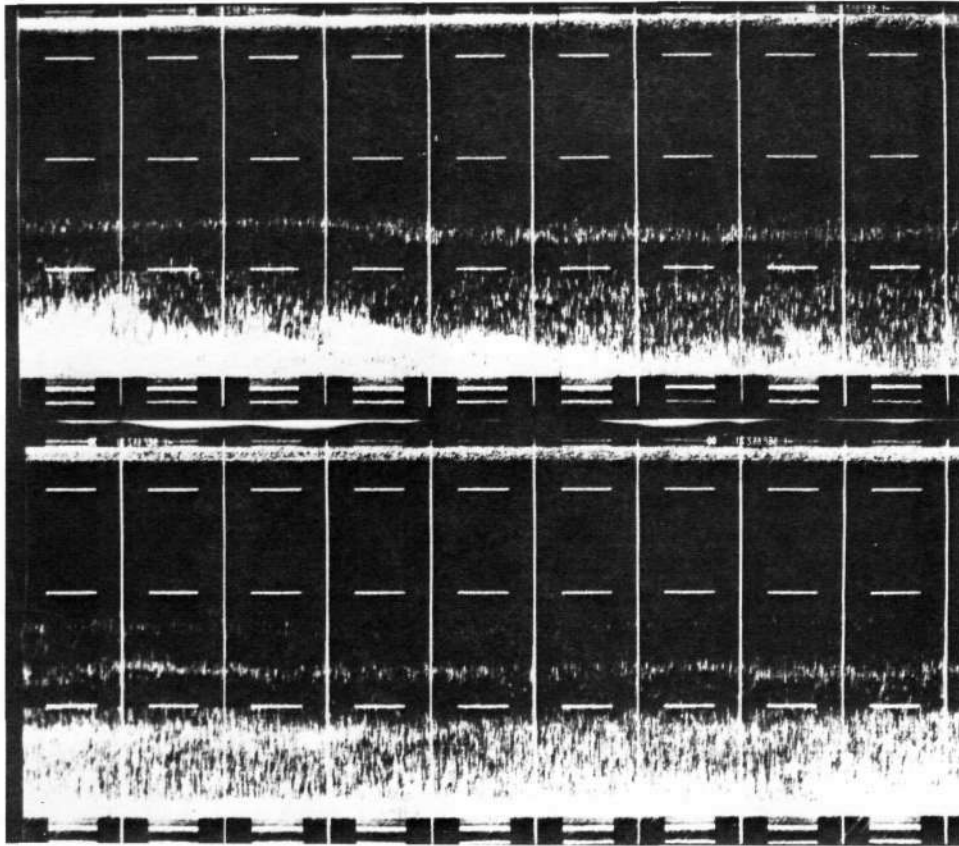
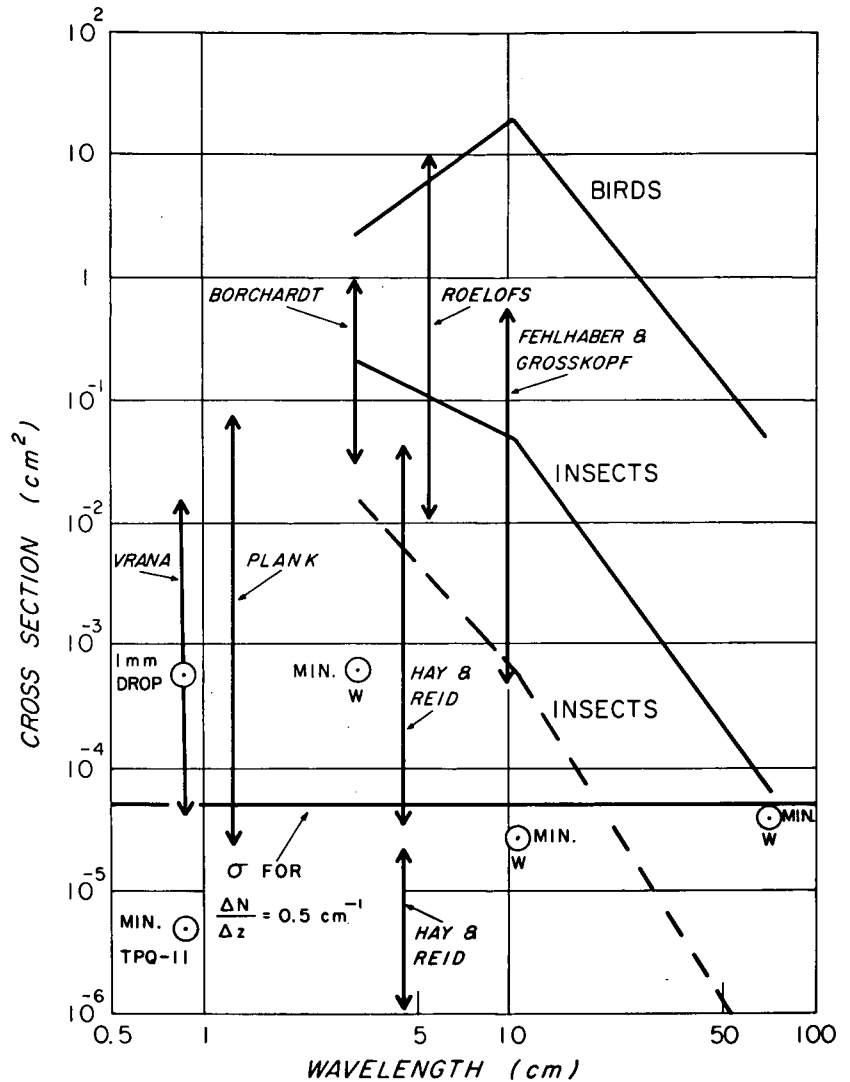


Fig. 2 Dot angels as seen with a vertically-pointing 0.86-cm TPQ-11 radar at Bedford, Mass., 1 Sept 1966, about 1600 E.S.T. The full vertical lines are at 5-min. intervals and the horizontal dashes correspond to 5000-foot height markers. (Courtesy Messrs. Wilbur H. Paulsen and Pio J. Petrocchi, Air Force Cambridge Research Laboratories, Bedford, Mass.)

radar backscattering cross-section of the dot angels. Certainly, dot angels were seen consistently with radars having wavelengths of less than 3 cm (Crawford, 1949; Plank, 1956; Vrana, 1961). However, at wavelengths of about 10 cm, only the recent more sensitive radars were able to detect the relatively small cross-section of the vast majority of dot angels.

Let us look at some of the observations of dot-angel cross-sections as reported by various investigators. These are indicated in Fig. 3. The data by Borchardt (1962), Roelofs (1963), and Fehlhaber and Grosskopf (1964) show cross-sections which range from about  $5 \times 10^{-4}$  to  $10 \text{ cm}^2$ . The cross-sections reported by Vrana (1961) and Plank (1956) vary from  $2 \times 10^{-5}$  to  $8 \times 10^{-2} \text{ cm}^2$ . Note that the minimum detectable cross-section of the TPQ-11 radar at a range of 1 km is almost 20 db less than the cross-section of a 1-mm diameter water drop. This radar could detect a single mosquito with ease at ranges of more than 2 km. The cross-sections of Hay and Reid (1962) cover a very large range of values. They use a particularly sensitive vertically pointing radar. But

Fig. 3 Cross-sections of dot angels, insects and birds as a function of wavelength. The insect and bird cross-sections are illustrated schematically. The minimum detectable cross-sections for the TPQ-11 radar and the Wallops Island radars are indicated by min. TPQ-11 and min. W respectively.



a vertically pointing radar is not capable of estimating the true cross-section of the target, because it is impossible to know where the target is relative to the beam axis. Thus, a large target near the fringes of the beam would have a small measured cross-section.

The results of cross-section measurements of insects and birds at various wavelengths are indicated schematically in Fig. 3. The curve for birds was chosen as a result of observations at three wavelengths on known birds as reported by Konrad and Hicks (1966) and of additional information presented by Glover and Hardy (1966). There is naturally a large variation in bird cross-sections. Even for the same bird, the cross-section can change by as much as  $\pm 10$  db especially at the shorter wavelengths. The general shape of the bird-curve, however, is believed to be quite representative for a large class of birds. The peak in the curve near 10-cm wavelength is probably due to the complicated wavelength dependence which is exhibited by Mie-type scatterers (i.e., the

particle size is of the same order as that of the radar wavelength).

The curves for known insects were similarly obtained from multiwavelength measurements using the Wallops Island radars (Glover, et al., 1966; Glover and Hardy, 1966). The two curves indicate a probable range of values for fairly large insects (maximum size equivalent to a worker honey bee). The cross-sections of insects having dimensions of less than 3 mm are generally undetectable with the Wallops Island radars. The insect cross-sections vary by about  $\pm 5$  db at wavelengths greater than 3 cm. There are no extensive cross-section measurements of known insects at wavelengths less than 3 cm. Nevertheless, the cross-sections of water spheres, which have volumes corresponding to those of a large class of insects, fall within the range of  $10^{-4}$  to  $10^{-1}$  cm<sup>2</sup> at wavelengths from 1-3 cm.

The data in Fig. 3 indicate that, taking into account the method of observation, all the cross-section measurements of dot angels fall within the range of values expected for insects or birds. Moreover, based on simultaneous multiwavelength measurements, Hardy, et al., (1966), Glover, et al., (1966), and Glover and Hardy (1966) have concluded that all of the dot angels observed in detail have characteristics which identify them as either insects or birds.

An alternative, but unsubstantiated, explanation for dot angels is that they are due to reflections from smooth pseudo-horizontal surfaces across which a large change in refractivity occurs. Atlas (1960, 1964, 1965) and Atlas and Hardy (1966) have described some of the clear-air atmospheric structures which would be required to explain the magnitude of the observed cross-sections. Assuming a refractivity gradient of  $0.5 \times 10^{-6}$  cm<sup>-1</sup> exists over a smooth surface which was smaller than the first Fresnel zone, then this surface would have a cross-section in the order of  $10^{-4}$  cm<sup>2</sup>. The power reflection coefficient of such a surface was assumed to vary as the square of the radar wavelength. From Fig. 3 we see that  $10^{-4}$  cm<sup>2</sup> is near the lower limit of the observed cross-sections of dot angels. This is in spite of the rather optimistic atmospheric structure which was assumed. Atlas (1965) has pointed out that curvature of a surface may result in considerable enhancement of the cross-section. This enhancement would apply to all wavelengths. However, the cross-sections of all dot angels observed at Wallops Island have been strongest at the shortest wavelengths (3.2 and 10.7 cm). Therefore, from the multiwavelength measurements at Wallops Island, there is no evidence of dot angels that are due to atmospheric reflections from sharp refractive-index gradients.

Chernikov (1966) has described some bistatic and depolarization investigations of dot angels. Contrary to his preliminary results, Chernikov (1966) now states that the experiments carried out provide convincing evidence that the overwhelming majority of dot-angel echo targets are insects and other particles introduced into the atmosphere. Fehlhaber and Grosskopf\* have arrived at the same conclusion after a reexamination of their bistatic measurements on dot angels. In summary, it would appear that insects or birds can account for the vast amount of observational radar-data on dot angels.

---

\* Private communication

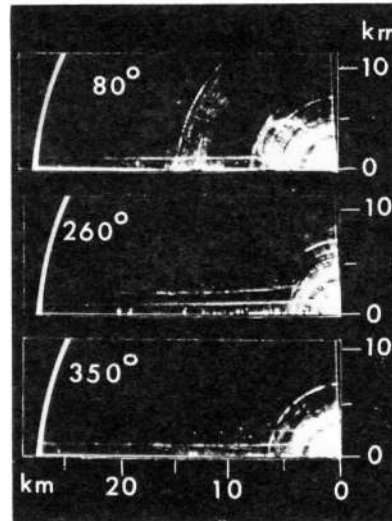
## 5. CLEAR-AIR ECHOES OF HORIZONTAL EXTENT

## 5.1 General Features

Atlas (1964) has reviewed some of the early results of radar echoes from stratified layers. These layers usually corresponded in height to regions having sharp vertical gradients in refractive index. Additional evidence for the existence of clear-air radar layers associated with large variations of refractive index is given by Saxton, et al., (1964), Ottersten (1964), and Hardy, et al., (1966).

Fig. 4 is an example of uniform, stratified layers as they appear on RHI photographs. These data were obtained with the 10.7-cm radar at Wallops Island at 0530 EST while the sky was perfectly clear. The layer near 1 km appears at all three azimuths and is coincident with a very pronounced inversion (Hardy and Glover, 1966). It is typical of the type of layer observed in the vicinity of very stable layers, but yet the variations of refractive index within the layer may be large (Lane, 1964).

Fig. 4 Photographs at three azimuths of the range-height indicators at a wavelength of 10.7 cm at Wallops Island, Va., 0530 E.S.T., 4 Sept 1965. The sky was perfectly clear at the time of the observation. The layer near 1 km is coincident with a very pronounced inversion. The circumferential arcs at short ranges are ground echoes seen by the side lobes. (From Hardy and Glover, 1966.)



The variation of the reflectivity of clear-air layers as a function of wavelength is shown schematically in Fig. 5. Some typical values of reflectivity observed with the Wallops Island 10.7 and 71.5-cm radars are indicated in the right-center of the figure. The slopes of the lines are close to the  $1/3$  power as expected for scatter from refractive index fluctuations (Eq. (1)), but in practice there is considerable variation in this slope for individual measurements. For comparison, the reflectivity-wavelength relationship observed in a particularly dense layer of insects (concentration of about  $5 \times 10^{-6} \text{ m}^{-3}$ ) is also indicated. It is evident that the two types of scatterers can be readily identified on the basis of their wavelength dependence (see also Fig. 1). Also indicated in Fig. 5 are the approximate maximum values of the 10-cm radar reflectivity as observed by Ottersten (1964) and by the Wallops Island 10.7-cm radar in regions which apparently were not contaminated with any insects.

Values of the coefficient  $C_n^2$  derived from Eq. (1) are shown on the scale at the right. The  $C_n^2$  values of the clear-air radar layers are usually in the range of  $10^{-15}$  -  $10^{-14} \text{ cm}^{-2/3}$ , but maximum values as high as  $10^{-12} \text{ cm}^{-2/3}$  may occur on rare occasions.

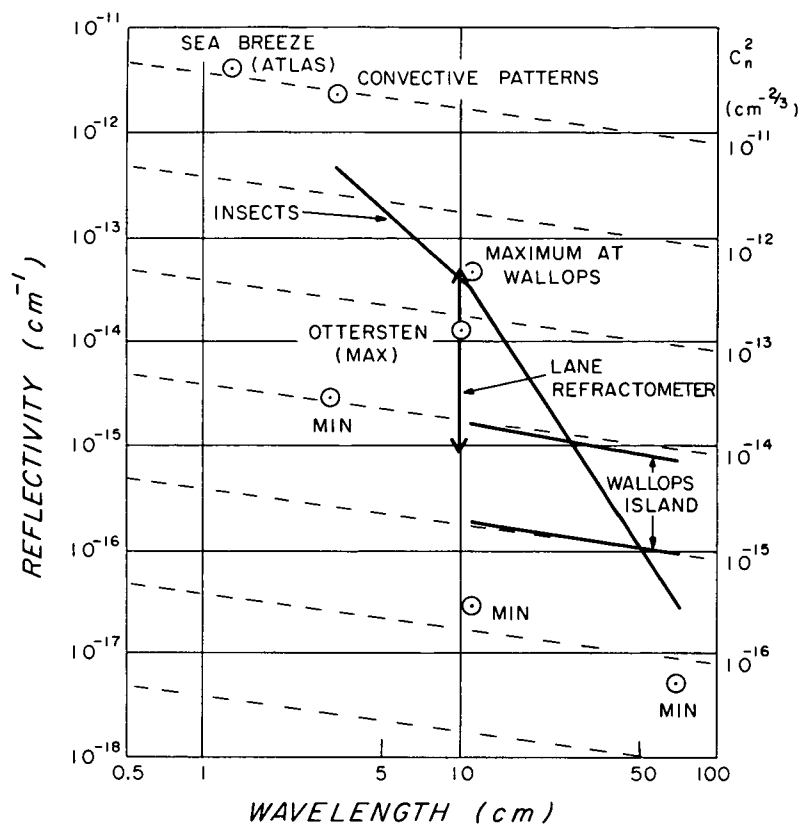


Fig. 5 Radar reflectivity as a function of wavelength for clear-air radar echoes. The values of the three-dimensional fluctuations in refractive index,  $C_n^2$ , as derived from theory are shown on the scale at the right. The reflectivity varies approximately as wavelength to the  $-1/3$  power for scattering from refractive-index fluctuations and wavelength to the  $-4$  power for insects. Values of reflectivity derived from direct measurements of refractivity spectra are consistent with the reflectivities observed with radar.

Balloon-borne refractometer soundings, carried out by Lane (1967) in England, have shown that at or near the base of elevated inversions and isothermal layers there are eddies within which unusually large values of variance  $\langle(\Delta n)^2\rangle$  are observed. Lane has performed a spectral analysis of 20 records, all of which were taken in layers which correlated with vertical-incidence 10-cm radar echoes. He then extrapolated values of  $\langle(\Delta n)^2\rangle F_n(k)$  corresponding to a radar wavelength of 10 cm ( $k = 4\pi/\lambda = 1.25\text{ cm}^{-1}$ ). From Eq. (3), he was able to estimate the reflectivity due to scattering from observed variations in refractive index. The range of reflectivity values thus computed for

the 20 spectra are indicated by the double-ended arrow at 10-cm wavelength in Fig. 5.

As seen in Fig. 5, the range of reflectivities expected from the direct refractivity measurements in England are in excellent accord with the reflectivities obtained from radar measurements in Sweden and the U.S. (Lane estimates crudely that the reflectivities, observed with the radar used in conjunction with his refractometer soundings, were also consistent with those observed by Ottersten.) Realizing that the data presented in Fig. 5 are subject to errors in the order of several db, it can, nevertheless, be seen that there is gross quantitative agreement between the radar observations and the corresponding direct atmospheric measurements.

There are two additional data points on Fig. 5 which have not been mentioned. These occur at wavelengths of 1.25 and 3.2 cm and correspond to  $C_n^2$  values of about  $10^{-11} \text{ cm}^{-2/3}$ . The 3.2-cm value was estimated from clear-air echoes during a time when insects were bountiful in the layer near the surface (Section 7). The value at 1.25 cm has been estimated from the radar observations of the sea-breeze reported by Atlas (1960a). Although refractive-index variations at a sea-breeze front are likely to be comparable to the maximum values which can exist in the atmosphere, it is difficult to picture more than an order of magnitude increase in  $C_n^2$  at a sea breeze front over the  $C_n^2$  observed in elevated layers. An alternative explanation is that a few insects were within the pulse volume and resulted in a significant contribution to the received signal. This possibility has appeal because of the relative ease at which short wavelength radars detect insects (Fig. 3), and it would obviate the need to explain refractive-index variations of more than an order of magnitude larger than those which have been observed or estimated by other techniques.

## 5.2 Experiments to Validate Theory

The expression given by Saxton, Eq. (3), states the relationship between radar reflectivity and the spectral density of refractive-index fluctuations. Tests have already been mentioned which have shown a qualitative association between regions of high variance in refractivity and the presence of clear-air echoes. Some experiments were also performed at Wallops Island which were directed toward a quantitative check of this theoretical relationship.

The technique used in these experiments involved tracking the meteorologically-instrumented aircraft with the radar, making radar measurements and meteorological measurements simultaneously. The radar automatically tracked the incoming aircraft with a tracking gate. A "data" gate was slaved to the tracking gate and was positioned just ahead of the aircraft; radar signal strength was measured in that volume of space determined by the data gate and radar beamwidths. The airplane flew into this volume about 10 seconds after the radar had a measure of its reflectivity. By taking this lag into account, one could compare radar reflectivity with the spectrum of the refractivity fluctuations.

Figure 6 shows the results of this experiment. Along the abscissa are values of  $\frac{\pi}{8} k^2 \langle (\Delta n)^2 \rangle F_n(k)$  and along the ordinate are values of radar reflectivity. The points showing the spectral values on the graph were obtained by

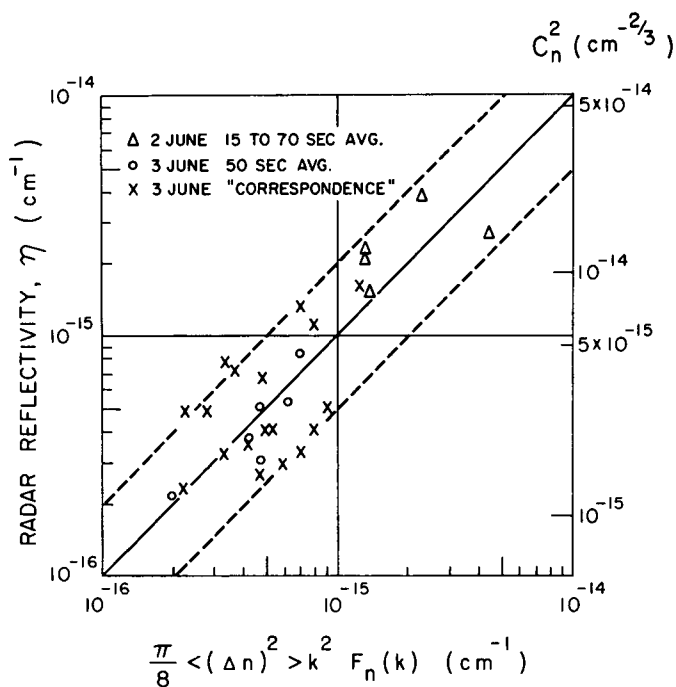


Fig. 6 Radar reflectivity as a function of spectral density or refractive index. Spectral density was obtained by extrapolating computed spectra down to wavenumber,  $k$ , corresponding to one-half the 10.7-cm radar wavelength. For almost all cases the radar reflectivity corresponds to within 3 db of that expected from direct refractometer measurements. (From Kropfli *et al.*, 1968.)

extrapolating the measured spectra to the appropriate wave number as was done by Lane (1967); this was necessary because the size of the sampling refractometer cavity precluded making direct measurements of the small atmospheric eddies. The solid line is the relationship expected from Eq. (3). It can be seen that most of the points fall within the 3 db bounds (shown as broken lines). It is possible to draw three conclusions from these results: (1) the "-5/3 law" is applicable to these atmospheric conditions, (2) the microscale cutoff is at a wave number greater than 5 cm, and (3) the theory which leads to Eq. (3) has been confirmed experimentally.

A continuation of this type of fine scale comparison is being planned. Clearly, it would be preferable to avoid extrapolation by measuring fluctuations in refractivity with devices sufficiently small that their frequency response lies in the appropriate region. This is already feasible using hot-wire anemometers and fine-wire thermometers. Rapid progress is being made in small-volume humidimeters and one is being installed for flights during the summer of 1968. To date, however, refractometers are unable to measure the atmosphere with the required resolution. It is strongly suggested that this is an area requiring active and high-priority research.

## 6. CONVECTIVE THERMALS

During clear days in the summer, convective patterns are observed consistently in the lower atmosphere with the 10.7 cm radar at Wallops Island. These patterns appear as wave-like perturbations on an RHI presentation and are illustrated in Fig. 7. The top photo (X-band, 3.2 cm) shows a few echoes at a height of about 800 m spaced 2-3 km apart. The corresponding echoes are much stronger in the middle photo (S-band, 10.7 cm), and this confirms that the scattering is from variations in refractive index (TABLE 1 and Fig. 1).

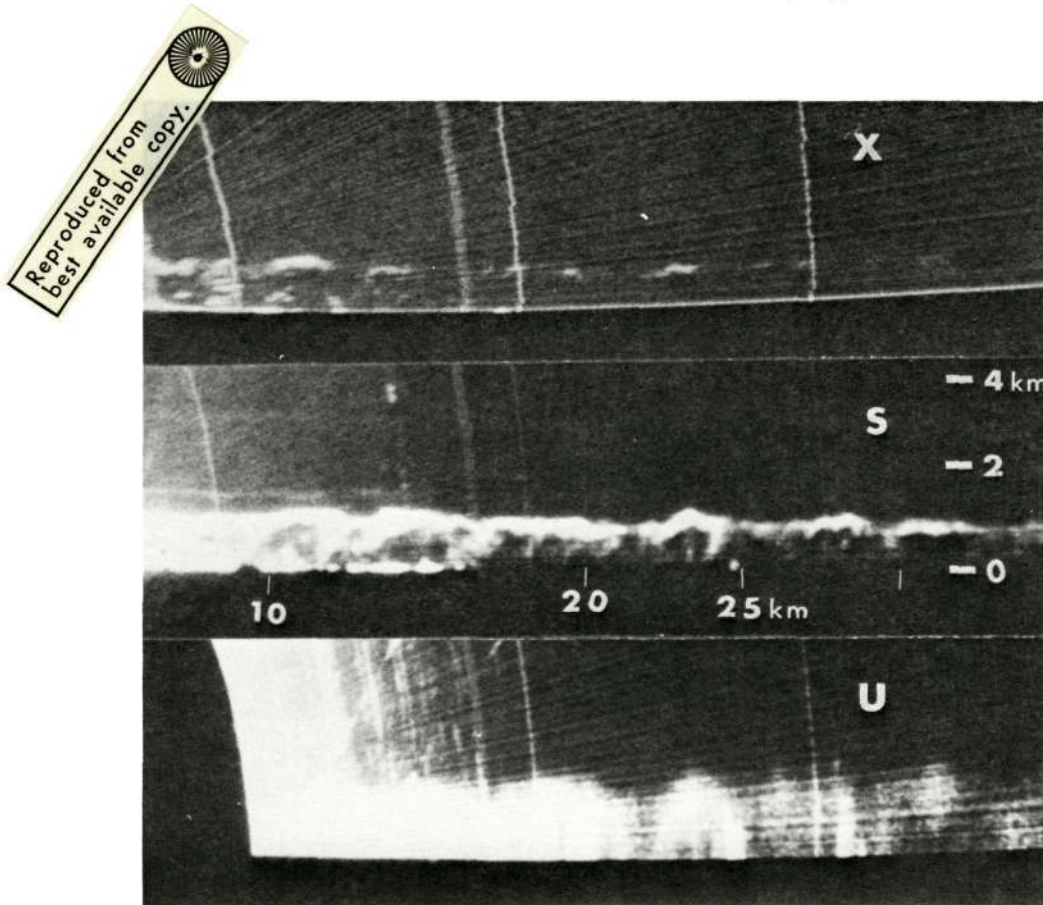


Fig. 7 Simultaneous photographs of range-height indicators at wavelengths of 3.2 cm (X-band), 10.7 cm (S-band), and 71.5 cm (UHF) taken while the sky was clear, 0850 E.S.T., 10 May 1966, at Wallops Island, Virginia; azimuth 250 deg. The definite wave-like perturbations are the boundaries of convective cells (Fig. 8a).

The bottom photo (UHF, 71.5 cm) shows extensive echoes out to a range of more than 30 km. Because of the broad 3-degree beam of the 71.5-cm radar (compared with the 0.5 degree beam of the 10.7-cm radar), the echoes are spread out at the longer wavelength.

The horizontal pattern of the echoes, shown in Fig. 8a, reveals that the echo-structure is actually circular or elliptical having diameters of 1-3 km and echo-free centers. There were cumulus clouds in the area at the time the photo shown in Fig. 8a was taken, and it is probable that many of the echoes are coming from cloudy regions. Nevertheless, the echoes are seen by virtue of scattering from refractive-index variations as established from the multi-wavelength measurements. Furthermore, essentially identical patterns have been observed during a perfectly clear day (Atlas and Hardy, 1966).

Figure 8b is a sketch of the atmospheric structure which might produce the observed echo pattern. It shows a rising plume of air or thermal. The sketch was derived not only from the data shown in Figs. 7 and 8a, but was also derived from a series of PPI photographs taken at successively increased ele-

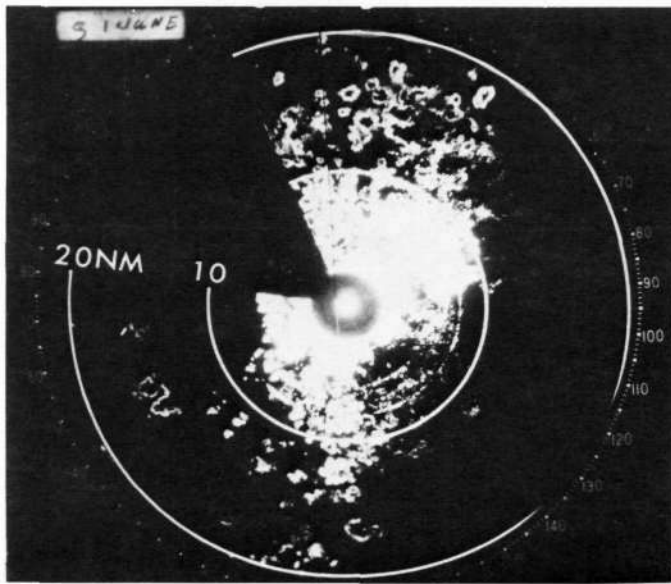


Fig. 8a Photograph of sector plan-position-indicator (PPI) at wavelength of 10.7 cm with 12 db attenuation; 1023 E.S.T., 1 June 1966, at Wallops Island, Virginia, elevation 5 deg., and range marks are at 10 n. mi. (18.5 km). Some of the intense echoes within 10 n.mi. are due to ground clutter. The radar beam cuts through the convective cells seen in Figure 7 showing that the cells are circular or elliptical with echo-free centers.

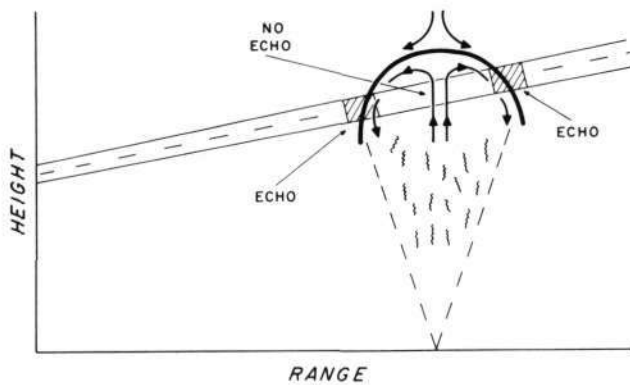


Fig. 8b Sketch of convective cell showing the refractivity structure which results in the observed doughnut-like echoes.

vation angles. These photos indicated that the hole regions became progressively more echo filled at greater heights in the atmosphere, and that the overall diameter of the echoes also diminished. The sketch indicates that the flow within the convective cell is upward in the center and that the relative flow around the periphery is downward. This model would be expected to give the maximum gradients of refractive index near the top of the cell, decreased gradients around the periphery, and relatively small gradients in the cell center where the air was fairly uniform.

## 7. BÉNARD-LIKE CONVECTION CELLS

The convective patterns described in the previous section had diameters in the order of 1-3 km, probably updrafts in their center, and were due to scattering from refractive index variations. In this section a different type of convective pattern is described.

Figure 9 is a photograph of a PPI of a CPS-9 (3.2 cm) radar taken at 0 degree elevation on 23 May 1966 at Sudbury, Massachusetts. Except for a few fair weather cumulus clouds (<1/10 coverage) the sky was clear at the time of

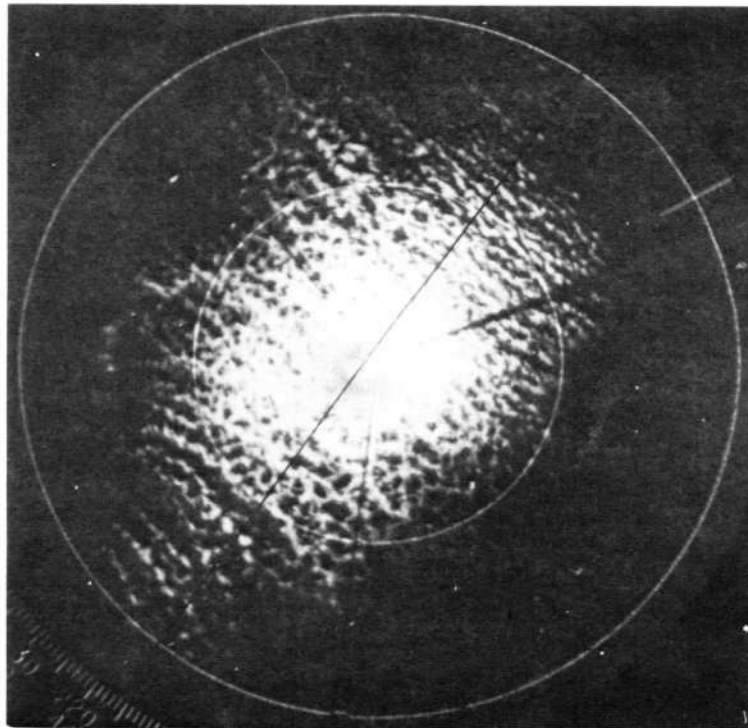


Fig. 9 PPI photo at 0 deg. elevation angle taken at 1120 E.S.T. on 23 May 1966 while the sky was essentially clear. The major range marks are at 25 n. mi. intervals. The radar is a 3.2-cm CPS-9 located at Sudbury, Massachusetts. A mesoscale cellular pattern, similar to the Bénard circulation patterns studied extensively in the laboratory can be seen. The individual cell has a diameter which varies from 5-10 km, a lifetime of at least 30 minutes, and is made up of several smaller cells. The echoes are due to scattering from insects which occurred in abnormally high concentrations during the observations. The insects apparently provide excellent tracers of the mesoscale atmospheric circulation.

the observation. A cellular pattern, similar to the Bénard Circulation patterns studied extensively in the laboratory (Brunt, 1951), is clearly evident. The diameters of the cells vary from 5-10 km and are similar to those discussed by Atlas (1959a). In contrast to the pattern shown in Fig. 7, an RHI of the Bénard-like echoes showed that the strongest reflectivities occurred near the surface. Furthermore, the boundary of each cell in Fig. 9 was composed of a series of intense cores spaced about 5 km apart and extending upward to a height of about 2 km. A study of the Bénard-like cells revealed that the flow pattern probably was slowly upward around the periphery of the cell and downward in the center. Superimposed on the upward peripheral motion were cores of more intense updrafts which had dimensions of, and resembled, the smaller convective thermals seen in Figs. 7 and 8a.

It is of interest to consider the source responsible for the clear-air

echoes evident in Fig. 9. It is estimated that their reflectivity is 15 db larger than the maximum clear-air reflectivity observed with the 3.2-cm radar at Wallops Island. This is illustrated in Fig. 5 which shows the reflectivity of the convective patterns to be considerably larger than the maximum clear-air reflectivity observed or estimated by other investigators. Because of this incredibly large reflectivity, it is not considered possible that the scattering is from variations in refractive index.

The only other echo source that might account for the Fig. 9 echoes is particulate matter and insects (Hardy, et al., 1966). To obtain a 3.2-cm reflectivity of  $3.2 \times 10^{-12} \text{ cm}^{-1}$  as observed (Fig. 5), insects would have had to be present which had a radar cross-section equivalent to that of a 0.5-cm diameter water sphere and which had a number concentration of about  $3 \times 10^4 \text{ km}^{-3}$ . If the insects were smaller, of 0.25-cm water sphere equivalent, then the required concentration would have been about  $3 \times 10^6 \text{ km}^{-3}$ . The latter concentration, in more reasonable units, is equivalent to 3 insects per cube having sides of 10 m length. This concentration is approximately equivalent to one insect per 20 people on a crowded beach! Insects the size of a small house fly or a flying ant have cross-sections in the 0.25 - 0.5-cm water sphere category (Hajovsky, et al., 1966). Of particular interest is the fact that, during the time the Fig. 9 patterns were observed, there was an abnormally large number of flying ants and other insects in the vicinity of the radar site. At the particular season of the year (May), it is common for a variety of insects to swarm. Thus it appears that insects were mainly responsible for the echoes shown in Fig. 9 and that, on occasion, the insects provide an excellent source of tracers for atmospheric flow circulations.

## 8. BREAKING GRAVITY WAVES

Hicks and Angell (1968) have investigated an apparent horizontally twisted or braided atmospheric structure which frequently appears in the RHI photographs. An example of such a braided structure, occurring at a height of 3.5 km (11,500 ft.) in a clear atmosphere, is shown in Fig. 10. The most reflecting portions of this echo structure slope upwards from right to left. That is, the echo strengths are not uniform along a single filament. Two filaments, however, combine to give the appearance of a braid.

During a six-week observational period in May and June, 1966, there were eleven occurrences of braided structures. The braided appearance persisted for at least several minutes, although adequate data to determine the actual lifetime of the phenomenon were never obtained. Since the braided appearance could be identified over a fairly large horizontal region, the rather obvious explanation that it is due to the intertwining of two filaments of increased refractivity must be ruled out. Other important features of this structure are that it shows a preference to be aligned in the direction of the wind shear, and it occurs in regions of relatively stable lapse rates or inversions. These environmental conditions are favorable to the formation, development, and breakdown of gravitational waves (Haurwitz, 1941), and the breakdown of gravitational waves is the explanation arrived at by Hicks and Angell.

The braided structure is sometimes preceded by the presence of stable waves which gives additional support to the breaking-wave explanation. Figure 11

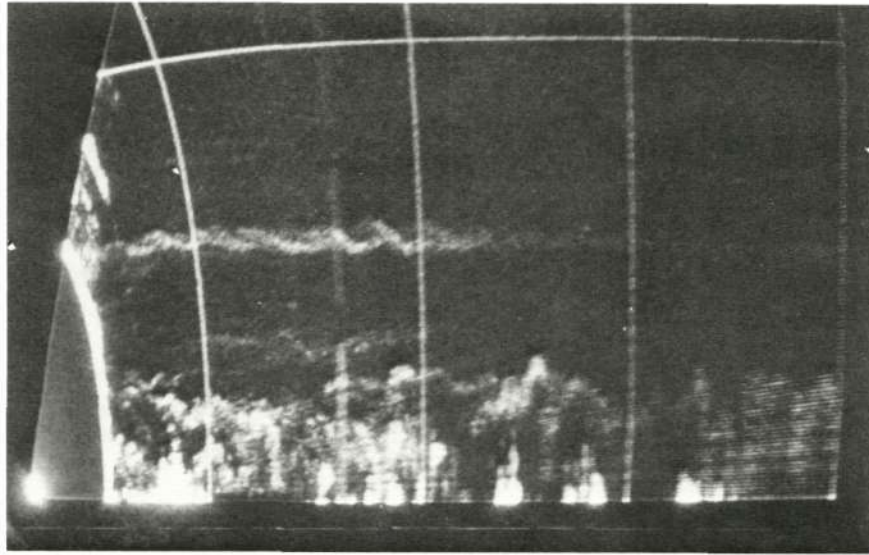
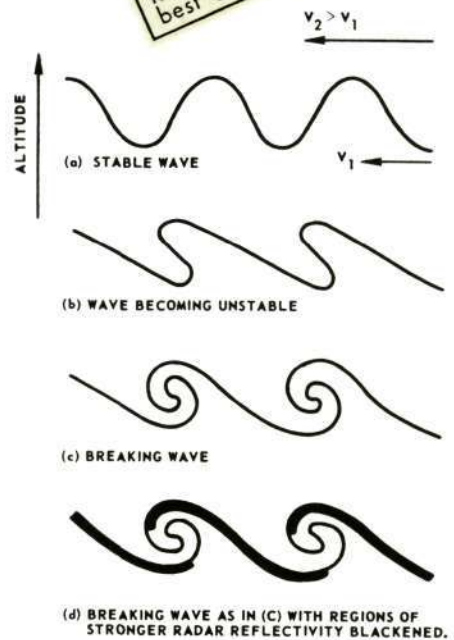


Fig. 10 Photograph of RHI scope of the 10.7-cm radar at Wallops Island taken on 1 June 1966, 1432 E.S.T., with 9 db attenuation, showing a twisted or braided structure near 11,500 ft. The height mark is near 20,000 ft. and the range marks are at 5 n.mi. intervals. The echoes below about 6,000 ft. are from cloudy regions, but the region near 11,500 ft. is probably clear. (From Hicks and Angell, 1968.)

Reproduced from best available copy.

Fig. 11 Sketch of gravitational wave embedded within a layer with winds increasing with height: (a) wave stable, (b) wave becoming unstable, (c) wave breaking and forming vortices (Fig. 12), and (d) same as (c) except with regions of stronger radar reflectivity blackened. (From Hicks and Angell, 1968.)



shows how breaking gravity waves, in cloudless regions, may give the appearance of braided structures when viewed with a radar. Figure 11a is a sketch of a stable gravity wave embedded in a layer having a velocity shear in the vertical,

11b depicts the wave becoming unstable, and 11c shows the wave breaking with the resultant forming of vortices. Figure 11d is the same as Fig. 11c, but now the solid portions of the breaking wave represent the stronger radar reflectivity and the lighter portions the weaker. This illustrates how a breaking gravity wave may actually appear as a braided structure on radar and yet is consistent with the observation of discontinuities which were evident in one of the braids.

Essentially the same structure seen by radar in a clear atmosphere is occasionally observed visually in cloud formations as the remarkable photograph of Fig. 12 illustrates. This picture was taken in Colorado, and the breaking waves are seen by virtue of the cloud droplets which provide excellent tracers for the air flow. Figure 12 is essentially identical to the structure depicted in Fig. 11c, and provides virtually irrefutable evidence that the mechanism proposed by Hicks and Angell for the braided radar structure is correct.

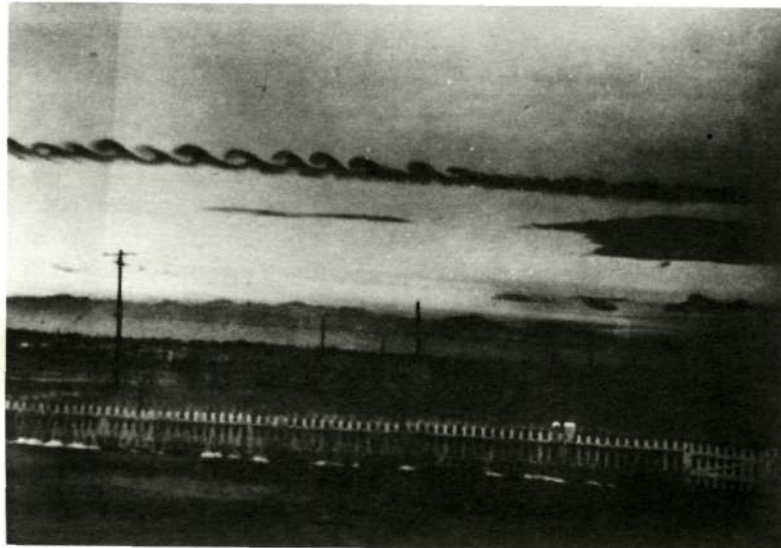


Fig. 12 Breaking gravitational waves seen visually by virtue of clouds defining the flow pattern. Note the similarity with the radar braided structure shown in Fig. 10. (Photo courtesy Mr. Paul E. Branstine. See Colson, D., 1954: *Weatherwise*, 34-35.)

## 9. CLEAR-AIR TURBULENCE

Usually the strongest clear-air radar echoes occur in the lower 3 to 4 km of the atmosphere. Such a result is expected from Eq. (5) because the very large mean gradients of refractive index are possible only in the lower few kilometers; that is, significant moisture gradients occur only in the lower troposphere and the refractive index is most sensitive to moisture. Moreover, the lower clear-air layers are usually not turbulent, at least not on the scale that affects aircraft. This has been confirmed by numerous aircraft flights in the lower 4 km made in conjunction with the radar observations at Wallops Island. Therefore, it is probable that, in the lower troposphere, the gradient of refractive index is usually the dominant factor determining

whether or not a clear-air layer will be detectable.

In spite of the predominance of clear-air radar layers in the lower troposphere, the layers of main concern in this section are those that occur in the upper troposphere or above approximately 6 km. Figure 13 shows one of these layers. It occurs at a height of 12 km out to a range of at least 30 km. From multiwavelength measurements it was determined that this layer was caused by scattering from refractive-index variations (Atlas *et al.*, 1966 b). The layer from about 7 to 10 km in altitude is cirrus cloud.

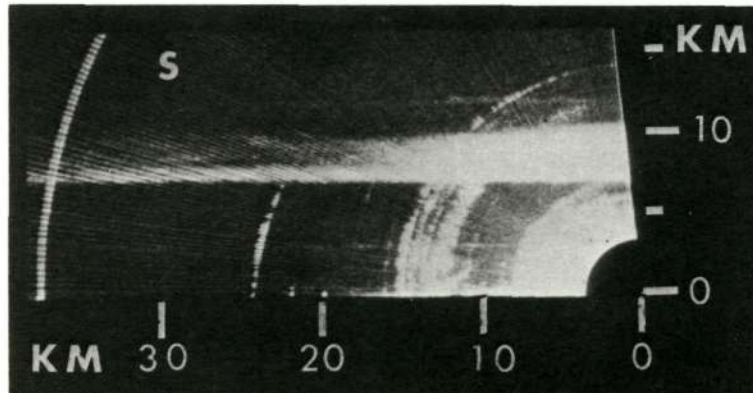


Fig. 13 Photograph of RHI at wavelength of 10.7 cm, 1030 E.S.T., 18 February 1966, at Wallops Island, Virginia, azimuth, 90 deg. The strong echo between 7 and 10 km is due to scattering from cirrostratus clouds. The echo layer near 12 km height occurs in a clear region and is associated with the tropopause. (From Atlas *et al.*, 1966b.)

The tropopause, at the time of the observation shown in Fig. 13, was at essentially the same height as the 12 km radar layer. Tropopause layers and clear-air layers above 6 km have been observed on numerous occasions during the winter months of 1966-67. A particularly interesting tropopause layer is shown in Fig. 14. Waves of fairly low amplitude are clearly evident within this layer. These non-breaking gravity waves at the tropopause level have been observed on one additional occasion in which the wave amplitude was considerably larger than that shown in Fig. 14. It was inferred by Atlas, *et al.*, (1966a and 1966b) that turbulence sufficiently intense to affect aircraft was necessary before the region at the tropopause level could be detected. This inference is supported by recent experimental results.

Hicks, *et al.*, (1967) have described experiments in which the high-altitude clear-air layers were probed with an uninstrumented F-106 aircraft. While the aircraft performed spiral ascents, descents or horizontal runs at the altitude of interest, the radar scanned in elevation in order to obtain data on all the echo layers within a vertical plane. The pilot reports provided a qualitative estimate of the location and severity of turbulence encountered.

The results of four aircraft flights and the corresponding 10.7-cm radar observations for regions above 6 km are summarized in Fig. 15. Cloud echoes

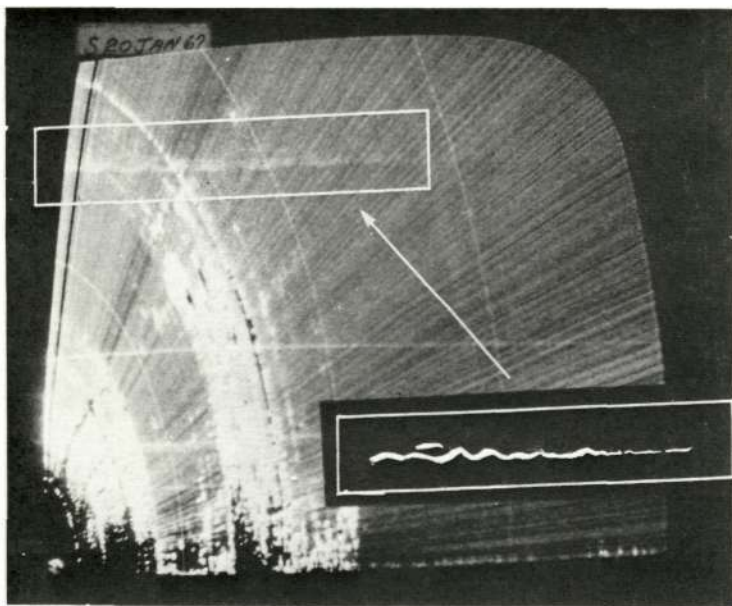


Fig. 14 Photograph of RHI at wavelength of 10.7 cm, 0912 E.S.T., 20 Jan 1967 at Wallops Island, Va., azimuth 70 deg. The range marks are at 5 n. mi. intervals and a height marker occurs at 20,000 ft. The low amplitude waves seen near 39,000 ft. occur in clear air (see inset for tracing of pattern) and are coincident with the height of the tropopause.

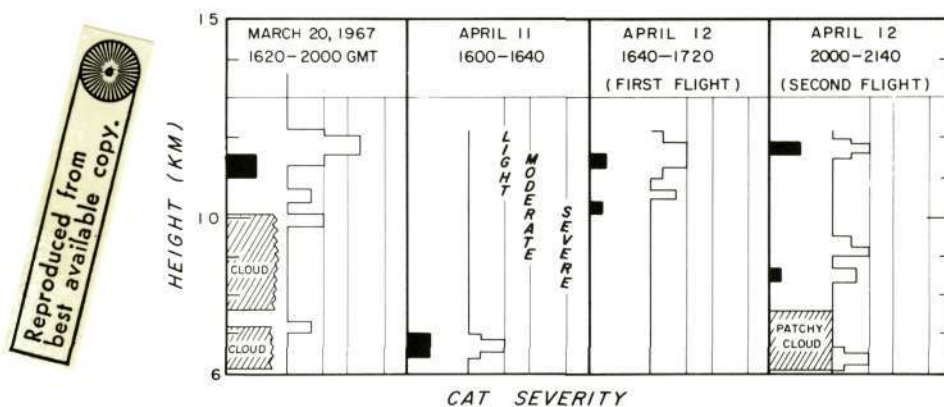


Fig. 15 Heights of radar echoes and reports of clear-air turbulence. Clear-air echoes are indicated by the solid areas, cloud echoes by the hatched areas, and the aircraft encounters with CAT by the open areas. The severity of CAT is indicated by a relative scale deduced from the pilot reports. The horizontal extent of the solid areas is roughly proportional to the radar reflectivity of the clear-air echoes. (From Hicks et al., 1967.)

are indicated by the hatched areas, clear-air echoes by the solid areas, and the aircraft encounters with clear-air turbulence (CAT) by the open areas. The correspondence in altitude between the clear-air radar echoes and the clear-air turbulence encounters is excellent. On all occasions, the regions of clear-air echoes above 6 km which were simultaneously probed with the aircraft were found to be turbulent. This appears to be the first time that aircraft and radar have probed the same region of space and confirmed the close relationship

between the high-altitude clear-air radar echoes and turbulent aircraft flight.

The high-altitude radar echoes were thin (200 to 600 m), stratified, and somewhat patchy (horizontal dimensions in the order of 5 to 15 km). Moreover, the echoes were not particularly persistent, often lasting for less than a few tens of minutes. The CAT was also reported to be in relatively thin layers, the maximum thickness being about 1.5 km centered near a height of 11.5 km during the first flight on 12 April. Although not determined precisely, the lateral extent of CAT was found to vary over narrow horizontal limits, usually less than 30 km. These dimensions are consistent with other aircraft probes of CAT (Reiter and Burns, 1966) emphasizing the patchiness which generally characterizes CAT. This patchiness is evident from both the radar and aircraft probes.

The results in Fig. 15 suggest that ultra-sensitive microwave radars can detect regions of CAT. A limitation, however, is the rather restricted range (less than 30 km) of the present CAT-detection capability. Moreover, as seen in Fig. 15, light CAT not detected with radars is encountered occasionally.

#### 10. METEOROLOGICAL RELEVANCE

Results thus far obtained on the multiwavelength high-power radar system discussed in this paper open vast new possibilities for the meteorologist. He can now investigate atmospheric processes, on scales up to 50 miles, in a 3-dimensional manner and practically instantaneously.

It has been stated previously that clear-air convective patterns are often observed both over land and water. The relationship between this clear-air pattern and subsequent cloud formation and development requires further investigation. A multiwavelength high-resolution ultra-sensitive radar facility provides a unique opportunity for studying clear-air structure, clouds, and precipitation and their interrelationships.

At present, meteorologists make wind velocity measurements by tracking balloons once every six hours. This yields a single wind speed at one point in space at each elevation. Photographs of clear-air radar echoes have shown wind fields in which the direction changes by perhaps 20 degrees within a 20-mile radius of the radar. This might indicate local convergence or divergence, for example. Observations like these may well lead to new methods for predicting cloud formation and dissipation.

By using the Doppler information, one could look for regions of high variance and thus find turbulence. This subject has already been discussed in this paper, but there are other aspects which are of interest. For example, a high-power Doppler radar could be used to determine gustiness over an airport to aid landing operations or in the region of a missile launcher to advise of appropriate meteorological launching conditions. Also, for a properly situated radar, one may well study such local effects as the sea breeze or make substantial contributions to solving the complex problem of air-sea interaction.

One may use remote radar probing techniques to shed light on diffusion processes. Since the radars detect regions of large variance in refractivity,

which implies mixing between two masses of air of originally different properties, it means that eddy diffusion is already in progress when detection takes place. Detection ceases when mixing is complete; homogeneous air does not lead to radar reflections. Thus the progression of the diffusion might well be determinable; more specifically, one may study diffusion coefficients under various conditions of stability.

The above illustrations indicate only a few of the possibilities. One way to summarize is to say that with high-power narrow-beam radars the clear atmosphere has become "visible". Motions and processes in the air, undetectable up to the present time except by single point sensors, are now susceptible to quantitative analysis.

## 11. FUTURE DEVELOPMENTS

### 11.1 Forward Scatter

Forward scatter experiments are being discussed in detail at other sessions. However, it should be mentioned here that several forward scatter paths are under consideration in connection with the Wallops Island radar site.

One proposed link is between Wallops Island and Valley Forge, Pennsylvania, a distance of about 250 km. The transmitter will operate at S-band and use a 50-foot precision parabola with ability to scan vertically. The receiving system will be the present S-band radar operated as a receiver only. It is anticipated that the two large antennas ( $1/2$  degree beams) will result in small enough common-volume resolution cells to facilitate identification of the reflecting layers.

The second path under consideration is an X-band link between Wallops Island and Westford, Massachusetts, using a mobile X-band transmitter at Wallops Island (6-foot antenna) and the 60-foot dish at Westford for reception.

One advantage stemming from a combined forward-scatter link and a high-power radar lies in the fact that the radar can identify the altitudes of the reflecting layers if they are within the detection range of the radar. Identification of the positions of the reflecting layers has thwarted interpretation of previous forward-scatter data.

Clearly, one could be more certain of successful interpretation on a forward scatter link by setting one up on a north-south path with the Wallops Island radars at the midpoint. This would assure identification of many high-altitude layers by backscatter radars; the positions of these layers could then be used to interpret the simultaneous forward-scatter signals.

### 11.2 Information Processing

One aspect which must be given attention is that of information display and utilization. Much can be said about the advantages of Doppler radars, but to date only a small proportion of Doppler data have been used for atmospheric research. The major difficulty lies in interpretation of the data. One can use a velocity-azimuth mode of operation which provides a wind speed at a

selected altitude. However, it has already been pointed out that wind velocity varies in both space and time in the hemisphere surrounding the radar. Although the velocity component toward the radar is measurable in the entire hemisphere and its spectrum (or velocity variance) is obtainable, the amount of information thus obtained is so large as to be unuseable. Methods must be devised to measure, analyze, digest, and put into useable form the 3-dimensional picture of the wind field. Presently available techniques are inadequate.

## 12. SUMMARY

This review describes some of the recent observations of radar echoes from the clear air with the object of substantiating the conclusions as to their origins and to illustrate how clear-air radar echoes can be used to investigate a wide range of atmospheric structures.

The radar cross-sections of dot angels at wavelengths from 0.86 to 71.5 cm are consistent with the range of cross-sections expected for insects or birds. Similarly, it has been concluded from simultaneous multiwavelength measurements and from recent bistatic depolarization studies that all of the dot angels observed in detail have characteristics which identify them as either insects or birds.

Powerful radars at 10-cm or longer wavelengths regularly detect narrow layers of clear-air echoes which have considerable horizontal extent. These layers correspond in height to regions having sharp vertical gradients in refractive index. The reflectivity-wavelength dependence is consistent with the theory that the scattering occurs from eddies having a spectrum of refractive index which is proportional to the  $-5/3$  power of the eddy wavenumber (Hardy, *et al.*, 1966; Atlas, *et al.*, 1966a). Moreover, excellent agreement has been found between the observed radar reflectivity and the reflectivity computed from the observed fluctuation-spectrum of refractive index. These results indicate, (1) scattering from the clear atmosphere can be described quantitatively in terms of the refractivity spectrum, and (2) the  $-5/3$  refractivity spectrum well represents the atmosphere out to limiting microscales smaller than 5 cm.

Clear-air convective thermals having diameters of 1-3 km are often observed with sensitive 10-cm radars. These thermals are seen by virtue of the scattering from refractive-index fluctuations, and in plan view, they typically appear circular or elliptical and have echo-free centers. It is suggested that the flow within these convective thermals is upward in the center and that the relative flow around the periphery is downward.

Bénard-like convective cells having diameters in the order of 10 km have also been observed occasionally using a 3.2-cm radar of moderate sensitivity. It is shown that the radar echoes on these occasions are due to an unusually large increase in the number of insects in the atmosphere. The atmospheric flow in these Bénard-like cells is probably upward around the periphery of the cells and downward within their centers.

An apparent horizontally braided atmospheric structure is sometimes

observed in the clear atmosphere with the 10.7-cm radar at Wallops Island. This structure shows a preference to be aligned in the direction of the wind shear, and it occurs in regions of relatively stable lapse rates or inversions. These features and the characteristics of the radar-echo structure have led to the conclusion that the braided appearance is caused by breaking gravity waves. Non-breaking waves have also been observed, and these often occur at the height of the tropopause.

In an effort to determine the degree of turbulence associated with the high-altitude clear-air layers observed with the Wallops Island radars, the regions have been occasionally probed with an aircraft. The pilot-reports provided a qualitative estimate of the location and severity of turbulence encountered. On all occasions, the regions of clear-air echoes above 6 km which were simultaneously probed with the aircraft were found to be turbulent. This experimental result is consistent with the conclusion previously inferred on theoretical grounds that turbulence sufficiently intense to affect aircraft appeared necessary before the regions of turbulence in the upper troposphere were detectable.

#### 14. ACKNOWLEDGMENTS

The research conducted at Wallops Island, Virginia, has been supported in part by the Laboratory Director's Fund, Air Force Cambridge Research Laboratories, and the National Aeronautics and Space Administration, Wallops Station.

#### REFERENCES

- Atlas, D., 1959: Radar studies of meteorological "angel" echoes, J. Atmospheric Terrest. Phys., 15, 262-287.
- Atlas, D., 1959a: Sub-horizon radar echoes by scatter propagation, J. Geophys. Res., 64, 1205-1218.
- Atlas, D., 1960: Possible key to the dilemma of meteorological "angel" echoes, J. Meteorol., 17, 95-103.
- Atlas, D., 1960a: Radar detection of the sea breeze, J. Meteor., 17, 244-258.
- Atlas, D., 1964: Advances in radar meteorology, Advan. Geophys., 10, 317-478.
- Atlas, D., 1965: Angels in focus, Rad. Sci. J. Res., NBS/USNC - URSI, 69D, No. 6, 871-875.
- Atlas, D., and K. R. Hardy, 1966: Radar analysis of the clear atmosphere: angels. Proc. XV General Assembly of URSI, Munich, Germany, 5-15 Sept., 401-469.
- Atlas, D., K. R. Hardy, and K. Naito, 1966: Optimizing the radar detection of clear-air turbulence. J. of Appl. Meteor., 5, 450-460.

- Atlas, D., K. R. Hardy, and T. G. Konrad, 1966a: Radar detection of the tropopause and clear air turbulence. Proc. 12th Weather Radar Conf., Amer. Meteor. Soc., Boston, 279-284.
- Atlas, D., K. R. Hardy, K. M. Glover, I. Katz, and T. G. Konrad, 1966b: Tropopause detected by radar. Science 153, 1110-1112.
- Booker, H. G., and W. E. Gordon, 1950: Theory of radio scattering in the troposphere. Proc. I.R.E., 38, 401-412.
- Borchardt, H., 1962: Wolkenbeobachtungen mit einem doppelwelligen Radargerät. Beit. Physik Atmosphäre 35, 43-68. See also Atlas (1964).
- Brunt, D., 1951: Experimental cloud formation. Compendium of Meteorology, Amer. Met. Soc., Boston, 1255-1262.
- Chernikov, A. A., 1966: Some new Soviet investigations of angel echoes. Proc. 12th Weather Radar Conf., Amer. Meteor. Soc., Boston, Mass., 291-292.
- Crawford, A. B., 1949: Radar reflections in the lower atmosphere, Proc. IRE, 37, 404-405.
- Fehlhaber, L., and J. Grosskopf, 1964: Untersuchung der Structure der Troposphäre mit einem Vertikalradar, Nachrichtentechnische Zeitschrift, 17(10), 503-507. English Translation - AFCRL, Bedford, Mass., TG-242, March 1965.
- Glover, K. M., and K. R. Hardy, 1966: Dot angels: insects and birds. Proc. 12th Weather Radar Conf., Amer. Meteor. Soc., Boston, 264-268.
- Glover, K. M., K. R. Hardy, T. G. Konrad, W. N. Sullivan, and A. S. Michaels, 1966: Radar observations of insects in free flight. Science, 154, 967-972.
- Hajovsky, R. G., A. P. Deam, and A. H. LaGrone, 1966: Radar reflections from insects in the lower atmosphere. IEEE Trans. on Antennas and Propagation, 14, 224-227.
- Hardy, K. R., and K. M. Glover, 1966: 24-hour history of radar angel activity at three wavelengths. Proc. 12th Weather Radar Conf., Boston, Mass., 269-274
- Hardy, K. R., D. Atlas, and K. M. Glover, 1966: Multiwavelength backscatter from the clear atmosphere. J. Geophys. Res., 71, 1537-1552.
- Haurwitz, B., 1941: Dynamic Meteorology, McGraw-Hill Book Co., Inc., New York.

## PROBING THE ATMOSPHERE WITH HIGH POWER, HIGH RESOLUTION RADARS

- Hay, D. R., and W. M. Reid, 1962: Radar angels in the lower troposphere, *Can. J Phys.*, 40, 128-138.
- Hicks, J. J., I. Katz, C. R. Landry, and K. R. Hardy, 1967: Simultaneous radar and aircraft observations of clear-air turbulence, *Science*, 157, 808-809.
- Hicks, J. J., and J. K. Angell, 1968: Radar observations of breaking gravitational waves in the visually clear atmosphere. *J. Appl. Meteor.*, 7, 114-121.
- Konrad, T. G., and J. Hicks, 1966: Tracking of known bird species by radar. *Proc. 12th Weather Radar Conf., Amer. Meteor. Soc., Boston, Mass.*, 259-263.
- Konrad, T. G., and D. Randall, 1966: Simultaneous probing of the atmosphere by radar and meteorological sensors. *Proc. 12th Weather Radar Conf., Amer. Meteor. Soc., Boston*, 300-305.
- Kropfli, R. A., I. Katz, T. G. Konrad, and E. B. Dobson, 1968: Simultaneous radar reflectivity measurements and refractive index spectra in the clear atmosphere. *Proc. 13th Radar Meteorology Conf., Montreal, Canada*.
- Lane, J. A., 1964: Small-scale irregularities of the radio refractive index of the troposphere. *Nature*, 204, 438-440.
- Lane, J. A., 1967: Radar echoes from tropospheric layers by incoherent back-scatter. *Electronic Letters*, 3, 173-174.
- Ottersten, H., 1964: Occurrence and characteristics of radar angels observed with a vertically-pointing pulse radar. *Proc. 11th Weather Radar Conf., Amer. Meteor. Soc., Boston*, 22-27.
- Petrocchi, J. J., and W. H. Paulsen, 1966: Meteorological significance of vertical density profiles of clouds and precipitation obtained with the AN/TPQ-11 radar. *Proc. 12th Weather Radar Conf., Amer. Meteor. Soc., Boston*, 467-472.
- Plank, V. G., 1956: A meteorological study of radar angels. *Geophys. Res. Paper 52*, 117 pp., Air Force Cambridge Research Laboratories, Bedford, Mass.
- Reiter, E. R., and A. Burns, 1966: The structure of clear-air turbulence derived from "TOPCAT" aircraft measurements. *J. Atmos. Sci.*, 23, 206-212.
- Saxton, J. A., J. A. Lane, R. W. Meadows, and P. A. Mathews, 1964: Layer structure of the troposphere - simultaneous radar and microwave refractometer investigations, *Proc. I.E.E.E.*, 3, 275-283.

- Tatarski, V. I., 1961: Wave propagation in a turbulent medium.  
McGraw-Hill Book Co., Inc., New York, N. Y., 285 pp.
- Villars, F., and V. F. Weisskopf, 1954: The scattering of electromagnetic waves by turbulent atmospheric fluctuations, *Phy. Rev.*, 94, 232-240.
- Vrana, N., 1961: Some characteristics of radar angel echoes.  
Center for Radiophysics and Space Research, Res. Rept. No. 32,  
29 pp., Cornell University, Ithaca, New York.

FURTHER REMARKS ON ATMOSPHERIC PROBING BY  
ULTRASENSITIVE RADAR

David Atlas

Department of Geophysical Sciences  
University of Chicago

ABSTRACT

This paper is supplementary to that of Hardy and Katz. It emphasizes the meteorological value of the various capabilities of ultrasensitive radar, highlights the points of agreement and disagreement, and focuses upon the directions of promising research. The theory of backscatter from a refractively turbulent region is said to be confirmed by the radar observations both with respect to magnitude and wavelength dependence. A reason for the apparent discrepancy between the results of some of the forward-scatter experiments and theory is suggested. Disagreement still exists with respect to the origin of clear air sea breeze echoes; the author does not agree with Hardy and Katz that they are due to insects. However, it is agreed that some unusually widespread echo displays on clear days are indeed due to insects. The meteorological value of ultrasensitive radars demonstrated by Hardy and Katz, here, and by others is so profound as to demand their use in remote atmospheric probing.

1. INTRODUCTION

These remarks are in comment upon the presentation of Drs. Hardy and Katz entitled "Probing the Atmosphere with High Power, High Resolution Radars." Their paper provides a fairly comprehensive review of the theoretical and experimental foundations for the use of ultrasensitive radars and for the interpretation of the observations in terms of meaningful atmospheric structures. I am in essential agreement with their presentation of the basic background material and have but a few reservations which I shall mention. Thus, my remarks will be directed primarily at: (1) focusing attention on the meteorological importance of the various observations of which ultrasensitive radars are

capable, (2) covering some of the points omitted by Hardy and Katz, and (3) pointing toward the directions which future research should take.

## 2. SOME POINTS OF AGREEMENT AND DISAGREEMENT

### 2.1 Confirmation of Theory of Turbulent Scatter

One of the most significant aspects of the Hardy-Katz (hereafter referred to as H-K) paper is the confirmation, at least for backscatter, of the theory of turbulent scatter of Tatarsky and others. This is vital if the reflectivity is to be interpreted quantitatively in atmospheric terms. H-K and their colleagues have presented an abundance of data which validate their Eqs. (1) and (3). In particular, all the radar data is in close accord with the  $\lambda^{-1/3}$  relationship, within experimental error, and thus justifies the use of the  $k^{-5/3}$  law for the one-dimensional spectrum of refractivity perturbations. The restriction, of course, is to wavelengths between 10 and 70 cm and to corresponding turbulent scales between 5 and 35 cm. Indeed, I believe it is mainly because the radar observations are concerned with the small scale (large wave number) end of the turbulence spectrum that the classical  $k^{-5/3}$  law of the inertial sub-range is applicable. It is of interest that Lawrence (1968) also reports the validity of the  $k^{-5/3}$  law in this range and somewhat beyond (i.e., to scales of millimeters) in his review of line-of-sight optical propagation.

### 2.2 Apparent Conflict with Tropo-Scatter

A long-standing question concerns the reasons why tropospheric radio scatter data fail to show general agreement with the  $k^{-5/3}$  spectrum. For example, Bolgiano's (1964) experiments at 3.2, 10.7, and 35.7 cm wavelengths show that a 3-D spectrum of  $k^{-11/3}$  (or  $k^{-5/3}$  for the 1-D spectrum) is applicable only to the median summer time conditions while  $k^{-9/2}$  (or  $k^{-5/2}$  in 1-D) represents the winter median. Two possible reasons are suggested: (1) Bolgiano's data correspond to filtered turbulence scales of 1.2 m, 3.9 m, and 13.2 m at the radio wavelengths of 3.2, 10.7, and 35.7 cm, respectively; these are considerably larger than those filtered by the radars of H-K. (2) The tropo data were taken along the Gt. Circle path where the signal contributions due to partial reflection from the mean vertical gradient of refractivity may readily mask those due to turbulence. Of course, no such contribution is possible in the H-K data except at vertical incidence. I am convinced that the latter is sufficient cause for the apparent discrepancy. The fact that  $k^{-9/2}$  (3-D) is applicable in winter is in itself strongly suggestive. This means that the apparent turbulence spectrum decreases more sharply with  $k$  than expected, thus producing relatively stronger signals at the longer wavelengths. Of course, we would expect the reflections from a stratified gradient of refractivity (i.e., an inversion) to increase with wavelength, and we know that such inversions are more common in the lower levels in winter than in summer.

But even in summer, when the median Bolgiano data accords with that of H-K, we may get simultaneous layer scatter in tropo paths along the Gt. Circle and turbulent scatter from the refractivity perturbations which tend to be collocated at the height of sharpest mean refractivity gradient. This is well demonstrated by the radar data of H-K, Lane (1964, 1967)\* and Saxton et al. (1964)\* which show incoherent layered echoes always associated with a stratum of sharp refractivity change. Also Lane's direct refractivity probes confirm the co-existence of strong refractivity perturbations and strong mean gradient. Accordingly, one might well regard Bolgiano's median summer findings of  $k^{-11/3}$  (3-D) as strong

---

\*See references in preceding article by Hardy & Katz

confirmation of the findings of H-K. While there may be other scatter experiments which can be cited in contradiction to the  $k^{-11/3}$  law, I believe that most of them can be questioned on grounds similar to those noted above. In any case, there are no data yet which refute the applicability of this law to radar wavelengths.

I might add that these remarks pertain as well to the tropo-scatter review by Cox\* who points out that the observations can frequently be explained either by turbulent scatter or layer reflection. In the light of our discussion, this is not at all surprising.

### 2.3 Reflectivity vs. Refractivity

Even more important than the confirmation of the wavelength dependence reported by H-K, is the validation of the magnitude of the radar measured reflectivity predicted by Eqs. (1) and (3) of H-K by the direct measurements of the refractivity spectrum as reported by Kropfli et al. (1968) (shown in Fig. 15 of the H-K paper). This and the similar confirmation by Lane (1967) leaves very little room for doubt. Together with the wavelength dependence, we therefore have a solid basis for interpreting reflectivity in terms of the magnitude of  $C_n^2$ . How to interpret  $C_n^2$  in terms of  $(\Delta n)^2$  - the mean square refractivity perturbation,  $L_0$  - the outer scale,  $\epsilon$  - the eddy dissipation rate, etc. is another question.

### 2.4 Refractivity Perturbations vs. Insects

There is one point in the H-K presentation which bothered me greatly and probably disturbed others as well. This is their contention that my 1.25 cm sea breeze echoes (Atlas, 1960) and their convective patterns (i.e., their Fig. 8) are due largely to insects and not to refractivity perturbations. Their argument is grounded solely on the fact that the required  $C_n^2$  of  $10^{-11} \text{ cm}^{-2/3}$  is too large to be meteorologically plausible. One might challenge this argument on the basis of Lane's 1965 direct measurements of  $(\Delta n)^2$  up to  $22 \times 10^{-12}$  at the base of a sharp inversion. Combined with a small outer scale  $L_0$  of the order of 1 m, this would produce the observed  $C_n^2$ . While such a small  $L_0$  seems implausible, it may be reasonable under a strong inversion where vertical motions are suppressed. Moreover, if a  $(\Delta n)^2$  of  $22 \times 10^{-12}$  has been measured, even larger values are probable. Thus, I would hesitate to exclude  $C_n^2$  values as large as  $10^{-11} \text{ cm}^{-2/3}$ , although it is admittedly a rare event.

More importantly, in the case of sea breeze radar observations, the radar pulse volume was a mere 70 ft off the ground and located at the shoreline with observers stationed on a 144 ft tower and on the ground with the express purpose of watching for birds and insects with binoculars. No insects were reported, and only a few birds. Admitting the possible difficulty of seeing insects the size of flies in concentrations of 3 per  $10^4$  to  $10^5 \text{ m}^3$  by eye, we must recall that our 1.25 cm radar beam was extremely narrow -  $0.3^\circ$  to half power points - and the pulse volume at the range of 0.8 Km amounted only to about  $700 \text{ m}^3$ . Accordingly, even with extreme concentrations of 1 per  $10^3 \text{ m}^3$ , we should have observed discrete point echoes. In fact the echoes were diffuse, solid, and virtually continuous. I am therefore unable to accept the Hardy-Katz thesis that insects were even partly responsible for the sea breeze echoes.

On the other hand, astounding though it may appear from their Fig. 8, I believe that insects may indeed be responsible for such echoes. The fact is that Lhermitte (1966), Lhermitte and Dooley (1966), and Browning and Atlas (1966)

---

\*See Section 5 these Proceedings

## ULTRASENSITIVE RADAR

obtained Doppler velocity records over extended periods and at heights up to 2 Km under clear sky conditions and with 3.2 and 5.5 cm radars of modest power. Typical records of Doppler velocity versus azimuth are shown in the original papers. They show that the echoes are discrete in velocity and/or azimuth and unlike the truly continuous corresponding records obtained in precipitation. Thus, the scatterers are indeed point targets, and though the Velocity-Azimuth Display (VAD) shows them to move with the wind, they are most probably insects. Indeed the average reflectivity measured by Lhermitte and Dooley for their Oklahoma data at 3.2 cm was  $3 \times 10^{-12} \text{ cm}^{-1}$ , identical to that of Hardy and Katz for the Massachusetts case. Moreover, they estimate a target concentration of 1 in  $10^4 \text{ m}^3$ , close to the concentration estimated by H-K. Independent Doppler observations by Browning and Atlas (1966) (also in Massachusetts) showed concentrations about 0.1 as large. Finally, since the Doppler targets were present for periods of 60 hours in Oklahoma and at least 7 hours in Massachusetts, and all the time moving with the wind, they must have been at least as spread in horizontal extent as shown in H-K's Fig. 8. Thus, we can be reasonably confident that those echoes are in fact due to insects.

This, at least, is my judgement. On the other hand, I think it equally likely that the 1.25 cm sea breeze data are due to refractivity perturbations and not insects. This implies that  $C_n^2 = 10^{-11} \text{ cm}^{-2/3}$  is probably valid under some sea breeze conditions.

I have spent some time on the insect versus refractivity question because it is central to the issue of deducing the true atmospheric structure from the radar observations. Clearly, since both may occur either separately or at one and the same time, means must be provided to distinguish one from the other. This means has been clearly denoted by Hardy and Katz and by Hardy, Atlas, and Glover (1966); namely, the use of two or more wavelengths simultaneously. Indeed, had two wavelengths been available during the observations discussed above, the question could have been readily resolved. Of course, two wavelengths are also required to distinguish cloud and precipitation echoes from those due to refractivity perturbations. This is especially important in understanding the interactions between clear air circulations and precipitation; a subject which was not treated by Hardy and Katz. With sensitive radars one may detect the clear air convection which is responsible for the subsequent development of clouds and precipitation. One may also detect cloud boundaries by virtue of their refractivity perturbations and the cloud cores by means of the scatter from developing precipitation. Obviously the two must be distinguished if any sense is to be made of the observations.

In short, ultrasensitive radars do indeed provide a heretofore unimagined potential for probing the structure of the atmosphere. At the same time, they have shown how very complex the atmosphere is. Unravelling its secrets will be a formidable task. But recognition of the atmosphere's complexity and of the magnitude of the effort required to explain its workings is a notable sign of progress.

### 3.0 SOME OMISSIONS

By and large Hardy and Katz have concentrated upon the clear air phenomena which are rendered detectable by powerful radars. I would therefore like to say a few words about other important phenomena which may be studied by such techniques.

### 3.1 Clouds and Precipitation

I have already alluded to clouds and precipitation in another context; now I should like to stress the value of sensitivity and resolution in detecting young and tenuous clouds. Few people will deny that our present day knowledge of precipitation processes and storm structure stems largely from radar observations. This is especially true in the case of convective storms whose internal structure is not readily observed by any other means. But our understanding of the earliest stages of convective precipitation has remained rudimentary because the particulates are not detectable by radars of ordinary sensitivity. The use of sensitive radars will extend our "sight" to these crucial early phases - both in terms of the sub-cloud circulations and the pre-precipitation cloud structure made visible by refractive index anomalies, and in terms of the smallest precipitation elements. At the same time, the increased resolution will permit us to dissect the small young clouds about as well as our broad beam "scalpels" now permit in the case of the larger storms. But increased resolution is equally important in the latter as well because existing beams present a highly degraded image of storm structure. I needn't belabor the point because the resulting distortions are obvious.

Increasing radar sensitivity by two to three orders of magnitude (i.e., the sensitivity ratio of the Wallops to "typical" existing meteorological radars) also extends our observational realm to a vast hierarchy of previously undetectable tenuous clouds. For example, the cirrus clouds shown so well in Fig. 1 of Hardy and Katz were rarely seen before by radar, and then only by fixed vertically pointing short wavelength systems. These and others are important both in their own right and by virtue of providing tracers of atmospheric motion. Their use opens up all sorts of interesting possibilities for studying turbulence, wave motions, and meso- and large-scale atmospheric circulations. The fact that we can now see clouds in the high troposphere and low stratosphere also suggests that we may be able to examine the dynamic links from one to the other. In short, dramatic though they are, the Wallops observations have only hinted at what greater radar sensitivity and resolution holds in store for the atmospheric sciences.

### 3.2 Turbulence Measurements

Hardy and Katz have suggested that the reflectivity of clear air echoes is related to  $\epsilon$ , the eddy dissipation rate of turbulent energy (their Eq. 5). While there is indeed some relationship, I believe that it will be obscured by the dependence upon the refractivity gradient. However, the point is not worth argument because we have the means of measuring turbulence directly.

The intensity of turbulence may be obtained directly from

$$\Sigma_v^2 = \sigma_{\langle v \rangle}^2 + \overline{\sigma_v^2} \quad (1)$$

after Rogers and Tripp (1964). Here  $\overline{\sigma_v^2}$  is the mean variance of the Doppler spectrum of the echoes and corresponds to scales of turbulence smaller than the pulse volume;  $\sigma_{\langle v \rangle}^2$  is the variance of the instantaneous mean Doppler velocity and corresponds to scales of turbulence larger than the pulse volume. Of course, the total turbulent energy is the sum of the two. While there are practical problems in deducing  $\sigma_{\langle v \rangle}^2$  from the total variance of the Doppler spectrum (because factors other than turbulence contribute to it - Atlas, 1964), these are minimized

in clouds of small particulates and snow. In addition to the direct measurement of turbulence intensity one may analyze the temporal or spatial variations of mean Doppler velocity to obtain the spectrum of large scale turbulence. Gorelik (1965) in the Soviet Union and Rogers and Tripp (1964) have exploited these ideas to provide previously unobtainable data on the characteristics of turbulence in the free atmosphere. (See the review by Lhermitte in these Proceedings for further details.)

Of course the techniques of radar turbulence measurement are not restricted to ultra-sensitive radars. However, the ability of such radars to detect both clear air echoes and tenuous clouds, especially in the high troposphere, greatly extends their turbulence probing utility. It seems clear that future studies of clear air turbulence should take advantage of this important capacity.

### 3.3 Wind Measurement

Lhermitte's review speaks extensively of the use of Doppler radar for wind measurement. It bears repeating here because ultra-sensitive radars can detect wind-borne scatterers - either cloud and precipitation elements or clear air turbulent eddies - through most of the troposphere and during a great part of the year. I venture to predict that a modest increase in sensitivity over that of the Wallops 10 cm radar will make it possible to detect wind-borne scatterers throughout the troposphere throughout the year, at least at short ranges. Thus, I suggest that we should be able to measure tropospheric winds effectively instantaneously and continuously. Such an observing capability would have a tremendous impact on our understanding of atmospheric circulations on all scales.

### 3.4 Lightning and Sferics

Very little work has been done in the way of radar lightning detection since the 1950's when Ligda (1956), Hewitt (1957), and Atlas (1958) showed that radars between 10 and 50 cm wavelength could detect and map lightning produced ionized paths and the radio noise (sferics) radiated therefrom. The new generation of radars have a great deal to offer in this regard. The greater sensitivity will permit the detection of much smaller electron densities and thus provide a means of studying both the earlier stages of electrification and the later phases of lightning decay. The use of two or more wavelengths will permit better discrimination between precipitation and lightning and show where in the storm electrification is initiated. Such observations should suggest how the precipitation mechanism controls or influences lightning, or as proposed by Moore, *et al.*, (1962), whether lightning triggers precipitation. We need also to learn how the lightning propagates within the storm cells, from one cell to another, from cloud to ground, and from cloud to ionosphere. Such data should be attainable by the clever use of several beams at two or more wavelengths.

The use of the radars as high resolution sferics receivers should also be most enlightening. First of all it should permit us to isolate the electrically active regions of clouds and storms in relation to their precipitation structure as seen by active radar. Surprisingly, we have only the crudest knowledge of this relationship. In addition, the combination of great sensitivity and high resolution will permit a search for and confirmation of the existence of the weak electrical discharges which are associated with particle coalescence and which may occur in clouds which never reach the thunderstorm stage (Sartor, 1964; see "Sferics" review by Pierce in these Proceedings). Finally, much can be learned of the fine scale structure of the discharges by studying both the

time-variation of the radiated signals and their dependence upon wavelength (see Pierce).

In short, it seems clear that we have much to learn about cloud and storm electrification; and the use of ultra-sensitive radars at two or more wavelengths offers us many interesting opportunities in this regard.

### 3.5 The "Pictorial" Value of Radar: A Lesson to be Learned

At the risk of stating the obvious, I consider it important to stress the value of the "pictorial" or mapping capacity of radar. Although the structure of precipitation echoes can be exceedingly complex, sense can be made of them because they are depicted in two or three dimensions and can be related readily to familiar structures which we have seen by eye. In short, the significance of a set of point observations in space or time remains obscure until they are pieced together as a unified entity. Satellite cloud photography is a dramatic example of the synergistic value of the whole cloud field in relation to that of the set of individual pieces of the puzzle.

This should teach us an important lesson in all approaches toward remote probing; namely, to map the observations in some familiar spatial coordinate system. In the case of radar, Hardy and Katz put it succinctly when they state: "Methods must be devised to measure, analyze, digest, and put into useable form the 3-dimensional picture of the wind field." Indeed, I feel quite strongly that much of the seeming complexity and ambiguity which has characterized tropospheric radio scatter measurements would be removed if we were to display the observations in time and/or space coordinates. Cox implicitly recognizes this problem in his review of tropo-scatter (in these Proceedings) when he states that the data are characterized by great variability and so reflect the variability and complexity of the atmosphere. Similarly, the suggestion by Hardy and Katz to utilize radar observations simultaneous with forward-scatter measurements emphasizes the need to combine various observational tools to provide greater significance than can be obtained from either alone.

### 4.0 CONCLUDING REMARKS

The reviews by Hardy and Katz and by Lhermitte, along with the supplementary remarks presented above, provide impressive evidence of the worth of ultra-sensitive multi-wavelength radars to the atmospheric sciences. But they provide only a hint of things to come.

We are now at a stage analogous to that of the early astronomers; the history of their progress has been linked to the power of their telescopes. The same is true in radio and radar astronomy, in electron microscopy, and in virtually every experimentally-based discipline. Thus, it is no longer a question as to whether or not to proceed to radars of greatly increased sensitivity and resolution, but how to proceed.

### REFERENCES

- Atlas, D., 1958: Radar lightning echoes and atmospheric in vertical cross-section. Recent Advances in Atmospheric Electricity, Pergamon Press, N.Y., 441-459.
- Atlas, D., 1960: Radar detection of the sea breeze. *J. Meteor.*, 17, 244-258.
- Atlas, D., 1964: Advances in Radar Meteorology. Advances in Geophysics, 10, Academic Press., N.Y., 317-478.

## ULTRASENSITIVE RADAR

- Bolgiano, R., Jr., 1964: A study of wavelength dependence of transhorizon propagation. Res. Rep. CRSR 188, Center of Radio Physics and Space Research, Cornell University, Ithaca, N.Y., 67 pp.
- Browning, K. A., and D. Atlas, 1966: Velocity characteristics of some clear air dot angels. J. Atmos. Sci., 23, 592-604.
- Gorelik, A.G., 1965: Atmospheric turbulence research by radar methods. Atmospheric Turbulence and Radio Wave Propagation, Nauka Publishing House, Moscow, (1967), 280-292.
- Hewitt, F. J., 1957: Radar echoes from inter-stroke processes in lightning. Proc. Phys. Soc. B, 70, 961-979.
- Kropfli, R.A., I. Katz, T. G. Konrad, and E. B. Dobson, 1968: Simultaneous radar reflectivity measurements and refractive index spectra in the clear atmosphere. Proc. 13th Weather Radar Conf., Amer. Meteor. Soc., Boston Aug. 20-23, 1968. In press.
- Lhermitte, R. M., 1966: Probing air motion by Doppler analysis of clear air returns. J. Atmos. Sci., 23, 575-591.
- Lhermitte, R. M. and J. T. Dooley, 1966: Doppler study of the motion of clear air targets. Proc. 12th Weather Radar Conf., Amer. Meteor. Soc., Boston, 293-299.
- Ligda, M.G.H., 1956: The radar observation of lightning. J. Atmos. Terr. Phys., 9, 329-346.
- Moore, C. B., B. Vonnegut, J. A. Machado, and H. J. Survilis, 1962: Observations of rain and hail gushes after lightning. J. Geophys. Res., 67, 208-220.
- Rogers, R. R., and B. R. Tripp, 1964: Some radar measurements of turbulence in snow. J. Appl. Meteor., 3, 603-610.
- Sartor, J. D., 1964: Radio observation of the electromagnetic emission from warm clouds. Science, 143, 948-950.

---

Note: References not listed above appear in the preceding paper by Hardy and Katz

N72-25364

ATMOSPHERIC PROBING BY DOPPLER RADAR

Roger M. Lhermitte  
Environmental Science Services Administration  
Research Laboratories  
Wave Propagation Laboratory

ABSTRACT

This paper is a survey of the application of Doppler techniques to the study of atmospheric phenomena. Particular emphasis is placed on the requirement of adequate digital processing means for the Doppler signal and the Doppler data which are acquired at a very high rate. The paper also discusses the need of a two or three Doppler method as an ultimate approach to the problem of observing the three-dimensional field of particle motion inside convective storms.

1. INTRODUCTION

Although conventional radar techniques have been extensively used for years in the study of atmospheric phenomena, Doppler radar techniques were introduced to this field only a decade or so ago. Experiments based on the use of continuous wave Doppler radar were conducted as early as 1958; however, this report will essentially deal with pulse Doppler radar techniques having the same ranging capabilities as conventional pulse radars. The radar wavelengths covered in this report range from X-band (3 cm) to S-band (10 m).

The first papers on the meteorological use of pulse Doppler radar techniques were presented in 1960 at the Eighth Weather Radar Conference and were concerned with the analysis of the vertical motion of precipitating particles using a vertically pointing beam.

Discussion of the earliest experiments, involving the use of a scanning Doppler radar beam for the purpose of analyzing wind field from observation of the motion of precipitation particles, was presented a year later at the Ninth Weather Radar Conference. Since the time of these early experiments, the number of pulse Doppler radars specifically designed for meteorological studies has been steadily increasing. There are now five meteorologically-oriented pulse Doppler radars in the United States, two in England and one in Japan. These radars were designed and built for the purpose of the study of atmospheric phenomena. The use of pulse Doppler radar for atmospheric physics studies has also been mentioned in the Russian literature on meteorological research. However, no information was provided as to the nature of the Doppler equipment involved in these experiments. More sophisticated equipment is now being built such as the Environmental Science Services Administration's planned system of three identical radar sets to be used for the study of the three-dimensional field of particle motion inside convective storms.

Considerable experience on the capabilities and usefulness of pulse Doppler radars has been acquired through their use. These experiments also have revealed the weaknesses and limitations of the single Doppler radar method which need to be overcome in order to increase the capabilities of the Doppler methodology toward its ultimate potential.

This report is a brief review of the meteorological Doppler technique, as well as a summary of the results which have already been acquired in several areas of atmospheric research. We will also propose improvements aimed towards the design of a more elaborate and appropriate Doppler radar methodology. The opinion of the writer is that the potential of the Doppler methods is far from being developed to its full capability and the use of more complex and sophisticated systems will provide us with a methodology capable of solving a large number of problems related to the study of micro-scale and mesoscale atmospheric phenomena. The design of multi-unit Doppler radar systems and the use of advanced data storing and processing techniques, compatible with large computers, will be an essential part of the proposed effort.

## 2. THE DOPPLER RADAR SPECTRUM

Numerous discussions of the Doppler radar method applied to the study of atmospheric phenomena have been given in various articles (Lhermitte 1963, Atlas 1964, Lhermitte 1966). It appears only necessary in this report to briefly mention the basic principles of the method. Only pulse Doppler radar techniques, having the same ranging capabilities as conventional radars, will be discussed.

In addition to the conventional radar capabilities of observing back-scattered signal amplitude, the pulse Doppler radar provides information on the rate of change of the phase,  $\phi$ , of the backscattered signal returned by the radar-detected target. By use of appropriate design of the Doppler circuits, the phase difference between transmitted and received signals, which is observed by the coherent radar, is a function only of the distance between the target and the radar. The rate of phase change,  $d\phi/dt$ , will therefore provide knowledge of the radial velocity  $dR/dt$  of the target. We can then write  $\frac{d\phi}{dt} = \frac{4\pi}{\lambda} \frac{dR}{dt}$  where  $\lambda$  is the wavelength of the transmitted signal. This expression shows that there is a complete cycle of phase change everytime the target moves by  $\lambda/2$ . The pulse Doppler radar is thus an accurate ranging device which provides knowledge of the rate of change of target range, i. e., the radial velocity. If the target is approaching the radar, the phase of the signal is increasing as a function of time and  $d\phi/dt$  is a positive quantity which is equivalent to an increase of the transmitted frequency of the radar. On the other hand if the target is receding  $d\phi/dt$  becomes a negative quantity which is equivalent to an effective decrease of the transmitter frequency. The sign of  $d\phi/dt$  is opposite to the sign of motion derived from the convention that kinematic divergence is a positive quantity. It therefore appears that it is more appropriate in meteorological work to consider that the receding targets have positive velocity. If the target moves in a direction different from the radar beam axis, only the radial velocity, i. e., the component of the target's vectorial velocity along the axis of the radar beam, will be measured. This statement reveals the ambiguities of dealing with radial velocities, which can partially or completely be overcome in certain ways described in this report.

Since we are discussing the application of Doppler techniques for the study of atmospheric phenomena, we are dealing with volume scattering due to an extended or "distributed" target composed of large numbers of scatterers.

The classical analysis of the backscattered signal received by conventional pulse radars from distributed targets, shows that the signal amplitude at any selected point in the radar range is due to the contribution of the signals re-radiated by scatterers existing inside a scattering volume defined by the cross-section of the radar beam and the pulse length of the radar. The pulse Doppler radar will be concerned with the same type of analysis but also provides information on signal phase.

Assuming the signal backscattered from a scatterer,  $i$ , has constant amplitude,  $\alpha_i$  and phase,  $\phi_i$ , the total backscatter signal,  $A(t)$ , will be given by the following expression:

$$A(t) = \sum_{i=1}^N \alpha_i e^{-j(\omega_0 t + \phi_i)} \quad (1)$$

$\omega_0 = 2\pi f_0$  with  $f_0$  being the transmitted signal frequency.

The signal phase,  $\phi$ , can be split into a component,  $\phi_0$ , corresponding to some conditions at the origin and a variable term  $\omega_d t$  where  $\omega_d = d\phi/dt$  (Doppler shift); therefore we can write:

$$A(t) = e^{-j \omega_0 t} \sum_{i=1}^N \alpha_i e^{-j(\omega_{di} t + \phi_{oi})} \quad (2)$$

The above relationship implies statistical independence of motion between scatterers and also implies that there is no collision processes between scatterers. It also relies on the fact that scatterers are moving freely for several radar wavelengths therefore leading to a clear definition of the Doppler shift. If the scatterers are submitted to a random displacement limited to a small fraction of the radar wavelength a different and more complicated expression of  $A(t)$  will be needed.

In the case of pulse radars, the time function  $A(t)$  is sampled at the radar pulse repetition rate. Selection of the signal at any radar range can be done by use of conventional range-sampling units assisted by signal-holding circuits which restore the time continuity of the signal between radar pulses and therefore provide a time function of the form of equation (1). However, the sampling and transformation of the signal in the radar circuits slightly modifies the spectral characteristic of the signal represented in  $A(t)$  especially for frequencies approaching half of the radar pulse-repetition rate. This effect is well known and usually is corrected by appropriate means.

Equation (1) shows that the power density spectrum of  $A(t)$  is the probability density function for the backscattered power expressed as a function of the Doppler shift and is called the Doppler spectrum. If the radar cross section of the scatterers exhibits time variations, the spectrum of  $A(t)$  will include the Fourier components generated by amplitude modulation due to this effect, Brook and Latham (1968).

Figure 1 shows an example of a Doppler spectrum obtained with a vertically pointing radar beam in falling snow conditions. This example illustrates the excellent velocity resolution of the radar system.

### 3. COHERENT RADAR DESIGN AND SPECTRUM RECORDING MEANS

Radar equipment capable of observing the phase difference between back-scattered and transmitted signals is called phase-coherent or simply "coherent".

The simplest method for comparing phases is based on mixing the signal returned by the moving target with the signal reflected by a fixed target at the same range. This "external-coherence" method, which is often used in airborne navigational Doppler radars, has been applied to the study of the motion of precipitating particles, Lhermitte (1960b). However, the usefulness of this method is seriously limited by the need for a fixed target to be at exactly the same range as the moving target under study. The transmitter

pulse signal can also be stored in microwave cavities but this technique is limited to short ranges by fast time decay of the stored signal. The above solutions have not been used extensively in the design of meteorological Doppler radars because they can be replaced by more appropriate systems described below.

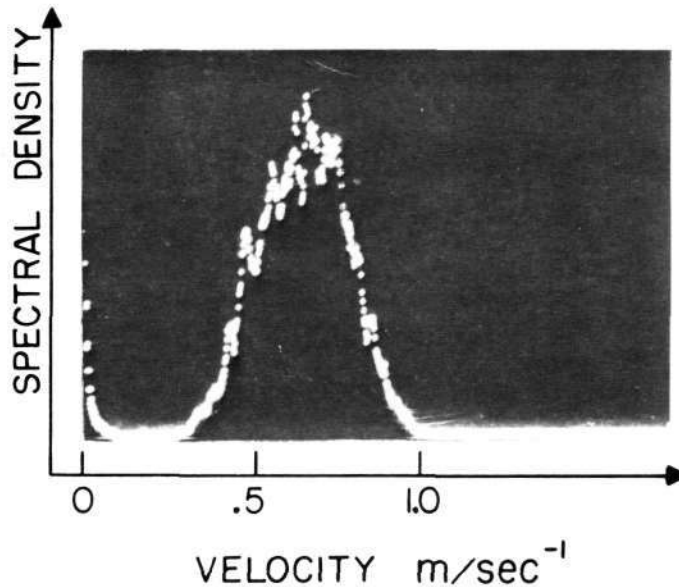


Figure 1. Doppler spectrum obtained in snow with a vertically pointing Doppler radar beam. Note the excellent velocity resolution of the system.

The most effective and accurate system is based on a primary stable microwave source called a STALO (Stable Local Oscillator). The microwave signal generated by the STALO is amplified, pulsed by a phase-coherent amplifier and radiated by the antenna. The scattered signal coming from the moving target is compared to the STALO signal and the signal phase analysis is performed by systems sensitive to the phase difference  $\Delta\phi$  between successive pulses. The quality of this system depends upon the frequency stability of the microwave oscillator during the time interval between radiation of a pulse and the return of the scattered signal. Therefore it involves only the "short term" frequency instabilities of the STALO. Relative frequency stabilities of  $10^{-10}$  can be easily achieved for longer than one millisecond and with Doppler phase jitter smaller than  $5 \times 10^{-3}$  radian.

System performance can be analyzed in terms of these estimated random phase instabilities occurring from pulse to pulse. If these phase instabilities are uncorrelated and limited to a small fraction of  $2\pi$ , they cause the presence, in the radar signal, of a radar-sampled white spectrum superimposed on the signal Doppler spectrum. The Doppler signal to noise ratio is given by the ratio between the signal phase variance (Doppler) and the contribution of the variance due to random phase instabilities, Lhermitte and Kessler (1964). If this is due to STALO phase instabilities, this ratio will typically be better than 50 db. We must emphasize that small STALO frequency instabilities will not limit the ability of the radar to observe very slow target motion which is only limited by the signal dwell time and the stability of the mean index of refraction in the path during this time. The instabilities

will only generate a phase noise which limits the dynamic range of the Doppler spectrum, and thereby inhibits the clear definition of the spectrum boundaries. The STALO contribution to phase instability increases systematically with target distance. In a well designed, fully coherent system, the STALO contribution to phase instabilities largely exceeds other contributions.

The need for a coherent microwave amplifier can be overcome by use of a conventional (but stable) magnetron microwave oscillator assisted by a transmitter phase-locked system (COHO) which stores the phase of the transmitter signal. This is the classical MTI radar which has been known and utilized for years. Phase-locking is usually done at the intermediate radar frequency and the basic requirements on the STALO remain the same as they are for fully coherent systems. High quality, commercially available magnetron oscillators have acceptable frequency stability. However, there is more phase noise generated by the magnetron and by the instabilities in phase-locking the COHO than in a system utilizing a STALO and a microwave coherent amplifier. The ratio of signal-phase to phase-noise, better than 50 db for fully coherent systems, is reduced to 30 to 35 db in the case of the MTI system. This phase noise contribution is independent of the radar range.

The above discussion shows that frequency analysis of the Doppler signal must be obtained prior to any reduction of the data. As discussed in section 8 of this report, multirange signal sampling and digitizing followed by digital computations of fast Fourier transforms offer the most flexible and effective means for this requirement. These techniques are, however, in a developing stage and have been temporarily replaced, in the present experimental work discussed in this report, by the following methods:

a. Range-gating associated with either a signal crossing technique which provides the spectrum's second moment, Lhermitte (1963), or a velocity tracking system which essentially processes the spectrum median frequency, Tripp (1964). This technique has the advantage of simplicity but it doesn't provide information on the spectrum width and shape, and is only acceptable in the case of narrow or, at least, symmetric spectra for which only the knowledge of the average frequency is required.

b. Range-gating associated with the use of multifilter frequency analyzer. This method leads to acceptable knowledge of the spectrum shape especially if integration means are provided for the signal at the output of every filter. It is, however, a slow process which doesn't match the requirements imposed by the study of atmospheric phenomena.

c. Coherent memory filter or velocity-indicator coherent integrator (VICI). The application of this device to meteorological work, which was first proposed by Chimera (1960), allows quick display of the distribution of the Doppler velocity as a function of radar range (Range velocity indicator, RVI). The device is extremely fast but it suffers from restricted range and velocity resolutions due to practical limitations of the system. The device is also unable to provide or display the signal power spectral density in a quantitative manner and therefore fails to indicate the Doppler spectrum shape. In its present form, the coherent memory filter also fails to produce data in a digital format which seems to be the only way to cope with the type of information provided by this system. An extension of its use for PPI display has been recently proposed by Armstrong and Donaldson (1968).

d. Time compression scheme. Several range gates can be Doppler analyzed in a short time by use of signal multiplexing techniques and time compression schemes. The digital time compression essentially allows that quick analysis of the spectra be done by use of fast scanning filters. The system is capable of analyzing the Doppler information at ten range gates in a time of the order of a few seconds. The complexity of this system, which involves digital techniques, approaches that of a purely digital system such as the one described in section 8 of this report. However, it doesn't have the flexibility of the digital computations and doesn't provide the digital output which is required for easy handling and processing of the data.

e. If real-time operation is not necessary, the recording of the Doppler signal by aid of a multi-track magnetic tape recorder offers a high rate of data acquisition which matches most of the requirements. Complementary informations can also be recorded on a separate track. The processing of the recorded signals can be done with the aid of specialized digital devices which provide a digital output. This seems to be the closest approach to the sophisticated digital system proposed in section 8 of this report.

#### 4. VERTICAL BEAM METHOD

The method, which was first proposed by Boyenval (1960), Probert-Jones (1960), Lhermitte (1960), relies on the operation of a fixed, vertically pointing, radar beam. The method is attractive from the point of view of data processing in that antenna orientation need not be recorded. The radar observes only the target's vertical motion by aid of a very narrow, perfectly vertical, radar beam. Smearing of the Doppler spectrum by the horizontal wind will occur in the case of a finite size beam. However, this effect is practically negligible for beam widths of the order of  $1^\circ$  if the tangential speed is limited to less than  $30 \text{ m sec}^{-1}$ .

Let us accept the fact that we are essentially dealing with the vertical velocity of the precipitating particles. The analysis of the data will still be ambiguous since the particles' vertical velocity is due to the contribution of both particle terminal speed and vertical air motion. In the case of stratiform precipitation, vertical air motion may be assumed to be negligible. Furthermore if we are observing raindrops, a relationship between particles' radar cross section and particles' vertical speed can be established thereby allowing the Doppler spectrum to be predicted on the basis of the knowledge of the particles' size distribution. The inverse proposition is true and the size distribution of raindrops have been derived from the vertical velocity Doppler data, Probert-Jones (1960), Rogers and Pilié (1962), Caton (1963), Rogers (1966).

For study of raindrop growth or evaporation in stratiform conditions this method of observing drop-size distribution is excellent. However, the results are very sensitive to the presence of air motion, especially where the speeds correspond to large drops whose terminal velocity is weakly related to drop diameters. In practice, this limits the method to nonconvective precipitation. Also, large particle scattering in case of limited signal dynamic range might overwhelm the weak contribution due to the smaller particles scattering and prevent accurate knowledge of the relative concentration of smaller size raindrops.

Provided that the antenna radiation pattern is excellent, fully coherent radar provides adequate spectrum dynamic range allowing good estimates of the presence of small raindrops. We may also mention that combined study of vertical velocity spectra and signal intensity in stratiform precipitation, Lhermitte and Atlas (1963), may lead to a better understanding of precipitation growth mechanisms.

Although the above comments indicate that the vertical beam method is useful, its systematic application to the study of convective storm processes is still very limited. In these cases it is unreasonable to expect that the altitude-time display of the particles' vertical velocity is significantly representative of the actual, time evolving, three-dimensional structure of the storm. Furthermore the vertical velocity observed by the radar will be difficult to resolve in its two components, the particle terminal speed and the vertical air motion.

To obtain estimates of the vertical air motion Rogers (1963) assumed an exponential (Marshall Palmer) model of raindrops size distribution of the form:

$$n(D)dD = N_0 e^{-\Lambda D} \cdot dD \quad (3)$$

where  $n(D)dD$  is the number of drops per unit volume in the diameter interval  $dD$ ,  $N_0$  is a constant, and  $\Lambda$  is a parameter that depends upon rainfall rate. By further assuming a relation between terminal fall velocity and size, Spilhaus (1948), and also Rayleigh scattering, Rogers arrived at an expression of the relationship between the average vertical velocity,  $\bar{V}_f$ , and radar reflectivity,  $Z$ , which is the following:  $\bar{V}_f = 3.8Z^{1/4}$ . He concluded that any departure from the above equation will be due to vertical air speed. The application of the above treatment seems to be only practical in stratiform rain, for average quantities obtained over long periods of time.

Similar assumptions have been made by Donaldson et al (1966) and Donaldson (1967a). In this work the analysis was restricted to regions where  $Z > 10$ , and the following expression between  $\bar{V}_f$  and  $Z$  was derived:

$$\bar{V}_f = 2 \log Z - 2 \quad (4)$$

The estimated vertical air speed,  $\hat{W}$ , was also derived from the following equation:

$$\hat{W} = \bar{V}_f + 2 \log Z - 2 \quad (5)$$

A different method to estimate updrafts has been used by Probert-Jones and Harper (1961) for the study of small convective storms. They suggested that above the  $0^\circ$  C level in the convective storm, precipitation was present in the form of large ice crystals or snow flakes. The assumption of a terminal fall velocity of  $1 \text{ m sec}^{-1} \pm 0.5 \text{ m sec}^{-1}$  provided Probert-Jones and Harper with means to estimate vertical air motion. They extended the analysis below the melting level by assuming continuity of air motion through the melting level and by further assuming that there was very little change of the terminal velocity of the drops between the melting level and the ground.

Although numerous assumptions were present in the analysis, the method showed a surprisingly well organized pattern of motion in the convective storm which could be used for a model of the structure of the air circulation within the storm. The model seems to have questionable application to larger convective systems where the melting level is not as clearly defined as in the convective storm analyzed by Probert-Jones and Harper.

A different approach to estimating updraft velocities has been used by Battan (1963a) and Battan and Theiss (1966, 1967). They suggested that the lowest part of the velocity spectrum is related to the small size precipitation particles which can be estimated by assuming a threshold of detection. Since the terminal speed for such precipitation particles was known, updraft could then be determined from this lower boundary of the vertical velocity spectrum. There is, however, some difficulty in estimating the lowest velocity boundary of the spectrum since its dynamic range is limited by the noise generated by or accepted in the radar circuit. This noise is mainly due to the radar phase noise generated by the radar equipment, but also includes contributions due to backscattering received outside the antenna main beam as allowed by the complex nature of the radiation pattern of the radar antenna. The spectrum dynamic range can also be degraded by signal processing such as the single sideband detection scheme used by Battan and Theiss (1966).

In spite of the restrictive assumptions, there is acceptable consistency in the published radar observations of vertical Doppler speed. These have covered a wide range of updraft speeds from  $4 \text{ m sec}^{-1}$  deduced by Probert-Jones and Harper (1961) in a weak convective storm, to  $20 \text{ m sec}^{-1}$  deduced by Battan and Theiss (1966). Updraft speeds larger than  $16 \text{ m sec}^{-1}$  have also been observed by Donaldson et al (1966). These observations reveal that updrafts are found mostly above the  $0^\circ \text{ C}$  level and downdrafts below this level.

The application of the previous methods to the estimate of updrafts and other processes inside storms is, however, questionable. Noticeable departure of the drop size distribution from the exponential Marshall Palmer mode, which will reduce the applicability of the updraft estimates, will occur in a variety of cases. Sorting of the precipitation particles is a frequent cause of drastic modification of spectrum size. The presence of hail will completely upset the estimated relationship between radar reflectivity and  $V_f$ , presented above.

The validity of the assumptions involved in estimating updraft speeds might be further questioned on the basis of some of the published results indicating very high air vertical velocity gradients  $dw/dz$ , Donaldson (1967). One sees that the Donaldson results shown in Figure 2 indicate that, between 1641 and 1642 EST,  $dw/dz$  was larger than  $10^{-2} \text{ sec}^{-1}$  at an altitude of 8 kms, therefore requiring that horizontal divergence of the same order of magnitude be present at this altitude. Results recently obtained by Donaldson (1968) indicate that  $dw/dz$  can reach a maximum value of  $3.10^{-2} \text{ sec}^{-1}$ .

The vertical beam method requires that some stratification or steady state process be realized for a reasonable length of time. These conditions will seldom be met in the case of convective storms.

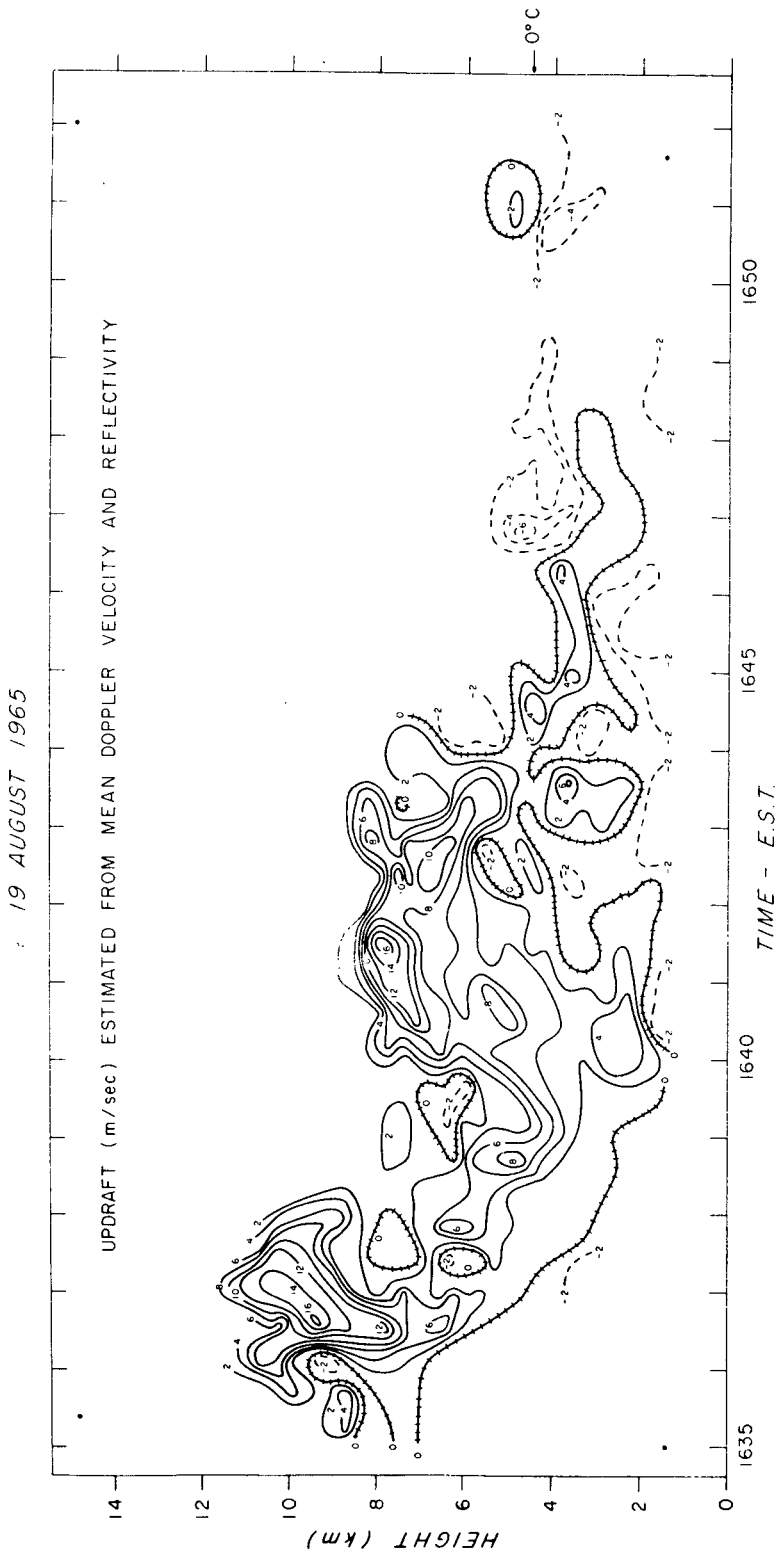


Figure 2. Vertical air motion field estimated from mean Doppler velocity and an assumed relationship between reflectivity and mean particle fall speed. Updrafts are solid contours, and downdrafts are dashed contours, with railroad tracks showing locations of zero vertical air motion. (After Donaldson, 1968).

In order to give meteorological significance to the Doppler data, the experimenter must rely on arbitrary assumptions which are not derived from sound physical reasoning. This attitude is reflected on the controversy surrounding the existence of a "balance level" proposed by Atlas (1966) and its significance as an important part of the storm processes. The balance level is characterized by the altitude at which the mean vertical Doppler velocity is zero. It is adventurous to specify such quantity without some knowledge of the spectrum shape. Furthermore, as indicated by Donaldson and Wexler (1968) the restricted significance of altitude-time cross sections does not allow any firm conclusion as to the presence of an accumulation zone or region of particle growth in the three-dimensional storm structure.

Since critical phases of the analysis of data derived from vertically pointing radar rely on arbitrary assumptions used as a substitute for the lack of knowledge of the storm processes outside of the region observed, the reader is referred to the above mentioned papers for a more detailed discussion on the significance of the balance level.

To summarize, it is the author's opinion that a single, vertically-pointing radar has and will continue to have severely limited application for the study of convective processes inside storms and should be replaced by the multiple Doppler radar method discussed at the end of this report.

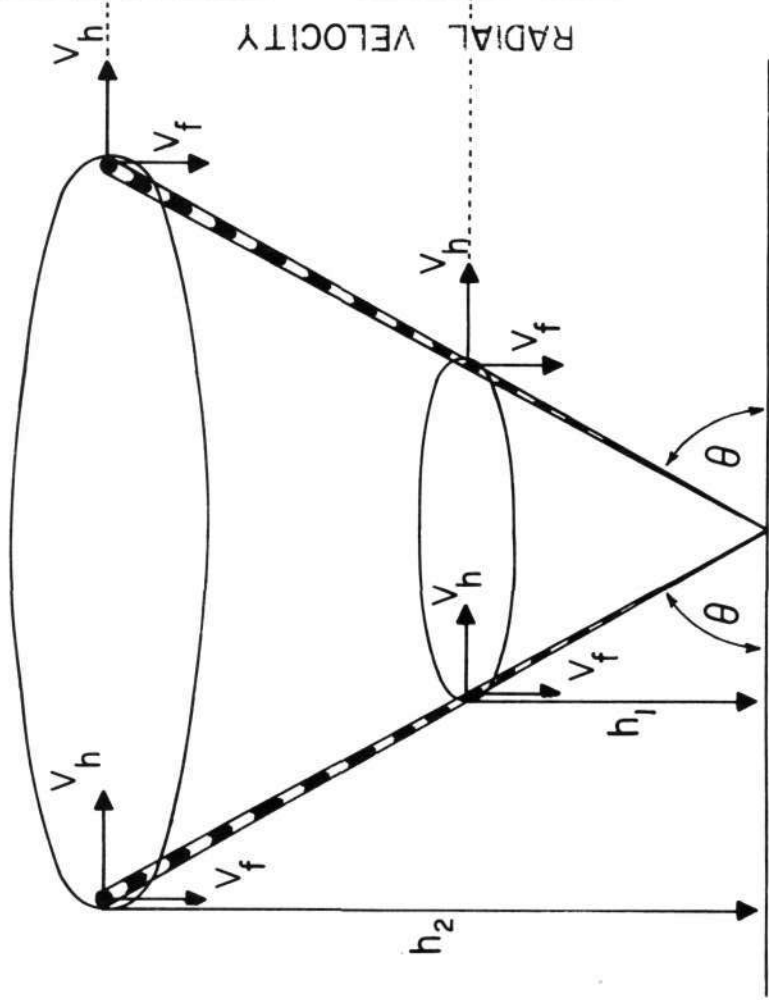
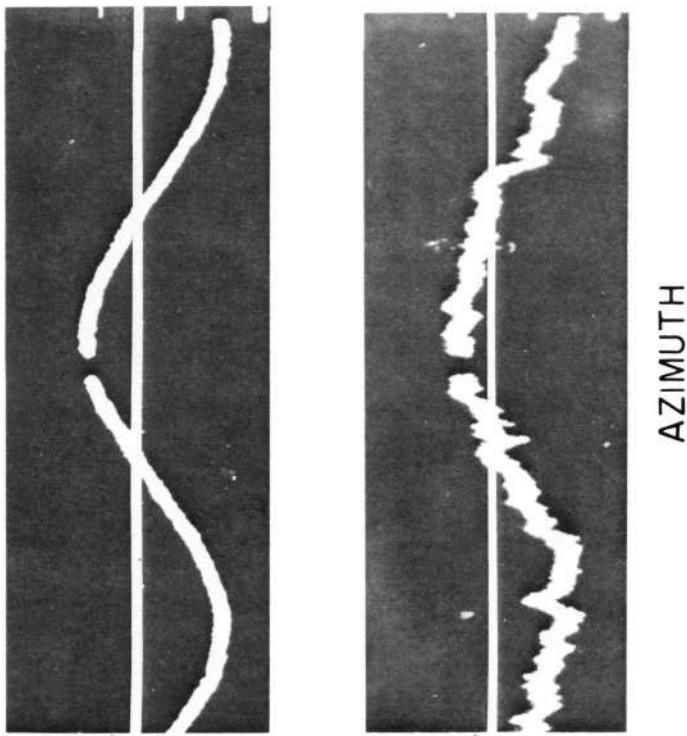
## 5. VAD METHODOLOGY

If we assume statistical homogeneity of the speed of the particles in the area covered by the radar equipment and if we are interested in deriving average properties of the wind field, it is appropriate to observe several radial components of the particle motion obtained in different directions, by means of azimuth scanning of the radar beam and display of the velocity azimuth function (Velocity-Azimuth-Display). With appropriate programming of the radar beam elevation angles and also selected ranges, the data can be representative of a range of altitude levels in the storm, thereby leading to a definition of the vertical distribution of the properties of the motion field.

The method was first proposed, Lhermitte and Atlas (1961), for the purpose of measuring the wind vertical profiles within a snow storm. An example of the method capability is shown in Figure 3. The particle radial velocity,  $V_R$ , at a certain altitude level in a snow storm is continuously recorded as a function of the azimuth of the radar beam,  $\beta$ .  $V_R$  is expressed as a function of the horizontal motion speed,  $V_h$ , and direction,  $\beta_0$ , the radar beam elevation angle,  $\theta$ , and the particle vertical velocity,  $V_f$ , by the following equation:

$$V_R = V_h \cos \theta \cos (\beta - \beta_0) + V_f \sin \theta \quad (6)$$

$V_R$  is in fact a spectrum whose variance is due to the contribution of  $V_h$  variance,  $\sigma_h^2$ ,  $V_f$  variance,  $\sigma_f^2$  (due mainly to the distribution of particle terminal speed), and the covariance between  $V_f$  and  $V_h$ . The estimate of the mean velocity  $\bar{V}_R$  (spectrum first moment) collected as a function of radar beam azimuth, offers means to determine a least square fit of equation (6) which permits a prediction of the average quantities:  $\bar{V}_h$ ,  $\bar{V}_f$  and  $\bar{\beta}_0$ .



$$V_R = V_h \cos \theta \cos (\beta - \beta_0) + V_f \sin \theta$$

Figure 3. Velocity azimuth display with examples of actual results.

There is, however, an ambiguity in the prediction of  $\bar{V}_f$  which is due to the possible presence of wind convergence in the wind field. This is easily shown by integrating  $V_R$  as a function of  $\beta$ . We have:

$$\int_0^{2\pi} V_R(\beta) d\beta = \cos\theta \int_0^{2\pi} V_h \cos(\beta - \beta_0) d\beta + \sin\theta \int_0^{2\pi} V_f d\beta \quad (7)$$

The term  $\int_0^{2\pi} V_h \cos(\beta - \beta_0) d\beta$  will be null only if there is no wind convergence.

We then can write:

$$\int_0^{2\pi} V_R(\beta) d\beta = \sin\theta \int_0^{2\pi} V_f d\beta \quad (8)$$

and therefore estimate  $\bar{V}_f$ . However, if there is wind convergence the term,

$$\int_0^{2\pi} V_h \cos(\beta - \beta_0) d\beta$$

will not be zero and will contribute to the term on the right hand of equation (7). By further manipulating the equations we can estimate the wind divergence,  $\text{div}_2 \vec{V}$  by the following expression:

$$\text{div}_2 \vec{V} = \frac{1}{\pi r} \int_0^{2\pi} \frac{V_R(\beta) d\beta}{\cos\theta} - \left( \frac{2 \bar{V}_f \tan\theta}{r} \right) \quad (9)$$

In this equation,  $r$  is the radius of the circle scanned by the radar beam at the selected range or altitude. The method is capable of an accurate estimate of the wind convergence if  $\theta$  is small and if the particle fall speed can be estimated accurately, i.e., (snowflakes falling in still air). For instance, if  $\theta = 10^\circ$  a change of the estimate of  $V_f$  by  $0.5 \text{ m sec}^{-1}$  will modify the convergence estimate by  $2 \cdot 10^{-5} \text{ sec}^{-1}$  at  $r = 15 \text{ kms}$ .

This method of measuring wind convergence has been first proposed and applied by Caton (1963). It reliably applies only to snow storms or the region of the atmosphere where the fall velocity of targets is either small or accurately estimated. Browning and Wexler (1966) have extended these computations to the study of other properties of the wind field such as deformation. Vorticity can not be observed with a single Doppler radar since it requires that the tangential component of the motion be known.

Wind fluctuations of smaller scale can also be estimated by classical Fourier analysis of the  $V_R(\beta)$  function and the Fourier components expressed in the following equation:

$$C_n = \int_0^{2\pi} V_R(\beta) e^{-jn\beta} d\beta \quad (10)$$

$C_n$  is indeed a complex quantity containing information of the phase and amplitude of the Fourier components.

$$C_0 = \int_0^{2\pi} V_R(\beta) d\beta \quad \text{is the "DC" term controlled by both the vertical velocity}$$

and the wind convergence which was discussed above. The method can bring information on the small scale variability of the wind, Lhermitte (1968b).

The design of the experiments with a program of elevation angles,  $\theta$ , provides more flexibility in analyzing the data since the relative contribution of the vertical and horizontal motion to the radial velocity will be modified by varying  $\theta$ .

The method is now largely being used for the study of mesoscale phenomena in widespread storms. Its capabilities of analyzing the wind field properties inside snowstorms are excellent. Mesoscale wind properties as well as turbulent eddy sizes and eddy dissipation rate can be observed and analyzed if the data are acquired at a high rate, simultaneously at different altitudes. However, in order to utilize the method to its full capabilities, the data have to be produced in digital form for efficient reduction by digital computers.

#### 6. COMMENTS ON THE USE OF A SINGLE DOPPLER RADAR FOR THE STUDY OF CONVECTIVE STORMS

Attempts have been made to analyze the horizontal wind field in a convective storm system from a slightly tilted Doppler radar beam. Donaldson (1967b) presented such experiments which were made by azimuth scanning of the convective cells, with elevation angle limited to  $1^\circ$ ,  $3^\circ$ , and  $5^\circ$ , for which the contribution due to particle vertical velocity was negligible. However, even if restricted to the storm's lowest levels the results are not representative of the storm circulation since only the radial particle velocity is observed. Even with assumptions about mean wind, whose significance is questionable in the strongly perturbed storm environment, the results do not show any convincing pattern leading to estimates of the storm wind field properties such as convergence and vorticity. The results obtained with such a technique will always be inconclusive except in the case where the azimuth scanning is limited to a small range of azimuth. One objective of such experiments might be to specify the scales of variance of the storm particle motion which can be used to assess the optimum sampling interval in future experiments involving the simultaneous use of several radars.

It is the writer's opinion that neither the vertical beam method nor the single radar horizontal scanning beam will provide significant improvements of the storm circulation knowledge. The prospects are much better if the measurements are based on a two radar system from which two radial components of the motion can be observed. By restricting the observations to low elevation angles, i.e., the storm's lowest levels, the analysis will bring a fairly good knowledge of the wind field leading to estimates of kinematic properties such as convergence. Vertical drafts can be estimated in the low levels of the storm by applying the equation of continuity to the wind fields observed at several altitude levels in the storm.

The Environmental Science Services Administration is developing a system of two compatible Doppler radars which will be tested during summer 1968 and should allow an assessment of the logistic problems involved. The two-Doppler radar method is a necessary step towards the design of a three-Doppler method described in section 9 of this report. Since the three-Doppler method retains the continuity of radar scanning it is more appropriate for the probing of the three-dimensional structure of a storm than the use of a network of vertically pointing Doppler radars, which was proposed by Browning (1966)\*.

## 7. DOPPLER STUDY OF CLEAR AIR MOTION

Doppler methods have also been used for the study of clear air targets (CAR) commonly called "Angels". The experiments were concerned with the observation of the speed of these targets for the purpose of identifying their nature and also the motion of the surrounding air. A much better identification of the target is possible with the phase information provided by the Doppler radar. For instance, birds species can be identified on the basis of the characteristics of the Doppler spectrum as related to the motion of their wings. On the other hand, insects which are smaller than the radar wavelength will only provide a small phase modulation of the signal, which can be used as information to recognize their nature. Although this sort of information would be helpful to entomologists and ornithologists interested in the migration of insects or birds species there has not been any real attempt to direct the analysis of the Doppler data to this use. Expected differences between the Doppler spectra might sometime resolve the controversy between the attribution of clear air radar returns to either sharp index of refraction discontinuity or the presence of small physical targets. It is, however, surprising to notice that there has been no published paper devoted to detailed analysis of the Doppler spectrum as means of identifying the targets detected in clear air. Only the mean Doppler frequency is usually observed and analyzed. The first data of this kind have been acquired with a vertically pointing beam, Battan (1960; 1963). The targets' vertical motion was observed as limited to  $+ 1 \text{ m sec}^{-1}$ . The analysis of the data was based on the assumption that the radar signals were due to air bubbles generated by thermal convection.

By use of the VAD technique described above Lhermitte (1966), Browning and Atlas (1966) were able to analyze the horizontal motion of the clear air targets. The Lhermitte observations, which are illustrated in Figure 5, were obtained in central Oklahoma and showed unambiguously that the targets were moving with the horizontal wind. Furthermore, the analysis showed that the method was capable of providing useful data on the vertical structure of the horizontal wind, almost continuously and over long periods of time. The low level jet frequent in central Oklahoma and northeastern Texas, when analyzed by use of this method, revealed a structure of the jet consistent with the classical studies of these boundary layer phenomena. Correlation between the clear air target horizontal motion and the presence of synoptic features such as cold fronts have been also analyzed by Lhermitte and Dooley (1966) for the spring and summer months in Oklahoma when the concentration of targets is very great. A summary of the observations of clear air target motion showed that vertical profiles of the wind can be often estimated by the method up to 1 or 2 km of altitude. The conclusions as to the nature of

\*Private communication.

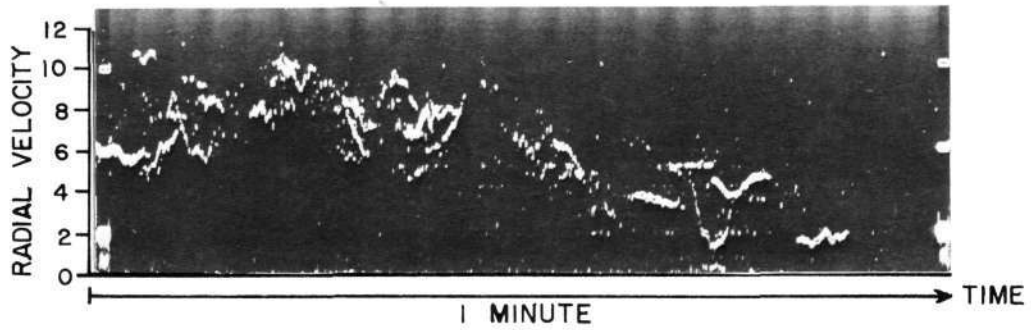


Figure 4. Time velocity variations of clear air target at a fixed point in space. Note the average trend which can be attributed to change of air motion speed.

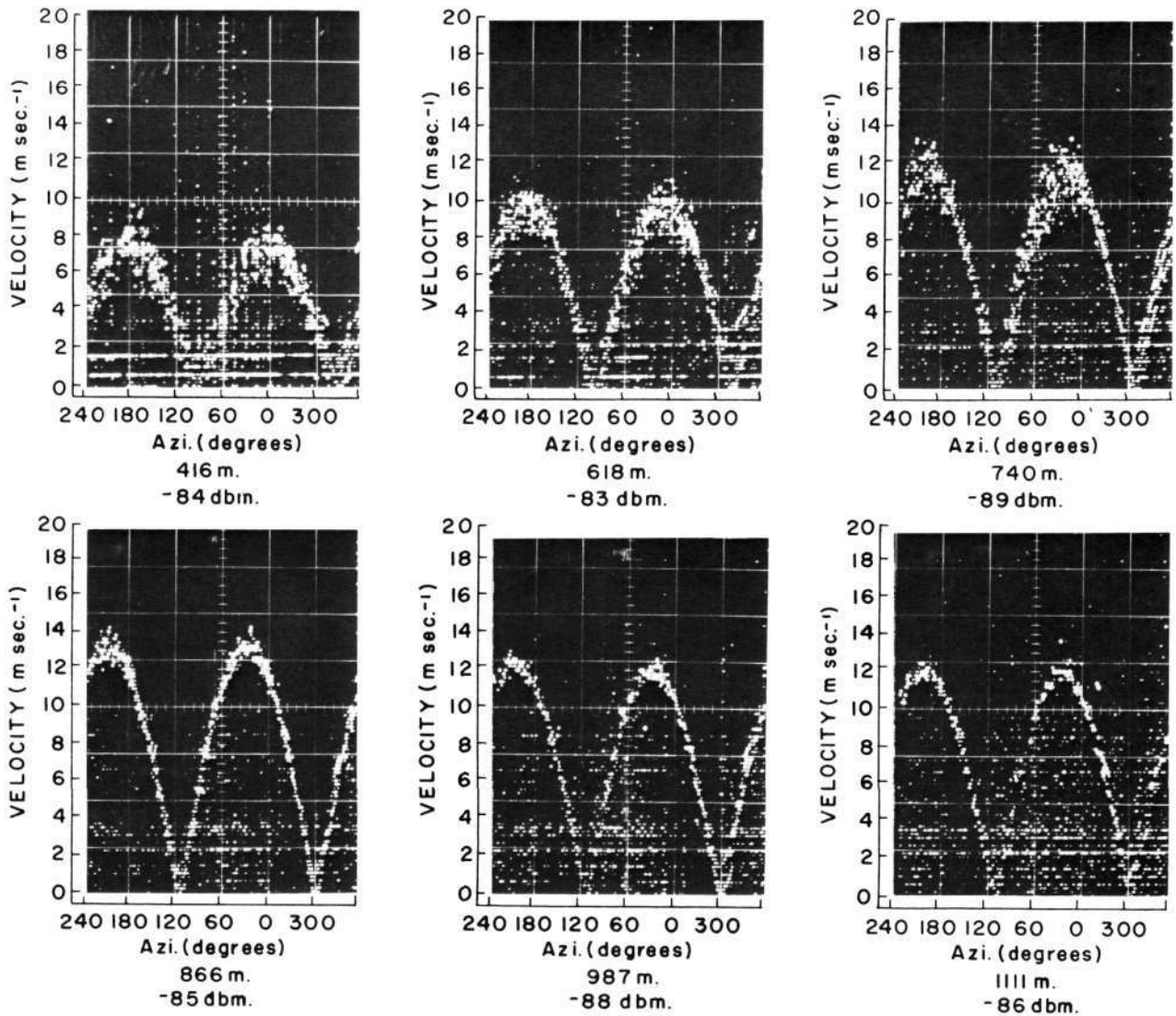


Figure 5. Velocity-Azimuth displays showing the CAR radial velocity at several altitudes. Radar beam elevation angle  $20^{\circ}$ . Radar site, Norman, Okla. Time 2023 to 2031 CST, 26 June. Signal mean intensity is indicated in -dbm.

the targets was uncertain although there was a high probability that they were insects drifting at air speed. In certain cases the space variance of the motion, with respect to the average wind, was so small that it would indicate very poor ability for these insects to react to the environment. More of these studies should be made to further specify the nature of the target and the capability of using the method for wind sounding techniques.

Tracers, such as "chaff" dipoles, offer an extremely interesting possibility for the probing of steady and turbulent air motion. The Doppler spectrum will be controlled by the turbulent processes and will contain information on turbulent parameters such as the eddy dissipation rate. Furthermore, by extending the observations to different regions of space by means of beam scanning, the study of turbulence homogeneity and large scale wind fluctuation can be performed. The material can be dispersed, either in bundles which will drift with the wind and expand through turbulent diffusion process, or introduced over large areas. The method will provide means to analyze the field of turbulent and steady clear air motion. The variance of the Doppler spectrum obtained under these conditions will be controlled by the variance of the horizontal motion,  $\sigma_h^2$ , the variance of vertical motion,  $\sigma_v^2$ , and the covariance between these two quantities. The covariance can be separated from the other variances by acquiring the Doppler information in such a way that positive and negative signs for the covariance will be available in the data analysis. The observation of the covariance between the horizontal and vertical component of the motion will provide means to probe the vertical transport of momentum in the friction layer, which is due to the interaction between the turbulent atmosphere and the earth's surface acting as a boundary, Lhermitte (1968b). The vertical distribution of the vertical motion variance,  $\sigma_v^2$ , can be easily obtained from a vertically pointing beam. Also the differences between Lagrangian (space variability) and Eulerian (time variability) scales of motion variance can be easily studied by comparing the cross correlation of covariance spectrum of the motion observed simultaneously at two points in space with the time autocorrelation or autocovariance of the individual motion sample. A scheme similar to this was presented by Gorelik (1965) and more recently by Boucher (1968). These methods present an extremely good prospect for the study of turbulent diffusion processes in critical areas where this is becoming an important factor (pollution zone). Surprisingly little work has been done in this research area and we recommend that such activity be included in research projects in the next few years. An X-band Doppler radar (or shorter wavelength) is appropriate for this kind of experiment. If the chaff is released by airplane the method also offers the possibility of probing the high altitude clear air turbulence.

## 8. ADVANCED DOPPLER SIGNAL PROCESSING AND DOPPLER DATA STORING

Most of the results which have been discussed in the previous section have been obtained through the use of relatively simple signal processing and data storing techniques which have severely limited the analysis of the data, and have prevented the use of the method to its full capability. Since most of the data have been hand reduced, an extremely time consuming analysis was needed, which has prevented the statistical treatment of the very large amounts of data provided by the method.

Recently, signal and data processing methods have drastically improved through the use of modern general purpose digital computers and also by the

aid of special purpose processing systems based on the use of modern digital hardware such as integrated circuits. The meteorological Doppler radar system, with its high rate of information flow, can benefit dramatically from the introduction of modern digital circuitry and methods for the processing and storing of the Doppler information. This section is devoted to analyzing the problems and predicting solutions which are expected to take place in the next few years for the treatment of the Doppler radar information to such an extent that the potential of the method will be fully realized.

As mentioned in the first part of this report, the Doppler signal which contains backscattering phase and amplitude information, must be processed to provide useful information on the spectrum of radial velocity of the scatterers. The transformation required is a conventional Fourier transform or its equivalent such as the processing of the signal by use of an analog type frequency analyzer.

Although digital computations of the Doppler signal power density spectrum have been involved in some of the experiments mentioned previously in this report, Battan (1964), they have not been widely used because of the time consuming nature of the operation. However, substantial progress has been made in the field of power density spectrum computation by digital computers, and efficient algorithms are now available which match the digital computer methods with the mathematics of the Fourier transform, Cooley, Tukey (1965). This fast Fourier method allows a substantial reduction of the time requirement for the digital computations of Fourier transforms.

The digital Fourier transform is based on the availability of digitized time samples,  $a_k$ , of the signal to be analyzed. The spectral power density estimates,  $S_j$ , are computed according to the following equations:

$$A_j = \sum_{k=1}^N a_k \cos 2\pi K_j / N$$

$$B_j = \sum_{k=1}^N a_k \sin 2\pi K_j / N$$

$$S_j = A_j^2 + B_j^2 \quad (11)$$

The method provides  $N$  non-redundant frequency samples from  $N$  time samples thus requiring that  $N^2$  multiplications be done per complete spectrum. It is usually admitted that 500 time samples are fairly representative of the spectral information in a time signal, requiring that 250,000 multiplications be done for each conventional Fourier transform. With modern fast digital computers the computing time will be on the order of, or less than, one second which is comparable to the signal dwell time required to build an acceptable knowledge of the spectrum. Therefore real-time digital computations by conventional Fourier algorithms are, at least, as effective as the filter bank method. In addition, the digital computer offers complete flexibility in the choice of appropriate frequency filter characteristics and the frequency coverage which is controlled by the signal sampling rate. See Blackman and Tukey (1958). Since it is based on the unambiguous Fourier transform mathematical expression, the digital frequency analyzer provides a well-defined answer

for the spectral density estimate which is easier to use in the analysis of the data.

The use of fast Fourier transform algorithms decreases the required number of multiplications to  $2 N \log_2 N$  instead of  $N^2$ . This will considerably reduce the computation time to much less than signal dwell time and thereby making it feasible to process several radar ranges in a time less than a few seconds. This involves the use of a high speed, elaborate system for multiplexing, and analog-to-digital conversion, of the Doppler signal. It also requires core memories which are organized in such a way that the sequence of the Fourier transforms can be easily computed, range after range, from the stored digital data. Such systems can be built at an acceptable cost by use of modern integrated circuit digital hardware. The expected maximum rate of data which can be processed by the system is on the order of 2,000 (20 ranges, 50 velocities) samples every two seconds. By use of a logarithmic scale only one BCD coded character will be necessary to represent the spectral density at a given range-velocity address. The storing of the Doppler data with range-velocity addresses will be done on magnetic tape with a format compatible with the requirement of general purpose digital computer (BCD format suitable for Fortran IV programming). Figure 6 illustrates the capabilities of the digital method for reducing and even presenting a three-dimensional display of the Doppler radar information. Such displays can be obtained in very short times by use of output devices usually associated with large computers.

The system is capable of processing signals recorded at an average speed of 10 to 20 spectra per second, which is compatible with the scanning capabilities of the radar beam and signal dwell time requirements (one or two beam width per second).

Let us inquire if the method has an acceptable observational speed to define convective storm processes known and anticipated. The evaluation of the number of points, which are needed to adequately sample the field of particle motion inside a convective storm, depends on the scale of the motion variance and the size of the storm. Although this information has to be acquired through actual experiments yet to be performed, it is reasonable to accept a few hundred meters as an appropriate space sampling interval.

This estimate is consistent with the radar angular resolution for nearby storms. If we analyze the problem in terms of the radar polar coordinates we will deduce that, (with a one degree beam width) an adequate description of the storm will be obtained with approximately 50 beam-widths in azimuth and 10 to 20 elevation angles. Assuming as mentioned before that the beam will stay in a fixed position for a time on the order of 0.5 second i.e., 20 to 30 spectra will be processed in one second, the total time required for exploring the storm will be on the order of 250 to 500 seconds or 4 to 8 minutes. This is marginal since the storm will be translating and evolving during this time. This effect can, however, be accounted for in the computation of radial velocity field estimates.

It is important to note that the rate at which the Doppler data are acquired and stored can be increased well beyond the limits expressed above. The expected availability of large scale integration (LSI) digital hardware along with the increasing speed capability of integrated circuits can increase

# ATMOSPHERIC PROBING BY DOPPLER RADAR

the data acquisition rate expressed above, by one order of magnitude. The capability of the system will still be limited to the scanning speed capabilities of radar antennas, although this, too, might ultimately be overcome by the development of electronic beam scanning techniques; but, isn't it dreaming??

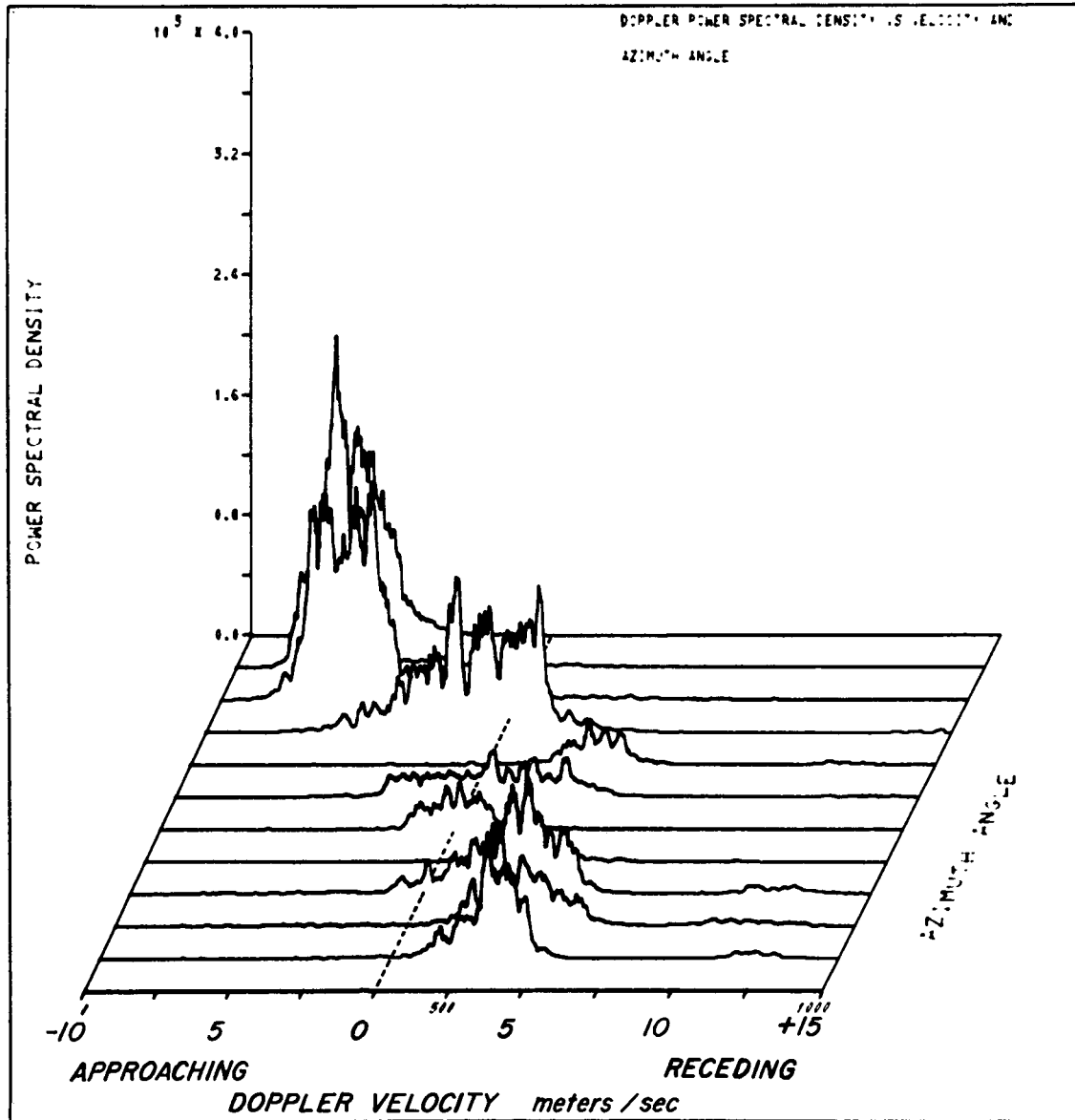


Figure 6. Three dimensional display of Doppler-azimuth patterns obtained with the cathode ray tube plotter of a CDC 3800 digital computer.

## 9. THE THREE DOPPLER RADAR METHOD

As mentioned in the previous section of the report the real weakness of the Doppler radar method is that it only provides the scatterers radial velocity. Since the vertical beam method is sensitive only to particle vertical velocity, it is less ambiguous and in the case of marked stratification, very useful. But, the method fails to exploit the outstanding capability of the radar, i.e., its ability to acquire data distributed in three coordinates of space. The observation of particle vertical velocity along a vertical coordinate is hardly representative of the storm processes except in the case of stratiform storms.

The use of a single radar scanning beam is useful and effective if assumptions about statistical homogeneities of particle motion in the region covered by the radar can be accepted. The most commonly employed scanning scheme is based on continuous azimuth scanning of the radar beam with a programmed elevation angle (VAD). The method, which was discussed in section 5 of the report, has an extremely good potential for the study of the dynamics of widespread storms by providing separate estimates of the mean properties of the horizontal wind field (magnitude, direction, convergence) and the vertical motion of the targets.

However, because of the absence of stratification and the non-uniformities of wind field, neither the vertical beam nor the VAD methods are applicable to observing the particle motion field inside convective storm systems. The understanding of the physical and dynamical processes involved in these storms fall in the most stimulating and unknown areas of meteorological research and have received a large attention from the meteorologist. However, progress on the study of storm dynamics has been slow mainly because of the lack of experimental data at the required scales. Theoretical work has always been limited to crude modeling far from the actual complexity of the storm's circulation patterns.

The main reason for this slow progress is the lack of appropriate means for observing the storm inner processes. The use of airplane as a means to acquire such data has been limited to a poor sampling of the storm environment since penetration of the storm was always questionable. Radiosonde networks have been useful to specify the condition of the storm environment and its link to the mesoscale or synoptic scale but, because of the techniques involved, they again provide only a poor time and space sampling far from the resolution required to adequately define the inner processes and evolution of a convective storm. Conventional radars have brought a much better understanding of the structure of the storm systems, which is still being developed, through the use of more elaborate quantitative processing of the radar signal.

As mentioned in section 6, the use of two Doppler radars, installed at different locations and simultaneously observing the same storm, drastically improves the capability of the single Doppler radar method. Figure 7 illustrates the concept. The same region of a storm is observed by two radars,  $R_1$  and  $R_2$ , installed at different locations thereby providing two radial components of the particles' motion,  $V_1$  and  $V_2$ . The two components,  $V_1$  and  $V_2$ , can be expressed by the following equations:

$$V_1 = V_h \cos\alpha \cos\theta_1 + (V_t + w)\sin\theta_1 \quad (12)$$

$$V_2 = \cos(\beta_1 + \beta_2 - \alpha)\cos\theta_2 + (V_t + w)\sin\theta_2 \quad (13)$$

In these equations  $\beta_1$  and  $\theta_1$  respectively are the azimuth and elevation angles for  $R_1$ ;  $\beta_2$  and  $\theta_2$  respectively are the azimuth and elevation angles for  $R_2$ ;  $V_h$  is the horizontal motion speed;  $\alpha$  is the azimuth angle between the direction of the motion and  $\beta_1$ ;  $V_t + w$ , the particles' vertical velocity ( $V_t$  is the terminal speed and  $w$  the air vertical motion). If the contribution to the Doppler due to vertical motion can be neglected, i.e.,  $(V_t + w)\sin\theta \approx 0$ , equations (12) and (13) can be solved for  $V_h$  and  $\alpha$  according to the following expressions:

$$V_h^2 = \frac{1}{\sin^2(\beta_1 + \beta_2)} \left[ \frac{V_1^2}{\cos^2\theta_1} + \frac{V_2^2}{\cos^2\theta_2} + \frac{2V_1V_2\cos(\beta_1 + \beta_2)}{\cos\theta_1 \cos\theta_2} \right] \quad (14)$$

$$\tan \alpha = - \frac{1}{\sin(\beta_1 + \beta_2)} \left[ \frac{V_2 \cos\theta_1}{V_1 \cos\theta_2} + \cos(\beta_1 + \beta_2) \right] \quad (15)$$

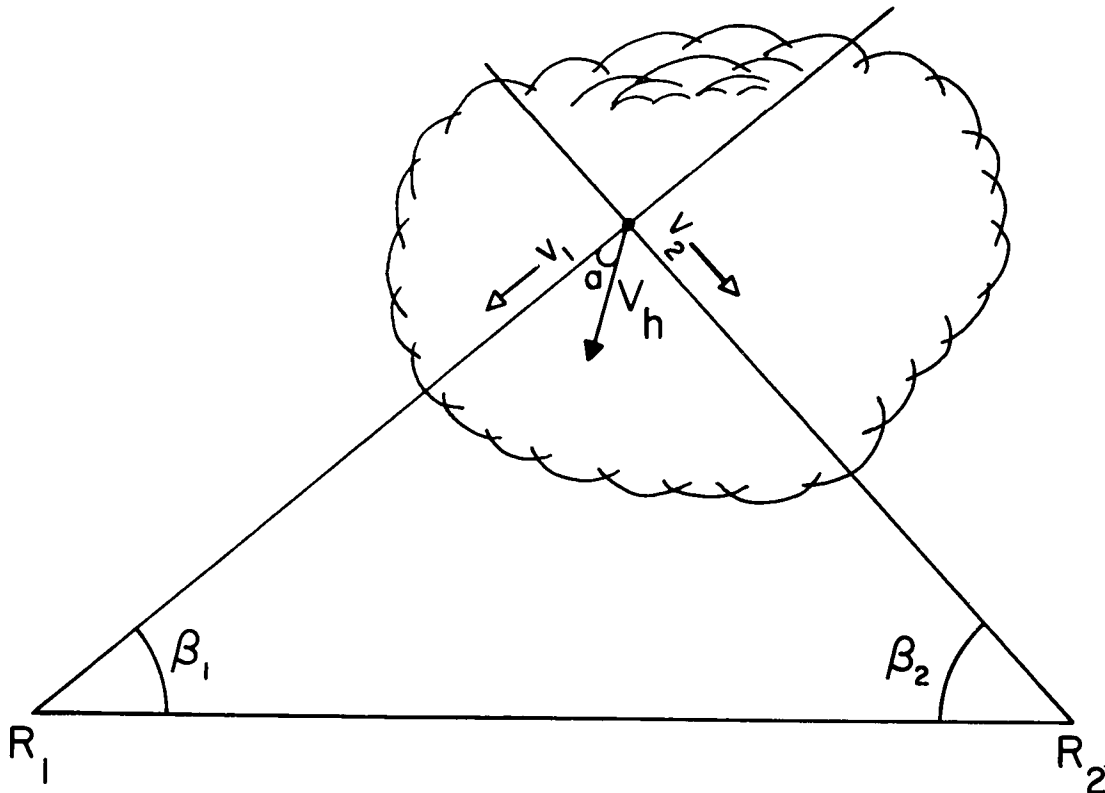


Figure 7. Measuring two-dimensional horizontal particle velocities by use of two Doppler radars observing the same storm from different directions.

The optimum spacing between the two radars depends on their characteristics but it is on the order of 20 to 60 kms.

The method offers excellent potential for mapping the particles' horizontal motion field inside convective cells for nearly horizontal radar beams. However, radar beam elevation angle smaller than 5° to 10° can be accepted in the scheme allowing the observation of the horizontal motion field up to altitudes on the order of 10,000 to 15,000 feet. The only assumption which is needed is to neglect the contribution due to particles' vertical motion. For targets which are outside of the line of sight between the two radars, the method offers accurate and non-ambiguous results which should clearly reveal convergence and vorticity patterns in the low levels of a convective storm.

If assumptions about the terminal velocity of the particles are adopted, the method can be extended to observations from larger elevation angles for which a significant contribution to the Doppler, due to the particles' vertical velocities, is likely. The method is also capable of providing estimates of the vertical air motion from convergence estimates made at several altitudes.

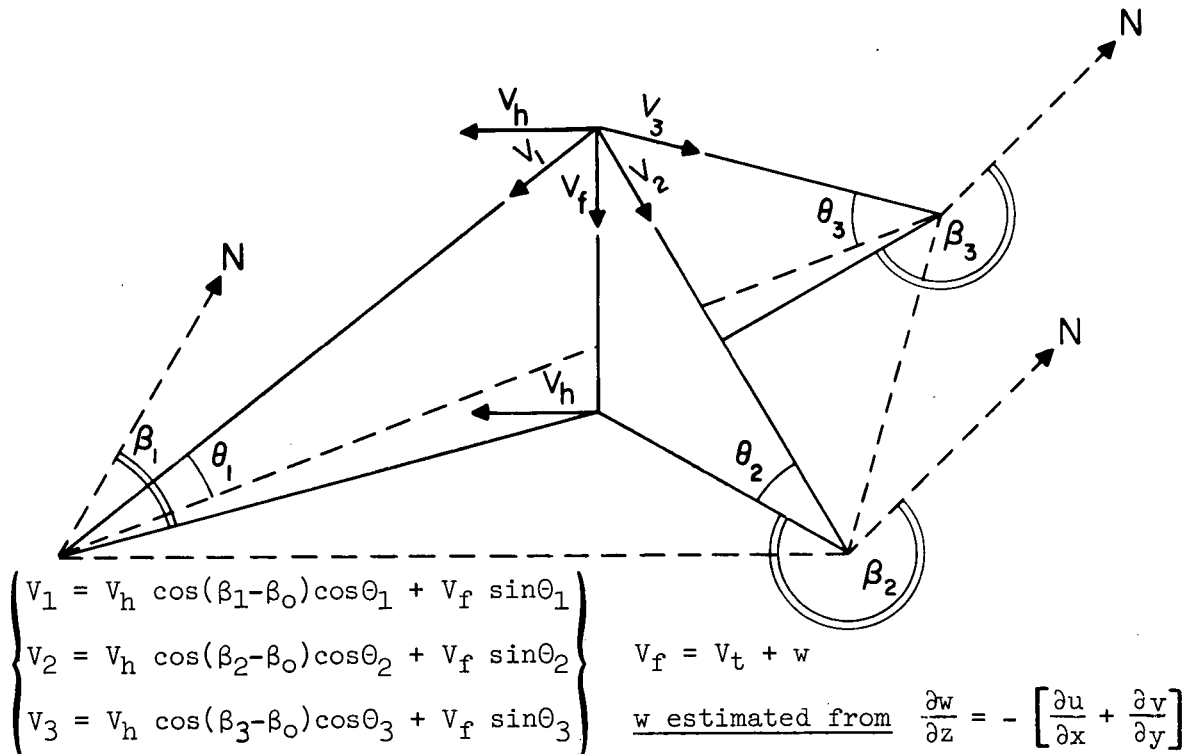


Figure 8. The three-Doppler radar method

Although it is a reasonable step towards the design of more elaborate systems, the dual Doppler radar method described above fails to provide useful horizontal wind information for targets situated on the line of sight between the two radars. It does not provide a complete knowledge of the three-dimensional field of the  $V_x$ ,  $V_y$ ,  $V_z$  components of the storm's particles' motion. This objective may be achieved from data collected by a well designed system of three Doppler radars, installed at three different locations which simultaneously observe the same convective storm. Figure 8 illustrates this concept and shows that the radial velocity at a given point in space can be observed from three different directions. The system of three equations indicated in Figure 6 provides the basis for computing the value of the three components of the motion. Therefore, by combining the radial velocity

information provided by the three Doppler radars, it is indeed possible to isolate and evaluate the three dimensional distribution, in Cartesian coordinates  $x, y, z$ , of  $V_x, V_y, V_z$ . This information can be sampled periodically provided that the storm is within the maximum range of the equipment. The time and space sampling capabilities are discussed below.

As an example of the unique capability of the method, the three dimensional field of particles' motion can be analyzed in the following manner:

First, it is assumed that precipitation particles are moving in the same direction and at the same speed as the horizontal wind. This assumption is valid except when particles are falling in regions of strong wind shear which might introduce a lag of the particles' velocity with respect to the environment. This effect is negligible for most of the precipitation particles; large hailstones are a marginal case. If we accept the above assumption, the particles horizontal motion field may be taken as that of the horizontal wind. The mean speed (first moment of the velocity spectrum) must be computed to provide basis for interpreting the two dimensional field. Theoretically, the estimated horizontal motion components do not include the variance due to particles' vertical speed distribution. The data are sorted according to their  $x, y$  and  $z$  coordinates evaluated from radar polar coordinates  $R, \beta$  and  $\Theta$ . The two dimensional estimates of the two quadratic components  $u$  and  $v$  of the estimated "wind" can then be defined at selected altitudes in the storm. The application of the equation of continuity, within the assumption of incompressibility, to the horizontal wind field, identified convergence with the estimates of air vertical velocity gradients,  $\partial w/\partial z$ . By integrating  $\partial w/\partial z$  with suitable boundary conditions, it is possible to estimate, not only one vertical updraft profile, but the complete structure of updrafts inside the whole storm. Details on the structure of updrafts will be controlled by the sharpness of the velocity gradients and the inherent velocity resolution of the radar equipment.

Comparison of the updrafts structure with the three dimensional distribution of the particles' vertical velocity (and its spectrum) which is derived simultaneously from the Doppler data, provides knowledge of the distribution of particles' terminal speed within the storm. This, in turn, provides means for defining, in any region of the observed storm the precipitation particles' terminal velocities and therefore their size distribution. The method has obvious application for the monitoring and study of such important processes as hail formation; its use should provide significant improvement of our knowledge of convective storm processes and provide a firm basis for a more efficient control of their behavior.

The three Doppler radar concept is far more complicated than the usual weather radar systems presently used in meteorological research. It can operate effectively only if efficient digital computer means are used to process the data. The Doppler information must by necessity be stored in a digital format compatible with computer use.

It is impractical and time consuming for the systematic scanning of a storm to restrict the Doppler observations obtained at a given time, to the intersection of the three radar beams in space. Indeed, when the radar beam is aimed in a fixed direction, a large number of ranges can be simultaneously

processed therefore adding to the Doppler information with respect to that provided by only one selected region. It is more appropriate that the radial velocity data provided by the three radars be acquired and processed separately, thereby leading to separate estimates of the three radial velocity fields. Since the process of scanning the storm will take an appreciable time, time-space interpolation techniques will be necessary to express the radial motion fields at the same time.

Radar beam scanning systems capable of systematically and automatically acquiring the Doppler data in limited angular regions controlled by the storm position with respect to the radar, are required for efficient use of the method. Digital control of a stepping radar beam must be preferred, as means for providing data easier to manipulate with digital computers.

The proposed method might seem to be difficult to implement because of the three-Doppler radar logistic problems involved. Let me make a few comments.

The velocity resolution of a well designed Doppler radar is sufficient to provide acceptable accuracy for estimating convergence or vorticity. If the radar beams are less than  $1^\circ$ , their cross section at distances of less than 50 kms ( $\leq 800$  m), will not seriously limit the value of the data and the experiments. Velocity ambiguities can be removed through assumption of continuity of the velocity field therefore providing large nonambiguous maximum ranges. Real-time processing of the data by digital computer in the field will bring serious logistic problems and might be beyond our present capabilities. They can be replaced by the processing, by a large computer, of the data stored on magnetic tape. The use of digital computer is recommended as providing objective methods for filtering, interpolating, and redigitizing the estimated least square field. In order to minimize the problems involved in directing three radar beams at the same time, to the same point in space, it is suggested that the X, Y, Z distribution of three radial velocity fields be separately estimated.

After the three radial velocity fields estimates are digitized in a three dimensional coordinates system common to the three radars, their combination in a set of equations aimed to restore the three components of the motion (and their spectra) will generate the X, Y, Z fields of the three components of particle speed discussed above.

It might be objected that the proposed scheme of three radars is much more sophisticated than the degree of complexity presently used in meteorological radar research. It really is, but it is still far from being as sophisticated as some military radars and certainly can be built at an acceptable cost. The approach to this objective is to design two mobile, low cost, radar prototypes using a wavelength leading to acceptable antenna size (X-band). The testing of these equipments in the field with appropriate Doppler signal recording systems will provide knowledge of the capabilities of the method and open the way for the three radar scheme.

Because of the unusual opportunities of the method and its unique potential for the study of three dimensionally distributed atmospheric phenomenon (such as convective storms), it is hoped that its implementation will represent the most significant contribution of Doppler radar techniques to the field of meteorology.

## 10. AIRBORNE PULSE DOPPLER RADAR

Ground-based equipment often suffers from lack of mobility e.g., when the observations require that the radar equipment be in close proximity of storms sparsely distributed over large areas. The airborne platform has the required mobility and can be used to analyze convective storm processes by pulse Doppler radar methods.

A vertical pulse Doppler radar beam can be carried by an airplane for the purpose of analyzing the observed vertical motion in a convective storm. The capability of the method is different from that of a ground-based vertically pointing Doppler radar, because the airplane can fly at a speed that is much higher than the storm motion. This capability would permit the vertical velocities of the storm particles to be observed and displayed in vertical cross section as the plane traverses the storm. Furthermore, this scheme could be repeated several times during the life of the storm therefore leading to an estimate of the three dimensional structure of particle vertical velocity. If medium ceiling airplanes are used, the scheme requires that the airplane fly through the storm, which is not applicable to the study of severe storms. However high-ceiling airplanes will have the capability of flying above the storm in regions where flight is not dangerous. The scheme was first proposed by Atlas (1962)\*. Logistic and technical problems were involved in the approach, which prevented actual experiments from being conducted. Since then, Doppler radar techniques have improved to the point that it is now feasible to consider that an airborne pulse Doppler radar can be developed at reasonable cost with acceptable chances of success. The magnetic tape recording of the signal aboard the airplane simplifies the scheme, and permits data acquisition techniques which are identical to the ones used by ground-based equipment.

The method can be extended to analyzing the wind field structure inside the storm by means of a side looking radar. Lhermitte and Weickmann (private communication) recommended that two airplanes, flying horizontally along perpendicular paths could look at the same storm, thereby providing the two components of the horizontal particle motion at flight level. This information will allow the estimate of the horizontal motion field, from which estimates of wind convergence can be derived. Slight tilt in the vertical plane of the side-looking radar beams, could provide some altitude scanning. This would allow the observation of the wind at different altitude levels without impairing the data by introducing significant vertical contribution due to the particle's velocities.

The airborne pulse Doppler radar scheme is particularly suited to the study of convective storms. The cost involved in conducting a feasibility study of the method can be held at a reasonable level by utilizing the techniques identical to these proposed for ground-based Doppler radars. Some of the problems related to the stability of the airborne platform can be solved by classical means or even by proper recording of the directional information for the radar antenna. The airplane is flying at a high speed (50 to 200 m per sec) therefore requiring that the beam be accurately perpendicular to the airplane motion. Smearing of the Doppler by the combination of the airplane's motion and the finite size of the beam will always occur. This effect can however be held to acceptable limits if the antenna width in

\*Private communication

the direction of the flight of the airplane is less than  $1^\circ$ . In view of the indicated potential it is therefore recommended that such studies be undertaken in the next few years.

## 11. CONCLUSION

It is hoped that this review of the applications of pulse Doppler radar techniques to the observation and study of atmospheric phenomena, has adequately demonstrated their excellent potential for solving urgent meteorological problems such as the monitoring and study of processes inside convective storms.

The present method of a ground-based single Doppler radar, with limited signal processing capabilities, suffers from two main weaknesses: (1) only the targets' radial velocity is observed; (2) the signal processing and attainable data reduction techniques fall far short of taking full advantage of the information pertaining to three dimensional fields of motion.

The opinion of the writer is that the subject of meteorological Doppler radars should be enlarged by extending the method to more sophisticated concepts, such as the design and application of a three Doppler radar technique assisted by adequate means for digital recording and processing of the Doppler spectrum. If we do so, the method will provide outstanding results in the study of currently undetectable and poorly understood meteorological phenomena such as convective storms and atmospheric turbulence.

Of course we should not forget that single Doppler radar techniques can also be used to improve the capabilities of conventional radar for the detection, monitoring, and tracking of storms.

The monitoring of hurricane evolution for instance, should be strengthened by continuous observations of the particle radial speed with a horizontal radar beam. Tornadoes might be more easily detected if information on particle radial speeds is added to the information on radar reflectivity. In order to retain the scanning capability of the radars, these techniques should preserve the two-dimensional display (PPI, RHI) of the information which is usual in conventional radar design. We therefore would recommend that radial velocity gating systems be used and that velocity contours be presented on PPI and RHI by use of appropriate methods.

## ACKNOWLEDGMENT

The author is indebted to Dr. C. Gordon Little for reviewing the manuscript and making helpful comments.

Mrs. Kathryn Kline deserves a special note of appreciation for her untiring assistance in preparing and typing of the manuscript.

REFERENCES

- Aoyagi, J., Fugiwara, M., Yangisawa, Z., and Kodaira, N., 1966: Doppler radar observations of snow showers; Proc. Twelfth Wea. Rad. Conf., Boston, American Met. Soc., 112-116.
- \*Aoyagi, Jiro, 1968: Mean Doppler Velocities of Precipitation near the Ground, 13th Radar Meteor. Conf., 22-25.
- \*Aoyagi, Jiro, 1968: A multi-channel Doppler frequency analyzer, 13th Radar Meteor. Conf., 324-327.
- \*Armstrong, Graham M., & Donaldson, R. J., Jr., 1968: A convenient indicator of tangential shear in radial velocity, 13th Radar Meteor. Conf., 50-52.
- Atlas, D., 1963: Radar analysis of severe storms, Meteor. Monograph, Vol. 5, No. 27, 177-220.
- Atlas, D., 1964: Advances in radar meteorology. Adv. Geo-phys., 10, New York Academic Press, 317-478.
- Atlas, D., Aoyagi, J., and Donaldson, R. J., Jr., 1965: Doppler analysis of the physical dynamics of a convective storm. Proc. Conf. Cloud Physics, Tokyo, 314-318.
- Atlas, D., 1966: The balance level in convective storms. J. Atmos. Sci., 23, 635-651.
- \*Atlas, D., and Tatehira, R., 1968: Precipitation-induced mesoscale wind perturbations, 13th Radar Meteor. Conf., 166-175.
- Battán, Louis J., 1963a: Some observations of vertical velocities and precipitation sizes in a thunderstorm. Proc. Tenth Weather Radar Conf., Boston, Amer. Meteor. Soc., 303-308.
- Battán, Louis J., 1963b: The vertical velocities of angel echoes. Proc. Tenth Weather Radar Conf., Boston, Amer. Meteor. Soc., 309-315.
- Battán, Louis J., 1964: Some observations of vertical velocities and precipitation sizes in a thunderstorm. J. Appl. Meteor., 3, 415-520.
- Battán, Louis J., and Theiss, J. B., 1967: Measurement of draft speeds in convective clouds by means of pulsed-Doppler radar, Univ. of Arizona, Inst. Atmos. Phys., Sci. Rept. No. 22, 23 pp.
- \*Battán, Louis J., and Theiss, John B., 1968: Measurement of draft speeds in convective clouds by means of pulsed-Doppler radar, 13th Radar Meteor. Conf., 26-29.
- Blackman, R. B., and Tukey, J. W., 1958: The measurement of power spectra. New York, Dover Publications, 190 pp.

- Boucher, R., Wexler, R. and Atlas, D. and Lhermitte, R., 1965: Meso-scale wind structure revealed by Doppler radar. *J. Appl. Meteor.*, 4, 590-597.
- \*Boucher, Roland J., 1968: Characteristics of turbulent structures observed by Doppler radar in snow., 13th Radar Meteor. Conf., 480-485.
- Boyenval, E. H., 1960: Echoes from precipitation using pulse Doppler radar, Proc. Eighth Wea. Radar Conf., Boston, Amer. Meteor. Soc., 57-64.
- Brantley, James Q., Jr., 1957: Some weather observations with a continuous wave Doppler radar. Proc. Sixth Wea. Radar Conf., Boston, Amer. Meteor. Soc., 297-306.
- \*Brook, Marx and Latham, D., 1968: The fluctuating radar echo. I. Modulation by vibrating Drops, 13th Radar Meteor. Conf., 2-7.
- \*Brown, Rodger A., and Peace, Robert L., Jr., 1968: Mesoanalysis of convective storms utilizing observations from two Doppler radars, 13th radar Meteor. Conf., 188-191.
- Browning, Keith A., and Atlas, D., 1966: Velocity characteristics of some clear air dot angels. *J. Atmos. Sci.*, 23, 592-604.
- Browning, K. A., and Wexler, R., 1966: The determination of kinematic properties of a wind field using a single Doppler radar. Proc. Twelfth Wea. Radar Conf., Boston Amer. Meteor. Soc., 125-127.
- Browning, K. A., and Wexler, R., 1968: A determination of kinematic properties of a wind field using Doppler radar. *J. Appl. Meteor.* 7, 105-113.
- \*Browning, K. A., Harrold, T. W., Whyman, A. M., and Beimers, J. G. D., 1968: Horizontal and vertical air motion, and precipitation growth, within a shower, 13th Radar Meteor. Conf., 122-127.
- Caton, P. G. G., 1963: The measurement of wind and convergence by Doppler radar. Proc. Tenth Wea. Radar Conf., Boston, Amer. Meteor. Soc., 290-296.
- Cooley, J. W. and Tukey, J., 1965: An algorithm for the machine calculation of complex Fourier series. *Mathematics of Computation*, 19, 297-301.
- Cox, E. G. and Groginsky, H. L., 1966: An analysis of the estimates of wind parameters using the VAD technique. Proc. Twelfth Wea. Rad. Conf., Boston Amer. Meteor. Soc. 44-51.
- Donaldson, R. J., Jr., Armstrong, G. M., and Atlas, D., 1966: Doppler measurements of horizontal and vertical motions in a paired instability line. Proc. Twelfth Conf. Radar Meteor., Boston Amer. Meteor. Soc., 392-397.
- Donaldson, R. J., 1967a: A preliminary report on Doppler radar observation of turbulence in a thunderstorm. Air Force Cambridge Research Laboratories Environmental Research Paper No. 255.

## ATMOSPHERIC PROBING BY DOPPLER RADAR

- Donaldson, R. J., 1967b: Horizontal wind measurement by Doppler radar in a severe squall line, Air Force Cambridge Research Laboratories, Proc. Conf. on Severe Local Storms, St. Louis, 89-98.
- Donaldson, R. J., Jr., 1968: Measurement of air motion in a thunderstorm anvil by Doppler radar. Paper presented at the 48th meeting Amer. Meteor. Soc., San Francisco.
- Donaldson, R. J., Jr., and Wexler, R. 1968: Notes on thunderstorm observation by fixed-beam Doppler radar. Journal of Atmos. Sci., Jan 1968, Vol 25, No. 1, 139-144.
- \*Donaldson, Ralph J., Jr., and Chmela, Albert C., 1968: Distribution of vertical velocity mean and variance in a thunderstorm, 13th Radar Meteor. Conf., 492-497.
- \*Dyer, Rosemary, 1968: Doppler measurements in stratiform rain, 13th Radar Meteor. Conf., 144-147.
- Easterbrook, C. C., 1967: Some Doppler radar measurement of circulation patterns in convective storms. J. Appl. Meteor., 6, 882-888.
- Glover, K., 1966: The feasibility of detecting shock waves by pulse Doppler radar, AFCRL-66-378, Environmental Research Paper #200.
- \*Glover, Kenneth M., Bishop, A. W., and Lob, W., 1968: Wind measurement by dual beam radar, 13th Radar Meteor. Conf., 456-463.
- Gorelik, A. G., 1965: Simultaneous measurements of Langrangian and Eulerian turbulence in snow precipitation. Atmospheric Oceanic Physics Series, Vol. 1, No. 9, 1965, 989-991, translated by Kenneth Syers.
- Gorelik, A. G., Kostarev, V. V., Chernikov, A. A., 1962: New possibilities of radar measurement of the wind. Meteorologiya i Gidrologiya, No. 7., Moscow, 1962, 34-39.
- Gorelik, A. G., Mel'Nichuk, V., Chernikov, A. A., 1965: The statistical characteristics of the radar echo as a function of the dynamic processes and microstructure of the meteorological entity, AFCRL August 1965, T-R-479.
- Gorelik, A. G., et al, 1965: The coordinate-Doppler method of wind observation, American Meteor. Soc., Boston, Dec. 1965.
- Gorelik, A. G. and Mel'Nichuk, V., 1966: Radar measurements of turbulent parameters in clouds and precipitations (Abstract only) Proc. Twelfth Wea. Radar Conf., Boston Amer. Meteor. Soc. 104.
- \*Gorelik, A. G., 1968: Wind structure investigations of boundary layer by radar "clear air" returns, 13th Radar Meteor. Conf., 248-251.
- \*Gorelik, A. G., and Logunov, V. F., 1968: Determination of vertical air motion velocity in rainfall by Doppler radar, 13th Radar Meteor. Conf. 18-21.

- Groginsky, H. L., 1966: Digital processing of the spectra of pulse Doppler radar precipitation echoes, Proc. Twelfth Wea. Rad. Conf., Boston Amer. Meteor. Soc., 34-43.
- \*Groginsky, Herbert L., 1968: Unambiguous measurement of updraft velocity and drop size distribution. 13th Radar Meteor. Conf., 30-34.
- \*Groginsky, Hervert L., 1968: Scanning requirements of the (VAD) operation of a pulse Doppler weather radar. 13th Radar Meteor. Conf., (abstract of late paper). p 35.
- Harrold, T. W., 1966: Measurement of horizontal convergence in precipitation using a Doppler radar - a case study. Quart. J. R. Meteor. Soc., 92, 31-40.
- Harrold, T. W., and Browning, K. A., 1967: Mesoscale wind fluctuations below 1500 meters, Meteorological Magazine, Vol. 96, 367-376.
- \*Harrold, T. W. and Browning, K. A., 1968: Low-level airflow at a cold front, 13th Radar Meteor. Conf., 222-225.
- Holmes, D. W., and R. L. Smith, 1958: Doppler radar for weather investigations. Proc. Seventh Wea. Radar Conf., Boston, Amer. Meteor. Soc. F-29 to F-33.
- Kodaira, Nobuhiko, 1964: A pulsed-Doppler radar for weather observations. Proc. Wea. Conf. on Rad. Meteor., Boston, Amer. Meteor. Soc., 300-303.
- Kodaira, N., and Zenji Yanagisawa, 1965: The MRI pulse Doppler radar. Proc. Internat. Conf. on Cloud Physics, Tokyo, 309-313.
- Lhermitte, Roger M., 1960a: Variations de la vitesse de chute des particules d'une précipitation étendue, a différents niveaux. Comptes Rendus des Séances de l'Académie des Sciences, 250, 899-901.
- Lhermitte, Roger M., 1960b: The use of a special pulse Doppler radar in measurement of particles fall velocities. Proc. Eighth Wea. Radar Conf., Boston, Amer. Meteor. Soc., 269-275.
- Lhermitte, Roger M., 1962: Note on wind variability with Doppler radar. J. Atmos. Sci., 19, 343-346.
- Lhermitte, Roger M., 1963: Weather echoes in Doppler and conventional radars. Proc. Tenth Wea. Radar Conf., Boston, Amer. Meteor. Soc., 323-329.
- Lhermitte, Roger M., 1964: Doppler radars as severe storm sensors. Bul. Amer. Meteor. Soc., 45, 587-596.
- Lhermitte, Roger M., 1966: Probing air motion by Doppler analysis of radar clear air returns. J. Atmos. Sci., 23, 575-591.
- Lhermitte, Roger M., 1966: Application of pulse Doppler radar technique to meteorology. Bul. Amer. Meteor. Soc., Vol. 47, No. 9, Sep 1966, 703-711.

ATMOSPHERIC PROBING BY DOPPLER RADAR

- Lhermitte, Roger M., 1966: Doppler observation of particle velocities in a snowstorm. Proc. Twelfth Wea. Rad. Conf., Boston, Amer. Meteor. Soc., 117-124.
- Lhermitte, Roger M., and Atlas, D., 1961: Precipitation motion by pulse Doppler radar, Proc. Ninth Wea. Radar Conf., Boston, Amer. Meteor. Soc., 218-223.
- Lhermitte, Roger M., and Atlas, D., 1963: Doppler fall speed and particle growth in stratiform precipitation. Proc. Tenth Wea. Radar Conf., Boston, Amer. Meteor. Soc., 297-302.
- Lhermitte, R. M., and Kessler, Edwin, 1964: An experimental pulse Doppler radar for severe storm investigations. World Conf. on Radio Meteor., Boston, Amer. Meteor. Soc., 304-309.
- Lhermitte, R. M., and Dooley, J., 1966: Study of the motion of clear air targets. Proc. Twelfth Wea. Radar Conf., Boston, Amer. Meteor. Soc., 293-299.
- \*Lhermitte, Roger M., 1968a: New developments in Doppler radar methods. 13th Radar Meteor. Conf., 14-17.
- \*Lhermitte, Roger M., 1968b: Turbulent air motion as observed by Doppler radar, 13th Radar Meteor. Conf., 498-503.
- \*Peace, Robert L., Jr., and Brown, Rodger A., 1968: Single and double radar velocity measurements in convective storms, 13th Radar Meteor. Conf., 464-470.
- Peace, Robert L., Jr., et al, 1968: Horizontal motion field observations with a single pulse Doppler radar, Cornell Aero. Lab Report.
- Pilié, R. J., Jiusto, J. E., Rogers, R. R., 1963: Wind velocity measurement with Doppler radar. Proc. Tenth Wea. Radar Conf., Boston, Amer. Meteor. Soc., 329a-329L.
- Probert-Jones, J. R., 1960: The analysis of Doppler radar echoes from precipitation. Proc. Eighth Wea. Radar Conf., Boston, Amer. Meteor. Soc., 377-385.
- Probert-Jones, J. R., and Harper, W. G., 1961: Vertical air motion in showers as revealed by Doppler radar. Proc. Ninth Wea. Radar Conf., Boston, Amer. Meteor. Soc., 225-232.
- Rogers, R. R., 1963: Investigation of precipitation processes. Technical Report, Cornell Aero Lab., Inc., 1-17.
- Rogers, R. R., 1964: An extension of the Z-R relationship for Doppler radar. World Conf. Rad. Meteor. and Eleventh Wea. Rad. Conf., 158-160.
- Rogers, R. R., 1966: Doppler radar investigation of Hawaiian rain. Proc. Twelfth Wea. Rad. Conf., Boston, Amer. Meteor. Soc., 128-134.

- Rogers, R. R., 1966: Project Hawaii - an investigation of rain on the island of Hawaii, Technical Report, CAL No. VC-2049-P-1, Cornell
- Rogers, R. R., and Chimera, A. J., 1960: Doppler spectra from meteorological radar targets. Proc. Eighth Wea. Radar Conf., Boston, Amer. Meteor. Soc., 377-385.
- Rogers, R. R., and Pilie, R. J., 1962: Radar measurements of drop size distribution. J. Atmos. Sci., 19, 503-506.
- \*Sloss, Peter W., and Atlas, David, 1968: Wind shear and reflectivity gradient effects on Doppler radar spectra, 13th Radar Meteor. Conf., 44-49.
- Spilhaus, A. F., 1948: The distribution of raindrops with size. J. Meteor., 5, 161-164.
- \*Tatehira, R., and Srivastava, R. C., 1968: Note on updraft estimation with Doppler radar, 13th Radar Meteor. Conf., 36-43.
- Theiss, J. B., 1963: More target data with sideband coherent data. Electronics, 36, 40-43.
- Tripp, Riley, 1964: The CAL pulse Doppler radar. World Conf. Radio Meteor., Boston, Amer. Meteor. Soc., 330-337.
- Wexler, R., Chemla, A. C., and Armstrong, G. M., 1967: Wind field observations by Doppler radar in a New England snowstorm, Published in December issue of Monthly Weather Review.
- \*Wexler, R., 1968: Doppler radar measurements in a rainstorm with a spiral band structure, 13th Radar Meteor. Conf., 192-193.
- Wilson, D., 1963: Drop size distribution as recorded by pulsed Doppler radar. U. of Arizona Masters' thesis.

---

\* presented at McGill University, Montreal, Canada, 13th Radar Meteorology Conference

PRECEDING PAGE BLANK NOT FILMED

N 72-25365

## COMMENTS ON DOPPLER RADAR APPLICATIONS

Edwin Kessler

National Severe Storms Laboratory  
Norman, Oklahoma

By correspondence from your Chairman, I have been invited to serve as a sort of "devil's advocate," and to contribute to a balanced view of Doppler radar applications. Since I substantially agree with Dr. Lhermitte, the brief comments below are presented only with the thought of shifting some of the points of emphasis.

Dr. Lhermitte's report, following the Terms of Reference of the Panel and the suggested format for review papers, discusses the experimental techniques before their meteorological relevance. There should be many competent scientists dedicated to the advance of scientific instrumentation, but we note the dichotomy that exists between groups whose first concern is with problems of applications and those groups which primarily consider the instrument to be applied. This situation is recognized in the Panel's Terms of Reference, which requests recommendations concerning "means of encouraging meteorological participation in remote sensing programs." However, some meteorologists may be legitimately uninterested in some kinds of remote atmospheric sensing, and we should consider the distinction between application of remote sensing data for understanding meteorological processes, and the use of such data by the weather science services. A panel of meteorologists might well encourage more participation by remote-sensing specialists in meteorology programs!

The relatively small size and transitory nature of severe local storms have been serious impediments to their observation by conventional means, and we are especially pressed to develop remote probes for use in these cases. I would certainly expect continuation of the kinds of multi-Doppler studies discussed by Dr. Lhermitte, with emphasis placed where there is most relevance to important theoretical or applied meteorological problems. For example, Doppler methods may provide improved estimates of the field of air motions in thunderstorms -- fundamental parameters are the rotational properties of thunderstorm air and the distribution and magnitude of air mass

## COMMENTS ON DOPPLER RADAR APPLICATIONS

sources and sinks. Measurements of air flow at particular points when linked with the equations of continuity for moisture and wind and the equations of dynamical meteorology, should help greatly to define the physical basis of severe local storms.

While having great interest and concern for advanced problems, let us not leap-frog apparently simpler problems which have great practical importance. For example, the community of aviation interests requires measurements of turbulence in storms, more representative than the indications of reflectivity measurements. The R-meter concept first developed at MIT over 10 years ago, but never fairly tried, offers one possibility for such turbulence measurement. The R-meter displays the rate of echo amplitude level crossings, which indicates the width of the Doppler spectrum. Full Doppler capability is not required for level crossing measurements, but only a conventional radar with a very stable magnetron. This approach might also enable us to identify a tornado, or better, an incipient tornado, more adequately than is done at present from radar reflectivity and echo shape. Since the Doppler spectrum of a tornado must be very wide, corresponding to the strong winds and wind gradients characteristic of that phenomenon, a relatively primitive Doppler capability might prove adequate for operational warning. Of course, the probable small reflectivity of the tornado funnel may be an important difficulty, but we will not really know how important such problems are until we undertake their systematic investigation. It should be noted also that methods for clearly identifying thunderstorms which harbor severe turbulence and tornadoes would have very important applications to basic research in meteorology.

The potential applications of radar to the detection of turbulence and tornadoes illustrate that Doppler-research capabilities of rather ordinary non-coherent radars, not to mention single Doppler radars, are far from exhausted. In fact, relatively simple equipment can be effectively utilized for many important theoretical and practical investigations, and deserves much more attention.

I would emphasize that radar-meteorology programs should be complemented by the inputs from a variety of sensors. Major interests today are more than ever directed to meteorological processes in their interaction rather than in isolation. For example, storm circulations cannot be properly understood without data concerning temperature, winds, and moisture in the clear air environment, and such data can probably not be adequately provided by radar. An observational program to gather meaningful data from a variety of sensors contemporaneously requires expensive facilities and a number of competent investigators working in cooperation toward a shared objective. The development of such cooperative relationships among investigators and the facilities available to them should continue to be encouraged.

Of course, we notice also that there are important singular problems which can be addressed on an ad hoc basis by an individual scientist with a highly specialized objective. Since there are many indirect probing facilities already developed in this country and utilized a rather low percentage of the time, I hope individual scientists will be encouraged to make use of these facilities, and to avoid, where practical, expensive new facilities programs.

N72-25366

COMMENTS ON HIGH-POWER HIGH-RESOLUTION RADARS

J. S. Marshall

McGill University

For observing precipitation, in terms of its intensity, increases in power and resolution could make good tools better. For precipitation intensity, however, it is not these changes that are vital, but rather a departure from use of a single attenuating wavelength (without lessening existing standards of resolution and sensitivity).

Angels: For angels, the situation is different. To move one step at a time, the situation was different when the Wallops Island Observations were undertaken by Atlas, et al. Let us define angels, for now at any rate, as targets yielding radar returns from a clear sky, distinguishing between true angels (inhomogeneities in the dielectric constant of the gaseous atmosphere, usually in the water-vapour concentration) and pseudo-angels (usually one or more birds or insects). True angels are related to the inhomogeneities that make possible radio scatter-propagation, and to those that are measured by "microwave refractometers", although distributions with frequency and gradient tend to differ for the three cases: radar, radio, refractometer. The situation, then, was that several scientists had a proper interest in true angels, and were busily engaged in observing angels, and interpreting them as true angels, even though this required some ingenuity. It was recognized, at the same time, that birds and insects could serve as radar targets; indeed, radar was being used by some to observe birds per se, and as hazards to aircraft. There had been fifteen years of debate as to the fraction of apparent angels that were biological rather than ethereal.

That was the state of affairs when Atlas designed and led in the execution of the Wallops Island experiment, using three radars having roughly the same beamwidth but differing in wavelength, and having enough power to see angels of one sort or another out to a good range. Some angels reflected better at a longer wavelength, so it was possible to remove the ambiguity between true and pseudo-angels, or to do so within those observations at any rate.

## COMMENTS ON HIGH-POWER HIGH-RESOLUTION RADARS

The experiment demonstrated the use of a "biological filter", based principally on variation of reflectivity with wavelength. It demonstrated the great field of observation available to radar installations several times larger than those assigned to meteorological studies in the past. At the same time, it made possible, by the new insights it provided, the more effective use of smaller, traditional installations.

The Wallops Island experiment was a perfect example of the opportune use for a scientific purpose of short-term-available scientific equipment. It does not follow that the equipment used then was the ideal establishment, either for solving the particular problem or for a continuing more general programme. One question that would arise, for example, is whether continued use of three wavelengths (rather than two) would be justified. Such questions can be raised usefully for conference discussion, but it could be unwise to base decisions directly on immediate answers.

Doppler radar gives the velocity of precipitation particles in a storm (or of any other point targets). More specifically, Doppler radar gives the radial component of such velocity, toward the radar, and usually quite reasonable and plausible assumptions can be made to convert radial component to vector velocity. Dr. Lhermitte would remove the need for these assumptions, by installing three radars at the points of a large triangle. The new tool thus created would be a powerful one. It would surely be complex.

I hope that Dr. Lhermitte's proposal can be supported, and I believe that it would be an excellent investment in major equipment. I hope at the same time that those of us who use radar without Doppler can carry on in our conservative habits with clear consciences. These hopes both have logical basis. Perhaps I may be permitted to use personalities and anecdotes to support them.

For myself, Lord Rayleigh's 1870 paper "on the light from the sky, its polarization and colour" is inspired gospel. It was written not only before the Lord was a Lord, but before Clerk Maxwell's equations. Thus, as I see it, weather radar was brought into the world to exploit Rayleigh scattering, with its simple relationship to particle size, and wavelength, and why the sky is blue. For me, the thing to measure is target intensity, as far out as storms can be seen over a curved earth. Suggestions that every radar should have a Doppler capability I resist, because I always suspect that with Doppler the radar is no longer optimal for intensity, or is reduced in the range to which it reaches. My opinion will change with enlightenment, but give me time.

For Roger Lhermitte, Doppler is a different matter. Doppler has been put to good use in weather radar by several scientists, and much credit goes

in particular to the unswerving interest in this technique of Dr. Lhermitte. Existing use, though, does tend to depend on assumptions, usually quite reasonable ones. Dr. Lhermitte sees a technical breakthrough that makes those assumptions unnecessary. This would make a world of difference in the case of the severe storm, where assumptions cannot be given great trust. The technical breakthrough involves one of those major jumps in the size of installation involved. This jump to a major installation is justified. In support of which claim, I recall an anecdote from the thirties, involving Queen Mary and the Chairman of the Board.

Actually, it is the ship Queen Mary that comes into the story. She was a much larger ship than anything before, and considerably faster. Her construction was complicated and delayed by the depression, and there was a need to justify her completion. The Chairman of Cunard made this justification, at the launching I believe it was. The Queen Mary, he said, was simply the smallest and slowest ship that, with just one sister, could maintain a weekly service between European ports and New York. Now, this comment could be put down to understatement for effect (and British understatement tends to be for effect, rather than self-effacement). But Sir Percy had a good point, worth remembering: is the proposed system the slowest and smallest that will do the job to a reasonable schedule; then is it worth the cost to get the job done?

Examples of this "Cunard criterion" can be found closer to home. Dr. Atlas has demonstrated in the Wallops Island experiment how one major experiment was just large enough in its capability to settle an argument that had continued through years of smaller-scale experimentation. Dr. Pierce, in another context and on a more modest scale, has indicated how a national sferics facility, somewhat larger than we are used to, might make a major increase in the effective use of sferics techniques. Dr. Lhermitte's proposal for a Doppler triangle impresses one as an economical solution to the problem of measuring vector velocities in a storm. Experience to date can give us confidence, on the one hand, that the proposal is the smallest and simplest that will do the job to a reasonable schedule, and on the other, that the state of the art is now quite ready for the undertaking.

SESSION 5

Radio  
Tropospheric  
Scatter

A REVIEW OF TRANSHORIZON PROPAGATION  
AS A POSSIBLE TOOL FOR  
REMOTE PROBING OF THE ATMOSPHERE

Donald C. Cox

Stanford Electronics Laboratories

ABSTRACT

This report reviews transhorizon propagation experiments from the viewpoint of their possible use as remote atmospheric probes. It is concluded that the state or structure of the atmosphere cannot be inferred unambiguously from measurement techniques used in experiments reported to date. Extensions or combinations of available techniques, however, appear promising for use in the remote probing of the atmosphere.

1. INTRODUCTION

This report considers the topic of transhorizon propagation or tropospheric scatter in the light of its possible use as a technique for the remote probing of the earth's atmosphere. This technique, like all radio techniques, can yield information only about the index of refraction or dielectric constant of the atmosphere. Since the mechanism which is usually involved in the transmission of these UHF or microwave radio signals beyond the optical horizon is the refractive index variations or fluctuations in the atmosphere, these variations or fluctuations are the parameters which can most readily be studied by this measurement technique. This report does not deal with the topics of "ducting" or other average refractive effects or with the effects of rain or other precipitation. Some of the atmospheric parameters which are possible candidates for study using transhorizon propagation measurements are

## TRANSHORIZON PROPAGATION

1. drift (wind) and internal motions as they affect the doppler spectrum or fading of the radio signals;
2. statistical characteristics or properties of the random fluctuations or variations in the atmosphere as they are related to frequency and angular dependence of the mean scattered power;
3. nonuniformities in the statistical characteristics of the atmosphere such as inhomogeneity or anisotropy which exist to a scale resolvable by practical measuring devices (usually antennas);
4. stratification tendencies in the atmosphere.

Currently these parameters cannot be determined with much certainty as will be seen in the following review of reported transhorizon propagation experiments.

In this report the term "remote probing" is interpreted to mean the unambiguous determination of the state or structure of the atmosphere or the quantitative determination of some atmospheric parameter from radio measurements made at locations (usually on the ground) remote from the region being investigated. All information necessary for determining the parameter value or atmospheric state should be contained in the radio measurements themselves or in other simultaneously made measurements, that is, it should not be necessary to include in the interpretation of the state or the parameter value any assumptions which are not supportable by the direct measurements themselves. The measured atmospheric parameters may be localized in time (fractions of seconds) or space (a few feet) or may be averaged over some larger region in space (hundreds or thousands of feet) or time (a few hours). Parameters averaged over extremes of space (for example the atmosphere from the earth's surface to the end of the sensible atmosphere) or time (over many hours or even days) are not considered useful in defining the state of the atmosphere with remote probing. Because of these quite definitive requirements placed on the interpretation of the words "remote probing" this report tends to be somewhat pessimistic in its view of results from transhorizon propagation experiments which have been conducted in the past.

Much of the early work in transhorizon radio propagation was concerned with communications system applications and the parameters which were measured in experiments were usually long-term averages which were not very useful for determining atmospheric characteristics at any given time. A screening of the literature has been made and experiments which deal with parameters which are of use only to communications system designers are not included in this review. That is, this report concerns itself

with the subject of transhorizon propagation only as it relates to remote probing of the atmosphere.

## 2. A BRIEF REVIEW OF THE THEORY OF TRANSHORIZON PROPAGATION

The theories which attempt to describe transhorizon propagation phenomena can usually be classified into two groups. The models which are used to describe the variations or fluctuations in the refractive index of the atmosphere are the major distinguishing features of the groups.

### 2.1 The Turbulence Theories

By far the greatest effort expended in trying to describe the transhorizon propagation phenomena has been based on a statistical description of turbulence in the atmosphere. A rather extensive review of this subject can be found in Staras and Wheelon (1959). The subject has been treated by many authors (for example, Booker and Gordon 1950; Staras 1952, 1955; Gordon 1955; Booker and de Bettencourt 1955; Villars and Weisskopf 1955; Balser 1957; Wheelon 1957, 1959; Bolgiano 1960). In the turbulence treatment, the refractive index (or dielectric permittivity) fluctuations are described as a small random change about mean level. Early work (for example, Booker and Gordon, 1950) dealt with the time fluctuations at a point in space; however, later work proceeds from the three-dimensional spatial variations (for example, Staras, 1955 or Wheelon, 1959). The formalism in either case proceeds along similar lines.

The dielectric permittivity can be expressed as  $\epsilon(\vec{r}, t) = \bar{\epsilon} + \Delta\epsilon(\vec{r}, t)$  where  $\vec{r}$  is a 3-dimensional space vector and  $\bar{\epsilon}$  is the mean of the permittivity. In most cases  $\Delta\epsilon(\vec{r}, t)$  is treated as a random process which is stationary in time and both homogeneous and isotropic in space. Associated with  $C(\vec{R}, t) = \langle \Delta\epsilon(\vec{r}, t) \cdot \Delta\epsilon(\vec{r} + \vec{R}, t) \rangle$ , the correlation function, is a spectrum  $\Phi(k)$  related to the correlation function by

$$C(\vec{R}) = \int_V \Phi(\vec{k}) \epsilon^{j\vec{k} \cdot (\vec{R})} d^3\vec{k}$$

with time variation suppressed. For the typical transhorizon propagation path geometry in Fig. 1, the wave equation is solved (Staras and Wheelon, 1959; Balser, 1957; Wheelon, 1959; Staras, 1952) using the Born (Single-scattering) approximation to yield an equation for the ratio of received power to transmitted power

$\frac{P_R}{P_T}$ . Omitting constants of proportionality,

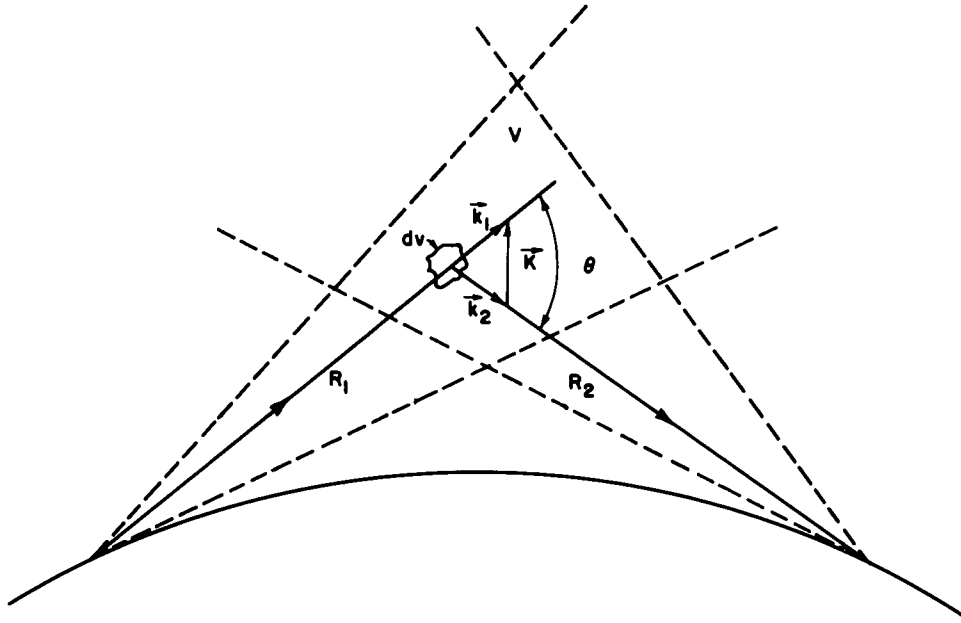


FIG. 1 PATH GEOMETRY FOR TURBULENCE THEORY

$$\frac{P_R}{P_T} \propto \frac{1}{\lambda^2} \int_V \frac{G_T G_R}{R_1^2 R_2^2} \Phi(\vec{K}) d^3 v$$

where the G's are gains of the transmitting and receiving antennas and K is the particular wavenumber  $|\vec{K}| = \frac{4\pi}{\lambda} \sin \frac{\theta}{2}$ . (Staras and Wheelon, 1959. This is often expressed as a function of scattering cross section  $\sigma(\vec{K})$  as

$$\frac{P_R}{P_T} \propto \lambda^2 \int_V \frac{G_T G_R}{R_1^2 R_2^2} \sigma(\vec{K}) d^3 v$$

where  $\sigma(\vec{K}) = \frac{\pi^2}{\lambda^4} \Phi(\vec{K})$  (Staras and Wheelon, 1959).

For antennas with beams sufficiently narrow so that  $\sigma(\vec{K})$  is approximately constant over the region in space,  $\Delta V$ , within

the half-power beamwidths of both antennas, the narrow-beam approximation can be applied and the integration can be reduced to a product

$$\frac{P_R}{P_T} \approx \lambda^2 \frac{G_T G_R}{R^4} \sigma(\vec{K}) \Delta V$$

Most of the experimental work reported in the literature is compared in some way with equations derived as described above.

For inhomogeneity in the statistics of the refractive index fluctuations, the spectrum  $\Phi(\vec{K})$  is in some way a function of the spatial coordinates  $(\vec{r})$ . For anisotropy in the statistics, the spectrum  $\Phi(\vec{K})$  is a function of the orientation of the  $\vec{K}$  vector as well as of its magnitude. Some effects of anisotropy have been treated theoretically (for example, see Staras 1955). Nonstationarity is a situation wherein the spectrum  $\Phi(\vec{K})$  is a function of time and is usually (but not always) slowly varying compared with the random fluctuations which make up the spectrum itself.

In the past much discussion has centered about the shape of the spectrum  $\Phi(\vec{K})$  but currently the Kolmogorov spectrum which exhibits an input range at small values of  $\vec{K}$ , an inertial subrange in which  $\Phi(\vec{K}) \propto \frac{1}{K^{11/3}}$ , and a dissipation range for large values of  $\vec{K}$  (for an example of this spectrum see Staras and Wheelon 1959) seems to be quite generally accepted. Since experiments do not appear to bear out the universal validity of this spectrum, however, (see the review of experiments in this report) another possibility which includes a buoyancy sub-range has been proposed by Bolgiano (1962). Various developments based on turbulence theory, such as synchronous beam swinging estimates (Booker and de Bettencourt 1955), have been made. In beam swinging, for example,  $\theta$  is varied in the experiment thus varying  $\Phi(\vec{K})$

since  $|\vec{K}| = \frac{4\pi}{\lambda} \sin \frac{\theta}{2}$ . The measured  $P_R$  is then proportional to  $\Phi(\vec{K})$ . In the general case where beams cannot be considered narrow the volume integration is quite difficult.

The subject of signal fading due to drift and internal motions has been treated only lightly in the literature as have other subjects such as transmission bandwidths and instantaneous signal estimates.

2.2 Layer Theories

These theories are based on partial reflection from stratified atmospheric layers which exhibit a relatively large change in refractive index (dielectric permittivity) over a short distance (usually height). Theoretical development based on this description of the variation in index of refraction has not been as extensive as that based on turbulence. Major contributions are contained in Bauer (1956), Friis, et al., (1957) and du Castel (1966).

The starting point for the layer theories is the amplitude (voltage) reflection coefficient for an abrupt, infinite dielectric discontinuity with index of refraction change across the discontinuity of  $\Delta n = |n_2 - n_1|$ . This reflection coefficient ( $\rho$ ) is derived in almost all texts in electromagnetic theory and for the small angles involved in the transhorizon propagation geometry it simplifies to  $\rho \approx \frac{2\Delta n}{\theta^2}$  where  $\theta$  is the scattering angle. (See Fig. 2).

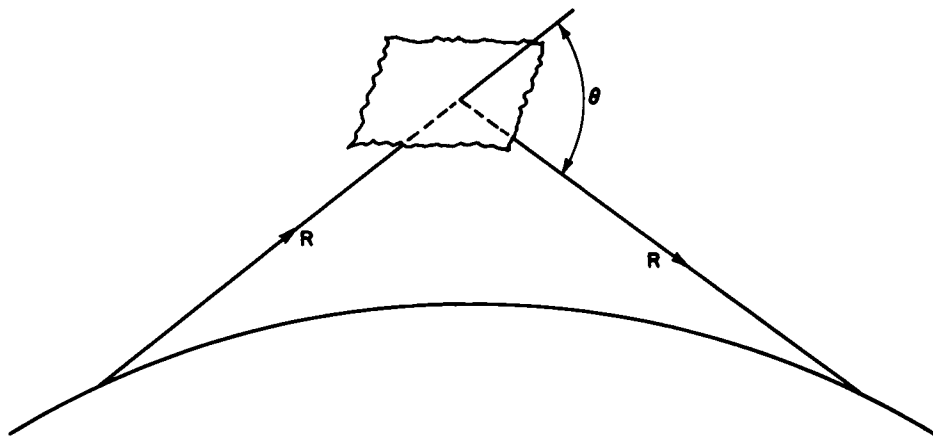


FIG. 2 PATH GEOMETRY FOR LAYER THEORY

If the discontinuity is gradual (as it probably is for the atmosphere) then the reflection coefficient takes on a frequency dependence, an angular dependence and layer thickness dependence (Wait 1964). The ratio of received power to transmitted power for an infinite layer is given by

$$\frac{P_R}{P_T} = \frac{G_T G_R}{64\pi^2} \frac{\lambda^2}{R^2} \rho^2$$

where again the G's are the antenna gains and R is the distance between receiver and transmitter. For finite layers Fresnel zone effects enter into this ratio and for layers small compared to a Fresnel zone a scattering cross-section situation exists again and

$$\frac{P_R}{P_T} = \frac{G_T G_R}{16\pi^2} \frac{\rho^2}{R^4} \left(A \frac{\theta}{2}\right)^2 \quad (\text{Friis, et al. 1957})$$

where the symbols are as before and A is the area of the layer.

Statistics may enter this theory, for example, in the spatial distribution of layers, in size and intensity distributions and in distributions of curvature for non-flat layers (du Castel 1966).

Layer theory results have been compared with experimental results by Crawford, et al., (1959). The agreement does not seem to be any better or any worse than the agreement between other experiments and theories based on turbulence models.

Signal level distributions, doppler spectrum, focusing effects, and instantaneous signal characteristics for sinusoidally shaped layers have been treated by Waterman and Strohbehn (1963) and Gjessing (1964). The possibility that large angular velocities may be produced by fleeting reflection points on irregular surfaces is demonstrated by these investigators. The treatment of signal characteristics in general from the viewpoint of layer theories is still in an elementary state.

The layer theories have been generally used to describe transhorizon signal characteristics in a deterministic manner while the turbulence theories inherently describe only the statistics of those signals.

This is by no means a comprehensive review of all the theory of transhorizon propagation but it includes most of the main areas of development and should provide a basis for viewing the experimental work in the next section. The theory of transhorizon propagation mechanisms is far from complete. The development of topics such as envelope fading and doppler spectrum of the radio signal has been barely started. It would appear that because of the variability in the results from different time periods the subject of transhorizon propagation theory might benefit at this time by being approached more strongly from the viewpoint of explaining each individual experimental observation for each limited time period, rather than by trying to find universal constants to fit averages over long time periods and over many experiments.

## 3. EXPERIMENTAL PROGRESS

Many of the early experiments in transhorizon radio propagation were conducted to determine the long-term statistical characteristics of the transhorizon signals because these parameters are of interest to designers of communications systems. In experiments of this type, parameters such as mean signal level, signal level distributions (for determining communications reliability), usable frequency bandwidths, and effective antenna size (aperture-to-medium coupling loss) were measured, usually as long term averages. These measurements were made at different frequencies and over transmission paths of different lengths over different terrains and with different minimum scattering angles. While these experiments were invaluable in the development of the transhorizon propagation mechanism as a communications medium, the long-term averages and simple parameters measured could be used almost equally well to support either theories based on atmospheric turbulence or theories based on reflection from atmospheric layers. It seems that for the purpose of probing the atmosphere, measurements which could be used to determine the state of the atmosphere over time periods of a few minutes to a few hours are desirable. Also because of the complex nature of the atmosphere it appears that the simultaneous measurement of several separate parameters is required to produce a good description of its state. For these reasons, experimental works in the field of transhorizon propagation have been screened and those which do not appear to contribute substantially to the question of remote probing (i.e., do not have sufficient "resolution") (for example: Ames, et al., 1955; Bullington, et al., 1955; Janes and Wells 1955; Rogers 1955; Yeh 1966; Mellen, et al., 1955) have not been included in this report. A number of works, however, whose major effort is along the communications system line but which also contain a few measurements of the types considered later in this section are included.

Experiments which involve the measurement of total path phase, doppler spectrum and group delay and which make use of phase-coherent measurements between precision frequency sources are omitted from this report because they are being reported on by Professor W. P. Birkemeier. This section will consider the types of measurements which have been made in transhorizon propagation experiments, conclusions which have been reached and possible limitations.

3.1 Beam Swinging Experiments

In its simplest form this type of experiment involves the "swinging," in azimuth or elevation, of a large, narrow-beam parabolic antenna which is being used either for transmitting or receiving. The receiver output is recorded during the swing to produce an angular response pattern for the antenna. Variations of this technique involve "swinging" both the transmitting and receiving antennas, or swinging the antenna feed, or using a large phased array with some means of appropriately varying phase shifts

in feed lines, or using antennas with multiple stationary feeds.

During a beam swing in either azimuth or elevation the significant scattering region changes position in the atmosphere. Also the effective scattering angle (i.e., the magnitude of the scattering wave vector  $\vec{K}$ ) changes. For a swing in azimuth the direction of the scattering wave vector  $\vec{K}$  also varies, but the wave vector direction remains constant or essentially constant during an elevation swing.

If the atmosphere were in a homogeneous, isotropic, stationary turbulent state during many elevation swings of a narrow beam, then the average of the angular response patterns from the swings would trace out the spectrum of the turbulence. Predictions of the form of averaged azimuth response patterns for such a turbulent state have been made. (Booker and de Bettencourt 1955; Strohbehn 1963; Koono, et al., 1962). The average patterns for both azimuth and elevation are generally broader than the patterns for the same narrow beam antennas used on a line-of-sight path. The exact modifications to theoretical response patterns to account for non-narrow beams or anisotropic or inhomogeneous turbulence do not seem to be directly available in the literature but some intuitive estimates of this effect can be made. Nonstationarity in signal statistics which is due either to nonstationary atmospheric conditions or to inhomogeneous atmosphere drifting through the scattering region presents a more formidable problem which has received little treatment.

Estimates of averaged angular response patterns for beam swinging experiments have been made for a layer theory (Friis, et al., 1957) but again uniformity in the distribution of layers and assumptions as to the distributions of layer sizes, orientations and intensities were required. Some estimates of the characteristics of angular response patterns for beam swings made in time periods short compared to changes in the atmosphere have been made (Strohbehn and Waterman 1964; Stein, et al., 1959) for both the turbulence theories and layer theories but the characteristics to be expected under many different atmospheric states are not clear from the existing theoretical work.

Table I is a listing of beam swinging experiments found in the literature. Figure 3 contains a few examples of beam swinging data. The early experiment reported by Waterman (1953, 1957) utilized a relatively broad receiving beam and a narrow-beam transmitting antenna (radar) which was rotated at a uniform azimuth rate so that the beam swing took less than 1/5 second. The near-instantaneous angular response patterns contain examples with multiple maxima and examples of broadened maxima which are indicative of signal arriving from azimuth angles slightly (of the order of  $1/2^\circ$ ) off the great circle path.

TABLE I  
BEAM SWINGING EXPERIMENTS

Author	Date Pub.	Path Location	Swing Az or El	Scan Period (sec.)	ALL EXPERIMENTS CONTAIN EXAMPLES OF AVERAGED RESPONSE PATTERNS						
					Swing Method	Swing Ant. Beamwidth (Deg.)	Freq. (Gc)	Path Length (miles)	Min. Scat. < (Deg.)	Met. Data	
Waterman, et al.	1953 1957	Calif.	Az	1/5	Rotate T Ant.	0.9	3	92 to 177	~ 1.7	None	
Trolese	1955	Ariz.	Az& El	Slow	Rotate R Ant.	1.75	9.4	46	--	Wind profiles 100 mi off path	
Chisholm, et al.	1955	Mass. N.J.	Az& El	Slow	Rotate R and T&R Ant.	0.7 T&R	3.7	188	--	None	
Waterman Strohbehn	1958 1963 1966	Calif. Calif.	Az	1/10	8 ele. phased array-rapid phase shifting	0.5 Az 5 El	3.1	101	0.91	Wind & N profiles 25 mi off path	
Crawford, et al.	1959	N.Y. N.J.	Az& El	15	Rotate R Ant.	0.3	4.1	171	--	Wx. map only	
Harai, et al.	1960	Japan	Az	Avg. pt. by pt.	Rotate T Ant.	1.0	2.1	147 214	1.55 2.7	--	

TABLE I (Continued)

Author	Date Pub.	Path Location	Swing Az or El	Scan Period (sec.)	ALL EXPERIMENTS CONTAIN EXAMPLES OF AVERAGED RESPONSE PATTERNS					Swing Method	Swing Ant. Beamwidth (Deg.)	Freq. (Gc)	Path Length (miles)	Min. Scat. < (Deg.)	Met. Data
Ortwein, et al.	1961	Calif.	Az&El	Avg. pt. by pt.	Rotates T & R Ant.	3/4 est.	9.4	190 144 78	--	N profiles extensive Wx.					
Chisholm, et al.	1962	East Coast U.S.	Az El	34° per sec. slow	Rotate T Ant.	2.8	0.4	618	6.7	--					
Koono, et al.	1962	Japan	Az El	1/60	Rotate R Feed	0.5	2.1	184	2.18	--					
Cox	1967	Calif.	El	1/100	Meas. $\Delta$ phase & amplitude compute beam	0.25 El 5 Az	3.2	102	0.84	--					
Kieburtz, Fantera	1966	N.Y.	Az & El	8 sample beams in space	Sample from 8 discrete beams	.32 Az&El	7.8	184	--	None					

See also: Bolgiano, 1963  
Gjessing 1960, 1963, 1964, 1966

Reproduced from best available copy.

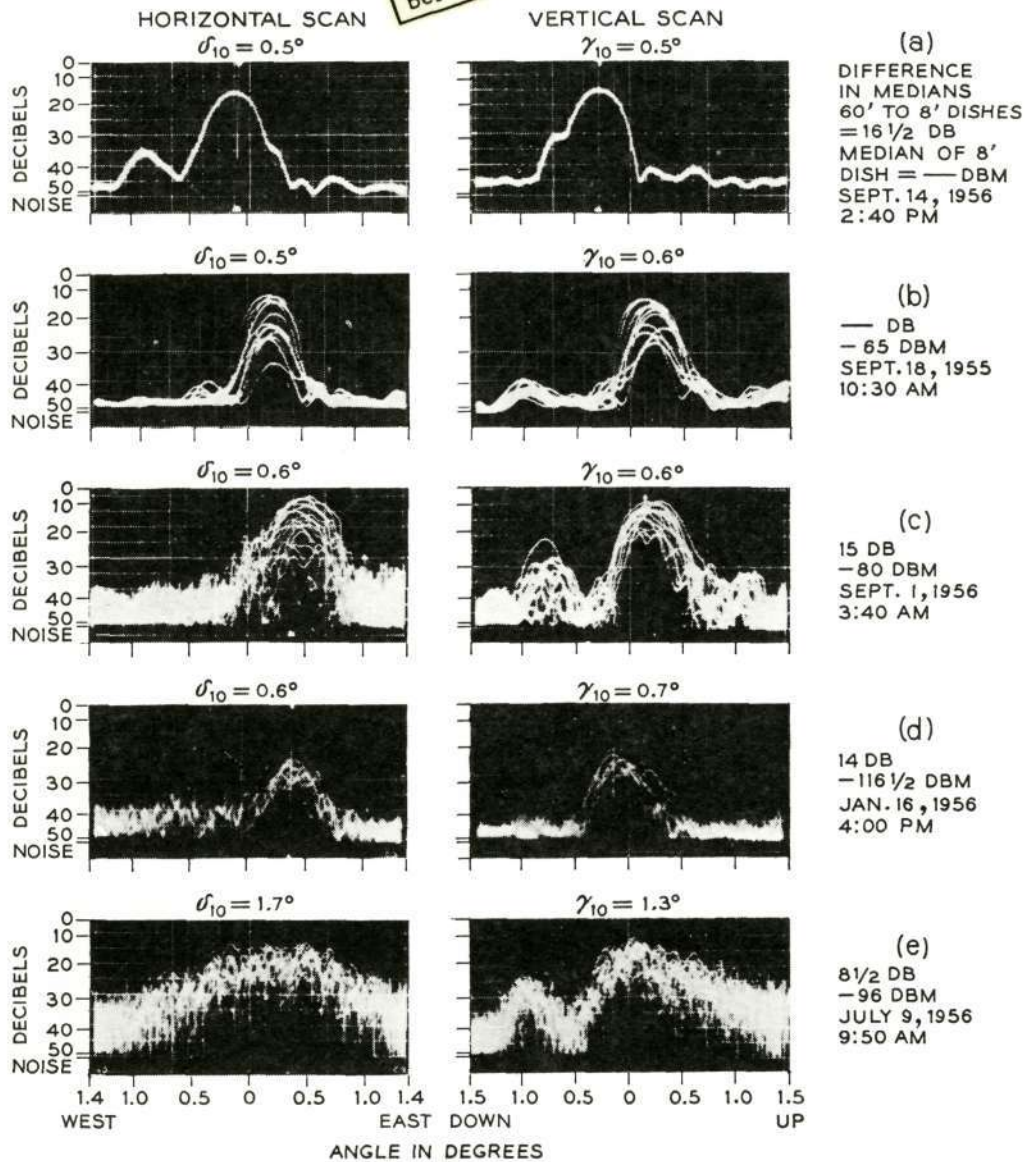


Fig. 3(a) ANGULAR RESPONSE PATTERNS

(From Crawford, A.B., et al., "Studies in Tropospheric Propagation Beyond the Horizon," *BSTJ*, Sept. 1959)  
(Copyright 1959, The American Telephone and Telegraph Co., reprinted by permission)

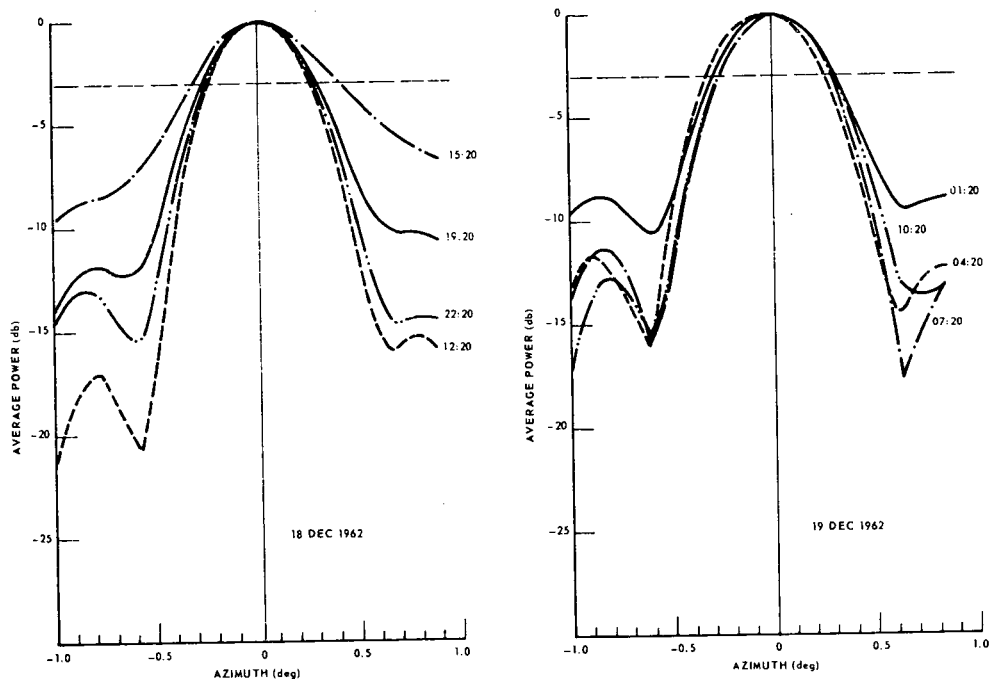


FIG. 38. AVERAGE ANTENNA-RESPONSE PATTERNS FOR 18-19 DEC 1962.

Fig. 3(b) AVERAGE ANTENNA-RESPONSE PATTERNS FOR 18-19 DEC 1962

(From Strohbehn, J.W., "Transhorizon-Propagation Measurements and Simulated Angular-Response Patterns," Final Report on Proj. 2270, Stanford Electronics Labs, Oct. 1963)

TRANSORIZON PROPAGATION

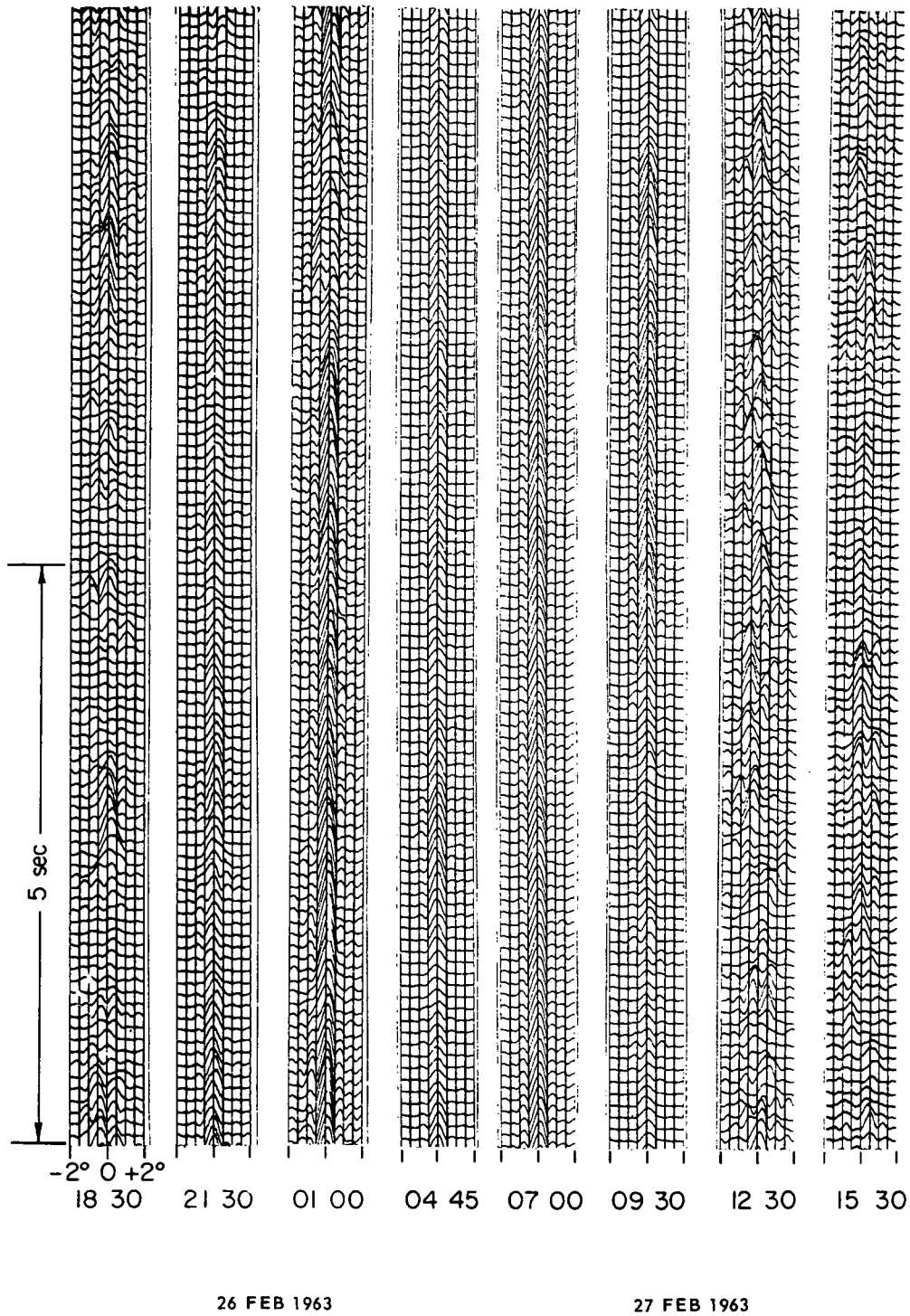


Fig. 3(c) AZIMUTH ANGULAR-RESPONSE PATTERNS

(From Strohbehn, J.W., "Transhorizon-Propagation Measurements and Simulated Angular-Response Patterns," Final Report on Proj. 2270, Stanford Electronics Labs, Oct. 1963)

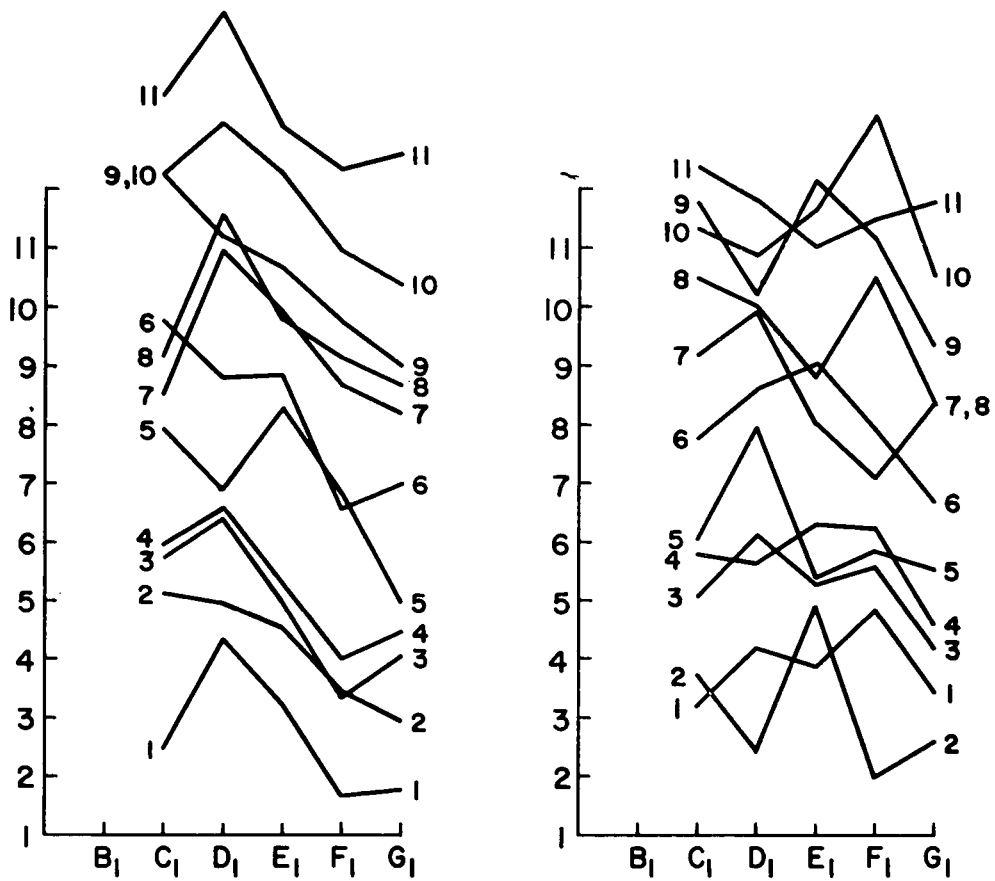


Fig. 3(d) INSTANTANEOUS INTENSITIES RECORDED FROM 5 NARROW BEAM ANTENNAS SEPARATED APPROXIMATELY 1/3 DEGREE IN AZIMUTH

(From Kieburz, R.B. & Fantera, I.A., "Angle-of-Arrival Measurements Performed Over a 296-KM Troposcatter Path," Radio Science, November 1966, by permission of author)

# TRANSHORIZON PROPAGATION

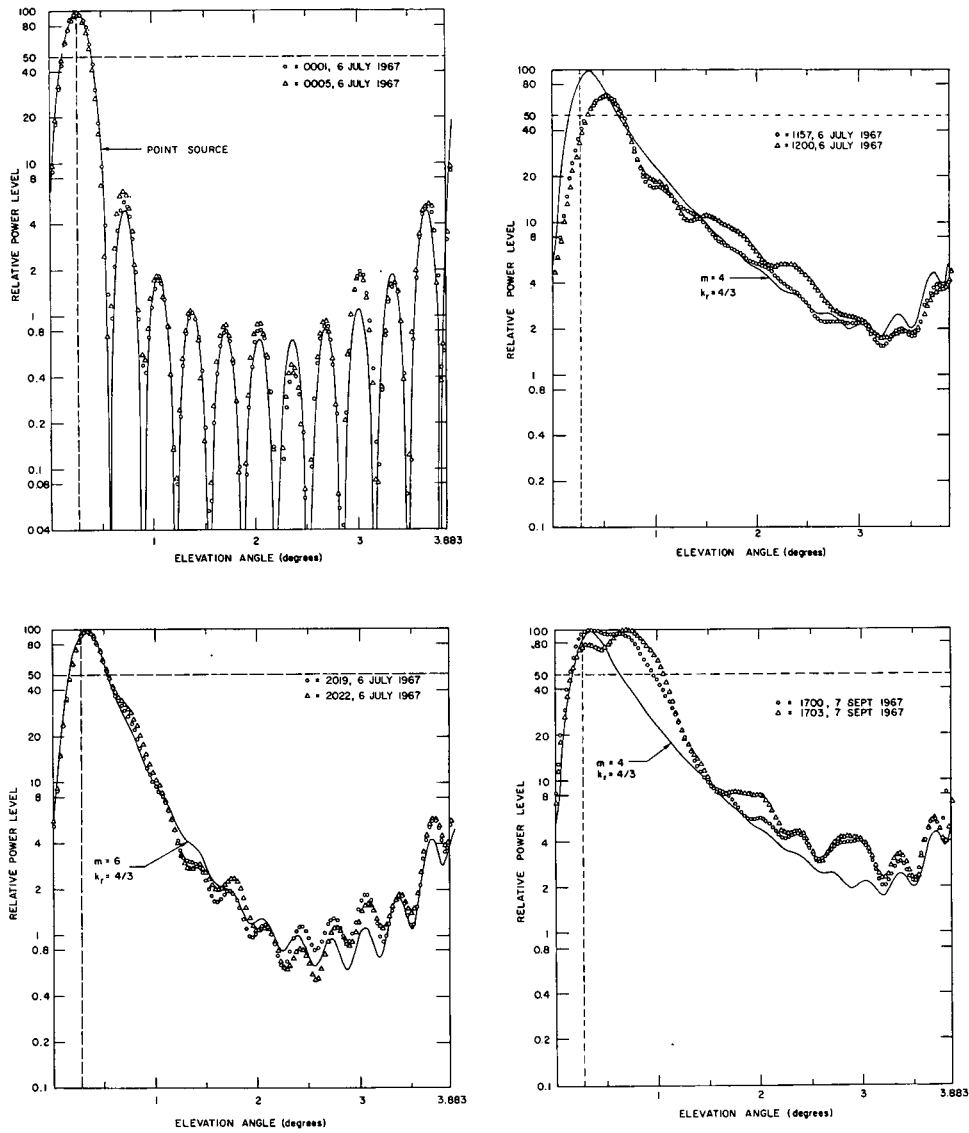


Fig. 3(e) AVERAGED ANGULAR RESPONSE PATTERNS IN ELEVATION

(From Cox, D.C., "Phase and Amplitude Measurements of Microwaves Propagated Beyond the Horizon," T.R. 2275-1, Stanford Electronics Labs, Dec. 1967)

The experiments reported by Chisholm, et al., (1955, 1962) and Trolese (1955) contain a few examples of beam swings which illustrate angular response patterns broader than the patterns for the same antennas used on line-of-sight paths (i.e., broadened beams). The experiment reported by Crawford, et al (1959) contains many examples of angular response patterns from beam swings both in azimuth and in elevation. Exact interpretation of the individual swings is complicated by the fact that the 15-second duration of each swing was not short compared to signal fading rates. Photographic integration was used to produce averaged response patterns from several swings. There is considerable variability between the different response patterns taken at different time periods. As an example, the function describing the decrease in received power with increasing elevation angle is different at different times. The experiments reported by Harai, et al., (1960) and Ortwein and Hopkins (1961) include averaged angular response patterns produced by swinging an antenna beam incrementally in angle and averaging the signal for periods of the order of minutes at each angular increment. The observed variability in the angular response patterns from one time period to another is again characteristic of such experiments although for some time periods nonstationarity in signal means hinders their interpretation.

Experiments reported by Waterman and Strohbehn (1958, 1963, 1966) include angular response patterns from azimuth beam swings with short (1/10 sec) periods and also averaged azimuth patterns made up of patterns from many rapid swings. The response patterns from the rapid swings show source regions in azimuth which are usually smaller than the  $1/2^\circ$  resolution of the beam, which occur individually or in simultaneous groups, which fade independently, and which move about sometimes at azimuth rates too fast (up to 600 mph at the minimum beam intersection point of the path) to represent transport of regions in the atmosphere. The characteristics of both the rapid swing patterns and the averaged patterns vary widely for different time periods but the averaged patterns are consistently narrower than would be predicted from a homogeneous turbulence theory. An experiment reported by Kono, et al., (1962) presents angular response patterns from rapid (1/60 sec) beam swings in azimuth and averaged response patterns in both azimuth and elevation. A peculiar phenomenon reported is the existence of propagation paths both along the great circle and off-axis in azimuth when the transmitting beam is oriented off-axis in azimuth. It would seem that transmitting antenna sidelobes might cause such an effect but no mention is made of checking sidelobe levels. Otherwise the response patterns contain the large variability from time period to time period and the broadened average responses observed by others.

The experiment reported by Kieburz and Fantera (1966) used 8 different beams oriented at different azimuth angles or different elevation angles to simultaneously sample the

## TRANSHORIZON PROPAGATION

power received from the different angles. The sampled angles are thus points along an angular response pattern. These fluctuate rapidly and average to an angular response pattern which is broad compared to the line-of-sight pattern of the antennas used. The averaged elevation patterns are complex. The average pattern characteristics are different for different time periods.

The experiment reported by Cox (1967) includes angular response patterns from elevation beam swings with periods of 0.01 sec and averaged elevation patterns made up of patterns from many rapid swings. The response patterns from the rapid swings show source regions in elevation which are usually smaller than the 0.30 resolution of the beam, which occur individually or in simultaneous groups and which fade independently. The characteristics of both the rapid swing patterns and the averaged patterns vary widely for different time periods. The variation in the elevation patterns runs from some which indicate average source regions much less than  $0.3^\circ$  wide in elevation to average source regions which appear to be inhomogeneous in elevation angle (vertical). These averaged angular response patterns precisely illustrate the different characteristics seen in practically all the other beam swinging experiments in elevation.

Additional experiments reported by Bolgiano (1963) and by Gjessing (1960, 1963, 1964, 1966) involve beam swinging but are discussed separately later.

The ideal beam swinging experiment would appear to be one in which narrow beams both in azimuth and elevation and at both transmitter and receiver are swung simultaneously and rapidly with respect to atmospheric motions to sweep out the entire scattering volume. Motion of scattering or reflecting regions could be accurately followed this way. Averaged two-dimensional response patterns could be produced which would yield the scattering cross section of the common volume as a function of spatial coordinates. A measurement of the degree of homogeneity and a measure of angular dependence of the turbulence spectrum plus a measurement useful in determining anisotropy of turbulence would result. Even such an extensive experiment, however, is not sufficiently powerful alone to uniquely determine the atmospheric structure.

All of the experiments reported exhibit some limitations when compared to an ideal experiment. In some (Harai, et al., 1960; Ortwein and Hopkins 1961) averages are taken at different angles at different times. Nonstationary signal means contaminate data taken this way. Some experiments swing a beam narrow in either azimuth or elevation but not both (Waterman 1958; Strohhahn 1963; Strohhahn and Waterman 1966; Cox 1967). None of the experiments rapidly swings both transmitting and receiving antennas in both azimuth and elevation over the same time period. In spite of these limitations, the experiments when reviewed as a

group show that

1. the experimental data contain much variability from one time period to another which is most probably indicative of different atmospheric states at different times.
2. the atmosphere exists in states which are sometimes quite homogeneous but at other times quite inhomogeneous in elevation angle (vertical direction).
3. extensive variations from time period to time period also exist in the azimuth angular response patterns (horizontal patterns) indicating either changes in homogeneity, isotropy, turbulence spectrum angular sensitivity, or even the scattering mechanism itself.
4. the experiments are not sufficiently definitive to differentiate between partial reflections from many layers and scattering from turbulent media since similar experiments can be shown to agree with predictions from both theories.
5. instantaneous scattering or reflecting regions small in extent move too rapidly at times to be caused by transport of atmosphere alone.

### 3.2 Pulse Transmission Experiments

The transmission of pulses over a transhorizon propagation path with precise timing at both ends should permit the determination of path length and thus an estimate of height of the scattering region or regions. Alternatively, if too many paths exist the resulting pulse distortion should give a measure of the extent of the scattering region.

Experiments involving the transmission of pulses were reported by Chisholm, et al., (1955, 1962) and are summarized in Table II. In these tests at times there was little or no broadening of pulse width even though during fades some pulse distortion occurred, at times more than one unbroadened discrete pulse was observed indicating more than one distinct scattering path and at times the pulses were broadened or smeared by multiple propagation paths. Differential delays of 2 to 8  $\mu$ sec were observed between discrete received pulses resulting from the same transmitted pulse. Pulses were observed which corresponded to paths - 20,000 ft to + 90,000 ft above the minimum beam intersection point of a path which was 640 miles long. Both pulse broadening and distortion were reduced by using narrow-beam antennas.

Although this technique appears quite good for exploring the extent of the active scattering region, very little

TABLE II  
PULSE TRANSMISSION EXPERIMENTS

<u>Author</u>	<u>Date Pub.</u>	<u>Path Location</u>	<u>Pulse Length Accuracy</u>		<u>Freq. (Gc)</u>	<u>Path Length (miles)</u>	<u>Min. Scat. &lt; (Deg.)</u>	<u>Met. Data</u>
Chisholm, et al.	1955	Mass. N.J.	1.5 $\mu$ sec. 0.1 $\mu$ sec.	[ Used different Ant. sizes ]	3.7	188	---	None
Chisholm, et al.	1962	East Coast U.S.	1 $\mu$ sec.	[ 10 $\mu$ sec. & 20 $\mu$ sec. PRF ]	0.4	640	$\approx$ 6.9	None

work has been done using it. Again it would appear that pulse transmission would need to be used in conjunction with other techniques (such as beam swinging) to produce a reasonable picture of the scattering mechanism at any given time.

### 3.3 Frequency Sweep Experiments

Rapid sweeping of the transmission frequency during transhorizon propagation experiments has been used to determine what frequency bandwidth can be used for information transfer. The width of the frequency band over which fading is correlated is related to the separation between actual scattering locations in the scattering volume since the rapid fading is caused by phase cancellation between the signals from the different scattering locations. Estimates of the separation between scattering regions were made by Crawford, et al., (1959) but there appears to be no extensive work relating these types of measurements to atmospheric characteristics. Frequency sweep experiments were run by Crawford, et al., (1959), by Tremblay (1962) and Strohbehn (1963). They all report that the signal fades at different wide-spaced frequencies (several Mc apart) at different times. The frequency separation for a given correlation of the fading at two different frequencies varies from time period to time period. The estimate of frequency separation for decorrelation made by Crawford, et al., on the basis of information from beam swinging measurements shows some agreement with measured frequency correlation widths. Chisholm, et al., (1962) transmitted 3 discrete modulation sidebands and measured the correlation of the fading between sidebands. His results also show a decrease in correlation between fading as the frequency separation increases. Table III summarizes these experiments.

### 3.4 Cross-Correlation Techniques

This type of experiment involves measuring the signal amplitude (or possibly phase) at two or more different antennas with different spacing and correlating the fluctuations between pairs of antennas. Ideally, measurements are made simultaneously at all antenna spacings of interest. The simultaneous measurements permit correlations to be compared with each other without contamination due to nonstationarity in the signal statistics. Predictions of correlation as a function of antenna spacing were made by Staras (1955). These were based on a uniform turbulence model which included some anisotropic effects and effects of height dependence of atmospheric fluctuation intensity. Table IV is a summary of experiments which measured spatial cross correlation.

Data from the experiment by Barsis, et al., (1954) is compared with theoretical curves in Staras (1955). In general these are long-term averages. Chisholm (1962) formed cross correlations as a function of horizontal antenna spacing for two spacings only. Again these were long-term averages.

TABLE III  
FREQUENCY SWEEP EXPERIMENTS

<u>Author</u>	<u>Date Pub.</u>	<u>Path Location</u>	<u>Sweep Width</u>	<u>Sweep Rate</u>		<u>Freq. (Gc)</u>	<u>Path Length (miles)</u>	<u>Met. Data</u>
Crawford, et al.	1959	N.Y., N.J.	20 Mc	30 cps	[28 ft Xmit. Ant. 60, 28 & 8 ft Rec. Ants.]	4.1	171	none
Tremblay	1962	France	200 Mc	1/20 sec/ sweep		3.4	187	--
Chisholm, et al.	1962	East Coast U.S.	[Discrete Frequencies 40, 60 & 100 Kc separation]			0.4	618	--
Strohbehn	1963	Calif.	20 Mc	312 cps	[wide Xmit. Ant. wide El but 0.5° Az Rec. Ant.]	3.1	101	--

TABLE IV  
CROSS CORRELATION TECHNIQUES

<u>Author</u>	<u>Date Pub.</u>	<u>Path Location</u>	<u>Vert Horiz</u>	<u>Total Elements</u>	<u>Ave. Time</u>	<u>Element Spacings</u>	<u>Element Size</u>	<u>Freq. (Gc)</u>	<u>Path Length (miles)</u>	<u>Min. Scat. &lt; (Deg.)</u>	<u>Met. Data</u>
Barsis, et al.	1954	Colo. Kansas	V&H					0.1 1.0			
Chisholm, et al.	1962	East Coast U.S.	H	2	-	100 ft 700 ft	Small	0.41	618	6.7	--
Fehlhaber	1966	Germany	V H V&H	3 3 3			30 ft (Small)	1.75	260	2.6	wind
Cox	1966	Calif.	V	12	6 min	4.5 ft up to 50 ft	4 ft	3.2	102	0.84	--

This technique has been exploited somewhat more extensively by Fehlhauer (1967) who used simultaneous measurements from 3 antennas in 3 different configurations (  $\circ \circ$  ;  $\circ \circ \circ$  ; and  $\circ \circ \circ$  ). The correlations show a large amount of variability from one time period to another. The comparisons of the correlation coefficient at a given vertical spacing with the correlation coefficient for horizontal antennas with the same spacing sometimes show evidence of anisotropy. For these comparisons the correlations were formed from data taken over the same time period. No evidence of vertical drift is seen in the vertical correlation functions. Shifts of the maxima of the horizontal correlation functions with time lag are a measure of horizontal drift velocity. This velocity correlates with some wind measurements.

Correlations of amplitude data taken simultaneously with 12 antennas spaced vertically were reported by Cox (1967). There is considerable variability in the shapes and widths of the correlation functions for different time periods. Characteristics in these functions are identifiable with characteristics observed in angular response patterns from beam swings produced by using the 12 antennas as a phased array. There is no evidence of vertical drift in the correlation functions with time lag. The correlation functions for some time periods agree quite well with the theoretical predictions of Staras (1955) but for other time periods the agreement is very poor.

This experimental technique, although quite powerful, is not sufficient to resolve the state of the atmosphere by itself. It has not been very widely used.

### 3.5 Examination of Fading Rates

Fading rates and Doppler spectra are closely tied to internal motions in the atmosphere and to drift of the atmosphere (wind). The subject of phase-coherent and frequency-coherent techniques is being reviewed by Professor Birkemeier and will be omitted here. A brief mention will be made, however, of the use of envelope fading to determine atmospheric motion. Three measures of envelope fading rate have been used. They are the number of positive-slope zero crossings per second, the width of the auto-correlation function, and power spectral density of the envelope. Table V summarizes these experiments.

In the experiment reported by Norton (1955) fading rates were found to be approximately proportional to transmitter frequency on the basis of 3 different frequencies. Fading rates correlated well with wind measurements.

Ortwein, et al, (1961) reported poor correlation between fading rates and wind measurement.

TABLE V  
FADING RATE EXPERIMENTS

<u>Author</u>	<u>Date Pub.</u>	<u>Path Location</u>	<u>Rate Parameter</u>	<u>Ave. Time</u>	<u>Element Size</u>	<u>Freq. (Gc)</u>	<u>Path Length (miles)</u>	<u>Min. Scat. &lt; (Deg.)</u>	<u>Met. Data</u>
Norton, et al.	1955	Colo. Kansas	No. of + slope crossings			0.2 0.1 1.0	70 to 225	--	wind
Ortwein, et al.	1961	Calif.	Envel. Auto. corr. & spectrum		0.78° 1.26° 2.0°	1.2 3.4 9.4	78 144 190	--	N profiles extensive Wx
Chisholm, et al.	1962	East Coast U.S.	Envel. Auto. corr.	~ 10 min	28 ft	0.41	188 350 618	--	--
Strohbehn & Waterman	1963 1966	Calif.	Envel. Auto. corr.	2-1/2 min	8 element array 0.5° Az 5° El	3.1	101	0.91	Wind & N profile 25 mi off path
Cox	1966	Calif.	Envel. Auto. corr.	6 min	4 ft (50)	3.2	102	0.84	--
Gjessing	1960 1964	Norway	Envel.		15 ft (.75°)	6	100 210		N profiles surface data

Chisholm (1962) reports that the fading rate increases when antennas are aimed off path.

Strohbehn and Waterman (1963, 1966) and Cox (1967) show many samples of envelope autocorrelation functions. These vary considerably from time period to time period. Strohbehn shows that the width of the autocorrelation function usually follows the trend of measured winds. Cox reports shorter correlation times during the day than at night.

Laaspere (1958) reviews the topic of fading rates.

In general there are experiments in this area for which the fading rates correlate well with measured wind and some for which the correlation is poor. There does not appear to have been sufficient effort (theoretical or experimental) in this area to form useful conclusions. Fading rate measurement should be a fruitful technique to use in conjunction with other techniques (such as beam swinging) to produce some measurement of atmospheric drift and/or internal motion. Interpretation of these rates is somewhat clouded by the rapidly moving reflection points or scattering regions observed by Waterman (1958) in a rapid beam swinging experiment in azimuth. It appears that reflection points may move at rates not related to actual transport of atmospheric material. If this effect occurs frequently, it most certainly will contaminate the quantitative measurement of actual atmospheric motions, both internal and drift (wind).

### 3.6 Multiple Frequency Experiments

Experiments of this type are designed to measure the wavelength dependence of the atmospheric turbulence spectrum  $\Phi(\vec{K})$ . In order to yield information about the same atmospheric region both the transmitting and receiving antennas must illuminate the same atmospheric region (i.e., be wavelength scaled). Table VI summarizes experiments using more than one frequency.

There are several experiments in the literature [for example, Bullington (1955); Chisholm, et al., (1955) and Crawford, et al., (1959)] which utilized more than one frequency but their results are not of a form which yields a direct interpretation of wavelength dependence over time periods of a few minutes (i.e., long enough to be statistically significant but short enough to avoid long-term drifts).

A multi-frequency experiment using antennas with similar beam patterns (antennas wavelength scaled) was conducted at Cornell University in 1956. According to Bolgiano (1959) at Cornell the results were not conclusive.

Bolgiano (1959) reported on an experiment by Chisholm, et al., (1957) which used scaled antennas (similar beam patterns)

TABLE VI  
MULTIPLE FREQUENCY

<u>Author</u>	<u>Date Pub.</u>	<u>Path Location</u>	<u>Element Scaling</u>	<u>Element Size</u>	<u>Freq. (Gc)</u>	<u>Path Length (miles)</u>	<u>Min Scat. &lt; (Deg.)</u>	<u>Met. Data</u>
Bullington Chisholm	1955 1955	(Two experiments utilizing 2 widely spaced frequencies)						
(Cornell Univ.)	1956	N.Y.		Scaled antennas		60		
Crawford, et al.	1959	(An experiment utilizing different frequencies)						
Bolgiano report of Chisholm et al. exp.	1959 1957	East Coast U.S.	Freq. scaled antennas	28 ft 5 ft	0.41 2.3	188	--	--
Ortwein	1961	Calif.	Freq. scaled antennas	2° beams	1.25 3.41 9.36	190		N profiles extensive weather
Bolgiano	1964	N.Y.	Freq. scaled antennas	28 ft 10 ft 4 ft	0.84 2.8 9.1	67	--	Soundings 150 mi from path

at two frequencies. The results indicate that the wavelength dependence is not constant but varies from one time period to another. The experiment reported by Bolgiano (1964) involved 3 frequencies and wavelength-scaled antennas. There was unquestionable variation in the wavelength dependence of the scattering mechanism observed in this experiment. This could be due to changes in the turbulence spectrum itself or possibly to nonuniformities in the atmosphere.

The technique of using more than one frequency in a transhorizon atmospheric probe is a powerful tool but it alone is not sufficient to resolve the question of atmospheric structure at any given time.

### 3.7 Measurement of Anisotropy and Inhomogeneity

An experiment reported by Bolgiano (1963) combined some aspects of the beam swinging and the multi-frequency experiments. Antennas with similar beam patterns (wavelength-scaled) were used at 3 widely separated frequencies (0.84 Gc, 2.8 Gc and 9.1 Gc). Averaged received power measurements were made with the 0.84 Gc antennas aimed  $3^\circ$  off the great circle path, the 9.1 Gc antennas aimed along the great circle, and the 2.8 Gc antennas swung in alternate half hours from along the great circle to  $3^\circ$  off the great-circle path. Average amplitude samples thus were taken of the scattering from the same two size (related to the wavenumber  $|\vec{k}|$ ) components of 3 meters and 1 meter with the  $\vec{k}$  vector vertical for the great circle path and at an angle of  $\approx 70^\circ$  from the vertical for the path  $3^\circ$  off the great circle. The results, which at times indicate different wavenumber (size) dependence for the different  $\vec{k}$  vector orientations are interpreted to mean that the atmosphere was anisotropic (i.e., that  $\phi(\vec{k})$  was a function of direction of  $\vec{k}$ ) for those time periods. At other time periods interpretation of the results indicates isotropic conditions. Again the variability from time period to time period is present. Since the data for a given comparison were not taken simultaneously, but at 1/2 hour intervals, one is forced to suspect that non-stationary conditions might have existed to contribute to the observed results, possibly in addition to conditions of anisotropy (or inhomogeneity). This experiment illustrates, however, that combinations of experimental techniques can be successfully applied to define better the state of the atmosphere over a given time period but it also points up the desirability or rather the necessity for measuring all required parameters simultaneously for a given interpretation.

An experiment reported by Gjessing (1960, 1963, 1964, 1966) involves carefully controlled synchronous swinging in azimuth and in elevation of both transmitter and receiver beams. The swinging is done in such a way that sometimes the scattering angle (i.e.,  $|\vec{k}|$ ) remains constant while the direction of  $\vec{k}$

varies (combined azimuth and elevation swing), sometimes swings are made so that the direction of  $\vec{k}$  remains constant while the scattering angle ( $|\vec{k}|$ ) varies (elevation swing only), and in other cases swings are made so that the scattering angle ( $|\vec{k}|$ ) remains constant and the direction of  $\vec{k}$  remains constant to within  $\approx 2^\circ$  (elevation swing only). In all cases the atmospheric scattering region varies during the swing. These measurements should indicate to some extent the degree of anisotropy and inhomogeneity and the angular dependence of the scattering cross section [and thus  $\phi(\vec{k})$ ]. Results of the experiments are interpreted to indicate that for some time periods the atmosphere is isotropic and homogeneous and for other time periods it is either anisotropic or inhomogeneous or both. A large amount of variability exists in the data from time period to time period. Interpretation of the data requires use of an inhomogeneity measurement to remove inhomogeneity from the isotropy data and the angular dependence data. Since the inhomogeneity may not be the same everywhere some error may result from this procedure. Also, again, all measurements are not made simultaneously--thus the specter of NONSTATIONARITY raised its head again. This experiment makes more complete use of the capabilities of synchronous beam swinging than does any other experiment reported to date and serves as a good example of the technique's versatility.

### 3.8 Meteorological Measurements for Comparison with Radio Measurements

For most of the transhorizon propagation experiments reported in the literature associated meteorological measurements either were not made at all or were gathered from existing, but usually not optimally located, weather stations. The experiments for which correlation between the radio observations and available meteorological observations was possible usually exhibit poor correlation. One exception to this experimental deficiency is noted in Ortwein, et al., (1961). During this experiment extensive surface weather data were collected, refractive index profiles were taken using airborne refractometers and supplementary balloon observations (pibals, Raobs and Rawindsondes) were made. Generally, the weather data were used to select time periods when turbulent conditions should exist. Radio data for these time periods were then compared with turbulence theory predictions. In general, effects of elevated inversions were noted on elevation angle beam swings but not on azimuth beam swings, large variations in atmospheric characteristics correlated with radio measurements and sometimes variations in wavelength dependence could be identified with variations in observed atmospheric structure.

Though the task is extremely difficult it appears that considerably more meteorological data need to be taken and more detailed meteorological analysis needs to be made than has been done in practically all propagation experiments conducted to date.

### 3.9 General Observations in the Experiments

The most striking feature observed in all the experiments is the wide range of variation in the measured parameters for different time periods regardless of what parameter or parameters were being measured in the experiment. This variation would indicate that all the experiments differentiate between different atmospheric states even though the states may be too complex to identify with the simple measurement or measurements made.

A second observation is that any given set of measurements can usually be interpreted in different ways. Examples are that beam swinging data with similar characteristics can be used to support both layer theories and turbulence theories, that data taken at different time periods can be combined and interpreted to indicate either inhomogeneity or nonstationarity due to changing atmospheric states or sometimes anisotropy, and that beam swinging data in elevation can be interpreted as an indication of different turbulence spectrum angular dependence or of a height dependence in the fluctuation intensity of turbulence (a kind of inhomogeneity). These problems result because there are not a sufficient number of measured parameters to permit the sorting out of all atmospheric states and assumptions of homogeneity or isotropy or stationarity are necessary to permit interpretation at all. Variations in one parameter like anisotropy which are "measured" in some experiments are assumed not to exist in the interpretation of other experiments.

A third observation, which must be made with care and caution because of the previous observation, is that during some time periods the atmosphere appears to be in a state of nearly isotropic, homogeneous, nonchanging (stationary) turbulence with a spectrum which is quite close to that predicted by Kolmogorov or Obukhov, while during other time periods the turbulence may be anisotropic and/or inhomogeneous and/or changing with time. During still other time periods the atmosphere may tend toward a stable state with the major irregularities being caused by stratified layers with different characteristics.

A fourth observation is that at times the significant scattering region is smaller than the resolution of angle- and distance-measuring instruments used in the experiments.

A fifth observation is that at times the measured parameters are quite stationary for time periods of the order of hours while at other times the measured parameters may change by a large amount in a few minutes.

A sixth observation is that the question of the mechanism of propagation (partial reflection or scattering from somewhat localized regions or scatterers) is not resolved. Evidence suggests that maybe there is not a unique mechanism but that scattering and partial reflection may both occur. This suggests that some problems in measuring atmospheric velocities

may be encountered if the velocity measured by radio methods is partially due to fleeting reflection points.

The last observation made by this author is that during the conduct of most transhorizon propagation experiments the measurement and analysis of meteorological parameters is not sufficient for determining the state of the atmosphere at the time of the experiment.

### 3.10 Requirements for Definitive Experiments

The only obvious general conclusions which result from a careful survey of reports describing past transhorizon propagation experiments are that either

1. It is not possible to determine anything very definitive about the state of the atmosphere or atmospheric motion from such measurements, or
2. The "tools" used in experiments so far were not sufficiently powerful or sufficiently numerous to define the states or motions in the atmosphere.

Choice of 1. runs contrary to the history of scientific measurements; therefore 2. would seem to be the most likely conclusion. With this in mind possible ways to strengthen such experiments will be explored.

The atmosphere exists in a variety of different complex states which are functions of both space and time. A logical development of experimental requirements might progress as follows:

The problem of resolving the changes of atmospheric state with time requires that all measurements must be made simultaneously and suggests that measurements should be made at rates greater than rates of change in the atmosphere.

The problem of defining the atmospheric state in a small region probably is approached best by using high-resolution (narrow beam) antennas. The antenna beamwidths at all frequencies should be the same. It appears desirable to measure independently two parameters which should produce identical dependence at least for some atmospheric states. A good possibility is the use of a number of frequencies to establish the wavelength dependence of the scattering mechanism in the small region and simultaneously, from several receiving sites, (see Fig. 4) determine the angular dependence of the scattering mechanism in the same region. Antenna beams at different sites need to be scaled to illuminate the same volume from all sites. If the mechanism were turbulence which was homogeneous in the small region then angular dependence and wavelength dependence should be the same. Other states would

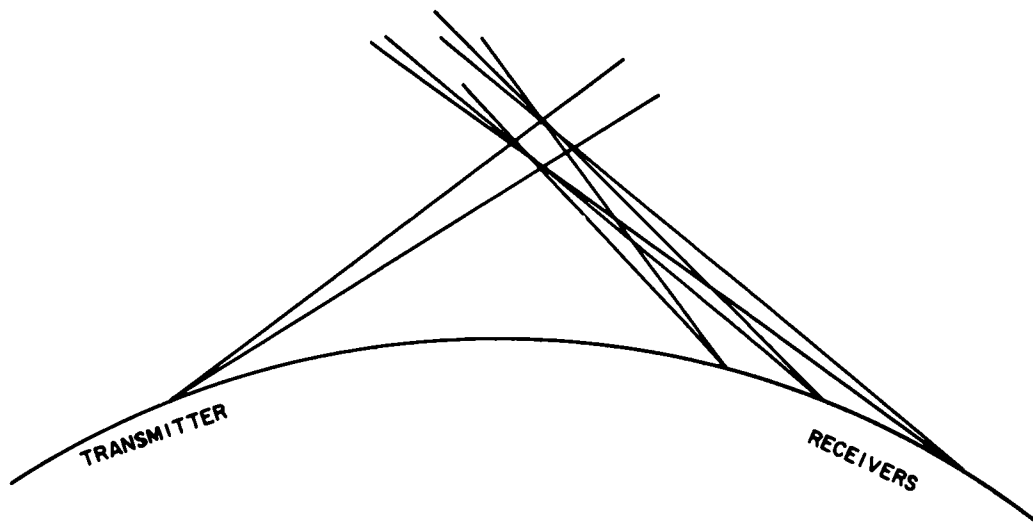


FIG. 4 GEOMETRY FOR DETERMINING ANGULAR DEPENDENCE

usually produce an angular dependence different from the wavelength dependence. The problem of describing the atmosphere throughout the entire volume accessible from the instrumentation sites might then be met by synchronously and rapidly sweeping the transmitting and receiving beams in such a way that the entire volume is swept out by the intersection region between the beams. This procedure should determine the extent of anisotropy and inhomogeneity in the entire volume. Height dependence of fluctuation intensities should also be resolvable. To produce a 3-dimensional picture of the atmosphere in the volume would require two sets of experimental apparatus operating perpendicularly to each other (crossed paths).

The measurement of doppler spectrum for velocity determination would require the precise generation of all frequencies. Since the procedure described above would permit the "tracking" of fleeting reflection points, the effects of these on the determination of actual atmospheric velocities from the doppler measurements could be defined.

So far these suggestions point to rather extensive experimental instrumentation and techniques which are extensions of techniques already applied individually. The data reduction requirements from such an effort also would be quite large since the instrumentation would produce something of a data explosion. It appears, however, that the collection of definitive data on

atmospheric state from transhorizon propagation experiments would require at least two and probably all of the experimental capabilities mentioned above to circumvent the need for making insupportable assumptions about the atmosphere in order to interpret data from more limited measurements.

In addition to such an extensive electromagnetic measurement program, extensive meteorological measurements both on the surface and within the scattering region should be made and analyzed to provide an independent check on the results from the transhorizon propagation probe.

The basic requirements then appear to be

- a. simultaneous rapid measurements
- b. high angular resolution (from an antenna array or large multi-feed antenna) with the same beamwidths at all frequencies
- c. multiple frequencies precisely determined
- d. synchronous pointing of transmitting and receiving antennas
- e. multiple receiving sites along the path line

It should be pointed out that even the pursuit of such an ambitious measurement program as that outlined above carries no guarantee of success at this time--it is only that such a program seems to be the most likely to succeed when viewed in the light of past experiments.

#### 4. ADVANTAGES AND LIMITATIONS OF TRANSHORIZON PROPAGATION PATHS AS REMOTE ATMOSPHERIC PROBES

Assuming that the technique of transhorizon propagation measurements were developed into a useful probing tool, two of its advantages would be

- a. Measurements could be made over a rather wide volume of space from one set of installations, and
- b. Requirements for site locations would not be critical. (No mountains or tall towers would be required as might be for a line-of-sight probe).

## TRANSHORIZON PROPAGATION

Some of the limitations of the technique would be

1. It is best suited to measuring characteristics averaged over regions in space defined by the intersection of two antenna beams (on the order of several hundred to a few thousand feet square).
2. It is not suited to making measurements near the ground. The useful region starts several hundred feet to a few thousand feet above the ground depending on the paths.
3. It is more sensitive to atmospheric characteristics at altitudes near the minimum beam intersection altitude of a given path and the sensitivity falls off quite rapidly above this altitude because of the angular-dependent nature of any of the scattering or reflecting mechanisms.
4. Some means must be provided for rejecting data taken when aircraft fly through the scattering region.

### 5. FACILITIES AVAILABLE

There are no facilities available with the complex capability suggested in section 4 of this report; however, there are some facilities intact which have been or are being used in trans-horizon propagation research. Below is a partial list of such facilities:

#### A. University of Wisconsin - Collins Radio

This facility is equipped with stable-frequency-generating equipment and is being used for path phase and doppler measurements. (See paper by Prof. Berkemeir in this Section.)

#### B. Stanford University, California

A large-aperture 12-element antenna array is available and is currently in use. The total aperture is adjustable but is currently set at 162.5 wavelengths (50 feet). The array is oriented vertically but can be positioned horizontally or even split for some horizontal and vertical resolution. The array and associated equipment must operate at 3.200 Gc because of the way both transmitter and receiver frequencies are generated. The frequencies are generated with sufficient precision to permit measuring the doppler spectrum. The basic data recorded are amplitude from each element and phase

difference between adjacent elements. These measurements are made at rates up to 100 samples from all 12 elements per second. (See Cox 1967).

C. University of Washington

A 10-element horizontal antenna array with an element spacing of 17 feet (aperture 153 feet) is being constructed. This array will operate at about 900 Mc when completed.

D. Cornell University, New York

Equipment for conducting experiments at 3 frequencies (840 Mc, 2.4 Gc and 9.1 Gc) with wavelength-scaled antennas (28 feet, 10 feet, and 4 feet in diameter) for both transmitting and receiving has been used at Cornell. Availability of the equipment is not known to this author. (See Bolgiano, 1964).

E. Rome Air Development Center, New York

Multiple Feed 28 foot parabolic reflectors with  $0.3^\circ$  beams for use at 7.8 Gc have been used recently for angle of arrival measurements. (Kieburtz, et al., 1966). Availability is unknown.

6. SUMMARY

Many attempts have been made at determining characteristics of the atmosphere from characteristics observed in radio signals propagated beyond the horizon. From the viewpoint of scientific investigation much progress has been made in defining the problem area in general, the mechanisms involved, the parameter characteristics and ranges and to some extent the relationship between the parameters and the atmosphere. From the viewpoint of remote atmospheric probing, however, the interpretation of any one set of radio measurements is not sufficiently definitive to permit the unambiguous determination of atmospheric state or structure or the quantitative determination of some atmospheric parameter. That is, the interpretation of all measurements made to date requires the use of assumptions about the atmosphere which are not directly supportable by the measurements themselves. The outstanding feature of the characteristics of the transhorizon signals is their extreme variability from one time period to another. This variability indicates that the signal characteristics are a good discriminator of changes in the atmosphere itself.

It would appear that too much theoretical and experimental effort has been expended trying to determine universal, gross, overall characteristics for the atmosphere such as the turbulence

## TRANSHORIZON PROPAGATION

spectrum  $\Phi(\vec{K})$  when the experimental data seem to indicate that such universal characteristics do not exist for the wavenumbers ( $\vec{K}$ ) involved in transhorizon propagation. More detailed and complex experiments seem to be required to provide a sufficient number of more or less independent parameters for use in sorting out the complex characteristics of the dielectric permittivity fluctuations in the atmosphere. These experiments should include sufficient meteorological measurements to provide a good check on the conclusions reached from radio signal measurements. Although results from past experiments suggest that the analysis of data from such complex experiments would yield a better description of the atmosphere than has been possible so far, there certainly is no guarantee that this success would be achieved.

Because of the present state of knowledge of transhorizon propagation phenomena, signals propagated beyond the horizon do not appear suitable for current use as remote atmospheric probes. Because of the variability in the characteristics of these signals, however, they do appear to hold considerable potential for such use. The development of this potential definitely should be continued. More definitive experiments which make use of combinations of measurement techniques and more complete theory to aid in the interpretation of the measurements are needed to develop this potential.

REFERENCES

1. Ames, L.A., Newman, P., and Rogers, T.F., "VHF Tropospheric Overwater Measurements Far Beyond the Radio Horizon," Proc. IRE, 43, 10, Oct. 1955, pp. 1369-1373.
2. Balser, M., "Some Observations on Scattering by Turbulent Inhomogeneities," IRE Trans. PGAP, AP-5, Oct. 1957, pp. 383-390. (See also: Stein, "Some Observations on Scattering by Turbulent Inhomogeneities," IRE Trans. PGAP, AP-6, July 1958, p. 299).
3. Barsis, A.P., Herbstreit, J.W., and Hornberg, K.O., "The Cheyenne Mountain Tropospheric Propagation Experiments," NBS Circular 554, Washington, D.C., Dec 1954.
4. Bauer, J.R., "The Suggested Role of Stratified Elevated Layers in Transhorizon Short-Wave Radio Propagation," Tech. Rep. No. 124, Lincoln Laboratories, M.I.T., Cambridge, Mass., 24 Sept 1956.
5. Bolgiano, R., Jr., "Wavelength Dependence in Transhorizon Propagation," Proc. IRE, 47, Feb 1959, p. 331.
6. Bolgiano, R., Jr., "A Theory of Wavelength Dependence in Ultrahigh Frequency Transhorizon Propagation Based on Meteorological Considerations," Jour. of Res. of Nat'l. Bureau of Stds. - D. Radio Propagation, 64 D, No. 3, May-June 1960, pp. 213-237.
7. Bolgiano, R., Jr., "Structure of Turbulence in Stratified Media," J. Geophys. Res., 67, 8, July 1962, pp. 3015-3023.
8. Bolgiano, R., Jr., "Evidence of Anisotropy in Tropospheric Microstructure," J. Geophys. Res., 68, 16, Aug 15, 1963, pp. 4873-4874.
9. Bolgiano, R., Jr., "A Study of Wavelength Dependence of Transhorizon Radio Propagation," Research Report CRSR 188, Center of Radio Physics and Space Research, Cornell University, Ithaca, N.Y., 15 June 1964.
10. Booker, H.G. and de Bettencourt, J.T., "Theory of Radio Transmission by Tropospheric Scattering Using Very Narrow Beams," Proc. IRE, 43, 3, March 1955, pp. 281-290.
11. Booker, H.G. and Gordon, W.E., "A Theory of Radio Scattering in the Troposphere," Proc. IRE, 38, April 1950, pp. 401-412.

## TRANSHORIZON PROPAGATION

12. Bullington, K., Inkster, W.J. and Durkee, A.L., "Results of Propagation Tests at 505 Mc and 4090 Mc on Beyond-Horizon Paths," Proc. IRE, 43, Oct. 1955, pp. 1306-1316.
13. du Castel, F., Tropospheric Radiowave Propagation Beyond the Horizon, Pergamon Press Ltd., First English ed., 1966.
14. Chisholm, J.H., Portmann, P.A., de Bettencourt, J.T., and Roche, J.F., "Investigations of Angular Scattering and Multipath Properties of Tropospheric Propagation of Short Radio Waves Beyond the Horizon," Proc. IRE, 43, 10, Oct 1955, pp. 1317-1335.
15. Chisholm, J.H., Morrow, W.E., Jr., Nichols, B.E., Roche, J.F., and Teachman, A.E., "Properties of 400 Mcps Long-Distance Tropospheric Circuits," Proc. IRE, 50, 1962, pp. 2464-2482.
16. Cox, D.C., "Phase and Amplitude Measurements of Microwaves Propagated Beyond the Horizon," Tech. Report No. 2275-1, (SEL-67-100), Stanford Electronics Laboratories, Stanford University, California, Dec 1967.
17. Crawford, A.B., Hogg, D.C., and Kummer, W.H., "Studies in Tropospheric Propagation Beyond the Horizon," Bell Sys. Tech. J., 38, Sept. 1959, pp. 1067-1178.
18. Fehlhaver, L., "Results of Scatter Experiments Over Land and Their Relation to Models of the Atmosphere," NATO Advanced Study Institute, Aberystwyth, Wales, Sept 1967.
19. Friis, H.T., Crawford, A.B., and Hogg, D.C., "A Reflection Theory for Propagation Beyond the Horizon," Bell Sys. Tech. J., 36, May 1957, pp. 627-644.
20. Gjessing, Dag T., "On the Determination of Permittivity Variations in the Troposphere by the Aid of Electromagnetic Measurements, Scatter Propagation Measurements on 6000 Mc over a 340 km Path," Rept. R-76, Norwegian Defense Research Establishment, Kjeller-Lillestrom, Norway, May 1960.
21. Gjessing, D.T., "An Experimental Determination of the Spectrum of Permittivity and Air Velocity Fluctuations along a Vertical Direction in the Troposphere Using Radio Propagation Methods," Rept. No. IR-E-7, Norwegian Defense Research Establishment, Kjeller-Lillestrom, March 1962.

22. Gjessing, D.T., "An Experimental Study of the Properties of the Tropospheric Permittivity and Wind Velocity Fields from the Point of View of Isotropy Using Radio-Propagation Methods," Rept. No. IR-E-6, Norwegian Defense Research Estab., Kjeller-Lillestrom, Norway, March 1963.
23. Gjessing, Dag T. and Irgens, F., "On the Scattering of Electromagnetic Waves by a Moving Tropospheric Layer Having Sinusoidal Boundaries," IEEE Trans. GAP, AP-12, 1, Jan 1964, pp. 51-73.
24. Gjessing, D.T. and Borresen, J.A., "Beamswing Experiments," NATO Advanced Study Institute, Aberystwyth, Wales, Sept 1967.
25. Gordon, W.E., "Radio Scattering in the Troposphere," Proc. IRE, 43, 1, Jan 1955, pp. 23-28.
26. Hirai, M., Nishikori, K., Fukushima, M., Kurihara, Y., Inoue, R., Ikeda, M., Niwa, S. and Kido, Y., "Studies in UHF Overland Propagation Beyond the Horizon," Jour. of Radio Res. Labs., Japan, 7, 31, May 1960, pp. 137-176.
27. Hirai, M., Inoue, R. and Kido, Y., "Variation in Received Signal Power with Narrow Beam Antennas Rotated Horizontally in UHF Beyond-the-Horizon Propagation," Jour. Radio Res. Labs, Japan, 7, 33, Sept. 1960, pp. 487-507.
28. Janes, H.B. and Wells, P.I., "Some Tropospheric Scatter Propagation Measurements Near the Radio Horizon," Proc. IRE, 43, 10, Oct. 1955, pp. 1336-1340.
29. Kieburztz, R.B. and Fantera, I.A., "Angle-of Arrival Measurements Performed Over a 296-Km Troposcatter Path." Radio Science, 1 (New Series), 11, Nov. 1966, pp. 1245-1252.
30. Koono, T., Hirai, M., Inoue, R., and Ishizawa, Y., "Antenna-Beam Deflection Loss and Signal Amplitude Correlation in Angle-Diversity Reception in UHF Beyond-Horizon Communications," J. Radio Res. Labs., Japan, 9, 41, Jan 1962, pp. 21-49.
31. Mellen, G.L., Morrow, W.E., Poté, A.J., Radford, W.H., and Weisner, J.B., "UHF Long-Range Communication Systems," Proc. IRE, 43, 10, Oct. 1955, pp. 1269-1280.

## TRANSHORIZON PROPAGATION

32. Norton, K.A., Rice, P.L., Janes, H.B. and Barsis, A.P., "The Rate of Fading in Propagation Through a Turbulent Atmosphere," Proc. IRE, 43, 10 Oct 1955, pp. 1341-1353.
33. Ortwein, N.R., Hopkins, R.U.F., and Pohl, J.E., "Properties of Tropospheric Scattered Fields," Proc. IRE, 49, 4, April 1961, pp. 788-802.
34. Rogers, T.F., "VHF Field Strength Far Beyond the Radio Horizon," Proc. IRE, 43, 5, May 1955, p. 623.
35. Smith, Paul L., Jr., "On Inferring the Refractive-Index Structure of the Troposphere from Electromagnetic Scattering Experiments," Radio Science J. Res. NBS/USNC-URSI, 69D, 6, June 1965, pp. 881-884.
36. Staras, H., "Scattering of Electromagnetic Energy in a Randomly Inhomogeneous Atmosphere," J. Applied Physics, 23, 10, Oct 1952, pp. 1152-1156.
37. Staras, H., "Forward Scattering of Radio Waves by Anisotropic Turbulence," Proc. IRE, 43, 10, Oct 1955, pp. 1374-1380.
38. Staras, H., "A Mathematical Study of Beyond the Horizon Scatter Propagation," Ph.D. Thesis, Univ. of Maryland, 1955, (Available University Microfilms, Ann Arbor, Michigan, Pub. No.: 15, 305).
39. Staras, H. and Wheelon, A.D., "Theoretical Research on Tropospheric Scatter Propagation in the United States, 1954-1957," IRE Trans. PGAP, AP-7, Jan 1959, pp. 80-87.
40. Stein, S., Johansen, D.E., and Starr, A.W., "Final Report on Theory of Antenna Performance in Scatter-Type Reception," Hermes Electronics Co., Cambridge, Mass., Sept 1951, pp. 132-156.
41. Strohbehn, J.W., "Transhorizon - Propagation Measurements and Simulated Angular-Response Patterns," Ph.D. Thesis, Final Report Proj. 2270, (SEL-63-083), Stanford Electronics Laboratories, Stanford, California, Oct 1963.
42. Strohbehn, J.W. and Waterman, A.T., Jr., "Simulated Angular Response Patterns for Transhorizon Propagation," Radio Science, J. Res. NBS/USNC-URSI, 68D, 2, Feb 1964, pp. 173-178.

43. Strohbehm, J.W. and Waterman, A.T., Jr., "Transhorizon Propagation Measurements from a Simultaneous Frequency and Angle Scan Experiment," Radio Science, 1 (New Series), 7, July 1966, pp. 729-741.
44. Trolese, L.G., "Characteristics of Tropospheric Scattered Fields," Proc. IRE, 43, 10, Oct 1955, pp. 1300-1305.
45. Villars, F. and Weisskopf, V.F., "On the Scattering of Radio Waves by Turbulent Fluctuations of the Atmosphere," Proc. IRE, 43, 10, Oct 1955, pp. 1232-1239.
46. Vogelman, J.H., Ryerson, J.L. and Bickelhaupt, M.H., "Tropospheric Scatter System Using Angle Diversity," Proc. IRE, 47, May 1959, pp. 688-696.
47. Wait, James R., "Coherence Theories of Tropospheric Radio Propagation," IEEE Trans. GAP, AP-12, 5, Sept 1964, pp. 649-650.
48. Wait, J.R., and Jackson, D.M., "Influence of the Refractive Index Profile in VHF Reflection from a Tropospheric Layer," IEEE Trans. GAP, AP-12, 4, July 1964, pp. 512-513.
49. Waterman, A.T., Jr., "A Note on Microwave Reception Well Beyond the Horizon," Tech. Rep. No. 8, NONR 225(10), Electronic Res. Labs., Stanford University, Stanford, Calif., Oct 15, 1953.
50. Waterman, A.T., Jr., Bryant, N.H., and Miller, R.E., "Some Observations of Antenna-Beam Distortion in Trans-Horizon Propagation," IRE Trans. PGAP, AP-5, July 1957, pp. 260-266.
51. Waterman, A.T., Jr., "A Rapid Beam-Swinging Experiment in Transhorizon Propagation," IRE Trans. PGAP, AP-6, Oct 1958, pp. 338-340.
52. Waterman, A.T., Jr. and Strohbehm, J.W., "Reflection of Radio Waves from Undulating Tropospheric Layers," TR No. 2270-4, (SEL-63-060), Stanford Electronics Laboratories, Stanford, Calif., May 1963.
53. Wheelon, A.D., "Relation of Radio Measurements to the Spectrum of Tropospheric Dielectric Fluctuations," J. Applied Physics, 28, 6, June 1957, pp. 684-693.
54. Wheelon, A.D., "Radio-Wave Scattering by Tropospheric Irregularities," J. Research Nat. Bureau Stds. - D. Radio Prop., 63D, 2, Sept. - Oct. 1959, pp. 205-233.

TRANSHORIZON PROPAGATION

55. Yeh, Leang P., "Experimental Aperture-to-Medium Coupling Loss," IEEE Trans. GAP, AP-14, 5, Sept 1966, pp. 663-665.

N72-25-368

## IDENTIFICATION OF ATMOSPHERIC STRUCTURE

BY COHERENT MICROWAVE SOUNDING

William P. Birkemeier

University of Wisconsin

### ABSTRACT

Two atmospheric probing experiments involving beyond-the-horizon propagation of microwave signals are reported. In the first experiment, Doppler-shift caused by the cross-path wind is measured by a phase-lock receiver with the common volume displaced in azimuth from the great-circle. Variations in the measured Doppler shift values are explained in terms of variations in atmospheric structure. The second experiment makes use of the pseudorandom sounding signal used in a RAKE communication system. Both multipath delay and doppler shift are provided by the receiver permitting the cross section of the layer structure of the atmosphere to be deduced. The angular dependance and the cross-path wind in each layer are displayed.

### 1. INTRODUCTION

This paper is concerned with the problem of identifying the structure and dynamics of the atmosphere from the coherent detection and analysis of sounding signals after their transmission through the scatter medium. Section I discusses the coherent CW soundings performed on the UW-Collins 230 km link. This work, which relies on the antenna beams for spatial resolution, has successfully identified cross-path winds in scattering strata at different heights and has led to a model which hopefully improves the understanding of the role of cross-path winds and atmospheric layer structure in the propagation mechanism. A model is presented which predicts the doppler shift of the

## IDENTIFICATION OF STRUCTURE BY MICROWAVE SOUNDING

received signals in terms of the cross-path motion of the scatterers through the family of ellipsoids of constant path delay. This model also predicts a unique amplitude vs. path delay and doppler-shift relationship for scatterers that are moving with a given horizontal cross-path wind speed in each strata.

Successful tests of amplitude vs. doppler shift for this model were performed by synchronously pointing the UW and Collins antennas off the great circle and noting that the average doppler shift increased appropriately with antenna beam displacement from the great circle.

A more useful test of the model which is discussed in Section II became possible with the results of certain RAKE channel sounding experiments described by Barrow, *et al.*, (1965) and Abraham, *et al.*, (1967). Interpreting the RAKE data in terms of the model yielded layer heights and wind speeds that compared favorably with the weather bureau sonde data available at the nearest times and location. Since the RAKE technique achieves spacial resolution by the use of wide-band, short correlation-time sounding signals rather than by small antenna beams, several system advantages are realized. These are discussed in Section 3, together with a hybrid system which would employ a vertical fanbeam.

### 2. CW SOUNDING ON THE UW-COLLINS LINK

In the UW experiment, a phase-stable 960 MHz, CW signal derived from a 1 MHz standard is transmitted at 10 kw from a 28 ft. steerable paraboloid at the Collins Communication Research Facility (CCRF) near Cedar Rapids, Iowa, to the University of Wisconsin Facility (UW) near Arlington, Wisconsin (Figure 1). The signal received at UW on a 28 ft. steerable paraboloid is phase-coherently retransmitted at 810 MHz and 1 kw from the same (duplexed) antenna to CCRF. The transponded signal is received at CCRF on a separate 28 ft. paraboloid slaved to the CCRF transmitting antenna. The round-trip signal is phase compared with the signal from the original standard in a linear phase-detection system. The phase difference, due almost entirely to the propagation path, is continuously recorded on two simultaneously available ranges ( $17.12\pi$  and  $60\pi$  radians). Each phase output automatically resets at its range limits, thereby providing linear, piece-wise continuous data over an unlimited number of cycles, (Figure 2). Residual phase noise of the closed-loop system is about  $30^\circ$  rms. Experimental error introduced by the antenna pointing systems is considered negligible. Antenna pattern measurements revealed a constant great-circle misalignment of approximately  $0.2^\circ$ . Data illustrated in Figures 3 through 9 have not been adjusted for this small error.

The signal phase behavior includes a wide range of variations (Birkemeier, *et al.*, 1965). Certain features are consistently noted. Phase "jumps" of up to, but not exceeding,  $\pi$  radians occur coincident with deep fades, indicating the interference nature of the fading phenomena. With the exception of these phase jumps and occasional periods of aircraft interference, the instantaneous phase rate never exceeds that which can be produced by tropospheric winds. When the antennas are aligned on the great-circle azimuth the phase has essentially zero average slope. Random variations over several minutes rarely exceed about  $10\pi$  radians (Figure 2). When the antennas are synchronously set to positions off the great-circle azimuth, the phase accumulates continually in one direction (Figure 2). Random phase variations about the average slope also become more rapid, suggesting that the phase spectrum of the received signal is dependent on the antenna pointing angle.

The average slope of the phase-versus-time record corresponds to an average doppler shift and at a given antenna angle is clearly defined over a few minutes (Figure 2).

A series of beam-swinging experiments revealed the average doppler shift to be a systematic function of the antenna pointing angle and the direction

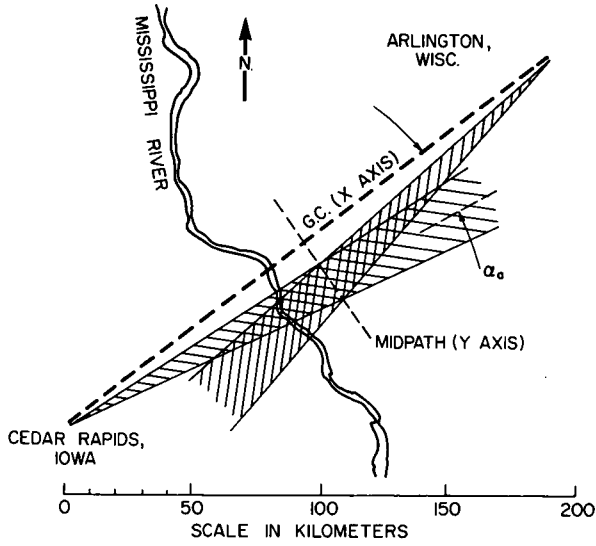


Figure 1. Plan view of closed-loop circuit illustrating geographic location, nominal antenna half-power beamwidth and azimuthal antenna-pointing angle,  $\alpha_a$ .

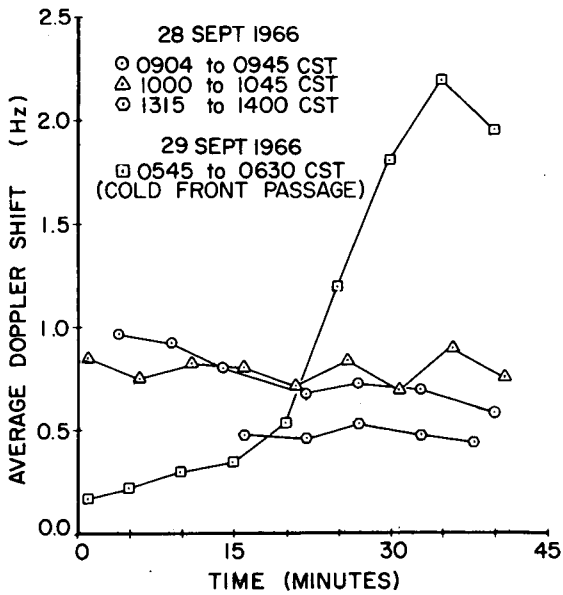


Figure 3. Measured average Doppler shifts vs. time for  $\alpha_a = 1.0^\circ$ .

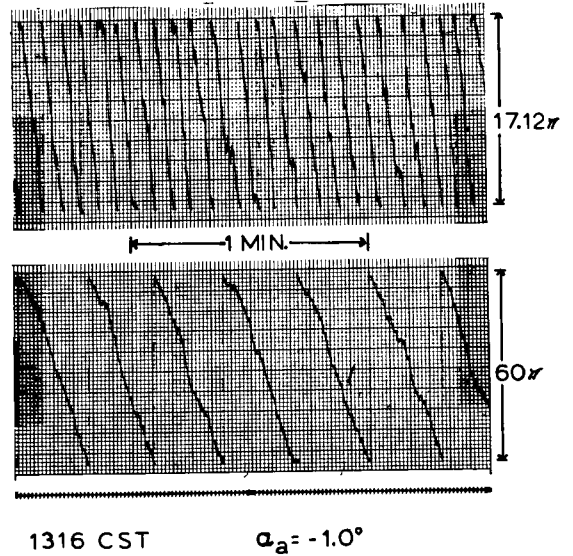
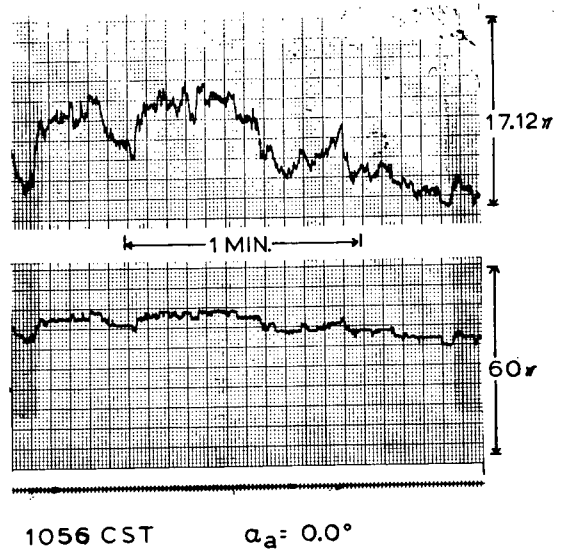


Figure 2. Typical strip-chart records of signal phase variations measured during experiment of 7 July 1966. Time markers at 1-s intervals.

IDENTIFICATION OF STRUCTURE BY MICROWAVE SOUNDING

Table 1  
Beam Swinging Experiments

Experiment	Date	Time (CST)	Time at Each Angle**	Sequence of Angles**
A	10 June 1966	1437-1750	1	1
B	7 July 1966	1015-1430	2	2
C	21 Sept. 1966	1211-1313	1	3
D	28 Sept. 1966	0431-0626	3	3
E	28 Sept. 1966	1840-1915	4	3
F	29 Sept. 1966	0230-0430	3	3
G	29 Sept. 1966	1055-1145	5	4
H	24 July 1967	2225-0230	5	3
I	25 July 1967	0440-0710	6	5
J	25 July 1967	1010-1115	7	3
K	25 July 1967	1115-1200	7	3
L	25 July 1967	1200-1315	7	3

\*Time at Each Angle  
 1. 10 minutes.  
 2. 15 minutes.  
 3. 10 minutes between 0.6° N & S, 5 minutes each larger angle.  
 4. 1.5 minutes.  
 5. 10 minutes between 0.4° N & S, 5 minutes each larger angle.  
 6. 4 minutes.  
 7. 3 minutes.

\*\*Sequence of Angles  
 1. 0.2° N & S, 0.4° N & S, etc.  
 2. 0.4° N & S, 1.0° N & S, 1.0° N & S, 1.0° N & S, 0.6° N & S.  
 3. Sequentially S to N.  
 4. Sequentially N to S.  
 5. Sequentially S to N from 5.0° S, then 5.0° S to 7.0° S.

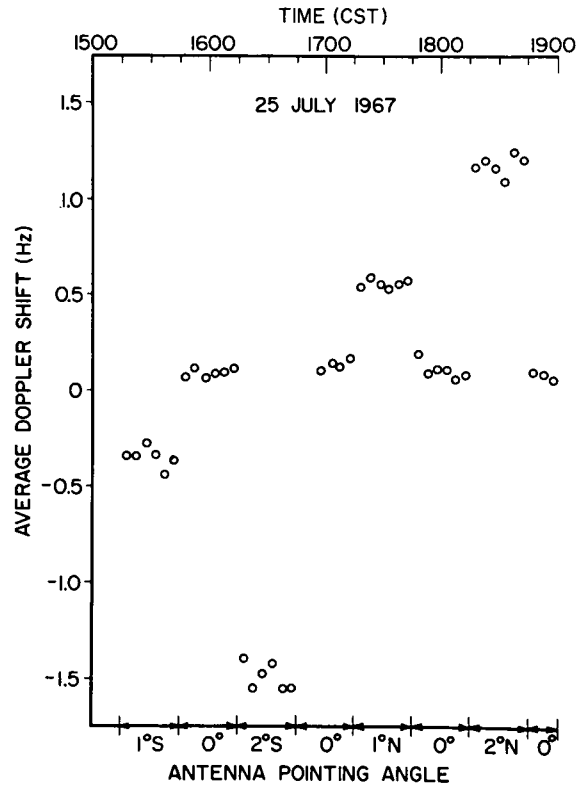


Figure 4. Measured average Doppler shifts vs. azimuthal antenna-pointing angle and time.

and magnitude of the crosspath wind. In each experiment the antennas were synchronously set for several minutes at a sequence of azimuthal angles. Experimental observations are summarized in Table 1 and Figures 5 through 9.

Doppler shifts measured at equal angles on opposite sides of the great circle are essentially identical in magnitude in Figures 5, 6 and 8. The sign of observed doppler shifts agrees with the direction of crosspath winds in the lower portion of the common volume, i.e., the received frequency is greater (less) than the transmitted when the antennas are pointed upwind (downwind). The symmetric, systematic, non-linear characteristic of these doppler shift versus antenna pointing angle curves cannot be ascribed to nonstationary meteorological processes. The daily to hourly variation in this curvature suggests dependence on the prevailing reflective angular dependence of the atmospheric refractive structure.

The observed data will be discussed in the context of the proposed doppler shift model which is developed in terms of the average crosspath wind. Concurrent wind data were obtained by tracking meteorological pilot balloons with a theodolite at launch intervals of 30 minutes to one hour. The analysis of tracking data included computation of vertical profiles of crosspath wind speed. Representative crosspath vertical profiles are shown in Figure 10. Balloons were normally launched from a field site at midpath beneath the common volume.

2.1 Doppler Shift Model

To each point in space there corresponds a ray-path length  $L(x,y,z)$  which is defined by a ray from the transmitter to receiver passing through the given

point. Surfaces of constant path length or phase are approximately ellipsoids of revolution having the radio terminals as foci (Figure 11). A signal obtained via any single moving point is shifted in frequency by an amount proportional to the rate at which the point cuts equiphase surfaces. Thus the "single-scatterer" doppler shift  $f$  is given by

$$f = -\frac{1}{\lambda} \frac{dL}{dt} = -\frac{1}{\lambda} \mathbf{V} \cdot \nabla L \quad (1)$$

where  $\lambda$  is the wavelength and  $V$  is the velocity of the moving scatterer. Assuming the simplest ray path of two straight lines through the scatterer,  $L$  is determined using the coordinate system illustrated (Figure 11) with origin at the midpoint of the straight (chordal) line between the terminals.

$$L = [(d+x)^2 + y^2 + z^2]^{1/2} + [(d-x)^2 + y^2 + z^2]^{1/2} \quad (2)$$

Applying (1) to (2) yields

$$f = -\frac{4}{\lambda L} \frac{ux(1 - 4d^2/L^2) + vy + wz}{1 - 16x^2d^2/L^4} \quad (3)$$

where  $(u,v,w)$  are the  $(x,y,z)$  components of  $V$ .

The relative importance of the various terms in (3) depends on the position of the scatterer and on the relative magnitude of the velocity components. The along-path ( $u$ ) contribution is negligible because the ellipsoids are longitudinally very "flat". The factor  $(1 - 4d^2/L^2)$  is small, and equal to  $4z_m^2/L^2 = 4h_m^2/d^2$ , where  $z_m$  and  $h_m$  are the midpath heights of an ellipsoid above the chordal axis and spherical earth, respectively. This factor ranges from  $10^{-4}$  to  $10^{-2}$  from the bottom to the top of the common volume for the path employed in these experiments.

At a given point, the average horizontal velocity normally greatly exceeds the average vertical velocity. We interpret our observations in terms of drift of scatterers with the average crosspath velocity  $v$ . Under these conditions, (3) predicts for a single scatterer in the vicinity of midpath,

$$f = -\frac{2}{\lambda} v \left(\frac{2y}{L}\right) = -\frac{2}{\lambda} v \sin \alpha = -\frac{2}{\lambda} v \alpha \quad (4)$$

where  $\alpha$  is the azimuthal angle of the single scatterer from the great circle. For a given crosspath wind speed, pointing the antennas to azimuthal angles away from the great circle tends to favor scatterers at larger angles  $\alpha$  which consequently increases the observed doppler shifts. There are many scatterers at various positions, however, which create a spectrum of doppler shifts in the received signal. It is necessary to specify the doppler spectrum and its dependence upon azimuthal antenna pointing angle  $\alpha_a$  in order to explain the shape of the curves of average doppler shift  $f$  vs.  $\alpha_a$ .

Consider numerous scatterers moving with the wind, each contributing a signal component having a doppler shift given by (4). Because of the longitudinal flatness of the ellipsoids, scatterers even widely displaced from midpath may be included with little error. For a given constant crosspath speed the doppler shift varies linearly with crosspath position and is independent of height. The shape of the doppler spectrum which results is principally determined by the relative strengths of scattered signals as a function of crosspath position. The signal power from a given position depends upon the combined antenna illumination pattern and upon the scattering cross section at the position. Let  $G(\alpha)$  denote the multiplied azimuthal pattern function of the antennas and  $W(\alpha)$  the scattered power per unit azimuthal angle. For synchronously pointed antennas with boresights at  $\alpha_a$ ,

IDENTIFICATION OF STRUCTURE BY MICROWAVE SOUNDING

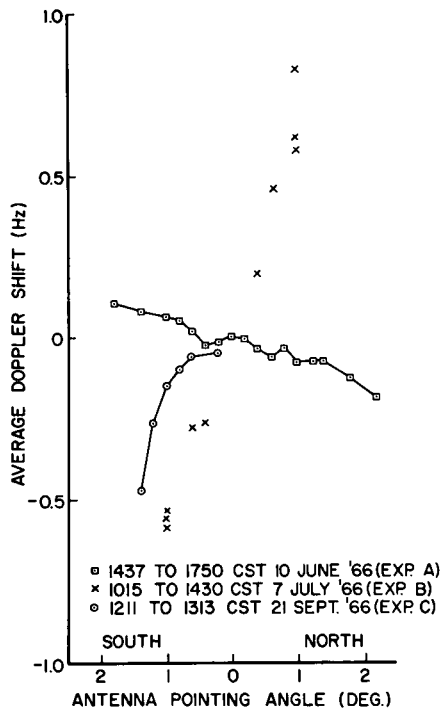


Figure 5. Measured average Doppler shifts vs. azimuthal antenna-pointing angle.

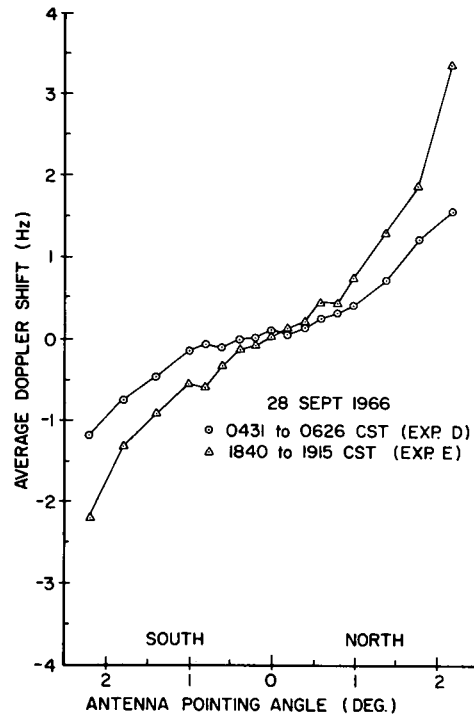


Figure 6. Measured average Doppler shifts vs. azimuthal antenna-pointing angle.

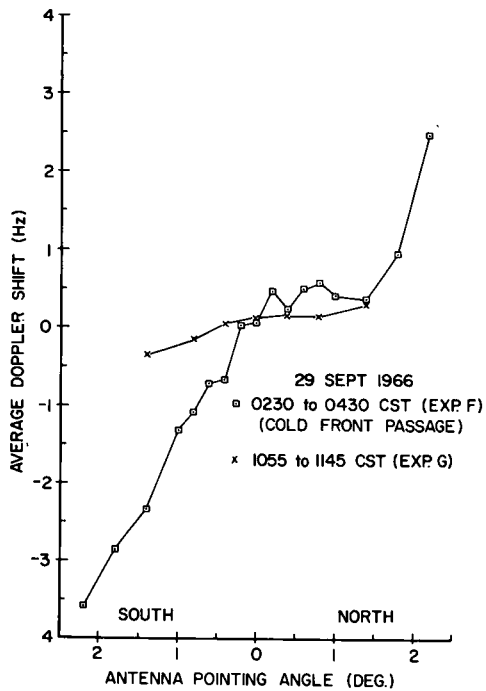


Figure 7. Measured average Doppler shifts vs. azimuthal antenna-pointing angle.

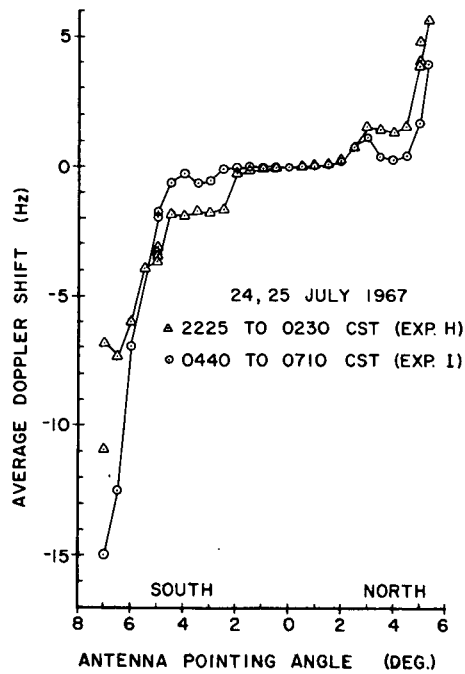


Figure 8. Measured average Doppler shifts vs. azimuthal antenna-pointing angle.

$$S(f) df - S_{\alpha}(\alpha, \alpha_a) d\alpha = G(\alpha - \alpha_a) W(\alpha) d\alpha \quad (5)$$

where  $S(f)$  is the doppler spectrum  $S_{\alpha}(\alpha, \alpha_a)$  is the doppler spectrum written in terms of  $\alpha$ , and  $f$  and  $\alpha$  are related by the scaling relation (4).

Bello (1965) gives the average doppler shift  $\bar{f}$  in terms of the doppler spectrum as

$$\bar{f} = \int f S(f) df / \int S(f) df \quad (6)$$

which according to (4) and (5) may be written

$$\bar{f} = - \frac{2v}{\lambda} \int \alpha G(\alpha - \alpha_a) W(\alpha) d\alpha / \int G(\alpha - \alpha_a) W(\alpha) d\alpha \quad (7)$$

This equation provides a relation between  $\bar{f}$  and  $\alpha_a$  in terms of the antenna patterns and the "angular dependence" function  $W$ .  $W$  includes the azimuthal dependence of scattering cross section and/or reflection coefficient depending on the degree of anisotropy of the atmospheric structure involved.  $W$  is assumed to decrease monotonically and symmetrically with increasing angle from great circle. The doppler spectrum  $S$  is weighted by  $W$  toward the great circle from  $\alpha_a$ , and the average doppler shift is reduced from the value associated with scatterers at  $\alpha_a$ .

An angular dependence function for reflectivity based upon the Tatarski (1961) model for a refractively turbulent medium is

$$\eta = \text{const} \quad \sin^2 \beta / \sin^{11/3}(\theta/2) \quad (11)$$

where  $\theta$  is the scattering angle and  $\beta$  is the angle between the electric field vector and the ray to the receiver. The combined wind and phase data suggested that dominant signal contributions were frequently propagated via a low layer of limited vertical extent. Supporting observations of tropospheric layer structure by Atlas, *et. al.* (1966) and Hardy, *et. al.* (1966) using radar backscatter, and by Lane (1966) using radar and radio refractometers, stimulated analysis of a thin, turbulent scattering layer. Using  $\eta$  (with  $\sin^2 \beta = 1$ ) and gaussian antenna patterns, the "doppler spectra" of Figure 12 were computed from (5). The peaks of  $S_{\alpha}(\alpha, \alpha_a)$  occur to the great-circle side of the pointing angle. These spectra are converted to doppler spectra by means of the scaling relation (4) for a given average crosspath wind velocity. Numerical integration of (7) for such doppler spectra yields the set of average doppler shift versus antenna pointing angle curves of Figure 13 for several heights of the thin, turbulent scattering layer. These curves are symmetric in  $\alpha_a$ , a property of (7) for symmetric  $W$  and  $G$ . A change in the magnitude or direction of the crosspath wind changes the vertical scale or the sign of the curves but not the shapes. The foregoing doppler shift model provides the qualitative features and correct orders of magnitude required to interpret the data.

## 2.2 Interpretation

The crosspath wind profiles have in several cases permitted identification of the height range of significant scattering.

During experiments conducted on 7 July 1966, 21 September 1966, 29 September 1966 and 24, 25 July 1967, the crosspath component of the wind was from the northwest (NW) at all altitudes. The sign of the average doppler shift corresponded to this direction, i.e., was positive (frequency increase) for antennas directed toward the windward side of the great circle, and negative (frequency decrease) for the leeward side. During the experiments of 25 July 1967 in which the beams were azimuthally swung in both an unelevated and elevated position, the average doppler shift was greater for the cases of elevated beams (Figure 9). The observed increase was in agreement with greater wind speeds

IDENTIFICATION OF STRUCTURE BY MICROWAVE SOUNDING

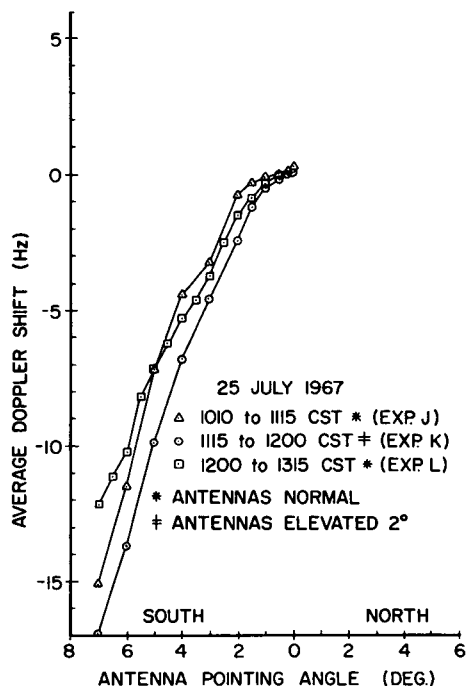


Figure 9. Measured average Doppler shifts vs. azimuthal antenna-pointing angle.

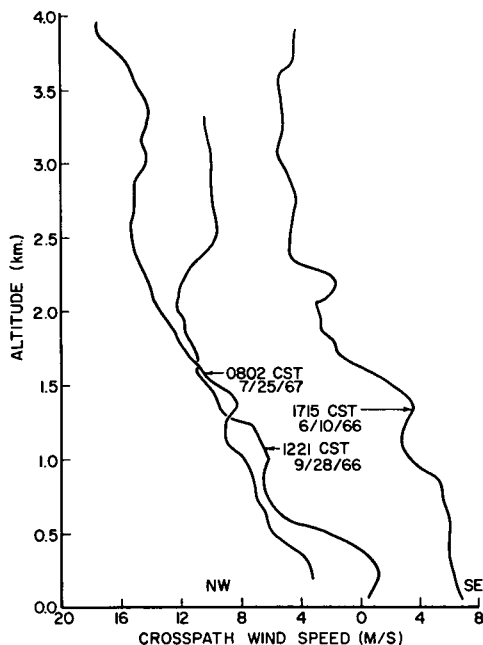


Figure 10. Typical crosspath wind profiles measured during varied meteorological conditions.

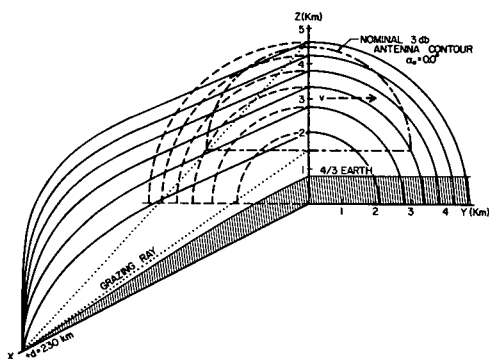


Figure 11. Longitudinal and transverse sections of propagation link and of ellipsoids of constant path length. Path length increment between ellipsoids is  $80\lambda$  shown for  $\lambda = 0.37$  m.

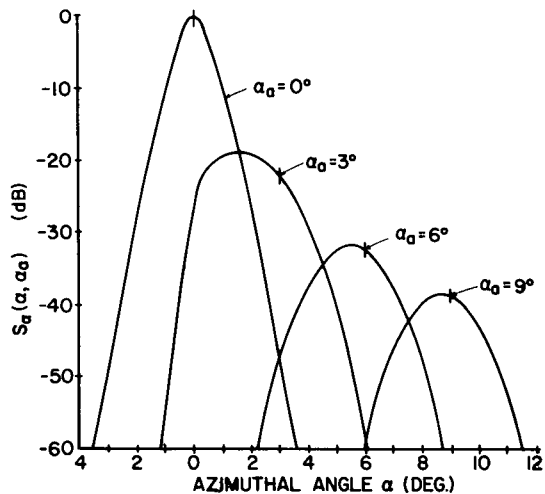


Figure 12. Theoretical Doppler spectra (written in terms of  $\alpha$ ) for different  $\alpha_a$  for a thin, turbulent scattering layer at 785 m above the earth, computed using Tatarski scattering cross section and Gaussian antenna patterns (each with  $3.0^\circ$  half-power beamwidth).

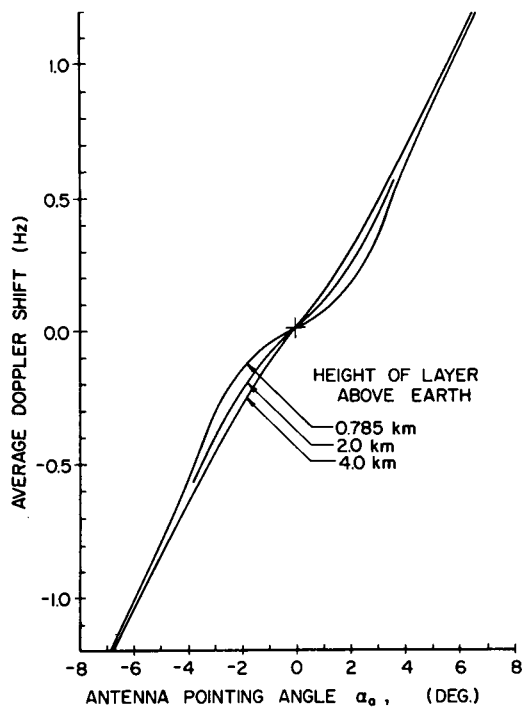


Figure 13. Theoretical average Doppler shift vs. antenna-pointing angle for the two-way path for thin, turbulent scattering layers, computed using Doppler spectra such as those of Fig. 12. Indicated heights are approximately at the bottom, middle and top of the nominal common volume,  $v = 1$  m/s.

measured at the higher altitudes.

Experiments on 28 September 1966 were conducted when the crosspath component was from the NW at all heights above approximately 400 m altitude but from the southeast (SE) between the surface and the reversal height (Figure 10). During the experiments the sign of the doppler shift corresponded to NW winds. Thus although a large percentage of the total propagation path is at altitudes below 400 m, this region did not appear to contribute the significant doppler-shifted signal components.

During the experiment of 10 June 1966, the crosspath component was SE below, and NW at all heights above 1.6 km. The sign of the average doppler shift corresponded to the SE winds in the lower portions of the common volume.

A vertical beam-swinging experiment in which the crosspath wind reversed direction from SW to NW at a height of approximately 1.5 km was conducted on 12 May 1967 and phase data is shown in Figure 15. With the antennas set  $2.0^\circ$  off the great-circle azimuth and at  $0.0^\circ$  elevation, the sign of the average doppler shift corresponded to the SE winds in the lower zone. When the beams were elevated to  $2.0^\circ$ , the average doppler shift reversed to the sense corresponding to the NW winds above 1.5 km. This result suggests that a crossed pair of bistatic, doppler-sensitive systems, measuring both crosspath wind components, might be used to remotely measure winds.

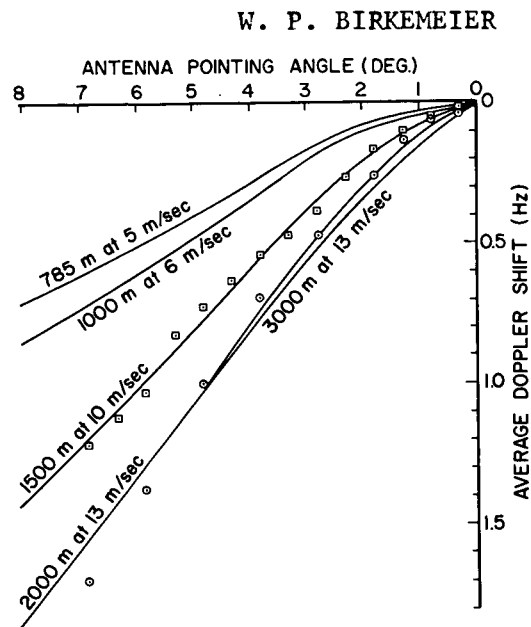


Figure 14. Comparison of data of experiments K and L (Fig. 9) with theoretical average Doppler shift for several layer heights. Wind speeds are average of those measured at the indicated heights during the experiment. Data are compensated for  $0.2^\circ$  constant misalignment.

## IDENTIFICATION OF STRUCTURE BY MICROWAVE SOUNDING

In their entirety these observations demonstrate that the dominant signal contributions were reradiated in the lower regions of the common volume, as distinct from either the upper portions of the common volume or the regions between the antennas and the common volume. This interpretation agrees with the conclusions of earlier studies based on statistical analysis of amplitude data by Ikegami (1960) and Fengler (1964). The next section on the RAKE data also confirms that stronger reflecting layers tend to be the lowest in elevation.

In Figure 14, theoretical curves, similar to those of Figure 13 but computed for single layers at different heights, are compared with the data of Figure 9. For clarity, only two data curves are included. The theoretical curves are scaled for the measured winds at the labeled heights. At low altitudes, where the wind speed increased with height, the height region of agreement is well resolved. The height of agreement for the case of elevated beams is poorly defined because the wind velocity was essentially constant between 2 and 3 km altitude. Good resolution was also obtained when the same procedure was applied to the data of Figure 6. The heights of agreement were about 1.5 and 2.0 km for experiments D and E respectively.

The model based on the Tatarski hypothesis is inadequate to explain features of the data of Figure 8 which were obtained during a stable, stratified nocturnal atmosphere. Stable layers may produce highly anisotropic space correlation functions of index of refraction that yield spectral energy only at wave numbers nearly normal to the earth's surface. This results in quasi-specular components arriving only via paths near the great circle plane. For this reason these components have nearly zero doppler shift independent of their scatterer's crosspath speed. Their contribution to the doppler spectrum is accounted for by emphasizing the angular dependence function  $W$  at small  $\alpha$ . Since many strata of scatterers with differing angular dependence functions and differing wind speeds would normally be included within the UW link's antenna beams, it is hazardous to try to associate the  $W$  function in a given experiment with a single layer. However, in the next section it will be shown that such an identification may be possible with RAKE probing even with large beams.

### 3. RAKE TROPOSCATTER SOUNDING

The experiments of Barrow (1965) and Abraham (1967) analyzed in this section were the first reported tests of the RAKE adaptive communication system applied to the troposcatter channel.

In its normal communicating mode of operation this system employs an estimator-correlator receiver containing a stored alphabet of reference signals. The decision as to which signal from the alphabet was transmitted in each signaling interval is determined by cross-correlating the received signal with each stored reference signal and selecting the one with the greater correlator output.

Since the received signal is distorted by the channel, the correlation process can be enhanced by predistorting the reference signals in the alphabet in an identical manner. To allow this, the receiver must learn the channel transfer characteristic and implement it as a delay-line model into which the reference signals are fed before cross-correlation with the arriving signal. It is the data from the channel sounding operation that is interpreted here in terms of the atmospheric layer structure and the crosspath winds.

To enable the RAKE receiver to learn the channel's transfer characteristic, i.e., its various paths, their delays, gains and doppler shifts, a 10 MHz wide phase-stable, periodic, pseudo-random sounding signal is transmitted continuously. Cross-correlation of this received signal with its replica at the receiver provides a correlation function which is proportional to the received signal intensity at those correlator delays which match the various path delays

of the channel. This cross-correlation function is the path-delay profile. A delay resolution of 0.1  $\mu$ sec. is provided in these data. Furthermore, the doppler shift associated with each path shows up as the beat-frequency of the cross-correlator output at that path delay setting. Figure 16 from Barrow (1965) shows an example of such a cross-correlation function produced by linearly increasing the reference signal delay at the rate of .1  $\mu$ sec. per second. Note the total channel path-delay profile width is about 2.8  $\mu$ seconds.

A systematic increase in doppler frequency with delay is clearly visible in the profile. This was plausibly interpreted by Barrow in terms of vertical wind velocities through the common volume, with higher vertical wind speeds at higher altitudes. However, it can be shown that the profile agrees closely with the result expected from a thin layer of scatterers moving essentially only with the horizontal wind. To show this, the doppler cycles in the profile were counted, starting at the first arrival, and the resulting function compared to that predicted by the model. To get the predicted function, consider a scattering point at (y,z). The path delay at the point relative to (0,z) is given by (2) and amounts to

$$\tau = (L - L_{\min}) / c = y^2 / c(d^2 + z^2)^{1/2} = ay^2 \quad (12)$$

Next, let the reference signal delay be varied linearly in real time t at the rate of p sec/sec. If the total number of doppler cycles appearing in the swept multipath delay profile is counted as a function of sweep time T, beginning with the first-arriving signals, the result is given by

$$N(T) = \int_0^T f_d(t) dt \quad (13)$$

where  $f_d(t)$  is the doppler beat frequency as a function of time.

Recalling that for the model the doppler shift varies linearly with cross-path displacement y and that the delay time  $\tau$  varies as the square of y, we have from (4) and the relation  $\tau = pt$ ,

$$f_d(t) = bvy = bv(\tau/a)^{1/2} = bv(p/a)^{1/2} t^{1/2} \quad (14)$$

where b, v, a and p are constants.

Finally,

$$N(T) = K \int_0^T t^{1/2} dt = \text{const } T^{3/2} \quad (15)$$

Figure 17 shows a log-log plot of N vs. T using the raw, counted data of the profile. A clear power-law dependence is demonstrated, with the empirical power equal to 1.58.

Further consideration of this multipath profile revealed the likelihood that the antennas of the RAKE link were both displaced about one-half beam-width to one side of the great-circle path. This was evidenced by the fact that, if the model is correct, the envelope of the multipath profile appears to violate the possible laws of angular dependence. The envelope peaks at about .8  $\mu$ seconds and then falls with increasing delay. No AGC was used. The total envelope amplitude change is also about 6 db, similar to the combined antenna patterns, suggesting the profile is due to a horizontal scattering layer lying near the bore-site intersection of the beams. Using the known antenna elevation angle, the suspected antenna position is shown superimposed on the cross-section of the ellipsoids of constant time-delay in Figure 18.

Meanwhile, continued data analysis by the original authors developed the doppler spectra for the signals arriving at 0.1 sec. time-delay intervals. These spectra revealed a consistent negative doppler shift. See, for example, Figure 19a. The prevailing cross-path winds were determined from weather bureau data to be from the West, indicating azimuthal antenna displacement to

IDENTIFICATION OF STRUCTURE BY MICROWAVE SOUNDING

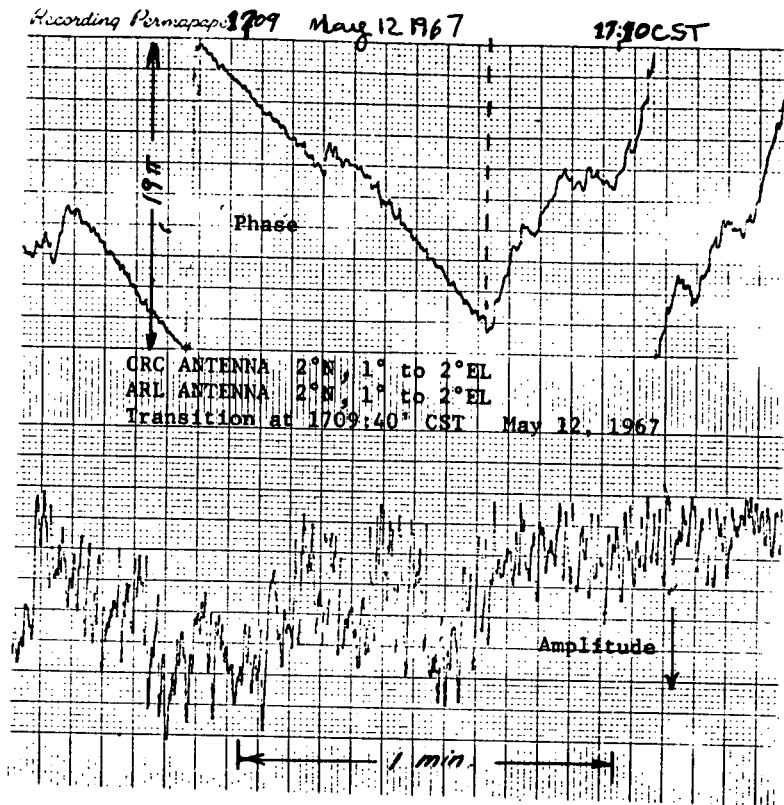


Figure 15. Doppler shift reversal with 2° antenna elevation. Clock offset was  $-23\pi$  rad/min.

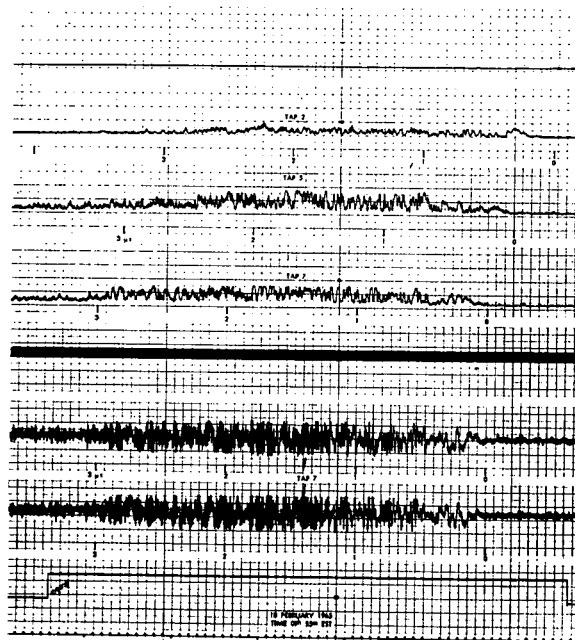


Figure 16. Quadrature components of swept multipath profile from Barrow, 1965. This profile followed scattering function 151 of Figure 19 in time by 6 hours.

Figure 16. Quadrature components of swept multipath profile from Barrow, 1965. This profile followed scattering function 151 of Figure 19 in time by 6 hours.

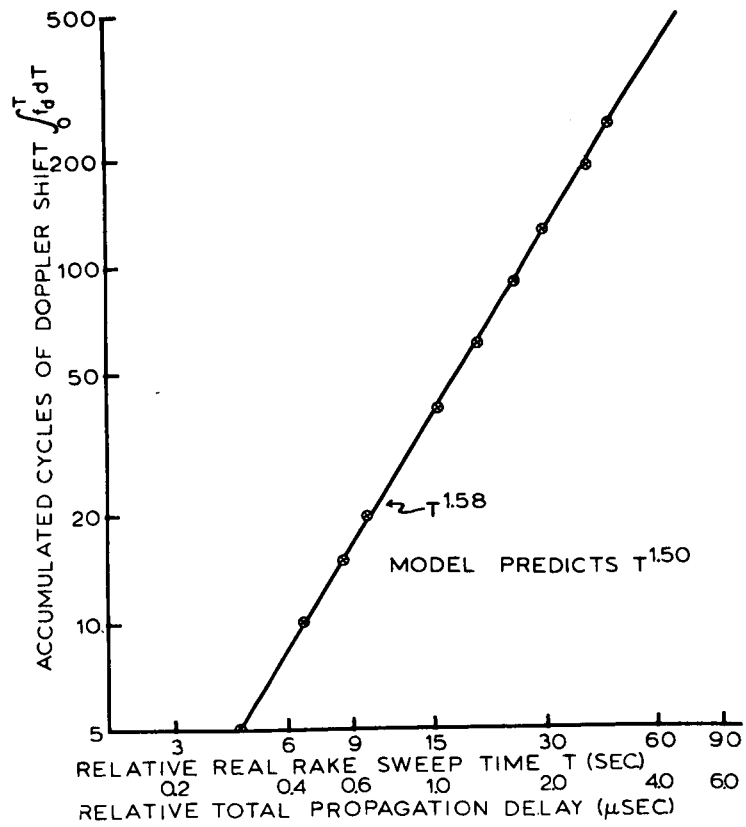


Figure 17. Plot of accumulated doppler-beat cycles vs. sweep time.

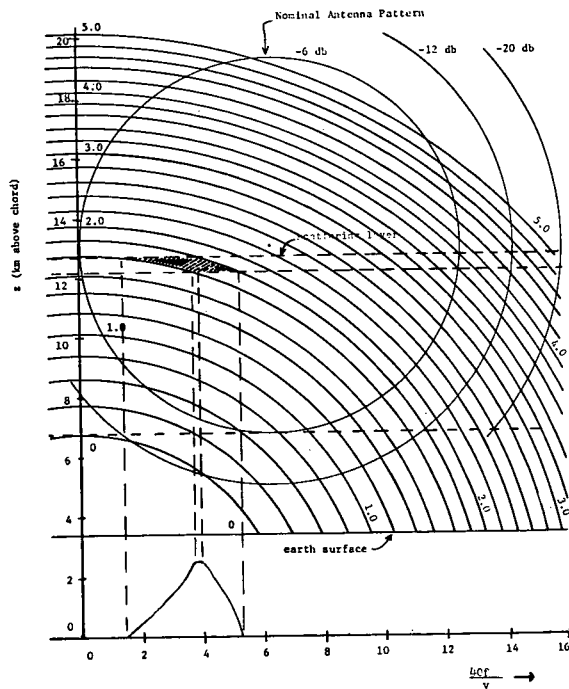


Figure 18. Apparent antenna position for RAKE link. Also shown is the construction of a doppler-spectrum from a single 0.1 μ sec time shell and a single scattering layer.

the East of the path. This predicted antenna displacement was consequently investigated by the original authors and the displacement to the East has been confirmed. The exact position is not known to this writer, however.

### 3.1 Atmospheric Structure From RAKE Profiles

In each of the RAKE scattering diagrams (Figures 19a, 23, 25) ridges of peaked doppler-spectra appear to follow parabolic loci in the time-frequency plane. Such loci are predicted by the model for each scattering strata by the fact that horizontally drifting scatterers increase their doppler shift linearly with  $y$  while their signal delay increases with  $y^2$ . Combining (12) with (4) and using the dimensions of the 480 km RAKE path, we obtain the delay-doppler locus for point scatterers at a height  $z$  and moving with cross-path wind speed  $v$  as

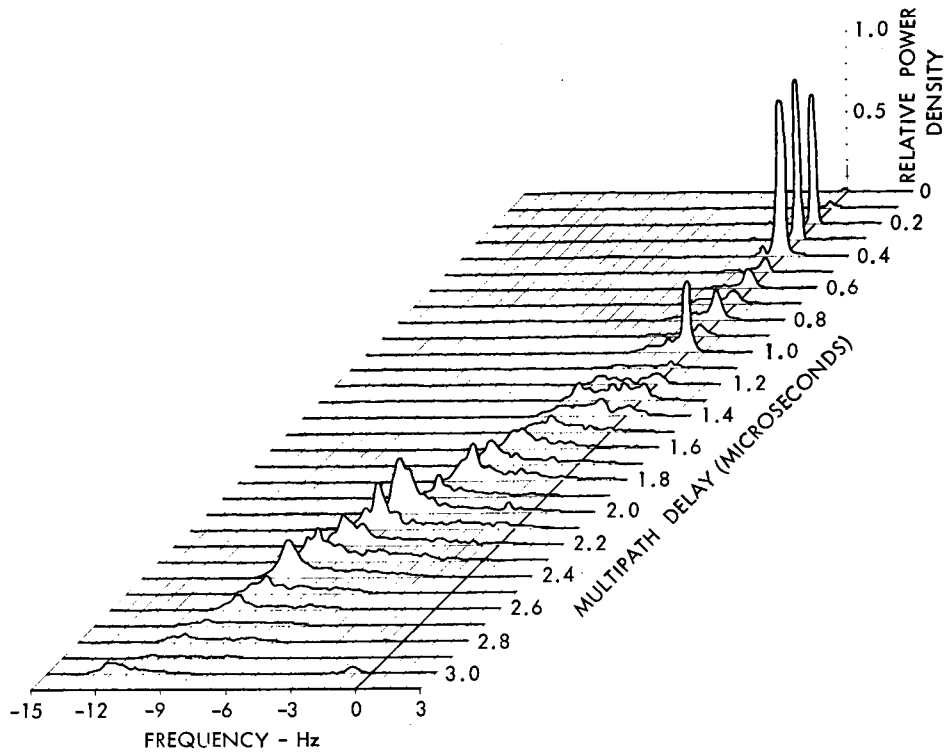
$$\tau = 21.8 f^2 / v^2 + z^2 / 72 - .64 \quad (16)$$

Here  $\tau$  is in microseconds relative to the ellipsoidal shell at the grazing ray intersection which represents the scattering location of the first possible arriving signals;  $f$  is in Hz,  $v$  is in meters/second, and  $z$  is in kilometers above the link chord.

To facilitate the interpretation of the RAKE profiles in terms of the implied layer structure, a program was written on the basis of the model to determine the theoretical ridge for an arbitrary layer height, thickness, and cross-path wind speed and angular dependence function. In this program the relative doppler power spectral density for a given delay shell is proportional to the vertical thickness of the scattering layer in the shell at a particular value of  $y$  (or  $f$ ), multiplied by the displaced antenna function and the angular dependence. Figure 18 shows the sketch of the spectrum obtained from a single shell. A theoretical ridge is shown in Figure 20 for a layer with Tatarski angular dependence, a height of 12.8 km, a thickness of 0.4 km, and a cross-path windspeed of 45 m/second. These values produce good agreement to the dominant ridge in the RAKE scattering function in Figure 19a. The spectrum at the origin in the RAKE diagram is assumed to have originated from signals scattered from near the great-circle plane at the grazing ray height. This determines the reference delay for each higher layer.

A number of additional parabolic tracks in this profile have been identified by plotting local spectra maxima for each shell. (See Figure 19b). Furthermore, several sharp spikes along the zero-doppler shift axis imply the existence of several specular layers as well. In an effort to compare these "radio identified" layers with the atmospheric structure in the vicinity of the link we resorted to the nearest weather bureau radio sonde profiles of wind, temperature, and humidity for the dates of the RAKE tests. Analysis of these data led to a set of probable layer heights together with their respective cross-path wind speeds. Using (16) each meteorologically identified layer's parabolic track was plotted and compared with the radio-deduced layer heights and winds. Figure 21 shows surprising agreement with the radio-detected layers since the sonde data precedes the radio run by eight hours. The result is nevertheless intriguing. Figure 22 based on the same profile shows the radio layers drawn in cross section across the antenna pattern. Wind profiles from the three weather stations are included for comparison to the radio-derived wind in each layer. The dashed lines indicate radio layers for which only the zero-doppler shift point on its track could be identified. The fact that such layers are likely to be specular agrees with the stable state of the atmosphere at their location as indicated by the sonde data.

In Figure 24 the radio layers corresponding to the parabolic tracks of the scattering function of Figure 23 are shown. It is apparent that the first 0.8



Scattering Function, Record No. 151

Figure 19a. Scattering diagram No. 151 (Abraham, 1967). Test data 2/18/65, 0821 GMT.

Figure 19b. Parabolic tracks of scattering diagram No. 151.

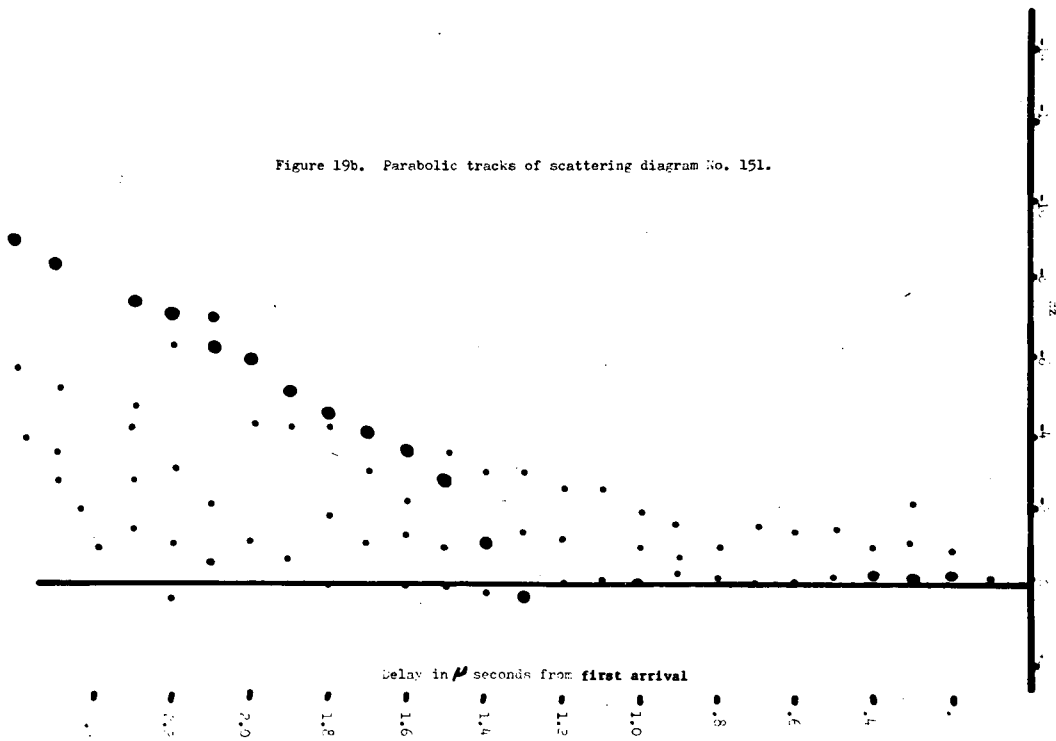


Figure 19b. Parabolic tracks of scattering diagram No. 151.

IDENTIFICATION OF STRUCTURE BY MICROWAVE SOUNDING

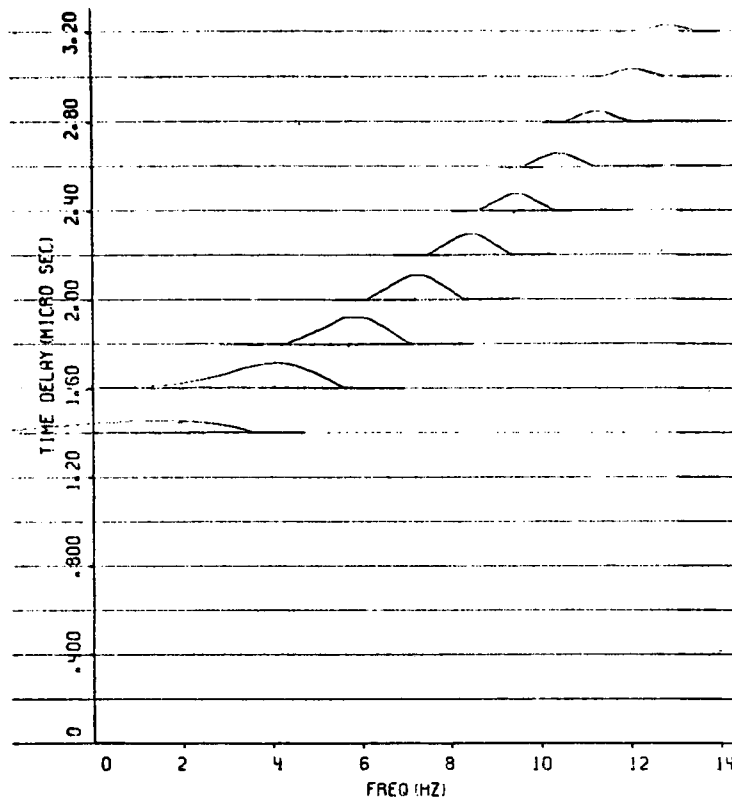


Figure 20. Theoretical scattering diagram for a layer of thickness = 0.4 km, height above chord = 12.5 km, and cross-path wind speed = 45 m/s.

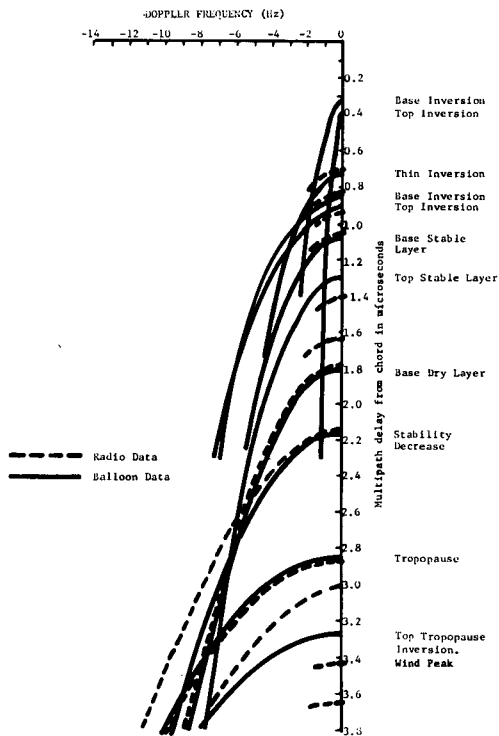


Figure 21. Comparison of RAKE parabolic tracks with tracks derived from meteorological sounding. Washington, D. C. sonde preceded radio run No. 151 by 8 hours.

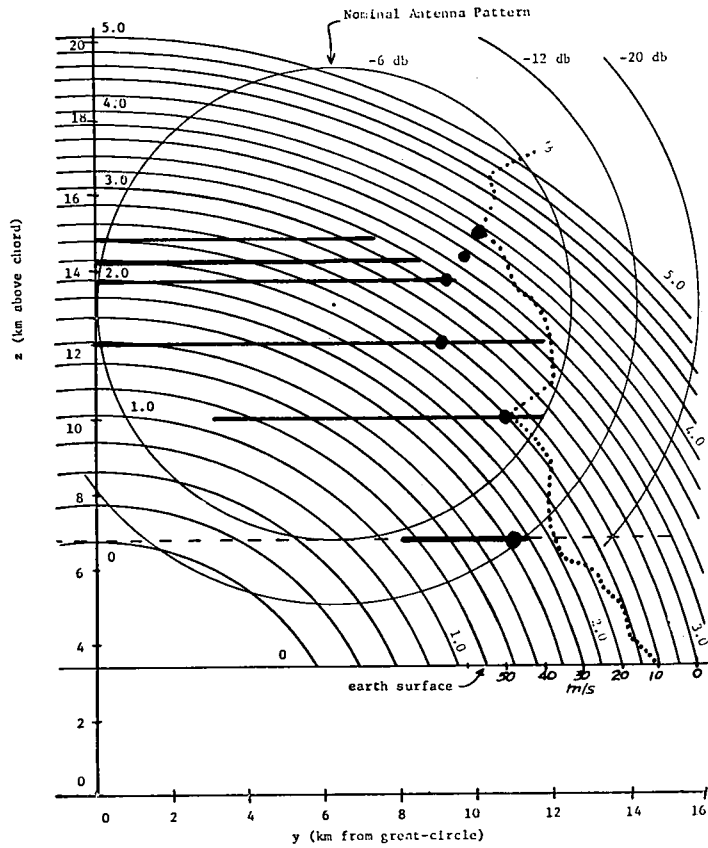


Figure 22. Atmospheric cross-section derived from Figure 19 (Scattering-function 151). Radio-derived wind-speed shown by large dots. Radio data 2/18/65 0821 GMT, Sonde data 3/18/65 0000 GMT.

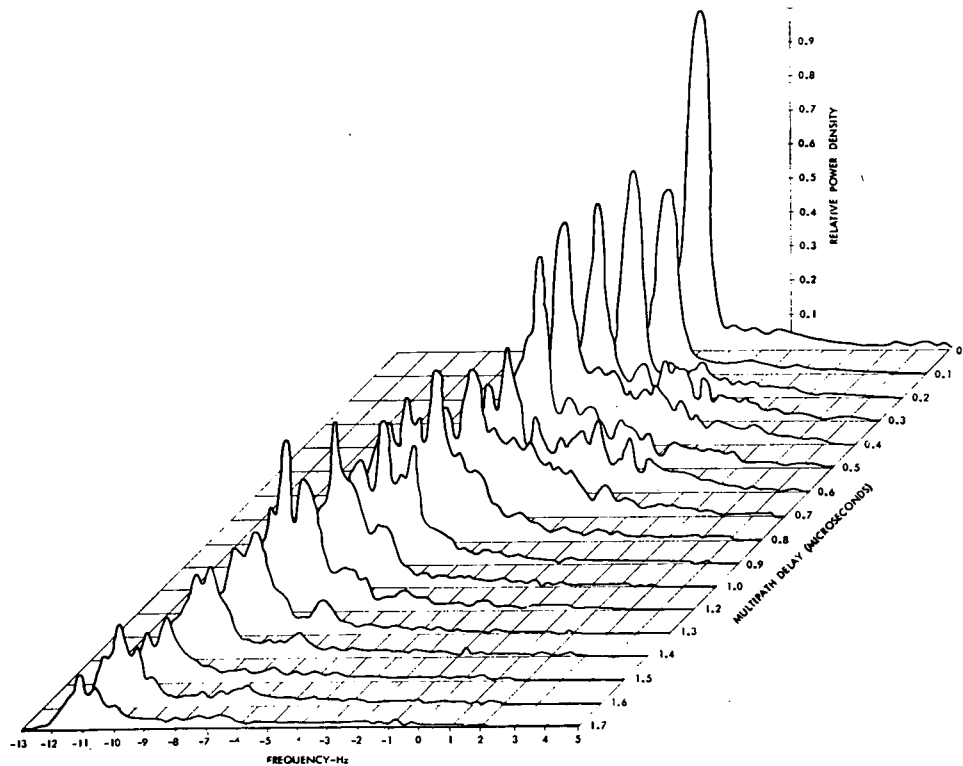


Figure 23. Scattering diagram No. 134 (Abraham, 1967).

IDENTIFICATION OF STRUCTURE BY MICROWAVE SOUNDING

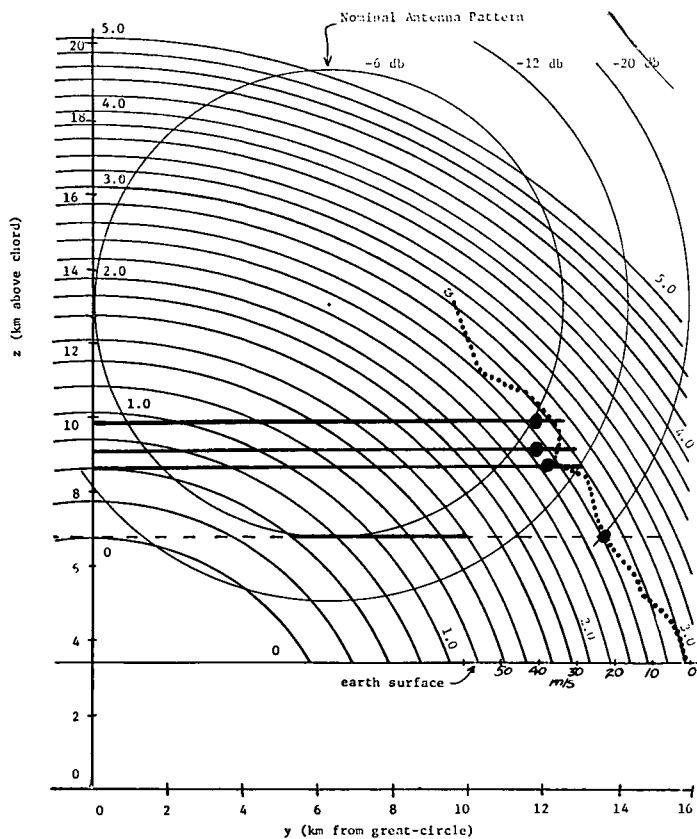


Figure 24. Atmospheric cross-section derived from Figure 23 (Scattering diagram 134). Radio data 2/17/65 2226 GMT, Sonde data 2/18/65

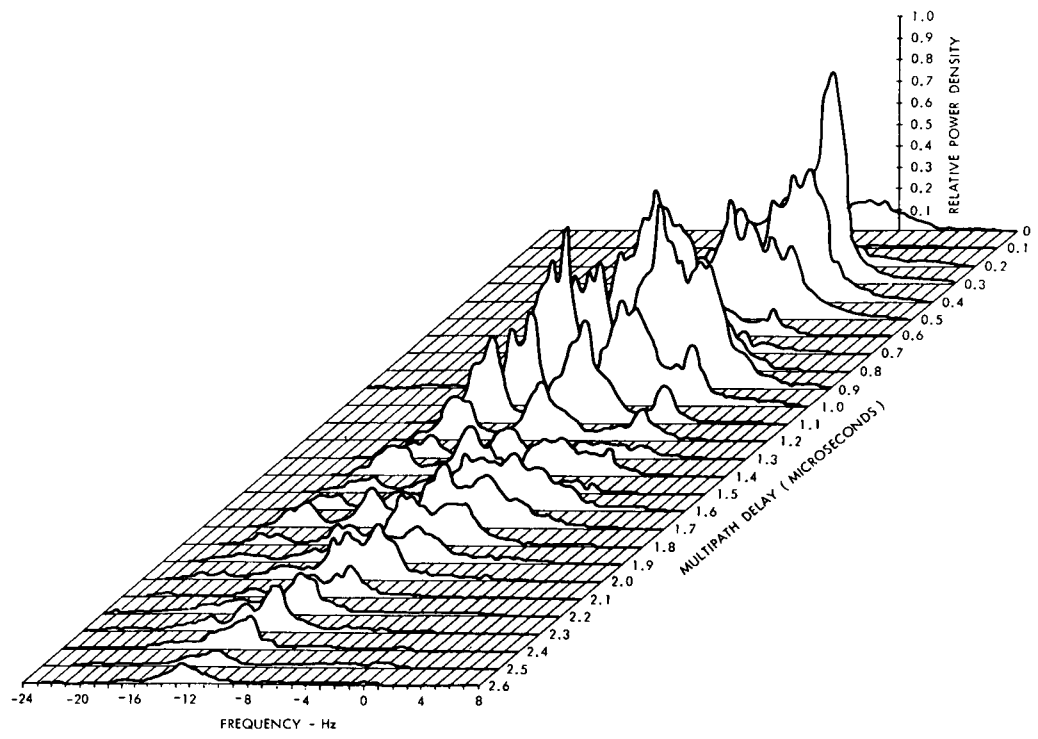


Figure 25. Scattering diagram No. 181 (Abraham, 1967).

microseconds are not included in the display. As such, the solid line segments indicate that part of the layer which contributed to the segment of the ridge in the scattering function.

The scattering function of Figure 25 appears to have coincided with a frontal passage. The cross-section derived is shown in Figure 26.

### 3.2 Considerations of Angular Dependence

Most of the parabolic ridges analyzed so far show general agreement with the  $-11/3$  power law. It is difficult to determine the power law exactly, however, since neither the antenna pattern nor its position is known accurately. Further RAKE studies performed carefully, however, may well allow the angular dependence to be determined for particular turbulent layers.

In certain RAKE data, strong angular dependence is implied by "spikes" along the zero-doppler shift axis in the RAKE scattering functions. An example is the scattering function shown in Figure 27. The analysis of this and similar profiles is in progress to evaluate the exact angular dependence function and, if possible, the degree of anisotropy of the space correlation function of the index of refraction in the layer.

### 3.3 Tilted Layers

Under certain atmospheric conditions, scattering layers may be uniformly slanted with respect to the horizon or layers may contain uniformly slanted "scatterers". If such scattering surfaces are visualized against the background of the ellipsoids of constant phase of path delay, it is apparent that maximum reflectivity will tend to occur off the great-circle at the point of greatest tangency of the scattering surfaces to the ellipsoids. A RAKE parabolic profile for such a layer (for antennas aimed along the great circle) should then peak to the side of the zero-doppler axis, indicating "slanted anisotropy" in the space correlation function of the refractive structure. There is the possibility that the antennas of the RAKE link were aligned under such a slanted atmospheric structure, accounting for their fixed misalignment.

## 4. PROPOSED HYBRID SYSTEMS

### 4.1 Measurement of Vertical Wind Velocities

An important limitation of the simplified model presented here, in spite of the apparent agreement with this particular RAKE data, is that it ignores turbulent velocity fluctuations in the wind. Such random variations in velocity become quite important if the cross-path wind component is small compared with the total wind speed. The effect of the velocity fluctuations is to spread the doppler spectra at the various RAKE delays. This greatly complicates the problem of calculating layer thickness from the RAKE data. A Scheme to measure the vertical velocity fluctuations by eliminating doppler shift due to horizontal motion is suggested by the link geometry. Both spatial resolution from the beams and time resolution from the RAKE are required. If the antennas are designed to produce vertical fan-beams sufficiently narrow to illuminate only the first Fresnel zone along the great-circle plane, then according to (3), doppler shift can occur only from vertical scatterer motion. (Tests with beams of  $0.3^\circ$  width will be attempted on the UW-Collins link in the near future) Combining such fan-beams with a RAKE system to provide height resolution should allow doppler-sensing of the vertical wind velocity field. Horizontal turbulent velocities may be measured similarly by azimuthally displacing the beams off the great circle, correcting for the vertical velocity fluctuations in the measured doppler shift fluctuations.

### 4.2 Total Wind Measurement by Crossed Links

IDENTIFICATION OF STRUCTURE BY MICROWAVE SOUNDING

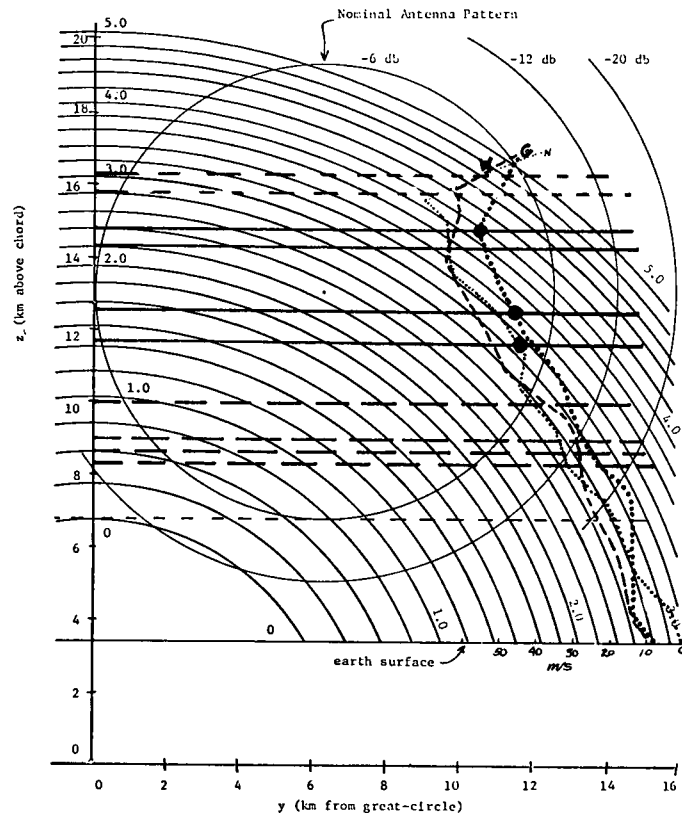


Figure 26. Atmospheric cross-section derived from Figure 25. (Scattering diagram 181). Radio data 2/19/65, 1831 GMT, Sonde data 2/19/65, 1200 GMT.

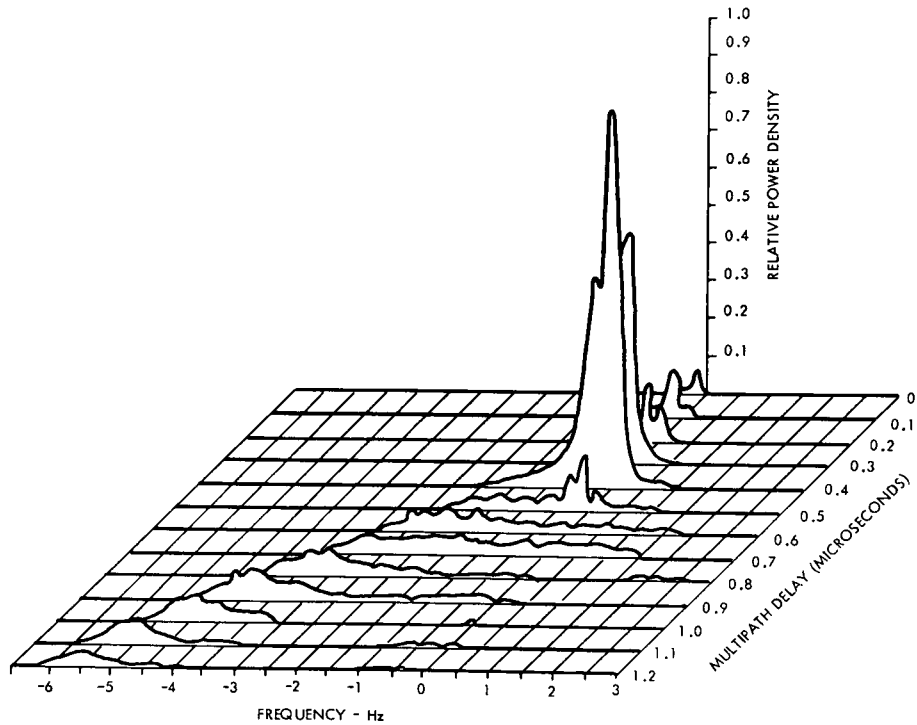


Figure 27. Scattering diagram No. 142 showing layer with strong angular dependence.

If two scatter links are arranged in parallel and spaced so that their ellipsoids of constant phase intersect orthogonally at approximately the height of the grazing ray intersection, it appears possible to measure the vertical and horizontal wind velocities simultaneously at a common point midway between the paths. This measurement is accomplished simply by forming the sum and difference of the phase outputs of the two links operating coherently on carrier-wave signals. Vertical profiles would be achieved by vertical beam swinging.

## 5. CONCLUSIONS

Forward-scatter atmospheric probing has been demonstrated to be potentially capable of providing useful structural information on the atmosphere. Much work needs to be done, but the combination of forward scatter's great sensitivity and the possibility of achieving spatial resolution through the use of signal processing techniques rather than by the use of large antennas makes the possibilities exciting indeed.

## ACKNOWLEDGEMENTS:

Section I is taken in part from a paper entitled "Observation of wind produced Doppler shifts in troposcatter" by Birkemeier, et. al. published in April, 1968 by Radio Science.

The author is indebted to the following persons for their able assistance: D. S. Sargeant, H. S. Merrill, A. B. Fontaine, D. Atlas, D. W. Thomson, G. T. Bergemann, C. M. Beamer, and I. H. Gerks. He also wishes to thank Dr. B. B. Barrow for his interest and cooperation in supplying the RAKE data which permitted this analysis.

The work was supported by the National Science Foundation, Atmospheric Science Division, under grants GP 667, GP 4352, and GA 1291, The Wisconsin Alumni Research Foundation, and the Collins Radio Company.

## REFERENCES

- Abraham, L. G., B. B. Barrow, W. M. Cowan, and R. M. Gallant, May, 1967: "Tropospheric Scatter Multipath Tests in the Caribbean," Sylvania Electronic Systems, Applied Research Laboratory, Waltham, Massachusetts.
- Atlas, D., K. R. Hardy and T. G. Konra, 1966: Radar Detection of the tropopause and clear air turbulence, Proc. XII Weather Radar Conf., 17-20 October 1966, Norman, Oklahoma.
- Barrow, B. B., L. Abraham, S. Stein and D. Bitzer, 16 April 1965: "Tropospheric-Scatter Propagation Tests Using a Rake Receiver," 1st Annual IEEE Communication Convention, Boulder, Colorado, June 7-9, 1965. Also available as Research Report 461, Applied Research Laboratory, Sylvania Electronic Systems, Waltham, Massachusetts.
- Barrow, B. B., L. Abraham, S. Stein and D. Bitzer, June 1965: "Preliminary Report on Tropospheric-scatter Propagation Tests Using a Rake Receiver," Proc. IEEE, vol. 53, no. 6, pp. 649-651.
- Bello, P., 1965: Some techniques for the instantaneous real-time measurement of multipath and doppler spread, IEEE Trans. COM-13, No. 3, 285-292.
- Birkemeier, W. P., H. S. Merrill, Jr., D. H. Sargeant, D. W. Thomson, C. M. Beamer, G. T. Bergemann, April, 1968: "Observation of Wind-Produced Doppler Shifts in Tropospheric Scatter Propagation," Radio Science, vol. 3, No. 4, pp. 309-317.

## IDENTIFICATION OF STRUCTURE BY MICROWAVE SOUNDING

- Birkemeier, W. P., D. H. Sargeant, J. P. Aasterud, H.S. Merrill, Jr., D.W. Thomson, I. H. Gerks, C. M. Beamer and G. T. Bergemann, 1965: A Study of the lower atmosphere using scattering of microwaves, Tech. Rep. 2, Depts. of Meteor. and Elect. Engr., Univ. of Wisc., Madison, Wisconsin.
- Bitzer, D. R., D. A. Chesler, R. Ivers and S. Stein, August 1966: "A Rake System for Tropospheric-scatter," IEEE Trans. on Comm. Tech., vol. COM-14, no. 4, pp. 499-506.
- Crawford, A. B., A. B. Hogg and W. H. Kummer, 1959: Studies in tropospheric propagation beyond the horizon, Bell Systems Tech. J., 38, 1067-1178.
- Du Castel, F. 1966: Tropospheric Radiowave Propagation Beyond the Horizon, Pergamon Press Ltd., Oxford, England.
- Fengler, G., 1964: Dependence of 500 Mc/s field strength values and fading frequencies on meteorological parameters, Proc. World Conf. on Radiometeorological parameters, 14-18 September 1964, Boulder, Colorado.
- Gjessing, D. T., 1964: An experimental study of the variations of the tropospheric scattering cross-section and air velocity with position in space, IEEE Trans., AP-12(1), 65-73.
- Hardy, K. R., D. Atlas and K. M. Glover, 1966: Multiwavelength backscatter from the clear atmosphere, J. Geophys. Res., 71, No. 6, 1537-1552.
- Ikegami, F., 1960: A preliminary study of radiometeorological effects on beyond-horizon propagation, J. R. NBS 64D (Radio Prop.), No. 3, 239-246.
- Koono, T., M. Hirai, R. Inoue and Y. Ishizawa, 1962: Antenna-beam deflection loss and signal amplitude correlation in angle-diversity reception in UHF beyond-horizon communication, J. Radio Res. Lab. 9, No. 41, 21-49.
- Laaspere, T., 1958: An analysis and re-evaluation of the role of horizontal drift in producing fading in tropospheric scatter propagation, Res. Rep. EEE-380, Cornell Univ., Ithaca, New York.
- Lane, J. A., 1966: Experimental investigations of refractive-index variations in the troposphere, XV General Assembly URSI, 5-15, Sept. 1966, Munich, Germany (Proc. to be published).
- Stein, S., 1966: in Schwarz, M., Bennett, W. R., and Stein, S. (1966), Communications Systems and Techniques, p. 360 (McGraw-Hill Book Company, Inc. New York, New York).
- Strohbehn, J. W. 1963: Transhorizon-propagation measurements and simulated angular response patterns, Res. Pre., SEL-63-083, Stanford Elect. Lab., Stanford, California.
- Tatarski, V. I., 1961: Wave Propagation in a Turbulent Medium McGraw-Hill Book Co., New York, New York.

N72-25369

THEORETICAL INTERPRETATIONS  
OF  
SCATTER PROPAGATION

Albert D. Wheelon  
Hughes Aircraft Company  
Culver City, California

The discovery of microwave propagation well beyond the radio horizon in the late forties created an immediate interest in its communication possibilities. The first decade (1950 - 1960) was characterized by a vigorous experimental and theoretical program aimed at mapping out those propagation features which were most relevant to the design of radio relay systems. Long term averages of mean signal level and their rough scaling with frequency and distance were of primary interest. Highly reliable signal levels were emphasized at the expense of unusually large, though infrequent signals. The fine structure of the signal was explored in a rough way, in order to set conservative bounds on the communication channel capacity. Space correlations of the signal were measured so as to establish appropriate separation distances for diversity transceivers. Theoretical explanations were tied either to a layered reflection model or to turbulence scattering schemes. The single scattering far field or cross section approximation was used almost exclusively to describe the latter, while signal variability had to be embroidered onto the stable layer theories by qualitative concepts of moving glint or reflection points. The two theories were first considered as competitive explanations of the same phenomenon, although gradually it was appreciated that a variable mixture of the two was probably responsible. Whatever the deficiencies of this program, one must admit that the combination of rough experiment and theory met the communication engineering needs of the first decade rather well.

The second decade beginning in 1960 is probably best described as a renaissance of the scientific interest which first stimulated the subject. The attractive possibility of using short term radio measurements as a means for inferring the instantaneous structure of the atmosphere through which the waves had passed was gradually appreciated. Important new experimental techniques also became available to improve such capabilities. Very stable oscillators were developed which made it possible to measure round trip signal phase on scatter paths (1). The time domain correlation or RAKE technique used by the Sylvania group (2) provides a unique means for examining particular range slices of the scattering volume. Multiple arrays of receiving antennas were used by the Stanford group (3) to study the azimuth and elevation fine structure of the propagation volume by the electronic synthesis of very narrow beams. Over and above these measurement techniques, data processing

capabilities have improved importantly since the early days when much of the data was hand reduced. The capacity to do high speed digital processing of wide band signals is central to the availability of substantial amounts of precision data on signal fine structure. Taken together, these experimental techniques provide a means for studying the atmospheric structure in three space dimensions and time with exciting precision. Nevertheless, our ability to design specific measurement programs to exploit this capability depends in large measure on our intrinsic understanding of the phenomenon.

Unfortunately, our theoretical understanding of the propagation mechanism has not kept pace with experimental progress. No adequate description of the signal fine structure has been developed thus far. We must still depend on two qualitative, competitive theories (layers vs. scatter) to explain the general features of the transmission, as discussed in Dr. Cox's review (4). Either a reconciliation or fusion of the two theories is needed to suggest the next step in an evolving understanding of the propagation. It may even be that the two models are simply different ways of describing the same basic mechanism which is as yet undiscovered. It is vital to separate the geometrical considerations of the propagation path from the physics of the layers and/or turbulent irregularities. Gaussian correlation models, chosen for their integrability, are no longer an adequate starting point. Nor is it appropriate to try to force all available data into universal turbulence theories which may or may not be primarily responsible at various times. Finally, the familiar restrictions on stationarity, homogeneity, and isotropy should be relaxed in a consistent way.

There has been a great deal of advanced theoretical research on line-of-sight propagation, both in Russia and the United States, stimulated in large measure by optical propagation using lasers. However, the geometries and signal statistical considerations for line-of-sight and transhorizon propagation are sufficiently different to make the recent research largely irrelevant to scatter propagation.

The general features of a theory for single scattering by turbulent irregularities which meets most of the above needs were described in 1959 (5). The fundamental physical notion is that the received signal is the integrated result of scattering/reflection events throughout the common volume. This leads naturally to an integral (equation) relation between the measured signal and the refractive structure producing it.

$$E_s(R) = -R^2 \int_V d^3r G(r, R) E_o(r, T) \Delta \epsilon(r, t) \quad (1)$$

where  $G(R, r)$  is the free space Green's function,  $V$  the common volume,  $\lambda = \frac{2\pi}{k}$  the electromagnetic wavelength,  $R$  the receiver and  $T$  the transmitter locations. Formally, this is just the Born approximation for scattering by a dielectric perturbation  $\Delta \epsilon$ . The problem is that  $\Delta \epsilon$  is the function that we wish to infer, not assume. Furthermore, it is usually a stochastic function of position and time, which is defined only by its statistical averages. The essential trick is to introduce a three dimensional Fourier transformation

$$\Delta z(r, t) = \int d^3 k \xi(k, t) e^{i \vec{k} \cdot \vec{r}} \quad (2)$$

in which the turbulence wavenumber  $\vec{k}$  decomposition of the turbulent irregularities  $\xi(k, t)$  is related to the more familiar wavenumber spectrum  $S(k)$  by:

$$\langle \xi(k, t) \xi(k', t) \rangle = \frac{\delta(k - k')}{(2\pi)^3} S(k) \quad (3)$$

If we substitute (2) into (1) and interchange the orders of integration, we achieve the crucial separation of propagation geometry and turbulence physics.

$$E_s(r) = \underbrace{-k^2 \int d^3 k \xi(k, t)}_{\text{Physics}} \underbrace{\int_V d^3 r e^{i \vec{k} \cdot \vec{r}} G(r, r) E_0(r, T)}_{\text{Geometry}} \quad (4)$$

Finally one can establish an explicit expression for the average scattered power by taking the magnitude of (4) and introducing Equation (3).

$$\langle |E_s|^2 \rangle = \frac{k^4}{(2\pi)^3} \int d^3 k S(k) \left| \int_V d^3 r e^{i \vec{k} \cdot \vec{r}} G(r, r) E_0(r, T) \right|^2 \quad (5)$$

It is this expression, rather than the cross section approximation, which provides the starting points for a more precise theory.

All of the electromagnetic and path geometrical features of the propagation are contained in the bracketed quantity in (5), which appears as a weighting function or kernel of the turbulent spectrum  $S(k)$ . The frequency and distance dependence of the scattered field are implicit in this weighting function via their appearance in the incident wave  $E_0$ , the Green's function, and their convolution with  $\exp(i \vec{k} \cdot \vec{r})$  over the scattering volume  $V$ . One can also exploit Equation (5) to describe more complicated experiments. For instance, by inserting appropriate Delta functions in the volume integration, it is possible to isolate those elements of the received signal corresponding to particular multipath components. An inhomogeneous field in which the intensity of turbulent irregularities varies with altitude is relevant to the real atmosphere and can be included in the above expression as height dependent shaping factors (i.e.  $\exp(-z/\lambda)$ ) in the geometrical integrals. The influence of a transmitter antenna pattern is contained naturally in the incident wave  $E_0$ , and can be included for the receiver by multiplying the free space Green's function  $G(R, r)$  by the pattern function describing ray propagation from the various scattering points  $r$  to the receiver  $R$ . The usual approximation for narrow beam geometries, in which the integrations are replaced by  $V$  times an average value of the integrand, can thus be checked. By further

complicating the geometry of Equation (5), one can describe beam swinging within or off the great circle plane. Unfortunately, this formalism has not yet been reduced to explicit expressions useful for comparison with experiment, and these calculations represent an ambitious program. However the important point to make is that it is essentially an exercise in integral calculus, one which can reliably provide the relationship between the scattered power and the still arbitrary spectrum  $S(\kappa)$  for any propagation path. The hope, of course, is that such integral relations can be inverted to deduce the spectrum  $S(\kappa)$  from the measured quantities.

It is of some interest to note that the bracketed weighting function in Equation (5) is a function of the three vector components of the wavenumber vector  $\vec{\kappa}$ . This occurs because of the different ways in which the propagation geometry integrals emphasizes the x, y, and z projections of  $\vec{\kappa}$  via the scattering mechanism. Through its argument, this produces a directional emphasis of the spectrum  $S(\kappa_x, \kappa_y, \kappa_z)$ , which must be considered together with non-isotropy of the turbulent field itself. The possible confluence of flat layers with large horizontal anisotropic blobs having short vertical correlation has been suggested before (6), and these two observations may provide an avenue to a common understanding of the phenomenon.

The basic signal statistical distribution of the received field should also provide a mechanism for distinguishing between: (1) scatter, and (2) layers plus scatter or glint. The usual assumption that the amplitude is Rayleigh distributed is not confirmed in any detail by experiment - nor should it be expected. The central limit theorem for the contributions of a large number of scattering elements does tell one that the orthogonal signal components of the scattered field

$$E_s = x(t) + iy(t) \tag{6}$$

ought to be distributed as follows:

$$dP(x,y) = \frac{dx dy}{2\pi\sigma^2\sqrt{1-\rho^2}} \exp\left[-\frac{x^2+y^2-2\rho xy}{2\sigma^2(1-\rho^2)}\right] \tag{7}$$

where  $\rho$  is the cross correlation coefficient of x and y and  $\sigma$  is the variance of each. Converting to polar amplitude and phase coordinates and integrating over the phase

$$dP(R) = \frac{R dR}{\sigma^2\sqrt{1-\rho^2}} I_0\left[\frac{\rho R^2}{2\sigma^2(1-\rho^2)}\right] \exp\left[-\frac{R^2}{2\sigma^2(1-\rho^2)}\right] \tag{8}$$

If the correlation  $\rho$  were zero, as usually assumed, this would reduce to the Rayleigh distribution. However, one can generalize Equation (5) to write an explicit expression for

$$\sigma_p^2 = \frac{R^4}{(2\pi)^3} \int d^3k S'(k) \left[ \int_V d^3r e^{i\vec{k}\cdot\vec{r}} \text{Re}(G E_0) \right] \times \left[ \int_V d^3r e^{i\vec{k}\cdot\vec{r}} \text{Im}(G E_0) \right] \quad (9)$$

In a mature theory this should be calculated as a function of geometry and compared with experiment. However, we must also note that a constant vector  $A$  added to a scattered component  $x + iy$  also produces a non-Rayleigh distribution. Starting from (6) and setting  $\rho = 0$  for contrast and temporary simplicity, we find

$$dP'(z) = \frac{R dR}{\sigma^2} I_0 \left[ \frac{RA}{\sigma^2} \right] \exp \left[ -\frac{R^2 + A^2}{2\sigma^2} \right] \quad (10)$$

which is what one ought to expect from a steady layer reflection plus a turbulent scatter component or a random glint from the layer. The hope is that a detailed comparison of short sample experimental data with the two predictions can distinguish between the mechanisms.

The relationship of signal amplitude and phase to one another at succeeding instants of time provides one of the most useful measures of signal fine structure. Included in such relationships are the time auto-correlation of amplitude and phase, plus their corresponding power spectra. The derivatives of these quantities lead to signal fading rates and doppler shifts, both of which are now available experimentally. The joint probability distribution of two time-displaced complex signals

$$E_s(t) = x_1 + iy_1$$

and

$$E_s(t+\tau) = x_2 + iy_2 \quad (11)$$

has been given before in its most general form (5). By converting to polar signal coordinates, it is possible to write an explicit expression for the joint distribution of amplitude  $R_1$ ,  $R_2$ , and phase  $\phi_1$  and  $\phi_2$ . From this one can compute all relevant experimental quantities by integration; viz  $\langle R_1 R_2 \rangle$ ,  $\langle (\phi_1 - \phi_2)^2 \rangle$ , etc. The coefficients in this probability distributions are functions of propagation geometry and the time displacement  $\tau$ . Explicit expressions for the coefficients which are time-displaced generalizations of equations like Equation (8) have been established (5) using the appropriate generalization of Eq. (3).

$$\langle S(k, t) S(k', t+\tau) \rangle = \frac{\delta(k - k')}{(2\pi)^3} S(k) e^{i\vec{k}\cdot\vec{u}\tau} C(k, \tau) \quad (12)$$

Here  $\vec{u}$  is the drift velocity of a frozen irregular structure and  $C(K, \tau)$  describes the time correlation of the turbulent internal rearrangement of the structure. Using this general decomposition, it is possible to write

$$\langle x(t) x(t+\tau) \rangle = \langle x_1 x_2 \rangle = \frac{R^4}{(c\tau)^3} \int d^3 k S'(k) e^{i\vec{u} \cdot \vec{k} \tau} \times C(K, \tau) \left| \int_V d^3 r e^{i\vec{k} \cdot \vec{r}} \nabla_k [G(r, \tau) E_0(r, \tau)] \right|^2 \quad (13)$$

and so on for the other components of the moment matrix which defines the coefficients in the general probability distribution function (5). Notice that these expressions also provide explicit separation of the turbulent physics and the path geometry. In point of fact, the integrals which occur in the time-displaced signal component correlations are the same as those required for the ordinary variances of  $x$  and  $y$  plus the cross correlation  $\langle xy \rangle$ .

The novel physical ingredient is the time autocorrelation of the turbulent structure  $C(K, \tau)$  describing the self motion. Most qualitative theories of fading on scatter paths have ignored this and dealt only with the horizontal wind vector  $\vec{u}$ . The intuitive justification is that the vertical transport velocity is negligible and that only off great circle scattering elements have significant horizontal components of  $\vec{k}$  via the weighting integrals in (13). This may be, but it is worth verifying by explicit calculation. The self-motion has no such projection, so that its vertical component is effective in producing time variability in the great circle plane. There is some reason (5) to believe that  $C(K, \tau)$  ought to be a function of  $K^{2/3} \tau$ , which would suggest a fading rate variation with carrier frequency of  $f^{2/3}$ , as compared to a linear variation for straight drift motion  $f$ . Experiment shows a sliding variability between the two extremes, suggesting a mixture. This kind of experiment ought to provide an exceedingly good means for studying the effect and relative strengths of the various propagation mechanisms. Furthermore, time variability measurements are probably easier to perform than beam swinging experiments because they do not require long times for antenna alignment and give one a chance to examine true snapshots of the atmospheric structure.

A final word about space and frequency correlations is in order. The basic probability distribution for signal components gathered at displaced antennas or at the same site on separated frequencies is given by the same expression referenced (5) above for time-correlated signals. The coefficients which occur in such distributions change by virtue of the modification of the geometrical integrals viz:

$$\begin{aligned}
 \langle x(\underline{r}) x(\underline{r} + \Delta \underline{r}) \rangle &= \langle x_1 x_2 \rangle = \frac{\rho^4}{(2\pi)^3} \int d^3 \underline{k} S(\underline{k}) \langle \\
 &\times \left\{ \int d^3 \underline{r}' e^{i \underline{k} \cdot \underline{r}'} \operatorname{Re} \left[ G(\underline{r}, \underline{r}') E_0(\underline{r}', \tau) \right] \right\} \\
 &\times \left\{ \int d^3 \underline{r}'' e^{i \underline{k} \cdot \underline{r}''} \operatorname{Re} \left[ G(\underline{r} + \Delta \underline{r}, \underline{r}'') E_0(\underline{r}'', \tau) \right] \right\} \quad (14)
 \end{aligned}$$

while the separated frequency expressions involve different electromagnetic wavenumbers  $\underline{k}$  in the Green's function and incident field. The calculation of these coefficients is part of the same unified analytical program suggested above.

Having pointed the way to a wider theory, it is appropriate to emphasize its deficiencies. Firstly, it refers only to the turbulent scatter component and not to a steady layer reflection. A comparable sophisticated theory is needed for the latter, plus a consistent means for predicting its time variability, space correlation, etc. We have also assumed single scattering in the common volume, and some have suggested that multiple scattering may be the dominant mode. While our expressions do allow for a non-isotropic turbulent spectrum  $S(\underline{k})$  depending individually on the three components of  $\underline{k}$ , we have no clear means for dealing with a non-stationary process. However, the primary deficiency of this proposal is that it is a plan and not a finished thesis. Perhaps the availability of new experimental data and the renaissance of genuine scientific interest in the subject will stimulate such research.

#### REFERENCES

- (1) William P. Birkemeier, "Identification of Atmospheric Structure by Coherent Microwave Scattering", April 1968 (this volume).
- (2) B. B. Barrow, L. Abraham, S. Stein, and D. Bitzer, "Preliminary Report on Tropospheric-Scatter Propagation Tests Using a Rake Receiver", Proc. IEEE, Vol. 53, No. 6, pp. 649-651; June 1965.
- (3) Donald C. Cox, "Phase and Amplitude Measurements of Microwaves Propagated Beyond the Horizon", Stanford Electronics Laboratories Technical Report No. 2275-1, December 1967; and J. W. Strohbehn and A. T. Waterman, Jr., "Transhorizon Propagation Measurements from a Simultaneous Frequency and Angle Scan Experiment", Radio Science, Vol. 7, pp. 729-741, (1966).
- (4) Donald C. Cox, "A Review of Transhorizon Propagation as a Possible Tool for Probing of the Atmosphere", March 1968 (this volume).
- (5) Albert D. Wheelon, "Radio Wave Scattering by Tropospheric Irregularities", J. Research NBS Part D, 63 D, p. 205, 1959.
- (6) Harold Staras and Albert D. Wheelon, "Theoretical Research on Tropospheric Scatter Propagation in the United States 1954-1957", IRE Trans. PGAP AP-7, 80 (1959).

COMMENTS ON THE POSSIBILITY FOR DETERMINING  
DETAILED ATMOSPHERIC STRUCTURE FROM TRANS-  
HORIZON RADIO PROPAGATION MEASUREMENTS

By

Richard B. Kieburzt

State University of New York at Stony Brook

The use of transhorizon radio propagation as a technique for investigation of the detailed structure of the upper atmosphere seems to me to have some serious difficulties. I am not optimistic that much more can be learned about detailed structure by use of transhorizon measurements alone, although in combination with other techniques this type of measurement may continue to provide useful information as it has in the past. At the session on transhorizon propagation Dr. Wheelon advocated the development of better theoretical techniques to relate experimental data to the actual structure of the atmosphere. He expressed some optimism that with a more powerful theoretical treatment, transhorizon measurements might be made to yield increased information as to detailed atmospheric structure. While I agree wholeheartedly on the need for development of better theoretical treatments in order to extract the maximum information from experimental data now available, and in order to intelligently plan future experiments, I cannot see how theoretical techniques can overcome the problems of lack of spatial stationarity of the refractive medium and lack of knowledge about the degree of anisotropy of the structure of the medium.

Transhorizon propagation measurements provide a signal which is related to the integrated properties of the atmosphere over a large volume. There is a definite limit on the minimum size of the common volume which is imposed by the antenna beam width and by scintillation errors in the antenna pointing angle due to the accumulated effects of refractivity variations along the propagation path. In experiments in which a signal of wide bandwidth is employed, such as is achieved with short pulses, a degree of spatial resolution within the common volume of the antenna beams is provided. However, this resolution is provided in only one dimension of an ellipsoidal coordinate system. Under circumstances in which it is known that the wind direction in the common volume does not have an appreciable vertical component, the resolution is improved through the use of coherent Doppler techniques. Although the predominance of the horizontal wind components is undoubtedly a valid assumption under most atmospheric conditions, doubt still remains that it will prevail under circumstances such as the passage of a front or the occurrence of thunder storms.

In order to utilize the information available from a transhorizon experiment to determine the structure of the atmosphere, two approaches can be taken. The first of these, which we might call a deterministic approach, assumes that the detailed structure of the atmosphere at any instant in time is to be determined. This determination is not possible unless some assumption is made as to the degree of anisotropy. In other words, if the atmosphere is assumed to exhibit variability in the structure of the refractive index only in one spatial dimension, then the experimental data can, in principle, be used to determine the structure subject to the limits of resolution of the experiment. The trouble with this type of treatment is that it is appropriate only when it is known from other independent measurements that layered structure is dominant as the scattering mechanism. Even in this case the resolution available from

## ATMOSPHERIC STRUCTURE FROM TRANS-HORIZON MEASUREMENTS

transhorizon measurements is severely limited. This is true because the vertical component of the wave vector, when the scattering angle is small, is itself small. The reciprocal of the vertical component of the wave vector provides a measure of the minimum dimension which can be resolved by the experiment.

A second way to relate the experimental data to atmospheric structure is through the assumption of a statistical model. In this case, the determination of the detailed structure at each instant is not the goal of the analysis of the data, but rather it is desired to determine the three dimensional spectrum of spatial wave numbers of the refractivity fluctuations and to determine the correlations which exist in this spectrum. Experience has shown that the gross structure of a statistical model is somewhat easier to determine from transhorizon propagation data than is the case with the deterministic model. Anisotropy which exists as a difference between the spectrum of fluctuations in vertical and horizontal directions, can, in principle, be measured by means of beam swinging experiments. The limitations of the statistical model have to do with the lack of spatial stationarity of the refractivity fluctuations in the atmosphere. To the degree that spatial stationarity is lacking, the problem is not amenable to a statistical treatment; thus it appears that the most powerful analytic techniques to relate experimental data from transhorizon propagation measurements to the structure of the atmosphere must involve a combination of statistical treatment and deterministic treatment. It does not appear to me, however, that even such a treatment will permit one to determine the detailed structure when both non-stationarity of the medium and possible anisotropy must be accounted for.

SESSION 6

Microwave  
Radiometry

N72-25371

A SELECTIVE REVIEW OF GROUND BASED PASSIVE  
MICROWAVE RADIOMETRIC PROBING OF THE ATMOSPHERE

William J. Welch

Radio Astronomy Laboratory  
Space Sciences Laboratory  
Department of Electrical Engineering  
University of California, Berkeley

ABSTRACT

This article reviews past and current work on probing of the atmosphere by ground based passive microwave radiometers. The absorption of the various atmospheric constituents with significant microwave spectra is reviewed. Based on the available data, an estimate is made of the uncertainty in the microwave absorption coefficients of the major constituents, water vapor and oxygen. Then there is an examination of the integral equations which describe the three basic types of observations: measurement of the spectrum of absorption of the sun's radiation by an atmospheric constituent, measurement of the emission spectrum of a constituent, and measurement at one frequency of the zenith angle dependence of the absorption or emission of the atmosphere. The weighting functions or kernels for observations of ozone, water vapor, and oxygen are discussed in terms of the height resolution they permit in studies of both constituent and temperature distribution. Radiometer sensitivities are reviewed, and the linear statistical inversion technique of Westwater and Strand

is discussed. It is concluded that the major source of error in carrying out the inversion will result from inaccuracies in the absorption coefficients. Past and current observation programs are reviewed and the prospects for future work are briefly discussed.

## 1. INTRODUCTION

In 1945 R. H. Dicke, employing a microwave radiometer developed by himself (Dicke, 1946), and his associates at the MIT Radiation Laboratory carried out the pioneer investigation of atmospheric absorption by passive microwave radiometric means (Dicke, et al., 1946). They measured the thermal emission from the atmosphere at 1.00, 1.25, and 1.50 cm wavelengths and compared their results with calculations based on simultaneous radiosonde measurements and the theoretical formulas for oxygen and water vapor absorption developed by Van Vleck (1947a, b). They found the agreement to be satisfactory with some qualifications. Following World War II and with the development of millimeter wave apparatus, atmospheric absorption measurements were carried out with greater precision and to higher frequencies, largely at the University of Texas and at the Bell Telephone Laboratories (Hogg, 1968). In addition, laboratory measurement of absorption by atmospheric constituents, work which was begun during the war, was pursued at a number of laboratories. It was then suggested that the microwave absorption of the atmospheric gases, now better understood, could serve as a tool for remotely probing the structure of the atmosphere (see Barrett, 1963). Barrett and Chung (1962) showed in detail how ground based studies of the emission by the 1.35 cm line of water vapor could provide data on the distribution of water vapor in the atmosphere, particularly at high altitudes. Also, Meeks and Lilley (1963) demonstrated that observations of the emission from the 5-6 mm band of oxygen at various heights in the atmosphere would yield data on the temperature distribution in the atmosphere. It is our purpose in this review to discuss the present state of these ideas and to suggest what some of the future developments may be.

Three different types of ground based observations have been suggested: measurement of the spectrum of absorption of the sun's radiation by an atmospheric constituent, measurement of the emission spectrum of an atmospheric constituent, and measurement at one frequency of the zenith angle dependence of the absorption or emission of the atmosphere. In each case a group of data are obtained which depend on the detailed distributions in the atmosphere of the absorbing constituents and the temperature and pressure. One then hopes to infer some information about these

distributions from the data. In the following we shall review the relevant factors: the absorption coefficients, the formal integral equations, the character of the kernels, the measurement accuracy of microwave radiometers, and the amount of information that one should expect from inverting the integral equations. We will then discuss past and current efforts and what the prospects for the future are.

## 2. ABSORPTION COEFFICIENTS

Figure 1 shows the run of the atmospheric absorption at the zenith. The curve is based on the best available data on water vapor and oxygen absorption. Rosenblum (1961) has reviewed all the experimental data on absorption by water vapor and oxygen prior to 1961. The water vapor lines at 13.5 mm, 1.63 mm and  $\lambda < 1$ mm are evident as are the oxygen band at 5-6 mm and the line at 2.5mm.

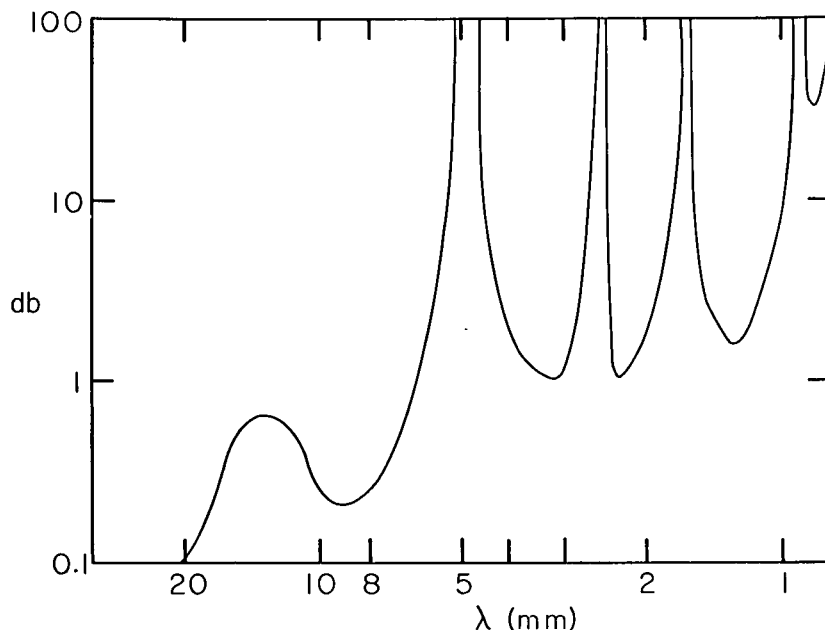


Fig. 1: Absorption of the atmosphere at the zenith due to water vapor and oxygen.

Table 1 lists the atmospheric constituents which absorb microwaves (Glueckauf, 1951). The approximate abundances and the wavelengths at which the constituents absorb are also shown. The right hand column gives an estimate of the peak absorption of a single strong line of each constituent near 1 cm, except for CO which has

GROUND BASED PASSIVE MICROWAVE PROBING

its longest wavelength line at 2.6 mm. With the exception of OH and O<sub>3</sub> the gases lie mostly within the troposphere where the mean line width, determined by pressure broadening, is in the range 800 - 2500 MHz. With this breadth and consequent poor contrast, the minor constituents are difficult to observe against the background of water vapor and oxygen absorption. The expected antenna temperature at the peak of each line may be estimated as follows: For an emission experiment the atmosphere acts like an absorber at about 280 °K and the antenna temperature will be approximately 280 times the peak absorption. If the sun is observed, the absorption dip in degrees will be approximately 5000 times the peak absorption. Observation at large zenith angles will give larger signals. Gases marked with an asterisk are largely industrial effluvia and are hence only transitory. Evidently, few of the trace components will be easily observed by microwave means. In contrast to the other traces, ozone lies in a layer above twenty kilometers where it produces a sharp line of about 200 MHz mean width, and it therefore stands out above the background. OH has a similar distribution but its probable abundance is too low for it to be detected. The final item in the table is water clouds. Liquid water is a good absorber near 1 cm, its absorption spectrum approximately proportional to  $\lambda^{-2}$ . If the clouds consist of small droplets, 0.3 mm or less in size, scattering within the clouds is unimportant and the cloud absorption spectrum will correspond to  $\lambda^{-2}$  (Kerr, 1951). Water clouds are readily detected by a microwave radiometer. On the other hand, cirrus clouds, composed of ice, are practically transparent.

Table 1: Atmospheric constituents that absorb microwaves. The wavelength intervals where the strongest lines lie are shown along with the peak absorption of a line near 1 cm estimated from the tables of Ghosh and Edwards (1956).

Component	Amount (cm-atmos.)	$\lambda$ (mm)	Peak Absorption
O <sub>2</sub>	167,400	5-6, 2.5	—
H <sub>2</sub> O	800-22,000	13.5, 1.63, $\lambda < 1$	.007-0.18
CO*	0.05-0.8	2.6, 1.3, etc.	.0004-.007
SO <sub>2</sub> *	0-1.0	4-16, <u>10</u>	$\leq$ .002
N <sub>2</sub> O	0.4	12, 6, 4	.001
O <sub>3</sub>	0.25	$\lambda < 30$	.0007
NO <sub>2</sub> *	.0004-.02	20, 12	.00001-.00007
NO	trace	—	—
OH	$\sim 10^{-5}$	—	—
water clouds	—	—	—

The formula for absorption by an isolated line of a gas was given by Van Vleck and Weisskopf (1945) as

$$\alpha = C \nu^2 \left\{ \frac{\Delta\nu}{(\nu-\nu_0)^2 + (\Delta\nu)^2} + \frac{\Delta\nu}{(\nu+\nu_0)^2 + (\Delta\nu)^2} \right\} \quad (1)$$

The constant  $C$  is proportional to the gas density, the population of the lower state of the transition, the square of the dipole matrix element, and the inverse temperature. It is assumed that the line is broadened by pressure. For moderate pressures  $\nu_0$ , the line center frequency, is constant and the line width  $\Delta\nu$  is proportional to pressure. A band of lines is given by a superposition of terms of the form (1). Measurements of absorption by atmospheric gases have generally been interpreted in terms of (1) with the data determining the parameters  $C$ ,  $\Delta\nu$ , and  $\nu_0$ . The temperature dependence of  $C$  and  $\Delta\nu$  are determined by both experiment and theory (Townes and Schawlow, 1955). At low and moderate pressures the line shape factor (1) fits the data quite well. The formula breaks down at very low pressures where the line broadening is due to the doppler effect. This occurs at pressures corresponding to altitudes of about 80 km or higher in the atmosphere. At pressures such that  $\Delta\nu$  is comparable to  $\nu_0$  agreement with (1) is obtained only if  $\Delta\nu$  is made a non-linear function of frequency and  $\nu_0$  is allowed to shift to zero frequency as the pressure is increased. These effects have been studied in the ammonia spectrum by Bleaney and Loubser (1950). At one atmosphere pressure these effects are small but not negligible in the spectra of water vapor and oxygen, the principal microwave absorbers in the earth's atmosphere.

Water vapor has strong absorption lines at 13.5 mm and 1.63 mm and a great many strong lines at wavelengths short of one millimeter. Inspection of (1) shows that when  $\nu_0 \gg \nu$ ,  $\alpha$  is proportional to  $\nu^2$ . Hence in the neighborhood of the 13.5 line the effect of the higher frequency lines should be representable by a single term proportional to  $\nu^2$ . Van Vleck (1947a) calculated the magnitude of this non-resonant term as well as the resonant 13.5 mm line and compared his results with the laboratory data of Becker and Autler (1946). Good agreement was obtained only if the magnitude of the non-resonant term was increased by about four times the calculated value. Subsequent measurements both in the field (Tolbert and Straiton, 1960) and in the laboratory at high pressures (Ho, et al., 1966) confirm this discrepancy. Ho, et al., (1966) also found a substantially different temperature dependence for the non-resonant term than the theoretical dependence. One may conclude that the water vapor absorption is best understood in the neighborhood of the 13.5 mm line. With the above adjustment in the non-resonant term and with temperatures near 300 °K the water vapor absorption formulas as summarized by Barrett and Chung (1962) are probably

correct within about 10% near the 1.35 cm line. More accurate measurements would be desirable particularly over a wider range of frequencies and temperatures.

Oxygen, the other principal atmospheric absorber, has a complex spectrum consisting of a band of lines in the range 5-6 mm, an isolated line at 2.5 mm, and non-resonant absorption ( $\nu_0 = 0$ ) which dominates at wavelengths longer than 3 cm. Measurements of the line frequencies and widths have been made in the laboratory at low pressures and pressures up to 1 atmosphere (Artman and Gordon, 1954, Anderson, *et al.*, 1952). Direct measurements of atmospheric absorption by oxygen have also been made (see Hogg, 1968). The measurements have been reviewed by Meeks and Lilley (1963) and more recently by Westwater and Strand (1967a). It was found that nitrogen is about 75% as effective as oxygen in broadening the oxygen absorption. In addition, whereas the line width was found to be about 1.95 MHz/mmHg at low pressure for all the lines, about half that value must be used in the Van Vleck-Weisskopf sum to predict the absorption at one atmosphere pressure. How the transition must be made is not yet understood, although Meeks and Lilley make the reasonable suggestion that the transition be assumed linear with height in the atmosphere between pressures of 19 mmHg and 207 mmHg. Even at one pressure and temperature the Van Vleck-Weisskopf sum with a single half-width parameter does not exactly fit the measurements. Figure 2 is taken from the atmospheric absorption studies of Crawford and Hogg (1956). The fit for a line width parameter of 600 MHz is good but not perfect. In view of this discrepancy and the uncertainty in the variation of the half width parameter with pressure, we may suppose that the accuracy with which the oxygen absorption coefficients may be predicted is not better than 5%. We shall see that this accuracy is not quite adequate for temperature sounding experiments.

In addition to further experimental studies to improve the precision of the absorption coefficients, theoretical work on the line shape function may be useful, particularly for the oxygen band and the infrared water vapor band. Recently, Ben Reuven (1965, 1966) has proposed a new line shape function and shown how it describes the absorption spectrum of ammonia much more adequately than the Van Vleck-Weisskopf formula, especially at high pressure. Even at low pressures Ben Reuven's formula predicts an absorption coefficient in the wings of the ammonia band that agrees better with measurement (see also Townes and Schawlow, 1955). The application of Ben Reuven's work to the oxygen band and to the sum of infrared water vapor lines, if possible, should prove fruitful.

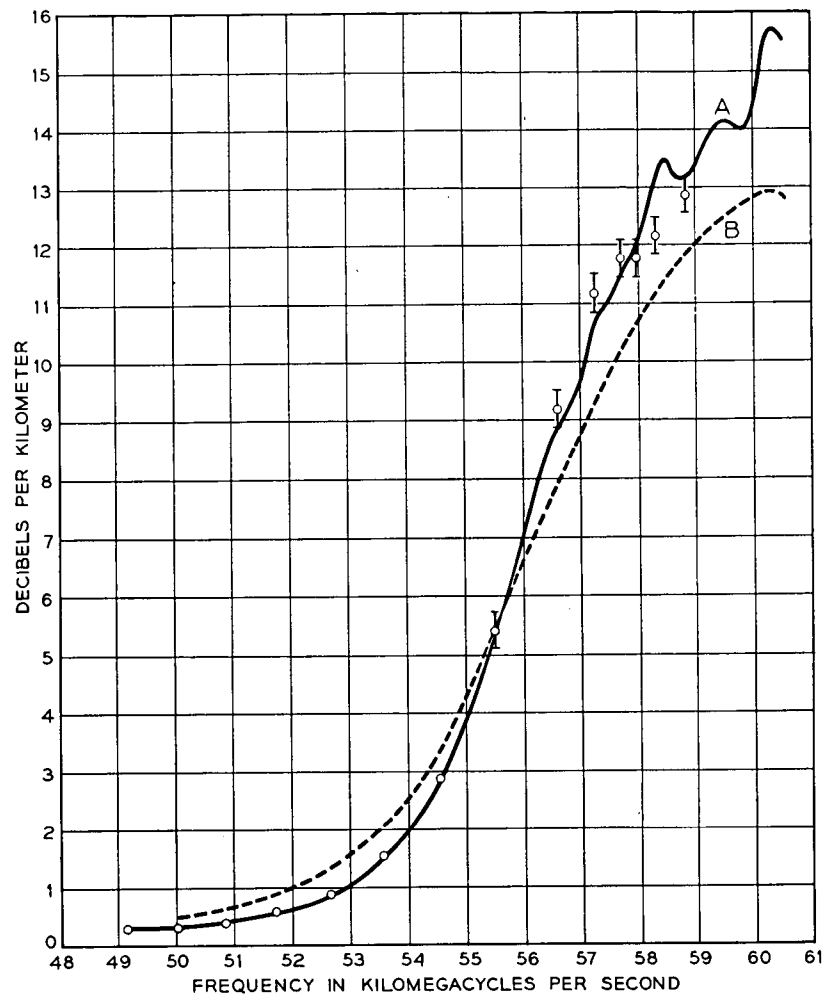


Fig. 2: Calculated and measured absorption by air at sea level. The dots represent the experimental data; the vertical lines indicate the spread in the measured values. Curves A and B are calculated curves of oxygen absorption using line breadth constants of 600 and 1200 MHz respectively. (After Crawford and Hogg, 1956).

## 3. THE INTEGRAL EQUATIONS

There are basically three different types of radiometric observations that may be made from the ground: a) One directs his antenna at the sun (or moon) and measures the spectrum of atmospheric absorption in the neighborhood of an absorption line or band. b) The antenna is oriented in a fixed direction away from the sun and the spectrum of the atmospheric emission is measured. c) The variation of the atmospheric emission is measured at one frequency as a function of the zenith angle of the antenna. In each case there results a group of data each datum of which results from a somewhat independent integration over the absorption coefficient of the atmospheric constituent and the temperature and pressure distributions in the atmosphere. Our program is then to invert this integral equation to obtain either the atmospheric temperature profile or the distribution of the absorbing constituent. The form of these equations follows from the theory of radiative transfer in the atmosphere.

The distribution of radiant intensity in the atmosphere is governed by the equation of radiative transfer (Chandrasekhar, 1960). With the assumption of local thermodynamic equilibrium and that scattering of microwaves in the atmosphere is negligible, the distribution of intensity,  $I_\nu$ , in the atmosphere obeys the simple equation

$$\frac{dI_\nu}{ds} + \alpha I_\nu = \alpha B_\nu(T) \quad (2)$$

where  $\alpha$  is the absorption coefficient and  $B_\nu(T)$  is the Planck function. In the microwave region of the spectrum  $B_\nu$  is directly proportional to  $T$  for all temperatures of physical interest.

$$B_\nu(T) \cong \frac{2kT\nu^2}{c^2} \quad (3)$$

where  $k$  is Boltzmann's constant. The equation takes on a simple form if we replace  $I_\nu$  by a brightness temperature  $T_B$  defined so that

$$I_\nu \equiv \frac{2kT_B}{\lambda^2} \quad (4)$$

We will assume the atmosphere to be horizontally homogeneous and essentially planar, having properties that are only a function of

the distance  $h$  above the surface of the earth. This model serves quite well for observations from the zenith to within about  $7^\circ$  of the horizon. The solution of (2) for the brightness temperature  $T_B$  of a pencil of radiation incident on the ground at a zenith angle  $z$  and azimuth angle  $\phi$  is

$$T_B(\nu, z, \phi) = T_E(\nu, z, \phi) e^{-\tau_0 \sec z} + \int_0^{\tau_0 \sec z} T(\tau) e^{-\tau \sec z} d(\tau \sec z) \quad (5)$$

where  $d\tau = \alpha(\nu, h)dh$ ,

$$\tau(h, \nu) = \int_0^h \alpha(\nu, h') dh' \quad \text{and} \quad \tau_0(\nu) = \int_0^H \alpha(\nu, h) dh. \quad (6)$$

$H$  is the extent of the atmosphere,  $T_E$  is the brightness of sources outside the atmosphere (such as the sun), and  $T(\tau)$  is the temperature of the atmosphere as a function of optical depth. If  $G(z, \phi; z', \phi')$  is the gain function of the antenna, the antenna temperature with the axis in the direction  $(z', \phi')$  is

$$T_A(\nu, z', \phi') = \frac{1}{4\pi} \int T_B(\nu, \phi, z) G(z, \phi; z', \phi') d\Omega \quad (7)$$

The three cases discussed above may now be considered separately. When the antenna is pointed toward the sun, the first term in (5) dominates because the brightness of the sun is much greater than that of the atmosphere.

$$T_A(\nu, z', \phi') \cong \frac{1}{4\pi} \int T_{ES} e^{-\tau_0 \sec z} G(z, \phi; z', \phi') d\Omega \quad (8)$$

If the entire main beam of the antenna lies within the solid angle of the sun, (8) becomes

$$T_A(\nu, z', \phi') = \eta_B T_{ES} e^{-\tau_0 \sec z'} \quad (9)$$

where  $\eta_B$  is the main beam efficiency (Kraus, 1966). Then

$$\tau_0(\nu) = - \frac{\partial [\ln(T_A(z', \nu))]}{\partial (\sec z)} \quad (10)$$

In general,  $\alpha(\nu, h)$  is nearly a linear function of the density of the absorbing gas, so that (6) and (10) may be combined to yield the following linear integral equation for the density  $\rho(h)$  (Staelin, 1966).

$$\int_0^h \rho(h) \left[ \frac{\alpha(\nu, h)}{\rho(h)} \right] dh = - \frac{\partial \{ \ln [ T_A(z', \nu) ] \}}{\partial (\sec z)} \quad (11)$$

If the pressure and temperature distributions with height are assumed,  $\alpha(\nu, h) / \rho(h)$  is a known function and (11) may be solved for  $\rho(h)$  (see Staelin, 1966, for a generalization of (11) to a non-planar atmosphere).

For case (b) the antenna is directed away from the sun, often toward the zenith, and  $T_E$  is just the weak isotropic cosmic background, approximately 2.7 °K (see e.g. Wilkinson, 1967). Because some of the sidelobes of the antenna pattern are directed at the ground, a term  $e(z, \phi) T_G$  should be added to (5) in (7).  $T_G$  is the ground temperature and  $e(z, \phi)$  is the ground emissivity. (7) then becomes

$$\begin{aligned} T_A(z', \nu) - \frac{1}{4\pi} \int_0^{\tau_0 \sec z} [ 2.7 e^{-\tau} + e(z, \phi) T_G ] G(z, \phi; z', \phi') d\Omega \\ = \frac{1}{4\pi} \int_0^{\tau_0 \sec z} \left\{ \int_0^{\tau} T(\tau) e^{-\tau(\nu)} d(\tau \sec z) \right\} G(z, \phi; z', \phi') d\Omega \end{aligned} \quad (12)$$

If  $G$  is a sharp function compared to the angular dependence of the term in the curly brackets, the right hand side of (12) may be approximated by

$$K(z') \int_0^{\tau_0 \sec z'} T(\tau) e^{-\tau} d(\tau \sec z') \quad (13)$$

$K(z')$  is a correction for the finite antenna beamwidth and probably can be worked out with sufficient accuracy with a standard model atmospheric distribution of  $T$  and  $\tau$ . If  $\tau(h)$  is assumed, (12) is an integral equation for  $T(h)$ . It will, in general, be slightly non-linear because  $\tau$  is somewhat a function of temperature. If  $\tau_0 \ll 1$ , as it will be for ozone, the exponential term in (13) is approximately unity, and (13) may be written

$$K(z') \sec z' \int_0^H \rho(h) \left[ \frac{T(h) \alpha(\nu, h)}{\rho(h)} \right] dh \quad (14)$$

Equation (12) is then essentially like equation (11). One important difference is that  $T_A$  on the left side of (12) must be measured absolutely whereas the zero point in the scale of  $T_A$  on the right side of (11) is unimportant.

For case (c), in which the antenna temperature as a function of zenith angle is measured at just one frequency, equation (12) applies. In order to attain sufficiently large values of  $\sec z'$ , the antenna must be able to look to within about one degree of the horizon. This requires an antenna with a complex sidelobe pattern. In this case the ground contribution term on the left hand side of (12) becomes both large and also difficult to evaluate.

Equations (11) and (12) are Fredholm integral equations of the first kind and may be written

$$T(x) = \int_a^b \rho(y) K(x, y) dy \quad (15)$$

where the kernel function  $K(x, y)$  is often called the weighting function. Before discussing the possible solutions to (15), it will be instructive to examine the weighting functions that occur in practice.

#### 4. CHARACTER OF THE WEIGHTING FUNCTIONS

An inspection of the kernel functions that occur in practice reveals how much information one can hope to recover from an actual inversion of the integral equation discussed above. A measurement of the spectrum of the absorption of solar radiation by a single line of ozone provides an example of an integral equation of type (a) discussed above. Furthermore, because the total abundance of telluric ozone is slight and hence  $\tau_o(\nu) \ll 1$ , a similar equation (see (14) above) is obtained for an emission measurement. The normalized ozone weighting functions for different frequencies in the neighborhood of the 37.8 GHz ozone line are shown in figure 3 (see Caton, et al., 1967). The functions are peaked with half widths of about 15 kms, suggesting that the mean ozone distribution at the right of the figure may be sliced into about 4 layers of about 10 kms thickness each with each layer contributing approximately independently to the integral in (11). Because of the width of the weighting functions, further resolution of the distribution in

GROUND BASED PASSIVE MICROWAVE PROBING

height is probably not possible. The weighting functions for Umkehr observations of ozone have the same width as these (Mateer, 1965). Hence, the spatial resolution of the microwave measurements and the Umkehr measurements is the same. Mateer (1965) finds,

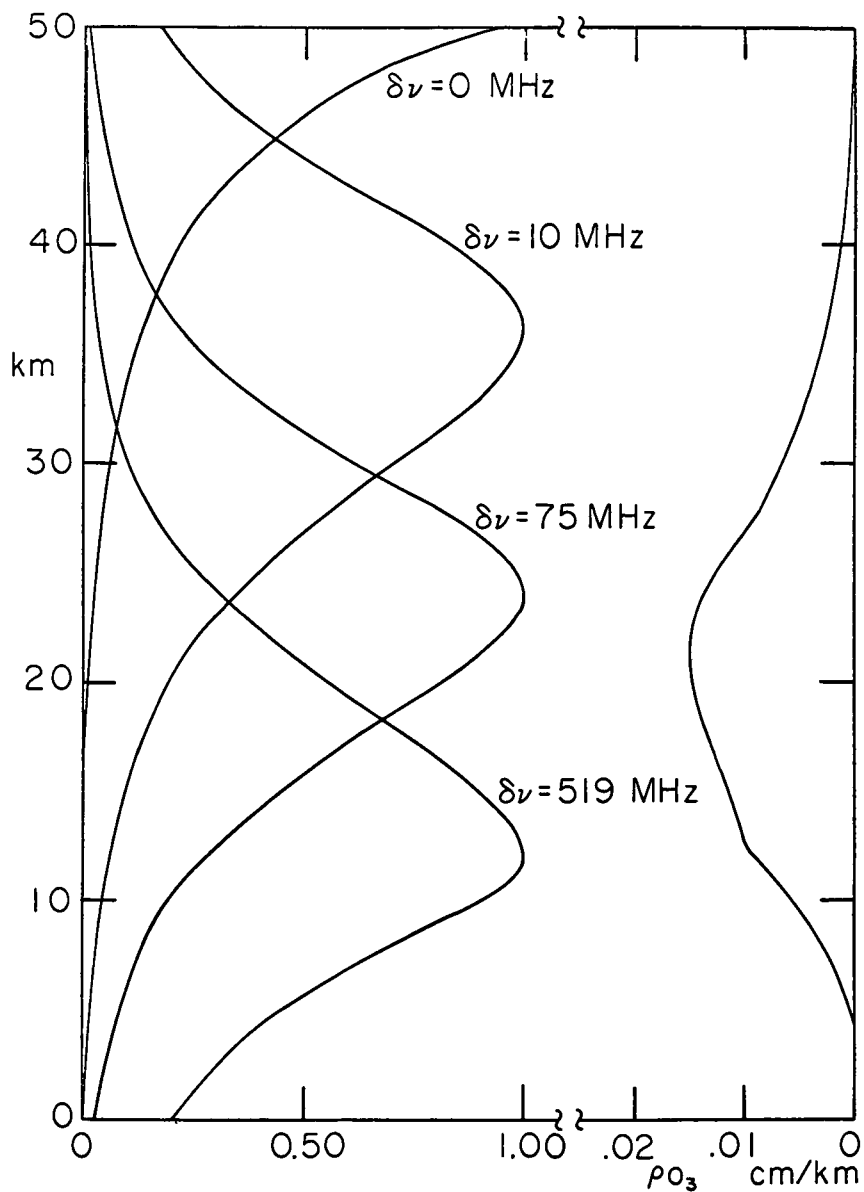


Fig. 3: The curves on the left are ozone weighting functions. The one on the right is a mean ozone distribution.

in fact, from a detailed investigation of the kernel for the Umkehr integral equation that at most four independent pieces of information about the ozone distribution may be obtained from an Umkehr measurement. The microwave weighting functions for water vapor have about the same width as those of ozone (Staelin, 1966). However, the water vapor is largely confined to a layer extending only up to about 8 km above the ground, and therefore only 2 or 3 independent data concerning the water vapor distribution may be obtained from a ground based microwave observation.

A study of the spectrum of emission at the zenith from the long wavelength wing of the 5-6 mm oxygen band provides an example of case (b) above. The unknown function in this case is the temperature distribution in the atmosphere, see (12). Figure 4 shows the normalized weighting functions at various frequencies next to a radiosonde temperature measurement taken at Oakland, California, December 10, 1967. It is clear that the best resolution is obtained near the ground and that only about 3 independent data concerning the temperature distribution may be obtained from the ground based observation. Because the resolution is best near the ground, one would hope to detect interesting distributions such as the temperature inversion which is evident in the figure.

An example of the kernel that one obtains using antenna elevation angle  $\epsilon$  rather than frequency as the measurement variable is shown in Figure 5 (Staelin, 1966). The effect of curvature of the earth is accounted for in the figure but not atmospheric refraction. Resolution comparable to that shown in Figure 4 is possible but requires that the antenna be tipped to within a degree of the horizon.

Normalization of the weighting functions in Figure 3 demonstrates the resolution in the observations but hides an important fact, namely, that the higher weighting functions are stronger. In fact, the function for the center of the line (the absorption coefficient for the center of the line) is proportional to  $(\Delta\nu)^{-1}$  and hence to  $p^{-1}$  and therefore increases approximately exponentially with height up to about 80 km above which  $\Delta\nu$  is determined by doppler broadening. As a result, absorption near the center of the line which takes place largely at the higher altitudes is intense even though the gas density may be low at those altitudes. Because microwave measurements permit very high resolution, it is possible to measure the intensity in the line core and hence to study the gas or temperature distribution at high altitudes.

GROUND BASED PASSIVE MICROWAVE PROBING

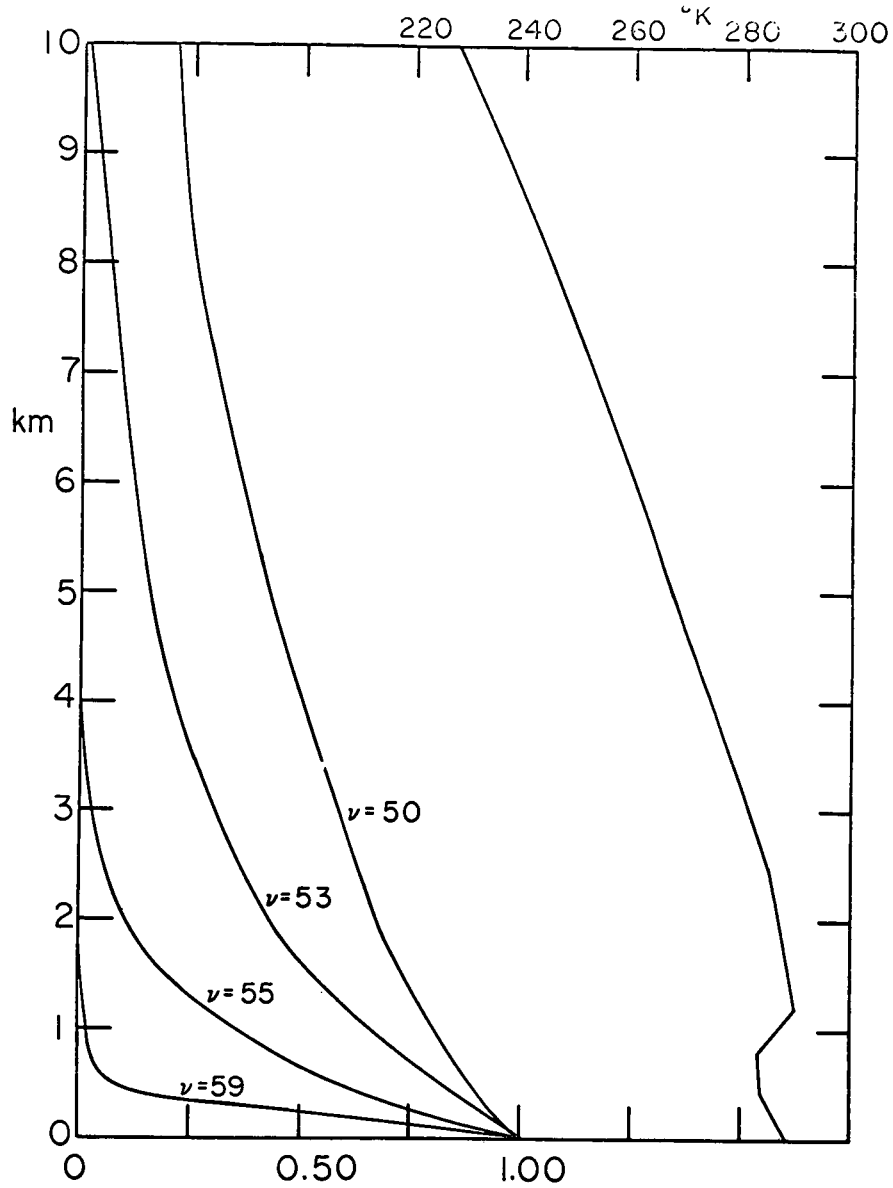


Fig. 4: Weighting functions for  $O_2$  are on the left for different frequencies (in GHz). The right hand curve is the radiosonde temperature profile at Oakland, California, Dec. 10, 1967.

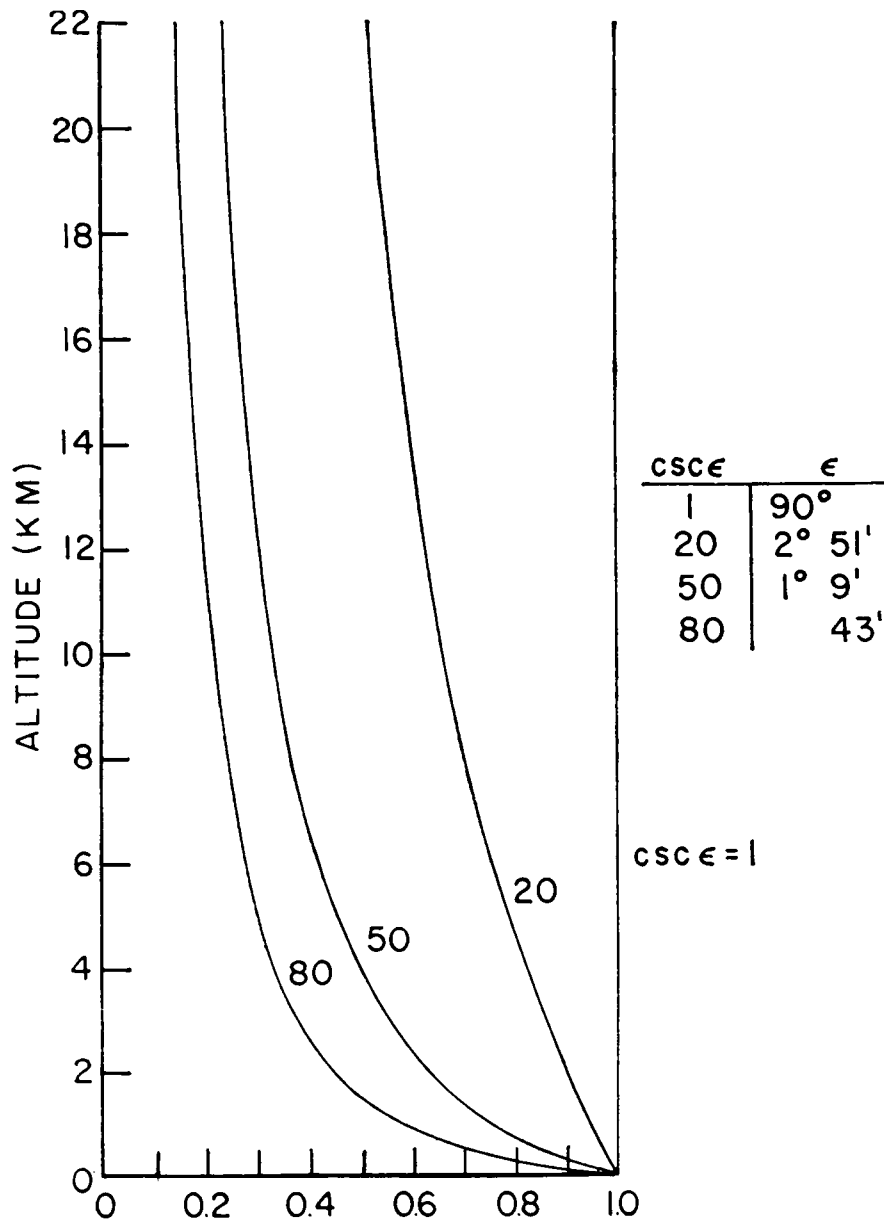


Fig. 5: Weighting functions for antenna tipping (after Staelin, 1966).

## 5. RADIOMETER SENSITIVITIES

Before discussing the details of the inversion further, let us consider the accuracy with which the radiation measurements can be made. The accuracy will have, of course, a strong bearing on the quality of the inference that can be drawn from the measurements. There are two types of uncertainty in radiometry: a) absolute calibration error, and b) error due to finite signal to noise ratio.

The signal to noise ratio of a radiometer is proportional to the system noise temperature and inversely proportional to the square root of the product of predetection bandwidth and integration time (Krauss, 1966). If absorption against the sun is being studied, the system temperature must include the solar brightness temperature, about 6000 °K or more. For an emission experiment, only the receiver noise temperature matters very much. For a crystal mixer it is not likely to be much less than 2000 °K in the millimeter range. On the other hand, parametric amplifiers or masers with noise temperatures of about 100 °K now appear to be possible in this wavelength range. Table 2 contains the expected radiometer output fluctuation for the above three system temperatures for an hour's integration time and for several typical bandwidths. The narrowest bandwidth is required for measuring a sharp line core as discussed in Section 4. As Table 1 shows, the ozone absorption is weak, having a peak emission temperature at the zenith of only 0.2 °K. Nevertheless, an inspection of Table 2 shows that measurement with a multichannel spectrometer and a low noise amplifier will

Table 2: Radiometer output fluctuation for various system temperatures and bandwidths and for 1 hour observation time.

System Temperature (°K)	Bandwidth (MHz)	$\Delta T$ (°K)
8000	2	.08
	10	.04
	100	.012
100	2	.001
	10	.0005
	100	.00016
2000	2	.02
	10	.01
	100	.003

permit observing an ozone emission profile with an accuracy of a few percent. Observation of the emission from atmospheric oxygen and water vapor can be made with better than 1 degree accuracy even with a 2000 °K system temperature.

The other source of radiometric uncertainty is absolute calibration error. For a narrow line like that of ozone, the continuum away from the line provides a reference. For wide lines or bands calibration must be made with respect to absolute black body terminations. These comparisons are difficult. Nevertheless, the recent experience of a number of workers in measuring the cosmic background radiation (see, for example, Wilkinson, 1967) has shown that absolute calibration accuracies of 0.5 °K or better are possible.

## 6. INFORMATION CONTAINED IN THE INTEGRAL EQUATIONS

If a single line is observed, such as that of ozone or of water vapor, the area under the profile depends only on the total amount of the absorber present and not on its distribution or on the pressure distribution. (There is a weak dependence on the temperature distribution along the path.) Hence the total abundance of the gas may be measured with an accuracy which is simply proportional to the radiometer accuracy and the certainty in the line strength. Such a determination will be simple for a narrow ozone line but much more difficult for the very broad water vapor profile which results from water vapor near the ground. It has been pointed out by Barrett and Chung (1962) that because water vapor appears to have a constant mixing ratio in the stratosphere this high altitude vapor should produce a narrow intense line superposed on the broad line associated with vapor in the troposphere. The total stratospheric abundance associated with such a narrow line should be readily determinable.

Working out the distribution of a constituent with height requires actual inversion of the integral equation, and in this case the effect of noise on the inferred distribution is somewhat obscure. In general, measurements will be made at a discrete set of frequencies or antenna elevation angles. Hence, in practice one replaces the integral equation (15) by an equivalent set of algebraic equations. Suppose, for example, one wished to infer the tropospheric vertical temperature structure from measurements of the spectrum of antenna temperatures at the zenith in the wing of the 5-6 mm oxygen band. The integral equation is of the form (12)

$$T_e(\nu) = \int T(h) K(h, \nu) dh \quad (16)$$

$T_e$  includes the ground and background radiation. The integral may be replaced by a sum either by dividing the atmosphere into slabs or by writing  $T(h)$  as a sum of known (possibly orthogonal) functions with unknown coefficients. In the former case one gets

$$T_{e_i} = \sum T_j K_{ij} \quad \text{or} \quad (T_e) = (K)(T) \quad (17)$$

It is well known that an attempt to invert (17) directly to obtain  $(T)$  will meet with disaster for two reasons. In the first place it should be clear from the form of the kernel functions that the data are somewhat coupled so that the matrix  $(K)$  is nearly singular. One finds, in fact, that if one does a model calculation, the round off error in even a large digital computer will produce errors of a few percent in the derived temperature distribution. The other source of difficulty is the uncertainty in the measurement of  $T_e$  and the inaccuracy in the absorption coefficients which go into  $(K)$ . The presence of noise in (17) makes the solution non-unique and aggravates the instability problem. Evidently, no useful solution may be extracted from the class of possible solutions without the a priori application of some constraint. The first work on this problem is that of Phillips (1962) who showed that a stable solution could be obtained if the solution is constrained to have a minimum second derivative. Twomey (1963) discussed other possible constraints including the least squares fit of the solution to some trial function. These ideas have been further developed by Twomey (1965), Twomey and Howell (1963), Mateer (1965), Wark and Fleming (1966), and most recently by Westwater and Strand (1967a, b).

Westwater and Strand argue that the inversion should be viewed as the improvement (by the radiation measurements) of the statistics of the temperature distribution. For example, daily measurements of the air temperature profile at many stations have been made with radiosondes for more than two decades. Thus for every station there is a yearly, seasonal, or monthly mean profile and a standard deviation of the temperature at each level in the atmosphere. Furthermore, because the profiles are continuous functions, there is significant correlation between the temperatures at nearby levels. The observations of the emission from the oxygen band are then to be used to find a solution to (17) such that the derived temperature distribution is a least squares fit to the temperature profile. The minimization is with respect to the joint probability distribution of the temperature profile and the observational error. The two or three independent pieces of data in the measurement are distributed over the profile reducing the variance where the weighting functions are the most sensitive. If  $T_0$  is the mean profile and  $S_T$  and  $S_e$  are the covariance matrices of the profile and the experimental data respectively, then the optimum linear estimate of  $(T)$  is given by Westwater and Strand, 1967a)

$$(T) = (T_o) + (X)^{-1}(K)^*(S_e)^{-1}[(T_e) - (T_{e0})] \quad , \quad (18)$$

$$\text{where} \quad (X) = (S_T)^{-1} + (K)^*(S_e)^{-1}(K) \quad (19)$$

The covariance matrix of  $(T - T_o)$  is given by  $(X)^{-1}$ . The diagonal elements of the latter are the mean-square variances at the different heights. Figures 6 and 7 are example model calculations by Westwater and Strand (1967b) appropriate to the oxygen sounding problem. The curves show the variance with height for profiles derived from sets of measurements at 5 frequencies with different assumed measurement errors,  $\sigma_e$ . The  $\sigma_e$  are absolute uncertainties in the antenna temperatures and are taken to be the same at each frequency. The curve for  $\sigma_e = \infty$  shows the a priori profile statistics. Figure 7 shows the results that are obtained if the ground temperature can be constrained by an independent measurement (perhaps with a thermometer).

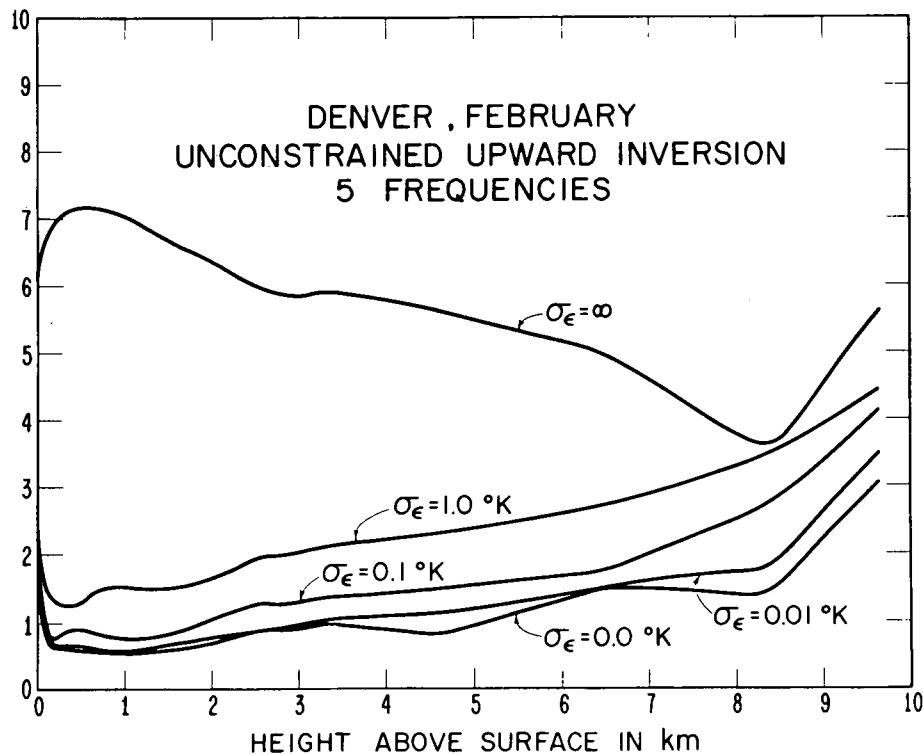


Fig. 6: Accuracies of several simulated upward inversions for temperature profiles for different levels of measurement error,  $\sigma_e = \infty$  shows the a priori profile statistics. The ordinate is °K. (Westwater and Strand, 1967).

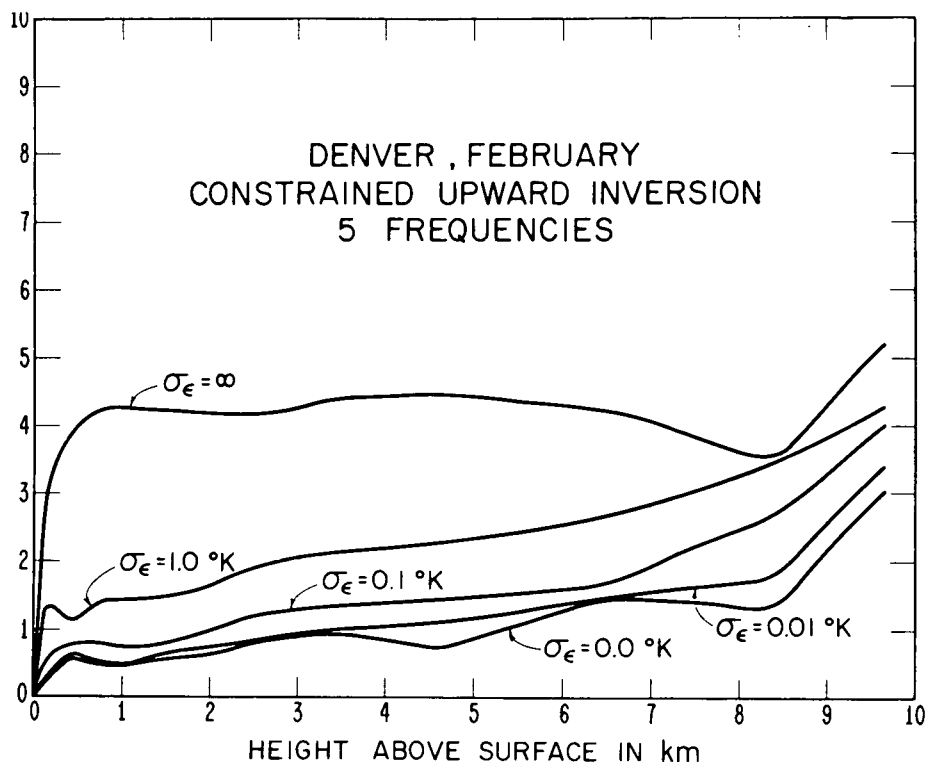


Fig. 7: Accuracies for several simulated upward inversions for temperature profile for different levels of measurement error,  $\sigma_\epsilon$ , with the surface temperature constrained. The ordinate is  $^\circ\text{K}$ . (Westwater and Strand, 1967).

It is clear from the figures that significant results may be obtained with measurement errors as large as  $1.0\text{ }^\circ\text{K}$ . One may well ask whether measurement errors as small as  $1.0\text{ }^\circ\text{K}$  are presently possible. In section 5 we concluded that an absolute accuracy of  $1.0\text{ }^\circ\text{K}$  was well within the capabilities of current radiometers. A more serious problem, particularly for the temperature sounding studies, is the inaccuracy in our knowledge of the absorption coefficients. For example, at 50 GHz the atmospheric optical depth is about 0.3 and hence the sky brightness temperature at the zenith is about  $100\text{ }^\circ\text{K}$ . If this opacity, which is mostly due to oxygen, is uncertain by 5%, an intolerably large error of  $5\text{ }^\circ\text{K}$  results. This error has the same effect as a measurement error.

## 7. PAST AND CURRENT PROGRAMS

To date, the observational possibilities in ground based passive microwave probing of the atmosphere have been only marginally exploited. Quite often the sky brightness is measured primarily so that the inferred atmospheric absorption can be used to correct astronomical observations (see, e.g. Shimabukuro, 1966; Tolbert, et al., 1965).

Wulfsberg (1964) measured sky brightness temperatures throughout a year at 15, 17, and 35 GHz. Falcone (1966) compared these data with theoretical temperatures based on concomitant radiosonde data and found that the correlation was best if an oxygen half-width parameter of 750 MHz at NTP was used. No attempt to invert this data has been published.

Staelin (1966) has published solar absorption spectra in the neighborhood of the 1.35 cm water vapor line for both clear and cloudy days. He shows how the abundance of the liquid water clouds, because of their characteristic  $\lambda^{-2}$  spectra, can be readily determined. For clear days he found that the difference between measured spectra and theoretical spectra from radiosonde data varied between 0 and 15%. The spectra are shown in Figure 8. As discussed in section 6 above, Barrett and Chung (1962) suggested that high altitude water vapor might be detectable as a narrow intense emission feature at 1.35 cm. Figure 9 shows some model distributions and corresponding spectra as calculated by Croom (1965). Bonvini, et al., (1966) reported measurements at Slough in which they did not detect the line and placed an upper limit of about 2 °K on the effect. Recently, Staelin (1968) has reported detecting a weak line at a lower level than 2 °K. The observed signal is in agreement with a constant stratospheric mixing ratio of about  $2 \times 10^{-6}$  as observed by balloon (Mastenbrook, 1968).

Both emission and absorption of ozone has been detected recently at Berkeley (Caton, et al., 1967), at the Ewen-Knight Corporation (Caton et al., 1968), and at MIT (Barrett, et al., 1967). The very strong 101.7 GHz line of ozone as seen against the sun by the Ewen-Knight group is shown in Figure 10. In each case only an approximate estimate of the total ozone abundance was obtained and no attempt at inversion was made. As in the case of stratospheric water vapor, the very high altitude ozone should produce a sharp central core. Hunt (1966) has estimated that the ozone abundance above 53 km should be enhanced at night, and Carver, et al., (1966) have reported detecting an enhancement with a rocket-borne UV spectrometer. A careful observation of the core of the microwave line may reveal these diurnal variations.

The current ground-based programs of which the author is aware are as follows: Multichannel studies of ozone and water vapor at MIT; Antenna tipping experiments at 4 mm at the University of Texas

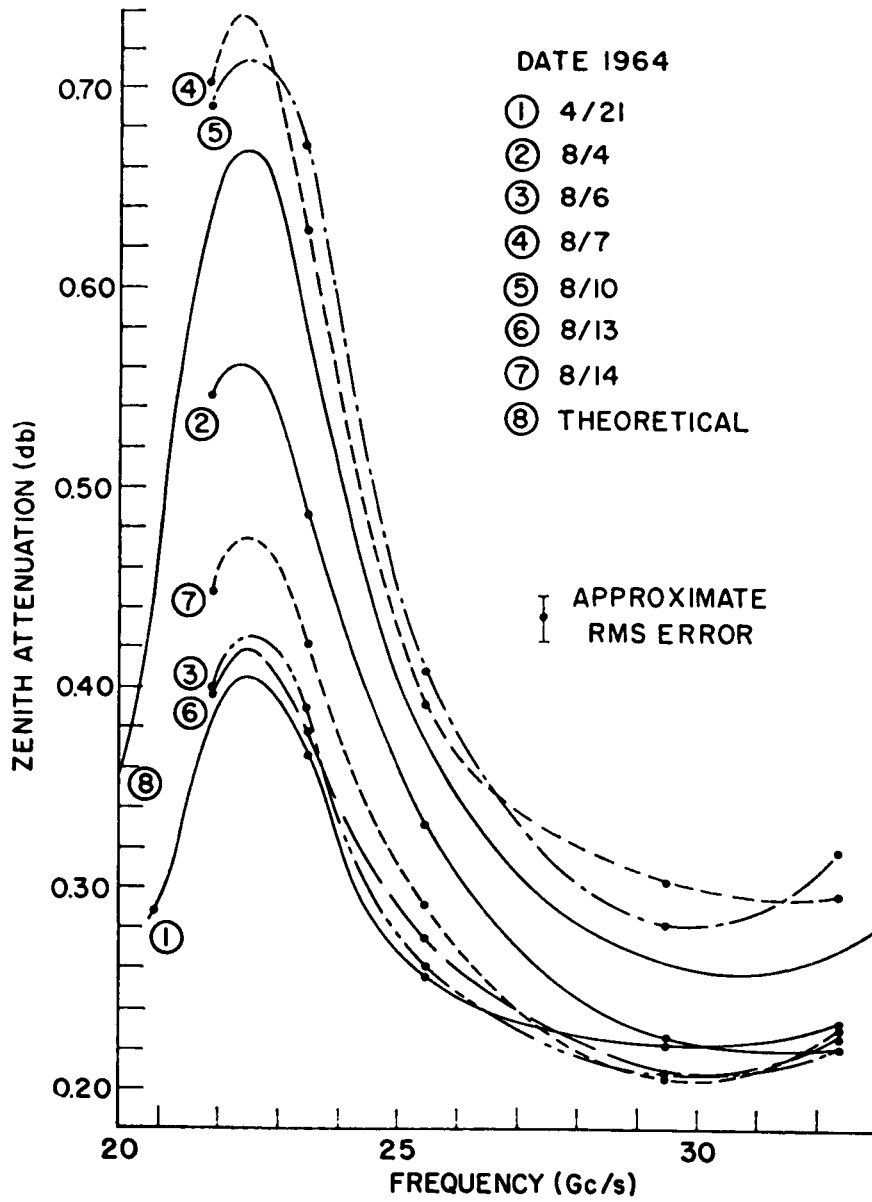


Fig. 8: Measured atmospheric absorption spectra (Staelin, 1966).

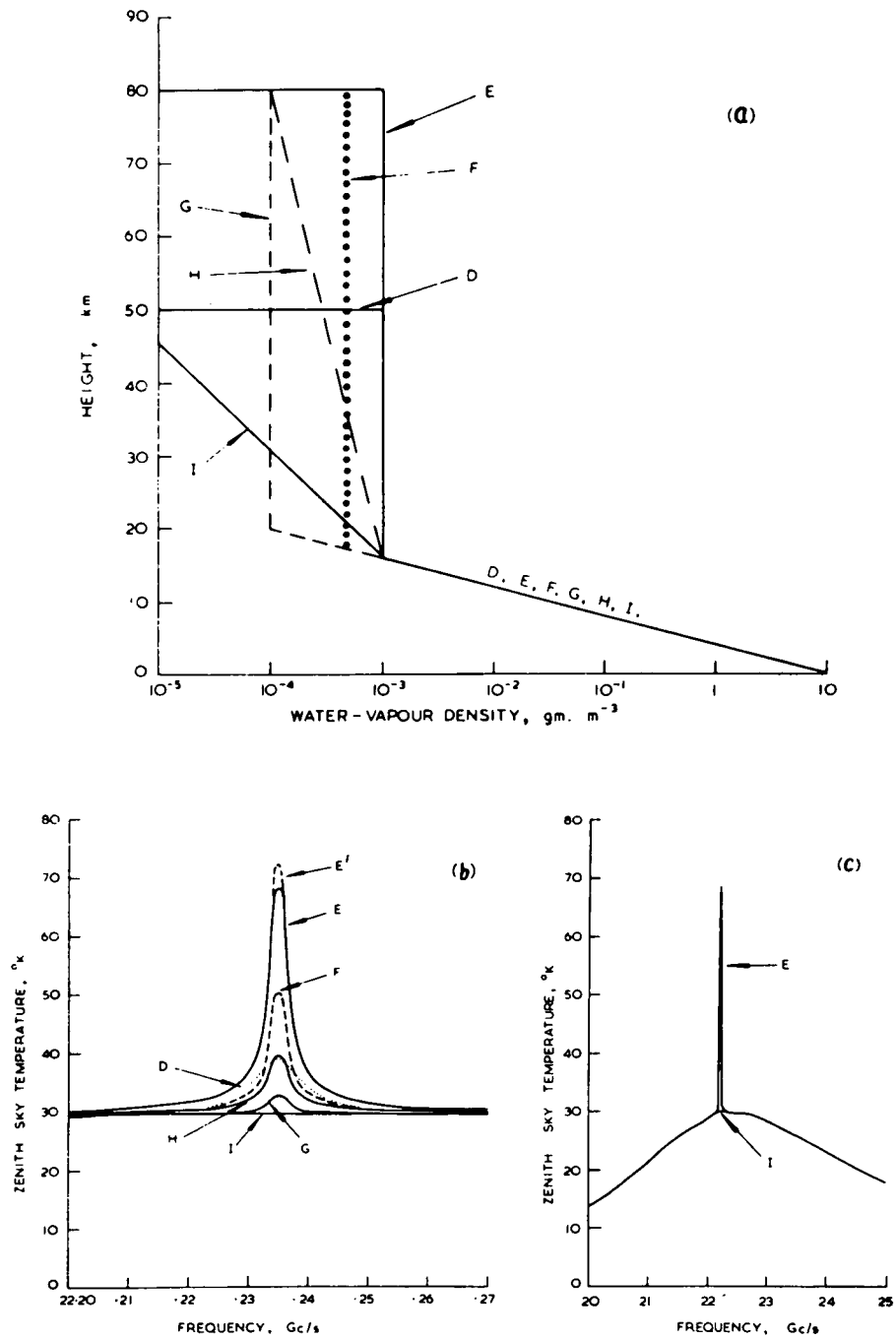


Fig. 9: Zenith sky emission spectra for six hypothetical water-vapor profiles. (a) Water-vapor profiles, (b) corresponding spectra on a fine frequency scale, (c) spectra E and I on a coarse frequency scale. (After Croom, 1965).

## GROUND BASED PASSIVE MICROWAVE PROBING

to obtain the tropospheric temperature profile; Both multi-frequency and antenna tipping experiments in Hawaii by the ESSA Boulder Laboratories; At UC Berkeley, multifrequency measurements in the oxygen band for the temperature profile, and multifrequency ozone line measurements.

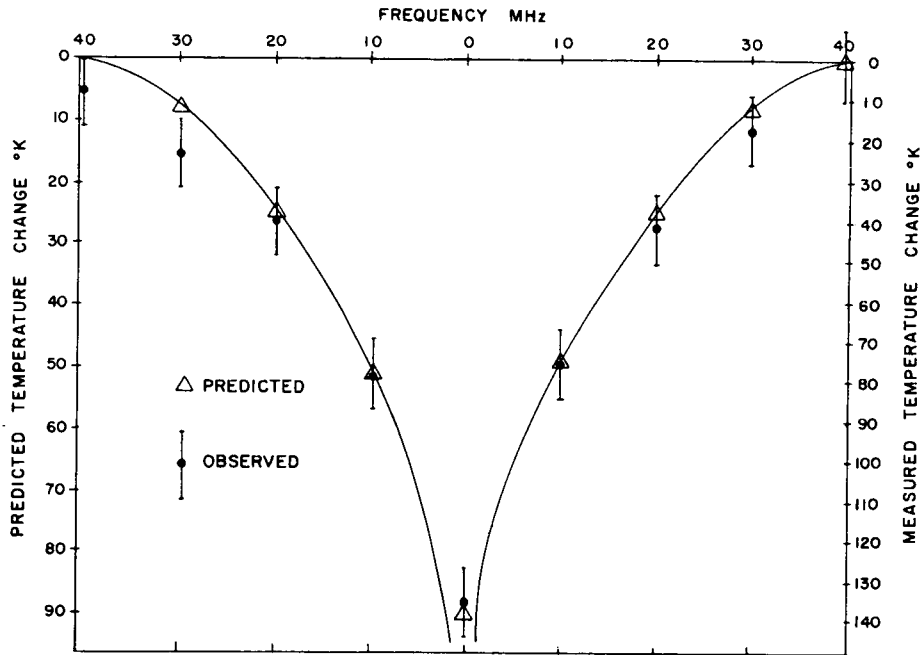


Fig. 10: Measured and predicted ozone profile for the 101.7 GHz ozone line. (After Caton, et al., 1968).

## 8. METEOROLOGICAL RELEVANCE

Ozone plays an important role in the heat balance of the atmosphere because of its absorption of ultra-violet radiation from the sun and infra-red radiation from the earth. Like Umkehr measurements, the microwave studies of the ozone from the ground will never provide the quality of spatial resolution afforded by balloon sampling. Only gross distribution features can be determined. Unlike the Umkehr observations which must be made at sunrise and sunset, the microwave emission studies can be made at any time of day or night. Hence they can be used for studies of hourly variations and, in particular, the night time high altitude enhancement. The total ozone content varies considerably during the year, especially at middle latitudes and it should be accurately measurable by microwave probing.

The influence of the different kinds of water clouds on the weather is familiar to everyone. There is probably no better way to remotely measure the amount of water in a cloud than with a microwave radiometer. The variable water vapor content can also, in principle, be measured quickly and accurately with a proper microwave radiometer. Furthermore, this vapor measurement can be made even in the presence of water clouds. In contrast, sounding in the infra-red fails in the presence of clouds because they are too opaque.

It is clear from the discussion of Sections 5 and 6 that measuring the emission from the oxygen band permits one to probe the temperature structure of just the first few kilometers. However, this is an important region because it is at these levels that the low lying temperature inversions form. The presence of such inversions is particularly important in urban areas because of the trapping of smog layers by inversions. Although radiosonde measurements naturally provide better resolution, the microwave probing technique offers some advantages: the measurements are more local and, in principle, may be done more quickly and more often.

## 9. SUMMARY

The prospects for making significant meteorological measurements by passive microwave probing seem to be very good. The measurement precision of radiometers that are currently available (or will soon be available) is adequate. On the other hand, the uncertainties in the gas absorption coefficients are presently too large. It may be that the microwave probing programs that are currently in progress will provide the data which can be used to improve the absorption coefficients. A better procedure is probably to make accurate absorption measurements in the laboratory. Further work such as that begun by Ho, et al., (1966) should be carried out; that is, accurate measurements of the temperature and pressure dependences of absorption in mixtures of gases should be made, and this program should be coupled with theoretical studies of the shape of microwave bands. Both the oxygen band and far infrared water vapor band are not sufficiently understood.

The theoretical machinery for inverting the radiometric data seems now to be well worked out. The observations for which the microwave probing techniques are especially well suited are: determination of total water vapor and ozone content, even in the presence of clouds, and determination of the water content of clouds.

## REFERENCES

- Anderson, R. S., W. V. Smith, and W. Gordy, 1952: Line-breadths of the microwave spectrum of oxygen. Phys. Rev., 87, 561-568.
- Artman, J. O., and J. P. Gordon, 1954: Absorption of microwaves by oxygen in the millimeter wavelength region. Phys. Rev., 96, 1237-1245.
- Barrett, A. H., and V. K. Chung, 1962: A method for the determination of high altitude water-vapor abundance from ground-based microwave observations. J. Geophys. Res., 67, 4259-4266.
- Barrett, A. H., 1963: Microwave spectral lines as probes of planetary atmospheres. Mémoires Soc. R. Sc. Liège, tome VII, 197-219.
- Barrett, A. H., R. W. Neal, D. H. Staelin, and R. M. Weigand, 1967: Radiometric detection of atmospheric ozone. Quart. Prog. Rept., Res. Lab. of Electronics, M.I.T. (July).
- Becker, G. E., and S. H. Autler, 1946: Water vapor absorption of electromagnetic radiation in the centimeter wave-length range. Phys. Rev., 70, 300-307.
- Ben Reuven, A., 1965: Transition from resonant to non-resonant line shape in microwave absorption. Phys. Rev. Letters, 14, 349-351.
- Ben Reuven, A., 1966: Impact broadening of microwave spectra. Phys. Rev., 145, 7-22.
- Bleaney, B., and J. H. N. Loubser, 1950: Proc. Phys. Soc., 63A, 438.
- Bonvini, L. A., D. L. Croom, and A. Gordon-Smith, 1966: A search for the 22.235 Gc/s emission line from stratospheric water vapour. J. Atm. Terr. Phy., 28, 891-896.
- Carver, J. H., B. H. Horton, F. G. Burger, 1966: Nocturnal ozone distribution in the upper atmosphere. J. Geophys. Res., 71, 4189.
- Caton, W. M., W. J. Welch, and S. Silver, 1967: Absorption and emission in the 8-mm region by ozone in the upper atmosphere. J. Geophys. Res., 72, 6137-6148.
- Caton, W. M., G. G. Mannella, P. M. Kalaghan, A. E. Barrington, H. I. Ewen, 1968: Radio measurement of the atmospheric ozone transition at 101.7 GHz. Astrophys. J., 151, L153-L156.
- Chandrasekhar, S., 1960: Radiative Transfer, Dover, New York.
- Coates, R. J., 1958: Measurements of solar radiation and atmospheric attenuation at 4.3 mm wavelength, Proc. IRE, 46, 122-126.
- Crawford, A. B., and D. C. Hogg, 1956: Measurement of atmospheric attenuation at millimeter wavelengths. Bell System Tech. Journal, 35, 907-916.
- Croom, D. L., 1965: Stratospheric thermal emission and absorption near the 22.235 Gc/s (1.35 cm) rotational line of water vapour. J. Atmos. Terr. Phys., 27, 217.
- Dicke, R. H., R. Beringer, R. L. Kyhl, and A. B. Vane, 1946: Atmospheric absorption measurements with a microwave radiometer, Phys. Rev., 70, 340-348.
- Dicke, R. H., 1946: The measurement of thermal radiation at microwave frequencies. Rev. Sci. Inst., 17, 268-275.
- Falcone, V. J., 1966: Calculations of apparent sky temperature at millimeter wavelengths. Radio Sci., 1, 1205-1208.

- Ghosh, S. N., and H. D. Edwards, 1956: Rotational frequencies and absorption coefficients of atmospheric gases. Airforce Surveys in Geophysics, No. 82, Geophysics Research Directorate, AFCRL.
- Gluekauf, E., 1951: The composition of atmospheric air, Compendium of Meteorology, Am. Meteorological Soc., Waverly Press, Boston.
- Ho, W., I. A. Kaufman, and P. Thaddeus, 1966: Laboratory measurement of microwave absorption in models of the atmosphere of Venus. J. Geophys. Research, 71, 5091-5107.
- Hogg, D. C., 1959: Effective antenna temperature due to oxygen and water vapor in the atmosphere. J. App. Phys., 30, 1417-1419.
- Hogg, D. C., 1968: Millimeter-wave communication through the atmosphere. Science, 159, 39-46.
- Hunt, B. G., 1966: Photochemistry of ozone in a moist atmosphere. J. Geophys. Res., 71, 1385-1398.
- Kerr, D. E., 1951: Propagation of Short Radio Waves, McGraw-Hill, New York.
- Kraus, J., 1966: Radioastronomy, McGraw-Hill, New York.
- Mastenbrook, H. J., 1968: Water vapor distribution in the stratosphere and high troposphere. J. Atm. Sci., 25, 299-311.
- Mateer, C. L., 1965: On the information content of Umkehr observations. J. Atm. Sci., 22, 370-381.
- Meeks, M. L., 1961: Atmospheric emission and opacity at millimeter wavelengths due to oxygen. J. Geophys. Research, 66, 3749-3757.
- Meeks, M. L., and A. E. Lilley, 1963: The microwave spectrum of oxygen in the earth's atmosphere. J. Geophys. Research, 68, 1683-1703.
- Phillips, D. L., 1962: A technique for the numerical solution of certain integral equations of the first kind. J. ACM, 9, 84-97.
- Rosenblum, E. S., 1961: Atmospheric absorption of 10-400 K Mc/s radiation. Microwave J., 4, 91-96.
- Shimabukuro, F. I., 1966: Propagation through the atmosphere at a wavelength of 3.3 mm. IEEE, AP-14, 228-235.
- Staelin, D. H., 1966: Measurements and interpretation of the microwave spectrum of the terrestrial atmosphere near 1-centimeter wavelength. J. Geophys. Research, 71, 2875-2881.
- Staelin, D. H., 1968: private communication.
- Straiton, A. W., and C. W. Tolbert, 1960: Anomalies in the absorption of radio waves by atmospheric gases. IEEE Proc., 48, 898-903.
- Tolbert, C. W., and A. W. Straiton, 1964: 35-Gc/s, 70-Gc/s and 94-Gc/s cytherean radiation. Nature, 204, 1242-1245.
- Townes, C. H., and A. L. Schawlow, 1955: Microwave Spectroscopy, McGraw-Hill, New York.
- Twomey, S., and H. B. Howell, 1963: A discussion of indirect sounding methods. Mon. Weather Rev., 91, 659-664.
- Twomey, S., 1963: On the numerical solution of Fredholm integral equations of the first kind by the inversion of the linear system produced by quadrature. J. ACM, 10, 97-101.

## GROUND BASED PASSIVE MICROWAVE PROBING

- Van Vleck, J. H., and V. F. Weisskopf, 1945: On the shape of collision broadened lines. Revs. Modern Phys., 17, 227-236.
- Van Vleck, J. H., 1947a: The absorption of microwaves by uncondensed water vapor, Phys. Rev., 71, 425-433.
- Van Vleck, J. H., 1947b: The absorption of microwaves by oxygen, Phys. Rev., 71, 413-424.
- Wark, D. Q., and H. E. Fleming, 1966: Indirect measurements of atmospheric temperature profiles from satellites. Mon. Weather Rev., 94, 351-362.
- Westwater, E. R., and O. N. Strand, 1967b: Statistical information content of radiation measurements used in indirect sensing. Preprint.
- Westwater, E. R., and O. N. Strand, 1967a: Application of statistical estimation techniques to ground-based passive probing of the tropospheric temperature structure. U.S. Dep't of Commerce, ESSA Technical Report IER 37 - ITSA 37. Boulder, Colorado.
- Wilkinson, D. T., 1967: Measurements of the cosmic microwave background at 8.56-mm wavelength. Phys. Rev. Letters, 19, 1195-1198.
- Wulfsberg, K. N., 1964: Apparent sky temperatures at millimeter wave frequencies. AFCRL Rpt. No. 64, 590.

N 72-25372

## GROUND-BASED MICROWAVE PROBING

Ed R. Westwater and Martin T. Decker  
Environmental Science Services Administration  
Research Laboratories  
Boulder, Colorado

### ABSTRACT

This report reviews the theoretical and experimental activities in remote sensing conducted by the Millimeter Wave Program, Wave Propagation Laboratory, of the ESSA Research Laboratories. The projects reported here are (1) the linear statistical inversion method, (2) determination of vertical temperature profiles from microwave emission measurements near 60 GHz, (3) determination of radio path length corrections from emission measurements at 20.6 GHz, and (4) determination of liquid water content of thunderstorm cells by emission measurements at 10.7 GHz.

### 1. INTRODUCTION

The possibilities of remote inference of temperature and water vapor profiles from microwave thermal emission measurements are well known (Meeks and Lilley, 1963; Barrett and Chung, 1962). The problems of inverting radiometer observations to obtain profiles has been solved for two frequently occurring situations:

- (1) a priori statistical knowledge of both the profile and experimental noise level, and complete knowledge of absorption coefficients are available (Rodgers, 1966; Strand and Westwater, 1968a, b).
- (2) simultaneous measurements of thermal emission and direct measurements of the profile can be obtained

## GROUND-BASED MICROWAVE PROBING

over a suitable ensemble of data. This technique, which is a multidimensional regression analysis, does not require knowledge of the absorption coefficient. The observational requirements of this technique, however, are not always practical.

Sections 2 and 3 of this report describe the linear inversion technique (1) and its use in evaluating the potential of ground - based probing in inferring temperature structure. A passive technique which corrects for range errors due to the refractive index of water vapor is described in Section 4. The remote inference of the liquid water content of discrete cloud structures by passive radiometry is discussed in Section 5.

### 2. THE LINEAR STATISTICAL INVERSION METHOD

Attempts to infer atmospheric profiles from measurements of emitted, absorbed, or scattered radiation have been described in the literature. Many of these problems can be reduced to solving an integral equation of the first kind in the presence of error in the measured quantity. Some of the difficulties in solving this type of equation are:

- a. Finite measurements. Only a finite (and usually small) number of measurements can be taken from which to infer an entire profile.
- b. Instability. Direct attempts to solve the equation by standard methods of matrix inversion can yield unstable solutions because of ubiquitous measurement errors, i. e., small errors in the measured quantity can yield large, physically unrealistic estimates of the inferred quantity.
- c. Nonuniqueness. In a mathematical sense, the solutions are not unique, since any function that can be integrated to yield the observed value to within the noise level of the sensor is mathematically (but not necessarily physically) a legitimate solution.
- d. Ill-Conditioning. Because kernel functions encountered in practical applications are smooth functions of physical parameters, measurements are often dependent, in the sense that certain measurements can be obtained from linear combinations of the others to within the noise level of the observations.
- e. As Twomey (1965) has shown, methods that attempt to approximate the profile by approximating its transform

are based on the incorrect premise that "nearness" to the transform implies "nearness" to the profile.

Some investigators, e.g., King (1964) have advocated nonlinear techniques to achieve useable results; others (Twomey, 1965) have used linear methods incorporating smoothing to reduce the instability. More recently (Alishouse, et al., 1967) empirical orthogonal functions have been used to maximize the information obtainable from the small number of determinable parameters. The minimum-rms inversion method (Rodgers, 1966; Strand and Westwater, 1968a, b) is linear, achieves smoothing by filtering the signal from the noise in a statistically optimum manner, and estimates the profile from the measurements at hand and the a priori statistical knowledge of both the profile and the noise level of the sensor. The essentials of this method may be described as follows:

The Fredholm integral equation of the first kind is written

$$g_e(x) = g(x) + \epsilon(x) = \int_a^b K(x, y)f(y) dy + \epsilon(x), \quad (1)$$

where  $g_e(x)$  is the measured value and is the sum of the amount contributed by the profile alone,  $g(x)$ , and the instrumental noise  $\epsilon(x)$ ;  $K(x, y)$  is the kernel (assumed to be known); and  $f(y)$  is the unknown. From measurements of  $g_e(x)$  at some set of values of  $x$ , say  $x_i$ ,  $i = 1, 2, \dots, n$ , it is wished to infer  $f(y)$ . Introduction of a suitable quadrature approximation to (1) yields the matrix equation

$$g_e = Af + \epsilon, \quad (2)$$

where

$$g_e = [g_e(x_1), g_e(x_2), \dots, g_e(x_n)]^T,$$

$$(A)_{ij} = K(x_i, y_j)w_j,$$

$$f = [f(y_1), f(y_2), \dots, f(y_m)]^T,$$

$$\epsilon = [\epsilon(x_1), \epsilon(x_2), \dots, \epsilon(x_n)]^T;$$

$w_j$  = quadrature weight associated with the point  $y_j$ , and the superscript T means matrix transposition. The minimum-rms inversion method does not attempt to solve (2); rather it attempts to use the data vector,  $g_e$ , to estimate the solution such that the average mean-square error in the

## GROUND-BASED MICROWAVE PROBING

estimation is as small as possible. Let

$$\eta \equiv f - f_o, \quad (3)$$

where  $f_o$  is the mean of  $f$ , obtained by averaging over a representative ensemble of profiles. If one assumes that the estimate to the profile,  $\hat{\eta}$ , can be expressed as a linear combination of the data,  $g_e$ , then the estimate that minimizes the expected mean-square error of  $\hat{\eta} - \eta$  is given by (Strand and Westwater, 1968b)

$$\hat{\eta} = S_f A^T H^{-1} (g_e - A f_o), \quad (4)$$

where

$$H = S_\epsilon + A S_f A^T,$$

$S_f$  = known covariance matrix of the profile

$$\equiv E \left\{ (f - f_o) (f - f_o)^T \right\}$$

(E denotes expected value operator),

and

$S_\epsilon$  = known covariance matrix of  
experimental observations.

In addition, the covariance matrix of the solution,  $S_{\hat{\eta} - \eta}$ , is given by

$$S_{\hat{\eta} - \eta} = X^{-1} \quad (5)$$

where

$$X = S_f^{-1} + A^T S_\epsilon^{-1} A.$$

The sum of the diagonal elements of  $S_{\hat{\eta} - \eta}$  is  $m$  times the expected mean-square error per quadrature point. The essential properties and requirements of the solution may be summarized as follows:

- a. The method requires knowledge of  $S_f$  and  $S_\epsilon$ . We can estimate  $S_f$  from past observations of  $f$  (usually direct observations);  $S_\epsilon$  can be determined experimentally by calibration of the sensor.

- b. Data with correlated errors can be treated by this method.
- c. The instability problem is completely eliminated: as  $S_{\epsilon} \rightarrow \infty$ ,  $\hat{\eta} \rightarrow 0$ , i. e., the best estimate of the profile is its mean.
- d. The average error of the solution can be determined immediately from properties of the equation of transfer, the measurement noise level, and the a priori information.
- e. The introduction of basis vectors to represent the solution is neither necessary nor desirable. A completely adequate representation of the solution is its values at each of the quadrature abscissas.
- f. The solution yields the best fit to the profile in the sense of minimum mean-square linear unbiased estimation when averaged over the joint probability distribution of  $f$  and  $\epsilon$ , where the components of  $f$  are assumed uncorrelated with those of  $\epsilon$ .
- g. A criterion for optimum observation ordinates (such as frequency or angle) may be given. From a large set of possible measurement locations, the optimum subset is the set that yields the minimum overall expected mean-square error ( $\text{Tr } S\hat{\eta} - \eta = \text{Tr } X^{-1}$ ). The optimum subset is a function of the kernel, the noise level of observations, the a priori information and the number of elements in the subset (Westwater and Strand, 1968).
- h. The method estimates the solution at each point along the profile. Thus, questions of "height resolution" can be answered only by reference to the correlation properties of the medium. For example, a profile "spike" of arbitrarily small thickness and lying outside the interval in which the kernel contributes to the integral could be inferred strictly on the basis of conditional probability if the medium had a correlation coefficient of unity between the two regions.
- i. The linear estimate is the optimum estimate, in the expected mean-square sense, if the profile and measurement error are jointly gaussian distributed

and if the integral equation is exactly a Fredholm equation (C. D. Rodgers, 1966).

### 3. GROUND-BASED TEMPERATURE PROBING BY PASSIVE MICROWAVE TECHNIQUES

Under clear-sky conditions, ground-based measurements of microwave thermal emission near 60 GHz can provide useful information about the temperature structure of the lower troposphere. Such information, obtainable on a time scale much finer than that provided by conventional radiosonde launches, could be useful in studying development of low altitude inversion layers, and in air pollution studies. In addition, ground-based passive probing for water vapor profiles requires knowledge of tropospheric temperature structure which could be provided by this technique. In this section, theoretical results of Westwater and Strand (1968) are presented to indicate the accuracies that might be expected from such a technique under clear-sky conditions.

Data vectors (i. e., thermal emission measurements) from which profiles can be extracted can be generated by either frequency or angular variation or both. A complete discussion of the comparative experimental accuracies achievable at present and in the future is beyond the scope of this paper. However, with statistical inversion methods, various choices of random experimental error, as embodied in the covariance matrix,  $S_{\epsilon}$ , can be made and the average effect of these measurement errors on the inferred profile can be determined. As an example of this type of calculation, Figures 1 and 2 show accuracies obtainable by ground-based probing using vertical emission measurements at five frequencies in the oxygen complex. In these figures, "constrained" refers to the use of the surface temperature to modify the estimate of the profile. With measurement accuracies of  $1^{\circ}\text{K}$ , only two, or at most three, of the measurements are independent (cannot be predicted to within the noise level by linear combinations of the remaining measurements), so that similar results could be obtained by a suitable choice of two or three channels. Figure 3 shows the accuracy expected from a fixed frequency variable-angle scheme at 53.8 GHz. The initial elevation angles ranged from  $1^{\circ}$  to  $90^{\circ}$  in equal increments of the cosecant of the elevation angle, spherical temperature stratification was assumed, and ray tracing based on Snell's law for a spherical atmosphere was used. The results indicate that, for the noise levels assumed here, the temperature profile can be determined to a standard deviation of  $2^{\circ}$  up to about 5 km. Above the 5 km, the results deteriorate rapidly, and the uncertainty approaches the a priori uncertainty.

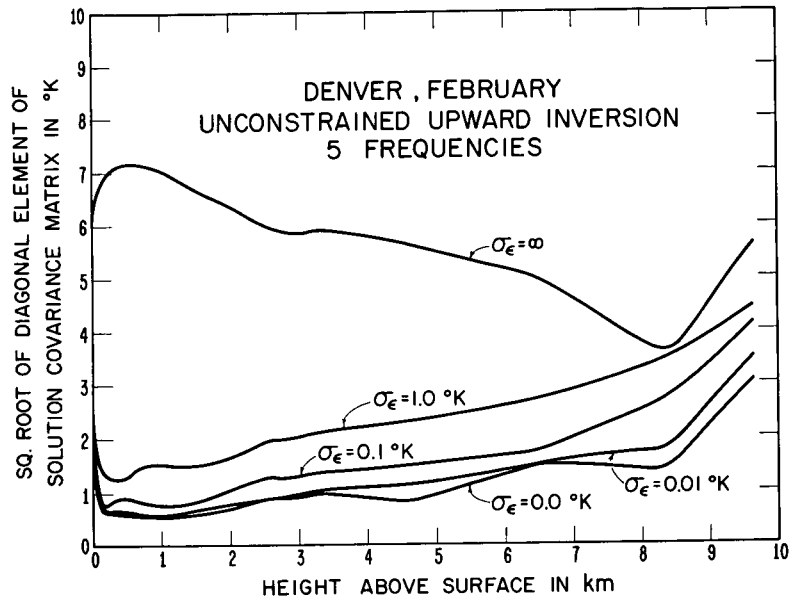


Figure 1. Accuracies obtainable by ground-based probing in the oxygen complex (unconstrained).

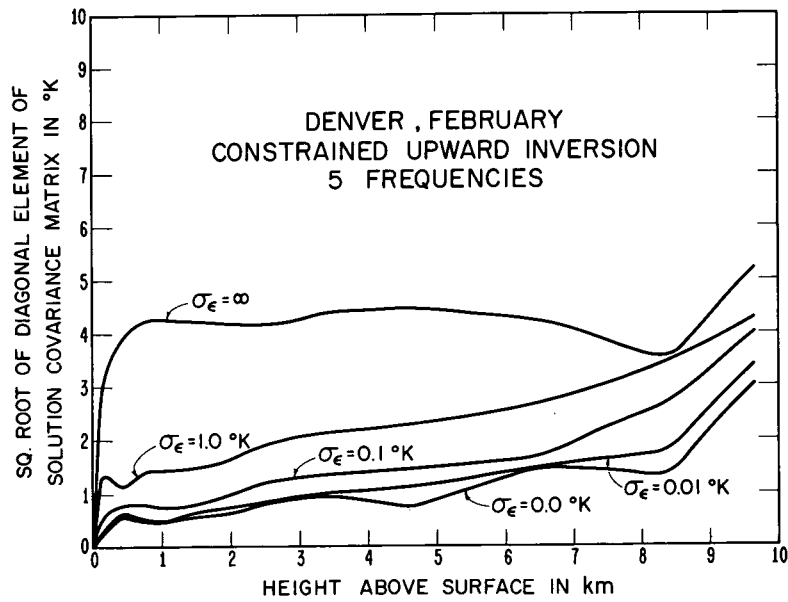


Figure 2. Accuracies obtainable by ground-based probing in the oxygen complex (constrained).

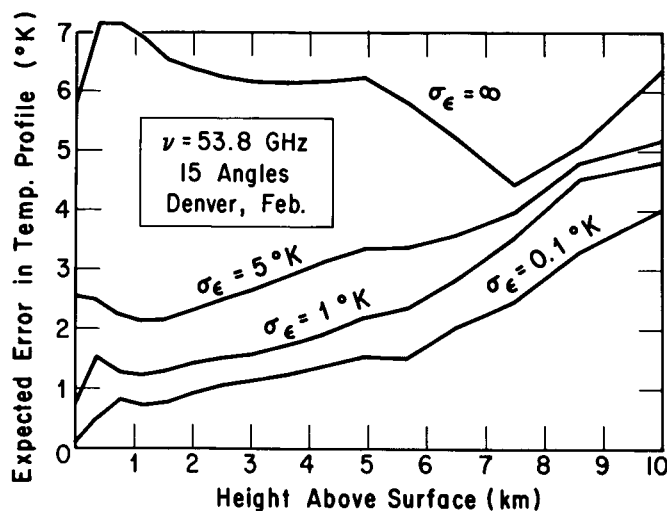


Figure 3. Information content of angular emission measurements in determining temperature profiles.

#### 4. DETERMINATION OF ATMOSPHERIC RANGE ERROR CORRECTION BY PASSIVE MICROWAVE RADIOMETRY

The accuracy of baseline-type tracking systems which measure range to missiles is limited by atmospheric refraction. The MARCOR (microwave atmospheric range correction) technique (Menius, *et al.*, 1964) corrects for range errors due to the wet component of atmospheric refractivity by using thermal emission measurements near the 1.35 cm water vapor line. These measurements are made by a radiometer pointing in the approximate direction of the tracked object, and related to the line integral of the wet refractivity. Theoretical results indicate that this technique can improve surface estimates of range correction by a factor of 5 to 10 (Westwater, 1967).

The Millimeter Wave Program Area of the Wave Propagation Laboratory and Tropospheric Physics Program Area of the Tropospheric Telecommunications Laboratory, ESSA Research Laboratories, have initiated a joint experimental effort to establish the feasibility of the MARCOR technique. Phase measurement techniques were used to measure apparent path length at frequencies near 10 GHz over a 64 km path from Upolu Point (elevation 30 m) on the island of Hawaii to Mt. Haleakala (elevation 3025 m) on the island of Maui. Variations of several meters in this measured path length, resulting from the changing atmospheric refractivity, were observed. Simultaneous measurements of atmospheric thermal emission were made at 20.6 GHz with a conical horn reflector having an aperture diameter of 1.2 m and directed along a path near that mentioned above. Meteorological data were taken at the surface, through the atmosphere with radiosondes, and

with an aircraft instrumented for refractivity and temperature soundings. Supplementary atmospheric emission and absorption measurements were made at 15, 31, and 53.8 GHz. The data are being analyzed to determine to what extent the radiometric data can predict the changes in apparent path length.

## 5. LIQUID WATER CONTENT OF THUNDERSTORM CELLS

Measurements of the thermal noise emission from Colorado thunderstorms by means of a 10.7 GHz radiometer and a 18 m diameter steerable parabolic antenna have been used to prepare contours of integrated liquid water content along radio rays passing through the storm (Decker and Dutton, 1968).

The experimental data consist of horizontal radiometric scans across the thunderstorm that make it possible to measure the difference in antenna temperature when the antenna is pointed at the clear atmosphere and the storm. In addition to the radiometric data, radar, radiosonde, and surface meteorological data were used to estimate the absorption that must have been occurring along a line of sight toward the clear sky and also when looking toward the storm. Subtracting the absorption due to the clear sky from that occurring when looking at the storm yielded an estimate of the absorption due to the storm itself. Since the storm absorption is proportional to the liquid water content with a known constant of proportionality dependent upon the temperature, the water content of the storm along the line of sight can be estimated.

Examples of contours of liquid water content, as seen from the radiometer site, plotted on an azimuth angle-elevation angle grid are shown in Figure 4. The contour values indicate the number of kilograms of liquid in a column of one square meter cross section along the entire path through the storm. Alternatively, one may estimate the average liquid water density in grams per cubic meter over the path length by dividing the contour values by an estimated length (in kilometers) through the storm.

The technique shows promise as a tool in the study of liquid water in clouds, although further work is needed to delineate its limitations. In particular, the effects of scattered energy should be evaluated, as well as the effects of ice particles with their different emitting and scattering properties.

GROUND-BASED MICROWAVE PROBING

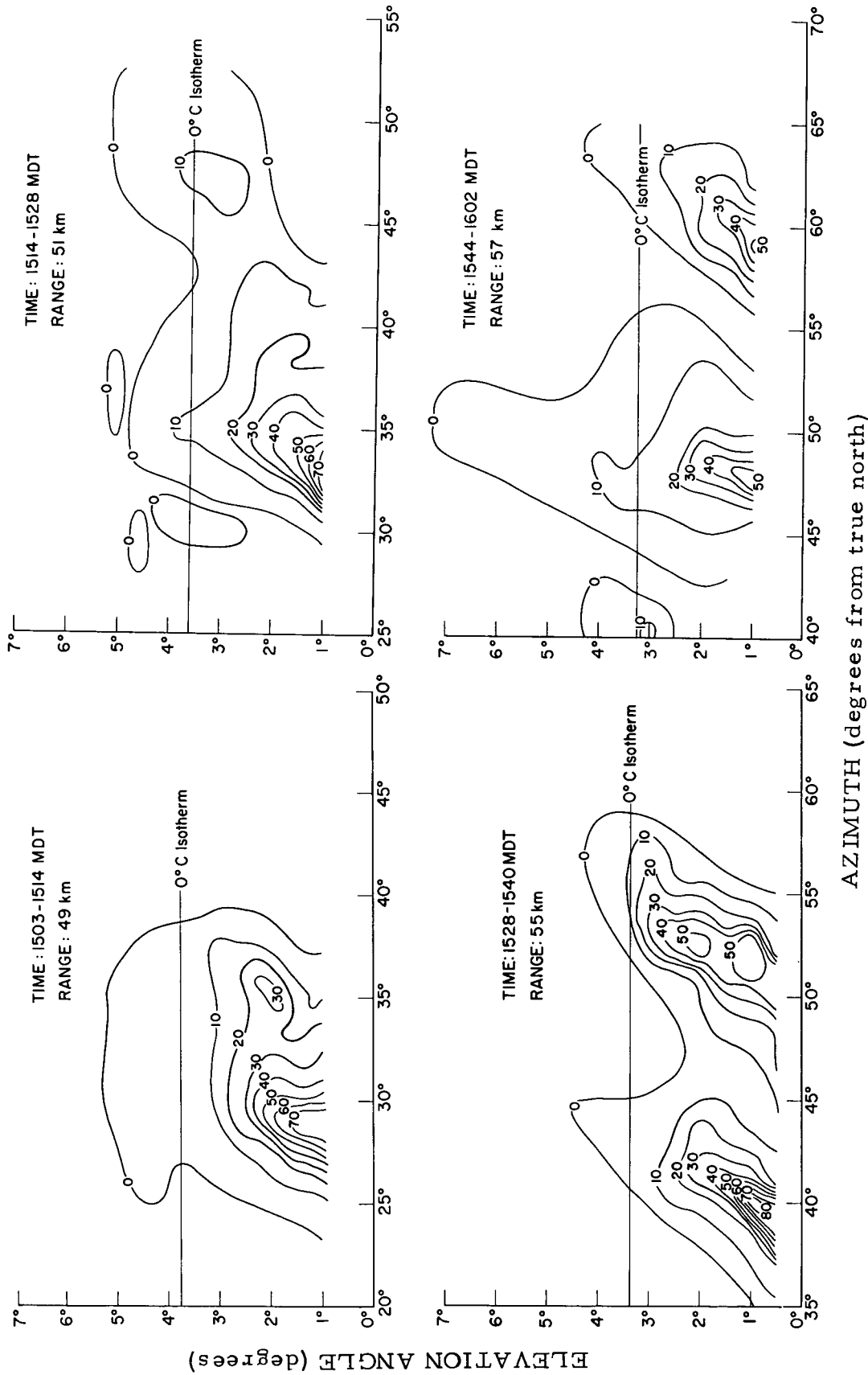


Figure 4. Liquid water content ( $\text{kg}/\text{m}^2$  column) of a July 18, 1967 thunderstorm near Boulder, Colorado.

REFERENCES

- Alishouse, J. C., L. J. Crone, H. E. Fleming, F. L. Van Cleef, and D. Q. Wark, 1967: A discussion of empirical orthogonal functions and their application to vertical temperature profiles. Tellus, XIX, 3, 477-482.
- Barrett, A. H., and V. K. Chung, 1962: A method for the determination of water vapor abundance from ground-based microwave observations. J. Geophys. Res. 67, 11, 4257-4266.
- Decker, Martin T., and E. J. Dutton, 1968: Radiometric observations of thunderstorm cells. Proc. Fifth Symp. Remote Sensing of Environ. (to be published)
- King, J. I. F., 1964: Inversion by slabs of varying thickness. J. Atmos. Sci. 21, 324-326.
- Meeks, M. L., and A. E. Lilley, 1963: The microwave spectrum of oxygen in the earth's atmosphere. J. Geophys. Res. 68, 1683-1703.
- Menius, A. C., C. F. Martin, W. M. Layson, and R. S. Flagg, 1964: Tropospheric refraction corrections using a microwave radiometer. PanAm. Airways Tech. Staff, Tech. Memo No. 19, ETV-TM-64-12.
- Rodgers, C. D., 1966: Satellite infrared radiometer - A discussion of inversion methods. Univ. of Oxford, Clarendon Laboratory Memorandum No. 66, 13, 625.
- Strand, O. N., and E. R. Westwater, 1968a: Statistical estimation of the numerical solution of a Fredholm integral equation of the first kind. J. ACM 15, 1, 100-114.
- Strand, O. N., and E. R. Westwater, 1968b: Minimum-rms estimation of the numerical solution of a Fredholm integral equation of the first kind. J. SIAM Num. Anal. 5, 2, 287-295.
- Twomey, S., 1965: The application of numerical filtering to the solution of integral equations encountered in indirect sensing measurements. J. Franklin Inst. 279, 2, 95-109.
- Westwater, E. R., 1967: An analysis of the correction of range errors due to atmospheric refraction by microwave radiometric techniques. ESSA Tech. Rept. IER 30-ITSA-30.

## GROUND-BASED MICROWAVE PROBING

Westwater, E. R., and O. N. Strand, 1967: Application of statistical estimation techniques to ground-based passive probing of tropospheric structure. ESSA Tech. Rept. IER 37-ITSA 37.

Westwater, E. R., and O. N. Strand, 1968: Statistical information content of radiation measurements used in indirect sensing. J. Atmos. Sci. 25, 5, 750-758.

N72-25373

## PASSIVE REMOTE SENSING AT MICROWAVE WAVELENGTH

David H. Staelin

Department of Electrical Engineering and  
Research Laboratory of Electronics  
Massachusetts Institute of Technology  
Cambridge, Massachusetts 02139

### ABSTRACT

Microwave meteorology is in part an outgrowth of radio astronomy techniques which have been developed for measuring and interpreting the intensity, polarization, and spectral properties of radio signals. In this review the ways in which radio signals are affected by meteorological parameters are described, as are methods for interpreting the signals, the state-of-the-art in instrumentation, the current state of development of the field, and some problems and prospects for the future. It is shown that the temperature profile of the atmosphere, water vapor and ozone distribution, cloud water content, and certain surface properties can be measured with sufficient accuracy to provide useful meteorological information. In some cases the information can not readily be obtained in any other way, and thus passive microwave techniques may open to study new areas of meteorology. Because of space constraints the review is composed primarily of summaries and conclusions, and it refers to the literature for most details.

### 1. INTRODUCTION

In this paper are reviewed ways in which the wavelength interval 0.1-100 cm can be utilized for passive ground-based or space-based meteorological measurements. Each region of the electromagnetic spectrum has unique properties which can be exploited for purposes of remote sensing, and in the microwave region these properties include an ability to penetrate clouds and to interact strongly with O<sub>2</sub>, H<sub>2</sub>O, and other atmospheric constituents. The interactions considered here are those of O<sub>2</sub>, H<sub>2</sub>O, O<sub>3</sub>, clouds, precipitation, sea state, surface temperature, and surface emissivity. Barrett (1962) has listed many other constituents which also interact, such as OH, CO, N<sub>2</sub>O, and SO<sub>2</sub>, but these are presently difficult to observe and are not considered in this review.

The review has two major parts, a technical section which reviews the physics of the interactions, the mathematics of data interpretation, and the state-of-the-art in instrumentation. The second part is applications-oriented and reviews the types, accuracy, and relevance of possible meteorological measurements. It also contains several suggestions for further work.

## 2. TECHNICAL REVIEW

### 2.1 Physics of the Interactions

The topics of this section include 1) the relevant equations of radiative transfer, 2) the absorption coefficient expressions for O<sub>2</sub>, H<sub>2</sub>O, O<sub>3</sub>, clouds, and precipitation, and 3) the microwave properties of the terrestrial surface. Both the theoretical expressions and the corresponding experimental verifications are described and referenced. In general only a fraction of all possible references are given.

#### 2.1.1 The Equations of Radiative Transfer

At wavelengths longer than 1 mm the Planck function can be simplified because  $h\nu \ll kT$  for all situations of meteorological interest. The symbols  $h$ ,  $\nu$ ,  $k$ ,  $T$  are Planck's constant, frequency, Boltzmann's constant, and temperature, respectively. In this paper rationalized MKS units are used unless stated otherwise. As a result of this low frequency approximation the power  $P$  (watts) received by a microwave radiometer equals  $kTB$ , where  $B$  is the bandwidth (Hz). Since temperature has direct physical significance, most radiometers are calibrated in terms of antenna temperature  $T_A$  (°K), which is the temperature a black body at the antenna terminals must have to produce a signal of the observed power  $P$ . That is,

$$T_A = P/kB \quad (1)$$

The measured antenna temperature  $T_A$  is in turn related to the angular distribution of power incident upon the antenna. The appropriately polarized power incident upon the antenna from any given direction can be described by an equivalent brightness temperature,  $T_B(\nu, \theta, \phi)$  (°K). The antenna temperature is then an average of the brightness temperature weighted over  $4\pi$  steradians according to the antenna gain function  $G(\nu, \theta, \phi)$ . That is

$$T_A(\nu) = \frac{1}{4\pi} \int_{4\pi} T_B(\nu, \theta, \phi) G(\nu, \theta, \phi) d\Omega \quad (2)$$

The gain of any particular antenna can be calibrated on an appropriate test range.

The equation of radiative transfer can be used to relate the brightness temperature  $T_B$  to the atmospheric composition and temperature  $T(z)$  along the line of sight, and to the brightness temperature  $T_o(\theta, \phi)$  of the medium beyond the atmosphere. To an excellent approximation the equation of radiative transfer for a slightly lossy medium is

$$T_B(\nu) = T_o e^{-\tau(\nu)} + \int_0^{z_{\max}} T(z) e^{-\int_0^z \alpha(z) dz} \alpha(z) dz \quad (3)$$

where scattering and variations in index of refraction have been neglected. The equation loses validity primarily in the presence of the relatively large particles like

raindrops or snowflakes, and at 1-mm wavelength in the presence of some clouds. In Equation (3)  $\tau(\nu)$  is the total opacity of the atmosphere, and  $\alpha(z)$  ( $\text{m}^{-1}$ ) is the absorption coefficient. Equation (3) expresses the fact that the brightness temperature in any given direction is the sum of the background radiation and the radiation emitted at each point along the ray trajectory, each component attenuated by the intervening atmosphere. The equations of radiative transfer with and without scattering are discussed by Chandrasekhar (1960) and are related to radio astronomy problems by Shklovsky (1960).

In certain cases the equations of radiative transfer is more appropriately expressed in matrix form. This form is desirable, for example, when describing the effects of Zeeman-split resonance lines upon the flow of polarized radiation. One such formulation was developed and applied by Lenoir (1967, 1968) to 5-mm wavelength measurements of the mesospheric temperature profile.

### 2.1.2 Opacity Expressions for Atmospheric Constituents

A general reference for microwave spectroscopy is the book by Townes and Schawlow (1955) and good references for general atmospheric and surface effects include the book by Stratton (1941) and the book edited by Kerr (1952). Expressions for the absorption coefficients of atmospheric constituents are usually formed by empirically choosing constants in the quantum-mechanical formulation for opacity in order to provide the best agreement with experiment. If experimental verification of the absorption coefficient expressions under all possible conditions were practical, one could dispense with quantum mechanics and electromagnetism entirely. The degree to which the absorption coefficients are presently based upon theory rather than upon experiment varies considerably, depending upon the constituents and the atmospheric conditions.

In the case of the oxygen complex near 5-mm wavelength the most widely used absorption coefficient is that of Meeks and Lilley (1963) who revised and updated the expressions developed by Van Vleck (1947). Gautier and Robert (1964) and Lenoir (1965) extended these expressions to include Zeeman splitting appropriate above 40 km altitude. The absorption coefficient was determined using the theoretical line-shape factor of Van Vleck and Weisskopf (1945), and those line-width parameters and line frequencies which were measured for the stronger lines. The line-widths have been measured at pressures near 1 atm and at low pressures. The dependence of line-width on pressure and temperature has also been measured. A complete bibliography by Rosenblum (1961) references the literature on microwave absorption by oxygen and water vapor up to 1961. Although much experimental work has been done, there is some need for still more precise laboratory measurements, particularly of atmospheric compositions over the full range of temperatures and pressures of meteorological interest.

The absorption coefficient of oxygen in the atmosphere can also be tested by direct measurement of antenna temperatures near 5-mm wavelength. Such measurements have been made from both ground-based and balloon-borne radiometers. The most recent such measurements are those of Lenoir *et al* (1968). They examined the  $9^+$  resonance line at 61.151 GHz with a three-channel microwave radiometer mounted on balloons which flew to altitudes of 35 km. Observations were made at zenith angles of  $60^\circ$ ,  $75^\circ$ ,  $120^\circ$ , and  $180^\circ$ , and at frequencies separated from 61.151 GHz by  $\pm 20$ ,  $\pm 60$ , and  $\pm 200$  MHz. The most precise tests of the theoretical opacity expressions are those measurements made looking upward. In this case differences between the theoretical and experimental values of atmospheric opacity as small as 5% could be

## PASSIVE REMOTE SENSING AT MICROWAVE WAVELENGTHS

detected in certain regions of the atmosphere. No discrepancies this large were noted 60 and 200 MHz from resonance when the balloon was in the altitude region 25-32 km. One such data set from Lenoir *et al* (1968) is shown in Figure 1. The experiments were less sensitive to opacity uncertainties in other regions of the atmosphere or spectrum. In these regions the differences between the theoretical and experimental brightness temperatures were generally less than 5°K, the approximate experiment accuracy.

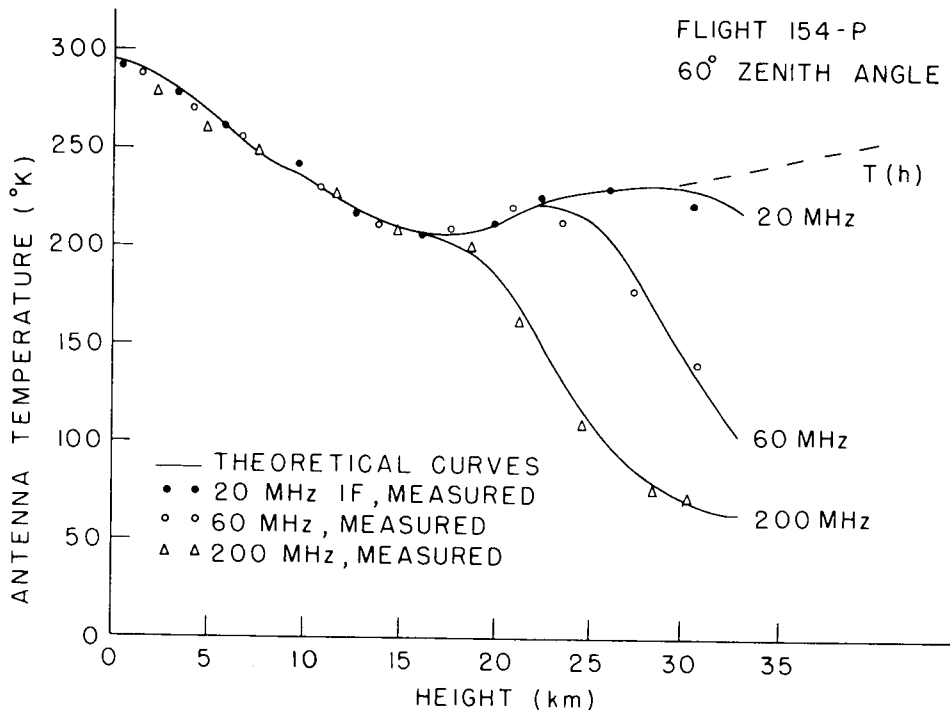


Figure 1. Experimental and theoretical values of antenna temperature at three i. f. frequencies for a 61.151 GHz radiometer mounted on a balloon.

Measurements at 53.4 - 56.4 GHz by Carter *et al* (1968) have permitted the Van Vleck-Weisskopf line shape to be refined slightly.

Water vapor has transitions at 22.237 and 183.3 GHz, in addition to many transitions at higher frequencies. The opacity expressions for the 22 GHz line were developed by Van Vleck (1947, 1951), and were refined by Barrett and Chung (1962) on the basis of the experimental findings of Becker and Autler (1946) and the theoretical calculations of Benedict and Kaplan (1959). Relatively good agreement between theory and experiment was obtained by combining the Van Vleck and Weisskopf (1945) line shape with a non-resonant term which corresponds to contributions from the far wings of all the resonances at other frequencies. The magnitude of the non-resonant term was selected to provide the best agreement with the measurements of Becker and Autler (1946), which were made at pressures near 1 atm. Gaut (1967) and Croom (1965a) have also developed expressions for the 22 GHz absorption coefficient.

Gaut (1967) has developed an expression for the absorption coefficient near the 183.310 GHz water vapor resonance. He included the effects of several neighboring lines by using in part the line strength calculations of King, Hainer, and Cross (1947), the Van Vleck-Weisskopf line shape, and measurements of Rusk (1965),

Frenkel and Woods (1966), and Hemmi (1966). Croom (1965a) has done similar calculations. The review and bibliography by Rosenblum (1961) is a useful reference.

Direct measurements of the atmosphere have been made primarily near 22 GHz. Most of these measurement programs have been handicapped because atmospheric water vapor varies somewhat more rapidly than the observing frequency can be changed, or more rapidly than accurate correlative measurements can be made. The remedy is improved instrumentation and stable meteorological conditions. An extensive series of observations has been made with a five-frequency radiometer by Staelin (1966) and Gaut (1967). Five frequencies were observed simultaneously in absorption against the sun and permitted opacity measurements with an approximate accuracy of 0.02 db or less than 5% of the total opacity. Meaningful comparison of the measured opacity spectrum and that spectrum expected on the basis of simultaneous rawinsondes was possible only on days characterized by very stable meteorological conditions. One such comparison made by Gaut (1967) is illustrated in Figure 2. Examination of 9 spectra measured under these stable conditions indicate that the theoretical expressions of Barrett and Chung (1962) are accurate to better than 5% for typical atmospheric conditions.

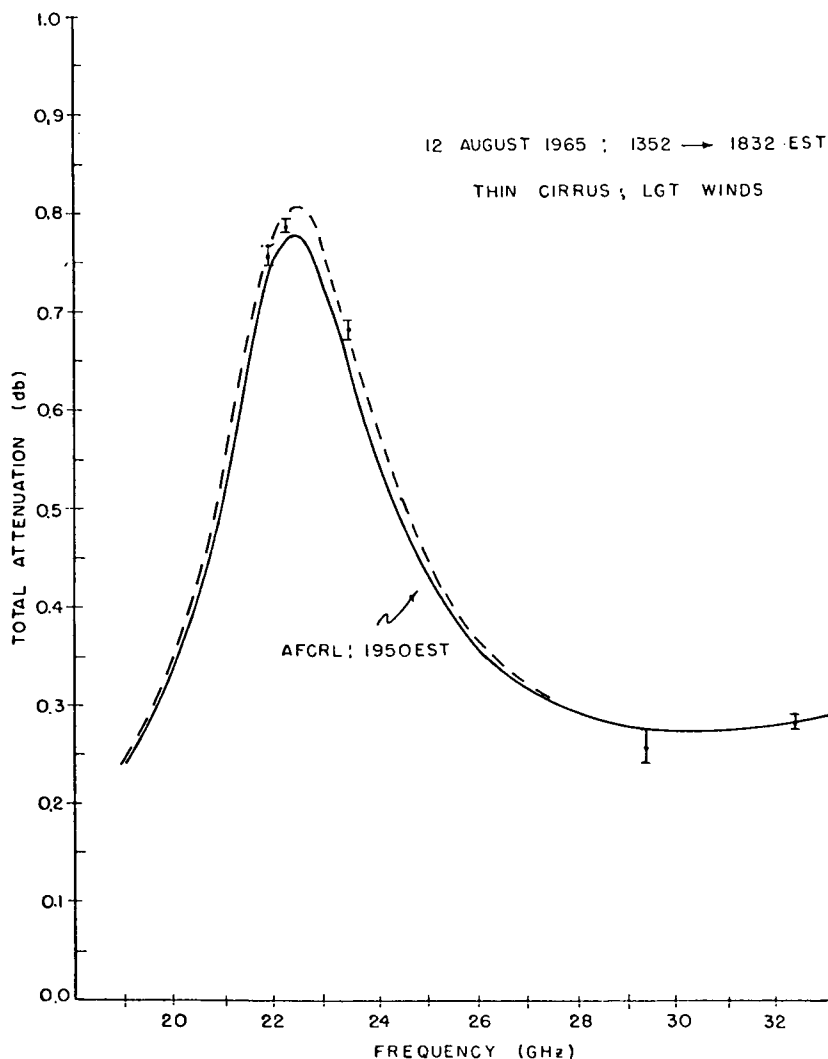


Figure 2. The observed spectrum and corresponding theoretical spectrum (based on simultaneous rawinsonde records) near the 22.234 GHz resonance of water vapor.

Ozone has many spectral lines at microwave frequencies, but because of the low abundance of ozone these lines are difficult to detect. Barrett (1962) listed resonances of ozone at frequencies (GHz) of 9.201, 10.226, 11.073, 15.116, 16.413, 23.861, 25.300, 25.511, 25.649, 27.862, 28.960, 30.052, 30.181, 30.525, 36.023, 37.832, 42.833, 43.654, 96.229, 101.737, and 118.364. Absorption coefficient expressions have been developed by Caton *et al* (1967), Caton *et al* (1968), and Weigand (1967). These theoretical expressions are based upon line frequencies and line strengths calculated by Gora (1959) and upon the Van Vleck-Weisskopf line shape assumption. At present 5 resonances in the terrestrial atmosphere have been observed. Mouw and Silver (1960) observed the 36.025 GHz line in absorption against the sun, Caton *et al* (1967) observed the 37.836 GHz line in absorption and the 30.056 GHz line in emission, Barrett *et al* (1967) observed the 23.861 GHz line in emission, and Caton *et al* (1968) observed the 101.737 GHz line in both emission and absorption. For spectral resolution of a few megahertz, the line amplitudes in emission at zenith are generally a few tenths of a degree Kelvin except for the line at 101.737 GHz, which had an amplitude of a few degrees. The most precise line measurement was that made at 101.737 GHz by Caton *et al* (1968), and their figure showing the line observed in absorption against the sun at 64° zenith angle is reproduced here in Figure 3. In order to match the theoretical and experimental curves they found it necessary to multiply the amplitude of the theoretical line by a factor of 1.5. It is uncertain whether this difference is due to errors in the opacity expression or errors in the assumed model atmosphere. More measurements of ozone would be very useful.

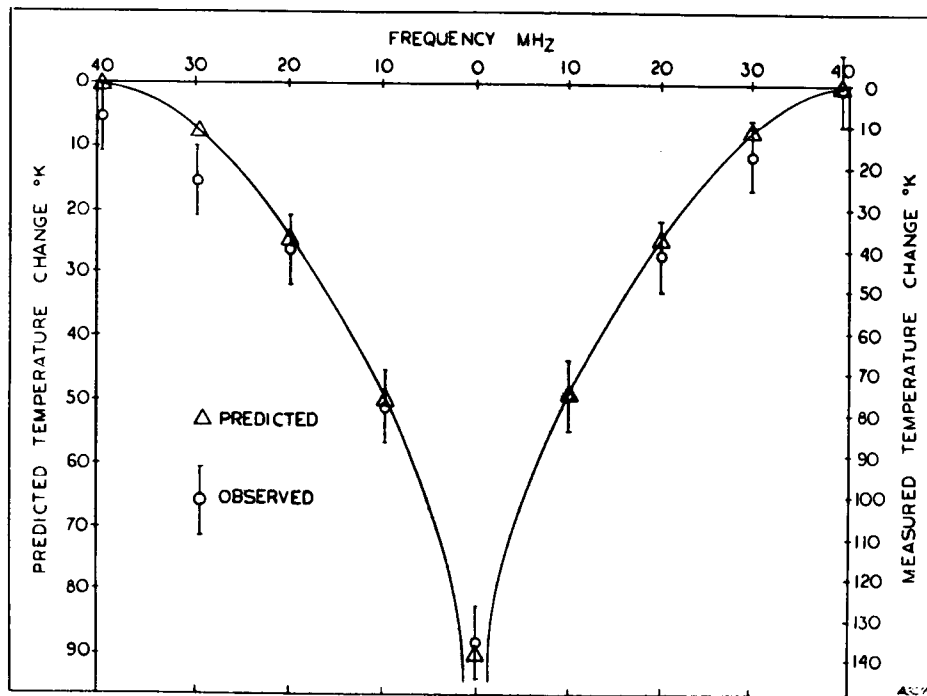


Figure 3. Experimental and theoretical changes in solar brightness temperature caused by ozone at 101.7 GHz. The predicted values were scaled by 1.5 to match the measured values.

Clouds exhibit no resonances in the microwave region of the spectrum but instead absorb by non-resonant processes. Scattering in clouds can generally be neglected if the wavelength is more than 30 times the droplet diameter.

Mie (1908), Stratton (1941), and others have developed expressions for the absorption and scattering cross-sections of dielectric spheres, Ryde and Ryde (1945) and Haddock (1948) have used the dielectric constants for water given by Saxton and Lane (1946) in order to compute the microwave absorption coefficients for clouds and rain. Goldstein (1951) and Atlas *et al* (1952) have reviewed and summarized much of this work. These equations can be extended to include snow and ice clouds through use of the refractive index of ice measured by Cummin (1952). These results were summarized by Atlas *et al* (1952) in a table plus footnotes which are reproduced here in Table 1.

TABLE 1  
Working Values of ATTENUATION in db. km<sup>-1</sup> (one way)

	Temp (C)	3.2 cm	1.8 cm	1.24 cm	0.9 cm
		RAIN* R in mm.hr <sup>-1</sup>	18**	0.0074R <sup>1.31</sup>	0.045R <sup>1.14</sup>
SNOW* R in mm.hr <sup>-1</sup> of melted water	0	3.3x10 <sup>-5</sup> R <sup>1.6</sup> + 68.6x10 <sup>-5</sup> R	3.32x10 <sup>-4</sup> R <sup>1.6</sup> + 12.2x10 <sup>-4</sup> R	1.48x10 <sup>-3</sup> R <sup>1.6</sup> + 1.78x10 <sup>-3</sup> R	5.33x10 <sup>-3</sup> R <sup>1.6</sup> + 2.44x10 <sup>-3</sup> R
	-10	3.3x10 <sup>-5</sup> R <sup>1.6</sup> + 22.9x10 <sup>-5</sup> R	3.32x10 <sup>-4</sup> R <sup>1.6</sup> + 4.06x10 <sup>-4</sup> R	1.48x10 <sup>-3</sup> R <sup>1.6</sup> + 0.59x10 <sup>-3</sup> R	5.33x10 <sup>-3</sup> R <sup>1.6</sup> + 0.81x10 <sup>-3</sup> R
	-20	3.3x10 <sup>-5</sup> R <sup>1.6</sup> + 15.7x10 <sup>-5</sup> R	3.32x10 <sup>-4</sup> R <sup>1.6</sup> + 2.80x10 <sup>-4</sup> R	1.48x10 <sup>-3</sup> R <sup>1.6</sup> + 0.41x10 <sup>-3</sup> R	5.3x10 <sup>-3</sup> R <sup>1.6</sup> + 0.56x10 <sup>-3</sup> R
WATER CLOUD M in gm.m <sup>-3</sup>	20	0.0483 M	0.128 M	0.311 M	0.647 M
	10	0.0630 M	0.179 M	0.406 M	0.681 M
	0	0.0858 M	0.267 M	0.532 M	0.99 M
	-8	0.112 M (extrapolated)			
ICE CLOUD M in gm.m <sup>-3</sup>	0	2.46x10 <sup>-3</sup> M	4.36x10 <sup>-3</sup> M	6.35x10 <sup>-3</sup> M	8.7x10 <sup>-3</sup> M
	-10	8.19x10 <sup>-4</sup> M	1.46x10 <sup>-3</sup> M	2.11x10 <sup>-3</sup> M	2.9x10 <sup>-3</sup> M
	-20	5.63x10 <sup>-4</sup> M	1x10 <sup>-3</sup> M	1.45x10 <sup>-3</sup> M	2x10 <sup>-3</sup> M

\* These are empirical equations. For the more exact relations on which they are based, see Atlas *et al* (1952).

\*\* The effect of temperature is discussed in Atlas *et al* (1952). The effect of non-sphericity on Q<sub>s</sub> and Q<sub>a</sub> has been neglected.

+ As long as snowflakes are in the Rayleigh region. A value of R-10 or R<sup>1.6</sup>-39 is an upper limit for snowfall rates.

Such theoretical calculations are approximate (Goldstein, 1951) because they must be based upon some assumed distribution of particle sizes, shapes, etc. The expressions are less sensitive to drop size at the longer wavelengths. The expressions are less sensitive to drop size at the longer wavelengths. The expressions are best tested by field measurements. Goldstein (1951) has reviewed several efforts to correlate rainfall rate with path loss measured along a short path. These measurements at wavelengths ranging from 0.62 to 3.2 cm are all within a factor of 2 of the predicted average attenuation. Emission spectra have been measured with a ground-based five-channel microwave radiometer observing at frequencies from 19.0 to 32.4 GHz (Toong, 1967). These spectra showed good agreement with the theoretical spectrum shapes, even through all but the heaviest rainfall. Data obtained at 30° elevation are compared with theoretical spectra in Figure 4. The cloud types inferred from these spectra were consistent with those characteristic of frontal passages.

### 2.1.3 The Terrestrial Surface

The terrestrial surface both emits and reflects radio waves, and the degree to which it does either is determined by the surface dielectric constant and the detailed structure of the surface. In some cases the emission and reflection coefficients calculated for smooth surfaces (Stratton, 1941) are good approximations. This is so far calm ocean and smooth homogeneous dirt surfaces, especially at longer wavelengths. Gaut (1967) and Marandino (1967) have calculated the emissivity of smooth water for a number of temperatures and wavelengths, and Marandino (1967) has made similar calculations for several solid surfaces.

Three interesting properties of the ocean surface are worthy of note, 1) the reflectivity is high, near 0.6, 2) the dielectric constant and hence the emissivity varies with temperature, and 3) the brightness temperature of the ocean surface is a function of surface roughness, which in turn is correlated with wind velocity. The high reflectivity results in a very low surface brightness temperature over most of the microwave spectrum, and thus spectral lines like H<sub>2</sub>O or O<sub>3</sub> can be seen in emission from space. The temperature dependence of the emissivity results in certain combinations of sea surface temperature and frequency having a surface brightness temperature independent of surface kinetic temperature, and at other combinations the dependence can be moderately strong. For water temperatures near 285°K this temperature dependence is weak for wavelengths of 1 and 20 cm, and is stronger near wavelengths of 3 cm. Yap (1965) and Stogren (1967) have calculated the dependence of surface brightness temperature upon equivalent wind speed, based upon the surface-slope statistics developed by Cox and Munk (1954). For example, Yap computed the effect at 3-cm wavelength at nadir to be approximately 0°K per knot equivalent wind speed and at 60° nadir angle to be 0.5°K for  $\vec{E}_\perp$  polarization, and 0°K for  $\vec{E}_{11}$  polarization.

Since land surfaces are difficult to analyze analytically, much emphasis must be placed on field measurement programs. Measurements by Porter (1966) of smooth asphalt and concrete are in reasonable agreement with theory. Measurements of rough surfaces have also been made, and qualitative agreement with intuition has been obtained. Very few well calibrated measurements have been made.

## 2.2 Mathematics of Data Interpretation

One of the central problems in remote sensing is conversion of the measurements into estimates of the desired atmospheric parameters with the smallest possible error. It is often called the inversion problem because it can be interpreted as the problem of

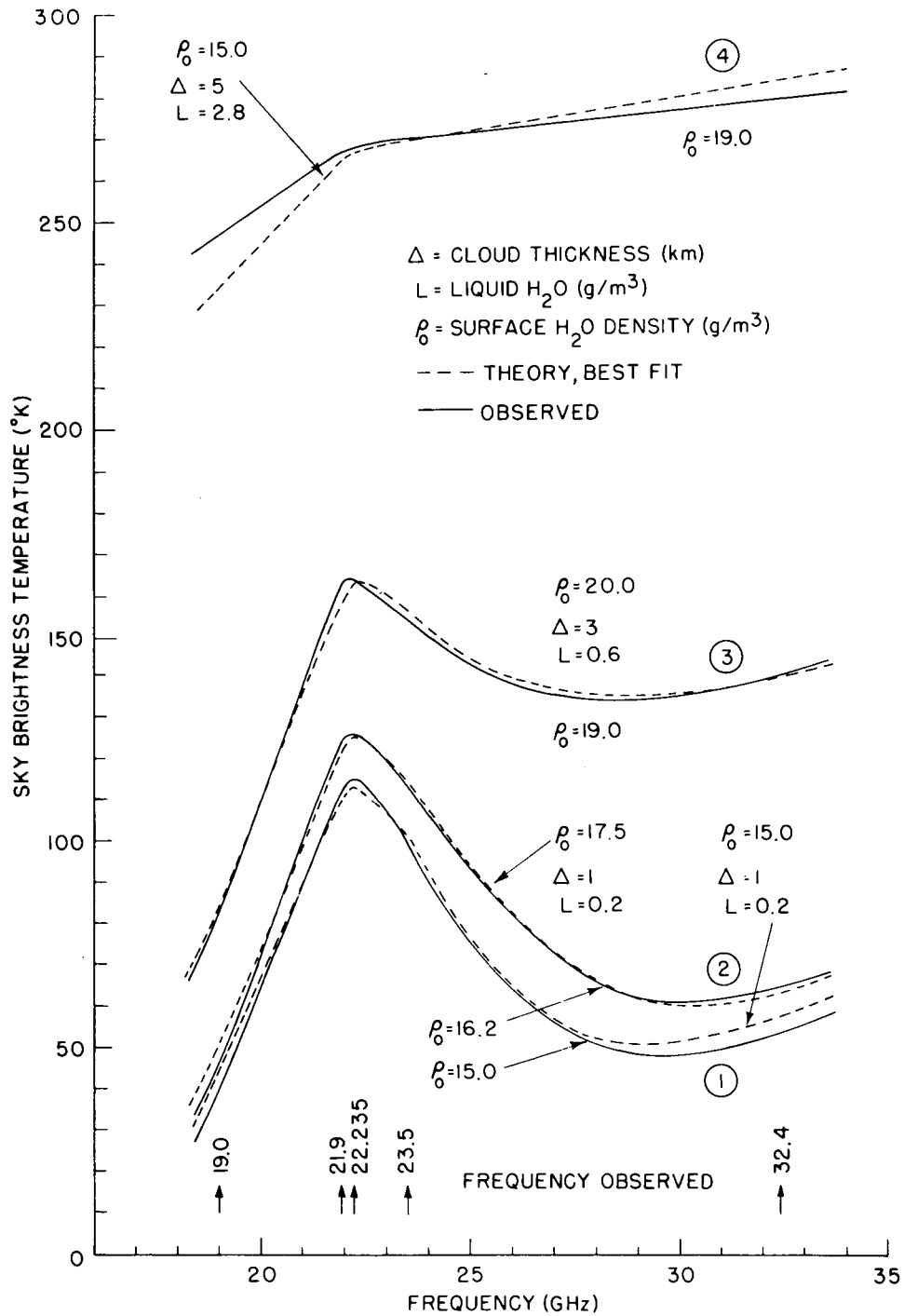


Figure 4. Experimental and best-fit theoretical emission spectra for the terrestrial atmosphere during a frontal passage. From Toong (1967).

inverting the equations of radiative transfer. There are several major approaches which have been taken toward solving this problem. These approaches include 1) the trial-and-error or library technique, 2) linear analytical procedures, 3) non-linear analytical procedures, 4) linear statistical methods, and 5) non-linear statistical methods.

The trial-and-error or library procedures, as the names imply, simply involve calculation of a large number of theoretical values for the measurements, and selection of that model atmosphere which provides the best agreement with the measurements actually obtained. Although the method is useful because of its conceptual simplicity, there are few inversion problems for which this technique produces completely useful results. Examples include the inversions of Toong (1967) and most studies of the atmospheres of other planets. These are cases where a priori data is not available or where accurate correlative measurements were not feasible.

Linear analytical procedures include those of King (1961), Fow (1964), Lenoir and Koehler (1967), and others. These methods consist primarily of the solution of a set of simultaneous linear equations which relate  $N$  atmospheric parameters to  $N$  measured parameters. Writing these equations usually involves linearizing the applicable equations of radiative transfer. These equations are then solved simultaneously to yield estimates for the unknown parameters. Because this may involve the inversion of a nearly singular matrix, it is necessary to have data that is not noisy or to incorporate boundary conditions which lead to a less singular matrix. If the matrix to be inverted is not singular, then the method is often satisfactory.

Non-linear analytical inversion procedures are similar to the linear procedures, except that non-linear equations are to be solved. For example, King (1964) considered the problem of approximating the atmospheric temperature profile by a set of slabs of varying thickness, or by a set of ramps. This technique has been extended by Florence (1968).

Linear statistical methods are similar to the linear analytical techniques, except that the final matrix which multiplies the data vector to yield the parameter vector is selected so as to minimize some error criterion, such as the mean-square estimation error. There are several approaches to the problem. One approach is that of Twomey (1965, 1966), in which the mean-square error between the true and estimated parameter vectors is minimized by heuristic adjustment of a smoothing parameter which represents the degree to which the estimate is smoothed and biased toward the a priori mean. This bias toward the a priori mean avoids inversion of singular matrices.

Perhaps a more elegant technique is that applied by Rodgers (1966) to inversions of atmospheric temperature profiles at infrared wavelengths. In this procedure, also discussed by Deutsch (1965), Strand and Westwater (1968), and others, the mean-square error between the estimated and true parameter vector is minimized without any heuristic parameters. A complete set of a priori statistics is required to implement the procedure, however. The technique can be described simply as follows. Let the measured data and the desired parameters be represented by the column vectors  $d$  and  $p$ , respectively. In order to reduce the dimensionality of  $p$ , a statistically orthogonal set of basis functions for  $p$ -space is sometimes sought, as discussed by Rodgers (1966) and others. Let  $p^*$  be the estimate of  $p$  based on a particular measured  $d$ , and let  $p^*$  be computed by multiplying  $d$  by the matrix  $D$ , where  $D$  is not necessarily a square matrix. The optimum matrix  $D$  may then be computed by finding that  $D$  which minimizes the mean-square error,  $E [(p^* - p)^t (p^* - p)]$ , where  $E$  is the expected-value operator and the superscript  $t$  means transpose. The optimum  $D$  can be shown to be given by

$$D^t = D_d^{-1} E [dp^t] \tag{4}$$

where  $C_d$  is the data correlation matrix,  $E [dd^t]$ . This procedure is equivalent to multi-dimensional regression analysis. In some cases the matrix  $C_d$  is sufficiently singular to degrade the inversion. In this case, as observed by Waters and Staelin (1968), the matrix  $d$  may be transformed to  $d'$  such that  $E [d' d'^t]$  is diagonal. It can be shown that  $d'$  is  $R^t d$ , where  $R^t$  is the transpose of the matrix formed from the normalized column eigenvectors of  $C_d$ . The estimate  $p^*$  then is given by  $D' d'$ . Those elements of  $d'$  corresponding to diagonal terms in  $C_d'$  less than the computational noise level can then be discarded.

Linear statistical estimation is optimum in a least-square sense only in special circumstances. The procedure of Rodgers (1966) is optimum if the parameter variations and the instrument errors are both jointly gaussian random processes. In general these conditions do not apply, and there is room for improvement. For example, in the infrared region of the spectrum the Planck function is inherently a non-linear function of atmospheric temperature. Even in the microwave region where the Planck function is linear, the equations of radiative transfer are somewhat non-linear. In addition, the parameter statistics are seldom jointly gaussian, although they often are approximately so. For non-linear or non-gaussian problems the optimum inversion procedure is generally non-linear.

One quite general non-linear statistical estimation procedure is Baye's estimate, as described for example by Helstrom (1960). The difficulty is that numerical evaluation of integrals over the parameter space can be impossibly time consuming for estimation problems involving several data points and many parameters. A more practical technique is the non-linear estimation procedure outlined by Staelin (1967) and Waters and Staelin (1968). This technique is similar to the linear statistical technique described above, except that the data vector  $d$  is replaced by the vector  $\phi(d)$ , where  $\phi_i(d)$  is any arbitrary function of  $d$ . This technique permits most non-linear relations between parameters and data to be inverted, and avoids the need for iteration which is sometimes employed with the linear procedures to obtain some of the benefits of non-linearity.

### 2.3 Instrumentation, State of the Art

The sensors used for microwave meteorology are generally adaptations of systems developed for radio astronomy, a field in which receiver development is quite active. The major problem areas include sensitivity, absolute accuracy, spectral response, and directional response. In addition, each application has constraints of cost, size, weight, power, availability, and operational simplicity.

Receiver sensitivity may be characterized by the receiver noise temperature  $T_R$ , the bandwidth  $B$ , an integration time  $\tau$ , a constant  $\alpha$  which is usually in the range 1-3, and the equivalent rms fluctuations at the receiver input  $\Delta T_{rms}$ . It can be shown (Kraus, 1966) that

$$\Delta T_{rms} = \frac{\alpha(T_A + T_R)}{\sqrt{B\tau}} \text{ } ^\circ\text{K} \quad (5)$$

This equation can be used to estimate an ultimate limit to receiver sensitivity. For example, a radiometer in space viewing the earth will see an antenna temperature of approximately 300°K. For a noiseless receiver with 1-sec integration, RF bandwidth  $10^8$  Hz, and  $\alpha$  equal 2, then  $\Delta T_{rms}$  is 0.06°K. If 1°K sensitivity is sufficient, then an integration time as short as 0.004 sec may be used. These limits have a strong

bearing on the ultimate spatial resolution and coverage which can be obtained by radiometers in space. For example, such a receiver in Earth orbit at 1000 km altitude could have spatial coverage no better than 50 spots per mile of ground track, with 1°K receiver sensitivity.

Although the receiver noise temperature  $T_R$  is not zero, the sensitivity of receivers is rapidly improving due to the development of improved solid-state components. At wavelengths longer than 3 cm receiver noise temperatures  $T_R$  of less than 150°K can be obtained with solid-state parametric amplifiers, and this performance is being extended to wavelengths near 1 cm. With masers receiver noise temperature lower than 40°K have been obtained in operational systems near 20-cm wavelength. At wavelengths shorter than 3 cm the most common type of receiver is the superheterodyne. These systems have noise temperatures ranging from several hundred degrees at 3-cm wavelength to perhaps 20,000°K at 3-mm wavelength. Recent improvements in Schottky-barrier diodes show promise of reducing superheterodyne noise temperatures to a few hundred degrees for wavelengths as short as 5 mm. Progress in this area is so rapid but unpredictable that planning more than five years in the future is difficult.

The absolute accuracy of most radiometers is generally much less than could be obtained with care. Perhaps the most careful measurements ever made were those performed to measure the cosmic background radiation, as described by Penzias and Wilson (1965), Wilkenson (1967), and others. In these experiments absolute accuracies of approximately 0.1-0.2°K (rms) were obtained for antenna temperatures of approximately 6°K. Since the calibration problem becomes simpler as the antenna temperature approaches the physical temperature of the radiometer, such accuracies are obtainable in situations of meteorological interest. Absolute accuracies of 1°K are readily obtainable without great care.

Almost any arbitrary spectral response can be obtained with a microwave radiometer, although most parametric or other low-noise amplifiers have instantaneous bandwidths approximately less than 200 MHz. Except for limitations imposed by the spectral response of low-noise amplifiers, bandwidths ranging from 1 to  $10^{10}$  Hz could be obtained over most of the microwave region of the spectrum. Receivers capable of observing 1-200 spectral intervals simultaneously have been built, in addition to single-channel frequency-scanning radiometers. For accurate observations of spectral lines the multi-channel radiometers generally are more accurate and permit shorter time variations to be monitored.

The directional response of antennas varies considerably depending upon wavelength and antenna size. The half-power beamwidth of most antennas is approximately  $1.3 \lambda/D$ , where  $\lambda$  is the wavelength and  $D$  is the antenna diameter. Thus a 5-mm wavelength radiometer with a 1-meter antenna could resolve 7-km spots from a 1000-km orbit. Still higher resolution could be obtained, but restrict most antennas to beamwidths greater than 1-5 minutes of arc. A second important property of an antenna is its sidelobe level, or the degree to which it is sensitive to radiation incident upon the antenna from directions outside the main beam. The fraction of energy accepted from outside the main beam of an antenna is called the stray factor, which varies between 0.05 and 0.4 for most antennas. Low sidelobes and stray factors are obtained at the expense of antenna size, although the antenna diameter seldom needs to be more than doubled to obtain reasonable performance. Most such low sidelobe antennas must be custom made, and such antennas are seldom used, although they could improve many meteorological experiments.

Some applications require scanned antennas. These antennas can be mechanically or electrically scanned. The advantages of mechanical scanning include a superior multi-frequency capability, lower antenna losses, and electronic simplicity. Electrically scanned antennas are more compact, need have no moving parts, and can scan more rapidly. The 19 GHz electrically scanned antenna system proposed for the Nimbus spacecraft has an antenna beamwidth of  $2.6^\circ$ , stray factor of 0.08, an insertion loss of 0.6 db, and scan angle of  $\pm 50^\circ$ , and is 18 x 18 x 3 in.

Reduction of size, weight, and power is expensive, and is warranted primarily for space experiments. Examples include the two-frequency radiometer which successfully observed Venus from the Mariner-2 space probe, (Barath et al 1962) and the single-frequency 5-mm wavelength radiometer described by Ewen (1967). The Mariner-2 radiometer weighed 20 pounds and consumed 5 watts average power and 10 watts peak power. The 5-mm wavelength radiometer weighed 16 lb., consumed 42 watts average power, and had a volume of 312 in<sup>3</sup>. Substantial reductions in size, weight, and power are expected over the next ten years.

### 3. METEOROLOGICAL APPLICATIONS OF PASSIVE MICROWAVE SENSING

Microwave experiments can be categorized in several different ways. Here they have been divided into 1) temperature profile measurements, 2) composition measurements, and 3) surface measurements. A review of several possible meteorological experiments from space is contained in a report edited by Ohring (1966).

#### 3.1 Measurement of the Atmospheric Temperature Profile.

The oxygen complex centered near 60 GHz offers opportunities to measure atmospheric temperature profiles from space or from the ground. This is so because the mixing ratio of oxygen in the terrestrial atmosphere is quite uniform and constant, and because the attenuation of the atmosphere varies from nearly zero to over 100 db. The possibilities for such temperature profile measurements were first explored by Meeks and Lilley (1963), and have been extended by Lenoir (1965) to higher altitudes. Westwater and Strand (1967) have applied statistical estimation techniques to ground-based probing of the atmosphere and Waters and Staelin (1968) have applied similar techniques to space-based measurements.

Meeks and Lilley (1963) cast the expression for brightness temperature  $T_B$  in the form of a weighting function integral, where  $W(h, \nu)$  is the weighting function and  $T(h)$  is the atmospheric temperature profile. That is,

$$T_B(\nu) = \int_0^{\infty} T(h) W(h, \nu) dh + T_0 e^{-\tau(\nu)} \quad (6)$$

where  $T_0 e^{-\tau}$  is the contribution of the background temperature. The weighting functions reveal the extent to which the brightness temperature measured at any particular frequency is sensitive to the kinetic temperature as a function of altitude. Lenoir (1965) has calculated many weighting functions appropriate to space-based microwave radiometers, and some of these are shown in Figure 5. The weighting functions above 50 km altitude are polarization dependent and vary in a predictable way with the terrestrial magnetic field. Parameters for several weighting functions computed by Lenoir (1965) are listed in Table 2. Examination of the half-widths  $\Delta h$  of these

PASSIVE REMOTE SENSING AT MICROWAVE WAVELENGTHS

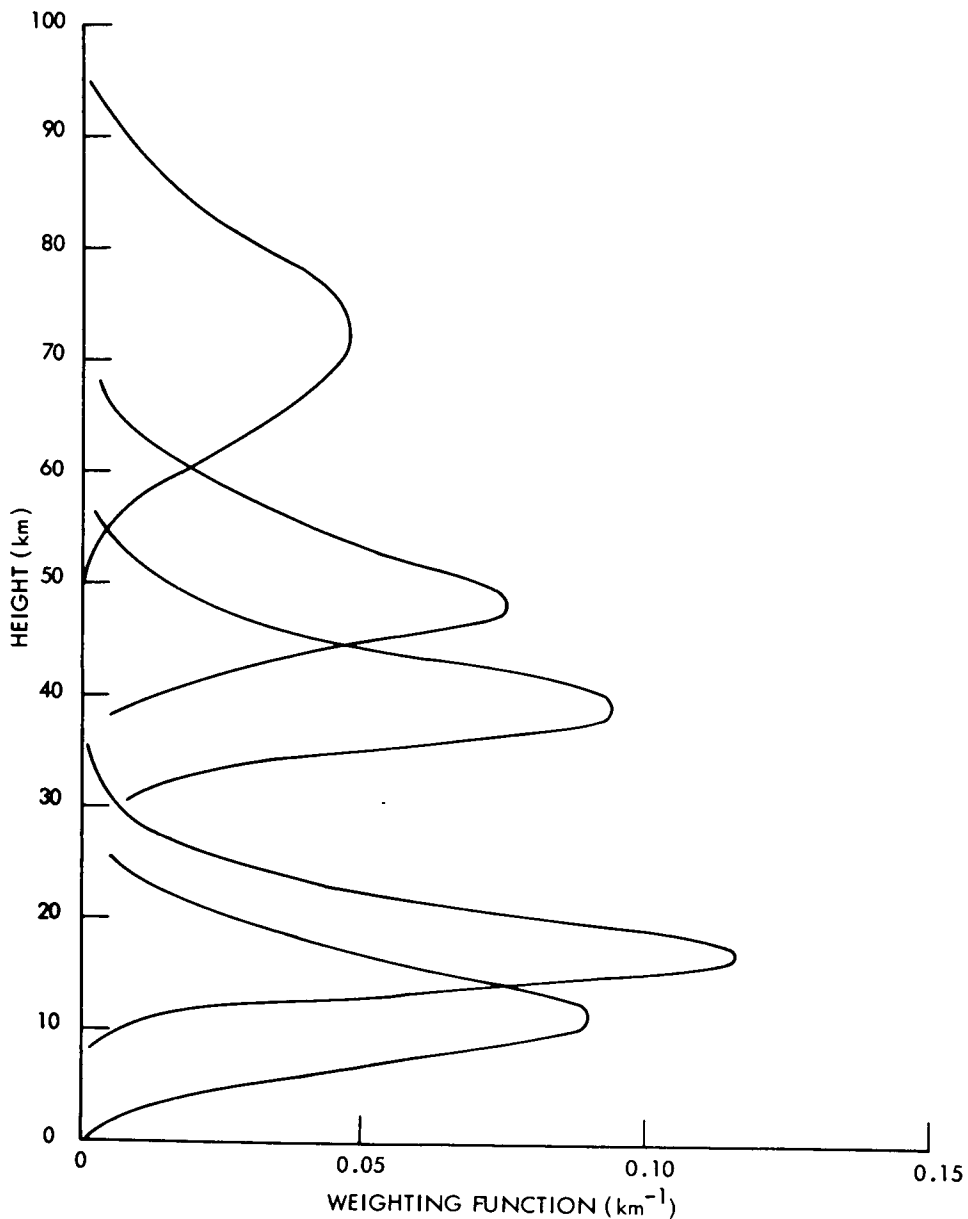


FIG.5 WEIGHTING FUNCTIONS, MAGNETIC EQUATOR

Figure 5. Temperature weighting functions for space-based observations at nadir. The frequencies are 64.47 and 60.79 GHz for the two lowest weighting functions, and straddle both the  $7^+$  and  $9^+$  resonances for the three other weighting functions, with the highest weighting function corresponding to 1.5 MHz bands centered on each of these two lines.

weighting functions indicates that altitude resolution of several kilometers can be obtained, depending upon the receiver sensitivity.

Waters and Staelin (1968) have applied statistical estimation techniques to the problem of inverting such microwave data. An example of the inversion accuracy is shown in Figure 6, where the priori standard deviation in the temperature is compared to the standard deviation obtainable with a seven-channel microwave radiometer

TABLE 2

Weighting Functions for Sounding the Atmospheric Temperature Profile

$\nu_0$ (GHz)	W (MHz)	$h_0$ (km)	$\Delta h$ (km)
64.47	200	12	11
60.82	200	18	7
58.388	30	27	9
60.4409	2.5	40	12
60.4365	1.0	50	20
63.5685 Equator	1.5	60	21
Pole		54	26
60.4348 Equator	1.5	73	20
Pole		66	26

RESULTS OF INVERSIONS FOR TEMPERATURE PROFILE  
BASED ON 100 SUMMER RADIOSONDES FROM PEORIA, ILL.

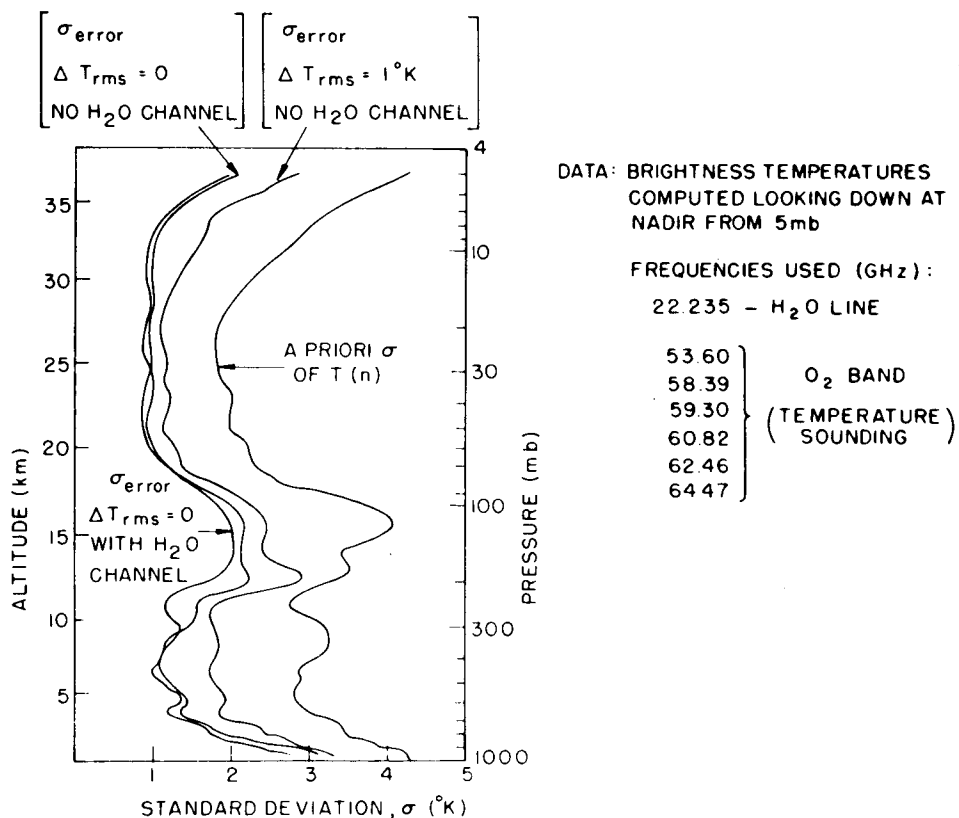


Figure 6. Results of 100 linear mathematical inversions showing a priori and a post-eriori standard deviations for no receiver noise, and 1°K rms noise. These inversions were computed for a height resolution of 0.5 km.

# PASSIVE REMOTE SENSING AT MICROWAVE WAVELENGTHS

of 1°K sensitivity. The six temperature weighting functions peaked at 4, 12, 18, 21, 27, and 31 km. One water vapor channel was also incorporated. These error statistics were computed on the basis of 100 summer radiosonde records from Peoria, Illinois. The decrease in accuracy in the bottom layer of the atmosphere is believed due to the frequent presence there of significant temperature changes over regions which are too narrow to be readily detected by this choice of observing frequencies or by weighting functions 10 km wide. If the temperature profile can be measured with an accuracy of 2-3°K on a global scale, then such microwave systems would be very useful for the collection of synoptic meteorological data. The water vapor channel provides not only water vapor information, as discussed later, but also permits improved inference of the temperature profile. It was assumed that the satellite was over ocean even though Peoria statistics were used, in order to permit the water vapor channel to be assessed. The height resolution of the radiosondes was 0.5 km. When the inferred  $T(h)$  and the true  $T(h)$  used for comparison were each smoothed by convolution with an 8-km gaussian, then the error performance was still better, as shown in Figure 7.

The effects of clouds and the terrestrial surface on such measurements can be estimated. In the preceding example only the weighting function which peaks at 4 km interacts appreciably with the terrestrial surface or with clouds. If the satellite is

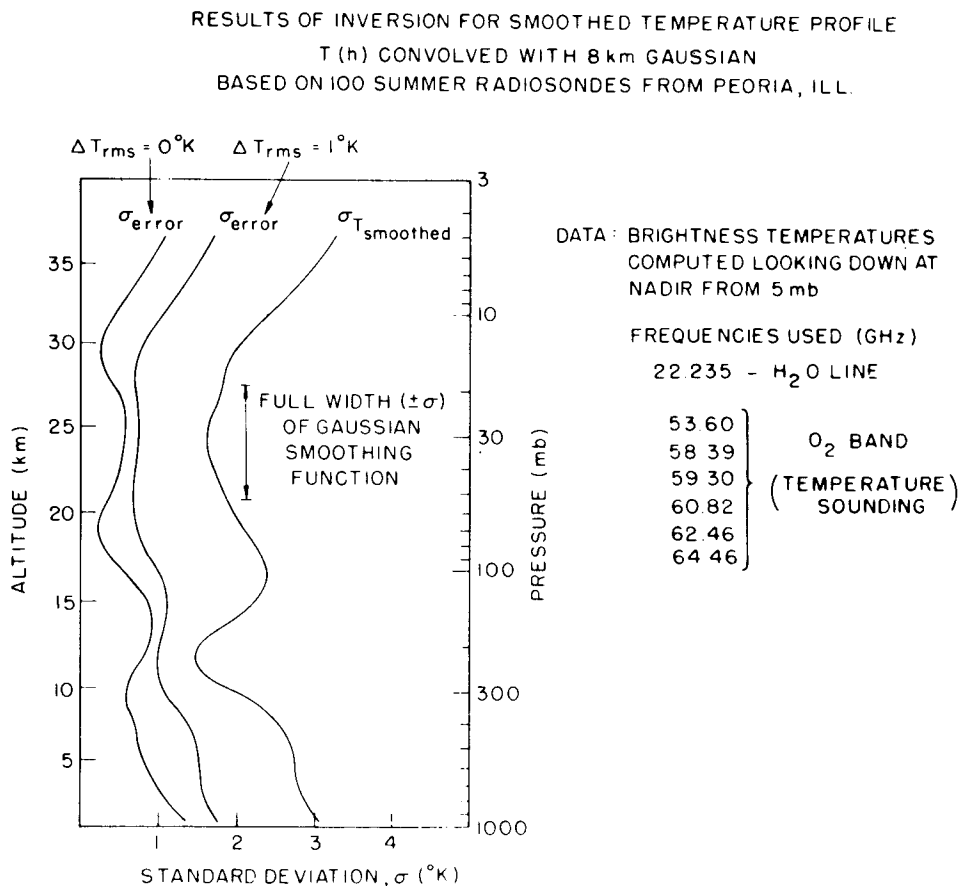


Figure 7. Results of 100 linear mathematical inversions showing a priori and a posteriori standard deviations for no receiver noise, and 1°K rms noise. The inferred  $T(h)$  and the true  $T(h)$  were each smoothed by convolution with a gaussian of width 8 km. These inversions were computed for a height resolution of 0.5 km.

over land then approximately 15% of the received radiation is received from the land, of which perhaps 95% represents the physical temperature of the land, and 5% is sky reflections, which have an effective temperature near 230°K. Thus a priori knowledge of the land temperature with 5°K rms uncertainty, plus knowledge of the emissivity within 1% rms reduces this contribution to the error in inferred atmospheric temperature at longer wavelengths can reduce this error still further. The effects of ice clouds are negligible, and even in the presence of heavy water clouds the error is small. For example, the heaviest non-raining cloud observed by Toong (1967) would have an approximate opacity of 1/2 at 5-mm wavelength, and thus would contribute an approximate error of less than 3°K, assuming the cloud were centered at 3-km altitude and that it were 20°K cooler than the surface. This same heavy cloud over ocean would have an even smaller effect because the cloud temperature in this case would be even closer to the brightness temperature flux moving upward at 3-km altitude. Thus even this heavy water cloud, approximately equivalent to a cumulus mediocris containing 0.18 gm/cm<sup>2</sup> H<sub>2</sub>O, would introduce no more than a few degrees error, even if it filled the entire antenna beam. Of course, if weighting functions were used which peaked nearer the surface, or if the bulk of the cloud were at much higher altitudes, then the effect could be larger.

Ground-based radiometers yield weighting functions which are quite different from those obtained for space-based measurements. These weighting functions are approximately exponentials with scale heights which depend upon the atmospheric opacity. This form of weighting function yields excellent height resolution near the observer, but the resolution is degraded at distances beyond 5-10 km. Westwater and Strand (1967) have calculated the errors expected for this example and find that for altitudes 0-10 km the rms errors range from 1.5°K to 4°K respectively, for 1°K receiver noise. Cloud effects for upward looking radiometers are more severe than for those systems looking down because the equivalent temperature of space is much colder and therefore offers more contrast to clouds than does land. The fast response of microwave radiometers plus their ability to scan and to observe continuously may enable ground-based microwave radiometers to provide meteorological information of a type not obtained before.

### 3.2 Measurement of Composition Profiles.

Composition measurements are usually made in semi-transparent regions of the microwave spectrum where the spectrum is more sensitive to the distribution of absorbers in the atmosphere than to the temperature profile. For those constituents with resonances the problem of determining the distribution profile can also be expressed in terms of weighting functions. For example, measurements of a spectral line in absorption against the sun can yield  $\tau(\nu)$ . If those contributions to  $\tau(\nu)$  from extraneous constituents are subtracted, then the remaining  $\tau_r(\nu)$  for the constituent of interest can be expressed as

$$\tau_r(\nu) = \int_0^{\infty} \rho(h) W(\nu, h) dh \quad (7)$$

where

$$W(\nu, h) = \alpha(\nu, h)/\rho(h)$$

and where  $\rho(h)$  is the constituent density profile,  $W(\nu, h)$  is the weighting function, and  $\alpha(\nu, h)$  is the absorption coefficient of the desired constituents. Staelin (1966) has computed such weighting functions for water vapor, as shown here in Figure 8. Very similar weighting functions result when the expressions are written for brightness

PASSIVE REMOTE SENSING AT MICROWAVE WAVELENGTHS

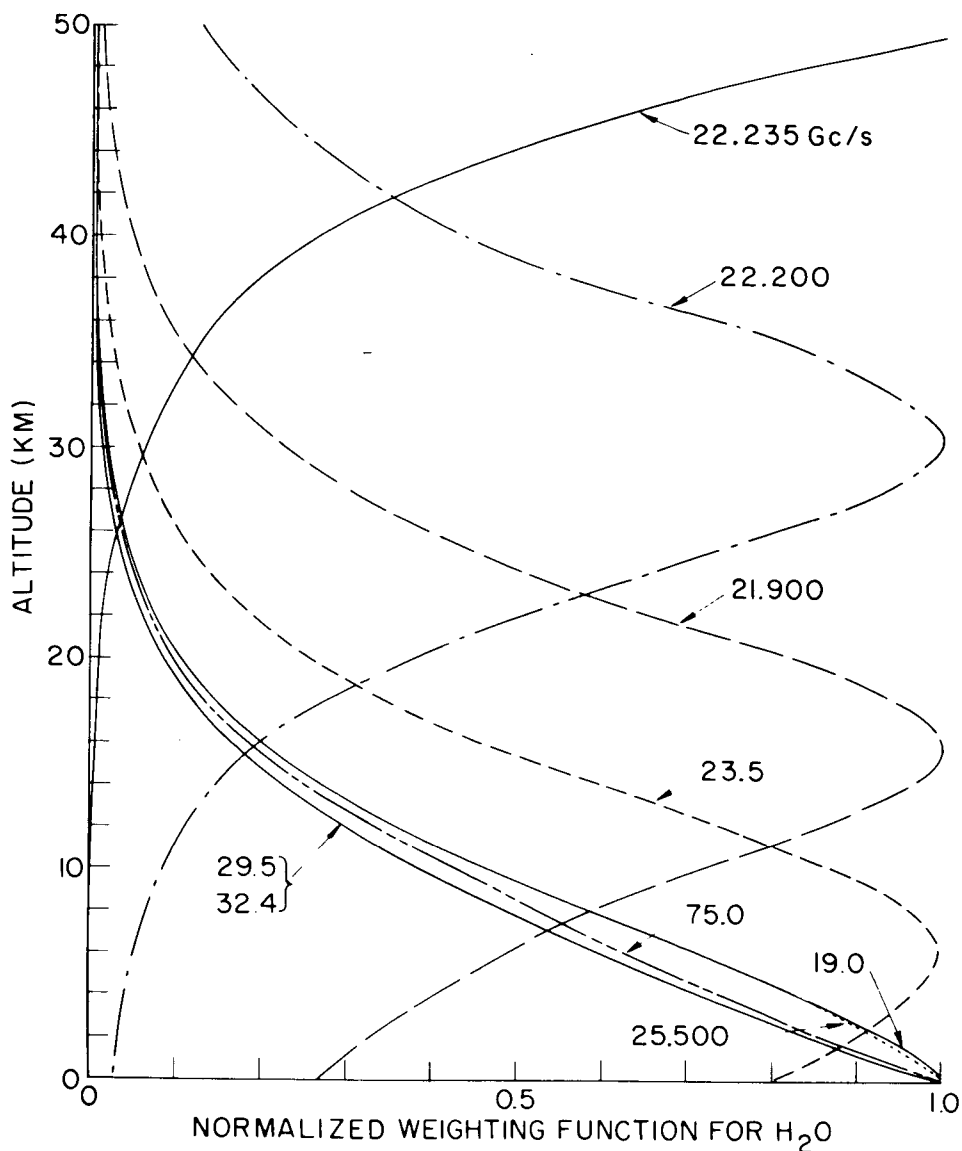


Figure 8. Normalized weighting functions for water vapor in the terrestrial atmosphere. These weighting functions were computed for interpreting opacity measurements.

temperature seen from the ground, or brightness temperature seen from space when over ocean. This is in contrast to the weighting functions found for the atmospheric temperature profile, which are quite different when observing from space or from the surface. Because the shape of the weighting function is determined almost exclusively by the variation of the line-width parameter with altitude, almost identical weighting function shapes would apply for  $O_3$ ,  $OH$ , or other trace constituents. The weighting function concept begins to break down, however, when the optical depth of the desired constituent is greater than 0.5, or when the background brightness temperature approaches the kinetic temperature of the atmosphere. Thus the weighting function concept can not readily be used to interpret the 183.3 GHz line of water vapor, nor any lines of trace constituents viewed from a spacecraft over land. Of course the development of weighting functions is not a prerequisite for use of the statistical estimation

procedures described earlier. The existence of weighting functions does imply a certain degree of linearity in the estimation problem however.

Gaut (1967) has applied the method of Rodgers (1966) to inversion of the solar absorption measurements of water vapor at 22 GHz, and Waters and Staelin (1968) have considered the problem of estimating water vapor by measuring brightness temperatures from space or from the ground. Recent preliminary calculations of Waters and Staelin are presented in Tables 3 and 4. These calculations of estimated inversion errors were based on assumed perfect knowledge of the absorption coefficient and statistics computed from 100 radiosonde records. The results in Table 3 were computed for 20 and 22 GHz ground-based observations at zenith on the basis of 100 radiosondes, half from Tucson and half from Kwajalein. These calculations indicate that the integrated water vapor abundance can be determined to  $0.1 \text{ gm/cm}^2$ . In Table 4 are presented similar results for observations from space over ocean. The atmosphere statistics were based upon 100 radiosondes from Huntington, Virginia, half in winter, and half in summer.

TABLE 3  
Inversion Performance for Ground-Based  
Viewing Zenith at 20.0 and 22.0 GHz. Radiometer

Parameter Water Vapor ( $\text{gm/cm}^2$ )	Parameter Statistics ( $\text{gm/cm}^2$ )		Inversion Errors	
	mean	$\sigma$	$\sigma (\Delta T_{\text{rms}} = 0^\circ\text{K})$	$\sigma (\Delta T_{\text{rms}} = 1^\circ\text{K})$
0-2 km	1.94	1.21	.14	.20
2-4 km	0.83	0.55	.13	.13
4-9.5 km	0.42	0.38	.11	.16
0-9.5 km	3.19	2.03	.02	.08

TABLE 4  
Inversion Performance for Space-Based Radiometer Viewing Nadir  
at 22, 31, 53.6, 60.8, and 64.5 GHz., over Smooth Ocean

Parameter Water Vapor ( $\text{gm/cm}^2$ )	Parameter Statistics		Inversion Errors	
	mean	$\sigma$	$\sigma (\Delta T_{\text{rms}} = 0^\circ\text{K})$	$\sigma (\Delta T_{\text{rms}} = 1^\circ\text{K})$
0-2 km	2.09	1.34	0.22	0.22
2-4 km	1.35	0.92	0.14	0.14
4-9.5 km	0.51	0.35	0.09	0.09
0-9.5 km	0.23	0.15	0.09	0.11

With the improved radiometric systems which should become available over the next few years, similar performance might be sought for ozone and stratospheric water vapor. The measurements of ozone were reviewed earlier in this paper. Stratospheric water vapor has tentatively been detected at 22 GHz (Law et al, 1968). Since no such meteorological data has been collected on the scale that passive microwaves should permit, the data will be quite unique. Spatial structure in three dimensions plus time variations should all be accessible.

Clouds and precipitation can also be measured. Because of the non-resonant nature of their absorption, however, it is difficult to measure altitude distribution or even to distinguish clouds from precipitation. Rain and cloud cover might be distinguished on the basis of form and intensity, and even on the basis of spectral shape, but the measurements of Toong (1967) indicate that such distinctions would be difficult to perform with any accuracy. Snow and ice might best be distinguished from water and rain on the basis of atmospheric temperature and climatology.

Non-resonant absorbers like clouds and precipitation can, however, be measured quantitatively and distinguished from water vapor or other resonant constituents. This was demonstrated theoretically by Staelin (1966) and experimentally by Toong (1967). Non-resonant constituents can best be measured from ground-based radiometers or from spacecraft over ocean. The accuracies which might be obtained can only be estimated. They are best expressed in terms of equivalent water cloud densities in  $\text{g/cm}^2$  at some nominal temperature, like  $283^\circ\text{K}$ . A ground-based 0.9-cm receiver with sensitivity  $1^\circ\text{K}$  looking at zenith could detect a cloud with  $0.005 \text{ g/cm}^2$ , if the water vapor abundance were known exactly. Since the clouds must be distinguished from water vapor on the basis of spectral shape, the cloud sensitivity might be degraded to  $0.01 \text{ g/cm}^2$ . The measurement accuracy would be further degraded by uncertainties in cloud temperature,  $5^\circ\text{K}$  representing  $\sim 15\%$  change in  $\alpha$ .

### 3.3 Measurement of Surface Properties.

Surface properties of interest include surface temperature, ground water, snow and ice cover, and sea state. Since the surface brightness temperature at long wavelengths is essentially the product of the surface emissivity and the surface temperature, the surface temperature can not be uniquely determined. If the surface brightness temperature is measured from space over a long period of time, then the surface emissivity may be averaged or calibrated out, and accurate measurements of temperature may be obtained. It is not known to what extent daily changes in emissivity may occur, but since the emissivity of most land surfaces is greater than 0.9, the variation is limited. The use of  $\vec{E}_1$  polarization near the Brewster's angle may increase the emissivity further. Improvement may also be obtained by simultaneous monitoring of  $\vec{E}_1$  and  $\vec{E}_{11}$  polarization so as to detect changes in emissivity and perhaps permit corrections to the inferred temperature. The presence of ground water should decrease the brightness temperature of  $\vec{E}_1$  radiation, and snow or ice should normally increase it. This is an area where more analysis and experiments are needed before performance can be accurately predicted.

Sea state may be measured from space by observing  $\vec{E}_1$  and  $\vec{E}_{11}$  polarization at a nadir angle near  $60^\circ$ . Since the change in brightness temperature with equivalent wind speed has been calculated to be approximately  $0.5^\circ\text{K}$  per knot for  $\vec{E}_1$  polarization at 3-cm wavelength, and since the accuracy of the measurement should be approximately  $1^\circ\text{K}$ , the equivalent wind speed might be inferred with an accuracy of 2 knots. The analysis on which this was based neglected features like whitecaps and foam, and assumed that the ocean surface was composed of smooth facets large compared to a

wavelength. Furthermore the sea surface properties depend not only upon wind speed, but also on fetch, current, surface pollution, etc. The true accuracy which might be obtained would best be determined by very carefully calibrated measurements at sea. Such measurements would be desirable not only at wavelengths where the atmosphere is nearly transparent, but also at wavelengths where the atmosphere absorbs up to one-half the radiation, because at these wavelengths that component of the brightness reflected from the sea surface into the antenna beam is quite sensitive to the surface slope probability distribution.

#### 4. METEOROLOGICAL RELEVANCE AND SUGGESTIONS FOR FURTHER WORK

There are several meteorological problem areas for which passive microwave sensors have unique capabilities.

1) Microwave sensors provide the only remote sensing technique capable of measuring atmospheric temperature profiles in the presence of clouds. This may be of crucial importance to global data collection for numerical weather prediction unless new techniques are developed which permit other remote sensors, super pressure balloons, etc. to operate more effectively in the 300-1000 mb region than do microwaves. Above 300 mb microwaves sensors also are a competitive technique.

2) Microwave sensors appear to be unique in their ability to measure the temperature profile above 50-km altitude. Synoptic mesospheric temperature data collected by satellite would be unparalleled as a tool for studying the mesospheric temperature structure.

3) Microwaves are unique in their ability to yield measurements of tropospheric water vapor in the presence of clouds. Although such sensors in space are effective only over ocean, the oceans cover over half the globe, and are very poorly monitored, in contrast to most land masses. Even in the absence of clouds the great sensitivity of microwaves to water vapor and the ability of microwave sensors to average water vapor spatially permits measurements of integrated water vapor abundances which are competitive with and perhaps superior to radiosondes, which appear to be handicapped by aliasing errors (Gaut, 1967). This averaging ability and ability to operate through clouds may make such instruments valuable on the ground also.

4) Microwaves are unique in their ability to measure water vapor above the tropopause and ozone on a continuous basis. Although this is difficult and has not yet been done, it is within the state-of-the-art. Again, until these experiments are done it is difficult to predict the meteorological significance. One might certainly hope to learn more about the distribution and variability of these constituents, and perhaps to use them as tracers for circulation in the upper atmosphere. Such experiments could be done from the surface or from space.

5) Microwaves provide a powerful tool for measuring the total liquid water content of clouds, and even though there may be some cloud-precipitation ambiguity, the data are still quite unique. If such data could be taken with a high-resolution imaging system on board a satellite, storm cells, squall lines, etc. could be mapped with a precision not always available with optical sensors. Proper choice of wavelength would permit very heavy clouds to be seen, or alternatively, perhaps almost all water clouds.

## PASSIVE REMOTE SENSING AT MICROWAVE WAVELENGTHS

6) Microwaves offer promise of land temperature measurements from space. Such data are of interest in their own right, and also as an aid to determining the temperature profile of the troposphere.

7) Microwaves offer promise of yielding such surface characteristics as sea state, snow cover, ice cover, ground water, etc. More research is needed to determine the true potential of such experiments, although the sea states measurements appear quite promising.

Still other applications exist, and no doubt new ones will develop as the field of microwave meteorology grows.

Several suggestions for further work appear quite obvious.

1) The expressions used for absorption coefficients of various atmospheric constituents should all be refined both experimentally and theoretically, particularly at millimeter wavelengths.

2) The microwave properties of the surface should be studied in a precise quantitative way in preparation for potential surface temperature measurements, sea state measurements, etc. from space.

3) The statistical inversion techniques should be improved and applied to a broader range of microwave problems, and to problems where microwave sensors are accompanied by infrared or other types of sensors.

4) Preparations for space experiments should continue.

5) Efforts to detect new spectral lines should continue as improved instruments become available.

6) Those lines which have been detected should become meteorological tools and studied as such, in particular, the stratospheric water vapor and the ozone lines should be observed.

7) Efforts should continue to improve the sensitivity, accuracy, and antenna characteristics of radiometric systems, particularly at millimeter wavelengths, while reducing their size, weight, and cost.

### ACKNOWLEDGEMENTS:

I am indebted to Joe W. Waters for the computation of the new inversion results discussed here, and to Alan H. Barrett and Norman E. Gaut for helpful discussions.

This work was supported by the National Aeronautics and Space Administration (Grant NsG-419).

## REFERENCES

- Atlas, D., V.G. Plank, W.H. Paulsen, A.C. Chmela, J.S. Marshall, T.W.R. East, K.L.S. Gunn, and W. Hirschfield (1952), "Weather Effects on Radar," Air Force Surveys in Geophysics, 23, Geophys. Res. Directorate, Air Force Camb. Res. Ctre., Cambridge, Mass.
- Barath, F. T., A.H. Barrett, J. Copeland, D.E. Jones, A. E. Lilley (1964) *Astron. J.*, 69, 49.
- Barrett, A.H., J.W. Kuiper, and W.B. Lenoir (1966) "Observations of Microwave Emission by Molecular Oxygen in the Terrestrial Atmosphere" *J. Geophys. Res.*, 71 (20), 4723.
- Barrett, A.H., and V.K. Chung, (1952) "A Method for the Determination of High-Altitude Water-Vapor Abundance from Ground-Based Microwave Observations," *J. Geophys. Res.*, 67 (11), 4259.
- Becker, G.E., and S.H. Autler (1946) "Water Vapor Absorption of Electromagnetic Radiation in the Centimeter Wave-Length Range", *Phys. Rev.*, 70, 300.
- Benedict, W.S. and L.D. Kaplan (1959) "Calculations of Line Widths in H<sub>2</sub>O-N<sub>2</sub> Collisions," *J. Chem. Phys.*, 30, 388.
- Carter, C.J., R.L. Mitchell, and E.E. Reber (1968) "Oxygen Absorption Measurements in the Lower Atmosphere," *J. Geophys. Res.*, 73 (10), 3113.
- Caton, W.M., W.J. Welch, S. Silver (1967) "Absorption and Emission in the 8-mm Region by Ozone in the Upper Atmosphere" *Space Sci. Lab.*, Ser. No. 8, Issue 42.
- Caton, W.M., G.G. Mannella, P.M. Kalaghan, A.E. Barrington, and H.I. Ewen (1968) "Radio Measurement of the Atmospheric Ozone Transition at 101.7 GHz," *Astrophys. J. (Letters)*, 151, 3, L153.
- Chandrasekhar, S. (1960), *Radiative Transfer*, Dover Publications, New York, New York.
- Cox, C.S., and W.H. Munk (1954), *J. Opt. Soc. Am.*, 44, 838.
- Croom, D.L. (1965a), "Stratospheric Thermal Emission and Absorption near the 22.235 GHz (1.35 cm) Rotational Line of Water-Vapour," *J. Atm. and Terr. Phys.*, 27, 217.
- Croom, D.L. (1965b), "Stratospheric Thermal Emission and Absorption near the 183.311 GHz (1.64 mm) Rotational Line of Water-Vapour," *J. Atm. and Terr. Phys.*, 27, 235.
- Deutsch, R. (1965) *Estimation Theory*, Prentice-Hall Inc., Englewood Cliffs, N. J.
- Even, H. E. (1967) personal communication.
- Fow, B.R. (1964) "Atmospheric Temperature Structure from the Microwave Emission of Oxygen," S.M. Thesis, Massachusetts Institute of Technology.

## PASSIVE REMOTE SENSING AT MICROWAVE WAVELENGTHS

- Florence, E.T. (1968) Paper presented at 3rd Interdisciplinary Workshop on Inversion of Radiometric Measurements, Florida State Univ., Tallahassee, Fla., February 26, 1968.
- Frenkel, L. and D. Woods (1966) "The Microwave Absorption by H<sub>2</sub>O Vapor and its Mixtures with Other Gases Between 100 and 300 GHz," Proc. I.E.E.E., 54, 4.
- Gaut, N.E. (1967) "Studies of Atmospheric Water Vapor by Means of Passive Microwave Techniques," Ph.D. Thesis, Dept. of Meteorology, Massachusetts Institute of Technology.
- Gautier, D. and A. Robert (1964) "Calcul du Coefficient d'Absorption des Ondes Millimetriques dans l'Oxygene Moleculaire en Presence d'un Champ Magnetique Faible. Application a l'Atmosphere Terrestre," Ann. Geophys., 20, 480.
- Gora, E.K. (1959) "The Rotational Spectrum of Ozone," J. Molecular Spectroscopy, 3, 78.
- Haddock, F.T. (1948) "Scattering and Attenuation of Microwave Radiation through Rain," Naval Research Laboratory, Wash., D.C. (unpublished manuscript).
- Helstrom, C.W. (1960) Statistical Theory of Signal Detection, Pergamon Press, MacMillan Co., New York.
- Hemmi, C. (1966) "Pressure Broadening of the 1.63-mm Water Vapor Absorption Line," Tech., Rept. 1, Elec. Eng. Res. Lab., Univ. of Texas.
- Kerr, D.E., (1951) editor, Propagation of Short Radio Waves, McGraw-Hill Book Co., New York, New York.
- King, J.I.F. (1961) "Deduction of Vertical Thermal Structure of a Planetary Atmosphere from a Satellite," Planetary Space Sci., 7, 423.
- King, J.I.F. (1964) "Inversion by Slabs of Varying Thickness," J. Atmos. Sci., 21, 324.
- King, G.W., R.M. Hainer, and P.C. Cross (1947) "Effective Microwave Absorption Coefficients of Water and Related Molecules," Phys., Rev., 71, 433.
- Kraus, J.D. (1966) Radio Astronomy, McGraw-Hill Book Co., New York, New York.
- Law, S.E., R. Neal, and D.H. Staelin (1968) "K-Band Observations of Stratospheric Water Vapor," Quarterly Progress Report No. 89, Research Laboratory of Electronics, Massachusetts Institute of Technology.
- Lenoir, W.B. (1965) "Remote Sounding of the Upper Atmosphere by Microwave Measurements," Ph.D. Thesis, Dept. of Elec. Eng., Massachusetts Institute of Technology.
- Lenoir, W.B. (1967) "Propagation of Partially Polarized Waves in a Slightly Anisotropic Medium," J. of Applied Phys., 38, 13, 5283.
- Lenoir, W.B. (1968) "Microwave Spectrum of Molecular Oxygen in the Mesosphere," J. of Geophys. Res., 73, 1, 361.
- Lenoir, W.B., J.W. Barrett, and D.C. Papa (1968) "Observations of Microwave Emission by Molecular Oxygen in the Stratosphere," J. of Geophys. Res., 73, 4, 1119.
- Lenoir, W.B. and R.F. Koehler Jr. (1967) "Inference of Temperature Profiles from Space-Based Microwave Measurements," manuscript submitted for publication.

- Marandino, G.E. (1967) "Microwave Signatures from Various Terrain," S.B. Thesis, Department of Physics, Massachusetts Institute of Technology.
- Meeks, M. L., and A.E. Lilley (1963) "The Microwave Spectrum of Oxygen in the Earth's Atmosphere," *J. Geophys. Res.*, 68, 1683.
- Mie, G. (1908) *Annalen der Physik* (4), 25, 377.
- Mouw, R.B., and S. Silver (1960) "Solar Radiation and Atmospheric Absorption for the Ozone Line at 8.3 Millimeters," *Inst. Eng. Res.*, ser 60, issue No. 277, Univ. of Calif., Berkeley, Calif.
- Ohring, G. editor (1966) "Meteorological Experiments for Manned Earth Orbiting Missions," *Geophys. Corp. of Am.*, Tech. Rept. No. 66-10-N, Final Report Contract No. NASW-1292 for N.A.S.A.
- Penzias, A.A., and R.W. Wilson (1965) *Astrophys. J.*, 142, 419.
- Porter, R.A. (1966) "Microwave Radiometric Measurements of Sea Water, Concrete, and Asphalt," Tech. Rept., June 20, Raytheon Co., Space and Inf. Sys. Div., Sudbury, Mass.
- Porter, R.A. (1966b) "Tech. Rept. Vol I for Microwave Radiometer Field Measurement Program," FR-66-293, Aug. 31, Raytheon Co., Space and Inf. Sys. Div., Sudbury, Mass.
- Rodgers, C.D. (1966) "Satellite Infrared Radiometer, A Discussion of Inversion Methods," Memorandum No. 66.13, Clarendon Lab., Univ. of Oxford.
- Rosenblum, E.S. (1961) "Atmospheric Absorption of 10-400 KMcps Radiation: Summary and Bibliography to 1961," *Microwave J.*, 4, 91.
- Rusk, J.R. (1965) *J. Chem. Phys.*, 42, 493 and *Letters, J. Chem. Phys.*, 43, 8, 2919.
- Ryde, J.W. And D. Ryde (1945) "Attenuation of Centrimetre and Millimetre Waves By Rain, Hail, Fogs, and Clouds," *British General Elec. Co.*, Rept. No. 8670.
- Saxton, J.A. and J.A. Lane (1946) "The Anomalous Dispersion of Water at Very High Frequencies" *Meteorological Factors in Radio Wave Propagation*, The Physical Society, London.
- Shklovsky, I.S. (1960) *Cosmic Radio Waves*, Harvard Univ. Press, Cambridge, Massachusetts.
- Staelin, D.H. (1966) "Measurements and Interpretation of the Microwave Spectrum of the Terrestrial Atmosphere near 1-Centimeter Wavelength," *J. of Geophys. Res.*, 71, 12, 2875.
- Staelin, D.H. (1967) "Interpretation of Spectral Data," *Quarterly Progress Report No. 85*, Research Lab. of Electronics, Massachusetts Institute of Technology, 15.
- Strand, O.N., and E.R. Westwater (1968) "The Statistical Estimation of the Numerical Solution of the Fredholm Integral Equation of the First Kind," *J. of the Assoc. Comp. Mach.*, 15, 1, 100.
- Stratton, J.A. (1941) *Electromagnetic Theory*, McGraw-Hill Book Company, New York, New York.
- Toong, H.D. (1967) "Interpretation of Atmospheric Emission Spectra Near 1-Cm Wavelength," 1967 NEREM Record, I.E.E.E. Cat. No. 61-3749, 214.

## PASSIVE REMOTE SENSING AT MICROWAVE WAVELENGTHS

- Townes, C.H. and A.L. Schawlow (1965) *Microwave Spectroscopy*, McGraw-Hill Book Co., New York, New York.
- Twomey, S. (1965) "The Application of Numerical Filtering to the Solution of Integral Equations Encountered in Indirect Sensing Measurements," *J. Franklin Inst.*, 279, 2, 95.
- Twomey, S. (1966) "Indirect Measurement of Atmospheric Temperature Profiles from Satellites: II. Mathematical Aspects of the Inversion Problems," *Mon. Weather Rev.*, 94, 6, 363.
- Van Vleck, J.H. (1947a) "The Absorption of Microwave by Oxygen," *Phys. Rev.*, 71, 413.
- Van Vleck, J.H. (1947b) "Absorption of Microwaves by Water Vapor," *Phys. Rev.*, 71, 425.
- Van Vleck, J.H., and V.F. Weisskopf (1945) "On the Shape of Collision Broadened Lines," *Revs. Modern Phys.*, 17, 227.
- Waters, J.W., and D.H. Staelin (1968) "Statistical Inversion of Radiometric Data," Quarterly Progress Report No. 89, Research Laboratory of Electronics, Massachusetts Institute of Technology.
- Weigand, R.M. (1967) "Radiometric Detection of Atmospheric Hydroxyl Radical and Ozone," S.M. Thesis, Dept. of Elec. Eng., Massachusetts Institute of Technology.
- Westwater, E.R., and O.N. Strand (1967) "Application of Statistical Estimation Techniques to Ground-Based Passive Probing of the Tropospheric Temperature Structure," E.S.S.A. Tech. Rept. IER 37-ITSA 37, Inst. for Telecomm. Sci. and Aeronomy, Boulder, Colorado.
- Wilkinson, D.T. (1967) "Measurement of Cosmic Microwave Background at 8.56-mm Wavelength," *Phys. Rev. Letters*, 19, 20, 1195.
- Yap, B.K. (1965) "Wind Velocity and Radio Emission from the Sea," S.M. Thesis, Dept. of Elec. Eng., Massachusetts Institute of Technology.

SESSION 7

Infrared  
Radiometry

N72-25374

# THE USE OF HIGH-FREQUENCY INFRARED RADIOMETRY FOR REMOTE ATMOSPHERIC PROBING WITH HIGH VERTICAL RESOLUTION

Lewis D. Kaplan

Department of Meteorology  
Massachusetts Institute of Technology

## 1. INTRODUCTION

The first experiment designed to obtain a three dimensional temperature sounding of the stratosphere and troposphere from a satellite is expected to be launched within a day or two of our meeting. The time, therefore, is particularly appropriate to look ahead to future satellite infrared measurements that will furnish the increasing requirements of a developing numerical weather prediction routine. In this paper I will discuss the two particularly important problems that we will eventually have to face: the necessity of obtaining soundings of temperature and water vapor content of the lower troposphere with sufficient vertical resolution to determine the exchange of heat and moisture between the surface and the atmosphere; and the necessity of obtaining these soundings even under the usual conditions of at least partial cloud cover. The means discussed for solving the first problem will be the use of emission measurements in the high frequency end of the thermal infrared, in particular in the  $4.3\mu$  band of  $\text{CO}_2$  and the  $6.3\mu$  band of  $\text{H}_2\text{O}$ . The means discussed for solving the second problem will be supplementary scanning with high area resolution.

## 2. THE PROBLEM OF VERTICAL RESOLUTION

The relevance of measurements at high frequency lies in the fact that the information-carrying quantity is not the transmission differential [e. g.  $(d\tau_\nu/d\ell np) d\ell np$ ] in which form weighting functions are usually presented but rather the increments of energy loss to space [i. e.  $B_\nu (d\tau_\nu/d\ell np) d\ell np$ ], or, more precisely, the differences of this latter quantity.

At microwave frequencies, where the black-body function  $B_\nu$  is a linear function of temperature, its effect on the weighting function is small. In contrast, the effect is appreciably and increasingly greater at higher frequencies, where  $B_\nu$  becomes proportional to  $\exp(-h\nu/kT)$ . In the  $4.3\mu$   $\text{CO}_2$  band the relative variation of  $B_\nu$  with temperature is 3.5 times as great as in the  $15\mu$   $\text{CO}_2$  band.

Thus, for measurements of thermal radiation in regions of the atmospheric emission spectra sufficiently far removed from each other, such as the  $4.3\mu$   $\text{CO}_2$  band, the  $15\mu$   $\text{CO}_2$  band and the 5 mm  $\text{O}_2$  band, the relative contribution of the different layers of the atmosphere will be markedly different from one band to another, even if the frequencies chosen are such as to have equal optical depths for the different bands.

In regions of the atmosphere where the temperature normally varies monotonically with height, the effect of the black-body function  $B_\nu$  is to sharpen the weighting function in the direction opposite to the

## PROBING WITH HIGH-FREQUENCY INFRARED RADIOMETRY

temperature gradient (i. e. on the low temperature side). Weighting functions, with and without the factor  $B_\nu$  are presented in Figure (1), which illustrates that this effect is particularly marked in the  $4.3\mu$   $\text{CO}_2$  band. The calculations were made by Dr. Robert A. McClatchey of AFCRL, assuming that the temperature distribution is given by the U. S. Standard Atmosphere.

It is seen that the effect of the  $B_\nu$  factor is to make the upper part of the tropospheric weighting functions much more horizontal. Since the temperature information is contained in the difference between consecutive weighting functions, it is evident that the effect of the  $B_\nu$  factor at these high frequencies is to restrict the information to very narrow strata of the atmosphere. I expect that satellite measurements at carefully chosen frequencies in the  $4.3\mu$  band of  $\text{CO}_2$  will allow a determination of the temperature structure of the lower troposphere with at least 100 mb resolution. Much higher vertical resolution will be obtained in the upper stratosphere. Such resolution would be impossible in practice from measurements in the  $15\mu$   $\text{CO}_2$  band or 5 mm  $\text{O}_2$  band, no matter how accurately they are made, because the wider weighting functions would not allow the determination of a unique sounding in comparable detail.

To obtain this vertical resolution from measurements in the  $4.3\mu$   $\text{CO}_2$  band, spectral band passes of about  $20\text{ cm}^{-1}$  width are required. Detectors having signal-to-noise values greater than 100 over such a band pass for incident radiation from sources with temperature  $210^\circ\text{ K}$  or greater are readily available; and, in fact, a spectrometer having these characteristics has been built and flown in a balloon (Shaw *et al.*, 1967).

Figure 2, which was also computed and prepared by Dr. McClatchey shows the weighting functions, with and without the black-body factor, for selected frequencies in the  $5.3\mu$  water vapor band. Again the U. S. Standard Atmosphere was assumed to represent the temperature distribution; the total water content was assumed to be  $2\text{ gm cm}^{-2}$ ; and its concentration in the troposphere was assumed to fall off with the third power of the pressure.

Again the effect of the factor  $B_\nu$  is seen to sharpen the upper part of the weighting function, although it is not so marked as in the higher frequency region near  $4.3\mu$ . However, because the decrease of mixing ratio with height has the same effect, the final weighting functions are quite similar to those of Figure 1. Thus the water vapor distribution in the lower troposphere can also be expected to be obtained with a resolution of 100 mb or better, by measurements in the  $6.3\mu$  band in conjunction with measurements in the  $4.3\mu$   $\text{CO}_2$  band.

The disadvantage of the high frequency bands in obtaining soundings is the insensitivity of the outgoing radiation to changes in temperature or humidity at the coldest levels of the atmosphere. To remedy this shortcoming, it will probably be necessary to supplement the high frequency measurements with a few measurements at lower frequencies, e. g., in the rotational water band and the  $15\mu$   $\text{CO}_2$  band, or, better yet, with use of microwave measurements in the region of  $\text{O}_2$  and  $\text{H}_2\text{O}$  lines. To obtain the best specification of the temperature and moisture field, an ideal sensing system would sample outgoing radiation at selected wave-lengths from  $3\mu$  to 3 cm.

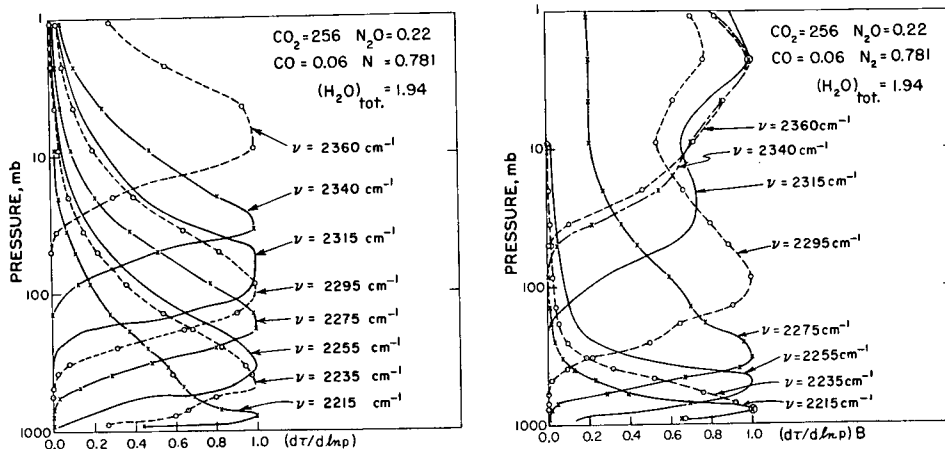


FIG. 1. Weighting functions for  $4.3\mu$  band of  $\text{CO}_2$ , without and with black-body factor (by R. A. McClatchey).

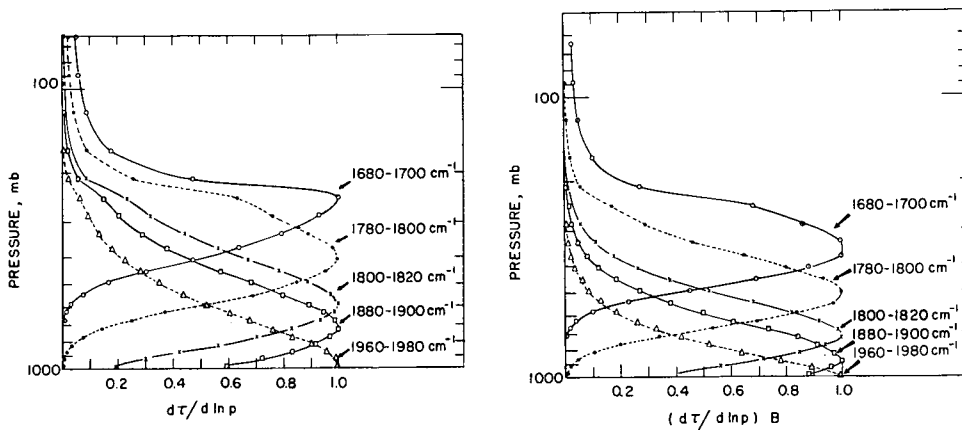


FIG. 2. Weighting functions for  $6.3\mu$  band of  $\text{H}_2\text{O}$ , without and with black-body factor (by R. A. McClatchey).

## 3. THE PROBLEM OF PARTIAL CLOUD COVER

The parts of the atmosphere below overcast cloud tops are inaccessible to infrared sounding from above, and a sounding of the entire atmosphere would require the use of microwave frequencies. However, for the reasons given above, it is essential that selected spectra of the higher frequency infrared flux be obtained wherever possible, including conditions of partial cloudiness, which are characteristic of most of the earth's area.

The resolution of the cloudiness problem probably requires area scanning of the field of view with considerably greater angular resolution than would be required for cloudless conditions. This is the procedure in a specific experiment suggested by W. L. Smith (1967, 1968). The increased angular resolution would be accomplished at the sacrifice of spectral resolution and therefore of the vertical resolution of the derived sounding. While this trade-off may be desirable in the immediate future to provide a useable coverage of the area of the earth, the highest possible vertical resolution will eventually be essential. I suggest that this can be accomplished in the presence of broken clouds by the supplementary use of broad-band, narrow-angle measurements. I understand from Dr. Sigmund Fritz that he is intending, along these lines, to use the HRIR measurements from NIMBUS B to help interpret those from the SIRS experiment in the presence of clouds.

In order to obtain maximum coherence of the broad-band with the narrow-band measurements, it is planned to include among the future modifications of the spectrometer system of Shaw et al. (1967) an array of broad band filters, centered at around  $5\mu$ , in the plane of the grating. They will have considerably smaller field-of-view and integration time than the narrow-band detectors, and will be oriented in such a fashion as to use the satellite motion to break the narrow-band field-of-view into say a five-by-five array of smaller areas. It is almost obvious that the combined system of narrow-band and wide-band measurements can be interpreted in terms of fractional cloud amount and temperature and height of the cloud tops, as well as the air temperature distribution, under conditions of one or two stratified layers of broken clouds. More complicated cloud distributions will probably require powerful inversion techniques, such as the one discussed in the next section and described in the appendix.

Two points should be mentioned concerning the effects of the cloudiness on the temperature inversion when use is made of the  $4.3\mu$   $\text{CO}_2$  band. The first is that the scattered sunlight during the daytime will interfere with the temperature inversion. In the absence of clouds, the bulk of the scattered and reflected light will come from the ground, and its effect on the spectrum of the total outgoing radiation will depend on the surface reflectivity, which can be determined by detectors located at atmospheric windows on both sides of the  $4.3\mu$  band. This will only affect the lower part of the sounding, as the atmosphere is completely opaque in the central part of the band. In the presence of daytime clouds, particularly high clouds, the entire spectrum will be affected, and it will be necessary to determine their amount, by the above-mentioned or other technique in order to determine the temperature inversion.

The second point is that the outgoing thermal radiation in the  $4.3\mu$  band is quite insensitive to small changes in cloudiness. This is because of the strong variation of the black-body radiation with temperature. As an example, if the inversion were performed neglecting the presence of a twenty per cent cloud cover at moderate altitude, the temperatures obtained would be off by less than  $5^\circ\text{C}$ .

Thus the strong temperature dependence of the black-body radiation at  $4.3\mu$  not only increases the temperature sensitivity of the measurements; it also makes the  $4.3\mu$   $\text{CO}_2$  band particularly appropriate for obtaining soundings in the presence of broken clouds.

#### 4. THE DETERMINATION OF THE PROFILE

The problem of obtaining the profile of temperature, moisture and clouds from the spectrum of outgoing radiation is very difficult. All of the published methods of solving this problem have following the original suggestion (Kaplan, 1959, 1961) of performing a matrix inversion and have tried to save computation time by linearization of the transfer equation. This has proved to be impossible without introducing damping functions, which would by their nature not allow the high vertical resolution that will eventually be necessary.

I wish to report at this time a beautiful and powerful new approach to this problem. Dr. M. T. Chahine has utilized an important physical property of the outgoing radiation to develop a relaxation method that should be much less sensitive to errors in measurement. It is highly convergent and does not require the time-consuming matrix inversion. I am attaching, as an Appendix to this report, a paper by Dr. Chahine describing his method for the special case of a temperature sounding under cloudless conditions determined from the spectrum of the  $4.3\mu$   $\text{CO}_2$  band. Note in particular the high vertical resolution obtained near the surface.

Chahine's method will be extended in an attempt to incorporate measurements in the  $15\mu$   $\text{CO}_2$  band, the 5 mm band of  $\text{O}_2$ , the  $6.3\mu$  and rotational bands of  $\text{H}_2\text{O}$ , and the effects of clouds. It should eventually be capable of incorporating all of this into real-time computations of the detailed state of the atmosphere.

The promise of obtaining sufficiently detailed soundings of the atmosphere for immediate use in numerical weather prediction routines appears to be very bright.

#### 5. SOUNDING FROM THE GROUND

Because of the pressure broadening of spectral lines, sounding from above allows the instrument to receive measurable amounts of radiation from all layers of the atmosphere. This characteristic of pressure-dependence of line shapes is a disadvantage for sounding from below. However, the technique may be of some use, under special circumstances, for

## PROBING WITH HIGH-FREQUENCY INFRARED RADIOMETRY

sounding the air in the immediate vicinity of the ground\* by measurements from a spectrometer or radiometer located at the surface. The strong temperature dependence of the black-body function at high frequencies again makes the  $4.3\mu$  CO<sub>2</sub> band and the  $6.3\mu$  H<sub>2</sub>O band particularly appropriate for this purpose.

In order to assess the feasibility of sounding from the ground, I have calculated the downward radiation at five frequencies in the  $4.3\mu$  CO<sub>2</sub> band as functions of the temperature distribution. The atmosphere has been divided into layers given by the first column of Table 1. For ease in computation, each layer was assumed to be isothermal and the spectrum was assumed to be composed of strong, randomly-spaced lines, so that the transmission could be represented by an approximation to Equation (9) of Kaplan (1953) in the form  $\tau = \exp(-a_{\nu} \sqrt{z})$ , where  $z$  is the height above the ground. The constants  $a_{\nu}$  were obtained from the laboratory data of Howard, Burch and Williams (1956), matched to a pressure of one atmosphere.

The downcoming radiation is plotted in Figure 3 for  $20 \text{ cm}^{-1}$  intervals centered at 2230, 2250, 2270, 2290 and  $2310 \text{ cm}^{-1}$ , and the points connected with straight lines. The bottom curve represents the "sounding" given by the second column of Table 1; the other curves are for the same sounding, except for a  $5^{\circ}\text{C}$  increase in the layer indicated.

It is seen from Figure 3 that the spectrum is quite sensitive, both quantitatively and qualitatively, to the temperature distribution in the first few hundreds of meters in the atmosphere. Thus measurements from below should provide data useful for determination of heat and moisture exchange between the atmosphere and the surface.

The results, in terms of percentage variation in downcoming radiation for a  $1^{\circ}\text{C}$  change of temperature in the specified layers, are also given in the last five columns of Table 1. It is seen that the sensitivity greatly decreases above the first kilometer. The approximations used to obtain the transmission function are such as to make the sensitivity to changes in the upper levels appear even greater than it is. Thus the sounding can be accomplished more easily and accurately by simpler means, such as direct sounding from tethered balloons or tall towers. The spectroscopic method may be the best from unmanned ocean buoys, however. It should be noted that, in contrast to sounding from satellites, microwave sounding from below may be competitive to the use of high-frequency bands. This is because of the possibility of obtaining higher measurement precision and because of the possibility of making almost monochromatic measurements in the wings of spectral lines, in which case the transmission function more nearly approximates the form  $\tau = \exp(-a_{\nu} z)$ .

---

\*Dr. Atlas has pointed out that surface observations of emission in transparent regions of the spectrum can be used to determine the temperatures of cloud bases and the sides of cumulonimbus clouds. This can be done with an accuracy of about  $1^{\circ}\text{C}$ .

TABLE 1. Percentage variation of downcoming radiation in selected spectral intervals for 1°C change in various atmospheric layers.

Layer (m)	T(°K)	Center of 20 cm <sup>-1</sup> interval (cm <sup>-1</sup> )				
		2230	2250	2270	2290	2310
0-50	290	0.7	1.0	1.7	3.1	4.2
50-100	290	0.7	0.8	1.1	0.8	0.0
100-225	285	0.6	0.6	0.6	0.2	
225-400	285	0.5	0.5	0.4	0.0	
400-900	280	0.8	0.7	0.3		
900-1600	270	0.5	0.4	0.1		
1600-2500	260	0.4	0.2	0.0		
2500-3600	250	0.2	0.1			
3600-4900	240	0.1	0.0			

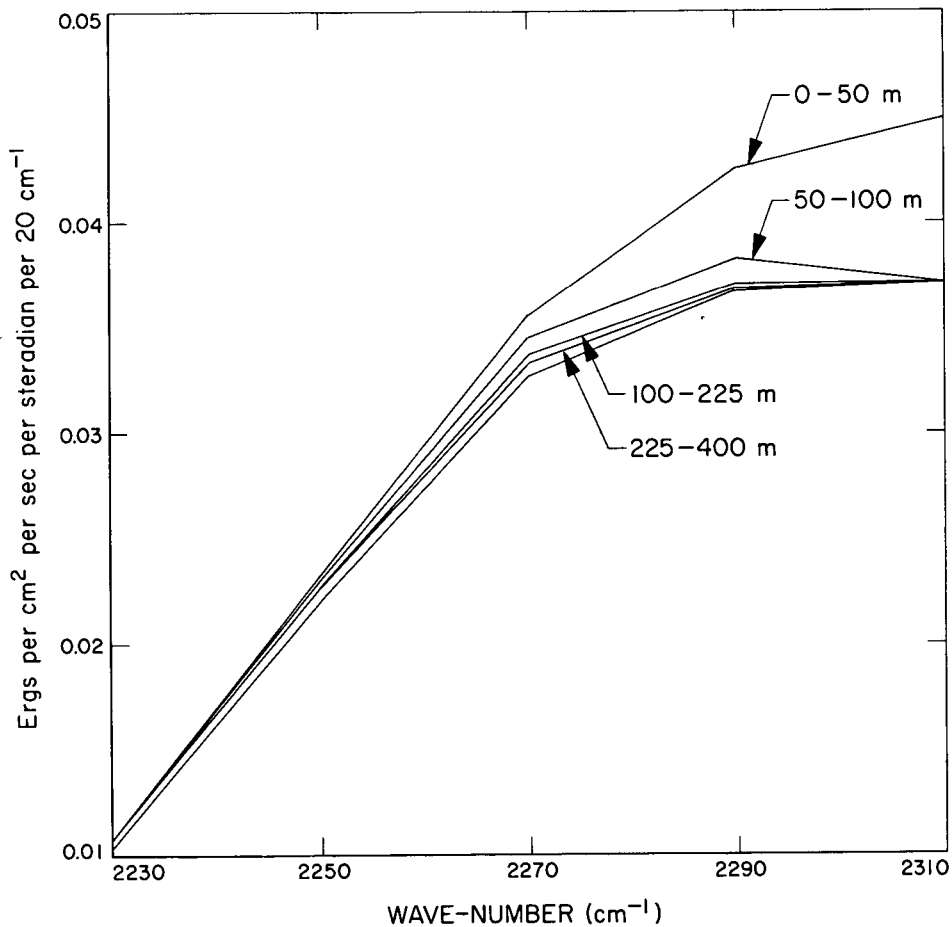


FIG. 3. Computed downward radiation for "sounding" of Table 1 (lower curve), and for same temperature distribution except for 5°C increase in indicated layer (upper curves).

# PROBING WITH HIGH-FREQUENCY INFRARED RADIOMETRY

## ACKNOWLEDGEMENTS

Grateful acknowledgements are due to Dr. Robert A. McClatchey for furnishing and allowing use of Figures 1 and 2, to Dr. Moustafa T. Chahine for allowing use of his paper as a contribution to this Section, and to the National Science Foundation for support under grant GA-1310X.

## REFERENCES

- Howard, J. N., Burch, D. E., and Williams, D., 1956: Infrared transmission of synthetic atmospheres. II. Absorption by carbon dioxide. J. Opt. Soc., 46, 237-241.
- Kaplan, L. D., 1953: A quasi-statistical approach to the calculation of atmospheric transmission. Proc. Toronto Met. Conf. (Roy. Met. Soc.), 43-48.
- Kaplan, L. D., 1959: Inference of atmospheric structure from remote radiation measurements. J. Opt. Soc., 49, 1004-1007.
- Kaplan, L. D., 1961: The spectroscope as a tool for atmospheric sounding by satellites. J. Quant. Spectrosc. Radiat. Transfer, 1, 89-95.
- Shaw, J. H., McClatchey, R. A., and Schaper, P. W., 1967: Balloon observations of the radiance of the earth between  $2100\text{ cm}^{-1}$  and  $2700\text{ cm}^{-1}$ . Appl. Opt., 6, 227-230.
- Smith, W. L., 1967: An iterative method for deducing tropospheric temperature and moisture profile from satellite radiation measurements. Mon. Wea. Rev., 95,
- Smith, W. L., 1968: An improved method for calculating tropospheric temperature and moisture from satellite radiometer measurements. Mon. Wea. Rev., 96,

N72-25375

DETERMINATION OF THE TEMPERATURE PROFILE  
IN AN ATMOSPHERE FROM ITS OUTGOING RADIATION

Moustafa T. Chahine  
Jet Propulsion Laboratory  
California Institute of Technology  
Pasadena, California

ABSTRACT

A highly convergent "relaxation" method for the inversion of the full radiative transfer equation has been developed. The results of the iterative solution indicate that convergence can be achieved over a wide range of initial "guesses," enabling the temperature profile of a relatively unknown atmosphere to be unambiguously determined. The method is illustrated by examples for the outgoing radiance in the earth's atmosphere for the region of the 4.3μ CO<sub>2</sub> band, but can be similarly applied in other frequency ranges.

1. INTRODUCTION

The total upward radiance  $I(\nu, \bar{P})$ , arriving vertically in a small solid angle ( $\omega \approx 0$ ) at a pressure level  $\bar{P}$  of an atmosphere in a given wave-number interval  $\nu$ , is obtained by formal integration of the fundamental radiative transfer equation (RTE), subject to a black-body boundary condition, and is conveniently reduced to read

$$I(\nu, \bar{P}) = \epsilon B[\nu, T(P_0)] \tau(\nu, P_0) + \int_{P_0}^{\bar{P}} B[\nu, T(P)] \frac{\partial \tau(\nu, P)}{\partial P} dP, \quad (1)$$

where  $B$  is the Planck function,  $\tau$  is the transmission function dependent on  $\nu, P$ , and the temperature distribution  $T(P)$  between  $\bar{P}$  and  $P$ ,  $P_0$  is the pressure at the lower boundary, and  $\epsilon$  is the emissivity at  $P_0$ .

Following a proposal made by Kaplan (1959) that the vertical distribution of atmospheric temperature,  $T(P)$ , can be inferred from measurements of outgoing radiance,  $\tilde{I}(\nu_i, \bar{P})$ ,  $i = 1, 2, \dots, n$ , a number of sophisticated but inconclusive attempts have been made to solve Eq. (1) for  $T(P)$ . The history of these attempts is extensively discussed and referenced in a series of articles by Wark and Fleming (1966). A review of these attempts further discloses the need for discovering and employing to advantage other physical and mathematical properties of the RTE that relate the measured radiance to the desired atmospheric

parameter, and to a general method of solution.

Past attempts to solve this problem, by linearizing the Planck function and reducing Eq. (1) to an  $n \times n$  system of linear equations, failed because the resulting system is always "ill-conditioned." In fact, our extensive studies of the above method applied to the  $\nu_3$  CO<sub>2</sub> band show that, without introducing any damping functions, the iterative solution converges only if the initial guess is made accurate to at least  $10^{-8}$  in  $T(P)$ . However, this author's past experience (Chahine, 1965) with the same family of Eq. (1) strongly suggests that the RTE in its integral form is "well-behaved," and that its reduction to a linear system of equations is improper.

The purpose of this work is to explore briefly an important property of the radiance emitted vertically from different layers of an atmosphere, and to apply it to the numerical solution of the complete RTE for the determination of the temperature profile.

## 2. GENERAL FORMULATION

The physical properties of outgoing radiation from various layers of an atmosphere are such that at any pressure level  $P$  within a wide range of pressures,  $P_2 < P < P_1$ , the total upward radiance can be related (e.g., from the mean value theorem) to the Planck function at  $P$  by

$$\frac{I(\nu, \bar{P})}{I^1(\nu, \bar{P})} \approx \frac{B[\nu, T(P)]}{B[\nu, T^1(P)]}, \quad (2)$$

where  $T(P)$  and  $T^1(P)$  are two different temperature profiles in the same atmosphere, resulting in radiance values  $I$  and  $I^1$ , respectively. This general feature is directly related to the fact that over a wide range of temperature profiles, the dependence of  $\tau(\nu, P)$  on changes in  $T(P)$  is negligible compared to that of the Planck function. Thus, if we select a set of  $i$  frequencies that satisfy Eq. (2) at an appropriate set of  $i$  pressure levels, we can readily use the above approximation to solve Eq. (1). In practice, it is more convenient to proceed first by factorizing the Planck function in terms of a function of temperature only and then use the latter as a universal variable of iteration.

To factorize the temperature in the Planck function we write

$$B(\nu, T) = a\nu^3 / (e^{b\nu/T} - 1) \quad (3)$$

$$= X(T)\beta(\nu)\delta(\nu, T), \quad (4)$$

with  $\delta(\nu, T) = O(1.0)$ . Since the temperature dependence of Eq. (3) appears as  $\sim e^{-b\nu/T}$ , we replace the argument  $-b\nu/T$ , within a small  $\nu$ - $T$  range, by its least-squares fit as

$$\frac{\partial}{\partial C_j} \int_{\nu'}^{\nu''} \int_{T'}^{T''} \left[ \frac{b\nu}{T} - C_1 - C_2\nu - \frac{C_3}{T} \right]^2 dT d\nu = 0, \quad (j = 1, 2, 3.) \quad (5)$$

The limits of integration reflect roughly the frequency range in use and the expected temperature variations in the atmosphere. Solution of the above  $3 \times 3$  system of equations gives

$$C_1 = -b \frac{\ln(T''/T')}{T'' - T'} \frac{v'' + v'}{2}, \quad (6-a)$$

$$C_2 = b \frac{\ln(T''/T')}{T'' - T'} \quad (6-b)$$

and

$$C_3 = b \frac{v'' + v'}{2}. \quad (6-c)$$

The scaled universal variable of iteration is then

$$X(T) = \exp \left( -C_1 - \frac{C_3}{T} \right) \quad (7)$$

The factorized Planck function becomes

$$\frac{B(v, T)}{av^3} \equiv X(T) \left[ \frac{\exp \left( -\frac{bv}{T} + C_1 + \frac{C_3}{T} \right)}{1 - e^{-bv/T}} \right], \quad (8)$$

in which the variation of  $X(T)$  with temperature can be several orders of magnitude larger than that of the second factor, as in the  $4.3\mu$  region of our example.

By substituting Eq. (8) into Eq. (1) and grouping, the RTE takes its final form as

$$I(v, \bar{P}) = X[T(P_0)] A(v, P_0) + \int_{P_0}^{\bar{P}} X[T(P)] K(v, P) dp, \quad (9)$$

in which the relatively weak dependence of  $A$  and  $K$  on changes in  $T(P)$  is not explicitly shown. Thus, the problem reduces now to solving Eq. (9) for  $X_i$  when  $\bar{P}$  is given together with a selected set of radiance values  $\tilde{I}_i(v, \bar{P})$  measured at  $i$  frequencies.

### 3. METHOD OF SOLUTION

We propose to solve Eq. (9) by iteration: We make a first guess  $T^0(P)$  for  $X_i^0$ , and using this as input to Eq. (9), evaluate  $I_i^0(v, \bar{P})$  for the given atmosphere. The mechanism for generating the iterative solution is obtained from Eqs. (8) and (2) as prescribed in the following relaxation equation:

$$X_i^n = X_i^{n-1} \frac{\tilde{I}_i}{I_i^{n-1}}, \quad (10)$$

where  $n$  is the order of iteration. From the above equation we determine  $X_i^1$ , then  $T^1(P_i)$ , substitute it into Eq. (9), and evaluate  $I_i^1$ . Using Eqs. (10) and (7) again, we evaluate  $X_i^2$ , then  $T^2(P_i)$ , and repeat the same procedure for the following iterations. It is important to point out here that when  $X_i^0(T)$  is

## RADIOMETRIC DETERMINATION OF ATMOSPHERIC TEMPERATURE PROFILES

reduced to temperature according to Eq. (7), the resulting values are temperatures at specific altitudes and are not average values taken over an atmospheric layer.

The rate of convergence is determined from the residuals

$$R_i^n = \frac{|\tilde{I}_i - I_i^n|}{\tilde{I}_i} \quad (11)$$

or their average value

$$\langle R^n \rangle_{av} = \frac{1}{i} \sum R_i^n \quad (12)$$

The solution converges when  $R_i^n \rightarrow 0$  for all  $v_i$ .

### 4. APPLICATIONS AND DISCUSSION

In the remaining part of this work we will demonstrate the way the above scheme can be used to determine the temperature distribution in the earth's atmosphere from the spectral distribution of vertically outgoing radiance in the region of the  $4.3\mu$   $\text{CO}_2$  band.

#### 4.1 Procedure

To set up the problem, we assume a temperature profile  $\tilde{T}(P)$ , determine the transmission function  $\tau$ , and use an accurate quadrature formula to evaluate the radiance  $\tilde{I}_i(v, P)$  for  $\epsilon = 1$ ,  $\bar{P}/P_0 = 0.009$ , and for the 39 frequencies from 2180 (5) 2370  $\text{cm}^{-1}$  (because our transmission subroutine had been designed to give  $\tau(v, P)$  at intervals of  $v$  equal to 5  $\text{cm}^{-1}$  in the above range). The aim now is to take the radiance at a set of selected frequencies as simulated experimental data and to investigate how accurately we can retrieve the temperature profile  $\tilde{T}(P)$ .

The results presented here were obtained according to the following sequence:

1. Select a set of 10 sounding frequencies ( $v_i = 2180, 2235, 2245, 2260, 2290, 2295, 2305, 2315, 2370, 2360$ ), corresponding to 10 pressure levels ( $P_i/P_0 = 1.0, 0.85, 0.60, 0.40, 0.20, 0.10, 0.04, 0.025, 0.0135, 0.009$ ). The selection of this set is not unique and the choice of its size is optional. The most efficient sounding frequencies, for numerical computation purposes, are those that satisfy Eq. (2) in the region where their contribution to the integrand of Eq. (9) is substantial.

2. Make an initial guess  $T^0(P)$  and solve Eq. (9); check the residuals  $R_i^n$  and  $\langle R^n \rangle_{av}$ , and satisfy convergence.

3. Compare the results with the exact answer,  $\tilde{T}(P)$ .

Other pertinent details of the above sequence will be presented along with our examination of the following results.

#### 4.2 Discussion of Numerical Results

Figure 1 shows the results of the fifth iteration using the U.S. Standard Atmosphere as initial guess. The temperature profile computed at 10 pressure levels (not layers) has an average accuracy of  $1^{\circ}\text{K}$ . In the calculations, the transmission function  $\tau$  was left unchanged from that of the Standard Atmosphere temperature profile. When  $\tau$  was recomputed after every iteration, to account for changes in the temperature profile, the results improved slightly. When other sets of  $\nu_i$  were used as sounding frequencies, the corresponding results compared favorably with those shown in Fig. 1, indicating the general prevalence of the feature given in Eq. (2). The numerical evaluation of the integral in Eq. (9) was performed by using a modified Simpson's rule and a second-order interpolation formula for the intermediate values of temperature.

The rate of convergence at each of the selected 10 sounding frequencies, as well as that at each of the remaining 29 $\nu$ , was checked after every iteration. The average rates of convergence  $\langle R^n \rangle_{av}$ , listed in Table I, were taken over all 39 $\nu$ . Examination of this list clearly reveals the two most important characteristic features of the iterative solution: stability and convergence.

A similar examination of the average rates of convergence of the temperature profile  $T^n(P)$  indicates that an average accuracy of  $1^{\circ}\text{K}$  is achieved when  $\langle R^n \rangle_{av} < 3\%$ , and that an average accuracy of  $2-3^{\circ}\text{K}$  can be achieved when  $5\% < \langle R^n \rangle_{av} < 7\%$ . The above results offer an initial indication of the effect on the accuracy of the final profile of errors in the measurements of radiance values.

Figure 2 shows the results of the eighth iteration using the same sounding frequencies as in Fig. 1, but using as initial guess any one of three isothermal temperature profiles, 280, 240, and  $200^{\circ}\text{K}$ . The transmission function  $\tau$  was recomputed during the first five iterations only and was kept unchanged afterward. After the fifth iteration, the results for all three (very different) initial guesses converged to the same profile, and became indistinguishable on the scale of Fig. 2. The fact that the same set of sounding frequencies gave equally good results for all the above cases demonstrates the strong persistence of the basic feature given in Eq. (2).

The rates of convergence for these three initial guesses were remarkably similar and the residuals decreased very sharply. The results listed in Table I show a spectacular example of convergence for the case of  $T^0(P) = 280^{\circ}\text{K}$ ; there, the average residual decreased from an initial value of 920.10% to 21.74% in just one iteration.

It was further noticed that convergence occurred first at the lower levels of the atmosphere, then spread upward. Thus, higher order iterations tended to improve convergence at the upper levels at the expense of accumulating truncation errors at the lower levels. We note in conclusion that the numerical results shown here do not represent the best in the art of computational refinements; we believe this method is capable of far greater accuracy.

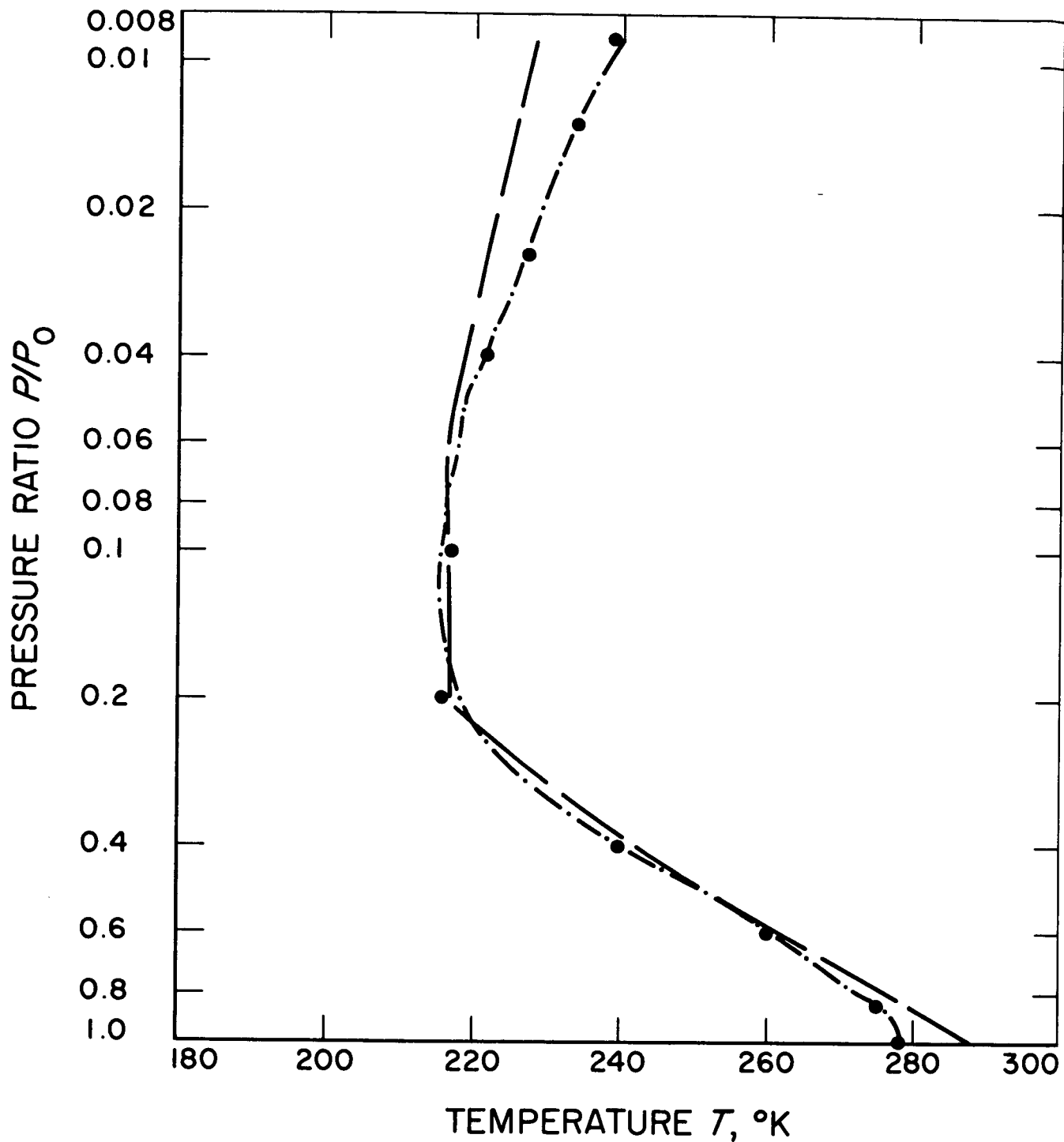


Fig. 1. Temperature profile, from 10 sounding frequencies, at the fifth iteration using the U.S. Standard Atmosphere as initial guess.  
 ••• , iterative solution. -•-•, exact profile.  
 — — , initial guess.

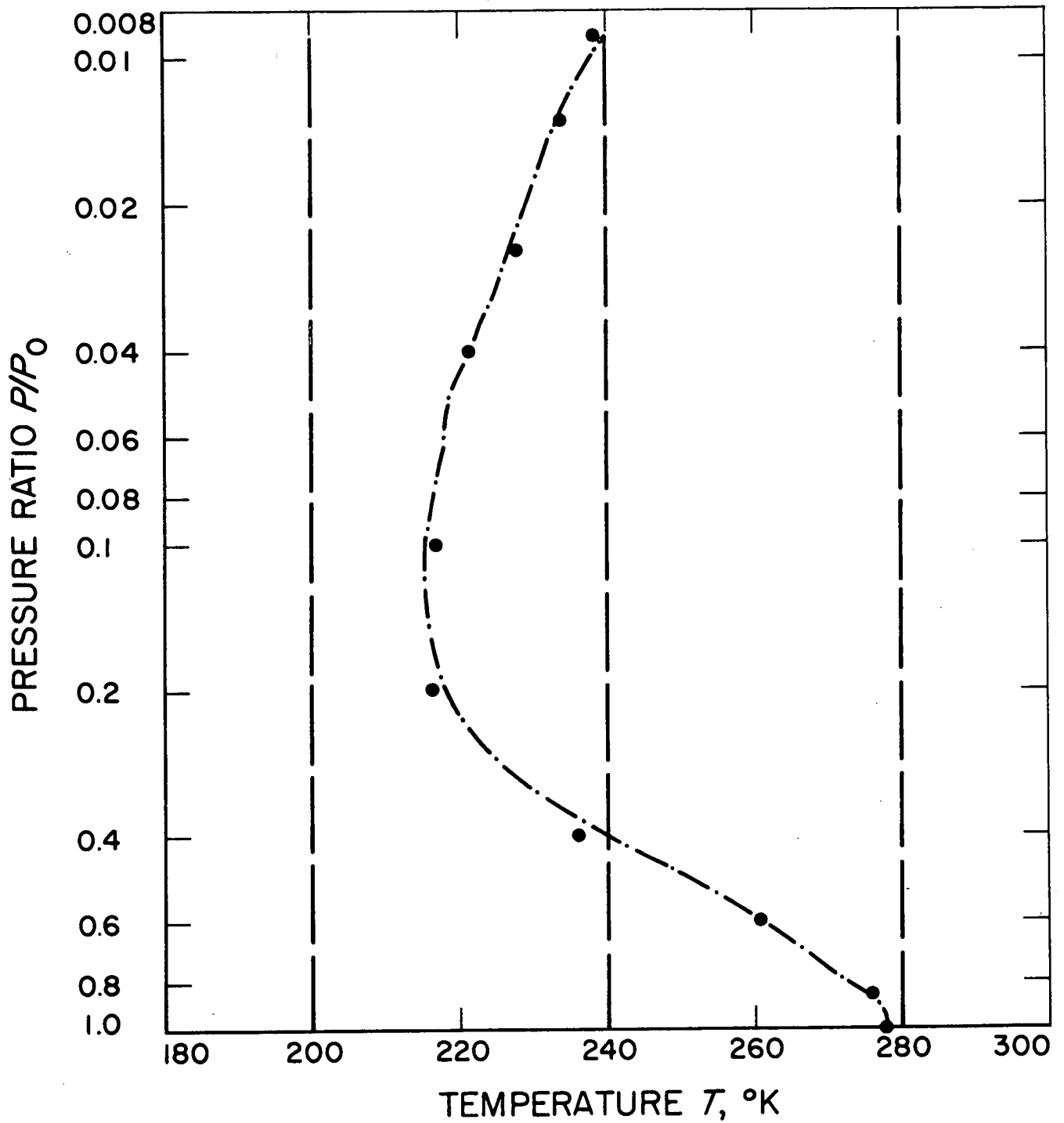


Fig. 2. Temperature profile, from 10 sounding frequencies, at the eighth iteration using as initial guess any one of three isothermal profiles: 280, 240, or 200°K.  $\dots$ , iterative solution.  $-\cdot-\cdot-$ , exact profile.  $- - -$ , initial guess.

RADIOMETRIC DETERMINATION OF ATMOSPHERIC TEMPERATURE PROFILES

TABLE I. Average Residuals  $R^n_{av}$ , %

Initial guess $T^0(P)$	Order of iteration, n									
	0	1	2	3	4	5	6	7	8	9
U.S. Standard Atmosphere	26.30	6.97	2.25	1.52	1.02	0.73	0.54	0.40	*	*
280°K	920.10	21.74	10.11	5.49	2.88	1.35	0.81	0.54	0.42	*
240°K	80.23	21.86	10.33	5.49	2.85	1.33	0.79	0.54	0.43	*
200°K	90.89	22.42	10.76	5.53	2.84	1.31	0.79	0.55	0.46	0.41

\*The relative error caused by the numerical quadrature precludes making the average residuals less than 0.39%.

5. CONCLUSION

The great advantage of the approach discussed here lies in the fact that it has exploited a dominant physical property of radiance occurring over a wide range of frequencies, and related this property to an efficient relaxation method of solution, and that it can be easily adapted for use in different frequency ranges, such as the 15  $\mu$  CO<sub>2</sub> band and the microwave regions.

The resulting inversion scheme provides a reliable tool for practical sounding of temperature with the accuracy required for use in numerical weather forecasting in the earth's atmosphere. Perhaps more important, this method is also suitable for unambiguous determination of temperature profiles of the comparatively unknown atmospheres of other planets. The time required for the reduction of a set of measured radiance values to the temperature profile shown here is very small, and the calculations are simple and can even be carried out on a desk calculator. Thus, a readily feasible system for the reduction of the measured radiance values can be arranged to produce temperature profiles in "real time" as data are accumulated.

6. ACKNOWLEDGMENT

The author wishes to express his deepest appreciation to Dr. C. B. Farmer for many long hours of helpful discussions, which were instrumental in the development of this work.

## REFERENCES

- Kaplan, Lewis D., 1959: Interference of atmospheric structure from remote radiation measurements. *J. Opt. Soc. Am.*, 49, 1004-1007.
- Wark, D. Q. and H. E. Fleming, 1966: Indirect measurements of atmospheric temperature profiles from satellites: I. Introduction. *Monthly Weather Review*, 94, 351-362.
- Chahine, Moustafa T., 1965: "Numerical Solution of the Complete Krook-Boltzmann Equation for Strong Shock Waves," in Methods in Computational Physics, Vol. 4, E. Alder, S. Fernbach, and M. Rotenberg, Eds. (Academic Press, New York).

TOWARDS AN OPTIMAL INVERSION METHOD FOR REMOTE  
ATMOSPHERIC SENSING

Jean I. F. King \*  
NAS/NRC Senior Resident Research Fellow  
Air Force Cambridge Research Laboratories  
Optical Physics Laboratory (CROI)  
L. G. Hanscom Field  
Bedford, Massachusetts 01730

ABSTRACT

The inference of atmospheric structure from satellite radiometric observations requires an inversion algorithm. The ideal inversion technique should be accurate, self-limiting, free from bias, stable against noise, flexible, and simple in application. A variety of techniques has been spawned to meet these demands. One class, the nonlinear inversion methods, copes with the serious problem of data noise in an unusual fashion. Unlike linear techniques which require a priori data smoothing, the nonlinear method can be applied directly to raw data. The algorithm discriminates the noise input by resolving the inferences into two types of solution, associating the real roots with atmospheric structure while ascribing the imaginary roots to noise.

The algorithm appears capable of further refinement with the possibility of inferring systematic noise structure, i.e. pinpointing a channel consistently in error. An example is given of this error-sensing ability of the nonlinear inversion technique.

---

\* On leave from GCA Corporation, Bedford, Massachusetts 01730

## 1. INTRODUCTION

The advent of meteorological satellites has led to intensive investigation of the possibilities and limitations inherent in remote atmospheric sensing. The upwelling radiation intercepted by the orbiting spectrometer is an integral transform of the physical state of the atmosphere, symbolically expressible as

$$I[\kappa(\nu)] = \Omega \{B[T(u)]\}, \quad (1)$$

with  $\kappa$  the monochromatic absorption coefficient at frequency  $\nu$  and  $B$  the Planck intensity, an implicit function of the vertical absorber distribution  $u$  through the temperature. For nadir frequency scanning in the far infrared, the integral operator  $\Omega$  follows from radiative transfer theory as a Laplace transform

$$I(0, 1/\kappa) = \int_0^{\infty} B(u) e^{-\kappa u} \kappa du = \kappa L[B(u)]. \quad (2)$$

Clearly the deduction of vertical thermal structure requires the solution of the inverse problem

$$B(u) = L^{-1} \left[ \frac{I(0, 1/\kappa)}{\kappa} \right]. \quad (3)$$

It might appear at first sight as if we were making a problem where none existed. Certainly the inverse Laplace transform is known for a variety of functions and extensive tabulations are readily accessible. Two features, both related to the observation of real data, intrude into the pure functional space of the mathematician. These are the unavoidable noise residing in the data and the finite number of sensing channels. The fact of noise is particularly pernicious, imposing a sharp upper limit to the information deduction. Inversion, akin to differentiation, tends to amplify data error. The finite channel number forces one to infer a continuous vertical structure from a limited sampling of the radiation field. Thus the goal of inversion cannot be to infer all the temperature structure. This is inaccessible in principle because of the presence of noise. Our aim must be the more modest one of seeking the optimum inversion technique which yields all the valid inferences inherent in the observations. A more subtle corollary to this is that the inversion algorithm must be capable of discriminating noise from the data, that is a proper attribution of the signals either to radiating atmospheric sources or to extraneous noise.

Let us set forth the requirements of an optimum, ideal inversion procedure

1) Accuracy: The inversion should reconstruct all the temperature structure inherent in the data.

2) Self-limiting: The inversion method should not infer more structure than that permitted by the noise level.

3) Freedom from bias: The inference should not be weighted towards any predetermined structure, such as a climatological set. Neither should the functional representation chosen force an unnatural configuration on the thermal profile.

4) Noise stability: The algorithm should be capable of discriminating noise from signals arising from emitting atmospheric sources.

5) Flexibility: The technique should be applicable to any meteorological situation and to any choice of channel sensing input.

6) Simplicity: The inversion procedure should be compatible for computer programming and real time temperature data readout.

It is a pleasure to report that a nonlinear inversion method has been developed which gives promise not only of fulfilling these stringent demands, but appears capable of discriminating between systematic and random errors. That is to say the inversion algorithm will go beyond indicating the presence of noise, by pinpointing which channel is in error and by how much! To indicate how this can be done, let us review the history of the inversion problem in sufficient depth to place this nonlinear Fourier inversion method in perspective.

## 2. INVERSION THEORY AND CRITIQUE

Most inversion methods are basically linear techniques modified in various ways to cope with the noise problem. They proceed by expanding the Planck intensity in a suitably chosen orthogonal polynomial set

$$B(u) = \sum_{j=1}^n B_j P_j(u). \quad (4)$$

Substituting this expression into Eq. (2) leads to a linear simultaneous set of equations which must be satisfied by the  $n$  measured intensities

$$I(0,1/\kappa_i) = \sum_{j=1}^n B_j p_j(\kappa_i) + \epsilon(\kappa_i) \quad i = 1, 2, \dots, n, \quad (5)$$

where  $p_j(\kappa) = \kappa L[P_j(u)]$  and  $\epsilon$  is the noise vector. Experience has shown that the best choice for representing the source is a set of empirical orthogonal functions based on climatological data. The solution consists of a matrix inversion to determine the  $n$  weights of the prechosen orthogonal members, with the data appropriately smoothed by the subtraction of the error vector  $\epsilon$ .

Nonlinear inversion is a completely different approach to the problem. Rather than specifying in advance the functional representation, the weights and members of the set are inferred directly from the intensity data. The data points are used to generate a unique characteristic equation whose eigenfunction solutions form the members of the set.

In the first application to nonlinear inversion, the Planck intensity was approximated by spline functions, i.e., a series of slabs (step functions) or ramps. Since the nonlinear inversion method using spline functions is documented elsewhere (King 1964), we shall merely epitomize its merits and demerits relative to linear methods before proceeding with the new approach.

Three advantages come to mind. First is the fact that the intensity data determine directly the choice of members of the set. For spline functions this corresponds to the slab thicknesses or the distance between successive ramps. The second feature, the uniqueness of the inferred profile, follows as a corollary of the first. The thicknesses are given by the algorithm as the  $n$  roots, necessarily unique, of an  $n$ th degree polynomial. Stated explicitly, for any suitably chosen  $2n$  intensities, there is one and only one array of  $n$  slabs which will fit the data. The third feature is the most subtle, most unexpected, and most important. This is the response of the algorithm to noise in the data. In this event one or more of the roots become negative. These inadmissible roots characteristically have small weights associated with them. The remaining valid roots are relatively unperturbed and preserve a high fidelity representation of the temperature profile. Thus the algorithm acts as a filter, discriminating between the rapidly varying noise components and the lower frequencies associated with temperature structure.

Balancing somewhat these three advantages of member choice, uniqueness, and noise discrimination vis-a-vis the linear methods are four restrictions associated with the nonlinear spline function inversion. First is the stipulation that the Planck intensity be approximated by a slab or ramp solution. For example, a constant tropospheric lapse-rate cannot be satisfactorily fit by a single ramp configuration. More serious, perhaps is the algorithm requirement that the channels be chosen at consecutive integral multiples of the absorption coefficient of the most transparent channel. The channel positions in practice are chosen out of engineering considerations, and it is highly unlikely that a choice on that basis would be optimal for the algorithm. A third condition is the need for an independent determination of the temperature at the top of the atmosphere [ $B(0)$ ] in the slab algorithm. For the ramp solution, inputs for both  $B(0)$  and  $B'(0)$  are necessary. Finally, the Prony algorithm is applicable only for transmittances of an exponential function type.

Certainly the most interesting and potentially the most useful feature of the nonlinear approach lies in its treatment of noise in the data. A natural question is whether the nonlinear technique has an underlying physical basis in transfer theory or if the inadmissible roots are mere artifacts of a solution algorithm. Accordingly, an effort was made to establish the constraints necessary to yield slab or ramp solutions to the transfer equation. The search proved fruitless. Indeed it appeared that solutions of the spline function type were incompatible with classical transfer theory.

The pursuit of this logic has led to the formulation of a new wave theory of radiative transfer which contrasts to the corpuscular approach of classical transfer theory. Although the preliminary outlines are clear, at this date (July 1968) the theory is not yet complete. The paper, "Remote Sensing and Inversion Techniques: State of Art, Kine (1967), indicates the progress and general direction of this research.

Our prime concern here is not transfer theory itself, but rather the insight it provides for inversion. In this vein it is a pleasure to report that the wave transfer theory has as a direct consequence a new inversion method based on nonlinear Fourier analysis. Let us back up a bit to see the problem and how the new inversion technique fulfills the need.

In the slab formulation the upwelling intensity is approximated by a set of exponentially weighted step functions of height  $B_j$  and thickness  $u_{j+1} - u_j$ .

$$\begin{aligned}
 I(0,1/\kappa) - B(0) &= \int_0^\infty e^{-\kappa u} dB(u) \\
 &= \sum B_j e^{-\kappa u_j} = \sum B_j x_j^\kappa, \tag{6}
 \end{aligned}$$

where we have substituted  $u_j = -\ln x_j$ . By specifying integral values of  $x_j$  we are led to a nonlinear simultaneous equation set which is mathematically equivalent to the moment problem in physics. This set

$$I(0,1/\kappa_i) - B(0) = \alpha_i = \sum B_j x_j^{\kappa_i} \quad \kappa_i = 0, 1, \dots, 2n-1 \tag{7}$$

possesses a unique solution of  $n$  slabs which can be obtained using the Prony algorithm.

We are led to ask the three questions

- 1) Are there other nonlinear sets soluble by a similar algorithm?
- 2) Are these sets more flexible, i.e., less rigid than the slab or ramp configurations?
- 3) Can the intensity sampling points be arbitrarily chosen, free from the Prony requirement of equally spaced intervals?

The answer to these questions is affirmative, leading to the hope that we are approaching the goal described earlier of an optimum inversion method.

### 3. NONLINEAR FOURIER INVERSION

#### 3.1 Application to Noise-Free Data

We begin by noting that the most general solution of the transfer equation involves waves, i.e., exponential functions of imaginary argument, as well as the attenuating exponentials of classical theory

$$I(u,1/\kappa) = c \left[ \sum_{j=1}^\infty \left( \frac{b_j e^{i\omega_j u}}{\kappa - i\omega_j} + \frac{b_j e^{-i\omega_j u}}{\kappa + i\omega_j} \right) + \frac{1}{\kappa} + u + Q \right]. \tag{8}$$

By specifying odd parity for the Planck intensity  $B(u)$ , the upwelling intensity  $I(0, 1/\kappa)$  and its inverse Laplace transform  $B(u)$  become

$$I(0, 1/\kappa) = c \left[ \sum_{j=1}^{\infty} \frac{\kappa b_j \omega_j}{2 \kappa + \omega_j} + \frac{1}{\kappa} \right],$$

$$B(u) = L^{-1} \left[ \frac{I(0, 1/\kappa)}{\kappa} \right] = c \left[ \sum_{j=1}^{\infty} b_j \sin \omega_j u + u \right]. \quad (9)$$

The form of these equations suggests that by fitting the intensity at  $2n$  channels we may obtain the unique set of  $n$  Fourier sine terms of amplitude  $b_j$  and frequency  $\omega_j$  prescribed by the observations.

Let us check the method with a quadratic case, seeing to what extent we can reconstruct the familiar profile

$$B(u) = 1 - \exp(-u) \quad (10)$$

on the basis of the four intensity observations

$$I(0, 1/\kappa_i) - B(0) = \alpha_i = \int_0^{\infty} e^{-u} dB(u) = \frac{1}{\kappa_i + 1} \quad \kappa_i = 1, 2, 3, 4. \quad (11)$$

Substitution of these values into Eq. (9) yields the following four relations which must be satisfied

$$\begin{aligned}\frac{1}{2} &= \frac{b_1\omega_1}{1+\omega_1^2} + \frac{b_2\omega_2}{1+\omega_2^2} \\ \frac{1}{3} &= \frac{2b_1\omega_1}{4+\omega_1^2} + \frac{2b_2\omega_2}{4+\omega_2^2} \\ \frac{1}{4} &= \frac{3b_1\omega_1}{9+\omega_1^2} + \frac{3b_2\omega_2}{9+\omega_2^2} \\ \frac{1}{5} &= \frac{4b_1\omega_1}{16+\omega_1^2} + \frac{4b_2\omega_2}{16+\omega_2^2}\end{aligned}\tag{12}$$

After clearing of fractions and eliminating  $b_1$  and  $b_2$  from the equations, we obtain the following two equations which must be satisfied

$$\begin{aligned}c_1 - c_2(\omega_1^2 + \omega_2^2) + c_3\omega_1^2\omega_2^2 &= 0 \\ c_4 - c_5(\omega_1^2 + \omega_2^2) + c_6\omega_1^2\omega_2^2 &= 0\end{aligned}\tag{13}$$

with

$$\begin{aligned}c_1 &= \frac{27\alpha_3}{5} - \frac{64\alpha_2}{5} + \frac{\alpha_1}{3} = \frac{17}{180} \\ c_2 &= \frac{3\alpha_3}{5} + \frac{16\alpha_2}{15} - \frac{\alpha_1}{3} = \frac{7}{180} \\ c_3 &= \frac{\alpha_3}{15} - \frac{4\alpha_2}{15} + \frac{\alpha_1}{3} = \frac{17}{180} \\ c_4 &= \frac{64\alpha_4}{7} - \frac{324\alpha_3}{35} + \frac{8\alpha_2}{5} = \frac{1}{21} \\ c_5 &= \frac{-4\alpha_4}{7} + \frac{36\alpha_3}{35} - \frac{2\alpha_2}{5} = \frac{1}{105}\end{aligned}\tag{14}$$

$$c_6 = \frac{\alpha_4}{28} - \frac{4\alpha_3}{35} + \frac{\alpha_2}{10} = \frac{1}{84}$$

The characteristic equation must be a binomial with roots at  $\omega_1^2$  and  $\omega_2^2$

$$(x - \omega_1^2)(x - \omega_2^2) = x^2 - (\omega_1^2 + \omega_2^2)x + \omega_1^2\omega_2^2 = 0. \quad (15)$$

This equation is compatible with the Eqs. (13) if and only if the following determinant vanishes

$$\begin{vmatrix} x^2 & x & 1 \\ c_1 & c_2 & c_3 \\ c_4 & c_5 & c_6 \end{vmatrix} = 0, \quad (16)$$

yielding as the characteristic equation

$$x^2 - \frac{c_1c_6 - c_3c_4}{c_2c_6 - c_3c_5} x + \frac{c_1c_5 - c_2c_4}{c_2c_6 - c_3c_5} = 0. \quad (17)$$

$$x^2 - \frac{85}{11} x + \frac{120}{55} = 0.$$

This equation possesses the roots

$$\omega_1^2 = 0.29350082, \omega_1 = \pm 0.54175716 \quad (18)$$

$$\omega_2^2 = 7.43377190, \omega_2 = \pm 2.72649443.$$

We determine  $b_1$  and  $b_2$  now by back substitution of these roots into any pair of Eqs. (12)

$$b_1 = 1.10607838, b_2 = 0.11364969 \quad (19)$$

Thus we have inferred from the four intensity measurements the following two Fourier sine terms

$$\begin{aligned}
 B(u) &= b_1 \sin \omega_1 u + b_2 \sin \omega_2 u \\
 &= 1.10607838 \sin 0.54175716u \\
 &\quad + 0.11364969 \sin 2.72649443u.
 \end{aligned}
 \tag{20}$$

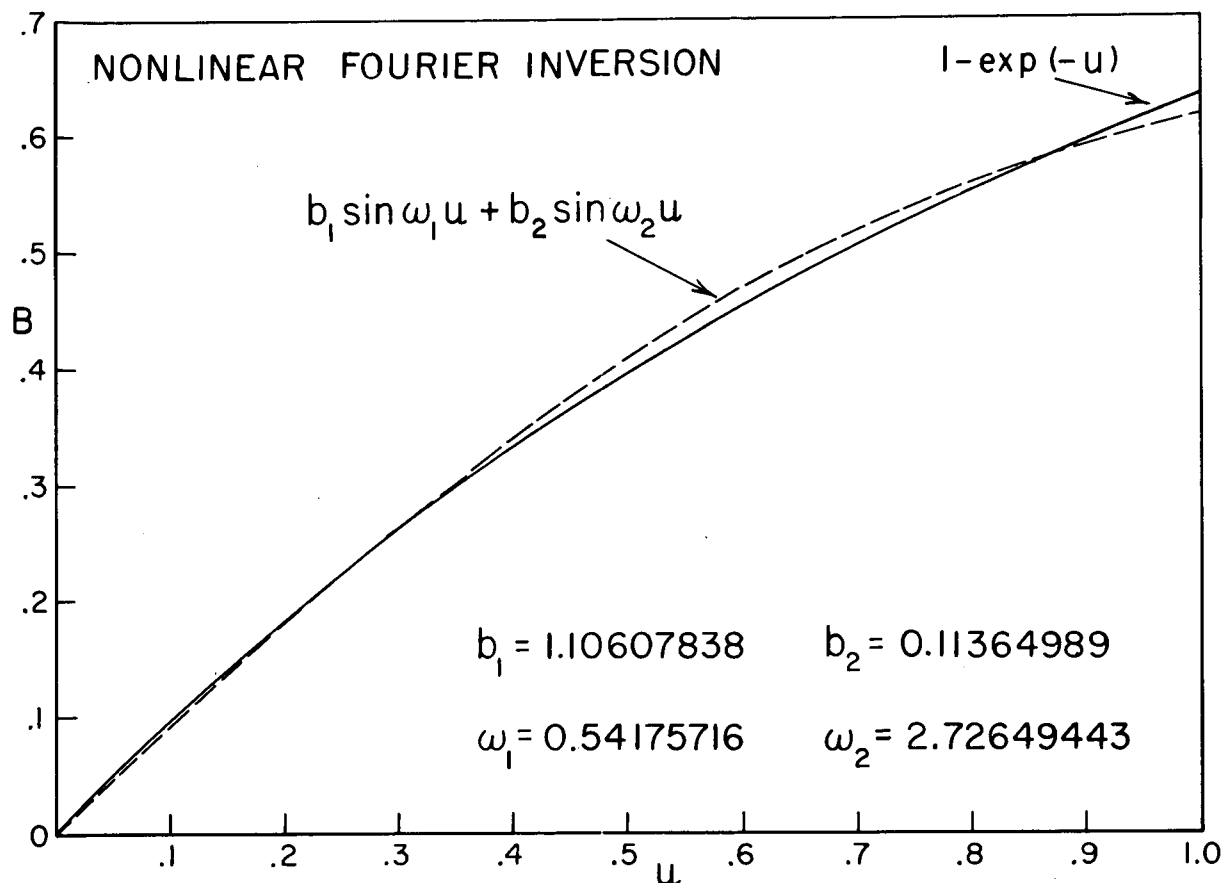


Figure 1. Nonlinear Fourier Inversion (inferred values versus actual profile.)

Figure 1 displays the inferred compared to the actual profile. The agreement is highly gratifying. Particularly encouraging is the fact that the lower frequency component has some eleven times the weight of the higher term, an indication that the method converges rapidly. Although the intensities were chosen at integral values of the absorption coefficient, this need not have been the case, since the inversion algorithm is independent of channel choice. Separation is desirable, however, to avoid near singular matrices.

Although the algebra becomes tedious as more Fourier terms are inferred it should be emphasized that once the channel sites are fixed, the routine

leading to the coefficient of the characteristic equation can be fixed once and for all. A program for direct time computer readout is certainly accessible.

The algorithm will surely respond to noise in the data by having one or more of the roots of the characteristic equation becoming negative. In fact one can expect that the algorithm not only will discriminate against noise but infer which one (or more) of the channels is in error. This could be considered the ultimate in inversion, a method which would not only infer all the valid information implicit in the observations but also which channels are in error and by how much.

### 3.2 Algorithm Response to Noise

Let us examine now the reaction of the nonlinear Fourier inversion to data noise. As a test case we have retained the intensities in three of the directions associated with the sample profile [Eq. (10)], perturbing the third channel alone. The intensities now read

$$\begin{aligned}\alpha_1 &= 1/2 \\ \alpha_2 &= 1/3 \\ \alpha_3 &= 1/3 \\ \alpha_4 &= 1/5.\end{aligned}\tag{21}$$

The straightforward application of the algorithm as before yields the perturbed characteristic equation [cf. Eq.(17)]

$$x^2 + \frac{2785}{361} x - \frac{1656}{361} = 0,\tag{22}$$

with the roots, one positive and one negative,

$$\begin{aligned}\omega_1^2 &= +0.55472626 \\ \omega_2^2 &= -8.26940770.\end{aligned}\tag{23}$$

We determine as well by back substitution the weights

$$\begin{aligned}b_{11}\omega_1 &= 0.78193720 \\ b_{22}\omega_2 &= 0.02138690.\end{aligned}\tag{24}$$

Our algorithm has therefore inferred from the perturbed intensity measurements, the following interpolation formula for the intensity

$$\begin{aligned}
 I(0,1/\kappa) &= \sum_{j=1}^2 \frac{\kappa b_j \omega_j}{\kappa^2 + \omega_j^2} \\
 &= \frac{0.78193720\kappa}{\kappa^2 + 0.55472626} + \frac{0.02138690\kappa}{\kappa^2 - 8.26940770},
 \end{aligned} \tag{25}$$

and the following temperature profile

$$\begin{aligned}
 B(u) &= \sum_{j=1}^2 b_j \sin \omega_j u \\
 &= 1.04986 \sin(0.7448u) + 0.007437i \sin(2.8757iu).
 \end{aligned} \tag{26}$$

These results deserve the closest attention and interpretation. We see from the intensity formula [Eq. (25)] that the algorithm has inferred a pole at  $1/\kappa = 1/\omega_2 = 0.34774$  to fit the erroneous measurement at  $1/\kappa = 1/3$ . The contribution of the negative root at  $1/\kappa = 1/3$  is

$$I_2(0,1/3) = \frac{0.02138690/3}{1-(8.26940770/9)} = .08781. \tag{27}$$

The actual displacement is  $(1/3)-(1/4) = (//12) = .08333$ , which is within 5% of the true value. Moreover we see that the negative root term affects only slightly the three valid channels. This high fitting specificity follows from the concentration of the amplitude excursion near the pole.

Turning now to the inferred temperature profile, [Eq. (26)] we see that there is only one valid term. The second term is deemed inadmissible because of the imaginary character of the amplitude and frequency. We note, however, that the contribution of the second term is down some two orders of magnitude from the first. The valid term that remains preserves with commendable fidelity the character of the actual profile.

The inadmissible root response of the inversion algorithm to data error is reminiscent of the spline function inversion. Physically this is evidence that there does not exist any Fourier sine pair of arbitrary amplitudes and frequencies which will yield the observed intensities [Eq. (21)]. Hence we must ascribe the negative root to some effect, such as data error, extrinsic to the atmospheric emitting sources.

## TOWARDS AN OPTIMAL INVERSION METHOD FOR REMOTE ATMOSPHERIC SENSING

These results underlie the optimism we feel that the ideal inversion procedure is within grasp and the expectation with which we view its application to real data.

### ACKNOWLEDGEMENTS

Research partially supported by NASA/GSFC under contract NAS5-3352

### REFERENCES

- King, Jean I. F., 1964: Inversion by Slabs of Varying Thickness. J. Atmos. Sci., 21, 324-326.
- King, Jean I. F., 1967: Remote Sensing and Inversion Techniques: State of the Art, pp. 253-265 in Proceedings of the Specialist Conference on Molecular Radiation and Its Application to Diagnostic Techniques, Marshall Space Flight Center, 5-6 October 1967. Document TMX-53711, ed. R. Goulard, NASA/MSFC, 489 pp.

N72-25377

EXPERIMENTAL APPROACHES TO REMOTE ATMOSPHERIC  
PROBING IN THE INFRARED FROM SATELLITES

William R. Bandeen  
Goddard Space Flight Center  
National Aeronautics and Space Administration  
Greenbelt, Maryland

ABSTRACT

Remote atmospheric probing in the infrared from satellites had its inception in October 1959 with the launch of Explorer VII carrying a simple wide field radiometer. Since that time much progress has been made in developing radiometric instruments of increasing spatial and spectral resolution. Thirteen different types of radiometric instruments either have been flown in orbit or are scheduled to fly on forthcoming satellites. A fourteenth type, a Very High Resolution Radiometer for Geosynchronous Altitude, is among several of the others whose development has been stressed for the Global Atmospheric Research Program (GARP) of the next decade. Hence, even though it is not yet approved for flight, this instrument is included in this survey of experimental approaches to remote atmospheric probing in the infrared from satellites, developed during the first decade of the space age.

Characteristics of each radiometric instrument and some applications of the different types of data are discussed.

1. INTRODUCTION

The era of remote atmospheric probing in the infrared from satellite began nearly ten years ago with the launch of Explorer VII carrying a rather simple array of hemispheric, omnidirectional sensors to measure the radiation balance of the earth. Since that time radiometric instruments of increasing spatial and spectral resolution, and hence of increasing complexity, have been flown in orbit on the TIROS and NIMBUS research satellites or scheduled for forthcoming flights through the remainder of the decade. With the orbital flight of these instruments has come a concurrent research effort to analyze and interpret the large amounts of radiation data acquired over the entire globe in terms of their physical significance. In addition to the objective of increasing our knowledge of atmospheric processes, a primary objective of these efforts is to develop instrumentation and techniques suitable for the national operational meteorological satellite system. Only recently have flat plate, wide field radiometers been added to the television instrumentation on the ESSA (Environmental Survey Satellite) operational satellites. The Goddard Space Flight Center/NASA will soon transmit electrically to the National Environmental Satellite Center/ESSA the High Resolution Infrared Radiometer (HRIR) data from NIMBUS III for preliminary operational use, and as an outgrowth of the research and development program three different types of radiometers are now being developed expressly for use on the second generation operational satellites.

The purpose of this paper is to survey the first ten years of remote atmospheric probing in the infrared from satellites. It was deemed advisable to include only those radiometric instruments—thirteen different types in all—which either have flown in orbit or are approved and scheduled for forthcoming flights. One exception was made. A fourteenth instrument, a Very High Resolution Radiometer for Geosynchronous Altitude, was included even though it is not yet part of an approved mission because of its importance to the concept of the Global Atmospheric Research Program (GARP) in the 1970's and because of the advanced technological developments involved in its design.

No attempt has been made to discuss each instrument and its results in detail. Rather the author's objective has been to present a broad overview, giving selected characteristics of each instrument which are of primary interest to the meteorologist or atmospheric physicist, and giving examples of the many possible applications of the data from the different instruments. An attempt has been made to list a comprehensive

Editor's Note

"Experimental Approaches to Remote Atmospheric Probing in the Infrared from Satellites" by William R. Bandeen, was written and distributed in advance to members of the National Academy of Sciences Panel on Remote Atmospheric Probing in preparation for a meeting of the Panel in Chicago on 16 May 1968. In writing the document it was presupposed that the Nimbus B spacecraft – carrying radiometric instruments numbered 4, 5, 6a, and 7a in Table I – would be placed successfully in orbit and thereby designated "Nimbus III" within a very few days of the meeting.

Because of a malfunction of the first stage of the rocket vehicle during the launch phase on 18 May 1968, the Nimbus B spacecraft was not placed in orbit. Therefore, all references in Table I and throughout the text to radiometric instruments having been flown on Nimbus III in May 1968 are erroneous.

A "Nimbus B2" mission which will carry the Nimbus B backup instruments numbered 4, 5, 6a, and 7a in Table I was authorized by the National Aeronautics and Space Administration on 27 June 1968. Nimbus B2 is scheduled to be launched in May 1969 and, if successfully injected into orbit, will be designated Nimbus III. The original report as reproduced herein should be read in this context.

bibliography wherein the reader may pursue a deeper interest in the design of a particular instrument or system or in particular applications of the different types of data.

## 2. BASIS FOR REMOTE ATMOSPHERIC PROBING

The basis for remote atmospheric probing in the infrared lies in the molecular absorption bands of the various gaseous constituents. The principal infrared absorber in the atmosphere is the variable gas  $H_2O$  with strong vibration-rotation bands centered near 1.1 microns, 1.38 microns, 1.87 microns, 2.7 microns, and 6.3 microns, and with a rotation band becoming effective, though weak, near 12 microns and intensifying increasingly out to about 65 microns. A second gaseous absorber of importance is  $CO_2$  with strong vibration-rotation bands centered near 2.7 microns, 4.3 microns, and 15 microns. Of particular importance to the concept of remotely sounding vertical profiles of temperature (and, as a subsequent step, the remote sounding of vertical profiles of the variable gases) is the observed constant (or nearly so) mixing ratio of  $CO_2$  from the surface to the vicinity of the mesopause. (This characteristic of the atmosphere is of primary importance to the application of radiometric instruments numbered 6, 7, 9, 10, and 12 in Table 1, all of which are intended for vertical sounding of the atmosphere.) Another important absorber is the variable gas  $O_3$  with a strong vibration-rotation band centered near 9.6 microns. In addition to the bands mentioned above, there are many other bands of  $H_2O$ ,  $CO_2$ , and  $O_3$  and of other gaseous constituents of the atmosphere, but they are not important for purposes of this discussion.

Infrared absorption spectra for the terrestrial atmosphere out to 15 microns are shown in Figure 1. The specific bands mentioned above are clearly identifiable along with other lesser bands. Also, of importance to remote sounding are the atmospheric "windows" where gaseous absorption is minimal. Two windows of consequence to the discussions of instruments that follow are one in the interval 3.5-4.1 microns and another (except for the absorption due to  $O_3$ ) in the interval 8.0-12.5 microns (cf. Figure 1).

Also of importance to remote atmospheric probing in the infrared are the absorption and scattering characteristics of liquid water droplets and ice crystals making up clouds and of other particulates in the atmosphere (see, for example, the discussion of the Filter Wedge Spectrometer below; No. 10 in Table 1).

## 3. RADIOMETRIC INSTRUMENTS FOR REMOTE ATMOSPHERIC PROBING IN THE INFRARED FROM SATELLITES

The fourteen types of radiometric instruments mentioned above and some examples of data from final satellite-borne or preliminary balloon-borne or aircraft-borne versions of the instruments are discussed in this Section. As previously pointed out, the discussion of a particular instrument and its data in a survey of this type must necessarily be limited, and an attempt has been made to include a sizeable bibliography to which the reader can refer for additional information. It was not possible to conduct an exhaustive literature search in compiling the bibliography. Rather it was assembled largely from sources immediately available to the author, and hence it seems inevitable that many excellent references have been inadvertently omitted. For these omissions the author should like to express his sincere regrets.

EXPER. APPROACHES INFRARED PROBING FROM SATELLITES

Table I  
Radiometric Instruments for Remote Atmospheric  
Probing in the Infrared from Satellites

No.	Radiometric Instrument	Satellite(s) (See Note A.)	Channel(s)	Detector(s)	Instantaneous Field of View (degrees of arc)	Linear Resolution at Subsatellite Point from (Nominal Orbital Height) for Indicated Satellite(s) (both in Km)	Application
1.	WIDE FIELD Sensors (See Note B.)	Explorer VII, TIROS III, IV, VII ESSA 3, 5, . . . etc.	1) Black (Long - and Short - Wave Radiation) 2) White (Long - Wave Radiation)	Hemispheres or Flat Plates - Thermistor Bolometers	Entire Earth's Disc	~50% from 1400(700) Expl., TIROS 2400(1400) ESSA	Radiation Balance (Long - Wave Emission, Albedo)
2.	Two Cone Low Resolution Radiometer	TIROS II, III, IV	1) Black (Long - and Short - Wave Radiation) 2) White (Long - Wave Radiation)	Thermistor Bolometers	50°	670 (700)	Radiation Balance
3.	Medium Resolution Radiometer [Scanning]	TIROS II, III, IV, VII	1) 6.0 - 6.5μ (TIROS II, III, IV) 14.8 - 15.5μ (TIROS VII) 2) 8.0 - 12.0μ 3) 0.2 - 6.0μ 4) 8.0 - 30.0μ (Not on TIROS IV) 5) 0.55 - 0.75μ	Thermistor Bolometers	5°	60 (700)	Cloud Cover Mapping Storm Tracking Surface Temp. Cloud Top Heights Radiation Balance Tropospheric Water Vapor and Circulation
4.	High Resolution Infrared Radiometer (HRIR) [Scanning]	Nimbus I, II, III	1) 3.5 - 4.1μ (Nimbus I, II) 3.5 - 4.1μ (Nimbus III) 0.7 - 1.3μ	PbSe Single - Stage, Radiatively - Cooled to 200°K	0.46°	9 (1100)	Cloud Cover Mapping Storm Tracking Surface Temp. Cloud Top Height (Absolute Emission Measurements, Nighttime Only)
5.	Medium Resolution (Infrared) Radiometer (MRIR) [Scanning]	Nimbus II, III	1) 6.4 - 6.9μ 2) 10.0 - 11.0μ 3) 14.0 - 16.0μ (Nimbus II) 14.5 - 15.5μ (Nimbus III) 4) 5.0 - 30.0μ (Nimbus II) 20.0 - 23.0μ (Nimbus III) 5) 0.2 - 4.0μ	Thermistor Bolometers	2.9°	55 (1100)	Cloud Cover Mapping Storm Tracking Surface Temp. Radiation Balance Tropospheric Water Vapor and Circulation
6a.	Infrared Interferometer Spectrometer (IRIS)	Nimbus III	1) 5 - 20μ; Spectrally Scanning; Reso- lution $\Delta\nu = 5 \text{ cm}^{-1}$ ( $\Delta\lambda = 0.1\mu @ 15\mu$ )	Thermistor Bolometer	8°	150 (1100)	Vertical Profiles (Temp., H <sub>2</sub> O, O <sub>3</sub> , etc.)
7a.	Satellite Infrared Spectrometer (SIRS)	Nimbus III	Total of 8 Chans: 7 in 15μ CO <sub>2</sub> Band; 1 in 11μ Window; Resolution $\Delta\nu = 5 \text{ cm}^{-1}$	Thermistor Bolometers	12°	230 (1100)	Vertical Temp. Profile
8.	ITOS High Resolution Radiometer [Scanning]	TIROS M ITOS A, B, . . . etc.	1) 10.5 - 12.5μ 2) 0.52 - 0.73μ	Thermistor Bolometer Silicon Cell	0.30° 0.16°	7 4 (1400)	Cloud Cover Mapping Storm Tracking Surface Temp. Cloud Top Heights Albedo
6b.	IRIS	Nimbus D	1) 6.3 - 50μ; Spectrally Scanning; Reso- lution $\Delta\nu = 3.0 \text{ cm}^{-1}$ ( $\Delta\lambda = 0.07\mu @ 15\mu$ )	Thermistor Bolometer	5°	90 (1100)	Vertical Profiles (Temp., H <sub>2</sub> O, O <sub>3</sub> , etc.)

Flown in Orbit (as of May 1968)

7b. SIRS	Nimbus D	Total of 14 Chans: 7 in 15μ CO <sub>2</sub> Band; 6 in Rot. H <sub>2</sub> O Band; 1 in 11μ Window; Resolution Δν = 5 cm	Thermistor Bolometers	12°	230 (1100)	Vertical Profiles (Temp., H <sub>2</sub> O)
9. Selective Chopper Radiometer (SCR)	Nimbus D	Total of 6 Chans: 6 in 15μ CO <sub>2</sub> Band; 1 Switchable to 11μ Window	Thermistor Bolometers	10°	190 (1100)	Vertical Temp. Profile
10. Filter Wedge Spectrometer (FWS)	Nimbus D	1) 1.2-2.4μ; 3.2-6.4μ Spectrally Scanning; Resolution λ/Δλ = 100 (Δλ = 0.05μ @ 5μ)	Pb Se Single-Stage, Radiatively-Cooled to 160°K	2°	38 (1100)	Determine Liquid Water or Ice Content of Clouds (1.2-2.4μ) Vertical Temp. Profile (4.3μ CO <sub>2</sub> Band) Vertical H <sub>2</sub> O Profile (6.3μ H <sub>2</sub> O Band)
11. Temperature Humidity Infrared Radiometer (THIR) [Scanning]	Nimbus D	1) 10.5-12.5μ 2) 6.5-7.0μ	Thermistor Bolometers	0.40° 1.20°	8 (1100) 23	Cloud Cover Mapping Storm Tracking Surface Temp. Cloud Top Heights Air Mass Discrimination - Vertical Motion Jet Stream Location
12. ITOS Vertical Temp. Profile Radiometer (VTPR)	ITOS (1970's)	Total of 8 Chans: 6 in 15μ CO <sub>2</sub> Band; 1 in Rot. H <sub>2</sub> O Band; 1 in 11μ Window	Thermistor Bolometer (Filter Wheel in Front of One Detector)	2°	50 (1400)	Vertical Temp. Profile
13. ITOS Very High Resolution Radiometer (VHRR) [Scanning]	ITOS (1970's)	1) 10.5-12.5μ 2) 0.6-0.7μ	HgCdTe; 2-Stage Radiatively-Cooled to 80°K Photodiode	0.034°	0.8 (1400)	Cloud Cover Mapping Storm Tracking Surface Temp. Cloud Top Heights Albedo
14. Very High Resolution Radiometer for Geosynchronous Altitude [Scanning]	Geosynchronous Satellite (Planning Only - Not An Approved Mission)	1) 10.5-12.5μ	HgCdTe; Cryogenically Cooled to 80°K	0.023°	15 (35,800)	Cloud Cover Mapping Storm Development/Tracking Surface Temp. Cloud Top Heights Upper Level Winds

Under Development for Forthcoming Flights

Proposed

Note A. Launch Dates for U. S. Meteorological Satellites Carrying Infrared Radiometric Instruments (Through 1970)

Explorer VII	13 October 1959
TIROS II	23 November 1960
TIROS III	12 July 1961
TIROS IV	8 February 1962
TIROS VII	19 June 1963
Nimbus I	28 August 1964
Nimbus II	15 May 1966
ESSA 3	2 October 1966
ESSA 5	20 April 1967
Nimbus III	May 1968
TIROS M	1st Quarter 1969
ITOS A	3rd Quarter 1969
Nimbus D	1st Quarter 1970

(Future odd-numbered ESSA satellites will carry wide field sensors. Additional ESSA satellites will be launched as required for the National Operational Meteorological Satellite System.)

(First of the Improved TIROS Operational Satellites - ITOS) (Followed by ITOS B, C, . . . as required for the National Operational Meteorological Satellite System in the 1970's)

Note B. Wide field sensors will also be flown on the second-generation operational meteorological satellites: TIROS M, ITOS A, B, C, . . .

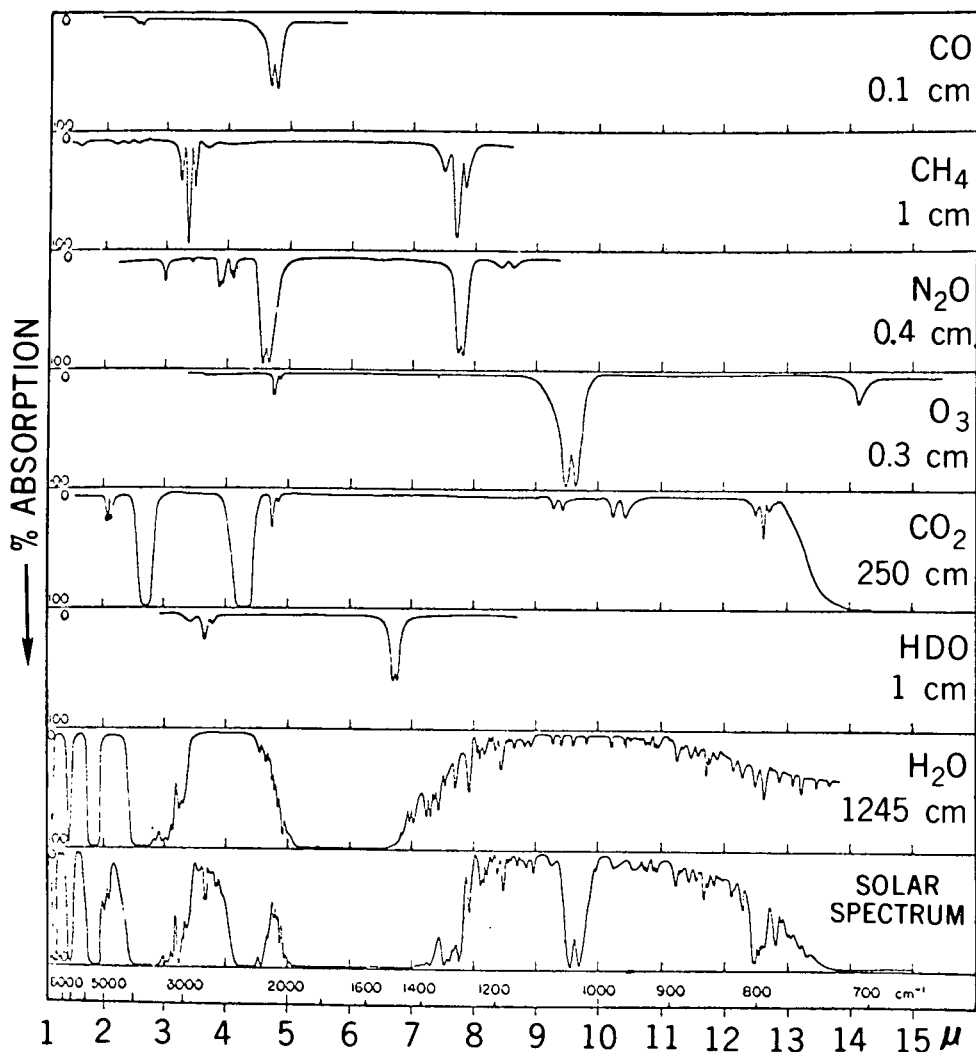


Figure 1. The near-infrared solar spectrum (bottom curve). Other curves are laboratory spectra of the molecules indicated. The approximate abundance of each gas in terms of cm NTP is indicated under the corresponding chemical formula; these are representative values for the highly variable gases H<sub>2</sub>O and O<sub>3</sub> (After Howard, Burch, and Williams, 1955).

The fourteen instruments and selected characteristics pertaining to them are listed in Table 1. This table virtually forms an outline of the paper, and it is intended that the reader refer to it often.

### 3.1 Wide Field Sensors

The first satellite-borne instrument to probe the atmosphere in the infrared was the thermal radiation balance experiment carried by the Explorer VII Satellite, launched on 13 October 1959 (Suomi, 1961; cf. Table 1, No. 1). This experiment, originally part of the International Geophysical Year 1957-58 Earth Satellite Program, was designed to measure the balance between long-wave radiation lost to space and short-wave solar radiation absorbed by the earth and atmosphere (Suomi, 1958). The resulting excesses and deficits in the radiation balance, and their spatial and temporal variations, make available the potential energy to drive the general circulation of the global atmospheric

"heat engine." Hence, their study is of primary importance in acquiring a deeper understanding of the thermal and dynamical characteristics of the atmosphere.

Explorer VII carried five hemispheric sensors in the form of hollow silver hemispheres. The hemispheres were thermally isolated from but in close proximity to special aluminized mirrors. The image of the hemisphere which appeared in the mirror made the sensor look like a full sphere. The spin of Explorer VII made the mirror-backed hemispheres act essentially as isolated spheres in space. Two of the hemispheres were provided with a black coating which made them respond about equally to solar and terrestrial radiation. One hemisphere was coated white, making it more sensitive to terrestrial radiation than to solar radiation. A fourth was gold-coated, making it more sensitive to solar radiation than to terrestrial radiation. The fifth hemisphere was tabor-surfaced and equipped with a shade to protect it from direct sunlight. In addition, a black sphere was mounted on the axis of the satellite at the top. It was used to determine any deterioration in the mirror surfaces by comparison with the blackened hemispheres. All temperature sensing elements were thermistors. The information telemetered to the earth was the sensor temperatures. The long-wave and short-wave radiation values were obtained by using these temperatures in heat balance equations. Even though the Explorer VII sensors viewed the entire earth's disc, the effective spatial resolution was considerably reduced by geometrical considerations, i.e., about 50% of the energy received at the nominal orbital height of 700 km originated within a radius of about 700 km from the subsatellite point.

An analysis of the nocturnal long-wave radiation lost to space as measured by the hemispheric sensors on Explorer VII is shown in Figure 2 (Weinstein and Suomi, 1961).

A variation of the Explorer VII experiment has been flown on several of the TIROS satellites which are also spin stabilized. In this variation a pair of hemispheric shells made of aluminum sheeting and backed by mirrors was used, one hemisphere with a black surface and the other with a white surface (House, 1965; Suomi, *et al.*, 1966). Another variation of the experiment is currently being flown on the odd-numbered ESSA satellites of the operational meteorological satellite system. (The ESSA satellites use the same basic spinning spacecraft as did the TIROS II, III, IV, and VII satellites. But whereas the spin axes of these TIROS satellites lay approximately within the orbital plane, the spin axes of the ESSA satellites are perpendicular to the orbital plane, causing them to be likened to a "cartwheel, rolling around the orbit.") In this variation flat plate sensors are used instead of hemispheres. Further, two versions of the flat plate sensors have been developed: (1) the basic radiometer consisting of one black and one white flat disc, and (2) the basic radiometer with cone optics added to restrict the field of view (Nelson and Parent, 1965; Operational Satellites Office, 1968). Because of the cosine dependence of a flat surface and because of the cone optics, the effective spatial resolution on the earth of the flat plate radiometer is less than that of an omnidirectional hemisphere for which the "Linear Resolution" values in Table 1, No. 1 were calculated. However, the principles applying to all variations are the same and the purpose of both the hemispheric and the flat plate sensors is to obtain low resolution measurements of the radiation balance of the earth-atmosphere system (Vonder Haar, 1968).

### 3.2 Two Cone Low Resolution Radiometer

A low resolution unchopped radiometer was flown on the TIROS II, III, and IV satellites (cf. Table 1, No. 2). The purpose of this radiometer was to measure the

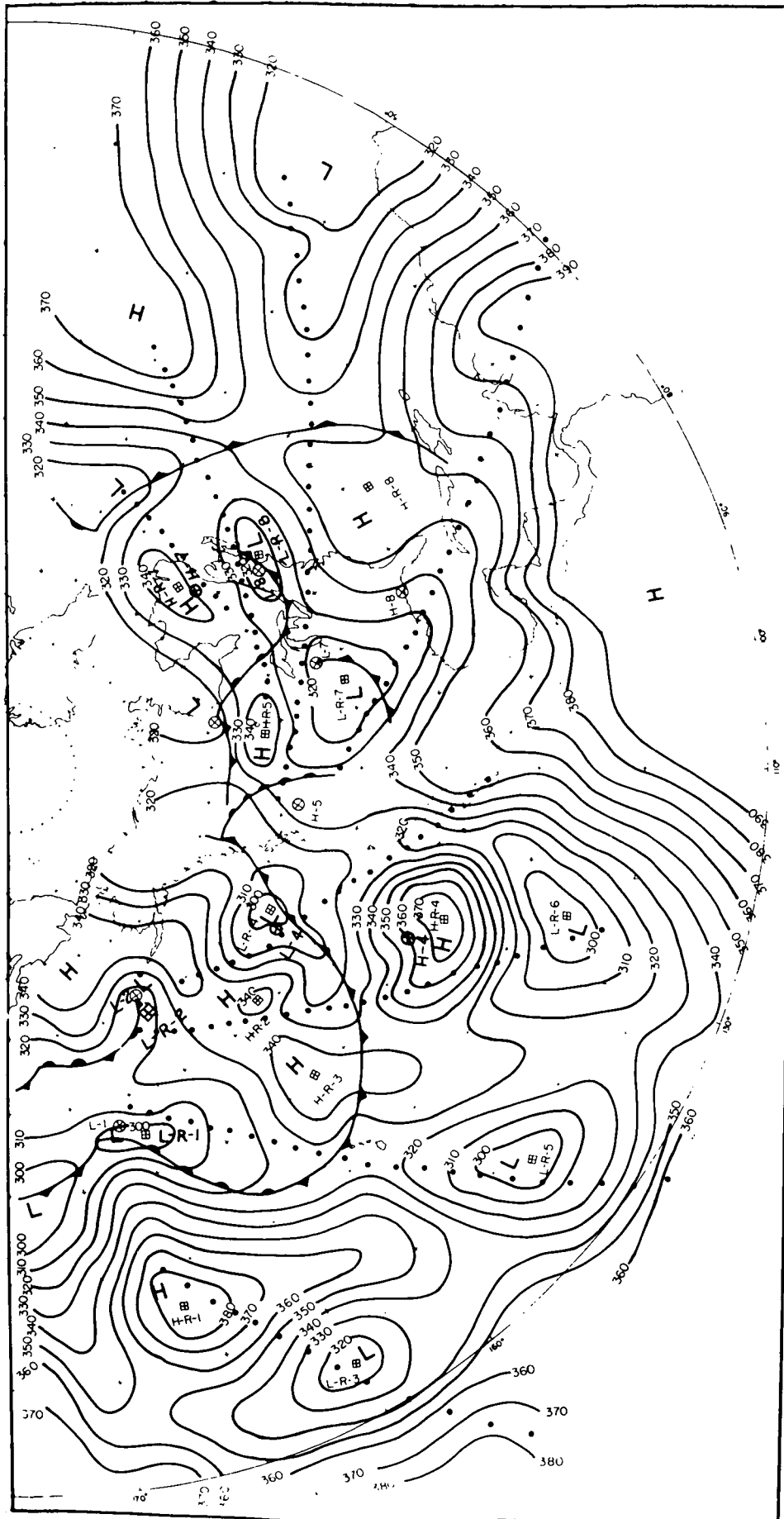


Figure 2. Long-wave radiation loss map, December 1, 1959. Lines are isolangleys, connecting equal long-wave radiation loss values in Langleys per minute  $\times 10^{-3}$ . Surface pressure centers and fronts are composite to the satellite passage time. Surface pressure centers, marked by circles, are designated L for Low and H for High, plus an arabic number (thus L-1). Radiation centers, marked by squares, are distinguished from surface centers by the inclusion of R (thus L-R-1 is radiation Low number 1 which is associated with surface Low L-1). Satellite observations points and orbit path are shown by dots (After Weinstein and Suomi, 1961).

equivalent blackbody temperature and albedo of the earth within its 50° field of view which was coaxial with the spin axis and with the optical axes of the two television cameras on the satellite (Bandeem, Hanel, et al., 1961).

The two low resolution channels consisted of a black and white thermistor detector each mounted in the apex of a highly reflective mylar cone. The black detector was equally sensitive to long-wave terrestrial radiation and reflected sunlight. The white detector was coated to be reflective in the visible and near infrared. The differences in the spectral emissivities of the two detectors yielded two independent energy balance equations from which the two unknowns, the equivalent blackbody temperature and the albedo within the field of view, could be solved (Hanel, 1961). The data analysis procedures and examples of analyzed data have been discussed by Bartko, Kunde, et al. (1964).

### 3.3 Medium Resolution Radiometer (TIROS)

In order to map radiometric data at considerably higher spatial resolutions than are possible with the two previously discussed instruments, the instantaneous field of view must be made smaller and it must be caused to scan over the earth beneath the satellite. The first radiometer of this type was the five-channel, medium resolution scanning radiometer flown on the TIROS II satellite, launched on 23 November 1960 (cf. Table 1, No. 3). The optical axes of the five channels were parallel and inclined by 45 degrees to the spin axis of TIROS. Viewing in both directions, they swept out two 45-degree half-angle cones around the spin axis on the "top" and "bottom" of the spacecraft as it spun at about 10 RPM. The intersection of these cones with the earth defined scan lines of varying shapes (depending upon the instantaneous nadir angle of the spin axis), and the progression of the satellite in orbit caused the advance of the individual scan lines. On the ground, then, it was possible to reconstruct the data in the form of maps of outgoing radiance in the direction of the satellite. The design of this radiometer has been described by Bandeem, Hanel, et al. (1961). The broad-band spectral intervals of the five channels and the nature of the radiation sensed are listed below:

1. 6.0-6.5 microns; water vapor absorption
2. 8.0-12.0 microns; atmospheric window
3. 0.2-6.0 microns; reflected solar radiation
4. 8.0-30.0 microns; thermal radiation
5. 0.55-0.75 microns; visible radiation (similar to the response of the television cameras)

The physical significance of these spectral regions has been discussed by Hanel and Wark (1961).

The same type of radiometer was subsequently flown on the TIROS III, TIROS IV, and TIROS VII satellites with several modifications. The most significant of these was the substitution of a channel responding to radiation in the interval 14.8-15.5 microns in lieu of the 6.0-6.5 micron channel on TIROS VII. The substitute channel sensed radiation within the 15 micron absorption band of carbon dioxide (cf. Fig. 1). The physical significance of this region has been reported by Hanel, et al. (1963), Bandeem, et al. (1963a), Nordberg, et al. (1965), and Warnecke (1966a). Detailed descriptions of the radiometers and of the available data are given in appropriate Manuals and Catalogs for each satellite (see, for example, Staff Members, 1964).

## EXPER. APPROACHES INFRARED PROBING FROM SATELLITES

The synoptic analysis of infrared data, including the mapping of cloud systems, the tracking of storms, and the inference of cloud top heights, both night and day, has received the attention of many workers. A sampling of studies in these areas includes papers by Fritz and Winston (1962), Nordberg, *et al.* (1962), Bandeen, *et al.* (1963b), Rao and Winston (1963), Allison, *et al.* (1964), Bandeen, *et al.* (1964), Hawkins (1964), Rasool (1964), Warnecke (1966b), Widger, *et al.* (1966), Allison and Thompson (1966b), Allison and Warnecke (1966c), and Allison and Warnecke (1967). Winston (1965) questioned some of the results of Rasool's (1964) analysis.

Allison and Warnecke (1967) interpreted synoptically the satellite-detected global radiation patterns in terms of a conventional weather analysis. Figure 3, taken from their paper, shows the equivalent blackbody temperature ( $T_{BB}$ , °K) pattern of outgoing 8.0-12.0 micron radiation from the earth's surface and the clouds above it measured by TIROS VII during the northern hemisphere winter and southern hemisphere summer. The cold areas which lie poleward of the 35 N and 40 S parallels are related to extratropical cyclonic activity; those near the equator indicate high cloud systems associated with the intertropical convergence zone. The presence of tropical cyclone "Danielle" under the high cloud shield at 40 S, 65 E indicates the beginning of hurricane activity in the southern hemisphere. The original figure, published by the authors in seven colors, was more impressive and informative than the black-and-white reproductions shown here.

The inference of ground surface temperatures from TIROS 8.0-12.0 micron measurements has been discussed by Wark, Yamamoto, and Lienesch (1962), Fritz (1963), and Buettner and Kern (1963). A promising method of specifying 500-mb heights from TIROS 8.0-12.0 micron data has been reported by Jensen *et al.* (1966), and correlations between TIROS 8.0-12.0 micron data and some diabatic properties of the atmosphere have been discussed by Davis (1965).

A method for inferring the mean relative humidity of the upper troposphere from coordinated measurements of the 6.0-6.5 micron and 8.0-12.0 micron channels was developed by Möller and Raschke (1964). An extension of this method to infer the water vapor mass above the 500-mb level, using conventional 500-mb temperature data in addition to the satellite data, was discussed by Bandeen, *et al.* (1965) and Bandeen (1966). Analyses of tropospheric moisture content utilizing this method have been published by Raschke (1967), Raschke and Bandeen (1967a), and Raschke and Bandeen (1967b). Figure 4 shows a map of the total water vapor mass above 500 mb in February 1962 determined by this method (Raschke and Bandeen, 1967b). The patterns indicate that the highest amounts of precipitable water vapor occur in the tropics and, particularly, in three regions, *vis.*, Southeast Asia, South America, and Central Africa. Fritz and Rao (1967), using data from the comparable "water vapor" and "window" channels of the NIMBIS II MRIR (*cf.* Table 1, No. 5) and conventional radiosonde data, discussed on both observational and theoretical grounds the problems involved in attempting to estimate atmospheric water vapor content above high clouds, especially cirrus, from such satellite measurements. In their discussion Fritz and Rao questioned some of the findings of Raschke and Bandeen (1967b).

A method for converting the 8.0-30.0 micron or 8.0-12.0 micron radiance measurements to total outgoing long-wave radiative flux was derived by Wark, *et al.* (1962). The original method, which employed a theoretically-determined limb darkening function, has

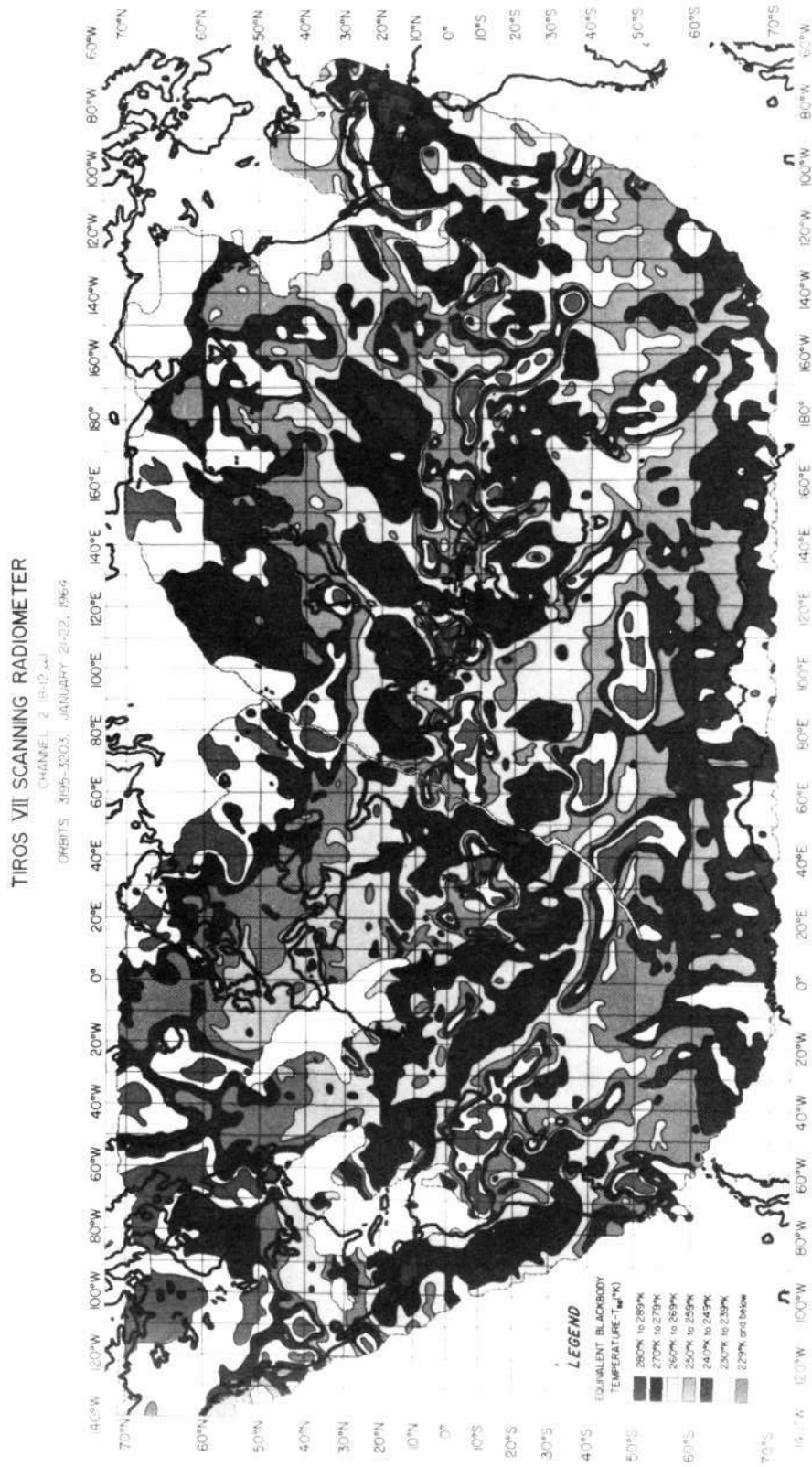


Figure 3. Composite map of radiation measured by the 8.0-12.0 micron channel of TIROS VII during nine consecutive orbits on January 21-22, 1964 (After Allison and Warnecke, 1967). The published figure is in seven shades of color.

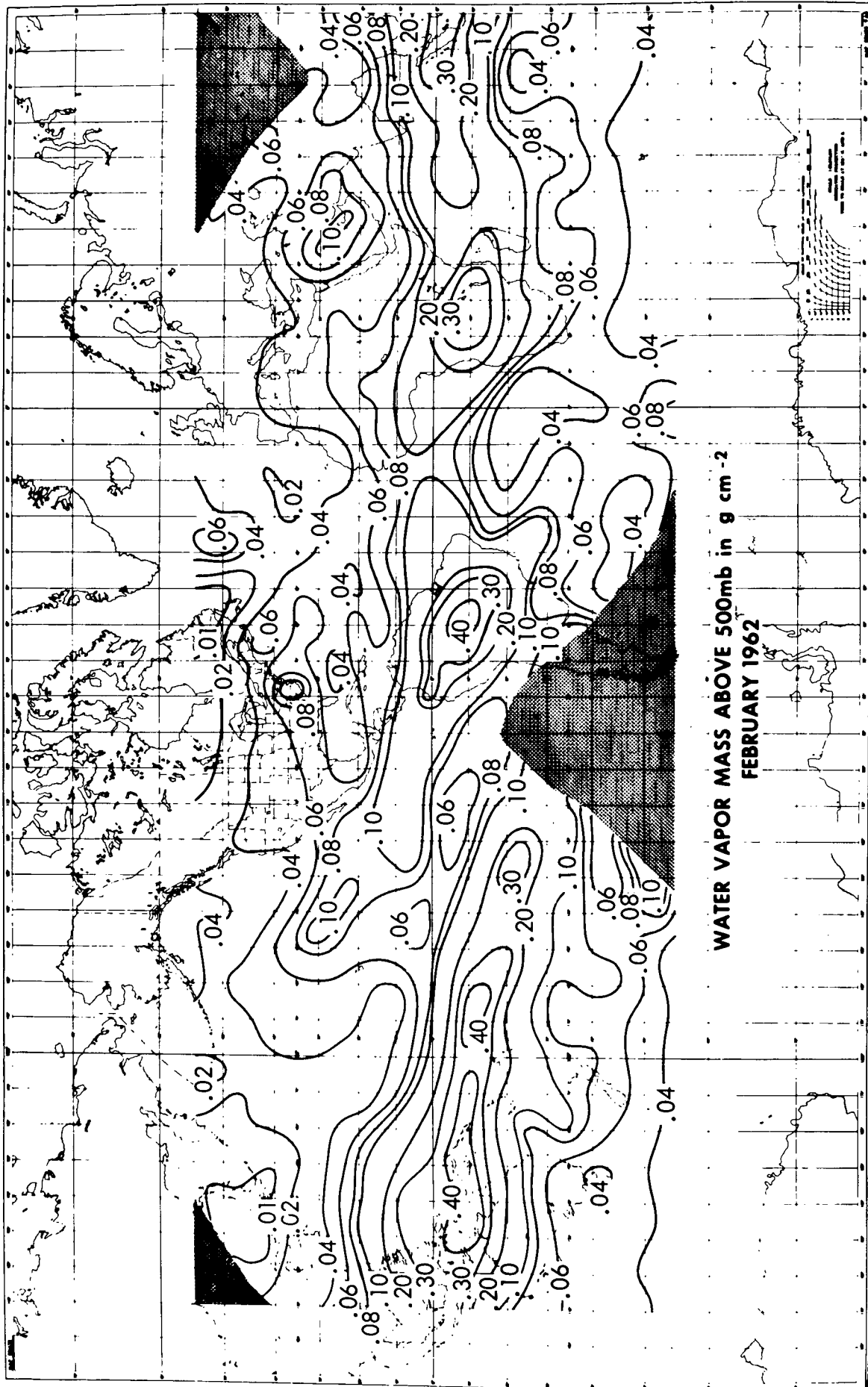


Figure 4. Quasi-global distribution of the water vapor mass above 500 mb during February 1962 inferred from coordinated TIROS IV 6.0-6.5 micron and 8.0-12.0 micron radiometric measurements (After Raschke and Bandeen, 1967b).

been improved by the application of a statistically-derived limb darkening function using infrared radiance data from the TIROS II, III, IV, and VII medium resolution scanning radiometers (Lienesch and Wark, 1967).

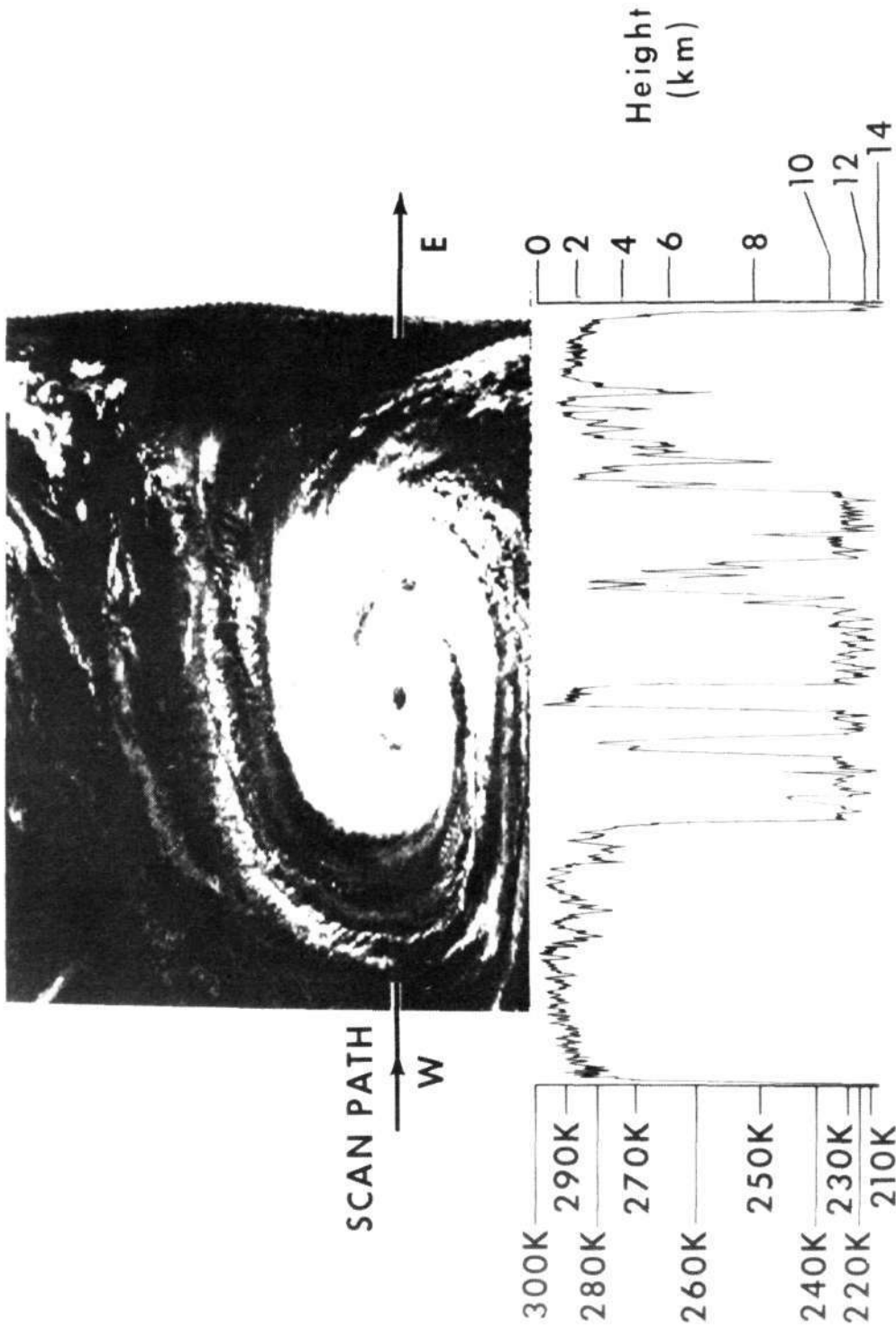
A number of analyses comparing the total outgoing long-wave radiative flux (deduced by the aforementioned method) with midtropospheric flow patterns, zonal kinetic energy, and available potential energy have been presented by Winston and Rao (1962), Winston and Rao (1963), Winston (1967a) and Winston (1967b). Also, by combining the total outgoing long-wave flux, inferred from the 8.0-30.0 micron or 8.0-12.0 micron measurements, with the albedo, inferred from the 0.2-6.0 micron or 0.55-0.75 micron measurements, analyses of the large-scale radiation balance have been carried out by Bandeen, et al. (1965), Rasool and Prabhakara (1966), and Vonder Haar (1968).

The 14.8-15.5 micron channel carried by the TIROS VII scanning radiometer measures emission from carbon dioxide in the atmosphere (cf. Figure 1). Because of the strength of the 15 micron band and because carbon dioxide is uniformly mixed (at least below the mesopause) in the atmosphere, the weighting function,  $d\tau/d \log p$  (where  $\tau$  is the mean normal transmittance to space over the effective spectral response and  $p$  is ambient pressure) of the 14.8-15.5 micron channel peaks at about 20 km (which is slightly higher than the peak of the weighting function for the spectrally broader 14.0-16.0 micron channel of the NIMBUS II MRIR shown in Figure 11). Thus, the 14.8-15.5 micron measurements can be interpreted in terms of mean temperatures of the lower stratosphere. Nordberg, et al. (1965), Warnecke (1966a), and Shen, et al. (1968) have discussed these data and shown that such events as sudden stratospheric warmings can be detected. Belmont, et al. (1968) have shown that a high correlation exists between the TIROS VII 15 micron data and 30 mb atmospheric temperatures. Kennedy and Nordberg (1967) made an harmonic analysis of the circumpolar temperature patterns and derived circulation features from the analysis.

### 3.4 High Resolution Infrared Radiometer (HRIR)

Nearly an order of magnitude increase in the linear resolution over previous satellite infrared radiometers was achieved with the launch of the first HRIR aboard NIMBUS I on 28 August 1964 (cf. Table 1, No. 4). In contrast to the TIROS medium resolution radiometer, the HRIR required a 45-degree rotating primary mirror to effect the transverse scan from the earth-oriented, three-axis stabilized NIMBUS spacecraft. The design of this instrument has been described by Foshee, et al. (1965). A description of the instrument is also given in the applicable Users' Guides (see, for example, NIMBUS II Users' Guide, 1966). The physical significance of the HRIR equivalent blackbody temperature measurements has been discussed by Kunde (1965), and investigations of the mesoscale resolutions possible and of characteristics of the HRIR data pertinent to such analyses have been carried out by Fujita and Bandeen (1965). Geophysical observations by the HRIR, such as cloud heights and sea surface and soil temperatures, have been discussed by Nordberg (1965), and HRIR measurements over the Antarctic ice pack and other polar features have been reported by Popham and Samuelson (1965).

The meteorological interpretation of HRIR data has been discussed by such authors as Nordberg and Press (1964), Widger, et al. (1965), Widger (1966), Nordberg, et al. (1966), and Allison, et al. (1966a). A photo facsimile depiction of hurricane Gladys and a single analog trace drawn to the same west-to-east scale are shown in Figure 5; hence,



### ANALOG TRACE OF SINGLE SCAN

Figure 5. An HRIR depiction of hurricane Gladys at 0422 UT, 18 September 1964. The HRIR photofacsimile picture of the hurricane is compared to a single HRIR analog trace through the eye of the hurricane. The analog trace is related to equivalent blackbody temperature ( $T_{BB}$ ) values given on the left. Geometric height above sea level is related to  $T_{BB}$  values by means of the 0000 UT 18 September 1964 radiosonde sounding from Kindley Air Force Base, Bermuda (After Allison et al., 1966a).

a given feature in the picture corresponds to the same feature in the analog trace underneath. The observed radiation intensities, expressed in °K, are measured along the left hand ordinate. The blackbody temperatures were converted to height on the basis of an actual temperature sounding. The corresponding heights are shown along the right hand ordinate (Allison, et al., 1966a).

The capability of the HRIR to detect and track storms at night is illustrated in Figure 6. Tropical storm Ruby was initially detected by the NIMBUS HRIR at 1500 UT, 31 August 1964, almost 21 hours before aerial reconnaissance located the storm. On four subsequent occasions in the week that followed, the HRIR tracked the course of Ruby across the Pacific until it passed full-blown over Hong Kong and dissipated over mainland China (Allison, et al., 1966a).

Another application of high resolution radiation data is the observation of sea surface temperatures and ocean currents. The importance of the temperature of the sea surface boundary has been emphasized by the Global Atmospheric Research Program (GARP) Report of the Study Conference held in Stockholm (1967). Under clear sky conditions, sea surface temperatures can be determined with an accuracy of  $\pm 1$  to  $2^\circ\text{K}$  (Warnecke, et al., 1968a). The remote detection of the Gulf Stream boundary by the NIMBUS II HRIR is shown in Figure 7, in which temperature gradients of  $5^\circ$  to  $10^\circ\text{K}$  over 20 km along the north wall were measured (Warnecke, 1968b).

In addition to the primary stored-data mode of operation, the HRIR experiments on NIMBUS II and III were adapted to the Automatic Picture Transmission (APT) system whereby local reception of the data in real time was possible the world over whenever the spacecraft came within line-of-sight range of a relatively simple and inexpensive groundstation (Nordberg, et al., 1966; Goldshlak, 1968).

Because of the intensity of the solar spectrum in the wavelength interval 3.5-4.1 microns, reflected solar radiation may be appreciable in daytime HRIR measurements, adding to the emitted radiation and making interpretations of the measurements in terms of surface temperatures ambiguous. Thus only nighttime measurements can be interpreted in terms of true surface temperatures. In order to eliminate possible ambiguities in daytime measurements, the NIMBUS III HRIR has a second passband, 0.7-1.3 microns, wherein reflected solar radiation predominates over emission at normal atmospheric and surface temperatures. However, at nighttime, the NIMBUS III HRIR makes measurements of emission only in the interval 3.5-4.1 microns, just as its two predecessors did. (For another view of NIMBUS HRIR data, see Figure 18.)

### 3.5 Medium Resolution (Infrared) Radiometer (MRIR)

The NIMBUS MRIR was similar in many respects to the earlier TIROS medium resolution scanning radiometer, but it represented an entirely new instrumental design, incorporating a 45-degree rotating primary mirror (similar to that of the HRIR) to effect the transverse scan necessary from the earth-oriented, three-axis-stabilized NIMBUS spacecraft. The first MRIR was launched aboard NIMBUS II on 15 May 1966 (cf. Table 1, No. 5). A description of the instrument is given in the applicable Users' Guides (see, for example, NIMBUS II Users' Guide, 1966).

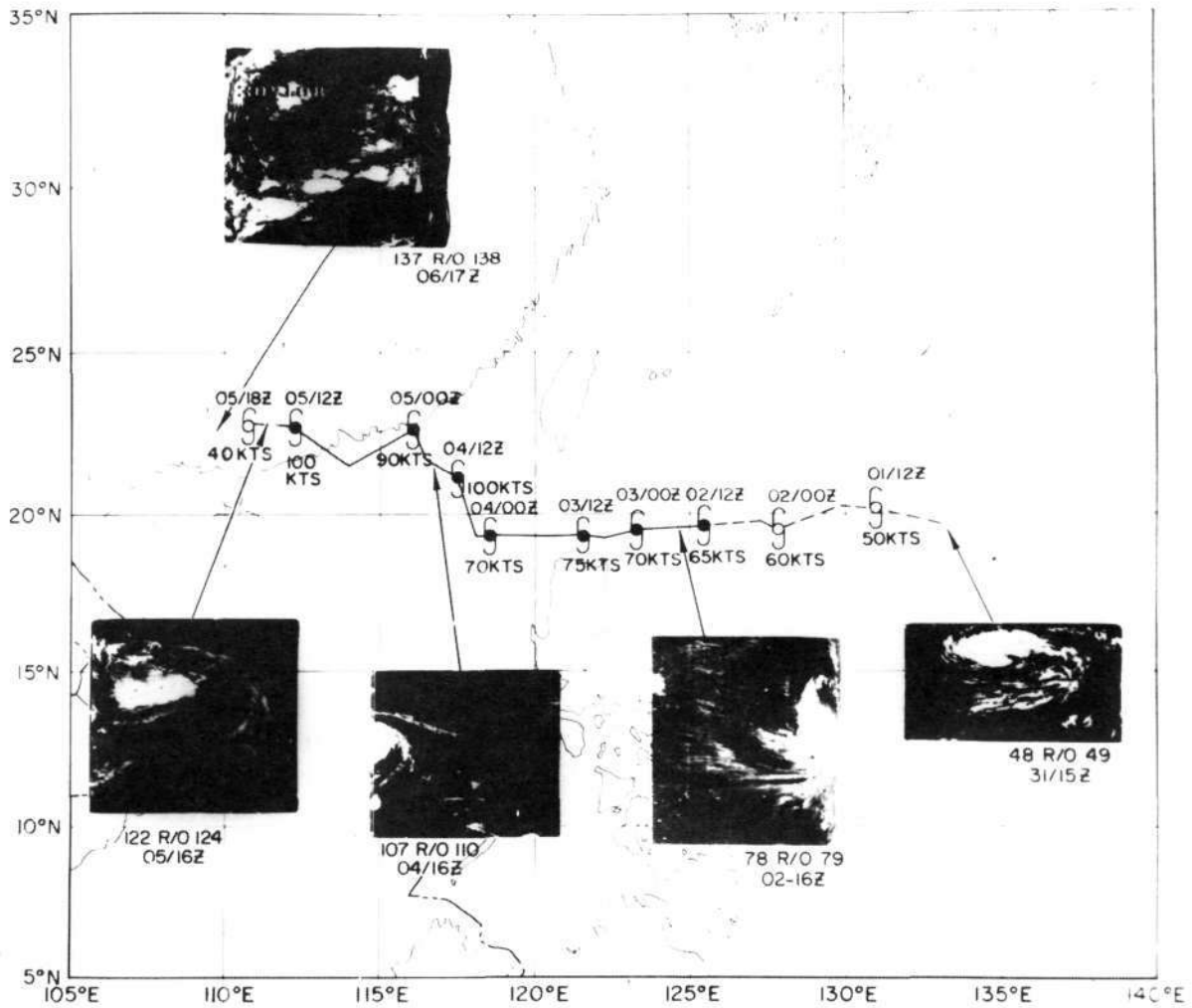


Figure 6. Track of typhoon Ruby from 31 August to 6 September 1964 with inserts of five Nimbus I HRIR photofacsimile depictions of Ruby in the western Pacific Ocean (After Allison et al., 1966a).

The application of the data is very similar to that of the earlier TIROS instrument. An advantage of the NIMBUS MRIR is that it views the entire globe, while the TIROS radiometer did not view poleward of about latitude  $63^\circ$  because of the lower inclination of the TIROS orbit. Global radiation balance studies have been carried out by Möller (1967), Raschke, Möller, and Bandeen (1968), Raschke and Pasternak (1968), and Raschke (1968).

An example of the total outgoing long-wave radiation inferred from the NIMBUS II 5.0-30.0 micron data by the method of Wark et al. (1962) is shown in Figure 8 (Raschke and Pasternak, 1968). The other component of the radiation balance, the absorbed solar radiation, follows from measurements of the albedo and a knowledge of the solar constant.

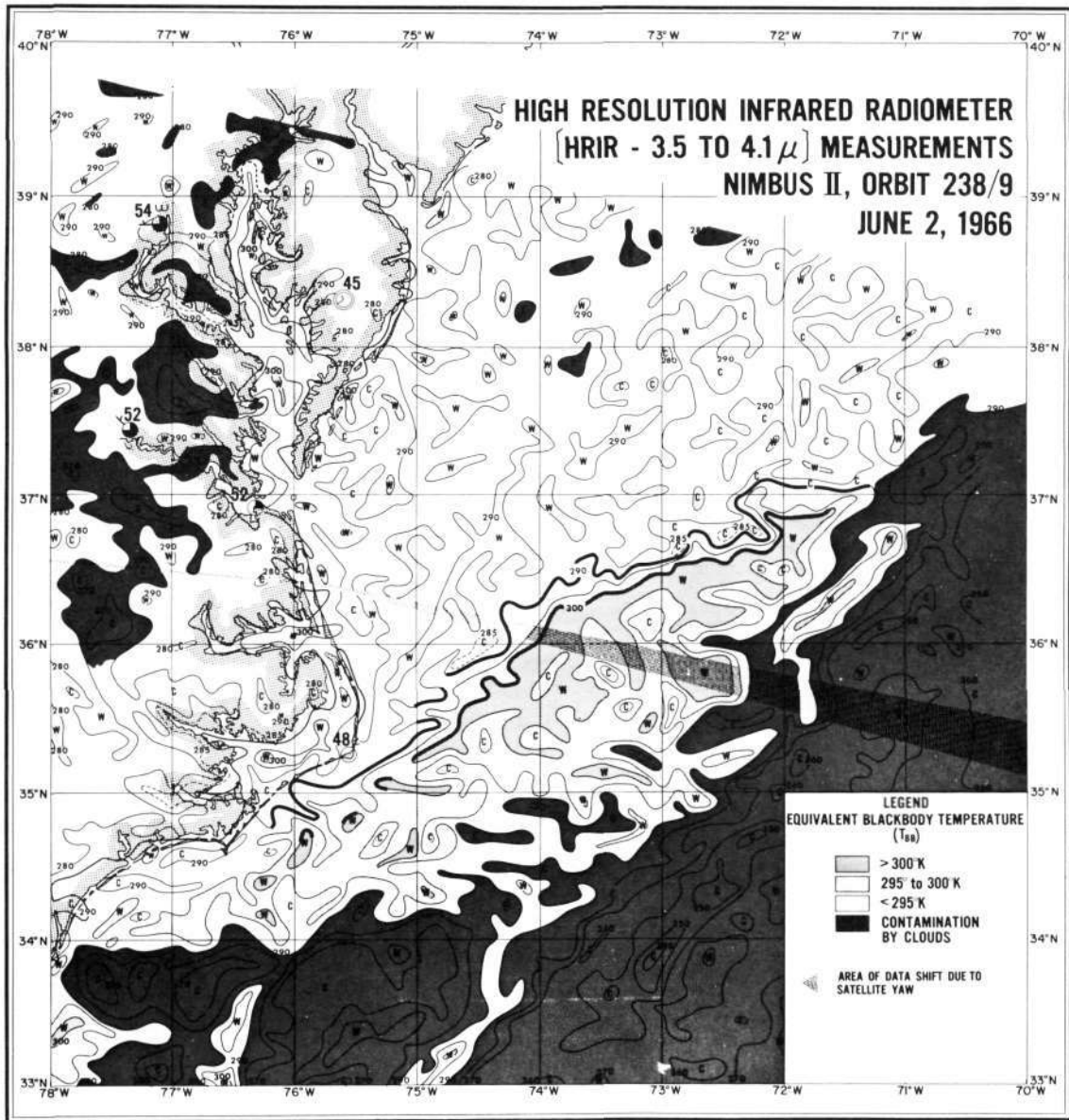


Figure 7. Remote detection of the Gulf Stream boundary by Nimbus II HRIR measurements (After Warnecke, 1968b).

The interpretation of the 15 micron channel measurements in terms of mean temperatures of the lower stratosphere and of stratospheric circulation patterns has been carried out, as it was previously for TIROS VII. The weighting function  $d\tau/d(\log p)$  for the 14.0-16.0 micron channel of NIMBUS II is shown by the dashed curve in Figure 11. (Because of the narrower spectral interval covered by the NIMBUS III 15 micron channel, its weighting function peaks about 2 km higher than the dashed curve of Figure 11.)

The capability of the NIMBUS II 15 micron data to map stratospheric temperatures on a global scale is shown in Figure 9. The maximum temperature of 240°K is centered over the summer North Pole and the isotherms in the Northern Hemisphere are generally zonal in character with gentle meridional gradients. In the Southern Hemisphere the isotherms are also zonal character but with much stronger meridional gradients in the intense winter polar vortex centered around the South Pole where the minimum temperature of 196°K is found (Warnecke and McCulloch, 1968c).

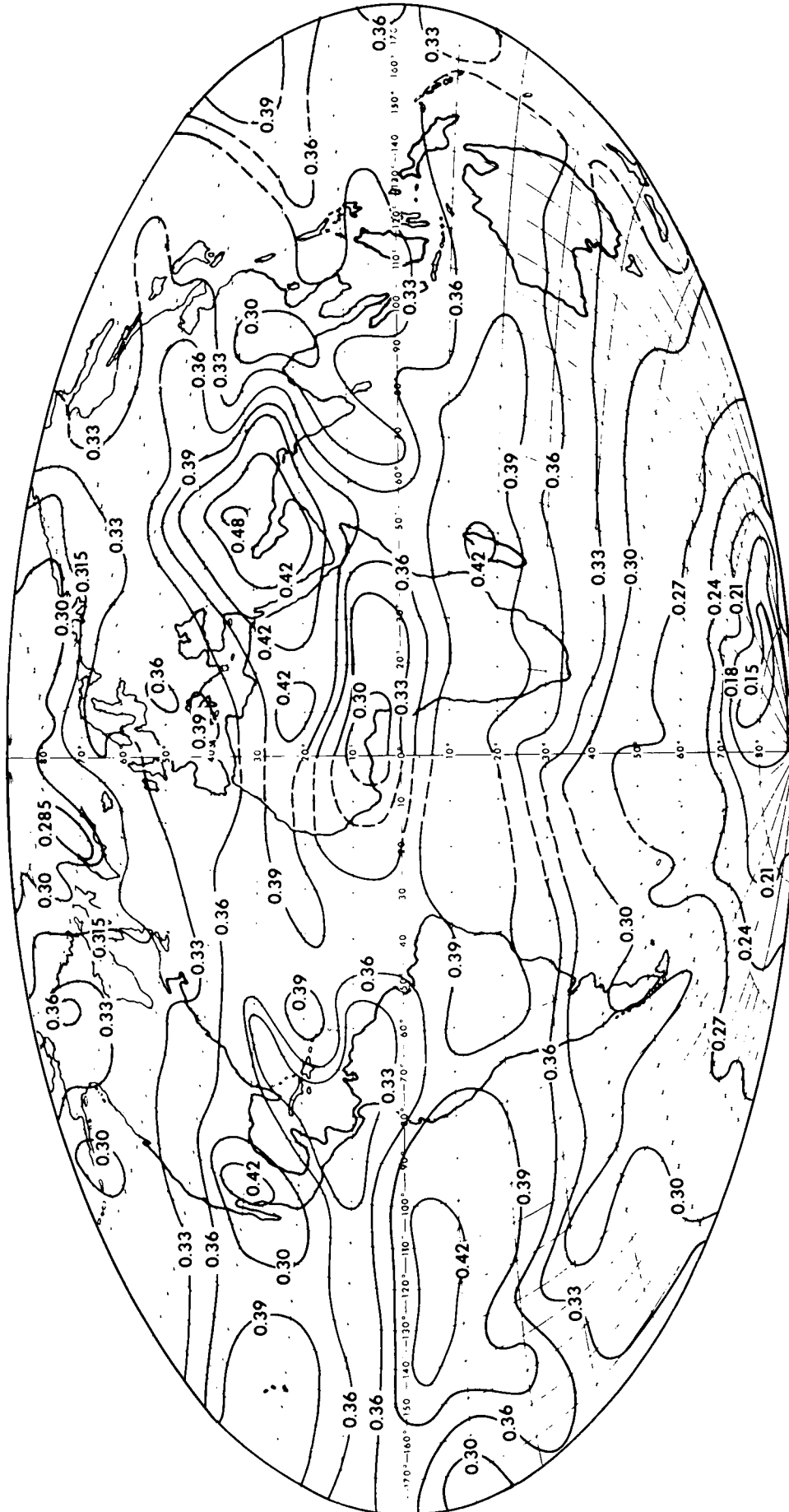


Figure 8. Outgoing total long-wave radiation in  $\text{cal cm}^{-2} \text{ min}^{-1}$ , inferred from the Nimbus II 5.0-30.0 micron data and averaged over the period 1-15 June 1966 (After Raschke and Pasternak, 1968).

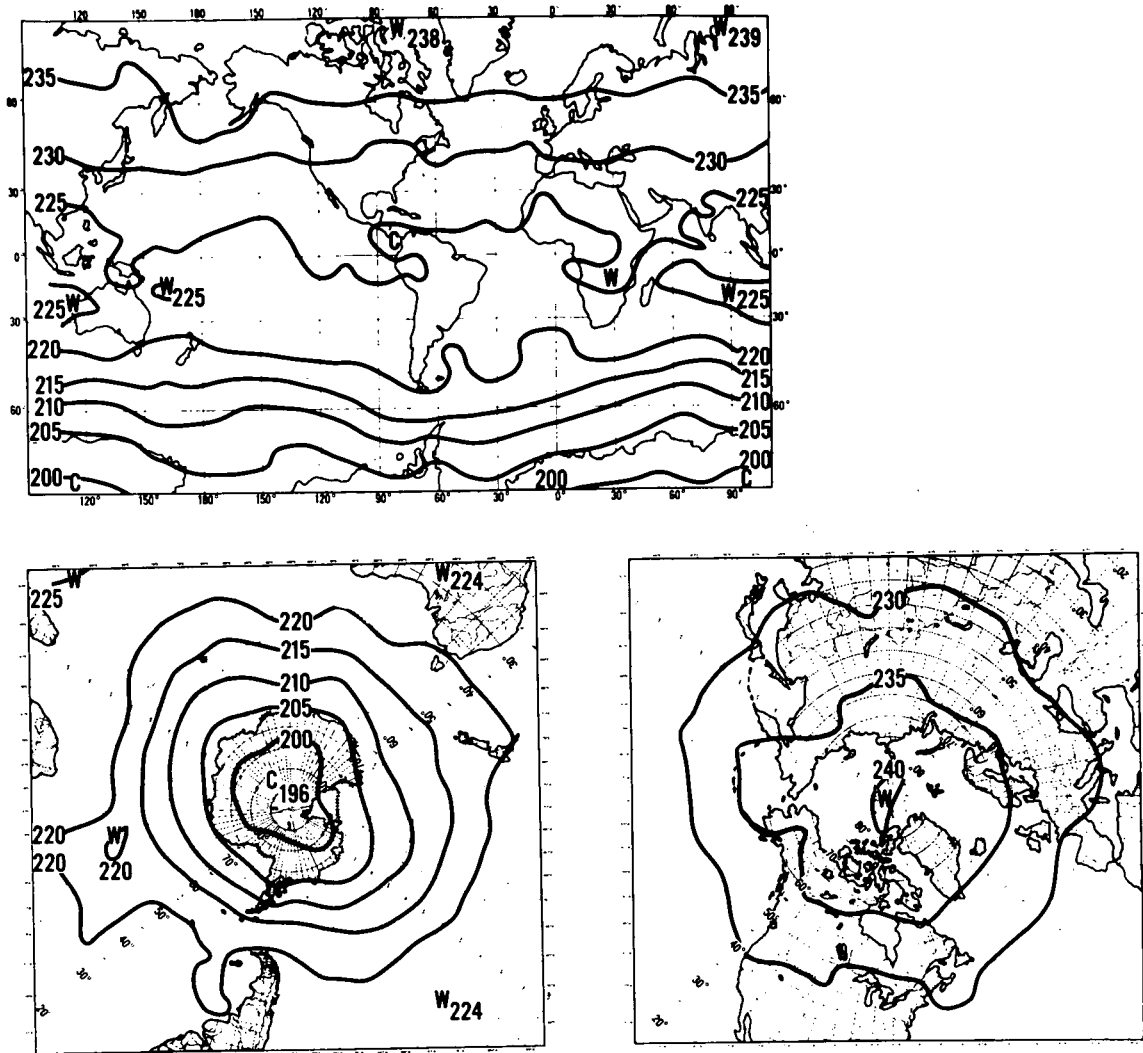


Figure 9. Global stratospheric temperature distribution ( $^{\circ}\text{K}$ ) from Nimbus II 15 micron measurements on 1 July 1966 (After Warnecke and McCulloch, 1968c).

Figure 10 (top) shows a composite of the cloud picture observed by the 11 micron channel in the belt  $30^{\circ}\text{N} - 30^{\circ}\text{S}$  at local noon on 5 June 1966 except for the two passes near  $140^{\circ}\text{E}$  and  $170^{\circ}\text{E}$  which were obtained at local midnight (Nordberg *et al.*, 1966). Although activity was relatively weak on this day the course of the ITCZ can be followed around the entire globe. The 6.4-6.9 micron water vapor channel observations shown in Figure 10 (bottom) were made simultaneously over the ITCZ. The dark regions on both sides of the cloud zone indicate strong subsidence. Near  $140^{\circ}\text{W}$  the northern band is quite narrow near  $30^{\circ}\text{N}$  over the Pacific and North America and is possibly indicative of the subtropical jet stream. Further east the northern zone of subsidence becomes considerably wider as is the entire southern zone. These wide, dry regions are indicative of the subtropical anticyclones. The warmest (driest) region observed in this channel is in the southern zone near  $40^{\circ}\text{W}$  over eastern Brazil where very strong downward motion can be inferred.

The NIMBUS III MRIR carries a channel sensing in the weakly absorbing 20.0-23.0 micron interval of the rotation band of water vapor (cf. Table 1, No. 5). Radiation sensed by this channel emanates from the lower tropospheric layers, in contrast to the radiation emanating from upper tropospheric layers (i.e., approximately 600 mb to 200 mb) detected

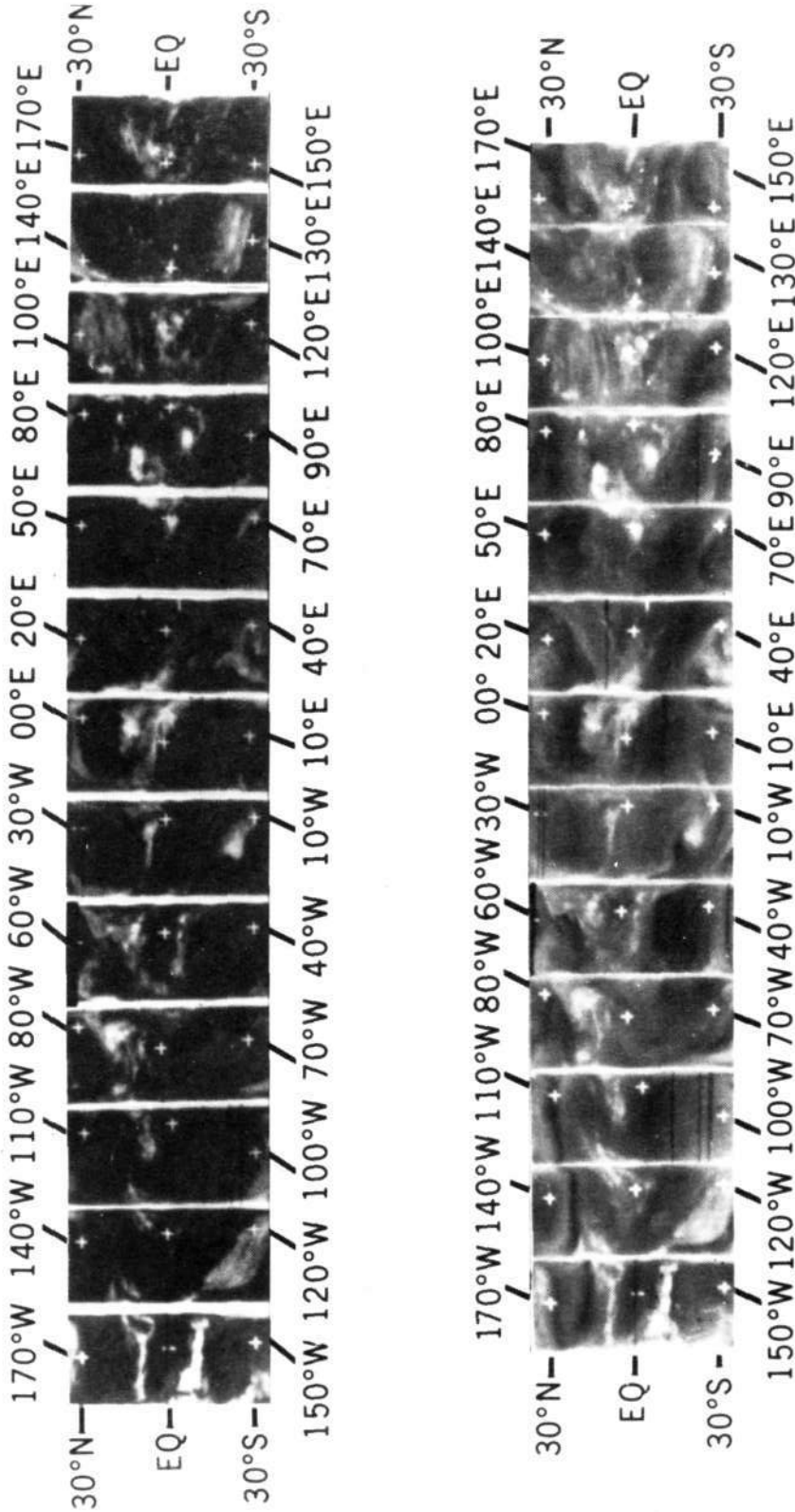


Figure 10. Cloud formations around the globe between 30°N and 30°S observed in the Nimbus II MRIR 10.0-11.0 micron channel (upper band) and 6.4-6.9 micron channel (lower band). Each band is composed of thirteen orbital passes. Reading from right to left, passes 3 through 13 were observed sequentially near local noon on 5 June 1966. Because daytime data over longitudes 130°E to 170°E were not acquired, passes 1 and 2 shown at the right were observed 12 hours later near local midnight (After Nordberg et al., 1966).

by the 6.4–6.9 micron channel, whose spectral interval is centered in a strongly absorbing part of the 6.3 micron band (cf. Figure 1). Although the satellite data are not yet available, it is expected that data from the two water vapor channels will yield additional information on the stratification of vertical motions and moist and dry layers.

### 3.6 General Discussion of Remote Vertical Sounding

The radiometric instruments discussed heretofore have all sensed radiation in relatively broad spectral intervals and have yielded data having a predominantly two dimensional character, e.g., maps of outgoing radiation originating either at cloud, ground, or water surfaces or within thick regions of the atmosphere. Examples of the latter are maps of mean stratospheric temperatures from the 14.0–16.0 micron channel of the NIMBUS II MRIR. The weighting function for this channel in the 1962 ARDC model atmosphere is shown by the dashed curve in Figure 11. At the half-amplitude points, this curve is more than 20 km thick. When the width of the spectral interval is reduced the shape of the weighting function becomes considerably more peaked and its thickness in the vertical smaller. This sharpening of the weighting function results from the lesser variability of the absorption coefficient over the narrower spectral interval as compared to the broader interval. (Note, however, that in the theoretical limit—for monochromatic radiation—the corresponding width of the weighting function is still about one scale height; cf. Figure 16.)

Five weighting functions for  $5\text{ cm}^{-1}$  intervals centered at the indicated wave numbers within the 15 micron carbon dioxide absorption band are shown by the solid curves in Figure 11. The weighting functions located high in the atmosphere correspond to strong absorption whereas those peaking at lower altitudes correspond to weaker absorption.

Although King (1956) originally suggested the possibility of inferring the vertical temperature profile from a nadir scan at one frequency, Kaplan (1959) first suggested the inference of the vertical temperature profile from a frequency scan in the nadir within the 15 micron carbon dioxide band at a spectral resolution of about  $5\text{ cm}^{-1}$ . Subsequently a number of authors discussed the problem of remotely inferring vertical atmospheric structure, among them Wark (1961), King (1964), Wark and Fleming (1966), Twomey (1966), Conrath (1967), and Conrath (1968).

The need for remotely sensed vertical profiles of temperature and other meteorological parameters for use in numerical models of the atmosphere during the World Weather Program of the 1970's, including the Global Atmospheric Research Program (GARP), was set forth in the GARP Report of the Stockholm Study Conference (1967). Five different instruments in Table 1 (No.'s 6, 7, 9, 10, and 12) have as a primary purpose the measurement of infrared radiances for inferring such vertical profiles. These will be discussed in turn below.

### 3.7 Infrared Interferometer Spectrometer (IRIS)

The IRIS is a Michelson interferometer employing a beamsplitter which divides the incoming radiation into two approximately equal components, one directed toward a fixed mirror and the other toward a moving mirror. After reflection from the mirrors, the two beams interfere with each other with a phase proportional to the optical path difference between both beams. The recombined components are then focused onto the

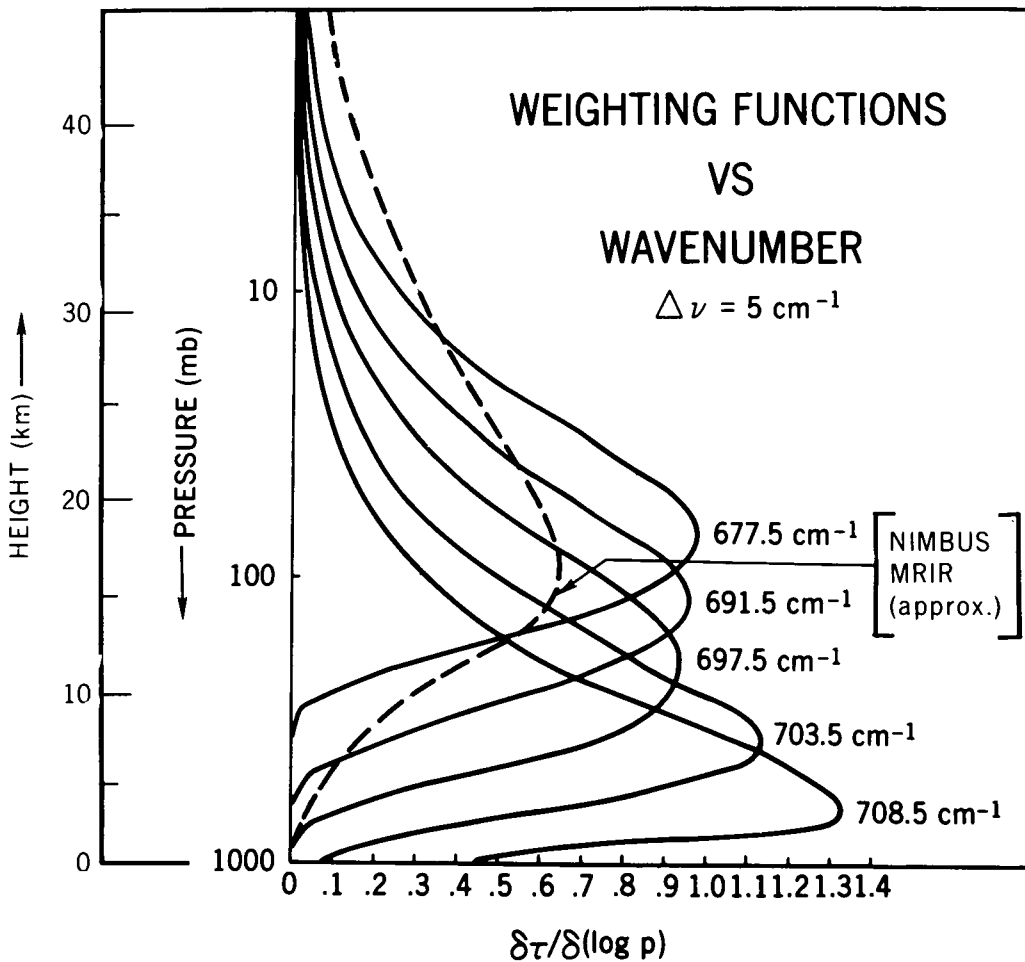


Figure 11. Fifteen micron carbon dioxide absorption band weighting functions (solid lines). The  $5 \text{ cm}^{-1}$  wide spectral intervals were chosen with mid-points at the indicated wavenumbers (After Conrath, 1968). The weighting function for the 14.0–16.0 micron channel of the Nimbus II MRIR (dashed line) is superimposed on the figure for comparison.

detector where the intensity is recorded as a function of the path difference. For a continuous spectrum, the superposition of many amplitudes of various frequencies takes place. The resultant combined signal is called the interferogram. The spectrum is reconstructed from the interferogram by applying an inverse Fourier transform.

The IRIS views in the nadir direction from the earth-oriented NIMBUS spacecraft. The first IRIS was launched aboard NIMBUS III in May 1968 (cf. Table 1, No. 6a). The design of the instrument has been described by Hanel and Chaney (1966). A description of the instrument is also given in the NIMBUS III User's Guide (1968).

Although at this writing satellite data are not yet available, data have been acquired from a breadboard version of the IRIS flown on a high altitude balloon from Palestine, Texas, on 8 May 1966. The balloon flight and some results from it have been discussed by Chaney, Drayson, and Young (1967). Conrath (1967) also has analyzed the balloon data in terms of inferred temperature and water vapor profiles.

A spectrum obtained with the breadboard version of the IRIS flown at the 7 mb level by the High Altitude Engineering Laboratory of the University of Michigan for the Goddard

Space Flight Center is shown in Figure 12. Included within the spectral interval of this instrument,  $500\text{ cm}^{-1}$  (20 microns) to  $2000\text{ cm}^{-1}$  (5 microns), are the water vapor absorption band centered at 6.3 microns, the 9.6 micron ozone band, and the 15 micron carbon dioxide band. Hence, information on atmospheric water vapor and ozone should be available from these data, as well as vertical temperature structure from the 15 micron band (Conrath, 1967).

A temperature inversion for the troposphere obtained from IRIS Palestine balloon flight data (such as those of Figure 12) is shown in Figure 13. For comparison data from the 1200 Z and 1800 Z flights of the nearest radiosonde station (Shreveport, Louisiana) are also plotted in Figure 13. At this point it is well to recall that there is some overlapping water vapor absorption in the 15 micron  $\text{CO}_2$  band (cf. Figure 1) which should be taken into account if accurate temperature inversions are to be obtained in the lower troposphere. Thus, the water vapor and temperature inversions are essentially coupled. In practice, one can take advantage of the relatively weak dependence of the temperature inversion on water vapor and use a first guess at the humidity profile to obtain a temperature inversion. The resulting temperature profile can be used to do a water vapor inversion in the 6.3 micron band. This procedure can be iterated as many times as necessary (Conrath, 1967).

A two-parameter water vapor mixing ratio inversion of IRIS data from the Palestine balloon flight is shown in Figure 14. Radiosonde data taken the same day at Shreveport are included in the figure (Conrath, 1967). In this trial water vapor inversion, the average temperatures from the two radiosonde runs furnished the necessary knowledge of the temperature profile. In actual operations using satellite data, this knowledge would be obtained from an inversion of 15 micron data, such as that performed to yield the profile of Figure 13.

Conrath (1967) also briefly discussed the problems attending the inversion of spectra in the 9.6 micron band to infer the vertical distribution of ozone. He points out that the atmosphere is not optically thick even in the strongest part of the 9.6 micron band and that the bulk of the ozone in a typical distribution is located at heights where the pressure broadening of individual lines is low. Weighting functions calculated by Bolle (1967) show widths greater than the characteristic heights over which the ozone concentration varies. Conrath (1967) concludes that it will be difficult to extract information on the vertical ozone distribution in any detail with IRIS data.

The second IRIS is scheduled to fly on NIMBUS D (cf. Table 1, No. 6b). It will be a somewhat modified version of the first instrument, e.g., the spectral coverage will be shifted to longer wavelengths to include the rotation band of water vapor, and both the spectral and spatial resolutions will be increased (Hanel, 1968).

### 3.8 Satellite Infrared Spectrometer (SIRS)

The SIRS is a modified Fastie-Ebert grating spectrometer. The radiant energy is detected behind each exit slit by a wedge-immersed thermistor bolometer. Design considerations leading to the satellite version have been discussed by Dreyfus and Hilleary (1962) and Hilleary, *et al.* (1966).

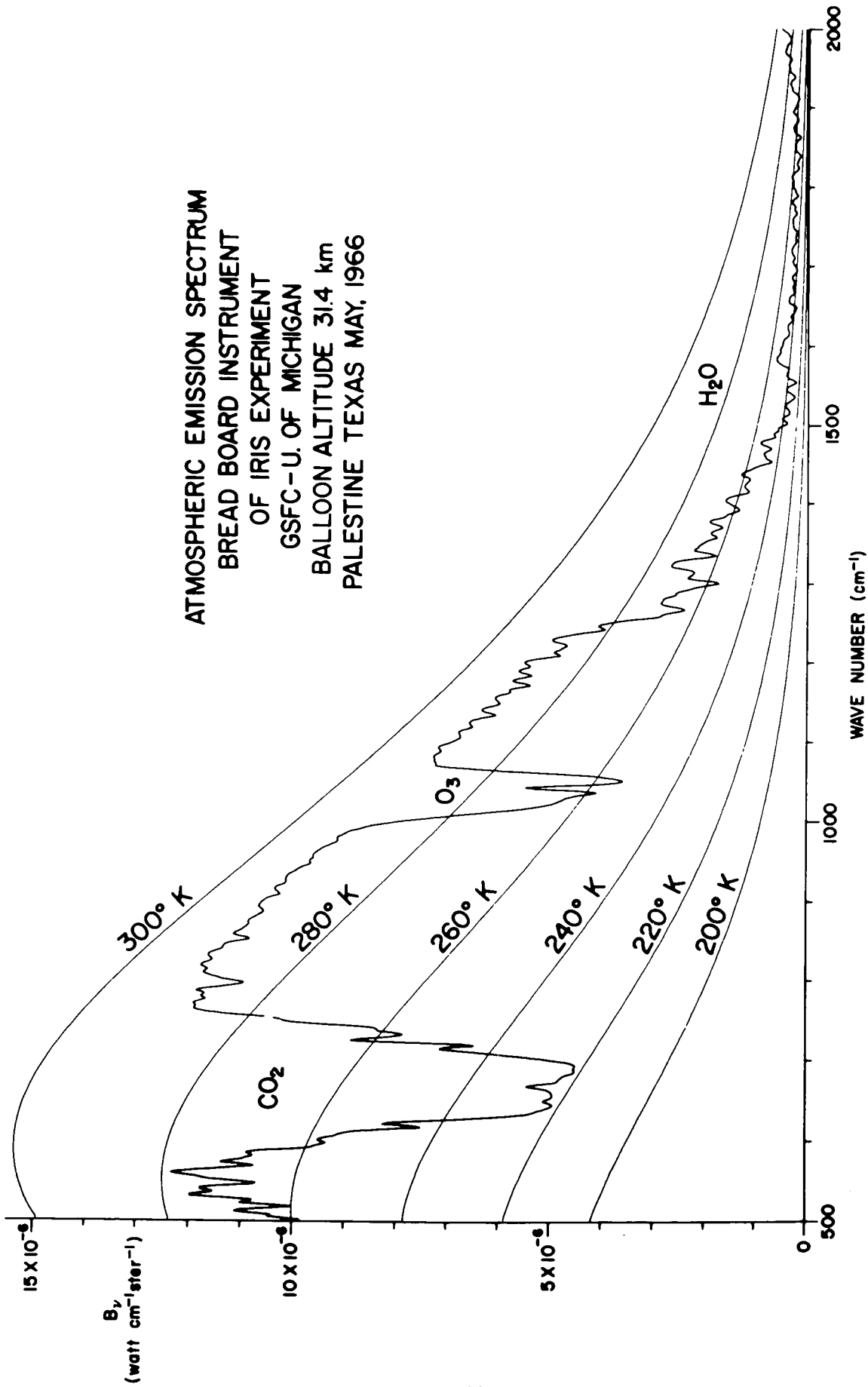


Figure 12. Atmospheric spectrum acquired with a breadboard version of an IRIS instrument in a balloon flight, 8 May 1966, from Palestine, Texas (After Conrath, 1967).

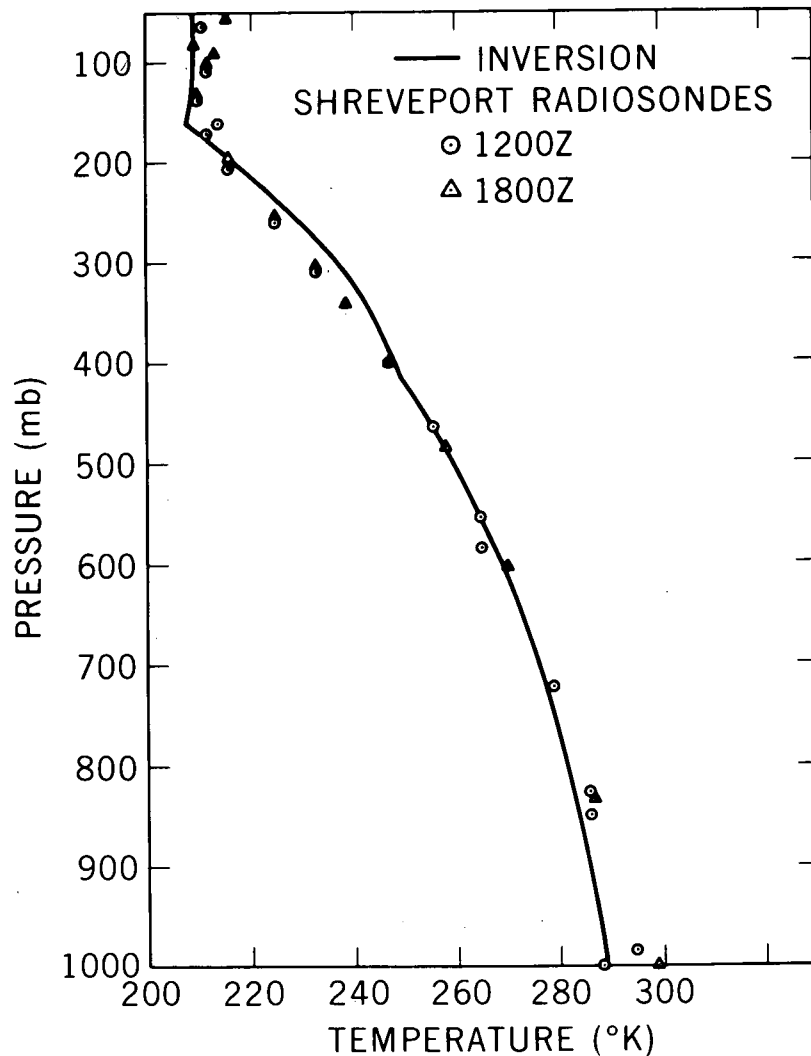


Figure 13. Tropospheric temperature inversion from IRIS data in the 15 micron carbon dioxide band. The data were acquired during the balloon flight on 8 May 1966 from Palestine, Texas (After Conrath, 1967).

The SIRS views in the nadir direction from the NIMBUS spacecraft. The first SIRS was launched aboard NIMBUS III in May 1968 (cf. Table 1, No. 7a). A description of the flight instrument and a discussion of the experiment are given in the NIMBUS III Users' Guide (1968). The mid-points of the  $5 \text{ cm}^{-1}$  wide spectral intervals sensed over the 15 micron carbon dioxide band are the following:  $669.0 \text{ cm}^{-1}$ ,  $677.5 \text{ cm}^{-1}$ ,  $692.0 \text{ cm}^{-1}$ ,  $699.0 \text{ cm}^{-1}$ ,  $706.0 \text{ cm}^{-1}$ ,  $714.0 \text{ cm}^{-1}$ , and  $750.0 \text{ cm}^{-1}$ . The eighth channel senses radiation in the atmospheric window, centered at  $899.0 \text{ cm}^{-1}$ .

Although at this writing satellite data are not yet available, analyses of data from ground-based instruments similar to SIRS have been carried out by James (1967) and Wolk and Van Cleef (1967), and results from balloon-borne versions of SIRS have been reported by Hilleary, *et al.* (1965) and Wark, *et al.* (1967). Figure 15 shows a temperature profile in clear skies deduced from data from a spectrometer flown on a balloon from Palestine, Texas, on 11 September 1964.

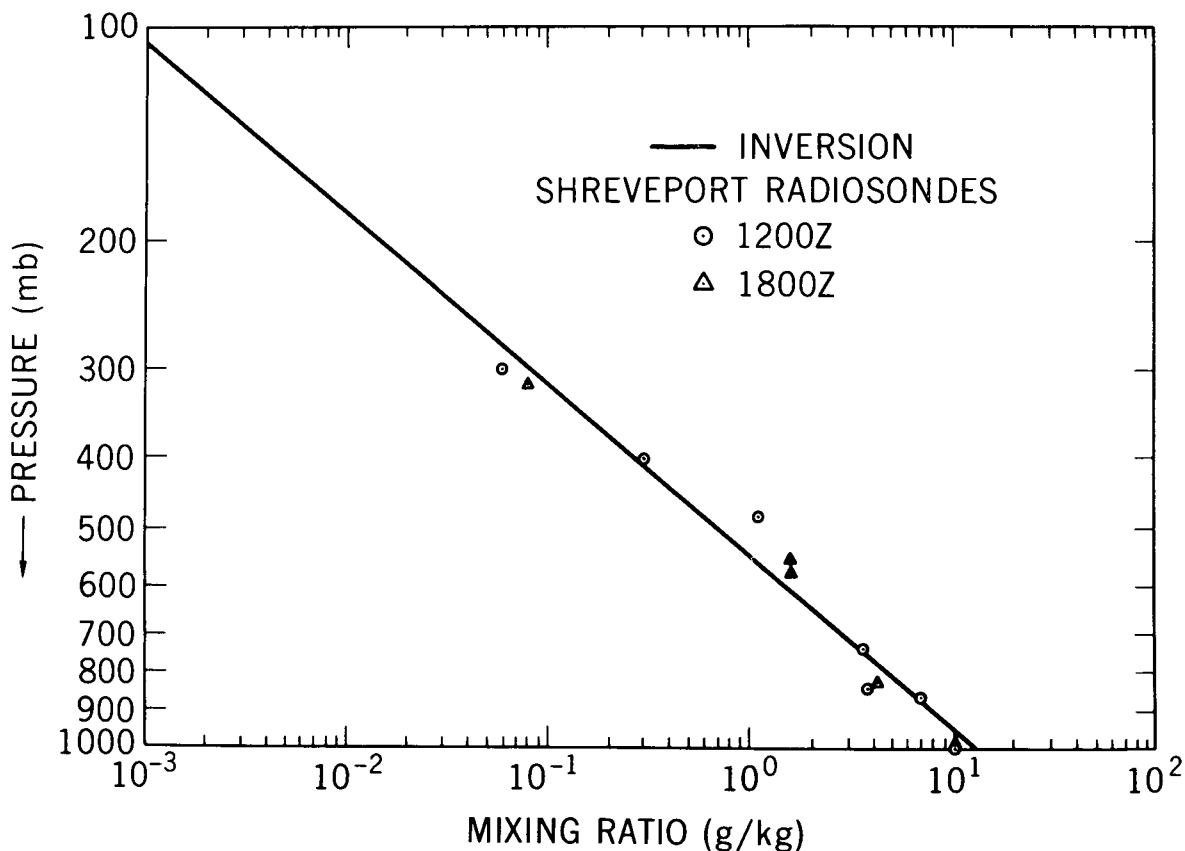


Figure 14. Two-parameter water vapor mixing ratio inversion from IRIS data in the 6.3 micron band. The data were acquired during the balloon flight on 8 May 1966 from Palestine, Texas (After Conrath 1967).

The second SIRS is scheduled to fly on NIMBUS D (cf. Table 1, No. 7b). It will be an augmented version of the first instrument, viz., in addition to the eight channels of the first SIRS, the second will have six channels sensing in  $5\text{ cm}^{-1}$  wide spectral intervals over the rotation band of water vapor. The mid points of these intervals are the following:  $280.0\text{ cm}^{-1}$ ,  $302.5\text{ cm}^{-1}$ ,  $290.5\text{ cm}^{-1}$ ,  $424.5\text{ cm}^{-1}$ ,  $488.0\text{ cm}^{-1}$ , and  $531.5\text{ cm}^{-1}$ . The purpose of adding the six additional channels is to acquire data for deducing water vapor (as well as temperature) profiles. Another significant modification in the NIMBUS D SIRS is a step-scanning feature by which the optical axis of the spectrometer will view at a nadir angle of  $25^\circ$ -to- $39^\circ$  to the left for one minute, followed by viewing in the nadir direction for a second minute, followed by viewing at a nadir angle of  $25^\circ$ -to- $39^\circ$  to the right for a third minute. This cycle will be repeated continuously, and the side-viewing nadir angles will be programmed to vary from  $39^\circ$  (at the equator) to  $25^\circ$  at high latitudes in order to effect an optimum grid spacing for computer input data for numerical modelling (Wark, 1968).

### 3.9 ITOS High Resolution Radiometer

A High Resolution Radiometer is being developed for the second generation operational meteorological satellite system, also called the Improved TIROS Operational Satellite System-ITOS (Operational Satellites Office, 1968). Selected characteristics of this radiometer are given in Table 1, No. 8. This instrument will be mounted on the earth-oriented, three-axis-stabilized platform of the gyro-magnetically controlled ITOS

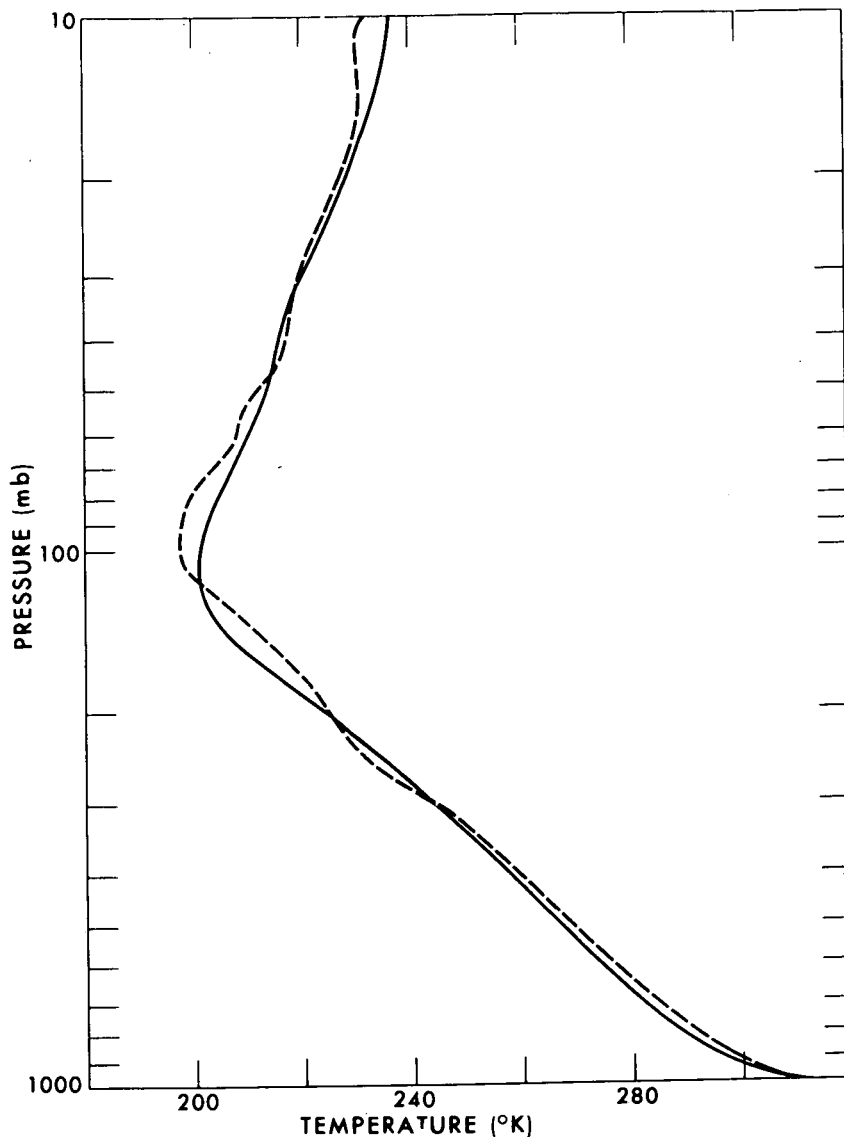


Figure 15. Deduced temperature profile in clear skies from data in the 15 micron carbon dioxide band acquired at 7:57 a.m. CST by a balloon borne version of SIRS (solid line). The balloon was launched to an altitude of 100,000 ft. on 11 September 1964 from Palestine, Texas. The dashed line is the noon CST profile from the Fort Worth radiosonde (After Wark et al., 1967).

vehicle and, therefore, will have a primary mirror scanning transverse to the spacecraft motion much like the NIMBUS HRIR and MRIR. The ITOS High Resolution Radiometer, although essentially duplicating spectrally two of the channels of the TIROS and NIMBUS Medium Resolution Radiometers, will have the advantage of a much higher spatial resolution (even somewhat higher than that of the NIMBUS HRIR). Hence, the quality of the photo-images should approach that of television cameras. Also, the probability in areas of partial cloud cover of either cloud elements or land or water surfaces completely filling the instantaneous field of view of the instrument will be vastly increased. Obviously under these conditions the interpretation of the data in terms of cloud top and land and sea surface temperatures will be more meaningful. Although the ITOS Radiometer is improved only slightly over the NIMBUS HRIR in spatial

resolution, it will be a decided improvement over the latter by being able to measure surface temperatures in the 10.5-12.5 micron interval equally well both day and night, and by being able to determine whether an area is cloud-free in the daytime by means of the synchronized visible channel measurements. Thus satellite measurements of land and sea surface temperatures and temperature gradients will be of increased accuracy and, consequently, increased usefulness in such applications as meteorology, oceanography, geomorphology, etc.

In addition to the stored-data mode of operation, the 10.5-12.5 micron channel of the ITOS High Resolution Radiometer will be adapted to the Automatic Picture Transmission (APT) system, constituting a Direct Readout of Infrared (DRIR) system. The DRIR system will operate throughout the entire orbit, reading out infrared imagery to APT stations all over the world in the nighttime and in the daytime as well (when the infrared data will be interleaved with the Standard APT pictures) (Operational Satellites Office, 1968).

### 3.10 Selective Chopper Radiometer (SCR)

A Selective Chopper Radiometer (SCR) is being developed to fly on NIMBUS D for the purpose of atmospheric temperature sounding (cf. Table 1, No. 9). The SCR will view in the nadir direction from the NIMBUS spacecraft. The basic optical system consists of a movable mirror, simple flapping choppers arranged in opposed pairs, germanium lens optical systems, interference filters, and a light pipe to condense radiation onto a thermistor bolometer detector. A description of the radiometer and a discussion of the experiment have been given by Peckham, et al. (1966) and by the Oxford Reading Group (1966).

A distinctive feature of the SCR is the use of very narrow band interference filters combined with CO<sub>2</sub> selective chopping and absorption cells to lessen the effective variation of the absorption coefficient over the spectral interval and, hence, to improve the height resolution of the weighting function and to make possible the measuring of the vertical temperature structure from the ground (or highest cloud top) to 50 km.

In connection with the channels associated with the two weighting functions peaking at the higher altitudes, a technique of selective chopping by CO<sub>2</sub> is used. The incoming radiation beam is switched between a cell containing CO<sub>2</sub> and a nearly-empty cell containing only a small amount of CO<sub>2</sub> at very low pressure. This technique has the effect of sensing only the radiation near the strongly-absorbing line centers (except the very centers of the lines, which are eliminated by the nearly-empty cell, thus further sharpening the weighting functions).

For the channels associated with the four weighting functions peaking at the lower altitudes, a single absorption cell is used to absorb out the line centers. This technique has the effect of sensing only the radiation toward the weakly-absorbing wings of the lines. A weighting function applying to a single absorption cell (C) is compared in Figure 16 with weighting functions applying to monochromatic radiation (M) and to a spectrometer (such as IRIS and SIRS) sensing over a spectral interval including many individual lines (S). An Elsasser band model was used in carrying out the calculations for Figure 16. It is seen that the absorbing cell weighting function differs very little from the monochromatic weighting function and is considerably sharper than the

THE USE OF SELECTIVE ABSORPTION TO IMPROVED HEIGHT  
RESOLUTION (Elsasser Model)

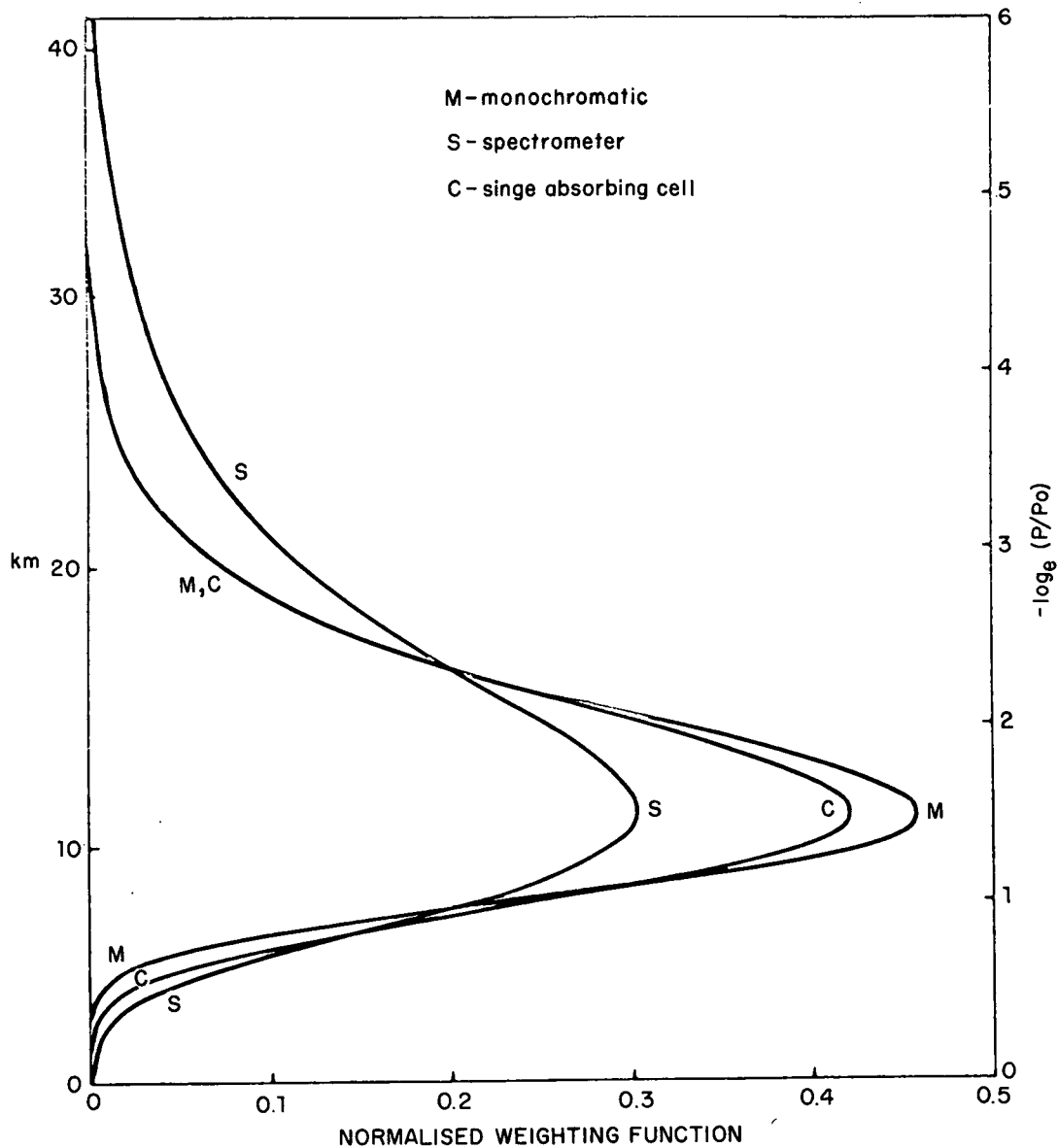


Figure 16. A comparison of weighting functions applying to monochromatic radiation (M), a spectrometer (S), and the single absorbing cell (C) of the Selective Chopper Radiometer (After Oxford-Reading Group, 1966).

spectrometer weighting function. One of the six channels of the SCR is switchable to 11 microns to provide surface temperature data for use in the inversion analysis.

A successful balloon flight of the SCR was made at 0300 hours on 9 June 1966. The balloon reached a height of 35 km over the southern counties of England. Satisfactory signals were received and indicated proper operation of the radiometer. The results of this flight and a complete discussion of the experiment and the instrument will soon be published in a series of papers in the open literature (Williamson, 1968).

### 3.11 Filter Wedge Spectrometer (FWS)

A Filter Wedge Spectrometer (FWS) is being developed to fly on NIMBUS D. Selected characteristics of the FWS are given in Table 1, No. 10. The FWS will view in the nadir direction from the NIMBUS spacecraft. The heart of the instrument is an interference filter wedge, consisting of a pair of halves of two filters—one covering the range 1.2-2.4 microns, and the other the range 3.2-6.4 microns. The assembly of two halves is necessary since present technology allows only one octave of spectrum to be covered on one disc, the same octave being covered twice in one 360° rotation (Hovis, Kley, and Strange, 1967). The instrument will utilize a lead selenide detector, radiatively cooled to 160°K.

The FWS will obtain continuous spectra at a resolution of  $\lambda / \Delta\lambda = 100$  of reflected solar and emitted thermal radiation from the earth and atmosphere in the two spectral intervals stated above. Three specific applications are identified. The first is to test the feasibility of determining whether a cloud is composed of ice crystals (cirrus) or water droplets. Blau, et al. (1966) reported among other features a characteristic minimum at 2.0 microns, observed in spectra of ice clouds taken from a high altitude aircraft. This minimum is absent in spectra of liquid-water clouds. In a series of flights of the NASA Convair-990 research aircraft in the spring of 1966, reflection and emission spectra were obtained by an aircraft version of the FWS over many types of clouds and other natural surfaces. The characteristic minimum at 2.0 microns was observed over cirrus clouds while over water clouds it was absent. This feature is evident in the three sequential spectra over cirrus clouds shown in Figure 17.

The second application is to infer the vertical temperature profile from spectral measurements in the 4.3 micron band of carbon dioxide in much the same manner as the temperature profile is inferred from measurements in the 15 micron band. A temperature profile of the atmosphere, determined from an analysis of measurements in the region of the 4.3 micron CO<sub>2</sub> band made by a balloon-borne grating spectrometer, and the techniques used and some of the problems encountered have been discussed by Shaw, McClatchey, and Schaper (1967).

The third application is to infer the water vapor profile from measurements in the region of the 6.3 micron band, having already determined the temperature profile. As mentioned in the discussion of the IRIS instrument, Conrath (1967) has investigated the problem of remotely inferring water vapor profiles.

### 3.12 Temperature Humidity Infrared Radiometer (THIR)

A Temperature Humidity Infrared Radiometer (THIR) is being developed to fly on NIMBUS D. Selected characteristics of the THIR are given in Table 1, No. 11. The scanner design uses an elliptically shaped plane scan mirror set at an angle of 45° (similar to that of the NIMBUS HRIR and MRIR and of the ITOS High Resolution Radiometer) and primary optics which are common to both channels. The two channels are separated by means of a dichroic beam splitter (McCulloch, 1968).

A 10.5-12.5 micron channel having a linear resolution at the subsatellite point of 7-to-8 km will be flown on TIROS M (cf. Table 1, No. 8); hence a test of the feasibility of a day-night operational cloud mapping instrument with high spatial resolution will have been accomplished prior to NIMBUS D. Therefore the purpose of this channel will largely be to provide supporting data for all scientific experiments on the spacecraft.

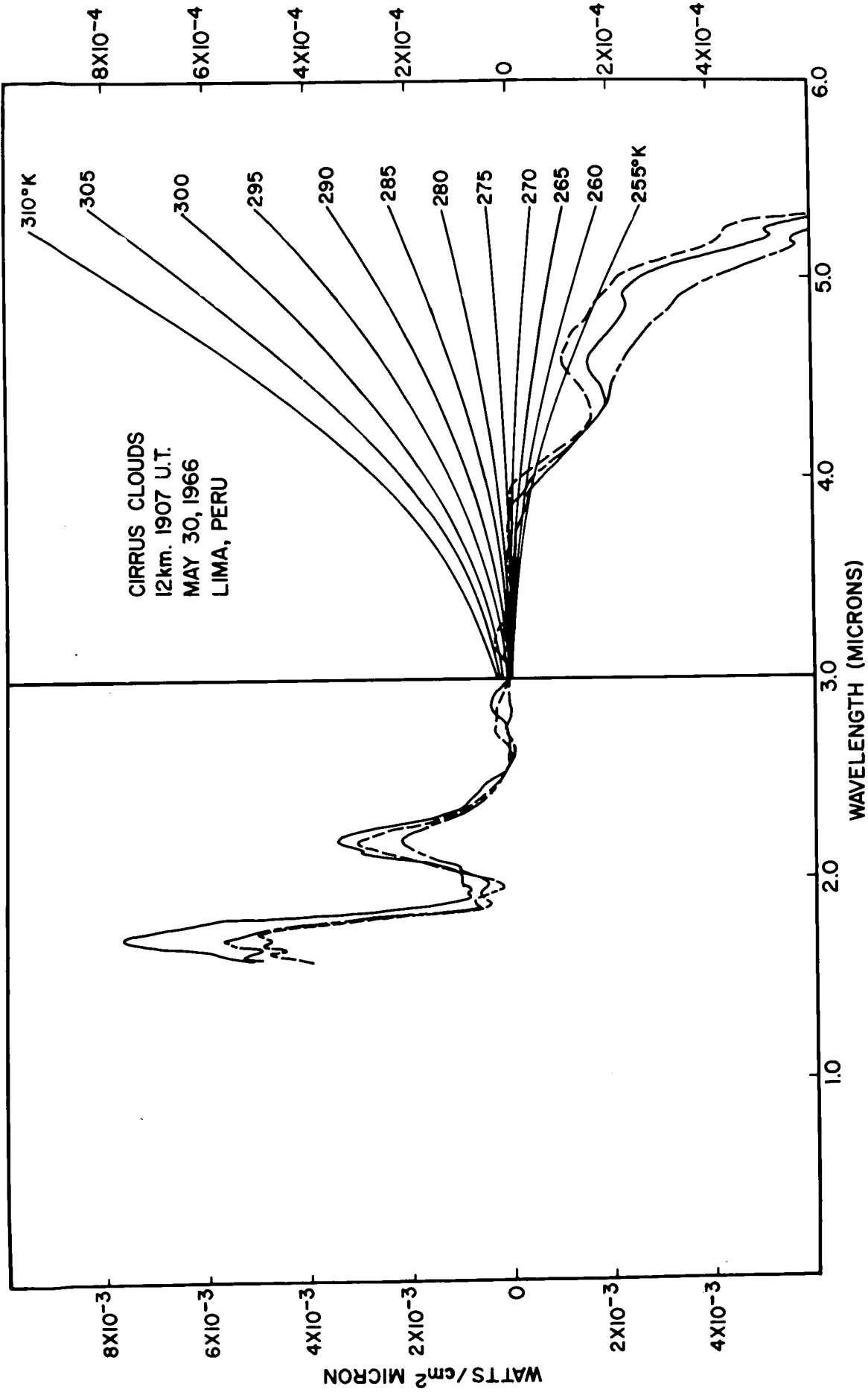


Figure 17. Three sequential spectra from a Filter Wedge Spectrometer on a jet aircraft over cirrus clouds, showing a characteristic minimum at 2.0 microns. The ordinate to the right of 3.0 microns is expanded ten-fold and blackbody curves are drawn for every 5°K (After Hovis and Tobin, 1967).

## EXPER. APPROACHES INFRARED PROBING FROM SATELLITES

The new and distinctive feature of the THIR is the 6.5-7.0 micron water vapor channel having better than twice the linear resolution of the comparable channel of the NIMBUS II and III MRIR. The inclusion of a water vapor channel will permit further studies at improved spatial resolution of the synoptic significance of the moisture patterns first detected in the 6.4-6.9 micron data of NIMBUS II as typified by Figure 10. Of particular interest will be the possibility of using the 6.5-7.0 $\mu$  data to trace air mass boundaries, vertical motions, and possibly the course of jet streams.

### 3.13 ITOS Vertical Temperature Profile Radiometer (VTPR)

A Vertical Temperature Profile Radiometer (VTPR) is being developed for the Improved TIROS Operational Satellite System-ITOS (Operational Satellites Office, 1968). Selected characteristics of this radiometer are given in Table 1, No. 12. The VTPR will view in the nadir direction from the earth-oriented platform of the ITOS vehicle. A final determination of the wave numbers at the mid-points of the eight channels has not been made, but there will probably be six channels ranging from about 669.0  $\text{cm}^{-1}$  to 750.0  $\text{cm}^{-1}$  in the 15 micron  $\text{CO}_2$  band, one channel sensing at about 532  $\text{cm}^{-1}$  in the rotation band of water vapor, and one channel sensing in the atmospheric window at 899  $\text{cm}^{-1}$ . The spectral resolution for all channels will be about 5  $\text{cm}^{-1}$ . This instrument is intended solely for the probing of the temperature profile from operational satellites, and it takes advantage of the latest advances in technology. For example, it utilizes one set of optics and one thermistor bolometer with a cone optic behind a filter wheel. The weight and power requirements of the instrument are notably small (about 10 pounds and 2 watts) compared to those of earlier instruments designed for vertical temperature probing (e.g., SIRS: 92 pounds and 20 watts, or IRIS: 28 pounds and 12 watts).

### 3.14 ITOS Very High Resolution Radiometer (VHRR)

A Very High Resolution Radiometer (VHRR) is being developed for the Improved TIROS Operational Satellite System-ITOS (Operational Satellites Office, 1968). Selected characteristics of this radiometer are given in Table 1, No. 13. The linear resolution on the ground of this instrument represents an order-of-magnitude improvement over that of the NIMBUS HRIR and ITOS High Resolution Radiometer and a nearly two-orders-of-magnitude improvement over that of the TIROS and NIMBUS Medium Resolution Radiometers (cf. Table 1). As such, the resolution of the VHRR is comparable to that of television systems currently flown on meteorological satellites. To achieve this resolution a mercury-cadmium-telluride detector, radiatively-cooled in two stages to 80°K will be used. But with the capability of the 10.5-12.5 micron channel to make measurements day and night, while the 0.52-0.73 micron channel is also making measurements in the daytime, the bit rate of the instrument far exceeds the capacity of any presently available tape recorder system. Therefore, the present plans are to read out the data directly (possibly via a relay geosynchronous satellite). Other possibilities include recording the VHRR data over only a portion of the orbit (a portion determined to be of high interest from other instruments) or recording a degraded form of the data over the entire orbit.

The applications of the data will be similar to those of the other scanning radiometers sensing in similar spectral intervals except that the much higher resolution will permit the study of smaller-scale phenomena such as the three-dimensional structure of cloud patterns and frontal systems and the possible distribution of multiple "hot tower" cumulus cells in hurricanes and typhoons.

### 3.15 Very High Resolution Radiometer for Geosynchronous Altitude

All of the radiometric instruments discussed to this point have been designed for single-satellite systems which permit observations of a given location on earth approximately once every twelve hours. However, there are many meteorological phenomena which have characteristic time periods much shorter than twelve hours, e.g., the development of hurricanes, typhoons, and other types of storms (most notably tornadoes whose whole life cycle can extend over only tens of minutes); the change in the motion of storm systems; and the change in identifiable cloud features which over a shorter period of time might serve as atmospheric tracers to determine winds and other kinematic properties of the atmosphere. The spin scan cloud cameras recently flown on the ATS-1 and ATS-3 satellites in geosynchronous orbits have indicated that a wealth of new information exists both because of the planetary view from the geosynchronous distance of 35,800 km and because of the time-lapse characteristic of the ATS pictures taken every twenty minutes. The possibility of determining flow patterns and wind velocities, and of studying the buildup and decay of short-lived systems and the interactions between hemispheres across the equator have been indicated (McQuain, 1967; Warnecke and Sunderlin, 1968d).

A Very High Resolution Radiometer for Geosynchronous Altitude has been proposed for future flight. Selected characteristics of this radiometer are given in Table 1, No. 14. The design of the proposed radiometer and other characteristics of the experiment have been discussed by Goldberg (1968). The radiometer has several important advantages over a camera that senses visible radiation. First the familiar "full earth" pictures made with the ATS cameras can be taken only during a small fraction of the day, while other pictures taken during the 24 hour period show varying smaller portions of the earth, depending on the location of the terminator. However, the radiometer system will take "full earth" pictures on every frame, independent of the position of the terminator.

Figure 18 attempts to illustrate how a radiometer "picture" of the earth at night (or in the daytime) might look. The model of the earth shown in Figure 18 was constructed by pasting orbital strips of NIMBUS II nighttime HRIR data in correct geographic sequence on a 10-inch-diameter globe (Warnecke, 1968b). The coldest areas are shaded white and the warmest are black with intermediate shades in between. Clearly identifiable are high white (cold) cloud patterns and dark (warm) ocean areas through clear skies. The Australian continent stands out in light shading (colder than the surrounding ocean at night) in the lower left part of the picture. There are marked distortions at the edges of the orbital strips because of the relatively low height of the NIMBUS satellite, but these do not seriously impair the general impression of a high resolution view of the earth in the spectral interval 10.5-12.5 microns from a geosynchronous satellite.

Another advantage of the radiometer over a camera is the capability of temperature measurement. Cloud top altitudes can be inferred from cloud top temperatures, and sea surface temperature variations such as those due to the Gulf Stream can be observed in cloud free regions. Also winds inferred from time-lapse movements of cloud patterns can be located approximately in height because of the temperature measuring capability of the radiometer. The importance of this type of experiment was set forth in the GARP Report of the Stockholm Study Conference (1967).

## REFERENCES

- Allison, Lewis J., Thomas I. Gray, Jr., and Guenter Warnecke, 1964: A Quasi-Global Presentation of TIROS III Radiation Data. Special Publication SP-53, NASA, Washington, D.C., 23 pp.
- Allison, Lewis J., George W. Nicholas, and James S. Kennedy, 1966a: Examples of the Meteorological Capability of the High Resolution Infrared Radiometer on the Nimbus I Satellite. Jour. Appl. Meteor., 5, 314-333.
- Allison, Lewis J. and Harold P. Thompson, 1966b: TIROS VII Infrared Radiation Coverage of the 1963 Atlantic Hurricane Season with Supporting Television and Conventional Meteorological Data. Technical Note TN D-3127, NASA, Washington, D.C., 48 pp.
- Allison, Lewis J. and Guenter Warnecke, 1966c: The Interpretation of TIROS Radiation Data for Practical Use in Synoptic Weather Analysis. Beiträge zur Physik der Atmos., 39, 165-181.
- Allison, Lewis J. and Guenter Warnecke, 1967: A Synoptic World Weather Analysis of TIROS VII Radiation Data. Technical Note TN D-3787, NASA, Washington, D.C., 34 pp.
- Bandeem, W. R., R. A. Hanel, J. Licht, R. A. Stampfl, and W. G. Stroud, 1961: Infrared and Reflected Solar Radiation Measurements from the TIROS II Meteorological Satellite. Jour. Geophys. Res., 66, 3169-3185.
- Bandeem, W. R., B. J. Conrath, and R. A. Hanel, 1963a: Experimental Confirmation from the TIROS VII Meteorological Satellite of the Theoretically Calculated Radiance of the Earth Within the 15-Micron Band of Carbon Dioxide. Jour. Atmos. Sci., 20, 609-614.
- Bandeem, W. R., B. J. Conrath, W. Nordberg, and H. P. Thompson, 1963b. A Radiation View of Hurricane Anna from the TIROS III Meteorological Satellite, pp. 224-233 in Proceedings of the First International Symposium on Rocket and Satellite Meteorology, ed. H. Wexler and J. E. Caskey, Jr., North-Holland Publishing Co., Amsterdam, 440 pp.
- Bandeem, W. R., V. Kunde, W. Nordberg, and H. P. Thompson, 1964: TIROS III Meteorological Satellite Radiation Observations of a Tropical Hurricane. Tellus, XVI, 481-502.
- Bandeem, W. R., M. Halev, and I. Strange, 1965: A Radiation Climatology in the Visible and Infrared from the TIROS Meteorological Satellites. Technical Note TN D-2534, NASA, Washington, D.C., 30 pp.
- Bandeem, W. R., 1966: Atmospheric Water Vapor Content from Satellite Radiation Measurements, pp. 229-249, in Satellite Data in Meteorological Research, NCAR-TN-11, ed. H. M. E. Van de Boogaard. National Center for Atmospheric Research, Boulder, Colorado, 349 pp.
- Bartko, Frank, Virgil Kunde, Clarence Catoe, and Musa Halev, 1964: The TIROS Low Resolution Radiometer. Technical Note TN D-614, NASA, Washington, D.C., 34 pp.

## EXPER. APPROACHES INFRARED PROBING FROM SATELLITES

- Belmont, A. D., G. W. Nicholas, and W. C. Shen, 1968: Comparison of 15- $\mu$  TIROS VII Data with Radiosonde Temperatures. Jour. Appl. Meteor., 7, 284-289.
- Blau, Henry H., Jr., Ronald P. Espinola, and Edward C. Reifenstein, III, 1966: Near Infrared Scattering by Sunlit Terrestrial Clouds. Appl. Optics, 5, 555-564.
- Bolle, H. J., 1967: Infrarotspektroskopie als Hilfsmittel und Gegenstand meteorologischer und planetarischer Forschung. Meteorologisches Institut der Ludwig-Maximilians - Universität München Forschungsbericht W 67-17 (July).
- Buettner, Konrad J. K. and Clifford D. Kern, 1963: Infrared Emissivity of the Sahara from TIROS Data. Science, 142 (Nov. 8), 671.
- Chaney, L. W., S. R. Drayson, and C. Young, 1967: Fourier Transform Spectrometer-Radiative Measurements and Temperature Inversion. Applied Optics, 6, 347-349.
- Conrath, Barney J., 1967: Remote Sensing of Atmospheric Water Vapor and Ozone Using Interferometry, pp. 277-296 in Proceedings of the Specialists Conference on Molecular Radiation and Its Application to Diagnostic Techniques, Marshall Space Flight Center, 5-6 October 1967. Document TM X-53711, ed. R. Goulard, NASA, Marshall Space Flight Center, 489 pp.
- Conrath, B. J., 1968: Inverse Problems in Radiative Transfer: A Review, pp. 339-360 in Proceedings of the XVIII International Astronautical Congress, Belgrade, October 1967. (Also available as Doc. X-622-67-57, NASA Goddard Space Flight Center.)
- Davis, Paul A. 1965: TIROS III Radiation Measurements and Some Diabatic Properties of the Atmosphere. Mo. Weather Rev., 93, 535-545.
- Dreyfus, M. G. and D. T. Hilleary, 1962: Satellite Infrared Spectrometer. Aerospace Engrg., February, 42-45.
- Foshee, L. L., I. L. Goldberg, and C. E. Catoe, 1965: The High Resolution Infrared Radiometer (HRIR) Experiment, pp. 13-22 in Observations from the Nimbus I Meteorological Satellite. Special Publication SP-89, NASA, Washington, D.C., 90 pp.
- Fritz, Sigmund and Jay S. Winston, 1962: Synoptic Use of Radiation Measurements from Satellite TIROS II. Mo. Weather Rev., 90, 1-9.
- Fritz, Sigmund, 1963: The Diurnal Variation of Ground Temperature as Measured from TIROS II. Jour. Appl. Meteor., 2, 645-648.
- Fritz, S. and P. Krishna Rao, 1967: On the Infrared Transmission Through Cirrus Clouds and the Estimation of Relative Humidity from Satellites. Jour. Appl. Meteor., 6, 1088-1096.
- Fujita, Tetsuya and William Bandeen, 1965: Resolution of the Nimbus High Resolution Infrared Radiometer. Jour. Appl. Meteor., 4, 492-503.

- Global Atmospheric Research Programme (GARP). Report of a Study Conference held at Stockholm, Sweden, 28 June - 11 July 1967, Jointly Organized by the ICSU/IUGG - Committee on Atmospheric Sciences and COSPAR and co-sponsored by the World Meteorological Organization; 144 pp.
- Goldberg, I. L., 1968: A Very High Resolution Radiometric Experiment for ATS F and G. Doc. X-622-68-26, NASA Goddard Space Flight Center.
- Goldschlak, L., 1968: Nimbus III Real Time Transmission Systems. Technical Report under Contract NAS 5-10343 with Allied Research Associates, Inc.
- Hanel, Rudolf A., 1961: Low Resolution Unchopped Radiometer for Satellites. ARS Journal, February, 246-250.
- Hanel, R. A. and D. Q. Wark, 1961: TIROS II Radiation Experiment and Its Physical Significance. Jour. Opt. Soc. Am., 51, 1394-1399.
- Hanel, R. A., W. R. Bandeen, and B. J. Conrath, 1963: The Infrared Horizon of the Planet Earth. Jour. Atmos. Sci., 20, 73-86.
- Hanel, R. A. and L. Chaney, 1966: The Merits and Shortcomings of a Michelson Type Interferometer to Obtain the Vertical Temperature and Humidity Profile. Proceedings of the XVII International Astronautical Congress, Madrid, 9-15 October 1966, Vol. II. (Also available as Doc. X-620-66-476, NASA Goddard Space Flight Center.)
- Hanel, R. A., 1968: Personal communication. Goddard Space Flight Center, Greenbelt, Md.
- Hawkins, R. S., 1964: Analysis and Interpretation of TIROS II Infrared Radiation Measurements. Jour. Appl. Meteor. 3, 564-572.
- Hilleary, D. T., D. Q. Wark, and D. G. James, 1965: An Experimental Determination of the Atmospheric Temperature Profile by Indirect Means. Nature, 205 (4970), 489-491.
- Hilleary, D. T., E. L. Heacock, W. A. Morgan, R. H. Moore, E. C. Mangold, and S. D. Soules, 1966: Indirect Measurements of Atmospheric Temperature Profiles from Satellites: III. The Spectrometers and Experiments. Mo. Weather Review, 94, 367-377.
- House, Frederick B., 1965: The Radiation Balance of the Earth from a Satellite. Ph.D. Thesis, Department of Meteorology, The University of Wisconsin, Madison, 69 pp. (Report to NASA under Contract NAS w-65.)
- Hovis, W. A., W. A. Kley, and M. G. Strange, 1967: Filter Wedge Spectrometer for Field Use. Applied Optics, 6, 1057-1058.
- Hovis, W. A. and M. Tobin, 1967: Spectral Measurements from 1.6 to 5.4 Microns of Natural Surfaces and Clouds. Applied Optics, 6, 1399-1402.

## EXPER. APPROACHES INFRARED PROBING FROM SATELLITES

- Howard, John Nelson, Darrell L. Burch, and Dudley Williams, 1955: Near-Infrared Transmission Through Synthetic Atmospheres. AFCRC-TR-55-213, Geophysical Research Papers No. 40, Air Force Cambridge Research Center, 244 pp.
- James, D. G., 1967: Indirect Measurements of Atmospheric Temperature Profiles from Satellites: IV. Experiments with the Phase 1 Satellite Infrared Spectrometer. Mo. Weather Review, 95, 457-462.
- Jensen, Clayton E., Jay S. Winston, and V. Ray Taylor, 1966: 500-MB Heights as a Linear Function of Satellite Infrared Radiation Data. Mo. Weather Rev., 94, 641-649.
- Kaplan, Lewis E., 1959: Inference of Atmospheric Structure from Remote Radiation Measurements. Jour. Opt. Soc. Am., 49, 1004-1007.
- Kennedy, James S. and William Nordberg, 1967: Circulation Features of the Stratosphere Derived from Radiometric Temperature Measurements with the TIROS VII Satellite. Jour. Atmos. Sci., 24, 711-719.
- King, Jean I. F., 1956: The Radiative Heat Transfer of Planet Earth, pp. 133-136 in Scientific Uses of Earth Satellites, ed. James A. Van Allen, University of Michigan Press, Ann Arbor, 316 pp.
- King, Jean I. F., 1964: Inversion by Slabs of Varying Thickness. Jour. Atmos. Sci., 21, 324-326.
- Kunde, Virgil G., 1965: Theoretical Relationship Between Equivalent Blackbody Temperatures and Surface Temperatures Measured by the Nimbus High Resolution Infrared Radiometer, pp. 23-36 in Observations from the Nimbus I Meteorological Satellite. Special Publication SP-89, NASA, Washington, D.C., 90 pp.
- Lienesch, J. H. and D. Q. Wark, 1967: Infrared Limb Darkening of the Earth from Statistical Analysis of TIROS Data. Jour. Appl. Meteor., 6, 674-682.
- McCulloch, A. W., 1968: Personal communication. Goddard Space Flight Center, Greenbelt, Md.
- McQuain, Robert H., 1967: ATS-1 Camera Experiment Successful. Bull. Am. Meteor. Soc., 48, 74-79.
- Möller, Fritz, and Ehrhard Raschke, 1964: Evaluation of TIROS III Radiation Data. Contractor Report CR-112, NASA, Washington, D.C., 114 pp.
- Möller, F., 1967: Eine Karte der Strahlungsbilanz des Systems Erde - Atmosphäre für Einen 14 Tägigen Zeitraum. Meteorologische Rundschau, 20 (4), 97-98.
- Nelson, David F. and Robert Parent, 1965: The Prototype Flat-Plate Radiometers for the ESSA III Satellite, Chap. 6 in Annual Report-1966 WBG-27 Amendment No. 1, Department of Meteorology, The University of Wisconsin, Madison.
- Nimbus II Users' Guide, 1966: National Space Science Data Center, Goddard Space Flight Center, NASA, Greenbelt, Md., 229 pp.

- Nimbus III User's Guide, 1968: National Space Science Data Center, Goddard Space Flight Center, NASA, Greenbelt, Md.
- Nordberg, W., W. R. Bandeen, B. J. Conrath, V. Kunde, and I. Persano, 1962: Preliminary Results of Radiation Measurements from the TIROS III Meteorological Satellite. Jour. Atmos. Sci., 19, 20-30.
- Nordberg, W. and Harry Press, 1964: The Nimbus I Meteorological Satellite. Bull. Amer. Meteor. Soc., 45, 684-687.
- Nordberg, William, 1965: Geophysical Observations from Nimbus I. Science, 150, 559-572 (Oct. 29).
- Nordberg, W., W. R. Bandeen, G. Warnecke, and V. Kunde, 1965: Stratospheric Temperature Patterns Based on Radiometric Measurements from the TIROS 7 Satellite, pp. 782-809 in Space Research V, ed. D. G. King-Hele, P. Muller, and G. Righini. North-Holland Publishing Co., Amsterdam, 1248 pp.
- Nordberg, W., A. W. McCulloch, L. L. Foshee, and W. R. Bandeen, 1966: Preliminary Results from Nimbus II. Bull. Amer. Meteor. Soc., 47, 857-872.
- Operational Satellites Office, 1968: Goddard Space Flight Center, Greenbelt, Md. Personal communication.
- Oxford-Reading Group, 1966: Selective Chopper Radiometer for Atmospheric Temperature Sounding for the Nimbus "D" Satellite. Joint Proposal by Oxford and Reading Universities to NASA for a Flight Experiment on Nimbus D, dated 15 April 1966.
- Peckham, G., C. D. Rodgers, J. T. Houghton, and S. D. Smith, 1966: Remote Temperature Sensing of the Earth's Atmosphere Using a Selective Chopper Radiometer, in Proceedings of the Symposium on Electromagnetic Sensing of the Earth from Satellites, Miami Beach, Florida, 22-24 November 1965.
- Popham, R. W. and R. E. Samuelson, 1965: Polar Exploration With Nimbus Meteorological Satellite. Arctic (Journal of the Arctic Institute of North America), 18, 246-255.
- Rao, P. Krishna and Jay S. Winston, 1963: An Investigation of Some Synoptic Capabilities of Atmospheric "Window" Measurements from Satellite TIROS II. Jour. Appl. Meteor., 2, 12-23.
- Raschke, Ehrhard, 1967: A Quasi-Global Analysis of the Mean Relative Humidity of the Upper Troposphere. Tellus, XIX, 214-218.
- Raschke, E. and W. R. Bandeen, 1967a: A Quasi-Global Analysis of Tropospheric Water Vapor Content and Its Temporal Variations from Radiation Data of the Meteorological Satellite TIROS IV, pp. 920-931 in Space Research VII, Vol. 2, ed. R. L. Smith-Rose, North-Holland Publishing Co., Amsterdam, 1479 pp.
- Raschke, Ehrhard and William R. Bandeen, 1967b: A quasi-Global Analysis of Tropospheric Water Vapor Content from TIROS IV Radiation Data. Jour. Appl. Meteor., 6, 468-481.

## EXPER. APPROACHES INFRARED PROBING FROM SATELLITES

- Raschke, Ehrhard, Fritz Möller, and William R. Bandeen, 1968: The Radiation Balance of Earth-Atmosphere System Over Both Polar Regions Obtained from Radiation Measurements of the Nimbus II Meteorological Satellite, pp. 42-57 in Scientific Papers Dedicated to Dr. Anders Ångström, Meddelanden, Serie B, Nr. 28, Sveriges Meteorologiska och Hydrologiska Institut, Stockholm. (Also available as Doc. X-622-67-460, NASA Goddard Space Flight Center.)
- Raschke, Ehrhard and Musa Pasternak, 1968: The Global Radiation Balance of the Earth-Atmosphere System Obtained from Radiation Data of the Meteorological Satellite Nimbus II, in Space Research VIII, ed. A. Dollfus, North-Holland Publishing Co., Amsterdam.
- Raschke, Ehrhard, 1968: The Radiation Balance of the Earth-Atmosphere System from Radiation Measurements of the Nimbus II Meteorological Satellite. Technical Note TN D-4589, NASA, Washington, D.C., 81 pp.
- Rasool, S. I., 1964: Cloud Heights and Nighttime Cloud Cover from TIROS Radiation Data. Jour. Atmos. Sci., 21, 152-156.
- Rasool, S. I. and C. Prabhakara, 1966: Heat Budget of the Southern Hemisphere, pp. 76-92 in Problems of Atmospheric Circulation, ed. R. V. Garcia and T. F. Malone. Spartan Books, Washington, D.C., 186 pp.
- Shaw, J. H., R. A. McClatchey, and P. W. Schaper, 1967: Balloon Observations of the Radiance of the Earth Between  $2100\text{ cm}^{-1}$  and  $2700\text{ cm}^{-1}$ . Applied Optics, 6, 227-230.
- Shen, W. C., G. W. Nicholas, and A. D. Belmont, 1968: Antarctic Stratospheric Warmings During 1963 Revealed by  $15\text{-}\mu$  TIROS VII Data. Jour. Appl. Meteor., 7, 268-283.
- Staff Members, Aeronomy and Meteorology Division, Goddard Space Flight Center, 1964: TIROS VII, Radiation Data Catalog and Users' Manual: Vol. 1. National Space Science Data Center, Goddard Space Flight Center, NASA, Greenbelt, Md., 255 pp.
- Suomi, V. E., 1958: The Radiation Balance of the Earth from a Satellite. pp. 331-340 in Annals of the IGY, VI, ed. L. V. Berkner. Pergamon Press, New York, 508 pp.
- Suomi, V. E., 1961: The Thermal Radiation Balance Experiment on Board Explorer VII, pp. 273-305 in JUNO II Summary Project Report. Volume I, Explorer VII Satellite. Technical Note TN D-608. NASA, Washington, D.C.
- Suomi, V., K. Hanson, and T. Vonder Haar, 1966: The Theoretical Basis for Low-resolution Radiometer Measurements from a Satellite, Chap. 4 in Annual Report-1966, WBG-27, Amendment No. 1, Department of Meteorology, The University of Wisconsin, Madison.
- Twomey, S., 1966: Indirect Measurements of Atmospheric Temperature Profiles from Satellites: II. Mathematical Aspects of the Inversion Problem Mo. Weather Review, 94, 363-366.

- Vonder Haar, Thomas H., 1968: Variations of the Earth's Radiation Budget, Ph.D. Thesis, Department of Meteorology, The University of Wisconsin, Madison, 118 pp. (Report to NASA under Contract NAS w-65.)
- Wark, D. Q., 1961: On Indirect Temperature Soundings of the Stratosphere from Satellites. Jour. Geophys. Res., 66, 77-82.
- Wark, D. Q., G. Yamamoto, and J. H. Lienesch, 1962: Methods of Estimating Infrared Flux and Surface Temperature from Meteorological Satellites. Jour. Atmos. Sci., 19, 369-384.
- Wark, D. Q. and H. E. Fleming, 1966: Indirect Measurements of Atmospheric Temperature Profiles from Satellites: I. Introduction. Mo. Weather Review, 94, 351-362.
- Wark, D. Q., F. Saiedy, and D. G. James, 1967: Indirect Measurements of Atmospheric Temperature Profiles from Satellites: VI. High-Altitude Balloon Testing, Mo. Weather Review, 95, 468-479.
- Wark, D. Q., 1968: Personal communication. National Environmental Satellite Center, ESSA, Suitland, Md.
- Warnecke, G., 1966a: TIROS VII  $15\mu$  Radiometric Measurements and Mid-Stratospheric Temperatures, pp. 215-227 in Satellite Data in Meteorological Research, NCAR-TN-11, ed. H. M. E. Van de Boogaard. National Center for Atmospheric Research, Boulder, Colorado, 349 pp.
- Warnecke, Guenter, 1966b: Synoptic Applications of Satellite-Borne Infrared Window Measurements, pp. 121-130 in Satellite Data in Meteorological Research, NCAR-TN-11, ed. H. M. E. Van de Boogaard. National Center for Atmospheric Research, Boulder, Colorado, 349 pp.
- Warnecke, Guenter, Lewis Allison, and Lonnie L. Foshee, 1968a: Observations of Sea Surface Temperatures and Ocean Currents from Nimbus II, in Space Research VIII, ed. A. Dollfus, North-Holland Publishing Co., Amsterdam.
- Warnecke, Guenter, 1968b: Personal communication. Goddard Space Flight Center, Greenbelt, Md.
- Warnecke, Guenter and Andrew W. McCulloch, 1968c: Stratospheric Temperature Patterns Derived from Nimbus II Measurements, in Space Research VIII, ed. A. Dollfus, North-Holland Publishing Co., Amsterdam.
- Warnecke, Guenter and Wendell S. Sunderlin, 1968d: The First Color Picture of the Earth Taken from the ATS-3 Satellite. Bull. Am. Meteor. Soc., 49, 75-83.
- Weinstein, Melvin and Verner E. Suomi, 1961: Analysis of Satellite Infrared Radiation Measurements on a Synoptic Scale. Mo. Weather Rev., 89, 419-428.
- Widger, W. K., Jr., J. C. Barnes, E. S. Merritt, and R. B. Smith, 1965: Meteorological Interpretation of Nimbus High Resolution Infrared (HRIR) Data. Contractor Report CR-352, NASA, Washington, D.C. 150 pp.

EXPER. APPROACHES INFRARED PROBING FROM SATELLITES

- Widger, William K., Jr., 1966: Weather from Way-Out. Weatherwise, 19, 100-111
- Widger, W. K., Jr., C. W. C. Rogers, and P. E. Sherr, 1966: Looking Down on Spirals in the Sky. American Scientist, 54, 288-314.
- Williamson, E. J., 1968: Personal communication. Goddard Space Flight Center, Greenbelt, Md.
- Winston, Jay S. and P. Krishna Rao, 1962: Preliminary Study of Planetary-Scale Outgoing Long-Wave Radiation as Derived from TIROS II Measurements. Mo. Weather Rev., 90, 307-310.
- Winston, J. S. and P. K. Rao, 1963: Temporal and Spatial Variations in the Planetary Scale Outgoing Long-Wave Radiation as Derived from TIROS II Measurements. Mo. Weather Rev., 91, 641-657.
- Winston, Jay S., 1965: Comments on "Cloud Heights and Nighttime Cloud Cover from TIROS Radiation Data." Jour. Atmos. Sci., 22, 333-338.
- Winston, Jay S., 1967a: Planetary-Scale Characteristics of Monthly Mean Long-Wave Radiation and Albedo and Some Year-to-Year Variations. Mo. Weather Rev., 95, 235-256.
- Winston, Jay S., 1967b: Zonal and Meridional Analysis of 5-Day Averaged Outgoing Long-Wave Radiation Data from TIROS IV Over the Pacific Sector in Relation to the Northern Hemisphere Circulation. Jour. Appl. Meteor., 6, 453-463.
- Wolk, M. and F. Van Cleef, 1967: Indirect Measurements of Atmospheric Temperature Profiles from Satellites: V. Atmospheric Soundings from Infrared Spectrometer Measurements at the Ground. Mo. Weather Review, 95, 463-467.

COMMENTS ON A PAPER BY W. R. BANDEEN

Comments by S. Fritz  
Environmental Science Services Administration  
National Environmental Satellite Center  
Suitland, Maryland

The paper presented and distributed by W. R. Bandeen was entitled "Experimental Approaches to Remote Atmospheric Probing in the Infrared from Satellites." The following comments will sometimes refer to specific sections in that document.

In the absence of calibration on-board a satellite, quantitative results are often questionable. In the case of the heat budget of the earth, quantitative results depend on the difference between the large amount of outgoing energy and the almost equally large amount of solar energy absorbed by the Earth. This lack of on-board calibration applies to the hemispherical and flat plate radiometers used on Explorer VII, TIROS, and ESSA satellites, (referred to as wide-field sensors in Section 3.1 of Bandeen's paper), as well as to the medium resolution infrared radiometers on the TIROS and Nimbus series mentioned in the same section and in Table 1. In the case of Nimbus, the on-board calibration was apparently adequate in some of the long-wave channels required to investigate the radiative budget of the earth; but calibration for the solar channels was lacking, so that the energy reflected from the earth is in more question.

It is well known that the wide-angle radiometers and the TIROS medium resolution radiometers did degrade with time; and in the absence of on-board calibration required accuracy in radiation values is lacking. This does not mean that a great deal of useful information was not obtained. For the relative distribution of the field of radiation from one place to another on any one day, and even from one day to another on adjacent days during which the calibration changed little, did indeed lend itself to a much useful research involving cloud forms, cloud patterns, the earth surface temperature, stratospheric temperature, etc.

More needs to be said about the water vapor determination using the 6 micron and 10 micron channels, the results of which are displayed in Figure 4. In his oral presentation Mr. Bandeen did discuss the limitations and agreed that the determination of water vapor in the presence of high, cold clouds by this method fails. Nevertheless, the so-called results of the water vapor distribution obtained by this method are shown in Figure 4. It is fairly obvious that Figure 4 is mainly a representation of the major cloud systems; the figure merely shows that where extensive clouds with large vertical development exist, as over the major tropical continents, then the amount of water vapor in mid-troposphere is high. This result could be obtained by the use of the 10 micron channel alone, or with one of a number of other channels. A more sophisticated method is not necessary for the correlation of pattern of radiation with the pattern of relative humidity or perhaps of other water vapor parameters.

In Section 3.4, Bandeen questions the use of the 3.5 to 4.1 micron radiation for determining the surface temperatures. It is quite possible that the ocean surface temperature could be determined even in daytime in the absence of clouds. This might be true because the reflectivity of solar radiation from the ocean surface at those wavelengths might be quite small so that the emitted radiation would dominate and might yield an accurate enough surface temperature. This has apparently not yet been tried, but should be.

REMOTE ATMOSPHERIC TEMPERATURE MEASUREMENT

There was a great deal of discussion, not only in Mr. Bandeen's paper but in several other papers at the meeting in Chicago, about the determination of the vertical temperature structure from a series of radiation measurements. In principle it is not possible to derive a unique set of temperatures from a set of radiation measurements alone. A unique solution is possible only after some assumption is made about the nature of the solution. The basic difficulty can be illustrated in the following way.

The radiance,  $I_i$ , measured by a satellite, at frequency,  $(\nu_i)$ , is given by

$$I_i = \int_0^1 B(\nu_i, T) d\tau(\nu_i) = \int_{\log p_0}^{\log 0.1} B \frac{\delta \tau}{\delta \log p} d \log p \quad (1)$$

where the symbols have standard meanings, and the "top of the atmosphere" is assumed to be at  $p = 0.1$  mb; this is an adequate "top" for the  $15\mu$   $CO_2$  band with resolution of about  $5 \text{ cm}^{-1}$ .

Now, for purposes of illustration, suppose we make measurements at two frequencies, "a" and "b". Assume that the Planck functions,  $B$ , have been normalized to a given reference frequency, and that we require the average temperature for two layers of the atmosphere. The average Planck function,  $B$ , will be closely related to the average temperatures in the layers. Therefore, from equation (1),

$$I_a = \left[ \begin{array}{c} B \frac{\delta \tau_a}{\delta \log p} \Delta \log p \\ \vdots \\ B \frac{\delta \tau_a}{\delta \log p} \Delta \log p \end{array} \right]_H + \left[ \begin{array}{c} B \frac{\delta \tau_a}{\delta \log p} \Delta \log p \\ \vdots \\ B \frac{\delta \tau_a}{\delta \log p} \Delta \log p \end{array} \right]_L \quad (2)$$

$$I_b = \left[ \begin{array}{c} B \frac{\delta \tau_b}{\delta \log p} \Delta \log p \\ \vdots \\ B \frac{\delta \tau_b}{\delta \log p} \Delta \log p \end{array} \right]_H + \left[ \begin{array}{c} B \frac{\delta \tau_b}{\delta \log p} \Delta \log p \\ \vdots \\ B \frac{\delta \tau_b}{\delta \log p} \Delta \log p \end{array} \right]_L \quad (3)$$

where "H" refers to the higher layer and "L" refers to the lower layer. The normalization factors for frequency have been incorporated into  $I_a$  and  $I_b$ . The averages have been performed with respect to  $\log p$ .

Now

$$\overline{B \left( \frac{\delta \tau_a}{\delta \log p} \right)} = \overline{B} \left( \frac{\delta \tau_a}{\delta \log p} \right) + \overline{B' \left( \frac{\delta \tau_a}{\delta \log p} \right)'} ,$$

where the primes refer to deviations from the average. Since

$$\overline{\left( \frac{\delta \tau_a}{\delta \log p} \right) \Delta \log p} = \Delta \tau_a$$

equation (2) becomes

$$I_a = \left[ \overline{B} \Delta \tau_a \right]_H + \left[ \overline{B} \Delta \tau_a \right]_L + \left[ \overline{B' \left( \frac{\delta \tau_a}{\delta \log p} \right)'} \Delta \log p \right]_H + \left[ \overline{B' \left( \frac{\delta \tau_a}{\delta \log p} \right)'} \Delta \log p \right]_L \quad (4)$$

with a corresponding equation for equation (3).

The solutions for  $\overline{B}_H$  and  $\overline{B}_L$  are, in matrix notation,

$$\begin{pmatrix} \overline{B}_H \\ \overline{B}_L \end{pmatrix} = A^{-1} \begin{pmatrix} I_a \\ I_b \end{pmatrix} - A^{-1} \begin{pmatrix} V_a \\ V_b \end{pmatrix} \quad (5)$$

Here,  $A^{-1}$  is the inverse of matrix A;

$$A = \begin{pmatrix} \Delta \tau_{aH} & \Delta \tau_{aL} \\ \Delta \tau_{bH} & \Delta \tau_{bL} \end{pmatrix}$$

and  $V_a$  is the sum of the last two terms in equation (4);  $V_b$  is the corresponding term in the equation involving frequency b.

From equation (5), it is thus evident that even without errors in the measured radiances, and even if only two average temperatures are sought from two spectral measurements, additional information is required in order to evaluate  $\bar{B}_H$  or  $\bar{B}_L$ . The additional information required is a knowledge of the magnitude of the terms  $V_a$  and  $V_b$ . These involve the co-variance between  $B'$  and  $(\delta\tau/\delta \log p)'$ , at the two frequencies. This co-variance term may perhaps be estimated from climatological data, or from synoptic data where radiosonde measurements exist. Perhaps it is sufficiently well correlated with  $\bar{B}$  itself or with the radiances. At any rate some estimate of it would be required.

From measurements at a few additional frequencies, additional average temperatures at a correspondingly larger number of layers can be evaluated. But always terms such as  $V_a$  will appear.

Where the number of levels, at which temperature is estimated, exceeds the number of radiances measured, it is even more obvious that some additional assumption is required. In practice, climatological data obtained from a long record of radiosonde data, or from a few days of actual radiance measurements over radiosonde stations, can serve to aid in acquiring the desired temperatures, if the radiances are sufficiently accurate. This was mentioned by several people at the Panel Discussions in Chicago.

N72-25378

SOME COMMENTS ON THE  
USE OF INFRARED RADIOMETRY FOR REMOTE ATMOSPHERIC PROBING

W. L. Godson

Meteorological Service of Canada, Toronto

ABSTRACT

This report represents primarily a critique of the lead paper by L.D. Kaplan on infrared radiometry. The following topics are analysed - the extent to which the desirable thermal resolution of the lower troposphere can be achieved, the effects of complex cloud structure on infrared data, the effective weighting function if linearisation is possible, remote sounding from below the atmosphere, first-guess fields and operational techniques to blend satellite infrared data into a mix of data from various meteorological systems, a simple inversion procedure for thermal structure, and problems arising from cloud and haze layers of variable amount and emissivity.

1. KEY PROBLEMS ACCORDING TO KAPLAN

Kaplan, in his lead paper on infrared radiometry, considers that two key problems in meeting the needs of numerical weather prediction are: "the necessity of obtaining soundings of temperature and water vapor content of the lower troposphere with sufficient vertical resolution to determine the exchange of heat and moisture between the surface and the atmosphere; and the necessity of obtaining these soundings even under the usual conditions of at least partial cloud cover".

To permit flux determinations, we need at least meso-scale resolution, which could be possible only by infrared probing from below. This could be both automated and remoted by using satellite interrogation of radiometric buoys or radiometric automatic land stations. However, we must bear in mind that the fluxes are needed in the numerical procedures not only at the moment of initial data, but for the next three or four weeks inside the computer as it races well ahead of the atmospheric

evolution. Within the computer, fluxes in the vertical near the ground will have to be parameterized. The divergence of these fluxes, plus advective and radiative processes, will then be used to modify local gradients over deep layers, from which new fluxes will again be calculated by parameterization. If this procedure is not possible, extended-range prediction for several weeks cannot be successful, and initial data on even a micro-scale will not contribute to the numerical prediction. Expressed in another way, meso-scale and micro-scale information decays rapidly in the atmosphere and must continually be re-synthesized by a numerical model. It therefore makes little or no difference whether such information is available initially or not.

The problem of a partial cloud cover is indeed a very complex one, to which we will return a little later. Essentially, the number of degrees of freedom associated with broken stratified clouds (amount and temperature for each distinct layer) is such that virtually no degrees of freedom will be available to specify either the tropospheric temperature or moisture fields. In other words, the radiative data do carry considerable information, but, relative to an informed first-guess field, such information deals almost entirely with the clouds themselves. Unfortunately, it may be very difficult to make an initial guess of the cloud characteristics, so that the method of solution will be slow and sensitive to errors. Moreover, space averages will certainly be involved and since the horizontal variability can be relatively great (clouds being sub-synoptic scale phenomena) there will be problems of non-linear averaging.

## 2. USE OF HIGH FREQUENCY INFORMATION

As Kaplan points out, in his lead paper, the upward intensity depends on the integral, over pressure, of the product of black-body intensity and the pressure derivative of the transmission function. If the problem can be solved by the use of a good initial guess-field the subsequent linearization replaces the black-body intensity by its temperature derivative. This derivative is also very sensitive to both frequency and temperature and behaves quite differently at high and low frequencies. At  $2000 \text{ cm}^{-1}$ , for example, the ratio of this derivative at  $300^\circ\text{K}$  to that at  $200^\circ\text{K}$  is about 53, whereas at  $667 \text{ cm}^{-1}$  the ratio is only 2.2. This means that the weighting functions for the 4.3 micron and 15 micron bands of  $\text{CO}_2$  will be quite different, so that the information from a second band will not be redundant and can permit an improved resolution of the thermal structure of the atmosphere.

If broken clouds are present, the use of two widely-separated spectral windows can also be very helpful. As an example, consider the case of a single layer covering one-half the sky at a temperature  $20^\circ\text{C}$  colder than the ground at  $260^\circ\text{K}$ . The effective radiating temperature at  $2500 \text{ cm}^{-1}$  will exceed that at  $900 \text{ cm}^{-1}$  by  $2.0^\circ\text{C}$ , with a standard error of about  $0.5^\circ\text{C}$ , assuming intensities have standard errors of one per cent. We thus have two relatively independent pieces of information, but unfortunately there are three unknown quantities. In the daytime one might

be able to estimate the cloud amount from data at visible wavelengths, or we may be able to guess the surface temperature from other meteorological data (especially over oceans for which this is a moderately conservative element).

Kaplan, in his lead article, suggests the use of a wide-band narrow-angle sub-scan over each element of area to determine intensity maxima (presumed to be clear skies) and minima (presumed to be overcast cloud). If true, both the ground and cloud temperature would be known, and narrow-band wide-angle window data would yield the effective average cloud amount. Knowing these three parameters, the effects of the broken clouds could be removed from non-window data. It is unlikely that this procedure would really be effective, but at least it could be checked if two pairs of wide-band and narrow-band windows were used. If both spectral regions yielded the same value for effective cloud amount, one would have considerably more confidence in the technique. If they did not agree, a more complex model would be needed, or else auxiliary information from non-infrared sensors. The correction technique suggested is very sensitive to the cloud-ground temperature difference, so that it would be necessary to be certain that truly overcast and truly clear areas were those of minimum and maximum intensity. If the two windows agreed on the effective radiating temperature of only one of these limits, the problem would still be soluble, however.

### 3. SOUNDING FROM BELOW

In his lead article, Kaplan draws attention to the information derivable from infrared sounding from below, and it is clear that microwave techniques are also effective in this mode. In both cases, resolution is good for layers for which sounding from above yields the least information. It is rather surprising that little serious attention appears to have been paid to the automating and remoting of a surface sounding system, using interrogating satellites and oceanic buoys plus automatic land stations in difficult or unpopulated areas. It is certain that radiosonde releases from unattended oceanic buoys are virtually impossible, while an unattended radiometric unit could well be feasible. Particularly over oceanic areas where conventional data have minimum density, such complex systems seem particularly attractive, especially in view of the fact that the platform itself and the telemetering capability, required for even the simplest observations, constitute a major expense, together with installation and subsequent inspection.

With a sun seeker added to the equipment, daytime observations of total aerosol, total water vapor and total ozone would seem feasible, and these may well be parameters of great significance for complex numerical models of the atmosphere. Total liquid water should be an extremely valuable parameter (perhaps from microwave observations) in addition to total vapor, since the sum of water in all phases would be an element whose careful budget inside a computer could greatly improve precipitation forecasts.

## 4. INCORPORATION OF INFRARED DATA INTO AUTOMATED ANALYSIS

If infrared data are to be used primarily in real time, all techniques and details should be based on this premise - with respect to both selection of channels and methods of processing. For both GARP and the eventual complete WWW, one can visualize two computer installations at a World Meteorological Centre. One will operate on a slowly advancing but quite complex model of the atmosphere at about real time, and will fit in all input data at their actual times by a very frequent objective analysis. At specified intervals, this computer will output complete observations and analyses for archiving, dissemination and input to the second computer which will do prediction, only, at very high speed and for variable time periods (e.g., once every few days to 30 days, but generally for much shorter periods). Both computers will deal, either directly or else indirectly by parameterization, with all significant processes and parameters, whether observed frequently (temperature, wind, etc.), infrequently (ozone distributions) or not at all (vertical motions). Both computers will have products that can be degraded by poor or insufficient initial data, but both can also operate in the absence of frequent specific data (by manufacturing synthetic data internally and/or carrying forward earlier data as the atmosphere would). After such an operation has run for a week or so in pseudo-real time, gathering in vast amounts of varied data, poor data will do more harm than no data.

We may conclude that at any time we will have available relatively good first-guess fields for temperature, water vapor and ozone - particularly if we have a full mix of data flowing to the computer: conventional surface and upper air data, merchant and fixed ship surface and upper air data, buoys and automatic stations, aircraft data (including dropsondes), floating balloon data and satellite radiometric observations. There will be no purpose in squeezing crude information from infrared sensors - such as ozone data or tropospheric temperatures and vapor concentrations under complex cloud conditions. In the latter case one would concentrate instead on deducing cloud information plus stratospheric temperatures.

Since the infrared data processing will require the products of the analysis computer and will feed data back in, all intermediate steps (on other computers) should be eliminated and the infrared data should go as directly as possible into the World Meteorological Centre. Not only should the frequencies be selected to provide maximum useful information to the analysis routine, but the processing must also be done in an optimum manner, fully consistent with the treatment of all other data. This implies space smoothing to remove sub-grid scale variance and prevent aliasing. Fortunately, this should simultaneously subdue random experimental and computational errors, but care will be needed to avoid degrading high-accuracy clear-sky data by averaging with lower-accuracy cloudy-sky data. Such problems will not be as severe as might be imagined in areas of persistent cloudiness, since the analysis routine will be able to produce, for such areas, relatively good estimates of cloud parameters.

With a good first-guess field for temperature, represented by a cap superscript, the governing equations become

$$\delta T_j = T_j - \hat{T}_j; \delta I_i = I_i - \hat{I}_i = \tau_{I(p)} \cdot \frac{\partial B_\nu}{\partial T} \cdot \delta T_B - \sum_j \delta T_j \int \frac{\partial B_\nu}{\partial T} \cdot \frac{\partial \tau_I}{\partial p} \cdot dp,$$

where we have an overcast cloud or ground surfact at  $(p_B, T_B)$ , and each of the  $j$  layers is a standard layer for the numerical model being used, for which  $\delta T_j$  is assumed effectively constant - since no finer resolution of temperature information is either achievable or desirable, in view of the vertical grid scale implied by the model. In any event, it would be quite reasonable to assume slow variations of  $\delta T$  in the vertical, uncorrelated with the weighting function in an individual layer. This would not be true for  $T_j$  or  $\hat{T}_j$ .

One problem that arises is how to ensure a stable solution yet extract maximum information from the infrared data, or how to match up the number of linearly independent frequency equations with a reasonable number of temperature departure parameters, to minimize errors in computed isobaric heights at all levels. If one uses frequencies from two bands to capitalize on significantly different behaviours of  $(\partial B_\nu / \partial T)$ , the number of frequencies may easily exceed the number of standard layers (perhaps about ten up to the 10 mb level). For some systems the number of frequencies may be less than ten and in any event one suspects that the number of degrees of freedom for a temperature departure field should be less than the number of standard layers. In other words, prior knowledge of an approximate temperature structure decreases the information content of the infrared data.

One possible procedure would be to treat as the unknowns smoothed temperature departures at a small number of selected pressure levels, and interpolate linearly between them to obtain the departures appropriate to each of the  $j$  standard layers. The  $i$  frequency equations could then be solved by a straightforward least-squares technique, and the final values of  $\delta T_j$  reformulated subsequently as the output. Such a procedure is statistically sound since the first-guess field can be assumed to be of roughly equal accuracy at all levels, and since any apparent loss in information due to under-resolution is compensated by increased accuracy of the set of departures deduced. The window frequency (or frequencies) would be used for the first guess of  $T_B$ , and  $p_B$  would be obtained from the assumed  $(p, T)$  relationship; the window frequency equations would also participate in the least-squares solution.

## 5. THE HAZE PROBLEM

The haze problem is largely an unknown one but may often be serious near the ground. It is certain that aerosol absorption of solar radiation is comparable to that by water vapor - although this fact has not been appreciated in the past. If this is the case, infrared attenuation is also inevitable, and will cause trouble in the inversion procedures. It may well be that aerosol data will have to be incorporated into future

## COMMENTS ON INFRARED PROBING

atmospheric numerical models, requiring good initial data as well as information on sources and sinks. If so, a combination of emission and backscatter sounding techniques (from above and/or below) may be required, and it might then be possible to correct infrared intensities for haze effects.

In the case of haze or cloud layers (whether black radiators or not), the key parameters are the temperature of the layered material and the product of emissivity and fraction of sky coverage for that layer (these two parameters cannot be separated, and need not be separated for the inversion problem). Further complications arise, particularly in the interpretation of window intensities, associated with the spectral variations in infrared emissivities of ground, cirrus cloud and haze. It is, nevertheless, quite apparent that two window spectral regions will be needed to minimize ambiguity (and permit an inversion solution) whenever the effective window temperature does not agree with a reasonable estimate of the ground temperature (after correction, of course, for radiative effects of atmospheric gases). It is to problems such as these that greatly increased attention appears to be warranted.

072-25317

# REMOTE DETECTION OF CAT BY INFRARED RADIATION

Robert W. Astheimer

Barnes Engineering Company

Several years ago, it was established by the work of P. W. Kadlec of Eastern Airlines (Project TRAPCAT, Ref. 1), that clear air turbulence was frequently associated with temperature gradients or discontinuities in the atmosphere. Barnes Engineering Company had just completed the development of the Satellite Infrared Spectrometer (SIRS) for the Weather Bureau for remote atmospheric temperature probing and it occurred to us that this technique might be adapted for the remote detection of CAT. To investigate this possibility an experimental airborne scanning infrared spectrometer was built under company sponsorship.

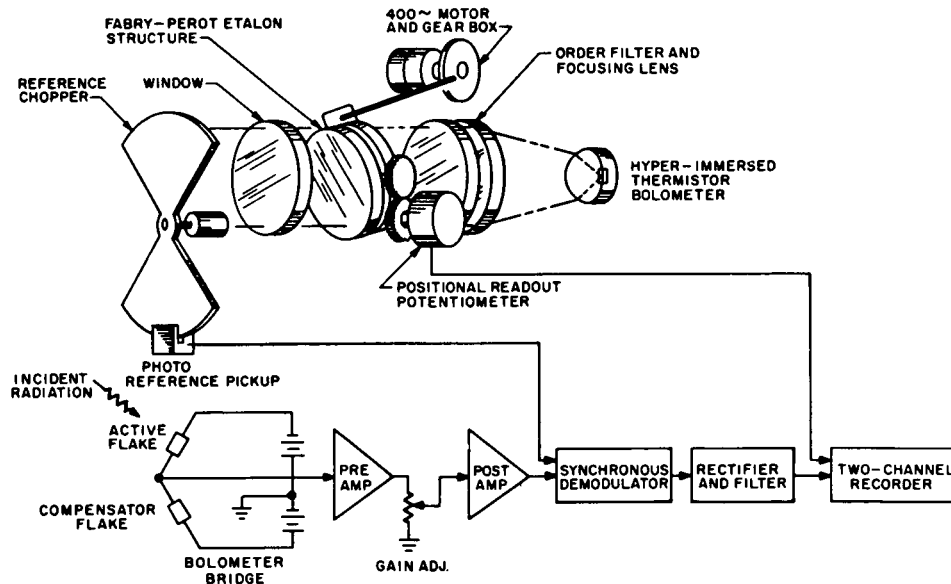


Figure 1 Fabry-Perot Spectrometer Optical-Electronic Schematic

A schematic drawing of this instrument is shown in Figure 1. It is essentially a Fabry-Perot interferometer with a narrow field of view directed along the flight path of the aircraft. The spectral bandwidth was  $0.3\mu$  and by rocking the Fabry-Perot etalon a spectral scan was obtained over the wing of

# REMOTE DETECTION OF CAT BY INFRARED RADIATION

the  $15\mu$   $\text{CO}_2$  absorption band. Distant temperature variations could be detected by comparing the signal received in a spectral region of low absorption with those in a high absorption region, the latter being an indication of the near or local air temperature which is used as a reference.

In the winter of 1966-7 a flight evaluation program using this instrument was funded by the FAA. The flights were conducted by the National Aeronautical Establishment of the National Research Council of Canada, using a T-33 Aircraft which was specially instrumented for turbulence measurements.

The results of these flight tests (Ref. 2) indicated a very high correlation between turbulence and temperature changes, and remote detection was obtained at distances up to about 10 miles. The instrument, however, was found to be extremely sensitive to pitch and only data taken when the aircraft was in very stable flight was useable.

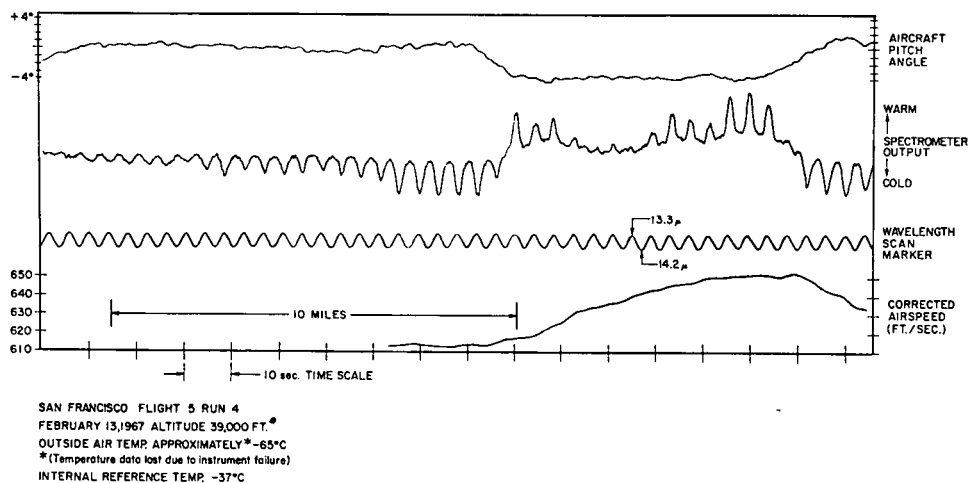


Figure 2 Sample Record Obtained with Fabry-Perot Spectrometer

Figure 2 shows one of the few records obtained where a turbulence encounter was preceded by a reasonably pitch-free period, so that the spectrometer record was not contaminated by pitch signals. The spectrometer output is a cyclic signal produced by the spectral scan, which was at the rate of 2 scans/second. When the temperature is uniform for a long distance ahead of the aircraft the spectrometer output remains constant over the spectral scan. As the turbulent region is approached, the associated temperature discontinuity is first sensed at the low absorption region of the spectral scan. This produces a 2 cps output which grows as the distance to the temperature anomaly shortens. It will be seen that the turbulence encounter in Figure 2 is first detected at a distance of about 10 miles. The spectrometer output after the turbulent region is entered is of no significance because of aircraft pitching.

Sensitivity to pitch is to be expected since when pitched down, the distant air viewed will be at a lower altitude and hence warmer than the local air and conversely when pitched up. However, the magnitude of the effect was much larger than expected. It was found that pitch changes of  $0.2^\circ$  would produce signals as large as a change in air temperature of about  $1^\circ\text{C}$  at a distance of 20 miles. It was concluded that a practical instrument would have to be pitch stabilized to better than  $\pm 0.2^\circ$  to avoid an unacceptable false alarm rate.

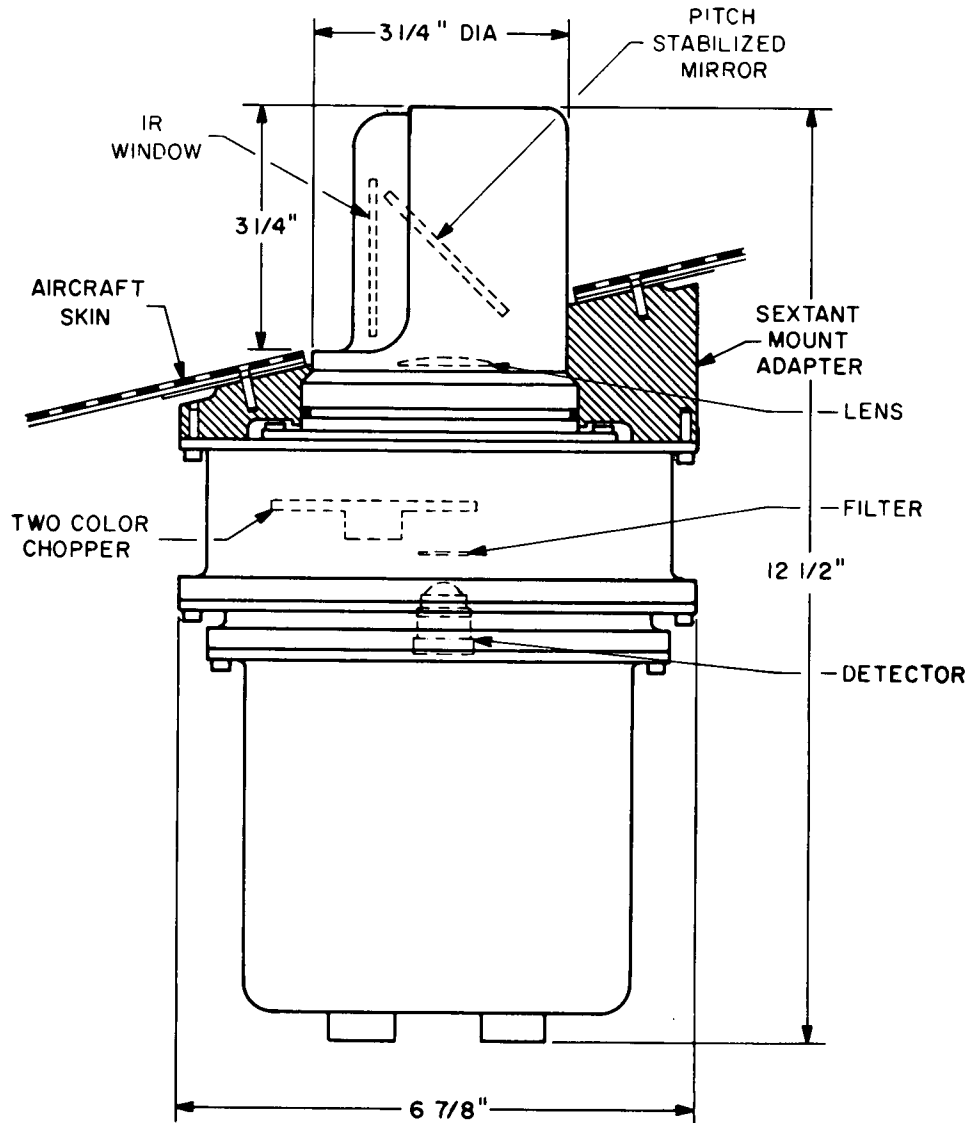
It also appeared from these flights that a continuous spectral scan was not necessary and that alternately sampling two bands was sufficient, one band in a region of high absorption indicating local air temperature, and the other band in a region of low absorption to sense distant air temperature with respect to the local air temperature reference. This would permit considerable simplification of the instrument and also increase the sensitivity since the electronic bandwidth could be reduced.

In 1967 a simplified instrument was constructed on these principles. A sketch of it is shown in Figure 3. The radiation is chopped by a wheel consisting of two filter sectors, one with a passband centered at the peak of the absorption band, and the other in a region on the wing of the band. The amplitude of the chopped signal is then proportional to the difference in radiation between the two spectral regions. This carrier is amplified, synchronously rectified, filtered and recorded as a slowly varying DC signal. When the air temperature is constant for a long distance ahead of the aircraft the radiation will be the same in the two bands and the output will be zero. A distant temperature anomaly will first appear in the filter on the wing of the band to produce a difference signal and hence a small DC output, which will increase as the anomaly is approached.

The field of view is  $1^\circ$  high and  $4^\circ$  wide. It is directed horizontally along the flight path of the aircraft and pitch stabilized to  $\pm 0.2^\circ$  by a  $45^\circ$  mirror which is servo controlled from the aircraft's vertical gyro reference. The receiver head was designed to be interchangeable with a sextant airlock fitting which is installed on the cockpit roof on many modern jet aircraft. Thus it can be conveniently mounted without cutting any metal on the aircraft.

CAT can extend horizontally over 50 miles or more, but is usually localized vertically to within a few thousand feet. This suggests that a change in altitude may be the best avoidance maneuver, and that a vertical search mode may be desirable. Since the instrument already has the servo-driven, pitch stabilizing mirror, it is easy to program this for a vertical search mode. A  $\pm 3^\circ$  vertical scan, with respect to the horizontal reference has been provided. A plot of the output normally to be expected with this scan is shown in Figure 4. The lapse rate of the atmosphere should produce a monotonic temperature increase as the scan moves downward. A turbulent zone might appear as "bump" or irregularity on this smooth curve as suggested in the figure.

REMOTE DETECTION OF CAT BY INFRARED RADIATION



A1158-012

Figure 3 IRCAT Sensor Head

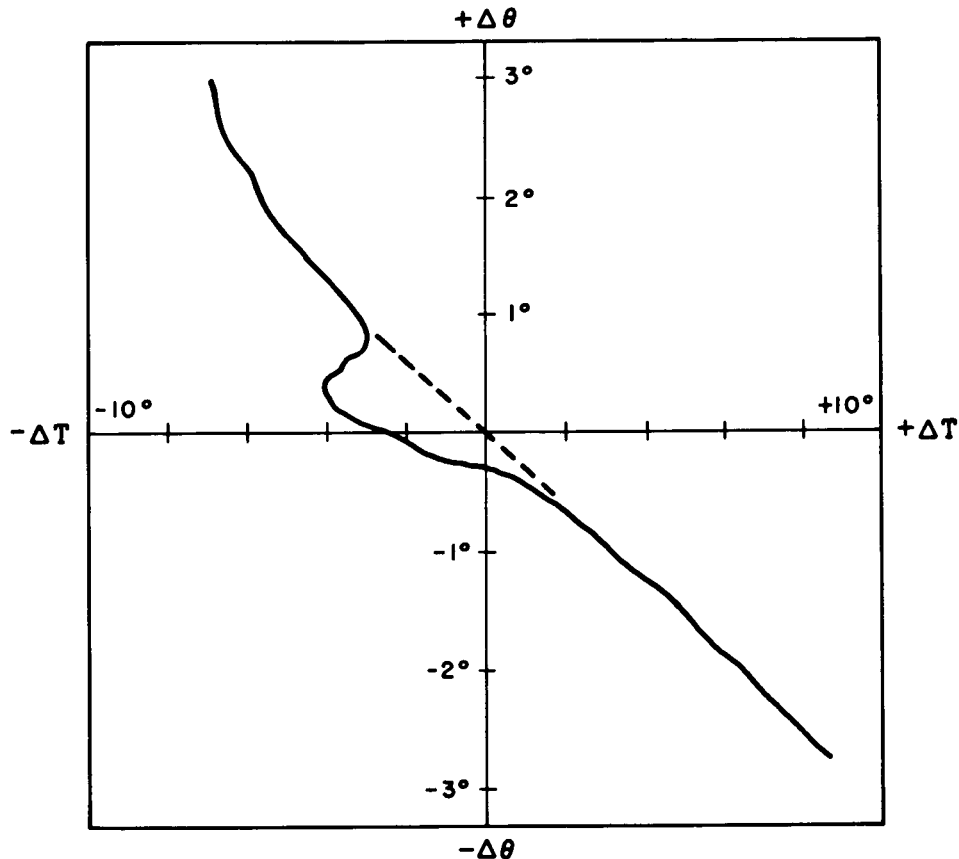


Figure 4 Vertical Search Mode Display

This instrument, which has been dubbed "IRCAT" was installed in the Canadian Research Council's T-33 and flown in the Denver area during February and March of 1968. Unfortunately, at least as far as instrument evaluation was concerned, no CAT was encountered. However, it was found that even with the line of sight stabilized, the residual pitch errors of less than  $\pm 0.2^\circ$  still produced disturbing signals.

The remaining pitch sensitivity is believed to be caused by the choice of spectral band, for the wing (or "far") filter. Figure 5 shows the transmission along a horizontal air path at 38,000 ft. for a variety of spectral bands. The contribution to signal of any distant slab of air is proportional to the difference in transmission between the two boundaries, which in the limit for an infinitesimally thick slab becomes the derivative of the transmission curve, known as the weighting function. We wish to optimize detection for the 20 - 40 mile interval. The difference in transmission or weighting function for this interval is shown in Figure 6 as a function of center wavelength for  $1\mu$  wide

REMOTE DETECTION OF CAT BY INFRARED RADIATION

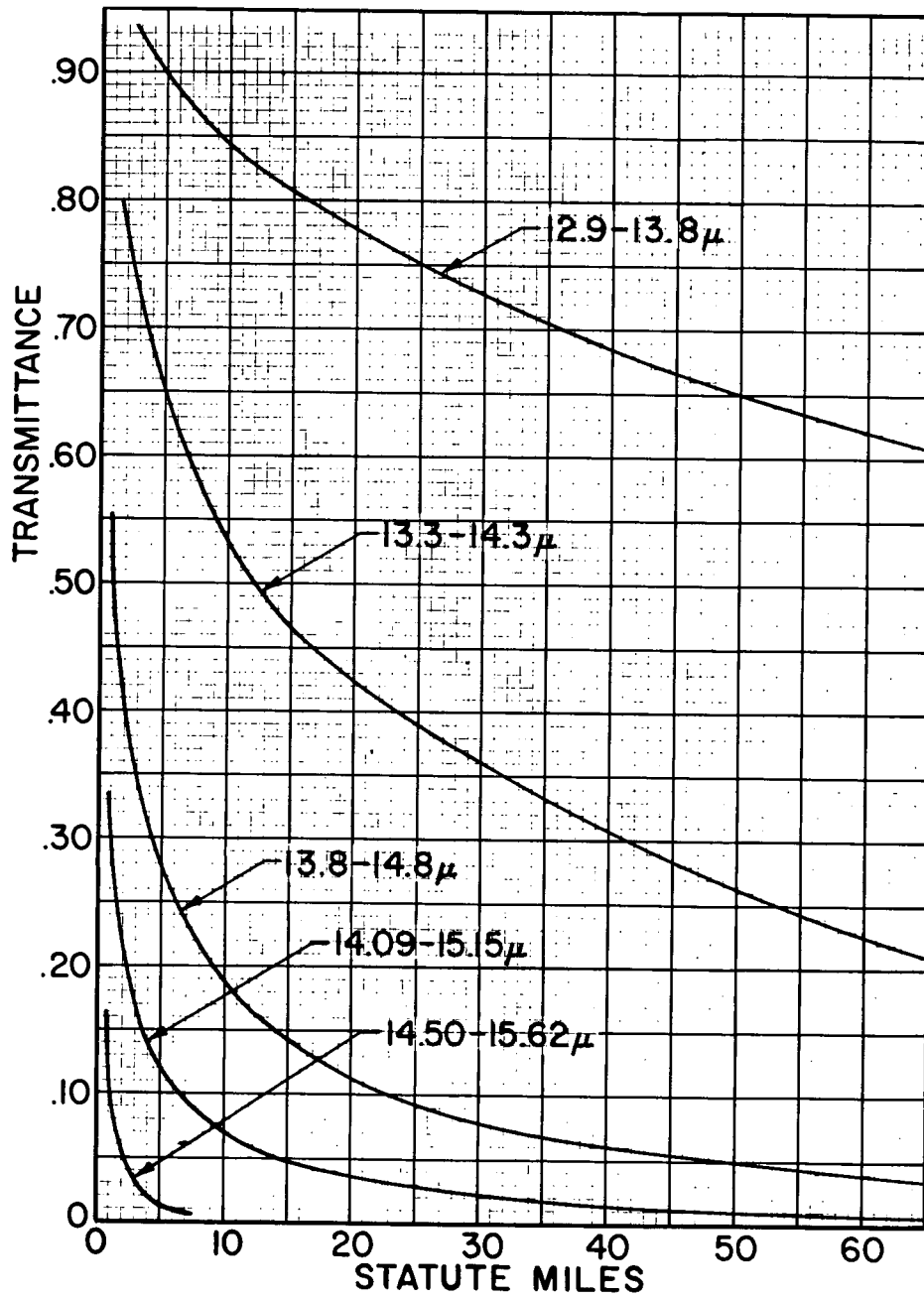


Figure 5 Horizontal Transmission of the Atmosphere at 38,000 Ft. Altitude

bandpasses, and for altitudes of 18K and 38K. A center wavelength of  $13.4\mu$  (actually  $12.9 - 13.8$ ) had been chosen as a good compromise over this altitude range.

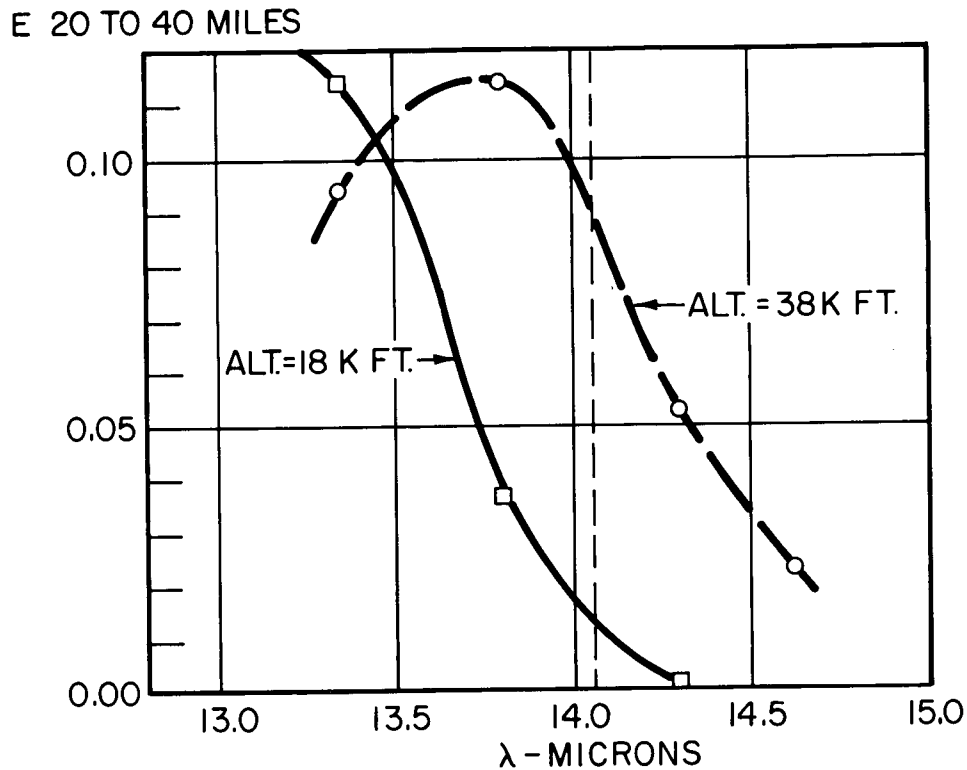


Figure 6 Effective Emissivity of a Slab of Air Extending from 20 to 40 Miles

However if we look at the transmission of this spectral region in Figure 5, we find that 68% of our signal comes from the air beyond 40 miles and 60% beyond 70 miles. Thus we were sensing mostly the very distant air, and because of the curvature of the earth are actually looking through the atmosphere, out to space. This long "lever arm" would be expected to make the signal highly sensitive to pitch.

To eliminate this condition the "far" spectral bandpass has been shifted to a center wavelength of  $14.1\mu$  where the absorption of  $\text{CO}_2$  is stronger. This will not cause much loss in sensitivity to temperature discontinuities in the 20 to 40 mile range as can be seen from Figure 6, but it will greatly reduce the contribution of the air beyond 40 miles. This spectral bandwidth will give degraded performance at low altitudes, but since long distance jet flights usually cruise at altitudes between 30K and 40K feet, it seems best to optimize the spectral region for this altitude range.

## REMOTE DETECTION OF CAT BY INFRARED RADIATION

This filter has now been installed and will be evaluated on the T-33. Also additional IRCAT instruments are under construction for evaluation by three major airlines to begin later this year.

### REFERENCES

1. Kadlec, P. W., Feb. 1966, "Exploration of the Relationship between Atmospheric Temperature Change and CAT," ION and SAE Conference on CAT, Washington, D. C.
2. Mather, G. K., May 1967, "Flight Evaluation of an Infrared Spectrometer as a CAT Detector," National Research Council of Canada, Nat. Aero. Establishment Ottawa Aeronautical Report LR 477.

SESSION 8

Crossed Beam  
Correlation  
Techniques

N72-25380

REMOTE SENSING OF WINDS AND ATMOSPHERIC  
TURBULENCE BY CROSS-CORRELATION OF  
PASSIVE OPTICAL SIGNALS

A. J. Montgomery  
IIT Research Institute  
Chicago, Illinois 60616

ABSTRACT

This paper describes a new method for the remote measurement of winds and atmospheric turbulence by the cross-correlation of passive optical signals. If small local variations in atmospheric density, temperature or other parameters cause fluctuations in scattered or thermal radiation detected by a radiometer on the ground, then the cross-correlation of the fluctuations detected by two radiometers with crossed fields of view can yield turbulence information pertaining to the region about this intersection point. When the fields of view are not quite crossed turbulent eddies will be convected through the fields of view sequentially, and the transit times of the eddies identified by the correlation procedure will yield wind information.

The successful application of this technique, detecting fluctuations in scattered sunlight, has demonstrated both the potential, and the present limitations of the method, which are discussed in this paper. Results for the power spectrum of the fluctuations and for winds at an altitude of 61

meters are shown, and the wind measurements are compared to similar measurements made with a standard anemometer located on top of a 61 meter tower.

## 1. INTRODUCTION

The determination of wind profiles, turbulence scales and three dimensional wave-number components is of great importance in numerical methods of weather prediction and in clear air turbulence studies. Some type of remote sensing system is quite clearly required if this information is to be obtained conveniently. In the case of wind measurements which are of particular importance in weather prediction for the tropical and subtropical regions of the earth, measurements at a sufficient number of grid points over a time interval of a few hours could be obtained only with a satellite remote sensing system.

At this time no proven technique is available by which wind fields may be remotely measured. However, a limited amount of wind field information may be inferred from some of the atmospheric parameters measured with presently orbiting meteorological satellites. This problem is discussed by W. Nordberg in COSPAR Transactions No. 3, "Status Report on the Applications of Space Technology to the World Weather Watch."

This paper describes a new technique presently under development which shows promise for the remote detection of winds directly. Wind components have been successfully determined at 200 and 400 foot altitudes from the cross-correlation of output signals of two photometers located on the ground with their fields of view intersecting at these altitudes. In these tests scattered sunlight was detected; however, extension of the technique to infrared measurements of water vapor, ozone or other possible atmospheric tracers is presently being studied.

This technique was first suggested by M. J. Fisher (1964) and has been developed by IIT Research Institute and NASA, Marshall Space Flight Center, for the measurement of convection speeds and turbulent flow properties in fluid flows. Since the power of the technique has very clearly been demonstrated in measurements of convection speeds, eddy scales, and eddy lifetimes, in turbulent shear layers produced by an air jet,

(Fisher and Krause, 1967), the basic method will be described with reference to these successful aerodynamic tests.

In the course of this paper we shall discuss:

- (1) The basic concept of the crossed-beam technique
- (2) Successful application to subsonic and supersonic aerodynamic flows
- (3) Methods of applying the technique to the atmosphere
- (4) Source of atmospheric fluctuations
- (5) Particular problems associated with the technique due to the unstationary nature of atmospheric phenomena
- (6) Initial measurements of winds and their comparison with data from meteorological towers
- (7) Some future developments which are currently being considered.

## 2. CROSSED-BEAM TECHNIQUE

The crossed-beam experimental configuration as used in the aerodynamic test program is shown in Figure 1. Two collimated

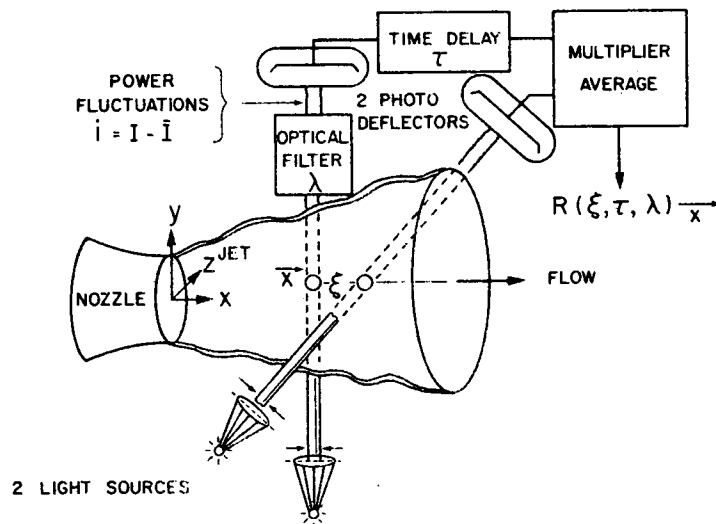


Figure 1. Space Fixed Crossed Beam Test Arrangements

beams from the two light sources shown intersect ( $\xi = 0$ ) at the point of interest in the flow. The spectral content of the radiation that is detected is selected by the optical filter or monochromator which precedes the detector in both beams, and the wavelength has to be chosen so that there are absorption or scattering losses from the beam during its passage through the flow. Since the flow is turbulent there will be variations in the numbers of absorbers or scattering agents along the two beams which will cause fluctuations in the detected signals. Measurement of the cross-correlation between the signals from the two detectors will yield information about the fluctuation level in the region of intersection of the two beams in the following manner. If a turbulent eddy having associated with it a higher or lower concentration of scatterers or absorbers than the surrounding medium passes through one of the beams it will cause fluctuations in the detected signal. Only if it passes through intersection point of the two beams will a zero time delay correlated fluctuation be produced. Thus it may be shown that the output of the correlator depends only on the properties of those eddies which pass through the beam intersection point. The correlation coefficient, which is normalized with respect to the uncorrelated fluctuations; depends as well on the eddy scales and the way in which the strength of the fluctuations in absorber or scatterer concentration vary along the two beams. Let us now consider one beam displaced a distance  $\xi$  down-stream from the other beam. An eddy convected along the line of minimum separation between the beams will cause fluctuations at one detector and a correlated fluctuation at the second detector a time  $\tau$  later, where  $\tau$  is the time for the eddy to be convected the distance  $\xi$ . Thus if the correlation between the two signals is measured as a function of time delay, this correlation function will be a maximum for  $t = \tau$ .

To put this discussion on a more formal footing, the mathematical basis of the technique will be briefly considered. Using the coordinate system shown in Figure 1, the point of beam intersection has coordinates  $(x, y, z)$ , where the  $y$  and  $z$  axis are orientated along the directions of the crossed beams. Distances from the point of intersection are denoted by  $\xi$ ,  $\eta$  and  $\zeta$  in the  $x$ ,  $y$ , and  $z$  directions, respectively. The intensity measured by the  $y$ -axis detecting system will be given by:

$$I_1(t) = I_0 \exp \left\{ - \int K(x, y + \eta, z, t, \lambda) d\eta \right\} \quad (1)$$

where  $I_0$  is the initial beam intensity and  $K$  is the extinction coefficient. The reduction in the intensity of the beam will result from both absorption and scattering losses. In a completely general case both scattering into the field of view of the detecting system and emission from within the field of

view have to be considered and, in fact, are of vital importance in the application of the crossed-beam technique to atmospheric measurements. However, the simple theory, only, will be considered here.

If the extinction coefficient,  $K$ , is divided into a mean and time varying part, equation (1) can be written

$$I_1(t) = I_0 \exp \left\{ - \int \langle K(x, y + \eta, z) \rangle d\eta \exp \left\{ - \int k(x, y + \eta, z, t) d\eta \right\} \right\} \quad (2)$$

Since the second integral in this expression will be, or can be made to be, very much less than unity, a linear expansion can be used, and the result obtained for the fluctuating signal at the detector is

$$i_1(t) = - \langle I_1 \rangle \int k(x, y + \eta, z, t) d\eta \quad (3)$$

The signal at the second detector will be of similar form and the covariance of the two detector signals will be given by

$$G(x, y, z) \equiv 1/T \int_0^T i_1(t) i_2(t) dt \quad (4)$$

where  $T$  is the period of integration which ideally is of sufficient length to yield a statistically stationary value of  $G(x, y, z)$ . Thus substituting for  $i_1(t)$  and  $i_2(t)$  we can write for the covariance of the signals that

$$G(x, y, z) = \langle I_1 \rangle \langle I_2 \rangle \int_{\eta} \int_{\zeta} 1/T \int_0^T k(x, y + \eta, z, t) k(x, y, z + \zeta, t) dt d\zeta d\eta \quad (5)$$

The term inside the time integral is clearly the covariance of the fluctuations in extinction coefficient at the points  $(x, y + \eta, z)$  and  $(x, y, z + \zeta)$  which will be significantly different from zero only within the correlated area about the beam intersection point. If the assumption is made that the fluctuations in the  $k$  do not vary appreciably over this correlation area then the covariance of the two detector signals can be written

$$G(x, y, z) = \langle I_1 \rangle \langle I_2 \rangle \overline{k^2(x, y, z, t)} L_y L_z \quad (6)$$

where  $L_y$  and  $L_z$  are the integral length scales in the  $y$  and  $z$  directions, respectively. This measured quantity is therefore related directly to the local turbulent intensities and the integral scales at the point of intersection of the beams.

# REMOTE SENSING OF WINDS AND ATMOSPHERIC TURBULENCE

A point to note here is that the spatial resolution is determined in theory by the beam diameters and that spatial resolutions obtained in turbulent intensity measurements are considerably less than the integral scale of the turbulence.

Other turbulent properties may be obtained from measurements of space-time correlations. In Figure 1 the second beam is displaced a distance  $\xi$  in the flow direction and the covariance of the two detector signals can be measured for different beam separation time delays  $\tau$ . Fisher and Krause have shown that, to a useful degree of approximation, the space time correlation coefficient that would be measured by two point probes located at the points A & B can be measured with the crossed-beam system,

$$r(\xi, \tau) = G(x + \xi, y, z, \tau) / G(x, y, z).$$

By measuring this space-time correlation coefficient over range of  $\xi$  and  $\tau$  such properties of interest as integral length scales, turbulent spectra, convection velocities, moving axis time scales and eddy lifetimes can be obtained.

This can most easily be understood with reference to some of the experimental results that have been obtained, as shown in Figure 2. Each of the individual curves is the correlation

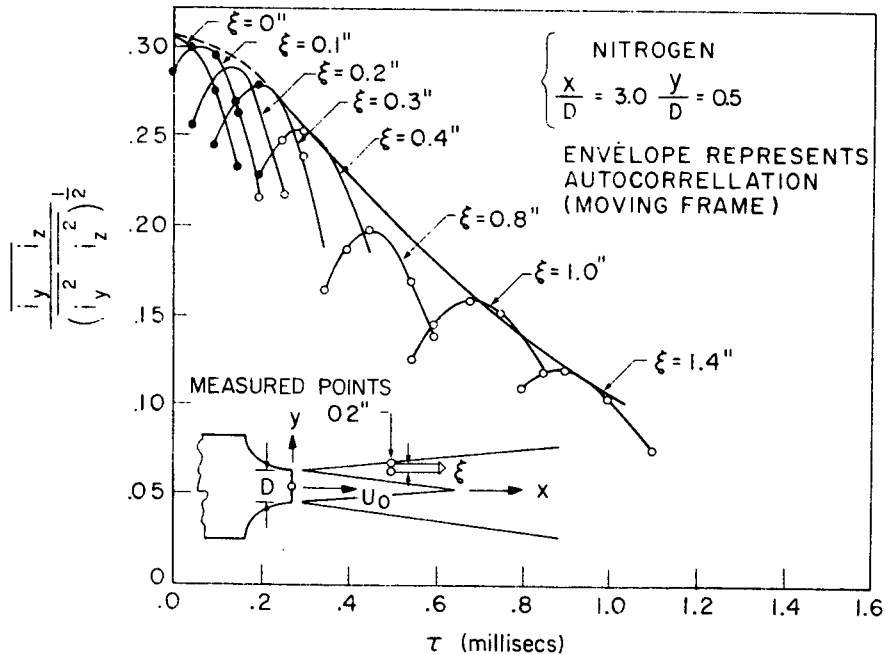


Figure 2. Crossed Beam Correlation in a Subsonic Jet

function obtained for one particular separation of the two beams. The convection velocity can be obtained from any of these curves, with the exception of the one in which  $\xi = 0$ , by dividing the known value of  $\xi$  by the time delay corresponding to the peak of the correlation function. The maximum value of the correlation function decreases as the beam separation increases. This behavior reflects the fact that as an eddy moves downstream it gradually loses its identity. The eddy-lifetime is defined as the time in which the envelope decreases to  $1/e$  of its initial value. The space correlation coefficient  $r(\xi, 0)$ , which can be generated by noting the points at which the individual cross-correlation curves intersect the  $\xi = 0$  axis, may be integrated over all  $\xi$  to obtain the integral scale of the turbulence, and the cross-power spectrum may be obtained by the Fourier transform of the cross-correlation function.

It was noted in the above discussion that the choice of optical wavelength has to be such that there is absorption or scattering along the beam so that turbulence effects therefore result in fluctuations in the detected signal. In supersonic flows, where there are significant variations in air density, some measurements were made at a wavelength of 1850A where oxygen absorbs. In subsonic flows, and in some experiments in supersonic flows, a tracer was introduced in the flow, and the fluctuations in visible light produced by variations in the number of tracer particles along the beam were detected.

In the subsonic case very good agreement was obtained with hot wire measurements, and this comparison also demonstrated the high spatial resolution that may be obtained using the crossed-beam technique. No comparison of the supersonic results with previously measured values is possible, since these measurements represent an advance in state of the art.

### 3. ATMOSPHERIC MEASUREMENTS

In the atmosphere the use of artificial light sources would be most undesirable since this would severely limit the application of the technique. Natural, distributed sources fall into three categories

- a) Scattered Sunlight
- b) Thermal Emission
- c) Non-Thermal Emission (for example, airglow).

Figure 3 shows the atmospheric radiation background for two altitudes. During daylight hours scattered sunlight predominates for wavelengths shorter than approximately 3 microns. At night scattered starlight, scattered moonlight and airglow are the main sources of radiation in the visible and near infrared portion of the spectrum.

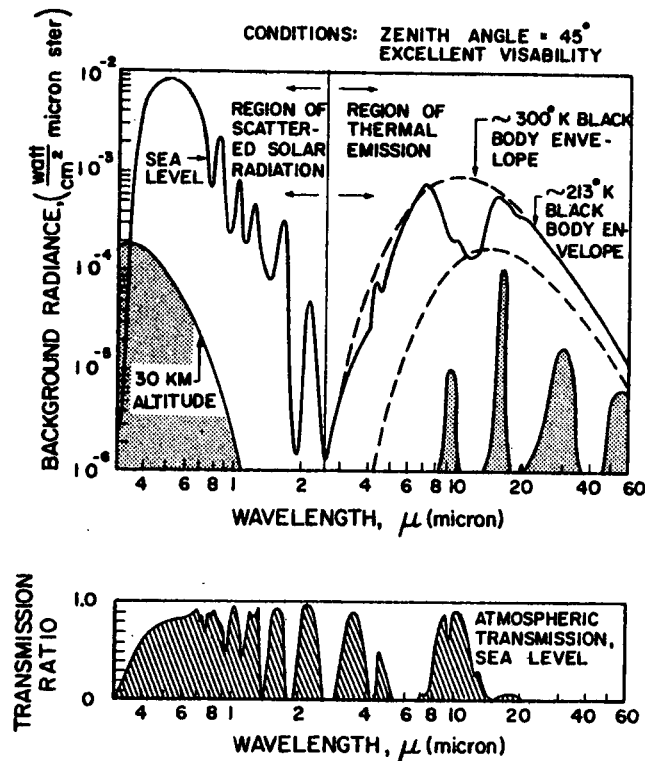


Figure 3. Emission Spectrum of Atmospheric Radiation Background for Two Altitudes.

To apply the crossed-beam technique to atmospheric measurements, the correlated portion of the detected fluctuations signals must be of such a magnitude that it can be pulled out of the noise in a reasonable integration time. The noise signal will consist of uncorrelated fluctuations from parts of the beam away from the intersection point, detector noise and shot noise associated with the mean level of radiation incident upon the detector. Ideally the design of the optical system would ensure that the predominant source of noise is due to atmospheric fluctuations, but if narrow spectral bandwidths have to be used in the infrared portion of the spectrum this may not be possible.

Even if the uncorrelated atmospheric fluctuations are the predominant noise source, it may not be possible to isolate the correlated portion of the signal in a reasonable integration time. The nonstationary nature of atmospheric phenomena limits the integration time, so that, if there are too many eddies along the field-of-view of the detector which significantly contribute to the atmospheric fluctuation level, it may not be possible 'pull out' the correlated signals by the cross-correlation, within times for which stationary conditions can be considered to obtain. For this reason, it is necessary to be selective in the type of measurement that is made so that the number of eddies

along the detector field-of-view which significantly contribute to the measured fluctuation level is limited.

In fact it would be difficult to choose a measurement wavelength for which there are equal contributions to the detected signal from different altitudes but the contribution from different altitudes is difficult to determine without a more comprehensive knowledge of turbulence scales, and temporal variations in density, aerosol concentration and temperature.

It was shown previously that the covariance of the signals from two detectors with crossed fields-of-view is given by

$$G(x, y, z) = \langle I_1 \rangle \langle I_2 \rangle \overline{\kappa^2(x, y, z, t)} L_y L_z .$$

This expression contains the square of the extinction-coefficient fluctuations and the product of two scale lengths. The magnitude of the extinction coefficient fluctuations will usually be greater near the ground because the air density and the aerosol concentration are greater, and because of the turbulence generated by flow over uneven terrain. On the other hand, the turbulence scales are less so that there will be a compensating effect, and the altitude region which contributes most significantly to the fluctuating signal is not clear-cut. There are obviously some severe problems in reliably computing contributions to the fluctuations from different altitudes, and this point will be clarified in the discussions of particular cases which follow.

### 3.1 Scattered Sunlight Measurements

A photometer on the ground pointing upwards will receive radiation which is scattered into its field-of-view by both air molecules and aerosol particles. The mean signal level recorded will depend on the elevation and azimuth of the field-of-view of the photometer relative to the angle of the sun and upon the meteorological conditions. Because of the presence of temperature and corresponding density variations in the air which will be convected through the photometer field-of-view by winds, there will be fluctuations superimposed upon the mean photometer output signal. The magnitude of these fluctuations will depend on the scales of these eddies and the absolute magnitude of the air density and/or aerosol density variations. For a constant eddy scale and percentage variation in scatterer concentration, the decrease in air density with height will reduce the molecular scatter contribution to the fluctuation level at the detector by a factor of 10 for eddies at an altitude of 8 kilometers as compared to fluctuations at ground level. The aerosol fluctuation contribution under similar conditions will fall off much more rapidly because of the much quicker relative decrease in aerosol concentration with altitude.

## REMOTE SENSING OF WINDS AND ATMOSPHERIC TURBULENCE

Using the turbid atmosphere model of Elterman (1964) the detected signal will be down a factor of 10 at an altitude of 1 kilometer.

However, since the eddy scales increase with altitude, the ability to detect fluctuations at an altitude of 1 kilometer by the cross-correlation of the photometer signals with the experimental arrangement shown in Figure 4 may not be more difficult than if the measurements are made with the beams crossed at an altitude of 50 meters to detect fluctuations at this level. In fact since scattering at low altitudes is dominated by atmospheric aerosols, and the aerosol concentration decreases very quickly with altitude as shown by the aerosol scattering coefficient in Figure 5, we expect the low altitude fluctuations to predominate and, for this reason, the experiments presently being carried out are aimed towards the measurements of winds and turbulence at altitudes up to about 1000 meters by detection of scattered sunlight.

In this discussion I have somewhat glossed over the origin of the fluctuations in scattered sunlight except to say that they are due to fluctuations in concentrations of aerosols and air molecules. Direct sunlight will be scattered by molecules and aerosols in the field-of-view of the detector so if there is a density increase or increase in concentration of aerosols in a volume element of the field-of-view, there will be an incremental increase in the direct scattered signal. However, light scattered into the field-of-view at higher altitudes may be scattered out of the beam and an increase in density or aerosol concentration in a volume element would therefore cause a decrease in detector signal. In addition there will be a contribution from multiple scattering into the 'beam'. The relative values of these different contributions will depend strongly on the atmospheric conditions and the angle of the sun with respect to the direction of view of the photometers.

If the direct scattered sunlight predominates it would be possible to obtain a positive correlation even in the complete absence of fluctuations in scatterer concentration in the region of the beam intersection point. The sunlight reaching this region has traversed a long path through the atmosphere and therefore there will be intensity fluctuations. Similar fluctuations will be present in the scattered sunlight which could result in a significant correlation between the two detected signals. However, when there is a lateral separation between the two beams as is necessary in wind measurement, this effect is minimized.

Midwest Research Institute (St. John, A. D. and Glauz, W. D. 1968) have performed some calculations to determine the relative contributions to the fluctuations in the detected signal. However, multiple scattering was not included, and further work is definitely necessary in this area.

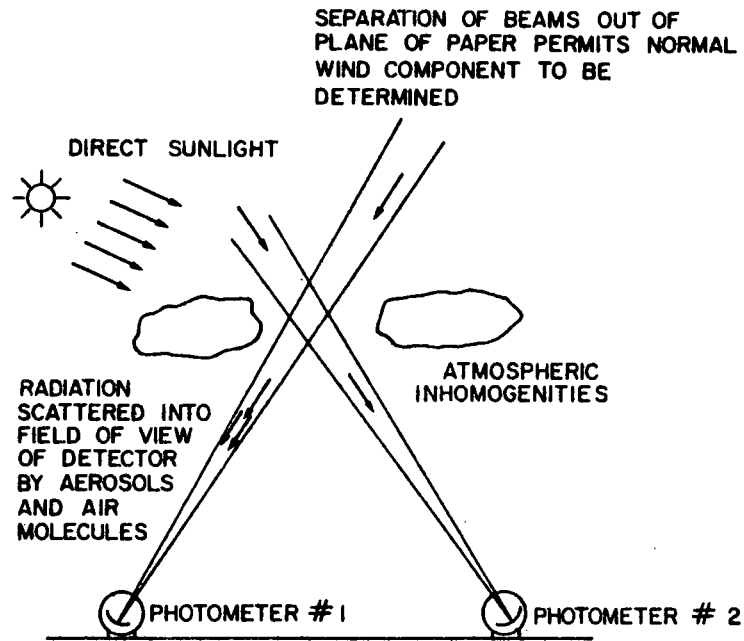


Figure 4. Application of Crossed Beam Technique to Measurement of Atmospheric Winds and Turbulence

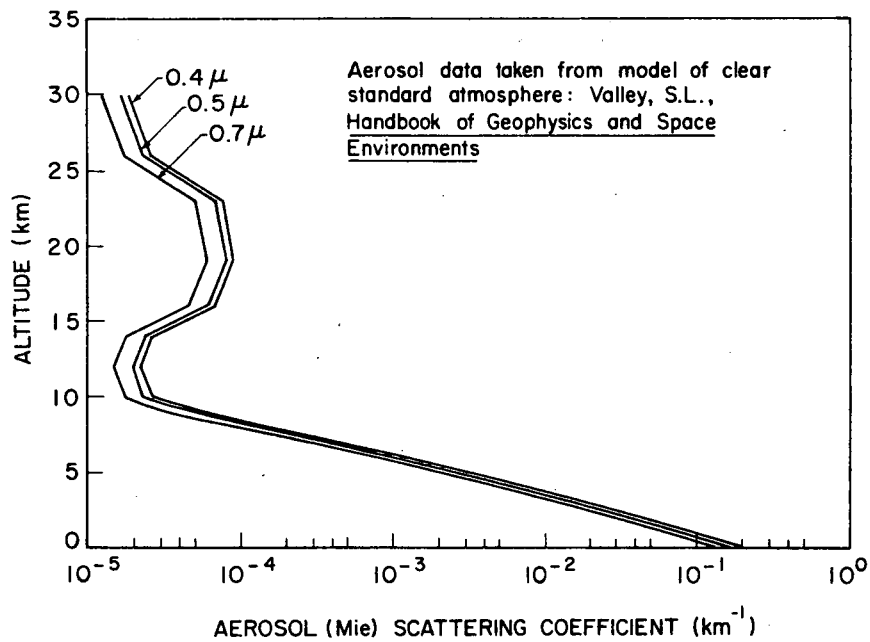


Figure 5. Aerosol (Mie) Scattering Coefficient vs. Altitude for Visible Wavelengths

3.2 Thermal Emission

Although successful measurements have been made detecting scattered sunlight in the visible portion of the spectrum, this particular method is restricted to substantially cloudless sky conditions. If an isolated cloud enters the field-of-view of the detecting system there is an increase by a factor of the order of 5 in the detected signal. With a response extending down to 0.01 cycles per second the recorded ac signal will also increase to a level which will be dependent upon the rate of movement of the cloud. When the cloud fills the field-of-view a main source of signal fluctuations will be the nonuniformities in the cloud itself.

If this signal were recorded the power associated with the fluctuations due to clouds would generally dominate the signals, and spurious cross-correlations would be measured. However, if clouds are in the field-of-view for only a small fraction of the recording time then this effect can be eliminated by setting the signal at zero whenever a cloud is in the field-of-view of either photometer system.

Potentially these problems can be largely overcome if water vapor is used as a tracer and measurements are made in the vicinity of the water vapor absorption band at 6.3 microns. The exact choice of wavelength will determine the relative signal received from volume elements at different distances from the detecting system. ESSA is presently studying this problem.

Measurements of wind profiles at higher altitudes could be made by detecting the thermal emission of ozone at 9.6 microns. Some preliminary calculations (Krause *et al.*, 1966) indicate that fluctuations of the order of 0.01% could be detected with 8 inch collector optics and state-of-the-art detectors. We are presently studying these approaches and plan field tests to determine their potential and to further increase the usefulness of the crossed-beam technique as applied to atmospheric measurements.

4. MEASUREMENTS OF SCATTERED SUNLIGHT FLUCTUATIONS

The photometer systems used in the atmosphere measurements of scattered sunlight have the following specifications:

Frequency Response	Variable within range 0.01-300 Hz
Mean Signal/RMS Noise	$10^4$
Field-of-View	5-30 minutes of arc
Spectral Response	0.4-1 micron
Spectral Bandpass	Variable (minimum 500A)

Details of the design of the photometer system are given in the appendix. A photograph of one of the photometers is shown in Figure 6 and the instrumentation van in Figure 7.

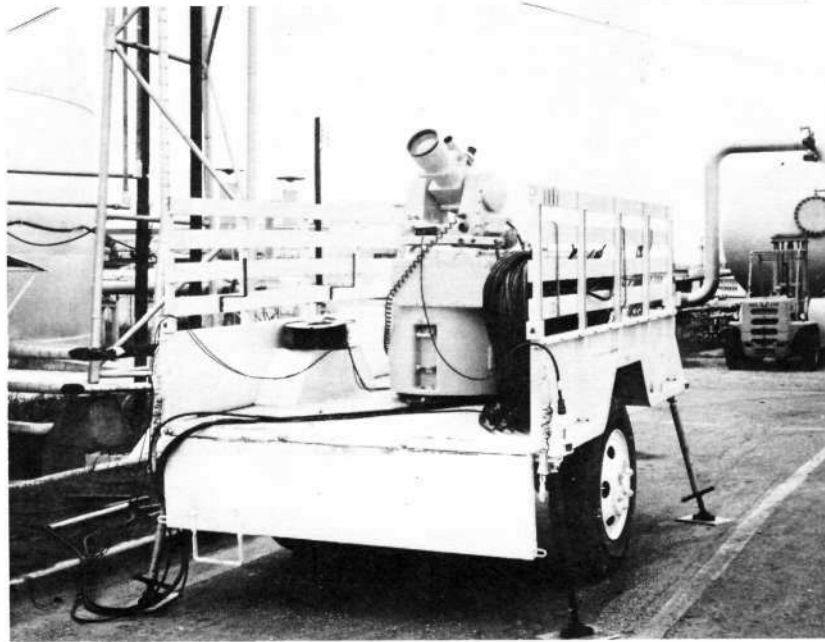


Figure 6. Photometer Trailers (by Courtesy of MSFC)

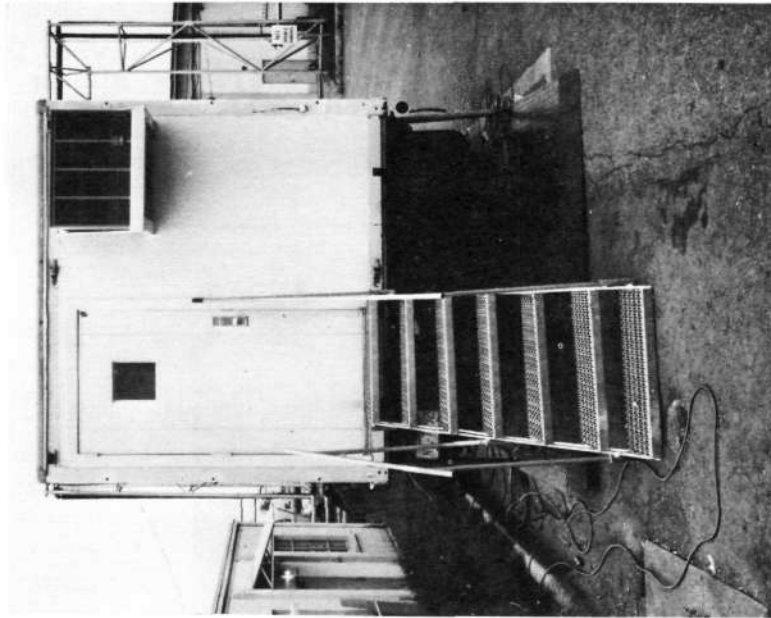


Figure 7. Instrumentation Van  
(By Courtesy of MSFC)



Power spectral density measurements of the fluctuations under clear sky conditions are shown in Figures 8, and in Figure 9 these results are replotted with the ordinate - power spectral density  $\times$  frequency. In this second plot the area underneath the curve in a particular frequency interval,  $\Delta f$ , is directly proportional to the energy in this frequency interval. These results were obtained by playing back the recorded signals through a variable bandpass filter and measuring the output level with a RMS voltmeter. It can be seen that the fluctuations follow quite closely a  $-6.5$  power law down to frequencies less than 0.1 cycles per second. The roll off beyond 0.01 cycles per second is due in part to the high pass filter which reduces the amplitude of the signal 3db at 0.01 cycles per second and winds down at the rate of 6db per octave.

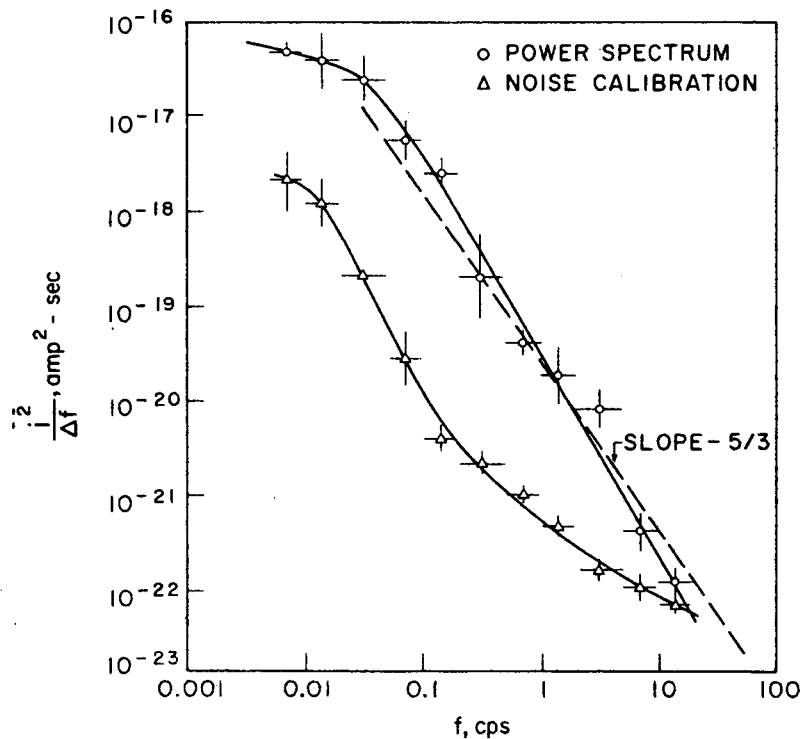


Figure 8. Single Beam Power Spectrum  $\frac{\overline{i^2}}{\Delta f}$  vs.  $f$

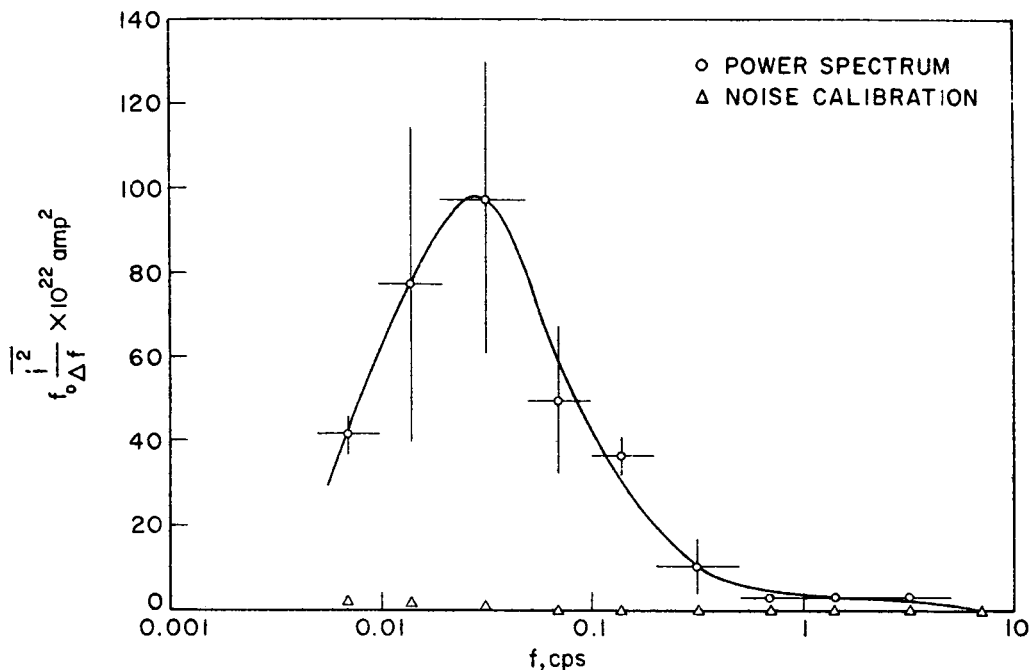


Figure 9. Single-Beam Power Spectrum,  $f_0 \frac{\overline{i^2}}{\Delta f}$  vs.  $f$

A line of slope  $-5/3$  is also shown in Figure 8 and it is evident that the results differ significantly from the  $-5/3$  dependence that would be expected in point measurements. This is not an unexpected result because of the integration along the line of sight. The contribution of an eddy, being convected through the field-of-view of the photometer system, to the fluctuating signal will be proportional to both the variation in the number of scatterers associated with the eddy, and the size of the eddy measured along the field-of-view of the detecting system. Because the contributions from different eddies are uncorrelated then the resulting rms fluctuation from  $n$  eddies along the line of sight will only be  $n$  times the contribution of a single eddy. This intuitive argument would indicate that a  $-8/3$  power law might be expected. At this time

there is no proven explanation of the  $-6.5/3$  power law that is actually measured, however, if the turbulent eddies were elongated in the flow direction, such a reduction in the power dependence could be observed. The effect of the increase in eddy scales and the decrease in the magnitude of the fluctuations with altitude would also be expected to change the power spectrum, but no attempt has yet been made to study the way in which these variables would effect it.

## 5. CROSSED-BEAM MEASUREMENTS OF WINDS

Since atmospheric crossed-beam measurements detecting scattered sunlight are continuing at the present time this paper is a status report of the results obtained to date. Successful wind measurements have been made, and this success has gone hand in hand with the development of suitable statistical methods to reduce the effects of non-stationarity in the data.

The geometry of the crossed-beam arrangement used in the atmospheric tests is shown in Figure 10. The location and

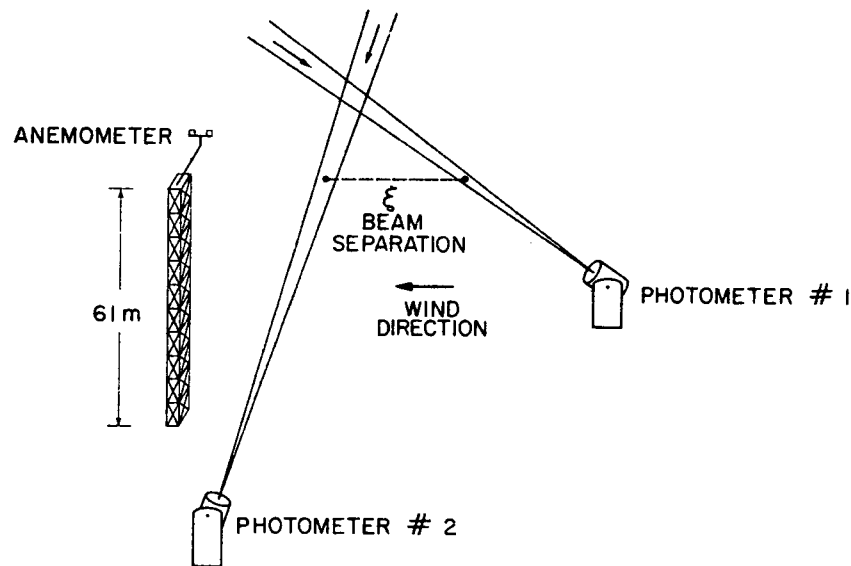


Figure 10. Geometry at Atmospheric Crossed Beam Arrangement.

## REMOTE SENSING OF WINDS AND ATMOSPHERIC TURBULENCE

viewing direction of the photometers are usually made to lie in two parallel vertical planes which are chosen to be approximately perpendicular to the wind direction. Most of the measurements to date have been made with the two beams crossed at an altitude corresponding to the top of the meteorological tower. Thus a direct comparison between the wind measured with an anemometer on top of the tower and that obtained from the crossed-beam measurements is possible. It should be noted that the altitude at which the wind is in fact measured depends on the wind direction. If the wind direction is perpendicular to the parallel vertical planes containing the lines of sight of the detector systems, then the altitude of measurement will be the height at which the beams would intersect if the two vertical planes were coincident. For all other wind directions an eddy can only traverse both 'beams' at a different altitude determined by the angle between the beams and the wind direction. Since in a practical case both the wind speed and the wind direction will be varying, the result obtained with the crossed-beam system represents a complex type of averaging over both altitude and time. If the wind direction is fairly constant within  $\pm 20^\circ$  of the plane of the beams then the altitude region over which the averaging will take place will be small, and the crossed-beam measurement can be considered to yield an average wind velocity at the crossing altitude.

Before describing some of the experimental results that have been obtained some comments about the fluctuation records, and the data processing are in order. Under clear skies the signal fluctuations with a bandpass from 0.01 - 10 Hz are typically of the order of 1% of the mean signal level. Although this fact is not completely established, the fluctuation levels appear to be less after a rain when the ground is still damp. This is not at all unlikely since the aerosol concentrations near the ground would be lower under these circumstances. In a 45 minute record it is usually found that there are portions of the record in which the fluctuation level is considerably higher than the average. Sometimes there is an obvious cause for this, such as a car going by on a nearby dirt road raising a considerable dust cloud which drifts through the detector field-of-view. At other times there is no apparent reason for the increased activity. In any case, if a straight averaging procedure were used in the data processing, the portions of the record in which the fluctuations are large tend to dominate the correlation results.

To avoid this problem the data are processed in the computer in 6 minute segments, and the time averaged cross product is normalized with respect to the rms levels in that segment of the record before the pieces are averaged through the entire record. In other words, the correlation function is found for each segment and this procedure successfully prevents any particular piece from dominating the entire record.

Despite these precautions, spurious correlations are still sometimes obtained which make identification of the peak in the

correlation function corresponding to the wind speed ambiguous. The so-called statistical error is utilized to help solve this problem. In simple terms a correlation function is found for each six minute piece of data throughout the record. These correlation functions are averaged and the rms variation in the value of the correlation function is found for each time delay. It is this rms variation, suitably weighted to obtain the desired statistical certainty in the result, which is called the statistical error.

Ideally, if a stationary situation existed, the statistical error would decrease as the square root of the number of pieces included; however, it is found in the atmospheric data that the error begins to decrease, but after some time period (usually between 30 minutes and one hour) the error either oscillates or starts to increase again. The integration time is therefore chosen as the time in which the statistical error reaches its minimum value.

Figure (11-14) shows some of the results obtained which have been previously presented by Stephens, Sandborn and Montgomery. Figure 11 is the result for a zero separation case with the fields-of-

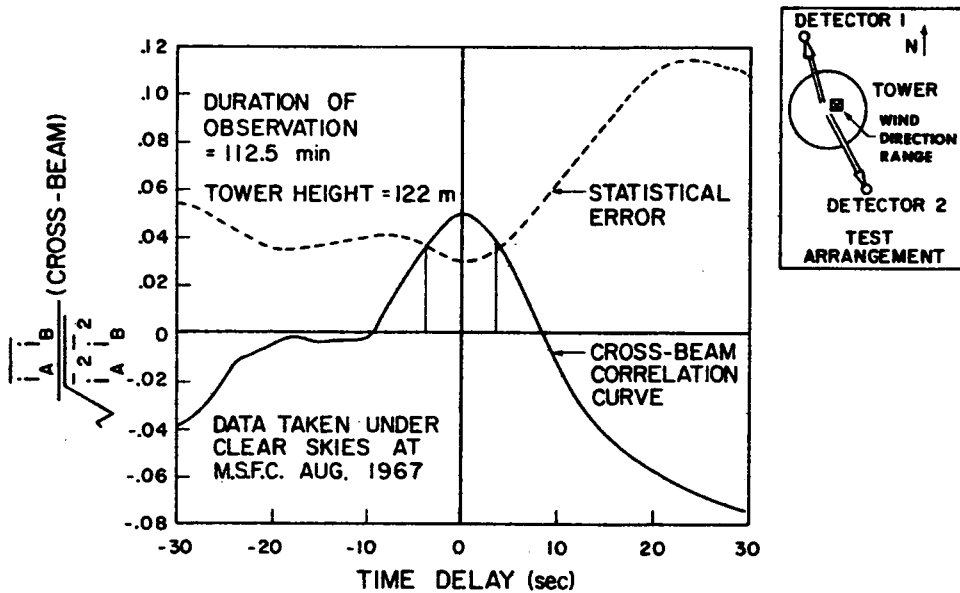


Figure 11. Cross Correlation Function - Zero Beam Separation

view of the two detectors intersecting at an altitude corresponding to the top of the meteorological tower at MSFC. No wind information is of course available from this measurement. The correlation coefficient is quite small  $\sim 0.05$  and the peak only slightly exceeds the statistical error. However, the peak does occur accurately at  $t = 0$  as would be expected in this measurement. The statistical error is associated, of course, with the value of the correlation function; hence with a 90% probability the correlation function at zero time delay is  $0.05 \pm 0.03$ . This statistical probability results from the choice of weighing factor applied to the rms variations in the correlation function. Plotting the results in this manner is used for ease of presentation.

The remaining wind measurements were made at the Colorado State University meteorological test site in the North Platte River Valley, located in northeastern Colorado, approximately fifteen miles east of the first major pressure rise of the Rocky Mountains.

Figure 12 shows the anemometer data plotted as a first order probability density of velocity, and the correlation function plotted in terms of a wind velocity. Since the beam separation was 30 meters the long tail of the cross-correlation curve

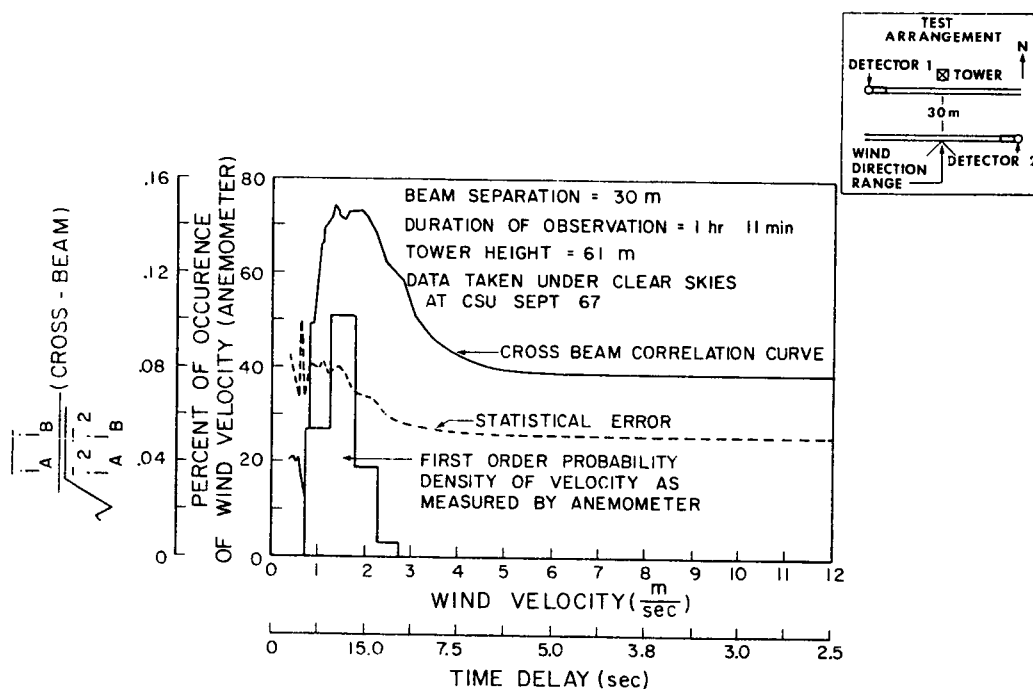


Figure 12. Light Wind Case  $\sim 3$  mph.

represents delay times from 2.5 to 5 seconds as compared with the 5-30 second time delay range covered by peak. Thus this tail results from the method of presentation and is not significant. There is quite good agreement between the anemometer and the crossed-beam results although the winds were light and variable.

Higher wind cases are shown in Figure 13 and 14 in which, once again, good agreement is shown between the anemometer and the crossed-beam results. In Figure 13 the statistical error is relatively small and the correlation coefficient at the peak is large. Under these windy conditions a greater concentration of aerosols might be expected to be present close to the ground, and this could weight the results by increasing the contribution to the fluctuating signal from low altitudes. This would have the effect of decreasing the number of eddies along the field-of-view of the photometers which contribute significantly to the fluctuation level, and therefore increase the correlation coefficient.

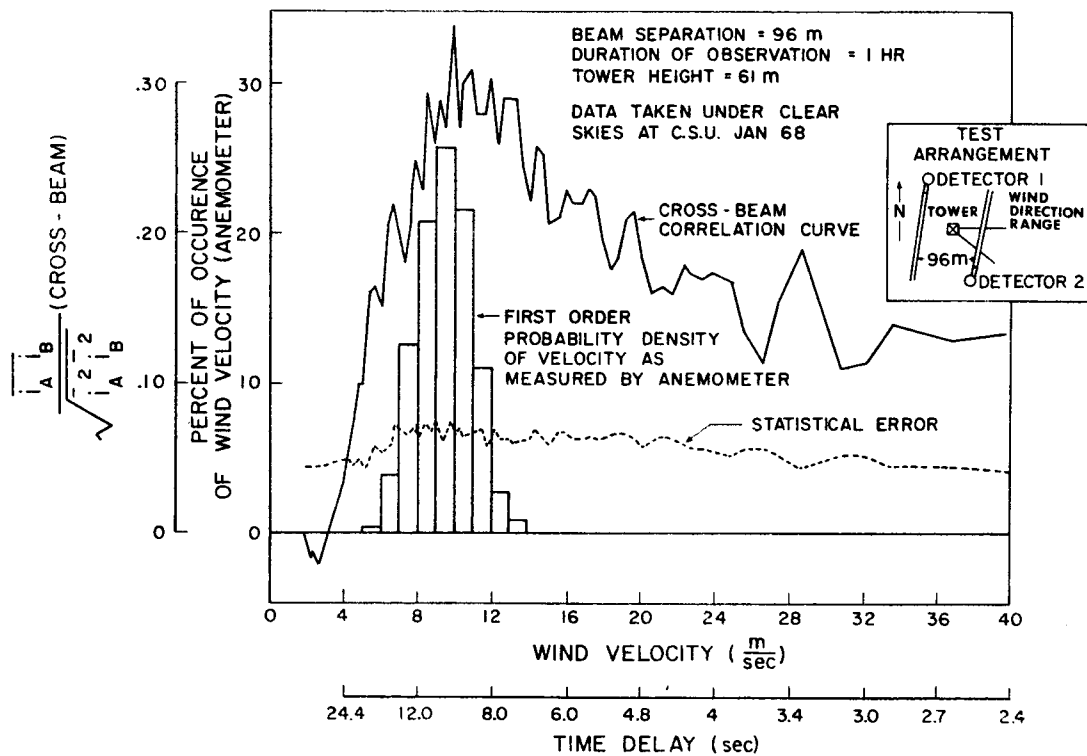


Figure 13. Medium Wind Case ~ 20 mph.

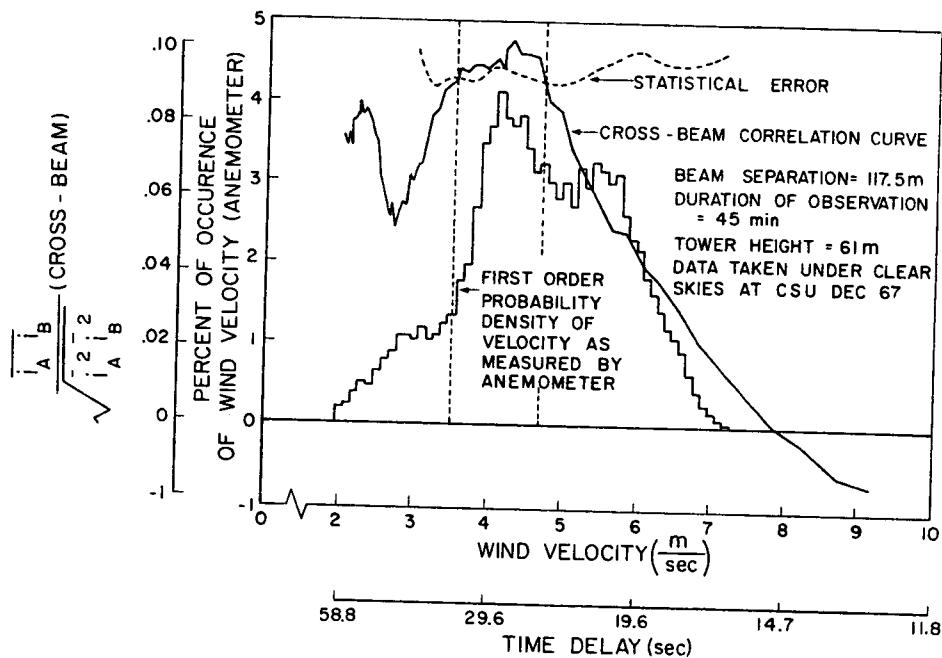


Figure 14. Low Wind - Large Beam Separation Case.

The results described above are summarized in the following table. There is encouragingly good agreement between the crossed-beam and the anemometer results. The field tests are continuing and it is hoped that results presently being analyzed will show the same promise of the results described in this paper.

## 6. FUTURE DEVELOPMENT OF THE CROSSED-BEAM TECHNIQUE

The immediate future developments of the crossed-beam technique have to be directed towards exploring the potential and the limitations of the method. For example, in order to remove some of the ambiguities which sometimes arise in determining the peak in the correlation function which corresponds to the wind speed, a multiple beam system is being developed. This will permit results for several beam separations to be obtained simultaneously, and in addition, because the beam will perform in a fan configuration, the wind direction can also be found if the correlation maxima are sufficiently well defined.

Table 1. X-BEAM AND ANEMOMETER COMPARISON

RUN	TEST CONDITIONS*							ANEMOMETER RESULTS				X-BEAM RESULTS		
	DATE	T <sub>START</sub> (hr)	T <sub>STOP</sub> (hr)	WIND CONDITIONS	DIR. FLUCT. (deg)	BEAM SEP. (m)	(U <sub>N</sub> ) MIN. (m/s)	(U <sub>N</sub> ) MAX. (m/s)	(U <sub>N</sub> ) (m/s)	(U <sub>N</sub> ) (m/s)	B (cps)	(U <sub>N</sub> ) (m/s)	(U <sub>N</sub> ) (m/s)	$\frac{(U_N)_{XB} - (U_N)_{AN}}{(U_N)_{AN}}$ (%)
I	9/29/67	0905	1038	LIGHT WIND FROM SOUTH	±23	30	0.7	2.5	1.6	1.3	.45		17.65	
II	1/03/68	1101	1203	LIGHT TO MODERATE WIND FROM EAST	±38	116	2.0	7.0	4.1	4.4	.50		6.82	
III	1/03/68	1343	1445	MODERATE TO STRONG WIND FROM SE	±25	96	6.0	13.0	9.5	9.7	.63		2.11	
IV	11/30/67	1235	1535	STRONG NW WIND	±30	71	8.0	20.0	14.6	13.6	.73		6.84	

\* ALL DATA TAKEN UNDER CLEAR SKIES IN ST. VRAIN RIVER VALLEY, COLORADO

## REMOTE SENSING OF WINDS AND ATMOSPHERIC TURBULENCE

To avoid the limitations imposed on the present system under the cloudy skies the potential of infrared measurements has to be explored. The physics of the problem in terms of trying to define the altitude contributions to the fluctuating signals in both the scattered sunlight and infrared cases has to be studied. This would permit estimates to be made of the altitude resolution and maximum altitudes for which useful wind data may be obtained.

Some new approaches in terms of the data reduction methods have to be developed. The use of the derivatives of the signals to effectively flatten the frequency spectra and narrow the correlation peak is presently being tried. Further examination of the statistical error, and the relative errors between correlations for different time delays obtained from the same data record have to be examined.

### 7. CONCLUSIONS

The potential future development of the crossed-beam technique once the feasibility of its application to atmospheric measurements has been demonstrated is very great. There are a large number of different types of measurements, some of which have been discussed above, that can usefully be made which will contribute to the understanding of atmospheric phenomena, and to improvement in weather forecasting.

Successful ground tests should be followed by measurements from aircraft. Clear air turbulence is of great importance as far as its effect on aircraft operations is concerned, and much could be learned of this phenomena by crossed-beam measurements from an aircraft. Of course in the aircraft case, instead of the fluctuations being produced by turbulence eddies being convected through stationary beams, the fluctuations will be largely produced by the movement of the "beams" or photometer field's of view through regions of atmospheric turbulence. The fluctuation frequencies will be considerably different. Also in the aircraft case, time delay tricks as illustrated in Figure 15 may remove the necessity of having two photometers separated in space.

The two photometers are mounted on a stabilized platform and have an angle  $\theta$  between their respective fields of view. If the turbulence structure is assumed to be frozen, then the fluctuations detected by photometer #1 originating from a height  $h$  above the aircraft will be repeated in signal from photometer #2 a time  $\tau$  later, where  $\tau$  is the distance  $d$  divided by the velocity of the aircraft. The altitude region of interest can therefore be studied by selecting the appropriate time interval  $\tau$ . To obtain wind speeds it is necessary to separate the photometer fields of view in a direction perpendicular to the plane of the

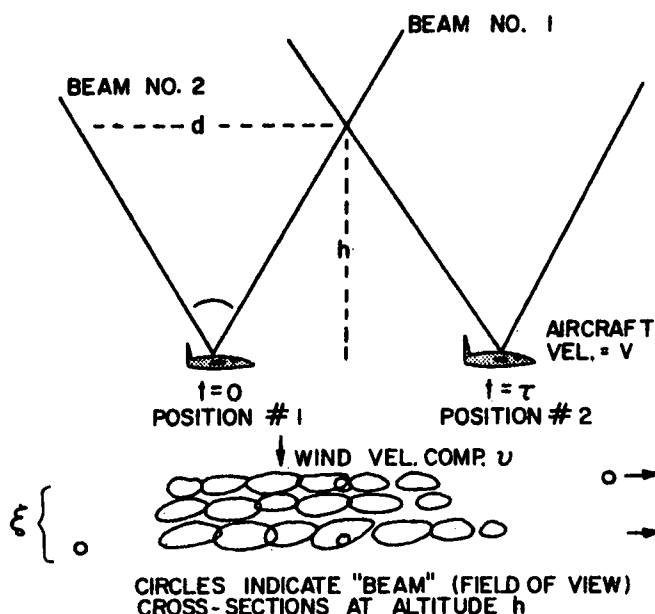


Figure 15. Scanning System Concept - For Particular Wind Speed  $u$  and Beam Separation  $\xi$  We have Time  $\tau$  for Line of Eddies Originally in Beam #1 to Reach Beam #2. At Height,  $h$ , Beam Delay is  $\tau$ , so a Maximum Correlation is Recorded For This Time Delay. With a Fan of Beam Giving Number of Different  $\xi$ 's the Wind Component as a Function of Altitude May Be Measured.

paper. An ambiguity is introduced here which can only be resolved by use of a fan of "beams" from one of the photometer systems. This problem has been discussed by Krause *et al.* (1966) and by Krause (1967) and will not therefore be considered further here.

The logical development of the technique through an aircraft operation phase together with the study of spectral regions in which signals are detected and which could be utilized by downward looking systems, would then enable the potential of satellite experiments to be accurately assessed.

ACKNOWLEDGEMENTS

In preparing this review paper I have drawn heavily on the work of my colleagues at IIT Research Institute, and friends and associates at Marshall Space Flight Center and Colorado State University.

The overall effort has been funded by NASA, George C. Marshall Space Flight Center. Dr. Fritz Krause is the NASA project monitor and he has made many significant technical contributions to this work.

The atmospheric crossed-beam instrumentation has been fabricated by IIT Research Institute while the recording and ancillary instrumentation has been supplied by MSFC. Check out and the first crossed-beam measurements were made by IIT Research Institute at Marshall Space Flight Center, and Colorado State University has been responsible for the field test program carried out in Colorado. All the digital data reduction has been done on MSFC computers.

It is not possible to acknowledge all the people who have made significant contributions to this program, however, particular mention should be made of M. J. Fisher and E. H. Klugman at IIT Research Institute, F. R. Krause and J. Heaman, R. R. Jayroe and J. B. Stephens at MSFC and V. Sandborn at Colorado State University.

REFERENCES

- Elterman, L., (1964), "Atmospheric Attenuation Model, 1964, in the Ultraviolet, the Visible and the Infrared Windows for Altitudes to 50 km," Environmental Research Paper No. 46, AFCRL.
- Fisher, M. J., (1964), "Measurement of Local Density Fluctuations in a Turbulent Shear Layer," IITRI Project Suggestion No. 64-107NX.
- Fisher, M. J. and Krause, F. R., (1967), "The Crossed-Beam Correlation Technique," J. Fluid Mech. 28, 705-717.
- Krause, F. R., Hu, S. S. and Montgomery, A. J., (1966), "On Cross-Beam Monitoring of Atmospheric Winds and Turbulence with Two Orbiting Telescopes," NASA TMX-53538.

Krause, F. R., (1967), "A Passive Optical Technique for Remote Sensing of Horizontal Wind Profiles and Atmospheric Turbulence," Presented at Forty-eighth Annual Meeting of the American Geophysical Union.

St. John, A. D. and Glauz, W. D., (1968), "Study of Atmospheric and AAP Objectives of Cross-Beam Experiments," NASA Contractor Report NASA CR-61191.

Stephens, J. B., Sandborn, V., Montgomery, A. J. "Remote Wind Detection With the Cross Beam Method at Tower Heights", Presented at the Third National Conference on Aerospace Meteorology May 6-9 (1968). New Orleans, La.

APPENDIX

DESIGN OF PHOTOMETERS FOR SCATTERED SUNLIGHT MEASUREMENTS

Optical Design -- The optical design of photometer system was based on the following specifications:

Frequency Response	0.001-300 cps
Mean Signal/RMS Noise	$10^4$
Field of View	5 - 30 minutes of arc
Spectral Response	0.4 - 1 micron
Spectral Bandpass	Variable (minimum 500A)

The system is shown schematically in Figure A1. The objective

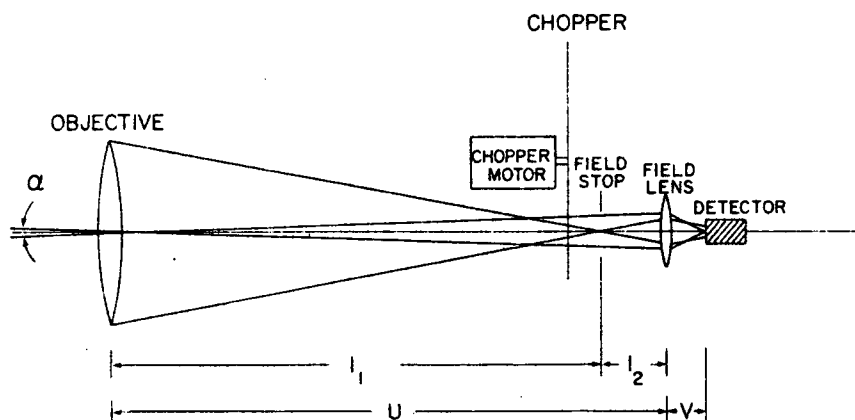


Figure A1. Optical System Schematic

## REMOTE SENSING OF WINDS AND ATMOSPHERIC TURBULENCE

(collector) lens has an aperture 17.5 cm and a focal length of 47.4 cm. The field stop which defines the field of view of the photometer is located in the focal plane of the collector lens, and is preceded by the chopper. To avoid any possible problems of nonuniform fields combined with variations in sensitivity over the detector area, a field lens is included which images the exit pupil of the objective on to the detector.

The chopper which has square blades is rotated by its motor approximately 3600 rpm and with 20 blades produces a signal frequency of 1200 cps. Use of such a chopper prevents the  $1/f$  noise of the silicon diode detector or of the preamplifier being the dominant noise source at low frequencies. It also prevents slow drifts, due for example to temperature changes, from being misinterpreted as a low frequency signal component.

Because the intensity of the radiation reaching the detector is relatively high, advantage could be taken of the much greater quantum efficiency available with a silicon diode as compared to a vacuum phototube or photodiode. The detector used is an EG&G SGD-444 silicon photodiode the quantum efficiency of which is compared to common photoemissive surfaces in Figure A2.

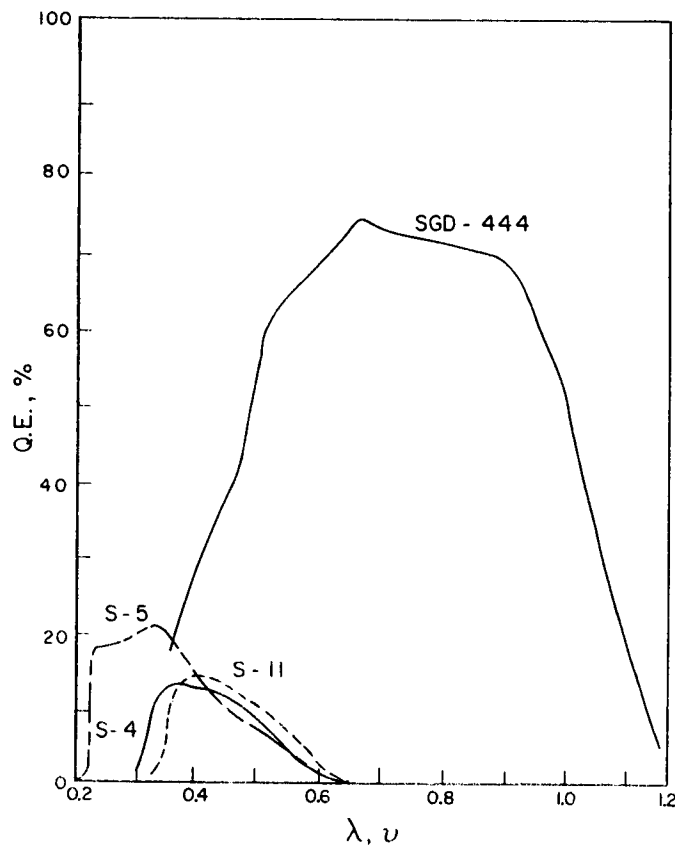


Figure A2. Comparison of Quantum Efficiencies of Several Photodetectors

Electronic Signal Processing--The signal processing electronics are shown in Figure A3. The signal from the detector is pre-amplified before being demodulated and the AC part of the demodulated signal is filtered and amplified. With the low-pass and high-pass filters in their zero position the passband is from 0.01 - 300 cps. Both the a.c. and the d.c. signals are recorded on magnetic tape using an Ampex CP100 tape recorder.

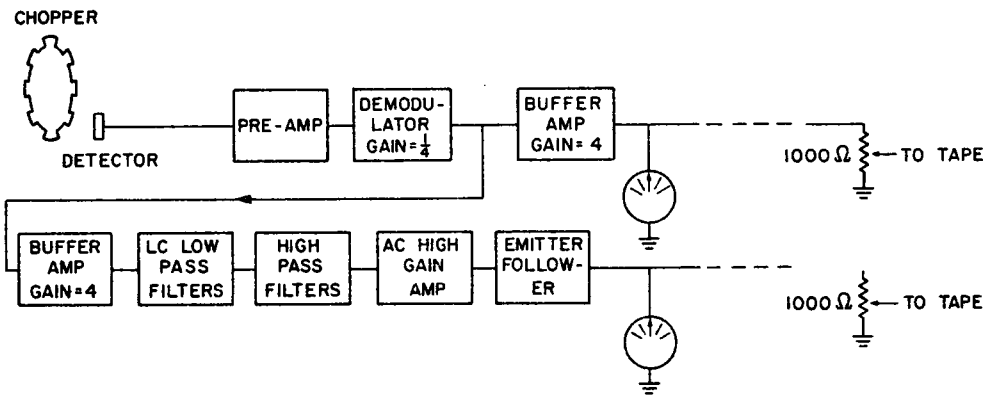


Figure A3. Block Diagram of Signal Processing Chain.

NOISE ELIMINATION BY PIECEWISE CROSS CORRELATION OF PHOTOMETER OUTPUTS

by

Fritz R. Krause and Benjamin C. Hablutzel

NASA, George C. Marshall Space Flight Center  
Huntsville, Alabama

ABSTRACT

A piecewise cross correlation technique has been developed to analyze the outputs of remote detection devices. The purpose of this technique is to eliminate the noise from optical background fluctuations, from transmission fluctuations and from detectors by calculating the instantaneous product of the detector output and a reference signal. Each noise component causes positive and negative oscillations of the instantaneous product and may thus be cancelled by an integration of the instantaneous product. The resultant product mean values will then contain the desired information on the spatial and temporal variation of emission, absorption and scattering processes in the atmosphere.

The piecewise correlation technique differs from previous digital analyses of stationary time series by separating statistical and temporal variations of product mean values. The statistical variations describe the amount of still uncancelled noise. The range of these variations is calculated by determining the frequency band width of the noise from the decrease of an accumulative statistical error with integration time. The temporal variations of the product mean values describe a change in the meteorological boundary conditions. They are indicated by the calculated errors which exceed the range of statistical variations that is expected for the given noise band width. Furthermore, such temporal variations set a level of irreducible noise components since the uncancelled noise cannot be distinguished from the temporal variations of the meteorological boundary

## NOISE ELIMINATION BY PIECEWISE CROSS CORRELATION OF PHOTOMETER OUTPUTS

conditions. However, the change of these boundary conditions may very often be suppressed by suitable normalization and trend removal techniques.

The accomplishments to date provide for automatic piecewise changes of gain factors and coordinate shifts which eliminate intolerable temporal variations of meteorological boundaries provided the signals do not exceed the dynamic range of the amplifier or the tape recorder.

Our recommendations are to continue the present studies on noise elimination in the presence of time dependent boundary conditions. Particular emphasis should be given to the temporal variations of product mean values which are caused by changes in aerosol concentrations, optical background fluctuations, variations of wind speed and changes of wind direction. Future development of piecewise correlation techniques should concentrate on noise elimination and interpretation of rapid scanning remote detection devices such that optical and meteorological phenomena might be monitored in real time.

### 1. INTRODUCTION

A new "piecewise" correlation technique has been developed to eliminate noise in photometer outputs. The need for such a program became apparent in crossed beam field tests [Montgomery, 1969, this Vol.] where temporal variations of meteorological boundary conditions sometimes produced irreducible noise components which were fatal. The new correlation techniques have subsequently isolated and eliminated temporal variations of meteorological boundary conditions by piecewise normalization and detrending procedures. The same techniques could also be applied to any other remote detection device or any other set of meteorological data.

The noise elimination is based on the integration of a lagged product between the photometer output and a reference signal. Section 3 gives a review of the usual noise elimination by product integration which is used for stationary time series where the boundary conditions are time invariant [Bendat and Piersol, 1966]. The piecewise correlation was developed to extend this classical product mean value calculation to meteorological boundary conditions which are time dependent. In this case, the calculated product mean values will be subject to both statistical and temporal variations. In theory, temporal and statistical variations could be separated by analyzing a large group of imaginary experiments which should all have identical time dependent boundary conditions [Crandall and Mark, 1963]. This theory is reviewed in Section 4. However, it cannot be applied directly, since meteorological conditions cannot be controlled to give many realizations of the same phenomenon. The best one can hope for is that temporal variations of meteorological conditions are of such a type that suitably modified portions of one long record could be treated as independent realizations. The conditions of stationarity and the results of this approximation are discussed in Section 5.

Our program is new in that the variations between different piecewise estimated time averages are used to calculate accumulative statistical errors

which should depend on the number of processed pieces in a universal way if the replacement of realizations with pieces is justified. Conversely, deviations from this behavior can be used to determine deviations from stationarity as discussed in Section 6. Temporal variations of meteorological boundary conditions restrict the noise elimination to the level of the temporal variations, since one cannot distinguish between statistical and temporal variations of product mean values. Fortunately, suitable normalization and trend elimination procedures are often sufficient to remove the temporal variations of boundary conditions. Piecewise variable ordinate shifts and gain factors have been proposed for trend elimination and normalization [Jayroe and Su, 1968]. The experience to date indicates that these piecewise modifications of photometer records were sufficient to remove temporal variations of boundary conditions and thereby increase the ability of noise elimination. The results are summarized in Section 7. Conclusions and recommendations are given in Section 8.

## 2. NOTATION

### a. Independent Variables

$t$	observation time
$T$	integration time
$\Delta T$	piece length
$i$	piece number ( $t/\Delta T$ )
$m$	accumulation number ( $T/\Delta T$ )
$f$	frequency
$\tau$	time lag between photometer output and reference signal
$\tau_M = 1/6 \Delta T$	maximum time lag
$k = 1, 2, \dots, N$	number of imaginary realizations.

### b. Dependent Variables

$I$	d.c. coupled photometer output
$i$	a.c. coupled photometer output
$x = i_A$	output from photometer A
$y = i_B$	reference signal or output from photometer B
$\sigma$	root mean square value of $i$
$R$	product mean value of $x$ and $y$

NOISE ELIMINATION BY PIECEWISE CROSS CORRELATION OF PHOTOMETER OUTPUTS

$\Delta R$  statistical error of product mean value

$\delta R = \frac{\Delta R}{\sigma_x \sigma_y}$  normalized statistical error of product mean value

P power inside frequency interval

$$-\frac{1}{4\tau_M} \leq f \leq \frac{1}{4\tau_M}$$

$\bar{s}_i = \bar{\tau} \bar{R}_i$  ordinate shift for piece i.

c. Operators

( ) Statistic

$$\overline{(\ )}_i = \frac{1}{\Delta T} \int_{(i-1)\Delta T}^{i\Delta T} (\ ) dt \quad \text{piecewise mean}$$

$$\overline{(\ )}_m = \frac{1}{m} \sum_{i=1}^m \overline{(\ )}_i \quad \text{accumulative mean}$$

$$\overline{\Delta(\ )}_m = \frac{1}{m-1} \sum_{i=1}^m \left( \overline{(\ )}_i - \overline{(\ )}_m \right)^2 \quad \text{piecewise statistical error}$$

$$\overline{\Delta(\ )}_m = \frac{\overline{\Delta(\ )}_m}{m} \quad \text{accumulative statistical error}$$

$$E[\overline{(\ )}] = \frac{1}{N} \sum_{k=1}^N (\ )^{(k)} \quad \text{sample of expected value or ensemble average for one group of N realizations}$$

$$(\sigma^{(1)})^2 = \frac{1}{N-1} \sum_{h=1}^N \left( \overline{(\ )}^{(h)} - E[\overline{(\ )}] \right)^2 \quad \text{sample of variance between realizations}$$

$$\overline{\overline{(\ )}} = \frac{1}{2\tau_{\max}} \int_{-\tau_{\max}}^{+\tau_{\max}} \overline{(\ )} d\tau \quad \text{average over time lags.}$$

## d. Subscripts

i	time interval $(i - 1) \Delta T \leq t \leq i\Delta T$
m	accumulation over all pieces up to $i = m$
x	from record x
y	from record y
a	straight time integration
w	weighting with piecewise variable gains
d	detrending with piecewise variable
c	ordinate shifts
C	combined piecewise shifts and gains.

## 3. NOISE ELIMINATION BY INTEGRATION OVER PRODUCTS

The subdivision of two data records into signal and noise components and the subsequent elimination of the noise are both based on the integration of instantaneous products. This is illustrated in Fig. 1 in terms of an idealized physical model that is used for the interpretation of crossed beam results [Krause, 1967]. Two data records,  $I_A(t)$  and  $I_B(t)$ , are obtained by monitoring the fluctuations of the radiative power which is received inside the narrow field of view of the two telescopes, A and B. Each time history,  $I$ , accounts for all sources of radiative power along the entire line of sight. The temporal changes of emission, scattering, or absorption processes will cause a fluctuation,  $i$ , in the recorded time history,  $I$ , which may be calculated by subtracting the mean value,  $\bar{I}$ , that is obtained for a certain recording period,  $\Delta T$ .

$$x(t, \dots) = I_A(t) - \frac{1}{\Delta T} \int_{t_1}^{t_1 + \Delta T} I_A(t) dt = I_A(t) - \bar{I}_A(t)$$

$$y(t, \dots) = I_B(t) - \bar{I}_B(t)$$
(1)

In our experiments this subtraction is done automatically by using a.c. coupled amplifiers. In this case  $\Delta T$  is proportional to the time constant of the a.c. coupling element ( $\approx 100$  seconds).

Local information from the area of minimum beam separation is retrieved from the two signals,  $x$  and  $y$ , by determining statistically which modulations are "common" to both beams. The concept of "common" signals has been developed in the analysis of communication signals and random vibrations [Bendat, Piersol, 1966] and is based on "lagged product calculations." The two modulations,  $x$  and  $y$ , are analyzed for common signals by multiplying them with each other and

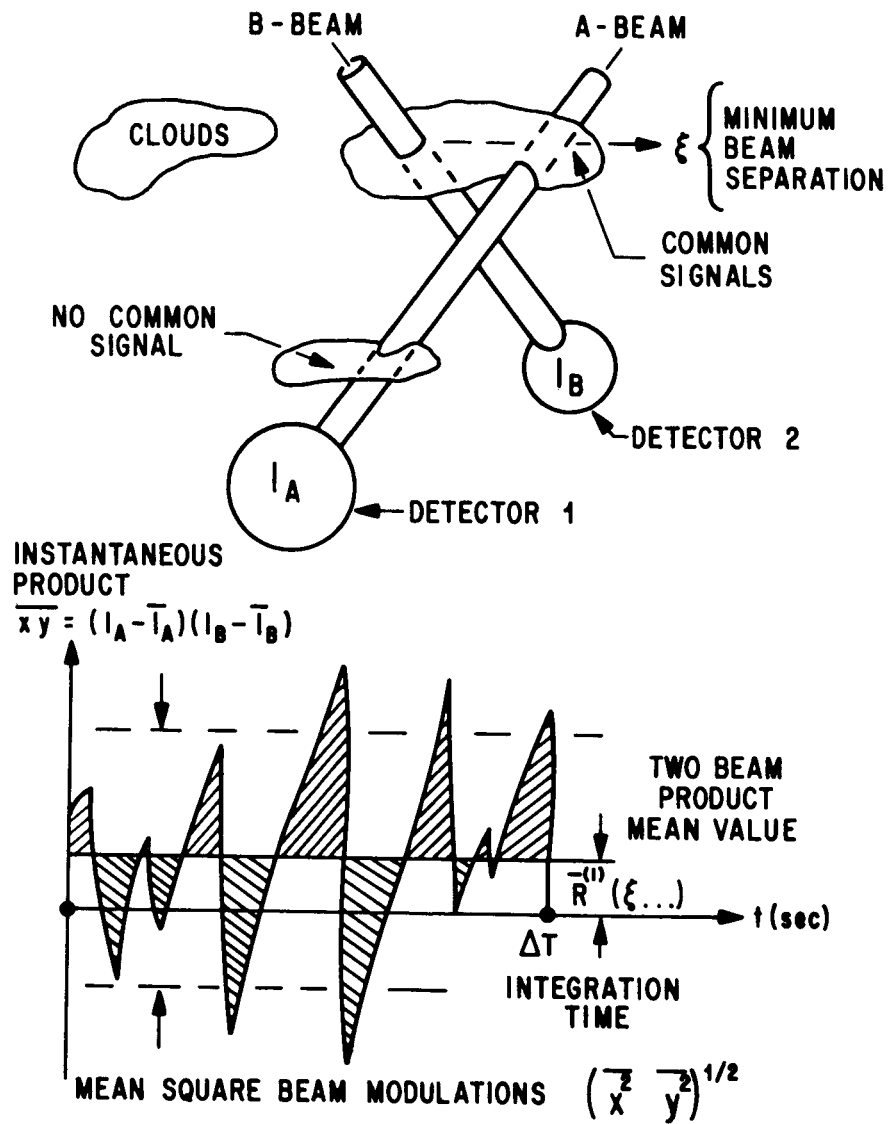


Figure 1. Retrieval of Common Signals.

by averaging this instantaneous product over time. This gives a "two-beam product mean value:

$$\bar{R}^{(1)}(t_1; \Delta T; \dots) = \overline{x(t; \dots)y(t; \dots)}^{(1)} = \frac{1}{\Delta T} \int_{t_1}^{t_1 + \Delta T} xy \, dt. \quad (2)$$

The instantaneous product oscillates between positive and negative values and these oscillations will cancel each other, at least partially, when the product is averaged by integrating it over time, as illustrated in Figure 1. Two beams are said to have no common modulations if the two-beam product mean value vanishes. This complete cancellation will occur when the increase or decrease of radiative power in one beam is independent of the power changes in the other beam in the sense that the change in the other beam may be positive or negative with equal likelihood. Typical examples for such independent beam modulations are the combined source and detector noise and any cloud which traverses only one beam without hitting the other beam. The partial cancellation of the oscillations of the instantaneous product is used to split a given time history,  $x(t)$ , into a "noise" component,  $x_N$ , and a "common" component,  $x_c$ . Both components are defined only with respect to a second reference signal,  $y$ . The noise component,  $x_N$ , of the first record,  $x$ , is that component which vanishes when multiplied with the reference signal

$$\overline{x_N y}^{(1)} = 0. \quad (3)$$

Conversely, the "common" component,

$$x_c = x - x_N, \quad (4)$$

is that component of signal,  $x$ , which is responsible for the finite value of the product mean value:

$$\overline{x y}^{(1)} = \overline{(x_c + x_N) y}^{(1)} = \overline{x_c y}^{(1)}. \quad (5)$$

The second signal could also be split into a common component,  $y_c$ , and a noise component,  $y_N$ , by taking the first signal,  $x$ , as the reference signal:

$$y = y_c + y_N. \quad (6)$$

Substituting Eq. (6) into Eq. (5), one finds that the product mean value is made up only of the common signals.

$$\overline{x y}^{(1)} = \overline{x_c y_c}^{(1)}. \quad (7)$$

The integration of the instantaneous product has thus eliminated the "noise" components and the resultant product mean value is contributed only by the signal component which is common to both data records,  $x$  and  $y$ . However, the word "common" does not mean that the components  $x_c$  and  $y_c$  are identical. It refers only to physical processes which produce a change simultaneously in both signals in such a way that the signs of these changes are either equal or opposite. A cloud which traverses two lines of sight (see Fig. 1) is a good example of such a physical process. Although this cloud will cause common changes in both photometer records  $x$  and  $y$ , these changes will be quite different since the two lines of sight intersect different portions of the same cloud.

#### 4. TEMPORAL AND STATISTICAL VARIATIONS OF PRODUCT MEAN VALUES

The value of a product mean value,  $\bar{R}$ , will depend in general on both the position,  $t$ , of the integration period and on the length,  $\Delta T$ , of the period. The variation with  $t$  reflects a temporal variation of the meteorological boundary conditions such as a change of wind speed and direction or a new type of lag in the area which is common to both lines of sight. The dependence on  $\Delta T$  may also reflect a temporal variation of the common signals. However, it is often more likely that the change is produced by the noise components which are not completely cancelled since any finite integration period will have over a finite number of oscillations of the instantaneous product. Such incomplete cancellation of extraneous noises reflects a change which may be classified as statistical, since it is associated with the uncontrollable change of physical phenomena other than the common physical process, i.e., a random change in boundary conditions. Both temporal and statistical variations will mostly occur simultaneously and are therefore very difficult to separate.

A detailed description of temporal and statistical variations of product mean values is possible, in theory, by treating the actual conducted experiments as one sample of a population of imaginary experiments which are all recorded for identical time dependent boundary conditions. Assume that  $k = 1, 2, 3, \dots, N$  realizations of the atmospheric field have been observed. Statistical averages may then be established by averaging over the different realizations instead of averaging over time. This "ensemble" average shall be denoted by the operator and will be called the "expected value":

$$E[(\ )] = \frac{1}{N} \sum_{k=1}^N (\ )^{(k)}. \quad (8)$$

Let  $x^{(k)}(t)$  and  $y^{(k)}(t)$  denote the photometer records of the  $k$ -th realization. The expected value of the product mean value would then be

$$E[\overline{xy}] = \frac{1}{N} \sum_{k=1}^N \frac{1}{\Delta T} \int_{t_1}^{t_1+\Delta T} x^{(k)}(t) y^{(k)}(t) dt = \frac{1}{N} \sum_{k=1}^N \overline{x^{(k)} y^{(k)}} = \bar{R}. \quad (9)$$

The temporal variations of this ensemble average can be determined since the time dependence of  $\bar{R}(t_1; \Delta T, \dots)$  is not cancelled when integrating across the ensemble.

The statistical variations of the experimentally accessible product mean value  $\bar{R}^{(1)}$  can also be established by analyzing the variations between the individual realization,  $k$ , and the expected value. The "expected" statistical variation of  $\bar{R}^{(1)}$  is provided by a mean square error calculation or "variance":

$$\text{Var } \bar{R}^{(1)} = \frac{1}{N-1} \sum_{k=1}^N \left\{ \bar{R}^{(k)} - E[\bar{R}] \right\}^2. \quad (10)$$

A sample of the variance between individual product mean values is thus given by

$$\begin{aligned} \text{Var } \bar{R}^{(1)} &= \frac{1}{N-1} \sum_{k=1}^N \left\{ \overline{x^{(k)} y^{(k)}} - E[x y] \right\}^2 \\ &= \frac{1}{N-1} \sum_{k=1}^N \left\{ \frac{1}{\Delta T} \int_{t_1}^{t_1+\Delta T} x^{(k)}(t) y^{(k)}(t) dt - \bar{R} \right\}^2. \end{aligned} \quad (11)$$

The associated standard deviation,  $(\text{Var } \bar{R}^{(1)})^{1/2}$ , describes one likely variation between the individual realization,  $\bar{R}^{(k)}$ , and the expected value,  $\bar{R}$ . Other variations will occur with other probabilities. Fortunately, the practical implications of the central limit theorem imply that the probability of mean value variations ought to follow the normal distribution. Knowing such a universal distribution, one can then calculate a certain limit,  $t_p (\text{Var } \bar{R}^{(1)})^{1/2}$ , which will not be exceeded by the individual variations  $\bar{R}^{(1)} - \bar{R}$  for the fraction  $p$  of all  $N$  realizations. These limits provide a confidence interval for the statistical variation between a single realization,  $k = 1$ , and the expected product mean value. The 80 percent confidence interval would be

$$\bar{R}^{(1)} - t_{0.90}(N) (\text{Var } \bar{R}^{(1)})^{1/2} \leq \bar{R} \leq \bar{R}^{(1)} + t_{0.90}(N) (\text{Var } \bar{R}^{(1)})^{1/2}. \quad (12)$$

The "percentile factors" of the normal distribution,  $t_p$ , are listed in Table 1.

Equation (12) gives the desired estimate for the expected statistical variations of individual product mean values. The associated confidence interval could be calculated if  $\text{Var } \bar{R}^{(1)}$  were accurately known. However, Eq. (11) gives only one sample of this variance. A new group of  $N$  realizations would give a different sample of  $\text{Var } \bar{R}^{(1)}$ . The accurate description of the statistical variations should therefore consider not only the variations between individual realizations of a single group but also the variation between different groups of realizations. Let  $(\bar{\sigma}^{(1)})^2$  denote the "population variance", which is calculated by taking the arithmetic mean of all samples of

TABLE 1

Percentile Factors and Confidence Intervals for Stationary Records

Student's t Distribution			$\chi^2$ -Distribution			
m	$t_{.90}$	$1/\sqrt{m}$	$\chi^2_{.90}$	$\chi^2_{.10}$	$\chi_{.90}/m$	$\chi_{.10}/m$
2	3.08	.707	2.71	.0158	.823	.063
3	1.89	.578	4.61	.211	.716	.153
4	1.64	.500	6.25	.584	.625	.191
5	1.53	.447	7.78	1.06	.558	.206
6	1.48	.408	9.24	1.61	.507	.211
7	1.44	.378	10.6	2.20	.465	.212
8	1.42	.353	12.0	2.83	.433	.210
9	1.40	.333	13.4	3.49	.407	.208
10	1.38	.317	14.7	4.17	.383	.204
12	1.35	.288	17.3	5.58	.347	.201
14	1.34	.267	19.8	7.04	.318	.190
16	1.33	.250	22.3	8.55	.295	.183
18	1.33	.236	24.8	10.1	.277	.179
20	1.32	.222	27.2	11.7	.261	.174
25	1.32	.200	33.2	15.7	.230	.160
30	1.31	.183	39.1	19.8	.028	.150
61	1.30	.128	74.4	46.5	.142	.112
$m \rightarrow \infty$	1.28	$1/\sqrt{m}$	m	m	$1/\sqrt{m}$	$1/\sqrt{m}$

Accumulative Means

$$\overline{(\ )}_m - t_p \overline{\Delta(\ )}_m \cong E[\overline{(\ )}] \cong \overline{(\ )}_m + t_p \overline{\Delta(\ )}_m .$$

Normalized Accumulative Error

$$\frac{\chi_{.10}}{m\sqrt{B\Delta T}} \cong \overline{\delta R}_m \cong \frac{\chi_{.90}}{m\sqrt{B\Delta T}} .$$

Var  $\bar{R}^{(1)}$ , i.e., the mean over all groups. The relative variation between the variance estimate from a single group and the average over all groups could then be expressed by the new variable,

$$\chi^2 = \frac{N \text{ Var } \bar{R}^{(1)}}{(\bar{\sigma}^{(1)})^2} . \quad (13)$$

The probability distribution of this variable is given by another universal distribution function, the  $\chi^2$ -distribution. Knowing this distribution, one can calculate a lower limit,  $\chi_{0.10}^2(N)$ , which will be exceeded by the  $\chi^2$  samples of all but 10 percent of the admitted groups. One can also calculate an upper limit,  $\chi_{0.90}^2(N)$ , which will exceed 90 percent of all  $\chi^2$  samples. Both limits together then give a confidence interval for the statistical variation of variance estimates between different groups of realizations. The 80 percent confidence interval would be

$$\frac{N \text{ Var } \bar{R}^{(1)}}{\chi_{0.90}^2(N)} \leq (\bar{\sigma}^{(1)})^2 \leq \frac{N \text{ Var } \bar{R}^{(1)}}{\chi_{0.10}^2(N)} . \quad (14)$$

The percentile factors  $\chi_{0.10}^2$  and  $\chi_{0.90}^2$  are also listed in Table 1. For  $N \geq 30$  they may be calculated from the equation [Spiegel, 1961]

$$\chi_p^2 = \frac{1}{2} (z_p + \sqrt{2(N-1) - 1})^2 = N(1 - \frac{3}{2N}) \left(1 + \frac{z_p}{\sqrt{2N-3}}\right)^2 . \quad (15)$$

In summary, we find that a single group of  $N$  realizations can provide the following samples:

- (a) The expected product mean value  $\bar{R}$ , Eq. (9).
- (b) One sample,  $\text{Var } \bar{R}^{(1)}$ , for the desired statistical variations between the individual product mean values from different realizations, Eqs. (11) and (12).
- (c) The confidence interval for the statistical variations of variance estimates between different groups of  $N$  realizations, Eq. (14).

All of these samples are based on universal distribution functions, which are independent from the particular physical process that produces the common signals. This universal behavior may therefore be used to separate the universal statistical variations of product mean values from specific temporal variations of these product mean values. One such possibility is discussed in Section 6.

## 5. STATISTICAL ERROR CALCULATION FOR STATIONARY DATA

Unfortunately, the results of the last section cannot be applied directly to experimental data, since meteorological boundary conditions cannot be adjusted to obtain many realizations of the same meteorological conditions. The alternative is then to assume that the meteorological boundary conditions are sufficiently time invariant during one experiment such that individual pieces of a long record represent statistically independent realizations of these invariant boundary conditions. For this purpose, a long record of length  $T$  is subdivided into  $i = 1, 2, \dots, m$  pieces of length  $\Delta T = T/m$ . The time average over one of these pieces may be expressed by

$$\overline{(\ )}_i = \frac{1}{\Delta T} \int_{t=(i-1)\Delta T}^{t=i\Delta T} (\ ) dt. \quad (16)$$

Each of these piecewise estimates is then treated as if it came from a new realization. This means that the summation over realizations is replaced with a summation over pieces

$$\overline{\overline{(\ )}}_m = \frac{1}{m} \sum_{i=1}^m \overline{(\ )}_i = \frac{1}{m\Delta T} \int_0^{m\Delta T} (\ ) dt = \frac{1}{N} \sum_{k=1}^N \overline{(\ )}^{(k)} = E[\overline{(\ )}]. \quad (17)$$

The following conditions [Bendat and Piersol, 1960] must be met to justify this replacement of realizations with pieces:

- (a) The time history of the statistic " $(\ )$ " is a self-stationary process.
- (b) The autocovariance function  $z(\tau)$  of this time history meets certain integrability conditions.
- (c) The individual piece length  $\Delta T$  exceeds the time lag range within which the autocovariance  $z(\tau)$  has become negligibly small.

Experimental data mostly meet the conditions (b) and (c). However, the condition (a) means that the replacement of realizations with pieces is only justified if the temporal variations of the product mean value are negligible. Such time histories are called stationary. For such stationary time series all remaining variations are statistical. This means that the variations between piecewise averages and the statistical variations between sets of pieces should all follow the universal probability distributions given in the last section. The "fit" of these distributions may thus be used as a criterion for stationarity. One such criterion is developed in the remainder of this section.

The desired criterion for stationarity considers the variations of "accumulative" averages which were defined in Eq. (17). The accumulative average of product mean values is derived by substituting Eq. (17) into Eq. (9).

$$\begin{aligned}
 \bar{R}_m &= \frac{1}{m} \sum_{i=1}^m \overline{(xy)}_i \\
 &= \frac{1}{T} \sum_{i=1}^m \int_{(i-1)\Delta T}^{i\Delta T} x(t) y(t) dt \\
 &= \frac{1}{N} \sum_{k=1}^N \overline{x^{(k)} y^{(k)}} = \bar{R}.
 \end{aligned} \tag{18}$$

The statistical variations of these accumulative averages are derived from the differences between pieces. A sample for the expected variance,  $(\bar{\sigma}^{(1)})^2$ , between any two pieces might be derived by substituting Eq. (17) into Eq. (10). This gives

$$\begin{aligned}
 \text{Var } \bar{R}^{(1)} &= \frac{1}{(N - 1)} \sum_{k=1}^N \left\{ \overline{x^{(k)} y^{(k)}} - \bar{R} \right\}^2 \\
 &= \frac{1}{(m - 1)} \sum_{i=1}^m \left\{ \overline{(xy)}_i - \bar{R}_m \right\}^2 \\
 &= \frac{1}{(m - 1)} \sum_{i=1}^m \left\{ \bar{R}_i - \bar{R}_m \right\}^2 = (\Delta \bar{R}_m^{(1)})^2.
 \end{aligned} \tag{19}$$

The associated standard deviation,  $\Delta \bar{R}_m^{(1)}$ , will be called the piecewise error. Any new group of  $m$  pieces or  $m$  realizations would give another sample of the piecewise error. A confidence interval for the statistical variations of piecewise errors between different groups of pieces is derived by substituting Eq. (19) into Eq. (14).

$$\frac{m(\Delta \bar{R}_m^{(1)})^2}{\chi_{0.90}^2(m)} \leq (\bar{\sigma}^{(1)})^2 \leq \frac{m(\Delta \bar{R}_m^{(1)})^2}{\chi_{0.10}^2(m)}. \tag{20}$$

The statistical error of the accumulative mean,  $\Delta \bar{R}_m$ , should be much smaller than the error of a piecewise mean,  $\Delta \bar{R}_m^{(1)}$ , since the statistical variations between pieces will partially cancel each other during the summation. For stationary data the reduction will be equal to  $1/m$ , since the cancellation accounts for  $m$  independent realizations of the same experiment. A sample of the mean square error of an accumulative mean is thus given by:

$$\begin{aligned} (\overline{\Delta(\ )}_m)^2 &= \frac{1}{m} (\overline{\Delta(\ )}_m)^2 \\ &= \frac{1}{m(m-1)} \sum_{i=1}^m \left\{ \overline{(\ )}_i - \overline{(\ )}_m \right\}^2. \end{aligned} \quad (21)$$

The associated standard deviation,  $\overline{\Delta R}_m$ , will be called the "accumulative error." Any new group of m pieces or m realizations would give a new sample of the accumulative error. A confidence interval for the statistical variations between these groups is derived by substituting Eq. (21) into Eq. (20) and by dividing with m. The result is

$$\frac{m(\overline{\Delta R}_m)^2}{\chi_{0.90}^2(m)} \leq \frac{(\overline{\sigma}^{(1)})^2}{m} \leq \frac{m(\overline{\Delta R}_m)^2}{\chi_{0.10}^2(m)}. \quad (22)$$

In most applications the accumulative error is normalized with the product of the accumulative root mean square values

$$\overline{\delta R}_m = \frac{\overline{\Delta R}_m}{\overline{(x^2)}_m^{1/2} \overline{(y^2)}_m^{1/2}} \quad (23)$$

The confidence interval for the normalized accumulative errors follows by dividing Eq. (23) with the product of the accumulative root mean square values:

$$\frac{m(\overline{\delta R}_m)^2}{\chi_{0.90}^2(m)} \leq \frac{(\overline{\sigma}^{(1)})^2}{m \overline{(x^2)}_m^{1/2} \overline{(y^2)}_m^{1/2}} \leq \frac{m(\overline{\delta R}_m)^2}{\chi_{0.10}^2(m)}. \quad (24)$$

Expressing the population variance of piecewise means in terms of a "noise" band width, B,

$$(\overline{\sigma}^{(1)})^2 = \frac{\overline{(x^2)}_m \overline{(y^2)}_m}{B \Delta T}, \quad (25)$$

and substituting this definition into the last inequality, one finds

$$\frac{m(\overline{\delta R}_m)^2}{\chi_{0.90}^2(m)} \leq \frac{1}{BT} \leq \frac{m(\overline{\delta R}_m)^2}{\chi_{0.10}^2(m)}. \quad (26)$$

However, the two factors,  $m/\chi_{0.90}^2$  and  $m/\chi_{0.10}^2$ , both asymptotically approach the value, 1, according to Eq. (14). Therefore, Eq. (25) gives the well known result that the relative statistical error of a product mean value should decrease with the inverse square root of integration time.

$$\delta \bar{R}_m = \frac{\Delta \bar{R}_m}{\overline{(x^2)}_m^{1/2} \overline{(y^2)}_m^{1/2}} \rightarrow \frac{1}{(BT)^{1/2}} . \quad (26a)$$

Direct calculations of the accumulative statistical error,  $\Delta \bar{R}_m$ , may thus be used to determine the noise band width, B, from the asymptotic decrease of this error with the inverse square root of integration time. Furthermore, the knowledge of this band width can then be used to calculate the confidence levels for the relative accumulative error. Rearranging the two inequalities of Eq. (26), one gets

$$\frac{\chi_{0.10}(m)}{m \sqrt{B \Delta T}} \leq \delta \bar{R}_m \leq \frac{\chi_{0.90}(m)}{m \sqrt{B \Delta T}} . \quad (27)$$

Figure 2 illustrates such a direct calculation of the confidence interval that is expected for stationary data. This example employs product mean values from a crossed beam test in a supersonic jet. The abscissa is given by the inverse square root of integration time, T, or accumulation number,  $m = T/\Delta T$ . The ordinate gives the relative statistical error which was calculated from Eq. (21). The actual data follow a straight line through the origin very closely as predicted by Eq. (26a). The slope of this line gives a noise band width of  $B = 22,276$  cps. This noise band width has been used to calculate the confidence intervals according to Eq. (27) and Table 1. All directly calculated statistical errors fall into this interval. One can thus say that the probability is better than 80 percent that the entire record was stationary.

By processing  $m = 14800$  pieces, it was also possible to reduce the statistical error  $\Delta \bar{R}_m$  of the accumulative product mean value,  $\bar{R}_m$ , to 0.2 percent of the mean square value of the actually recorded integrated signals. This demonstrates the surprising power of digital correlation techniques to retrieve very small signals out of noise. The successful development of the associated "piecewise" correlation computer program and the success of crossed beam detection of wind profiles and turbulence parameters in subsonic and supersonic jets [Fisher, Krause, 1967] with the program provided the basis and the starting point for extending crossed beam measurements into the atmosphere.

## 6. DEVIATIONS FROM STATIONARITY AND IRREDUCIBLE NOISE

Fluctuation measurements with winds, humidity, and temperature sensors on meteorological towers indicate that the power spectra of these fluctuations may contain significant energy for frequencies down to 0.01 cps, i.e., for periods as long as 2 minutes. The length of one piece should be two to five times larger than this period if such pieces are to be treated as independent realizations of the same meteorological conditions. We chose a piece length

NOISE ELIMINATION BY PIECEWISE CROSS CORRELATION OF PHOTOMETER OUTPUTS

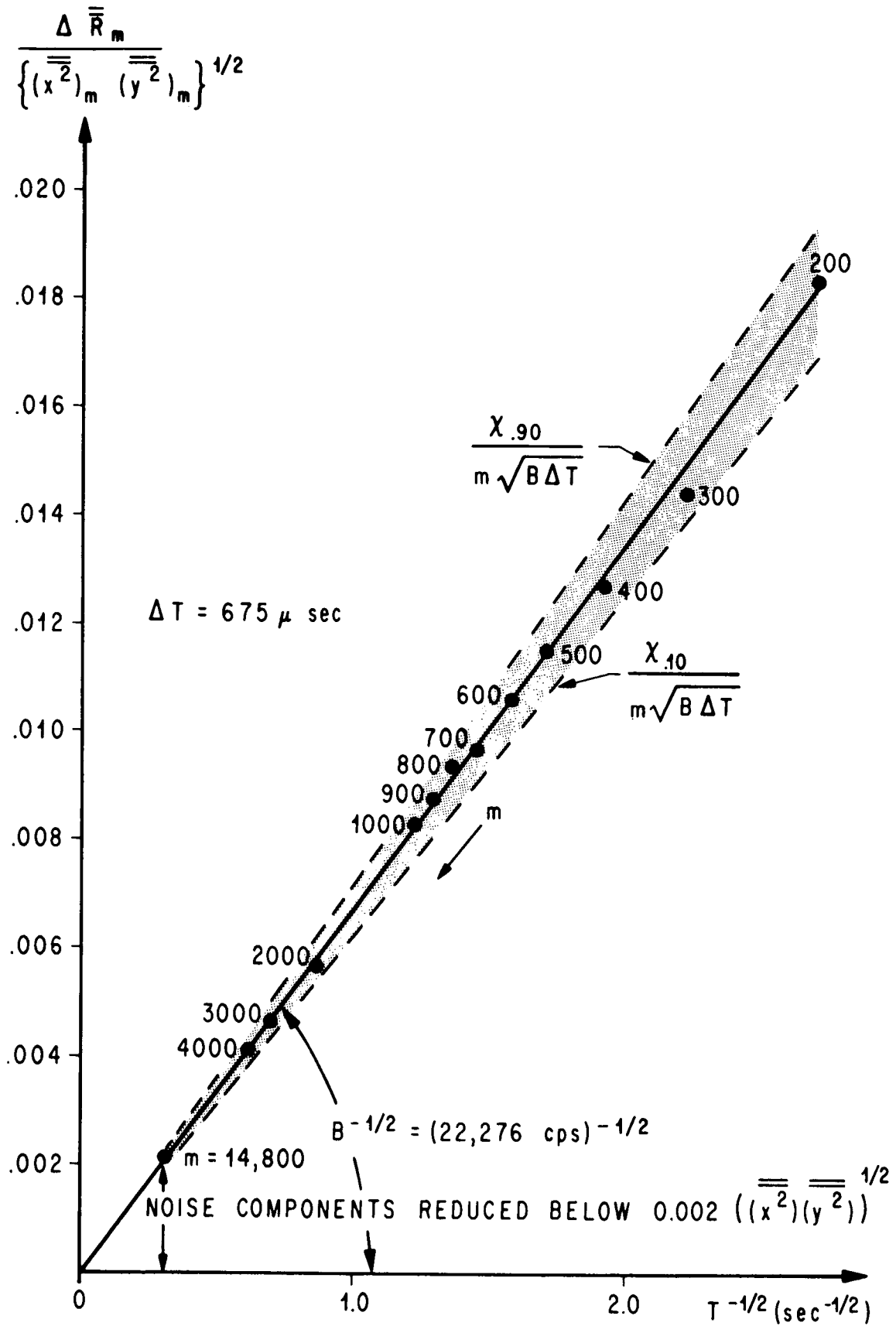


Figure 2. Noise Elimination for Stationary Wind Tunnel Data.

of  $\Delta T = 450 \text{ sec} = 7.5 \text{ minutes}$  for most of our work. At least 5 different realizations of a physical phenomenon are then required to establish the level or irreducible noise components and nonstationarities from the statistical variations between these pieces.

We have chosen to illustrate the noise and stationarity analysis for a marginal case where only 6 pieces are available. The test conditions and the photometer records  $x(t)$  and  $y(t)$  are shown in Fig. 3. The piecewise means of photometer output "A",  $\bar{x}_i$ , are shown in Fig. 4a together with the accumulative mean,  $\bar{x}_6$ , of these means. Furthermore, the statistical error of the individual piecewise mean,  $\Delta\bar{x}_6$ , is added and subtracted from each piecewise mean. The striking observation is that the mean of piece 6 makes a sudden jump which is so large that it exceeds the statistical errors. In case of stationary data, the different values of the piecewise means should stay within the confidence interval given by Eq. (12). The observed large jumps fall, however, outside such an interval; therefore, it is unlikely that these jumps are of a statistical origin. One should rather anticipate sudden changes in the meteorological boundary conditions.

The deviation from stationarity, which is anticipated because of the large jump of the sixth piecewise mean, is clearly indicated by the accumulative error of these means. These errors were calculated according to Eq. (21) and plotted against  $T^{-1/2}$  as shown in Fig. 4b. The expected stationary process was then defined by fitting the calculated points with a straight line through the origin. The slope of this line gives a noise band width of  $B = 0.19 \text{ cps}$ , which is then used to calculate the 80 percent confidence interval according to Eq. (27). However, the directly calculated errors increase suddenly between pieces 5 and 6 and exceed the confidence interval. This exceedance illustrates clearly the deviation from stationarity that was anticipated from the above visual inspection of Fig. 4a.

The exceedance of the confidence interval can be used to define and analyze a deviation from stationarity in many different ways. Fig. 4b illustrates the most simple of all classifications which completely disregards the shape of the actual error curve. A period of a record is called stationary if the accumulative error falls within the 80 percent confidence interval of the expected stationary process. Conversely, a period of a record is called nonstationary if the calculated errors exceed the expected confidence interval. The experience which was gained with this classification is summarized in Table 2.

The second important aspect of the accumulative error curves is the estimate of the irreducible amount of noise. Such an analysis is based on the results of the last section, which should apply within a period of stationarity. According to the discussion of equations (9) and (11), the accumulative statistical error will be contributed predominantly by the uncanceled noise components, since the meteorological boundary conditions are time invariant in a period of stationarity. The finite extent of the period of stationarity means, therefore, that an irreducible amount of noise exists which is equal to the lower limit of the accumulative statistical error inside the given period. The calculation of statistical error curve,  $\Delta\bar{x}_m(T)$ , will therefore provide a direct estimate of the irreducible noise for each period of stationarity as illustrated in Fig. 4b.

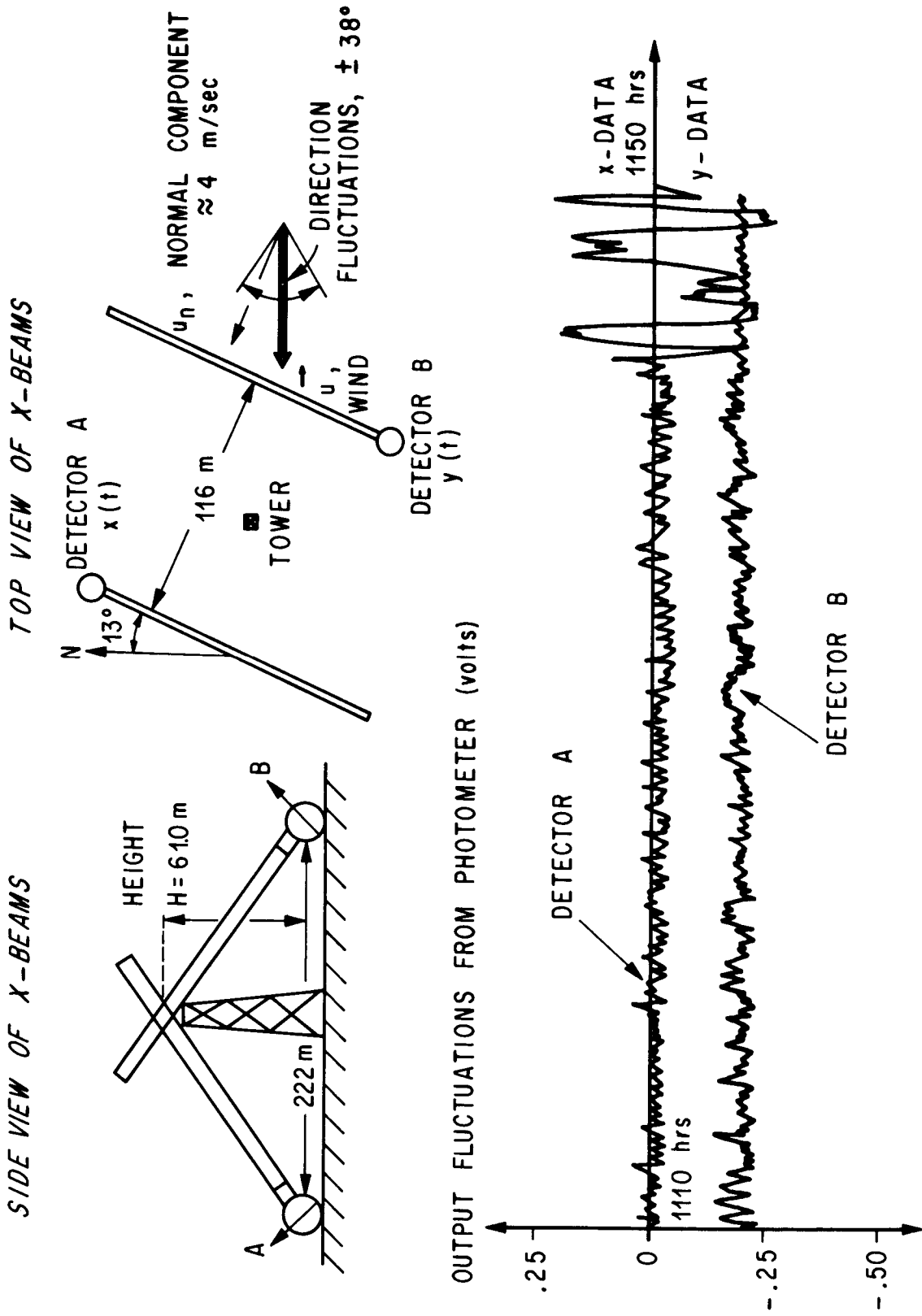
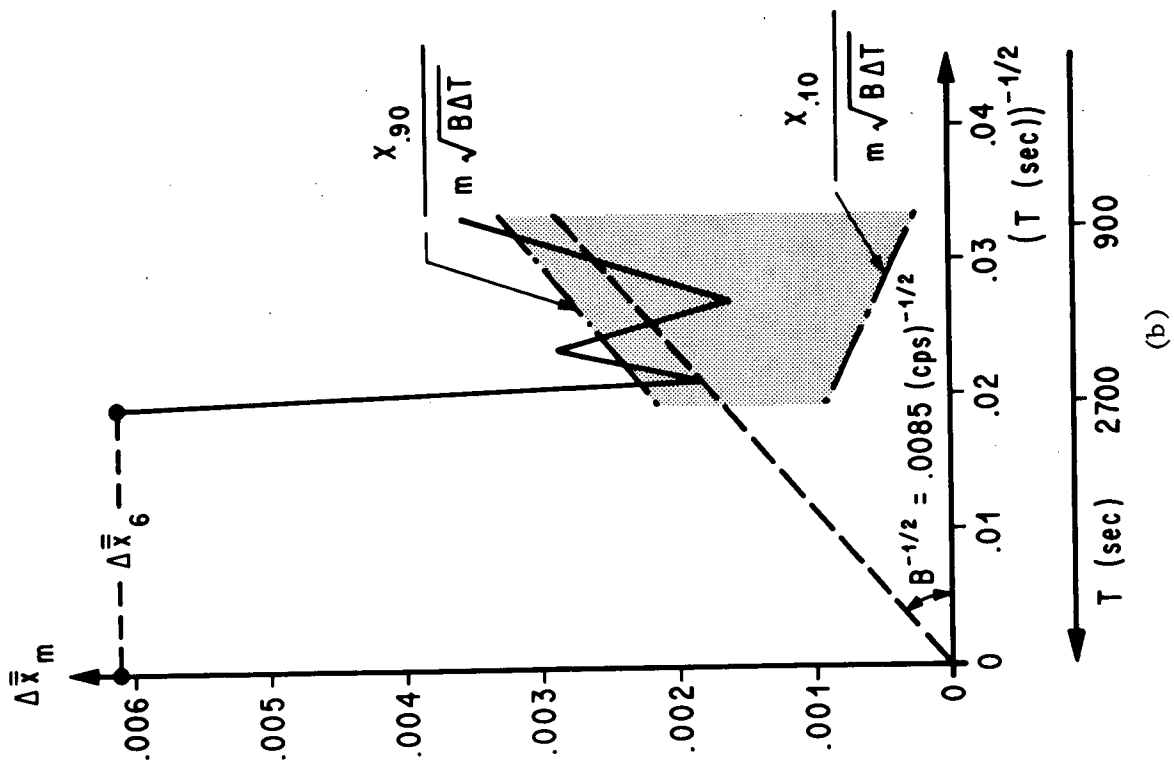
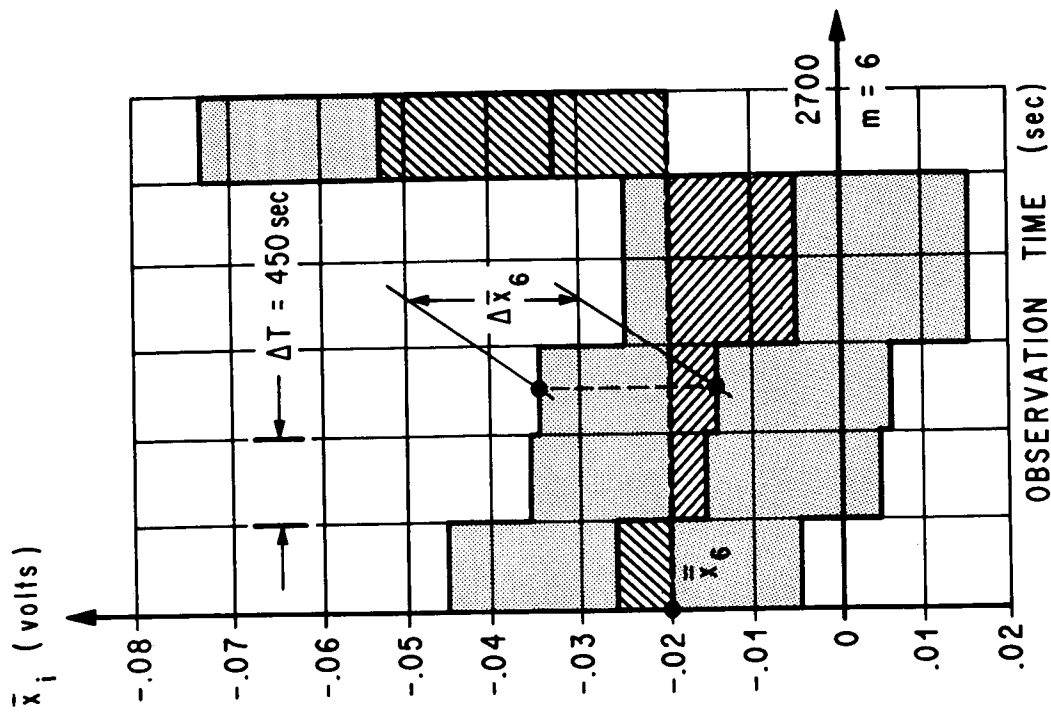


Figure 3. Example of Cross-Beam Experiment.



(a)



(b)

Figure 4. Piecewise Means (a) and Accumulative Statistical Error (b) of Photometer Output  $x$ .

Table 2

Preliminary Experience on Temporal Product Mean Value Variations

Run	T <sub>max</sub> (sec)	B (cps)	Straight Time Integration				Piecewise Gain Change			
			T <sub>1</sub> (sec)	T <sub>2</sub> (sec)	$\frac{T_1-T_2}{T_{max}}$ (%)	(δR) <sub>min</sub>	T <sub>1</sub> (sec)	T <sub>2</sub> (sec)	$\frac{T_1-T_2}{T_{max}}$ (%)	(δR) <sub>min</sub>
A	6750	.063	NA	NA	0	NA	0	6750	100	.050
B	4050	.044	NA	NA	0	NA	0	4050	100	.067
C	4500	.045	3600	4500	20	.078	0	4500	100	.052
D	7200	.063	2250	7200	62	.060	0	7200	100	.046
E	3240	.063	NA	NA	0	NA	0	3240	100	.065
F	4950	.012	0	4950	100	.060	450	4950	91	.045
G	4500	.111	NA	NA	0	NA	0	4500	100	.044
H	10350	.250	NA	NA	0	NA	0	10350	100	.019
I	2700	.063	NA	NA	0	NA	0	2700	100	.040

T<sub>1</sub> = start of stationary period

T<sub>2</sub> = end of stationary period

$$\frac{T_2 - T_1}{T_{max}} = \text{percentage of stationarity}$$

NA = not applicable.

7. PARTIAL REMOVAL OF TEMPORAL VARIATIONS BY PIECEWISE ORDINATE SHIFTS AND GAIN FACTORS

The existence of an irreducible amount of noise would be fatal to crossed beam experiments if this irreducible noise exceeds the small levels of the common signal. However, the results of the last section imply that the "irreducible" amount is inversely proportional to the length of the period of stationarity. If one could partially remove the temporal variations of the meteorological boundary conditions, then the amount of "irreducible" noise might be further reduced by allowing a longer period of stationarity. In other words, the term "irreducible" applies only to a straight time integration as described by Eq. (16). Averaging procedures other than time integration might provide smaller "irreducible" noise levels by removing the time dependence of boundary conditions through suitable normalization and trend

elimination procedures. Jayroe and Su proposed the concept of "accumulative" means which differ from straight time integration by employing piecewise variable ordinate shifts and gain factors [Jayroe and Su, 1968]. The applications of these shifts and gains will now be discussed for the same test run that has already been used.

A piecewise variable ordinate shift may be described as an attempt to remove large scale (i.e., low frequency) trends. Consider lagged product mean values which differ from the product mean values of Eq. (2) only by delaying signal x relative to signal y:

$$\bar{R}_i(\tau) = \overline{x(t - \tau) y(t)}_i = \frac{1}{\Delta T} \int_{(i-1)\Delta T}^{i\Delta T} x(t - \tau) y(t) dt. \quad (28)$$

This lagged product mean value (or temporal correlation function) is calculated for equally spaced time lags and truncated at a time lag

$$\tau_{\max} = \frac{1}{6} \Delta T.$$

Figure 5a shows such a piecewise estimated correlation function for piece 1 of our test run (Fig. 3). The ordinate of this correlation curve shall then be shifted by an amount  $\bar{P}_i(0)$  which makes the area under the shifted curve vanish.

$$\bar{P}_i(0) = \frac{1}{2\tau_{\max}} \int_{-\tau_{\max}}^{+\tau_{\max}} \bar{R}_i(\tau) d\tau. \quad (29)$$

This ordinate shift is equal to the cross power inside the narrow frequency band

$$\begin{aligned} -\frac{1}{4\tau_M} &\leq f \leq \frac{1}{4\tau_M} : \\ \Delta f \cdot S(f \rightarrow 0) &= \frac{1}{2\tau_M} \cdot \lim_{f \rightarrow 0} \int_{-\infty}^{+\infty} \bar{R}_i(\tau) e^{-i2\pi f\tau} d\tau \\ &= \frac{1}{2\tau_M} \int_{-\infty}^{+\infty} \bar{R}_i(\tau) d\tau = \bar{P}_i(0). \end{aligned} \quad (30)$$

The ordinate shift  $\bar{P}_i(0)$  therefore removes all power at frequencies below  $1/4\tau_M$ , i.e., all slowly varying trends. The ordinate shift may thus be

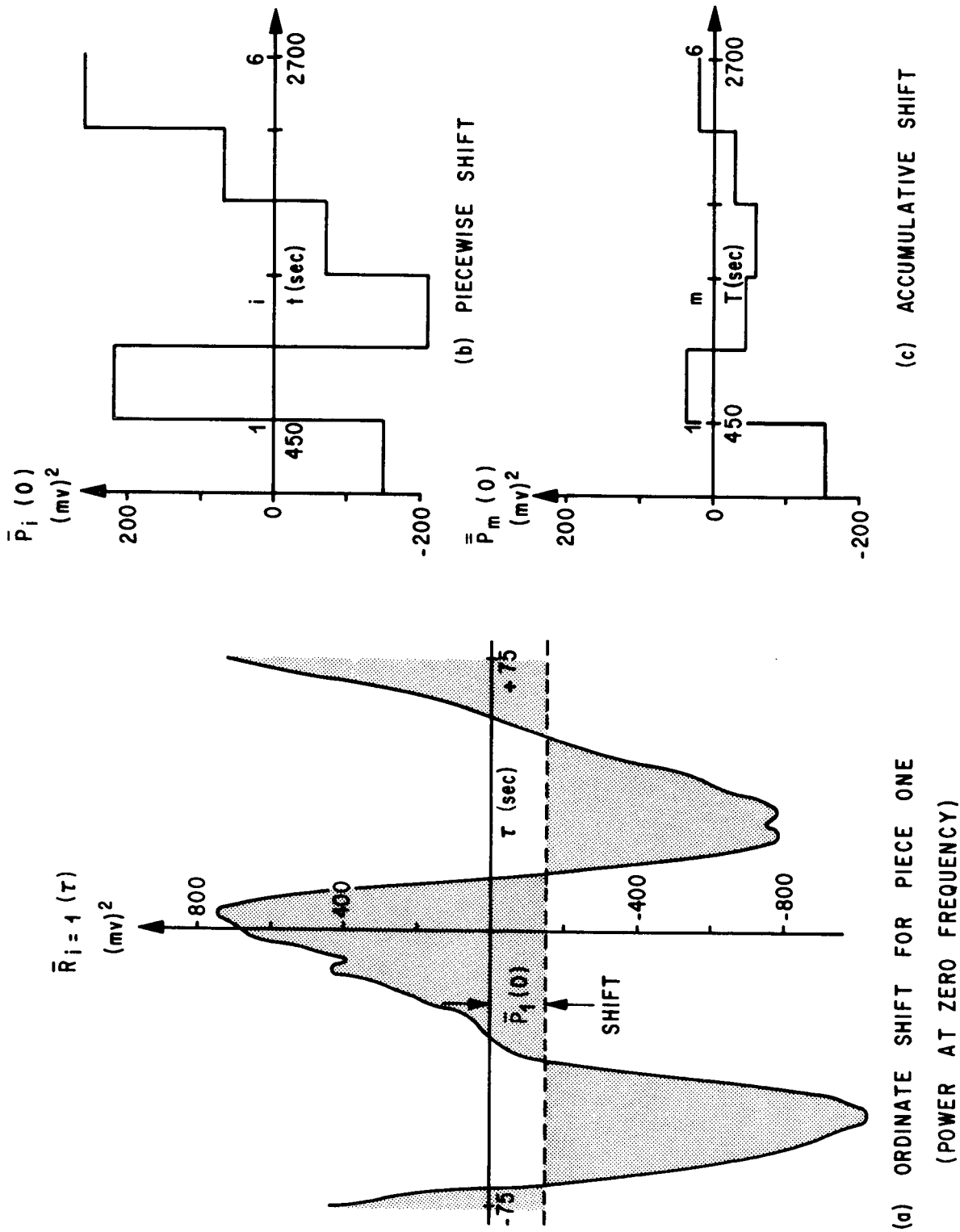


Figure 5. Removal of Low Frequency Components Through Piecewise Ordinate Shifts.

described as a piecewise trend elimination method. The application of this detrending procedure leads to the following accumulation average:

$$(\bar{R}_m)_d = \frac{1}{m} \sum_{i=1}^m (\bar{R}_i - \bar{P}_i(0)). \quad (31)$$

Figure 5b shows the ordinate shifts,  $\bar{P}_i(0)$ , which have been calculated for the six pieces of our test run. These shifts oscillate between positive and negative values in such a way that the accumulative shift,  $\bar{P}_m(0)$ , stays very small. Apparently, the temporal variations of product mean values (Fig. 5c) may be insignificant, although the temporal variations of the mean values (Fig. 4a) are large.

Piecewise ordinate shifts are effective in removing trends. However, in many cases the temporal variations of the boundary conditions will also cause changes at higher frequencies. One change that was observed often is a piecewise jump of fluctuation amplitudes. The average fluctuation amplitude,  $\sigma$ , for a piece is given by the root mean square value

$$\bar{\sigma}_{xi}^2 = \frac{1}{\Delta T} \int_{(i-1)\Delta T}^{i\Delta T} x^2 dt. \quad (32)$$

Temporal variations of fluctuation amplitude are then indicated by the variations of this root mean square value. Figure 6 illustrates this variation for the test run. The temporal variation of the boundary condition that was discovered (Fig. 4b) also, apparently, causes a large jump of the amplitude between pieces 5 and 6. However, the effect of this jump could be minimized by normalizing with the associated root mean square value. This would reduce the fluctuations of the normalized signal  $x/\bar{\sigma}_{xi}$  to the level of the previous pieces. The opposite would be true with a piece that is characterized by a sudden decrease of fluctuation levels. Temporal variations of signal amplitudes can thus be suppressed effectively by using a piecewise variable gain factor which is proportional to  $1/\bar{\sigma}_i$ . Such a nondimensional gain factor has been defined by multiplying  $1/\bar{\sigma}_i$  with the accumulative root mean square value

$$\bar{\bar{\sigma}}_m^2 = \frac{1}{m} \sum_{i=1}^m \bar{\sigma}_i^2. \quad (33)$$

The application of this gain,  $\bar{\bar{\sigma}}/\bar{\sigma}$ , leads to a new type of accumulative average which may be denoted by

$$(\bar{R}_m)_w = \frac{\bar{\bar{\sigma}}_{xm} \bar{\bar{\sigma}}_{ym}}{m} \sum_{i=1}^m \frac{\bar{R}_i}{\bar{\sigma}_{xi} \bar{\sigma}_{yi}}. \quad (34)$$

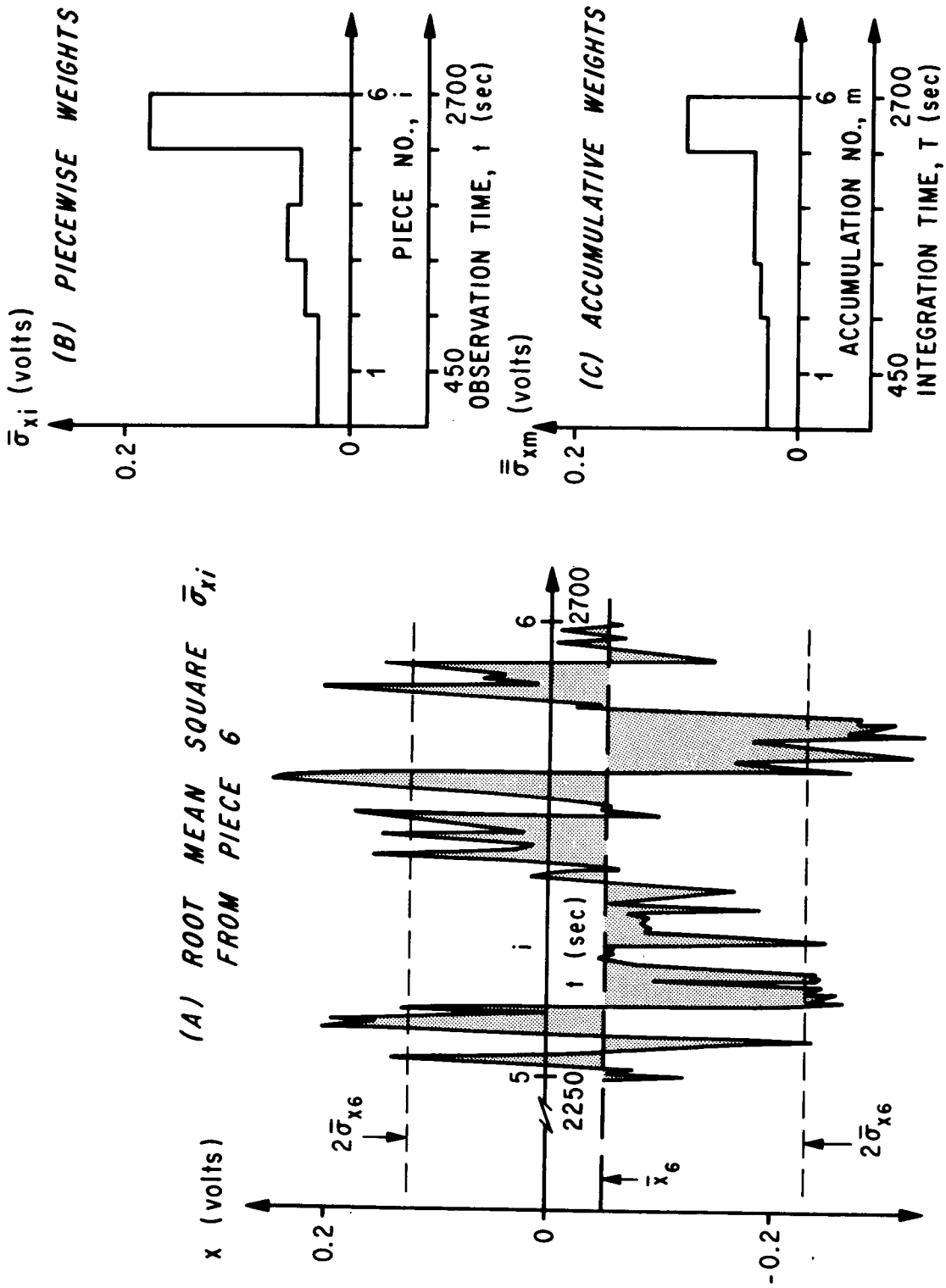


Figure 6. Piecewise gains.

Combined weighting and detrending gives a fourth type of accumulative average:

$$(\bar{R}_m)_c = \frac{\bar{\sigma}_{xm} \bar{\sigma}_{ym}}{m} \sum_{i=1}^m \frac{\bar{R}_i - \bar{P}_i(0)}{\bar{\sigma}_{xi} \bar{\sigma}_{yi}}. \quad (35)$$

All of these different accumulation procedures may be summarized by the use of a unified accumulative average,

$$\bar{R}(\tau; m; \dots) = \frac{\bar{\sigma}_{xm} \bar{\sigma}_{ym}}{m} \sum_{i=1}^m \frac{\bar{R}_i - \bar{s}_i}{\sigma_x \sigma_y}, \quad (36)$$

which allows for a free choice of gain factors,  $\bar{\sigma}/\bar{\sigma}$ , and ordinate shifts,  $\bar{s}$ . The various options that have been tried to this date are characterized by the following choices:

Straight time integration: subscript a

$$\sigma_x = \bar{\sigma}_{xm}; \quad \sigma_y = \bar{\sigma}_{ym}; \quad \bar{s}_i = 0.$$

Piecewise detrending: subscript d

$$\sigma_x = \bar{\sigma}_{xm}; \quad \sigma_y = \bar{\sigma}_{ym}; \quad \bar{s}_i = P_i(0).$$

Piecewise weighting: subscript w

$$\sigma_x = \bar{\sigma}_{xi}; \quad \sigma_y = \bar{\sigma}_{yi}; \quad \bar{s}_i = 0.$$

Combined detrending and weighting: subscript c

$$\sigma_x = \bar{\sigma}_{xi}; \quad \sigma_y = \bar{\sigma}_{yi}; \quad \bar{s}_i = P_i(0).$$

The value of these choices may be judged from the behavior of the associated accumulative statistical error,

$$(\delta \bar{R}(\tau; T; m))^2 = \left( \frac{\Delta \bar{R}(\tau, T, m)}{\bar{\sigma}_{xm} \bar{\sigma}_{ym}} \right)^2 = \frac{1}{m(m-1)} \sum_{i=1}^m \left\{ \frac{\bar{R}_m - \bar{s}_i - (\bar{R}_m - \bar{s}_m)}{\bar{\sigma}_x \bar{\sigma}_y} \right\}^2. \quad (36)$$

The desired accumulation procedure should suppress the temporal variation of meteorological boundary conditions. According to section 6, this suppression may be judged by fitting the tail (m large) of the error curve with a straight line. The best accumulation procedure is the one that gives the best fit. Furthermore, the slope of that line gives the noise band width, B, of the piecewise modified noises and can be used to calculate the confidence interval for the entire error curve from Eq. (27). The whole procedure is illustrated in Fig. 7 for the test run and differs from the illustration given in Fig. 4 in the following aspects:

- (a) The statistical error refers to product mean values, not mean values.
- (b) The time lag dependence of the product mean value has been cancelled by integration:

$$\overline{\delta R^2}(T; m) = \frac{1}{2\tau_{\max}} \int_{-\tau_{\max}}^{+\tau_{\max}} \overline{\delta R^2}(\tau; T; m) d\tau \quad (37)$$

- (c) Four different error curves have been calculated using the different options for piecewise shifts and gains that were identified above by the subscripts a, d, w and c.

The straight time integration, curve a, indicates that both the beginning and the end of the record are strongly affected by temporal variations of the boundary conditions. These variations cannot be described by low frequency trends since the piecewise detrending, curve d, is not effective to alter the shape of the error curve. Only the use of piecewise gains produces error curves (c and a) which approximate a straight line through the origin. The slope of this line gives a bandwidth  $B = 0.063$  cps, which in turn is used to calculate the confidence interval  $\propto \sqrt{mB\Delta T}$ . Both curves w and c fall into this interval; i.e., the piecewise modified photometer records are stationary with a probability exceeding 80 percent. The smallest error of these curves,  $\tau \overline{\delta R} \approx 0.075$ , gives then the irreducible amount of noise that is left after accumulating over a period of  $T = 45.00 = 2700$  seconds. A further noise reduction would require a longer record.

The use of piecewise gains proved to be a very powerful tool in cases where the meteorological boundary conditions were known to be highly time invariant. One of the more dramatic changes of meteorological conditions under clear skies is the change of wind direction. Fig. 8 provides an example of piecewise gain changes for moderate fluctuations of wind directions ( $\pm 22^\circ$ , run H). Without piecewise gains we get a curve that fits the confidence interval; however, this curve does not exhibit the desired straight line fit. The use of piecewise gains improves the approximation of a stationary record significantly and also slightly improves the noise elimination. Figure 9 provides an example for extreme temporal variations of boundary conditions ( $\pm 180^\circ$ , run A). The wind was blowing from all directions during the

SYMBOL	ACCUMULATION METHOD
●	STRAIGHT TIME INTEGRATION $(\bar{\quad})_i = \bar{R}_i, \sigma = (\overline{x^2})_m^{1/2}; (\overline{y^2})_m^{1/2}$
□	PIECEWISE GAINS $(\bar{\quad})_i = \bar{R}_i, \sigma = (\overline{x^2})_i^{1/2}; (\overline{y^2})_i^{1/2}$
■	PIECEWISE SHIFTS $(\bar{\quad})_i = \bar{R}_i - \bar{P}_i(0), \sigma = (\overline{x^2})_m^{1/2}; (\overline{y^2})_m^{1/2}$
▲	COMBINED PIECEWISE GAINS AND SHIFTS $(\bar{\quad})_i = \bar{R}_i - \bar{P}_i(0), \sigma = (\overline{x^2})_i^{1/2}; (\overline{y^2})_i^{1/2}$

NORMALIZED STANDARD ERROR

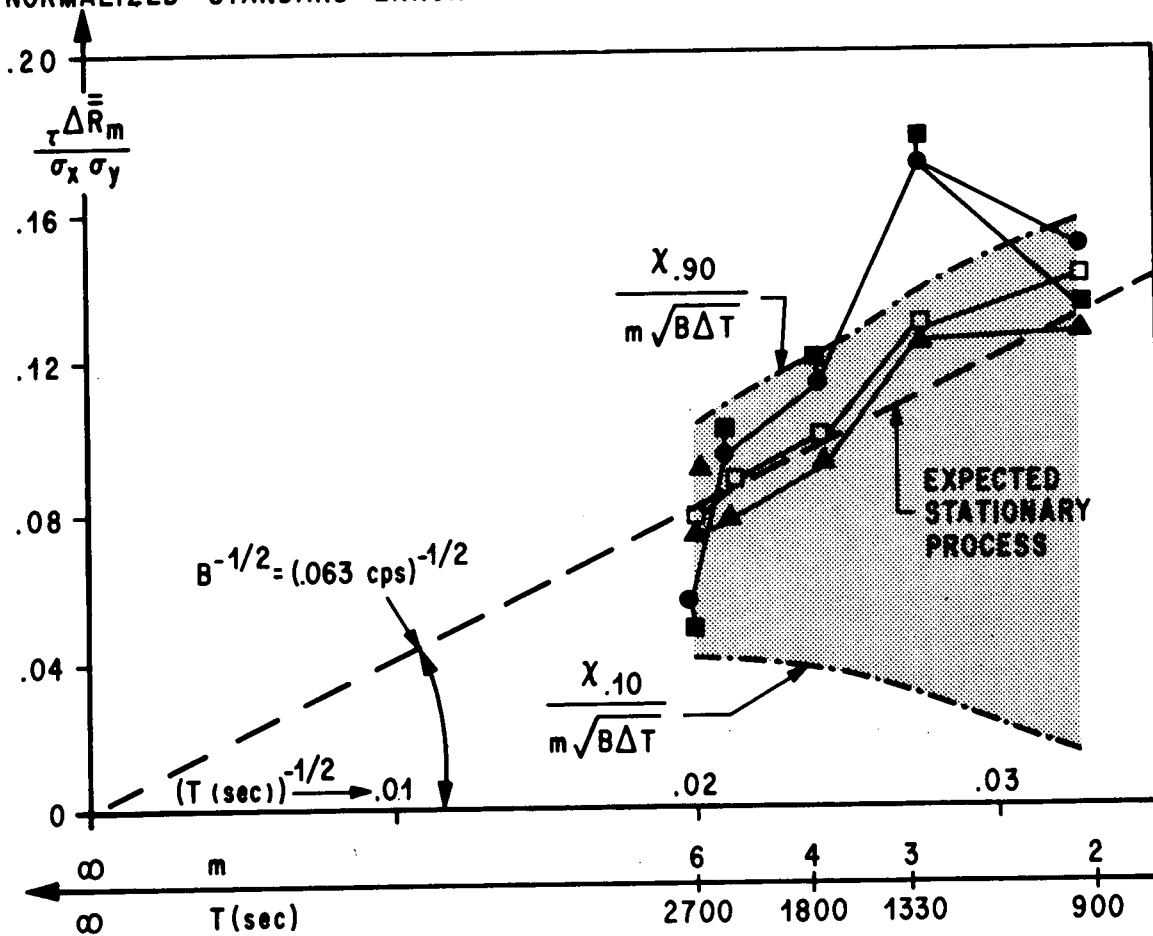


Figure 7. Application of Piecewise Shifts and Gains to Test Runs.

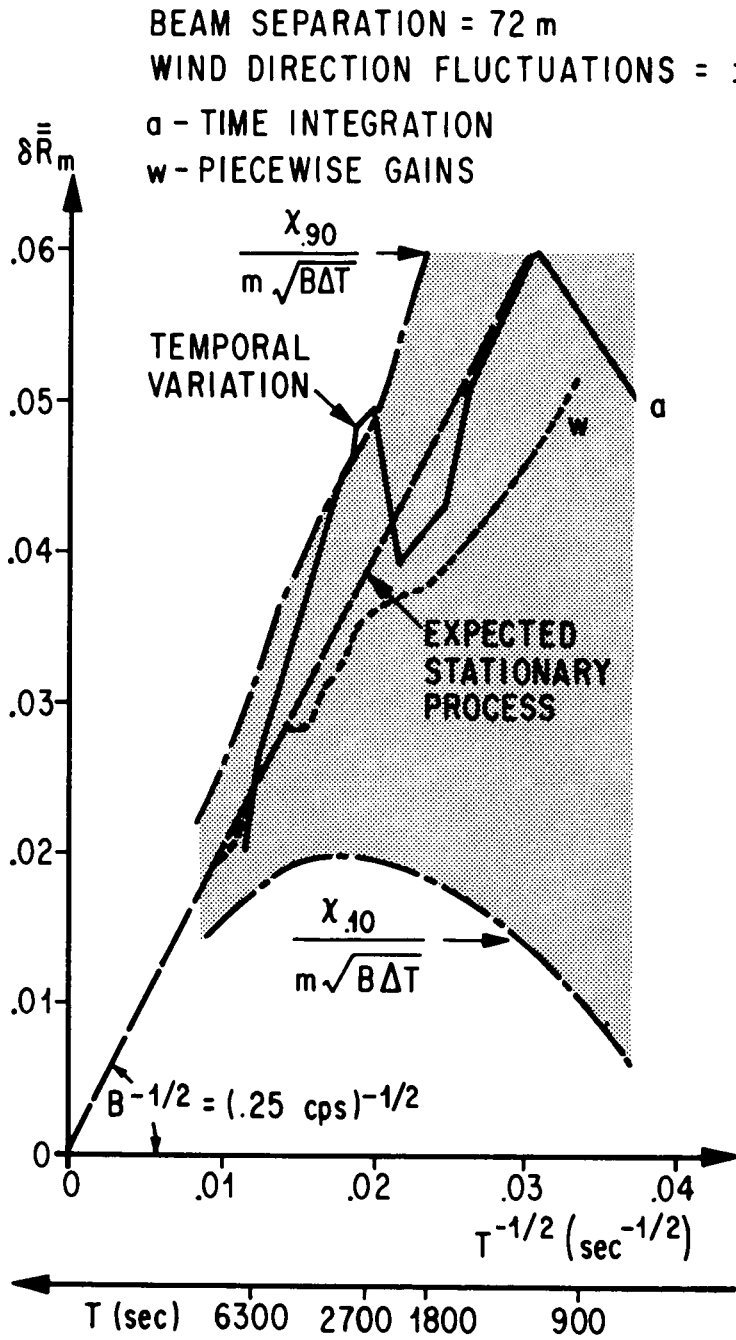


Figure 8. Removal of Temporal Product Mean Value Variations with Piecewise Gains (Run H).

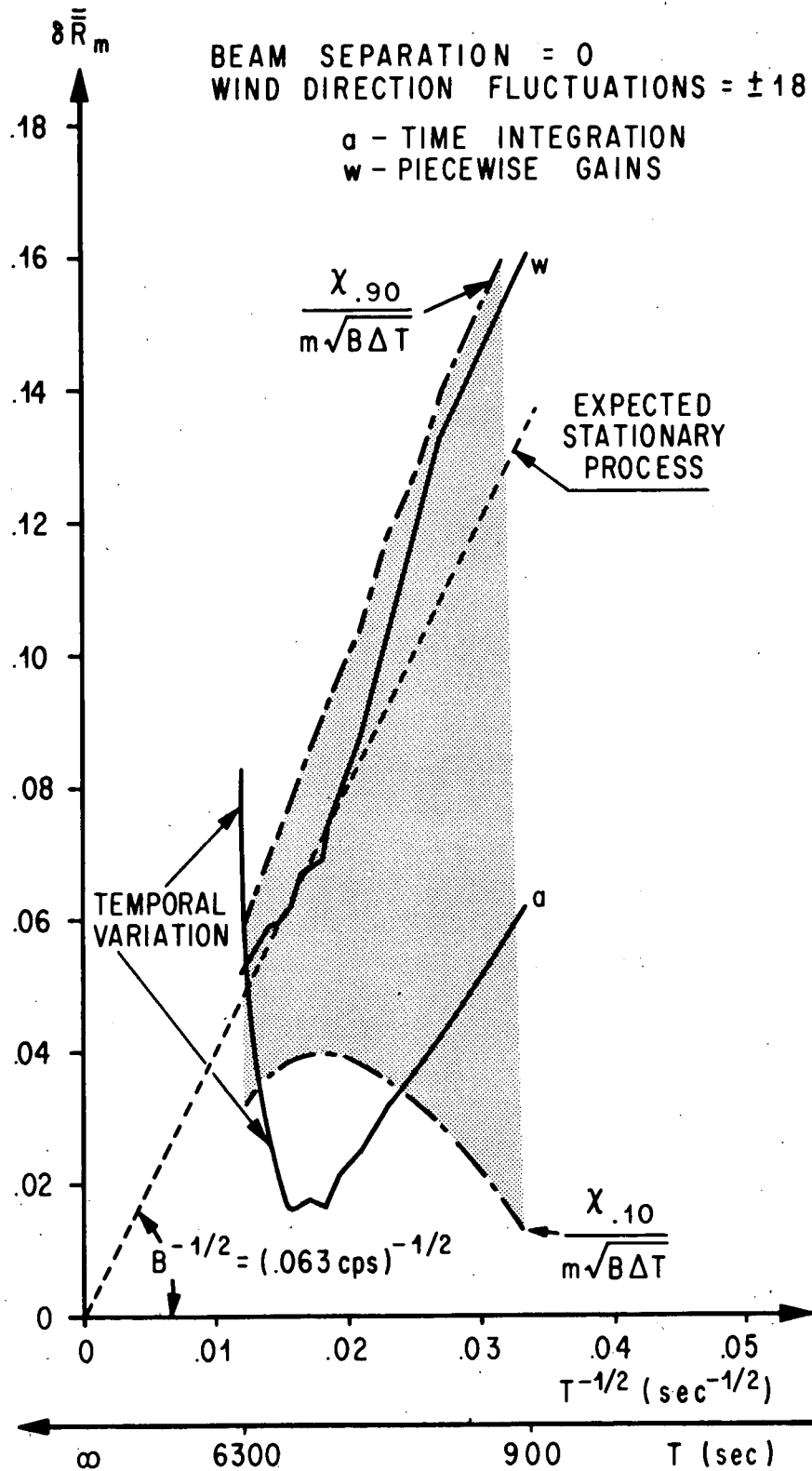


Figure 9. Removal of Temporal Product Mean Value Variations with Piecewise Gains (Run A).

C.11

## NOISE ELIMINATION BY PIECEWISE CROSS CORRELATION OF PHOTOMETER OUTPUTS

recording period. In this case, the straight time integration produces an error curve which does not resemble a stationary process at all. However, even in this extreme case the use of piecewise gains proves sufficient to eliminate the temporal fluctuations of product mean values.

Our preliminary experience with the application of piecewise correlation methods indicates that temporal variations of product mean values occur quite frequently for observation periods between 1/2 and 2 hours. Table 2 gives a summary of the first 9 runs where statistical and temporal product mean value variations were separated. In six out of nine runs the temporal variations of stationarity did not exist at all. Two of the six cases are illustrated in Figs. 7 and 9.

For record lengths up to 2 hours, the use of piecewise gains and ordinate shifts has always been sufficient to remove temporal variations of product mean values provided that the amplifier or tape recorder is not driven into saturation by these temporal variations. Saturation by a large temporal variation of meteorological conditions however always occurred and was the dominant factor which determined the maximum record length,  $T$ . Elimination of this saturation problem should allow longer recording times and thereby contribute to a further reduction of noise below the values of  $(\delta R)_{\min}$  that are listed in Table 2.

### 8. CONCLUSIONS AND RECOMMENDATIONS

The piecewise correlation technique was developed to eliminate noise in the output of remote detection devices. The noise is reduced by multiplying the photometer output with a reference signal and by integrating this instantaneous product over time. This method is quite common for stationary time series where the boundary conditions of the experiment are time invariant. The piecewise correlation technique is new by extending this elimination of noise to meteorological boundary conditions which are time dependent. The simple time integration of products cannot reduce the noise level below the level of temporal variations, since one cannot distinguish between statistical and temporal variations of the product mean value.

The mathematical theory of product mean value variations is based on the difference between a large group of imaginary experiments, all of which have the same time dependent boundary conditions. This theory cannot be applied directly since meteorological conditions cannot be controlled to repeat themselves many times. However, individual pieces of a long record may often be normalized and detrended in such a way that the resultant piecewise modified data behave as if they belonged to independent realizations of the same meteorological boundary conditions. Piecewise correlation techniques are thus based on the premise that one can, in most cases, find suitable piecewise modifications of the photometer outputs and the reference signal which produce two new signals that are stationary although the experiment itself is quite nonstationary.

The effect of piecewise modifications of the photometer outputs may be judged by curve fitting the resultant accumulative error curve with a straight line. The modifications have been successful if the accumulative error decreases linear with the inverse square root of integration time. The slope

of the straight line fit gives the frequency band width of the noise components which one wishes to suppress. Knowing this band width, one can also calculate a confidence interval that should contain most of the calculated statistical errors. Temporal variations of product mean values are then indicated by those errors which fall outside this confidence interval.

The experience gained with piecewise correlation techniques indicates that significant temporal variations of product mean values do occur quite frequently (50 percent of all runs). However, these temporal variations have been removed successfully by employing piecewise changes of gain factors and piecewise ordinate shifts. The proposed automatic changes of gains and ordinates are thus suitable piecewise modifications. They have successfully reduced the temporal variations of product mean values below the level of the statistical variations in all cases where the temporal variations of the meteorological boundary conditions did not drive the amplifier or the tape recorder into saturation.

The piecewise correlation technique provides a new tool that can distinguish between statistical and temporal variations of product mean values. The statistical variations are due to the still uncanceled noise and the temporal fluctuations are caused by a temporal change in meteorological boundary conditions. We recommend continuing the present studies of noise elimination in the presence of time dependent meteorological boundary conditions. Particular emphasis should be given to the temporal variations of product mean values which are caused by changes in aerosol concentrations, optical background fluctuations, variations of wind speeds and changes of wind direction.

The above recommendation is based on the technical problems that were encountered in our first cross beam field tests. These problems and the proposed solutions may be described as follows.

Temporal variations of local scattering process were frequently observed under clear skies which are so large that both the a.c. amplifiers and tape recorders are driven into saturation. Amplifier saturation is being reduced by installing a new coupling circuit with a stepwise variable time constant that is triggered by the incoming signal. Tape recorder saturation will be eliminated by replacing the analog recorder with an on-line digital data logging system.

Temporal variations of the optical background radiation were caused by distant clouds and haze which drift through the photometer's field of view. The associated background noise far exceeds the signal contributions from the desired target layers and may be so large that it cannot be reduced sufficiently by integration of products. In crossed beam tests these background fluctuations have been suppressed by pointing the telescopes to the horizon beneath the cloud level. Infrared photometer systems are now being assembled which should suppress the background fluctuations by setting the monochromator band-pass to a spectral region where the optical path length terminates below the cloud level.

Temporal variations of wind speeds have often caused the dominant temporal variations of product mean values. One promising approach to eliminate noise in the presence of speed fluctuation is to replace the photometer output with its time derivative. The correlation of time derivatives is presently being employed to retrieve the probability density of wind component fluctuations.

## NOISE ELIMINATION BY PIECEWISE CROSS CORRELATION OF PHOTOMETER OUTPUTS

Large temporal variations of wind directions change the altitudes where the common signals originate. A single-beam fan arrangement is being assembled which sets a fan of six narrow fields of view by mounting a plurality of photodiodes in the focal plane of the collector optics. A new piecewise correlation program is being coded for multichannel operation to process the output from several detectors simultaneously. The fan system will then be used to study the altitude distribution of the common signals and the restrictions on altitude resolution that are imposed by large wind direction changes.

A successful elimination of noise in the presence of time dependent meteorological boundary conditions would provide an opportunity to extend remote detection techniques to the description of dynamic phenomena such as winds and turbulence. In particular, the theory of a rapid scanning crossed beam system [Krause, et al., 1966] indicates that wind and turbulence profiles could conceivably be monitored in real time with a single flyby. Furthermore, a crossed beam system which is mounted on an airplane or a satellite moves so rapidly that temporal variations of wind speed and wind direction should no longer interfere with the noise elimination [St. John and Blauz, 1968]. Our recommendation for future studies is therefore to develop piecewise correlation techniques and onboard computer systems for rapid scanning remote detection devices such that space and time variations of optical and meteorological phenomena might be monitored in real time in regions where balloons are not available.

We hope to continue our present field test programs to collect design information that could be used for the development of rapid scanning remote detection devices. The long range objective of these field tests is to isolate the space time variations of local emission, absorption and scattering processes at various altitudes and to determine the irreducible amount of noise which is imposed by the variations of the meteorological boundary conditions. The design of airplane instrument packages and of on-line computer systems should be initiated as soon as the results of the continued field tests indicate the feasibility of such a step.

### ACKNOWLEDGEMENTS

The development of the piecewise correlation program would have been impossible without significant contributions from our colleagues at the Marshall Space Flight Center (MSFC) and the Nortronics-Huntsville Division (N-H). Analog data acquisition systems were provided by J. P. Heaman, MSFC. Software and analog digital conversion systems were made available by J. A. Jones, MSFC. Computer operations and development of program options were provided by J. Pooley, N-H. The concepts of piecewise ordinate shifts and piecewise gain factors have been contributed by R. R. Jayroe, MSFC, and M. Y. Su, N-H. Most experimental data were collected by V. A. Sandborn, Colorado State University.

- Bendat, J. S. and A. G. Piersol, 1966: Measurement and Analysis of Random Data, John Wiley & Sons, New York.
- Crandall, S. H. and W. D. Mark, 1963: Random Vibrations in Mechanical Systems, Academic Press, New York.
- Fisher, M. J. and F. R. Krause, 1967: The crossed beam correlation method, J. Fluid. Mech., Vol. 28, p. 705.
- Jayroe, R. R. and M. Y. Su, 1968: Optimum averaging times of meteorological data with time dependent means, AIAA Conference on Aerospace Meteorology, New Orleans, May 5-9.
- Krause, F. R., S. S. Hu and A. J. Montgomery, 1966: On cross beam monitoring of atmospheric winds and turbulence with two orbiting telescopes, NASA TM X-53538, November.
- Krause, F. R., 1967: Mapping of turbulent fields by crossing optical beams, Invited paper, American Physical Society, Div. of Fluid Mech., Bethlehem, Pa., November.
- Montgomery, Anthony J., 1969: Remote sensing of winds and atmospheric turbulence by cross correlation of passive optical signals, Atmospheric Exploration by Remote Probes, Vol. 2, National Academy of Sciences - National Research Council, Washington, D. C.
- St. John, A. D. and W. D. Blauz, 1968: Study of atmospheric and AAP objectives of cross beam experiments, NASA CR-61191, February.
- Spiegel, M. R., 1961: Theory and Problems of Statistics, Schaum Publ. Co., New York.

FIELD TESTS OF THE OPTICAL CROSS-BEAM SYSTEM

V. A. Sandborn  
Colorado State University

ABSTRACT

Recent detailed evaluation of the use of an optical cross-beam system to measure convective wind velocities are reported. Low level measurements, where the optical system is looking at either the earth surface or cloud banks, are demonstrated. Further information on the nature and scale of the light fluctuations is reviewed.

1. INTRODUCTION

The measurement of convective wind speeds with the optical cross-beam system is demonstrated by Montgomery (1969). These preliminary measurements were limited to clear skies at elevations of 61 meters or greater. Operation of the optical system under cloudy skies had proven difficult, due to the extreme large variation in light intensity. In recent experiments it has been found that sufficient light fluctuations are present at low levels to allow operation even against distant cloud backgrounds. The present paper demonstrates the operation of the optical system during the cloud conditions.

2. FIELD TESTS

Field tests of the ground based cross-beam system were conducted at a Colorado State University meteorological field site on the St. Vrain Creek in northeastern Colorado. The general location is in the North Platte River Valley. It is located approximately 15 miles east of the first pressure rise of the Rocky Mountains. A 61 meter high tower is set up at the site.

The optical instruments and general arrangement of the equipment are reported by Montgomery (1969). (See first paper, Section 8, this volume)

2.1 Measurements with Ground and Cloud Backgrounds - The report of Montgomery (1969) has demonstrated the operation of the cross-beam system for

FIELD TESTS OF THE OPTICAL CROSS-BEAM SYSTEM

ideal sky conditions. Current measurements are presently being conducted to evaluate the system operation during adverse light conditions. Two conditions; one looking at distant hills and the other looking at distant cloud banks, have been investigated. At low levels the amount of light fluctuation due to scattering is much greater than at high levels. Thus, the cross-beam system is found to give good results for these two adverse conditions.

The magnitude and frequency of light fluctuations are found to change with time and from day to day. However, at no time are the fluctuations found to be absent. Figure 1 shows a typical trace of the fluctuations in light seen by a telescope. Figure 1 is from a telescope looking in a south direction at an elevation of  $52^{\circ} 12'$  above the horizon. The light fluctuations are from a band of 4500 to 6500 Å in optical wave length. Figure 2 shows the energy spectra of the light fluctuations measured both for the trace shown in Figure 1 (noted as Unit No. 1 on Figure 2) and for the second telescope that was looking into the north sky. The spectral function is defined as

$$\int_0^{\infty} F(f) df = 1 \quad . \quad (1)$$

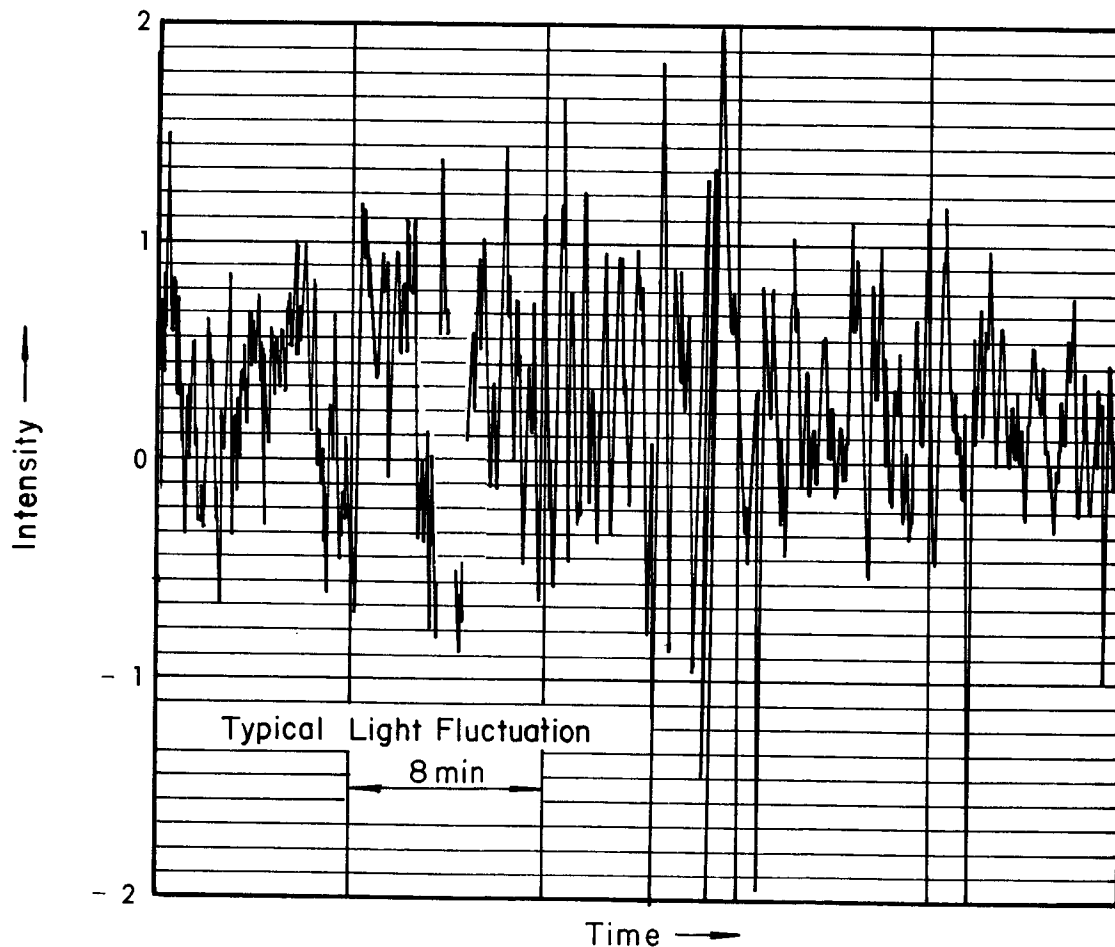


Figure 1. Typical light intensity fluctuations.

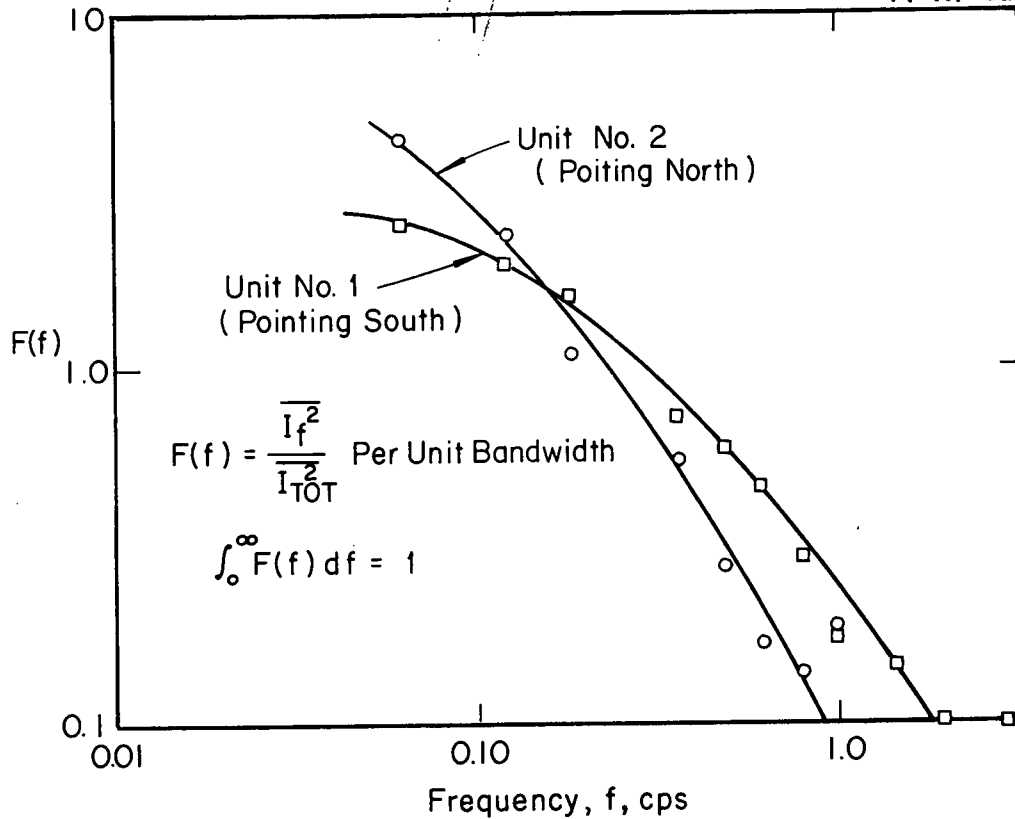


Figure 2. Spectra of light fluctuations.

Using the Taylor turbulent scale definition

$$L_x = \int_0^{\infty} R_x dx \tag{2}$$

together with the Fourier transformation

$$F(f) = \frac{4}{U} \int_0^{\infty} R_x \cos \frac{2\pi fx}{U} dx \tag{3}$$

where  $R_x$  is the x-distance correlation and  $U$  is the wind velocity, the turbulent scale may be written as

$$L_x = \frac{F(0)U}{4} \tag{4}$$

where  $F(0)$  is the value of  $F(f)$  at zero frequency. The spectrum curve of Figure 2 does not go to zero frequency; however as a first approximation the maximum value of  $F(f)$  might be used. For Unit No. 1  $F(f)_{max} \approx F(0) \approx 3$ .

For a wind velocity of approximately 15 meters/sec measured with cup anemometers at the time the recording was taken, equation (4) gives a scale length of 11.2 meters. This indicates that the fluctuations that dominate the record of Figure 1 come from heights of the same order of magnitude as the turbulent scale. Thus, the major part of the fluctuations most likely come from the first 10 or 20 meters in the atmosphere.

Figure 3 shows an autocorrelation curve for the signals of Figure 1. Using the transformation,  $Ut = x$ , the autocorrelation is equivalent to the space correlation  $R_x$ . Evaluation of  $L_x$  from equation (2) and the autocorrelation curve give a scale of 10.8 meters, which is in good agreement with the spectrum measurements. The autocorrelation curve falls to zero correlation after 5 seconds, indicating information on scales as great as  $(5 \times 15)$  75 meters are contributing to the signal. Thus, there is information in the light fluctuations from high elevations as well as from the lower levels.

Figure 4 shows a cross-correlation curve for the two light beams operating parallel to the ground. Both beams are looking at the distant hills beyond the river valley. The cross-correlation was obtained with a Princeton Research Associates time correlator. The two beams are separated by a distance of 67.8 meters. The common volume of the two beams is 209.8 meters. This is a very large volume of common intersection; however, the cross-correlation coefficient reaches a maximum of 0.10. The small correlation coefficient is due to the large magnitude of background fluctuations which are not correlated. The delay time to peak correlation agrees well with the observed wind velocity of approximately 10 meters per second. This run shown in Figure 4 was taken on a very cloudy day. If the overall light level were fluctuating along with the local levels seen by the beam, a peak in the correlation curve would also be observed at zero time delay. Zero time delay peaks have been observed for runs such as shown in Figure 4.

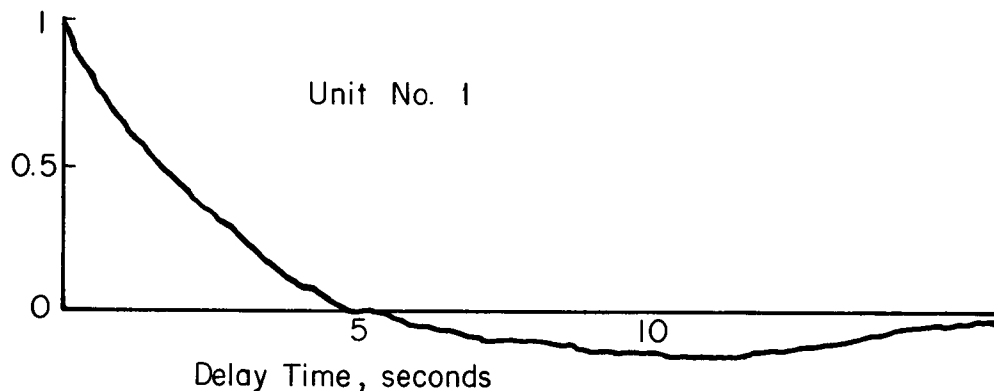


Figure 3. Autocorrelation of the light fluctuation.

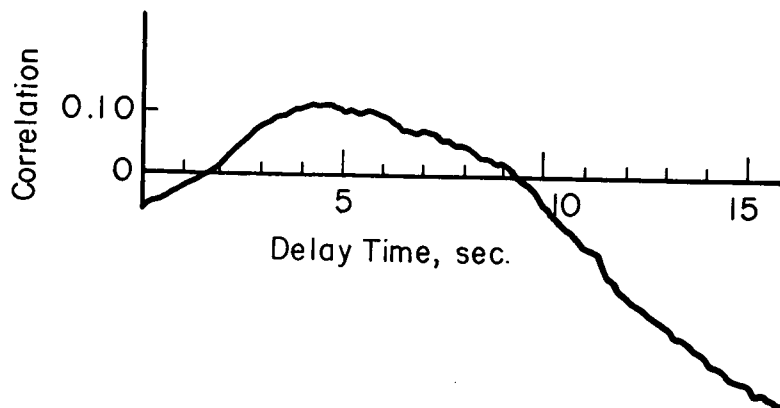


Figure 4. Cross correlation for two beams separated by 67.8 meters and parallel to the ground at a height of approximately 3 meters.

Figure 5 shows a cross-correlation curve for the two light beams operating at a low level of elevation (No. 1 Unit  $6^{\circ} 28'$ , No. 2 Unit  $7^{\circ} 54'$ ). The height of their common intersection point is 13.1 meters. The two beams are separated by 67.8 meters. Both beams are looking into clouds. Although the light fluctuations were very large for this particular test run, the peak of the cross-correlation curve is at the right time for a wind velocity of approximately 5 meters per second. One of the major difficulties encountered with the cross beam application to the atmosphere has been the large dynamic range of the light fluctuations. The present electronic operation of the photodiodes is not adequate to handle large fluctuations caused by clouds. Only near the surface, where there are large local light fluctuations, can the instruments be operated in the presence of clouds. Modification of the electronic circuits should improve the operation of the system in the presence of clouds.

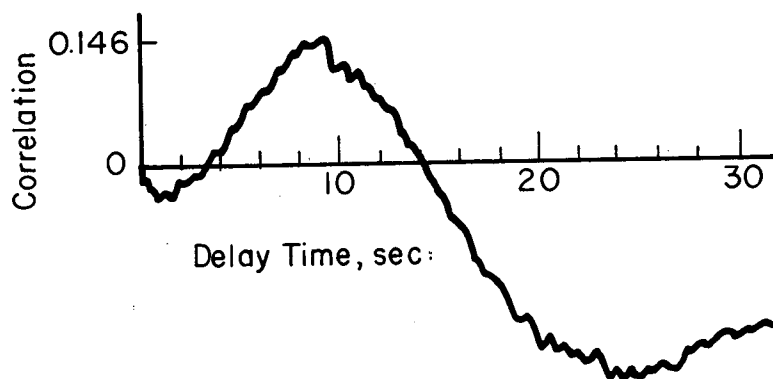


Figure 5. Cross correlation for two beams separated by 67.8 meters at a height of 13.1 meters.

### 3. RECOMMENDATIONS

The cross-beam technique has been demonstrated to measure convective velocities of the wind under specific conditions. It is important to keep in mind the fact that this technique may be employed with almost any atmospheric sensing instrument. The correlation technique could produce a convective velocity for any tracer that can be sensed by optical, infrared, or micro-wave techniques.

3.1 Continuing Studies - The optical cross beam system is presently being compared with cup anemometers. The system will be developed and evaluated by a means of measuring local velocity distributions above the surface.

3.2 Future Studies - The optical cross beam system should be able to evaluate a great deal of information about the turbulent structure of the atmosphere. Further studies of the measurement of the scale of turbulence from cross correlation data will be undertaken. The cross beam measurements are to be compared with turbulence evaluated from hot-wire anemometer data.

## FIELD TESTS OF THE OPTICAL CROSS-BEAM SYSTEM

3.3 Special Facilities - The field tests are being run through the joint cooperation of NASA and ESSA. Further studies will be conducted at the ESSA Gun Barrel hill site. A special digital converter system is being developed to improve the evaluation of the measurements.

### 4. CONCLUSIONS

The cross beam optical system has been proven as a technique to measure convective winds in the atmosphere. It is also demonstrated that low level winds can be measured using either surface or cloud backgrounds. Further development of the instruments should make it a very flexible measuring tool.

### ACKNOWLEDGMENTS:

The field tests reported in this paper were conducted under NASA Contract DCN 1-7-75-20042 (IF) for the George C. Marshall Space Flight Center of the National Aeronautics and Space Administration. The work is administered under the technical direction of the Aero-Astroynamics Laboratory with Dr. Fritz Krause acting as project manager.

### REFERENCE

Montgomery, A. J., 1969: Remote sensing of winds and atmospheric turbulence by cross correlation of passive optical signals, Atmospheric Exploration by Remote Probes, Vol. 2, National Academy of Science - National Research Council, Washington, D. C.

SESSION 9

Sferics

N72-25383

SFERICS

E. T. Pierce  
Stanford Research Institute, Menlo Park, California

ABSTRACT

The properties of sferics--the electric and magnetic fields generated by electrified clouds and lightning flashes--are briefly surveyed, the source disturbance and the influence of propagation being examined. Methods of observing sferics and their meteorological implications are discussed. It is concluded that close observations of electrostatic and radiation fields are very informative, respectively, upon the charge distribution and spark processes in a cloud; that ground-level sferics stations can accurately locate the positions of individual lightning flashes and furnish valuable knowledge on the properties of the discharges; but that satellite measurements only provide general information on the level of thundery activity over large geographical regions. It is recommended that simultaneous investigations of sferics and other--possibly associated--meteorological phenomena be encouraged and that immediate consideration be given to the establishment of a National Sferics Facility; this would consist of a network of ground stations capable of locating every lightning flash in the U.S.A. as it occurs.

1. INTRODUCTION

In meteorology "sferics" studies are usually considered to involve investigations of the electromagnetic signals radiated by distant lightning flashes, and to have as their prime objective the location of the positions of the flashes. Most of this review will be concerned with such studies. However,\* some attention will also be given to observations of the electrical field-changes generated by close lightning, and to investigations of the fields accompanying electrified clouds but not directly associated with lightning occurrence.

---

\* In accordance with the request of Professor David Atlas, Chairman, Panel on Remote Atmospheric Probing.

It is usual to define the electric moment  $M$  of an electrified cloud by  $M = 2 \sum qh$  where the summation involves every elementary charge  $q$ , at altitude  $h$ , associated with the cloud. If the net electrification of the cloud can be represented by a point charge  $Q$  at a height  $H$  then the vertical electrostatic field,  $E_s$ , produced at the surface of the earth by the cloud is given by

$$E_s = \frac{1}{4\pi\epsilon_0} \frac{2QH}{(H^2 + D^2)^{3/2}} = \frac{1}{4\pi\epsilon_0} \frac{M}{(H^2 + D^2)^{3/2}} \approx \frac{1}{4\pi\epsilon_0} \left( \frac{M}{D^3} \right) \text{ for } H \ll D \quad (1)$$

where  $D$  is the distance along the ground from below the cloud to the point of observation, and  $\epsilon_0$  is the permittivity of free space. When either  $Q$  or  $H$  are changing rapidly then--in addition to the electrostatic component  $E_s$ --the electric field,  $E_t$ , at time  $t$  has appreciable induction ( $E_I$ ) and electromagnetic radiation ( $E_R$ ) components. An approximate representation is

$$E_t = E_s + E_I + E_R = \frac{1}{4\pi\epsilon_0} \left\{ \frac{M_t}{D^3} + \frac{dM_t/dt}{cD^2} + \frac{d^2M/dt^2}{c^2D} \right\} \quad (2)$$

where  $c$  is the velocity of light, and retarded values at time  $(t - D/c)$  are used for  $M_t$ . Equation (2) is a useful guide to general behavior but is of limited applicability. It involves implicitly the assumption that  $D$  is appreciably greater than the dimensions of the cloud. Also if  $\lambda$  is the wavelength of any electromagnetic radiation described by Eq. (2) then  $\lambda$  should considerably exceed the length of the radiating channel involved; in practice this implies that the validity of Eq. (2) decreases rapidly for  $\lambda$  less than about 10 km (frequency greater than 30 kHz). Equation (2) applies to an infinite vacuum half-space above a perfectly conducting ground; it will thus be increasingly modified with increasing distance by the finite electrical properties of the earth and the effect of the ionosphere. The ionosphere has the influence--very important in sferics studies--of channelling radio signals at some frequencies around the earth.

It is instructive to note that if  $M_t$  is assumed to alter at a frequency  $f$  then the three terms in Eq. (2) are equal in magnitude when  $D = c/2\pi f$ . Thus at 10 kHz,  $E_R$  will dominate in Eq. (2) for  $D$  greater than about 5 km; at 100 Hz on the other hand  $E_s$  will still be the largest component for  $D \leq 450$  km.

Sferics signals are naturally emitted from electrified clouds and are therefore in themselves meteorological information.\* A received sferics signal consists of the original source disturbance subsequently modified during propagation. Close to the origin the propagational effects will be slight; the source characteristics are relatively uncontaminated, and since these characteristics are complicated a variety of observational techniques must be employed if they are to be accurately defined. Propagation tends to eliminate or to smooth out many of the source characteristics so that as distance increases sferics become more uniform and so--in consequence--do the techniques for their observation. Some of the source effects are preserved to very great distances, but with others their identification becomes difficult if the length of the propagation "filter" is large.

---

\* This is not always appreciated by meteorologists.

For the above reasons it is convenient to consider separately close and distant sferics observations, and to divide the latter category into ground-based and satellite measurements. However, before these topics are discussed, it is appropriate to present some established and relevant background information.

## 2. BACKGROUND INFORMATION

### 2.1 Thunderstorm Behavior

The characteristics of thunderstorms relevant in sferics studies have been reviewed by Dennis (1964) and--more briefly--by Pierce (1967a). Most theories of thunderstorm electrification envisage a time of some 10 to 30 minutes as elapsing between the onset of unusual electrification in a developing thundercloud and the occurrence of the first lightning discharge. This development time is in agreement with electrical observations. The electrification develops in active cells; each has a diameter of perhaps 6 km but the most intense activity is often more concentrated. A cell has a typical lifetime of some 30 minutes; during this time the flashing rate within the cell varies from under one per minute to a maximum which is usually less than 10 per minute but which can be as high as 50 per minute. An average flashing rate is about 3 per minute.

Electrically active cells may occur anywhere within a complex having a diameter of some 30 to 40 km. The complex essentially defines the thunderstorm extent. Within the complex the flashing rate does not differ greatly from that for a single cell since it is rare for more than two cells to be active simultaneously. In most synoptic circumstances complexes are separated by about a hundred kilometers; sometimes they are disposed along a frontal system thus producing a line storm situation which may persist for a day or more.

During the build-up period prior to the first lightning flash only minor sparks--by definition--occur within the cloud. Thus the transient  $E_I$  and  $E_R$  fields (Eq. 2) will be small, but the semi-permanent  $E_S$  field can be large.

### 2.2 Lightning Flashes

A thundercloud normally contains a net positive charge in its upper portions while the base of the cloud is negatively charged. These are two common types of lightning discharge--the flash to ground and the intracloud discharge. The former usually removes negative charge to earth, while the intracloud flash tends to neutralize the overall electrification of the cloud either by upward movement of the lower negative charge or by downward motion of the upper positive charge.

The electrical effects accompanying a lightning discharge are of considerable duration. For both flashes to earth and intracloud discharges, the average duration exceeds 0.25 s. During most of this time leader processes are occurring. These involve the advance of a charge-carrying channel by a series of comparatively minor sparks which occur in rapid succession. The most intense of these minor sparks are the well-known "steps"; these are often present during the advance, from the base of the cloud to the earth, of the leader-streamer which initiates the flash to ground. Usually--and particularly for streamer processes within a cloud--it is difficult to distinguish the

electrical signal associated with each small spark involved in advancing the streamer; it is only the aggregate electrostatic effect or the radiated electromagnetic "noise" that can easily be recognized.

If an advancing charge-carrying leader encounters a concentration of charge of opposite sign, there is a rapid recoil surge of current backwards along the advancing channel. The electrical and luminous effects produced by such surges are readily identified. In the case of intracloud discharges, the phenomena accompanying the sudden surges are described as K changes. These are pronounced but far more intense effects accompany the return-strokes of the flash to ground. In an earth discharge, the initial leader-channel carries negative charge downward from the cloud. When contact with the ground is made a very intense upward surge of luminosity towards the cloud occurs; this is a return-stroke. There may be several return-strokes contained within a flash to earth. During the intervals between return-strokes it is believed that leader streamers carrying positive charge probe into the cloud from the upper part of the channel energized by the return-stroke. If such a positive leader encounters a medium sized concentration of negative charge within the cloud, there is a recoil streamer giving a K change. Occasionally the recoil may be sufficiently intense to extend as far as the ground; in these instances the recoil streamer is known as a dart leader. In its passage, the dart leader recharges the original channel negatively, so that when the dart reaches the earth the conditions are suitable for another return-stroke to surge upwards. It is noteworthy that K changes are present both for intracloud discharges and for flashes to earth (between return-strokes or after the final return-stroke). On the other hand true return-strokes only occur for the discharge to earth, since it is solely in this case that one extremity of the spark is a large homogeneous, good, electrical conductor.

Equation (2) shows that at close distances and extremely low frequencies the field-change is dominated by the electrostatic component. However for  $D$  greater than some 15 km and frequencies exceeding 3 kHz, it is the radiated field that is important. The structure of the electromagnetic radiation due to a single discharge shows interesting variations with frequency; these are illustrated in Fig. 1. [Pierce (1967b)]. At VLF (3-30 kHz) the pulses are discrete and are generated principally by return-strokes or recoil streamers (K-changes). As frequency increases so does the number of pulses per flash to reach a maximum of about  $10^4$  per discharge at a frequency in the VHF range (30-300 MHz); the disturbance accompanying the flash is then quasi-continuous. With a further increase in frequency there is a sharp decrease in the number of pulses, until at centimetric wavelengths (radar-GHz) the pulses are again well separated and associated with macroscopic features such as return-strokes. Peak pulse amplitudes are reached, for a flash to earth, at about 5 kHz. With increasing frequency up to at least  $10^4$  MHz there is a general decrease in amplitude which approximately follows an inverse frequency dependency; however over substantial sections of the spectrum between 10 kHz and  $10^4$  MHz there are probably appreciable deviations from this simple law. Figures 2 and 3 which are taken from a recent review by Oetzel and Pierce (1968) illustrate the amplitude variation with frequency of the radio emission from close lightning. The results--which represent information from several sources--have been normalized to a distance of 10 km. Figure 2 represents the amplitude spectrum,  $S(f)$ , while Fig. 3 is the peak amplitude,  $e_p$ , for a receiver of bandwidth of 1 kHz. The relation between  $S(f)$  and  $e_p$  is complicated; however,

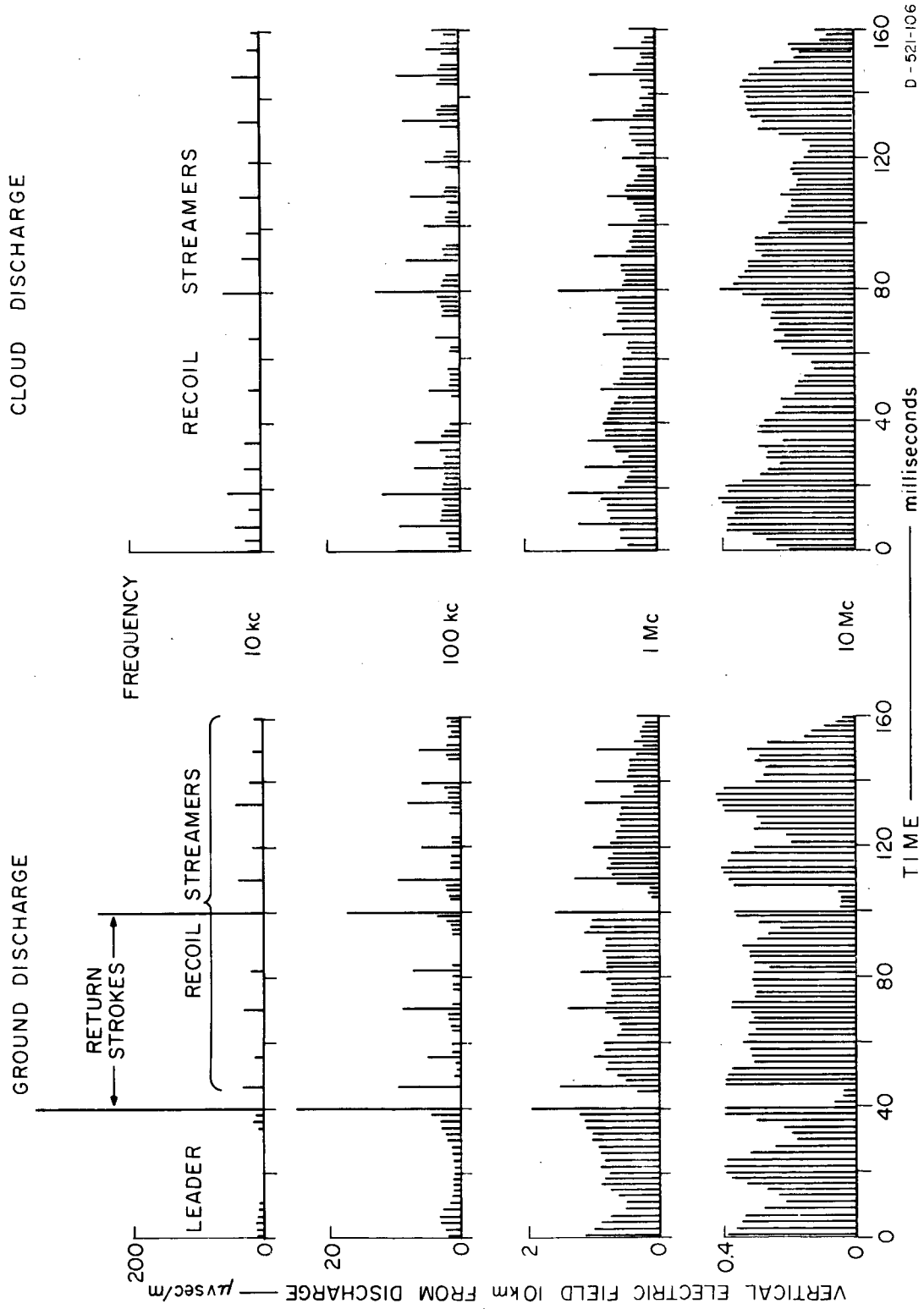


Figure 1. Response of Narrow Band Receivers to a Close Lightning Flash.

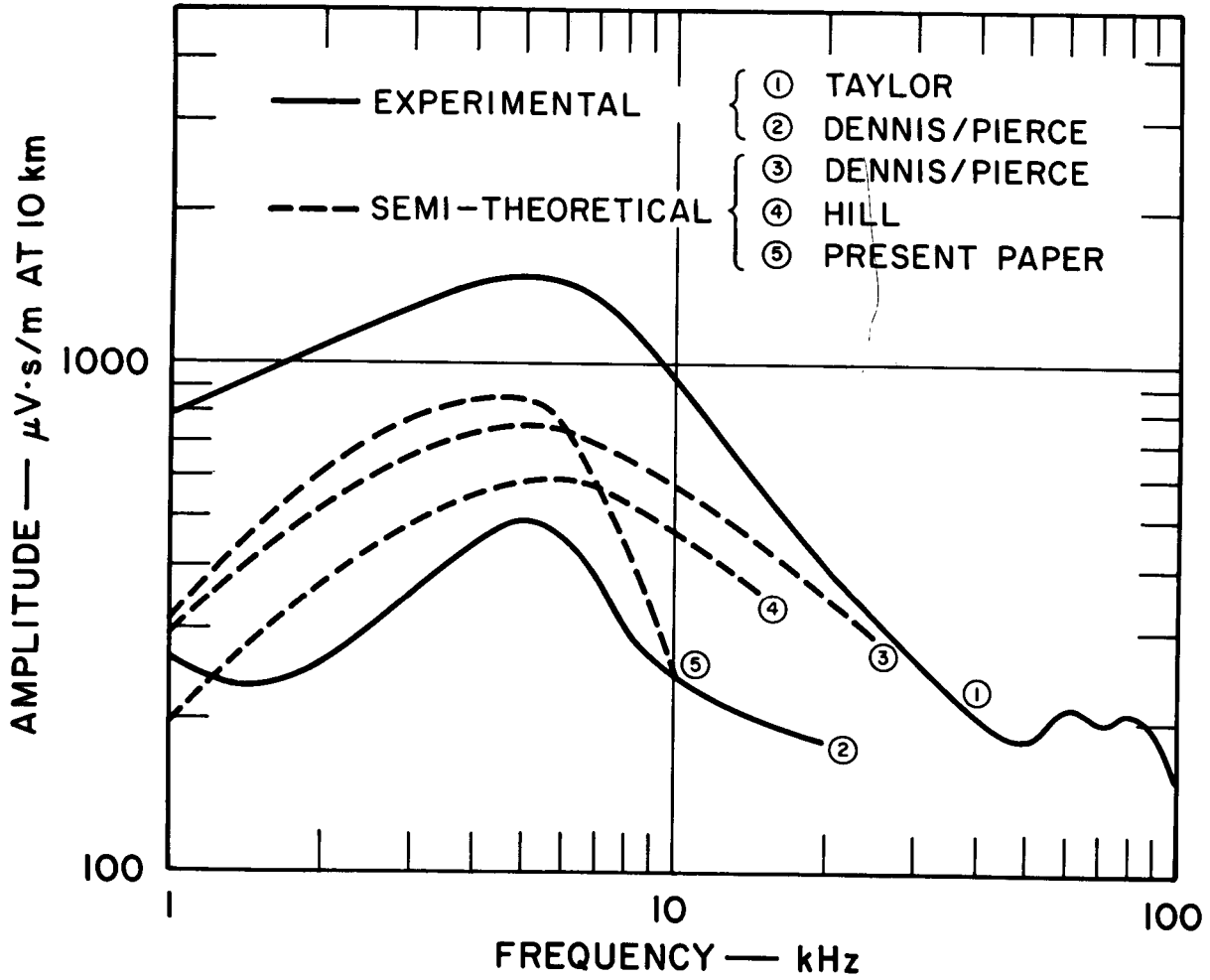


Figure 2. Amplitude Spectra of Return-Stroke Pulses.

Fig. 2 can be approximately interconnected to Fig. 3 if the ordinate scale of Fig. 2 is multiplied by  $10^3$ . Note that Fig. 2 represents the spectrum of the return-stroke pulse; at 5 kHz this exceeds the spectrum of a K change pulse by more than an order of magnitude, but at 100 kHz the two spectra are much more comparable.

The behavior of the radio emissions from close lightning may be summarized by stating that a multitude of subsidiary sparks of many different types is involved: the larger the current peak in a given type of spark, the longer the energized channel, the lower the frequency at which peak signal is radiated, and the less frequent the occurrence of the particular kind of spark. High current channels tend to be orientated vertically (especially the return-stroke); minor subsidiary discharges are, however, much more randomly disposed.

### 2.3 Propagation Effects

If sferics signals are to reach ground receivers at great distances from the thunderstorms generating the sferics then the propagation must be almost entirely by ionospherically reflected rays. This implies a restriction to frequencies below the HF bank (3-30 MHz). At HF and MF (0.3-3 MHz) there are very considerable temporal variations in long distance radio propagation and losses are always substantial; at still lower frequencies, however, there are two frequency ranges, of especial importance in sferics studies, at which propagation conditions are relatively stable and attenuation is minimal.

For frequencies below about 100 kHz radio signals travel between the earth and the lower ionosphere as in a quasi-waveguide. The variation in signal strength  $E$  (mv/m) with distance  $D$ , can often be approximated when  $D$  is large by the equation

$$E \approx \frac{300}{h} \left\{ \frac{P \lambda}{a \sin(D/a)} \right\}^{\frac{1}{2}} \exp(-\alpha_f D) \quad (3)$$

In Eq. (3),  $\lambda$  is the wavelength involved,  $a$  is the radius of the earth,  $h$  the effective width (earth-ionosphere) of the guide,  $P$  the radiated power from the flash (kW). The attenuation coefficient  $\alpha_f$  depends principally on frequency,  $f$ , but is also affected by the electrical characteristics of the earth and lower ionosphere; by the temporal changes that occur in the ionosphere; and by the orientation of the propagation path with respect to the geomagnetic field. Usually  $\alpha_f$  has two pronounced minima which occur in the frequency range of 10 to 30 kHz and at frequencies below about 300 Hz; this behavior is illustrated in Fig. 4b. If the source disturbance has the spectrum shown in Fig. 4a, (for a typical return-stroke pulse), then the frequency-selective propagational attenuation tends to remove components at frequencies above 30 kHz and between 300 Hz and 10 kHz. Thus the sferic received from a distant lightning flash tends to consist of distinct VLF and extremely low frequency (ELF) signals. The propagation is dispersive with the VLF signal traveling the more rapidly; thus a sferic as recorded using a broad-band system (Fig. 4c) consists of a VLF oscillation succeeded by an ELF perturbation (sometimes known as the "slow tail").

With the advent of satellites sferics propagation through the ionosphere has obviously become of importance. Radio signals can penetrate the ionosphere if their frequency exceeds the ionospheric critical frequency  $f_c$ ;

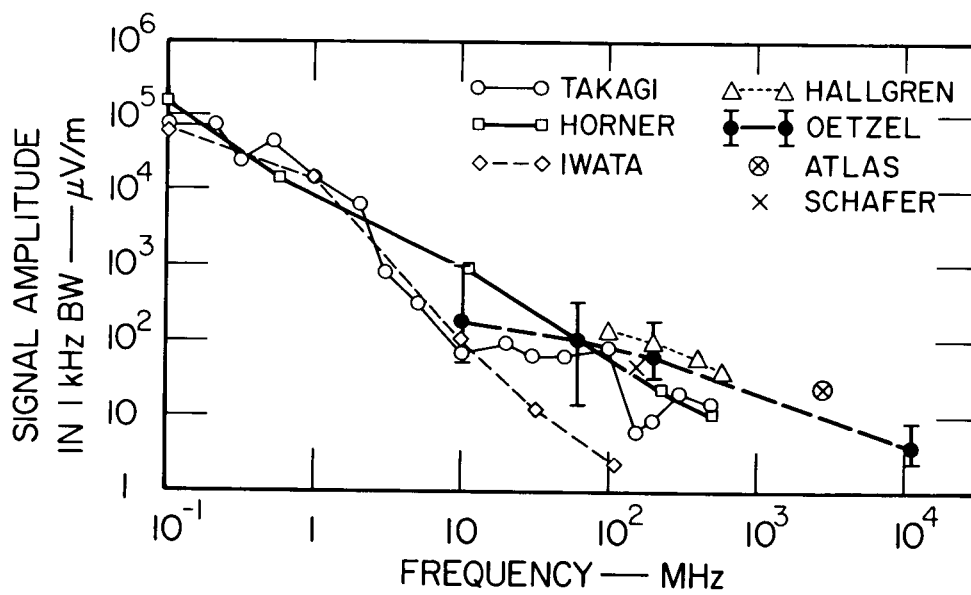


Figure 3. Peak Amplitude of Radiation from Lightning, 0.1 MHz to 10<sup>4</sup> MHz. Data have been normalized to 1 kHz bandwidth and 10 km range.

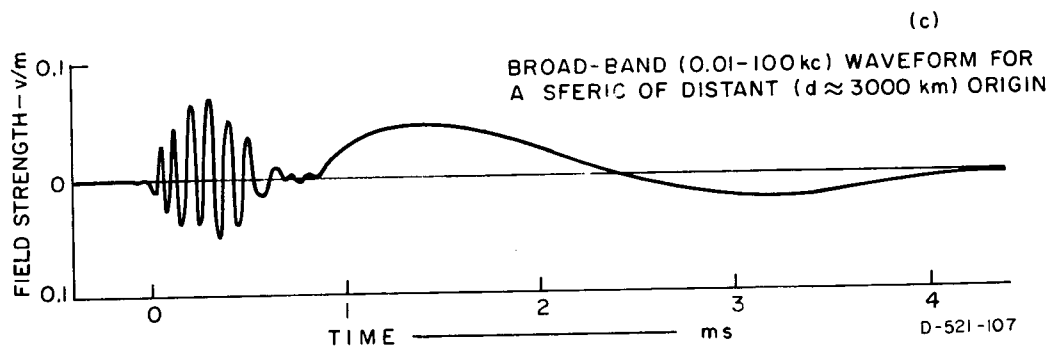
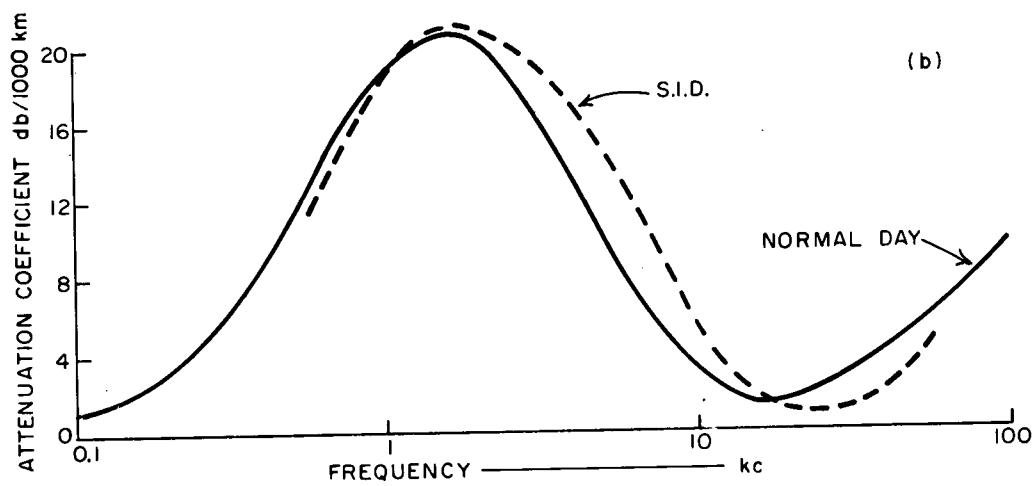
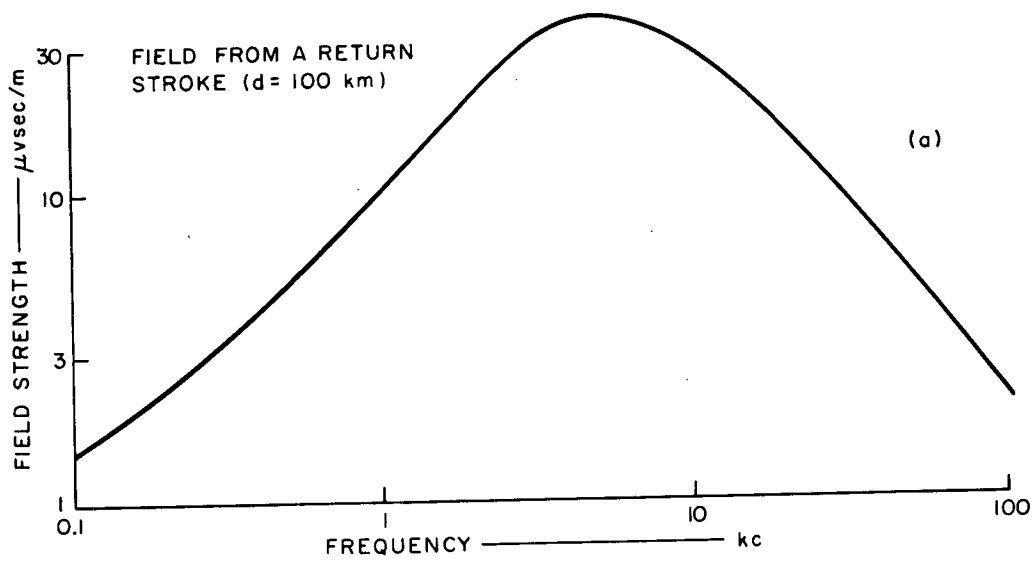


Figure 4. Illustrating some Factors in the Formation of a Sferic.

$f_c$  is normally a few megahertz. Penetration is also possible for some frequencies less than  $f_c$  by means of the whistler mode. In this mode of propagation the signals travel in a guided fashion along geomagnetic field lines. Whistler mode propagation is particularly effective at VLF. The main propagation is along the earth-ionosphere waveguide but there is a continual leakage from the upper boundary of the guide into the whistler mode.

At frequencies exceeding  $f_c$  where penetration of the ionosphere is possible the attenuating and other effects of the ionosphere decrease in magnitude as  $f$  increases. However, it is likely that  $f$  must be more than 100 MHz at least before the influence of the ionosphere can be ignored and the propagation considered as line-of-sight. When  $f$  is not much greater than  $f_c$  (say  $4f_c > f > f_c$ ) the ionosphere acts in an interesting way to limit the ground area from which sferics signals can be received in an overhead satellite. For oblique upward radio propagation with an angle of incident  $\phi$  upon the ionosphere penetration occurs if  $f$  is greater than  $f_c \sec \phi$ . It follows that a satellite at height  $x$  will be receiving signals from an area  $A_f$  below given approximately by

$$A_f = \pi x^2 \left( \left( \frac{f}{f_c} \right)^2 - 1 \right) \quad (4)$$

### 3. SFERICS OBSERVATIONS OF CLOSE LIGHTNING

The techniques [Chalmers (1967)] for studying the electric and magnetic signals generated by a nearby lightning flash are so diverse and specialized that their description must inevitably deal in generalities if it is not to be intolerably prolix. When a thunderstorm is close the difficulties imposed by the unpredictability, in position and time, of lightning occurrence are most pronounced: the relative size of the electrostatic, induction, and radiation field components changes very rapidly with distance and with the frequency band at which observations are being made: the time resolution required ranges from much less than a microsecond for certain features of the discharge (e.g. the return-stroke pulse), to perhaps a second if the overall effects of flashes and thunderstorms are being investigated: while the dynamic recording range must be large embracing, for instance, currents of from tens of amperes (in leader stages) to well over  $10^4$  A (return-strokes).

A common practice among investigators of close lightning is to employ broad-band equipment which either extends in frequency response from a fraction of a cycle per second to an upper cutoff at a few kHz, or responds to a higher frequency range (possibly 3-300 kHz). With the former frequency coverage the recorded fields and field-changes essentially represent the electrostatic component and can therefore be interpreted in terms of charge magnitudes and locations: however, if the higher frequency range is selected, the signals are dominantly transient radiated fields and their examination is thus primarily informative upon spark characteristics (especially when individual pulses such as those due to K processes or return-strokes can be identified). Simultaneous recording using two broad-band but separated frequency ranges can be particularly instructive [Kitagawa and Brook (1960)].

At frequencies exceeding perhaps 1 MHz noise interference usually precludes wide band recording except at certain ideal sites. Narrow band experiments

give useful but restricted information.

Much valuable knowledge regarding thundercloud electrification can be derived from observations of the field variations occurring during the course of a storm but not generated by or coincident with lightning. This fact is apparent in the pioneer electrostatic field measurements of C. T. R. Wilson. It has long been realized that as the electrostatic fields grow during the developmental stage of a thunderstorm magnitudes will be attained at which points at the surface of the earth will break into corona; corona and micro-sparking can also occur for drops within the cloud. Such minute discharges generate radio emissions [Pierce (1962)]; these have been experimentally detected, at frequencies of some tens of megahertz, from thunderclouds several minutes before the first lightning flash, [Zonge and Evans (1966)] and even from shower clouds which never develop into thunderstorms [Sartor (1964)].

In sferics studies of close lightning, there are many modern ways of improving basic techniques. Appropriate antenna arrays can be employed at the higher frequencies, while the use of broad-band tape recorders is especially profitable in that it enables sferics signals to be processed at leisure in several ways long after the occurrence of the thunderstorm. Simultaneous measurements at several ground stations have some advantages; these can be extended to the height dimension with aircraft, balloons, or rockets. However, the complexities of interpretation are sometimes such that more is lost by multi-station work than is gained; this is particularly so if redundant information is being obtained.

It is evident from the preceding paragraphs that observations of the signals from close lightning is rarely a routine matter, and that the optimum techniques to be used largely depend upon the primary objectives of the individual experimenter. Perhaps the only simple instrument by which useful data on some electrical characteristics of local thunderstorms can be routinely obtained is a lightning-flash counter. These instruments count whenever the incoming signal produced by a lightning discharge exceeds a certain threshold  $E_T$ ;  $E_T$  can be statistically related to an effective counter range  $R$ . Counters must never be regarded as precise instruments but they can yield valuable information, especially if counters of identical design are employed under similar circumstances at different geographical locations. Horner (1967), for example, has demonstrated how counter results can establish the diurnal variation of lightning activity, and can be used to refine and to replace the common meteorological statistic of the thunderstorm day.

#### 4. SFERICS OBSERVATIONS OF DISTANT LIGHTNING

##### 4.1 Ground-Based Techniques

An atmospheric received at a ground station from a distant thunderstorm consists predominantly of VLF and ELF components (Fig. 4c). Methods-- of various levels of refinement--for recording such atmospherics are well established. In meteorology, networks of VLF sferics ground stations have been very extensively and profitably used [Horner (1964)] to determine the position of the original lightning discharge responsible for an atmospheric incident over the network, and thus to track thunderstorms. The flash is located by analysis, either of times of arrival, or of bearings recorded, for the incoming sferic at each network station.

Considerable efforts have been made to develop methods whereby the origin of a sferic can be established from a single station. The approach is usually to combine a bearing observation with the measurement of some distance-dependent characteristic of the incoming atmospheric. The techniques of Frisius, Heydt, and Volland [see for example Volland (1965)] are especially sophisticated; using these techniques the distribution of amplitudes and group time delays for incoming sferics can be recorded as a function of azimuth and frequency, and the information then analyzed to give thunderstorm positions. Even with this refined approach, however, the accuracy of the results obtained is much less than that achieved by a multi-station fixing network.

Studies of the characteristics of VLF sferics that have traveled a long distance tend to be more informative on radio propagation at VLF than on the source disturbance. However, some meteorological data can be obtained. Most VLF sferics can be identified as originating in return-strokes or K streamers, and sferic measurements such as amplitude and phase spectra can be analyzed, after allowing for the propagational modifications, to yield estimates of the form and magnitude of the current surges in the corresponding source pulses. Information on the relative magnitudes and time separations of the individual return strokes and K processes in discharges is fairly easily obtainable, and this information can be applied to determine whether a sequence of VLF sferics was generated by an intracloud discharge or by a flash to earth.

Investigations of sferics at ELF ("slow tails") have been surprisingly neglected in recent years; there are present signs, however, of a revived interest [Hughes (1967)]. Bearing information can be obtained just as effectively at ELF as at VLF. Furthermore, since propagation at ELF depends less on variations in ground conductivity, path orientation with respect to the geomagnetic field, and temporal changes in the ionosphere, than does VLF propagation, it is easier to allow for the propagational modifications when attempting to extrapolate back to source properties.

There are two specialized aspects of sferic studies which merit at least passing mention. Several stations at various locations in the world monitor radio noise at selected frequencies [ITU (1964)]. The results from the radio-noise stations can be used to determine crudely the temporal variations in position and strength for the main global thundery areas. Similar approximate information can be deduced from investigations of the Schumann resonances. These resonances of the earth-ionosphere cavity, which occur at frequencies of about 8, 14, 20, 26 Hz and upward, are excited by lightning flashes. The strengths of the resonances at a given station are related to the rate of occurrence (activity) of the discharges, and their locations with respect to the observing point.

#### 4.2 Satellite Techniques

Sferic measurements in satellites have great apparent attractions but a little consideration soon reveals their very real limitations. The radio signals that contain most information about the lightning source are those at the lower frequencies (especially in the VLF band); it is these frequencies that are most influenced by the propagation through the ionosphere, so that much of the source information is lost. For signals at frequencies (above)

perhaps 100 MHz), that are relatively unaffected in their passage through the ionosphere, the original radiation is of low amplitude (Fig. 3), and contains only crude information on the lightning flash.

The flashing characteristics of a cell impose severe restrictions on the effectiveness of the surveillance of individual thunderstorms by low-altitude (say 1000 km) sferics satellites. For such satellites the orbital speed is about 7 km/s; thus with an antenna system resolving a cloud area comparable with that of a thunderstorm cell the area is only monitored for about a second. Since the interval between flashes is typically 20s, one second is a time quite insufficient for a cloud to be identified as thundery or not.

High altitude--stationary would be 37,000 km -- orbits, in conjunction with elaborate antenna scanning systems might enable fairly small areas of the earth's surface to be examined. However, at 37,000 km sferics signals must be identified within a framework of strong background noise. There may be advantages in using optical ( $H\alpha$ ) sensors but the discussion of these is beyond the scope of this report.

Summarizing, sferics satellites seem incapable of yielding useful information on individual lightning flashes or thunderstorms. They can monitor large areas (diameter ca 1000 km), and hence determine approximately the degree of thundery activity within these areas. Thus the main potential use of sferics satellites is in improving our knowledge of temporal variations in the strengths and positions of the main global thunderstorm regions.

Sferics sensors in satellites might operate either at VLF, HF, or VHF. At VLF the source radiation is strong, but propagation is by the whistler mode so that the received sferic penetrates the ionosphere along the geomagnetic field line through the satellite position; before entry into the ionosphere the sferic propagates, from the originating lightning discharge, below the ionosphere in the earth-ionosphere quasi-waveguide. This complicated path entails difficulties in identifying the location of the lightning flash generating the sferic. The geomagnetic path control has some remarkable implications; for example, a satellite 1000 km above the equator would tend to receive VLF signals from equatorial thunderstorms via a path below the ionosphere as far as a latitude of  $20^\circ$  N or S, and then through the ionosphere along the appropriate field line.

At HF the sferics signals received in satellites above the ionosphere are well above the ambient background in strength. The ionosphere itself defines the area upon the surface of earth that is being monitored (Eq. 4). If several narrow-band receivers tuned to various frequencies within the HF band are employed then the recorded noise can be associated with different areas and the value of the results enhanced. A multi-frequency experiment of this kind, presently being carried on the Ariel III satellite, is already yielding useful data [Bent (1968)]. One aspect of HF sferics sensors is that the results are equally revealing upon the characteristics of the ionosphere as upon those of the thundery activity beneath. Indeed, if the latter information is to be deduced then the ionospheric effects must first be reliably estimated.

The main drawback to using sensors at frequencies ( $>$  say 100 MHz)

essentially unaffected by passage through the ionosphere is the low ratio of sferics signal to other noise. This other noise can be of cosmic, solar, terrestrial (thermal) or manmade (including receiver) origin. Pierce (1967a) has estimated that for a satellite at an altitude of 1000 km the signal/noise ratio deteriorates from about 10/1 at 100 MHz to perhaps 2/1 at 600 MHz; this decrease is principally due to the drop in the lightning signal as frequency increases (Fig. 3). If the satellite altitude becomes greater the signal/noise ratio becomes less; this is because, at best the sferics signal varies inversely with distance (Eq. 2), while several noise sources (cosmic, solar, receiver) are independent of distance.

It is perhaps appropriate in this section to query whether sferics satellites are really necessary since the information they can supply is possibly being already obtained by other satellite experiments. For example, there are indications that large-scale thunderstorms with massive convection can be identified from cloud-photographing satellites. This identification might become more positive, if comparisons were made between the cloud photographs and the considerable amount of sferics data that has already been obtained in satellites (Lofti, Ogo, Alouette, Ariel, etc.). Certainly this comparison should be performed before elaborate schemes for specialized sferics satellites are considered.

#### 5. METEOROLOGICAL INFORMATION POTENTIALLY OBTAINABLE FROM SFERICS.

Sferic observations can furnish direct information on the electrical characteristics of individual lightning flashes, and on the temporal changes in the level of electrical activity for single thunderstorms or for thundery regions. They can also be used to locate the positions of active storm centers. Non-electrical meteorological information can be deduced from sferics results, but the validity of such deductions is often questionable since the degree of association between electrical and other meteorological phenomena is seldom well established, and may indeed in many instances be very slight.

Three classes of sferics observations have been identified in the preceding text. Of these, satellite measurements seem primarily capable only of improving our climatological knowledge of the main global thundery regions. However, such information, which essentially establishes the spatial and temporal variations of thunderstorm activity, has important basic and applied implications. In the former category, the most obvious use is in improving our definition of the qualities of the global thunderstorm generator controlling the universal aspects of atmospheric electricity. Again, in the basic field, accurate knowledge of thunderstorm climatology may assist our understanding of the general atmospheric circulation and of the distribution of atmospheric contaminants since it is possible that the large convective clouds of intense thunderstorms play a vital role in exchanges between the troposphere and the stratosphere. Practical applications of satellite sferics measurements tend to be non-meteorological; two such applications are in improving the estimation of atmospheric noise interference to radio communication, and in establishing approximately the optimum degree of lightning protection required for electrical power transmission lines to be located in remote areas of the world.

Ground-level sferics techniques can locate the positions of individual lightning flashes and therefore of active thunderstorms, while the examina-

tion of incoming sferics is informative upon the electrical characteristics of the flashes in storms. Radio noise and Schumann resonance measurements give information on the locations and strengths of active thundery areas, comparable in refinement with that obtained by satellite techniques; however, a VLF sferics network yields incomparably more accurate fixes. This improved location precision enables VLF sferics data to be applied in ways for which cruder results would be unsuitable. Among these uses are the selection of optimum safe routing for aircraft, and the estimation of forest fire hazards after lightning strikes. A standard VLF sferics network with station separations of the order of 1000 km can continuously locate lightning flashes, and record the waveforms (for example) of the corresponding sferics, over a region with a dimension of several thousand kilometers. The pulses within the individual sferics can be usually recognized as due to return-strokes or K processes; consequently, an identification with intracloud or cloud-ground discharges can be established. Detailed examination of the time separations and structure of the pulses yields some estimate of the currents and charges involved in the sferic (flash). Flashing-rates can obviously be derived for individual thunderstorms, and lead to estimates of the violence of the storm; this in turn is possibly related to such specialized meteorological phenomena as the occurrence of unusual hydrometeors (large hail). It is especially interesting to note that thunderstorms containing active tornadoes could perhaps be identified by distant sferics measurements, since tornadoes appear to produce very high flashing rates and to possess an unusual spectral distribution, in the VLF and LF bands, of the sferic source disturbance [see for example Jones (1965)].

Observations of close thunderstorms are naturally more informative on thunderstorm characteristics than are measurements at a distance. All the knowledge that can be deduced from records of distant VLF sferics, and more, can be determined from short range observations of radiation fields. This VLF information is enhanced by measurements of the electromagnetic radiation at other radio frequencies which propagate relatively poorly so that the signals are readily detectable only close to the source. Observations of radiation fields over a very wide frequency range are necessary in order to build up a complete picture of all the spark processes associated with lightning. At short distances ionospheric influences are unimportant; it is thus possible by employing suitable antenna arrangements to determine the polarization and hence the orientation of a large discharge channel. Electrostatic fields are only dominant (Eq. 2) when  $D$  is small. Records of such fields are by far the most direct way of estimating the magnitudes and heights of the charges in a thundercloud and the manner in which the electrical activity varies with time; this includes the growth phase before the first lightning flash. The radio emissions during the growth phase are potentially informative on the development of micro-discharges (for example between water-drops) within the cloud; however, these emissions are very weak and therefore difficult to study, while their identification with specific processes involving cloud constituents is not yet definitely established. Indeed the latter deficiency applies very generally; little is known of the association, if any, between electrical characteristics and other thunderstorm information such as height, rainfall-rates, updrafts, et cetera.

## 6. DISCUSSION AND SUGGESTIONS FOR FUTURE WORK

There are many facets of sferics that have been thoroughly investigated;

there are others that have been extensively studied but still merit further examination; while some aspects have been relatively neglected. This section will discuss the extent of our knowledge, and indicate how any deficiencies might be remedied. Specific recommendations, which appear to deserve priority in action, are listed in the following section.

Sferics satellites and their meteorological uses are a presently fashionable topic. Any system for the reception of sferics in a satellite must examine the nature of the disturbance generated at the source; the modification of the signals during their propagation to the satellite; the background noise above which the sferics must be identified; the technical aspects of the reception in the satellite; and the limitations imposed on the obtainable information by satellite orbits and thunderstorm characteristics. All these aspects need to be considered to comparable degrees in the design of a sferics satellite system. It is disturbing to find systems described that treat one specific aspect with extreme sophistication, while accepting crude idealized models for the other aspects; indeed papers have appeared demonstrating that the authors, if they had been aware of the true physical picture for these other aspects, would have realized that their sophisticated approach in one respect was quite inapplicable! Much knowledge is now available upon all the problems connected with sferics satellites; the difficulty is to ensure that all this information--and not merely a biased selection--is employed. There is perhaps only one obvious investigation which could provide a valuable supplement to existing knowledge regarding sferics satellites; this is a comparison of radio noise data already taken in satellites with low-level cloud and thunderstorm information.

Turning to ground level observations of distant sferics, the techniques of location using VLF signals and a network of stations have become standardized; so also have methods--often very sophisticated--for recording waveforms and other characteristics of the individual sferics [Grubb (1967)]. The problems of extending location coverage to a very large geographical area by interlinking sferics networks are organizational rather than technical and scientific. The ELF frequency band apparently offers some advantages for position location and other investigation of sferics of distant origin; more observational results at these frequencies are needed. Extensive work has shown that establishment of thunderstorm position from a single sferics station cannot be done easily with any accuracy [Horner (1964)]; it seems futile to pursue any further the simple techniques so far considered in this connection. Sophisticated methods [Volland (1965)] may eventually enable single station location to be achieved; however, it should be decided whether very complicated equipment at one station is any real improvement over several much simpler instruments placed at a few stations within a network, particularly when it is considered that the automation of such a network is not difficult. Any deductions regarding thunderstorm climatology that can be obtained from radio noise or Schumann resonance measurements are likely to be crude; thus there is little reason--from a meteorological point-of-view--to encourage research in these fields.

There have been many investigations of the field-changes due to close lightning in which either the electrostatic component or the VLF radiation fields have been studied; further work in these areas is unlikely to be very profitable. Lightning research should concentrate primarily upon studies of the electromagnetic fields radiated at frequencies above about 50 kHz; the

changes in structure as frequency increases from 50 to 500 kHz, and again between 10 to 200 MHz, deserve special attention. Another frequency range that has been relatively neglected in researches on close lightning is that from 100 Hz to 3 kHz; it is surprising that we are still somewhat uncertain which phases of the lightning flash are involved in the generation of ELF sferics. Measurements of the fields occurring during thunderstorm growth and decline but not directly associated with lightning need more attention; such observations should include data obtained simultaneously for both electrostatic and radiation components. Indeed, simultaneous recordings using well-separated frequency bands are immensely advantageous in lightning research. This is particularly so if one measurement is continuous and the other intermittent; it is pointless, for example, to obtain a triggered high time-resolution record of lightning radiation at VHF, unless the phase of the complete lightning discharge at which the triggered record occurred can be established by comparison with, for instance, a continuous registration of the electrostatic field. Simultaneity of records should not be confined to electrical phenomena; only an inter-comparison of data from electrical and other--notably radar-sensors, can resolve the urgent question of how closely the electrical characteristics of a thundercloud are associated with the other meteorological phenomena of the storm. In this latter connection, and also for some practical reasons, it is often desirable to be able to locate lightning positions at distances of up to about 100 km; over this range conventional VLF methods are relatively ineffective, and while other techniques are promising they still need development. Finally, it is perhaps appropriate to mention that the human observer of thunder and lightning is still in many ways a useful standardized instrument capable of yielding reliable statistical information on the gross electrical characteristics of local thunderstorms; only a simple lightning-flash counter, possibly, can give comparable information as easily and as cheaply.

## 7. SPECIFIC RECOMMENDATIONS

These recommendations are limited to the items that seem presently of most importance; the previous section has indicated some other areas in which action is desirable but not a matter of urgency.

(a) Immediate consideration should be given to establishing a National Sferics Facility (Nasfa?)\* This would locate--in real time--every lightning flash occurring over the continental U.S.A. and adjacent areas; simultaneously the characteristics of the associated sferic would be recorded. There are no technical difficulties involved in achieving the facility by means of a ground network of VLF sferics stations; the received information could be continuously displayed and/or stored at a central master control point. A National Sferics Facility would supplement or partially replace--especially in routine functions--the existing sferics activities of many institutions; these establishments include government departments, universities, non-profit organizations, and industrial laboratories. Existence of the Facility would lead to identification and detailed warning of potentially dangerous meteorological

---

\* Details of a possible practical arrangement for such a Facility are given in the Appendix. This Appendix was submitted as the original input to the Panel on Remote Atmospheric Probing in September 1967. Since the Appendix includes material not appearing in the present review it is being reproduced as a supplement.

## SFERICS

situations; the resulting national economic benefits in aviation, public safety, and forestry--to name only a few areas--would be immense.

(b) Every proposal for sferics measurements from satellites should be very carefully scrutinized in order ensure that all relevant factors have been considered. The implementation of any elaborate scheme for sferics satellites should be deferred until existing radio noise data already obtained in satellites has been analyzed and its relation to surface meteorological conditions established.

(c) Observations of close thunderstorms should concentrate on inter-linking the various electrical phenomena, and--especially--on relating these phenomena to other meteorological effects. Simultaneous recording using several sensors is to be encouraged; investigations in which only a specialized fine-structure aspect of sferics is being studied should receive little support.

(d) It seems time to replace the meteorological statistic of the thunderstorm day by some more refined and quantitative parameter. A convenient way of achieving this replacement is by the routine use of a simple standardized lightning-flash counter and recorder.

## APPENDIX †

### REMOTE ATMOSPHERIC PROBING TECHNIQUES\* SFERICS OBSERVATIONS

#### 1. INTRODUCTION

An atmospheric or more colloquially a "sferic" is the radio disturbance generated by a lightning discharge and modified by propagation influences during its travel towards an observing station. The signal at the lightning source is complicated, since it represents the combined effects of a multiplicity of sparks, all different in character, and occurring over the considerable (approaching a second) duration of the discharge. However, the main features of the radio emissions associated with an individual flash are isolated impulses of large amplitude at frequencies in the VLF band (3-30 kc/s) and below; a transition to a quasi-continuous succession of pulses of less amplitude than those at VLF as frequency increases to HF (3-30 Mc/s); and a gradual reversion to isolated pulses but now of very small amplitude as frequency further increases to UHF (300-3000 Mc/s).

Radio signals at frequencies exceeding about 30 Mc/s follow quasi line-of-sight paths and are therefore of little use for remote probing. Signals in the MF (0.3-3 Mc/s) and HF bands can travel around the earth through ionospheric returns, but the propagation characteristics are very temporally variable especially between day and night. However, radio waves at lower fre-

---

\* It is assumed that the probing is only to consider ground-based equipment, and that "remote" implies an equipment location essentially unaffected by the atmospheric conditions being probed.

† See footnote on page immediately preceding.

quencies, particularly in the VLF band, propagate well under almost all conditions in the quasi-waveguide formed by the earth and lower ionosphere. Since the source signals at VLF are large discrete pulses and the propagation is good, VLF atmospherics are easily received many thousands of kilometers away from their thunderstorm origin.

In meteorology it is almost tacitly assumed that sferics observations imply measurements in the VLF band; this interpretation will be followed in the ensuing text. The basic meteorological objective of measurements on VLF atmospherics is to locate the thunderstorm sources of the sferics.

## 2. DESCRIPTION OF TECHNIQUE

Sferics location techniques using a network of stations are well established in theory and have been thoroughly tested in practice. Most commonly each station fixes the direction of the incoming VLF sferic by means of a crossed loop antenna arrangement; triangulation using the directions established respectively at the various network stations then fixed the origin of the sferic. In a rather more accurate technique the times of arrival of the VLF sferic at any pair of network stations are compared; a given difference in the arrival times defines a hyperbola, and the intersection of the hyperbolas fixes the sferic position.

Many techniques for locating areas of sferic activity from a single station have been suggested; none of these have yet reached the stage where they are suitable for routine operation. The most promising approach is probably in further development of the work of Heydt and Volland. In this research the statistical distribution of incoming impulse magnitudes is recorded as a function of azimuth for several selected frequencies in the VLF and LF bands.

## 3. APPLICATION TO ATMOSPHERIC PROBLEMS

Sferics observations can readily identify the position of a lightning flash at distances of up to a few thousand of kilometers from the locating stations. By definition, if a lightning discharge is fixed then so is a thunderstorm position, while the rate of occurrence of flashes in a specific area is an indicator of the strength of thundery activity in that area. If a thunderstorm region is located then, by association, it is an area of violent atmospheric convection and turbulence within which such unusual hydrometeors as large hailstones are likely to occur.

Sferics techniques are the only way in which ground measurements can establish the positions of distant thunderstorms. Information upon the spatial and temporal variations of thunderstorm activity has both basic and applied implications. Among basic problems are those of the general atmospheric circulation and the vertical distribution of atmospheric contaminants, since it is believed that the large cumulonimbus clouds of intense thunderstorms play a vital role in exchanges between the stratosphere and troposphere. Another fundamental problem is that in atmospheric electricity of the qualities of the global thunderstorm generator.

Among applied areas lightning location information is useful in forestry (fire hazard); in assessing the need for protection of electrical power

## SFERICS

transmission lines; in aviation by enabling optimum safe routing to be easily selected; in estimating atmospheric noise interference to radio communication; and in other ways. A specially interesting application is the remote location of tornadoes; this can be achieved because tornadoes are identifiable since they seem to produce a very much higher flashing (sferics occurrence) rate than do conventional thunderstorms.

### 4. FACILITIES

Even within the confines of the U.S.A. there are far too many establishments making sferics measurements of one kind or another for any comprehensive listing to be appropriate in a brief note of this kind. There are certainly--at a conservative estimate--well over fifty establishments recording sferics data. The agencies concerned include government departments (e. g., Air Force, Navy, ESSA); Universities (e.g. Montana State, Oklahoma); non-profit organizations and industry (e.g., SRI and Litton). Unfortunately, there is little standardization of measurements and co-operation between the various active establishments.

Before any estimate of the cost of a central sferics remote probing facility can be made, some definition of the function and scope for such a facility must be made. Suppose we arbitrarily consider a facility consisting of a master station situated in the heartland of the U.S.A. with several peripheral sub-stations. Let the function of the facility be to locate all thunderstorms occurring within the continental U.S.A., and a major proportion of those active in the immediately contiguous areas. Furthermore, the information is to be presented at the master station with a time delay of a few minutes at most.

A network comprising a master station in the St. Louis area, with eight sub-stations in the vicinities of Seattle, San Diego, Boulder, Colorado, El Paso, N. Dakota, Florida, Washington, D.C., and Maine, would cover the continental U.S.A. very adequately while also providing a desirable degree of redundancy. A standard sferics direction-finding set costs well under \$10,000; installation and addition of an output stage giving a signal, representing the D-F information and/or pulse magnitude, that can be readily applied to a radio or telephone link, is unlikely to cost more than \$5,000. It seems likely that the sub-stations could be located at establishments, e.g., colleges, where the equipment would be gladly accepted as an addition to the local research facilities, so that personnel and other charges for maintenance and routine operation would be low; perhaps \$1,000 a month per sub-station would be adequate. The sub-station signals must be conveyed to the master station with a delay which is less than a few milliseconds and known with fair accuracy if confusion between separate sferics is to be avoided; a leased telephone line (typical cost \$1,250 a month) is a simple and reliable solution. At the master station the technique of combining the incoming information might range from plotting by operatives to an elaborate fully automated display. There would be a balancing between personnel and capital equipment costs; perhaps \$40,000 per annum for the former and \$80,000 for the latter is a suitable compromise. It is assumed that the master station could be housed at an appropriate establishment without appreciable costs specifically attributable to the sferics work.

Summarizing, the national sferics facility might cost \$200,000 to set

up initially and \$250,000 per annum to operate thereafter. Although the latter figure is substantial, it should be realized that once a national facility is functioning, many other systems presently in operation would be free to concentrate upon specific detailed investigations, and to eliminate some of their more routine functions. The savings from this elimination, and the national economic benefits in--to give only a few areas--aviation, public safety, and forestry, cannot be accurately assessed; however, even the most conservative estimate suggests that they should very considerably exceed \$250,000 per annum.

## REFERENCES

- Bent, R. B., 1968: Investigations of global thunderstorm activity from the Ariel III satellite. Paper prepared for the Fourth International Conference (Tokyo, Japan, May 1968) on Universal Aspects of Atmospheric Electricity.
- Chalmers, J. A., 1967: Atmospheric Electricity. New York, Pergamon Press, 515 pp.
- Dennis, A. S., 1964: Lightning observations from satellites. Final Report SRI Project 4877, Prepared for National Aeronautics and Space Administration, Contract NAS r49- (18). Stanford Research Institute, Menlo Park, California, 94025, U.S.A.
- Grubb, R. N., 1967: A digital data collection system for transient waveforms in the 1-100 kilohertz band and its application to the study of atmospheric. Paper prepared for the M.F., L.F., and V.L.F. Radio Propagation Conference, November, 1967, IEE, Savoy Place, London.
- Horner, F., 1964: Radio noise from thunderstorms. Advances in Radio Research, Vol. 2, New York, Academic Press, 121-215.
- , 1967: Analysis of data from lightning-flash counters. Proc. IEE, 114, 916-923.
- Hughes, H.G., 1967: Nonreciprocal attenuation rates at ELF from slow tail measurements. J. Geophys. Res., 72, 5383-5388.
- International Telecommunication Union, 1964: World distribution and characteristics of atmospheric radio noise. CCIR Report 322, Document X, Plenary Assembly (1963), Geneva.
- Jones, H. L. 1965: The tornado pulse generator. Weatherwise, 18, 78-85.
- Kitagawa, N. and M. Brook, 1960: A comparison of intracloud and cloud-to-ground lightning discharges. J. Geophys. Res., 65, 1189-1201.
- Oetzel, G. N. and Pierce, E. T., 1968: The radio emissions from close lightning. Paper prepared for the Fourth International Conference (Tokyo, Japan, May 1968) on Universal Aspects of Atmospheric Electricity.
- Pierce, E. T., 1962: Sources of atmospheric noise in lightning. Radio Noise of Terrestrial Origin, Amsterdam, Elsevier, 55-71.

## SFERICS

- Pierce, E. T., 1967a: Atmospherics-their characteristics at the source and propagation. Progress in Radio Science 1963-1966, Proceedings XVth General Assembly (Munich 1966), URSI, 987-1039.
- , 1967b: Spherics (sferics). Encyclopaedia of Atmospheric Sciences and Astrogeology, New York, Reinhold, 935-939.
- Sartor, J. D. 1964: Radio observations of the electromagnetic emission from warm clouds, Science, 143, 948-950.
- Volland, H., 1965: Long range detection of thunderstorms. The Controller, 4, 35-36.
- Zonge, K. L. and W. H. Evans, 1966: Prestroke radiation from thunderclouds. J. Geophys. Res., 71, 1519-1523.

## REFERENCES (FOR APPENDIX)

- Heydt, G. and H. Volland, 1965: Long range detection of thunderstorms, The Controller (IFATCA Journal), 4, 2, 35-37.
- Pierce, E. T. 1966: The determination by radio methods of global thunderstorm characteristics, Report for the National Academy of Sciences (Committee on Atmospheric Sciences, Panel on Atmospheric Electricity), Stanford Research Institute, Menlo Park, California.

COMMENTS ON THE PAPER BY E. T. PIERCE

Heinz W. Kasemir

Atmospheric Physics and Chemistry Laboratory  
ESSA Research Laboratories  
Environmental Science Services Administration  
Boulder, Colorado

In general I agree with Dr. Pierce's paper therefore I can limit myself to only a few points where I deviate from his opinion or where I think the emphasis should be shifted. My remarks will be to the following topics:

1. Sferics Satellite
2. Sferics ground network
3. Lightning counter
4. Analysis of the electric field of near lightnings

1. Sferics satellite. Even considering the limitations of the satellite such as lack of resolving power to pinpoint an individual storm, the loss of a faithful reproduction of the sferics signal by frequency cutoff by the ionosphere, the one task the satellite can do very well, namely scanning rapidly the large thundery areas of the globe would be an important achievement and worthwhile effort. True that the same result could be obtained by a world-wide sferics network, but the satellite would be independent of international organization of such a network and its political ramifications.

2. Sferics ground network. The establishment of a national sferics network with the capability of recording the location of each lightning discharges in the U. S. A. and in the neighboring countries would be indeed a very rewarding enterprise. Here I would like to shift the emphasis to tornado tracking and short range forecasting. I believe that the tremendous number of lightnings produced by a tornado should be identifiable by a sferics network. A government agency like ESSA with its facilities and know-how could be suggested for establishing and operating such a network.

3. Lightning Counter. I support to the fullest Dr. Pierce's recommendation of the wider use of the lightning stroke counter. This instrument is inexpensive, almost maintenance free, and would lift the much needed thunderstorm statistic from a poor estimate to a measured parameter.

4. Analysis of the electric field of nearby lightnings. I disagree with the statement on page 610 of Dr. Pierce's paper: "There have been many investigations of the field changes due to close lightning in which either the electrostatic component or the VLF radiation fields have been studied; further work in these areas is unlikely to be very profitable". I think the electrostatic field of a close lightning is one of the best sources of information of the electric structure of the lightning discharge as well as the charge

distribution in the thundercloud. Recording instruments with a frequency range from to about 100 KHz are commercially available and well in the state of the art. The evaluation of the data is handicapped by the lack of an adequate theory. The widely used formulas of the oscillating dipole, referred to at the beginning of Dr. Pierce's paper, are not even sufficient as a first approximation. Therefore much information is still hidden in the electrostatic field records of the nearby lightning discharge.

SESSION **10**

Acoustics

072-25384

ACOUSTIC METHODS OF REMOTE PROBING OF THE LOWER ATMOSPHERE

C. G. Little

Environmental Science Services Administration  
Research Laboratories  
Boulder, Colorado

ABSTRACT

Stimulated by the experimental acoustic radar work of McAllister, this paper reviews the potential usefulness of acoustic methods for the remote probing of the lower atmosphere. Starting with a comparison of the effects of temperature, wind, and humidity fluctuations upon the refractive index of air to electromagnetic and acoustic waves, it is shown that the fluctuations in acoustic refractive index may be expected to be about one thousand times stronger than in the radio case. Since the scattered power is proportional to the square of the refractive index fluctuations, the scatter of acoustic waves may be expected to be roughly one million times stronger than for radio waves. In addition, the million-fold ratio between the velocities of electromagnetic and acoustic waves results in an acoustic system requiring one million times less bandwidth to interrogate a given atmospheric volume. Since the ambient noise levels per cycle per second in the two types of receivers are likely to be approximately equal, this results in an overall reduction in interfering noise power for the acoustic case of about a factor of one million. The net result is that the acoustic signal-to-noise ratio from a given scattering region (for equal radiated powers, antennas and wavelengths), is likely to be some twelve orders of magnitude stronger than in the radio case!

The system parameters required to achieve an effective acoustic radar are discussed, using the theoretical work of Kallistratova, and including the effect of absorption. It is concluded that the acoustic radar technique could be developed to provide continuous information on the profile of wind speed and direction, the profile of mechanical turbulence (and hence of atmospheric diffusion), the profile of temperature inhomogeneity, (and therefore of optical refractive index inhomogeneity), the existence, location, and intensity of temperature inversions, and the variation of humidity with height. Limitations to the acoustic radar technique include its limited range (up to about 1500 meters) and the probability of serious loss of sensitivity due to increased noise level during periods of strong wind or rain or hail.

## 1. INTRODUCTION

Remote probing of the lower atmosphere by acoustic or electromagnetic waves involves the interaction of the waves with the atmosphere. The interaction of electromagnetic waves with the gases of the lower atmosphere is in general rather weak (except in certain largely-unused regions of the spectrum where absorption is strong), hence sensitive and sophisticated equipments are often required to measure these interactions. It is important to recognize that the interaction of sound waves with the lower atmosphere is very much stronger than that for most parts of the electromagnetic spectrum, and that relatively simple equipment can be used.

The sensitivity of the interaction may be expressed in terms of the magnitude of the fluctuations in refractive index of the medium, i.e. of the phase velocity of the wave in the medium relative to the phase velocity for standard conditions (vacuum for electromagnetic waves, 1 atmosphere pressure of dry air at 0° C for acoustic waves). Thus, a 1° C fluctuation in temperature is equivalent to about 1700 N units change in sonic velocity (1 N unit equals 1 part in  $10^6$ ), whereas for radio wavelengths the resultant change is of the order 1 N unit. For wind, the situation is even more striking; the electromagnetic waves are unaffected by the wind, whereas acoustic waves experience a 3000 N unit change for a 1 meter/second variation in wind speed. For humidity, the changes are again relatively large; for sound waves a 1 mb change in water vapor pressure corresponds to about a 140 N unit change in refractive index; for radio wavelengths the corresponding change is about 4 N units and for optical wavelengths about 0.04 N units. From these figures, it will be seen that the fluctuations in refractive index of air to sound waves tend to be dominated by the wind and temperature fluctuations, with humidity fluctuations relatively unimportant; for electromagnetic waves the wind fluctuations of course have no effect; at optical frequencies the temperature fluctuations are dominant but at radio frequencies both temperature and humidity fluctuations may be important.

From the above figures, it will be seen that the diurnal variation of sonic velocity is likely to be of the order 1 part in 100, as opposed to roughly 1 part in  $10^5$  for optical and radio waves. Refraction effects are also likely to be extremely severe for acoustic waves; the 157 N units/kilometer decrease in refractivity required to give a horizontal ray a curvature equal to the curvature of the earth's surface would be produced by a temperature gradient of only  $+ 0.1^\circ$  C per kilometer, or by an increase of wind speed on only 5 cm/sec per kilometer of height! Thus sound waves usually cannot be considered as travelling in straight lines.

In the case of the scatter of acoustic or electromagnetic waves by atmospheric irregularities, the scattered power is proportional to  $(\Delta n/n)^2$ . For acoustic waves, the scattering cross section is therefore of the order 1 million times greater than for electromagnetic waves.

These relatively strong interactions of acoustic waves with the lower atmosphere therefore suggest that increased attempts should be made to use them for remote probing purposes.

## 2. PASSIVE RECEPTION OF ACOUSTIC WAVES OF NATURAL ORIGIN

As described by Dr. R. K. Cook in a companion paper, acoustic pressure fluctuations of natural origin have been studied for many years, particularly in the infrasonic range of frequencies. Such waves propagate with very low attenuation, and may be observed at distances of many thousands of kilometers. Since this topic is covered in his paper, and since relatively little atmospheric information has been derived using natural sources of acoustic waves, it is not discussed further here.

## 3. LINE-OF-SIGHT PROPAGATION EXPERIMENTS

The velocity,  $V$ , of sound deduced by a stationary observer will be the sum of the velocity of sound,  $C$  relative to the air, plus the velocity of the air  $W$  relative to the observer. Thus

$$\vec{V} = \vec{C} + \vec{W}$$

The velocity of sound in dry air is given by

$$C + 20.05 \sqrt{T} \text{ meters/second}$$

where  $T$  is the absolute temperature of the air.

In moist air the velocity of sound is slightly increased, by an amount proportional to the partial pressure of the water vapor.

$$C_{\text{moist}} = C_{\text{dry}} \left( 1 + 0.14 \frac{e}{p} \right),$$

where  $e/p$  is the ratio of water vapor pressure  $e$  to total pressure  $p$ . The total contribution of the atmospheric water vapor to the phase velocity of sound is typically of the order 1 meter/second.

The sensitivity of sound velocity to changes in wind, temperature, and humidity is such that the humidity fluctuations can almost always be ignored. For remote probing purposes one is therefore left with the problem of being able to identify separately the effects of wind and temperature fluctuations. This can readily be done by using the fact that the wind is a vector quantity, while the temperature is scalar; thus measurements of the time of arrival of pulse, or of the phase of a received CW acoustic signal, taken on a ring of microphones surrounding a central loudspeaker could be used to measure both the mean temperature (from the average time delay around the ring) and the mean wind and wind direction (from the variation of time delay around the ring). The data from the various microphones could also be used to derive information on the spatial scales of the turbulence and on the power spectra of the fluctuations in time. Using a CW system, considerable sensitivity in mean wind speed and temperature could be achieved. A 100 meter radius circle around which the relative phase of 100 Hz acoustic signal could be measured to an accuracy of  $(1/100)\lambda \approx 3.6^\circ$  would give mean wind speeds to about 10 cm/sec. Temperature measurements to an accuracy of  $0.2^\circ$  C could be made, provided the partial pressure of water vapor was known to an accuracy of about 1 mb.

The above discussion relates to the measurement of atmospheric parameters at the surface of the earth. In addition, the line-of-sight propagation technique has been extensively used to derive information on atmospheric winds and temperatures in the height range 30-80 Km, using grenades released from a rocket as sources of sound (see for example Strand, et al. 1956). Since the present paper deals with remote probing of the lower atmosphere, this technique is not discussed further.

#### 4. THE USE OF SCATTER FOR REMOTE ACOUSTICAL PROBING

The scatter of sound by irregularities in the atmospheric wind or temperature fields has been discussed by several workers.

Following Kallistratova (1960) we can write for the scatter of sound by inhomogeneities in dry air

$$d\sigma = 2 \pi k^4 V \cos^2 \theta \left[ \frac{1}{C^2} E(\vec{K}) \cos^2 \frac{\theta}{2} + \frac{1}{4T^2} \varphi(\vec{K}) \right] d\Omega \quad (1)$$

where  $d\sigma$  is the fraction of the incident acoustic power which is scattered by irregularities in volume  $V$  through an angle  $\theta$  into a cone of solid angle  $d\Omega$ ;  $k = 2\pi/\lambda$  is the wave number of the acoustic wave;  $\vec{K} = 2k(\sin \theta/2)$  is the effective wave number at which an acoustic radar scattering through angle  $\theta$  interrogates the medium.  $C$  and  $T$  are the mean velocity of sound and mean temperature of the scattering volume, and  $E(\vec{K})$  and  $\varphi(\vec{K})$  are respectively the spectral intensity of the wind fluctuations and the temperature fluctuations at wave number  $\vec{K}$ .

For a Kolmogorov spectrum of turbulence this reduces to

$$\sigma(\theta) = 0.03 k^{1/3} \cos^2 \theta \left[ \frac{C_V^2}{c^2} \cos^2 \frac{\theta}{2} + 0.13 \frac{C_T^2}{T^2} \right] \left( \sin \frac{\theta}{2} \right)^{-11/3} \dots \text{Eq. 1}$$

where  $\sigma(\theta)$  is now the scattered power, per unit volume, per unit incident flux, per unit solid angle at an angle  $\theta$  from the initial direction of propagation.  $C_V$  and  $C_T$  may be obtained from measurements of the structure functions:

$$D_W = \overline{[W(x) - W(x+r)]^2} = C_V^2 r^{2/3}$$

$$D_T = \overline{[T(x) - T(x+r)]^2} = C_T^2 r^{2/3}$$

where  $W(x)$  and  $T(x)$  are the instantaneous wind speed and temperature at point  $x$ ,  $W(x+r)$  and  $T(x+r)$  the corresponding instantaneous values at point  $(x+r)$ .

The above equation shows that the scattered acoustic power resulting from illumination of a Kolmogorov spectrum of turbulence:

- a. varies relatively weakly with wavelength,

$$(\sigma \propto \lambda^{-1/3}),$$

- b. is the sum of two terms, one due to the wind fluctuations (normalized by the mean velocity of sound in the medium) and one due to the temperature fluctuations, (normalized by the mean temperature of the medium),
- c. both wind- and temperature-scattering terms are multiplied by  $\cos^2 \theta$ , which therefore means that no power will be scattered at an angle of  $90^\circ$ ,
- d. the wind term includes a  $\cos^2 (\theta/2)$  multiplying term, which means that the wind fluctuations produce no scatter in the backward direction ( $\theta = 180^\circ$ ),
- e. both the wind and temperature components of the scatter are multiplied by a  $(\sin \theta/2)^{-11/3}$  factor, i.e. most of the scatter is in the forward hemisphere.

This equation therefore indicates that a full measurement of the scattered power as a function of wave number and scatter angle would permit measurement of:

- a.  $\varphi(\vec{K})$ , the intensity of temperature fluctuations at the three dimensional wave number  $\vec{K}$ , as a function of direction, wave number, and height, and time. Note that this parameter is of considerable communication and atmospheric importance, being directly proportional to the refractive index fluctuations which are responsible for the scintillation of optical sources.
- b.  $E(\vec{K})$ , the intensity of velocity fluctuations at wave number  $\vec{K}$ , as a function of wave number, direction and height and time. Note that this three dimensional spectrum is of immediate concern to the meteorologist and those concerned with atmospheric turbulence, diffusion, and pollution.
- c. The mean wind speed and direction could be measured as a function of height, using Doppler techniques. These could be measured, free of ambiguity due to the fallrate of hydrometeors or chaff, either using a monostatic radar in the velocity-azimuth display mode, or by using a bistatic system. The measurements of Doppler frequency would provide information on the velocity field of the atmosphere surrounding the radar with spatial resolution determined by the pulse length and beamwidth, and could therefore be used for studies of large-scale atmospheric turbulence. In addition, the width of the Doppler spectrum of the echo from a given range element would be a measure of the velocity variation within the pulse volume (a one-degree beam with 100 millisecond pulses would give scatter volumes of the order 15-20 meter cube at 1 kilometer range).
- d. The formation, location, and intensity of temperature inversion layers would be identified and evidenced by marked aspect sensitivity and narrowing of the frequency spectrum on a vertically directed monostatic radar, and would be readily distinguishable from regions of increased turbulence. In addition, a marked difference in wavelength dependence would be expected, with the echo strength increasing with increasing wavelength, as opposed to a  $\lambda^{-1/3}$  law for a Kolmogorov spectrum of turbulence.

In this connection it is interesting to note that humidity layers would tend to reflect the acoustic energy weakly - and would not show the null in scatter through a  $90^\circ$  angle.

The continuous remote measurement of temperature inversions would appear to be of great significance to meteorologists generally and especially to those concerned with atmospheric turbulence, diffusion, and pollution.

## 5. ON THE FEASIBILITY OF ACOUSTIC RADAR

The above discussion of the conceivable potential of acoustic radar for remote atmospheric probing makes it desirable to estimate the system requirements.

The equation, applied to the monostatic case, gives the received power  $P_r$  as

$$P_r = P \cdot \sigma \cdot c\tau/2 \cdot A_r \cdot 1/R^2 \cdot L$$

where  $P$  is the radiated acoustic power,  $\sigma$  is the scattering cross section of Eq. (1) with  $\theta = 180^\circ$ ,  $C$  is the velocity of sound in the scattering region,  $\tau$  is the pulse length,  $A_r$  is the collecting area of the receiving antenna,  $R$  is the range to the scattering region, and  $L$  is an attenuation factor which takes into account antenna and transducer inefficiencies and any atmospheric attenuation along the double path to and from the scattering region.

Assuming for the moment

$$P = 10 \text{ watts}$$

$$\tau = 10^{-2} \text{ seconds (3.3 meter long pulse)}$$

$$R = 150 \text{ meters}$$

$$A_r = 1 \text{ square meter}$$

then

$$P_r = 7.3 \times 10^{-2} \sigma L.$$

For the backscatter case, Eq. (1) reduces to

$$\sigma = 0.0039 (2\pi/\lambda)^{1/3} (C_T / T)^2$$

Taking  $\lambda = 2\pi \text{ cms}$  ( $f \approx 5 \text{ KHz}$ )

$$C_T = 10^{-2} \text{ degree cm}^{-1/3} \text{ (typical of the boundary layer)}$$

$$T = 300^\circ \text{ K}$$

$$\sigma = 4.4 \times 10^{-12} \text{ cm}^2 \text{ per cm}^3$$

Using this value of  $\sigma$ , we have

$$P_r = 3.2 \times 10^{-13} L \text{ watts}$$

In considering the detectability of this received power, we must first estimate  $L$  and then estimate the interfering noise power against which the signal must be detected.

The attenuation factor  $L$  is made up of the efficiency factor of the receiving antenna (i. e. the ratio of output electrical power from the microphone transducer to the acoustical power incident upon the geometrical area of the receiving antenna) and the absorption of acoustical energy occurring on the propagation path.

The efficiency factor of a loudspeaker at the focus of a paraboloid is likely to be of the order 0.05, based on an effective collecting area of about 0.5 of the geometrical area and a transducer efficiency of about 0.1.

The absorption of sound by the atmosphere is a strong function of frequency. It is conventional to divide this into two components; a classical absorption due to the sum of viscosity, conduction, diffusion, and radiation terms, and a non-classical component due to the presence of water vapor. In the frequency range 1 KHz to 10 KHz, the classical absorption is usually the smaller, and can be well predicted; at 5 KHz it is about 1.0 dB for the round trip path to a height of 150 meters.

Detailed results for the classical and anomalous absorption of sound in air as a function of humidity and temperature have been presented by Harris (1964). Figure 1 is representative of one of the many diagrams in his paper and shows that at 20° C and 50 per cent humidity, the total attenuation at a frequency of 5 KHz would be about 10 dB for the round trip to 150 meters height. This figure decreases with increasing temperature and with increasing relative humidity.

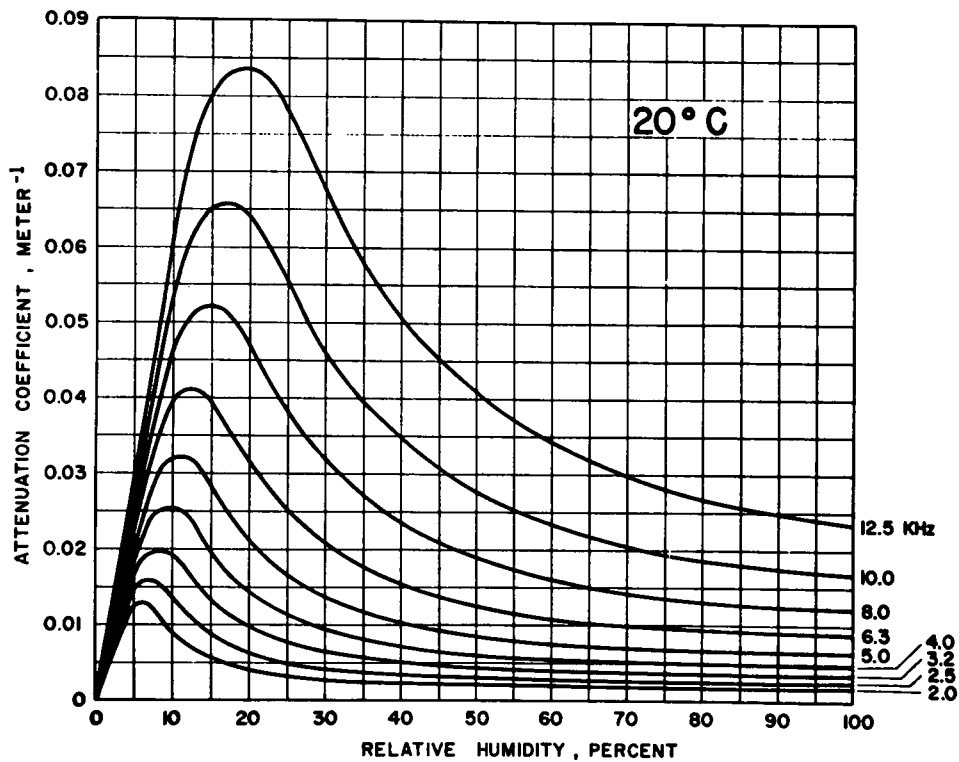


FIG. 1 Total attenuation coefficient,  $m$ , versus percent relative humidity for air at 20° C and normal atmospheric pressure for frequencies between 2.0 and 12.5 KHz at 1/3 octave intervals. To obtain the attenuation in dB/meter, multiply the ordinate by 4.34

Using the above values of receiving antenna efficiency and of atmospheric attenuation,

$$L = 5 \times 10^{-3}$$

whence

$$P_r = 1.6 \times 10^{-15} \text{ watts}$$

This electrical signal is now to be compared with the interfering noise level existing at the input to the preamplifier.

Five potential sources of noise must be considered in identifying the signal-to-noise ratio to be expected on an acoustic radar. The ultimate, ineluctable limit, to be achieved only under ideal conditions, will be set by the random pressure fluctuations experienced by the microphone due to the random thermal motion of the atmospheric molecules. The available acoustic noise power is given by

$$P_a = kTB$$

where  $k$  = Boltzmann's constant,  $T$  = absolute temperature of air, and  $B$  = observing bandwidth. For a bandwidth of 100 Hz and normal atmospheric temperatures this thermal acoustic noise power would be about  $4.2 \times 10^{-19}$  watts. This would, however, be reduced by the transducer inefficiency factor to about  $4.2 \times 10^{-20}$  watts of electrical noise power.

Electron shot noise in the receiving preamplifier must also be considered. At audio frequencies there should, however, be no difficulty in building a preamplifier which generates no more noise than that of a resistor at room temperature. For a 100 Hz bandwidth, this is therefore about  $4.2 \times 10^{-19}$  watts.

Wind noise on the receiving microphone is likely to prove a more serious limit to the sensitivity of the radar. This can, however, be greatly reduced by placing it as close to the surface of the earth as practicable, by using an array of microphones (since the wind noise will not be correlated on microphones more than a wavelength apart), and by screening the microphone from the wind. A combination of these techniques may be expected to reduce this problem until it is no longer limiting, at least under low wind conditions.

In addition to wind-induced noise created at the microphone itself, atmospheric turbulence may create pressure fluctuations which propagate as sound waves of natural atmospheric origin. Pressure fluctuations of sub-audible frequencies attributable to the jet stream, severe storms, etc., have been detected at considerable ranges; it is believed that the intensity of these pressure fluctuations drops off rapidly with frequency. It is not

known to what extent acoustic noise generated by atmospheric turbulence may at times limit the sensitivity of an acoustic radar, but if this should occur, it should be recognized that the technique may provide a new passive method of sensing atmospheric turbulence.

The final noise limitation to be considered is that of acoustical energy from non-atmospheric sources such as vehicles, insects, etc. This may be estimated as follows from data summarized by Stevens and Baruch (1957), who show that the ambient acoustic noise power at a quiet site is of the order 20 dB above  $10^{-16}$  watt  $\text{cm}^{-2}$  for an octave band centered at 1 KHz. This noise power decreases by about 5 dB per octave increase in frequency. Using these figures, an acoustic noise power of about +8 dB per octave at 5 KHz would be expected; for a 100 Hz bandwidth at 5 KHz the noise power flux would be of the order -9 dB relative to  $10^{-16}$  watts  $\text{cm}^{-2}$  or  $1.25 \times 10^{-17}$  watts  $\text{cm}^{-2}$ . Assuming that the noise is isotropic in origin, the effective collecting area for this noise will be  $\lambda^2/4\pi = 3 \text{ cm}^2$  leading to an acoustic noise power of  $3.75 \times 10^{-17}$  watts. This acoustic noise power is, however, reduced to  $3.75 \times 10^{-18}$  electrical watts after allowing for transducer inefficiency. This result suggests that even at a quiet site the electrical noise level due to 5 KHz acoustical interference is likely to be some 10 dB above the equivalent electrical noise input power due to the preamplifier noise.

The expected received signal power of  $1.6 \times 10^{-15}$  watts electrical power exceeds the predicted interference noise power of about  $4 \times 10^{-18}$  watts electrical power by a factor of 400, or +26 dB.

## 6. CHOICE OF THE OPTIMUM FREQUENCY RANGE FOR AN ACOUSTIC RADAR

The optimum frequency range for an acoustic radar will be a compromise between the increase in directivity, the improved Doppler resolution and the reduced interference noise-level all potentially available at the higher frequencies, and the undesired increase in attenuation experienced as one goes to higher frequencies. The optimum frequency will be a strong function of the range over which the radar is to work, being lower for the larger ranges. Thus the calculations above give a predicted 26 dB signal-to-noise ratio for a range of 150 meters and a frequency of 5 KHz. At ten times the range, the atmospheric absorption would be 100 dB instead of 10 dB, making it imperative to come down in frequency. Computations similar to the above indicate that a back-scattered signal-to-noise ratio of 20 dB could still be obtained at a range of 1.5 Km, but would require 100 watt, 100 millisecond 1 KHz acoustic pulses radiated and received on a  $100 \text{ m}^2$  acoustic antenna.

It should be noted that the above signal-to-noise estimates are based on backscatter, i.e. on the least favorable case. For  $\theta \neq 180^\circ$  the echo strength is likely to be stronger (except near  $\theta = 90^\circ$ ), due to the appearance of scatter due to wind turbulence, and to the  $(\sin \theta/2)^{-1/3}$  angle dependence of both wind and temperature scattering terms. This suggests that the acoustic analogue of the electromagnetic forward scatter systems could be used to measure atmospheric parameters to heights and distances considerably greater than the 1500 meters mentioned above.

## 7. A POSSIBLE TECHNIQUE FOR THE MEASUREMENT OF HUMIDITY PROFILES

As indicated above, the scattering cross section for acoustic waves in the inertial subrange of the Kolmogorov spectrum of turbulence varies relatively weakly with wavelength ( $\sigma \propto \lambda^{-1/3}$ ). The molecular absorption of the sound, however, varies quite strongly with frequency and humidity. This fact suggests that measurements of the received echo strength as a function of frequency and height could be used to derive information on the variation of humidity with height. A possible method is outlined below.

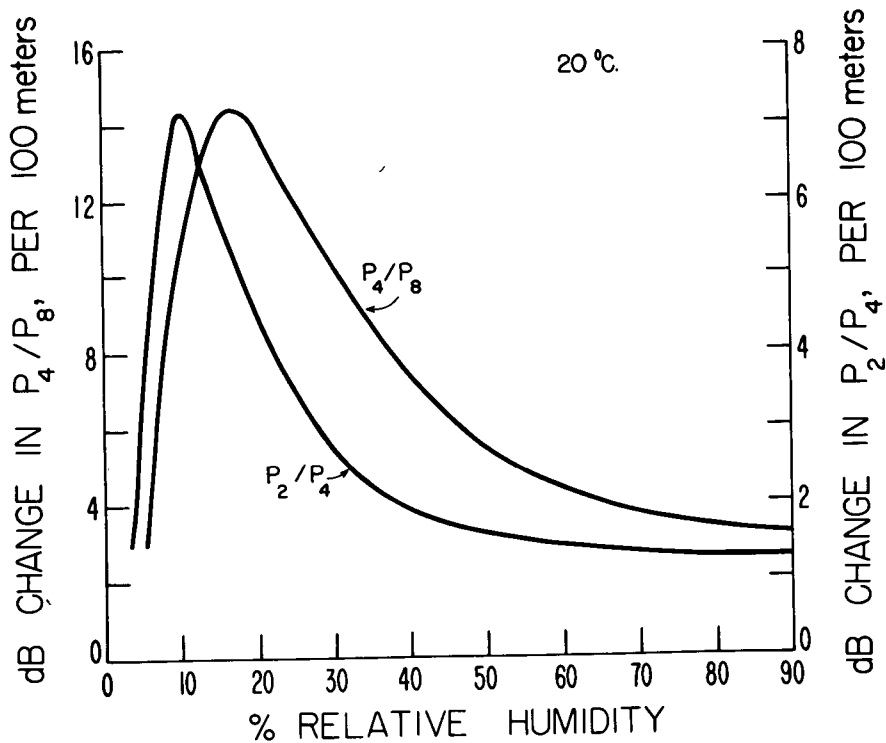


FIG. 2 Variation with relative humidity of the increase, per 100 meters increase in height, of the ratio of echo powers  $P_2/P_4$  and  $P_4/P_8$  for acoustic radars operating at 2, 4, and 8 KHz. Atmospheric temperature assumed to be 20° C.

Consider the case in which two acoustic radars are used in the back-scatter mode to obtain echoes successively from the same volume of space on two frequencies of 4 KHz and 8 KHz. Let us suppose that the same peak power, antennas, transducer efficiencies, etc. apply to each radar. In the absence of any atmospheric attenuation, the 8 KHz radar echoes should be 1 dB stronger than the 4 KHz echoes at all heights, because of the  $\lambda^{-1/3}$  increase in effective scattering cross section. The classical absorption of acoustic energy would result in a weakening of the 8 KHz echoes relative to the 4 KHz

by a known amount (approximately 1 dB per 100 meters increase in height). Any additional decrease in the ratio of 8 KHz to 4 KHz echo power with height could be attributed to molecular absorption due to water vapor; the known dependence of this absorption upon humidity could be used to derive the humidity profile. Thus Figure 2 indicates that a 5.75 dB decrease in the ratio of 8 KHz echo power to 4 KHz echo power, per 100 meters increase in height, implies a 50% relative humidity if the temperature is 20° C. Ambiguity might occur for values near twelve dB change in echo ratio per 100 meter, which could be interpreted as about 12% or about 30% relative humidity; this ambiguity could be fully resolved if the radar could also operate at 2 KHz. In this case the right hand scale shows that the 4 KHz/2 KHz change in ratio would either be 7 dB/100 meters for 12% relative humidity or 2.8 dB/100 meters for 30% relative humidity, a difference which could presumably be readily resolved.

One obvious weakness of this method is the assumption of an isotropic homogeneous Kolmogorov spectrum of turbulence. However, the effect of temperature inversions could be identified and avoided by using different elevation angles; and checks of the spectrum of turbulence could also be made using bistatic systems.

## 8. SUMMARY

Hitherto, with the notable exception of the rocket grenade techniques, relatively little use has been made of acoustic waves for the remote probing of the atmosphere. The above discussion indicates that acoustic techniques, and especially acoustic radar techniques, offer exciting promise for the remote probing of the atmospheric boundary layer. In view of the emphasis of this paper upon this potential, it is perhaps appropriate to end the paper with an indication of some of the limitations of the technique.

The primary limitation to the acoustic radar technique is likely to be one of range (to heights of 1 Km or so); in addition, the radar is likely to be very susceptible to the adverse effects of strong wind, rain, and hail as they increase the ambient noise level at the receiver. The problem of the susceptibility of the radar to man-made noise, and of man to the acoustic signals from the radar, has not been adequately discussed; some preliminary tests by the author of a low side-lobe acoustic antenna suggest that these need not be a serious problem.

In balance, then, the author concludes that the acoustic radar technique offers a uniquely important (though clearly finite) opportunity to the atmospheric scientist for remote sensing of important lower atmospheric parameters, and that its potential should therefore be vigorously explored and exploited.

## REFERENCES

- Harris, C. M., 1966: Absorption of sound in air versus humidity and temperature. J. Acoust. Soc. Am., 40, No. 1, 148-159.
- Kallistratova, M. A., 1961: Experimental investigation of sound wave scattering in the atmosphere. Trudy instituta fizika atmosfery, Atmosfer'naya turbulentnost, No. 4, 203-256.

Stevens, K. N., and J. J. Baruch, 1957: Community noise and city planning. Handbook of Noise Control, Chapter 35, (Ed. C.M. Harris), McGraw-Hill.

Strand, W. G., W. Nordberg, and J. R. Walsh, 1956: Atmospheric temperatures and winds between 30 and 80 Km. J. Geophys. Res., 61, 45-56.

N72-25-385

PRECEDING PAGE BLANK NOT FILMED

ATMOSPHERIC SOUND PROPAGATION

Richard K. Cook

Geoacoustics Group, Research Laboratories  
Environmental Science Services Administration  
Rockville, Maryland 20852

ABSTRACT

The propagation of sound waves at infrasonic frequencies (oscillation periods 1.0 - 1000 seconds) in the atmosphere is being studied by a network of seven stations separated geographically by distances of the order of thousands of kilometers. One of the typical stations, in Washington, D. C., has an array of five microphones separated by distances of about 7 kilometers. Each microphone is at ground level and is connected to the central station by means of a leased telephone line. In effect the array is "steered" to look for sound waves in a programmed sequence of search directions. The station measures the following characteristics of infrasonic waves passing through Washington: (1) the amplitude and waveform of the incident sound pressure, (2) the direction of propagation of the wave, (3) the horizontal phase velocity, and (4) the distribution of sound wave energy at various frequencies of oscillation. Some infrasonic sources which have been identified and studied include the aurora borealis, tornadoes, volcanos, gravity waves on the oceans, earthquakes, and atmospheric instability waves caused by winds at the tropopause. Waves of unknown origin seem to radiate from several geographical locations, including one in the Argentine.

# ATMOSPHERIC SOUND PROPAGATION

## 1. INTRODUCTION

Sound waves have two principal uses to which acoustical researches have been directed intensively during the last fifty years. The first use, a very ancient one, is in the art of communication between men and the handling of everyday affairs, by hearing and speech. Audio-frequency waves, those audible to man in the frequency range from 15 to 17000 Hz, are necessary for this purpose. They are propagated through the atmosphere for relatively short distances. But unwanted sounds — noise — of the same frequencies interfere with communication and indeed with other aspects of man's activity. The importance of audible sound to man has led to an extensive technology for the quantitative measurement, analysis, and display of such sound waves. Researchers have developed equipment and methods for producing controlled amounts of sound and vibration, and for reducing noise.

A more recent use for sound waves is for researches into the structure and properties of matter — solids, liquids, and gases. Generally speaking, high-frequency sound (at ultrasonic frequencies) is used for studying solids and liquids. Industry has found ultrasonic waves valuable for location of flaws in thick pieces of metal, by measurement and display of the scattered sound from the flaws. Sound waves offer the only practical method for exploring the contours of the sea bottoms, and for locating underwater objects such as submarines at distances more than a few feet away. But for researches on gases, including the atmosphere, sound waves have been found useful over a wide range of frequencies. The microstructure of gases is studied in the laboratory with ultrasound. Waves at audible and infrasonic frequencies, some as low as  $10^{-4}$  Hz, are studied in the free atmosphere. When the details of propagation through a medium are known, then properties of the source itself can be deduced from the sound it radiates, measured at distant points.

Researches on the two principal uses for sound are dependent upon, and unified by, (a) modern electroacoustics which makes the controlled generation of sound waves and accurate measurements of them possible, and (b) the theory of sound propagation and its mathematical-physical formulation.

We are considering in particular propagation through the atmosphere. Some studies aim at measuring the influence of unwanted sound, e.g., aircraft noise on man. Others look towards measurement of atmospheric properties by probing — remote sensing — with sound waves. Still others seek to determine the properties of distant sources of sound. But all researches on atmospheric

sound must depend on theoretical analysis of sound propagation, coupled with measurements of sound at only a relatively few available locations, to arrive at useful results.

We concentrate our attention on infrasound in the atmosphere — sound waves whose frequencies of oscillation are less than the lowest frequency, about 15 Hz, that can be heard. Of particular interest are those waves whose oscillation periods lie in the range of 1.0 to 1000 sec, because such waves propagate for distances of thousands of kilometers without substantial loss of energy. Sounds at these frequencies are almost always present at measurable intensities. Those of natural origin have many causes, including tornadoes, volcanic explosions, earthquakes, the aurora borealis, waves on the seas, and large meteorites. Man-made sources include powerful explosions and the shock waves from vehicles moving through the atmosphere at supersonic speeds, at altitudes below about 125 km.

## 2. PRINCIPAL FEATURES OF SOUND PROPAGATION

### 2.1 Sound Pressure

The passage of an infrasonic wave causes pressure oscillations as it traverses the atmosphere. For infrasound of natural origin, the amplitude  $p$  of the sound pressure is often in the range of 0.1 to 100 dyn/cm<sup>2</sup>, and infrasonic microphones are usually designed to respond to such pressures. The atmospheric pressure  $B \approx 10^6$  dyn/cm<sup>2</sup>.

A microphone converts the sound pressure at a particular point into electric current variations having the same waveform. The passage of a sound wave is also accompanied by small vibratory displacements and small variations in temperature of the atmosphere. Microphones have been designed which respond to one or the other of these parameters of the sound wave. For example, the hot-wire microphone responds to the vibratory particle velocity of the air. But any microphone must be located in principle out-of-doors, and it therefore responds to the variable pressure effects of the turbulent eddies associated with the wind, in addition to the effects of the sound wave. An examination of the generation of noise pressure variations caused by turbulent flow shows that the ratio of the desired acoustical signal to unwanted flow noise is greater (by at least an order of magnitude) for the sound pressure than is the ratio for the particle velocity. Therefore measurements of atmospheric sound are always made with pressure microphones.

## 2.2 Speed of Sound

The square of the phase velocity  $c^2$  for sound in a gas at a uniform temperature is the ratio of the gas's modulus of elasticity to its density:  $c^2 = \gamma B / \rho$  where  $B$  (see above) is the atmospheric pressure in dynes per square centimeter, and  $\rho$  is the density in grams per cubic centimeter. For air, the adiabatic gas constant  $\gamma = 1.402$  (dimensionless).  $\gamma B$  is the adiabatic modulus of elasticity for the atmosphere. But the equation of state for air is  $B = \rho R K$ , where  $K$  is the absolute temperature and  $R$  is a constant. Therefore  $c^2 = \gamma B / \rho = \gamma \rho R K / \rho = \gamma R K$ , and so finally

$$c = \text{constant} \times \sqrt{K} \quad (1)$$

Equation (1) shows that the speed of sound is independent of the density of the atmosphere, but directly proportional to the square root of the absolute temperature. For air at a temperature of  $20^\circ\text{C} = 293^\circ\text{K}$ , the speed  $c$  is about 344 m/sec. From this, the sound velocity can be found at other temperatures by means of Eq. (1). The formula is applicable for all sound waves from the low infrasonic frequency of  $f = 0.01$  Hz (wavelength  $\lambda = 34$  km) through audible frequencies,  $f \approx 1000$  Hz, to ultrasonic frequencies,  $f > 20,000$  Hz.

Although the sound speed  $c$  is an important parameter, the propagation of sound waves through the atmosphere cannot be characterized by a single unique speed. It is useful to distinguish between four velocities of sound. The phase velocity  $c$  (see above) is the speed at which a surface of constant phase travels through the atmosphere for a sinusoidal oscillation having  $\omega = 2\pi f$  ( $f$  is the frequency). The local phase velocity of sound is fixed only by the temperature of the atmosphere in the vicinity of the region of interest. For long waves extending vertically in the atmosphere with its substantial differences in temperature, the phase velocity is a function of the entire temperature distribution (see the next sub-section 2.3). In such cases, the phase velocity depends upon the wavelength  $\lambda$ , and hence upon  $k = 2\pi/\lambda$ . The group velocity is defined in acoustics as  $c_g = d\omega/dk$ . The signal velocity is defined by  $c_s = D/T$ , where  $D$  is the distance from the source of sound to the microphone, and  $T$  is the time between the radiation from the source and the emergence (at the microphone) of the signal from noise. In general, the signal velocity differs from both the phase velocity and the group velocity; the relationships between them depend on the structure of the entire atmospheric path, including winds.

The fourth velocity is directly measured at an infrasonic station. Infrasonic microphones are usually on the earth's surface and therefore approximately in the same plane. The speed of a line of constant phase for a sound wave traveling over the earth's surface can be determined from the output of the several microphones. This speed  $c_h$  is usually called the horizontal trace velocity. It depends on the elevation above the horizon of the ray direction for incident plane waves. When the angle of incidence is  $\theta$  (elevation angle =  $\pi/2 - \theta$ ), then  $c_h = c/\sin\theta$ .

### 2.3 Effect of Temperature Distribution

The atmosphere is never in an isothermal state, but is approximately horizontally stratified with the variation in temperature being a function principally of altitude above the surface. In fact the first evidence for a region of warm air at an altitude of about 50 km, at the same or a slightly higher temperature than that at ground level, came from early observations on the anomalous audibility of sounds from large explosions heard at distances greater than about 100 km from the explosive source. The audible waves were in effect used to remotely sense the temperature at the 50 km altitude of the mesosphere.

The phase velocity therefore varies with altitude since the temperature does, see Eq. (1). This variation is a gross feature of the atmosphere and substantially affects the propagation to great distances. The data on the atmosphere obtained from sound propagation measurements, and from instrumented rockets and satellites, show that the temperature, and hence the local phase velocity, depend on location on the earth's surface as well as on altitude, and also vary with time. The average properties have been incorporated into various "standard atmospheres." The distribution of temperature and sound speed with altitude for the 1962 U. S. Standard Atmosphere is shown in Figure 1. The curves should be regarded as averages over all seasons of the year for northern temperate latitudes. The standard atmosphere is useful for analytical investigations into sound propagation.

A detailed mathematical analysis for the propagation of sound shows that the speed minimum in the stratosphere results in waves emitted at low altitudes being "channeled" between the ground and the layer of relatively high sound speed at 50 km altitude. Loosely speaking, the layer serves as a reflector, albeit a poor one. For the shorter waves,  $T < 15$  sec (approximately), sound-ray trajectories are useful for studying propagation.

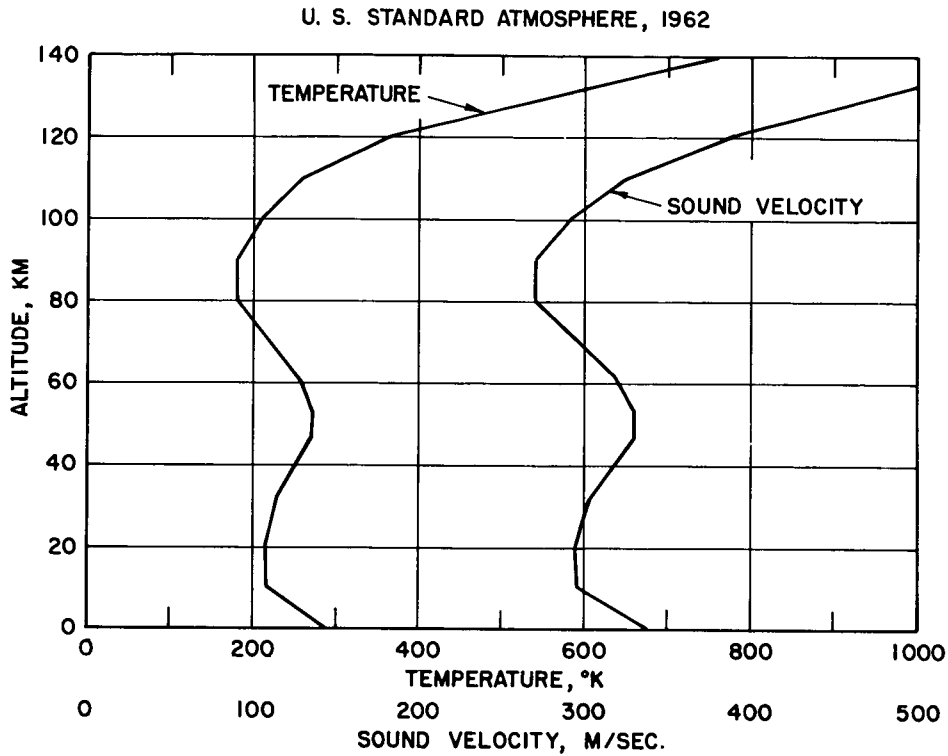


Figure 1. Temperature and sound velocity in the 1962 U. S. Standard Atmosphere. Details of the real atmosphere vary with location on the earth's surface and with the seasons.

In general, the rays emitted at low elevation angles  $\theta$  from a source at ground level are alternately reflected between the layer at 50 km altitude and the surface of the ground.

#### 2.4 Influence of Gravity

Since the atmosphere is in the gravitational field of the earth, its density decreases approximately exponentially with altitude  $z$  above the surface. For an isothermal atmosphere with a sound velocity  $c = 333$  m/sec, the density will decrease as  $\exp(-z/H)$ , where  $H =$  scale height of the atmosphere  $\approx 8.1$  km. The sound pressure for a plane wave of sound sent vertically upward will decrease as  $\exp(-z/2H)$ , but the particle velocity will increase as  $\exp(+z/2H)$ , so that the sound intensity would remain constant. If the frequency of oscillation is decreased until  $T_R = 4\pi c/\gamma g = 305$  sec, ( $\gamma = 1.40$ ,  $g = 9.8$  m/sec<sup>2</sup>), then the phase velocity of the upward traveling wave becomes infinite. But for waves of period shorter than about 100 sec (frequencies greater than about  $10^{-2}$  Hz), gravity effects on sound speed

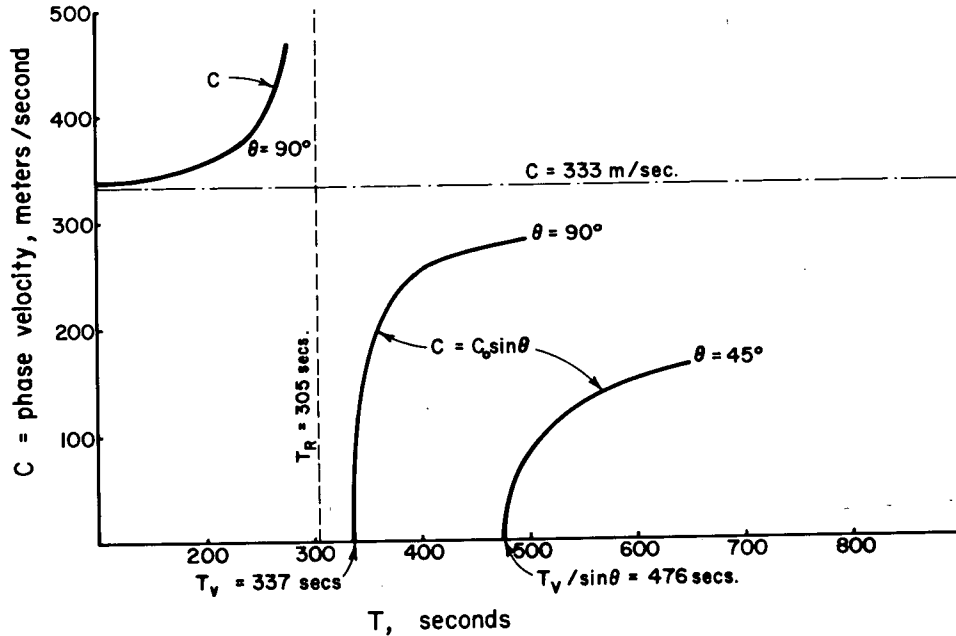


Figure 2. Phase velocities for sound waves in the atmosphere at very low frequencies.  $\theta$  = angle of incidence for plane waves.

are not significant.

$T_R$  is the resonant period for vertical oscillations of the atmosphere. Another important resonant period is the Väisälä period  $T_V = 337$  sec, for the isothermal atmosphere ( $c = 333$  m/sec) under consideration.  $T_V$  is the natural period of oscillation for a small parcel of air which is displaced adiabatically in a vertical direction, in an isothermal atmosphere horizontally stratified by gravity. Plane sinusoidal waves of periods  $T > 337$  sec are usually called "acoustic-gravity" waves, although the atmospheric motions satisfy the same equations of motion as do the sound waves of shorter period  $T < T_R$ . Because the phase velocity is substantially less than the high-frequency velocity  $c = 333$  m/sec, the waves might be called subsonic oscillations. The phase velocity is furthermore, for a particular period  $T$ , a function of the angle  $\theta$  between the direction of propagation and the horizontal plane. See Figure 2 for curves showing how the speeds of plane acoustic-gravity waves vary with frequency and angle  $\theta$ .

In general the speeds are low enough so that wind and temperature gradients can have a strong effect on the propagation. In fact, it appears that acoustic-gravity waves have never been detected with certainty more than a hundred kilometers or so away from the source. For example, vertical

## ATMOSPHERIC SOUND PROPAGATION

oscillations of the jet stream at an altitude of about 10 km produce strong subsonic pressure oscillations, at periods  $T > 300$  sec, at ground level over a large area of the eastern seaboard of the United States. But these occur only when the jet stream is vertically overhead. Acoustic-gravity waves are probably scattered and absorbed strongly by wind and temperature gradients in the atmosphere, and so are not propagated with measurable intensities over global distances away from the source area.

### 2.5 Atmospheric Absorption

The absorption of infrasound in the atmosphere, due to viscosity and heat conduction, is considerably less than the absorption for audible sounds because of the low frequency of oscillation. The absorption coefficient  $\alpha$ , defined by the spatial variation of  $p$ ,  $|p(x)| = p_0 \exp(-\alpha x)$ , is about  $1.6 \times 10^{-4}/T^2 B$  decibels (dB)/m.  $B$  is the barometric pressure in  $\text{dyn/cm}^2$ . For a plane wave of sound in the lower atmosphere at  $T = 10$  sec, the absorption is, therefore, less than  $2 \times 10^{-9}$  dB/km. Hence the loss due to this absorption mechanism is totally insignificant, even for propagation over distances of thousands of kilometers. The absorption in the upper atmosphere is substantially greater because of the lower barometric pressure. At an altitude of 90 km, where the barometric pressure  $\approx 1 \text{ dyn/cm}^2$ , the absorption  $\approx 2 \times 10^{-3}$  dB/km for waves of 10-sec periods.

Up to altitudes of about 10 km in the troposphere, the absorption due to water vapor should be considered. The exact variation of this absorption with barometric pressure is not accurately known for infrasonic frequencies. We estimate that at sea level (altitude = 0 km) the absorption coefficient might be as large as  $5 \times 10^{-9}/T^2$  dB/m, which is about 30 times greater than the absorption for viscosity and heat conduction, as indicated previously. But the absorption due to water vapor is still insignificant for infrasound at  $T = 10$  sec, being only  $5 \times 10^{-8}$  dB/km. This corresponds to an energy loss of less than one percent after propagation half-way around the earth, a distance of 20,000 km.

At very low frequencies, there is an absorption due to relaxation of the thermal energy stored in vibrations of the diatomic molecules in air. We estimate the absorption coefficient to be almost 1000 times greater than that of the viscosity-heat-conduction loss. Therefore, waves in the lower atmosphere at  $T = 10$  sec have  $\alpha \approx 10^{-6}$  dB/km. Again, this is an insignificant loss.

The atmosphere has inhomogeneities in temperature and density arising, for example, from solar heating of the ground. Inhomogeneities in density and motion are associated with turbulence in the wind as it passes over trees, buildings, hills, etc. Furthermore, sound waves are scattered by such obstacles as well as by the atmospheric inhomogeneities. All of these effects cause attenuation of sound-wave energy. But, the attenuation is estimated to be quite small when the wavelength is greater than about 1 km.

The net result is that the total attenuation for infrasound in the atmosphere is small enough so that propagation can occur over thousands of kilometers without substantial loss of energy. An example of this is the sound from the tremendous explosion of the volcano Krakatoa in the East Indies in 1883. The absorption of infrasound from the explosion was low enough so that the waves were still detectable after having traveled around the earth several times. Even though electroacoustic equipment suitable for measurement of infrasound did not then exist, the inaudible sound waves from this disturbance had sound pressures so great that readable deflections were produced on barographs all over the world.

## 2.6 Influence of Winds

The wind speed  $w$  near the surface of the earth is rarely a substantial fraction of the speed of sound  $c$ . The wind Mach number  $\beta = w/c$  is usually less than 0.05. But when the jet stream blows at the tropopause at an altitude of about 12 km, then  $\beta$  is at least 0.1 and sometimes as great as 0.25.

Winds near the stratopause at an altitude of 50 km can be even stronger, and  $\beta = 0.35$  occasionally. At the stratopause the phase velocity of sound has a maximum, since there is a temperature maximum at that level (see Figure 1). Therefore the wind speed and its direction with respect to the direction of sound propagation have important influences on the channeled propagation of sound between the surface of the earth and the stratopause.

In temperate latitudes in the northern hemisphere, there are strong westerly winds for a long regime (about five months) during the winter. There is a shorter regime of strong easterlies during the summer, about two and one-half months. The following is a short table of winds at the stratopause over the continental United States.

Table 1

East-West (Zonal) Winds at Several Geometric Altitudes

Altitude km	Mean values of wind speed in m/sec. (+) = towards east, (-) = towards west			
	16 Oct. to 31 March	1 April to 31 May	1 June to 15 Aug.	16 Aug. to 15 Oct.
50	+52	+2	-42	0
55	+58	-5	-47	+2
60	+61	-8	-51	+5

The mean north-south (meridional) wind components are less than 10 m/sec at any time of the year, and have an annual average speed of 6 m/sec toward the north. Fuller details on the winds at various altitudes have been published by the Air Force Cambridge Research Laboratories (1965).

We see that the effective speed of sound at the stratopause for propagation to the east during the winter is  $330 + 57 = 387$  m/sec (see Figure 1 and Table 1), whereas at the surface the speed is much less,  $c = 335$  m/sec. But for propagation to the west, the effective speed at the stratopause is  $330 - 57 = 273$  m/sec, and the speed at the surface is substantially greater. In brief, the conclusion is that over the continental United States the 50-km thick atmospheric layer between the stratopause and the surface of the earth serves as a waveguide for eastward propagation of sound energy during the winter, but not for westward propagation. In summer the opposite is true; the waveguide effect is only for westward propagation.

For sound waves generated by a source near the earth's surface, the signal velocity  $c_s$  for propagation eastward will generally differ from that westward. The amount of the difference will of course vary with the seasons, because of the seasonal changes in the stratopause winds. In addition because of the difference in waveguide properties, the attenuation of infrasonic waves for eastward propagation will differ from westward propagation. For example, the westward attenuation in winter will be much greater.

Analytical expressions for the effect of stratopause winds on infrasonic signal velocity and attenuation need to be developed. We suggest that such expressions, applied properly to data on propagation of infrasound, could be used to remotely sense winds at the stratopause.

C.12

### 3. MEASUREMENTS OF INFRASOUND

#### 3.1 Measurement System

The electroacoustic system used at each of the infrasonic stations in the ESSA network consists of an array of at least four microphones, associated electronic filter-amplifiers, and recorders. The system is designed for determining four characteristics of infrasonic waves passing through the station area: (1) the amplitude and waveform of the incident sound pressure, (2) the direction of propagation of the wave, (3) the horizontal phase velocity, and (4) the distribution of sound wave energy at various frequencies of oscillation.

The microphones are located at ground level, approximately in the same plane, and about 7 km apart. See Figure 3 for the station at Washington, D. C. Effects on each microphone of pressure fluctuations caused by local

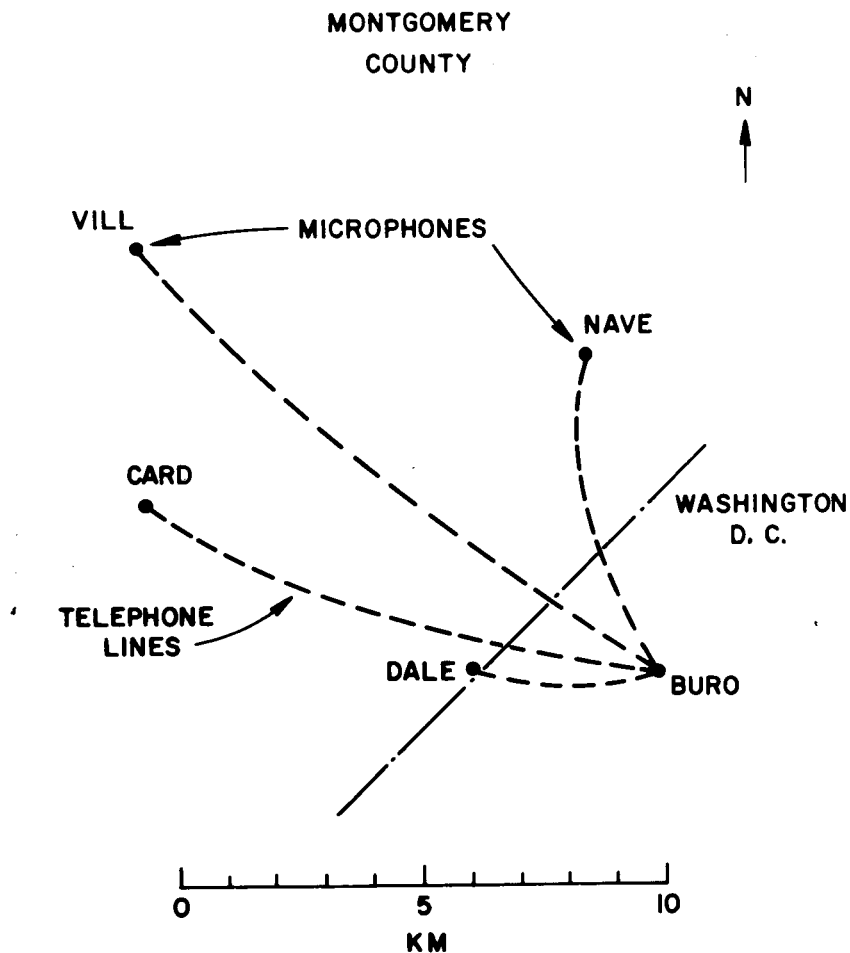


Figure 3. Location of line-microphones at the infrasonics station in Washington, D.C. Recordings are made at the Buro site.

## ATMOSPHERIC SOUND PROPAGATION

turbulent wind eddies are minimized by noise-reducing lines of pipe which are about 300 m long, have capillary inlets, and are connected to the inlet to the microphone. The theory of this noise-reducing line has been described by Daniels (1959). For sound waves of wavelength greater than about 3 km, the line microphone is essentially nondirectional and does not attenuate the sound pressure appreciably. However, noise due to random pressure fluctuations in the period range of 1.0 to 30 sec, such as that caused by wind turbulence, is reduced considerably.

The microphones are of the electrostatic condenser type, and produce frequency-modulated voltages, on a carrier frequency of about 1500 Hz, proportional to the incident sound pressure. These voltages are transmitted by telephone wires to a central location where they are demodulated, amplified, and recorded by several means that will be described below. Band-pass filters are introduced into the amplifiers when a higher signal-to-noise ratio is desired for the sound under study. Earthquake waves, for example, are best studied with a band-pass filter passing sounds having periods of oscillation between 0.4 and 20 sec, as in Figure 4.

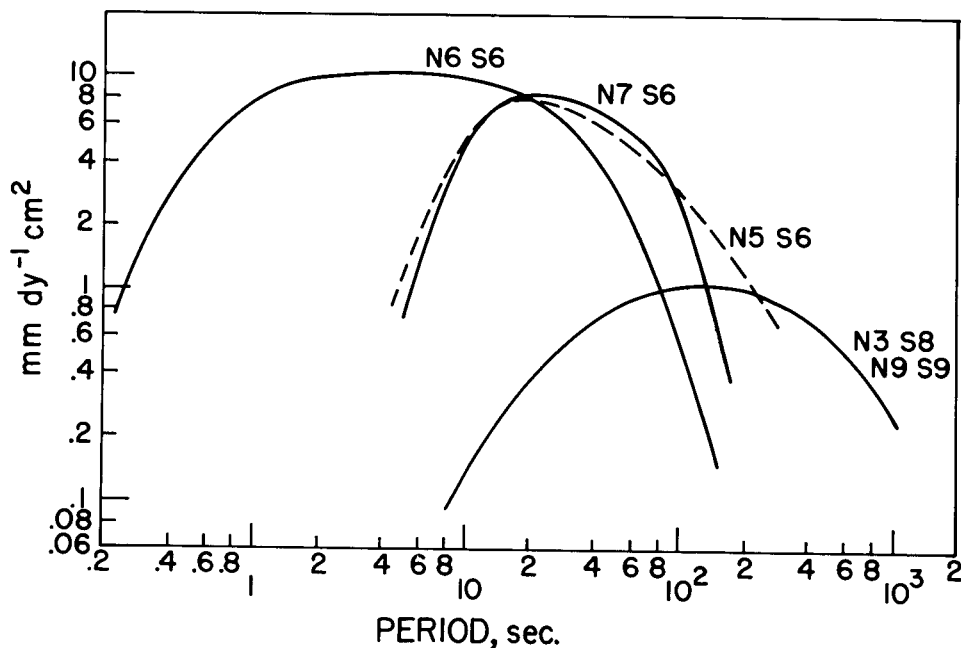


Figure 4. Response curves of some filters used with an infrasonic microphone system. The ordinate scale applies to ink-on-translucent-paper chart recordings.

Calibration of each microphone is done by connecting its inlet through a short hose to a calibrating barrel with a volume of about  $0.19 \text{ m}^3$ . An oscillating piston on top of the barrel produces accurately known sinusoidal sound pressures within it at various low frequencies.

### 3.2 Recording on Paper Charts

A convenient recording scheme has been in use for many years. It is in analog form, in real time, as ink-on-translucent-paper traces. Each line-microphone is recorded on its own paper chart. The waveform of each recording is that of the sound pressure as modified by the gain, as a function of frequency, of the microphone and electronic filter combination. An important feature of the scheme is the accurate timing trace for each recording.

The four characteristics of the sound wave (see the preceding subsection 3.1) are obtained from the ink-on-paper traces by a procedure based on visual congruence (correlation) between pairs of recordings, which are matched by superposition on a transparent table top illuminated from below, for example. At "best correlation," time differences are obtained for arrival of the same sound waveform at the several pairs of microphones. The direction of propagation and the horizontal phase velocity are found from these differences by a simple geometrical procedure described by Matheson (1966). The sound pressure amplitude is obtained from a calibration of the microphone-recording system with an oscillating piston source, and the dominant periods are found by inspection of the recorded waveform. The success of the correlation scheme depends on the fact that almost all sound waves coming from distant sources have approximately plane wavefront surfaces of constant phase.

### 3.3 Magnetic Tape Recording

With the magnetic tape scheme, sound pressures at the several line-microphones are recorded in analog form on parallel channels (tracks) on the tape along with time. When a sound wave is present, its direction of propagation and horizontal phase velocity are obtained from the magnetic tape recording by means of an automatic multichannel correlator. This is essentially an analog computing instrument which receives the magnetic tape recording and produces an output trace (on paper tape) proportional to the average of the cross-correlations between pairs of microphone voltages.

## ATMOSPHERIC SOUND PROPAGATION

Variable time delays are mechanically introduced into each microphone channel, with the delays corresponding to a systematic search for correlation at all azimuths and over a range of horizontal phase velocities between  $c$  = the speed of sound and  $c\sqrt{2}$ . Details on the automatic correlator have been given by Brown (1963). The direction of propagation and the horizontal phase velocity are read from the output trace of the correlator.

### 4. RESULTS OF OBSERVATIONS ON INFRASONIC WAVES

We proceed to describe infrasound caused by the following geophysical disturbances: volcanic explosions, the aurora borealis, earthquakes, microbaroms due to ocean waves, subsonic oscillations of the jet stream, and shock waves from the entry of meteorites and satellites into the atmosphere.

There are other natural sources of infrasound not yet fully studied. In particular severe storms such as tornadoes (Cook and Young, 1962), and the passage of winds over certain mountainous areas, give rise to infrasonic waves in the atmosphere. Two areas of "mountain" waves seem to be the Pacific coast of North America between north latitudes  $40^\circ$  and  $60^\circ$ , and the region of Argentina east of the Andes Mountains between south latitudes  $25^\circ$  and  $35^\circ$ .

#### 4.1 Volcanic Explosions

Sufficiently strong volcanic explosions occur frequently enough to provide many useful data on the propagation of infrasound over global distances through the atmosphere. We mentioned earlier the tremendous explosion of Krakatoa in the East Indies in 1883, whose infrasonic waves were still detectable after having traveled around the earth several times. Following are a few of the volcanos whose explosions radiated substantial amount of infrasound: Bezymyanny in eastern Siberia in 1956, reported by Passechnik (1959); Mt. Agung on the island of Bali in 1963, reported by Goerke et al (1965); Mt. Redoubt in southern Alaska in 1966, reported by Wilson (1966); the caldera on Isla Fernandina in the Galapagos Islands in the spring of 1968, still under study.

The sound waves from Mt. Agung were observed at three infrasonic stations in the continental U.S.A. The essential features of the data are shown in Table 2 and Figure 5.

Table 2

Sound Waves from the Explosion of Mt. Agung  
8.3° south lat., 115.5° east long.,  
at 0855 h, May 16, 1963 (UT).

	Infrasonic Stations		
	Boulder, Colo.	Boston, Mass.	Washington, D.C.
Location	40.1°N 105.2°W	42.5°N 71.2°W	39.0°N 77.1°W
Short great-circle distance from Mt. Agung, km	14,700 25,300*	16,200	16,300
Observed infrasonic arrival, UT	2301 h, May 16 0757 h,* May 17	0028 h, May 17	0150 h, May 17
Signal velocity m/sec	288 305*	289	268 †
Maximum amplitude, dyn/cm <sup>2</sup>	>6.6 2.4*	10.6	9.0
Measured azimuth of sound wave arrival	304° 111° *	350°	347° ‡
Azimuth of great- -circle to Mt. Agung	300.5° 120.5° *	348.3°	336.4°

\* Via great-circle path through antipode

† Uncertain because start of received signal was obscured by noise.

‡ Observed about 2 1/2 hr. after start of signal.

The sound pressure at each station emerged slowly from noise, and so the measured transit times might be somewhat greater than the "true" (least) time. In particular, the rather low signal velocity deduced from the Washington data is due to masking of the early part of the infrasound by wind noise. The low signal velocity of 288 m/sec deduced from the Boulder and Boston data (short great-circle paths) might be due in part to easterly winds at the stratopause over the Pacific Ocean and the continental United

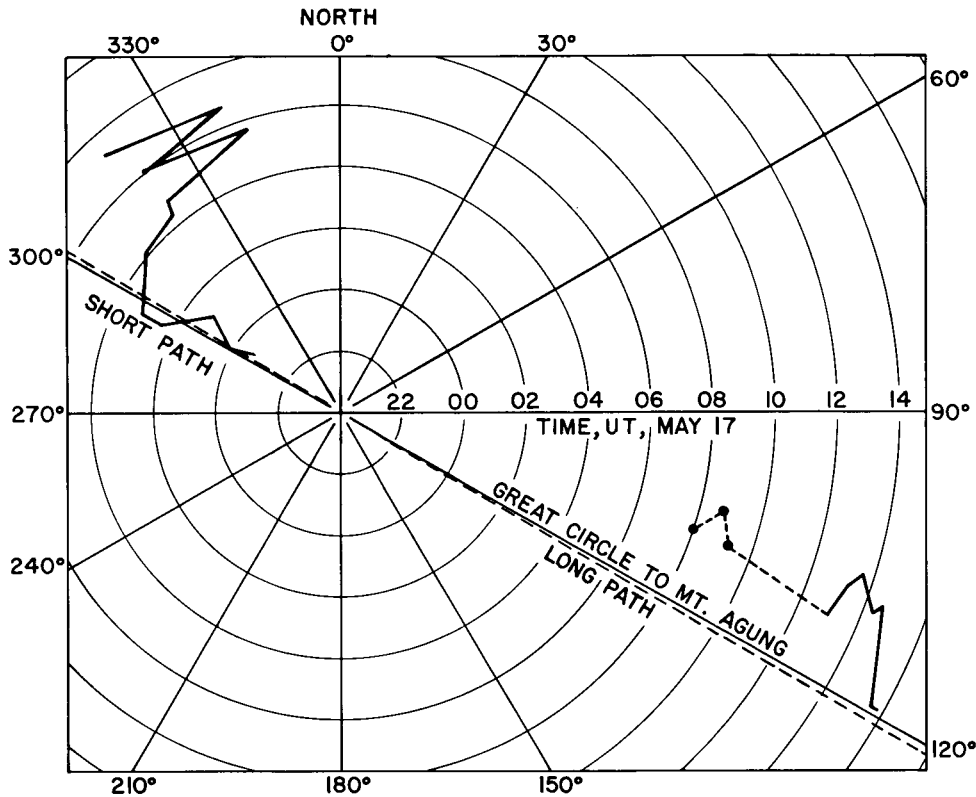


Figure 5. Variations of azimuth for arrival of infrasound from Mt. Agung in Boulder on May 16 - 17, 1963. The three points are for sporadic appearances of sound waves in noise at about 0800 - 0900 h.

States, (see Table 1).

About two-thirds of the antipodal (long) great-circle path to Boulder is in the southern hemisphere, where much less is known of the upper atmosphere winds. The infrasonic signal velocity of 305 m/sec is a little higher than the average of 300 m/sec for the wind-free atmosphere. We therefore estimate that the stratopause winds at the 50 km altitude in the southern hemisphere, during the infrasound transit in May, must have been mainly toward the west, at an average speed no greater than  $-10$  m/sec.

But this conclusion is at variance with the deduction from Webb's (1964) hypothesis that the southern hemisphere winds can be deduced by symmetry from the northern hemisphere data. The hypothesis would lead to strong winds, at the southern hemisphere stratopause, toward the east at  $+50$  m/sec over about half of the infrasonic propagation path. Furthermore, such strong adverse winds, if present, would have reduced the antipodal sound intensity by a much greater amount than was actually observed.

The reader should note that the wind data published by the AFCRL (1965) for the stratopause are based on measurements made with vertically ascending rockets at a number of geographical locations. In other words, the wind measurements were made at isolated points on the earth's surface, separated by thousands of kilometers. Measurements of sound propagation offer the potentiality (not yet realized in full) of obtaining average winds over long paths in the atmosphere. These propagation data should be useful supplements to the rocket data.

#### 4.2 Auroral Infrasonic Waves

Two types of infrasonic waves caused by the auroral borealis are found in the atmosphere of the northern hemisphere at temperate and high latitudes. The first type is found at mid-latitudes during sufficiently strong magnetic storms even in the absence of a visible aurora at the geographical location of the infrasonic station. The second type of infrasonic wave, found near the auroral oval at high latitudes when visible sharply-defined auroral forms travel overhead across the station location at supersonic speeds, has directions of propagation and horizontal trace velocities very nearly the same as those of the visible auroral form. Before discussing these two types of waves, we digress to present a short description of a magnetic storm and related phenomena.

With the advent of a solar flare or a sun storm, electromagnetic radiation reaches the earth almost immediately. An ionized-gas cloud sometimes arrives one or two days later. This plasma cloud perturbs the magnetic field of the earth. Mid-latitude observatories see a rise in the horizontal component of the magnetic field, followed by a larger decrease and a recovery lasting several days. The strong and erratic variations that result are known as magnetic storms, magnetic activity, or disturbance variations. A measure of this solar-particle radiation effect is furnished by the planetary magnetic index  $K_p$  which is derived from data from a number of participating magnetic observatories. One of a series of numbers from 0 to 9 is given to each three-hour interval of each day, a larger number indicating a greater departure from undisturbed conditions. During large magnetic storms, magnetic fluctuations with periods from a few seconds to several minutes occur, radio communications are disturbed, x-rays are observed with instruments carried in balloons, and the aurora is observed in mid-latitudes.

Waves recorded during the magnetic storm of February 11, 1958, at

ATMOSPHERIC SOUND PROPAGATION

Washington, exhibited a more-or-less typical behavior pattern. The storm began on February 11 at 0126 UT. It was accompanied by an intense red aurora visible in Washington. The first distinguishable sound waves arrived about 0642 UT from a north-northwest direction and had a trace velocity of 775 m/sec. Measurements at 0905 UT indicated a direction slightly more from the west and a trace velocity of 750 m/sec. The sound waves decreased in amplitude and disappeared between 1100 and 1200 UT. Comparison of the large trace velocity, usually greater than 400 m/sec at the mid-latitudes of Washington and Boulder, with the local speed of sound is often enough to distinguish these waves from other infrasound. There are variations with time in the apparent direction and trace velocity of the waves. There is an apparent short-period cutoff near  $T = 15$  sec.

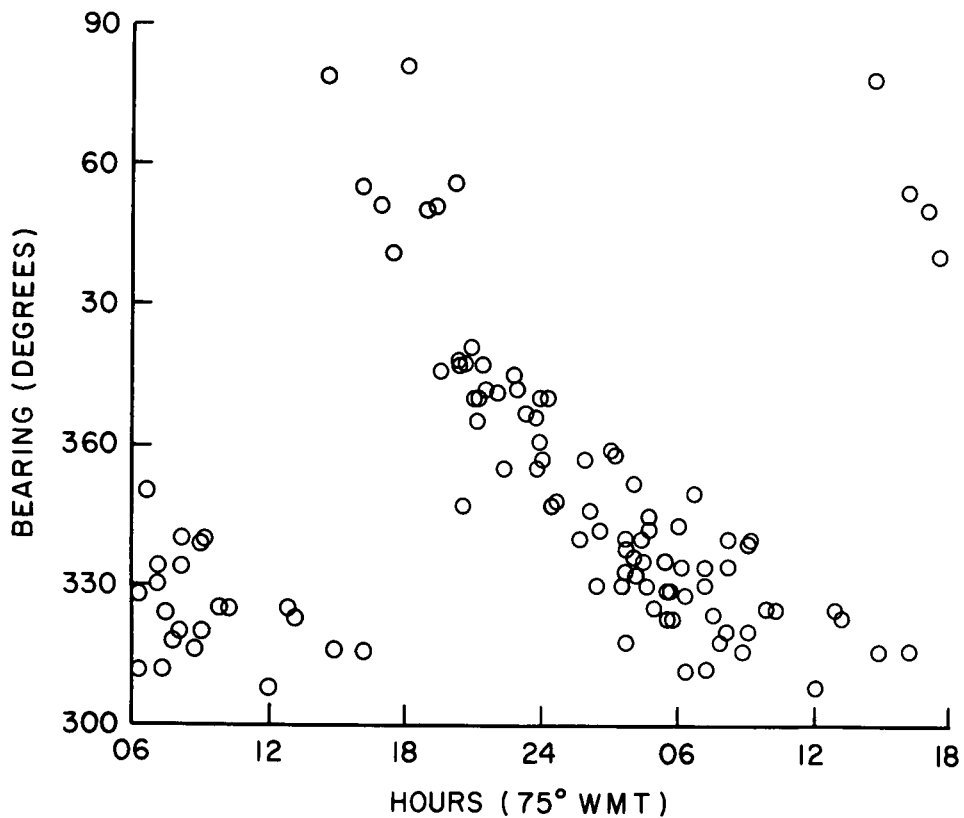


Figure 6. Azimuth of auroral infrasound arriving during magnetic storms, as a function of local time in Washington, D.C. Bearing (= azimuth) = angle, in degrees east of north, to the direction from which the sound comes. The open circles are measured azimuths during 1956 - 1962.

The remarkably consistent changes in direction of arrival with time of day are shown in Figure 6. Direction changes from the northeast in the evening, through north about midnight, then northwest in the morning, and to the northeast again somewhat suddenly after local noon. The data in this figure were restricted to signals with trace velocities above 390 m/sec to help prevent possible confusion with sound from other sources.

Sound waves usually arrive at Washington, D. C., within 5 or 6 hr of rise of  $K_p$  to a value of 5 or higher. Predominant periods range from 20 to several hundred seconds. The pressure amplitude is usually less than  $3 \text{ dyn/cm}^2$ , but is sometimes 7 or greater. Durations range from 1 or 2 hr to more than 24 hr, with a mean of about 6 hr. During the active solar years 1960 and 1961, auroral infrasonic waves were observed for more than 200 hr each year at Washington, D. C. Additional details are given by Chrzanowski et al (1961, 1962).

A very simple hypothesis may serve to explain qualitatively the experimental observations on these sound waves at mid-latitudes. Imagine a somewhat diffuse source in the lower ionosphere and fixed in geomagnetic latitude on the side of the earth opposite the sun. Let the magnetic latitude of the center of the source be that of the auroral zone, or about  $66^\circ$ . Waves from the source spread out through the ionospheric plasma at supersonic speeds. Sound waves leak out from the lower surface of the plasma and therefore have the supersonic horizontal trace velocities observed at mid-latitudes. The earth will turn underneath the source once each day. This qualitatively explains the diurnal change of direction of infrasound observed at Washington, D. C. The relative absence of short periods and the large trace velocity suggest a high-altitude source where the mean free path of the molecules is long and the modes excited in the atmospheric wave guide have wave normals with a vertical component. This picture is, of course, oversimplified. Since the aurora moves south with increasing geomagnetic activity, it is possible that the sound source may vary in geomagnetic latitude with strength of the disturbance. Fluctuations in longitude of the source may also occur.

On the basis of the above hypothesis and the observations of duration and amplitude at Washington, D. C., it seems reasonable to assume that perhaps one quarter of the earth's surface is simultaneously bathed in acoustic radiation with an average pressure of about  $1 \text{ dyn/cm}^2$ . This suggests an acoustic source of roughly  $10^9 \text{ W}$  during a typical magnetic storm.

## ATMOSPHERIC SOUND PROPAGATION

The other type of infrasonic waves, caused by visible aurorae, has been observed by C. R. Wilson and his colleagues (1967a, 1967b) at the infrasonic station at College, Alaska. The basic observations are: (a) the horizontal trace velocity is supersonic,  $c_h > 450$  m/sec; (b) the transient pulses of sound have about the same direction of propagation and velocity as fast-moving auroral arcs overhead at Alaska, measured with an all-sky camera; (c) the dominant period of oscillation is about 20 sec; (d) peak sound pressure is typically  $5 \text{ dyn/cm}^2$ ; and (e) each pulse is of only a few minutes duration.

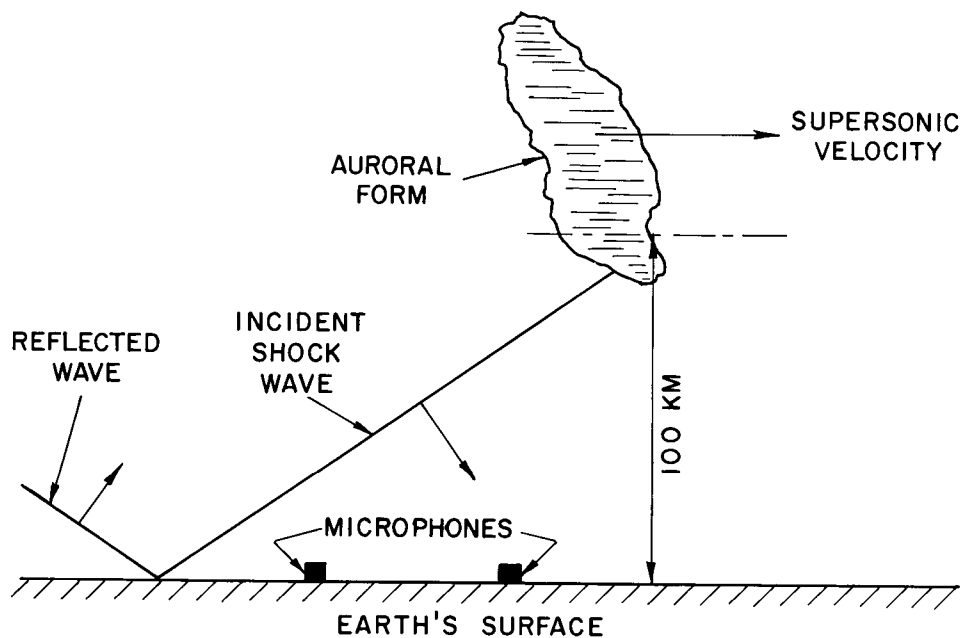


Figure 7. Acoustical shock wave caused by supersonic motion of the leading edge of an auroral form.

The observations can be very well explained by means of Wilson's shock wave model, in which the supersonic motion of the leading edge of an auroral wave gives rise to an acoustical shock wave (see Figure 7). The lower edge of the aurora serves as a line source (perpendicular to the plane of the paper). A particular pulse arrived at the ground station microphones 420 sec after an auroral arc passed overhead. The 420-sec delay corresponds to a source altitude of 140 km for an assumed average  $c = 300$  m/sec and measured  $c_h = 680$  m/sec. This altitude is to be compared with the known heights of visible auroral arcs, which in most instances have streamers extending from 110-km to 145-km altitudes.

Auroral infrasound is apparently not propagated into the equatorial zone. The infrasonic stations at Huancayo, Peru ( $12^{\circ}$  S lat.) and La Paz, Bolivia ( $17^{\circ}$  S lat.) have not yet detected infrasound from either the aurora borealis or the aurora australis. The station at Tel Aviv, Israel ( $32^{\circ}$  N lat.) has observed auroral infrasound on only two or three occasions. These observations are consistent with the leakage of acoustic waves from an ionospheric disturbance originating in the auroral zone.

#### 4.3 Earthquakes

After a strong earthquake, traveling waves spread from it over the earth's surface and radiate sound into the atmosphere as well. The vertical component of the earth's surface motions gives rise to the sound radiation. There are several different types of earthquake waves, and they all travel with speeds much greater than the velocity of sound in air. As a consequence, the sound radiations are propagated upward in a direction almost perpendicular to the earth's surface. The strongest surface motions at locations away from the epicenter of the earthquake are those caused by Rayleigh waves. These travel entirely on the surface of the earth and have periods of oscillation  $T$  between about 10 and 50 sec. The phase velocities  $c_o$  of these waves when traveling over continental surfaces are about 3.5 km/sec. The sound from Rayleigh waves is occasionally strong enough to reach the ionosphere and cause substantial motions there.

The sound radiated by strong earthquakes can be measured at infrasonic stations. Usually the detected sound is that locally radiated by earthquake waves passing through the geographical area of the station. But from a very strong earthquake, sound radiated directly from the epicentral area into the atmosphere can be measured at an infrasonic station several thousand kilometers away. This occurred at the time of the great Alaskan earthquake in 1964, whose epicentral sound was readily measured at the Washington, D. C. infrasonic station.

Let us look into the characteristics of a few of the waves which spread out from the focus of an earthquake. The focus is the location on or near the surface at which the earthquake occurs (Figure 8). The epicenter is the point on the surface where a radius vector terminates on passing from the center of the earth through the focus. There are three waves of principal interest to our discussion. The first wave to arrive at a distant location is a longitudinal wave which has passed through the body of the earth; this

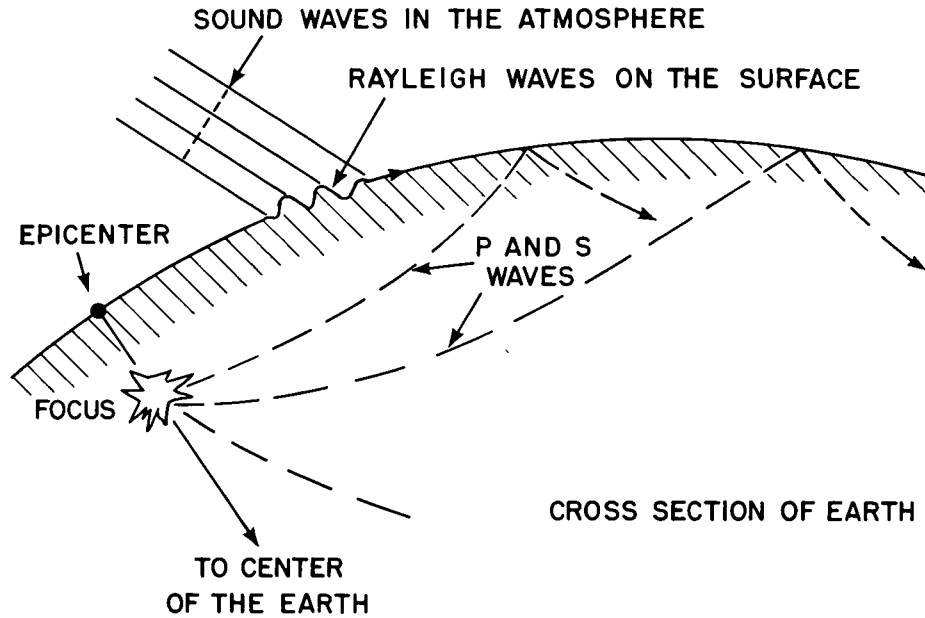


Figure 8. Seismic waves from the focus of an earthquake, and sound radiated into the atmosphere by the seismic waves.

is called a P wave. The second to arrive is a transverse or shear wave traveling more slowly and designated as an S wave. The third wave, which travels entirely on the surface, is the Rayleigh wave. These three are accompanied by many others, for example, by P and S waves reflected from the boundary between the mantle and core 2900 km below the surface. From measurements of arrival times of the waves received at several seismological stations, the epicenter and focal depth of an earthquake can be determined very accurately.

#### Montana Earthquake

The great earthquake in Montana at 0637.27 UT on August 18, 1959, produced seismic waves strong enough in the Washington, D. C. area to cause easily measured infrasonic waves in the atmosphere. The epicenter in Montana was 2860 km away from the Washington infrasonic station on a great-circle bearing 66° west of north.

The sound radiated by the P wave arrival was obscured by wind noise and microbaroms and could not be distinguished with certainty. The arrival of the S waves (shear waves) produced measurable infrasound, from which it was deduced that the shear waves came from 44° west of north with a period of oscillation of 11 sec and a horizontal trace velocity of 6.0 km/sec. The

arrival was from a direction  $22^\circ$  north of the great-circle bearing. The earth's displacement in Washington, deduced from a peak-to-peak sound pressure of  $0.8 \text{ dyn/cm}^2$ , was 0.34 mm.

The very strong Rayleigh waves had periods initially of about 15 sec, which shortened to about 8 sec after a minute or so. This change came about because the group velocity of the 8-sec waves was less than for the 15-sec waves, and so it took longer for the 8-sec waves to travel across the country to Washington. The earth's displacement, calculated from the large peak-to-peak sound pressure of  $5 \text{ dyn/cm}^2$ , was 3.0 mm. The average trace velocity of the Rayleigh waves was 3.8 km/sec. They came mainly from the great-circle direction of the epicenter, with the later waves coming from a slightly more northerly direction.

We can only conjecture about the reason for the arrival of the seismic waves from directions mostly north of the great-circle bearing. Refraction on passing from the Appalachian Mountains onto the Piedmont Plateau might have been the cause.

#### Acoustical Radiation Zones

An interesting feature of the sound radiated into the atmosphere by Rayleigh waves is that the sound pressure at any point on the surface is due to the integrated effect of an extensive area of the traveling waves. This is in contrast to a seismometer, which measures the earth's displacement only at the spot where the instrument is located.

We present the results of an analysis showing how much of the traveling wave motion is effective in producing sound pressure at a point just above the surface. For a long train of sinusoidal surface waves of wavelength  $\lambda_0$ , the waves in a circular area of radius  $4 \lambda_0$  contribute at least 70 percent to the amplitude of the sound pressure at the center of the circle. We call this circular area the "radiation zone" for the sound pressure produced by the surface waves. If the Rayleigh waves have a period  $T = 25$  sec, then  $\lambda_0 = 88$  km, and so  $R = 4 \lambda_0 \approx 350$  km; this is the radius of the radiation zone for such long waves. Fuller details have been given by Cook (1965).

#### Ionospheric Motions

At the time of the Alaskan earthquake on March 28, 1964, Rayleigh waves of considerable amplitude passed across the United States. The sound waves which they produced at infrasonic frequencies were propagated upward and

caused substantial motions of the ionosphere.

We examine first the equation for propagation of a sound wave into the less dense regions of the upper atmosphere. We recall that the sound wave travels almost vertically upward in a direction  $\arcsin(c/c_0) \approx 6^\circ$  from the vertical. The main features of the propagation can therefore be seen from a consideration of plane waves of sound traveling vertically upward parallel to the  $z$  - axis in an approximately isothermal atmosphere. The differential equation for the particle velocity  $v$  in the waves is

$$\frac{\partial^2 v}{\partial z^2} - \frac{\gamma g}{c^2} \frac{\partial v}{\partial z} = \frac{1}{c^2} \frac{\partial^2 v}{\partial t^2} \quad (2)$$

In this  $c^2/\gamma g = H =$  the scale height of the atmosphere  $\approx 8.4$  km (in the lower atmosphere), for  $\gamma = 1.40$ , and  $g = 9.8$  m/sec<sup>2</sup>,  $c = 340$  m/sec. The density  $\rho$  of the atmosphere as a function of altitude  $z$  is given by  $\rho = \rho_0 \exp(-z/H)$ . The particle velocity  $v$ , obtained from equation (2) for sinusoidal waves ( $\omega = 2\pi/T$ ) is

$$v = |v_0| \exp(z/2H) \cos \left[ \omega t - z \sqrt{k^2 - (1/2H)^2} \right], \quad (3)$$

where  $|v_0|$  = amplitude of vibration at ground level ( $z=0$ ). From this we see that for vertically traveling sound waves in the atmosphere, the amplitude of vibration varies inversely as the square root of the atmospheric density.

Let us see how this applies to the Rayleigh waves from the Alaskan earthquake. The infrasonic stations at Boulder and Washington measured sound pressures of about 20 dyn/cm<sup>2</sup>, the period  $T$  of the waves being of the order of 25 sec. These very substantial sound pressures correspond to vertical surface motions  $|v_0| \approx 0.5$  cm/sec. A wave that starts out with an amplitude of 0.5 cm/sec will increase to an amplitude of about  $10^4$  cm/sec at an altitude of 160 kilometers.

A little before it reaches this altitude the sound wave becomes a discontinuous shock wave. From the analysis that follows we can estimate the altitude  $z$  at which this occurs. In a real gas the pressure-crests in a sound wave continually gain on the troughs, since the crests have the excess velocity  $|v|$  computed above. The atmospheric waves start out sinusoidal, and the time  $T'$  at which the crests overtake the troughs and discontinuity begins is given by

$$\frac{\lambda}{2\pi} = \int_0^{T'} |v| dt = \int_0^{T'} |v_0| \exp(ct/2H) dt = 2(H|v_0|/c) [\exp(cT'/2H) - 1]. \quad (4)$$

The foregoing is based on Lord Rayleigh's (1945) analysis. Continuing, we find that the altitude  $z$  is approximately

$$z = cT' = 2H \log [1 + c\lambda/4\pi |v_0| H] \approx 138 \text{ km.} \quad (5)$$

From the foregoing analysis we estimate that the oscillatory vertical motions of the atmosphere at higher altitudes, caused by the Rayleigh waves, are of the order of hundreds of meters per second.

We consider next the results of observations on ionospheric motions near Boulder, Colorado. These observations were made by Mr. Donald M. Baker of ESSA's Boulder Laboratories. He sent radio waves almost vertically upward and observed the waves reflected from the ionosphere back down to a receiving station on the ground. At the time the Rayleigh waves passed through the Boulder area, Doppler shifts of more than 3 Hz occurred for the radio waves at 4 MHz. Such shifts correspond to a vertical motion of the ionosphere, at the 4 MHz reflection height of about 240 kilometers, of more than 200 meters per second. Similar Doppler shifts occurred in the 10-MHz radio wave propagated from the standard-frequency station WWV in Hawaii and received in Boulder, but it is difficult to estimate the geographical area of the ionosphere from which reflections might have occurred.

The Doppler shifts started about 9 min after the Rayleigh waves arrived at Boulder. The sound waves travel vertically upward with an average velocity  $\underline{c}$  of about 1/3 km/sec up to an altitude of 140 km. At higher altitudes the velocity  $\underline{c}$  is about 700 m/sec. The computed transit time to the ionosphere at an altitude of 240 km is therefore less than 10 min, which is confirmed by the observed transit time of 9 min.

We conclude from the foregoing that the Rayleigh waves traveling across the continental United States from the Alaskan earthquake produced sound waves which, on propagation upward through the atmosphere, caused substantial motions of the ionosphere.

The absorption and dissipation into heat energy of the sound waves takes place in the ionosphere. This can be seen from the results of the measurements. These show that the intensity on entering the ionosphere is at least of the same order of magnitude as the computed intensity, the latter being based on no absorption in the lower atmosphere. We can estimate the total energy dissipated. The intensity of the sound waves traveling upward was about 10 erg/(cm<sup>2</sup>sec) for about 300 sec. Therefore the total sound energy carried up into the ionosphere, and there dissipated as heat, was roughly

## ATMOSPHERIC SOUND PROPAGATION

$6 \times 10^{20}$  ergs for the area of North America (about 20,000,000 km<sup>2</sup>). This surprisingly large energy is to be compared with the total estimated seismic energy released by the Alaskan earthquake, which was about  $10^{24}$  ergs.

### 4.4 Microbaroms

Natural sounds in the atmosphere having dominant periods of oscillation between 4 and 7 sec seem to be particularly widespread and are commonly called microbaroms. They are characterized by their persistence at a given geographic location for many hours, by a rather constant period of oscillation, and by an amplitude which seldom exceeds 3 or 4 dyn/cm<sup>2</sup> in the area of Washington, D. C. Microbaroms of 4-sec periods were observed by Gutenberg and Benioff (1941) at Pasadena in southern California. They found the microbaroms to be sound waves traveling approximately parallel to the earth's surface and coming from a direction southwest of Pasadena. Saxer (1945, 1953-54) and Dessauer et al (1951) observed microbaroms at Fribourg in Switzerland. They found the waves traveling parallel to the earth's surface to come from a direction northwest of Fribourg, with periods  $\approx 5$  sec, and sound pressures  $\approx 0.5 - 1$  dyn/cm<sup>2</sup>. Furthermore, the sound pressures seemed to be correlated with the heights of water waves in the north Atlantic Ocean due to storms and with the strength of microseisms in the earth observed at Strasbourg (about 200 km north of Fribourg). Observations on microbaroms in the Washington area will be discussed later.

What causes microbaroms? Similarities between them and microseisms on the earth's surface suggest that one causes the other. But it can be easily shown that, on the one hand, the sound waves radiated into the atmosphere by microseisms are much weaker than microbaroms. On the other hand, sound pressure of the latter on the earth's surface is not strong enough to produce observable microseisms (Cook and Young, 1962).

It had long been conjectured (e.g., Daniels, 1962) that the gravity waves created by storms on the surfaces of the seas radiate sound into the atmosphere. In the analysis that follows we shall introduce quantitative expressions showing that long trains of such waves cannot radiate sound power, because their phase velocities are less than the phase velocity  $c$  of sound in the atmosphere. On the other hand sound power radiation can occur (a) when the waves come to an abrupt stop as, for example, on the beach, and (b) when waves traveling in different directions have an interference pattern which causes periodic oscillations in the potential energy of the atmosphere over the waves.

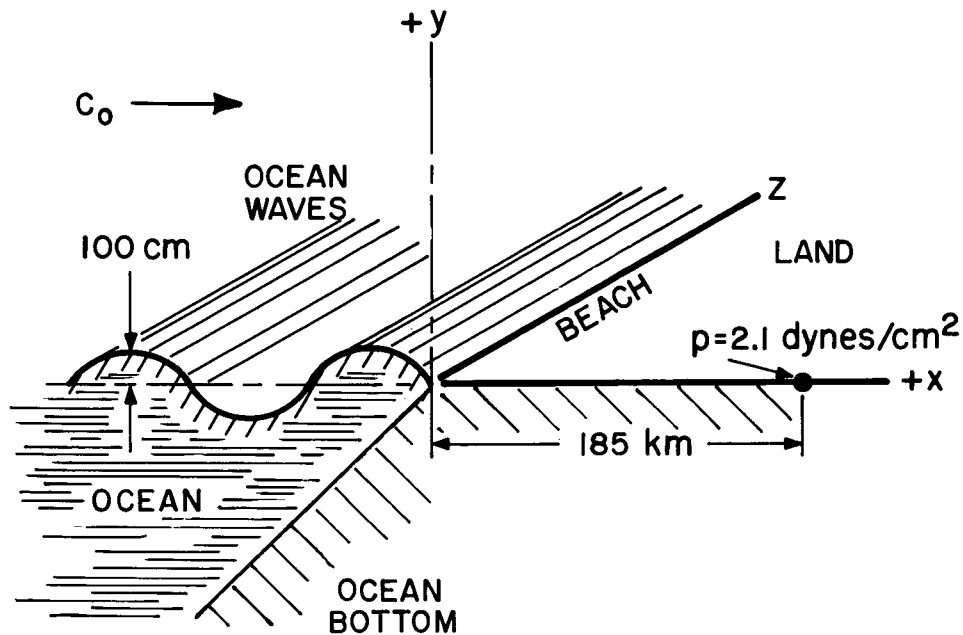


Figure 9. Radiation of infrasound by a semi-infinite wave train on a water surface.

Radiation by an infinite train of surface waves on water

We consider first a sinusoidal gravity wave on water, of amplitude  $A$  and period  $T$ , the wave fronts being straight lines parallel to the  $z$ -axis. (See Figure 9). We suppose the depth to be substantially greater than  $\frac{1}{k_0} = \lambda_0/2\pi$  ( $\lambda_0$  = wavelength), and so the deep-water wave speed is  $c_0 = gT/2\pi = g/\omega$ , where  $g$  = acceleration of gravity. Therefore the surface displacement can be represented by

$$y_0 = A \exp i(\omega t - k_0 x) \tag{6}$$

for all  $x$ .

In the atmosphere above the water a distribution of sound pressure and particle motions is caused by the surface wave. The velocity potential for this distribution must satisfy the sound wave equation and the boundary condition at the water surface. The final result is that the sound pressure in the atmosphere above the water is

$$p = \frac{\rho c \omega A}{\sqrt{\beta^2 - 1}} \exp \left[ -\sqrt{k_0^2 - k^2} y + i(\omega t - k_0 x) \right] \tag{7}$$

## ATMOSPHERIC SOUND PROPAGATION

where  $\rho$  = density of the atmosphere,  $c$  = speed of sound,  $\beta = c/c_0$ , and  $k = \omega/c$ .

Note that the sound pressure at the water surface is in phase with the displacement. Hence no net work is done and no sound power is radiated into the atmosphere.

For water waves of period  $T = 2\pi = 6.28$  sec,  $\omega = 1.0/\text{sec}$ ,  $c_0 = 9.80$  m/sec, and  $\lambda_0 = 61$  meters. Suppose the displacement amplitude  $A = 100$  cm. Then the sound pressure at the water surface is  $|p| \approx 120$  dyn/cm<sup>2</sup>. But at a height of 100 m above the surface the sound pressure is reduced by a factor of  $e^{-10} \approx 1/22000$  to less than  $10^{-2}$  dyn/cm.

### Radiation by a semi-infinite wave train

We consider next a sinusoidal gravity wave on water coming from  $-\infty$  and stopping abruptly at  $x = 0$ , the wavefronts again being straight lines parallel to the  $z$ -axis (see Figure 9). The surface displacement  $y_0$  is the same as in Eq. (6) for  $-\infty < x < 0$ , and  $y_0 = 0$  for  $x > 0$ . We imagine the line  $x = 0$  in the  $xz$ -plane to be the beach, and the region  $x > 0$  to be the landward side.

The velocity potential  $\psi$  for the total wave field at  $y = 0$  is readily found by superposition of the hemicylindrical waves generated by each line element, parallel to the  $z$ -axis and of width  $du$ , of the surface waves.

$$\psi = -\frac{\omega A e^{i\omega t}}{2} \int_{-\infty}^0 [J_0(kx - ku) - i Y_0(kx - ku)] e^{-ik_0 u} du \quad (8)$$

for  $x > 0$ .

A good approximation to this integral is found as follows. We first replace the Bessel functions  $J_0$  and  $Y_0$  by the first terms of their asymptotic expansions. This leads to a Fresnel integral expression for  $\psi$ , whose asymptotic form for large  $x$  yields

$$\psi \sim \frac{cA}{\sqrt{2\pi}(\beta-1)} \frac{(-ie^{\pi i/4} e^{i(\omega t - kx)})}{\sqrt{kx}} \quad (9)$$

From this we find the sound pressure on the landward side ( $x \gg 0$ ) to be

$$|p| = \frac{\rho c A}{(\beta-1)T} \sqrt{\frac{\lambda}{x}}, \quad (10)$$

where  $\lambda$  = wavelength of the atmospheric sound. As before we suppose the water waves to have a period  $T = 2\pi$  sec and  $A = 100$  cm. Then  $\beta = 35$  and  $\lambda = 2130$  m. At a distance  $x = 185$  km from the beach, the sound pressure will be  $2.1$  dyn/cm<sup>2</sup>.

Suppose the wave starts abruptly at the beach  $x = 0$  and travels towards  $x = -\infty$ . We find the sound pressure on the landward side to be almost the same as before; for such a wave the factor  $\beta - 1$  in Eq. (10) above is replaced

by  $\beta + 1$ . Therefore a standing wave caused by reflection of an incoming wave by a beach will also give rise to a radiated sound field.

Since an infinite wave train radiates no sound power, whereas there is radiation by a semi-infinite train stopping abruptly at  $x = 0$ , we can imagine that the radiated power is due to a line source on the beach. The assumption is not strictly correct, but we can use it to estimate the power by means of Eq. (10). For the water waves of the period  $T$  and amplitude  $A$  considered above, we find the radiated sound power to be about 30 kW per kilometer of beach.

#### Radiation by a standing wave

A theory, analogous to the Longuet-Higgins analysis for the generation of microseisms, explains the generation of microbaroms by standing water waves associated with marine storms. The theory is based on the vertical oscillations of the center of gravity of the atmosphere immediately above the standing waves, which might be near a beach as well as out at sea. The frequency of oscillation of the atmosphere's gravitational potential energy is twice that of the ocean waves. The varying potential energy has a radiated sound field associated with it, with sound waves at twice the ocean wave frequency. Full details of the analysis have been given by Posmentier (1967) and by Brekhovskikh (1968).

#### Comparison with observed microbaroms

The foregoing (for waves on a beach) analysis is for the idealized case of straight-line wavefronts of infinite length, the waves being perpendicularly incident on a straight-line beach. But natural beaches are not very straight; the waves arriving at one point might not be coherent with those arriving at a point on the beach a few kilometers away; the strength of the wave can be affected by reflection from the upper atmosphere; etc. The mathematically derived sound field of Eq. (10) can therefore be expected to yield only order-of-magnitude estimates for sound pressures at a large distance from a beach.

Microbaroms have been observed in the Washington area with the infrasonic system described in Section 3. The Atlantic Ocean beach is 185 km east-south-east of the infrasonic station. Generally speaking, the microbarom sound waves come from the east and travel parallel to the earth's surface. They appear at almost all times of the year, and occasionally have sound pressures as great as  $6 \text{ dyn/cm}^2$ . For a typical recording made on March 11, 1961,  $T \approx 5.5$  sec and  $p \approx 1 \text{ dyn/cm}^2$ . On the basis of the analysis given above, microbaroms

## ATMOSPHERIC SOUND PROPAGATION

at Washington could be caused by waves on the Atlantic Ocean beaches ranging in amplitude from about 20 cm to 100 cm.

Fribourg (Switzerland) is about 650 km from the Atlantic Ocean beach on the west coast of France. Microbaroms observed at Fribourg often had daily average sound pressures  $\approx 0.4 \text{ dyn/cm}^2$ . From the above analysis the expected pressure at Fribourg due to ocean waves of  $A = 100 \text{ cm}$  would be  $1.0 \text{ dyn/cm}^2$ . But the sound waves were reported as arriving from a northwest direction. The Atlantic Ocean is about 1500 km away in this direction, beyond north Ireland and Scotland. It seems that the standing-wave hypothesis can account for the microbaroms observed at Fribourg by Saxer and Dessauer.

### 4.5 Subsonic Oscillations

The passage of a jet stream in the atmosphere over the eastern (Atlantic) seaboard of the United States is occasionally accompanied by large oscillations in barometric pressure at infrasonic frequencies. The jet stream is a thin layer of fairly high speed wind. The location of the layer in the atmosphere is in the neighborhood of the tropopause, at an altitude of about 10 km. The thickness of the stream is about three kilometers. The wind speed along the axis is at least 30 m/sec, and sometimes as great as 80 m/sec. The wind blows towards a direction between northeast and southeast, and the width of the stream (in a direction transverse to the direction of flow) is generally at least 100 km.

An important characteristic is that the periods of oscillation are usually greater than the resonant period  $T_R \approx 300 \text{ sec}$  of the atmosphere (see Section 2.4). Since, as we recall, the phase velocities for plane waves of such long periods are substantially less than the high-frequency sound velocity, the waves may be called subsonic oscillations.

The results of observations made at our station in Washington show that almost all sound waves coming from subsonic oscillations of the jet stream have wavefront surfaces of constant phase which are almost plane. The sound pressure has the following features when the jet stream is blowing. (1) The direction of propagation of lines of constant-phase sound pressure across the Washington area is very close to the direction of the jet stream over Washington. (2) The horizontal phase velocity  $c_o = 30 \text{ to } 100 \text{ m/sec}$  is about the same as the speed of the jet. (3) The sound pressures are mainly in the range  $50 - 400 \text{ dyn/cm}^2$ . (4) Periods of oscillation  $T = 300 \text{ to } 1000 \text{ sec}$ .

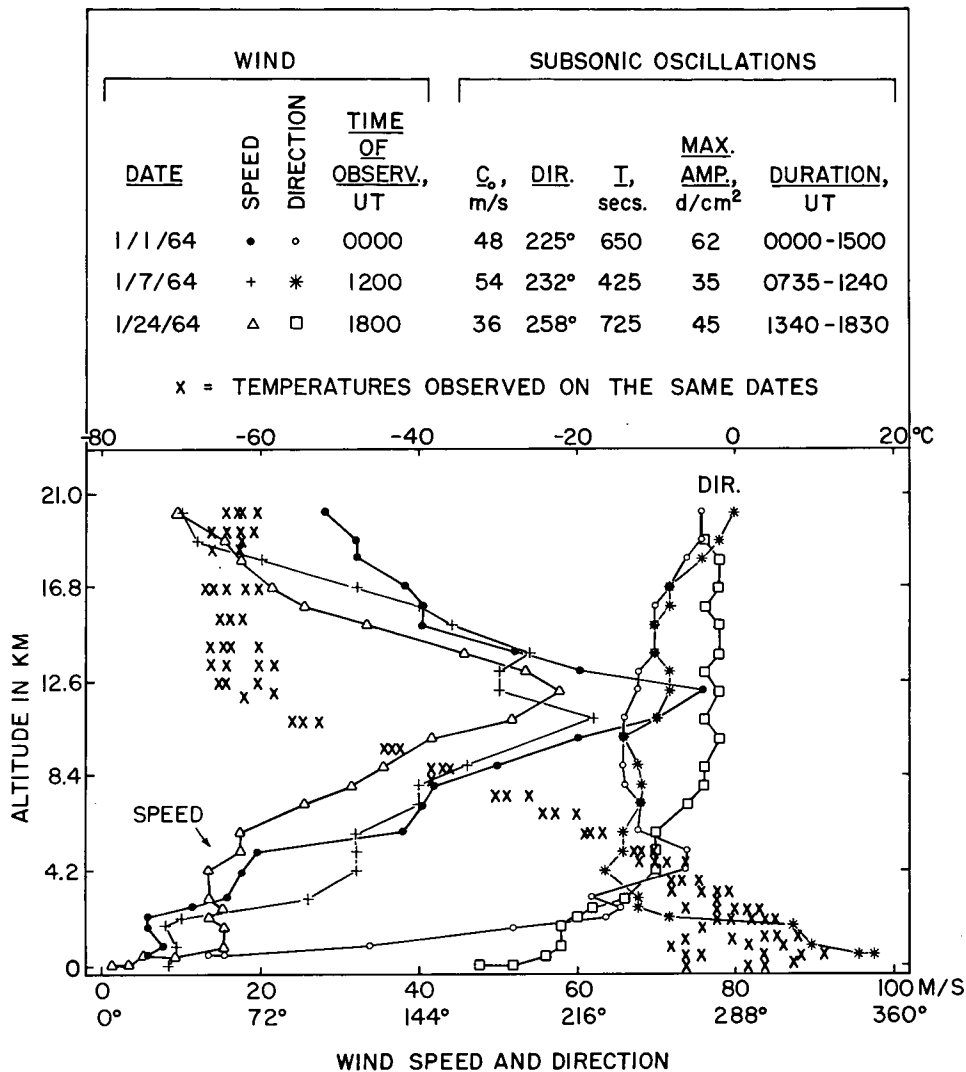


Figure 10. Observations on jet stream oscillations.

A brief summary of a few observations made in Washington is given in Figure 10. The data show the correlations between the features of the sound pressure, and the characteristics of the jet stream causing the sound pressure. The waves observed at the Washington station have been studied in detail by Mary W. Hodge and her associates (1968). Further data on the Washington waves have been summarized by A. J. Bedard, Jr. (1966). Sound pressures caused by the jet stream have been also observed elsewhere; a comprehensive report on waves in the Boston, Massachusetts, area has been prepared by Elizabeth A. Flauraud and her associates (1954).

The sound pressure probably has its origin in flow instability of the jet stream. The mechanism of the instability is not known. We can conjecture

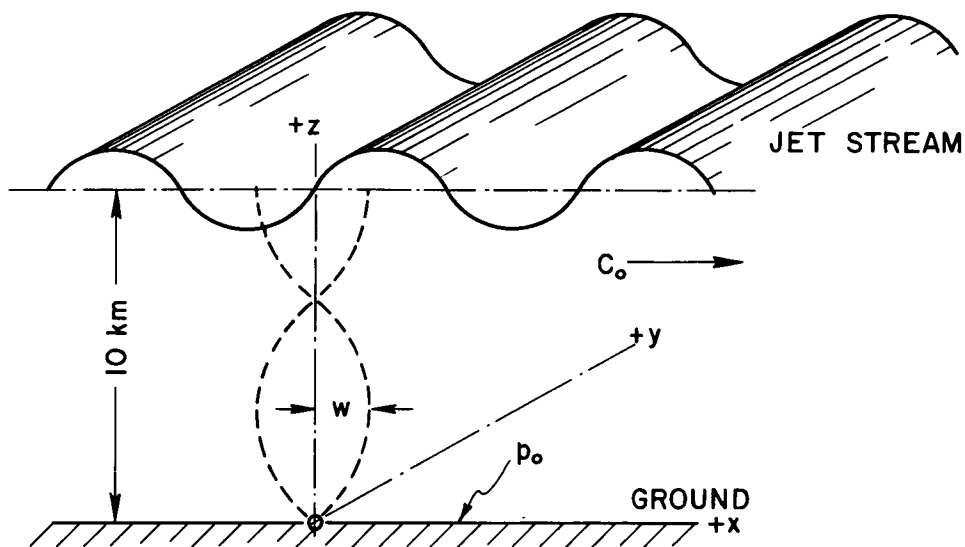


Figure 11. Radiation of sound pressure by jet stream oscillations.  $w$  = vertical component of the atmospheric particle velocity at altitude  $z$ .  $P_0$  = pressure at ground level.

that it arises from a combination of viscous shear between the jet stream and the surrounding atmosphere, and unstable temperature gradients. We assume that the jet stream oscillations force the atmosphere into oscillation. The well-known equations of motion for sound waves in a wind-free atmosphere (see Lamb, 1945) can be used to determine the relationship between the sound pressure measured at the ground and the assumed oscillatory displacement of the jet. The basic idea is that the atmosphere between the oscillating jet stream and the surface of the ground is filled with downward-traveling plane waves, and reflected upward-traveling waves, with both waves having a forward component of phase velocity the same as the speed of the jet stream. Figure 11 is a schematic drawing for the mathematical analysis that has been carried out in detail by Cook (1968), under the following physical assumptions. (1) The atmosphere is isothermal and wind-free. (2) The waves are sinusoidal in time, and all quantities vary like  $\exp(i\omega t)$ . (3) All motions are in the  $x$ - $z$  plane, and so the particle velocity, with components  $u$ ,  $v$ ,  $w$ , has its  $y$ -component  $v \equiv 0$ . (4) The traces of the straight lines of constant-phase sound pressure on the  $x$ - $y$  plane have a phase velocity  $c_0 = \omega/k_0$ , and so all quantities vary as  $\exp(-ik_0 x)$ ; the waves are advancing in the  $(+x)$  direction. The equations of motion finally yield the following expression for the amplitude of the vertical component of particle displacement at the altitude  $z = 10$  km of the jet stream:

$$\Delta z = 2H(k_0^2 - k^2) |P_0| / \beta \gamma B k^2 \quad (11)$$

where  $H$  = scale height of the atmosphere =  $c^2/\gamma g = 8.1$  km for an isothermal atmosphere with  $c = 333$  m/sec. Also  $c = \omega/k$ ,  $\gamma = 1.40$ , and  $\beta$  is a real number for a typical subsonic oscillation. As an example, consider a wave with  $T = 500$  sec,  $c_0 = 33$  m/sec ( $\approx c/10$ ), and  $|P_0| = 200$  dyn/cm<sup>2</sup>. We find  $\Delta z = 60$  m, which must be the jet stream's vertical oscillatory displacement at an altitude of 10 km necessary to produce the measured sound pressure at the ground.

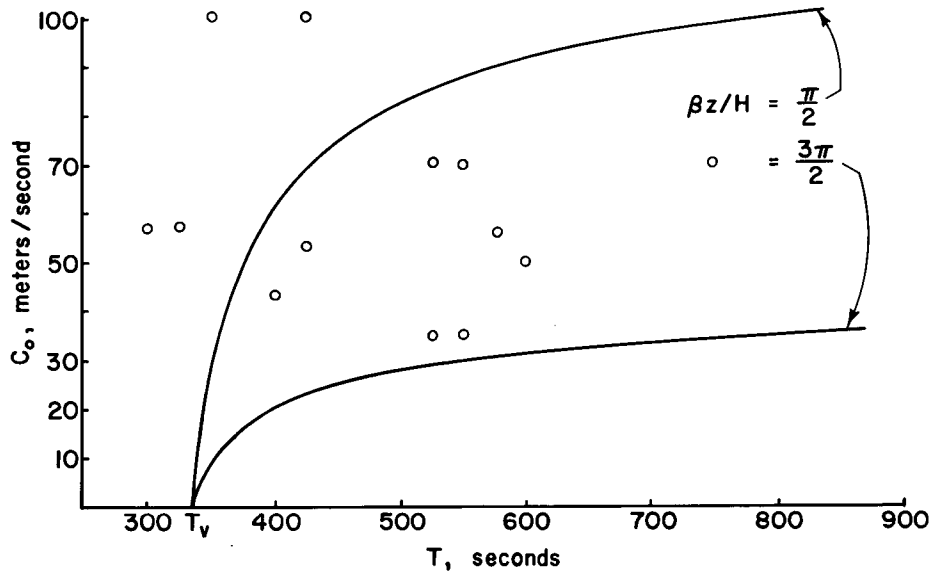


Figure 12. Horizontal phase velocities at various oscillation periods. Solid lines = theoretical velocities.  $\circ$  = observed velocities.

#### Standing-Wave Hypothesis

The mechanism of the oscillation is not known, and there is no obvious limitation on the vertical component  $\beta/H$  of the wave-number vectors. We examine the conjecture that the vertical component  $w$  of the particle velocity (which is zero at the ground) has a maximum at the jet stream's nominal altitude of 10 km (see Figure 11). The analysis shows that this occurs approximately when

$$\beta z/H = \pi/2, 3\pi/2, 5\pi/2, \dots \quad (12)$$

Use of these values for  $\beta$  leads to a series of curves showing how the horizontal trace velocity  $c_0$  varies with the period of oscillation  $T$ . Two of the curves are shown in Figure 12. The curves all start with  $c_0 = 0$  at  $T_v = 337$  sec, this being the Väisälä period of stability oscillations for the isothermal atmosphere ( $c = 333$  m/sec) under consideration. Also plotted are some

## ATMOSPHERIC SOUND PROPAGATION

observed values of horizontal phase velocities corresponding to well-defined periods of oscillation for the jet stream over Washington during January 1964. The data do not seem to confirm the hypothesis of Eq. (12). But gravitational forces evidently play a substantial role in the generation mechanism, since most of the observed oscillations occur at periods greater than the Väisälä  $T_v$ .

### Propagation to the Ionosphere

The displacement and velocity amplitudes in the jet-stream oscillation can be expected to serve as sources for radiation of subsonic wave power upward into the ionosphere. The equations of motion show that the amplitude of the vertical component  $\underline{w}$  of the particle velocity increases exponentially with altitude.

$$|w| = w_j \exp[(z-10)/2H] , \quad (13)$$

where  $w_j = (2\pi/T) \Delta z$  = the amplitude at  $z = 10$  km. For the example given above,  $T = 500$  sec, etc., we find that at an altitude of  $z = 100$  km,  $|w| \approx 100$  m/sec and  $\Delta z \approx 9$  km. This estimate for  $|w|$  is greater than the phase velocity of the wave ( $\approx 30$  m/sec). It appears that subsonic waves traveling upward will probably undergo substantial waveform changes, e.g., taking on a shock-wave configuration, well before reaching the ionosphere.

#### 4.6 Shock Waves from Satellite Entry

The entry of a meteorite, artificial satellite, or other solid object into the upper atmosphere at supersonic speeds will generally produce an acoustical shock wave. Sometimes the shock wave strength is great enough so that it can be measured at an infrasonic station. For example, the entry of the Cosmos 213 rocket body into the atmosphere on April 19, 1968, was accompanied by a Mach cone whose shock wave was observed and measured at ESSA's infrasonic station in Boulder, Colorado. The paper-chart recordings of the shock wave's sound pressure at ground level resembled a single sine wave — a pseudo N-waveform — with a peak-to-peak sound pressure of  $1.2 \text{ dyn/cm}^2$  and a duration of about 2.5 sec. The rocket body passed overhead through the ionosphere near Boulder at an elevation of 112 km, on a path almost parallel to the earth's surface.

The measurement system used at Boulder was the same as that described earlier (see Section 3.1). The band-pass filter was N6 S6 (see Figure 4). But an N-waveform of duration 2.5 sec has a Fourier transform with a substantial spectral density at higher frequencies, outside the N6 S6 "window." In short, the paper-chart recording was that of the N-waveform sound pressure

appreciably modified by the filter.

If an N-waveform is recorded and measured accurately, it can be used to deduce some information about the object producing the wave. For example, one can obtain the altitude of an artificial satellite during atmospheric entry, even if its large Mach number  $\approx 25$  is not accurately known. This is because the shock strength and duration in the so-called far field, at a miss-distance  $h$  (= altitude) moderately large relative to the greatest linear dimension  $l$  of the object, is determined essentially by the following factors: (1) The geometrical size and shape of the object. (2) The ambient atmospheric pressure  $B$  at the altitude of the object. (3) The Mach number  $M$  of its supersonic speed. (4) The miss-distance  $h$ . The pressure jump at the head of the N-waveform is given by

$$\Delta p = B(M^2 - 1)^{1/8} \times (l/h)^{3/4} \times (K_s D/l) \quad , \quad (14)$$

where  $D$  = an equivalent maximum diameter for the object, and  $K_s$  = its aerodynamic shape factor for supersonic speeds. The pressure jump  $\Delta p$  observed will be increased, because of the approximately exponential increase in ambient pressure, by a factor of about  $e^{h/2H}$  when the shock wave propagates down to the ground. It will be increased also by a factor of 2 because of reflection at the ground surface.

#### REFERENCES

- Air Force Cambridge Research Laboratories staff, 1965: Handbook of geophysics and space environments. Published by AFCRL of the U.S. Air Force.
- Bedard, A. J., Jr., 1966: Some observations of traveling atmospheric pressure disturbances. National Bureau of Standards Report No. 9364.
- Brekhovskikh, L. M., 1968: Radiation of infrasound into the atmosphere by ocean waves. Izvestiya Akademii Nauk SSSR, Fizika Atmosfery i Okeana, 4, 444-450.
- Brown, R. F. Jr., 1963: An automatic multichannel correlator. National Bureau of Standards J. Research, 67C, 33-38.
- Chrzanowski, P., G. Greene, K. T. Lemmon, J. M. Young, 1961: Traveling pressure waves associated with geomagnetic activity. J. Geophys. Res., 66, 3727-3733.
- Chrzanowski, P., J. M. Young, G. Greene, K. T. Lemmon, 1962: Infrasonic pressure waves associated with magnetic storms. J. Phys. Soc. of Japan, 17, Suppl. A-2, 9-13.

## ATMOSPHERIC SOUND PROPAGATION

- Cook, R. K., 1965: Radiation of sound by earthquakes. Reports of the 5<sup>e</sup> Congrès International d'Acoustique, Liège, Belgium, Report No. K 19.
- Cook, R. K., J. M. Young, 1962: Strange sounds in the atmosphere. Part 2. Sound, 1, No. 3, 25 - 33.
- Cook, R. K., 1968: Subsonic atmospheric oscillations. Reports of the 6th International Congress on Acoustics, Tokyo, Japan, Report No. H-5-17.
- Daniels, F. B., 1959: Noise-reducing line microphone for frequencies below 1 cps. J. Acoust. Soc. Am., 31, 529 - 531.
- Daniels, F. B., 1962: Generation of infrasound by ocean waves. J. Acoust. Soc. Am., 34, 352 - 353.
- Dessauer, F., W. Graffunder, J. Schaffhauser, 1951: On atmospheric pulsations. Archiv. Meteorol. Geophys. u. Bioklimatol. Series A 3, 453.
- Flauraud, E. A., A. H. Mears, F. A. Crowley, Jr., A. P. Crary, 1954: Investigation of microbarometric oscillations in Eastern Massachusetts. Geophysical Research Papers No. V 27 of the Air Force Cambridge Research Center.
- Goerke, V. H., J. M. Young, R. K. Cook, 1965: Infrasonic observations of the May 16, 1963, volcanic explosion on the Island of Bali. J. Geophys. Res., 70, 6017-6022.
- Gutenberg, B. H., H. Benioff, 1941: Atmospheric pressure waves near Pasadena. Trans. Am. Geophys. Union, 22, 424-426.
- Hodge, M. W., D. T. Volz, 1968: Possible relation of mesoscale surface pressure waves to the jet stream region and to clear air turbulence. Third Nat. Conf. on Aerospace Meteor., 557-563.
- Lamb, H., Hydrodynamics. Dover Publications, New York (1945)
- Matheson, H., 1966: A nomogram for determining azimuth and horizontal trace velocity from tripartite measurements. Earthquake Notes, 37, 33-37.
- Passechnik, I. P., 1959: Seismic and airwaves which arose during an eruption of the volcano Bezmyanny, on March 30, 1956. Bull. Acad. Sci. USSR, Geophys. Ser., (English trans.) No. 9, 650-653.
- Posmentier, E. S., 1967: A theory of microbaroms. Geophys. J. Roy. Astr. Soc., 13, 487-501.
- Rayleigh, 1945: Theory of Sound, Vol. II, page 36. Dover Publications, New York.
- Saxer, L., 1945: Electrical measurement of small atmospheric pressure oscillations. Helv. Phys. Acta., 18, 527.

- Saxer, L., 1953-1954: Archiv. Meteorol. Geophys. u. Bioklimatol. Series A 6, 451-463.
- U. S. Standard Atmosphere, 1962. Published by NASA, U. S. Air Force, and U. S. Weather Bureau.
- Webb, W. L., 1964: Stratospheric solar response. J. Atmospheric Sci., 21.
- Wilson, C. R., S. Nichparenko, R. B. Forbes, 1966: Evidence of two sound channels in the polar atmosphere from infrasonic observations of the eruption of an Alaskan volcano. Nature, 211, 163-165.
- Wilson, C. R., S. Nichparenko, 1967a: Infrasonic waves and auroral activity. Nature, 214, 1299-1302.
- Wilson, C. R., 1967b: Infrasonic pressure waves from the aurora: a shock wave model. Nature, 216, 131-133.

N72-25386

PRECEDING PAGE BLANK NOT FILMED

VERTICAL PROFILES OF WIND AND TEMPERATURE BY  
REMOTE ACOUSTICAL SOUNDING

Herbert L. Fox

Bolt Beranek and Newman Inc.

ABSTRACT

Sound generated at the earth's surface is refracted in the atmosphere as a consequence of the variation with altitude of the wind and temperature. The sound which is refracted back to the earth can be used to obtain information on the vertical profiles of wind and temperature. The spatial distribution of refracted intensity does not appear to be a sufficiently accurate indicator of the vertical profiles, but adequate definition and detail appear to be obtainable by processing transit times from a multiplicity of receivers. We report the current state of an analytical study of the feasibility of such a method of remote probing of the atmosphere.

1. INTRODUCTION

We are investigating an acoustical method for obtaining meteorological soundings that is based on the refraction due to the vertical variation of wind and temperature. The method has the potential of yielding horizontally averaged measurements of the vertical variation of wind and temperature up to heights of a few kilometers; the averaging takes place over a radius of 10 to 15 km.

The investigation is a modest feasibility study which we hope to follow with an experimental program. The results thus far are very encouraging. We report here an outline of the basic concepts and some of the results that we have already obtained.

## 2. ACOUSTICAL SOUNDING

The velocity of sound in still air depends on the sonic temperature (a weighted linear combination of the virtual and absolute temperature). When the sound travels in moving air the motion of the air in the direction of the propagation must be added to the proper velocity of sound. Hence, if an acoustic signal propagates through a parcel of air in which the temperature or wind are not homogeneous, the sound is refracted. As a direct consequence of the atmosphere having its principal variation of temperature and wind in the vertical direction, sound traveling obliquely with respect to the earth tends to be refracted downward or upward depending on whether the effective sound velocity (the proper sound velocity added to the wind in the direction of propagation) is greater or lesser aloft.\* An example of how sound, propagating along a given azimuth, is refracted is shown in Figure 1. Two measurable characteristics of the sound refracted to the ground that relate to the vertical variation of the wind and temperature are (1) the acoustical intensity at a point on the ground and (2) the time required for signals to traverse the distance from source to receiver.

### 2.1 Previous Investigations

The distribution of intensity on the ground is strongly influenced by a variety of effects other than refraction. Ingard (1953) showed how temperature fluctuations, propagation into the shadow zone, attenuation in a humid atmosphere, ground absorption and turbulent scattering influence the intensity distribution. Buell (1966) examined the short- and long-term variation of meteorological parameters and showed the unreliability of estimates of sound intensity based on the wind and temperature profiles. Thus we conclude that the distribution of acoustic intensity on the ground can only be used qualitatively. The qualitative use of intensity distributions to investigate the diurnal variation of an upper channel wind was reported to this panel by Posmentier of Lamont. For detailed quantitative profile determination we have turned to using measurements of time of arrival at arrays of receivers.

Fox (1966) found that sound-ranging data in the form of time differences between signals received at an array of microphones could be used not only for determining target locations but also to estimate winds and temperatures. The altitudes and the ranges involved in that investigation are similar to those in the present study; however earlier workers had used similar techniques for high altitude studies. Whipple (1935) attempted an experimental determination of temperature profiles up to 60 km. He measured the total

---

\*Except where indicated otherwise, we appropriately use geometrical acoustics.

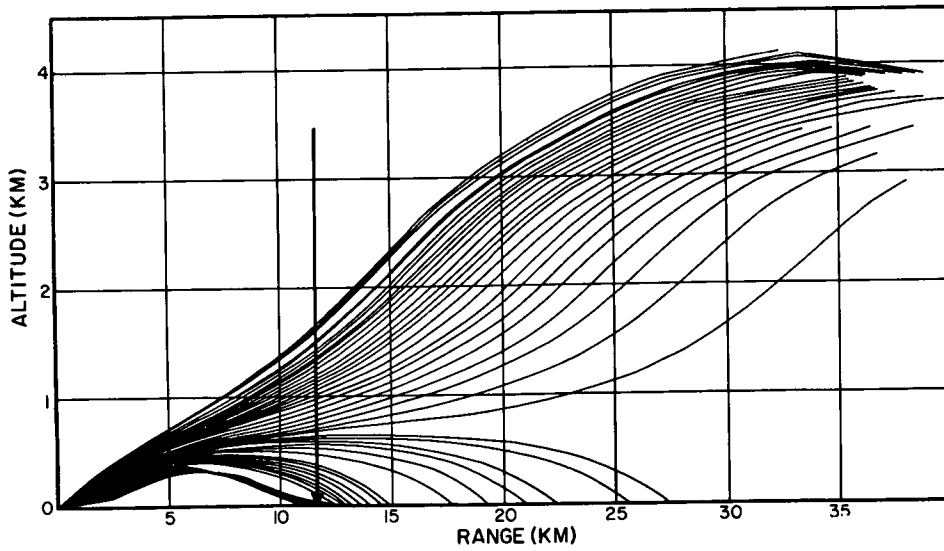
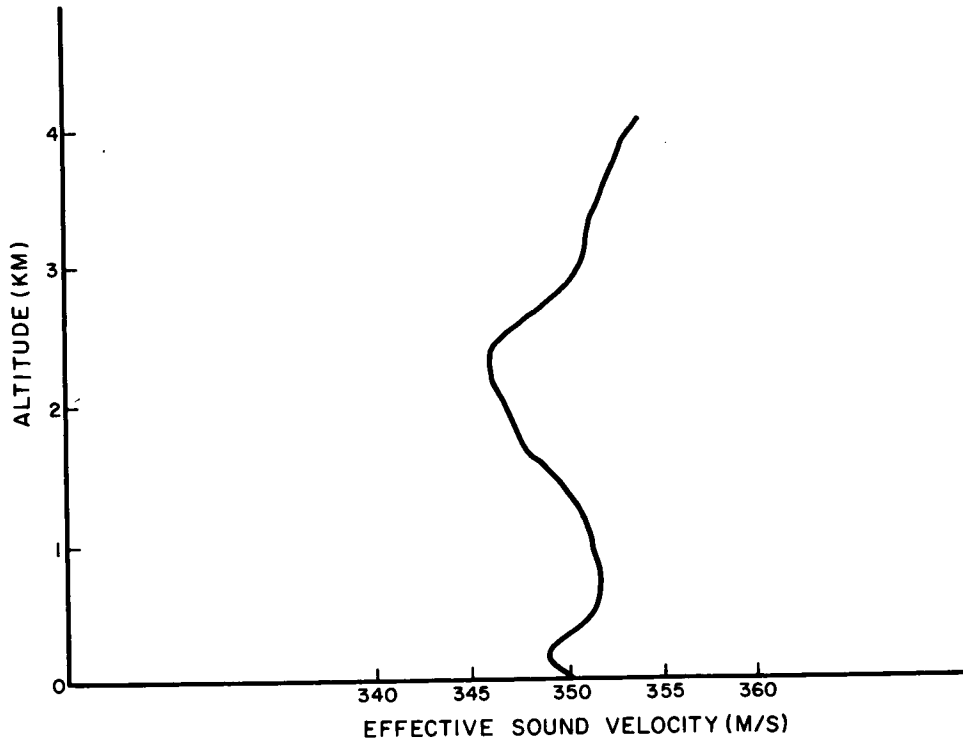


Figure 1. Principal ray bundles created by refraction related to profile above.

transit time and the angle of descent of the sound rays along a single azimuth at ranges up to several hundred kilometers. Using balloon data up to 20 km and neglecting winds entirely he assumed that the temperature profile above 20 km consisted of an isothermal layer above which there was a constant positive-gradient layer. He used the sound data to match the parameters of his model and thereby determined that the isotherm extended to about 40 km and that the temperature of the next layer matches the ground temperature at a height of about 60 km. Subsequently, Gutenberg (1939) and Cox (1945) used Whipple's technique.

The first attempt at using an acoustical method to obtain both wind and temperature aloft appears to be that of Crary (1950). For acoustic sources he used detonations (200 and 500 pound bombs). He measured the time of arrival and the angle of descent of the sound signals on several azimuths up to ranges of several hundred kilometers. As with the previous investigators he used the known profile up to 20 km but above that he assumed a profile consisting of a negative-slope layer followed by a positive-slope layer. He was not able to make a unique determination; however, by correlating with other data and using a least-squares method, he was able to obtain estimates of the temperature and wind profiles. His method was subsequently used by Richardson and Kennedy (1952) to obtain wind and temperature profiles in the upper atmosphere over Colorado and by Johnson and Hale (1953) to measure the upper atmosphere over Arizona. The importance of measurements of time intervals between multiple arrivals was emphasized in an experimental program carried out by Rothwell (1966). He used shells exploded at various altitudes and a ground-based gun.

## 2.2 The Basic Theory

To determine the vertical profiles of effective sound velocity along a given azimuth, we require several arrays of receivers located along the azimuth. Three parameters can be determined by each array: (1) the time of arrival of the acoustic signals at the array\*, (2) the angle of descent of the acoustic ray as it crosses the array (for a horizontally uniform atmosphere this is the angle of elevation of the ray as it leaves the source), and (3) the ratio of the effective sound velocity at any height to the cosine of the angle of elevation of the ray trajectory at that height (a constant of the motion by Snell's law). Detailed derivations of these quantities and the relationships between them and the parameters of the profile are presented in Lukes (1942). From the basic equations one can systematically determine parameters for an assumed form of the effective sound - velocity profile. To extract the wind and temperature the effective sound velocity is

---

\*We assume that the sound source is controlled by the experimenters and thus it is possible to measure the times of transit from the sound source to the receiver and not just times differences between sets of receivers. This is not however restrictive. Our results are adaptable to time-difference data.

required for at least three azimuths in order to separately determine the wind speed, wind azimuth, and temperature. However more than three azimuths can be used with a least-mean-squares technique.

### 3. PRELIMINARY RESULTS

Figure 2 presents results obtained when we assume that the effective sound velocity profile can be described by two layers. We used synthetic acoustic data that was generated assuming the profile of four layers shown in the figure. Our scheme also produces estimates of the precision with which the calculated profile matches the actual profile. More-complex models than the two-layer profile are presently being investigated.

A problem of extreme importance is the question of the likelihood of receiving acoustic energy at the surface. To examine this question and to determine an optimum microphone configuration we calculated the intensity distribution that would have occurred on four occasions where the profiles were characteristic of those that are important in air pollution. The predicted zones of refracted sound are shown in Figure 3. On the basis of these data we have established the distribution of arrays illustrated in Figure 4. Here we assume the sound source to be at the center. Each dot represents an array. An array consists of at least three receivers; two on the ground along the azimuth and one elevated. The actual spacing between the receivers will be determined by the spectrum of the sound source. Presently we envision using a low-frequency to subsonic impulsive source which will be masked by nearby background noise, but which will be effective in the acoustical sounding technique.

### 4. RECOMMENDATIONS AND CONCLUSIONS

#### 4.1 Continuing Studies

Using the profiles referred to in Figure 3, we are simulating the data that would be obtained by arrays placed as shown in Figure 4. The calculated vertical profiles of wind and temperature are then to be compared with the available balloon soundings.

We are investigating the effect of fluctuations, that is, horizontal and temporal inhomogeneities. The technique should be effective, in spite of the fluctuations, because of our averaging procedures.

# REMOTE ACOUSTICAL SOUNDING

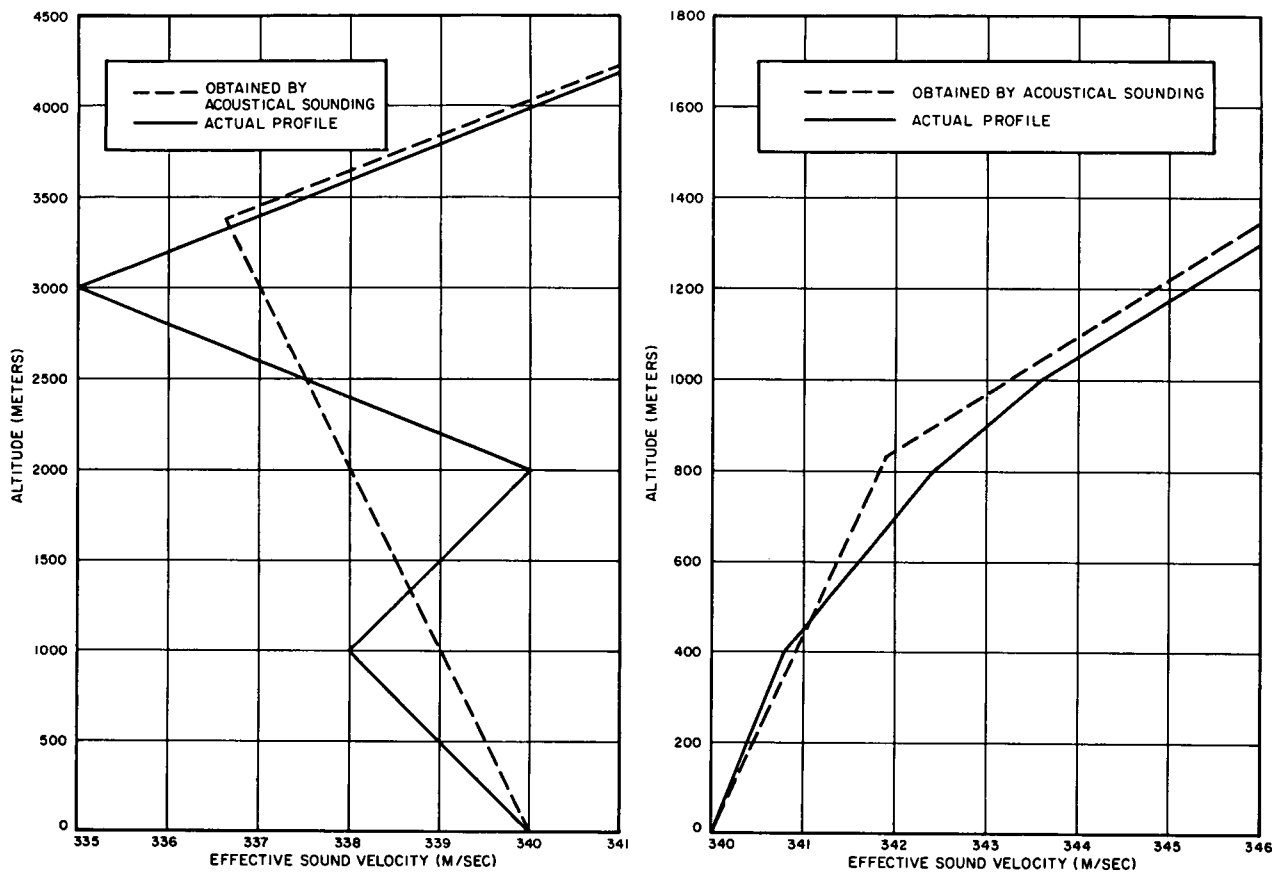
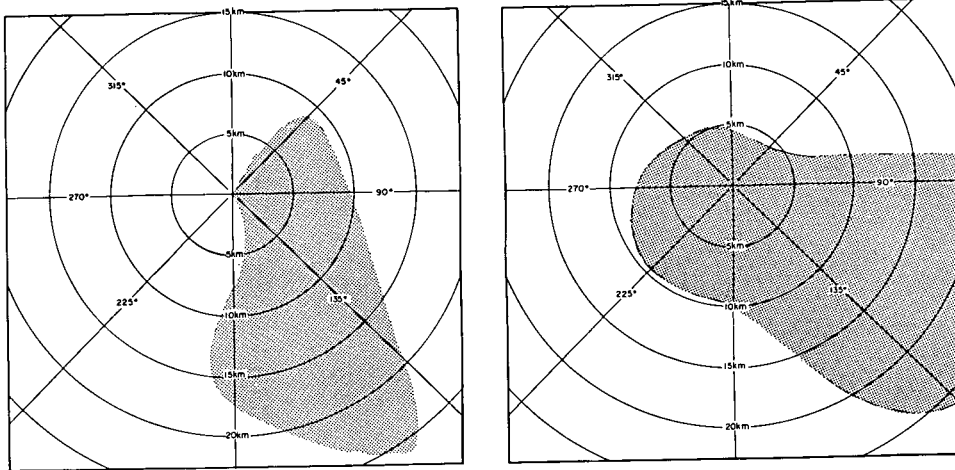


Figure 2. Examples of two layer profile obtained when actual profile has four layers.

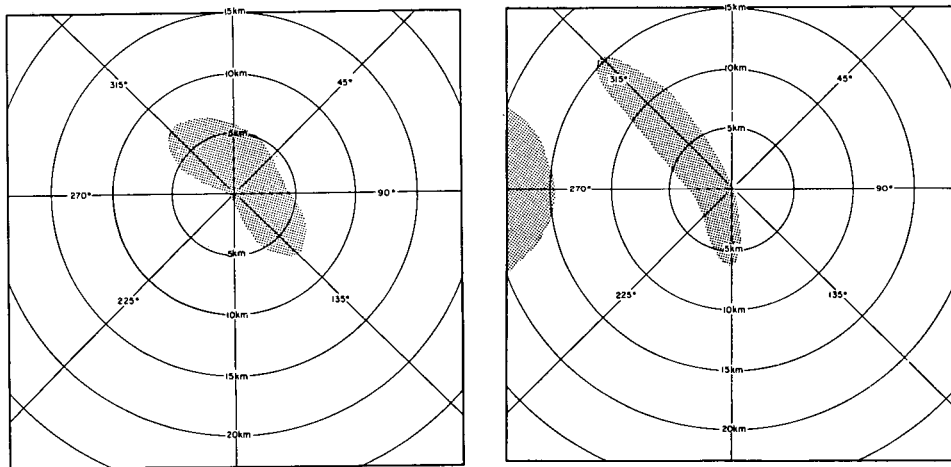


Dayton, Ohio

August 9, 1967

Dayton, Ohio

September 12, 1967



Dayton, Ohio

October 2, 1967

J. F. K.

November 22, 1967

Figure 3. Zone of refracted sound from a point source.

REMOTE ACOUSTICAL SOUNDING

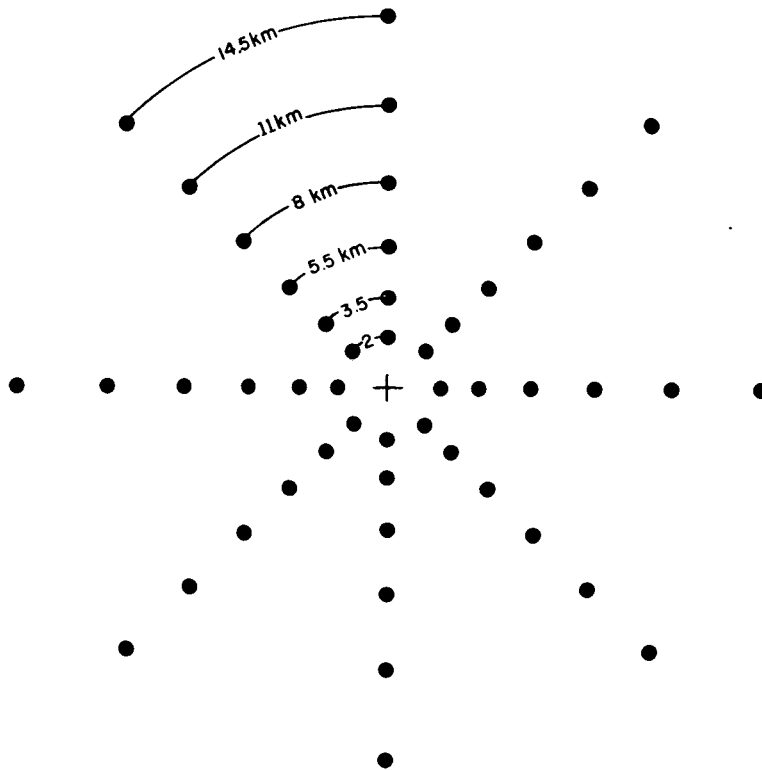


Figure 4. Proposed distribution of arrays.

## 4.2 Future Studies

We advise an experimental program to compare acoustical soundings with balloon soundings. The problems of scattering by large objects on the ground and of secondary sources of sound can be studied separately from the basic problem of how accurately one can assess the vertical variation of wind and temperature by acoustical methods if we use a region free of large buildings and secondary sound sources. Further experiments should then be conducted in the more troublesome environment of a city.

ACKNOWLEDGEMENTS: Much of the work in the present investigation has been performed by R. Abilock of our staff. The project is funded by the National Center for Air Pollution Control of the Public Health Service. Mr. Charles Hosler is the project officer.

## REFERENCES

- Buell, C. E., 1966: Variability of Sound Propagation Prediction Due to Atmospheric Variability. NASA CR-61160.
- Cox, E. F., 1949: Upper Atmosphere Temperatures from Helgoland Big Bang. J. Of Meteor., 6, 300.
- Crary, A. P., 1950: Stratosphere Winds and Temperatures from Acoustical Propagation Studies. J. of Meteor., 7, 233.
- Fox, H. L., 1966: Meteorological Techniques for Sound Ranging: Conceptual Basis. U. S. Army ECOM-00151-4.
- Gutenberg, B., 1939: The Velocity of Sound Waves and the Temperature in the Stratosphere in Southern California. Bull. Amer. Meteor. Soc., 20, 192.
- Ingard, U., 1953: The Physics of Outdoor Sound. Proc. Nat. Noise Abatement Symposium, 4, 11.
- Johnson, C. T. and Hale, F. E., 1953: Abnormal Sound Propagation Over the Southwestern United States. JASA, 25, 642.
- Lukes, G. D., 1942: Sound Ranging for Artillery. (Vol. I and II) U. S. Army SCL Eng. Report No. 753.
- Richardson, J. M., and Kennedy, W. B., 1952: Atmospheric Winds and Temperatures to 50-Kilometers Altitude as Determined by Acoustical Propagation Studies. JASA, 24, 731.
- Rothwell, P., 1956: Sound Propagation in the Lower Atmosphere. JASA, 28, 656.
- Whipple, F. J. W., 1935: The Propagation of Sound to Great Distances. Quart. J. of Roy. Meteor. Soc., 61, 285.

PRECEDING PAGE BLANK NOT FILMED

PROBING THE ATMOSPHERE WITH INFRASOUND<sup>1</sup>

Eric S. Posmentier<sup>2</sup> and William L. Donn

Lamont Geological Observatory  
Columbia University

#### ABSTRACT

Recent studies of atmospheric infrasound at Lamont Geological Observatory have contributed to our knowledge of atmospheric structure and have established the practicality of infrasonic techniques for probing the atmosphere to heights of 120 km or more. Temporal variations of the amplitude of continuously generated natural infrasound of 0.1 - 0.4 Hz (microbaroms) provide information about wind variations in the E-layer, including atmospheric tidal winds. Infrasound in the same frequency range produced by space-launch rockets yields further data on upper atmospheric structure. The dispersion of longer-period explosions is an additional source of information about temperatures and winds to high altitudes.

#### INTRODUCTION

The effects of the temperature and wind-stratification of the atmosphere on low frequency acoustic waves are regional focusing and defocusing, and geometric dispersion. Conversely, spatial variations of sound intensity, or velocity dispersion of waves from impulsive sources, can both provide information about atmospheric structure. Sound is thus a useful tool for probing the atmosphere. Infrasound (sound below audible frequencies), because of its ability to propagate long distances without attenuation through the upper atmosphere, has proven particularly useful for such atmospheric investigations.

For each class of infrasound used to probe the atmosphere, an appropriate theory of propagation must be developed. The atmosphere's structure may then be surmised, through the theory, from observed propagation characteristics. The purpose of this

1. Lamont Geological Observatory (Columbia Univ.) Contribution No. 1245
2. Now at New York University, Dept. of Meteorology and Oceanography.

## PROBING THE ATMOSPHERE WITH INFRASOUND

paper is to review such observations of a few types of infrasound, the theories used to account for the propagation of infrasound, and the deduced atmospheric structures.

### 2. MICROBAROMS

Microbaroms are atmospheric acoustic waves associated with marine storms; they have periods of 2.5 - 10 sec and amplitudes of a few microbars (dynes/cm<sup>2</sup>). They were first reported by Benioff and Gutenberg (1939). More recently, Donn and Posmentier (1967) reported their observations of concurrent high activity of both microbaroms and microseisms (background seismic motion in the same frequency band as microbaroms). They concluded that both microbaroms and microseisms had been generated by ocean waves in a marine storm, by a common mechanism which determined their identical spectral characteristics. Posmentier (1968a) proposed that microbaroms are generated by interfering waves in storm areas, by a mechanism similar to that suggested by Longuet-Higgins (1950) for the generation of microseisms. The validity of this explanation is confirmed by a more recent study of several months of microbarom/microseism ocean wave data (Posmentier and Donn, 1968).

Microbaroms are applicable to the problem of acoustic probing of the atmosphere through the study of their long-range propagation. Time variations of microbaroms received from a continuous source have already led to an independent confirmation of semidiurnal atmospheric tidal winds above 100 km. Figure 1 shows a cross-section of a 24-hour seismic-type drum record of infrasound. There is an apparent semi-diurnal variation of the amplitude of the infrasound, which has been identified as microbaroms from a source to the northeast of the detector array in Palisades, New York. Donn (1968) suggested that semidiurnal tidal winds in the upper atmosphere caused these amplitude variations. This explanation requires that the phase of the semidiurnal amplitude variations depend on the direction of the source. Such a dependence has been confirmed by measuring the phases of the amplitude variations of microbaroms from sources whose directions span three quadrants, and by comparing the phases with those predicted by the ray theory of sound propagation in a time-varying wind-and-temperature-stratified atmosphere (Posmentier, 1968b)

By applying the ray theory of sound propagation to microbaroms in a wind-and-temperature-stratified model atmosphere including both ambient and semidiurnally varying winds, it is possible to test the model's adequacy in explaining observed microbarom amplitude variations. Table I describes such a model atmosphere which represents a consensus among several observations and theories of atmospheric circulation (both ambient and tidal) and temperature structure.

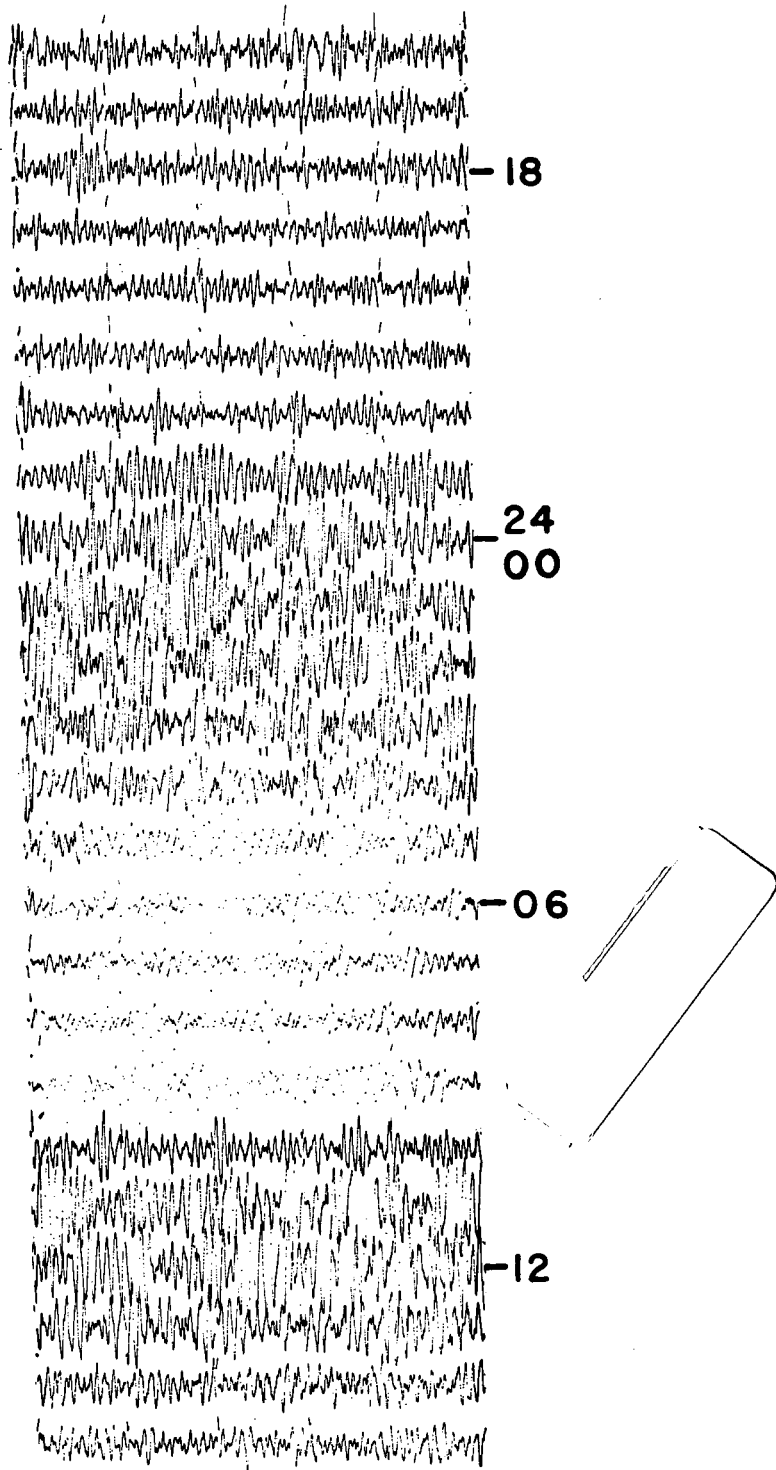


Figure 1. Cross section of a drum record of microbaroms, showing a 5-minute signal sample every hour. Time is indicated in EST

PROBING THE ATMOSPHERE WITH INFRASOUND

TABLE I

<u>Z</u>	<u>T</u>	<u>U</u>	<u>V<sub>w</sub></u>	<u>P<sub>w</sub></u>	<u>V<sub>s</sub></u>	<u>P<sub>s</sub></u>
0	275	2	0.1	1.00	0.1	10.0
10	215	39	0.2	1.00	0.2	10.0
25	215	10	0.6	1.00	0.6	10.0
30	215	21	0.7	1.00	0.7	10.0
40	240	43	1.0	7.00	1.0	4.00
50	265	65	2.5	7.00	3.2	4.00
65	283	41	5.0	7.00	6.6	4.00
80	200	16	7.5	7.00	10.0	4.00
90	200	10	11.0	7.00	15.0	4.00
100	200	-10	15.0	7.00	20.0	4.00
105	237	-15	19.4	6.25	25.0	3.25
120	350	0	30.0	4.00	40.0	1.00

---

Z Altitude, km

T Temperature, °K

U Ambient westerly wind speed, mps. (Ambient northerly winds are sufficiently small to be neglected here).

V<sub>w</sub> Speed of semidiurnal component of westerly wind, mps.

P<sub>w</sub> Local time at which semidiurnal component of westerly wind increases through zero.

V<sub>s</sub> Speed of semidiurnal component of northerly wind, mps.

P<sub>s</sub> Local time at which semidiurnal component of northerly wind increases through zero.

This table applies to winter months at  $45^{\circ}\text{N}$ . Sources of the observations and theories used to form this model are Murgatroyd (1956), Batten (1961), Stolov (1955), Kantor and Cole (1964), Manring, et. al., (1964), and reviews by Khvostikov (1964) and Craig (1965).

Assuming that wind speeds and temperatures vary linearly between the altitudes specified in Table I, ray paths representing propagation from the northeast at  $1\frac{1}{2}$  hour intervals were computed based on Fermat's principle. The results indeed show that optimum and minimum conditions for propagation from the northeast exist at six hour intervals, at 1030 or 2230, and 0430 or 1630 local time, respectively (Figs. 2 and 3) in approximate agreement with observations exemplified by Fig. 1.

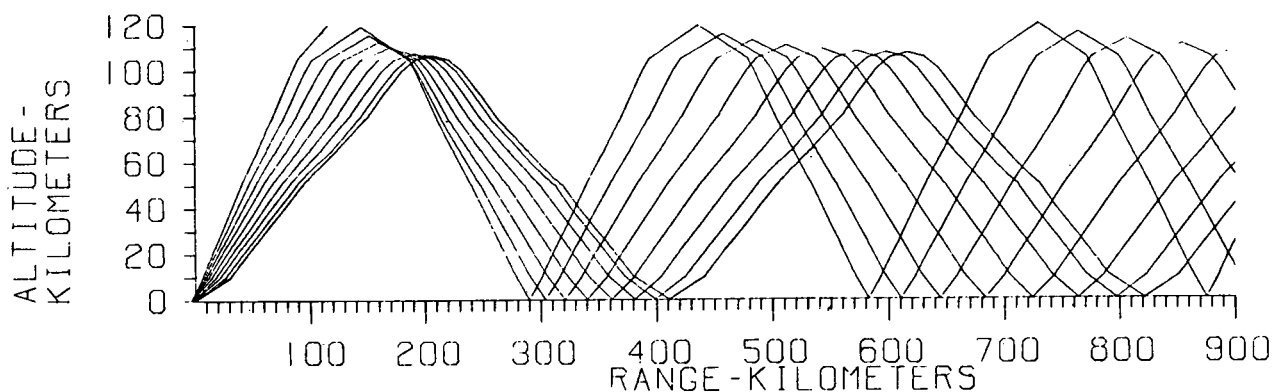


Figure 2. Ray tracing at 1030 (or 2230) local time, showing rays with initial elevation angles of  $0^{\circ}$  through  $40^{\circ}$  inclusive.

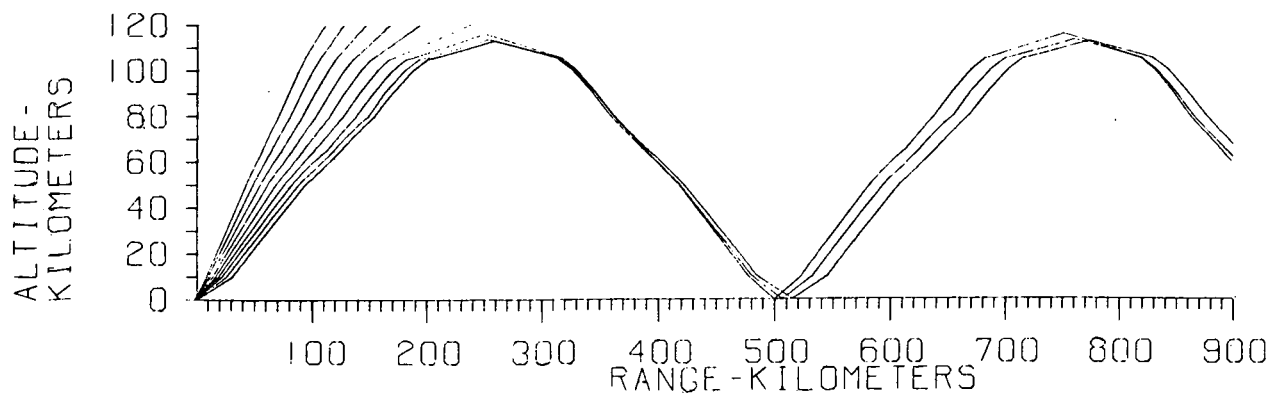


Figure 3. Same as Figure 2, for 0430 (or 1630) local time.

Through the ray theory of acoustic propagation, it is thus possible to conclude that the atmospheric model used here can account for observed time variations of sound propagation through the atmosphere. A more detailed experimental and theoretical study should lead to the refinement of our present knowledge of upper atmospheric motions.

## PROBING THE ATMOSPHERE WITH INFRASOUND

### 3. INFRASOUND FROM ROCKETS

Artificially produced infrasound opens further possibilities for probing the upper atmosphere. Rockets, for example, are small sources of infrasound which follow known trajectories at known times, in contrast with natural infrasound such as microbaroms, which are generated continuously over large areas. Artificial infrasound thus offers the advantage of known sources, but has the difficulty that large rockets and bombs are programmed primarily for reasons other than the acoustic probing of the atmosphere.

Infrasound produced by Scout, Atlas, Agena, and Saturn rockets have been observed at ranges exceeding 1000 miles by Fehr (1967) and Donn et al., (1968). The sources of the infrasound may be rocket ignition, ballistic energy, and possibly rocket exhaust during flight. Generation and propagation above the E-layer of infrasound of a few seconds period have been documented.

The effect of the stratification of the atmosphere on the propagation of acoustic signals from rockets is quite significant causing regions of focusing and de-focusing on the ground, and alternately preventing and enhancing the return of acoustic energy to the ground from the rocket as it travels upward through sound channels. Conversely, a knowledge of time and distance variations of the acoustic signal from a rocket can be used to infer the temperature and wind structure of the propagating medium. Bushman and Smith (1966) have computed wind profiles up to 85 km, based on acoustic data from a Saturn rocket flight.

### 4. ACOUSTIC-GRAVITY WAVES FROM NUCLEAR EXPLOSIONS

Nuclear explosions in the atmosphere have provided a powerful tool for the study of the propagation of acoustic-gravity waves in the atmosphere and of the coupling between the neutral atmosphere and the ionosphere.

Most of the experimental study of waves generated by nuclear tests has been by means of surface pressure sensors which detect the passage of acoustic-gravity waves. For the largest explosions, these waves have been detected after several circuits of the earth.

The property of acoustic-gravity waves of greatest value is that of wave dispersion. This is a systematic dependence of group velocity on wave period. On records of pressure perturbation related to acoustic-gravity waves dispersion is indicated by a wave train showing period decreasing with time (normal dispersion) or increasing with time (inverse dispersion). When group velocity is plotted against period, a group velocity dispersion curve is obtained whose shape and position depends on the appropriate propagation parameters of the atmosphere, the

most important of which are temperature and wind. In order to determine the structure of the atmosphere along the path of wave propagation, an empirically determined dispersion curve is compared with curves determined theoretically from a variety of atmosphere models. Presumably, the model providing the best fit between theory and observation is most indicative of the atmosphere along the wave path. However, some ambiguity exists in the results that can be obtained from the choice of models.

Analysis of records of acoustic-gravity waves as well as theoretical solutions indicate that the wave trains are normally composed of a number of modes. Following the classification of Pfeffer (1963) we identify them as the fundamental, acoustic or gravity modes. The acoustic modes are those which disappear when the medium is assumed to be incompressible. Gravity modes disappear when the acceleration of gravity is assumed to be zero.

In general, theoretical resolution of modes exceeds that of experimental analysis. At Lamont we have obtained the best analysis by making a "running" Fourier amplitude analysis of successive overlapping sections of the signal, as described by Balachandran and Donn (1968).

Theoretical group velocity dispersion curves for acoustic-gravity waves were determined through the application of the method developed initially in the study of seismic surface waves. Our best results were obtained by the application of normal mode theory to the propagation of waves in a multi-layer model of the atmosphere. In the model, temperature and wind are held constant in each unit layer, but with the necessary difference from layer to layer to define the temperature and wind gradients used. A complete statement of the theory is given by Balachandran (1968) and summarized with results by Balachandran and Donn (1968)

The kind of comparison obtained between theory and observations for the Soviet nuclear test of August 5, 1962, is indicated in Fig. 4.

In the generalization of the theoretical dispersion curves, the vertical temperature profile was taken from the COSPAR model atmosphere to an elevation of 300 km. Winds included in the model were adequate to generate the necessary theoretical curves. In general, the theory of Balachandran (1968) appears capable of explaining most of the features of acoustic-gravity waves observed at the ground.

In summary of the comparison of theory with observations, the main features of acoustic-gravity waves up to a period of about 400 miles can be explained by an atmospheric model with only one (lower) temperature sound channel, and related winds. The upper, second sound channel must be included to explain waves of periods greater than 400 sec. Inverse dispersion of

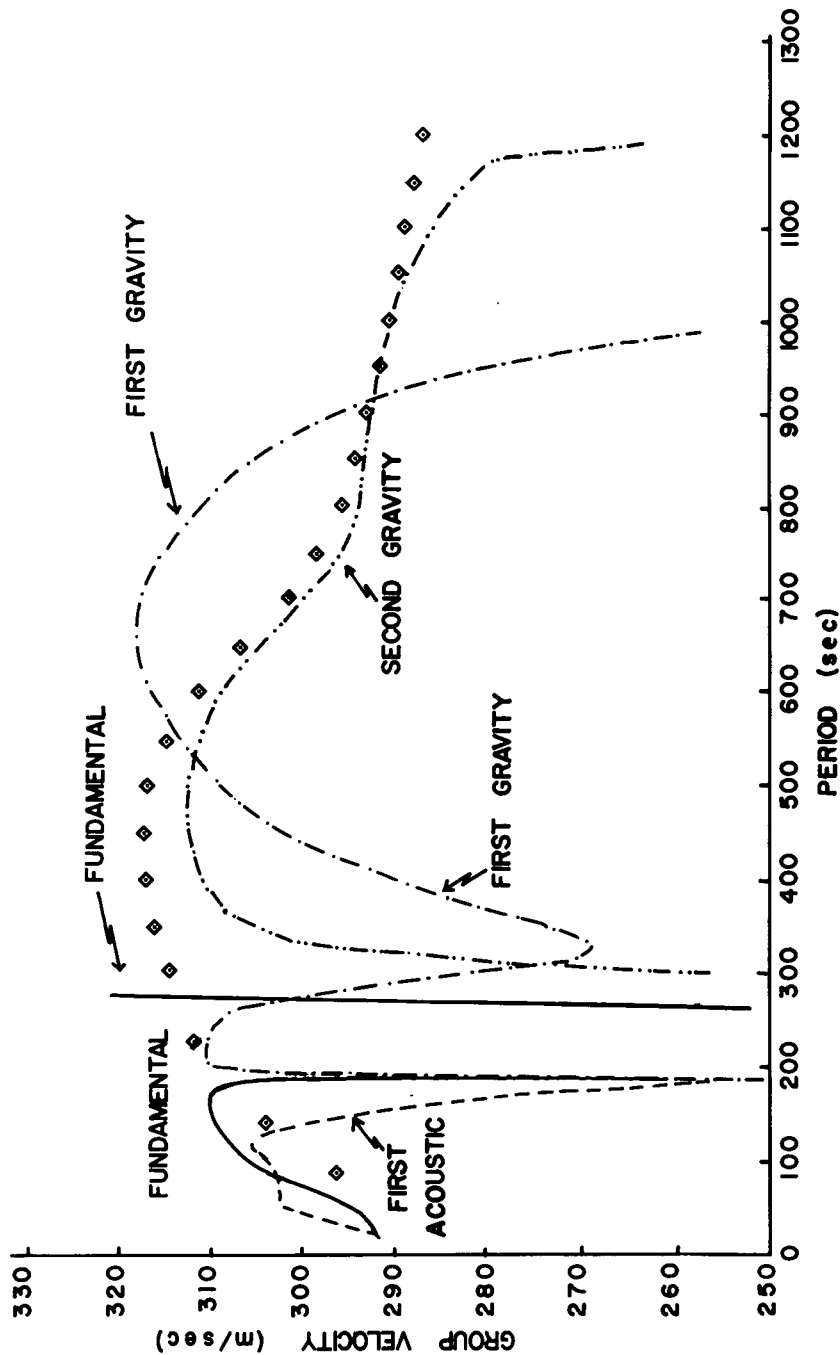


Figure 4. Comparison of empirical dispersion (points) with theoretical acoustic-gravity waves for the Soviet explosion of August 5, 1962. (from Balachandran and Donn, 1968)

long period waves are produced by high positive winds in the upper sound channel (at about 100 km) or by high negative winds in the bottom part of the lower sound channel.

Davies and Baker (1966) reported observations of unexplained ionospheric disturbances soon after the times of nuclear explosions. Following publication of the comprehensive report on atmospheric waves from nuclear explosions by Donn and Shaw (1967), Baker (1968) recognized that the ionosphere disturbances were produced by the passage of acoustic-gravity waves from nuclear explosions. Balachandran and Donn (1968) then subjected Doppler-sonde signals from Boulder, Colorado and pressure signals from Berkley, California, and Poughkeepsie, New York from the nuclear explosion of October 30, 1962 to running spectrum analysis. Results should show strikingly similar dispersion patterns for both surface pressure and ionospheric signals. The study of this coupling effect is continuing.

## 5. CONCLUDING REMARKS

Research in atmospheric acoustics has advanced a great deal in recent years, contributing to our knowledge of the generation and propagation of low-frequency pressure disturbances in the atmosphere, and of the structure of the atmosphere. Of the many developing methods of acoustic probing of the atmosphere discussed in this paper and by other panel members, several offer great potential. In order that the continuing efforts in this branch of geophysics be most fruitful, it is necessary that gains thus far achieved be consolidated, and that future work be done with a minimum of duplication and a maximum of cooperation.

Continuing research in atmospheric acoustics will undoubtedly make many valuable contributions to our knowledge of general and day to day atmospheric structure and motions.

## ACKNOWLEDGEMENTS

The research described in this report was supported by the National Science Foundation and the U.S. Army Research Office Durham under NSF GA 1333 and AROD DAH C04-67C- 0037 respectively.

REFERENCES

- Baker, D. 1968: Acoustic waves in the ionosphere following nuclear explosions. Proceedings Symposium on Acoustic-Gravity Waves, Boulder, Colorado. (in press)
- Balachandran, N.K., 1968: Acoustic-gravity wave propagation in a temperature-wind-stratified atmosphere. J. Atmos. Sci., 25, 5.
- Balachandran, N.K. and W.L. Donn, 1968: Dispersion of acoustic-gravity waves in the atmosphere. Proceedings Symposium on Acoustic-Gravity Waves, Boulder, Colorado. (in press).
- Batten, E.S., 1961: Wind systems in the mesosphere and lower ionosphere, J. Meteorology., 18, 283.
- Benioff, H. and B. Gutenberg, 1939: Waves and currents recorded by electromagnetic barographs, Bull. Am. Met. Soc., 20, 421.
- Bushman, W.W. and O.E. Smith, 1966: An acoustic wind measuring technique. Paper presented at AIAA, Fourth Aerospace Sciences Meeting, Los Angeles, California, June 27-29, 1966.
- Craig, R.A., 1965: The Upper Atmosphere, Academic Press, New York.
- Davies, K. and D. Baker, 1966: On frequency variations of ionospherically propagated HF radio signals, Radio Science, 1, 545-556.
- Donn, W.L. and D. Shaw, 1967: Exploring the atmosphere with nuclear explosions, Rev. Geophys. 5, 53-82.
- Donn, W.L. and E.S. Posmentier, 1967: Infrasonic waves from the marine storm of April 7, 1966. J. Geophys. Res., 72, 1.
- Donn, W.L., E.S. Posmentier, U. Fehr, and N.K. Balachandran, 1968: Infrasound from long range from Saturn V, 1967. (submitted to Science).
- Fehr, U., 1967: Measurements of infrasound from artificial and natural sources. J. Geophys. Res. 72, 2403-2417.
- Kentor, A.J. and A.E. Cole, 1964: Zonal and meridional winds to 120 kilometers. J. Geophys. Res., 69, 5131.
- Khvostikov, I.A., 1964: The Upper Layers of the Atmosphere, National Aeronautics and Space Administration, TT F-315, Washington, D.C.
- Manring, E., J. Bedinger, H. Knoflich, and D. Layzer, 1964: An experimentally determined model for the periodic character of winds from 83 to 135 km, National Aeronautics and Space Administration, Cf-36, Washington, D.C.

N72-25388

E. S. Posmentier, W. L. Donn

- Murgatroyd, R.J., 1957: Winds and temperatures between 20 Km and 100 Km, Rev. Quart. J. Roy. Meteorol. Soc., 83, 417.
- Pfeffer, R., and J. Zarichny, 1963: Acoustic-gravity wave propagation in an atmosphere with two sound channels. Geofisica Pura et Applicata, 55, 175-199.
- Posmentier, E.S., 1968a: A theory of microbaroms. Geophys. J. Roy. Astron. Soc., 13, 487-501.
- Posmentier, E.S., 1968b: Natural atmospheric infrasound of 0.1-0.4 Hz. PhD dissertation, Columbia University.
- Posmentier, E.S. and W.L. Donn, 1968: Natural atmospheric infrasound of 0.1-0.4 Hz. J. Geophys. Res. (submitted)
- Stolov, H., 1955: Tidal wind fields in the atmosphere, J. Meteorology., 12, 117.

THE HUDSON LABORATORIES MICROBAROGRAPH SYSTEM:  
RESULTS AND FUTURE TRENDS

I. Tolstoy and T. Herron  
Hudson Laboratories of Columbia University  
Dobbs Ferry, New York 10522

ABSTRACT

An outline of the Hudson Laboratories Microbarograph system is given, with mention of some results and problems for periods ranging from a few minutes to a few hours.

1. THE HUDSON LABORATORIES MICROBAROGRAPH ARRAY

In late 1965 the development of an ultra-low frequency ( $10^{-4}$  Hz  $< f < 1$  Hz) microbarograph array was undertaken at Hudson Laboratories, Columbia University. Since we desired to include periods up to 90 min or so, we had to make our own microbarographs. This was done during the fall of 1965 and early 1966, following a design suggested and already partially tested by J. Young and R. Cook of the ESSA infrasonics groups in Washington, D. C. Since 1966, the number of sensors operating in the field has varied between 1 and 16, depending upon the particular experiment being conducted. On the whole, the system has steadily grown to its present size of 16 microbarographs. A map showing the distribution of sensors as of spring 1968 is given in Fig. 1.

In addition to the microbarographs, the system includes one Doppler-shift type ionosounder and magnetometers at the Catskill (New York), Thornhurst (Pennsylvania), and Lebanon (New Jersey) sites.

All instrument outputs are transmitted by telephone lines to the central recording station at Hudson Laboratories in Dobbs Ferry. The data are recorded in digital form (BCD) on magnetic tape, with a total capacity of 32 channels capable of recording one four-digit number each twice a second.

2. TYPE OF PHENOMENA INVESTIGATED SO FAR. SOME RESULTS.

Most of the system's work to date has been oriented toward a study of background pressure fluctuations for periods of 5 min to 90 min, approximately. Velocities of propagation for naturally occurring disturbances in this band appear to vary from about  $10 \text{ m sec}^{-1}$  to several hundred  $\text{m sec}^{-1}$ . The corresponding wavelengths therefore vary from a few km to  $10^3$  km or so. This scale of dimensions corresponds to what the meteorologists refer to as the mesoscale, somewhere between meteorological phenomena proper at one end and boundary layer turbulence and wind effects at the other (micrometeorological effects, see, e. g., Lumley and Panofsky, 1964). Insofar as the acoustician is concerned, periods  $1 \text{ sec} < T < 10 \text{ min}$  are in the infrasonic domain. Periods  $T > 10 \text{ min}$ , when they do correspond to wave phenomena, belong to the internal gravity wave part of the spectrum.

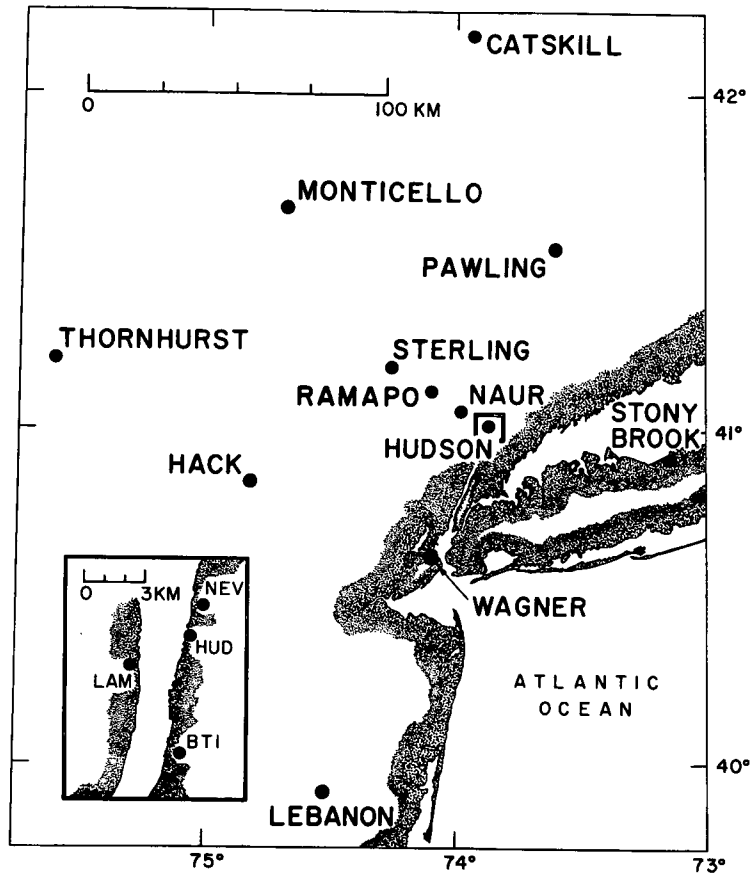


Figure 1. Microbarograph array.

The spectral distribution of the background energy given by our studies is typified by the average, smoothed, type of behavior shown in Fig. 2. This particular curve is an average over many weeks of data. It is representative of hundreds of curves of this type obtained by us over a period of about two years. It is also consistent with earlier results of Gossard (1960), Golitsyn (1964), and Pinus *et al.* (1967).

As a result of studies performed in the summer and fall of 1967, using the small scale network of microbarographs shown in the inset of Fig. 1, we have succeeded in showing quite conclusively that much of the energy input into this band comes from the jet stream (Herron and Tolstoy, 1968; Tolstoy and Herron, 1968). Thus, for lengthy periods of time (often for weeks on end) the direction of travel of pressure perturbations in this part of the spectrum closely follows that of the jet stream winds aloft. The velocities of propagation, in the  $20\text{--}50\text{ m sec}^{-1}$  are also of the same order. In addition, a preliminary calculation indicates that the correct order of magnitude for ground level pressure perturbations, as well as the main spectral characteristics, are obtained if one assumes that the wind fluctuation power spectrums obtained from flying aircraft (Kao and Woods, 1964; Reiter, 1963) correspond to internal gravity wave systems being shed by the jet stream. This shedding could occur near the core or, as suggested by Claerbout (1967), near the level of least stability below the core itself. Figure 3 shows a comparison of our calculation with some of our mean and extremal power spectrums. It is seen that this mechanism not only yields the correct orders of magnitude for the pressure fluctuations, but also appears to explain the typical knee appearing on all pressure power spectrums in this band of periods.

Figure 2. A typical single spectrum (24 hour sample) and a monthly mean power spectrum for background pressure fluctuations at Hudson Laboratories.

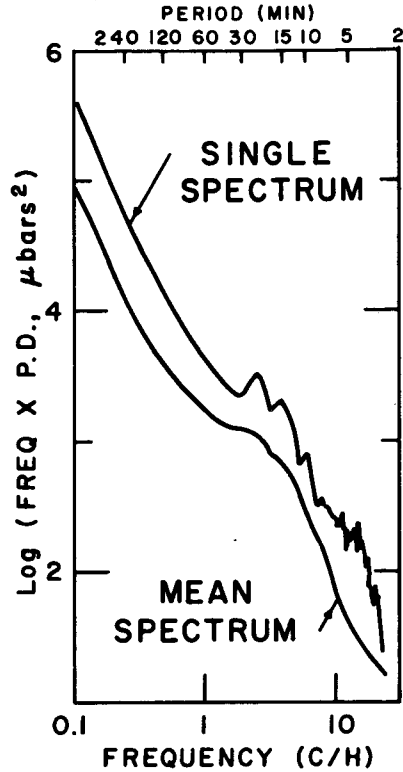
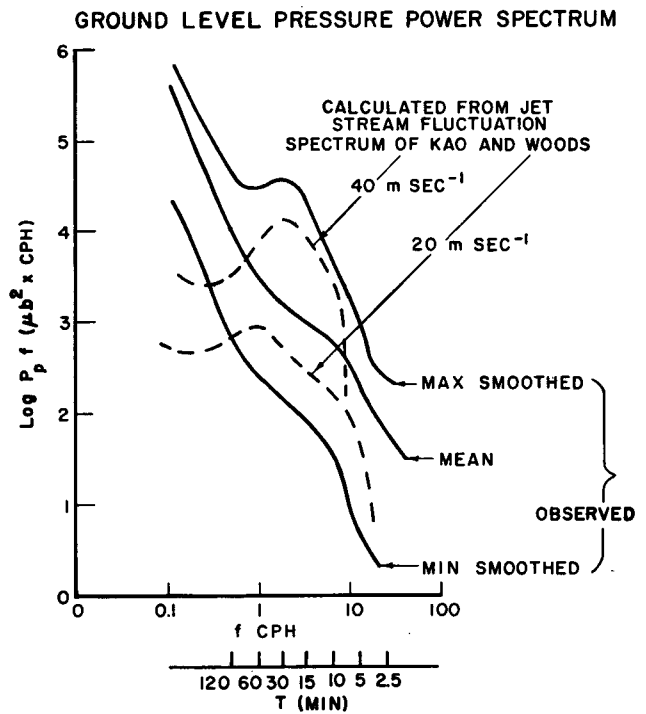


Figure 3. Comparison of mean and smoothed extremum power spectra for pressure with calculated power spectra, based upon a simplified mechanism of internal gravity wave generation by the jet stream, for two different assumptions for the stream velocity (dashed lines).



## 3. SOME FURTHER PROBLEMS TO BE INVESTIGATED

Insofar as larger-scale phenomena are concerned, the use of beam forming techniques on the full array of Figure 1 indicates the existence of disturbances having periods of 15 to 50 min, traveling at speeds of the order of  $300 \text{ m sec}^{-1}$ . A systematic study of these processes is underway. If this is a wave phenomenon, as appears probable, then one is dealing with internal gravity waves of wavelengths between 300 and 1000 km.

Apart from long wavelength internal gravity waves of this type and short wavelength ones of the kind generated by the jet stream, there exist other processes for the propagation of pressure disturbances in the mesoscale range. Obvious candidates are wind-borne convection systems, large-scale eddies, etc. There is also another fairly obvious wave phenomenon, i.e., that of stability (or instability!) waves in shear flows. This type of disturbance is well known to hydrodynamical theorists (see, e.g., Lin, 1955). Clearly the tropospheric wind system which culminates in the jet stream at 10 km altitude represents a steady shear flow capable of supporting waves of this kind. A more thorough theoretical and experimental study of the relevance of these waves is desirable.

## ACKNOWLEDGMENTS

This work was supported by the Office of Naval Research and the Advanced Research Projects Agency under Contract Nonr-266(84). Reproduction in whole or in part is permitted for any purpose of the United States Government. It is Hudson Laboratories of Columbia University Contribution No. 327.

## REFERENCES

- Lumley, J. L., and H. A. Panofsky, 1964: The Structure of Atmospheric Turbulence. New York, Interscience Publishers, 239 p.
- Gossard, E. E., 1960: Spectra of atmospheric scalars. J. Geophys. Res., 65, 3339-3351.
- Golitsyn, G. S., 1964: On the time spectrum of micropulsations in atmospheric pressure. Izv. Geophys. Ser., 8, 1253.
- Pinus, N. Z., E. R. Reiter, G. N. Shur, and N. K. Vinnichenko, 1967: Power spectra of turbulence in the free atmosphere. Tellus, 19(2), 206.
- Herron, T. J., and I. Tolstoy, 1968: Tracking jet stream winds from ground level pressure signals. J. Atmos. Sci., in Press.
- Tolstoy, I., and T. J. Herron, 1968: A model for atmospheric pressure fluctuations in the mesoscale range. J. Atmos. Sci., in Press.
- Kao, S. K., and H. D. Woods, 1964: Energy spectra of mesoscale turbulence along and across the jet stream. J. Atmos. Sci., 21, 513.
- Reiter, E., 1963: Jet-Stream Meteorology. U. of Chicago Press, 515 p.
- Claerbout, J. F., 1967: Electromagnetic Effects of Atmospheric Gravity Waves. Massachusetts Institute of Technology thesis.
- Lin, C. C., 1955: The Theory of Hydrodynamic Stability. Cambridge U. Press, 155 p.

## AUTHOR INDEX

Aarons, J. . . . .	89
Astheimer, R. W. . . . .	517
Atlas, D. . . . .	245
Bandeen, W. R. . . . .	465
Barrett, E. W. . . . .	173
Beard, C. I. . . . .	79
Birkemeier, W. P. . . . .	337
Chahine, M. T. . . . .	443
Clemesha, B. R. . . . .	201
Collis, R. T. H. . . . .	147
Cook, R. K. . . . .	633
Cox, D. C. . . . .	295
Decker, M. T. . . . .	397
Deitz, P. H. . . . .	119
Donn, W. L. . . . .	681
Fox, H. L. . . . .	671
Fried, D. L. . . . .	133
Fritz, S. . . . .	507
Godson, W. L. . . . .	511
Grams, G. . . . .	207
Hablutzel, B. C. . . . .	555
Hardy, K. R. . . . .	217
Harp, J. C. . . . .	21
Herron, T. . . . .	693
Hufnagel, R. E. . . . .	145
Ishimaru, A. . . . .	87

Kaplan, L. D.	435
Kasemir, H. W.	617
Katz, I.	217
Kessler, E.	287
Kieburtz, R. E.	367
King, J. I. F.	453
Krause, F. R.	555
Lawrence, R. S.	91
Lee, R. W.	21
Lhermitte, R. M.	253
Little, C. G.	619
Lucy, R. F.	125
Marshall, J. S.	291
Montgomery, A. J.	525
Pierce, E. T.	595
Portman, D. J.	111
Posmentier, E. S.	681
Reagan, J. A.	213
Sandborn, V. A.	589
Schotland, R. M.	179
Staelin, D. H.	409
Strohbehn, J. W.	1
Tolstoy, I.	693
Welch, W. J.	369
Westwater, E. R.	397
Wheelon, A. D.	359